frontiers | Research Topics

Targeted cancer therapies, from small molecules to antibodies, volume II

Edited by
Zhe-Sheng Chen, Yunkai Zhang, Jian-ye Zhang and Yan-yan Yan

Published in
Frontiers in Oncology
Frontiers in Pharmacology

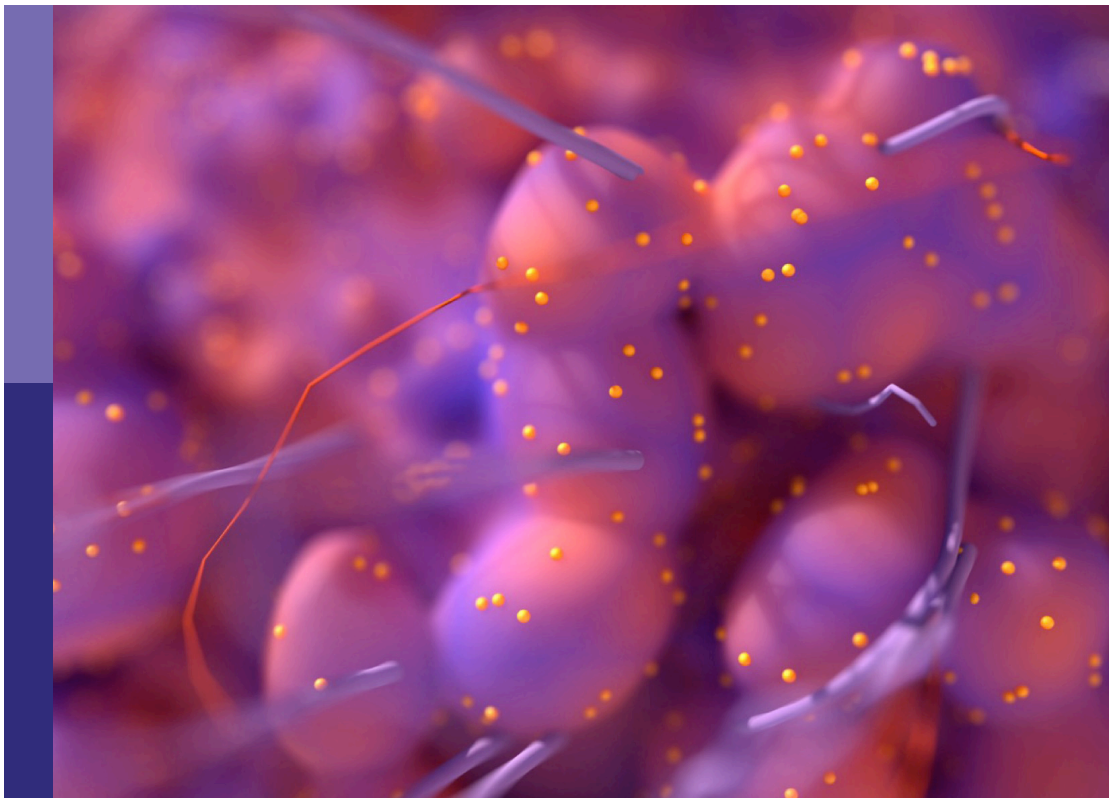

ISSN 1664-8714
ISBN 978-2-8325-3003-0
DOI 10.3389/978-2-8325-3003-0

About Frontiers

Frontiers is more than just an open access publisher of scholarly articles: it is a pioneering approach to the world of academia, radically improving the way scholarly research is managed. The grand vision of Frontiers is a world where all people have an equal opportunity to seek, share and generate knowledge. Frontiers provides immediate and permanent online open access to all its publications, but this alone is not enough to realize our grand goals.

Frontiers journal series

The Frontiers journal series is a multi-tier and interdisciplinary set of open-access, online journals, promising a paradigm shift from the current review, selection and dissemination processes in academic publishing. All Frontiers journals are driven by researchers for researchers; therefore, they constitute a service to the scholarly community. At the same time, the *Frontiers journal series* operates on a revolutionary invention, the tiered publishing system, initially addressing specific communities of scholars, and gradually climbing up to broader public understanding, thus serving the interests of the lay society, too.

Dedication to quality

Each Frontiers article is a landmark of the highest quality, thanks to genuinely collaborative interactions between authors and review editors, who include some of the world's best academicians. Research must be certified by peers before entering a stream of knowledge that may eventually reach the public - and shape society; therefore, Frontiers only applies the most rigorous and unbiased reviews. Frontiers revolutionizes research publishing by freely delivering the most outstanding research, evaluated with no bias from both the academic and social point of view. By applying the most advanced information technologies, Frontiers is catapulting scholarly publishing into a new generation.

What are Frontiers Research Topics?

Frontiers Research Topics are very popular trademarks of the *Frontiers journals series*: they are collections of at least ten articles, all centered on a particular subject. With their unique mix of varied contributions from Original Research to Review Articles, Frontiers Research Topics unify the most influential researchers, the latest key findings and historical advances in a hot research area.

Find out more on how to host your own Frontiers Research Topic or contribute to one as an author by contacting the Frontiers editorial office: frontiersin.org/about/contact

Targeted cancer therapies, from small molecules to antibodies, volume II

Topic editors

Zhe-Sheng Chen — St. John's University, United States
Yunkai Zhang — BioSpatula LLC, United States
Jian-ye Zhang — Guangzhou Medical University, China
Yan-yan Yan — Shanxi Datong University, China

Citation

Chen, Z.-S., Zhang, Y., Zhang, J.-y., Yan, Y.-y., eds. (2023). *Targeted cancer therapies, from small molecules to antibodies, volume II*. Lausanne: Frontiers Media SA. doi: 10.3389/978-2-8325-3003-0

Table of contents

frontiers | Frontiers in Pharmacology

TYPE Editorial
PUBLISHED 30 June 2023
DOI 10.3389/fphar.2023.1147488

OPEN ACCESS

EDITED AND REVIEWED BY
Filippo Drago,
University of Catania, Italy

*CORRESPONDENCE
Yun-Kai Zhang,
mail@ykzhang.com
Zhe-Sheng Chen,
chenz@stjohns.edu

†These authors have contributed equally to this work

RECEIVED 18 January 2023
ACCEPTED 23 June 2023
PUBLISHED 30 June 2023

CITATION
Su C-Y, Yan Y-Y, Zhang J-Y, Zhang Y-K and Chen Z-S (2023), Editorial: Targeted cancer therapies, from small molecules to antibodies, volume II.
Front. Pharmacol. 14:1147488.
doi: 10.3389/fphar.2023.1147488

Editorial: Targeted cancer therapies, from small molecules to antibodies, volume II

Chao-Yue Su[1†], Yan-Yan Yan[2†], Jian-Ye Zhang[3], Yun-Kai Zhang[4*] and Zhe-Sheng Chen[5*]

[1]Department of Pharmacy, The Fifth Affiliated Hospital, Sun Yat-sen University, Zhuhai, Guangdong, China, [2]School of Medicine, Shanxi Datong University, Datong, China, [3]Guangzhou Municipal and Guangdong Provincial Key Laboratory of Molecular Target and Clinical Pharmacology, The NMPA and State Key Laboratory of Respiratory Disease, School of Pharmaceutical Sciences and the Fifth Affiliated Hospital, Guangzhou Medical University, Guangzhou, China, [4]BioSpatula LLC, Telford, PA, United States, [5]Department of Pharmaceutical Sciences, College of Pharmacy and Health Sciences, St. John's University, New York, NY, United States

KEYWORDS

cancer, target, small molecules, antibodies, therapy

Editorial on the Research Topic
Targeted cancer therapies, from small molecules to antibodies, volume II

Rapid advances in molecular biology have enabled an unprecedented understanding of the genes that drive tumorigenesis and progression, making innovative targeted therapy an attractive new strategy for treating cancers. By creating medications that target tumor-specific targets, such as small molecule drugs and monoclonal antibodies, the drug resistance and cytotoxicity of conventional chemotherapy drugs will be greatly reduced. Therefore, this Research Topic "*Targeted Cancer Therapies, from Small Molecules to Antibodies, Volume* II" focuses on the role of novel targets and targeted anticancer drugs in reducing tumor therapy resistance and precise tumor therapy. To these ends, 32 articles, including 2 case reports, 10 reviews and 20 original research articles, were ultimately accepted for publication in this Research Topic.

The development of tumor resistance mechanisms is multifaceted and highly heterogeneous at the intratumoral or intercellular level. Due to clonal selection or evolution under therapeutic pressure, "off-target effects" frequently arise with a single tumor-targeting therapy, which may be related to novel genetic alterations in the targeted oncogene or other related oncogenes. Therefore, the combination of two targeted drugs is very necessary for tumor treatment. Wang et al. emphasized the use of dual-targeted therapy, that is, to deal with non-genetic drug resistance during tumor treatment by simultaneously inhibiting two or more related targets or pathways. The study by Wang et al. found that AZD5153, a small molecule inhibitor, targeting the DNA damage repair regulator MUS81, could enhance the antitumor efficacy of talazopanib. Mechanistically, AZD5153 impaired the activation of the ATR/CHK1 cell cycle signaling pathway and promoted gastric cancer cells with talazoparib-induced DNA damage to continue mitosis. Interestingly, a study performed by Fu et al. showed that antihypertensive drug amlodipine combined with gefitinib can synergistically inhibit the proliferation of non-small cell lung cancer (NSCLC) A549 cells by blocking the cell cycle. Similarly, Xia et al. uncovered that hypolipidemic drug simvastatin combined with DNA methyltransferase inhibitor 5-Aza-2'-deoxycytidine to mediate pyroptosis via GSDME (a pyroptotic effector) to exert anti-tumor effect. Li et al.

showed that the combination of fruquintinib and sintilimab (anti-PD-1 antibody) greatly inhibits colorectal cancer growth by altering tumor immune microenvironment. Zhang et al. provided a case report, showing that the combination of the PARP inhibitor olaparib with EGFR TKI dacomitinib could significantly benefit a NSCLC patient with osimertinib-resistant brain and leptomeningeal metastases who had EGFR mutations combined with TP53 and ERBB2 mutations. In addition, double-dose icotinib exposure has also been shown to respond well to the treatment of targetable TKIs including almonertinib or osimertinib, in patients with emerging EGFR exon 20 T790M mutations (Chen et al.). Liu et al. showed that gemcitabine plus anlotinib was more effective and safe compared with gemcitabine plus docetaxel in advanced soft tissue sarcoma.

Additionally, several studies have shown that the drug delivery system could be used to enhance the active targeting capacity of drugs to improve the anti-tumor effect. For example, anti-CD47 antibody conjugated with valine-citrulline-monomethyl auristatin E (VCMMAE), named anti-CD47-VCMMAE, had a greater therapeutic effect on NSCLC tumors with high expression of *CD47* gene. Combining VCMMAE with anti-CD47 mAb was a novel and promising immunotherapy approach to directly kill NSCLC (Chiang et al.). Xie et al. highlighted the conjugation of chemotherapeutic agents to targeting ligands as a unique treatment approach for osteosarcoma. The selection of these targeting ligands was diverse, including antibodies, aptamers, peptides, saccharide, vitamin, bisphosphonates, hyaluronic acid and folate. Interestingly, Canals Hernaez et al. showed that PODO447 (a novel antibody targeting podocalyxin) conjugated to monomethyl auristatin E, could be used as a highly specific and potent antibody-drug conjugate to kill ovarian, pancreatic, glioblastoma, and leukemia cell lines. Therefore, PODO447-antibody drug conjugates served as precise tumor-specific and highly effective immunotherapeutic agents for targeting human tumors. In addition, Diao et al. prepared liposomes of peanut agglutinin-conjugated irinotecan hydrochloride and capecitabine with a stronger ability to target MUC1 (tumor-associated antigen mucin 1)-positive liver cancer cells.

Over the past decade, a great deal of research has been directed at RNA-based therapeutics. Therapeutic targeting of noncoding RNAs (ncRNAs), such as microRNAs (miRNAs) and long noncoding RNAs (lncRNAs), is propelling the future advancement of biomarker development, as well as represents an attractive approach for the treatment of human tumor. In those review articles, Fu and Xu summarized the emerging role of transfer RNA-derived small RNAs (tsRNAs) as cancer diagnostic and prognostic biomarkers. In addition, N6-methyladenosine (m6A), as a major internal epigenetic modification in eukaryotic mRNA, is a promising therapeutic target for malignant tumors. Zhu et al. introduced the molecular mechanism of m6A methylation involved in regulation and its role in tumor therapy. Wang et al. showed that silencing of lncRNA CHRM3-AS2 expression inhibited the malignant progression of glioma by regulating miR-370-5p/KLF4 expression. Another study showed that lncRNA TMPO-AS1 was overexpressed in endometrial cancer (EC) tissues and was closely related to the proliferation, invasion, glycolysis and paclitaxel resistance of EC cells. Dysregulation of lncRNA TMPO-AS1-miR-140/miR-143 axis promoted glycolysis and drug resistance in EC cells by upregulating GLUT1 expression (Dong et al.). It is worth noting that many recent studies have focused on the role of circular RNAs (circRNAs) in regulating gene transcription and splicing and encoding proteins. CircRNAs exert competitive endogenous RNA (ceRNA) to sponge miRNA and thus play an integral role in tumorigenesis. Shi et al. showed that silencing circOMA1 inhibits osteosarcoma progression by sponging miR-1294 to regulate c-Myc expression.

With the development of targeted therapy and immunotherapy, more and more cancer-related targets and signal transduction pathways have been examined. Designing and investigating small molecule inhibitors or antibodies by targeting these oncogenes or signaling pathways provides new opportunities for developing new therapeutic strategies in personalized oncology. For example, the c-Met gene is overexpressed in many human tumors and is related to the proliferation, differentiation, invasion and drug resistance of tumor cells. Anti-tumor therapies targeting c-Met, such as TKIs, monoclonal Antibodies and adoptive immunotherapy have shown remarkable effects in the treatment of digestive system tumors (Zhang et al.). Two review articles highlighted the crucial roles of the transmembrane proteins 88 (TMEM88) and 16A (TMEM16A) in tumorigenesis, progression, metastasis, proliferation and apoptosis, respectively (Guo et al.; Cai et al.). Therefore, inhibitors targeting TMEM88 and TMEM16A are expected to become new strategies in the treatment of malignant tumors. Wu et al. discovered a new potential therapeutic target for bladder cancer: vaccinia-related kinase 1, and confirmed that it could significantly inhibit the proliferation of bladder cancer cells *in vivo* and *in vitro*. Overexpression of SEMA3C played an important role in promoting cancer cell survival, which could be used as a new therapeutic target or diagnostic marker in pancreatic cancer, especially in tumors harboring specific KRAS G12D mutation. Zhang et al. discovered a gene named SEMA3C was highly expressed in pancreatic cancer cell lines and patients with a G12D mutation in KRAS. Of note, a case report performed by Luo et al. identified the expression of a novel *FGFR2-KIAA1217* fusion gene in gastrointestinal stromal tumors. PI3K/AKT is an important cancer-related pathway and designing new anti-tumor targeted drugs by targeting this pathway is a very promising therapeutic prospect. Peng et al. reviewed that aberrant activation of the PI3K/AKT/mTOR pathway has a significant role in carcinogenesis. Guo et al. showed that hinokiflavone, a natral double flavone compound, inhibits the growth of esophageal squamous cell carcinoma by regulating PI3K/AKT/mTOR signal pathway to induce apoptosis. Hinokiflavone can be used as a complementary/alternative agent for ESCC therapy. Another similar study also highlighted the importance of targeting the PI3K/AKT signaling pathway in tumor therapy. Vemurafenib suppresses breast cancer by targeting PI3K/AKT signaling pathway to inhibit immune evasion biomarker BCL2A1 (Dai et al.).

Recent studies have found that epigenetic enzyme-mediated transcriptional dysregulation of oncogenes or tumor suppressor genes is closely related to the occurrence, progression and prognosis of tumors. Small molecule compounds targeting epigenetic regulatory enzymes such as DNA methylases, histone modifiers (methylation and acetylation), enzymes that specifically recognize post-translational modifications, and post-transcriptional regulators have emerged as promising therapeutic approaches (Jin et al.). Ma et al. showed that histone deacetylase inhibitor I13 could significantly inhibit proliferation and colony formation of acute myeloid leukemia cells by inducing cell differentiation coupled with

cell-cycle exit at G0/G1. It had also been shown that the natural product pectolinarigenin inhibited the proliferation of glioblastoma by inhibiting ribonucleotide reductase subunit M2 to induce cell cycle arrest (Jiang et al.). In addition, Guo et al. highlighted the critical role of adenylyl cyclase, a protease superfamily associated with cancer drug resistance and progression, in mediating tumor drug resistance and prognostic therapeutic targets. What's more, developing anticancer compounds that could inhibit DNA or RNA repair enzymes was also a promising approach to fighting cancer. Kirsanov et al. found that 7-methylguanine (7-MG) could competitively inhibit DNA repair enzyme poly (ADP-ribose) polymerase and RNA-modifying enzyme tRNA-guanine transglycosylase and represents a potential anticancer drug candidate. Xing et al. designed a novel compound targeting aminopeptidase N (a type II membrane bound metalloprotease, also known as CD13), which could be used as a tumor chemosensitizer and a lead compound for cancer stem cell-based therapy.

In summary, the research topic of "*Targeted Cancer Therapies, from Small Molecules to Antibodies, Volume* II" emphasized the significance of both new small molecules and antibodies in cancer targeting therapy. With a deeper understanding of oncogenes or tumor suppressor genes and the elucidation of tumor-related signal transduction pathways, we anticipated that more and more anticancer small molecules and antibodies will be developed, opening up a new avenue of precise cancer therapy.

Author contributions

C-YS conducted the literature collection and drafted the manuscript. Y-YY, J-YZ, and Y-KZ made important revisions to the manuscript. Z-SC revised and approved the final version of the manuscript for publication. All authors contributed to the article and approved the submitted version.

Conflict of interest

Y-KZ was empolyed by BioSpatula LLC.

The remaining authors declare that the research was conducted in the absence of any commercial or financial relationships that could be construed as a potential conflict of interest.

Publisher's note

frontiers in Oncology

ORIGINAL RESEARCH
published: 01 February 2022
doi: 10.3389/fonc.2022.833719

Hinokiflavone Inhibits Growth of Esophageal Squamous Cancer By Inducing Apoptosis *via* Regulation of the PI3K/AKT/mTOR Signaling Pathway

Jida Guo[†], *Shengqiang Zhang*[†], *Jun Wang*, *Pengfei Zhang*, *Tong Lu* and *Linyou Zhang*[*]

Department of Thoracic Surgery, The Second Affiliated Hospital of Harbin Medical University, Harbin Medical University, Harbin, China

OPEN ACCESS

Edited by:
Zhe-Sheng Chen, St. John's University, United States

Reviewed by:
Shuang Fan, University Medical Center Göttingen, Germany
Yanan Song, First Affiliated Hospital of Zhengzhou University, China

***Correspondence:**
Linyou Zhang
lyzhang@hrbmu.edu.cn

[†]*These authors have contributed equally to this work*

Specialty section:
This article was submitted to Cancer Molecular Targets and Therapeutics, a section of the journal Frontiers in Oncology

Received: *12 December 2021*
Accepted: *10 January 2022*
Published: *01 February 2022*

Citation:
Guo J, Zhang S, Wang J, Zhang P, Lu T and Zhang L (2022) Hinokiflavone Inhibits Growth of Esophageal Squamous Cancer By Inducing Apoptosis via Regulation of the PI3K/AKT/mTOR Signaling Pathway. Front. Oncol. 12:833719. doi: 10.3389/fonc.2022.833719

Background: Globally, esophageal cancer ranks as the seventh most common cancer. Esophageal squamous cell carcinoma (ESCC) is one of its major histological types. ESCC accounts for the vast majority of cases in China, and the mortality rate is high. Cisplatin, the standard adjuvant chemotherapy drug for ESCC, has a modest response rate due to the development of drug resistance. Hinokiflavone (HF) is a natural biflavonoid compound with anti-melanoma activity. However, its anti-tumor effect on ESCC and the underlying mechanisms remain largely unknown.

Methods: The ESCC cell lines KYSE150 and TE14 were used. The cell counting kit-8 assay and flow cytometry analysis, along with colony formation, EdU, wound healing, and Transwell migration assays, were performed to assess cell characteristics (viability, migration, invasion, and apoptosis) following treatment with HF. Gene Ontology (GO), Kyoto Encyclopedia of Genes and Genomes (KEGG), western blotting, and molecular docking were used to investigate the pathways potentially modulated by HF. *In vivo* anti-tumor effects of HF were also investigated using a mouse xenograft model.

Results: Our findings revealed that HF inhibited ESCC cell proliferation. Hoechst 33342 staining, annexin V-FITC/PI staining, and western blotting confirmed that HF causes caspase-dependent apoptosis. KEGG pathway enrichment analysis and western blotting indicated that the PI3K/AKT/mTOR pathway played an important role in the process of HF-induced apoptosis. Furthermore, HF effectively impaired the migration and invasion abilities of KYSE150 cells and downregulated the expression of the matrix metalloproteinases (MMP) MMP2 and MMP9. HF inhibited tumor growth and exhibited minimal toxicity in the organs of the KYSE150 xenograft model.

Conclusion: This is the first study to demonstrate the inhibition of ESCC growth and progression by HF. The underlying mechanism is through blocking the PI3K/AKT/mTOR signaling pathway, thereby inhibiting cell proliferation and inducing apoptosis. HF can be used as a complementary/alternative agent for ESCC therapy.

Keywords: esophageal cancer, hinokiflavone, apoptosis, KEGG analysis, molecular docking, PI3K/AKT/mTOR signal pathway

INTRODUCTION

Esophageal cancer is the sixth leading cause of cancer-related deaths and the seventh most common cancer worldwide (1). It is well known that there are two dominant histological types of esophageal cancer: esophageal adenocarcinoma and esophageal squamous cell carcinoma (ESCC). ESCC accounts for 90% of all esophageal cancer cases in Asia and Africa (1). In recent years, despite the development of multimodal treatment including surgery combined with chemoradiotherapy and targeted therapy, the prognosis of esophageal cancer patients remains poor due to the strong malignancy of this cancer (2, 3). Therefore, the development of novel therapeutic approaches for this disease is urgent and necessary.

Natural products have a long history of use for the treatment of human disease, which is of great value for drug discovery and development (4). Moreover, many common chemotherapeutic compounds have been derived from natural products (5, 6). Hinokiflavone (HF) (**Figure 1A**, $C_{30}H_{18}O_{10}$) has been extracted from several plants, including *Selaginella tamariscina, Juniperus phoenicea*, and *Rhus succedanea*, with high stability. It exhibits several biological activities including cytotoxicity (7), anti-HIV-1 reverse transcriptase activity (8), and antioxidant activity (9). Sui et al. (10) reported that the ethyl acetate extract of *Selaginella doederleinii* Hieron inhibits proliferation of A549 cell lines by inducing apoptosis. Magne et al. (11) also identified natural flavonoids in HF that are useful therapeutic agents for breast cancer. In addition, HF might also be a novel compound to treat melanoma by cell cycle arrest, inducing apoptosis and blocking cell migration and invasion (12). However, the antitumor effect of HF in ESCC and its specific targeted signaling pathways have not been investigated.

Multiple studies have demonstrated that phosphoinositides, the multiphosphorylated derivatives of phosphatidylinositol, are membrane-bound signaling molecules that play a crucial role in a variety of cellular biological processes (13–15). Under general physiological conditions, phosphatidylinositol-3-kinase (PI3K) activates AKT (protein kinase B) by phosphorylating Thr 308 and Ser 473 (p-AKT) (16, 17). p-Akt then phosphorylates several of its downstream effector proteins, such as tuberous sclerosis complex 2 (TSC2) and glycogen synthase kinase 3 (GSK3α/β), and these activated proteins subsequently regulate cell growth, survival, and apoptosis (18, 19). Whereas mammalian target of rapamycin (mTOR) was shown to be the major signaling molecule downstream of TSC2, targeting regulation of the PI3K/Akt/mTOR pathway has been proven effective in cancer therapies (20, 21). Accumulating evidence has also shown that the PI3K/Akt signaling pathway is activated in multiple tumor types and contributes to tumor progression by promoting tumor cell proliferation, apoptosis resistance, and distant metastasis (22, 23). Moreover, the PI3K/AKT signaling pathway plays a vital role in ESCC growth and metastasis (24, 25).

In the current study, we extensively explored the anti-tumor effects of HF on human esophageal cancer cells *in vitro* and *in vivo* as well as the underlying molecular mechanisms. We found that HF exhibited a strong growth inhibitory effect on two ESCC cell lines (KYSE150 and TE14) and the PI3K/AKT/mTOR signaling pathway plays a crucial role in HF-induced apoptosis in these cells. These results indicate that HF has potential anti-tumor activity, which can be exploited to develop effective therapeutic strategies for ESCC.

MATERIALS AND METHODS

Reagents, Antibodies and Kits

HF of 98% purity was purchased from Chengdu Biopurify Phytochemicals, Ltd. (Chengdu, China). Dimethylsulfoxide (DMSO), RPMI 1640 medium, and fetal bovine serum (FBS) were purchased from Sigma Chemical Co. (St Louis, MO, USA). Antibodies against β-actin, phosphorylated PI3K [p-PI3K (Tyr458 and Tyr199)], PI3K, phosphorylated AKT [p-AKT (Ser473 and Thr308)], AKT, cleaved Caspase 3 (c-Caspase 3), phosphorylated mTOR [p-mTOR (Ser2448)], mTOR, matrix metalloproteinase-2 (MMP2), and MMP9 were purchased from Cell Signaling Technology, Inc. (Danvers, MA, USA). Antibodies against Bcl-2 and Bax were purchased from Proteintech Group, Inc. (Chicago, IL, USA). RIPA lysis buffer, phenylmethanesulfonyl fluoride (PMSF), and the bicinchoninic acid (BCA) protein assay kit were from Beyotime (Nanjing, China). Enhanced chemiluminescence detection reagent was obtained from GE Healthcare Life Sciences Inc. (Marlborough, MA, USA). SC-79 (AKT activator) was purchased from MedChemExpress (Shanghai, China). Cell Counting Kit-8 (CCK-8) was obtained from Dojindo Laboratories (Kumamoto, Japan). Hoechst33342 and BeyoClick™ EdU Cell Proliferation Kit with Alexa Fluor 594 and the Annexin V-fluorescein isothiocyanate (FITC)/propidium iodide (PI) apoptosis detection kit were purchased from Beyotime Biotechnology (Jiangsu, China).

A stock solution of HF dissolved in DMSO (40 mM) was stored at -20°C and diluted with medium for experimental applications.

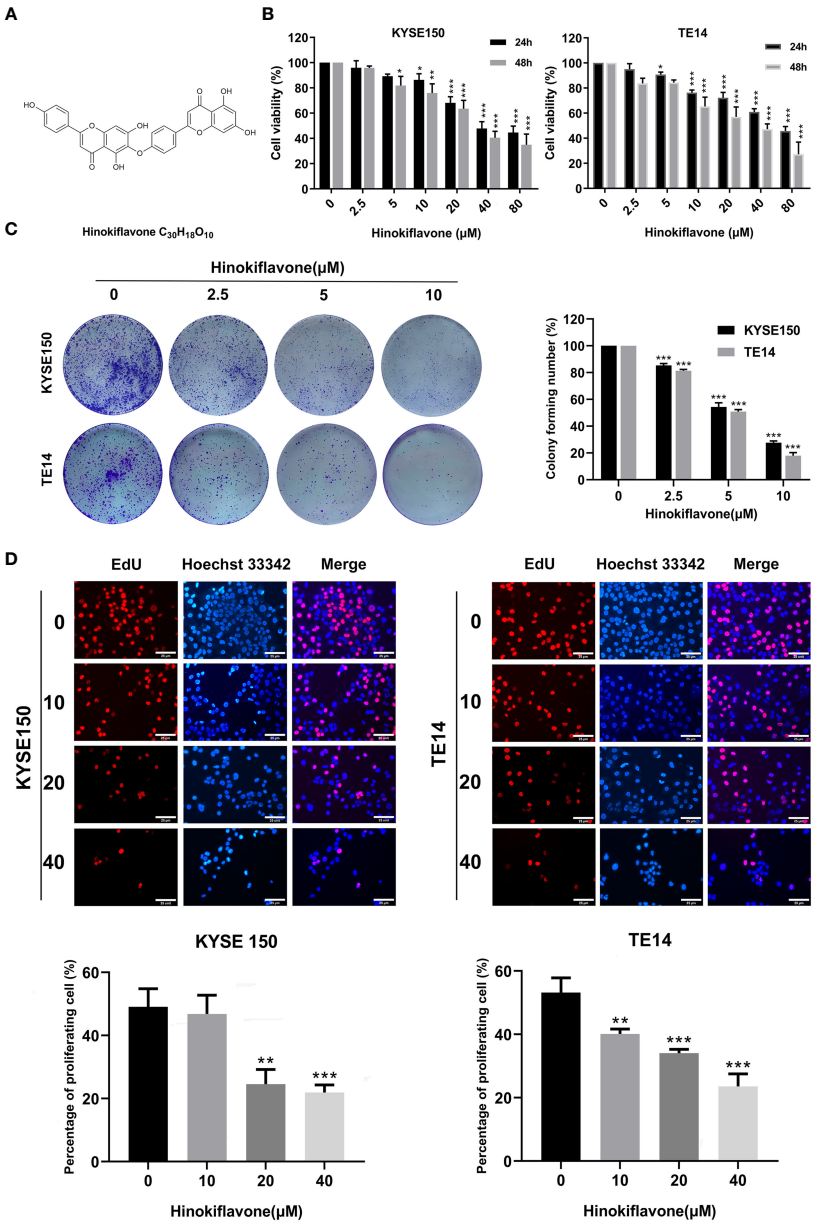

FIGURE 1 | Effect of hinokiflavone (HF) on the proliferation of esophageal squamous cell carcinoma (ESCC) cells. **(A)** Two-dimensional chemical structure of HF ($C_{30}H_{18}O_{10}$). **(B)** KYSE150 and TE14 cell lines were incubated with different concentrations of HF for 24 and 48 h Cell viability was evaluated using the CCK-8 assay. **(C)** HF reduced colony formation of ESCC cells. KYSE150 and TE14 cells were treated with 0, 2.5, 5, and 10 μM of HF and cultured for 9 days to form colonies. Colonies were stained with crystal violet and counted. **(D)** EdU assay analyzed the antiproliferative effect of HF on ESCC cells. Hoechst 33342 cell nuclei dye presented as blue fluorescence cells represent total cells, and EdU positive cells presented as red fluorescence represent proliferating cells. Magnification, ×200; scale bars = 25 μm. All the above experimental data are presented as the mean ± SD of three independent experiments. *$P < 0.05$; **$P < 0.01$; ***$P < 0.001$ compared to vehicle control (0 μM) group.

Cell Culture

KYSE150 and TE14 cell lines were purchased from the Cell Bank of the Chinese Academy of Sciences. Cells were cultured in RPMI 1640 medium with 10% FBS and 1% penicillin-streptomycin at 37°C in a humidified incubator with 5% CO_2 and 95% humidity.

Cell Proliferation Assay

Cell viability was determined using the CCK-8 assay. KYSE150 and TE14 cells were seeded at a density of 1×10^4 cells/well in 96-well plates. After 24 h of incubation, the cells were treated with 0, 2.5, 5, 10, 20, 40, and 80 μM of HF. Controls were treated with

RPMI medium containing DMSO only. After 24 h and 48 h, old medium was aspirated and 100 μL of CCK-8 working solution, diluted to 10% in culture medium, was added to each well and further incubated for 4 h at 37°C in a humidified incubator. The absorbance at 450 nm was measured using a microplate reader. IC_{50} values were calculated with Graphpad Prism 8 using data obtained from three independent experiments.

Colony Formation Assay

KYSE150 and TE14 cells were plated in 6-well plates (1.0×10^3 cells/well). After 24 h of incubation, the cells were incubated with various concentrations (0, 2.5, 5, and 10 μM) of HF for 9 days. Cells were fixed with 4% paraformaldehyde and then stained with 0.5% crystal violet for 15 min, after which a dissecting microscope was used to count colonies (> 50 cells).

EdU Assay

The EdU assay was performed to analyze proliferating cells by evaluating the incorporation of fluorescent labeled EdU into replicating DNA in the S phase of cell cycle. The BeyoClick™ EdU Cell Proliferation Kit with Alexa Fluor 594 was used for this purpose, according to the manufacturer's instructions. The maximum excitation wavelength of Alexa 594 is 590 nm, and the maximum emission wavelength is 615 nm. Briefly, KYSE150 and TE14 cells were seeded in 96-well plates at a cell density of 5.0×10^3 cells/well and treated with different concentrations of HF for 24 h. Edu was added to the culture medium and brought to a final concentration of 10 μM, and the cells were cultured for an additional 2.5 h at 37°C. Afterwards, cells were washed twice using phosphate-buffered saline (PBS) and fixed by 4% paraformaldehyde for 15 min at approximately 25°C. After co-staining with Hoechst 33342, the cells were imaged using a fluorescence microscope (Leica, Wetzlar, Germany).

Morphological Analysis by Hoechst 33342 Staining

Alterations in cell morphology, including cell shrinkage and apoptotic body formation, were analyzed after Hoechst 33342 staining to identify apoptotic cells. KYSE150 and TE14 cells were seeded in 96-well plates at a density of 5.0×10^3 cells/well and cultured for 24 h. After treatment with different concentrations of HF (0, 10, 20, and 40 μM) for 24 h, the cells were washed twice using PBS and fixed in 4% paraformaldehyde for 15 min. Then, the cells were stained using Hoechst 33342 working solution diluted well according to the instructions for 15 min at 25°C and analyzed under a fluorescence microscope (Zeiss, Axiovert 200, Oberkochen, Germany).

Quantification of Apoptosis

Further verification of HF-induced apoptosis was carried out using the Annexin V-FITC/PI apoptosis detection kit. After treatment with HF (0, 10, 20, and 40 μM) for 24 h, KYSE150 and TE14 cells at a cell density of 1.0×10^6 cells/well were trypsinized, collected by centrifugation, and washed twice with ice-cold PBS. The cells were then co-stained with 5 μL FITC-Annexin V and 5 μL PI for 15 min at 20–25 °C in the dark. The apoptosis rate was measured by flow cytometry (CytoFLEX, Beckman Coulter, Brea, CA, USA).

Gene Ontology and Kyoto Encyclopedia of Genes and Genomes Pathway Enrichment Analyses

A total of 355 and 100 potential targets for HF were searched from the Pharma Mapper (http://www.lilab-ecust.cn/pharmmapper/) and Swiss target prediction (http://www.swisstargetprediction.ch/) databases, respectively. GO and KEGG pathway enrichment analyses was performed using the DAVID database (26, 27).

Molecular Docking

The 3D structures of PI3K (code 6pys) and AKT1 (code 4ejn) were downloaded from the Protein Data Bank (https://www.rcsb.org/). Chemical structure data of HF was obtained from PubChem (http://pubchem.ncbi.nlm.nih.gov/). Molecular docking was implemented using the LibDock module of the Discovery Studio 2016, and the results were evaluated using the LibDock score. A higher libdock score indicates a higher activity of the small molecule (such as HF) binding to the target protein.

Western Blot Analysis

KYSE150 and TE14 cells at a cell density of 5.0×10^6 cells/well were treated with various concentrations of HF (0, 10, 20, and 40 μM) for 24 h. Cells were washed twice using PBS and lysed by adding RIPA cell lysis buffer containing PMSF. The cell lysate was centrifuged at 12,000 × *g* for 20 min at 4°C, after which the supernatant was gently aspirated using a pipette. The total protein content in the supernatant was measured using the BCA protein assay kit. Equal amounts of protein (20 μg) were separated by SDS-PAGE (8%–12%). The separated proteins were then transferred onto a PVDF membrane. The membranes were blocked with Quickblock blocking buffer (Beyotime Biotechnology, China) for 0.5 h and incubated with specific primary antibodies overnight at 4°C on a shaker. Membranes were washed three times for 10 min each with Tris-buffered saline-Tween 20 (TBST), completed by incubation with horseradish peroxidase (HRP)-conjugated secondary antibody for 1 h at approximately 25°C. Our study used the following primary antibodies: β-actin (1:1,000), phosphorylated PI3K (p-PI3K) (Tyr458, 1:1,000 and Tyr199, 1:1,000), PI3K (1:1,000), phosphorylated AKT (p-AKT) (Ser473, 1:1,000; Thr308, 1:1,000), AKT (1:1,000), c-Caspase 3 (1:1,000), p-mTOR (Ser2448, 1:1,000), mTOR (1:1,000), matrix metalloproteinase-2 (MMP2) (1:1,000), MMP9 (1:1,000), Bcl-2 (1:2,000), and Bax (1:1,000). The secondary antibody was HRP-conjugated goat anti-rabbit antibody (1:10,000; Cell Signaling Technology, Inc.). After three 10 min washes with TBST, the protein band was visualized using enhanced chemiluminescence detection reagent (GE Healthcare Life Sciences). Finally, protein bands were quantified by densitometric analysis using ImageJ software, and the protein amounts were expressed relative to the corresponding reference protein.

Wound-Healing Migration Assay

KYSE150 cells were grown to a density of approximately 80-90% in 6-well plates, after which the cell monolayer was scraped using a sterile 100-μL pipette tip to create "wounds". Reduced serum medium (1 mL) containing HF (0, 10, 20, or 40 μM) was gently added to the wells along the lateral wall to ensure that it covered the entire bottom. After incubation for 24 h in an incubator, the cells were washed and fixed with 4% paraformaldehyde (1 mL/well), and images were acquired under a microscope (Zeiss, Jena, Germany). Cell movement distances were measured by ImageJ (v1.8.0).

Cell Migration and Invasion Assay

Transwell migration and invasion assays were implemented by using Boyden chamber (8 μm pore size, Corning, NY, USA). For migration assay, KYSE150 cells (2.0×10^4 cells in 100 μL serum-free medium) were added into the upper chamber, and 600 μL of medium with 10% FBS was added into the lower chamber. For invasion assay, the upper surface of the Transwell membrane was coated with Matrigel (BD Biosciences, Franklin lakes, NJ, USA) diluted 1:8 with serum-free medium before adding cells. For both assays, various concentrations of HF (0, 10, 20, and 40 μM) were added into the lower chamber. After incubation for 24 h, the medium was discarded, the cells were gently removed from the upper surface of the Transwell membrane with a cotton swab, and the migrated or invaded cells on the lower surface were fixed with 4% paraformaldehyde, after which they were stained with 0.5% crystal violet. Using microscopy, the number of stained cells on the lower surface was counted in five random fields per Transwell membrane (×100 magnification), and the Image J software was used to enumerate the migrated/invaded cells.

Mouse Xenograft Model

All experimental procedures and manipulations involving animals were performed in compliance with the guidelines of the National Institutes of Health Guide for the Care and Use of Laboratory Animals. Moreover, all animal experiments were approved by the Institutional Animal Care and Use Committee of the Second Affiliated Hospital of Harbin Medical University (SYDW2021-046). Female BALB/c-nu athymic mice, at 6 weeks and weighing 14-17 g, were purchased from Beijing Vital River Laboratory Animal Technology Co., Ltd. (Beijing, China). Mice were maintained in a specific pathogen-free (SPF) grade rearing environment using sterile water and food feeding. KYSE150 cells (1.0×10^7 cells in 100 μL PBS) were injected subcutaneously into the right shoulders of the mice (n=18). Tumor size was measured every 3 days using a caliper. The formula for calculating tumor volume was as follows: $V = 0.5 \times L \times W^2$ (L, tumor longest diameter; W, tumor shortest diameter). When the tumor volume reached 50 mm^3, mice were randomized into three groups (n=6/group; control, 25 mg/kg HF, and 50 mg/kg HF). Next, HF (25 mg/kg and 50 mg/kg in 200 μL saline) was administered by intraperitoneal injection to the two treatment group mice daily for 21 days. The control mice received saline alone. The body weight and tumor volume of mice were measured every 3 days. After completion of drug administration, all animals were fed normal diet for another 3 days, after which they were euthanized by cervical dislocation. The tumors were excised, weighed, and immunohistochemical staining was performed. The internal organs were collected for hematoxylin and eosin (H&E) staining.

Immunohistochemistry

Tumor tissues from mice were formalin fixed, then embedded in paraffin and sectioned at 4 μm thin sections were used for examination. For staining, tissue sections were deparaffinized and rehydrated following standard protocols. Antigen retrieval of tissues in our study was performed by boiling in sodium citrate buffer (10 mM, pH 6.0) for 10 min, after which the samples were treated with 3% H_2O_2 for an additional 10 min. Each section was blocked with 10% goat serum albumin in a humidified chamber for 1 h at approximately 20–25°C. Then, tissue sections were incubated with specific primary antibodies (p-AKT, p-mTOR, Bax, and c-Caspase 3) overnight at 4°C in a humidified chamber. After further washing, the sections were incubated with secondary antibody for 30 min at approximately 25°C, followed by incubation with 3,3'-diaminobenzidine and counterstaining with hematoxylin. Stained sections were imaged under a microscope (Leica, DM4000B).

H&E Staining

Mouse organs (heart, liver, spleen, lung, and kidney) were fixed in formaldehyde, embedded in paraffin, and sectioned at 4 μm thickness. After deparaffinization and rehydration, tissue sections were stained with hematoxylin for 10 min, 1% ethanol-hydrochloric acid for 30 s, and eosin solution for 3 min. The sections were dehydrated in graded alcohol, after which they were cleared with xylene and finally mounted using neutral balsam.

Statistical Analysis

All data are presented using the mean ± SD of three independent experiments. Statistical analysis was performed using GraphPad Prism version 8 (GraphPad Software, San Diego, CA, USA). Student's *t*-test was used to compare two groups, and one-way analysis of variance was used for multiple comparisons. Statistically significant *P*-values are labeled as follows: *P < 0.05, **P < 0.01, ***P < 0.001.

RESULTS

HF Inhibits the Proliferation of ESCC Cells

The chemical structure of HF was drawn with ChemDraw software as shown in **Figure 1A**. KYSE150 and TE14 cell lines were treated with HF at different concentrations (0, 2.5, 5, 10, 20, 40, or 80 μM) for 24 or 48 h, and cell proliferation was assessed by CCK-8 assay, as described in the Methods. As shown in **Figure 1B**, HF significantly inhibited the cell viability of both ESCC cell lines in a concentration- and time-dependent manner. Furthermore, the IC_{50} values for KYSE150 cells treated with HF for 24 h and 48 h were 27.92 μM and 24.91 μM, respectively,

while the respective values for TE14 cells were 26.21 μM and 22.07 μM. Long-term cell viability assays (colony formation assays) showed that KYSE150 and TE14 cells formed significantly fewer colonies with increasing HF concentrations. (**Figure 1C**). The anti-proliferative activity of HF was further verified using an EdU assay. As shown in **Figure 1D**, the proportion of proliferating KYSE150 and TE14 cells decreased from 49.1% and 53.2% to 21.9% and 23.6%, respectively, after 40 μM HF treatment for 24 h. Taken together, these results indicate that HF effectively inhibits ESCC cell proliferation.

HF Induces Apoptosis in ESCC Cells

We next explored whether HF induces apoptosis in ESCC cells. Induction of apoptosis by HF was first evaluated by Hoechst

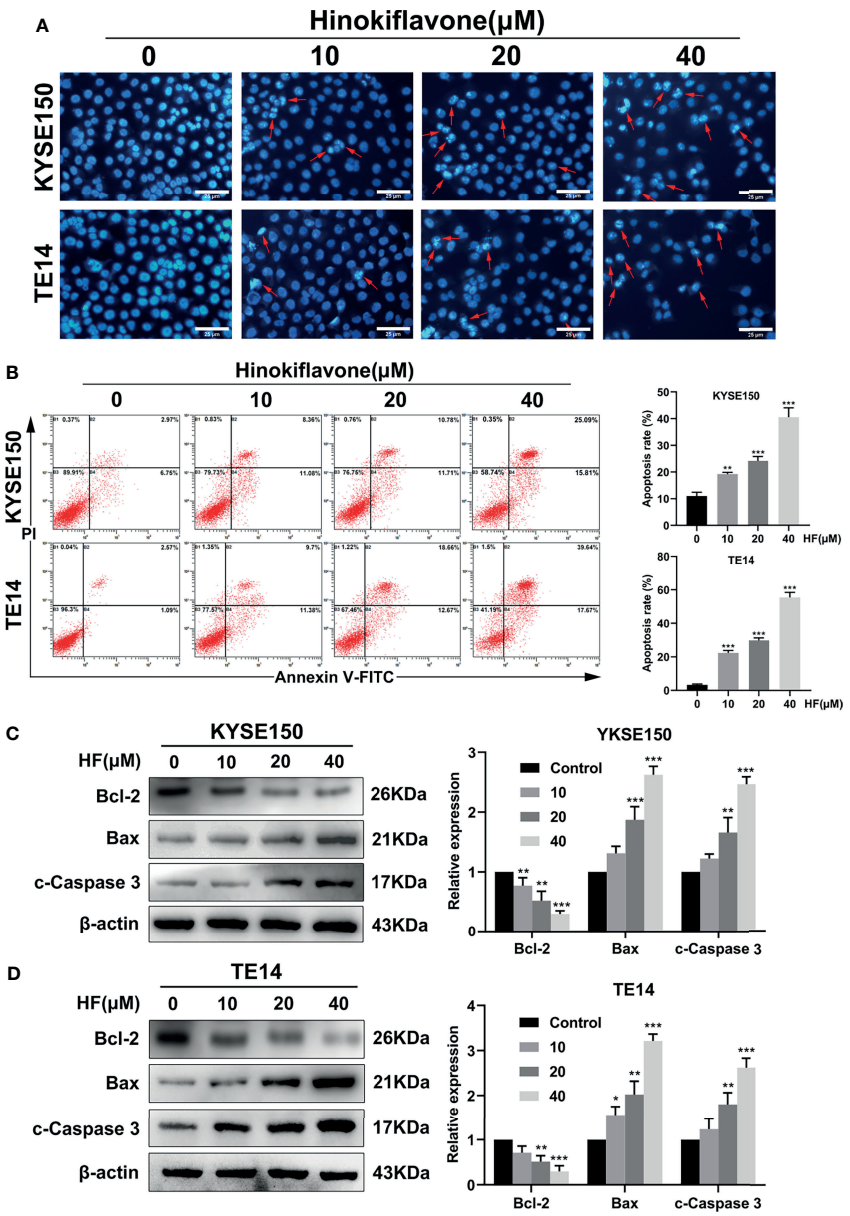

FIGURE 2 | Induction of apoptosis in ESCC cells by HF. **(A)** Hoechst 33342 nuclear dye was used to stain the KYSE150 and TE14 cells and utilized fluorescence microscopy to detect HF induced apoptotic nuclear morphological alterations (indicated by red arrows). Magnification, ×200; scale bars = 25 μm. **(B)** Percentage of KYSE150 and TE14 cells apoptosis after HF treatment was measured using Annexin V-fluorescein isothiocyanate (FITC)/propidium iodide (PI) double staining and analyzed by flow cytometry. **(C, D)** Expression levels of Bcl-2, Bax, and c-Caspase 3 were detected by western blot and quantitated *via* densitometric analysis using ImageJ software, while the expression level of β-actin was used as an internal control. The relative expression of experimental histones was calculated according to the protein scale set to 1 for 0 μM control group. All the above experimental data are presented as the mean ± SD of three independent experiments. $^{*}P < 0.05$; $^{**}P < 0.01$; $^{***}P < 0.001$ compared to vehicle (0 μM) group.

33342 staining assay. As shown in **Figure 2A**, HF-treated KYSE150 and TE14 cell cultures contained dense and heavily stained apoptotic cells, suggesting that HF might cause various degrees of cell shrinkage, nuclear fragmentation, and condensed nuclei formation. Furthermore, flow cytometric analysis of Annexin V-FITC and PI staining revealed that the ratio of early and late apoptotic cells increased in a dose-dependent manner after treatment with HF for 24 h. As shown in **Figure 2B**, the mean apoptosis ratios (from three independent experiments) were 11.0% (0 μM), 19.2% (10 μM), 24.2% (20 μM), 40.6% (40 μM) for KYSE150 cells; 3.3% (0 μM), 22.3% (10 μM), 29.9% (20 μM), and 55.6% (40 μM group) for TE14 cells.

Next, apoptosis-related proteins Bcl-2 (anti-apoptotic) and Bax (pro-apoptotic) were analyzed by western blot. Caspase-3, which is a member of the caspase family and is cleaved during apoptosis (28–30), was also analyzed by western blot. Treatment of KYSE150 and TE14 cells with HF significantly reduced the protein level of Bcl-2, while increasing the protein levels of Bax and c-Caspase 3 in a dose-dependent manner (**Figures 2C, D**). These results indicate that HF induced apoptosis of ESCC cells involves the mitochondrial pathway.

GO and KEGG Pathway Enrichment Analyses

GO enrichment analysis of HF was performed on the 355 putative targets of HF that were collected from the Pharma Mapper database to determine the relative significance with regards to biological processes, cell components, and molecular functions. The top 20 significantly enriched GO terms are listed in **Figures 3A–C** and **Table S1**. KEGG pathway enrichment analysis of HF was performed, and the top 20 targets are listed in **Figure 3D** and **Table S2**. The results show pathway enrichment for the GO and KEGG terms "negative regulation of apoptotic process," "pathways in cancer," and "PI3K-AKT signaling pathway," based on the Pharma Mapper database. Similarly, we obtained 100 putative targets of HF from the Swiss database. The GO enrichment analysis of the Swiss database is shown in **Figures S1A–C** and **Table S3**, and the KEGG pathway enrichment analysis is shown in **Figure S1D** and **Table S4**. Interestingly, the results analyzed according to the Swiss database were similar to those analyzed by the Pharma Mapper database. In summary, the analysis results of both databases indicate that HF might target the PI3K-AKT signaling pathway, leading to induction of apoptosis.

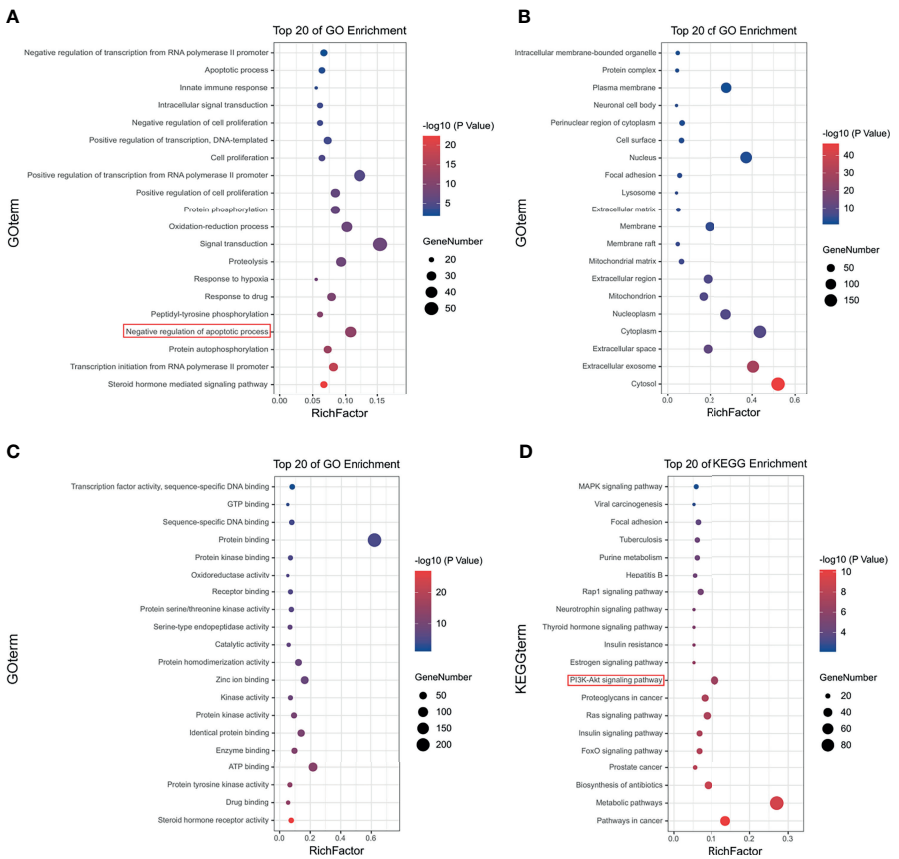

FIGURE 3 | Gene Ontology (GO) and Kyoto Encyclopedia of Genes and Genomes (KEGG) pathway analyses of HF. Top 20 signaling pathways of HF in **(A)** GO-BP pathway analysis, **(B)** GO-CC pathway analysis, and **(C)** GO-MF pathway analysis. **(D)** Top 20 signaling pathways of HF in KEGG enrichment pathway analysis.

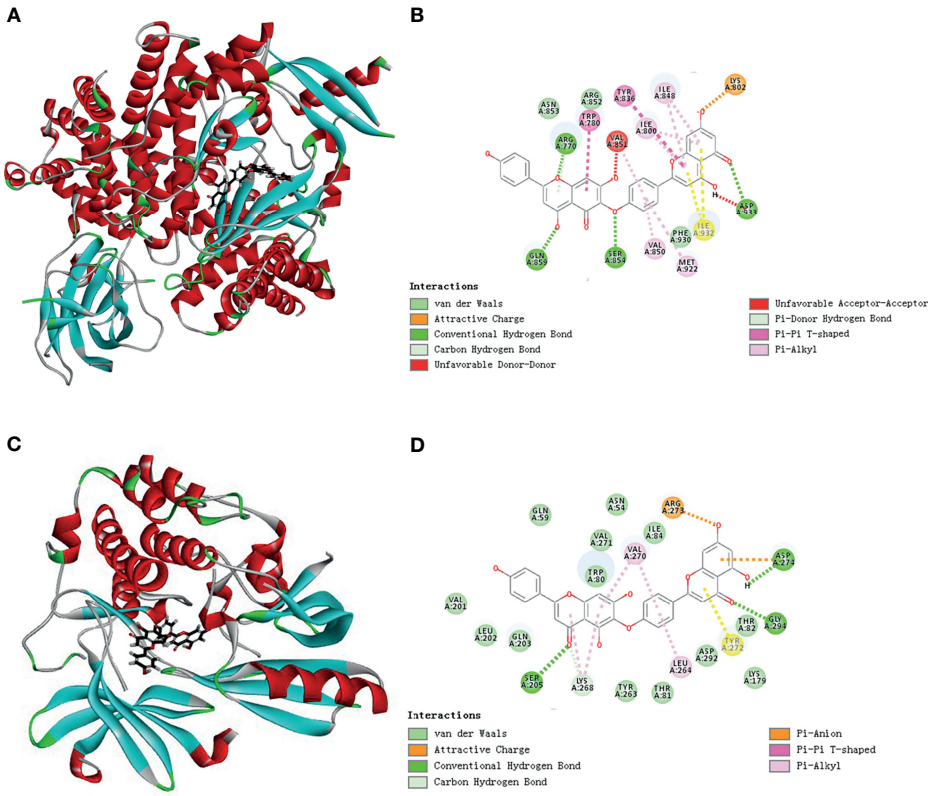

FIGURE 4 | Schematic representation of three- and two-dimensional molecular docking models. **(A)** Three-dimensional view of HF and PI3K docking scenario. **(B)** Two-dimensional view of HF and PI3K docking scenario. **(C)** Three-dimensional view of HF and AKT1 docking scenario. **(D)** Two-dimensional view of HF and AKT1 docking scenario.

HF Is Predicted to Have Direct Interaction With PI3K and AKT1

To predict the possible mutual binding mode of HF with PI3K and Akt, we further used molecular docking analysis. As shown in **Figure 4A**, HF was predicted to have a strong interaction with PI3K (LibDock score 115.982). The molecular docking of other conformations of HF with the protein PI3K is shown in **Figures S2A, B**. The binding affinity was attributed to the following: hydrogen bonding with the ARG-770, GLN-895, SER-854, and ASP-933 residues; the pi-pi T-shaped interaction with the TRP-780 and TYR-836 residues; the pi-alkyl interactions with the ILE-800, ILE-848, VAL-850, and MET-922 residues of PI3K (**Figure 4B**). Moreover, the analysis results show that HF could also interact strongly with protein AKT1 (LibDock score 143.752, **Figure 4C**). Molecular docking of other conformations of HF with AKT1 is shown in **Figures S2C, D**. The binding affinity was attributed to the following: hydrogen bonding with the SER-205, GLY-294, and ASP-274 residues; the pi-alkyl interactions with the LYS-268, VAL-270, and LEU-264 residues, and pi-anion interactions with the ARG-273 and ASP-274 residues of AKT1 (**Figure 4D**). Therefore, in common with the results of KEGG pathway enrichment analysis, HF showed high binding activity with PI3K and AKT in this study.

HF Inhibits the PI3K/AKT/mTOR Pathway in ESCC Cells

To verify the interaction of HF with PI3K/AKT, we analyzed HF-treated KYSE150 and TE14 cells *via* western blotting. Our results showed that the protein levels of p-PI3K, p-AKT, and p-mTOR in KYSE150 and TE14 cells were significantly reduced by HF treatment at 10, 20, and 40 μM, whereas total expression levels of PI3K, AKT, and mTOR were not significantly changed (**Figures 5A–C**). To verify whether HF induces apoptosis through the inhibition of PI3K/AKT/mTOR pathway, KYSE150 cells were treated with HF in the presence or absence of SC-79, a specific AKT activator (31). As shown in **Figures 5D, E**, SC-79 effectively enhanced the levels of phosphorylated proteins including p-AKT and p-mTOR. Meanwhile, pretreatment with SC-79 improved the inhibitory effect of HF on the protein expression of p-AKT, p-mTOR, and Bcl-2. Furthermore, the effect of HF to increase the expression amounts of apoptosis-related proteins (Bax and c-Caspase 3) could be reversed by pretreatment with SC-79 as well. We also found an increased viability of KYSE150 cells in the HF and SC-79 co-treatment group compared with HF alone treatment (**Figure 5F**), suggesting that activation of AKT attenuated the ability of HF to inhibit cell proliferation. These results indicate

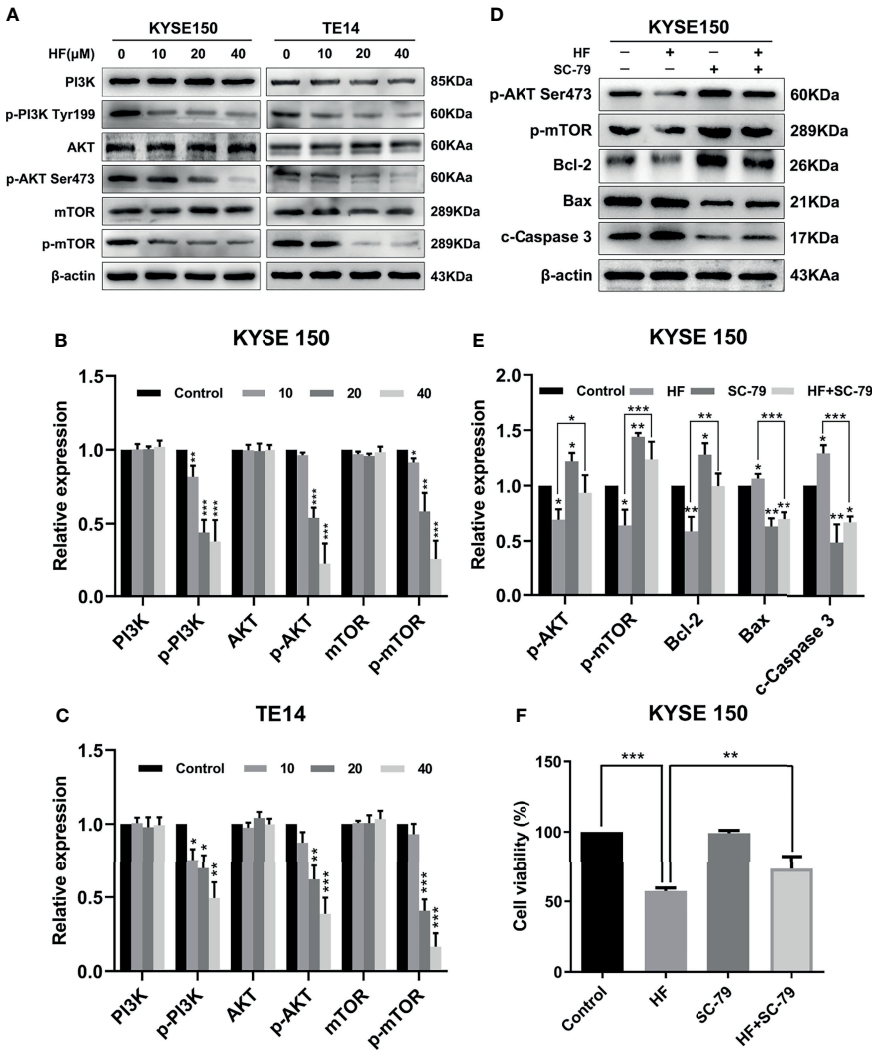

FIGURE 5 | HF induces apoptosis of ESCC cells by negatively regulating the PI3K/Akt/mTOR pathway. **(A–C)** KYSE150 and TE14 cells received various concentrations of HF intervention for 24 h, and the expression of pathway related proteins PI3K, p-PI3k, Akt, p-Akt, mTOR, and p-mTOR was detected by western blotting and quantified *via* densitometric analysis. **(D, E)** KYSE150 cells were pretreated with SC-79 (10 μM) for 24 h, and the expression of apoptosis related proteins Bcl-2, Bax and c-caspase 3 was determined by western blotting. **(F)** KYSE150 cells were first cultured with HF with or without addition of SC-79 (10 μM) for 24 h, and cell viability was detected using CCK-8 assays. The above experimental data are presented as the mean ± SD of three independent experiments. $^{*}P < 0.05$; $^{**}P < 0.01$; $^{***}P < 0.001$ compared to the control group.

that the anticancer effect of HF on ESCC involves regulation of PI3K/AKT/mTOR pathway.

HF Suppresses Migration and Invasion in ESCC Cells

Esophageal cancer patients with distant metastases have a very poor prognosis (32), and the migration and invasion abilities of tumor cells are vital factors affecting the process of tumor metastasis (33). Therefore, we evaluated whether HF could inhibit the migration and invasion of ESCC cells. As revealed by wound-healing assay (**Figure 6A**), the migratory ability of KYSE150 cells gradually became weaker with higher HF concentrations. Moreover, compared with the control group, HF treatment significantly inhibited the Transwell migration and invasion of ESCC cells in a dose-dependent manner (**Figure 6B**). Studies have shown that MMP family proteins play an important role in the regulation of cell migration and invasion abilities, and that MMPs are always upregulated in invasive epithelial cancers (34, 35). Therefore, we explored whether the protein levels of MMP2 and MMP9 are associated with alterations in ESCC cell migration and invasion following treatment with HF. As shown in **Figures 6C, D**, we found that HF significantly downregulated the expression of MMP2 and MMP9 in ESCC cells. Altogether, these results suggest that HF possesses an effective ability to inhibit ESCC cell migration and invasion.

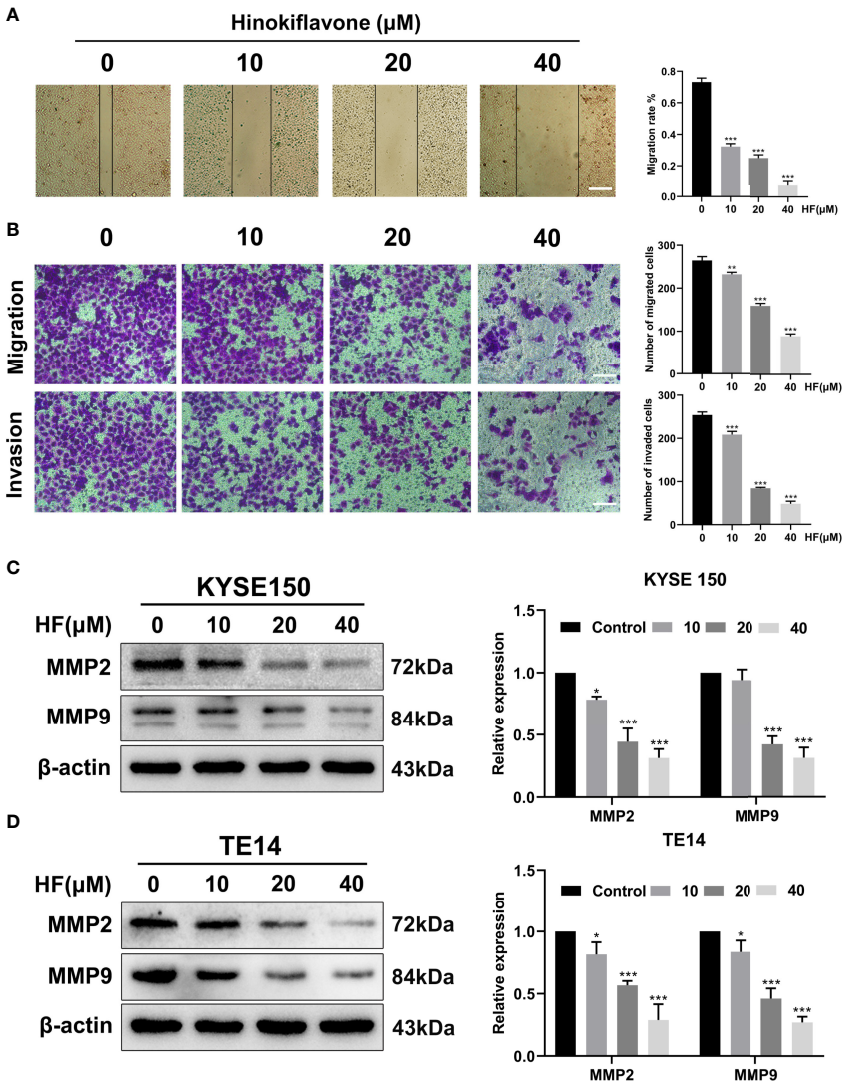

FIGURE 6 | HF inhibits ESCC cell migration and invasion. **(A)** Cell migration was measured in a scratch-wound assay. KYSE150 cells were cultured until reaching approximately 80-90% cell density, the culture was scratched as described in Methods, and further cultured with various concentrations of HF (0, 10, 20, and 40 μM) for 24 h, after which the cells were fixed and photographed. Magnification, ×100; scale bars = 100 μm. The distance of cell migration from the same region was quantified using ImageJ. **(B)** KYSE150 cells were placed in the top chamber on the Transwell membrane with serum-free medium and the upper surface of the Transwell membrane was coated with/without Matrigel. Cells were treated using HF with a concentration gradient for 24 h, and then the cells were fixed and photographed using a microscope after crystal violet staining. Magnification, ×100; scale bars = 100 μm. Migrated and invaded cells were counted as described in the Methods. **(C, D)** KYSE150 cells and TE14 cells were treated with various concentrations of HF for 24 h, and then the cells were collected for protein extraction. The extracted proteins were later used for western blot analysis to determine the protein expression levels of MMP2 and MMP9. All the above experimental data are presented as the mean ± SD of three independent experiments. $^{*}P < 0.05$; $^{***}P < 0.001$ compared to 0 μM vehicle group.

Antitumor Effect of HF in Mouse Xenograft Model of ESCC

To investigate whether the antitumor effect of HF *in vivo* is consistent with its *in vitro* effects, ESCC xenografts were established by subcutaneously transplantation of KYSE150 cells into BALB/c-nu mice, followed by treatment with HF (saline control, 25 mg/kg HF, 50 mg/kg HF) for 3 weeks, as described in the Methods (**Figure 7A**). Results from the animal experiments showed that transplanted tumors in the HF intervention groups grew much slower than those in the control group (**Figures 7B–D**). The mean size (or weight) of the tumors in HF 25 mg/kg, and HF 50 mg/kg group was reduced to 348.9 mm^3 (or 0.315 g) and 126.9 mm^3 (or 0.08 g), compared with 738.9 mm^3 (or 0.525 g) in the control group (**Figures 7B, D**). As a crucial indicator of health, the average body weights of the control and HF-treated mice were not significantly different at all time points (**Figure 7E**). Moreover, immunohistochemical analysis showed that HF suppressed the protein expression levels of p-AKT and p-mTOR, while upregulating those of Bax and c-Caspase 3 (**Figure 7F**). As shown in **Figure 7G**, the results of H&E staining experiments

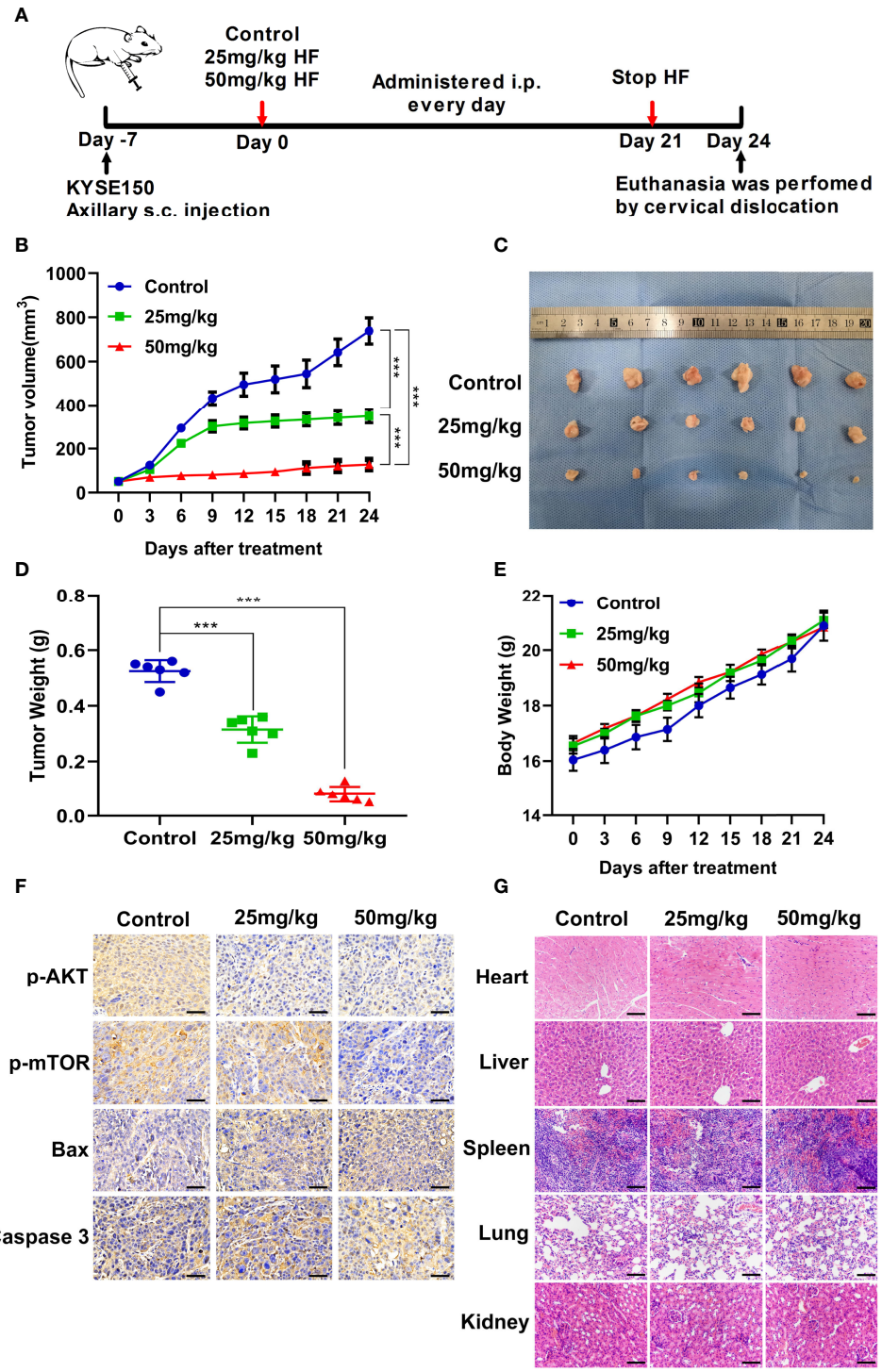

FIGURE 7 | HF suppresses the growth of mouse ESCC xenograft tumors. **(A)** BALB/c-nu mice implanted with KYSE150 xenograft tumors were treated daily with an equal volume of saline (control group) or HF (25 or 50 mg/kg) by intraperitoneal injection for total 21 days. **(B)** The tumor volume was measured every 3 days, and the difference in tumor volume between HF treated and control mice is shown. ***$P < 0.001$. **(C)** After euthanasia of mice, subcutaneous xenografts were removed and photographed. **(D)** The removed xenograft tumors were weighed and graphed for statistical analysis. ***$P < 0.001$ vs the control group. **(E)** Body weights of tumor-bearing mice were measured every 3 days in the HF-treated and control groups. **(F)** Expression levels of p-AKT, p-mTOR, Bax, and cleaved-Caspase 3 were detected by immunohistochemistry in the xenograft tumors. Magnification, ×400; scale bars = 50 μm. **(G)** H&E staining of the heart, liver, spleen, lung, and kidney of experimental mice shows no pathological changes in the organ tissues of any group. Magnification, ×200; scale bars = 100 μm.

on the heart, liver, spleen, lung, and kidney of mice exhibited no obvious pathological changes, such as necrosis, edema, or hemorrhage, indicating that HF possessed no major organ-related toxicity. Consistent with the experimental results *in vitro*, these data suggest that HF inhibits tumor growth by inducing apoptosis and does not have apparent adverse effects at the dose tested.

DISCUSSION

Despite progressive advances in the treatment of esophageal cancer, its mortality rate remains high worldwide. Currently, surgery and chemotherapy remain the main treatment modalities for esophageal cancer patients. However, since chemotherapeutics have their own disadvantages, such as drug resistance and systemic toxicity, more effective therapeutic strategies with fewer side-effects are urgently needed. Many studies have demonstrated the promising antitumor activity of some naturally active compounds (36). Our study is the first to indicate that HF inhibits the growth of ESCC cells. Furthermore, we comprehensively and profoundly explored the detailed molecular mechanisms underlying the antitumor effects of HF on ESCC *in vitro* and *in vivo* experiments.

In this study, the CCK-8 and colony formation assays demonstrated that HF had an effective anti-proliferative effect on KYSE150 and TE14 cells, which was validated by the EdU assay results. To investigate the anti-proliferation mechanism of HF in ESCC cells, we used Hoechst 33342 staining assay to identify apoptotic features of cell shrinkage, nuclear fragmentation, and condensed nuclei formation in HF-treated KYSE150 and TE14 cells. Flow cytometric analysis further illustrated induction of apoptosis in ESCC cells by HF in a concentration-dependent manner. Apoptosis is an orderly enzymatic cascade that induces DNA fragmentation into characteristic nucleosome fragments and culminates in cell death (30, 37, 38). Previous study has shown that apoptosis *via* the mitochondrial pathway is commonly regulated by Bcl-2 family proteins, with representative proteins such as the anti-apoptotic protein Bcl-2 and the pro-apoptotic protein Bax (39). In this context, our experimental results proved that HF intervention can cause a decreased expression of Bcl-2 protein and an increase in Bax and c-Caspase 3 expression, suggesting that HF induced apoptosis of ESCC cells occurs through the mitochondrial pathway.

We next used two databases, the Pharma Mapper and Swiss database, to screen the putative molecular targets of HF. The GO functional enrichment analysis showed that the predicted potential targets of HF were significantly enriched in "negative regulation of apoptotic process." Furthermore, KEGG pathway analysis revealed that HF might affect the PI3K-AKT signaling pathway. Our molecular docking analysis further indicated that HF can dock with PI3K and AKT1. Western blot analysis demonstrated a progressive decrease in p-PI3K, p-AKT, and p-mTOR protein levels with increasing concentrations of HF in KYSE150 and TE14 cells (**Figure 5A**). Interestingly, western blot analysis showed that the activation (phosphorylation) of PI3K, as indicated by levels of p-PI3K, was inhibited by HF, whereas expression of PI3K protein itself was not significantly altered. This suggested that HF can regulate post-translational modification of PI3K by physically interacting with the protein, as shown by the results of the GO enrichment, KEGG pathway, and molecular docking analyses. It is plausible that HF may directly attenuate the phosphorylation of PI3K at tyrosine 199, as reported in another study (40). The PI3K/Akt/mTOR pathway is a crucial signaling cascade in living organisms that has to be activated in a variety of cancers and to regulate cell proliferation, invasion, and migration (20, 41). We observed (**Figures 5D–F**) that SC-79 usage could activate the PI3K/AKT/mTOR pathway and partially counteract the pro-apoptotic and anti-proliferative effects of HF in ESCC cells. Overall, our results clearly show that the PI3K/AKT/mTOR pathway was inhibited by HF, which induced apoptosis in ESCC cells.

Metastasis is known to be a multistep biological process wherein subsets of cancer cells spread from the primary tumor to distant tissues or other organs to form metastases affects the body's normal physiological functions, which is the leading cause of cancer-related death (42). Moreover, for esophageal cancer patients, approximately 50% have already developed distant metastasis by the time of initial diagnosis (43, 44). Members of the MMP family of proteins, particularly MMP2 and MMP9, play a crucial role in cancer metastasis (34, 45, 46). The results of the migration and invasion assay we performed showed HF exhibited an obvious inhibitory effect on the metastatic potential of ESCC cells. We also found that HF significantly reduced MMP2 and MMP9 expression in KYSE150 and TE14 cells. These results suggest that HF can significantly hinder the metastasis of ESCC cells.

Finally, to verify the antitumor effect of HF *in vivo*, an esophageal cancer cell xenograft model was used in our study. Our experimental results showed that HF treatment significantly inhibited xenograft tumor growth in mice. In addition, the body weight of the experimental group mice receiving HF treatment was not significantly different from that of the control group mice. H&E staining also revealed no significant histopathological alterations in the heart, liver, lung, and kidney tissues of HF treated BALB/c-nu mice, indicating that HF did not induce significant systemic toxicity at the tested doses.

CONCLUSION

Data from our *in vitro*, in silico, and *in vivo* experiments showed that HF exerts antitumor effects against ESCC by inhibiting tumor growth and promoting apoptosis through the PI3K/AKT/mTOR signaling pathway. HF may also possibly inhibit metastasis by regulating MMPs. Overall, these findings reveal the underlying mechanisms by which HF inhibits the growth of human ESCC and provide new evidence supporting therapeutic potential of HF in ESCC.

DATA AVAILABILITY STATEMENT

The datasets presented in this study can be found in online repositories. The names of the repository/repositories and accession number(s) can be found in the article/**Supplementary Material**.

ETHICS STATEMENT

The animal study was reviewed and approved by the Institutional Animal Care and Use Committee of The Second Affiliated Hospital of Harbin Medical University (SYDW2021-046).

AUTHOR CONTRIBUTIONS

JG, SZ, and LZ contributed to the conception and design of this research. JG and SZ performed the experiments. JG and SZ analyzed the results. JG, SZ, JW, PZ, TL, and LZ wrote the paper. All authors contributed to the article and approved the submitted version.

SUPPLEMENTARY MATERIAL

The Supplementary Material for this article can be found online at: https://www.frontiersin.org/articles/10.3389/fonc.2022.833719/full#supplementary-material

REFERENCES

1. Sung H, Ferlay J, Siegel RL, Laversanne M, Soerjomataram I, Jemal A, et al. Global Cancer Statistics 2020: GLOBOCAN Estimates of Incidence and Mortality Worldwide for 36 Cancers in 185 Countries. *CA Cancer J Clin* (2021) 71(3):209–49. doi: 10.3322/caac.21660
2. Bang YJ, Van Cutsem E, Feyereislova A, Chung HC, Shen L, Sawaki A, et al. Trastuzumab in Combination With Chemotherapy Versus Chemotherapy Alone for Treatment of HER2-Positive Advanced Gastric or Gastro-Oesophageal Junction Cancer (Toga): A Phase 3, Open-Label, Randomised Controlled Trial. *Lancet* (2010) 376(9742):687–97. doi: 10.1016/S0140-6736(10)61121-X
3. Yang H, Liu H, Chen Y, Zhu C, Fang W, Yu Z, et al. Neoadjuvant Chemoradiotherapy Followed by Surgery Versus Surgery Alone for Locally Advanced Squamous Cell Carcinoma of the Esophagus (NEOCRTEC5010): A Phase III Multi-Center, Randomized, Open-Label Clinical Trial. *J Clin Oncol* (2018) 36(27):2796–803. doi: 10.1200/JCO.2018.79.1483
4. Newman DJ, Cragg GM. Natural Products as Sources of New Drugs Over the 30 Years From 1981 to 2010. *J Nat Prod* (2012) 75(3):311–35. doi: 10.1021/np200906s
5. Rane R, Karpoormath R. "Discovery and Development of New Anticancer Drugs Inspired From Natural Product Leads" Part 1. *Anticancer Agents Med Chem* (2015) 15(5):536. doi: 10.2174/1871520615050514130306
6. Rane R, Karpoormath R. "Discovery and Development of New Anticancer Drugs Inspired From Natural Product Leads" Part 2. *Anticancer Agents Med Chem* (2015) 15(8):932. doi: 10.2174/1871520615080150817112012
7. Lin YM, Chen FC, Lee KH. Hinokiflavone, a Cytotoxic Principle From Rhus Succedanea and the Cytotoxicity of the Related Biflavonoids. *Planta Med* (1989) 55(2):166–8. doi: 10.1055/s-2006-961914
8. Lin YM, Anderson H, Flavin MT, Pai YH, Mata-Greenwood E, Pengsuparp T, et al. *In Vitro* Anti-HIV Activity of Biflavonoids Isolated From Rhus Succedanea and Garcinia Multiflora. *J Nat Prod* (1997) 60(9):884–8. doi: 10.1021/np9700275
9. Wang G, Yao S, Zhang XX, Song H. Rapid Screening and Structural Characterization of Antioxidants From the Extract of Selaginella Doederleinii Hieron With DPPH-UPLC-Q-TOF/MS Method. *Int J Anal Chem* (2015) 2015(undefined):849769. doi: 10.1155/2015/849769
10. Sui Y, Li S, Shi P, Wu Y, Li Y, Chen W, et al. Ethyl Acetate Extract From Selaginella Doederleinii Hieron Inhibits the Growth of Human Lung Cancer Cells A549 *via* Caspase-Dependent Apoptosis Pathway. *J Ethnopharmacol* (2016) 190(undefined):261–71. doi: 10.1016/j.jep.2016.06.029
11. Magne Nde CB, Zingue S, Winter E, Creczynski-Pasa TB, Michel T, Fernandez X, et al. Flavonoids, Breast Cancer Chemopreventive and/or Chemotherapeutic Agents. *Curr Med Chem* (2015) 22(30):3434–46. doi: 10.2174/0929867322666150729115321
12. Yang S, Zhang Y, Luo Y, Xu B, Yao Y, Deng Y, et al. Hinokiflavone Induces Apoptosis in Melanoma Cells Through the ROS-Mitochondrial Apoptotic Pathway and Impairs Cell Migration and Invasion. *BioMed Pharmacother* (2018) 103(undefined):101–10. doi: 10.1016/j.biopha.2018.02.076
13. Boss WF, Im YJ. Phosphoinositide Signaling. *Annu Rev Plant Biol* (2012) 63(undefined):409–29. doi: 10.1146/annurev-arplant-042110-103840
14. Wymann MP, Schneiter R. Lipid Signalling in Disease. *Nat Rev Mol Cell Biol* (2008) 9(2):162–76. doi: 10.1038/nrm2335
15. Engelman JA, Luo J, Cantley LC. The Evolution of Phosphatidylinositol 3-Kinases as Regulators of Growth and Metabolism. *Nat Rev Genet* (2006) 7(8):606–19. doi: 10.1038/nrg1879
16. Vanhaesebroeck B, Stephens L, Hawkins P. PI3K Signalling: The Path to Discovery and Understanding. *Nat Rev Mol Cell Biol* (2012) 13(3):195–203. doi: 10.1038/nrm3290
17. Vicinanza M, D'Angelo G, Di Campli A, De Matteis MA. Phosphoinositides as Regulators of Membrane Trafficking in Health and Disease. *Cell Mol Life Sci* (2008) 65(18):2833–41. doi: 10.1007/s00018-008-8353-2
18. Inoki K, Li Y, Zhu T, Wu J, Guan KL. TSC2 is Phosphorylated and Inhibited by Akt and Suppresses Mtor Signalling. *Nat Cell Biol* (2002) 4(9):648–57. doi: 10.1038/ncb839
19. Cross DA, Alessi DR, Cohen P, Andjelkovich M, Hemmings BA. Inhibition of Glycogen Synthase Kinase-3 by Insulin Mediated by Protein Kinase B. *Nature* (1995) 378(6559):785–9. doi: 10.1038/378785a0
20. Serra V, Markman B, Scaltriti M, Eichhorn PJ, Valero V, Guzman M, et al. NVP-BEZ235, a Dual PI3K/Mtor Inhibitor, Prevents PI3K Signaling and Inhibits the Growth of Cancer Cells With Activating PI3K Mutations. *Cancer Res* (2008) 68(19):8022–30. doi: 10.1158/0008-5472.CAN-08-1385
21. Roulin D, Waselle L, Dormond-Meuwly A, Dufour M, Demartines N, Dormond O. Targeting Renal Cell Carcinoma With NVP-BEZ235, a Dual PI3K/Mtor Inhibitor, in Combination With Sorafenib. *Mol Cancer* (2011) 10(undefined):90. doi: 10.1186/1476-4598-10-90
22. Ko FC, Chan LK, Tung EK, Lowe SW, Ng IO, Yam JW. Akt Phosphorylation of Deleted in Liver Cancer 1 Abrogates Its Suppression of Liver Cancer Tumorigenesis and Metastasis. *Gastroenterology* (2010) 139(4):1397–407. doi: 10.1053/j.gastro.2010.06.051
23. Vivanco I, Sawyers CL. The Phosphatidylinositol 3-Kinase AKT Pathway in Human Cancer. *Nat Rev Cancer* (2002) 2(7):489–501. doi: 10.1038/nrc839
24. Li B, Tsao SW, Li YY, Wang X, Ling MT, Wong YC, et al. Id-1 Promotes Tumorigenicity and Metastasis of Human Esophageal Cancer Cells Through Activation of PI3K/AKT Signaling Pathway. *Int J Cancer* (2009) 125(11):2576–85. doi: 10.1002/ijc.24675
25. Hong P, Liu QW, Xie Y, Zhang QH, Liao L, He QY, et al. Echinatin Suppresses Esophageal Cancer Tumor Growth and Invasion Through Inducing AKT/Mtor-Dependent Autophagy and Apoptosis. *Cell Death Dis* (2020) 11(7):524. doi: 10.1038/s41419-020-2730-7
26. Huang DW, Sherman BT, Lempicki RA. Systematic and Integrative Analysis of Large Gene Lists Using DAVID Bioinformatics Resources. *Nat Protoc* (2009) 4(1):44–57. doi: 10.1038/nprot.2008.211
27. Huang DW, Sherman BT, Lempicki RA. Bioinformatics Enrichment Tools: Paths Toward the Comprehensive Functional Analysis of Large Gene Lists. *Nucleic Acids Res* (2009) 37(1):1–13. doi: 10.1093/nar/gkn923
28. Pawlowski J, Kraft AS. Bax-Induced Apoptotic Cell Death. *Proc Natl Acad Sci USA* (2000) 97(2):529–31. doi: 10.1073/pnas.97.2.529
29. Kirsch DG, Doseff A, Chau BN, Lim DS, de Souza-Pinto NC, Hansford R, et al. Caspase-3-Dependent Cleavage of Bcl-2 Promotes Release of Cytochrome C. *J Biol Chem* (1999) 274(30):21155–61. doi: 10.1074/jbc.274.30.21155

30. Dolka I, Krol M, Sapierzynski R. Evaluation of Apoptosis-Associated Protein (Bcl-2, Bax, Cleaved Caspase-3 and P53) Expression in Canine Mammary Tumors: An Immunohistochemical and Prognostic Study. *Res Vet Sci* (2016) 105:124–33. doi: 10.1016/j.rvsc.2016.02.004
31. Jo H, Mondal S, Tan D, Nagata E, Takizawa S, Sharma AK, et al. Small Molecule-Induced Cytosolic Activation of Protein Kinase Akt Rescues Ischemia-Elicited Neuronal Death. *Proc Natl Acad Sci USA* (2012) 109 (26):10581–6. doi: 10.1073/pnas.1202810109
32. Tanaka T, Fujita H, Matono S, Nagano T, Nishimura K, Murata K, et al. Outcomes of Multimodalitytherapy for Stage IVB Esophageal Cancer With Distant Organ Metastasis (M1-Org). *Dis Esophagus* (2010) 23(8):646–51. doi: 10.1111/j.1442-2050.2010.01069.x
33. Friedl P, Wolf K. Tumour-Cell Invasion and Migration: Diversity and Escape Mechanisms. *Nat Rev Cancer* (2003) 3(5):362–74. doi: 10.1038/nrc1075
34. Chang C, Werb Z. The Many Faces of Metalloproteases: Cell Growth, Invasion, Angiogenesis and Metastasis. *Trends Cell Biol* (2001) 11(11):37–43. doi: 10.1016/s0962-8924(01)02122-5
35. Huang W, Dong Z, Wang F, Peng H, Liu JY, Zhang JT. A Small Molecule Compound Targeting STAT3 DNA-Binding Domain Inhibits Cancer Cell Proliferation, Migration, and Invasion. *ACS Chem Biol* (2014) 9(5):1188–96. doi: 10.1021/cb500071v
36. Atanasov AG, Waltenberger B, Pferschy-Wenzig EM, Linder T, Wawrosch C, Uhrin P, et al. Discovery and Resupply of Pharmacologically Active Plant-Derived Natural Products: A Review. *Biotechnol Adv* (2015) 33(8):1582–614. doi: 10.1016/j.biotechadv.2015.08.001
37. Ou L, Lin S, Song B, Liu J, Lai R, Shao L. The Mechanisms of Graphene-Based Materials-Induced Programmed Cell Death: A Review of Apoptosis, Autophagy, and Programmed Necrosis. *Int J Nanomed* (2017) 12 (undefined):6633–46. doi: 10.2147/IJN.S140526
38. Elmore S. Apoptosis: A Review of Programmed Cell Death. *Toxicol Pathol* (2007) 35(4):495–516. doi: 10.1080/01926230701320337
39. Cory S, Adams JM. The Bcl 2 Family: Regulators of the Cellular Life-or-Death Switch. *Nat Rev Cancer* (2002) 2(9):647–56. doi: 10.1038/nrc883
40. Katase N, Nishimatsu SI, Yamauchi A, Yamamura M, Fujita S. DKK3 Knockdown Confers Negative Effects on the Malignant Potency of Head and Neck Squamous Cell Carcinoma Cells *via* the PI3K/Akt and MAPK Signaling Pathways. *Int J Oncol* (2019) 54(3):1021–32. doi: 10.3892/ijo.2018.4667
41. Mi Y, Xiao C, Du Q, Wu W, Qi G, Liu X. Momordin Ic Couples Apoptosis With Autophagy in Human Hepatoblastoma Cancer Cells by Reactive Oxygen Species (ROS)-Mediated PI3K/Akt and MAPK Signaling Pathways. *Free Radic Biol Med* (2016) 90(undefined):230–42. doi: 10.1016/j.freeradbiomed.2015.11.022
42. Chen YQ. Cancer and Metastasis Reviews. Introduction. *Cancer Metastasis Rev* (2013) 32(null):3–4. doi: 10.1007/s10555-012-9411-7
43. Enzinger PC, Mayer RJ. Esophageal Cancer. *N Engl J Med* (2003) 349 (23):2241–52. doi: 10.1056/NEJMra035010
44. Horner MJ, Ries LAG, Krapcho M, Aminou R, Howlader N, Altekruse SF, et al. *Seer Cancer Statistics Review, 1975–2006*. Bethesda, MD: National Cancer Institute (2009). Available at: http://seer.cancer.gov/csr/1975_2006/.
45. Liu F, Cao J, Wu J, Sullivan K, Shen J, Ryu B, et al. Stat3-Targeted Therapies Overcome the Acquired Resistance to Vemurafenib in Melanomas. *J Invest Dermatol* (2013) 133(8):2041–9. doi: 10.1038/jid.2013.32
46. Xia Y, Lei Q, Zhu Y, Ye T, Wang N, Li G, et al. SKLB316, a Novel Small-Molecule Inhibitor of Cell-Cycle Progression, Induces G2/M Phase Arrest and Apoptosis *In Vitro* and Inhibits Tumor Growth *In Vivo*. *Cancer Lett* (2014) 355(2):297–309. doi: 10.1016/j.canlet.2014.09.042

Conflict of Interest: The authors declare that the research was conducted in the absence of any commercial or financial relationships that could be construed as a potential conflict of interest.

Publisher's Note: All claims expressed in this article are solely those of the authors and do not necessarily represent those of their affiliated organizations, or those of the publisher, the editors and the reviewers. Any product that may be evaluated in this article, or claim that may be made by its manufacturer, is not guaranteed or endorsed by the publisher.

frontiers in Oncology

REVIEW
published: 04 March 2022
doi: 10.3389/fonc.2022.843345

Targeted Delivery of Chemotherapeutic Agents for Osteosarcoma Treatment

Duoli Xie[1,2,3†], *Zhuqian Wang*[1,2,3†], *Jie Li*[4], *De-an Guo*[5], *Aiping Lu*[2,3,6,7*] *and Chao Liang*[1,2,3*]

[1] Department of Biology, School of Life Sciences, Southern University of Science and Technology, Shenzhen, China, [2] Institute of Integrated Bioinfomedicine and Translational Science (IBTS), School of Chinese Medicine, Hong Kong Baptist University, Hong Kong, Hong Kong SAR, China, [3] Law Sau Fai Institute for Advancing Translational Medicine in Bone and Joint Diseases, School of Chinese Medicine, Hong Kong Baptist University, Hong Kong, Hong Kong SAR, China, [4] Department of Laboratory Medicine, Peking University Shenzhen Hospital, Shenzhen, China, [5] National Engineering Laboratory for Standardization of Traditional Chinese Medicine, Shanghai Institute of Materia Medica of the Chinese Academy of Sciences, Shanghai, China, [6] Institute of Arthritis Research in Integrative Medicine, Shanghai Academy of Traditional Chinese Medicine, Shanghai, China, [7] Guangdong-Hong Kong-Macau Joint Lab on Chinese Medicine and Immune Disease Research, Guangzhou, China

OPEN ACCESS

Edited by:
Jian-ye Zhang, Guangzhou Medical University, China

Reviewed by:
Anubhab Mukherjee, Principal Scientist, Hyderabad, India
Silvio Naviglio, University of Campania Luigi Vanvitelli, Italy

***Correspondence:**
Chao Liang
liangc@sustech.edu.cn
Aiping Lu
aipinglu@hkbu.edu.hk

[†]*These authors have contributed equally to this work*

Specialty section:
This article was submitted to Cancer Molecular Targets and Therapeutics, a section of the journal Frontiers in Oncology

Received: *25 December 2021*
Accepted: *07 February 2022*
Published: *04 March 2022*

Citation:
Xie D, Wang Z, Li J, Guo D-a, Lu A and Liang C (2022) Targeted Delivery of Chemotherapeutic Agents for Osteosarcoma Treatment. Front. Oncol. 12:843345. doi: 10.3389/fonc.2022.843345

Since osteosarcoma (OS) is an aggressive bone cancer with unknown molecular pathways of etiology and pathophysiology, improving patient survival has long been a challenge. The conventional therapy is a complex multidisciplinary management that include radiotherapy, chemotherapy which followed by surgery and then post-operative adjuvant chemotherapy. However, they have severe side effects because the majority of the medicines used have just a minor selectivity for malignant tissue. As a result, treating tumor cells specifically without damaging healthy tissue is currently a primary goal in OS therapy. The coupling of chemotherapeutic drugs with targeting ligands is a unique therapy method for OS that, by active targeting, can overcome the aforementioned hurdles. This review focuses on advances in ligands and chemotherapeutic agents employed in targeted delivery to improve the capacity of active targeting and provide some insight into future therapeutic research for OS.

Keywords: osteosarcoma, targeted delivery, chemotherapeutic agents, ligand-based delivery systems, antibodies

INTRODUCTION

Osteosarcoma (OS) is a relatively rare malignant mesenchymal origin bone cancer that 70%–80% of OS patients are adolescents and young adults and is distinguished by the formation of immature osteoid extracellular matrix (1). The disease has a 1–3 case per 1,000,000 population incidence and accounts for 20% of all primary malignant bone tumors in the world (2). OS is most common in the metaphysis of long, tubular bones like the proximal humerus, distal femur, and proximal tibia. It is very rare in the spine, pelvis, and sacrum, but it can be found in the metaphysis of some other bones (3). More than 85% of individuals with localized illness will develop a local or distant recurrence, most commonly in the lungs (85-90%) (4). Clinically, the development of disease is marked primarily by local discomfort and swelling, with occasional joint dysfunction (5) (**Figure 1**).

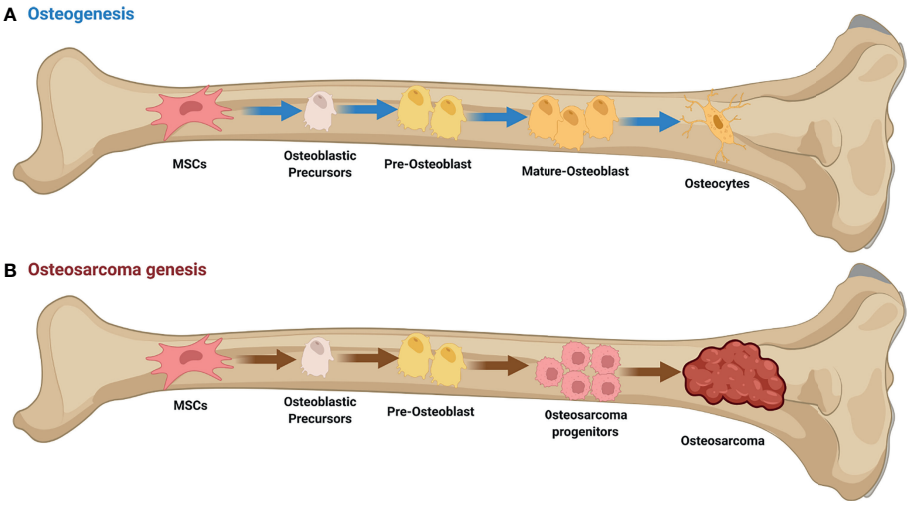

FIGURE 1 | Osteogenesis and Osteosarcoma genesis. **(A)** Initiation of osteogenic differentiation from mesenchymal stem cells (MSCs). MSCs are multipotent bone marrow cells that are capable of differentiating to bone (osteoblast/osteocyte), fat (adipocyte), and cartilage (chondrocyte) tissues. **(B)** Defects in osteogenesis lead to osteosarcoma genesis. Genetic alterations probably interfere with the normal osteogenic process, resulting in incompletely differentiated osteoblasts or osteocytes in bone. These defects disrupt the balance between proliferation and differentiation, and may cause a group of cells to display uncontrolled cell proliferation. Osteosarcoma progenitors may arise from these cells and expand to form osteosarcoma. This figure was created with BioRender.com.

Chemotherapy, followed by total surgical resection and then post-operative adjuvant chemotherapy as well as radiotherapy, is currently the standard treatment strategy for OS. Methotrexate (MTX), doxorubicin (DOX), cisplatin (CDDP), ifosfamide (IFO), and etoposide are commonly used chemotherapeutic agents recommended by The National Comprehensive Cancer Network guidelines, which increased the survival rate in patients with localized resectable tumors by up to 60-70% (1); However, most clinical applications of chemotherapeutics for patients with advanced and metastatic OS have been limited due to a lack of selectivity and sensitivity to tumor cells, toxicity towards normal cells, multidrug resistance (MDR), poor pharmacokinetic performance (6), and other factors that limit treatment efficacy and result in severe adverse effects on vital organs (7). With these combination therapy, the overall 5-year survival percentage for individuals with primary metastatic or relapsed cancer is less than 20% (8). Despite numerous clinical trials over the last three decades, cure rates for those with OS have not considerably improved, and survival for patients with metastatic or recurrent disease remains bleak (9). In the meantime, there are many NCT clinical trials in progress, pending follow-up (**Table 1**).

As a result, the development of some new anticancer medicines with reduced toxicity and higher tumor-killing effectiveness is desirable in order to increase patient survival and quality of life (10). A potent treatment with rational delivery vehicle and a surface ligand are often included in a ligand-based drug delivery system (11). Drugs might be delivered to tumor sites by receptor-mediated endocytosis once the individual ligands have contacted the corresponding tissue *in vivo*, allowing for tailored distribution of unique effector molecules while reducing adverse effects (12). Ligands such as antibodies, aptamers, peptides (13), saccharide, vitamin, bisphosphonates (BP) (14, 15), hyaluronic acid (HA) (16) and folate (17) have been reported to be used in the development of OS targeted drug delivery systems that mediate delivery vehicle and drug interactions with and internalization into OS cells with high specificity and efficiency (7). Some of them have a strong affinity for hydroxyapatite and can be employed as ligand in bone (7). In terms of drug carrier, liposomes which Alec D. Bangham developed in 1965, served as the first therapeutic nanoparticles to receive FDA approval, are now the most widely used (18). Liposomes have been extensively explored since they are capable of holding both hydrophilic and lipophilic pharmaceuticals (19). Mepact–liposomal mifamurtide which had been commercialized by Takeda Pharmaceuticals in 2004, is indicated for the treatment of high-grade, nonmetastasizing, resectable osteosarcoma following complete surgical removal in children, adolescents, and young adults (20). For further development in the similar line of thought, liposomes combined with chitooligosaccharides with a disulphide linker were developed by Yin et al. (21); Similarly, a reduction-responsive liposome decorated with COS and functionalised with oestrogen has been synthesised to preferentially target MG63 cells (22); Haghiralsadat et al. synthesised a thermo- and pH- sensitive liposome for nanoformulation of DOX which could inhibit the proliferation of MG63 cells and reduce cytotoxicity to healthy bone cells (23). As above mentioned, the advantages of traditional anti-OS chemotherapy are expected to be overcome by these drug delivery systems. In this review, we will look at the different types of ligands that can specifically bind to the matching receptors in OS and cause receptor-mediated endocytosis. Furthermore, the drug conjugates produced by chemically conjugating drugs were explained using studies that were available. This will spark new ideas for the development of more effective therapeutic options.

TABLE 1 | Ongoing NCT clinical trials of OS.

Clinical Trial NCT No.	Phase	Title	No. of patients	Status; Estimated completion date	Cancer Type	Sponsor
NCT01459484	II	ABCB1/P-glycoprotein Expression as Biologic Stratification Factor for Patients with non metastatic Osteosarcoma (ISG/OS-2)	225	Active, not recruiting; October 30, 2021	Non-metastatic extremity high-grade osteosarcoma	Italian Sarcoma Group
NCT03006848	II	A Phase II Trial of Avelumab in Patients with Recurrent or Progressive Osteosarcoma	19	Active, not recruiting; January 31, 2023	Recurrent/Refractory osteosarcoma	St. Jude Children's Research Hospital
NCT04154189	II	A Study to Compare the Efficacy and Safety of Ifosfamide and Etoposide with or Without Lenvatinib in Children, Adolescents and Young Adults with Relapsed and Refractory Osteosarcoma	72	Active, not recruiting; December 31, 2022	Relapsed or Refractory Osteosarcoma.	Eisai Inc.
NCT02484443	II	Dinutuximab in Combination with Sargramostim in Treating Patients with Recurrent Osteosarcoma	41	Active, not recruiting; N.A.	Metastatic Malignant Neoplasm in the Lung Metastatic/Recurrent Osteosarcoma	National Cancer Institute (NCI)
NCT02470091	II	Denosumab in Treating Patients with Recurrent or Refractory Osteosarcoma	56	Active, not recruiting; September 30, 2022	Metastatic/Recurrent/ Refractory Osteosarcoma Stage IV/IVA/IVB Osteosarcoma AJCC v7	Children's Oncology Group
NCT02432274	I/II	Study of Lenvatinib in Children and Adolescents with Refractory or Relapsed Solid Malignancies and Young Adults with Osteosarcoma	117	Active, not recruiting; March 31, 2022	Tumors Solid Malignant Tumors Osteosarcoma Differentiated Thyroid Cancer (DTC)	Eisai Limited
NCT02243605	II	Cabozantinib S-malate in Treating Patients with Relapsed Osteosarcoma or Ewing Sarcoma	90	Active, not recruiting; N.A.	Metastatic/Recurrent/ Unresectable Ewing Sarcoma Recurrent/Metastatic/ Unresectable Osteosarcoma Stage III/Stage IV/Stage IVA/Stage IVB Osteosarcoma AJCC v7	National Cancer Institute (NCI)
NCT04690231	N.A.	Apatinib + Ifosfamide and Etoposide for Relapsed or Refractory Osteosarcoma	79	Active, not recruiting; June 1, 2021	Relapsed or Refractory Osteosarcoma	Peking University People's Hospital
NCT00470223	III	Combined Chemotherapy With or Without Zoledronic Acid for Patients With Osteosarcoma (OS2006)	318	Active, not recruiting; December 2025	Osteosarcoma	UNICANCER
NCT01953900	I	iC9-GD2-CAR-VZV-CTLs/Refractory or Metastatic GD2-positive Sarcoma and Neuroblastoma (VEGAS)	26	Active, not recruiting; October 31, 2034	Osteosarcoma Neuroblastoma	Baylor College of Medicine
NCT02357810	II	Pazopanib Hydrochloride and Topotecan Hydrochloride in Treating Patients With Metastatic Soft Tissue and Bone Sarcomas	178	Active, not recruiting; June 2022	Adult/Metastatic/Recurrent Liposarcoma Metastatic/Recurrent Osteosarcoma Recurrent /Stage IV Adult Soft Tissue Sarcoma	Northwestern University

MAIN CONTENT

Antibodies as Targeting Ligands

Antibody-drug conjugates (ADCs) are monoclonal antibodies (mAbs) that have been chemically linked to cytotoxic medications and are directed onto a cancer cell surface antigen, delivering and releasing cytotoxic chemicals at the tumor site with low systemic toxicity (24, 25). The FDA has currently approved a number of ADCs for clinical use in cancer therapy (26). In addition, the ADCs are well equipped for pharmacological agents in OS.

Microtubules are dynamic filamentous cytoskeletal proteins. For decades, until the advent of targeted therapy, microtubules were the only alternative to DNA as a therapeutic target in cancer (27). The most widely used pharmacological agents conjugated to antibodies are DNA-targeting and tubulin-targeting medicines, which cause DNA alkylation or double-strand break and prevent tubulin depolymerization, respectively (28).

The cytotoxic component of the dimeric protein ricin, one of the most potent and deadliest plant poisons generated from Ricinus communis seeds, is A chain (RTA). RTA has been investigated as a potential option for cancer treatment in the form of immunotoxins, as well as an approach for *in vivo* macrophage depletion (29). Gp72 is a cell surface antigen discovered on the surface of tumors such as osteogenic

sarcomas (30). The anti-gp72 mAb 79IT/36 conjugates with MTX or RTA as therapeutic moieties demonstrate substantial results in treating OS (30), and better results were obtained with 79IT/36-RTA. Mice treated with the 79IT/36-RTA immunotoxin for five days, tumor growth was significantly suppressed *in vivo*.MM

The transmembrane protein glycoprotein non-metastatic b (gpNMB) plays a physiological role in bone differentiation and remodeling. gpNMB was found to be abundant in OS samples, implying that gpNMB could be a suitable target for antibody-mediated drug delivery in OS (31). Glembatumumab vedotin is an ADC that combines the anti-gpNMB mAb targeting characteristics with the payload of the antimitotic microtube inhibitor MMAE. The glembatumumab vedotin has shown strong preclinical activity in *in vitro* and *in vivo* studies (32), whereas in a phase II clinical trial, it shows limited efficacy in relapsed and/or refractory OS (31).

CD184 (CXCR4) is a G-protein coupled receptor discovered on the surface of metastatic tumor cells. In patients, CXCR4 expression is a poor predictor of survival and a high predictor of tumor relapse (33). It could be efficiently absorbed when the ligand binds. A recombinant anti-CD184 mAb coupled to MMAE demonstrated significant toxicity *in vitro* on metastatic OS cells derived from lung metastasis (34). Similarly, an anti-CXCR4 IgG–auristatin ADC demonstrated superior activity against metastatic SJSA-1-met-luc cells (OS lung metastasized cells from mouse) (35). This ADC is capable of eradicating tumors in mice receiving the immunoconjugate in a tumor xenograft lung-seeding model.

The CD248 (endosialin/TEM1) receptor is a transmembrane glycoprotein found on pericytes and fibroblasts during embryogenesis. It has been associated to tumor angiogenesis and inflammation, making it a molecular and therapeutic target for OS (36, 37). Two anti-endosialin ADCs were investigated in preclinical OS models (28). The anti-endosialin-MC-VC-PABC-MMAE was investigated for antitumor effectiveness in two endosialin-positive human cell lines and one sarcoma xenograft model. *In vitro*, a completely human anti-CD248 mAb coupled to MMAE inhibited the development of CD248 overexpressing OS cells (37).

TGF induces leucine-rich repeat containing 15 (LRRC15), a member of the Leucine-Rich Repeat superfamily, on activated fibroblasts (SMA+) and mesenchymal stem cells (MSC), which is associated with cell adhesion, invasion, and immunological responses. LRRC15 is a new cancer-associated fibroblast and mesenchymal marker that is overexpressed in OS tissue samples and is being investigated as a potential therapeutic target for ADC-based sarcoma treatment (38, 39). Samrotamab vedotin (ABBV-085) is an ADC made up of an anti-LRRC15 humanized IgG1 antibody (Ab1) linked to the anti-mitotic medication MMAE *via* a protease cleavable valine-citrulline (vc) linker. In preclinical studies, samrotamab vedotin extended event-free life in patient-derived xenograft (PDX) models (40), which may target cancer cells over LRRC15-positive cancer-associated fibroblasts due to the cell-permeable characteristics of MMAE. However, data from this unique stromal-targeting ADC's phase 1 clinical trial are mixed (38).

CD13, also known as aminopeptidase-N (APN) and alanyl aminopeptidase (ANPEP), is a metallopeptidase that was initially discovered to be a myeloid-specific hematological marker (41). A number of studies have found that CD13 plays a role in tumor growth, metastasis, and angiogenesis. By conjugating anti-CD13 monoclonal antibody (mAb) TEA1/8 to the marine chemical PM050489, a novel ADC, MI130110, was created. The MI130004 shown exceptional effectiveness in numerous murine xenograft models for OS (42).

Endothelial growth factor (VEGF) antibody was chosen as the targeted agent for the elevated production of VEGF antigen in OS cells (43), which plays a significant role in tumor angiogenesis processes. For the treatment of OS, an iron oxide nanoparticle complex conjugated to VEGF antibody and the ligand cluster of differentiation 80 (CD80) was developed (44). This combination approach would be able to target not just the extensively expressed VEGF antigen in OS cells, but also the increased expression of the surface cell receptor cytotoxic T lymphocyte-associated antigen-4 (CTLA4) (44).

The anti-CD11c mAb interacted with the CD11c receptor, which is abundant in OS cell lines. The functionalized nanoparticles of mesoporous silica nanoparticles (MSNPs) loaded with DOX and coupled with the anti-CD 11c mAb may considerably boost cellular absorption, resulting in an increased toxic and antiproliferative potential (45).

A transmembrane glycoprotein from the immunoglobulin family, activated leukocyte cell adhesion molecule (CD166/ALCAM), can be employed as a cell surface receptor for targeting OS. In SCID mouse xenograft models, the anticancer efficacy of a mAb anti-CD166 conjugation to DOX-loaded liposomal nanoparticles targeting CD166 in OS cell lines was investigated *in vivo*. When compared to non-targeted medicines, these antibody-targeted medications demonstrated an increase in cytotoxicity for OS cells (7, 13).

The B7-H3 receptor was significantly overexpressed in OS specimens, implying the possibility of targeting this receptor for therapeutic purposes (46). ADCs targeting B7-H3 are also being developed, such m276-PBD (47). This drug carries a PBD payload containing a DNA-damaging agent and elicited full responses in two of five OS PDX models (47). MGC018 is another ADC targeting B7-H3 that has a DNA alkylating payload (duocarmycin) that is now being tested in OS PDX models (48). Preliminary data showed a controllable safety profile and signs of action in four of the twenty OS patients included. (**Table 2** and **Figure 2**)

Aptamers as Targeting Ligands

Aptamers are single-stranded, synthetic DNA or RNA molecules that may fold into unique three-dimensional conformations to attach to specific target molecules with great affinity (51). Through SELEX, a repetitive *in vitro* process of sequential selection and amplification steps, aptamers could be selected from DNA or RNA libraries and function like "chemical antibodies". They are excellent candidates for targeted delivery of therapeutic agents due to their high selectivity and specificity, low immunogenicity, ease of synthesis with low cost and high

TABLE 2 | Targeted delivery based on antibody as ligands.

Ligands	Targets	Therapeutic agents	References
gp72 mAb	gp72	MTX/RTA	(30, 49)
gpNMB mAb	gpPNMB	MMAE	(32)
anti-CD184 mAb	CXCR4	MMAE/auristatin	(35, 50)
anti-endosialin Ab	CD248	MMAE	(28, 37)
anti-LRRC15 humanized IgG1 kappa antibody Ab1	LRRC15	MMAE	(38, 40)
anti-CD13 mAb	CD13	PM050489	(42)
anti-VEGF mAb	VEGF	N/A	(44)
anti-CD11c mAb	CD11c	DOX	(45)
anti-CD166 mAb	CD166	DOX	(7, 13)
B7-H3 mAb	CD276	PBD/duocarmycin	(47, 48)

gpNMB, glycoprotein non-metastatic b; CD, cluster of differentiation; LRRC15, Leucine-rich repeat containing 15; VEGF, Vascular endothelial growth factor; MTX, Methotrexate; RTA, ricin toxin A chain; MMAE, monomethyl auristatin E; DOX, Doxorubicin; PBD, pyrrolobenzodiazepine.

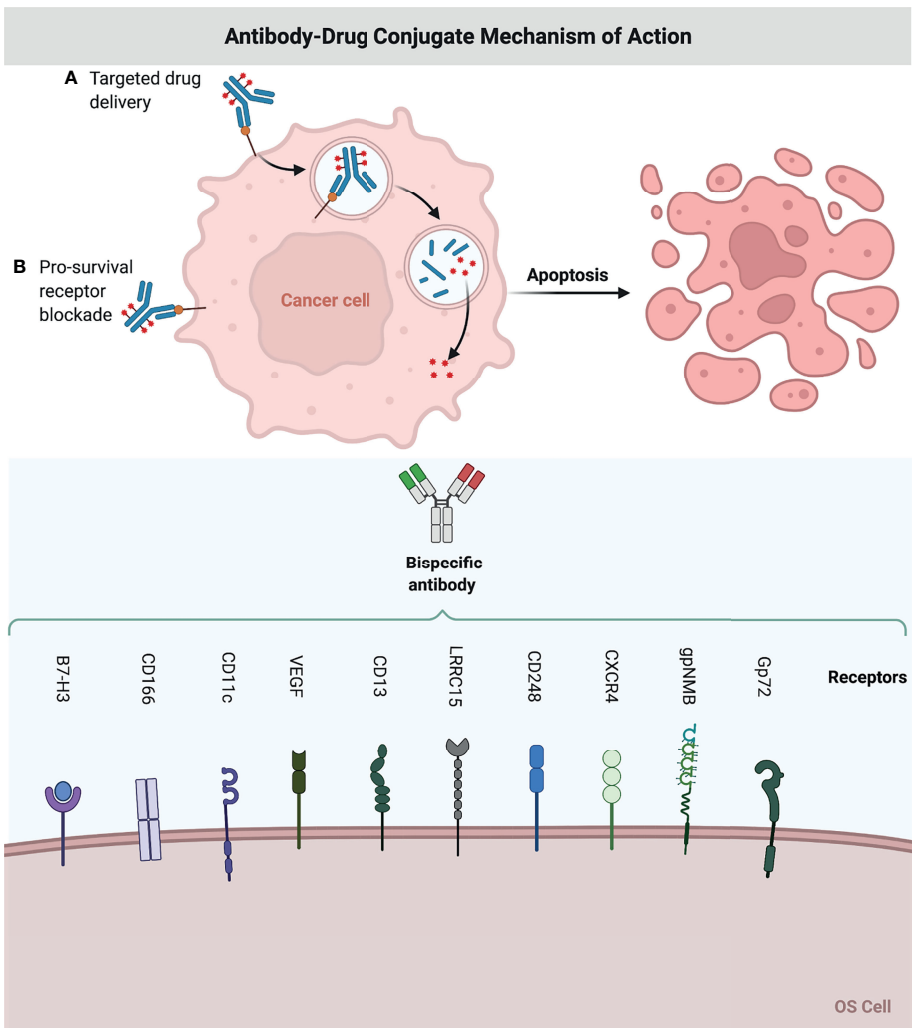

FIGURE 2 | Antibody-Drug Conjugate Mechanism of Action. A chemodrug is coupled to an antibody that specifically targets a certain OS antigen. Antibodies attach themselves to the antigens on the surface of cancerous cells. The biochemical reaction between the antibody and the target protein (antigen) triggers a signal in the OS cell, which then inhibits OS cell growth, or internalizes the antibody together with the linked chemo drug and eliminates the OS cell. This figure was created with BioRender.com.

reproducibility, relatively rapid tissue penetration with no toxicity (52, 53); As a result, they are typically utilized in conjunction with anticancer medications to target tumor cell surfaces (7), which may result in more promising outcomes when compared to aptamer-free competitors. Aptamer-drug conjugates (ApDCs) are an efficient technique of reducing OS growth *in vitro* and *in vivo* due to advances in technology (54).

Vascular Endothelial Development Factor A (VEGF A) overexpression was linked to tumor growth and angiogenesis. Our research has created an OS cell-targeted aptamer (LC09) that binds to VEGFA-positive K7M2 OS cells but not to mice normal hepatocytes (AML12) or peripheral blood mononuclear cells (PBMCs). After *in vivo* delivery, this aptamer may reduce non-specific liver and PBMC uptake. LC09-modified lipopolymers that were loaded with CRISPR/Cas9 plasmids containing VEGFA gRNA and Cas9 showed that they were only found in OS and lung metastasis. This led to a decrease in VEGFA expression and secretion, as well as a decrease in OS malignancy and lung metastasis (55, 56).

CD133 is a transmembrane glycoprotein that is thought to be a cancer stem cell (CSC) marker in OS and other cancers (57–59). As a result, CD133 aptamers have been employed as targeted ligands for OS CSC monitoring (60, 61). CD133-functionalized polymeric nanoparticles loaded with salinomycin could precisely and efficiently transport anticancer medicines to CD133 positive OS CSCs, greatly inhibiting OS development by eliminating CD133+ OS CSCs (62).

Due to the fact that amplification of the epidermal growth factor receptor (EGFR) is a frequent genetic aberration in OS, EGFR became a feasible target in the disease. EGFR aptamers were used to create OS-targeted medication delivery vehicles. Yu et al. (63) found that EGFR-SNPs, which are aptamer-conjugated polymer-lipid hybrid NPs that are loaded with salinomycin, effectively stopped the formation of tumorspheres and reduced the number of CD133-positive OS CSCs. This led to an even stronger cytotoxic effect than with non-targeted SNPs and salinomycin. Chen et al. (60) engineered salinomycin-entrapped lipid-polymer nanoparticles (CESP) with CD133 and EGFR aptamers to specifically target OS cells and CSCs. CESP demonstrated superior cytotoxicity to single-targeted or untargeted salinomycin-loaded nanoparticles in OS cells and CSCs. In OS-bearing mice, *in vivo* administration of CESP inhibited tumor growth more than other controls (**Table 3** and **Figure 3**).

Peptides as Targeting Ligands

Peptides are short chains of amino acids linked by peptide bonds that are typically thought to be harmless due to their low immunogenicity and non-toxic metabolites (85). Peptides are thought to be swiftly broken by proteolytic enzymes and removed from the bloodstream by the liver and kidney. Different ways to modification and stabilization can be used to alter these pharmacodynamic features (86). Lipidation, which involves the incorporation of fatty acids into the peptide, is one of the most well-known principles in peptide stabilization. Fatty acids attachment could induce a more extended circulation period (87). As carrier molecules, peptide-drug conjugates (PDCs) have various advantages. The straightforward synthesis allows for reasonable optimization of side chains and backbone structures, which might result in improved binding affinities and direct influence of physicochemical attributes (88). Furthermore, their low molecular weight allows for greater penetration into solid tissues, leading in a more effective anti-tumor impact (89, 90).

Conventional chemotherapeutic medicines linked with peptides present greater pharmacokinetics and reduced cytotoxic. Chemotherapeutic drugs utilized in PDCs are divided into three types. The chemicals first bind to and interact with cellular DNA or DNA-protein complexes. As a result, transcription and DNA replication are disrupted, resulting in the activation of apoptosis. The cytotoxicity of the second class

TABLE 3 | Targeted delivery based on aptamers, peptides, saccharide, vitamin or bisphosphonates as ligands.

Ligands	Targets	Therapeutic agents	References
LC09 aptamer	VEGFA	plasmids encoding VEGFA gRNA and Cas9	(56)
CD133 aptamer	CD133	salinomycin	(60–62)
EGFR aptamer	EGFR	salinomycin	(60, 63)
YSA peptide	EphA2	DOX	(64)
VIP peptide	VPAC1R and VPAC2R	DOX	(65)
RGD peptide	Integrins	DOX	(13, 66, 67)
iRGD peptide	NRP-1	N/A	(68, 69)
KRP	RPS6KA2	DOX	(70, 71)
HA	CD44	DOX	(16, 16, 72)
FA	FRs	MTX and/or DOX	(73–76)
Alendronate	/	DOX or PTX	(77–79)
Bisphosphonate prodrug	/	DOX	(80)
Phospholipid	/	MDP	(81)
Bisphosphonate	/	DOX	(56, 82)
Pamidronate	hydroxyapatite	DOX	(83)
Medronate	/	DOX	(77, 82)
pamidronate	/	DOX	(84)

VEGFA, Vascular Endothelial Growth Factor A; EGFR, epidermal growth factor receptor; EphA2, ephrin type-A receptor 2; VIP; vasoactive intestinal peptide; RGD, Arg-Gly-Asp; CD, cluster of differentiation, DOX; doxorubicin; iRGD, Internalizing Arg-Gly-Asp; NRP-1, αv integrins and neuropilin-1; HA, Hyaluronic acid; FA, Folate or folic acid; FRs, folate receptors; MTX, methotrexate; MDP, Methylene diphosphonate.

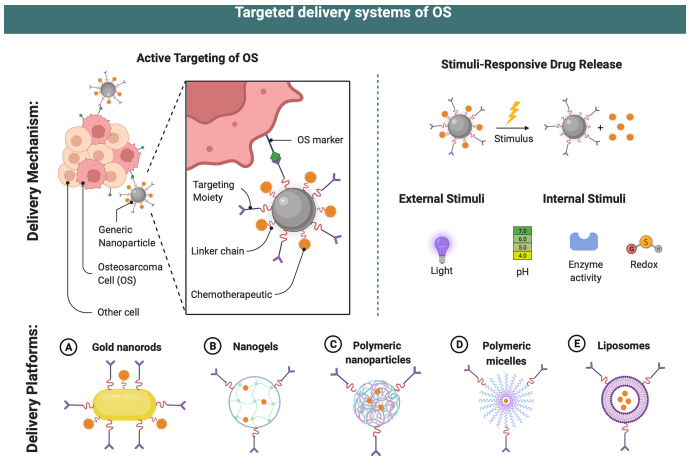

FIGURE 3 | Targeted delivery systems of OS. Different delivery systems have ideal properties for chemodrugs transport and delivery. Targeting ligands may be attached to the surface allowing an active targeting strategy and an increase in efficiency of the therapeutic payloads in OS therapy. After internalization, dissociation occurs at a proper microenvironment due to different stimuli (enzyme, redox, etc.), drug payloads are released into the cytosol of cancer cells. This figure was created with BioRender.com.

of commonly used toxophores is conveyed through blocking DNA biosynthesis. These antimetabolites include the folate derivative MTX, which inhibits the dihydrofolate reductase enzyme. Anti-mitotic drugs, which operate on microtubules, comprise the third class of chemotherapeutics (91).

By loading the same medication DOX, several new peptide-based targeted delivery systems were produced. The 12-amino acid peptide YSA (YSAYPDSVPMMS) is an ephrin A1 mimic and ligand for ephrin type-A receptor 2. (EphA2). Ephrins are a large family of tyrosine kinase receptors with well-documented roles in cancer proliferation and metastasis. They are emerging as intriguing prospective targets for cancer therapeutic methods (92, 93). Surface molecule EphA2a is extensively expressed in both primary and metastatic OS cells (94). In comparison to doxorubicin-free and non-targeted L-doxorubicin, DOX-loaded liposomes modified with the YSA peptide may more effectively target human Saos2 OS cells, hence increasing toxicity and cellular absorption (64). When D-aspartic acid octapeptide conjugate to micelles includes the medication DOX, it effectively promotes DOX accumulation in OS while having minimal side effects (65). The vasoactive intestinal peptide (VIP) receptors (VPAC1R and VPAC2R) are significantly expressed in Saos2. To treat OS cells, a new lipid analog (lipopeptide) coupled with VIP was created. It was proposed that the lipopeptide could be a good molecule for OS (65).

RGD, an integrin selectivity and affinity tripeptide, can be employed as an effective cancer therapeutic ligands as it can accomplish dual targeting for angiogenic endothelial cells and various tumor cells *via* the receptors integrin v3 and v5, respectively (95, 96). Integrins, which are abundantly expressed in OS cell lines, connect the extracellular matrix to the intracellular cytoskeleton to mediate cell adhesion, migration, and proliferation (97). RGD peptides have the advantage of having a low risk of immunological reactivity, being simple and affordable to synthesize, and having tight control over ligand presentation (66), as well as active OS cell targeting capacity (13, 67). A study by Fang et al. (13) found that RGD-DOX polymeric micelles were more effective in eliminating osteoblasts than nontargeted micelles, demonstrating their ability to target and kill OS cells *in vitro*. Beyond RGD, internalizing Arg-Gly-Asp peptide (iRGD) combines RGD's tumor-homing ability with C-end Rule's tissue penetrating characteristic, allowing for the targeting of extravascular tumor parenchyma (68). The iRGD mechanism consists of three steps: The RGD motif binds to v integrins on tumor endothelial cells, and subsequently iRGD is proteolytically cleaved, gaining the ability to bind to neurophilin-1 and so achieving tissue penetration (68). Malignancies overexpressing v integrins and neuropilin-1 that internalize RGD (iRGD) may have increased vascular and tissue permeability (NRP-1). Increased expression of v integrins and NRP-1 in OS may serve as a predictor for therapeutic treatment optimization through the discovery of these two genes (69).

It was found that when KRP-DOX was combined with doxorubicin, it had multiple synergistic functions *in vitro* and *in vivo*, including good biocompatibility and biodistribution, selective accumulation of tumor tissues, and an ability to remain in tumor tissues and be internalized by cancer cells in the presence of KRP. KRP-DOX complex also evaded lysosomal breakdown and exhibited cytotoxicity in OS cells (70). OS mice were given KRP-DOX, which was shown to be more effective than either saline or DOX alone in controlling RPS6KA2 expression (71) (**Table 3** and **Figure 3**).

Saccharide as Targeting Ligands

Proteoglycans, such as glycoproteins, are typically found on the outer surface of cancer cells, making saccharides or polysaccharides ideal ligands for OS-targeted drug delivery (98).

Biodegradable and biocompatible linear polysaccharides, such as hyaluronic acid (HA), are naturally biodegradable and biocompatible linear polysaccharides composed of glucuronic acid and N-acetyl d-glucosamine linked by alternating -1,4 and -1,3 glycosidic connections (99–102). The cluster determinant 44 (CD44) HA receptor is substantially expressed on MG-63 cells (103, 104), implying that HA could be a promising targeting agent for drug delivery in OS treatment. Nanocarriers with HA-CD44 interactions have recently been employed for tumor-targeted medicine delivery due to the obvious leaky vasculature of solid tumors (105, 106). Redox-sensitive, HA-functionalized liposomal nanocarriers have been developed by Chi et al. (16) to improve OS therapy. It was shown that HA-modified liposomes were more able to penetrate OS MG63 cells than regular human hepatocytes. Non-HA-coated nanoparticles, on the other hand, showed a decrease in tumor formation and an increase in tumor suppression. Dox administration in OS therapy can be improved by using a CDDP-crosslinked HA nanogel (CDDPHANG) (72). Redox-sensitive and CD44-targeted liposomes were developed in another study (Chol-SS-mPEG/HA-L). Liposomes loaded with DOX were coated with noncovalent HA, showing that the easily manufactured Chol-SS-mPEG/HA-L was demonstrated to be an efficient intracellular drug delivery system that may circulate for long periods of time and release GSH-triggered cytoplasmic drug (16). Beyond HA, recently a study demonstrated that chitooligosaccharides modified liposome loaded with DOX presented a good therapeutic effect in MG63 cell-bearing nude mice (21) (**Table 3** and **Figure 3**).

Vitamin as Targeting Ligands

Vitamins are a group of chemical molecules and nutrients that are essential for the survival of all living cells. Rapid multiplication of tumor cells, in particular, need an excess of specific vitamins, such as folate and retinoic acid (RA), in order to support their rapid development. On the tumor cell surface, the receptors involved in vitamin absorption are consequently increased when compared to normal cells. As a result, these vitamin receptors are useful target substrates for tumor-targeted medication delivery.

Coenzymes that assist the transfer of one-carbon units from donor molecules into essential biosynthetic pathways such as methionine, purine, and pyrimidine biosynthesis require folic acid (FA), also known as water-soluble vitamin B9, vitamin M and vitamin Bc (107, 108). Furthermore, it is involved in the interconversion of serine and glycine, as well as histidine catabolism (108). The principal method of cellular internalization *via* high affinity folate receptors (FRs) is receptor-mediated endocytosis. For ligand-based targeted treatment, folate receptor-targeted drug delivery vehicles have been revealed to transport anticancer medications into cells *via* receptor-mediated endocytosis, making FA an ideal alternative (109, 110). Through receptor-mediated endocytosis, high-affinity folate receptors (FRs) are involved in the cellular uptake of these nutrients (73). As a result, folate-functionalized nanocarriers were employed in OS-targeted treatment (17, 74, 111). Through the interaction of FA-FRs, these nanosystems may preferentially aggregate in tumor masses and suppress tumor development.

Nanocrystalline apatite substrates coupled with FA and MTX were employed in the human SAOS-2 OS cell line (75). For OS treatment, Ai et al. (112) produced FA surface modified-titanium dioxide NPs (FA-TiNP) that displayed a superior anticancer impact compared to TiNP.

Folate-targeted gold nanorods (GNRs) are being developed as an OS treatment. To act as coating agents for GNRs, an amphiphilic polysaccharide-based graft-copolymer (INU-LA-PEG-FA) and an amino derivative of the, poly(N-2-hydroxyethyl)-D,L-aspartamide functionalized with folic acid (PHEA-EDA-FA) were produced. In tridimensional (3-D) OS models, the role of folate-targeted GNRs is investigated (111). Another study looked at the anticancer potential of curcumin and C6 ceramide (C6) when both were enclosed in a bilayer of liposomal nanoparticles. With C6-curcumin-FA liposomes, a substantial reduction in tumor size was reported using pegylated liposomes to enhance plasma half-life and tagging with folate (FA) for targeted distribution *in vivo (*17). A hybrid nanoporous microparticle (hNP) carrier based on calcium carbonate and biopolymers derivatized with FA and carrying DOX as a chemotherapeutic drug model was created and evaluated on the human OS MG-63 cell line, which demonstrated reduced cell viability (76) (**Table 3** and **Figure 3**).

Bisphosphonates as Targeting Ligands

Hydroxyapatite is a mineral needed for bone formation. BP have a high affinity for the hydroxyapatite matrix of bone because they chelate with the divalent calcium ions (Ca^{2+}) in it (15, 113, 114). BP may be a promising targeted drug for treating bone cancer since it accumulates in bone and helps to limit osteoclast recruitment and adherence to the bone matrix, which diminishes osteoclast half-life and directly suppresses its activity.

Multifunctional alendronate-drug conjugates delivery systems are an emerging notion for successful OS targeted therapy. Morton et al. (77) demonstrated that alendronate-coated nanoparticles bind and internalize fast in human OS 143B cells. Pull-(GGPNle—PTX) was created by covalently conjugating PTX with pullulan and alendronate. This pullulan-alendronate-coated medication delivery method significantly reduced breast cancer growth, migration, and angiogenesis, as well as OS bone metastases (78). Zhao et al. created a new PTX NP coated with polydopamine and grafted with alendronate as a ligand for OS targeted therapy. *In vitro* experiments demonstrated that targeting NPs were more hazardous to K7M2 WT OS cells than non-targeting NPs (79). In another study, alendronate (ALN) was conjugated with hyaluronic acid and DSPEPEG2000COOH *via* a bioreducible disulfide linker (SS) to produce an ALNHASSL loaded with DOX. *In vitro*, ALNHASSLL/DOX shown increased cytotoxicity to human OS MG-63 cells, as well as high and quick cellular uptake; *in vivo*, ALNHASSLL/DOX demonstrated excellent tumor growth suppression and prolonged survival time for orthotopic OS nude mouse models. This work showed that ALNHASSLL/DOX, which has bone-and CD44-dual-targeting properties as well as redox sensitivity, could be a potential OS-targeted treatment (14).

Several BP-conjugated polymeric nanocarriers were created to carry chemotherapeutic medicines to OS, and their tumor-

targeting and anticancer activities were tested *in vivo*. With the exception of free DOX or nontargeted DOX nanocarriers, these functionalized, DOX-loaded nanoparticles showed increased, longer tumor accumulation and dramatically better anticancer effectiveness (77, 82). Katrin et al. (80) created a DOX BP prodrug to target bone metastases. In human plasma, the prodrug exhibits rapid DOX release and appropriate stability over many hours. For about the first time, researchers found that using DOX-conjugated BP NPs reduced tumor growth 40% more effectively than using free DOX in a xenograft mouse model of human Saos-2 OS (82). It has been widely employed in the detection of bone formation and remodeling diseases, including bone cancers, using Methylene diphosphonate (MDP), a significant radiopharmaceutical agent (115). Wu et al. (81) created a phospholipid liposome coupled with MDP for *in vivo* targeting of OS and single photon emission computed tomography trace. By targeting OS, this method reduces toxicity to normal tissue while increasing cancer uptake (116). Recently, hydroxyapatite NPs functionalized with medronate (the smallest BP) as a bone-targeting moiety in OS focused treatment have been reported. *In vitro* studies revealed that JQ1-loaded hydroxyapatite NPs effectively suppressed OS cell migration and invasion while being less hazardous to primary fibroblasts (15). Bone-targeted rather than OS targeted, BP may have the capacity to suppress osteoclasts and bone homeostasis throughout their extended stay in bone tissue (113, 117).

OS tumors are more likely to accumulate DOX-loaded NPs when a combination of pamidronate and NP EPR is used to target bone (83). Yin et al. (84) demonstrated the use of pamidronate-functionalized nanoparticles to transport DOX to the bone microenvironment for the targeted treatment of OS. (**Table 3** and **Figure 3**).

CONCLUSION

OS treatment is hindered by its unknown origin, high genetic instability, large histological heterogeneity, lack of diagnostic biomarkers, high local aggressiveness, and potential for rapid spread. Certain negative effects, including tissue damage, medication resistance, and rapid blood clearance are associated with chemical treatments for OS. It is possible to improve the capacity of medications to target cancer by using active targeting strategies, such as ligand-mediated tumor targeting. An eligible ligand is critical in this progression. We reviewed commonly utilized ligands as well as other compounds in this review; these conjugates are used as emerging tools for the treatment of OS. Although significant advances in the creation of new multifunctional ligand-chemical platforms may hold enormous promise for the treatment of OS in the future, these conjugates are not yet well-developed for usage in OS patients. The majority of them are still in the cellular and animal experimental stages, and there is a lengthy transition period before they can be used in humans. However, due to improved therapeutic effects and reduced side effects, as well as the growing use of next-generation sequencing and emerging technologies such as single-cell sequencing, which has resulted in the discovery of a large number of OS heterogeneity and novel targets, the active targeting strategy of ligand-based chemicals is doomed to play an important role in the treatment of OS.

FUTURE PERSPECTIVES

Beyond targeted ligand-chemodrug conjugates, surgery is a significant component in the treatment of OS. OS resection is tough due to the varied placement of tumors and its closeness with adjacent tissues. It also carries a considerable risk of postoperative complications. According to Ma et al., to overcome the difficulty of precise OS resection, computer-aided design was employed to create patient-specific guidance templates for OS resection based on CT scans and magnetic resonance imaging of human OS. The guiding templates were then created using a 3D printing technology. The OS surgery was directed by the guiding templates, which occurred in more exact removal of the tumorous bone and placement of the bone implants, less blood loss, a shorter operation duration, and less radiation exposure throughout the procedure. Patients recovered sufficiently enough to achieve a mean Musculoskeletal Tumor Society score, according to follow-up investigations (118). Bone grafts, which can be autogenous (from the own body of patient), homogeneous (from other individuals), or xenografts (from other species), are currently used to replace bone after surgery. Because each of these techniques has its own set of limitations, research has concentrated on the use of synthetic grafts that are both safer and more cost-effective (119). To be acceptable for bone regeneration, synthetic osteo-regenerative scaffolds must be biocompatible and have the requisite porosity, degradability, compositional, and mechanical qualities (120). The above conditions are achieved by 3D printing. 3D printed scaffolds can be precisely designed to mimic bone tissue morphologically (120) and provide control over scaffold pore shape and size (121), as well as facilitate the incorporation of other functional agents within the scaffold, making them an advantageous method for fabricating implantable scaffolds for bone regeneration (120). According to Jing et al., cisplatin/hydrogel-loaded 3D-printed titanium alloy implants are safe and effective for treating OS-related bone defects and should be explored for clinical application.

However, treating bone abnormalities caused by surgical resection may not be enough. There is still a chance that some tumor cells are left over, which could lead to OS recurrence. To address this, Fu et al. 3D printed a bioceramic free carbon-embedding larnite (larnite/C). The free carbon was added to aid a photothermal effect when an NIR laser was used to excite it. *In vivo*, the scaffold was able to kill human OS cells, slow tumor growth in naked mice, and encourage new bone production. *In vitro*, expression of rat bone mesenchymal stem cells may be aided by the scaffolds (122). Scaffolds made of different carbon sources, such as graphene oxide, may also have photothermal conversion characteristics. Ma et al. created graphene oxide (GO)-modified-tricalcium phosphate (GO-TCP) composite scaffolds with photothermal properties. *In vitro*, photothermal impacts caused considerable MG-63 OS cell death and reduced tumor growth in mice. Furthermore, as compared to plain-TCP

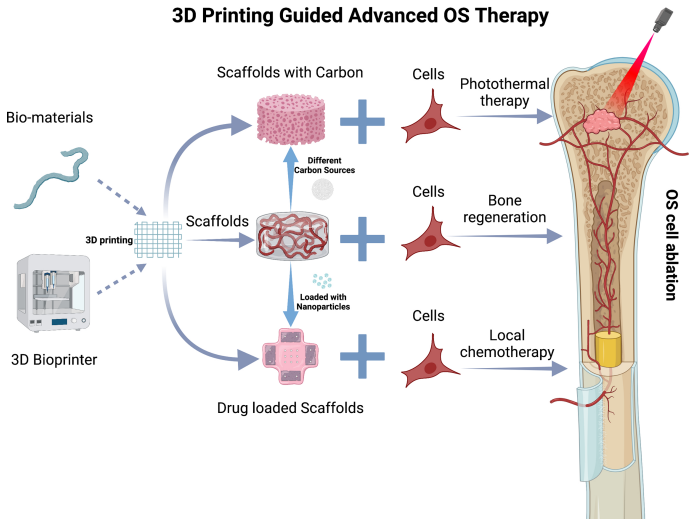

FIGURE 4 | 3D Printing guided advanced OS therapy. 3D printing scaffold and various types of carbon sources or nanocariers that may be incorporated. The nanocarriers and carbon sources are included in a 3D printed scaffold. The scaffold is then implanted into the critical defect site in the tibial due to OS resection to present bone regeneration, photothermal therapy, and local chemo release. This figure was created with BioRender.com.

scaffolds, the GO-TCP scaffolds showed superior osteogenic differentiation and new bone production (123).

Drug-loaded implants currently combine active pharmaceuticals with a biocompatible carrier and slowly release the drug after being implanted, allowing for local treatment (124). As a result, high drug concentrations at the location of interest are achieved while systemic drug exposure is reduced, avoiding undesired side effects in OS treatment (125). In this circumstance, the high degree of flexibility and controllability of 3D printing technique allows for the creation of complex forms with individualized dosages with variable release profiles, which improves local treatment. Fahimipour et al. recently developed a 3D printed gelatin/alginate/-TCP scaffold. The scaffold was subsequently coated with poly (D,L-lactic-co-glycolic acid), which encapsulated VEGF for long-term release (126). Wang et al. also created a unique technique based on 3D printed poly L-lactic acid drug carriers that has the ability to realize the potential of tailored local chemotherapy in the treatment of OS and could serve as a universal platform for anti-OS therapy (124).

Among these emerging insights to facilitate OS therapies, it should be noted that 3D printed scaffolds pose an opportunity with high potential. They may be used to provide templates in order to achieve precise OS resection, to enhance bone regeneration, to target residual OS cells after surgical resection, and to induce sustained release platforms for drugs (**Figure 4**).

AUTHOR CONTRIBUTIONS

CL and AL supervised and revised the manuscript. DX and ZW wrote and edited the manuscript. DG and JL provided the professional expertise. All authors contributed to the article and approved the submitted version.

FUNDING

This review is supported by the National Natural Science Foundation Council of China (82172386 and 81922081 to CL), the Croucher Foundation (CAS14BU/CAS14201 to A.L.), the Department of Education of Guangdong Province (2021KTSCX104 to CL), the 2020 Guangdong Provincial Science and Technology Innovation Strategy Special Fund (Guangdong-Hong Kong-Macau Joint Lab) (2020B1212030006 to AL), the Guangdong Basic and Applied Basic Research Foundation (2020A1515011450 to JL), the Shenzhen Project of Science and Technology (JCYJ20190809094007719 to JL), the National Natural Science Foundation of China (82104216 to JL) and the Science, Technology and Innovation Commission of Shenzhen (JCYJ20210324104201005 to CL).

REFERENCES

1. Mercatelli D, Bortolotti M, Bazzocchi A, Bolognesi A, Polito L. Immunoconjugates for Osteosarcoma Therapy: Preclinical Experiences and Future Perspectives. *Biomedicines* (2018) 6:1–10. doi: 10.3390/biomedicines6010019
2. Hernandez Tejada FN, Zamudio A, Marques-Piubelli ML, Cuglievan B, Harrison D. Advances in the Management of Pediatric Sarcomas. *Curr Oncol Rep* (2021) 23(1):3. doi: 10.1007/s11912-020-00995-8
3. Corre I, Verrecchia F, Crenn V, Redini F, Trichet V. The Osteosarcoma Microenvironment: A Complex But Targetable Ecosystem. *Cells* (2020) 9:1–25. doi: 10.3390/cells9040976

4. Meazza C, Scanagatta P. Metastatic Osteosarcoma: A Challenging Multidisciplinary Treatment. *Expert Rev Anticancer Ther* (2016) 16:543–56. doi: 10.1586/14737140.2016.1168697
5. Isakoff MS, Bielack SS, Meltzer P, Gorlick R. Osteosarcoma : Current Treatment and a Collaborative Pathway to Success. *J Clin Oncol* (2015) 33:3029–36. doi: 10.1200/JCO.2014.59.4895
6. Athanasou WN, Bielack S, de Alava E, Tos APD, Ferrari S, Paulussen M, et al. Clinical Practice Guidelines Bone Sarcomas : ESMO Clinical Practice Guidelines for Diagnosis, Treatment and Follow-Up Clinical Practice Guidelines. *Ann Oncol* (2010) 21:204–13. doi: 10.1093/annonc/mdq223
7. Desai SA, Manjappa A, Khulbe P. Drug Delivery Nanocarriers and Recent Advances Ventured to Improve Therapeutic Efficacy Against Osteosarcoma: An Overview. *J Egypt Natl Canc Inst* 33(1):4. doi: 10.1186/s43046-021-00059-3
8. Meazza C, Bastoni S, Scanagatta P. What is the Best Clinical Approach to Recurrent/Refractory Osteosarcoma? *Expert Rev Anticancer Ther* (2020) 20:415–28. doi: 10.1080/14737140.2020.1760848
9. Hattinger CM, Patrizio MP, Magagnoli F, Luppi S, Serra M. An Update on Emerging Drugs in Osteosarcoma: Towards Tailored Therapies? *Expert Opin Emerg Drugs* (2019) 24:153–71. doi: 10.1080/14728214.2019.1654455
10. Wang SY, Hu HZ, Qing XC, Zhang ZC, Shao ZW. Recent Advances of Drug Delivery Nanocarriers in Osteosarcoma Treatment. *J Cancer* (2020) 11:69–82. doi: 10.7150/jca.36588
11. Bahrami B, Hojjat-Farsangi M, Mohammadi H, Anvari E, Ghalamfarsa G, Yousefi M, et al. Nanoparticles and Targeted Drug Delivery in Cancer Therapy. *Immunol Lett* (2017) 190:64–83. doi: 10.1016/j.imlet.2017.07.015
12. Chen J, Almo SC, Wu Y. General Principles of Binding Between Cell Surface Receptors and Multi-Specific Ligands : A Computational Study. *PloS Comput Biol* (2017) 13(10):e1005805.
13. Fang Z, Sun Y, Xiao H, Li P, Liu M, Ding F, et al. ScienceDirect Targeted Osteosarcoma Chemotherapy Using RGD Peptide-Installed Doxorubicin-Loaded Biodegradable Polymeric Micelle. *BioMed Pharmacother* (2017) 85:160–8. doi: 10.1016/j.biopha.2016.11.132
14. Feng S, Wu ZX, Zhao Z, Liu J, Sun K, Guo C, et al. Engineering of Bone- and CD44-Dual-Targeting Redox-Sensitive Liposomes for the Treatment of Orthotopic Osteosarcoma. *ACS Appl Mater Interf* (2019) 11:7357–68. doi: 10.1021/acsami.8b18820
15. Wu VM, Mickens J, Uskoković V. Bisphosphonate-Functionalized Hydroxyapatite Nanoparticles for the Delivery of the Bromodomain Inhibitor JQ1 in the Treatment of Osteosarcoma. *ACS Appl Mater Interf* (2017) 9:25887–904. doi: 10.1021/acsami.7b08108
16. Chi Y, Yin X, Sun K, Feng S, Liu J, Chen D, et al. Redox-Sensitive and Hyaluronic Acid Functionalized Liposomes for Cytoplasmic Drug Delivery to Osteosarcoma in Animal Models. *J Control Release* (2017) 261:113–25. doi: 10.1016/j.jconrel.2017.06.027
17. Dhule SS, Penfornis P, He J, Harris MR, Terry T, John V, et al. The Combined Effect of Encapsulating Curcumin and C6 Ceramide in Liposomal Nanoparticles Against Osteosarcoma. *Mol Pharm* (2014) 11:417–27. doi: 10.1021/mp400366r
18. Allen TM, Cullis PR. Liposomal Drug Delivery Systems: From Concept to Clinical Applications. *Adv Drug Delivery Rev* (2013) 65:36–48. doi: 10.1016/j.addr.2012.09.037
19. Saraf S, Jain A, Tiwari A, Verma A, Panda PK, Jain SK. Advances in Liposomal Drug Delivery to Cancer: An Overview. *J Drug Delivery Sci Technol* (2020) 56:101549. doi: 10.1016/j.jddst.2020.101549
20. Singh AP, Biswas A, Shukla A, Maiti P. Targeted Therapy in Chronic Diseases Using Nanomaterial-Based Drug Delivery Vehicles. *Signal Transduct Target Ther* (2019) 4:1–21. doi: 10.1038/s41392-019-0068-3
21. Yin X, Chi Y, Guo C, Feng S, Liu J, Sun K, et al. Chitooligosaccharides Modified Reduction-Sensitive Liposomes: Enhanced Cytoplasmic Drug Delivery and Osteosarcomas-Tumor Inhibition in Animal Models. *Pharm Res* (2017) 34:2172–84. doi: 10.1007/s11095-017-2225-0
22. Yin X, Feng S, Chi Y, Liu J, Sun K, Guo C, et al. Estrogen-Functionalized Liposomes Grafted With Glutathione-Responsive Sheddable Chotooligosaccharides for the Therapy of Osteosarcoma. *Drug Delivery* (2018) 25:900–8. doi: 10.1080/10717544.2018.1458920
23. Haghiralsadat F, Amoabediny G, Sheikhha MH, Zandieh-doulabi B, Naderinezhad S, Helder MN, et al. New Liposomal Doxorubicin Nanoformulation for Osteosarcoma: Drug Release Kinetic Study Based on Thermo and pH Sensitivity. *Chem Biol Drug Des* (2017) 90:368–79. doi: 10.1111/cbdd.12953
24. Wolska A, Tadeusz W. Safety and Tolerability of Antibody – Drug Conjugates in Cancer. *Drug Saf* (2019) 42:295–314. doi: 10.1007/s40264-018-0775-7
25. Mukherjee A, Waters AK, Babic I, Nurmemmedov E, Glassy MC, Kesari S, et al. Antibody Drug Conjugates: Progress, Pitfalls, and Promises. *Hum Antibodies* (2018) 27:53–62. doi: 10.3233/HAB-180348
26. Chau CH, Steeg PS, Figg WD. Therapeutics Antibody – Drug Conjugates for Cancer. *Lancet* (2019) 394:793–804. doi: 10.1016/S0140-6736(19)31774-X
27. Dumontet C, Jordan MA. Microtubule-Binding Agents: A Dynamic Field of Cancer Therapeutics. *Nat Rev Drug Discov* (2010) 9:790–803. doi: 10.1038/nrd3253
28. Polito L, Calafato G, Bortolotti M, Bolognesi A, Olivari CC, Maiello S. Antibody Conjugates for Sarcoma Therapy : How Far Along Are We ? *Biomedicines* (2021) 9(8):978.
29. Alipour M, Pucaj K, Smith MG, Suntres ZE. Toxicity of Ricin Toxin a Chain in Rats. *Drug Chem Toxicol* (2013) 36:224–30. doi: 10.3109/01480545.2012.710624
30. Tumor H, Lines C. Sensitivity and Selectivity of Ricin Toxin A Chain-Monoclonal. *Cancer Res* (1986) 46:5524–8.
31. Kopp LM, Malempati S, Krailo M, Gao Y, Buxton A, Weigel BJ, et al. Phase II Trial of the Glycoprotein Non-Metastatic B-Targeted Antibody–Drug Conjugate, Glembatumumab Vedotin (CDX-011), in Recurrent Osteosarcoma AOST1521: A Report From the Children's Oncology Group. *Eur J Cancer* (2019) 121:177–83. doi: 10.1016/j.ejca.2019.08.015
32. Kolb EA, Gorlick R, Billups CA, Hawthorne T, Kurmasheva RT, Houghton PJ, et al. Initial Testing (Stage 1) of Glembatumumab Vedotin (CDX-011) by the Pediatric Preclinical Testing Program. *Pediatr Blood Cancer* (2014) 61:1816–21. doi: 10.1002/pbc.25099
33. Darash-Yahana M, Pikarsky E, Abramovitch R, Zeira E, Pal B, Karplus R, et al. Role of High Expression Levels of CXCR4 in Tumor Growth, Vascularization, and Metastasis. *FASEB J* (2004) 18:1240–2. doi: 10.1096/fj.03-0935fje
34. Kularatne SA, Deshmukh V, Ma J, Tardif V, Lim RKV, Pugh HM, et al. A CXCR4-Targeted Site-Specific Antibody-Drug Conjugate. *Angew Chemie* (2014) 126:12057–61. doi: 10.1002/ange.201408103
35. Bottaro LB. A CXCR4-Targeted Site-Specific Antibody-Drug Conjugate. *Bone* (2008) 23:1–7. doi: 10.1002/anie.201408103.A
36. Guo Y, Hu J, Wang Y, Peng X, Min J, Wang J, et al. Tumour Endothelial Marker 1/Endosialin-Mediated Targeting of Human Sarcoma. *Eur J Cancer* (2018) 90:111–21. doi: 10.1016/j.ejca.2017.10.035
37. Rouleau C, Gianolio DA, Smale R, Roth SD, Krumbholz R, Harper J, et al. Anti-Endosialin Antibody-Drug Conjugate: Potential in Sarcoma and Other Malignancies. *Mol Cancer Ther* (2015) 14:2081–9. doi: 10.1158/1535-7163.MCT-15-0312
38. Purcell JW, Tanlimco SG, Hickson J, Fox M, Sho M, Durkin L, et al. LRRC15 Is a Novel Mesenchymal Protein and Stromal Target for Antibody – Drug Conjugates. *Cancer Res* (2018) 78(14):4059–73. doi: 10.1158/0008-5472.CAN-18-0327
39. Cui J, Dean D, Wei R, Hornicek FJ, Ulmert D, Duan Z. Expression and Clinical Implications of Leucine-Rich Repeat Containing 15 (LRRC15) in Osteosarcoma. *J Orthop Res* (2020) 38:2362–72. doi: 10.1002/jor.24848
40. Hingorani P, Roth ME, Wang Y, Zhang W, Gill JB, Harrison DJ, et al. ABBV-085, Antibody – Drug Conjugate Targeting LRRC15, Is Effective in Osteosarcoma : A Report by the Pediatric Preclinical Testing Consortium. *Mol Cancer Ther* (2021) 20(3):535–41. doi: 10.1158/1535-7163.MCT-20-0406
41. Petrovic N, Schacke W, Gahagan JR, O'Conor CA, Winnicka B, Conway RE, et al. CD13/APN Regulates Endothelial Invasion and Filopodia Formation. *Blood* (2007) 110:142–50. doi: 10.1182/blood-2006-02-002931
42. Domínguez JM, Pérez-chacón G, Guillén MJ, Muñoz-alonso MJ, Somovilla-crespo B, Cibrián D, et al. CD13 as a New Tumor Target for Antibody- Drug Conjugates : Validation With the Conjugate MI130110. *J Hematol Oncol* (2020) 7:1–15.
43. Liu Y, Zhang F, Zhang Z, Wang D, Cui B, Zeng F, et al. High Expression Levels of Cyr61 and VEGF Are Associated With Poor Prognosis in

Osteosarcoma. *Pathol Res Pract* (2017) 213:895–9. doi: 10.1016/j.prp.2017.06.004
44. Kovach AK, Gambino JM, Nguyen V, Nelson Z, Szasz T, Liao J, et al. Prospective Preliminary in Vitro Investigation of a Magnetic Iron Oxide Nanoparticle Conjugated With Ligand CD80 and VEGF Antibody As a Targeted Drug Delivery System for the Induction of Cell Death in Rodent Osteosarcoma Cells. *Biores Open Access* (2016) 5:299–307. doi: 10.1089/biores.2016.0020
45. Shahabi S, Döscher S, Bollhorst T, Treccani L, Maas M, Dringen R, et al. Enhancing Cellular Uptake and Doxorubicin Delivery of Mesoporous Silica Nanoparticles *via* Surface Functionalization: Effects of Serum. *ACS Appl Mater Interf* (2015) 7:26880–91. doi: 10.1021/acsami.5b09483
46. Wang L, Zhang Q, Chen W, Shan B, Ding Y, Zhang G, et al. B7-H3 is Overexpressed in Patients Suffering Osteosarcoma and Associated With Tumor Aggressiveness and Metastasis. *PloS One* (2013) 8:4–11. doi: 10.1371/journal.pone.0070689
47. Seaman S, Zhu Z, Saha S, Zhang XM, Yang MY, Hilton MB, et al. Eradication of Tumors Through Simultaneous Ablation of CD276/B7-H3-Positive Tumor Cells and Tumor Vasculature. *Cancer Cell* (2017) 31:501–515.e8. doi: 10.1016/j.ccell.2017.03.005
48. Scribner JA, Brown JG, Son T, Chiechi M, Li P, Sharma S, et al. Preclinical Development of MGC018, a Duocarmycin-Based Antibody–Drug Conjugate Targeting B7-H3 for Solid Cancer. *Mol Cancer Ther* (2020) 19:2235–44. doi: 10.1158/1535-7163.MCT-20-0116
49. Byers VS, Pimm MV, Scannen PJ, Pawluczyk I. (1987), 5042–6.
50. Adam M, Range K, Y DM. 基因的改变nih Public Access. *Bone* (2008) 23:1–7. doi: 10.1002/art.30444.Collagen-Induced
51. Sun H, Zu Y. Aptamers and Their Applications in Nanomedicine. *Small* (2015) 11:2352–64. doi: 10.1002/smll.201403073
52. Chen K, Liu B, Yu B, Zhong W, Lu Y, Zhang J, et al. Advances in the Development of Aptamer Drug Conjugates for Targeted Drug Delivery. *Wiley Interdiscip Rev Nanomed Nanobiotechnol* (2017) 9(3). doi: 10.1002/wnan.1438
53. Moosavian SA, Sahebkar A. Aptamer-Functionalized Liposomes for Targeted Cancer Therapy. *Cancer Lett* (2019) 448:144–54. doi: 10.1016/j.canlet.2019.01.045
54. Ravichandran G, Rengan AK. Aptamer-Mediated Nanotheranostics for Cancer Treatment : A Review. *ACS Appl Nano Mater* (2020) 3(10):9542–59. doi: 10.1021/acsanm.0c01785
55. Liu T, Yan Z, Liu Y, Choy E, Hornicek FJ, Mankin H, et al. CRISPR-Cas9-Mediated Silencing of CD44 in Human Highly Metastatic Osteosarcoma Cells. *Cell Physiol Biochem* (2018) 46:1218–30. doi: 10.1159/000489072
56. Liang C, Li F, Wang L, Zhang Z, Lu A, Zhang G. Biomaterials Tumor Cell-Targeted Delivery of CRISPR/Cas9 by Aptamer-Functionalized Lipopolymer for Therapeutic Genome Editing of VEGFA in Osteosarcoma. *Biomaterials* (2017) 147:68–85. doi: 10.1016/j.biomaterials.2017.09.015
57. Li J, Zhong XY, Li ZY, Cai JF, Zou L, Li JM, et al. CD133 Expression in Osteosarcoma and Derivation of CD133+ Cells. *Mol Med Rep* (2013) 7:577–84. doi: 10.3892/mmr.2012.1231
58. Akbari M, Shomali N, Faraji A, Shanehbandi D, Asadi M, Mokhtarzadeh A, et al. CD133: An Emerging Prognostic Factor and Therapeutic Target in Colorectal Cancer. *Cell Biol Int* (2020) 44:368–80. doi: 10.1002/cbin.11243
59. Aghajani M, Mansoori B, Mohammadi A, Asadzadeh Z, Baradaran B. New Emerging Roles of CD133 in Cancer Stem Cell: Signaling Pathway and miRNA Regulation. *J Cell Physiol* (2019) 234:21642–61. doi: 10.1002/jcp.28824
60. Chen F, Zeng Y, Qi X, Chen Y, Ge Z, Jiang Z, et al. Targeted Salinomycin Delivery With EGFR and CD133 Aptamers Based Dual-Ligand Lipid-Polymer Nanoparticles to Both Osteosarcoma Cells and Cancer Stem Cells. *Nanomed Nanotechnol Biol Med* (2018) 14:2115–27. doi: 10.1016/j.nano.2018.05.015
61. Gui K, Zhang X, Chen F, Ge Z, Zhang S, Qi X, et al. Biomedicine & Pharmacotherapy Lipid-Polymer Nanoparticles With CD133 Aptamers for Targeted Delivery of All-Trans Retinoic Acid to Osteosarcoma Initiating Cells. *BioMed Pharmacother* (2019) 111:751–64. doi: 10.1016/j.biopha.2018.11.118
62. Cai G. Poly (Lactic-Co-Glycolic Acid) Nanoparticles Conjugated With CD133 Aptamers for Targeted Salinomycin Delivery to CD133 + Osteosarcoma Cancer Stem Cells. *Int J Nanomed* (2015) 10:2537–54.
63. Yu Z, Chen F, Qi X, Dong Y, Zhang Y, Ge ZHE, et al. Epidermal Growth Factor Receptor Aptamer – Conjugated Polymer – Lipid Hybrid Nanoparticles Enhance Salinomycin Delivery to Osteosarcoma and Cancer Stem Cells. *Exp Ther Med* (2018) 15(2):1247–56. doi: 10.3892/etm.2017.5578
64. Haghiralsadat F, Amoabediny G, Naderinezhad S, Nazmi K, de Boer JP, Zandieh-doulabi B, et al. EphA2 Targeted Doxorubicin-Nanoliposomes for Osteosarcoma Treatment. *Pharm Res* (2017) 34(12):2891–900. doi: 10.1007/s11095-017-2272-6
65. Low SA, Yang J, Kopeček J. Bone-Targeted Acid-Sensitive Doxorubicin Conjugate Micelles as Potential Osteosarcoma Therapeutics. *Bioconjug Chem* (2014) 25:2012–20. doi: 10.1021/bc500392x
66. Bellis SL. Advantages of RGD Peptides for Directing Cell Association With Biomaterials. *Biomaterials* (2011) 32:4205–10. doi: 10.1016/j.biomaterials.2011.02.029
67. Lu Y, Li L, Lin Z, Li M, Hu X, Zhang Y, et al. Enhancing Osteosarcoma Killing and CT Imaging Using Ultrahigh Drug Loading and NIR-Responsive Bismuth Sulfide@Mesoporous Silica Nanoparticles. *Adv Healthc Mater* (2018) 7:1–12. doi: 10.1002/adhm.201800602
68. Sugahara KN, Teesalu T, Karmali PP, Kotamraju VR, Agemy L, Girard OM, et al. Tissue-Penetrating Delivery of Compounds and Nanoparticles Into Tumors. *Cancer Cell* (2009) 16:510–20. doi: 10.1016/j.ccr.2009.10.013
69. Zhu H, Cai H, Tang M, Tang J. Neuropilin-1 is Overexpressed in Osteosarcoma and Contributes to Tumor Progression and Poor Prognosis. *Clin Transl Oncol* (2014) 16:732–8. doi: 10.1007/s12094-013-1141-y
70. Yu M, Li X, Huang X, Zhang J, Zhang Y, Wang H. New Cell-Penetrating Peptide (KRP) With Multiple Physicochemical Properties Endows Doxorubicin With Tumor Targeting and Improves Its Therapeutic Index. *ACS Appl Mater Interf* (2019) 11:2448–58. doi: 10.1021/acsami.8b21027
71. Yu M, Wang H. Peptide KRP Conjugated With Doxorubicin Exerts Anti-Tumor Activity by Regulating RPS6KA2 in Osteosarcoma. (2021), 1–17.
72. Zhang Y, Wang F, Li M, Yu Z, Qi R, Ding J, et al. Self-Stabilized Hyaluronate Nanogel for Intracellular Codelivery of Doxorubicin and Cisplatin to Osteosarcoma. *Adv Sci (Weinh)* (2018) 5(5):1700821. doi: 10.1002/advs.201700821
73. Kamen BA, Capdevila A. Receptor-Mediated Folate Accumulation is Regulated by the Cellular Folate Content. *Proc Natl Acad Sci USA* (1986) 83:5983–7.
74. Wang R, Li D, Wang L. Nanoscale Polysaccharide Derivative as an AEG-1 siRNA Carrier for Effective Osteosarcoma Therapy. *Int J Nanomed* (2018) 13:857–75.
75. Ia M, Pascaud-mathieu P, Adamiano A, Montesi M, Panseri S, Marsan O, et al. Interaction of Folic Acid With Nanocrystalline Apatites and Extension to Methotrexate (Antifolate) in View of Anticancer Applications. *Langmuir* (2018) 34(40):12036–48. doi: 10.1021/acs.langmuir.8b02602
76. Bosio VE, Cacicedo ML, Calvignac B, León I, Beuvier T, Boury F, et al. Colloids and Surfaces B : Biointerfaces Synthesis and Characterization of CaCO 3 – Biopolymer Hybrid Nanoporous Microparticles for Controlled Release of Doxorubicin. *Colloids Surfaces B Biointerf* (2014) 123:158–69. doi: 10.1016/j.colsurfb.2014.09.011
77. Morton SW, Shah NJ, Quadir MA, Deng ZJ, Poon Z, Hammond PT. Osteotropic Therapy *via* Targeted Layer-by-Layer Nanoparticles. *Adv Healthc Mater* (2014) 3:867–75. doi: 10.1002/adhm.201300465
78. Bonzi G, Salmaso S, Scomparin A, Eldar-Boock A, Satchi-Fainaro R, Caliceti P. Novel Pullulan Bioconjugate for Selective Breast Cancer Bone Metastases Treatment. *Bioconjug Chem* (2015) 26:489–501. doi: 10.1021/bc500614b
79. Zhao L, Bi D, Qi X, Guo Y, Yue F, Wang X, et al. Polydopamine-Based Surface Modification of Paclitaxel Nanoparticles for Osteosarcoma Targeted Therapy. *Nanotechnology* (2019) 30(25):255101. doi: 10.1088/1361-6528/ab055f
80. Hochdörffer K, Abu Ajaj K, Schäfer-Obodozie C, Kratz F. Development of Novel Bisphosphonate Prodrugs of Doxorubicin for Targeting Bone Metastases That are Cleaved pH Dependently or by Cathepsin B: Synthesis, Cleavage Properties, and Binding Properties to Hydroxyapatite

as Well as Bone Matrix. *J Med Chem* (2012) 55:7502–15. doi: 10.1021/jm300493m
81. Wu D, Wan M. Methylene Diphosphonate-Conjugated Adriamycin Liposomes: Preparation, Characteristics, and Targeted Therapy for Osteosarcomas *In Vitro* and *In Vivo*. *BioMed Microdevices* (2012) 14:497–510. doi: 10.1007/s10544-011-9626-3
82. Rudnick-Glick S, Corem-Salkmon E, Grinberg I, Margel S. Targeted Drug Delivery of Near IR Fluorescent Doxorubicin-Conjugated Poly(Ethylene Glycol) Bisphosphonate Nanoparticles for Diagnosis and Therapy of Primary and Metastatic Bone Cancer in a Mouse Model. *J Nanobiotechnol* (2016) 14:1–11. doi: 10.1186/s12951-016-0233-6
83. Maeda H, Nakamura H, Fang J. The EPR Effect for Macromolecular Drug Delivery to Solid Tumors: Improvement of Tumor Uptake, Lowering of Systemic Toxicity, and Distinct Tumor Imaging *In Vivo*. *Adv Drug Deliv Rev* (2013) 65:71–9. doi: 10.1016/j.addr.2012.10.002
84. Yin Q, Tang L, Cai K, Tong R, Sternberg R, Yang X, et al. Pamidronate Functionalized Nanoconjugates for Targeted Therapy of Focal Skeletal Malignant Osteolysis. *Proc Natl Acad Sci USA* (2016) 113:E4601–9. doi: 10.1073/pnas.1603316113
85. Ahrens VM, Beck-sickinger AG. Peptides and Peptide Conjugates : Therapeutics on the Upward Path. *Future Medicinal Chem* (2012) 4 (12):1567–86.
86. Zhang L, Bulaj G. Converting Peptides Into Drug Leads by Lipidation. *Curr Med Chem* (2012) 18:1602–18.
87. Frokjaer S, Otzen DE. Protein Drug Stability : A Formulation Challenge. *Nat Rev Drug Discov* (2005) 4:298–306. doi: 10.1038/nrd1695
88. Erak M, Bellmann-sickert K, Els-heindl S, Beck-sickinger AG. Bioorganic & Medicinal Chemistry Peptide Chemistry Toolbox – Transforming Natural Peptides Into Peptide Therapeutics. *Bioorg Med Chem* (2018) 26:2759–65. doi: 10.1016/j.bmc.2018.01.012
89. Firer MA, Gellerman G. Targeted Drug Delivery for Cancer Therapy : The Other Side of Antibodies. *J Hematol Oncol* (2012) 5:1. doi: 10.1186/1756-8722-5-70
90. Hock MB, Thudium KE, Schwabe NF. Meeting Report Immunogenicity of Antibody Drug Conjugates : Bioanalytical Methods and Monitoring Strategy for a Novel Therapeutic Modality. *AAPS J* (2014) 17(1):35–43. doi: 10.1208/s12248-014-9684-6
91. Hoppenz P, Els-heindl S, Beck-sickinger AG. Peptide-Drug Conjugates and Their Targets in Advanced Cancer Therapies. *Front Chem* (2020) 8:1–24. doi: 10.3389/fchem.2020.00571
92. Lodola A, Giorgio C, Incerti M, Zanotti I, Tognolini M. Targeting Eph/ephrin System in Cancer Therapy. *Eur J Med Chem* (2017) 142:152–62. doi: 10.1016/j.ejmech.2017.07.029
93. Saha N, Robev D, Mason EO, Himanen JP, Nikolov DB. Therapeutic Potential of Targeting the Eph/ephrin Signaling Complex. *Int J Biochem Cell Biol* (2018) 105:123–33. doi: 10.1016/j.biocel.2018.10.006
94. Posthumadeboer J, Piersma SR, Pham TV, van Egmond PW, Knol JC. Surface Proteomic Analysis of Osteosarcoma Identifies EPHA2 as Receptor for Targeted Drug Delivery. *British J Cancer* (2013) 109:2142–54. doi: 10.1038/bjc.2013.578
95. Zitzmann S, Ehemann V, Schwab M. Arginine-Glycine-Aspartic Acid (RGD)-Peptide Binds to Both Tumor and Tumor-Endothelial Cells *In Vivo*. *Cancer Res* (2002) 62:5139–43.
96. Danhier F, Le BA, Préat V. RGD-Based Strategies to Target Alpha(V) Beta (3) Integrin in Cancer Therapy and Diagnosis. *Mol Pharm* (2012) 9:2961–73. doi: 10.1021/mp3002733
97. Hynes R. Integrins : A Family of Cell Surface Receptors. *Cell* (1987) 48:549–54.
98. Jain K, Kesharwani P, Gupta U, Jain NK. A Review of Glycosylated Carriers for Drug Delivery. *Biomaterials* (2012) 33:4166–86. doi: 10.1016/j.biomaterials.2012.02.033
99. Pouyani T, Prestwich GD. Functionalized Derivatives of Hyaluronic Acid Oligosaccharides: Drug Carriers and Novel Biomaterials. *Bioconjug Chem* (1994) 5:339–47. doi: 10.1021/bc00028a010
100. Prestwich GD, Marecak DM, Marecek JF, Vercruysse KP, Ziebell MR. Controlled Chemical Modification of Hyaluronic Acid: Synthesis, Applications, and Biodegradation of Hydrazide Derivatives. *J Control Release* (1998) 53:93–103. doi: 10.1016/S0168-3659(97)00242-3
101. Oh EJ, Park K, Kim KS, Kim J, Yang JA, Kong JH, et al. Target Specific and Long-Acting Delivery of Protein, Peptide, and Nucleotide Therapeutics Using Hyaluronic Acid Derivatives. *J Control Release* (2010) 141:2–12. doi: 10.1016/j.jconrel.2009.09.010
102. Rosso F, Quagliariello V, Tortora C, Di Lazzaro A, Barbarisi A, Iaffaioli RV. Cross-Linked Hyaluronic Acid Sub-Micron Particles: *In Vitro* and *In Vivo* Biodistribution Study in Cancer Xenograft Model. *J Mater Sci Mater Med* (2013) 24:1473–81. doi: 10.1007/s10856-013-4895-4
103. Eliaz RE, Nir S, Marty C, Szoka FC. Determination and Modeling of Kinetics of Cancer Cell Killing by Doxorubicin and Doxorubicin Encapsulated in Targeted Liposomes. *Cancer Res* (2004) 64:711–8. doi: 10.1158/0008-5472.CAN-03-0654
104. Kim JH, Moon MJ, Kim DY, Heo SH, Jeong YY. Hyaluronic Acid-Based Nanomaterials for Cancer Therapy. *Polymers (Basel)* (2018) 10:1–15. doi: 10.3390/polym10101133
105. Plattt VM, Szoka FC. Anticancer Therapeutics: Targeting Macromolecules and Nanocarriers to Hyaluronan or CD44, a Hyaluronan Receptor. *Mol Pharm* (2008) 5:474–86. doi: 10.1021/mp800024g
106. Maeda H. Macromolecular Therapeutics in Cancer Treatment: The EPR Effect and Beyond. *J Control Release* (2012) 164:138–44. doi: 10.1016/j.jconrel.2012.04.038
107. Leamon CP, Low PS. Folate-Mediated Targeting: From Diagnostics to Drug and Gene Delivery. *Drug Discovery Today* (2001) 6:44–51. doi: 10.1016/S1359-6446(00)01594-4
108. Lucock M. Folic Acid: Nutritional Biochemistry, Molecular Biology, and Role in Disease Processes. *Mol Genet Metab* (2000) 71:121–38. doi: 10.1006/mgme.2000.3027
109. Gupta A, Kaur CD, Saraf S, Saraf S. Targeting of Herbal Bioactives Through Folate Receptors: A Novel Concept to Enhance Intracellular Drug Delivery in Cancer Therapy. *J Recept Signal Transduct* (2017) 37:314–23. doi: 10.3109/10799893.2016.1147581
110. Wei X, Liao J, Davoudi Z, Zheng H, Chen J, Li D, et al. Folate Receptor-Targeted and Gsh-Responsive Carboxymethyl Chitosan Nanoparticles Containing Covalently Entrapped 6-Mercaptopurine for Enhanced Intracellular Drug Delivery in Leukemia. *Mar Drugs* (2018) 16(11):439. doi: 10.3390/md16110439
111. Giammona G. Near-Infrared Light Responsive Folate Targeted Gold Nanorods for Combined Photothermal-Chemotherapy of Osteosarcoma. *ACS Appl Mater Interfaces* (2017) 9(16):14453–69. doi: 10.1021/acsami.7b03711
112. Ai J, Liu W, Liu B. Folic Acid-Tagged Titanium Dioxide Nanoparticles for Enhanced Anticancer Effect in Osteosarcoma Cells. *Mater Sci Eng C* (2017) 76:1181–7. doi: 10.1016/j.msec.2017.03.027
113. Rotman SG, Grijpma DW, Richards RG, Moriarty TF, Eglin D, Guillaume O. Drug Delivery Systems Functionalized With Bone Mineral Seeking Agents for Bone Targeted Therapeutics. *J Control Release* (2018) 269:88–99. doi: 10.1016/j.jconrel.2017.11.009
114. Leu C, Luegmayr E, Freedman LP, Rodan GA, Reszka AA. Relative Binding Affinities of Bisphosphonates for Human Bone and Relationship to Antiresorptive Efficacy. *Bone* (2006) 38:628–36. doi: 10.1016/j.bone.2005.07.023
115. Bonewald LF, Harris SE, Rosser J, Dallas MR, Dallas SL, Camacho NP, et al. Von Kossa Staining Alone is Not Sufficient to Confirm That Mineralization *In Vitro* Represents Bone Formation. *Calcif Tissue Int* (2003) 72:537–47. doi: 10.1007/s00223-002-1057-y
116. Yu L, Cai L, Hu H, Zhang Y. Experiments and Synthesis of Bone-Targeting Epirubicin With the Water-Soluble Macromolecular Drug Delivery Systems of Oxidized-Dextran. *J Drug Target* (2014) 22:343–51. doi: 10.3109/1061186X.2013.877467
117. Li CJ, Liu XZ, Zhang L, Chen LB, Shi X, Wu SJ, et al. Advances in Bone-Targeted Drug Delivery Systems for Neoadjuvant Chemotherapy for Osteosarcoma. *Orthop Surg* (2016) 8:105–10. doi: 10.1111/os.12238
118. Ma L, Zhou Y, Zhu Y, Lin Z, Wang Y, Zhang Y, et al. 3D-Printed Guiding Templates for Improved Osteosarcoma Resection. *Sci Rep* (2016) 6:2–10. doi: 10.1038/srep23335
119. Martin V, Bettencourt A. Bone Regeneration: Biomaterials as Local Delivery Systems With Improved Osteoinductive Properties. *Mater Sci Eng C* (2018) 82:363–71. doi: 10.1016/j.msec.2017.04.038

120. Wang C, Huang W, Zhou Y, He L, He Z, Chen Z, et al. 3D Printing of Bone Tissue Engineering Scaffolds. *Bioact Mater* (2020) 5:82–91. doi: 10.1016/j.bioactmat.2020.01.004
121. Ghorbani F, Li D, Ni S, Zhou Y, Yu B. 3D Printing of Acellular Scaffolds for Bone Defect Regeneration: A Review. *Mater Today Commun* (2020) 22:100979. doi: 10.1016/j.mtcomm.2020.100979
122. Fu S, Hu H, Chen J, Zhu Y, Zhao S. Silicone Resin Derived Larnite/C Scaffolds *via* 3D Printing for Potential Tumor Therapy and Bone Regeneration. *Chem Eng J* (2020) 382:122928. doi: 10.1016/j.cej.2019.122928
123. Ma H, Jiang C, Zhai D, Luo Y, Chen Y, Lv F, et al. A Bifunctional Biomaterial With Photothermal Effect for Tumor Therapy and Bone Regeneration. *Adv Funct Mater* (2016) 26:1197–208. doi: 10.1002/adfm.201504142
124. Wang Y, Sun L, Mei Z, Zhang F, He M, Fletcher C, et al. 3D Printed Biodegradable Implants as an Individualized Drug Delivery System for Local Chemotherapy of Osteosarcoma. *Mater Des* (2020) 186:108336. doi: 10.1016/j.matdes.2019.108336
125. Zhou H, Hernandez C, Goss M, Gawlik A, Exner AA. Biomedical Imaging in Implantable Drug Delivery Systems. *Curr Drug Targets* (2015) 16(6):672–82
126. Fahimipour F, Rasoulianboroujeni M, Dashtimoghadam E, Khoshroo K, Tahriri M, Bastami F, et al. 3D Printed TCP-Based Scaffold Incorporating VEGF-Loaded PLGA Microspheres for Craniofacial Tissue Engineering. *Dent Mater* (2017) 33:1205–16. doi: 10.1016/J.DENTAL.2017.06.016

Conflict of Interest: The authors declare that the research was conducted in the absence of any commercial or financial relationships that could be construed as a potential conflict of interest.

Publisher's Note: All claims expressed in this article are solely those of the authors and do not necessarily represent those of their affiliated organizations, or those of the publisher, the editors and the reviewers. Any product that may be evaluated in this article, or claim that may be made by its manufacturer, is not guaranteed or endorsed by the publisher.

frontiers in Oncology

ORIGINAL RESEARCH
published: 11 March 2022
doi: 10.3389/fonc.2022.856381

Silencing of lncRNA CHRM3-AS2 Expression Exerts Anti-Tumour Effects Against Glioma *via* Targeting microRNA-370-5p/KLF4

*Dong Wang, Qiang Chen, Jun Liu, Yuqing Liao and Qiuhua Jiang**

Department of Neurosurgery, Ganzhou People's Hospital, Ganzhou, China

OPEN ACCESS

Edited by:
Zhe-Sheng Chen,
St. John's University, United States

Reviewed by:
Yu Li,
Peking University Shenzhen Hospital, China
Hao Zhang,
University of Pennsylvania, United States

***Correspondence:**
Qiuhua Jiang
jiangqh1968@126.com

Specialty section:
This article was submitted to Cancer Molecular Targets and Therapeutics, a section of the journal Frontiers in Oncology

Received: *17 January 2022*
Accepted: *21 February 2022*
Published: *11 March 2022*

Citation:
Wang D, Chen Q, Liu J, Liao Y and Jiang Q (2022) Silencing of lncRNA CHRM3-AS2 Expression Exerts Anti-Tumour Effects Against Glioma via Targeting microRNA-370-5p/KLF4. Front. Oncol. 12:856381. doi: 10.3389/fonc.2022.856381

Objectives: Long non-coding RNAs (lncRNAs) are key regulators involved in the progression of glioma, and many functional lncRNAs are yet to be identified. This study aimed to explore the function of CHRM3-AS2, a rarely reported lncRNA, in glioma, as well as the underlying mechanisms involving miR-370-5p/KLF4.

Methods: Differentially expressed RNAs (DERs) were screened from two gene expression profiles of glioblastoma (GBM). Fluorescence *in situ* hybridisation was performed to determine the subcellular localisation of CHRM3-AS2. Cell viability, colony formation, apoptosis, migration, and invasion were evaluated using cell counting kit-8, colony counts, flow cytometry, wound healing, and Transwell assays, respectively. mRNA and protein expression of specific genes were measured using quantitative real-time polymerase chain reaction and western blotting, respectively. Dual luciferase reporter gene, RNA immunoprecipitation, and RNA pull-down assays were performed to identify the target relationships. A mouse xenograft model was established for *in vivo* validation.

Results: CHRM3-AS2 was screened as a prognosis-associated DER in GBM. CHRM3-AS2 expression was up-regulated in glioma cells, and CHRM3-AS2 was localised in the cytoplasm. Silencing of CHRM3-AS2 expression inhibited cell viability, colony formation, migration, and invasion and promoted apoptosis of U251 and SHG-44 cells. In addition, CHRM3-AS2 targeted miR-370-5p/KLF4 in glioma cells. The anti-tumour effect of CHRM3-AS2 silencing was weakened by miR-370-5p silencing or KLF4 overexpression. *In vivo*, silencing of CHRM3-AS2 expression inhibited tumour growth and Ki67 expression in mice. Overexpression of KLF4 also weakened the anti-tumour effect of CHRM3-AS2 silencing in mice.

Conclusions: Silencing of CHRM3-AS2 expression inhibited the malignant progression of glioma by regulating miR-370-5p/KLF4 expression.

Keywords: glioma, differentially expressed RNAs, CHRM3-AS2, miR-370-5p, KLF4

INTRODUCTION

Glioma is a prevalent type of primary intracranial carcinoma, accounting for 81% of malignant brain tumours (1). Based on pathological features, glioma can be classified into the following subtypes: astrocytoma, oligodendroglioma, oligoastrocytoma, ependymoma, glioblastoma (GBM), and mixed tumours (2). Conventional therapeutic strategies, including surgical resection, chemotherapy, and radiotherapy, are still limited in improving the prognosis of patients with glioma (3). In addition, grade IV GBM, the most common and malignant form of glioma, is more likely to be accompanied with poor prognosis because GBM stem-like cells are resistant to conventional therapy and easily undergo recurrence (4). For GBM patients receiving current standard treatments, the median overall survival is approximately 12–18 months (5). Therefore, discovery of novel therapeutic targets for glioma is urgently needed.

Long non-coding RNAs (lncRNAs), i.e. non-coding RNAs that are > 200 nucleotides in length, play important regulatory roles in biological processes at the transcriptional, post-transcriptional, and epigenetic levels (6). lncRNAs are also implicated in the occurrence and progression of glioma in the aspects of stemness, hyperproliferation, angiogenesis, and drug resistance (7). Expression of many lncRNAs has been shown to be dysregulated in glioma, such as the up-regulation of NEAT1, HOTAIR, FOXM1-AS, H19, SOX2OT, and HCP5 expression and the down-regulation of GAS5, NBAT-1, and CASC2 expression (8). These lncRNAs exert critical regulatory roles in the development of the malignant features of glioma cells. For example, NEAT1 knockdown inhibits the proliferation of glioma cells both *in vitro* and *in vivo* (9). Up-regulation of H19 expression promotes the proliferation, migration, invasion, and angiogenesis of glioma cells (10). Overexpression of GAS5 inhibits cell proliferation, migration, and invasion and promotes the apoptosis of glioma cells (11). Despite these findings, many functional lncRNAs remain to be identified. The expression of CHRM3-AS2, an lncRNA, has been reported to be down-regulated in ovarian carcinoma (12). CHRM3-AS2 is considered to be an independent prognostic factor in the prognosis of ovarian carcinoma (12). However, the functions of CHRM3-AS2 in glioma remain unclear.

MicroRNAs (miRNAs) are small, non-coding, 18–25-nucleotide long RNAs that are closely associated with glioma tumourigenesis and development. A meta-analysis found that cell-free miRNAs, especially miR-21, -125, and -222, in cerebrospinal fluid and blood are potential non-invasive biomarkers for the early diagnosis of glioma (13). Another meta-analysis revealed that increased expression of miR-15b, -21, -148a, -196, -210, and -221 and decreased expression of miR-106a and -124 are correlated with poor outcomes in patients with glioma (14). In addition, certain miRNAs have been noted to be the therapeutic targets of glioma through regulation of malignant characteristics. These targets include miR-451 (15), -93 (16), -320a (17), -27b-3p (18), and -6869-5p (19). miR-370-5p serves as an anti-oncogene in breast cancer (20), lung cancer (21), hepatocellular carcinoma (22), and ovarian cancer (23). However, the functions of miR-370-5p in glioma and related mechanisms have not been explored.

lncRNAs are considered to be competing endogenous RNAs that can competitively bind to miRNAs, thereby regulating the expression of downstream target genes of miRNAs at the post-transcriptional level (24). To date, emerging regulatory axes involving lncRNA/miRNA/mRNA have been determined to be involved in glioma progression, such as H19/miR-138/HIF-1α (10), BCYRN1/miR-619-5p/UEDC2 (25), PVT1/miR-128-3p/GREM1 (26), and SNHG16/miR-373/EGFR (27). KLF4 is a core component of the pluripotency transcription network that is involved in the regulation of cell cycle following DNA damage (28). A recent study has proved that KLF4 can be targeted by lncRNA XIST/miR-152 in regulating stemness in GBM (29). In this study, a screened prognosis-associated differentially expressed RNA (DER), CHRM3-AS2, was analysed in glioma. Then, the action mechanisms of CHRM3-AS2 involving miR-370-5p/KLF4 were evaluated. Our findings may reveal potential molecular targets for the treatment of glioma.

METHODS

Bioinformatic Analysis

A GBM gene expression profile was downloaded from The Cancer Genome Atlas. Samples of 162 tumour tissues with clinical prognostic information and 5 normal solid tissues were used as a training dataset. Another GBM gene expression profile was downloaded from the Chinese Glioma Genome Atlas. Samples of 237 tumour tissues were used as a validation dataset. lncRNAs and mRNAs were annotated based on HUGO Gene Nomenclature Committee recommendations (30). Immune infiltration grouping (immunity_H and immunity_L) was established *via* single sample gene set enrichment analysis (ssGSEA) using GSVA package (31). The stromalScore, immuneScore, and ESTIMATEScore were analysed using the Estimate package (32). DERs were isolated using Limma package (FDR < 0.05 and |log2FC| > 0.5) (33). Prognosis-associated DERs were isolated by univariate and multivariate Cox regression analyses using Survival package (log-rank $p < 0.05$) (34) and then screened using Penalized package based on Cox-Proportional Hazards model (35).

Cell Transfection

A normal human glial cell line (HEB), and four glioma cell lines (U251, SHG-44, U87, and T98) were purchased from the American Type Culture Collection (ATCC, Manassas, VA, USA). Cells were cultured in Dulbecco's Modified Eagle's Medium (DMEM) containing 10% foetal bovine serum (FBS), 100 U/mL penicillin, and 100 U/mL streptomycin at 37°C with 5% CO_2. pMKO.1-GFP vector carrying shRNA-CHRM3-AS2 (sh-CHRM3-AS2, GCCAGTTCTGCTGAGAATTAT) and corresponding empty vector (sh-NC), pcDNA3.1 vector carrying full length CHRM3-AS2/KLF4 (oe-CHRM3-AS2/KLF4) and corresponding empty vector (oe-NC), miR-370-5p inhibitor (GUAACUGCAGAGACGUGACCUG) and inhibitor NC (TAACACGTCTATACGCCCA), as well as miR-370-5p mimic (CAGGUCACGUCUCUGCAGUUAC) and mimic NC (GAUGGCAUUCGAUCAGUUCUA) were packaged into lentivirus (RiboBio, Guangzhou, China) and used for

transfection. Cell transfection was performed using HighGene transfection reagent (ABclonal, Wuhan, China) following the manufacturer's instructions.

Fluorescence *In Situ* Hybridisation

The subcellular localisation of CHRM3-AS2 was determined using FISH. Cells were fixed with 4% paraformaldehyde for 15 min, permeabilised with 0.1% Triton X-100 for 15 min, soaked in 2 × SSC solution for 30 min, and dehydrated in a graded ethanol series (3 min in each concentration). Subsequently, cells were hybridised with 1 ug/mL of probe (CY3-GCTGACAAACTCT CTTGCCC) at 37°C overnight. After incubation with 0.4 × SSC containing 0.3% Triton X-100 for 2 min at 65°C, cells were counterstained with DAPI for 5 min in the dark. Stained cells were observed under a confocal microscope (ULTRAVIEW VOX, Perkin Elmer, Waltham, MA, USA).

Cell Viability Assay

Cell viability was determined using Cell Counting Kit-8 (CCK-8, Beyotime, China). Transfected cells were seeded into 96-well plates and cultured for 24, 48, and 72 h. Cells in each well were then incubated with 10 μL CCK-8 solution for 2 h at 37°C. The optical density at 450 nm was detected using a microplate reader (SpectraMax M4, MolecularDevices, CA, USA).

Colony Formation Assay

Colony formation assays were performed to measure cell proliferation. Transfected cells were seeded into 6-well plates at a density of 200 cells/well. After 7 days of culture, the colonies generated were fixed with 10% methanol for 15 min and then stained with 1% crystal violet for 20 min at 25°C. Stained colonies were observed and counted under a microscope (BX53M, Olympus, Japan).

Cell Apoptosis Assay

Cell apoptosis was detected using the Apoptosis Detection Kit (Beyotime). Transfected cells were re-suspended in 300 μL binding buffer, then incubated with 5 μL Annexin V-FITC for 15 min, and subsequently incubated with 10 μL propidium iodide for 10 min at 25°C in the dark. The apoptosis rate was detected *via* flow cytometry (CytoFLEX S, Beckman, Miami, FL, USA) using Cell Quest software (BD Biosciences, NJ, USA).

Wound Healing Assay

Wound healing assays were performed to measure cell migration. Transfected cells were seeded into 6-well plates and cultured overnight (to 80–90% confluence). An artificial wound (scratch) was made in each well using a pipette tip. After 24 h of culture, the wound was observed under a microscope (BX53M, Olympus). The migration rate was calculated according to the healing distance before and after wounding.

Cell Invasion Assay

Cell invasion was detected using Transwell chambers. Transfected cells in serum-free medium were added into Matrigel-coated upper chambers, and DMEM containing 10% FBS was added into the lower chamber. After being cultured for 24 h, cells in the lower chamber were fixed with methanol for 30 min and then stained with crystal violet for 20 min. The stained cells were observed under a microscope (BX53M, Olympus) and counted in five random fields.

Quantitative Real-Time Polymerase Chain Reaction

Total RNA was extracted from cells or tissues using TRIzol reagent (Invitrogen, CA, USA). After reverse transcription using FastKing First-strand cDNA Synthesis Mix (TiangenI, China), cDNA was used as template for qRT-PCR. Using the SYBR Green qPCR Kit (Lifeint, China), qRT-PCR was performed on an Mx3000P Real-Time PCR instrument (Stratagene, CA, USA) with the following thermocycling program: 95°C for 3 min, followed by 40 cycles of 95°C for 12 s and 62°C for 40 s. The relative expression of target genes was calculated *via* the $2^{-\Delta\Delta Ct}$ method. U6 was used as an internal control for miR-370-5p, and GAPDH was the internal control for CHRM3-AS2 and KLF4. The primers used in qRT-PCR are shown in **Table 1**.

Western Blotting

Cell or tissue samples were lysed in RIPA Lysate (Beyotime) to extract total proteins. The protein samples were separated *via* 10% sodium dodecyl sulphate–polyacrylamide gel electrophoresis and then transferred onto polyvinylidene difluoride membranes. After blocking with 5% non-fat milk for 1 h, the membrane was incubated with anti-KLF4 antibodies (1:500, Abcam, Cambridge, UK) at 4°C for 12 h. The membrane was then incubated with horseradish peroxidase (HRP)-conjugated IgG (goat anti-rabbit, 1:2000, Abcam) for 1 h at 25°C in the dark. Protein bands were visualised using ECL reagent (Thermo Fisher Scientific, CA, USA) and images were captured using a Gel Imaging System (Tanon, China).

Target Prediction

The miRNA targets of CHRMS-AS2 were predicted using ENCORI (https://starbase.sysu.edu.cn/index.php). Between two potential targets, miR-370-5p, an anti-oncogenic miRNA was selected for analysis. Similarly, the mRNA targets of miR-370-5p were subsequently predicted using miRDB (http://www.mirdb.org/mirdb/index.html). Among 360 targets, KLF4 (rank 11, score 94) with an important role in glioma was selected for analysis.

TABLE 1 | The primers used in qRT-PCR.

Primers	Sequences
CHRM3-AS2-F	5'-TGTTCACCACTGCACACTCA-3'
CHRM3-AS2-R	5'-CGTTGTGGGCCCGTGATAAT-3'
miR-370-5p-F	5'-ACACTCCAGCTGGGCAGGTCACGTCTCTGC-3'
miR-370-5p-R	5'-CTCAACTGGTGTCGTGGAGTCGGCAATTCAGTTGAGGTAACTGC-3'
KLF4-F	5'-CCCACATGAAGCGACTTCCC-3'
KLF4-R	5'- CAGGTCCAGGAGATCGTTGAA-3'
U6-F	5'-AAAGCAAATCATCGGACGACC-3'
U6-R	5'- GTACAACACATTGTTTCCTCGGA-3'
GAPDH-F	5'- TGTGGGCATCAATGGATTTGG-3'
GAPDH-R	5'- ACACCATGTATTCCGGGTCAAT-3'

Dual Luciferase Reporter Gene Assay

Target relations involving miR-370-5p and CHRM3-AS2/KLF4 were determined using DLR assays. CHRM3-AS2 and KLF4 carrying wild-type binding sites (WT-CHRM3-AS2, ugaaaaa gguuGCUGUGACCUg; WT-KLF4, uccgaucaacauuuaUGAC CUAa) or mutant binding sites (MT-CHRM3-AS2, ugaaaaagg uuGUGCACUGGUg; MT-KLF4, uccgaucaacauuuaUCUGGUc) were integrated into dual luciferase vectors (Beyotime). U251 cells were co-transfected with WT/MUT-CHRM3-AS2/KLF4 and miR-16-5p mimic/mimic NC for 48 h. The relative luciferase activity (Firefly/Renilla luciferase) was detected using Cypridina-Firefly Luciferase Dual Assay Kit (Thermo Fisher Scientific).

RNA Immunoprecipitation Assay

RIP assays were performed to verify the target relationship involving miR-370-5p and CHRM3-AS2. Briefly, U251 cells were lysed in RIPA lysis reagent and then incubated with anti-Ago2 or IgG-conjugated beads (Millipore, Billerica, MA, USA) at 4°C overnight. The precipitates were incubated with proteinase K for 30 min at 55°C and immunoprecipitated RNAs were then extracted using TRIzol reagent. The expression of CHRM3-AS2 and miR-370-5p was detected using qRT-PCR, as described earlier.

RNA Pull-Down Assay

The target relationship between miR-370-5p and CHRM3-AS2 was also verified *via* RNA pull-down assays. Wild-type (cAGGUCA cgucucugcaguuac) or mutant miR-370-5p (cUCCAGUcgucucu gcaguuac) were labelled with biotin-conjugated RNA (WT/MT-miR-370-5p) and transfected into U251 cells. After 48 h of transfection, cells were lysed in RIPA reagent and incubated with Nucleic Acid Compatible Streptavidin Magnetic Beads (Thermo Fisher Scientific) at 25°C for 30 min in the dark. The beads were further incubated with Biotin Elution buffer for 30 min, and the eluents were collected for RNA extraction. The expression of CHRM3-AS2 was quantified using qRT-PCR as described earlier.

Murine Tumour Xenograft Model

Female BALB/c nude mice (4 weeks old, 14 ± 2 g, HFK Bioscience, Beijing, China) were used for the establishment of a tumour xenograft animal model. Mice were fed at 25–27°C and 45–50% relative humidity with free access to water and food. Mice were subcutaneously injected with 0.1 mL transfected U251 cells at a density of 1×10^7 cells/mL (n = 6 for each group). Tumour diameters were measured every 3 days using Vernier callipers, and tumour volumes were calculated as follows: (longest diameter × shortest diameter^2)/2. Twenty-one days after injection, mice were sacrificed by intraperitoneal injection of 150 mg/kg pentobarbital sodium. The resected tumour xenografts were weighed and then used for histological examination. All animal experiments were approved by the ethics committee of our hospital in accordance with the Guide for the Care and Use of Laboratory Animals.

Immunohistochemistry and Immunofluorescence

The expression of Ki-67 in tumour tissues was detected *via* IHC and IF. Resected tumour tissues were fixed in 4% paraformaldehyde for 24 h, dehydrated in a graded ethanol series, embedded in paraffin, and sectioned to 5–7 μm. After dewaxing in xylene and rehydration with graded ethanol, the sections received microwave irradiation in citrate buffer at 95°C for 15 min, following which they were soaked in 3% H_2O_2 for 20 min. The sections were blocked with 5% goat serum for 15 min and then incubated with specific anti-Ki67 antibody (1:200, Abcam) at 4°C overnight. Subsequently, the sections were incubated with secondary antibody (HRP-IgG for IHC, 1:500; Alexa Fluor® 647-IgG for IF, 1:200, Abcam) for 1 h at 25°C. For IHC, positive cells were visualised with diaminobenzidine and then observed under a microscope (BX53M, Olympus). For IF, positive cells were counterstained with DAPI and then observed under a confocal microscope (ULTRAVIEW VOX, Perkin Elmer).

Statistical Analysis

Statistical analysis was performed using GraphPad Prism v.7 software. Data are presented in the form of mean ± standard deviation. Comparisons among different groups were performed *via* one-way or two-way analysis of variance followed by Tukey's test. $P < 0.05$ was considered to be statistically significant.

RESULTS

Identification of DERs in GBM Samples

Bioinformatics analysis was performed to determine the research objective of this study. Based on two GBM gene expression profiles, a total of 788 lncRNAs and 15,788 mRNAs were annotated. In aspect of immune infiltration, ssGSEA showed that GBM samples could be divided into two clusters, including immunity_H (72 samples) and immunity_L (90 samples) (**Figure 1A**). The stromalScore, immuneScore, and ESTIMATEScore were significantly higher in immunity_H samples than those in immunity_L samples ($P < 0.001$, **Figure 1B**). The immune cell types were also significantly different between immunity_H and immunity_L samples ($P < 0.05$, **Figure 1C**). Moreover, between immunity_H and immunity_L samples, 585 DERs were identified, and between tumour and normal samples, 798 DERs were identified. A total of 222 overlapping DERs were screened, including 12 lncRNAs and 210 mRNAs (**Figure 1D**). After being analysed *via* univariate and multivariate Cox regression analyses, 2 lncRNAs and 9 mRNAs independently associated with clinical prognosis were obtained. Furthermore, 9 DERs were confirmed *via* Cox-Proportional Hazards modelling (**Figure 1E**). CHRM3-AS2 was finally selected as the research objective for the following assays.

CHRM3-AS2 Was Up-Regulated in Glioma Cells and Localised Cytoplasmically

To determine the role of CHRM3-AS2 in glioma, the expression of CHRM3-AS2 was firstly quantified in glioma cells. qRT-PCR showed that the expression of CHRM3-AS2 was significantly higher in glioma cell lines (U251, SHG-44, U87, and T98) than that in HEB cells ($P < 0.05$, **Figure 2A**). Subsequently, the subcellular localisation of CHRM3-AS2 in glioma cells was determined using FISH. As

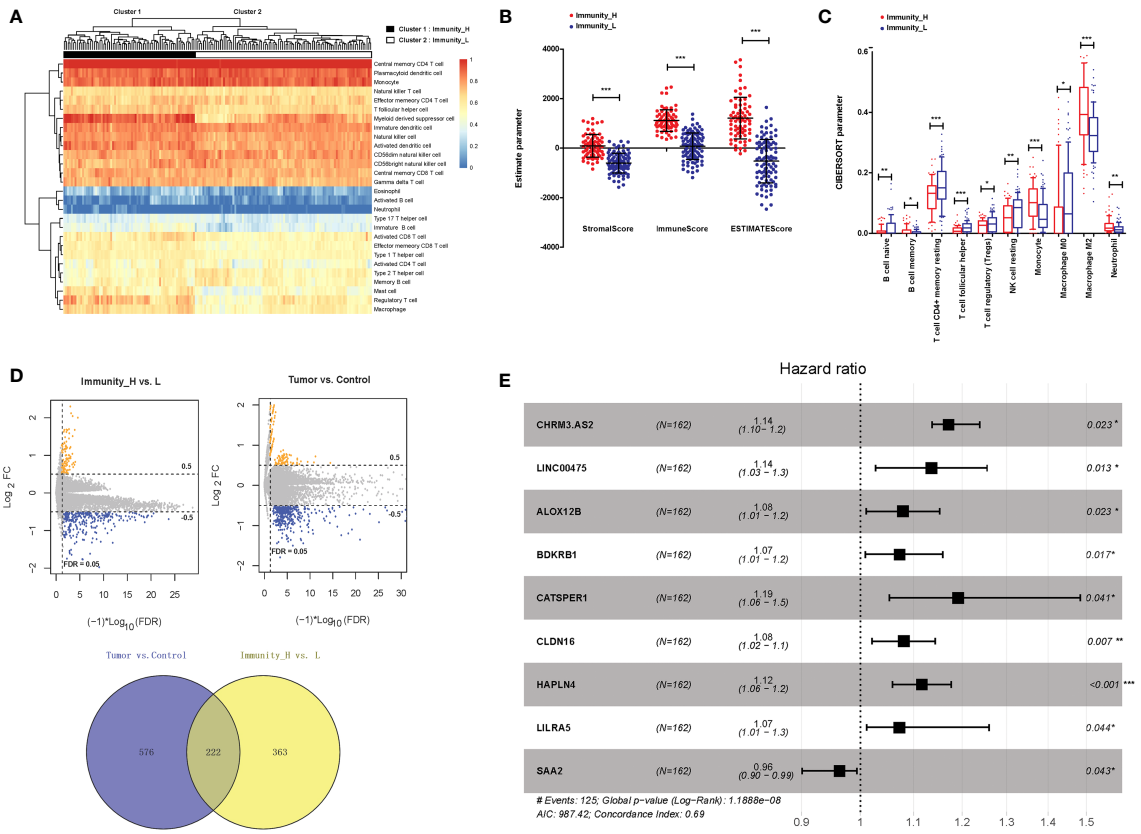

FIGURE 1 | Isolation of DERs in GBM samples. **(A)** Immune infiltration grouping of GBM samples. **(B)** The stromalScore, immuneScore, and ESTIMATEScore in immunity_H and immunity_L samples. **(C)** Immune cell types in immunity_H and immunity_L samples. **(D)** DERs between immunity_H and immunity_L samples and between tumour and normal samples. **(E)** Forest plots of 9 prognosis-associated DERs (2 lncRNAs and 7 mRNAs). *P < 0.05, ** P < 0.01, ***P < 0.001.

shown in **Figure 2B**, CHRM3-AS2 was mainly distributed in the cytoplasm of U251 and SHG-44 cells. U251 cells, with a relatively high change of CHRM3-AS2 expression, and SHG-44 cells, with relatively low change of CHRM3-AS2 expression, were selected for subsequent functional assays.

CHRM3-AS2 Acted as an Oncogene in Glioma Cells

To understand the function of CHRM3-AS2 in glioma, CHRM3-AS2 was silenced or overexpressed in U251 and SHG-44 cells. qRT-PCR determined that transfection of sh-CHRM3-AS2 significantly decreased the expression of CHRM3-AS2, and transfection of oe-CHRM3-AS2 significantly increased the expression of CHRM3-AS2 in U251 and SHG-44 cells ($P < 0.05$, **Figure 3A**). These findings proved the effective transfection efficiency of sh-CHRM3-AS2 and oe-CHRM3-AS2 in glioma cells. As per the functional assays performed, CHRM3-AS2 silencing inhibited cell viability, colony formation, and promoted cell apoptosis in U251 and SHG-44 cells ($P < 0.001$, **Figures 3B–D**). The migration and invasion of U251 and SHG-44 cells were also significantly decreased by CHRM3-AS2 silencing ($P < 0.001$, **Figures 3E, F**). In contrast, transfection of oe-CHRM3-AS2 elicited contrary effects in U251 and SHG-44 cells, compared with transfection of sh-CHRM3-AS2 ($P < 0.001$, **Figures 3B–F**). The above regulatory effects of CHRM3-AS2 on the malignant characteristics of U251 and SHG-44 cells indicated an oncogenic role of CHRM3-AS2 in glioma.

CHRM3-AS2 Regulated miR-370-5p/KLF4 in Glioma Cells

To understand the mechanism of action of CHRM3-AS2 in glioma, the miRNA targets of CHRM3-AS2 were predicted using Starbase 3.0. MiR-370-5p, a potential miRNA target of CHRM3-AS2, was selected for analysis. qRT-PCR showed that the expression of miR-370-5p was significantly lower in glioma cells (U251, SHG-44, U87, and T98) than that in HEB cells ($P < 0.001$, **Figure 4A**). The target relationship between CHRM3-AS2 and miR-370-5p was further identified by DLR, RIP and RNA pull-down assays. DLR assay showed that miR-370-5p mimic significantly decreased the luciferases activity in U251 cells transfected with WT-CHRM3-AS2 ($P < 0.001$), but not in cells transfected with MUT-CHRM3-AS2 (**Figure 4B**). RIP assay showed that CHRM3-AS2 was immunoprecipitated with miR-370-5p in U251 cells ($P< 0.01$, **Figure 4C**). RNA pull-down assay

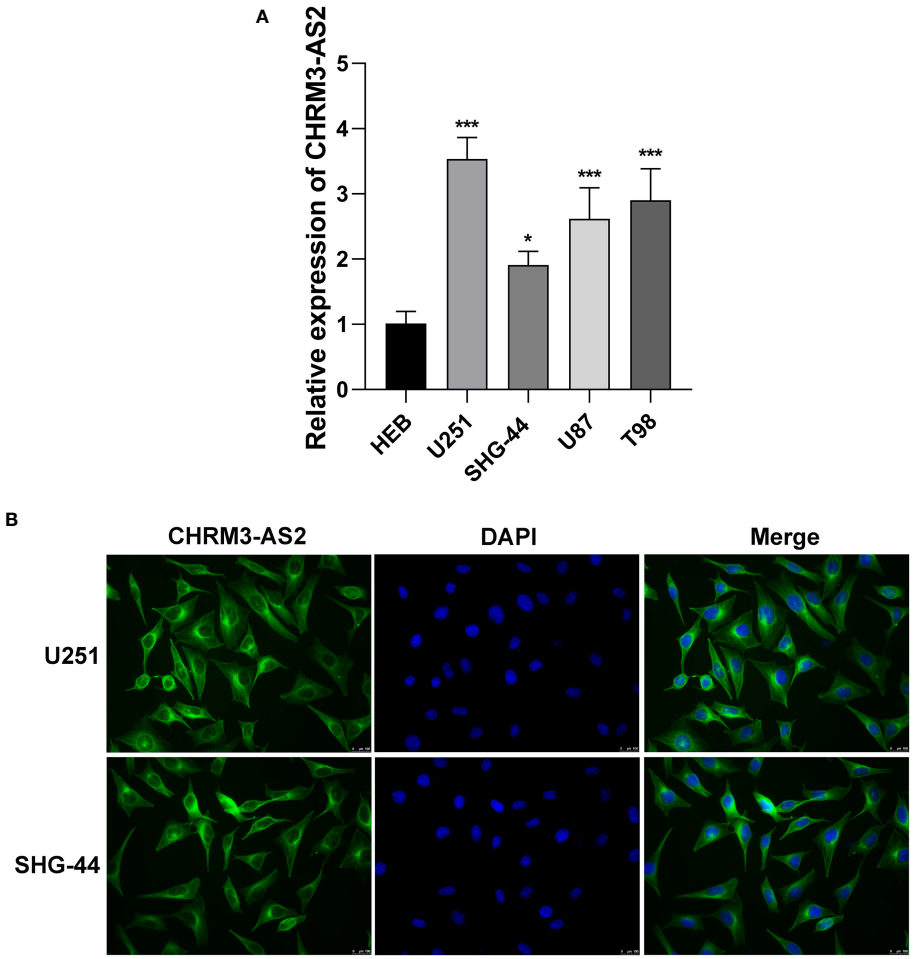

FIGURE 2 | Up-regulation of expression of CHRM3-AS2 localised in the cytoplasm of glioma cells. **(A)** Expression of CHRM3-AS2 in a normal human glial cell line (HEB) and four glioma cell lines (U251, SHG-44, U87, and T98) was quantified *via* qRT-PCR. **(B)** Subcellular localisation of CHRM3-AS2 was determined *via* FISH in U251 and SHG-44 cells. *P < 0.05, ***P < 0.001 vs. HEB.

further determined that CHRM3-AS2 was pulled down by WT-miR-370-5p, but not by MUT-miR-370-5p (P< 0.001, **Figure 4D**). In addition, silencing of CHRM3-AS2 expression significantly up-regulated miR-370-5p expression (P < 0.001) and overexpression of CHRM3-AS2 significantly down-regulated miR-370-5p expression in U251 and SHG-44 cells (P < 0.05, **Figures 4E, G**). These findings indicated that CHRM3-AS2 negatively regulated its target miR-370-5p in glioma cells. Furthermore, the use of miR-370-5p inhibitor reversed the effects of sh-CHRM3-AS2 transfection (i.e. down-regulation of CHRM3-AS2 expression and up-regulation of miR-370-5p expression) (P < 0.01, **Figure 4F**). The use of miR-370-5p mimic reversed the effects of oe-CHRM3-AS2 transfection (i.e. up-regulation of CHRM3-AS2 expression and down-regulation of miR-370-5p expression) (P < 0.01, **Figure 4H**). These results further indicated that miR-370-5p could also reversely regulate CHRM3-AS2.

Subsequently, the mRNA targets of miR-370-5p were predicted using TargetScan 7.1. KLF4, a potential mRNA target of miR-370-5p, was selected for analysis. Compared with HEB cells, glioma cells (U251, SHG-44, U87, and T98) exhibited significantly higher expression levels of KLF4 at both the mRNA and protein levels (P < 0.01, **Figure 5A**). DLR assay confirmed the target relationship between miR-370-5p and KLF4, evidenced by decreased the luciferases activity in U251 cells co-transfected with miR-370-5p mimic and WT- KLF4 (P < 0.001, **Figure 5B**). In addition, the mRNA expression of KLF4 was significantly decreased by transfection of sh-CHRM3-AS2 (P < 0.05) and increased by transfection of oe-CHRM3-AS2, in U251 and SHG-44 cells (P < 0.001, **Figures 5C, E**). The use of miR-370-5p inhibitor alleviated the inhibitory effects of sh-CHRM3-AS2 on the expression of KLF4 in U251 cells (P < 0.05, **Figure 5D**). MiR-370-5p mimic weakened the promoting effects of oe-CHRM3-AS2 on KLF4 expression in SHG-44 cells (P < 0.001, **Figure 5F**). These results indicated the presence of CHRM3-AS2/miR-370-5p/KLF4 axis in glioma cells.

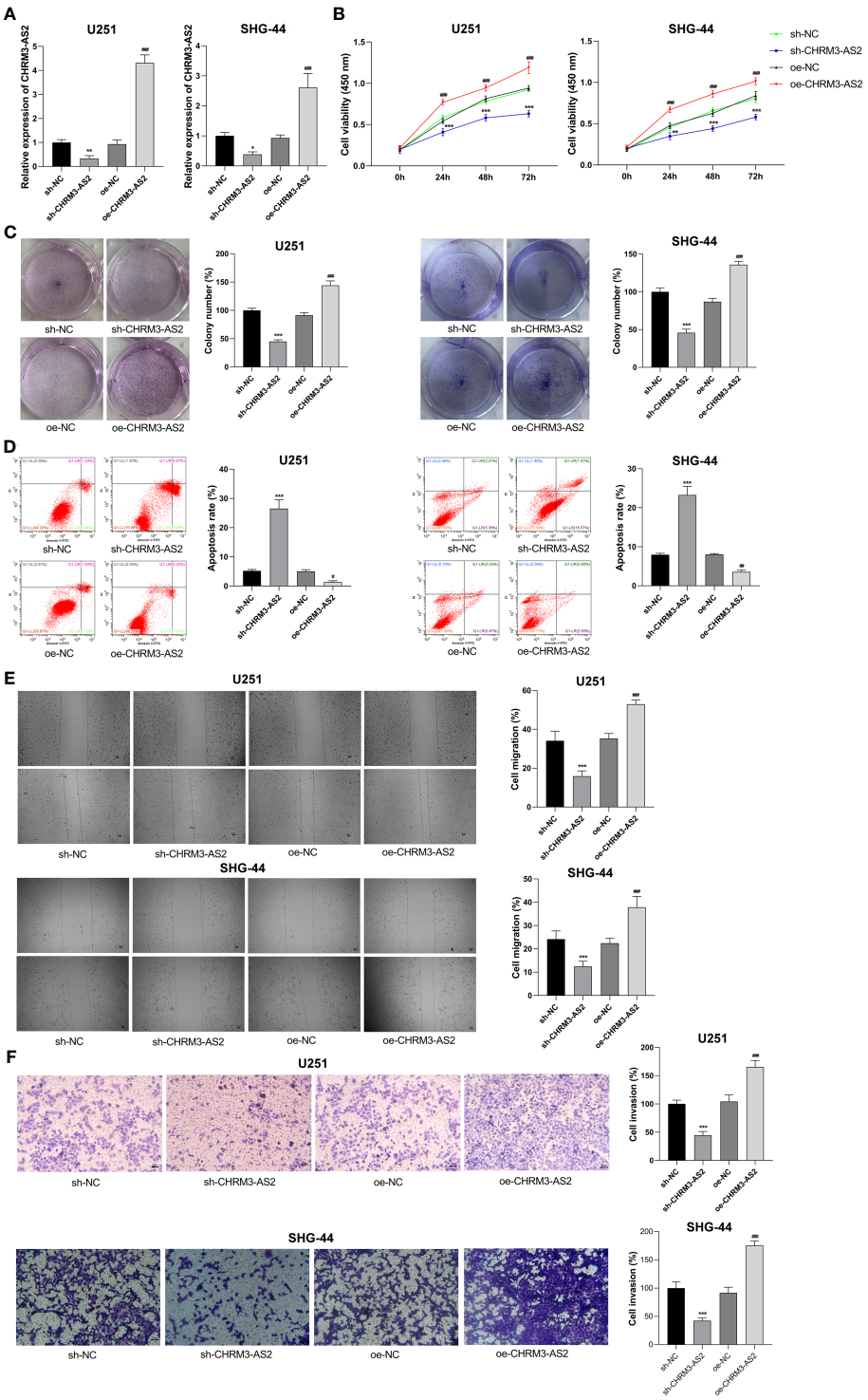

FIGURE 3 | CHRM3-AS2 inhibited the malignant characteristics of glioma cells. **(A)** Expression of CHRM3-AS2 was quantified *via* qRT-PCR. **(B)** Cell viability was measured using CCK-8 assays. **(C)** Colony numbers were measured using colony formation assays. **(D)** Cell apoptosis was evaluated *via* flow cytometry. **(E)** Cell migration was evaluated using wound healing assays. **(F)** Cell invasion was analysed using Transwell assays. U251 and SHG-44 cells were transfected with sh-CHRM3-AS2/sh-NC or oe-CHRM3-AS2/oe-NC. *P < 0.05, ** P < 0.01, ***P < 0.001 vs. sh-NC; $^{\#\#}$P < 0.01, $^{\#\#\#}$P < 0.001 vs. oe-NC.

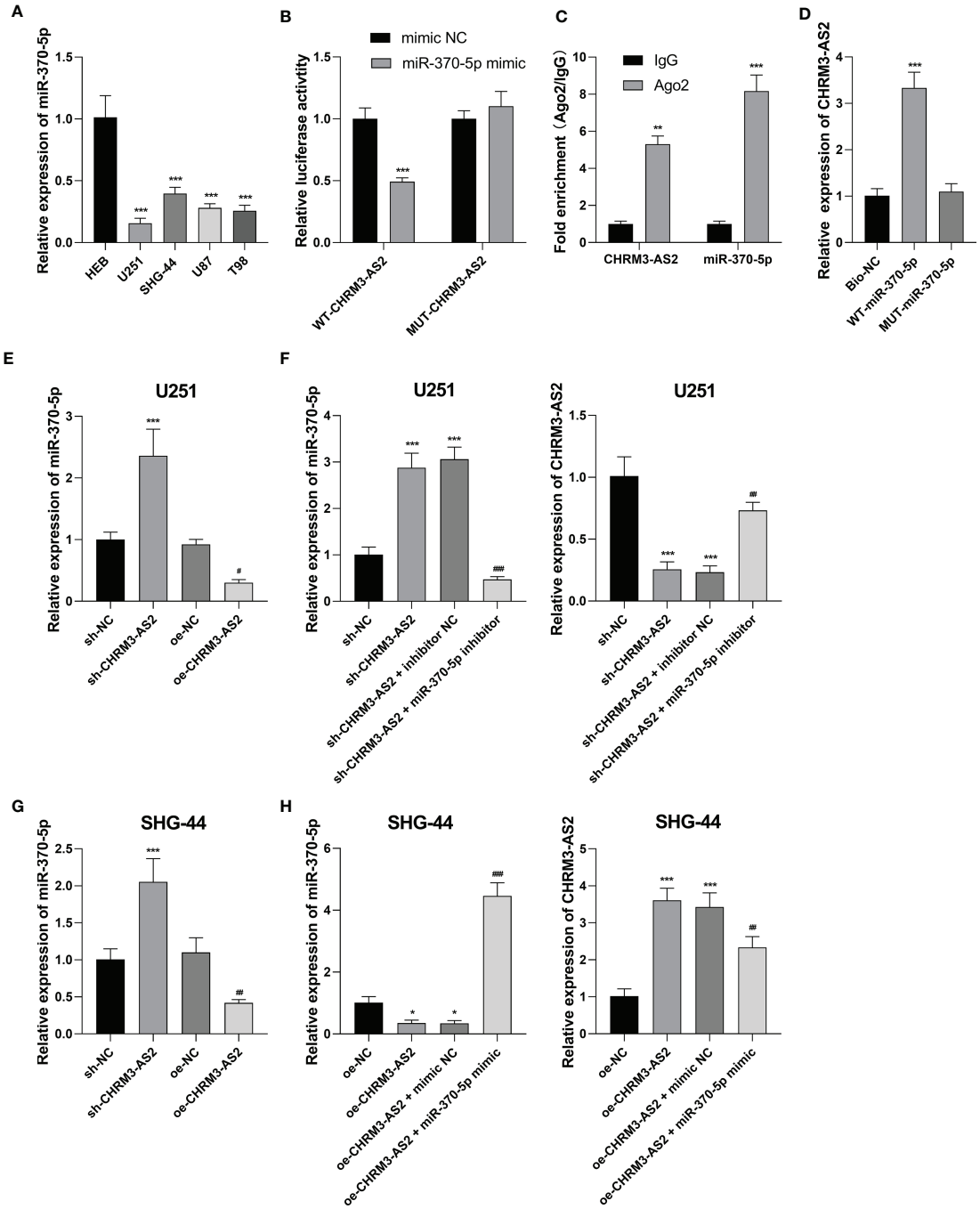

FIGURE 4 | CHRM3-AS2 targeted miR-370-5p in glioma cells. **(A)** The expression of miR-370-5p in a normal human glial cell line (HEB) and four glioma cell lines (U251, SHG-44, U87, and T98) was quantified *via* qRT-PCR; ***P < 0.001 vs. HEB. **(B)** The relationship between CHRM3-AS2 and miR-370-5p was determined *via* DLR assays; ***P < 0.001 vs. mimic NC. **(C)** The relationship between CHRM3-AS2 and miR-370-5p was determined *via* RIP assays; **P < 0.01, ***P < 0.001 vs. IgG. **(D)** The relationship between CHRM3-AS2 and miR-370-5p was determined *via* RNA pull-down assays; ***P < 0.001 vs. Bio-NC. **(E)** Expression of miR-370-5p in U251 cells transfected with sh-CHRM3-AS2/sh-NC or oe-CHRM3-AS2/oe-NC was quantified *via* qRT-PCR; ***P < 0.001 vs. sh-NC; $^{\#}$P < 0.05 vs. oe-NC. **(F)** Expression of miR-370-5p and CHRM3-AS2 in U251 cells transfected with sh-CHRM3-AS2/sh-NC and miR-370-5p inhibitor/inhibitor NC was quantified *via* qRT-PCR; ***P < 0.001 vs. sh-NC; $^{\#\#}$P < 0.01, $^{\#\#\#}$P < 0.001 vs. sh-CHRM3-AS2. **(G)** Expression of miR-370-5p in SHG-44 cells transfected with sh-CHRM3-AS2/sh-NC or oe-CHRM3-AS2/oe-NC was quantified *via* qRT-PCR; ***P < 0.001 vs. sh-NC; $^{\#\#}$P < 0.01 vs. oe-NC. **(H)** Expression of miR-370-5p and CHRM3-AS2 in SHG-44 cells transfected with oe-CHRM3-AS2/oe-NC and miR-370-5p mimic/mimic NC was quantified *via* qRT-PCR; *P < 0.05, ***P < 0.001 vs. oe-NC; $^{\#}$P < 0.05, $^{\#\#}$P < 0.01, $^{\#\#\#}$P < 0.001 vs. oe-CHRM3-AS2.

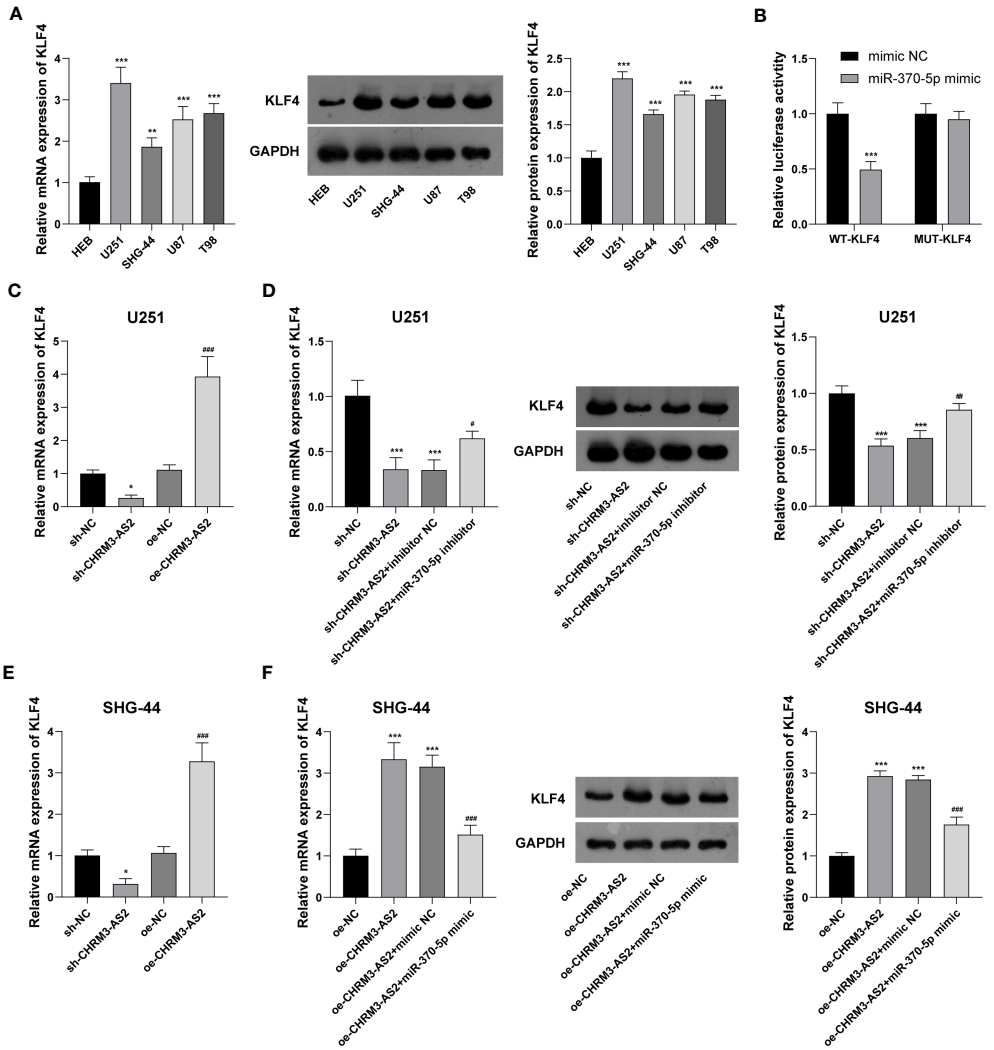

FIGURE 5 | CHRM3-AS2 targeted miR-370-5p/KLF4 axis in glioma cells. **(A)** KLF4 mRNA and protein expression levels in a normal human glial cell line (HEB) and four glioma cell lines (U251, SHG-44, U87, and T98) were quantified *via* qRT-PCR and western blotting, respectively. $^{**}P < 0.01$, $^{***}P < 0.001$ vs. HEB. **(B)** The relationship between miR-370-5p and KLF4 was determined *via* DLR assays; $^{***}P < 0.001$ vs. mimic NC. **(C)** KLF4 mRNA expression in U251 cells transfected with sh-CHRM3-AS2/sh-NC or oe-CHRM3-AS2/oe-NC was quantified *via* qRT-PCR; $^{*}P < 0.05$ vs. sh-NC; $^{###}P < 0.001$ vs. oe-NC. **(D)** KLF4 mRNA and protein expression in U251 cells transfected with sh-CHRM3-AS2/sh-NC and miR-370-5p inhibitor/inhibitor NC was quantified *via* qRT-PCR and western blotting, respectively. $^{***}P < 0.001$ vs. sh-NC; $^{#}P < 0.05$, $^{##}P < 0.01$ vs. sh-CHRM3-AS2. **(E)** KLF4 mRNA in SHG-44 cells transfected with sh-CHRM3-AS2/sh-NC or oe-CHRM3-AS2/oe-NC was quantified *via* qRT-PCR; $^{*}P < 0.05$ vs. sh-NC; $^{###}P < 0.001$ vs. oe-NC. **(F)** KLF4 mRNA and protein expression in SHG-44 cells transfected with oe-CHRM3-AS2/oe-NC and miR-370-5p mimic/mimic NC was quantified *via* qRT-PCR and western blotting, respectively. $^{***}P < 0.001$ vs. oe-NC; $^{###}P < 0.001$ vs. oe-CHRM3-AS2.

CHRM3-AS2/miR-370-5p/KLF4 Axis Regulated Malignant Characteristics of Glioma Cells

In view of the discovery of CHRM3-AS2/miR-370-5p/KLF4 axis in glioma cells, we suspected that CHRM3-AS2 silencing may exert inhibitory effects on glioma cells through regulating miR-370-5p/KLF4. As expected, the transfection of miR-370-5p inhibitor or oe-KLF4 significantly increased cell viability and colony formation, and decreased cell apoptosis, in sh-CHRM3-AS2-transfected U251 cells ($P < 0.001$, **Figures 6A–C**). In addition, the migration and invasion of sh-CHRM3-AS2-transfected U251 cells were significantly promoted by miR-370-5p silencing or KLF4 overexpression ($P < 0.001$, **Figures 6D, E**). These results further illustrated the regulatory role of CHRM3-AS2/miR-370-5p/KLF4 axis in glioma cells.

Silencing of CHRM3-AS2 Inhibited Growth of Tumour Xenografts in Mice *via* Regulation of miR-370-5p/KLF4

In addition to *in vitro* experiments, the anti-tumour potential and mechanisms of CHRM3-AS2 silencing was further investigated in a mouse tumour xenograft model *in vivo*. As

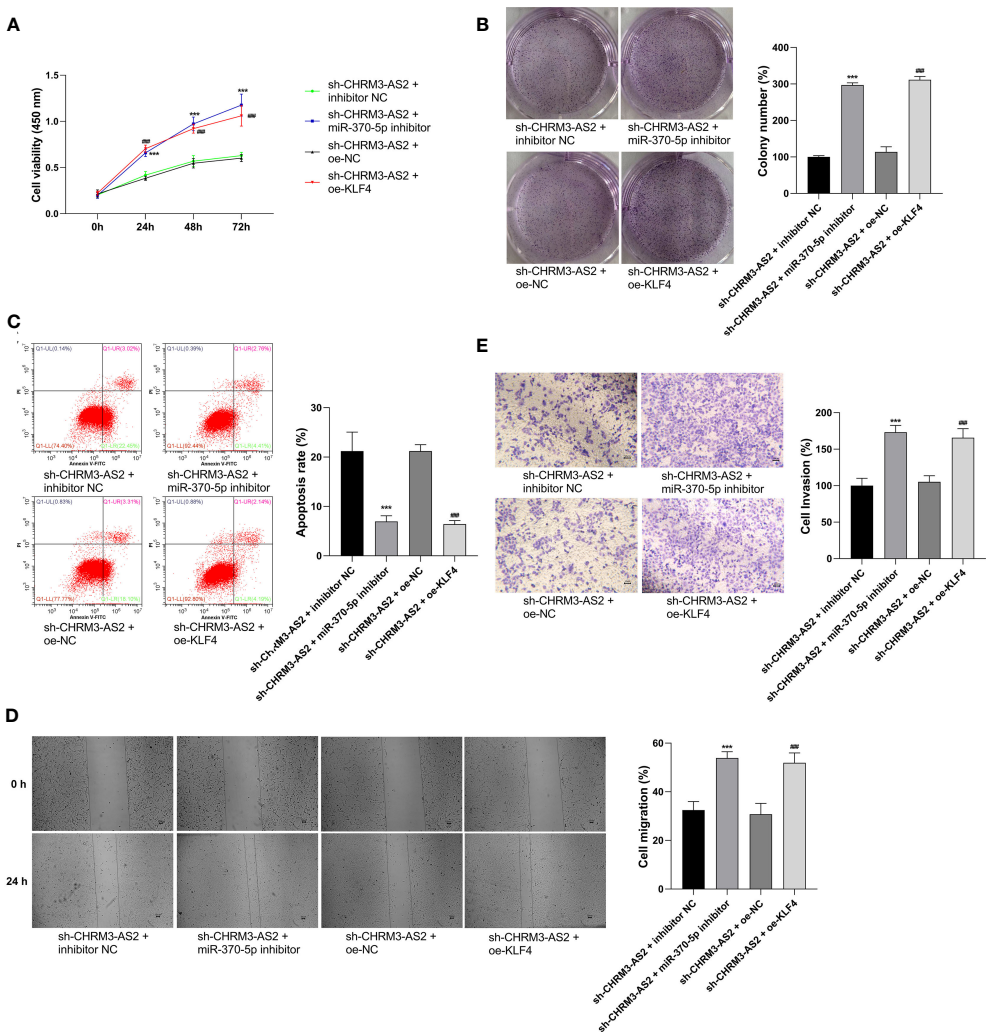

FIGURE 6 | Regulatory role of CHRM3-AS2/miR-370-5p/KLF4 axis in malignant characteristics of glioma cells. **(A)** Cell viability was evaluated *via* CCK-8 assays. **(B)** Colony numbers were quantified *via* colony formation assays. **(C)** Cell apoptosis was evaluated *via* flow cytometry. **(D)** Cell migration was evaluated *via* wound healing assays. **(E)** Cell invasion was evaluated *via* Transwell assays. U251 cells were co-transfected with sh-CHRM3-AS2 and miR-370-5p inhibitor/inhibitor NC or oe-KLF4/oe-NC. ***P < 0.001 vs. sh-CHRM3-AS2 + inhibitor NC; $^{###}$P < 0.001 vs. sh-CHRM3-AS2 + oe-NC.

shown in **Figures 7A–C**, silencing of CHRM3-AS2 expression significantly decreased tumour weights and volumes in mice (P < 0.001). The intervention of sh-CHRM3-AS2 also significantly down-regulated CHRM3-AS2 and KLF4 expression and up-regulated miR-370-5p expression in tumour xenografts (P < 0.01, **Figures 7D–F**). In addition, sh-CHRM3-AS2-induced down-regulation of KLF4 expression was reversed by the intervention of oe-KLF4 in tumour xenografts (P < 0.001, **Figure 7F**). Overexpression of KLF4 also weakened the inhibitory effects of sh-CHRM3-AS2 on tumour weight and volume (P < 0.01, **Figures 7A–C**). These results illustrated that CHRM3-AS2 silencing can inhibit tumour growth *in vivo via* regulating miR-370-5p/KLF4. Furthermore, Ki67, a robust marker of cell proliferation was detected in tumour xenografts by IF and IHC. The results showed that the expression of Ki67 was down-regulated by CHRM3-AS2 silencing in tumour xenografts, and this inhibitory effect was weakened by KLF4 overexpression (**Figures 7G, H**).

DISCUSSION

lncRNAs are important regulators involved in glioma tumourigenesis and progression. To date, numerous lncRNAs have been demonstrated to play tumour-inhibiting or tumour-promoting roles in glioma. Nevertheless, numerous lncRNAs are yet to be identified. In this study, a total of 12 differentially expressed lncRNAs were screened from two GBM gene expression profiles, based on tumourigenesis and immune infiltration. Furthermore, CHRM3-AS2 and LINC00475 were

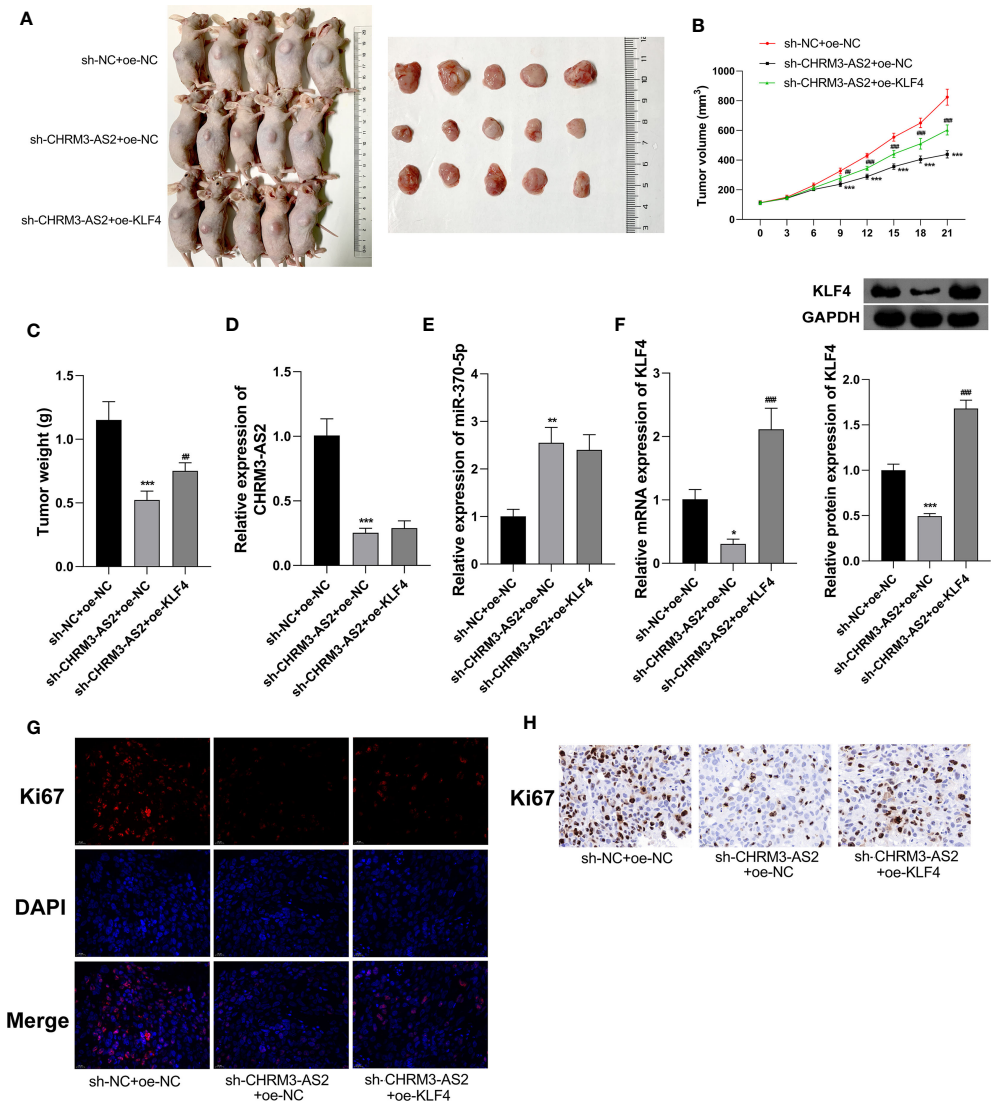

FIGURE 7 | Silencing of CHRM3-AS2 expression inhibited tumour growth in a mouse tumour xenograft model by regulating miR-370-5p/KLF4 axis. **(A)** Tumour morphology. **(B)** Tumour volume. **(C)** Tumour weight. **(D)** Expression of CHRM3-AS2 was quantified *via* qRT-PCR. **(E)** Expression of miR-370-5p was quantified *via* qRT-PCR. **(F)** The mRNA and protein expression of KLF4 was quantified *via* qRT-PCR and western blotting, respectively. **(G)** Expression of Ki67 was detected *via* IF. **(H)** Expression of Ki67 was detected *via* IHC. Mice were injected with U251 cells co-transfected with sh-CHRM3-AS2/sh-NC and oe-KLF4/oe-NC. *P < 0.05, **P < 0.01, ***P < 0.001 vs. sh-NC + oe-NC; $^{\#\#}$P < 0.01, $^{\#\#\#}$P < 0.001 vs. sh-CHRM3-AS2 + oe-NC.

identified to be DERs that were independently associated with disease prognosis. Previous studies have proved that LINC00475 expression is up-regulated in glioma and can promote the progression of glioma (36, 37). As the role of CHRM3-AS2 expression in glioma is still unknown, CHRM3-AS2 was selected as the research target of this study. Similar to LINC00475, we found that CHRM3-AS2 expression was up-regulated in glioma cells. Subsequent functional assays showed that silencing of CHRM3-AS2 expression inhibited proliferation (viability and colony formation), migration, and invasion and promoted the apoptosis of glioma cells. In contrast, overexpression of CHRM3-AS2 exacerbated the malignant characteristics of glioma cells. These results indicated that CHRM3-AS2 is an oncogene in glioma, similar to NEAT1 (9), H19 (10), PVT1 (26), and DLGAP1-AS2 (38). Furthermore, silencing of CHRM3-AS2 expression inhibited the growth of tumour xenografts in mice, presenting decreased tumour weight and volume, as well as down-regulated Ki67 expression. Our findings illustrated that CHRM3-AS2 silencing is effective in inhibiting the malignant progression of glioma both *in vitro* and *in vivo*.

lncRNAs are known as endogenous sponges that can regulate the expression of specific miRNAs (39). Previous studies have proved that miR-370-5p is involved in the tumourigenesis of various tumours by acting as a target of lncRNAs such as SNHG3/

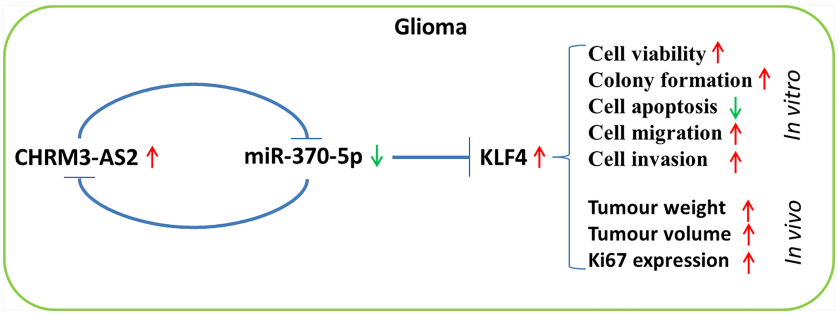

FIGURE 8 | A flow chart of the regulatory axis of CHRM3-AS2/miR-370-5p/KLF4 in glioma.

miR-370-5p in colorectal carcinoma, LINC00511/miR-370-5p in ovarian cancer, and LINC01232/miR-370-5p in pancreatic adenocarcinoma. In this study, miR-370-5p was identified as a target of CHRM3-AS2 in glioma. miR-370-5p is an anti-oncogene that has been reported to be down-regulated in breast, lung, liver, and ovarian cancers (20–23). Decreased expression of miR-370-5p was consistently observed in glioma cells. In addition, studies have confirmed the anti-tumour role of miR-370-5p, with respect to the malignant characteristics of cancer cells. Sang et al. showed that overexpression of miR-370-5p suppresses the proliferation and invasion of breast cancer cells (20). Li et al. found that overexpression of miR-370-5p inhibits cell proliferation, migration, and invasion and induces cell-cycle arrest in non-small-cell lung carcinoma cells (21). Zhang et al. (22) revealed that knockdown of miR-370-5p enhances the proliferative and invasive rates of colorectal cancer cells. As miR-370-5p expression is down-regulated by CHRM3-AS2, we suspect that the anti-tumour effect of CHRM3-AS2 silencing in glioma cells is associated with the up-regulation of miR-370-5p expression. Our subsequent feedback experiments determined that the use of miR-370-5p inhibitor promoted cell proliferation, migration, and invasion and inhibited cell apoptosis in glioma cells with CHRM3-AS2 knocked down. Therefore, we conclude that silencing of CHRM3-AS2 expression inhibits the malignant progression of glioma cells *via* up-regulation of miR-370-5p expression.

As lncRNAs and miRNAs are both non-coding RNAs, their regulatory role in cancer is mainly achieved *via* modulation of target genes. To date, many miR-370-5p-associated regulatory axes have been identified in different cancers, including miR-370-5p/LUC7L3 in breast cancer (20), miR-370-5p/p21 in lung cancer (21), and SNHG3/miR-370-5p/EZH1 in colorectal carcinoma (40). In this study, KLF4 was identified as a downstream target of miR-370-5. KLF4 is a zinc finger transcription factor that functions as a tumour suppressor (in lung, gastric, and colorectal cancers) or a tumour promoter (in breast ductal carcinoma and oral/skin squamous cell carcinoma), depending on cancer type (41). KLF4 also acts as a key regulator in GBM. Wang et al. (42) have shown that KLF4 promotes spare respiratory capacity of human GBM cells by inducing mitochondrial fusion. Gong et al. revealed that SRC-1 promotes GBM stemness through KLF4 activation (29). Wang et al. found that HIF1/2α-induced KLF4 expression enhances the malignant progression of GBM by promoting stemness and cell cycle arrest (42). In this study, KLF4 was found to be up-regulated in glioma cells, indicating a tumour-promoting potential. In addition, KLF4 expression was down-regulated by miR-370-5p and up-regulated by CHRM3-AS2. Given the combination of interactions of CHRM3-AS2 and miR-370-5p with KLF4 expression, we suggest that miR-370-5p-mediated KLF4 expression is part of the underlying mechanism of action of CHRM3-AS2 on glioma cells. Furthermore, the overexpression of KLF4 was noted to weaken the anti-tumour effects of CHRM3-AS2 silencing both *in vitro* and *in vivo*. These results implied that silencing of CHRM3-AS2 expression inhibits the malignant progression of glioma by regulating the miR-370-5p/KLF4 axis.

CONCLUSION

In conclusion, CHRM3-AS2, a prognosis-associated DER in GBM, is an oncogene that is up-regulated in glioma cells. miR-370-5p-mediated KLF4 expression is targeted by CHRM3-AS2. Importantly, silencing of CHRM3-AS2 expression inhibited the malignant progression of glioma through regulation of the miR-370-5p/KLF4 axis. The CHRM3-AS2/miR-370-5p/KLF4 axis involved in the progression of glioma may represent a potential therapeutic target (**Figure 8**). However, the regulation of miR-370-5p/KLF4 axis is not the only action mechanism involving CHRM3-AS2 in glioma. The detailed mechanisms of action of CHRM3-AS2, as well as the clinical value of CHRM3-AS2 in glioma, require further investigation.

DATA AVAILABILITY STATEMENT

The original contributions presented in the study are included in the article/**Supplementary Material**. Further inquiries can be directed to the corresponding author.

ETHICS STATEMENT

The animal study was reviewed and approved by the Ethics Committee of Ganzhou People's Hospital.

AUTHOR CONTRIBUTIONS

DW and QJ performed the conception and design of the research. QC, JL, and YL acquired and analysed data. DW and QC draft the manuscript. DW and QJ revised the manuscript and obtained the funding. All authors contributed to the article and approved the submitted version.

FUNDING

This work was supported by the Natural Science Foundation of Jiangxi Province [20181BAB205057]; the Scientific research project of Ganzhou Health Committee [2020-2-7].

SUPPLEMENTARY MATERIAL

The Supplementary Material for this article can be found online at: https://www.frontiersin.org/articles/10.3389/fonc.2022.856381/full#supplementary-material

REFERENCES

1. Ostrom QT, Bauchet L, Davis FG, Deltour I, Fisher JL, Langer CE, et al. The Epidemiology of Glioma in Adults: A "State of the Science" Review. *Neuro Oncol* (2014) 16:896–913. doi: 10.1093/neuonc/nou087
2. Louis DN, Ohgaki H, Wiestler OD, Cavenee WK, Burger PC, Jouvet A, et al. The 2007 WHO Classification of Tumours of the Central Nervous System. *Acta Neuropathol* (2007) 114:97–109. doi: 10.1007/s00401-007-0243-4
3. Xu S, Tang L, Li X, Fan F, Liu Z. Immunotherapy for Glioma: Current Management and Future Application. *Cancer Lett* (2020) 476:1–12. doi: 10.1016/j.canlet.2020.02.002
4. Wen PY, Reardon DA. Neuro-Oncology in 2015: Progress in Glioma Diagnosis, Classification and Treatment. *Nat Rev Neurol* (2016) 12:69. doi: 10.1038/nrneurol.2015.242
5. Bush NA, Chang SM, Berger MS. Current and Future Strategies for Treatment of Glioma. *Neurosurg Rev* (2017) 40:1–14. doi: 10.1007/s10143-016-0709-8
6. Huang Y. The Novel Regulatory Role of lncRNA-miRNA-mRNA Axis in Cardiovascular Diseases. *J Cell Mol Med* (2018) 22:5768–75. doi: 10.1111/jcmm.13866
7. Xi J, Sun Q, Ma L, Kang J. Long Non-Coding RNAs in Glioma Progression. *Cancer Lett* (2018) 419:203–9. doi: 10.1016/j.canlet.2018.01.041
8. Peng Z, Liu C, Wu M. New Insights Into Long Noncoding RNAs and Their Roles in Glioma. *Mol Cancer* (2018) 17:61. doi: 10.1186/s12943-018-0812-2
9. Li Y, Wang X, Zhao Z, Shang J, Li G, Zhang R. LncRNA NEAT1 Promotes Glioma Cancer Progression via Regulation of miR-98-5p/BZW1. *Biosci Rep* (2021) 41(7):BSR20200767. doi: 10.1042/BSR20200767
10. Liu ZZ, Tian YF, Wu H, Ouyang SY, Kuang WL. LncRNA H19 Promotes Glioma Angiogenesis Through miR-138/HIF-1alpha/VEGF Axis. *Neoplasma* (2020) 67:111–8. doi: 10.4149/neo_2019_190121N61
11. Li G, Cai Y, Wang C, Huang M, Chen J. LncRNA GAS5 Regulates the Proliferation, Migration, Invasion and Apoptosis of Brain Glioma Cells Through Targeting GSTM3 ExpressionThe Effect of LncRNA GAS5 on Glioma Cells. *J Neurooncol* (2019) 143:525–36. doi: 10.1007/s11060-019-03185-0
12. Li Y, Huo FF, Wen YY, Jiang M. Screening and Identification of an Immune-Associated lncRNA Prognostic Signature in Ovarian Carcinoma: Evidence From Bioinformatic Analysis. *BioMed Res Int* (2021) 2021:6680036. doi: 10.1155/2021/6680036
13. Wang J, Che F, Zhang J. Cell-Free microRNAs as Non-Invasive Biomarkers in Glioma: A Diagnostic Meta-Analysis. *Int J Biol Markers* (2019) 34:232–42. doi: 10.1177/1724600819840033
14. Zhang Y, Chen J, Xue Q, Wang J, Zhao L, Han K, et al. Prognostic Significance of MicroRNAs in Glioma: A Systematic Review and Meta-Analysis. *BioMed Res Int* (2019) 2019:4015969. doi: 10.1155/2019/4015969
15. Nan Y, Guo H, Guo L, Wang L, Ren B, Yu K, et al. MiRNA-451 Inhibits Glioma Cell Proliferation and Invasion Through the mTOR/HIF-1alpha/VEGF Signaling Pathway by Targeting Cab39. *Hum Gene Ther Clin Dev* (2018) 29:156–66. doi: 10.1089/humc.2018.133
16. Liu DK, Wei YJ, Guo Y, Wang J, Wang GH. MiRNA-93 Functions as an Oncogene in Glioma by Directly Targeting RBL2. *Eur Rev Med Pharmacol Sci* (2018) 22:2343–50. doi: 10.26355/eurrev_201804_14825
17. Xiong W, Ran J, Jiang R, Guo P, Shi X, Li H, et al. miRNA-320a Inhibits Glioma Cell Invasion and Migration by Directly Targeting Aquaporin 4. *Oncol Rep* (2018) 39:1939–47. doi: 10.3892/or.2018.6274
18. Miao W, Li N, Gu B, Yi G, Su Z, Cheng H. MiR-27b-3p Suppresses Glioma Development via Targeting YAP1. *Biochem Cell Biol* (2020) 98:466–73. doi: 10.1139/bcb-2019-0300
19. Wang F, Zhang H, Liu B, Liu W, Zhang Z. miR-6869-5p Inhibits Glioma Cell Proliferation and Invasion *via* Targeting Pgk1. *Mediators Inflammation* (2020) 2020:9752372. doi: 10.1155/2020/9752372
20. Sang K, Yi T, Huang X, Pan C, Zhou J, Yu L. MiR-370-5p Inhibits the Progression of Breast Cancer via Targeting LUC7L3. *J Recept Signal Transduct Res* (2021) 41:442–50. doi: 10.1080/10799893.2020.1819319
21. Li C, Ge Q, Liu J, Zhang Q, Wang C, Cui K, et al. Effects of miR-1236-3p and miR-370-5p on Activation of P21 in Various Tumors and Its Inhibition on the Growth of Lung Cancer Cells. *Tumour Biol* (2017) 39(6):1010428317710824. doi: 10.1177/1010428317710824
22. Zhang L, Liu Y, Tao H, Zhu H, Pan Y, Li P, et al. Circular RNA Circube2j2 Acts as the Sponge of microRNA-370-5P to Suppress Hepatocellular Carcinoma Progression. *Cell Death Dis* (2021) 12(11):985. doi: 10.1038/s41419-021-04269-4
23. Wang K, Zhu G, Bao S, Chen S. Long Non-Coding RNA LINC00511 Mediates the Effects of ESR1 on Proliferation and Invasion of Ovarian Cancer Through miR-424-5p and miR-370-5p. *Cancer Manag Res* (2019) 11:10807–19. doi: 10.2147/CMAR.S232140
24. Li D, Zhang J, Li J. Role of miRNA Sponges in Hepatocellular Carcinoma. *Clin Chim Acta* (2020) 500:10–9. doi: 10.1016/j.cca.2019.09.013
25. Mu M, Niu W, Zhang X, Hu S, Niu C. LncRNA BCYRN1 Inhibits Glioma Tumorigenesis by Competitively Binding With miR-619-5p to Regulate CUEDC2 Expression and the PTEN/AKT/p21 Pathway. *Oncogene* (2020) 39:6879–92. doi: 10.1038/s41388-020-01466-x
26. Fu C, Li D, Zhang X, Liu N, Chi G, Jin X. LncRNA PVT1 Facilitates Tumorigenesis and Progression of Glioma *via* Regulation of MiR-128-3p/GREM1 Axis and BMP Signaling Pathway. *Neurotherapeutics* (2018) 15:1139–57. doi: 10.1007/s13311-018-0649-9
27. Zhou XY, Liu H, Ding ZB, Xi HP, Wang GW. lncRNA SNHG16 Promotes Glioma Tumorigenicity Through miR-373/EGFR Axis by Activating PI3K/AKT Pathway. *Genomics* (2020) 112:1021–9. doi: 10.1016/j.ygeno.2019.06.017
28. Shie JL, Chen ZY, Fu M, Pestell RG, Tseng CC. Gut-Enriched Kruppel-Like Factor Represses Cyclin D1 Promoter Activity Through Sp1 Motif. *Nucleic Acids Res* (2000) 28:2969–76. doi: 10.1093/nar/28.15.2969
29. Gong M, Wang X, Mu L, Wang Y, Pan J, Yuan X, et al. Steroid Receptor Coactivator-1 Enhances the Stemness of Glioblastoma by Activating Long Noncoding RNA XIST/miR-152/KLF4 Pathway. *Cancer Sci* (2021) 112(2):604–18. doi: 10.1111/cas.14685
30. Yates B, Braschi B, Gray KA, Seal RL, Tweedie S, Bruford EA. Genenames.org: The HGNC and VGNC Resources in 2017. *Nucleic Acids Res* (2017) 45:D619–25. doi: 10.1093/nar/gkw1033
31. Li BL, Wan XP. Prognostic Significance of Immune Landscape in Tumour Microenvironment of Endometrial Cancer. *J Cell Mol Med* (2020) 24:7767–77. doi: 10.1111/jcmm.15408

32. Hu D, Zhou M, Zhu X. Deciphering Immune-Associated Genes to Predict Survival in Clear Cell Renal Cell Cancer. *BioMed Res Int* (2019) 2019:2506843. doi: 10.1155/2019/2506843
33. Ritchie ME, Phipson B, Wu D, Hu Y, Law CW, Shi W, et al. Limma Powers Differential Expression Analyses for RNA-Sequencing and Microarray Studies. *Nucleic Acids Res* (2015) 43(7):e47. doi: 10.1093/nar/gkv007
34. Wang P, Wang Y, Hang B, Zou X, Mao JH. A Novel Gene Expression-Based Prognostic Scoring System to Predict Survival in Gastric Cancer. *Oncotarget* (2016) 7:55343–51. doi: 10.18632/oncotarget.10533
35. Goeman JJ. L1 Penalized Estimation in the Cox Proportional Hazards Model. *Biom J* (2010) 52:70–84. doi: 10.1002/bimj.200900028
36. Yu L, Gui S, Liu Y, Qiu X, Qiu B, Zhang X, et al. Long Intergenic Non-Protein Coding RNA 00475 Silencing Acts as a Tumor Suppressor in Glioma Under Hypoxic Condition by Impairing microRNA-449b-5p-Dependent AGAP2 Up-Regulation. *Ther Adv Med Oncol* (2020) 12:1758835920940936. doi: 10.1177/1758835920940936
37. Yu M, Yi B, Zhou W, Gong W, Li G, Yu S. Linc00475 Promotes the Progression of Glioma by Regulating the miR-141-3p/YAP1 Axis. *J Cell Mol Med* (2021) 25:463–72. doi: 10.1111/jcmm.16100
38. Miao W, Li N, Gu B, Yi G, Su Z, Cheng H. LncRNA DLGAP1-AS2 Modulates Glioma Development by Up-Regulating YAP1 Expression. *J Biochem* (2020) 167:411–8. doi: 10.1093/jb/mvz108
39. Zhao Z, Sun W, Guo Z, Zhang J, Yu H, Liu B. Mechanisms of lncRNA/microRNA Interactions in Angiogenesis. *Life Sci* (2020) 254:116900. doi: 10.1016/j.lfs.2019.116900
40. Zhang Y, Li L, Lu KX, Yu LB, Meng J, Liu CY. LncRNA SNHG3 Is Responsible for the Deterioration of Colorectal Carcinoma Through Regulating the miR-370-5p/EZH1 Axis. *Eur Rev Med Pharmacol Sci* (2021) 25:6131–7. doi: 10.26355/eurrev_202110_26891
41. Tang G, Liu D, Xiao G, Liu Q, Yuan J. Transcriptional Repression of FOXO1 by KLF4 Contributes to Glioma Progression. *Oncotarget* (2016) 7:81757–67. doi: 10.18632/oncotarget.13184
42. Wang P, Zhao L, Gong S, Xiong S, Wang J, Zou D, et al. HIF1alpha/HIF2alpha-Sox2/Klf4 Promotes the Malignant Progression of Glioblastoma via the EGFR-PI3K/AKT Signalling Pathway With Positive Feedback Under Hypoxia. *Cell Death Dis* (2021) 12:312. doi: 10.1038/s41419-021-03598-8

Conflict of Interest: The authors declare that the research was conducted in the absence of any commercial or financial relationships that could be construed as a potential conflict of interest.

Publisher's Note: All claims expressed in this article are solely those of the authors and do not necessarily represent those of their affiliated organizations, or those of the publisher, the editors and the reviewers. Any product that may be evaluated in this article, or claim that may be made by its manufacturer, is not guaranteed or endorsed by the publisher.

frontiers in Oncology

ORIGINAL RESEARCH
published: 17 March 2022
doi: 10.3389/fonc.2022.841977

Fruquintinib Enhances the Antitumor Immune Responses of Anti-Programmed Death Receptor-1 in Colorectal Cancer

Qingli Li[1†], Xiaojiao Cheng[1†], Cong Zhou[1], Yao Tang[1], Fuli Li[1], Baiwen Zhang[1], Tinglei Huang[1], Jianzheng Wang[2] and Shuiping Tu[1*]*

[1] State Key Laboratory of Oncogenesis and Related Genes, Department of Oncology, Renji Hospital, School of Medicine, Shanghai Jiao Tong University, Shanghai, China, [2] Department of Oncology, Henan Cancer Hospital, The Affiliated Cancer Hospital of Zhengzhou University, Zhengzhou, China

Background: Programmed death receptor-1 (PD-1) blockade shows little benefit in patients with microsatellite-stable colorectal cancer (MSS-CRC). Fruquintinib is a China-made anti-angiogenic drug which is approved for the third line therapy in mCRC. This study investigates the effect of the combination of fruquintinib and PD-1 blockade on MSS-CRC and its relative mechanisms.

Methods: The mouse allograft tumor models that represent MSS and microsatellite instability (MSI) CRC were established using murine CT26 and MC38 colon cancer cells, respectively, to assess the treatment efficacy. The percentages of immune cells were detected in the peripheral blood, spleen and tumor tissues in the tumor-bearing mice by flow cytometry analysis. Angiogenesis in tumor tissues was detected by immunofluorescence. The safety of drug treatment was evaluated by histopathology analysis in murine main organs. The efficacy of the combination of fruquintinib and sintilimab were verified in the treatment of MSS-CRC patients.

Results: Our results showed that the combination of fruquintinib and sintilimab exhibited the strongest inhibition of tumor growth and achieved the longest survival time in mice bearing MC38 or CT26 xenograft tumors, compared to fruquintinib and sintilimab alone. Mechanistically, the combination of fruquintinib and sintilimab reduced angiogenesis, reprogramed the vascular structure, enhanced the infiltration of $CD8^+$T cells ($p<0.05$), $CD8^+TNF\alpha^+$ ($p<0.05$) T cells and $CD8^+IFN\gamma^+$ ($p<0.05$) T cells and reduced the ratios of MDSCs and macrophages in mice. There was no obvious toxicity observed in the main organs of the tumor-bearing mice with the combined treatment. Moreover, the treatment using the combination of fruquintinib and sintilimab achieved effective response in five patients with refractory advanced MSS CRC.

OPEN ACCESS

Edited by:
Zhe-Sheng Chen,
St. John's University, United States

Reviewed by:
Zhihui Song,
Fox Chase Cancer Center, United States
Edmund Waller,
Emory University, United States
Xueqian Qian,
Zhejiang University, China

****Correspondence:***
Shuiping Tu
tushuiping@yahoo.com
Jianzheng Wang
46962384@qq.com

†These authors have contributed equally to this work and share first authorship

Specialty section:
This article was submitted to Cancer Molecular Targets and Therapeutics, a section of the journal Frontiers in Oncology

Received: *23 December 2021*
Accepted: *15 February 2022*
Published: *17 March 2022*

Citation:
Li Q, Cheng X, Zhou C, Tang Y, Li F, Zhang B, Huang T, Wang J and Tu S (2022) Fruquintinib Enhances the Antitumor Immune Responses of Anti-Programmed Death Receptor-1 in Colorectal Cancer. Front. Oncol. 12:841977. doi: 10.3389/fonc.2022.841977

Conclusion: Our results show that the combination of fruquintinib and sintilimab greatly inhibits CRC growth by altering tumor immune microenvironment. This study provides the rational for using the combination of fruquintinib and anti-PD-1 antibody for the treatment of advanced CRC.

Keywords: fruquintinib, sintilimab, immunotherapy, microsatellite stable colorectal cancer, anti-angiogenesis

INTRODUCTION

Colorectal cancer is the second most common cause of cancer-related death worldwide (1).The latest research results have showed that the use of pembrolizumab as the first-line therapy for metastatic colorectal cancer (mCRC) with high microsatellite instability (MSI-H) or deficiency mismatch repair (dMMR) gene few treatment-related adverse events (2). Nivolumab plus ipilimumab demonstrated high response rates, promoting progression-free survival, manageable safety, and meaningful improvements in patients with dMMR/MSI-H mCRC (3). Although immunotherapy has achieved significant effects on advanced colon cancer- MSI-H or dMMR (4–6), the therapy is limited in 80%-90% advanced colon cancer patients-with low microsatellite instability(MSI-L) or proficiency mismatch repair genes (pMMR) (4, 7, 8). The results of the clinical trial IMblaze370 have underlined the challenge of immunotherapy in patients with microsatellite-stable metastatic colorectal cancer (9).

The significant effect of anti-PD-1 antibody treatment in patients with MSI-H colon cancer can be explained by its high tumor mutation burden (4–6). However, the tumor mutation burden alone cannot fully explain the lack of response of MSS to PD-1 antibodies (10, 11). Compared with other types of cancers, including cervical cancer, hepatocellular carcinoma, breast cancer and so on, that have similar mutation burden observed in MSS colon cancer patients, the anti-PD-1 antibody response rate is between 5.7%and 61.7% (10), indicating that there may be other factors that influence the immunity response. Our previous studies showed that bone marrow–derived myofibroblasts (BMFs)-rich tumors had relatively poor response to PD-L1 blockade immunotherapy and provided a novel insight into the mechanism tumor resistance to immunotherapy (12). Angiogenesis is critical in the process of colon carcinogenesis. One of the most important factors for angiogenesis is the VEGF/VEGFR axis.VEGF secreted by cancer cells stimulates the proliferation and survival of endothelial cells leading to change of vascular permeability and neo-angiogenesis (13).VEGF can have a direct effect on multiple immune cells, including T cells, regulatory T cells, dendritic cells, and myeloid derived suppressor cells (14). There are two major approaches for targeting VEGF/VEGFR axis as anti-cancer therapies: the neutralization antibody of VEGF (monoclonal antibodies) and the small molecule inhibitors that block the activity of VEGFR kinases. Bevacizumab is the most successful antibody for neutralizing VEGF.

The combination of immunotherapy with anti-angiogenesis agents is one of the many strategies currently under investigation to improve tumor response to immunotherapy (15). Fruquintinib (HMPL-013) is a small molecule inhibitor with strong potency and high selectivity against VEGFR1, 2, and 3 and was approved for the third line therapy in metastatic colon cancer in China. Fruquintinib is currently being registered in clinical study for the third line therapy in metastatic colon cancer outside China (16, 17). It has good safety and effectiveness in clinical patients. However, it is not known whether combining fruquintinib and anti-PD-1 therapy could enhance its effectiveness in CRC. The effect of the combination of fruquintinib and anti-PD-1 in MSS colon cancer has not been examined and the detailed mechanism of action has not been elucidated. The REGONIVO study found that nivolumab plus regorafenib had an ORR of 36% and a median PFS of 7.9 months in 25 patients with metastatic colorectal cancer who progressed after standard therapies (18). Our previous results have indicated that the MDSCs are important in the early stages of gastric carcinogenesis because of its pro-inflammatory role (19).

Here, we hypothesized that the combination of anti-PD-1 treatment with fruquintinib could enhance the antitumor immune response in MSS CRC. We explored whether fruquintinib could synergize with anti-PD-1 in MSS CRC by reducing angiogenesis and improving the tumor immune environments.

MATERIALS AND METHODS

Cells and Culture Conditions

The MC38 and CT26 murine colorectal cancer cells and HUVECs were from the American Type Culture Collection (ATCC). These cell lines were cultured in complete RPMI-1640 medium, supplemented with 10% fetal bovine serum, 2mM L-glutamine, 1% (v/v) penicillin/streptomycin and maintained at 37°C in 5% CO_2.

Animals

The 6-week-old female C57BL/6J and BALB/c mice were purchased from Shanghai Laboratory Animal Center (Shanghai, China). Animal experiments were approved in accordance with the guidelines issued by the Animal Ethics Committee of Ruijin Hospital, Shanghai Jiaotong University School of Medicine (Shanghai China).

Tumor Models

For the subcutaneous tumor mouse models, 1 x 10^6 MC38 or CT26 colorectal cancer cells were resuspended in 200ul of serum-free RPMI-1640 medium and injected subcutaneously into the right flank of C57BL/6J and BALB/c mice, respectively. Six or

eight days after MC38 and CT26 cell inoculation, the tumor-bearing mice were randomly assigned to four or six groups (n = 5-6 per group) according to mean tumor volume. Tumor volumes were monitored every three days with a Venire caliper, and the body weight of mice was monitored every three days. Tumor volumes were calculated using the formula (length x width x width)/2. All data were represented as means± SD.

Drugs Information and Treatments

Fruquintinib (HMPL-013) was a gift from Hutchison MediPharma Limited (Shanghai, China). The anti-PD-1antibody- Sintilimab (cat: 11430) was a gift from Innovent Biologics Suzhou, China. CMC-Na (carboxymethyl cellulose–Na solution) was purchased from Sangon Biotech (Shanghai, China) and 0.5%CMC-Na (w/v) dissolved in sterilized water was used for oral gavage (po. 200ul every day, total 21 days) as control treatment. Fruquintinib was completely dissolved in 0.5%CMC-Na and was gavaged as 2.5mg/kg,5mg/kg or 10mg/kg (200ul every day, total 21 days); Sintilimab, an anti-PD-1 antibody, provided by Innovent Biologics, was diluted to 2.5mg/kg (200ul,twice a week, total two weeks).The treatment was began at day 8.or day 6 after tumor cell inoculation.

Single Cell Suspensions

Tumor tissues were washed in phosphate buffered saline (PBS), minced into small fragments and then incubated in collagenase solution (1 mg/mL collagenase IV obtained from Sigma in PBS) and DNase (500ug/ml) at 37°C for 30 min. The spleen and peripheral blood were homogenized and passed through a 70 μm cell strainer to achieve single cell suspensions. Red blood cells were lysed.

Flow Cytometry Analysis

Single-cell suspensions were incubated with anti-mouse CD16/32 antibody (clone 93; Biolegend, San Diego, CA) for 5 minutes prior to staining for immune cell markers for 15 minutes at room temperature. The following monoclonal antibodies were used: APC-CY7 conjugated anti-mouse CD45 (BD Biosciences Cat:557659 Clone:30-F11), FITC conjugated anti-mouse CD11b (Biolegend Cat:101205 Clone:M1/70), APC conjugated anti-mouse Gr1(Biolegend Cat:108412,Clone: RB6-8C5), FITC conjugated anti-mouse CD8a(Biolegend Cat:100706 Clone:53-6.7), PE conjugated anti-mouseCD4(BD Biosciences Cat:553048 Clone: RM4-5), APC conjugated anti-mouse PD-L1(Biolegend Cat:124311 Clone: 10F.9G2), and IFN-γ (XMG1.2).The flow cytometry analyses were performed using a BD Fortessa Flow Cytometer (BD Fortessa). BD FACS Diva software V.5.0.1 (BD) or Flow Jo (Tree Star) was used for data processed. For cytokine staining, harvested cells were incubated in RPMI-1640 medium with cell activation cocktail with brefeldin A (Bio legend) for 6 hours at 37°C, and stimulated cells were stained as described above.

Immunohistochemistry and Immunofluorescence

Resected tumor tissues were fixed in 4% paraformaldehyde or embedded either in paraffin or in optimal cutting temperature compound and frozen. Vascular endothelial staining was performed using anti-CD31 antibody (clone DIA-310; for immunofluorescence [IF]), pericytes were identified with antibody against α-smooth muscle actin (SMA) (Sigma-Aldrich), and anti-rabbit secondary antibodies (Jackson ImmunoResearch) as appropriate. Cell nuclei were identified with 4′,6-diamidino-2-phenylindole (DAPI; Thermo Fisher Scientific). The total number of vessels and pericyte-covered vessels were counted in five random fields using a 200x magnification lens. Organoids (tumor tissues) were fixed in 4% formaldehyde for 15 minutes. Then, organoids were washed 3 times with PBS and immunostained. Primary antibodies targeting CD8a (1:600; Cell Signaling Technology cat: 98941), were added to the sections, which were incubated at 4°C overnight. Then, HRP-conjugated secondary antibodies (Dako, K4003), were applied to the corresponding primary antibody. Afterward, we stained the samples with diaminobenzidine (DAB; CST8059) and hematoxylin for nuclei staining. IF images were analyzed using a microscope (Leica),.

The Combination of Fruquintinib and Sintilimab for the Treatment of CRC Patients

Five patients with refractory mCRC were given fruquintinib (3mg orally, once daily for 3 weeks, followed by 1 weeks off in a 4-week cycle) and sintilimab (200mg intravenously, once every 3 weeks). Before treatment, peripheral blood samples were collected and next-generation sequencing was performed to detect the gene profile of patients. Each of the patients signed an informed consent before the therapy. All the patients treated were not part of a prospective clinical trial.

Statistical Analysis

Data are presented as Mean ± SD. One way ANOVA with Turkey multiple comparison post-test and the Student's t- test were used for statistical comparisons using Graph PadPrizm8.Statistical significance was determined at the < 0.05 level (*p<0.05, **p< 0.01, and ***p<0.001, or $^{\#}$p<0.05, $^{\#\#}$p< 0.01, and $^{\#\#\#}$p<0.001). Survival was defined as the time from treatment to death of mice due to excess tumor burden.

RESULTS

Fruquintinib Inhibits CRC Tumor Growth in a Dose-Dependent Manner

We first examined the effects of different doses of fruquintinib (Fru) on colon cancer syngeneic in the tumor mouse models. We treated the mice bearing MC38 tumor with three different doses of fruquintinib (2.5mg/kg, 5mg/kg, and 10mg/kg) every day for a total of three weeks. The results showed that fruquintinib could inhibit MC38 allograft tumor growth in a dose-dependent manner and the strongest inhibition was observed in the Fru 10mg/kg treatment group (**Figures 1A, B**). We examined immune cells of the spleen and peripheral blood in the mice with MC38 tumor, and found that the fractions of $CD11b^{+}Gr1^{+}$MDSCs (Myeloid-derived suppressor cells) were significantly reduced in the spleen (**Figure 1C**) and peripheral blood (**Figure 1F**) of mice in the Fru 10mg/kg treatment group.

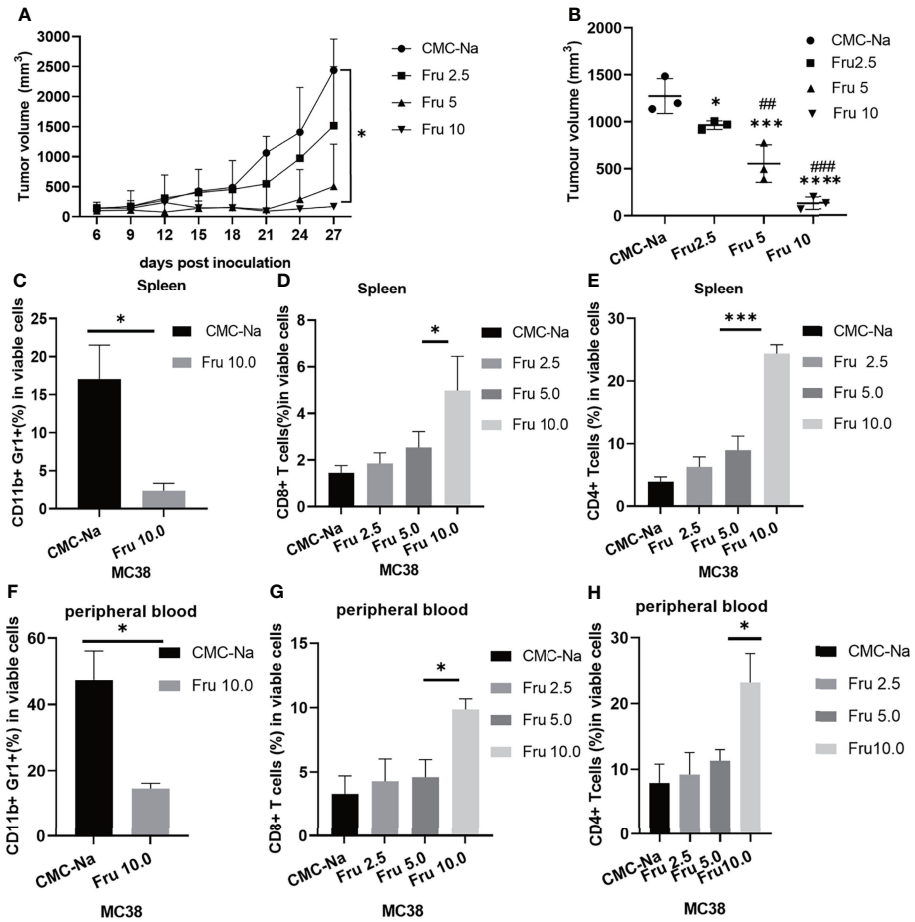

FIGURE 1 | Fruquintinib inhibits tumor growth in mouse CRC allograft tumor models. Tumor-bearing mice were treated with different doses (2.5, 5, and 10mg/kg) of fruquintinib or CMC-Na control by oral gavage daily for a total of 21days. Tumor volume and immune cells were analyzed on days 14 after fruquintinib treatment (n = 3 per group). **(A)** The tumor growth curve of MC38 tumor-bearing mice ($p = 0.026$). **(B)** the tumor volume measured at the 28th day after treatment ($p < 0.0001$). **(C)** MDSCs were analyzed in spleen on day14 after fruquintinib treatment. **(D, E)** $CD8^+$T cells and $CD4^+$Tcells were analyzed in spleen. **(F)** MDSCs were analyzed in peripheral blood on day14 after fruquintinib treatment. **(G, H)** $CD8^+$T cells and $CD4^+$Tcells were analyzed in peripheral blood on day14 after fruquintinib treament. *$p < 0.05$, ***$p < 0.001$, ****$p < 0.0001$. $^{\#\#}p < 0.01$,$^{\#\#\#}p < 0.001$. (* compared to control group, #compared to Fru2.5 group).

As the dose of fruquintinib increased, the proportion of $CD8^+$ T cells and $CD4^+$ T cells increases in the spleen (**Figures 1D–G**) and peripheral blood (**Figures 1E–H**) of mice. These results suggest that Fruquintinib inhibits CRC MC38 tumor growth and enhances antitumor immune response.

Fruquintinib Enhances the Anti-Tumor Effect of Anti-PD-1 Antibody and Prolongs Survival of the CRC Mice

Next, we determined the effects of the combination therapy on MC38 and CT26 colon cancer mouse models. Tumor-bearing mice were treated with fruquintinib at two different doses (Fru, 2.5mg/kg, and Fru, 5mg/kg) every day for a total of three weeks, sintilimab (2.5mg/kg) twice a week for a total of two weeks, or their combination. We found that single-agent treatment and combination treatment significantly inhibited tumor growth, and the combination treatment exhibited the strongest inhibition of tumor growth in the MC38 (**Figures 2A, C**) and CT26 (**Figures 2B, D**) allograft tumor models. The representative tumors from MC38 allograft tumor-bearing mice were shown in **Figure 2E**, and the tumor weight were shown in **Figure 2F**. Moreover, fruquintinib and sintilimab alone significantly increased the median survival time (MST) in MC38 (**Figure 2G**) and CT26 (**Figure 2H**) tumor-bearing mice, and the combination therapy achieved the longest MST in both models (**Figures 2E, F**).

Combination Treatment of Fruquintinib and Anti-PD-1 Reprograms the Immune Microenvironment and Enhances Antitumor Immunity *In Vivo*

Next, we investigated the mechanisms by which fruquintinib enhances the effects of anti-PD-1 antibody in CRC mouse models. We first evaluated whether combination therapy increases

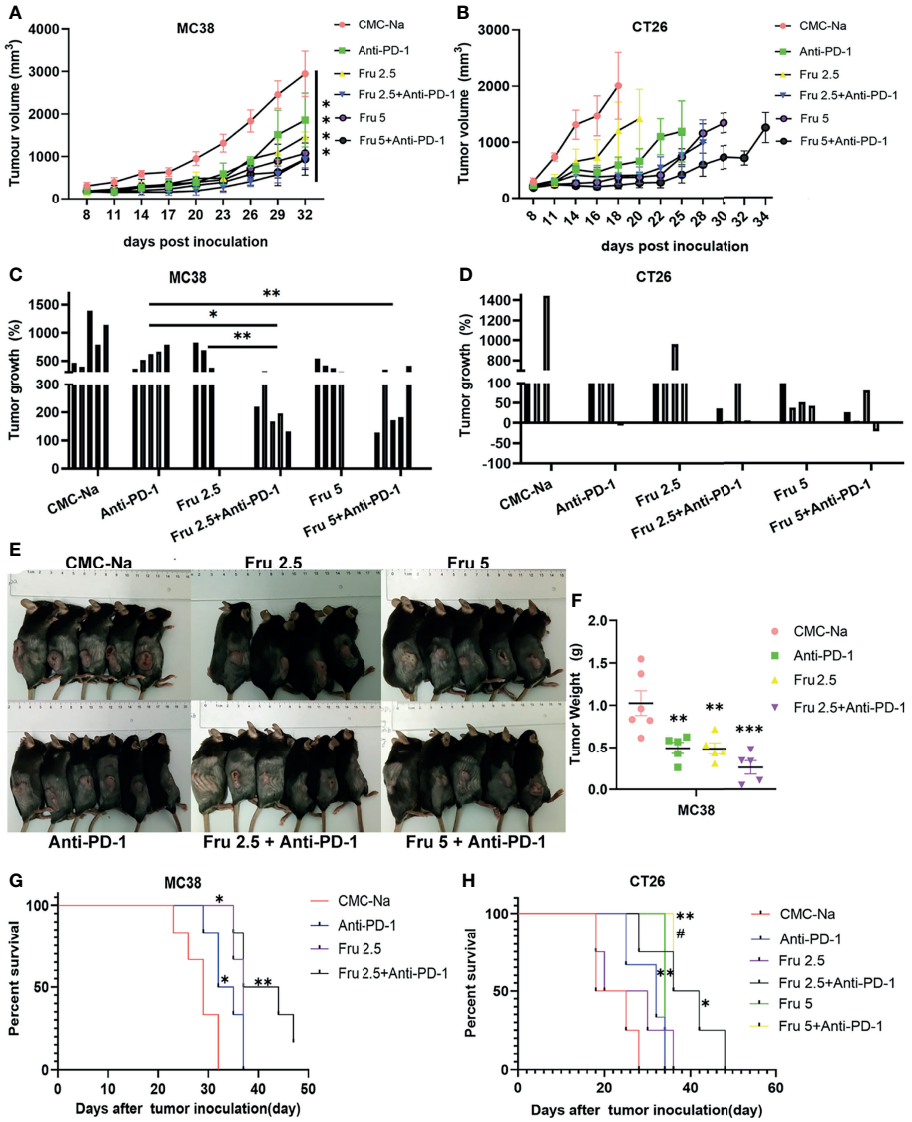

FIGURE 2 | Fruquintinib enhances the anti-tumor effect of anti-PD-1 in CRC mouse models. **(A, B)** Tumor growth curve of the subcutaneously implanted tumors in MC38 and CT26 mouse models after treatment (n = 4-6). **(C, D)** Tumor volume of the subcutaneously implanted tumors in each mouse showed in 28 days after treatment **(E)** Diagram depicting the tumor volume of MC38 allograft tumor model. **(F)** Tumor weight in the MC38-bearing mice. *p < 0.05, **p < 0.01, ***p < 0.001, ****p < 0.0001 **(G, H)** Overall survival of MC38 and CT26 tumor-bearing mice. Kaplan-Meier survival curves were shown in each group of implanted tumors #p < 0.05, compared to Fru2.5 group).

lymphocyte infiltration. We found that the number and proportion of CD8+ T lymphocytes, $CD8^+TNF\alpha^+$T lymphocytes and $CD8^+INF\gamma^+$ lymphocytes were significantly increased in tumor-bearing mice treated with fruquintinib or sintilimab alone or combination therapy (**Figure 3A**). Moreover, the combination treatment showed the strongest effect on increasing the infiltration of CD8+ T, $CD8^+TNF\alpha^+$ T and $CD8^+INF\gamma^+$ lymphocytes (**Figures 3A, B**). Immunohistochemistry staining further confirmed a markedly increase of $CD8^+$T lymphocytes in tumor tissues in combined treatment group (**Figure 3C**). Furthermore, treatment with the combination of fruquintinib and sintilimab significantly reduced the fraction of $CD11b^+Gr1^+$MDSCs and $CD11b^+F4/80^+$tumor-associated macrophages in CT26 allograft tumor compared to fruquintinib or sintilimab alone (**Figure 3D**). These results suggest that fruquintinib enhance the effect of anti-PD-1 to reprogram the tumor immune microenvironment and enhances antitumor immunity in CRC.

Fruquintinib Reduces Angiogenesis in CRC Both *In Vitro* and *In Vivo*

Previous studies suggested that fruquintinib could inhibit tubular sprouting and prevent angiogenesis *in vitro* (16). We investigated the

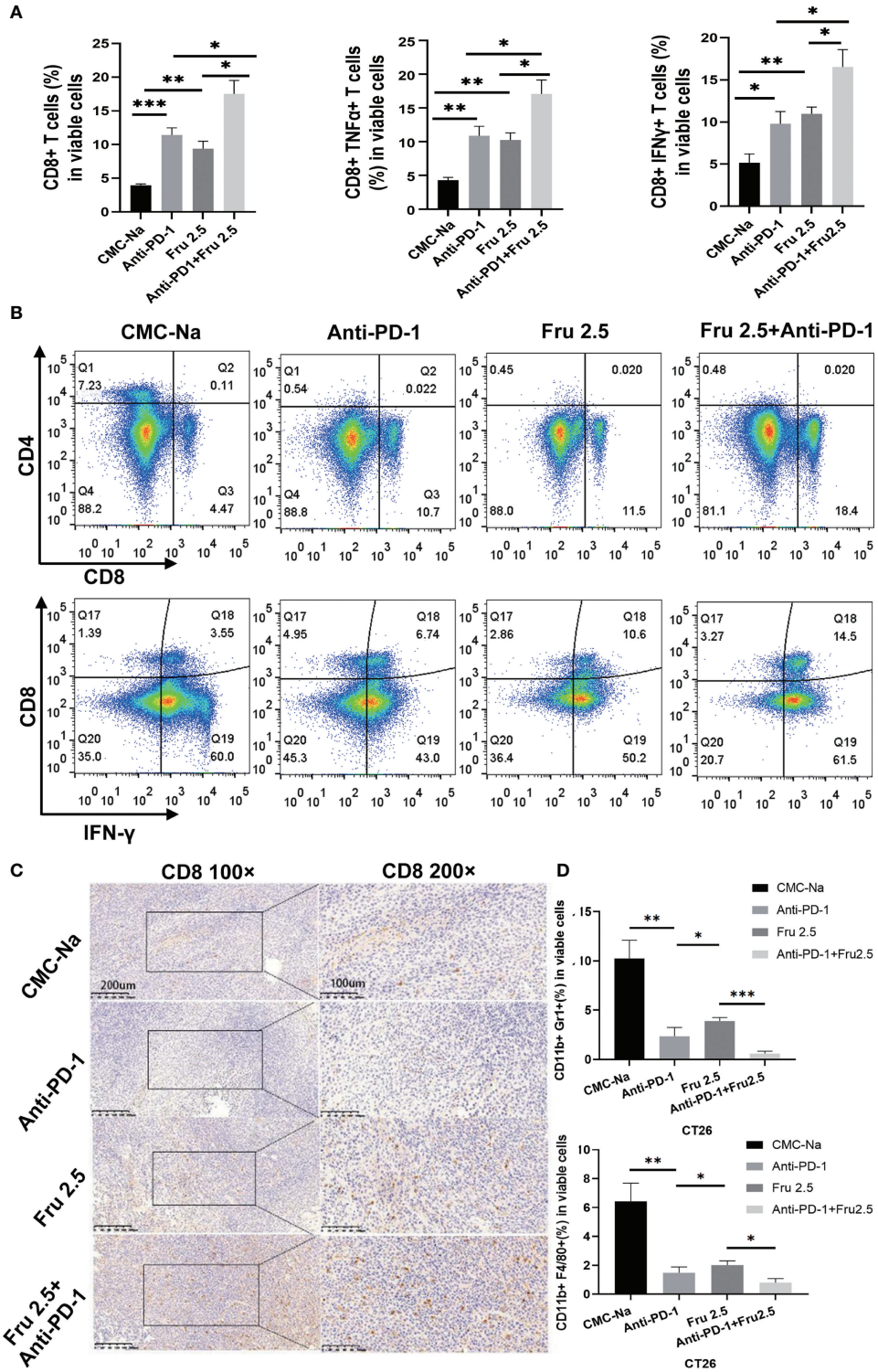

FIGURE 3 | Fruquintinib enhances the effect of sintilimab to reprogram the immune microenvironment and enhance antitumor immunity in CRC. **(A)** Percentages of $CD8^+$T cells, $CD8^+TNF\alpha^+$T cells,$CD8^+IFN\gamma^+$ T cells in tumor tissues determined by FACS in CT26 tumor-bearing mice treated with indicated drugs (shown as fractions of $CD45^+$ cells) in tumors treated with control CMC-Na, anti-PD-1, Fru2.5, arnti-PD-1 and Fru 2.5, measured by flow cytometry at day 14. **(B)** Representative images of the FACS plots of $CD8^+$ and $CD8^+IFN\gamma^+$ CTLs. **(C)** IHC images for CD8 staining of tumor sections on day14. Scale bar, 200um. **(D)** Percentage of MDSCs ($CD11b^+Gr1^+$) and TAM ($CD11b^+F4/80^+$) in each groups on day 14. *p < 0.05, **p < 0.01, ***p < 0.001.

effect of fruquintinib on tubular formation in HUVEC *in vitro*. Fruquintinib suppressed the tube branching in a dose-dependent manner in HUVEC (**Figure 4A**). The tubule length of HUVECs significantly decreased in the fruquintinib treatment group compared to the control group. In addition, we investigated the changes of intratumoral vessels in CT26 mouse model. We treated the tumor-bearing mice with low-dose of fruquintinib (2.5mg/kg, thereafter referred to as "Fru 2.5") or 0.5% CMC-Na as a control *via* oral gavage 14 days after tumor cell inoculation, and then evaluated the tumor vasculature. The dual staining of alpha-smooth muscle actin (a-SMA) and CD31 showed that tumor vessels were significantly less in the Fru 2.5 group compared with the control group in the CT26 allograft tumor model (**Figure 4B**). Furthermore, we assessed the tumor vessels by angiography in ultrasound machine on the 14th day after treatment. SonoVue was injected into the tail vein of mice (n=3) to display the mouse tumor vascular perfusion. We found that fruquintinib reduced tumor vascular formation in CT26 colon cancer-bearing mice (**Figure 4C**).

Safety of the Combination of Fruquintinib and Anti-PD-1 *In Vivo*

We further determined the safety of the combination of fruquintinib and sintilimab *in vivo*. No toxicity, allergy or cachexia was observed in the tumor-bearing mice treated with the combination of fruquintinib and sintilimab. There was no significantly decreased in the body weight (**Figure 5A**). Blood cell analysis,liver and kidney function and histopathological analysis showed that no obvious damage in the murine major organs, such as the heart, liver, lung,

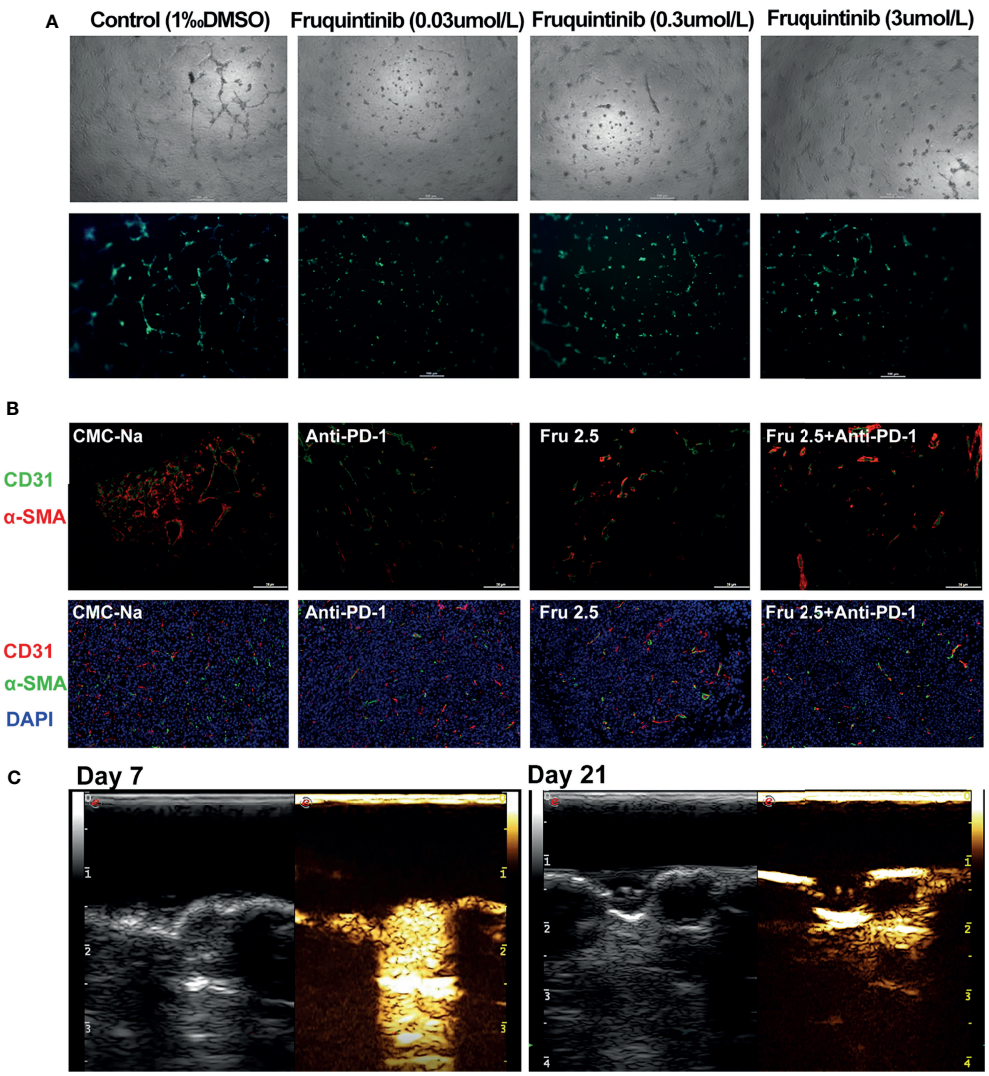

FIGURE 4 | Fruquintinib reduces angiogenesis in CRC both *in vitro* and *in vivo*. **(A)** The effect of fruquintinib on tubular formation in HUVEC *in vitro* with different doses (0.03,0.3, and 3umol/l) of fruquintinib or CMC-Na control. **(B)** Representative immunofluorescent staining of sections from different treatment groups on day14. Red, CD31; α-SMA staining; green; blue, DAPI staining. **(C)** Fruquintinib reduces tumor vascular formation in CT26 colon cancer-bearing mice by angiography using ultrasound machine on day 7 and day 21 after treatment.

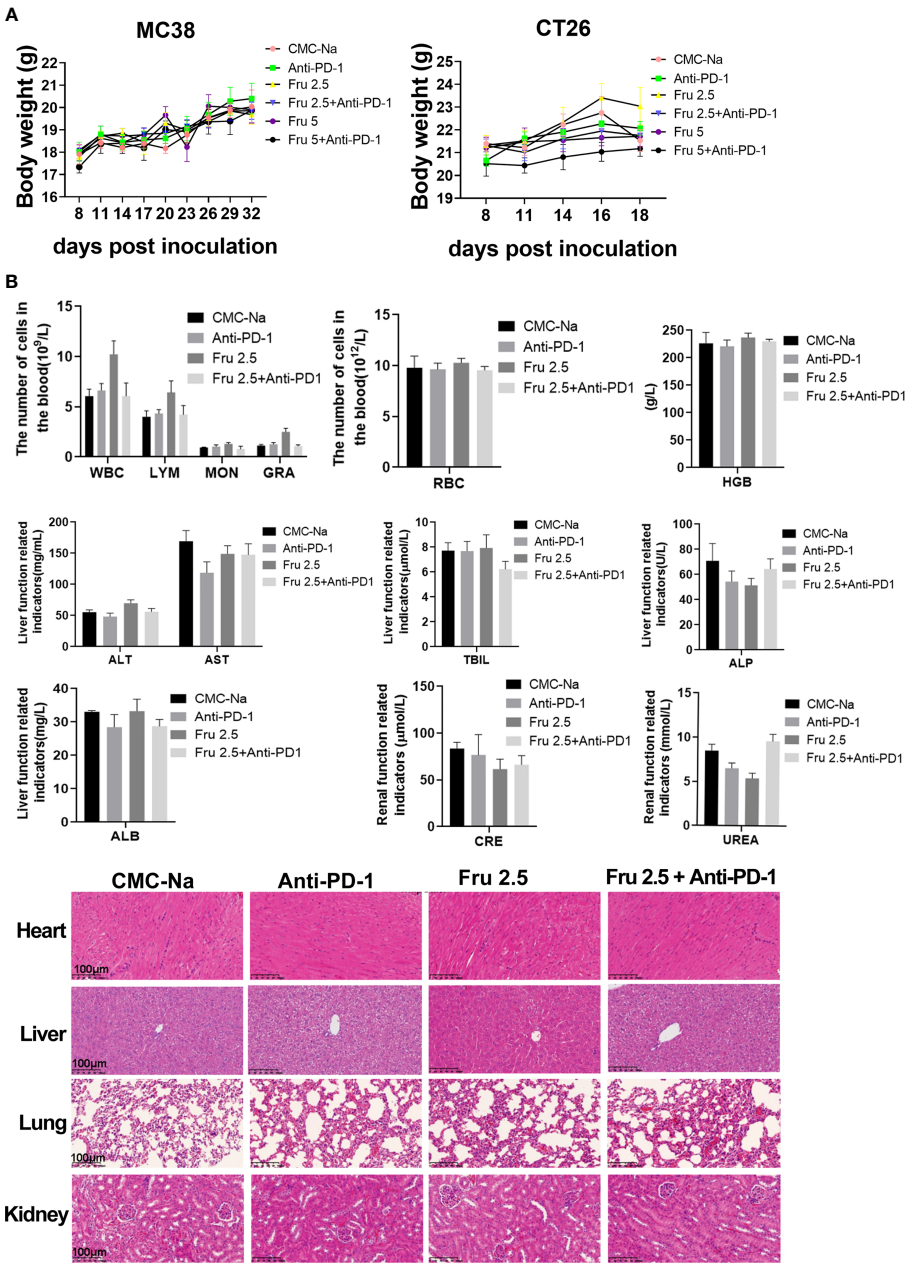

FIGURE 5 | A safety of the combination of fruquintinib and anti-PD-1 *in vivo*. **(A)** Body weight of tumor-bearing mice in each group. The weight was measured every three days. **(B)** Blood cell analysis,liver and kidney function and histopathology morphology of the murine major organs (heart, liver, lung, kidney) in the mouse models.

and kidney (**Figure 5B**). These results suggest that fruquintinib in combination with sintilimab is well tolerated.

The Combination of Fruquintinib and Anti-PD-1 Shows Antitumor Activity in Refractory Advanced CRC Patients

Based on our preclinical data from the animal experiments, we observed the effect of the combination of fruquintinib and anti-PD-1 on 5 patients with metastatic colorectal cancer who failed in more than two lines of standard treatment. Among the 5 patients, all are MSS mCRC, 2 cases CRC patients with lung metastasis, 2 cases with liver metastasis, and 1 case with abdominal wall metastasis (see **Table 1** in details). We assessed the efficacy of treatment every 3 cycles. The longest follow-up time for the patients was 18 weeks. Two CRC patients with lung metastatic lesions and one CRC with abdominal wall metastasis

TABLE 1 | The summary of outcomes for all treated patients.

NO.	Age	Metastasis size	Efficacy
Case1	**68y**	lung metastasis	**PR**
Case2	**48y**	lung metastasis	**PR**
Case3	**56y**	liver metastasis	**SD**
Case4	**56y**	liver metastasis	**SD**
Case5	**40y**	abdominal wall metastasis	**PR**

Individual clinical outcomes and the 5 patients enrolled by therapeutic responses (assessed via RECIST v1.1). No, patient number; y, years old; PR, partial response; SD, stable disease; PD, progressive disease.

achieved partial response (PR). Two CRC patients with liver metastatic lesions showed stable disease (SD). The total disease control rate (DCR) was 100% (**Figure 6A**). All the included patients experienced at least one treatment-related adverse event (AE). The majority of these AEs were mild and tolerable. All patients were still on treatment and alive at the time we prepare this manuscript. More CRC patients are being recruited in the clinical study.

DISCUSSION

Immune checkpoint inhibitors have shown good anti-tumor effects since they were applied to clinical use, especially in solid tumors such as melanoma, renal clear cell carcinoma and liver cancer (20–22). Anti-PD-1 antibodies have achieved significant effects on advanced colon cancer with high microsatellite instability (MSI-H) or missing mismatch repair genes (dMMR) (4–6), but its response rate for 80%-90% of low microsatellites (MSI-L) or mismatch repair gene wild (pMMR) colon cancer is limited (4).The clinical trial IMblaze370 showed no improved overall survival with atezolizumab plus cobimetinib or atezolizumab versus regorafenib. The results of IMblaze370 have underlined the challenge of extending the benefit of immunotherapy to CRC patients whose tumors have low baseline levels of immune inflammation, such as those with microsatellite-stable metastatic colorectal cancer (9).Optimized combinatorial strategies could expand the use of anti-PD-1 based immunotherapy in colon cancer (23–25). One of the combinatorial strategies is anti-angiogenesis drug, with the basic theory of blood vessel normalization can optimize the tumor immune microenvironment and may synergize with immunotherapy to enhance anti-tumor immunity (26).These effects remain unclear in MSS mCRC, a disease where several anti-angiogenesis drugs (fruquintinib and regorafenib) are standard treatment (17, 27). The potential of anti-angiogenesis drugs to enhance antitumor immunity in combination with immunotherapy in patients has been postulated by our preclinical data and clinical trials of others (18).

In this study, we explored the effect of the anti-angiogenesis drug fruquintinib in combination with anti-PD-1 antibody for the treatment of colon cancers, particularly in MSS CRC. Based on the past research results, we have chosen clinically relevant mouse models using the CT26 and MC38 mouse colon cancer cells, that represent for MSS CRC and MSI CRC, respectively (28, 29). We addressed one critical issue that fruquintinib can be successfully combined with anti-PD-1 to increase its efficacy in both MSI and MSS CRC. For MSS CRC, this question is in time and is in line with promising phase 1b clinical trial data in CRC patients, which showed promising high response rates in a phase1 trial (18). Based on the research that antiangiogenic agents demonstrate dose- and time-dependent influence on tumor vasculature (30, 31), we investigated the effects of distinct doses of fruquintinib on intratumoral vessels and immune components ahead of the experiments for combination treatment. We observed a favorable proinflammatory microenvironment for immunotherapy 14 days after low-dose (2.5mg/kg) fruquintinib immunotherapy treatment. Similarly, earlier studies stated that anti-angiogenesis had immune modulatory effects and combinational strategy might help to overcome resistance to anti–PD-1/PD-L1 (32, 33). We thus hypothesized that a low dose of fruquintinib might be more effective when combined with anti-PD-1immunotherapy. The work presented here is a proof that under optimal conditions, PD-1 blockade combined with antiangiogenic agents, such as fruquintinib can induce enhanced therapeutic effect. Our results from *in vivo* combination treatment experiments confirmed this hypothesis.

We showed that fruquintinib therapy not only reduced angiogenesis but also increased the proportion of T lymphocytes in our size-matched mouse tumor samples. These combination treatment interactions led to reprogramming of the immune microenvironment of CRC. Furthermore, we showed that fruquintinib not only reduced angiogenesis, but also mediated antitumor immunity by influencing lymphocyte ratio and eliminate immunosuppressive cells, such as MDSCs and TAMs. Our findings were in consistent with several previous reports in various tumor models (31, 34, 35).

In addition, we evaluated the toxicity and safety of fruquintinib, no major toxicity was found in the mouse models. Moreover, we retrospectively analyzed 5 patients with MSS mCRC, the toxicity of fruquintinib was tolerable. One of the patients' PFS was 18 months when the data were collected. Our findings demonstratted that low-dose fruquintinib reduced immunosuppressive components and enhanced tumor immunotherapy. The preliminary clinical results further support our hypothesis. Our study is limited by using the mouse models to mimic the human TME and the study of the patient's therapy is not a prospective clinical trial. More animals experimental systems and prospective clinical trials for further evalution are warranted.

In summary, our results suggested that fruquintinib, a VEGFR1, 2, and 3 inhibitor, when administrated at a lower dose, could optimize the immunosuppressive TME and increase the therapeutic response to immunotherapy both in mice colon cancer models and in clinical colon cancer patients. Further evaluation in randomized clinical trials are warranted.

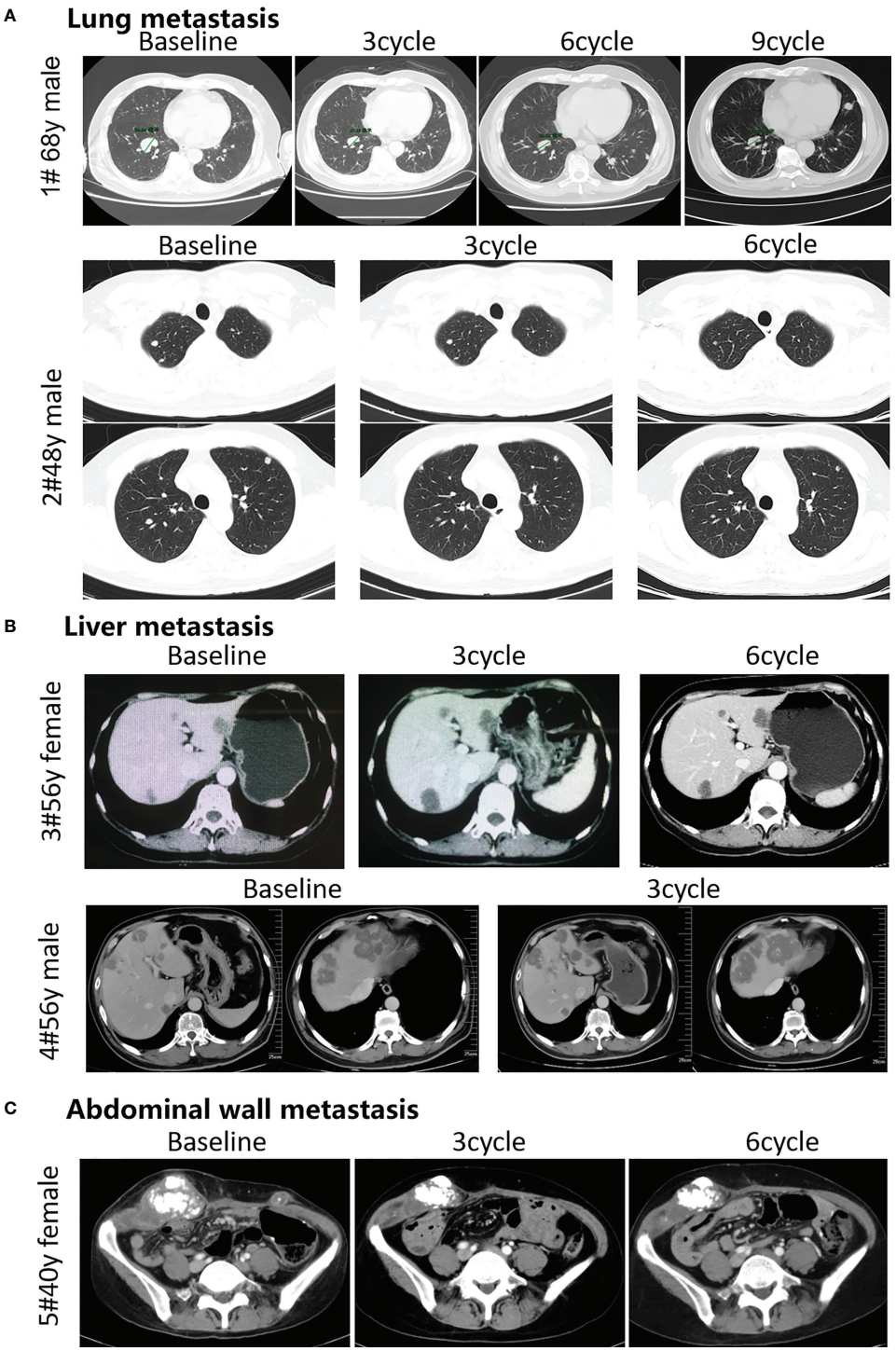

FIGURE 6 | Efficacy of the combination therapy of fruquintinib and anti-PD-1 in patients in MSS mCRC. Radiologic evidence of the 5 patients who achieved PR or SD after the combination treatment. CT scans were performed at the baseline and subsequent treatment cycles. **(A)** Two CRC patients with lung metastasis: (case 1 # and case 2) were treated with anti-PD-1 and Fruquintinib, and the lesions were significantly reduced (PR). **(B)** Two CRC patients with liver metastasis: (case 3and case 4) were treated with anti-PD-1 and fruquintinib, the liver metastases showed stable morphological changes, the density became uniform and reduced, the edge became clear, and the peripheral edge enhancement disappeared. **(C)** One CRC patient with abdominal wall metastasis (case 5) were treated with anti-PD-1 and fruquintinib, and the lesions were significantly reduced (PR). Individual clinical outcomes and the 5 patients enrolled by therapeutic responses (assessed via RECIST v1.1) in **Table 1**. No, patient number; y, years old; PR, partial response; SD, stable disease; PD, progressive disease.

DATA AVAILABILITY STATEMENT

The original contributions presented in the study are included in the article/**Supplementary Material**. Further inquiries can be directed to the corresponding authors.

ETHICS STATEMENT

The patients/participants provided their written informed consent to participate in this study. The animal study was reviewed and approved by The Animal Ethics Committee of Ruijin Hospital, Shanghai Jiaotong University School of Medicine (Shanghai China). Written informed consent was obtained from the individual(s) for the publication of any potentially identifiable images or data included in this article.

AUTHOR CONTRIBUTIONS

ST designed the study, analysized data and revised the manuscript. QL carried out the most of experiments, analysized original data and drafted the manuscript. XC collected and analyzied the samples and the clinical data. JW collected the clinical data and revises the manuscirpt.YT, FL, BZ, and TH participated the coordination of research. CZ drafted the manuscript. All authors contributed to the article and approved the submitted version.

FUNDING

The project was supported by National Science Foundation of China (NSFC 81773259,Chinese Society of Clinical Oncology Foundation (Y-Q201802-073, Y-XD202001-0318), the Science and Technique Foundation of Henan Province (No. 202102310121 for JW), Medical Science and Technology Co-construction Project of Henan Province (No. LHGJ20200167).

ACKNOWLEDGMENTS

We thank Jun Wu, Yihua Gu, and Ke Wang for the technical assistance. We are grateful to Hutchison MediPharma Limited providing fruquintinib and Innovent Biologics providing anti-PD-1antibody- Sintilimab was a gift from Innovent Biologics.

SUPPLEMENTARY MATERIAL

The Supplementary Material for this article can be found online at: https://www.frontiersin.org/articles/10.3389/fonc.2022.841977/full#supplementary-material

REFERENCES

1. Sung H, Ferlay J, Siegel RL, Laversanne M, Soerjomataram I, Jemal A, et al. Global Cancer Statistics 2020: GLOBOCAN Estimates of Incidence and Mortality Worldwide for 36 Cancers in 185 Countries. *CA Cancer J Clin* (2021) 71(3):209–49. doi: 10.3322/caac.21660
2. André T, Shiu KK, Kim TW, Jensen BV, Jensen LH, Punt C, et al. Pembrolizumab in Microsatellite-Instability-High Advanced Colorectal Cancer. *N Engl J Med* (2020) 383(23):2207–18. doi: 10.1056/NEJMoa2017699
3. Overman MJ, Lonardi S, Wong KYM, Lenz HJ, Gelsomino F, Aglietta M, et al. Durable Clinical Benefit With Nivolumab Plus Ipilimumab in DNA Mismatch Repair-Deficient/Microsatellite Instability-High Metastatic Colorectal Cancer. *J Clin Oncol* (2018) 36(8):773–9. doi: 10.1200/JCO.2017.76.9901
4. Le DT, Uram JN, Wang H, Bartlett BR, Kemberling H, Eyring AD, et al. PD-1 Blockade in Tumors With Mismatch-Repair Deficiency. *N Engl J Med* (2015) 372(26):2509–20. doi: 10.1056/NEJMoa1500596
5. Overman MJ, McDermott R, Leach JL, Lonardi S, Lenz HJ, Morse MA, et al. Nivolumab in Patients With Metastatic DNA Mismatch Repair-Deficient or Microsatellite Instability-High Colorectal Cancer (CheckMate 142): An Open-Label, Multicentre, Phase 2 Study. *Lancet Oncol* (2017) 18(9):1182–91. doi: 10.1016/S1470-2045(17)30422-9
6. Le DT, Durham JN, Smith KN, Wang H, Bartlett BR, Aulakh LK, et al. Mismatch Repair Deficiency Predicts Response of Solid Tumors to PD-1 Blockade. *Science* (2017) 357(6349):409–13. doi: 10.1126/science.aan6733
7. Topalian SL, Hodi FS, Brahmer JR, Gettinger SN, Smith DC, McDermott DF, et al. Safety, Activity, and Immune Correlates of Anti-PD-1 Antibody in Cancer. *N Engl J Med* (2012) 366(26):2443–54. doi: 10.1056/NEJMoa1200690
8. Yamamoto N, Nokihara H, Yamada Y, Shibata T, Tamura Y, Seki Y, et al. Phase I Study of Nivolumab, an Anti-PD-1 Antibody, in Patients With Malignant Solid Tumors. *Invest New Drugs* (2017) 35(2):207–16. doi: 10.1007/s10637-016-0411-2
9. Eng C, Kim TW, Bendell J, Argilés G, Tebbutt NC, Di Bartolomeo M, et al. Atezolizumab With or Without Cobimetinib Versus Regorafenib in Previously Treated Metastatic Colorectal Cancer (IMblaze370): A Multicentre, Open-Label, Phase 3, Randomised, Controlled Trial. *Lancet Oncol* (2019) 20(6):849–61. doi: 10.1016/S1470-2045(19)30027-0
10. Yarchoan M, Hopkins A, Jaffee EM. Tumor Mutational Burden and Response Rate to PD-1 Inhibition. *N Engl J Med* (2017) 377(25):2500–1. doi: 10.1056/NEJMc1713444
11. Chalmers ZR, Connelly CF, Fabrizio D, Gay L, Ali SM, Ennis R, et al. Analysis of 100,000 Human Cancer Genomes Reveals the Landscape of Tumor Mutational Burden. *Genome Med* (2017) 9(1):34. doi: 10.1186/s13073-017-0424-2
12. Huang T, Li F, Cheng X, Wang J, Zhang W, Zhang B, et al. Wnt Inhibition Sensitizes PD-L1 Blockade Therapy by Overcoming Bone Marrow-Derived Myofibroblasts-Mediated Immune Resistance in Tumors. *Front Immunol* (2021) 12:619209. doi: 10.3389/fimmu.2021.619209
13. Ferrara N. Vascular Endothelial Growth Factor and Age-Related Macular Degeneration: From Basic Science to Therapy. *Nat Med* (2010) 16(10):1107–11. doi: 10.1038/nm1010-1107
14. Khan KA, Kerbel RS. Improving Immunotherapy Outcomes With Anti-Angiogenic Treatments and Vice Versa. *Nat Rev Clin Oncol* (2018) 15 (5):310–24. doi: 10.1038/nrclinonc.2018.9
15. Apte RS, Chen DS, Ferrara N. VEGF in Signaling and Disease: Beyond Discovery and Development. *Cell* (2019) 176(6):1248–64. doi: 10.1016/j.cell.2019.01.021
16. Sun Q, Zhou J, Zhang Z, Guo M, Liang J, Zhou F, et al. Discovery of Fruquintinib, a Potent and Highly Selective Small Molecule Inhibitor of VEGFR 1, 2, 3 Tyrosine Kinases for Cancer Therapy. *Cancer Biol Ther* (2014) 15(12):1635–45. doi: 10.4161/15384047.2014.964087
17. Li J, Qin S, Xu RH, Shen L, Xu J, Bai Y, et al. Effect of Fruquintinib vs Placebo on Overall Survival in Patients With Previously Treated Metastatic Colorectal Cancer: The FRESCO Randomized Clinical Trial. *Jama* (2018) 319(24):2486–96. doi: 10.1001/jama.2018.7855

18. Fukuoka S, Hara H, Takahashi N, Kojima T, Kawazoe A, Asayama M, et al. Regorafenib Plus Nivolumab in Patients With Advanced Gastric or Colorectal Cancer: An Open-Label, Dose-Escalation, and Dose-Expansion Phase Ib Trial (REGONIVO, Epoc1603). *J Clin Oncol* (2020) 38(18):2053–61. doi: 10.1200/JCO.19.03296
19. Tu S, Bhagat G, Cui G, Takaishi S, Kurt-Jones EA, Rickman B, et al. Overexpression of Interleukin-1beta Induces Gastric Inflammation and Cancer and Mobilizes Myeloid-Derived Suppressor Cells in Mice. *Cancer Cell* (2008) 14(5):408–19. doi: 10.1016/j.ccr.2008.10.011
20. Callahan MK, Kluger H, Postow MA, Segal NH, Lesokhin A, Atkins MB, et al. Nivolumab Plus Ipilimumab in Patients With Advanced Melanoma: Updated Survival, Response, and Safety Data in a Phase I Dose-Escalation Study. *J Clin Oncol* (2018) 36(4):391–8. doi: 10.1200/JCO.2017.72.2850
21. Nivolumab Approved for Liver Cancer. *Cancer Discovery* (2017) 7(11):Of3. doi: 10.1158/2159-8290.CD-NB2017-138
22. Topalian SL, Hodi FS, Brahmer JR, Gettinger SN, Smith DC, McDermott DF, et al. Five-Year Survival and Correlates Among Patients With Advanced Melanoma, Renal Cell Carcinoma, or Non-Small Cell Lung Cancer Treated With Nivolumab. *JAMA Oncol* (2019) 5(10):1411–20. doi: 10.1001/jamaoncol.2019.2187
23. Mahoney KM, Rennert PD, Freeman GJ. Combination Cancer Immunotherapy and New Immunomodulatory Targets. *Nat Rev Drug Discovery* (2015) 14(8):561–84. doi: 10.1038/nrd4591
24. Chowdhury PS, Chamoto K, Honjo T. Combination Therapy Strategies for Improving PD-1 Blockade Efficacy: A New Era in Cancer Immunotherapy. *J Intern Med* (2018) 283(2):110–20. doi: 10.1111/joim.12708
25. Sanmamed MF, Chen L. A Paradigm Shift in Cancer Immunotherapy: From Enhancement to Normalization. *Cell* (2018) 175(2):313–26. doi: 10.1016/j.cell.2018.09.035
26. Zhao S, Ren S, Jiang T, Zhu B, Li X, Zhao C, et al. Low-Dose Apatinib Optimizes Tumor Microenvironment and Potentiates Antitumor Effect of PD-1/PD-L1 Blockade in Lung Cancer. *Cancer Immunol Res* (2019) 7(4):630–43. doi: 10.1158/2326-6066.CIR-17-0640
27. Li J, Qin S, Xu R, Yau TC, Ma MB, Pan H, et al. Regorafenib Plus Best Supportive Care Versus Placebo Plus Best Supportive Care in Asian Patients With Previously Treated Metastatic Colorectal Cancer (CONCUR): A Randomised, Double-Blind, Placebo-Controlled, Phase 3 Trial. *Lancet Oncol* (2015) 16(6):619–29. doi: 10.1016/S1470-2045(15)70156-7
28. Castle JC, Loewer M, Boegel S, de Graaf J, Bender C, Tadmor AD, et al. Immunomic, Genomic and Transcriptomic Characterization of CT26 Colorectal Carcinoma. *BMC Genomics* (2014) 15(1):190. doi: 10.1186/1471-2164-15-190
29. Kim K, Skora AD, Li Z, Liu Q, Tam AJ, Blosser RL, et al. Eradication of Metastatic Mouse Cancers Resistant to Immune Checkpoint Blockade by Suppression of Myeloid-Derived Cells. *Proc Natl Acad Sci USA* (2014) 111(32):11774–9. doi: 10.1073/pnas.1410626111
30. Hamzah J, Jugold M, Kiessling F, Rigby P, Manzur M, Marti HH, et al. Vascular Normalization in Rgs5-Deficient Tumours Promotes Immune Destruction. *Nature* (2008) 453(7193):410–4. doi: 10.1038/nature06868
31. Huang Y, Yuan J, Righi E, Kamoun WS, Ancukiewicz M, Nezivar J, et al. Vascular Normalizing Doses of Antiangiogenic Treatment Reprogram the Immunosuppressive Tumor Microenvironment and Enhance Immunotherapy. *Proc Natl Acad Sci USA* (2012) 109(43):17561–6. doi: 10.1073/pnas.1215397109
32. Manegold C, Dingemans AC, Gray JE, Nakagawa K, Nicolson M, Peters S, et al. The Potential of Combined Immunotherapy and Antiangiogenesis for the Synergistic Treatment of Advanced NSCLC. *J Thorac Oncol* (2017) 12(2):194–207. doi: 10.1016/j.jtho.2016.10.003
33. Allen E, Jabouille A, Rivera LB, Lodewijckx I, Missiaen R, Steri V, et al. Combined Antiangiogenic and Anti-PD-L1 Therapy Stimulates Tumor Immunity Through HEV Formation. *Sci Transl Med* (2017) 9(385):eaak9679. doi: 10.1126/scitranslmed.aak9679
34. Wallin JJ, Bendell JC, Funke R, Sznol M, Korski K, Jones S, et al. Atezolizumab in Combination With Bevacizumab Enhances Antigen-Specific T-Cell Migration in Metastatic Renal Cell Carcinoma. *Nat Commun* (2016) 7:12624. doi: 10.1038/ncomms12624
35. Tian L, Goldstein A, Wang H, Ching Lo H, Sun Kim I, Welte T, et al. Mutual Regulation of Tumour Vessel Normalization and Immunostimulatory Reprogramming. *Nature* (2017) 544(7649):250–4. doi: 10.1038/nature21724

Conflict of Interest: The authors declare that the research was conducted in the absence of any commercial or financial relationships that could be construed as a potential conflict of interest.

frontiers in Oncology

REVIEW
published: 24 March 2022
doi: 10.3389/fonc.2022.819128

PI3K/Akt/mTOR Pathway and Its Role in Cancer Therapeutics: Are We Making Headway?

*Yan Peng[1], Yuanyuan Wang[2], Cheng Zhou[3], Wuxuan Mei[2] and Changchun Zeng[3]**

[1] Department of Obstetrics, Longhua District Central Hospital, Shenzhen, China, [2] Xianning Medical College, Hubei University of Science and Technology, Xianning, China, [3] Department of Medical Laboratory, Shenzhen Longhua District Central Hospital, Guangdong Medical University, Shenzhen, China

Cancer is a severe public health issue that is a leading cause of mortality globally. It is also an impediment to improving life expectancy worldwide. Furthermore, the global burden of cancer incidence and death is continuously growing. Current therapeutic options are insufficient for patients, and tumor complexity and heterogeneity necessitate customized medicine or targeted therapy. It is critical to identify potential cancer therapeutic targets. Aberrant activation of the PI3K/AKT/mTOR pathway has a significant role in carcinogenesis. This review summarized oncogenic PI3K/Akt/mTOR pathway alterations in cancer and various cancer hallmarks associated with the PI3K/AKT/mTOR pathway, such as cell proliferation, autophagy, apoptosis, angiogenesis, epithelial-to-mesenchymal transition (EMT), and chemoresistance. Importantly, this review provided recent advances in PI3K/AKT/mTOR inhibitor research. Overall, an in-depth understanding of the association between the PI3K/AKT/mTOR pathway and tumorigenesis and the development of therapies targeting the PI3K/AKT/mTOR pathway will help make clinical decisions.

Keywords: PI3K/Akt/mTOR pathway, targeted therapy, precision medicine, cancer, oncogenic alterations

OPEN ACCESS

Edited by:
Yan-yan Yan,
Shanxi Datong University, China

Reviewed by:
Enrique Gonzalez Billalabeitia,
Hospital Universitario 12 de Octubre, Spain
Xiaoyong Fu,
Baylor College of Medicine, United States

****Correspondence:***
Changchun Zeng
zengchch@glmc.edu.cn

Specialty section:
This article was submitted to Cancer Molecular Targets and Therapeutics, a section of the journal Frontiers in Oncology

Received: *20 November 2021*
Accepted: *04 March 2022*
Published: *24 March 2022*

Citation:
Peng Y, Wang Y, Zhou C, Mei W and Zeng C (2022) PI3K/Akt/mTOR Pathway and Its Role in Cancer Therapeutics: Are We Making Headway? Front. Oncol. 12:819128. doi: 10.3389/fonc.2022.819128

INTRODUCTION

The mammalian target of rapamycin complex 1 (mTORC1) and the mammalian target of rapamycin complex 2 (mTORC2) are two distinct complexes formed by the mTOR. Growth factors, rapamycin, insulin, phosphatidic acid, certain amino acids, and oxidative stress affect the activity of mTOCR1, which is comprised of mTOR, Raptor, MLST8, PRAS40, and DEPTOR. The most classical targets downstream of mTOCR1 are S6K and 4EBP1, which play critical roles in protein synthesis, nutritional response, and tumor development. mTORC2 is composed of mTOR, RICTOR, mLST8, PROTOR1/2, DEPTOR, and mSIN1. mTORC2 interacts with PDK1 to activate AKT *via* phosphorylating it. Moreover, mTORC2 plays a critical role in the actin cytoskeleton, cell cycle, and survival (1–5). Receptor tyrosine kinases (RTKs), alterations in PIK3CA and its effectors, reduced PTEN expression, and other events contribute to oncogenic stimulation of the PI3K/Akt/mTOR pathway (6–8). In this review, we mainly described the genetic alterations of the PI3K/Akt/mTOR pathway. The mutations and amplification of PIK3CA are the most occurring events in cancer, and abnormal PI3K activity is a transforming event in the disease process (9). Alteration in AKT can cause an abnormal increase in the phosphorylated level of Akt in cancer cells (10). PTEN is another component of the PI3K/Akt signaling pathway, and its dysregulation

can enhance cell growth, proliferation, and survival. Loss of heterozygosity (LOH), mutations, promoter methylation, and post-translational inhibition of PTEN are events in tumors and are involved in the pathogenesis of tumors (11, 12).

In this era of precision medicine, there are some advances in tailored, targeted therapies that inhibit specific pathways, potentially halting the evolution and spread of cancer. Understanding the abnormal expression of cancer pathway genes that play a vital role in cancer genesis and progression will contribute to cancer therapies. Based on current cancer genomic investigations, several critical cancer pathways are abnormally regulated (13). The PI3K/AKT/mTOR signaling pathway has been described as one of the most commonly disrupted pathways in cancer, making it an attractive candidate for therapeutic intervention. The PI3K/AKT/mTOR pathway is crucial for cell motility, growth, survival, and metabolism in cancer (14, 15). The current commercially accessible targeted inhibitors for cancer patients with abnormal activation of the PI3K/AKT/mTOR pathway include everolimus (mTOR inhibitor), sirolimus (mTOR inhibitor), temsirolimus (mTOR inhibitor), alpelisib (PI3K inhibitor), duvelisib (PI3K inhibitor), copanlisib (PI3K inhibitor), idelalisib (PI3K inhibitor), umbralisib (PI3K inhibitor). Phase III clinical trials of AKT inhibitors, such as capivasertib and ipatasertib, have been proceeded in cancer (**Figure 1** and **Table 1**) (6, 16, 17). Preclinical and clinical trials have shown encouraging outcomes for these targeted medicines. However, resistance to these medications is a drawback to their clinical usage. The rising prevalence of cancer necessitates the development of increasingly effective targeted medicines. Additionally, drugs targeting the PI3K/AKT/mTOR pathway in combination with chemotherapy drugs or other targeted drugs can inhibit tumor development (18). This review highlights the importance of the PI3K/AKT/mTOR pathway in

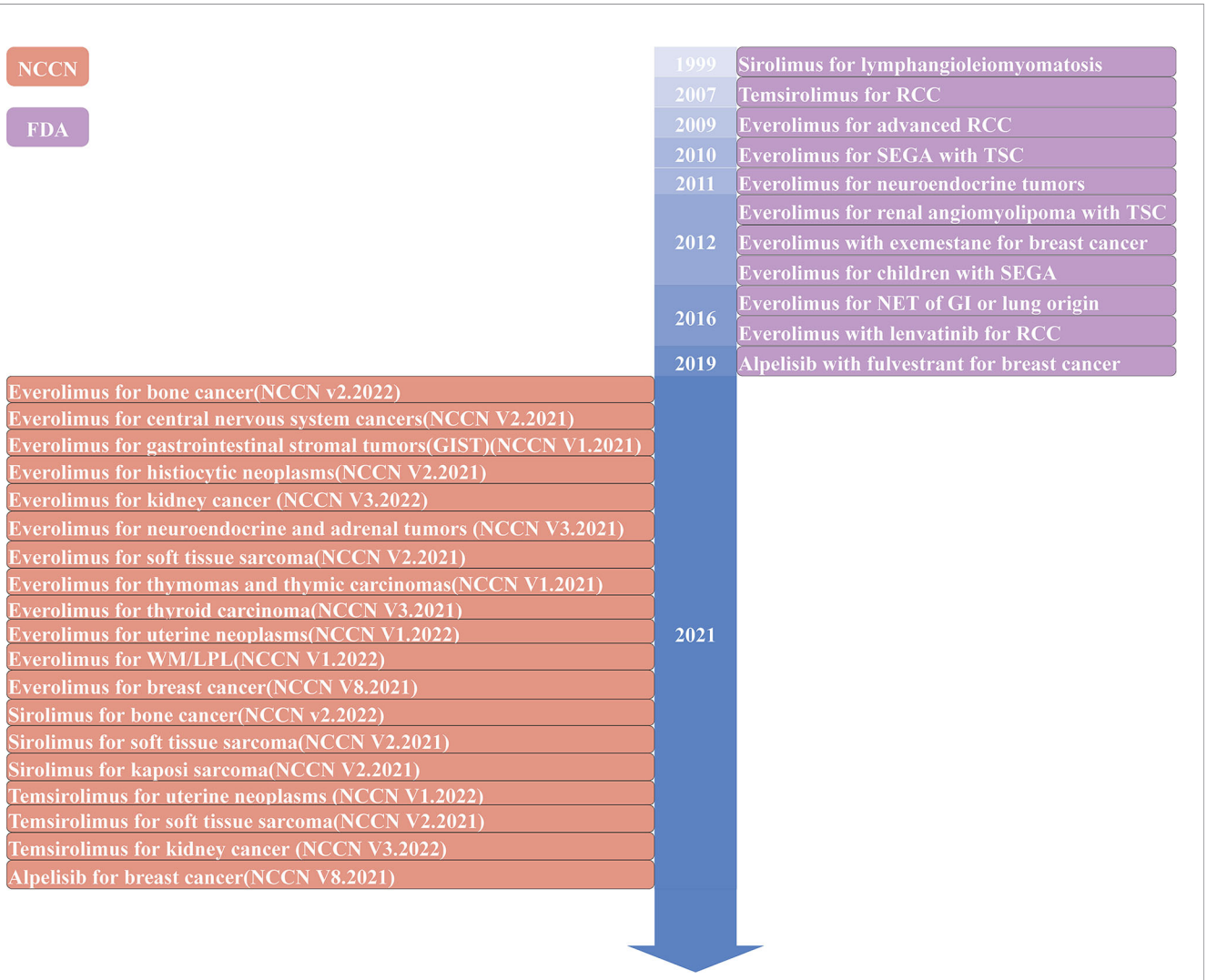

FIGURE 1 | Timeline of The Food and Drug Administration (FDA)-approved or the National Comprehensive Cancer Network (NCCN) recommended inhibitors targeting the PI3K/AKT/mTOR pathway in solid tumors. WM, Waldenstrom macroglobulinemia; LPL, lymphoplasmacytic lymphoma; RCC, renal cell carcinoma; SEGA, subependymal giant cell astrocytoma; TSC, tuberous sclerosis complex; NET, neuroendocrine tumor; GI, gastrointestinal.

TABLE 1 | PI3K/AKT/mTOR pathway inhibitors.

Inhibitors	Targets	FDA-approved status	Clinical trial	Condition
Piqray (alpelisib) 2019 year	PI3Kα	Yes	NCT02437318(Phase III)	In combination with fulvestrant for postmenopausal women, and men, with HR-positive, HER2-negative, PIK3CA-mutated, advanced or metastatic breast cancer.
Copiktra (duvelisib) 2018 year	PI3Kδ, PI3Kγ	Yes	NCT02004522(Phase III);NCT02204982 (Phase III)	Adult patients with relapsed or refractory CLL or SLL or FL after at least two prior therapies.
Aliqopa (copanlisib) 2017 year	PI3Kδ, PI3Kα	Yes	NCT01660451(Phase II)	Copanlisib for the treatment of adult patients with relapsed FL.
Zydelig (idelalisib) 2014 year	PI3Kδ	Yes	NCT01539512(Phase III)	Chronic lymphocytic leukemia, relapsed follicular B-cell non-Hodgkin lymphoma, and relapsed small lymphocytic lymphoma.
Ukoniq (umbralisib) 2021year	PI3Kδ, CK1ε	Yes	NCT02793583 (Phase II/III)	MZL and FL.
Sonolisib (PX-866) 2015 year	PI3Kα, PI3Kγ, PI3Kδ	No	NCT01259869(Phase II)	Glioblastoma multiforme at the time of first relapse or progression.
Buparlisib (NVP-BKM120) 2018 year	PI3Kα, PI3Kβ, PI3Kγ, PI3Kδ	No	NCT01633060(Phase III)	In combination fulvestrant, in postmenopausal women with HR-positive HER2-negative aromatase inhibitor-treated, locally advanced or metastatic breast cancer who progressed on or after mTOR inhibitor-based treatment.
Afinitor (everolimus) 2009 year	mTORC1, mTORC2	Yes	NCT00863655(Phase III); NCT00510068 (Phase III); NCT01524783(Phase III); NCT00412061(Phase III); NCT00410124 (Phase III)	Advanced HR+, HER2- breast cancer; PNET; progressive NET of gastrointestinal or lung origin; advanced renal cell carcinoma; SEGA and renal angiomyolipomas associated with tuberous sclerosis.
Rapamune (Sirolimus) 1999 year	mTORC1, mTORC2	Yes	NCT00414648(Phase III)	The prophylaxis of organ rejection in patients aged 13 years or older receiving renal transplants, and LAM.
Torisel (temsirolimus) 2007year	mTORC1, mTORC2	Yes	NCT00065468(Phase III)	Advanced renal cell carcinoma.
Capivasertib (AZD5363) 2020 year	AKT1, AKT2, AKT3	No	NCT03997123(Phase III)	Locally advanced or metastatic triple-negative breast cancer
Ipatasertib (GDC-0068) 2021 year	AKT1, AKT2, AKT3	No	NCT03072238(Phase III)	Ipatasertib plus abiraterone and prednisolone in metastatic castration-resistant prostate cancer
MK-2206 2020 year	AKT1, AKT2, AKT3	No	NCT01042379(Phase II)	HER2-positive and/or HR-negative breast cancer

HR: hormone receptor; HER2: epidermal growth factor receptor 2; CLL: chronic lymphocytic leukemia; SLL: small lymphocytic lymphoma; FL: follicular lymphoma; MZL: marginal zone lymphoma; PNET: progressive neuroendocrine tumors of pancreatic origin; NET: neuroendocrine tumors; SEGA: subependymal giant cell astrocytoma; LAM: lymphangioleiomyomatosis.

cancer genesis and progression and summarizes inhibitors of this axis for cancer prevention and treatment.

ONCOGENIC PI3K/AKT/MTOR PATHWAY ALTERATIONS IN CANCER

Genetic Alterations in the PIK3CA Gene

The p110 α (p110α) subunit encoded by the PIK3CA gene is the most prevalent altered catalytic subunit of the phosphatidylinositol 3-kinase (PI3K) isoform in cancer. PI3K, comprised of a catalytic subunit (p110α) and a regulatory subunit (p85α), is a class of lipid kinases that participates in cellular functions, including cell proliferation, growth, differentiation, migration, and survival (**Figure 2A**). Numerous receptor tyrosine kinases, such as ERBB2, EGFR, MET, RET, and VEGFR, transform extracellular stimuli into intracellular signals and bind PI3K to the plasma membrane through scaffold proteins like IRS1 or by activation of RAS. After being stimulated, PI3K-110α transforms its lipid substrate phosphatidylinositol-4,5-bisphosphate (PIP2) to phosphatidylinositol- 3,4,5-bisphosphate (PIP3), triggering the AKT/mTOR pathway (19).

According to various studies, the mutation frequency of the PIK3CA gene ranges from 11% to 14% in cancer. PIK3CA activation mutations are identified in multiple tumor types, such as breast cancer, uterine corpus endometrial carcinoma, carcinoma of the uterine cervix, colorectal carcinoma, esophageal carcinoma, gallbladder carcinoma, non-small cell lung cancer, ovarian carcinoma, and gastric cancer (**Table 2**). 13% (1354/10336) of patients harbored PIK3CA mutations in MSK-

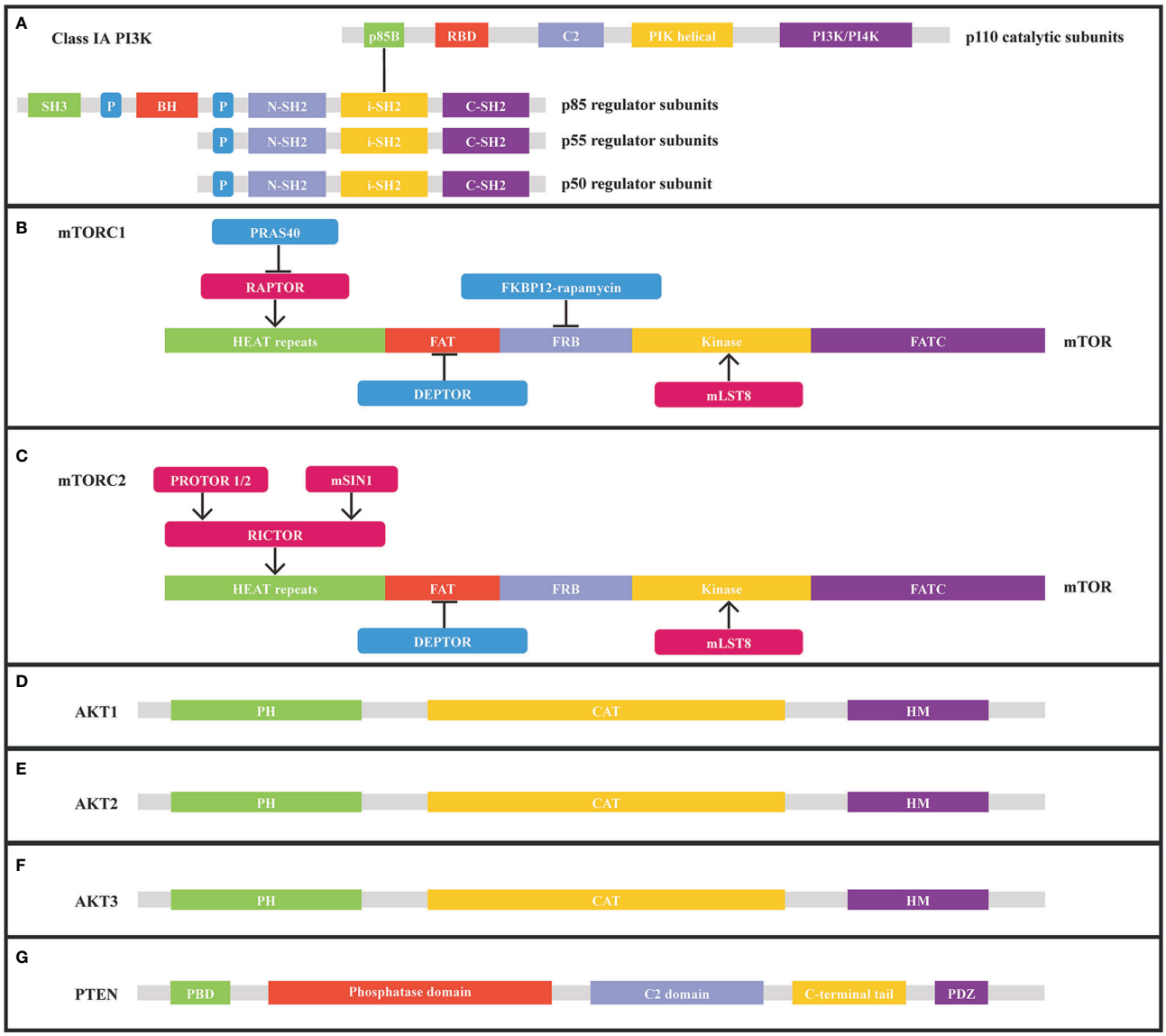

FIGURE 2 | Structure of class IA PI3K, mTORC1, mTORC2, AKT1, AKT2, AKT3, and PTEN from Uniprot.org. **(A)** class IA PI3K consists of catalytic and regulatory subunits. **(B)** mTORC1 subunits and corresponding binding sites on mTOR. **(C)** mTORC2 subunits and corresponding binding sites on mTOR. **(D)** Structure of AKT1. **(E)** Structure of AKT2. **(F)** Structure of AKT3. **(G)** Structure of PTEN. RBD, Ras binding domain; P, proline-rich domain; BH, breakpoint cluster homology domain; C2, membrane-interacting domain; iSH2, inter-SH2 domain; FRB, FKBP12-rapamycin-binding; HEAT, Huntingtin/Elongation factor 3/a subunit of protein phosphatase2A/TOR1; mSIN1, mammalian stress-activated; PH, pleckstrin homology; CAT, catalytic domain; HM, hydrophobic motif.

IMPACT Clinical Sequencing Cohort, while 11% (1143/10194) of patients harbored PIK3CA mutations in China Pan-cancer Cohort (OrigiMed2020) (20, 22). The most common mutations in PIK3CA are in the helix domain (E542/E545) and the kinase domain (H1047) (22–24). PIK3CA mutations are prevalent in breast cancer, with 35.7% (2261/6338) of tumors carrying the mutations, most common in estrogen receptor-positive breast cancer. H1047R (35%), E545K (17%), E542K (11%), N345K (6%), and H1047L (3%) were the five mutations that accounted for 73% of all PIK3CA mutations (25). PIK3CA H1047R and H1047L are hotspot mutations within the PI3K/PI4K kinase domain of the Pik3ca protein. Moreover, the E545K and E542K mutations in the PIK helical domain of the Pik3ca protein are also hotspot mutations. Besides, PIK3CA N345K lies in the Pik3ca protein's C2 PI3K-type domain. H1047R, H1047L, E545K, E542K, and N345K contribute to enhanced Akt and Mek1/2 phosphorylation, cell survival, and transformation (26, 27). PIK3CA amplification is a frequent genetic event in various cancers such as lung squamous cell carcinoma, cervical squamous cell carcinoma, esophageal adenocarcinoma, breast carcinoma, and is usually mutually exclusive with PIK3CA mutations. Increased PIK3CA copy number is strongly

TABLE 2 | Genetic alterations of the PIK3CA, mTOR, PTEN, AKT1, AKT2, and AKT3 genes in human cancers.

PIK3CA			
Cancer Type	**Number of Cases**	**Mutation Frequency**	**Amplification Frequency**
Endometrial Carcinoma	586	44.54%	4.10%
Cervical Squamous Cell Carcinoma	251	22.71%	11.55%
Invasive Breast Carcinoma	1084	30.72%	1.85%
Head and Neck Squamous Cell Carcinoma	523	13.58%	11.85%
Colorectal Adenocarcinoma	594	24.75%	–
Bladder Urothelial Carcinoma	411	20.44%	2.68%
Non-Small Cell Lung Cancer	1053	5.41%	15.95%
Ovarian Epithelial Tumor	584	0.86%	19.35%
Esophagogastric Adenocarcinoma	514	14.20%	5.06%
Diffuse Glioma	513	8.19%	0.78%
Glioblastoma	592	6.25%	2.53%
Melanoma	444	4.73%	0.45%
Prostate Adenocarcinoma	494	2.02%	2.23%
mTOR			
Cancer Type	Number of Cases	Mutation Frequency	Amplification Frequency
Melanoma	444	11.94%	0.90%
Endometrial Carcinoma	586	10.58%	0.85%
Esophagogastric Adenocarcinoma	514	6.42%	1.75%
Colorectal Adenocarcinoma	594	6.73%	–
Renal Clear Cell Carcinoma	511	6.07%	–
Non-Small Cell Lung Cancer	1053	4.18%	0.19%
PTEN			
Cancer Type	Number of Cases	Mutation Frequency	Delation Frequency
Endometrial Carcinoma	586	58.02%	2.56%
Glioblastoma	592	22.13%	8.95%
Prostate Adenocarcinoma	494	2.63%	15.59%
Melanoma	444	9.46%	5.86%
Cervical Squamous Cell Carcinoma	251	7.57%	4.78%
Esophagogastric Adenocarcinoma	514	6.03%	4.28%
Invasive Breast Carcinoma	1084	5.17%	4.98%
Non-Small Cell Lung Cancer	1053	5.60%	4.75%
Sarcoma	255	2.35%	5.88%
Colorectal Adenocarcinoma	594	5.22%	2.36%
Bladder Urothelial Carcinoma	411	3.89%	3.16%
Ovarian Epithelial Tumor	584	1.20%	4.45%
Diffuse Glioma	513	4.68%	0.97%
Hepatocellular Carcinoma	369	1.90%	3.52%
Head and Neck Squamous Cell Carcinoma	523	2.29%	2.87%
AKT1			
Cancer Type	Number of Cases	Mutation Frequency	Amplification Frequency
Endometrial Carcinoma	586	3.24%	1.02%
Ovarian Epithelial Tumor	584	3.94%	0.17%
Invasive Breast Carcinoma	1084	2.49%	1.11%
Melanoma	444	2.70%	–
Cervical Squamous Cell Carcinoma	251	1.59%	1.20%
Non-Small Cell Lung Cancer	1053	0.85%	1.71%
AKT2			
Cancer Type	Number of Cases	Mutation Frequency	Amplification Frequency
Pancreatic Adenocarcinoma	184	0.54%	7.07%
Endometrial Carcinoma	586	3.58%	3.57%
Ovarian Epithelial Tumor	584	0.17%	5.31%
Cervical Squamous Cell Carcinoma	251	1.99%	3.59%
Sarcoma	255	0.39%	3.53%
Non-Small Cell Lung Cancer	1053	1.14%	3.32%
Esophagogastric Adenocarcinoma	514	2.14%	1.17%
Bladder Urothelial Carcinoma	411	0.97%	2.43%
AKT3			
Cancer Type	Number of Cases	Mutation Frequency	Amplification Frequency
Invasive Breast Carcinoma	1084	0.74%	9.78%
Endometrial Carcinoma	586	5.29%	2.73%
Hepatocellular Carcinoma	369	0.27%	5.96%
Melanoma	444	2.48%	2.93%

(Continued)

TABLE 2 | Continued

PIK3CA Cancer Type	Number of Cases	Mutation Frequency	Amplification Frequency
Ovarian Epithelial Tumor	584	5.65%	–
Non-Small Cell Lung Cancer	1053	1.14%	3.51%
Esophagogastric Adenocarcinoma	514	1.75%	1.36%
Pancreatic Adenocarcinoma	184	0.54%	2.17%
Colorectal Adenocarcinoma	594	2.19%	0.51%

The Cancer Genome Atlas (TCGA) PanCancer Atlas Studies included 32 studies selected (10967 samples) (20, 21).

associated with increased PIK3CA expression and PI3K activity in malignancies. In addition, breast cancer patients with high PIK3CA copy numbers have a worse prognosis (22–24, 28).

Genetic Alterations in the mTOR Gene

The mTOR protein, which is encoded by the mTOR gene, belongs to a serine-threonine kinase that controls cell responses to stressors such as growth factors, nutrient deprivation, and DNA damage and regulates tumor growth, survival, and metabolic signaling (**Figures 2B, C**). mTOR activation mutations enhance the kinase activity of mTOR, resulting in the overactivation of downstream pro-proliferative pathways. MTOR mutations are common in malignant tumors, such as endometrial carcinoma, melanoma, esophagogastric adenocarcinoma, colorectal adenocarcinoma, renal cell carcinoma, and bladder cancer (**Table 2**) (29). In MSK-IMPACT Clinical Sequencing Cohort, MTOR is mutated at a rate of 3% (329/10336) in metastatic cancer, which is also observed at the similar rate (2.9%, 292/10194) observed in China Pan-cancer Cohort (OrigiMed2020) (20, 22). Nonsynonymous mTOR mutations are present in 10.4% (N=412) of melanoma patients and are associated with a poor prognosis (30). Besides, 6% of clear-cell renal cell carcinoma patients with mTOR mutation were identified (31). The predicted mutation incidence was 3% (N=8630) for mTOR in head and neck cancer (32). The mTOR missense mutations are found in a wide variety of malignancies, most notably in roughly 7.5% of lung adenocarcinomas, 6% of clear cell renal cell carcinomas, 5% of endometrial carcinomas, and 4% of colorectal carcinomas (33). The most prevalent alterations of MTOR in malignant tumors are E1799K, S2215F, and amplification (29). Mutations in key regions such as HEAT repeat, FAT domain, and kinase domain make the mTOR gene highly tumorigenic. Moreover, mTOR W1456R, M938T, V2284M, T2294I, V2291I, P2273S, G1479N, and E2288K mutants dramatically elevated the activity of protein kinase. Besides, the mTOR/p70S6K pathway was significantly increased in the W1456R, P2273S, and E2288K mutants. In addition, the W1456R, P2273S, and E2288K mutants affected the mTOR/p70S6K and Akt pathways (34).

Genetic Alterations in the AKT Gene

AKT1, AKT2, and AKT3, as members of the AGC kinase family, are serine/threonine protein kinases and downstream effectors of the PI3K signaling pathway (**Figures 2D–F**). Following PI3K activation, cytosolic AKT1 is transported to the membrane where it interacts with PIP3 (PtdIns3,4,5-P3), resulting in AKT1 phosphorylation and activation. AKT1 can stimulate a variety of downstream effectors, including GSK3, FOXO, and mTORC1, all of which are crucial for cell survival, growth, and metabolism. AKT1 can be negatively regulated as a result of PTEN phosphatase activity inhibiting PI3K. Besides, activation of the PI3K pathway or inactivation of PTEN can cause AKT1 activation in cancers. AKT1 activation mutations and AKT1 infrequent amplification enable AKT1 activation independent of phosphoinositide (14, 35, 36). The activating mutations of AKT2 and AKT3 induce disruption of intramolecular pleckstrin homology domain (PH) and kinase domain (KD) interactions, resulting in AKT oncogenic activation (37). AKT1, AKT2, AKT3 aberrations were identified in 1.8% (183/10336), 1.6% (163/10336), and 1.4% (149/10336) of patients in the MSK-IMPACT Clinical Sequencing Cohort, respectively. While AKT1, AKT2, AKT3 aberrations were identified in 1.4% (138/10194), 2% (206/10194), and 1.2% (122/10194) of patients in China Pan-cancer Cohort (OrigiMed2020) (20, 22). AKT1 E17K is a hotspot mutation, the most frequent AKT1 mutation in breast cancer, and a highly recurrent AKT1 mutation in many other cancer types. 6.3% (N=619) of breast cancer patients carry the AKT1 E17K mutation, associated with increased mortality (38). AKT1 E17K mutation boosts the binding of Akt1 to the phosphatidylinositol-3,4,5-trisphosphate (PIP3) ligand, which facilitates Akt transport from the cytoplasm to the cell membrane, and further stimulates Akt phosphorylation on the cell membrane. Activated AKT relocates in the cytoplasm, nucleus, or other intracellular locations phosphorylates a wide variety of substrate proteins and consequently modulates cell activity. Besides, AKT1 E17K mutation accelerates cell migration and resistance to chemotherapeutic treatments in luminal breast cancer cells (39, 40). The oncogene AKT2 is triggered by amplification or overexpression in a variety of malignant tumors, thus facilitating tumor invasion and metastasis (41, 42). More prevalent amplification of the oncogene AKT3 has been detected in many cancers, such as breast carcinoma, endometrial carcinoma, melanoma, ovarian epithelial tumor, cholangiocarcinoma, and non-small cell lung cancer (**Table 2**) (22, 23).

Genetic Alterations in the PTEN Gene

PTEN is a tumor suppressor gene that can negatively regulate the PI3K/AKT/mTOR pathway and is one of the most common mutated genes in cancer (**Figure 2G** and **Table 2**). PTEN functions as a phosphatase on the cell membrane, converting phosphatidylinositol (3–5)-triphosphate (PIP3) to phosphatidylinositol (4, 5)-diphosphate (PIP2). PTEN dysfunction caused by inactivation mutations, homozygous deletions, loss of heterozygosity (LOH), or

epigenetic modifications accumulates PIP3 and activates catabolic downstream AKT/mTOR signaling, thereby stimulating cell proliferation and survival. In addition, nuclear PTEN can modulate RAD51 expression, which is tightly associated with homologous recombination (HR) and DNA double-strand breaks (DSBs). Furthermore, PTEN deficiency may also result in increased genomic instability, allowing for the accumulation of deleterious mutations (43). Nedd8 interacts with PTEN at high glucose levels, inducing PTEN neddylation and resulting in nuclear import of PTEN without impairing PTEN stability. Neddylated PTEN mainly aggregates in the nucleus and dephosphorylates the fatty acid synthase (FASN), suppresses FASN ubiquitylation and degradation through TRIM21, and subsequently enhances fatty acid synthesis. Besides, PTEN neddylation was closely associated with tumor development and a worse prognosis in breast cancer (44). Germline PTEN mutations are found in approximately 80% of patients with the cancer predisposition syndrome Cowden, which is associated with a high incidence of breast and thyroid cancer events (45, 46). The PTEN mutation is one of the most prevalent cancer mutations, frequently found in endometrial carcinoma, glioblastoma, and prostate adenocarcinoma. PTEN mutations occurred in 9% (888/10336) of patients in the MSK-IMPACT Clinical Sequencing Cohort, while PTEN was altered in only 5% (534/10194) of patients in China Pan-cancer Cohort (OrigiMed2020) (20, 22). PTEN mutations or deletions are detected in 45% of endometrial cancer and are more frequent in endometrioid endometrial cancer than in other histological subtypes (47). PTEN mutations were found in 29.0% (N=303) of glioblastoma patients, and PTEN deletions were identified in 39.6% (N=260) of glioblastoma cases. 13.5% (N=260) of cases had concomitant PTEN mutation and deletions (48). PTEN mutations and/or deletions are identified in 30% of prostate cancer cases. PTEN silencing lowers H3K27me3 and H3K27Ac enrichment in the Nkx3.1 promoter region and promotes alterations in DNA CpG methylation and transcriptome gene expression, associated with various inflammatory and immunological pathways in the development of prostate cancer (49). PTEN Y240 phosphorylation mediated by FGFR2 prevents cells from DNA damage *via* enabling DNA repair. PTEN Y240 phosphorylation facilitates homologous recombination (HR)-mediated DNA double-strand break (DSB) repair through enhancing RAD51 filament synthesis or stabilization. PTEN Y240 phosphorylation interacts with chromatin and recruits RAD51 to facilitate DNA repair. Inhibiting Y240 phosphorylation can make glioblastoma more sensitive to ionizing radiation (IR), thus extending glioblastoma survival time (50).

THE PI3K/AKT/MTOR PATHWAY AND DIFFERENT CELLULAR PROCESSES IN CANCER

Cell Proliferation

PI3K/Akt/mTOR signaling pathway involved in cell survival, growth, and proliferation is the commonly activated signaling pathway in human cancers. Dysregulated mTOR activation is a frequent observation in cancer and represents a process in cancerogenesis. mTOR interacts with other proteins and is a component of two protein complexes, mTOR complex 1 and mTOR complex 2, that control various cellular activities. Both mTORC1 and mTORC2 contain subunits that mediate different but overlapping activities. mTORC1 is triggered by a variety of nutrients and can be stimulated by PI3K signaling. mTORC1 is an upstream regulator, whereas mTORC2 is a downstream effector of Akt. Akt is an essential substrate of mTORC2, which is often shown to be overactive in malignancies. Akt accumulates signals from the PI3K/mTORC2 and PI3K/PDK1 to enhance cell survival, growth, and proliferation (51). mTORC1 regulates the phosphorylation of downstream translation effectors such as the ribosomal protein S6 kinase B1 (S6K1) and the eukaryotic translation initiation factor 4E (eIF4E)-binding protein 1 (4E-BP1) to control cell growth and proliferation. mTORC2 controls cell survival and proliferation *via* phosphorylating Akt Ser473. Small molecules, such as hormones and growth factors, can activate Akt, mTORC2, and then mTORC1 through an Akt-dependent phosphorylation pathway. Nutrients can activate Akt, mTORC2, and directly stimulate mTORC1 through an Akt-independent phosphorylation pathway. Glycogen synthase kinase-3 beta (GSK3) is a significant Akt substrate, and its deactivation is induced by phosphorylation. GSK3 promotes cell proliferation by modulating the stability and production of proteins involved in the G1/S cell cycle phase transition, such as cyclin D1. FKBP4 enhances cell proliferation in breast cancer by increasing Akt phosphorylation at Ser473 and Thr308 through PI3K/PDK1 and mTORC2 (52). GSK3 collaborates with mTORC1 by increasing p70S6K1 activity by phosphorylating at Ser371 inside the p70S6K1 turn motif, which enhances mTORC1- mediated Thr389 phosphorylation. GSK3 may serve as an inducer of malignant cell growth and survival. Phosphorylation of some GSK3 substrates is critical for cell proliferation or survival and produces a phosphorylated protein recognized by E3 ubiquitin ligase, causing the phosphorylated protein to be degraded by the proteasome. After Rictor is phosphorylated by GSK3 and interacts with FBXW-7, it is degraded through a ubiquitination/proteasome-dependent pathway. When PI3K/Akt signaling inactivates GSK3, Rictor expression, and mTORC2 assembly increase, boosting mTORC2 activity (53). Rictor functions as an upstream kinase for many members of the AGC (cAMP-dependent, cGMP-dependent, and protein kinase C) protein family, such as Akt, SGK, and PKC, and is a critical component of mTORC2. Stimulation of Rictor/mTORC2 affects the structure of actin and enhances cell proliferation by phosphorylating the substrates. When used in conjunction with rapamycin, Rictor down-regulation significantly decreased cell proliferation, increased cell cycle arrest, and induced apoptosis by inhibiting the AktSer473 feedback phosphorylation (54). Activation of the mTORC2 subunit p-AKT (Ser473) and RICTOR stimulate the esophageal squamous cell carcinoma. Inhibiting RICTOR may increase esophageal squamous cell carcinoma cell sensitivity to PP242 (a pan-mTOR inhibitor) as well as RAD001 (a mTORC1 inhibitor) (55).

Autophagy

Autophagy is a critical homeostatic cellular recycling process that degrades damaged or dysfunctional cellular proteins and organelles. As a result of the dysregulation of the PI3K/Akt/

mTOR pathway, autophagy can be triggered in malignancies, allowing them to adapt to low-nutrient environments and proliferate (56). mTOR is a regulator that inhibits autophagy, and anticancer therapies that disrupt the PI3K/Akt/mTOR pathway promote autophagy. mTORC1 inhibits catabolism *via* suppressing autophagy and lysosome formation, which are two processes critical for lysosome-dependent macromolecule degradation. mTORC1 inhibits autophagy and lysosomal degradation *via* phosphorylating ULK1, a critical autophagy modulator, and TFEB, a modulator of lysosomal gene expression. The activity of mTORC1 can be modulated by energy levels, nutrient status, and hypoxic settings *via* the AMPK/TSC pathway, which affects autophagy. The mTORC1 downstream effectors' elongation factor 4E-BP1 and p70S6 kinase control protein synthesis. Stimulated mTORC1 phosphorylates the autophagy protein complex (ULK1/2) to suppress the downstream autophagy cascade. AMPK activated by AMP or LKB1 can promote autophagy by inhibiting the activity of mTORC1 through phosphorylation of TSC1/2. The intracellular flow of essential amino acids may limit autophagy by stimulating mTORC1. Additionally, MEK/ERK signaling promotes starvation-induced autophagy and ROS-dependent ERK activation boosts autophagy and induces cell death (57). PI3KCI stimulates Akt, which can attenuate the inhibitory impact of the TSC1/2 heterodimer on Rheb, thereby activating mTORC1 and inhibiting autophagy. Akt is triggered by mTORC2, which further inhibits autophagy. Moreover, PTEN promotes autophagy by suppressing the production of PIP3, which in turn triggers the PI3K/Akt/mTOR signaling. GTP-Ras suppresses autophagy *via* activating PI3KCI and the RAF/MEK/ERK pathway (58). The cyclin–CDK inhibitor CDKN1B (also known as p27Kip1) enhances starvation-induced autophagy *via* a mTORC1-dependent pathway. A portion of p27Kip1 is transported to lysosomes in amino acid-derived cells, where it cooperates with LAMTOR1, an essential component of the Ragulator complex, to stimulate mTORC1. When p27Kip1 binds to LAMTOR1, regulatory assembly and mTORC1 stimulation are inhibited, thereby facilitating autophagy. In p27 −/− cells, elevated mTORC1 activity contributes to cytoplasmic retention of TFEB, impaired lysosomal function, and decreased autophagy flux, ultimately improving cell survival (59). Gαq, a component of the mTOR/Raptor/p62 complex, regulates autophagy by promoting the assembly of the active mTORC1 complex through PB1-mediated Gαq/p62 interaction in the presence of nutrients (60).

Apoptosis

Apoptosis is a type of programmed cell death that enables the body to clear abnormal or unneeded cells in an orderly manner. Caspases are critical to the apoptotic mechanism as the initiators and executors of apoptosis, which can be activated by the extrinsic death receptor pathway, the intrinsic mitochondrial pathway, and the intrinsic endoplasmic reticulum pathway. The extrinsic death receptor pathway begins with the binding of death ligands (TNF and FasL) to death receptors (TNFR1 and Fas). The binding of the death ligand to the death receptor promotes the formation of the death-inducing signaling complex (DISC), a ligand-receptor-conjugating protein complex that further leads to the assembly and activation of caspase 8. The activated caspase 8 serves as an initiator caspase, which triggers apoptosis by cleaving other downstream caspases. Moreover, internal stimuli such as genetic damage, hypoxia, excessive cytosolic Ca2+ concentrations, and severe oxidative stress may cause elevated mitochondrial permeability and the production of pro-apoptotic substances such as cytochrome-c into the cytoplasm, stimulating the intrinsic mitochondrial pathway. Cytoplasmic release of cytochrome c activates caspase 3 *via* forming an apoptosome complex, composed of cytochrome c, Apaf-1, and caspase 9. The intrinsic mitochondrial pathway is tightly regulated by the Bcl-2 family proteins, mainly composed of pro-apoptotic proteins and anti-apoptotic proteins. Anti-apoptotic proteins such as Bcl-2, Bcl-XL, Bcl-W, BFL-1, and McL-1 regulate apoptosis by inhibiting the release of cytochrome c from mitochondria, while pro-apoptotic proteins such as Bax, Bak, Bad, Bcl-XS, Bid, Bik, Bim, and Hrk enhance the release of cytochrome c from mitochondria. Both extrinsic and intrinsic pathways are closely associated with various signaling proteins, such as NK-kB and p53-MDM2, and converge to caspases. Additionally, the intrinsic endoplasmic reticulum pathway is caspase 12-dependent and mitochondria-independent. Overall, the mechanisms of apoptosis evasion and carcinogenesis are mediated by the imbalance of Bcl-2 family proteins, reduced caspases expression, disrupted death receptor signaling pathway, p53 defects/mutations, and overexpression of inhibitor of apoptosis proteins (IAPs) such as BIRC1 (NAIP), BIRC2 (c-IAP1), BIRC3 (c-IAP2), BIRC4 (XIAP), BIRC5 (Survivin), BIRC6 (Apollon/BRUCE), BIRC7 (Livin/MLIAP) and BIRC8 (ILP2) (61, 62). mTOR inhibitors can rapidly inhibit 4E-BP1 phosphorylation *via* DR5/FADD/Caspase-8 axis and trigger the extrinsic apoptotic pathway in colorectal cancer cells. High dosages of mTOR inhibitors result in a significant reduction of 4E-BP1 phosphorylation and mTOR activity, all of which may be factors in ER stress, C/EBP homologous protein (CHOP), and death receptor 5 (DR5) and consequent cancer cell death. Besides, mTOR inhibitors have a substantial synergistic effect with tumor necrosis factor-related apoptosis-inducing ligand (TRAIL) and chemotherapy in inducing Fas-associated protein with death domain (FADD) and DR5-dependent apoptosis. Generally, mTOR inhibitors may have an anti-tumor effect *via* stimulating the extrinsic apoptotic pathway (63).

Angiogenesis

Angiogenesis is the formation of new blood vessels, enabling oxygen and nutrients to be delivered to the body's tissues. Angiogenesis is critical in the development of cancer, which requires the development of new blood vessels to grow and metastasize. Endogenous angiogenesis regulators mainly include growth factors, cytokines, proteases, protease inhibitors, trace elements, oncogenes, and endogenous modulators. A balance of activators such as vascular endothelial growth factor (VEGF), basic fibroblast growth factor (bFGF), platelet-derived endothelial cell growth factor (PD-ECGF), tumor necrosis factor (TNF)-α, angiogenin, transforming growth factor (TGF)-α, TGF-β, granulocyte colony-stimulating factor (G-

CSF), placental growth factor (PGF), hepatocyte growth factor (HGF), interleukin-8 (IL-8), and epidermal growth factor (EGF) and inhibitors such as angiostatin, interferon, endostatin, platelet factor 4 (PF4), thrombospondin (TSP), and tissue inhibitors of metalloproteinases (TIMPs) regulates angiogenesis (64–66). mTOR, a crucial switch that regulates anabolism and catabolism of endothelial cells, is critical in angiogenesis. Shear stress and coordinated interactions between endothelial growth factors (VEGF, PDGF-B, ANG2, ANG1, bFGF, ephrin-B2, and TGF-beta superfamily), intracellular signaling molecules (NOTCH1 and COUP-TFII), and intercellular connections (VCAM1) contribute to tumor angiogenesis, which may activate the PI3K/Akt/mTOR pathway in cancer cells. Hypoxia stabilizes HIF-1α, which triggers tumor cells to produce more vascular endothelial growth factor (VEGF). Stimulation of the PI3K/AKT pathway in tumor cells may boost the production of VEGF *via* hypoxia-inducible factor 1 (HIF-1) dependent and independent pathways. Besides, the PI3K/AKT pathway also regulates other angiogenic factors such as angiopoietins and nitric oxide. Angiogenic tumor cells release more bFGF and VEGF than non-angiogenic tumor cells. Increased VEGF levels may enhance vascular permeability, resulting in leaky vessels, slow blood flow, and high interstitial pressure. The binding of VEGF to receptors stimulates the PI3K/AKT/mTOR pathway, which is critical for cell migration (67). Suppression of the mTOR pathway prevents VEGF-mediated angiogenesis and cell proliferation by decreasing VEGF production and secretion, and VEGFR2-mediated signaling. Rutacecarpine suppresses angiogenesis *via* targeting VEGFR2 and the Akt/mTOR/p70s6k signaling pathways regulated by VEGFR2 (68). Rapamycin inhibits angiogenesis and lymphangiogenesis in melanoma by inhibiting the expression of VEGF-A/VEGFR-2 and VEGF-C/VEGFR-3 (69). VEGF stimulation increased the expression of Sox7 and Sox17 in angiogenesis through the mTOR pathway. Additionally, Sox7 and Sox17 increased the expression of VEGFR2 in angiogenic vessels (70).

Epithelial-to-Mesenchymal Transition

Epithelial-mesenchymal transition (EMT) refers to the transition of cells from epithelial to mesenchymal phenotypes, which results in functional alterations in cell migration and invasion. EMT is a vital step through which epithelial cells develop mesenchymal, fibroblast-like features characterized by decreased intercellular adhesion and enhanced motility. EMT-like processes play a significant role in tumor growth and malignant transformation, causing cancer cells to become more aggressive and spread (71, 72). During EMT, the expression of epithelial markers (E-cadherin) decreases, and the expression of mesenchymal markers (vimentin and fibronectin) increases. Snail, ZEB, and Twist regulate these markers by blocking the CDH1 gene encoding E-cadherin. Cumulative evidence indicates that the AKT/mTOR pathway is closely associated with the EMT process (73, 74). Phosphorylation and activation of EMT transcription factors are a result of AKT activation. Increased AKT activation causes decreased E-cadherin expression, partly attributable to the Snail accumulation in the nucleus. Besides, AKT may trigger Twist expression, which decreases E-cadherin expression and inhibits cell migration. Activation of NF-kB *via* AKT may cause the accumulation of ZEB-1, which acts as a repressor of E-cadherin expression. Growth factors, specific proteins, and aberrant tumor suppressors may stimulate AKT and regulate EMT transcription factor expression and EMT activation. Cancer cells experience dramatic remodeling of the actin cytoskeleton during the EMT process. mTORC2 modulates the actin cytoskeleton of the cell and EMT *via* regulating the phosphorylation status of Protein Kinase C (PKC) and activating Akt (75). TGF-receptors interact with the regulatory p85 subunit of PI3K, triggering the PI3K/AKT pathway. TGF-β has the potential to cause EMT *via* activating the mTOR pathway (76–79).

Chemoresistance

The druggable metabolic vulnerability is mediated by mTORC1, which inhibits autophagy and enhances resistance to chemotherapy and targeted drugs (80–82). The mTOR pathway regulates FANCD2, which leads to cancer cells' resistance to DNA double-strand breaks (83). The combination of adriamycin/cisplatin and mTOR inhibitor (torisel) blocked 4EBP-1 and p70S6K phosphorylation, elevated γH2AX expression indicative of DNA damage, and induced cell cycle arrest at G2/M and apoptosis, indicating a potential role of mTOR inhibitors in rebuilding chemosensitivity to adriamycin/cisplatin (84). FOXD1-AS1 facilitated the translation of FOXD1 protein *via* the eIF4G-eIF4E-eIF4A translational complex. Moreover, FOXD1-AS1 modulated 4E-BP1 phosphorylation and enhanced eIF4G-eIF4E interaction *via* triggering the PI3K/AKT/mTOR pathway. Overall, FOXD1-AS1 increases FOXD1 translation through PI3K/AKT/mTOR signaling, thereby exacerbating gastric cancer development and resistance to chemotherapy (85). Chemotherapy-resistant epithelial ovarian cancer cells exhibit EMT and increased expression of tumor stem cell markers due to stimulation of the PI3K/Akt/mTOR signaling pathway. In combination with cisplatin, BEZ235, an anti-PI3K/mTOR inhibitor, might be a viable therapeutic approach for epithelial ovarian cancer chemoresistance (86). Aurora-A expression was positively correlated with phosphorylated AKT/4E-BP1 expression in endometrial cancer tissues. Aurora-A triggers the AKT/mTOR pathway in endometrial cancer, which stimulates cell proliferation and causes chemoresistance, suggesting that Aurora-A inhibitor and AKT/mTOR inhibitor in combination with chemotherapy intervention may be a therapeutic strategy for Aurora-A overexpressed endometrial cancer (87).

RECENT ADVANCES IN PI3K/AKT/MTOR INHIBITOR RESEARCH

Because of the significant rise in the number of novel therapeutic drugs that target molecular pathways, targeted therapeutic agents are now more precise than traditional chemotherapy agents. The PI3K/AKT/mTOR pathway is critical for cell growth, proliferation, and survival, and it is one of the most frequently

disrupted pathways in malignancies, making it a desirable target for treatment (**Figure 3**). In this review, we reviewed the research progress of PI3K/AKT/mTOR inhibitors and presented the representative PI3K/AKT/mTOR inhibitors in **Table 1**.

PI3K Inhibitors

Phosphatidylinositol 3–kinases (PI3Ks) are a class of lipid kinases that control signaling and intracellular vesicular trafficking *via* phosphorylating intracellular inositol lipids. PI3Ks are classified into three groups based on their structural characteristic and substrate specificity. Class I PI3Ks synthesize 3-phosphoinositide lipids that activate signal transduction pathways directly. Class I PI3Ks are classified into subclasses IA and IB according to their regulatory mechanisms. Class IA PI3Ks are heterodimers with a catalytic subunit of p110 and a regulatory subunit of p85. The class IA catalytic isoforms p110α, p110β, and p110δ are encoded by the PIK3CA, PIK3CB, and PIK3CD genes, respectively. The class IB PI3K are the heterodimers with a catalytic subunit of p110γ and a regulatory subunit of p101 or p87. The class IB isoforms p110γ, p101, or p87 are encoded by the PIK3CG, PIK3R5, and PIK3R6 genes, respectively. The class I PI3Ks are frequently activated in malignant tumors, associated with translation, cell growth, glucose metabolism, cytoskeletal motility, cell survival, transformation. Cellular processes such as growth, cell migration, primary cilium function, glucose metabolism, cell survival, and angiogenesis are modulated by the Class II PI3Ks. The class II catalytic isoforms PI3KC2α, PI3KC2β, and PI3KC2γ are encoded by the PIK3C2A, PIK3C2B, and PIK3C2G genes, respectively. Autophagy, endosomal trafficking, and phagocytosis are dependent on the class III PI3K. The class III PI3Ks are the heterodimers with a catalytic subunit of VPS34 encoded by PIK3C3 and a regulatory and accessory subunit of VPS15 encoded by PIK3R4. Presently, several types of PI3K-specific inhibitors have been developed. PI3K inhibitors are divided into three categories according to their pharmacokinetic characteristics and capacity to interact with ATP-binding clefts: pan-PI3K inhibitors, isoform-selective PI3K inhibitors, and dual PI3K/mTOR inhibitors.

Pan-Class I inhibitors can block catalytic properties of p110 isoforms. The use of pan-PI3K inhibitors was restricted owing to the adverse pharmacological event caused by off-target effects, and on-target consequences of blocking all class I PI3K isoforms, independent of their role in carcinogenesis. PX-866, a derivative

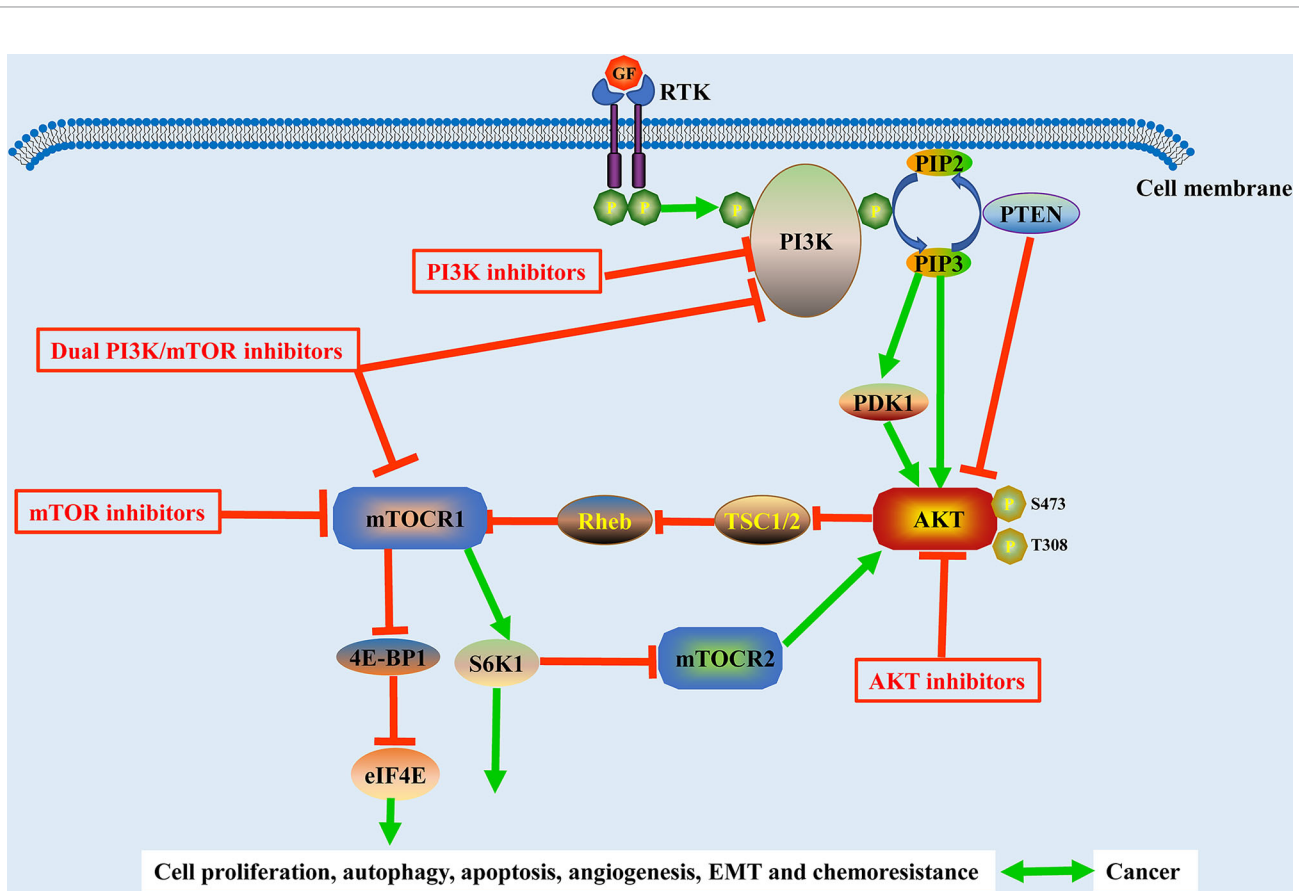

FIGURE 3 | Schematic representation of the PI3K/Akt/mTOR pathway and its related inhibitors in solid tumors. The activation of the PI3K/Akt/mTOR pathway is associated with cell proliferation, autophagy, apoptosis, angiogenesis, EMT, and chemoresistance in solid tumors. GF, growth factor; EMT, epithelial-to-mesenchymal transition; RTK, tyrosine kinase receptor.

of Wortmannin, is a physiologically stable pan-PI3K inhibitor that targets the PI3K pathway and has shown improved antineoplastic activity and favorable pharmacokinetic properties in a variety of tumors (88). In glioblastoma, blockage of the PI3K pathway by PX-866 results in cell growth suppression and reduced stimulation of downstream pathways. PX-866 was generally well tolerated. However, it failed to achieve the efficacy endpoints. 21% of individuals with recurrent glioblastoma had sustained stable disease. However, there are no biomarkers that can distinguish participants (89). Buparlisib (NVP-BKM120) is a pan-PI3K inhibitor targeting all class I PI3K isoforms. Based on the safety profile of buparlisib with fulvestrant in the BELLE-3 trial, further studies on buparlisib with fulvestrant in postmenopausal, hormone-receptor-positive, HER2-negative, advanced breast cancer patients pretreated with endocrine treatment and mTOR inhibitors are not recommended. However, the efficacy of buparlisib with fulvestrant supports the use of PI3K inhibitors combined with endocrine therapy in individuals with PIK3CA mutations, indicating that PIK3CA mutations may be a biomarker of PI3K inhibitor efficacy (90). Buparlisib had limited single-agent efficacy in PI3K-activated recurrent glioblastoma. The lack of efficacy of buparlisib was attributed to inadequate blockage of the PI3K pathway, despite the drug's substantial brain penetration. Further studies on PI3K inhibitors with more pathway blocking are needed (91). In the BERIL-1 study, patients with relapsed or metastatic head and neck squamous cell carcinoma treated with buparlisib in combination with paclitaxel had a median progression-free survival of 1.1 months longer than those treated with placebo plus paclitaxel (4.6 months *vs.* 3.5 months). Although the adverse events were considered manageable, patients treated with buparlisib plus paclitaxel had more grade 3 or 4 adverse events. Buparlisib plus paclitaxel seemed to be an effective second-line therapy for patients with platinum-pretreated recurrent or metastatic head and neck squamous cell carcinoma (92). In 2017, the Food and Drug Administration (FDA) granted approval to copanlisib (a pan-PI3K inhibitor) based on results from the CHRONOS-1 trial for the treatment of adult patients with recurrent follicular lymphoma who have undergone at least two previous systemic therapies (93). In addition to PX-866, buparlisib, and copanlisib, other pan-PI3K inhibitors include CH5132799, pilaralisib, ZSTK474, sonolisib, pictilisib, B591, TG-100-115, and RIDR-PI-103. Further clinical trials are needed to evaluate the efficacy of pan-PI3K inhibitors in solid tumors. The wide activity of pan-PI3K inhibitor may increase the risk of adverse effects and toxicity.

Isoform-selective PI3K inhibitors targeting one of the PI3K isoforms have enhanced, precise targeting and decreased toxicity compared with pan-PI3K inhibitors. Isoform-specific PI3K inhibitors may need appropriate patient identification according to sensitivity and resistance markers. In 2014, Idelalisib (a PI3Kδ inhibitor) is approved by the FDA for the treatment of chronic lymphocytic leukemia, relapsed follicular B-cell non-Hodgkin lymphoma, and relapsed small lymphocytic lymphoma (94). In 2018, the FDA approved duvelisib (an isoform-specific inhibitor targeting PI3Kγ and PI3Kδ) based on results from the DUO and DYNAMO for adult patients with relapsed or refractory chronic lymphocytic leukemia or small lymphocytic lymphoma after more than two previous therapies (95, 96). In 2019, the FDA approved alpelisib (a PI3Kα inhibitor) in combination with fulvestrant for postmenopausal women, and men, with hormone receptor-positive, human epidermal growth factor receptor 2 -negative, PIK3CA-mutated, advanced or metastatic breast cancer based on the results from the SOLAR-1 trial (97). According to the results of the CBYL719X2101 trial, alpelisib exhibited an acceptable safety and promising antitumor activity in patients with PIK3CA-mutant malignancies, indicating that selective PI3K inhibitors in conjunction with additional antineoplastic drugs may be effective for the treatment of PIK3CA-mutant malignancies (98). In 2021, the FDA approved umbralisib (a PI3Kδ/CK1ϵ inhibitor) for the treatment of marginal zone lymphoma and follicular lymphoma based on the results from the UTX-TGR-205 trial (99). In addition to idelalisib (δ), alpelisib (α), duvelisib (δ/γ), and umbralisib (δ), other isoform-selective PI3K inhibitors include serabelisib (a PI3Kα inhibitor), GSK2636771 (a PI3Kβ inhibitor), Zandelisib (a PI3Kδ inhibitor), AMG319 (a PI3Kδ inhibitor), linperlisib (a PI3Kδ inhibitor), parsaclisib (a PI3Kδ inhibitor), leniolisib (a PI3Kδ inhibitor), eganelisib (a PI3Kγ inhibitor), tenalisib (a PI3Kδ/γ inhibitor), taselisib (a PI3Kα/δ/γ inhibitor), AZD8186 (a PI3Kβ/δ inhibitor), and AZD8835 (a PI3Kδ/α inhibitor).

Akt Inhibitors

AKT, an effector of the PI3K/AKT/mTOR pathway to activate tumors, is a promising target. The Akt kinase family comprises the AKT1, AKT2, and AKT3 isoforms. AKT activity is controlled in an Akt-dependent manner *via* phosphorylation and dephosphorylation. Akt inhibitors have been classified into three categories depending on how they impede Akt activity. ATP-competitive inhibitors reduce the phosphorylation of Akt by competing with ATP. Allosteric inhibitors prevent Akt from interacting with its substrate by causing conformational transitions in enzymic structure. Irreversible inhibitors are another less common type of Akt inhibitor. ATP-competitive inhibitors (GSK690693, ipatasertib, uprosertib, and capivasertib) and allosteric inhibitors (MK-2206) have demonstrated the more potent inhibition of Akt in malignant cells. ATP-competitive inhibitors attach to the active conformation of Akt, in which the pleckstrin homology (PH) domain has swung away from the kinase domain and exposed the ATP-binding pocket, thereby blocking the activity of Akt. Allosteric inhibitors can impede the localization of AKT to the plasma membrane and prevent the phosphorylation and activation of AKT.

In the EAY131-Y trial, the objective response rate of single-agent capivasertib (AZD5363) was 28.6% (N=35) in patients with an AKT1 E17K-mutated tumor. One patient with endometrioid endometrial cancer had a complete response and was still on treatment after 35.6 months. Moreover, 46% (N=35) of patients had stable disease, and 6% (N=35) of patients had progressive disease, suggesting that capivasertib shows clinically substantial efficacy in refractory malignant tumors (100). Adding

pan-AKT inhibitor capivasertib to docetaxel and prednisolone did not improve a composite progression-free survival in metastatic castration-resistant prostate cancer regardless of whether the PI3K/AKT/PTEN pathway was activated or not in the ProCAID trial (101). After a median follow-up of 4.9 months, median progression-free survival was 10.3 months for patients with metastatic, estrogen-receptor-positive breast cancer treated with capivasertib plus fulvestrant compared with 4.8 months for patients treated with fulvestrant plus placebo in the FAKTION trial (102). The combination of capivasertib and paclitaxel for metastatic triple-negative breast cancer can contribute to significantly prolonged progression-free survival (5.9 months *vs*. 4.2 months) and overall survival (19.1 months *vs*. 12.6 months) compared with paclitaxel plus placebo in the PAKT trial. The results suggested that capivasertib plus paclitaxel has potential as a first-line treatment for metastatic triple-negative breast cancer. In PIK3CA/AKT1/PTEN-altered patients, median progression-free survival with capivasertib plus paclitaxel was 9.3 months while placebo plus paclitaxel was only 3.7 months. Severe adverse events (grade 3-4) were more common in patients treated with capivasertib plus paclitaxel ($P < 0.01$). The most common adverse events with capivasertib plus paclitaxel versus paclitaxel plus placebo were diarrhea (13% *vs*. 1%), infection (4% *vs*. 1%), neutropenia (3% *vs*. 3%), rash (4% *vs*. 0%), and fatigue (4% *vs*. 0%) (103).

Targeting AKT signaling ipatasertib (GDC-0068) exhibited an acceptable safety profile and significant disease control in patients with AKT-activated solid tumors (104). After a median follow-up of 19 months, the inhibition of PI3K/AKT and androgen-receptor dual pathways by ipatasertib (an ATP-competitive AKT inhibitor) plus abiraterone can improve the median radiographical progression-free survival of metastatic prostate cancer patients with PTEN loss compared with placebo plus abiraterone (18·5 months *vs*. 16·5 months) in the IPATential150 trial. 39% (21/546) of patients treated with the placebo plus abiraterone and 70% (386/551) of patients treated with ipatasertib plus abiraterone experienced grade 3 or higher adverse events. Adverse events led to drug discontinuation in 5% (28/546) of patients treated with the placebo plus abiraterone and 21% (116/551) of patients treated with ipatasertib plus abiraterone (105). In the intention-to-treat population, the combination of ipatasertib and paclitaxel for triple-negative breast cancer can result in significantly prolonged median progression-free survival compared with paclitaxel plus placebo (6.2 months *vs*. 4.9 months) in the LOTUS trial. Median progression-free survival in PTEN-low patients with ipatasertib plus paclitaxel was 6.2 months compared to placebo plus paclitaxel in 3.7 months. Serious adverse events occurred in 28% (17/61) of patients in the ipatasertib plus paclitaxel group and 42% (26/62) of patients in the placebo plus paclitaxel group. The ipatasertib plus paclitaxel group was mainly associated with severe adverse reactions related to infections and gastrointestinal effects, while the placebo plus paclitaxel group was mainly associated with severe adverse reactions related to infections (106).

In the I-SPY 2 trial, MK-2206 (an allosteric inhibitor) combined with standard neoadjuvant chemotherapy contributed to higher pathologic complete response rates in human epidermal growth factor receptor 2 (HER2)-positive, hormone receptor (HR)-negative early-stage breast cancer. Substantial skin adverse reactions are observed, but adverse events, such as rash, can be controlled. Although MK-2206 is not currently being explored further in breast cancer, this type of Akt inhibitor is still promising for clinical use (107).

mTOR Inhibitors

The mTOR kinase family mainly consists of three functional components: mTOR1, mTOR2, and mTOR3. mTOR1 and mTOR2 are linked with cancer. mTORC1 serves as a downstream effector for several commonly disrupted oncogenic pathways, including the PI3K/AKT and MAPK pathways, and the mTOR pathway is overactive in various tumor types, making mTOR a target for cancer treatment. mTOR inhibitors are a type of drug that works by selectively inhibiting mTOR activity. Generally, mTOR inhibitors are classified into two categories: rapamycin and its analogs (rapalogs), and ATP-competitive mTOR kinase inhibitors. The former is capable of suppressing mTORC1, and the latter can suppress mTORC1/2.

Rapamycin (Sirolimus), a rapalog, was initially used as an immunosuppressant in patients experiencing organ transplantation and it also has anti-proliferative properties. A phase I/II study of pemetrexed in combination with sirolimus in recurrent, metastatic non-small cell lung cancer revealed synergistic benefits when sirolimus was added to pemetrexed (108). In 2007, temsirolimus (CCI-779) was the first rapalog to be approved by the Food and Drug Administration (FDA) for the treatment of advanced renal cell carcinoma (109). FDA approves everolimus (a rapalog) for treatment of various diseases, such as renal cell carcinoma, progressive neuroendocrine tumors of pancreatic origin (PNET), postmenopausal women with advanced hormone receptor-positive, HER2-negative breast cancer, neuroendocrine tumors (NET) of gastrointestinal (GI) or lung origin, tuberous sclerosis complex (TSC)-associated partial-onset seizures, TSC-associated subependymal giant cell astrocytoma (SEGA) and TSC-associated renal angiomyolipoma. In the MIRACLE study, the progression-free survival of patients with HR-positive, ERBB2-negative premenopausal advanced breast cancer treated with everolimus plus letrozole was substantially longer than that of patients treated with letrozole (19.4 months *vs*. 12.9 months; P=0.008), suggesting the effectiveness of everolimus among patients who experienced disease progression and took the same endocrine therapy (110). Compared to fulvestrant plus vistusertib (a dual mTORC1 and mTORC2 inhibitor) or fulvestrant alone, the combination of fulvestrant and everolimus (a mTORC1 inhibitor) resulted in a substantially longer progression-free survival in patients with hormone receptor-positive metastatic breast cancer. Adding vistusertib to fulvestrant failed to show a benefit in the MANTA study (111). In the AcSé-ESMART trial, the CDK4/6 inhibitor ribociclib combined with topotecan and temozolomide (TOTEM) or everolimus was well-tolerated in children with advanced malignancies (112).

The development of resistance to rapamycin analogs seems inevitable due to compensatory activation of the PI3K/Akt pathway. Several drugs have been developed as ATP competitors that block the catalytic activity of mTOR to overcome the ineffectiveness of rapamycin in antitumor therapy. Researchers are now focused on developing mTORC1/2 complex inhibitors such as vistusertib (AZD2014), sapanisertib (TAK-228), AZD8055, and PP242 to overcome this shortcoming of rapamycin analogs (113). 118 postmenopausal women with hormone receptor-positive, human epidermal growth factor receptor 2 negative advanced/metastatic breast cancer participated in a phase IB/II study (NCT02049957) in which the safety, tolerability, and antitumor activity of sapanisertib plus exemestane or fulvestrant were assessed. The combination of sapanisertib with exemestane or fulvestrant has a maximum tolerable dosage of 4 mg once daily. Sapanisertib plus exemestane or fulvestrant showed therapeutic benefit in postmenopausal women with pretreatment everolimus-sensitive or everolimus-resistant breast cancer with clinical benefit rate at 16 weeks (CBR-16) of 45% versus 23% in everolimus-sensitive versus everolimus-resistant subgroups. Molecular analysis revealed a positive correlation between the presence of an AKT1 mutation and improved effectiveness (114). In comparison to the combination of fulvestrant and vistusertib, or to fulvestrant alone, fulvestrant with everolimus showed a substantially longer progression-free survival in patients with hormone receptor-positive metastatic breast cancer. The addition of the dual mTORC1 and mTORC2 inhibitor vistusertib to fulvestrant failed to show any advantage in the MANTA trial (111). Besides, vistusertib was well tolerated in children with advanced malignancies. However, the study arms were discontinued due to the lack of tumor responses and a failure to engage the target (113). Nonetheless, dual mTORC1 and mTORC2 inhibitors targeting the PI3K/AKT/mTOR pathway in the treatment of malignant tumors are still being investigated.

Dual PI3K/mTOR Inhibitors

Dual PI3K/mTOR inhibitors interact with the ATP-binding cleft of both PI3K and mTOR, reducing the kinase activity of both enzymes and impacting pathway activities more effectively than mTOR kinase inhibitors alone. Dual PI3K/mTOR inhibitors have shown some promise in the early-stage trial. Additional research is required to establish whether dual PI3K/mTOR inhibitors are more effective than mTOR inhibitors. Dual PI3K/mTOR inhibitors such as dactolisib (BEZ235), apitolisib (GDC-0980), gedatolisib (PF-05212384), bimiralisib (PQR309), paxalisib (GDC-0084), and voxtalisib (SAR245409, XL765) have shown substantial anticancer efficacy in various tumor xenografts (9, 115–117).

Treatment with dactolisib (BEZ235), when compared to everolimus, has not been shown to improve effectiveness in patients with advanced pancreatic neuroendocrine tumors who have not previously received mTOR inhibitor treatment, and it may have a worse tolerability profile. The limited effectiveness and poor tolerability of dual PI3K/mTOR inhibitors may restrict their potential for clinical applications (118). In a phase Ib trial (NCT01634061), individuals with castration-resistant prostate cancer were administered dactolisib (BEZ235) plus abiraterone acetate. Eighteen individuals (N=25) were randomized to receive dactolisib plus abiraterone acetate at the first dosage level (200 mg bid) in the dactolisib plus abiraterone acetate arm (NCT01634061). Five dose-limiting toxicities were found in nine individuals. Dactolisib plus abiraterone acetate in castration-resistant prostate cancer will not be studied further due to the available pharmacokinetics, safety, and effectiveness evidence (119). A phase Ib dose-escalation trial (NCT01508104) showed that dactolisib with everolimus was neither efficacious nor tolerable enough in patients with advanced malignancies. Systemic exposure to dactolisib increased in a dose-proportional manner, whereas oral bioavailability was poor, perhaps due to gastrointestinal toxicity (120). Additionally, the combination of gedatolisib (dual PI3K/mTOR inhibitor) with carboplatin and paclitaxel was tolerated in patients with advanced solid tumors, and preliminary effectiveness was seen particularly in clear cell ovarian cancer in a phase I dose-escalation trial (121). In a phase II study (MAGGIE), the efficacy of apitolisib (a dual PI3K/mTOR inhibitor) was assessed in patients with advanced endometrial cancer. The anticancer efficacy observed with apitolisib was restricted by its tolerability. A comprehensive molecular profile revealed that 57% (N=46) of patients had at least one PIK3CA, PTEN, or AKT1 mutation. Each of the three individuals who had a confirmed response had at least one PI3K pathway gene mutation, indicating that patients with mutations in the PI3K pathway may have benefited more with apitolisib. The most common grade 3 or higher adverse events were rash (maculopapular, acneiform). Two serious adverse events due to grade 3 rash were associated with MK-2206 (122). In addition, enrichment for PI3K pathway biomarkers may be beneficial for future research of more selective inhibitors in PI3K/mTOR signaling.

CONCLUSION AND PROSPECT

Multiple studies have revealed significant genetic alterations in cancer cases. Due to the heterogeneity and complexity of tumors, the mechanism of carcinogenesis remains undetermined. Targeted treatment is developed as an evolving strategy to improve the survival of cancer patients. The PI3K/AKT/mTOR pathway is the most commonly disrupted in cancer. This hyperactive pathway offers possibilities and opportunities for drug research and discovery. The previous studies have exhibited that significant PI3K/AKT/mTOR axis is significantly altered in cancer and targeting this axis with multiple inhibitors can modulate a variety of cellular processes such as cell proliferation, autophagy, apoptosis, angiogenesis, EMT, and chemoresistance. Pharmaceutical research has contributed to the development of various types of inhibitors that target distinct components of this axis. mTOR inhibitors, PI3K inhibitors, Akt inhibitors, and dual PI3K/mTOR inhibitors have all been studied as monotherapy or in combination with other inhibitors in the treatment and prevention of cancer. Despite substantial advancements, effective management of

cancer remains a challenge due to the heterogeneity of cancer and proper patient identification for targeted therapy.

There are still many issues in this review that deserve attention or need to be further explored. For example, most of the data on precision medicine come from developed countries in Europe and the United States, while data from other regions, such as Asia, are relatively rare. Differences in data on precision medicine from different populations need to be explored more widely. Besides, multiple TCGA datasets included more primary tumors, and the genetic profiles of primary tumors may differ from those of advanced or metastatic tumors. Moreover, combination with PARP inhibitors or immune checkpoint inhibitors is a promising direction that needs further exploration. Additionally, multiple combinations of targeted therapy strategies are appropriate only for specific cancer types. For example, dactolisib plus abiraterone acetate (a CYP17 inhibitor) is mainly used to treat castration-resistant prostate cancer. Capivasertib plus fulvestrant (an estrogen receptor antagonist) is primarily used to treat metastatic, estrogen-receptor-positive breast cancer. Furthermore, PI3K/AKT/mTOR inhibitor resistance and its mechanism need to be further elucidated.

Targeted therapy targeting the PI3K/AKT/mTOR pathway may produce a variety of adverse reactions and is prone to progress due to drug resistance. Tumor-specific research should be a severe issue, and appropriate dosing regimens need to be explored to make PI3K/AKT/mTOR inhibitors more tolerable and efficient. Increasing the number of clinical studies is an effective way to tailor treatments for cancer patients. Further research is needed to uncover the resistance mechanisms of PI3K/AKT/mTOR inhibitors, explore how to overcome resistance to PI3K/AKT/mTOR inhibitors, and develop new, more rational therapeutic combinations.

AUTHOR CONTRIBUTIONS

YP, YW, CZ, WM, and CCZ designed the study and supervised. YP, CZ, and YW collected data. YP performed statistical analysis. YP, WM, and YW interpreted data and drafted the manuscript. CCZ contributed to administrative and technical and material support. All authors contributed to the article and approved the submitted version.

FUNDING

This work was supported by the National Natural Science Foundation of China (81660755); and the Science and Technology Project of Shenzhen of China (JCYJ20170307160524377 and JCYJ20190808162605484).

REFERENCES

1. Foster KG, Fingar DC. Mammalian Target of Rapamycin (mTOR): Conducting the Cellular Signaling Symphony. *J Biol Chem* (2010) 285 (19):14071–7. doi: 10.1074/jbc.R109.094003
2. Kim LC, Cook RS, Chen J. Mtorc1 and Mtorc2 in Cancer and the Tumor Microenvironment. *Oncogene* (2017) 36(16):2191–201. doi: 10.1038/onc.2016.363
3. Lee BJ, Boyer JA, Burnett GL, Thottumkara AP, Tibrewal N, Wilson SL, et al. Selective Inhibitors of Mtorc1 Activate 4EBP1 and Suppress Tumor Growth. *Nat Chem Biol* (2021) 17(10):1065–74. doi: 10.1038/s41589-021-00813-7
4. Luciani A, Stagi M. How Mtorc1 Makes Sense of Nutrients. *Kidney Int* (2021) 99(2):295–8. doi: 10.1016/j.kint.2020.07.052
5. Wipperman MF, Montrose DC, Gotto AM Jr, Hajjar DP. Mammalian Target of Rapamycin: A Metabolic Rheostat for Regulating Adipose Tissue Function and Cardiovascular Health. *Am J Pathol* (2019) 189(3):492–501. doi: 10.1016/j.ajpath.2018.11.013
6. Li H, Prever L, Hirsch E, Gulluni F. Targeting PI3K/AKT/mTOR Signaling Pathway in Breast Cancer. *Cancers (Basel)* (2021) 13(14):3517. doi: 10.3390/cancers13143517
7. Pungsrinont T, Kallenbach J, Baniahmad A. Role of PI3K-AKT-mTOR Pathway as a Pro-Survival Signaling and Resistance-Mediating Mechanism to Therapy of Prostate Cancer. *Int J Mol Sci* (2021) 22(20):11088. doi: 10.3390/ijms222011088
8. Martorana F, Motta G, Pavone G, Motta L, Stella S, Vitale SR, et al. AKT Inhibitors: New Weapons in the Fight Against Breast Cancer? *Front Pharmacol* (2021) 12:662232. doi: 10.3389/fphar.2021.662232
9. Vanhaesebroeck B, Perry MWD, Brown JR, Andre F, Okkenhaug K. PI3K Inhibitors are Finally Coming of Age. *Nat Rev Drug Discov* (2021) 20 (10):741–69. doi: 10.1038/s41573-021-00209-1
10. Hua H, Zhang H, Chen J, Wang J, Liu J, Jiang Y. Targeting Akt in Cancer for Precision Therapy. *J Hematol Oncol* (2021) 14(1):128. doi: 10.1186/s13045-021-01137-8
11. Khorasani ABS, Pourbagheri-Sigaroodi A, Pirsalehi A, Safaroghli-Azar A, Zali MR, Bashash D. The PI3K/Akt/mTOR Signaling Pathway in Gastric Cancer; From Oncogenic Variations to the Possibilities for Pharmacologic Interventions. *Eur J Pharmacol* (2021) 898:173983. doi: 10.1016/j.ejphar.2021.173983
12. Fusco N, Sajjadi E, Venetis K, Gaudioso G, Lopez G, Corti C, et al. PTEN Alterations and Their Role in Cancer Management: Are We Making Headway on Precision Medicine? *Genes (Basel)* (2020) 11(7):719. doi: 10.3390/genes11070719
13. Yip HYK, Papa A. Signaling Pathways in Cancer: Therapeutic Targets, Combinatorial Treatments, and New Developments. *Cells* (2021) 10(3):659. doi: 10.3390/cells10030659
14. Hoxhaj G, Manning BD. The PI3K-AKT Network at the Interface of Oncogenic Signalling and Cancer Metabolism. *Nat Rev Cancer* (2020) 20 (2):74–88. doi: 10.1038/s41568-019-0216-7
15. Harsha C, Banik K, Ang HL, Girisa S, Vikkurthi R, Parama D, et al. Targeting AKT/mTOR in Oral Cancer: Mechanisms and Advances in Clinical Trials. *Int J Mol Sci* (2020) 21(9):3285. doi: 10.3390/ijms21093285
16. Duan Y, Haybaeck J, Yang Z. Therapeutic Potential of PI3K/AKT/mTOR Pathway in Gastrointestinal Stromal Tumors: Rationale and Progress. *Cancers (Basel)* (2020) 12(10):2972. doi: 10.3390/cancers12102972
17. Iksen, Pothongsrisit S, Pongrakhananon V. Targeting the PI3K/AKT/mTOR Signaling Pathway in Lung Cancer: An Update Regarding Potential Drugs and Natural Products. *Molecules* (2021) 26(13):4100. doi: 10.3390/molecules26134100
18. Zhong L, Li Y, Xiong L, Wang W, Wu M, Yuan T, et al. Small Molecules in Targeted Cancer Therapy: Advances, Challenges, and Future Perspectives. *Signal Transduct Target Ther* (2021) 6(1):201. doi: 10.1038/s41392-021-00572-w
19. Bader AG, Kang S, Zhao L, Vogt PK. Oncogenic PI3K Deregulates Transcription and Translation. *Nat Rev Cancer* (2005) 5(12):921–9. doi: 10.1038/nrc1753
20. Gao J, Aksoy BA, Dogrusoz U, Dresdner G, Gross B, Sumer SO, et al. Integrative Analysis of Complex Cancer Genomics and Clinical Profiles

Using the Cbioportal. *Sci Signal* (2013) 6(269):pl1. doi: 10.1126/scisignal.2004088
21. Cerami E, Gao J, Dogrusoz U, Gross BE, Sumer SO, Aksoy BA, et al. The Cbio Cancer Genomics Portal: An Open Platform for Exploring Multidimensional Cancer Genomics Data. *Cancer Discov* (2012) 2(5):401–4. doi: 10.1158/2159-8290.CD-12-0095
22. Zehir A, Benayed R, Shah RH, Syed A, Middha S, Kim HR, et al. Mutational Landscape of Metastatic Cancer Revealed From Prospective Clinical Sequencing of 10,000 Patients. *Nat Med* (2017) 23(6):703–13. doi: 10.1038/nm.4333
23. Robinson DR, Wu YM, Lonigro RJ, Vats P, Cobain E, Everett J, et al. Integrative Clinical Genomics of Metastatic Cancer. *Nature* (2017) 548 (7667):297–303. doi: 10.1038/nature23306
24. Bolton KL, Ptashkin RN, Gao T, Braunstein L, Devlin SM, Kelly D, et al. Cancer Therapy Shapes the Fitness Landscape of Clonal Hematopoiesis. *Nat Genet* (2020) 52(11):1219–26. doi: 10.1038/s41588-020-00710-0
25. Martinez-Saez O, Chic N, Pascual T, Adamo B, Vidal M, Gonzalez-Farre B, et al. Frequency and Spectrum of PIK3CA Somatic Mutations in Breast Cancer. *Breast Cancer Res* (2020) 22(1):45. doi: 10.1186/s13058-020-01284-9
26. Dogruluk T, Tsang YH, Espitia M, Chen F, Chen T, Chong Z, et al. Identification of Variant-Specific Functions of PIK3CA by Rapid Phenotyping of Rare Mutations. *Cancer Res* (2015) 75(24):5341–54. doi: 10.1158/0008-5472.CAN-15-1654
27. Ng PK, Li J, Jeong KJ, Shao S, Chen H, Tsang YH, et al. Systematic Functional Annotation of Somatic Mutations in Cancer. *Cancer Cell* (2018) 33(3):450–62.e10. doi: 10.1016/j.ccell.2018.01.021
28. Gonzalez-Angulo AM, Chen H, Karuturi MS, Chavez-MacGregor M, Tsavachidis S, Meric-Bernstam F, et al. Frequency of Mesenchymal-Epithelial Transition Factor Gene (MET) and the Catalytic Subunit of Phosphoinositide-3-Kinase (PIK3CA) Copy Number Elevation and Correlation With Outcome in Patients With Early Stage Breast Cancer. *Cancer* (2013) 119(1):7–15. doi: 10.1002/cncr.27608
29. Zhang Y, Kwok-Shing Ng P, Kucherlapati M, Chen F, Liu Y, Tsang YH, et al. A Pan-Cancer Proteogenomic Atlas of PI3K/AKT/mTOR Pathway Alterations. *Cancer Cell* (2017) 31(6):820–32.e3. doi: 10.1016/j.ccell.2017.04.013
30. Kong Y, Si L, Li Y, Wu X, Xu X, Dai J, et al. Analysis of mTOR Gene Aberrations in Melanoma Patients and Evaluation of Their Sensitivity to PI3K-AKT-mTOR Pathway Inhibitors. *Clin Cancer Res* (2016) 22(4):1018–27. doi: 10.1158/1078-0432.CCR-15-1110
31. Brugarolas J. Molecular Genetics of Clear-Cell Renal Cell Carcinoma. *J Clin Oncol* (2014) 32(18):1968–76. doi: 10.1200/JCO.2012.45.2003
32. Moura AC, Assad DX, Amorim Dos Santos J, Porto de Toledo I, Barra GB, Castilho RM, et al. Worldwide Prevalence of PI3K-AKT-mTOR Pathway Mutations in Head and Neck Cancer: A Systematic Review and Meta-Analysis. *Crit Rev Oncol Hematol* (2021) 160:103284. doi: 10.1016/j.critrevonc.2021.103284
33. Kandoth C, McLellan MD, Vandin F, Ye K, Niu B, Lu C, et al. Mutational Landscape and Significance Across 12 Major Cancer Types. *Nature* (2013) 502(7471):333–9. doi: 10.1038/nature12634
34. Murugan AK, Alzahrani A, Xing M. Mutations in Critical Domains Confer the Human mTOR Gene Strong Tumorigenicity. *J Biol Chem* (2013) 288 (9):6511–21. doi: 10.1074/jbc.M112.399485
35. Manning BD, Toker A. AKT/PKB Signaling: Navigating the Network. *Cell* (2017) 169(3):381–405. doi: 10.1016/j.cell.2017.04.001
36. Vivanco I, Sawyers CL. The Phosphatidylinositol 3-Kinase AKT Pathway in Human Cancer. *Nat Rev Cancer* (2002) 2(7):489–501. doi: 10.1038/nrc839
37. Parikh C, Janakiraman V, Wu WI, Foo CK, Kljavin NM, Chaudhuri S, et al. Disruption of PH-Kinase Domain Interactions Leads to Oncogenic Activation of AKT in Human Cancers. *Proc Natl Acad Sci USA* (2012) 109(47):19368–73. doi: 10.1073/pnas.1204384109
38. Rudolph M, Anzeneder T, Schulz A, Beckmann G, Byrne AT, Jeffers M, et al. AKT1 (E17K) Mutation Profiling in Breast Cancer: Prevalence, Concurrent Oncogenic Alterations, and Blood-Based Detection. *BMC Cancer* (2016) 16:622. doi: 10.1186/s12885-016-2626-1
39. Beaver JA, Gustin JP, Yi KH, Rajpurohit A, Thomas M, Gilbert SF, et al. PIK3CA and AKT1 Mutations Have Distinct Effects on Sensitivity to Targeted Pathway Inhibitors in an Isogenic Luminal Breast Cancer Model System. *Clin Cancer Res* (2013) 19(19):5413–22. doi: 10.1158/1078-0432.CCR-13-0884
40. Chen Y, Huang L, Dong Y, Tao C, Zhang R, Shao H, et al. Effect of AKT1 (P. E17K) Hotspot Mutation on Malignant Tumorigenesis and Prognosis. *Front Cell Dev Biol* (2020) 8:573599. doi: 10.3389/fcell.2020.573599
41. Sharma M, Dey CS. Role of Akt Isoforms in Neuronal Insulin Signaling and Resistance. *Cell Mol Life Sci* (2021) 78(23):7873–98. doi: 10.1007/s00018-021-03993-6
42. Pereira L, Horta S, Mateus R, Videira MA. Implications of Akt2/Twist Crosstalk on Breast Cancer Metastatic Outcome. *Drug Discov Today* (2015) 20(9):1152–8. doi: 10.1016/j.drudis.2015.06.010
43. Song MS, Salmena L, Pandolfi PP. The Functions and Regulation of the PTEN Tumour Suppressor. *Nat Rev Mol Cell Biol* (2012) 13(5):283–96. doi: 10.1038/nrm3330
44. Xie P, Peng Z, Chen Y, Li H, Du M, Tan Y, et al. Neddylation of PTEN Regulates its Nuclear Import and Promotes Tumor Development. *Cell Res* (2021) 31(3):291–311. doi: 10.1038/s41422-020-00443-z
45. Hollander MC, Blumenthal GM, Dennis PA. PTEN Loss in the Continuum of Common Cancers, Rare Syndromes and Mouse Models. *Nat Rev Cancer* (2011) 11(4):289–301. doi: 10.1038/nrc3037
46. Moliere S, Mathelin C. The Cowden Syndrome. *N Engl J Med* (2020) 382 (15):e29. doi: 10.1056/NEJMicm1910478
47. Alexa M, Hasenburg A, Battista MJ. The TCGA Molecular Classification of Endometrial Cancer and Its Possible Impact on Adjuvant Treatment Decisions. *Cancers (Basel)* (2021) 13(6):1478. doi: 10.3390/cancers13061478
48. Choi SW, Lee Y, Shin K, Koo H, Kim D, Sa JK, et al. Mutation-Specific Non-Canonical Pathway of PTEN as a Distinct Therapeutic Target for Glioblastoma. *Cell Death Dis* (2021) 12(4):374. doi: 10.1038/s41419-021-03657-0
49. Wang C, Feng Y, Zhang C, Cheng D, Wu R, Yang Y, et al. PTEN Deletion Drives Aberrations of DNA Methylome and Transcriptome in Different Stages of Prostate Cancer. *FASEB J* (2020) 34(1):1304–18. doi: 10.1096/fj.201901205RR
50. Ma J, Benitez JA, Li J, Miki S, Ponte de Albuquerque C, Galatro T, et al. Inhibition of Nuclear PTEN Tyrosine Phosphorylation Enhances Glioma Radiation Sensitivity Through Attenuated DNA Repair. *Cancer Cell* (2019) 35(3):504–18.e7. doi: 10.1016/j.ccell.2019.01.020
51. Tian T, Li X, Zhang J. mTOR Signaling in Cancer and mTOR Inhibitors in Solid Tumor Targeting Therapy. *Int J Mol Sci* (2019) 20(3):755. doi: 10.3390/ijms20030755
52. Mange A, Coyaud E, Desmetz C, Laurent E, Beganton B, Coopman P, et al. FKBP4 Connects Mtorc2 and PI3K to Activate the PDK1/Akt-Dependent Cell Proliferation Signaling in Breast Cancer. *Theranostics* (2019) 9 (23):7003–15. doi: 10.7150/thno.35561
53. Evangelisti C, Chiarini F, Paganelli F, Marmiroli S, Martelli AM. Crosstalks of GSK3 Signaling With the mTOR Network and Effects on Targeted Therapy of Cancer. *Biochim Biophys Acta Mol Cell Res* (2020) 1867 (4):118635. doi: 10.1016/j.bbamcr.2019.118635
54. Bian YH, Xu J, Zhao WY, Zhang ZZ, Tu L, Cao H, et al. Targeting Mtorc2 Component Rictor Inhibits Cell Proliferation and Promotes Apoptosis in Gastric Cancer. *Am J Transl Res* (2017) 9(9):4317–30.
55. Lu Z, Shi X, Gong F, Li S, Wang Y, Ren Y, et al. RICTOR/mTORC2 Affects Tumorigenesis and Therapeutic Efficacy of mTOR Inhibitors in Esophageal Squamous Cell Carcinoma. *Acta Pharm Sin B* (2020) 10(6):1004–19. doi: 10.1016/j.apsb.2020.01.010
56. Yoshida GJ. Therapeutic Strategies of Drug Repositioning Targeting Autophagy to Induce Cancer Cell Death: From Pathophysiology to Treatment. *J Hematol Oncol* (2017) 10(1):67. doi: 10.1186/s13045-017-0436-9
57. Al-Bari MAA, Xu P. Molecular Regulation of Autophagy Machinery by mTOR-Dependent and -Independent Pathways. *Ann N Y Acad Sci* (2020) 1467(1):3–20. doi: 10.1111/nyas.14305
58. Janku F, McConkey DJ, Hong DS, Kurzrock R. Autophagy as a Target for Anticancer Therapy. *Nat Rev Clin Oncol* (2011) 8(9):528–39. doi: 10.1038/nrclinonc.2011.71
59. Nowosad A, Jeannot P, Callot C, Creff J, Perchey RT, Joffre C, et al. P27 Controls Ragulator and mTOR Activity in Amino Acid-Deprived Cells to Regulate the Autophagy-Lysosomal Pathway and Coordinate Cell Cycle and

Cell Growth. *Nat Cell Biol* (2020) 22(9):1076–90. doi: 10.1038/s41556-020-0554-4
60. Cabezudo S, Sanz-Flores M, Caballero A, Tasset I, Rebollo E, Diaz A, et al. Galphaq Activation Modulates Autophagy by Promoting Mtorc1 Signaling. *Nat Commun* (2021) 12(1):4540. doi: 10.1038/s41467-021-24811-4
61. Wong RS. Apoptosis in Cancer: From Pathogenesis to Treatment. *J Exp Clin Cancer Res* (2011) 30:87. doi: 10.1186/1756-9966-30-87
62. Carneiro BA, El-Deiry WS. Targeting Apoptosis in Cancer Therapy. *Nat Rev Clin Oncol* (2020) 17(7):395–417. doi: 10.1038/s41571-020-0341-y
63. He K, Zheng X, Li M, Zhang L, Yu J. mTOR Inhibitors Induce Apoptosis in Colon Cancer Cells *via* CHOP-Dependent DR5 Induction on 4E-BP1 Dephosphorylation. *Oncogene* (2016) 35(2):148–57. doi: 10.1038/onc.2015.79
64. Nishida N, Yano H, Nishida T, Kamura T, Kojiro M. Angiogenesis in Cancer. *Vasc Health Risk Manag* (2006) 2(3):213–9. doi: 10.2147/vhrm.2006.2.3.213
65. Lugano R, Ramachandran M, Dimberg A. Tumor Angiogenesis: Causes, Consequences, Challenges and Opportunities. *Cell Mol Life Sci* (2020) 77 (9):1745–70. doi: 10.1007/s00018-019-03351-7
66. Zuazo-Gaztelu I, Casanovas O. Unraveling the Role of Angiogenesis in Cancer Ecosystems. *Front Oncol* (2018) 8:248. doi: 10.3389/fonc.2018.00248
67. Karar J, Maity A. PI3K/AKT/mTOR Pathway in Angiogenesis. *Front Mol Neurosci* (2011) 4:51. doi: 10.3389/fnmol.2011.00051
68. Ji L, Wu M, Li Z. Rutacecarpine Inhibits Angiogenesis by Targeting the VEGFR2 and VEGFR2-Mediated Akt/mTOR/p70s6k Signaling Pathway. *Molecules* (2018) 23(8):2047. doi: 10.3390/molecules23082047
69. Wang M, Xu Y, Wen GZ, Wang Q, Yuan SM. Rapamycin Suppresses Angiogenesis and Lymphangiogenesis in Melanoma by Downregulating VEGF-A/VEGFR-2 and VEGF-C/VEGFR-3 Expression. *Onco Targets Ther* (2019) 12:4643–54. doi: 10.2147/OTT.S205160
70. Kim K, Kim IK, Yang JM, Lee E, Koh BI, Song S, et al. SoxF Transcription Factors Are Positive Feedback Regulators of VEGF Signaling. *Circ Res* (2016) 119(7):839–52. doi: 10.1161/CIRCRESAHA.116.308483
71. Roche J. The Epithelial-To-Mesenchymal Transition in Cancer. *Cancers (Basel)* (2018) 10(2):52. doi: 10.3390/cancers10020052
72. Yang J, Antin P, Berx G, Blanpain C, Brabletz T, Bronner M, et al. Guidelines and Definitions for Research on Epithelial-Mesenchymal Transition. *Nat Rev Mol Cell Biol* (2020) 21(6):341–52. doi: 10.1038/s41580-020-0237-9
73. Chen HT, Liu H, Mao MJ, Tan Y, Mo XQ, Meng XJ, et al. Crosstalk Between Autophagy and Epithelial-Mesenchymal Transition and its Application in Cancer Therapy. *Mol Cancer* (2019) 18(1):101. doi: 10.1186/s12943-019-1030-2
74. Herrerias MM, Budinger GRS. Revisiting mTOR and Epithelial-Mesenchymal Transition. *Am J Respir Cell Mol Biol* (2020) 62(6):669–70. doi: 10.1165/rcmb.2020-0109ED
75. Annunziata MC, Parisi M, Esposito G, Fabbrocini G, Ammendola R, Cattaneo F. Phosphorylation Sites in Protein Kinases and Phosphatases Regulated by Formyl Peptide Receptor 2 Signaling. *Int J Mol Sci* (2020) 21 (11):3818. doi: 10.3390/ijms21113818
76. Karimi Roshan M, Soltani A, Soleimani A, Rezaie Kahkhaie K, Afshari AR, Soukhtanloo M. Role of AKT and mTOR Signaling Pathways in the Induction of Epithelial-Mesenchymal Transition (EMT) Process. *Biochimie* (2019) 165:229–34. doi: 10.1016/j.biochi.2019.08.003
77. Hao Y, Baker D, Ten Dijke P. TGF-Beta-Mediated Epithelial-Mesenchymal Transition and Cancer Metastasis. *Int J Mol Sci* (2019) 20(11):2767. doi: 10.3390/ijms20112767
78. Choi D, Kim CL, Kim JE, Mo JS, Jeong HS. Hesperetin Inhibit EMT in TGF-Beta Treated Podocyte by Regulation of mTOR Pathway. *Biochem Biophys Res Commun* (2020) 528(1):154–9. doi: 10.1016/j.bbrc.2020.05.087
79. Lamouille S, Connolly E, Smyth JW, Akhurst RJ, Derynck R. TGF-Beta-Induced Activation of mTOR Complex 2 Drives Epithelial-Mesenchymal Transition and Cell Invasion. *J Cell Sci* (2012) 125(Pt 5):1259–73. doi: 10.1242/jcs.095299
80. Gremke N, Polo P, Dort A, Schneikert J, Elmshauser S, Brehm C, et al. mTOR-Mediated Cancer Drug Resistance Suppresses Autophagy and Generates a Druggable Metabolic Vulnerability. *Nat Commun* (2020) 11 (1):4684. doi: 10.1038/s41467-020-18504-7
81. Murugan AK. mTOR: Role in Cancer, Metastasis and Drug Resistance. *Semin Cancer Biol* (2019) 59:92–111. doi: 10.1016/j.semcancer.2019.07.003
82. Rascio F, Spadaccino F, Rocchetti MT, Castellano G, Stallone G, Netti GS, et al. The Pathogenic Role of PI3K/AKT Pathway in Cancer Onset and Drug Resistance: An Updated Review. *Cancers (Basel)* (2021) 13(16):3949. doi: 10.3390/cancers13163949
83. Shen C, Oswald D, Phelps D, Cam H, Pelloski CE, Pang Q, et al. Regulation of FANCD2 by the mTOR Pathway Contributes to the Resistance of Cancer Cells to DNA Double-Strand Breaks. *Cancer Res* (2013) 73(11):3393–401. doi: 10.1158/0008-5472.CAN-12-4282
84. Gaur S, Chen L, Yang L, Wu X, Un F, Yen Y. Inhibitors of mTOR Overcome Drug Resistance From Topoisomerase II Inhibitors in Solid Tumors. *Cancer Lett* (2011) 311(1):20–8. doi: 10.1016/j.canlet.2011.06.005
85. Wu Q, Ma J, Wei J, Meng W, Wang Y, Shi M. FOXD1-AS1 Regulates FOXD1 Translation and Promotes Gastric Cancer Progression and Chemoresistance by Activating the PI3K/AKT/mTOR Pathway. *Mol Oncol* (2021) 15(1):299–316. doi: 10.1002/1878-0261.12728
86. Deng J, Bai X, Feng X, Ni J, Beretov J, Graham P, et al. Inhibition of PI3K/Akt/mTOR Signaling Pathway Alleviates Ovarian Cancer Chemoresistance Through Reversing Epithelial-Mesenchymal Transition and Decreasing Cancer Stem Cell Marker Expression. *BMC Cancer* (2019) 19(1):618. doi: 10.1186/s12885-019-5824-9
87. Wu J, Cheng Z, Xu X, Fu J, Wang K, Liu T, et al. Aurora-A Induces Chemoresistance Through Activation of the AKT/mTOR Pathway in Endometrial Cancer. *Front Oncol* (2019) 9:422. doi: 10.3389/fonc.2019.00422
88. Hong DS, Bowles DW, Falchook GS, Messersmith WA, George GC, O'Bryant CL, et al. A Multicenter Phase I Trial of PX-866, an Oral Irreversible Phosphatidylinositol 3-Kinase Inhibitor, in Patients With Advanced Solid Tumors. *Clin Cancer Res* (2012) 18(15):4173–82. doi: 10.1158/1078-0432.CCR-12-0714
89. Pitz MW, Eisenhauer EA, MacNeil MV, Thiessen B, Easaw JC, Macdonald DR, et al. Phase II Study of PX-866 in Recurrent Glioblastoma. *Neuro Oncol* (2015) 17(9):1270–4. doi: 10.1093/neuonc/nou365
90. Di Leo A, Johnston S, Lee KS, Ciruelos E, Lonning PE, Janni W, et al. Buparlisib Plus Fulvestrant in Postmenopausal Women With Hormone-Receptor-Positive, HER2-Negative, Advanced Breast Cancer Progressing on or After mTOR Inhibition (BELLE-3): A Randomised, Double-Blind, Placebo-Controlled, Phase 3 Trial. *Lancet Oncol* (2018) 19(1):87–100. doi: 10.1016/S1470-2045(17)30688-5
91. Wen PY, Touat M, Alexander BM, Mellinghoff IK, Ramkissoon S, McCluskey CS, et al. Buparlisib in Patients With Recurrent Glioblastoma Harboring Phosphatidylinositol 3-Kinase Pathway Activation: An Open-Label, Multicenter, Multi-Arm, Phase II Trial. *J Clin Oncol* (2019) 37 (9):741–50. doi: 10.1200/JCO.18.01207
92. Soulieres D, Faivre S, Mesia R, Remenar E, Li SH, Karpenko A, et al. Buparlisib and Paclitaxel in Patients With Platinum-Pretreated Recurrent or Metastatic Squamous Cell Carcinoma of the Head and Neck (BERIL-1): A Randomised, Double-Blind, Placebo-Controlled Phase 2 Trial. *Lancet Oncol* (2017) 18(3):323–35. doi: 10.1016/S1470-2045(17)30064-5
93. Dreyling M, Santoro A, Mollica L, Leppa S, Follows GA, Lenz G, et al. Phosphatidylinositol 3-Kinase Inhibition by Copanlisib in Relapsed or Refractory Indolent Lymphoma. *J Clin Oncol* (2017) 35(35):3898–905. doi: 10.1200/JCO.2017.75.4648
94. Brown JR, Byrd JC, Coutre SE, Benson DM, Flinn IW, Wagner-Johnston ND, et al. Idelalisib, an Inhibitor of Phosphatidylinositol 3-Kinase P110delta, for Relapsed/Refractory Chronic Lymphocytic Leukemia. *Blood* (2014) 123 (22):3390–7. doi: 10.1182/blood-2013-11-535047
95. Flinn IW, Hillmen P, Montillo M, Nagy Z, Illes A, Etienne G, et al. The Phase 3 DUO Trial: Duvelisib vs Ofatumumab in Relapsed and Refractory CLL/SLL. *Blood* (2018) 132(23):2446–55. doi: 10.1182/blood-2018-05-850461
96. Flinn IW, Miller CB, Ardeshna KM, Tetreault S, Assouline SE, Mayer J, et al. DYNAMO: A Phase II Study of Duvelisib (IPI-145) in Patients With Refractory Indolent Non-Hodgkin Lymphoma. *J Clin Oncol* (2019) 37 (11):912–22. doi: 10.1200/JCO.18.00915
97. Andre F, Ciruelos E, Rubovszky G, Campone M, Loibl S, Rugo HS, et al. Alpelisib for PIK3CA-Mutated, Hormone Receptor-Positive Advanced

Breast Cancer. *N Engl J Med* (2019) 380(20):1929–40. doi: 10.1056/NEJMoa1813904
98. Juric D, Rodon J, Tabernero J, Janku F, Burris HA, Schellens JHM, et al. Phosphatidylinositol 3-Kinase Alpha-Selective Inhibition With Alpelisib (BYL719) in PIK3CA-Altered Solid Tumors: Results From the First-In-Human Study. *J Clin Oncol* (2018) 36(13):1291–9. doi: 10.1200/JCO.2017.72.7107
99. Fowler NH, Samaniego F, Jurczak W, Ghosh N, Derenzini E, Reeves JA, et al. Umbralisib, a Dual PI3Kdelta/CK1epsilon Inhibitor in Patients With Relapsed or Refractory Indolent Lymphoma. *J Clin Oncol* (2021) 39 (15):1609–18. doi: 10.1200/JCO.20.03433
100. Kalinsky K, Hong F, McCourt CK, Sachdev JC, Mitchell EP, Zwiebel JA, et al. Effect of Capivasertib in Patients With an AKT1 E17K-Mutated Tumor: NCI-MATCH Subprotocol EAY131-Y Nonrandomized Trial. *JAMA Oncol* (2021) 7(2):271–8. doi: 10.1001/jamaoncol.2020.6741
101. Crabb SJ, Griffiths G, Marwood E, Dunkley D, Downs N, Martin K, et al. Pan-AKT Inhibitor Capivasertib With Docetaxel and Prednisolone in Metastatic Castration-Resistant Prostate Cancer: A Randomized, Placebo-Controlled Phase II Trial (ProCAID). *J Clin Oncol* (2021) 39(3):190–201. doi: 10.1200/JCO.20.01576
102. Jones RH, Casbard A, Carucci M, Cox C, Butler R, Alchami F, et al. Fulvestrant Plus Capivasertib Versus Placebo After Relapse or Progression on an Aromatase Inhibitor in Metastatic, Oestrogen Receptor-Positive Breast Cancer (FAKTION): A Multicentre, Randomised, Controlled, Phase 2 Trial. *Lancet Oncol* (2020) 21(3):345–57. doi: 10.1016/S1470-2045(19)30817-4
103. Schmid P, Abraham J, Chan S, Wheatley D, Brunt AM, Nemsadze G, et al. Capivasertib Plus Paclitaxel Versus Placebo Plus Paclitaxel As First-Line Therapy for Metastatic Triple-Negative Breast Cancer: The PAKT Trial. *J Clin Oncol* (2020) 38(5):423–33. doi: 10.1200/JCO.19.00368
104. Saura C, Roda D, Rosello S, Oliveira M, Macarulla T, Perez-Fidalgo JA, et al. A First-In-Human Phase I Study of the ATP-Competitive AKT Inhibitor Ipatasertib Demonstrates Robust and Safe Targeting of AKT in Patients With Solid Tumors. *Cancer Discov* (2017) 7(1):102–13. doi: 10.1158/2159-8290.CD-16-0512
105. Sweeney C, Bracarda S, Sternberg CN, Chi KN, Olmos D, Sandhu S, et al. Ipatasertib Plus Abiraterone and Prednisolone in Metastatic Castration-Resistant Prostate Cancer (IPATential150): A Multicentre, Randomised, Double-Blind, Phase 3 Trial. *Lancet* (2021) 398(10295):131–42. doi: 10.1016/S0140-6736(21)00580-8
106. Kim SB, Dent R, Im SA, Espie M, Blau S, Tan AR, et al. Ipatasertib Plus Paclitaxel Versus Placebo Plus Paclitaxel as First-Line Therapy for Metastatic Triple-Negative Breast Cancer (LOTUS): A Multicentre, Randomised, Double-Blind, Placebo-Controlled, Phase 2 Trial. *Lancet Oncol* (2017) 18 (10):1360–72. doi: 10.1016/S1470-2045(17)30450-3
107. Chien AJ, Tripathy D, Albain KS, Symmans WF, Rugo HS, Melisko ME, et al. MK-2206 and Standard Neoadjuvant Chemotherapy Improves Response in Patients With Human Epidermal Growth Factor Receptor 2-Positive and/or Hormone Receptor-Negative Breast Cancers in the I-SPY 2 Trial. *J Clin Oncol* (2020) 38(10):1059–69. doi: 10.1200/JCO.19.01027
108. Komiya T, Memmott RM, Blumenthal GM, Bernstein W, Ballas MS, De Chowdhury R, et al. A Phase I/II Study of Pemetrexed With Sirolimus in Advanced, Previously Treated Non-Small Cell Lung Cancer. *Transl Lung Cancer Res* (2019) 8(3):247–57. doi: 10.21037/tlcr.2019.04.19
109. Motzer RJ, Hudes GR, Curti BD, McDermott DF, Escudier BJ, Negrier S, et al. Phase I/II Trial of Temsirolimus Combined With Interferon Alfa for Advanced Renal Cell Carcinoma. *J Clin Oncol* (2007) 25(25):3958–64. doi: 10.1200/JCO.2006.10.5916
110. Fan Y, Sun T, Shao Z, Zhang Q, Ouyang Q, Tong Z, et al. Effectiveness of Adding Everolimus to the First-Line Treatment of Advanced Breast Cancer in Premenopausal Women Who Experienced Disease Progression While Receiving Selective Estrogen Receptor Modulators: A Phase 2 Randomized Clinical Trial. *JAMA Oncol* (2021) 7(10):e213428. doi: 10.1001/jamaoncol.2021.3428
111. Schmid P, Zaiss M, Harper-Wynne C, Ferreira M, Dubey S, Chan S, et al. Fulvestrant Plus Vistusertib vs Fulvestrant Plus Everolimus vs Fulvestrant Alone for Women With Hormone Receptor-Positive Metastatic Breast Cancer: The MANTA Phase 2 Randomized Clinical Trial. *JAMA Oncol* (2019) 5(11):1556–64. doi: 10.1001/jamaoncol.2019.2526
112. Bautista F, Paoletti X, Rubino J, Brard C, Rezai K, Nebchi S, et al. Phase I or II Study of Ribociclib in Combination With Topotecan-Temozolomide or Everolimus in Children With Advanced Malignancies: Arms A and B of the AcSe-ESMART Trial. *J Clin Oncol* (2021) 39(32):3546–60. doi: 10.1200/JCO.21.01152
113. Morscher RJ, Brard C, Berlanga P, Marshall LV, Andre N, Rubino J, et al. First-In-Child Phase I/II Study of the Dual Mtorc1/2 Inhibitor Vistusertib (AZD2014) as Monotherapy and in Combination With Topotecan-Temozolomide in Children With Advanced Malignancies: Arms E and F of the AcSe-ESMART Trial. *Eur J Cancer* (2021) 157:268–77. doi: 10.1016/j.ejca.2021.08.010
114. Lim B, Potter DA, Salkeni MA, Silverman P, Haddad TC, Forget F, et al. Sapanisertib Plus Exemestane or Fulvestrant in Women With Hormone Receptor-Positive/HER2-Negative Advanced or Metastatic Breast Cancer. *Clin Cancer Res* (2021) 27(12):3329–38. doi: 10.1158/1078-0432.CCR-20-4131
115. Mishra R, Patel H, Alanazi S, Kilroy MK, Garrett JT. PI3K Inhibitors in Cancer: Clinical Implications and Adverse Effects. *Int J Mol Sci* (2021) 22 (7):3464. doi: 10.3390/ijms22073464
116. Hillmann P, Fabbro D. PI3K/mTOR Pathway Inhibition: Opportunities in Oncology and Rare Genetic Diseases. *Int J Mol Sci* (2019) 20(22):5792. doi: 10.3390/ijms20225792
117. Yang J, Nie J, Ma X, Wei Y, Peng Y, Wei X. Targeting PI3K in Cancer: Mechanisms and Advances in Clinical Trials. *Mol Cancer* (2019) 18(1):26. doi: 10.1186/s12943-019-0954-x
118. Salazar R, Garcia-Carbonero R, Libutti SK, Hendifar AE, Custodio A, Guimbaud R, et al. Phase II Study of BEZ235 Versus Everolimus in Patients With Mammalian Target of Rapamycin Inhibitor-Naive Advanced Pancreatic Neuroendocrine Tumors. *Oncologist* (2018) 23 (7):766–e90. doi: 10.1634/theoncologist.2017-0144
119. Massard C, Chi KN, Castellano D, de Bono J, Gravis G, Dirix L, et al. Phase Ib Dose-Finding Study of Abiraterone Acetate Plus Buparlisib (BKM120) or Dactolisib (BEZ235) in Patients With Castration-Resistant Prostate Cancer. *Eur J Cancer* (2017) 76:36–44. doi: 10.1016/j.ejca.2017.01.024
120. Wise-Draper TM, Moorthy G, Salkeni MA, Karim NA, Thomas HE, Mercer CA, et al. A Phase Ib Study of the Dual PI3K/mTOR Inhibitor Dactolisib (BEZ235) Combined With Everolimus in Patients With Advanced Solid Malignancies. *Target Oncol* (2017) 12(3):323–32. doi: 10.1007/s11523-017-0482-9
121. Colombo I, Genta S, Martorana F, Guidi M, Frattini M, Samartzis EP, et al. Phase I Dose-Escalation Study of the Dual PI3K-Mtorc1/2 Inhibitor Gedatolisib in Combination With Paclitaxel and Carboplatin in Patients With Advanced Solid Tumors. *Clin Cancer Res* (2021) 27(18):5012–9. doi: 10.1158/1078-0432.CCR-21-1402
122. Makker V, Recio FO, Ma L, Matulonis UA, Lauchle JO, Parmar H, et al. A Multicenter, Single-Arm, Open-Label, Phase 2 Study of Apitolisib (GDC-0980) for the Treatment of Recurrent or Persistent Endometrial Carcinoma (MAGGIE Study). *Cancer* (2016) 122(22):3519–28. doi: 10.1002/cncr.30286

Conflict of Interest: The authors declare that the research was conducted in the absence of any commercial or financial relationships that could be construed as a potential conflict of interest.

frontiers in Oncology

REVIEW
published: 28 March 2022
doi: 10.3389/fonc.2022.848221

Targeting Epigenetic Regulatory Enzymes for Cancer Therapeutics: Novel Small-Molecule Epidrug Development

Ye Jin[1†], *Tianjia Liu*[1†], *Haoming Luo*[1], *Yangyang Liu*[2*] *and Da Liu*[1*]

[1] School of Pharmacy, Changchun University of Chinese Medicine, Changchun, China, [2] Affiliated Hospital of Changchun University of Chinese Medicine, Changchun, China

OPEN ACCESS

Edited by:
Zhe-Sheng Chen,
St. John's University, United States

Reviewed by:
Oronza Antonietta Botrugno,
San Raffaele Scientific Institute (IRCCS), Italy
Zhihui Liu,
National Cancer Institute (NIH), United States

***Correspondence:**
Yangyang Liu
lyyccucm@163.com
Da Liu
liuda_1986@163.com

[†]These authors have contributed equally to this work

Specialty section:
This article was submitted to Cancer Molecular Targets and Therapeutics, a section of the journal Frontiers in Oncology

Received: 10 January 2022
Accepted: 04 March 2022
Published: 28 March 2022

Citation:
Jin Y, Liu T, Luo H, Liu Y and Liu D (2022) Targeting Epigenetic Regulatory Enzymes for Cancer Therapeutics: Novel Small-Molecule Epidrug Development. Front. Oncol. 12:848221. doi: 10.3389/fonc.2022.848221

Dysregulation of the epigenetic enzyme-mediated transcription of oncogenes or tumor suppressor genes is closely associated with the occurrence, progression, and prognosis of tumors. Based on the reversibility of epigenetic mechanisms, small-molecule compounds that target epigenetic regulation have become promising therapeutics. These compounds target epigenetic regulatory enzymes, including DNA methylases, histone modifiers (methylation and acetylation), enzymes that specifically recognize post-translational modifications, chromatin-remodeling enzymes, and post-transcriptional regulators. Few compounds have been used in clinical trials and exhibit certain therapeutic effects. Herein, we summarize the classification and therapeutic roles of compounds that target epigenetic regulatory enzymes in cancer treatment. Finally, we highlight how the natural compounds berberine and ginsenosides can target epigenetic regulatory enzymes to treat cancer.

Keywords: epigenetic regulatory enzymes, cancer therapeutics, inhibitors, small molecule, epidrug development

1 INTRODUCTION

The concept of epigenetics was first introduced in 1942 by Waddington, a British scientist who defined "epigenetics" as changes in the phenotype without underlying genotypic changes to explain altered growth and development (1). Epigenetics is now widely recognized as the regulatory mechanisms by which a heritable phenotype is changed without altering the DNA sequence.

Abbreviations: AML, acute myeloid leukemia; BBR, berberine; BET, BRD-extra terminal protein; BRD, bromodomain; CHD, chromo-ATPase/helicase-DNA-binding; CDY, chromodomain Y; CpGI, CpG island; CRC, colorectal cancer; DNMT, DNA methylase; DNMTi, DNMT inhibitor; DOT1, disruptor of telomeric silencing 1; DOT1L, DOT1-like; EZH1/2, enhancer of zeste homologs 1/2; FAD, flavin adenine dinucleotide; GNAT, GCN5-related N-acetyltransferase; HAT, histone acetyltransferase; HDAC, histone deacetylase; HMT, histone methyltransferase; HMTi, HMT inhibitor; HP1, heterochromatin protein 1; JmjC, Jumonji C; KDM, lysine demethylase; KMT, lysine methyltransferase; LSD, lysine-specific demethylase; MBD, methyl-CpG-binding domain; MBP, methyl-CpG-binding protein; MBT, malignant brain tumor; mC; miRNA, microRNA; MLL, mixed lineage leukemia; MM, multiple myeloma; MTase, methyltransferase; MYST, MOZ, YBF2/SAS3, SAS2, and TIP60; NA, nucleoside analog; NB, neuroblastoma; ncRNA, noncoding RNA; NHL, non-Hodgkin's lymphoma; PHD, plant homeodomain; PRMT, protein arginine methyltransferase; PRMTi, PRMT inhibitor; PWWP, Pro-Trp-Trp-Pro; SAM, S-adenosylmethionine; SCLC, small cell lung cancer; SET, su(var) 3-9, enhancer of zeste, and trithorax; SIRT, sirtuin; TET, ten-eleven translocation.

Epigenetic changes, including DNA/RNA methylation, histone modifications, nucleosome localization, non-coding RNA (ncRNA) expression, and chromatin 3D structure, are involved in cellular growth, development, and function (2). These epigenetic modifications constitute the specific epigenome of an individual organism and provide a regulatory mechanism for cellular diversity. Recently, epigenetics has gained attention in fields such as medicine, exerting a profound impact on the research and treatment of diseases such as cancer.

Epigenetic modifications catalyzed by epigenetic regulatory enzymes are important for regulating chromatin structure and gene expression. Imbalanced gene expression can be one of the main mechanisms underlying diseases such as cancer. In particular, thee aberrant expression of oncogenes, tumor suppressor genes, or cancer-related genes by dysregulated epigenetic regulatory enzymes can trigger tumorigenesis by modulating basic processes, such as DNA repair, cell proliferation, and mortality (3, 4). Therefore, epigenetic marks such as DNA methylation, histone modifications, and ncRNA expression have been identified as potential biomarkers for the early diagnosis and prognosis of cancers (5, 6). In recent years, many small-molecule compounds targeting epigenetic regulatory enzymes have been discovered, some of which are promising anticancer drugs.

The discovery and development of inhibitors targeting epigenetic regulatory enzymes are extensively described in this review. Further, we summarize the functions of berberine (BBR) and ginsenosides, natural compounds capable of targeting epigenetic enzymes in cancer. Additionally, we discuss promises and challenges that lie ahead of us.

2 DNA METHYLATION AND ITS ROLE IN CANCER TREATMENT

2.1 DNA Methylation

DNA methylation is a stable epigenetic event in intracellular processes, such as cell differentiation, and is involved in the lineage classification and quality control of stem cells (7). In humans, DNA methylation occurs almost exclusively at cytosine residues in CpG sequences. These dinucleotides are dispersed unevenly across the genome, and most are heavily methylated. In contrast, CpG-rich regions known as CpG islands (CpGIs) remain largely unmethylated, especially in promoter regions (8). However, altered CpGI methylation patterns during cancer progression result in both genome-wide hypomethylation and site-specific CpGI hypermethylation (9). Therefore, DNA methylation provides a useful molecular marker for cancer diagnosis and therapeutics (10). In mammals, DNA methyltransferases (DNMTs) are responsible for transferring methyl donor S-adenosyl-L-methionine (SAM) to the 5′-residue of cytosine (5′-C) in DNA (**Figure 1A**). The DNMT family includes DNMT1, DNMT2, DNMT3A, DNMT3B, and DNMT3L, which differ based on their structural characteristics and functional domains (**Figure 1B**). For example, the Pro-Trp-Trp-Pro (PWWP) domain of DNMT3A/3B recognizes the di- or

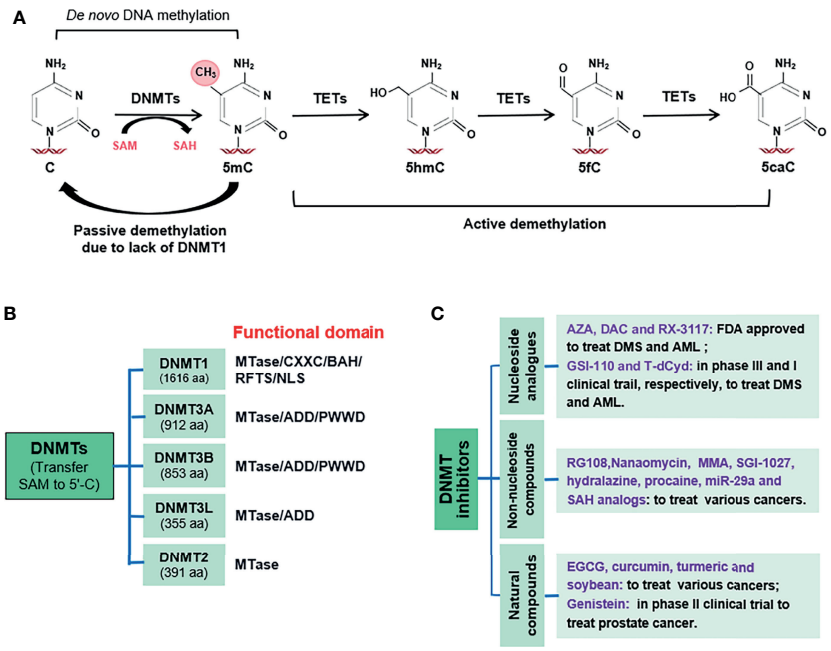

FIGURE 1 | Types of DNA methyltransferases (DNMTs) and antitumor activity of its inhibitors: **(A)**. Schematic of DNA methyltransferases (DNMTs) transferring methyl donor S-adenosyl-L-methionine (SAM) to cytosine (5 ‘C) 5′- residues in DNA or removing SAM from DNA. **(B)**. Functional domains of DNMTs. (DNMT1, DNMT2, DNMT3A, DNMT3B and DNMT3L) **(C)**. Three types of DNMTs inhibitors.

tri-methylation of histone H3 lysine 36 (H3K36) to activate gene expression (11, 12), whereas the ATRX-like domain of DNMT3A and XXC-BAH1 domain of DNMT1 interact with deacetylase HDAC1 to repress gene expression (13, 14). Further, the C-terminal catalytic methyltransferase (MTase) domain of DNMT3A mediates homo- and heterodimerization to regulate progressive DNA methylation (15, 16). Cleavage between the N- and C-terminal domains reportedly affects the relative preference of DNMTs for unmethylated and hemi-methylated DNA (17). DNMTs preferentially bind to hemi-methylated CpG sites (18).

DNA demethylation can occur either passively or actively. DNA demethylation or "erasing DNA methylation" can occur passively when DNA is replicated and the modification is not re-established. One example of passive DNA demethylation is the absence of methylation owing to a lack of DNMT1, whereas another is the removal of methyl groups from cytosine (5-mC) by ten-eleven translocation proteins (TETs) in a replication-independent manner. TETs mainly oxidize 5-mC to form 5-hydroxymethylcytosine (5hmC), 5-formylcytosine (5fC), and 5-carboxycytosine (5caC) (19, 20). The catalytic domain of TETs consists of a double-stranded β-helix domain and cysteine-rich domain at the carboxyl end (21). In addition, TET1 and TET3 contain CXXC domains at their N-terminus, which are composed of two Cys4-type zinc finger motifs that promote DNA binding (22). Importantly, DNA methylation can be recognized by methyl-CpG-binding proteins (MBPs), which bind and interpret methylated DNA to initiate gene silencing by recruiting other factors (23). MBPs can be classified as methyl-CpG-binding domain (MBD) proteins as follows: su (var) 3-9, enhancer of zeste, and trithorax (SET), RING-associated, and zinc finger (24). To date, 11 proteins in the MBD family have been identified, including methyl-CpG-binding protein 2, MBDs 1–6, SETB1/2, and BAZ2A/B (25). In addition to the MBD domain, SETB1/2 and BAZ2A/B also contain other domains, such as SET, DNA-binding homeobox and different transcription factors, plant homeodomain (PHD), and bromodomain (BRD). Although they cannot interact with 5mC residues, MBPs can bind to methylated or acetylated histones to participate in heterochromatin formation and transcriptional inhibition by coordinating H3K9 demethylation, histone H4 deacetylation, and DNA methylation, which are essential for the epigenetic silencing of ribosomal DNA (26, 27).

2.2 Inhibitors Targeting DNMTs (DNMTis)

In view of the hypermethylation of CpGIs in the promoter region of most cancers, DNMT inhibitors (DNMTis) have been developed for tumor treatment. DNMTis are mainly divided into three types, nucleoside analogs (NAs), non-nucleoside compounds, and natural compounds (**Figure 1C**) (28). Compounds that inhibit DNMTs lead to hypomethylation across cell divisions, subsequently inducing the expression of tumor suppressors. Using methylation-specific PCR, Chan et al. demonstrated substantial demethylation of all latent and lytic Epstein-Barr virus promoters in nasopharyngeal cancer patients after treatment with 5-azacytidine (a DNMTi) (29). DNMTis such as azacitidine, decitabine, guadecitabine, and 4-thio-2-deoxycytidine have been examined in clinical anti-tumor trials (30–32) (**Table 1**). Non-nucleoside compounds with various chemical scaffolds have also been studied (63). Compounds such as RG108, nanaomycin A, mithramycin A, SGI-1027, hydralazine, procaine, S-adenosyl-L-homocysteine analogs, and miR-29a have been shown to suppress the activity of DNMTs (33–40). Among these, hydralazine has been shown to be an effective demethylation agent and tumor suppressor gene transcriptional reactivator (36). In a phase II clinical study, hydralazine in combination with standard cytotoxic chemotherapy reactivated tumor suppressor genes silenced by DNA methylation and increased chemotherapy efficacy in prostate cancer (33). Interestingly, some natural compounds, such as (-)-epigallocatechin-3-gallate, curcumin, and genistein from green tea/soybean, also reportedly block the activity of DNMTs (36, 37). Genistein and related soy isoflavones reportedly reactivate methylation-silenced genes to delay the progression of breast or prostate cancer by directly blocking DNMT. Although many DNMTis have been identified, few have been applied clinically as current DNMTis are nonselective cytosine analogs that induce cytotoxic side effects (64).

3 HISTONE METHYLATION AS AN ANTICANCER TARGET

3.1 Histone Methylation

Histone methylation, a unique post-translational modification catalyzed by histone MTases (HMTs), occurs at both lysine (K) and arginine (R) residues. Abnormal histone methyl modification plays an important role in the proliferation, apoptosis, differentiation, and invasion of tumor cells. Thus, blocking these abnormal modifications has become a new direction in tumor therapeutics (65, 66). The key steps of the histone methylation process, including HMT inhibitors (HMTis) and histone lysine demethylases (KDMs), are shown in **Figures 2A, B**. Lysine methylation occurs in mono-, di-, and tri-states, whereas arginine methylation only occurs in mono- and di-states. These methyl marks contribute to transcriptional regulation and serve as platforms for the recruitment of effector proteins. Most HMTs contain the SET domain. Methylation occurs at lysine residues K4, K9, K27, K36, and K79 of histone H3 and K20 of histone H4 (**Figure 2B**). In general, methylation at H3K9, H3K27, and H4K20 correlates with transcriptional repression, whereas methylation at H3K4, H3K36, and H3K79 corresponds with gene transcription (67). H3K9me2/me3, H3K27me2/me3, and H4K20me3 often appear on heterochromatin where genes remain silent (68).

There are two families of histone demethylases, lysine-specific demethylases (LSDs) and Jumonji C (JmjC) domain-containing lysine demethylases (JmjC-KDMs). The LSD family includes LSD1/KDM1A and LSD2/KDM1B proteins, which contain the N-terminal Swi3p, Rsc8p, and Moira (SWIRM) domains, a flavin adenine dinucleotide-binding motif (FAD), and a C-terminal amine oxidase domain that is responsible for LSD activity in an FAD-dependent manner (69). Both LSD1 and LSD2 function as corepressors through the demethylation of mono- or di-methyl

TABLE 1 | Small molecule compounds targeting epigenetic regulatory enzymes.

Compound	Type	Tumor types	Status	Ref.
DNMTi				
5-azacytidine/AZA	NA	DMS/AML	Phase I	(29)
5-aza-2'deoxycytidine/DAC	NA	DMS/AML	Phase I	(29)
RX-3117	NA	DMS/AML	Phase I	(30)
Guadecitabine/SGI-110	NA	AML	Phase II	(31)
4-Thio-2-deoxycytidine	NA	Cancer	N/A	(32)
RG108	NNC	Prostate cancer	N/A	(33)
Nanaomycin A	NNC	Colorectal cancer	Phase III	(33)
Mithramycin A/MMA	NNC	Lung cancer	N/A	(33)
SGI-1027	NNC	Cancer	N/A	(34)
Procaine	NNC	Human cancer	N/A	(35)
Hydralazine	NNC	Prostate cancer	Phase I	(36)
SAH analogs	NNC	MDS	N/A	(37)
MiR-29a	NNC	AML	N/A	(38)
EGCG	Natural compounds	Colon Cancer	Phase I	(39)
Curcumin/Genistein	Natural compounds	Breast Cancer	Phase II	(39)
Soybean	Natural compounds	Prostate Cancer	Phase II	(40)
HMTi				
BIX-01294	G9a-GLP inhibitors	Prostate/colon cancer	N/A	(41)
Chaetocin	Non-specific inhibitor	Glioma cancer	N/A	(41)
GSK343	LIS	Osteosarcoma	CTT	(42)
CPI-1205/UNC0321	LIS	Solid tumors/BCL	Phase I	(43)
UNC1999	LIS	Bladder cancer	CTT	(25)
EPZ005687/GSK-126/EL	LIS	DLBL	CTT	(25)
Tazemetostat/EPZ6438	LIS	Solid tumors/BCL	Phase I	(44)
Tazemetostat	LIS	follicular lymphoma	Phase 2	(45)
Tazemetostat	LIS	Papillary thyroid cancer	N/A	(46)
EPZ004777	DOT1L inhibitor	Leukemia	N/A	(47)
EPZ-5676	DOT1L inhibitor	Leukemia	Phase I	(48)
SYC-522	DOT1L inhibitor	AML	N/A	(49)
PRMTi				
DB75	Type I PRMT Inhibitor	Malaria	Phase I	(44)
GSK3368715	Type I PRMT Inhibitor	Solid tumors	Phase I	(50)
TP-064/EZM2302	CARM1 inhibitor	MM	N/A	(51)
GSK3235025/EPZ015666	PRMT5 inhibitor	NHL	N/A	(52)
GSK3326595/EPZ015938	PRMT5 inhibitor	Breast cancer	Phase II	(52)
Ly -283	PRMT5 inhibitor	NHL	N/A	(53)
GSK3203591	PRMT5 inhibitor	Breast cancer	N/A	(54)
KDMi				
PCPA	LSD1 inhibitor	Cancer	N/A	(55)
INCB059872	LSD1 inhibitor	Myeloid leukemia	Phase I	(56)
IMG-7289	LSD1 inhibitor	Acute myeloid leukemia	Phase I	(57)
CC-90011	LSD1 inhibitor	Prostatic cancer	Phase I/II	(58)
Thieno[3,2-b]pyrrole-5-carboxamides	LSD1 inhibitor	Human leukemia	N/A	(59)
GSK2879552	PCPA derivatives	AML/SCLC	Phase I	(60)
ORY-1001	PCPA derivatives	AML/SCLC	Phase I	(61)
HCI-2059	PCPA derivatives	MYCN-amplified neuroblastoma	N/A	(62)

AML, Acute Myeloid Leukemia; BCL, B-cell lymphoma; CTT, Clinical trial termination; DLBL, Diffuse large B-cell lymphoma; EGCG, (-)-epigallocatechin-3-gallate; LIS, Lyridine-indazole scaffold; MDS, Myelodysplastic syndrome; MM, Multiple myeloma; NA, Nucleoside analogues; NHL, Non-Hodgkin's lymphoma; NNC, Non-nucleoside compounds; SCLC, Small cell lung cancer.

marks on H3K4 (70). However, LSD1 can also act as a coactivator of the androgen receptor *via* the demethylation of H3K9me1/me2 (71). The JmjC-KDM family includes iron- and α-ketoglutarate-dependent dioxygenases, which can be divided into KDM 2–8 subfamilies. Members of the JmjC-KDM family are responsible for the demethylation of all statuses of H3K4, H3K9, H3K27, H3K36, H3K79, and H4K20 through the co-substrate 2-oxoglutarate, dioxygen, and Fe (II) as a cofactor (42, 72). The lysine residues mentioned previously herein are prone to methylation and play critical roles in tumorigenesis (73, 74).

3.2 Histone Methyltransferase Inhibitors (HMTis)

Histone methylation is a hot topic in tumor epigenetic modification. This modification is associated with the biological behavior of tumor cells and plays a role in the development of tumors. In this section, we focus on a subclass of epigenetic regulators, namely histone methyltransferases. To date, hundreds of HMTs have been identified, including lysine and arginine MTases (47). Several HMTs have been linked to different types of cancer. However, in most cases, we only have limited knowledge regarding the molecular

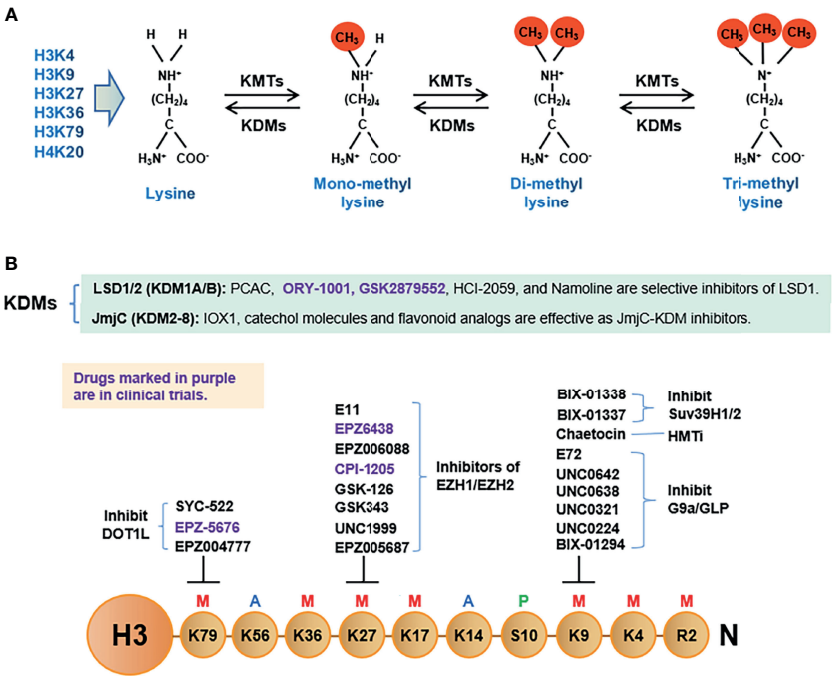

FIGURE 2 | The histone methylation process, inhibitors of histone lysine methyltransferases (HMTs) and histone lysine demethylases (KDMs). **(A)**. Schematic diagram of three states of lysine methylation: mono, di, and tri states. **(B)**. A summary of the histone methylation process and inhibitors of HMTs and KDMs.

mechanisms by which the HMTs contribute to disease development. HMTis can be classified according to their specificity for different types of methyltransferases. Here, we summarize the current knowledge regarding some of the best validated examples of HMTis inhibiting tumorigenesis and discuss their potential mechanisms of action.

3.2.1 Inhibitors of H3K9 HMTs

Most HMTs are present as closely homologous pairs. For example, the catalytic SET domains of G9a and GLP share 77% sequence identity and are present as a stoichiometric heterometric complex (75). In cells, they are responsible for H3K9 methylation and G9a/GLP-mediated H3K9me2, which are highly associated with transcriptional repression (76). A recent study reported high expression of G9a in various cancers, such as prostate/colon/lung cancers, multiple myeloma, and lymphocytic leukemia, indicating that G9a inhibitors might suppress cancer proliferation (41, 77). BIX-01294 was first found as a G9a/GLP-specific inhibitor that can modulate global H3K9me2 levels in cells (78). Although specific G9a/GLP inhibitors, such as UNC0224, UNC0321, E72, UNC0638, and UNC0642, have been developed, they have not been used in clinical trials because of their cell toxicity or poor bioavailability.

3.2.2 Inhibitors of H3K27 HMTs

In mammals, polycomb repressive complex 2 exhibits HMT activity on H3K27 *via* catalytic subunits enhancer of zeste homologs 1/2 (EZH1/2) (79). In *Drosophila*, EZH1 and 2 are mainly responsible for maintaining the spatial expression pattern of homeobox (*HOX*) genes (80). Aberrant EZH2 expression has been associated with various human cancers. For example, the overexpression of EZH2 has been detected in prostate, breast, and other cancers, suggesting that it might serve as a prognostic marker for cancers (43, 81). Further, wild-type and mutant EZH2 cooperatively regulate and maintain the hypertrimethylation of H3K27, which inhibits the proliferation of lymphoma cells by abnormally silencing PCR2-target genes (47).

Inhibitors of EZH1/2 can be classified into three groups according to their basic skeleton structure as follows: those with the pyridone-indazole scaffold, which includes EPZ005687, UNC1999, and GSK343 (48); those with the pyridone-indole scaffold, which includes GSK-126, CPI-1205, and E11 (41, 78); and those with the pyridone-phenyl scaffold, which includes EPZ006088 and EPZ6438 (tazemetostat) (45). More recently, several non-SAM-derived inhibitors of the catalytic activity of EZH2 have been discovered. Among them are GSK126 and EPZ005687, inhibitors effective against EZH2 mutant lymphomas, and EI1, a low MW inhibitor that blocks diffuse large B-cell lymphoma proliferation (46). Tazemetostat has been recently approved for relapsed/refractory after two or more lines of therapy in the presence of an EZH2 mutation or independent of an EZH2 mutation in the absence of other options (82). Combined tazemetostat and MAPKis enhances the differentiation of papillary thyroid cancer cells harboring BRAFV600E by synergistically decreasing the global trimethylation of H3K27me (44). UNC1999, a modified

inhibitor, improves the specificity of EZH2 and achieves better oral bioavailability (83). As a second-generation compound, EPZ6438 shows improved potency, pharmacokinetic properties, and selectivity for EZH1 than EPZ005687 (81). Both EPZ6438 and CPI-1205 are currently undergoing clinical trials for solid tumors or B-cell lymphoma (84) (**Table 1**).

3.2.3 Inhibitors of H3K79 HMTs

DOT1-like protein (DOT1L), an enzyme responsible for H3K79 methylation, does not contain the SET catalytic domain and displays a class I SAM-dependent MTase fold (85). In cells, DOT1/DOT1L-mediated H3K79 methylation is involved in various biological processes, including gene transcription, the cell cycle, and DNA damage repair (86). DOT1L interacts with mixed lineage leukemia (MLL) translocation fusion proteins, such as AF10, ENL, AF9, and AF4, resulting in the DOT1L-mediated H3K79 methylation of target genes. Therefore, DOT1L has become a potential target for developing therapeutic drugs to treat leukemia.

To date, more than 20 DOT1L inhibitors have been reported. Among them, EPZ004777 was first found to selectively kill leukemic cells by repressing DOT1L-mediated H3K79 methylation (87). EPZ-5676, an optimized version of EPZ004777, forms hydrogen bonds with residues Asp222, Glu186, Gly163, and Asp161 of DOT1L to prevent cellular H3K79 methylation. EPZ-5676 has been used against leukemia in phase I clinical trials (88). Another DOT1L inhibitor, SYC-522, effectively delayed the progression of MLL in the preclinical phase by suppressing H3K79 methylation and reducing the expression of two important leukemia-related genes, *HOXA9* and *MEIS1*. Additionally, SYC-522 significantly reduces the expression of *CCND1* and *BCL2L1*, which are important regulators of the cell cycle and anti-apoptotic signaling pathways (49) (**Table 1**).

3.3 Inhibitors Targeting Protein Arginine Methyltransferases (PRMTis)

The protein arginine MTase (PRMT) family includes nine enzymes divided into three types, type I PRMT, CARM1, and PRMT5. In cells, PRMTs catalyze the methylation of arginine residues on histones. PRMT dysfunction is associated with the occurrence of several cancers.

PRMTis are also classified into three types based on their corresponding PRMT type and have been investigated in the early preclinical stage (**Table 1**). Type I PRMTis include AMI-1, AMI-6, DB75, GSK3368715, and MS023 (50, 89). MS049, TP-064, and EZM2302 exhibit the highly selective inhibition of CARM1 (PRMT4) (51), and the latter two compounds can be effectively used to treat multiple myeloma (MM) by selectively blocking CARM1 (90, 91). Interestingly, PRMT5 inhibitors, such as EPZ015666 (GSK3235025), EPZ015938 (GSK3326595), and LLY-283, possess high anti-tumor activities. EPZ015666 was used against NHL in clinical trials by blocking SmD3 methylation (52–54).

3.4 Inhibitors Targeting Histone Lysine Demethyltransferases (KDMis)

Many small-molecule compounds have emerged as lysine demethyltransferase inhibitors (KDMis), some of which have entered different clinical stages as anti-tumor drug candidates (**Table 1**). Inhibitors of both the LSD/KDM and JmjC-KDM family proteins have been shown to block the catalytic domain to reduce catalytic activity. One of the most potent LSD1 inhibitors, tranylcypromine (PCPA), causes the irreversible inhibition of LSD1 by forming a covalent adduct with the FAD cofactor of LSD1 (92). This process destroys the catalytic group of the histone lysine demethyltransferase, which inhibits the activity of the enzyme and inactivates it. Based on the chemo-type scaffold, a series of PCPA derivatives have been designed and shown to exert anti-tumor effects (55). Two recently developed PCPA derivatives, ORY-1001 and GSK2879552, promoted the differentiation of acute myeloid leukemia (AML) and limited the growth of small cell lung cancer (SCLC) in a phase 1 clinical trial aimed to assess their roles against AML and SCLC (60, 61). These two PCPA derivatives exhibit higher selectivity for LSD1 than for PCPA (93). Therefore, PCPA derivatives have the potential to become new epigenetic anticancer drugs. In addition, HCI-2509, a potent small-molecule inhibitor of LSD1, hinders the growth of and exerts the cytotoxic effects on neuroblastoma (NB) cells *via* p53 (62). Of the thieno[3,2-b]pyrrole-5-carboxamides, novel reversible inhibitors of KDM1A, that showed a remarkable anti-clonogenic cell growth effect on MLL-AF9 human leukemia cells (59) (**Table 1**).

Various structural scaffolds, including hydroxamic acid, hydroxyquinoline analogs, and cyclic peptides, reportedly function as effective JmjC-KDM inhibitors (25). For example, the 8-hydroxyquinoline derivative IOX1 can block many KDM isoforms (94). Several catechol molecules and flavonoid analogs have also been identified as JmjC-KDM inhibitors (25). However, the aforementioned compounds are still in the developmental phase.

3.5 Inhibitors Targeting Specific Functional Domains of Methyl-Lysine Readers

The methylation of lysine residues in N-terminal tails of histones H3 and H4 widely mediates biological processes in cells. In recent decades, various proteins containing specific functional domains that recognize methyl-lysine on histones have been identified, such as methyl-lysine reader proteins. Methyl-lysine readers are approximately categorized into chromodomain, PHD finger domain, Tudor domain, PWWP domain, WD40 repeat (WDR) domain, and malignant brain tumor (MBT) domain families (5). These proteins exhibit different abilities to recognize methylated lysine residues according to their different functional domains.

Chromodomain proteins are further classified into heterochromatin protein 1 (HP1)/polycomb (Pc), chromo-ATPase/helicase-DNA-binding (CHD), chromobarrel domain, and chromodomain Y (CDY) families (5). Both HP1/Pc and CDY proteins show strong preference for trimethylated H3K9 and H3K27 (68). Moreover, CHD proteins recognize methyl-lysine residues on H3K4 (95), whereas chromobarrel domain proteins interact with methylated H3K36 and H4K20 (96). In addition, both PHD and MBT domain proteins recognize methylated H3K4 (97).

Methyl-lysine reader proteins play important roles in regulating many cellular processes, such as development, the cell cycle, stress responses, and oncogenesis, and have increasingly become the focus of epigenetic research. Inhibitors of methyl-lysine reader proteins, such as MS37452A, SW2_110A, and UCN3866, have been found to inhibit the growth of cancer cells as selective inhibitors of Pc chromobox (CBX) and CDY proteins (98, 99). Additionally, several compounds have been identified as PHD inhibitors (100). For example, macrocyclic calixarenes can disrupt the binding of ING2 PHD to H3K4me, disulfiram, amiodarone, and tegaserod to prevent interactions between JARID1A PHD3 and H3K4me3 (2, 6). Moreover, benzimidazole can be selectively docked in methylated H3K4, preventing the binding of the Pygo-BCL9 chromatin reader to H3K4me PHD (101). Thus, many proteins targeting methyl-lysine readers have been shown to exert anticancer effects (102).

4 HISTONE ACETYLATION AS A TARGET FOR ANTI-TUMOR DRUG DEVELOPMENT

4.1 Histone Acetylation

Acetylation of the ε-amino group of a lysine residue was first discovered with histones in 1968, but the responsible enzymes, histone acetyltransferases and deacetylases, were not identified until the mid-1990s (103). Histone acetylation is a reversible process that occurs *via* the addition of an acetyl group to the ε-amino of the lysine residue at the midamino end and tail of the histone. This process is dynamically controlled by histone acetyltransferases (HATs), lysine acetyltransferases, and histone deacetylases (HDACs) (**Table 2**). Lysine residues on histones are prone to acetylation, resulting in a decrease in the positive charge and weakening of the interaction between histones and DNA (104).

There are three major families of HATs, general control non-derepressible 5 (Gcn5)-related N-acetyltransferases (GNATs), p300/CBP, and MYST proteins. p300 (adenoviral E1A-associated protein of 300 kDa) and CBP (CREB-binding protein) form a pair of paralogous transcriptional co-activators. Members of the GNAT family include HAT1, yeast Gcn5, and its metazoan orthologs GCN5 and PCAF (p300/CBP-associated factor) (103). HATs are classified into types A and B based on their cellular location. Type A is responsible for acetylating histones associated with chromatin, whereas type B acetylates newly translated histones in the cytoplasm. Nuclear HATs can be divided into two categories based on their sequence homology and shared structural features. The GCN5-related N-acetyltransferase (GNAT) family, which includes GCN5 and p300/CBP-associating factor (PCAF), can acetylate lysine residues on histones H2B, H3, and H4. Meanwhile, the MOZ, YBF2/SAS3, SAS2, and TIP60 (MYST) families of proteins are characterized by a highly conserved MYST domain (105).

Acetyl groups on lysine residues must be removed by HDACs. Dependent on sequence similarity and cofactor dependency, HDACs are grouped into four classes and two families, the classical and silent information regulator 2 (Sir2)-related protein (sirtuin) families. In humans, members of the classical family include HDAC1, 2, 3, and 8 (class I); HDAC4, 5, 6, 7, 9, and 10 (class II); and HDAC11 (class IV). They share sequence similarity and require Zn^{2+} for deacetylase activity. The sirtuin family contains seven members (SIRT1–7, class III), which show no sequence resemblance to members of the classical family and require NAD+ as the cofactor (106, 107).

4.2 Inhibitors Targeting Histone Acetyltransferases (HATis)

Imbalanced HAT expression and acetylation levels in tumorigenesis make HATs suitable targets for drug development. In preclinical experiments, many small-molecule compounds have been screened as potential HATis to regulate histone acetylation and reduce tumor growth (**Table 3**). These compounds include isothiazolone-based chemical compounds, the natural compounds garcinol and embelin (108, 109), the pyrazolone-containing small molecule C646 (124), and the pyridoisothiazole derivatives PU139 and PU141, which block

TABLE 2 | Classification of histone deacetylases (HDACs) and their inhibitors.

Classification		Locations		Inhibitors
Zn++ Dependent	Class I	HDAC1	Nucleus	pan-HDAC inhibitors approved by FDA to treat CTCL, PTCL, AML:
		HDAC2	Nucleus	Vorinostat (SAHA),
		HDAC3	Nucleus/cytoplasm	Belinostat (PXD-101),
		HDAC8	Cytoplasm	Panobinostat (LBH589),
	Class IIa	HDAC4	Cytoplasm/nucleus	Pracinostat (MEI pharma),
		HDAC5	Cytoplasm/nucleus	Romidepsin (FK228)
		HDAC7	Cyto–/mto-/nucleus	Chidamide (CS055, HBI-8000)
		HDAC9	Cytoplasm/nucleus	pan-HDAC inhibitors are being evaluated clinically:
	Class IIb	HDAC6	Cytoplasm	Resminostat (4SC-201) →for Hodgkin's lymphoma;
		HDAC10	Cytoplasm/nucleus	Givinostat (ITF2357) →for polycythemia;
	Class IV	HDAC11	Nucleus	Quisinostat (JNJ-26481585), Entinostat and Mocetinostat →for various cancers.
				pan-HDAC inhibitor in preclinical stage: Trigustatin A
NAD+ Dependent	Class III	SIRT 1	Cytoplasm	SIRTs inhibitors for against breast cancer:
		SIRT 2	Cytoplasm/nucleus	Sirtinol and Nicotinamide
		SIRT 3	Mitocondria	
		SIRT 4	Mitocondria	
		SIRT 5	Mitocondria	
		SIRT 6	Nucleus	
		SIRT 7	Nucleus	

PCAF and/or p300 (110). For example, PU139 retards the growth of NB by blocking Gcn5, PCAF, CBP, and p300 (110).

4.3 Inhibitors Targeting Histone Lysine Deacetylases (HDACis)

Global histone acetylation levels are frequently decreased in cancer cells. Correcting imbalanced acetylation in tumor cells can be achieved by reducing the activity of HDACs using HDACis (**Table 3**). The first HDACi discovered was trichostatin A, a dienohydroxamic acid obtained from *Streptomyces* that effectively suppressed zinc-dependent HDACs in the preclinical stage (111). Notably, numerous pan-HDAC inhibitors (P-HDACi) such as vorinostat (also known as suberoylanilide hydroxamic acid, SAHA) (112), belinostat (PXD-101) (113), panobinostat (LBH589) (114), pracinostat (MEI Pharma) (115), romidepsin (FK228) (116), and chidamide (CS055, HBI-8000) (117), have been approved by the FDA to treat different cancers, including primary cutaneous T-cell lymphoma, peripheral T-cell lymphoma, MM, and AML. Moreover, several P-HDACis, including resminostat (4SC-201) (118), givinostat (ITF2357) (119), quisinostat (JNJ-26481585) (120), entinostat (121), and mocetinostat (122), have been evaluated clinically for Hodgkin's lymphoma, polycythemia, ovarian cancer, and other carcinomas. Furthermore, both sirtinol and nicotinamide have exhibited activity against breast cancer as SIRT inhibitors (123, 125) (**Table 3**). In addition to the compounds mentioned, novel HDACis are constantly being developed (25).

4.4 Inhibitors Targeting Specific Functional Domains of Acetyl-Lysine Readers

Acetyl-lysine on histones can also be recognized by readers with specific functional domains, such as PHD finger, Yaf9, ENL, AF9, Taf14, and Sas5 (YEATS), and BRD. PHD finger proteins recognize acetylated, un-acetylated, or methylated histones, with the PHD finger domains in MLL4 (KMT2D) and MLL3 (KMT2C) targeting H4K16 acetylation and involved in the interaction between MLL4/3 and males absent on the first (MOF) (1278). YEATS proteins interact with acetylated histones H3K9, H3K14, and H3K27 (126).

Many BRD proteins are involved in chromatin-remodeling or chromatin-modifying enzymes. BRDs in HATs act as protein–protein interaction modules that specifically recognize acetylated histones to regulate gene transcription, including H4K5, H4K8, H4K12, H4K16, H4K20, H3K14, and H3K36 (5). BRD proteins are the most widely studied acetyl-lysine readers and have been found in many nuclear proteins, including HATs, HMTs, chromatin-remodeling enzymes, and transcriptional co-activators (127). At present, several inhibitors that target the acetyl-binding pocket of BRDs or BRD extraterminal proteins (BETs) have been discovered (25) (**Table 4**). Among them, BET inhibitors such as RVX-208 (RVX00022), I-BET762 (GSK525762), FT-1101, CPI-0610, BAY1238094, INCB054329, PLX51107, GSK2820151, ZEN003694, BMS-986158, BI 894999, ABBV-075, GS-5829 (128, 129), and OTX015 (MK-8628) have been tested for their anti-tumor effects against numerous types of cancers in clinical trials (130, 131) (**Table 4**). Moreover, several novel BRD inhibitors, including I-BRD9, BI-7273, and BI-9564, can specifically target BRD9 and possess anti-tumor activity (132, 133).

5 EPIGENETIC ENZYMES AS ANTICANCER TARGETS OF NATURAL COMPOUNDS AND THEIR ACTIVE COMPONENTS

Natural compounds and their active components have been widely used in traditional medicine in China, Japan, South Korea, and other countries for their various pharmacological effects. Increasing natural compounds have demonstrated high anticancer activity, providing potential candidates for developing multifunctional tumor-targeted drugs. However, their precise mechanisms of

TABLE 3 | Compounds targeting histone acetylation exert anti-tumor activity.

Compound	Types	Tumor types	Status	Ref.
HATi				
Garcinol	Natural compound	Breast cancer	Preclinical	(108)
Embelin	Natural compound	Prostate cancer	Preclinical	(109)
PU139	A pyrazolone containing small molecule C646	Neuroblastoma	Preclinical	(110)
PU141	Pyridoisothiazole derivatives	Neuroblastoma	Preclinical	(110)
HDACi				
Trigustatin A	Zinc-dependent HDACs inhibitors	NA	Preclinical	(111)
Vorinostat/SAHA	P-HDACi	CTCL	Phase II	(112)
Belinostat/PXD-101	P-HDACi	PTCL	Approved by FDA	(113)
Panobinostat/LBH589	P-HDACi	MM	Approved by FDA	(114)
Pracinostat/MEI pharma	P-HDACi	AML	Phase II	(115)
Romidepsin/FK228	P-HDACi	CTCL	Phase II	(116)
Chidamide/CS055/HBI-8000	P-HDACi	AML	Phase I	(117)
Resminostat/4SC-201	P-HDACi	Solid tumors	Phase I	(118)
Givinostat/ITF2357	P-HDACi	Polycythemia	N/A	(119)
Quisinostat/JNJ-26481585	P-HDACi	Solid tumors	Phase I	(120)
Entinostat	P-HDACi	HL	Phase II	(121)
Mocetinostat	P-HDACi	HL	Phase II	(122)
Sirtinol/Nicotinamide	SIRTs inhibitors	Breast cancer	Phase I	(123)

CTCL, Cutaneous T-cell lymphoma; HL, Hodgkin lymphoma; MPNs, myeloproliferative neoplasms; P-HDACi, Pan-HDAC inhibitors; PTCL, peripheral T-cell lymphoma.

TABLE 4 | BRD-extraterminal proteins inhibitors (BETi) display the roles against tumors.

Compound	Tumor types	Status	Ref.
GSK525762/I-BET762	Breast Cancer	Phase I	(128)
FT-1101	AML	Phase I	(128)
CPI-0610	MM	Phase I	(128)
BAY1238094	N/A	N/A	(128)
INCB054329	Solid Tumors	Phase I/II	(128)
PLX51107/GSK2820151	Solid Tumors	Phase I	(129)
ZEN003694	Prostate Cancer	Phase I	(129)
BMS-986158/GS-5829	Solid Tumor	Phase I	(129)
BI 894999	Neoplasms	Phase I	(129)
ABBV-075	Breast Cancer	Phase I	(129)
MK-8628/OTX015	AML	Phase I	(130)

action remain unclear. Here, we focus on BBR (C20H18NO4) and ginsenosides, natural compounds that have undergone extensive preclinical investigation and play anti-tumor roles by targeting epigenetic enzymes and ncRNAs (**Figure 3**).

5.1 Berberine, a Natural Compound With Epigenetic Regulatory Activity

BBR, the main alkaloid in the herbal medicine *Coptis*, and its derivatives exhibit effective anti-tumor activity (**Table 5**). The functional mechanism of BBR is closely related to its regulation of epigenetic chromatin-modifying enzymes, as the activities of multiple enzymes involved in histone acetylation and methylation, such as CBP/p300, SIRT3, KDM6A, SETD7, and HDAC8, are altered when myeloma U266 cells are treated with BBR (138). Furthermore, BBR treatment leads to the increased acetylation of histones H3 and H4 and suppresses total HDAC activity, further retarding the growth of human lung cancer A549 cells (139). Chen et al. demonstrated that BBR reduces the expression of both EZH2 and H3K27me3 in esophageal carcinoma (134). Further, pseudodehydrocorydaline (a protoberberine alkaloid) selectively suppresses the activity of HMT G9a and decreases the expression of H3K9me2 in MCF-7 breast cancer cells *via* CT13 occupation of the binding site of histone H3, suggesting that CT13 might provide a novel scaffold for synthetic G9a inhibitors (135). In addition to modifying histones, BBR also regulates DNMTs. BBR reportedly accesses chromatin in hepatoma HepG2 cells, resulting in increased global genome methylation and reduced methylation in promoter region CpG sites of cytochrome P450 2B6 (*CYP2B6*), cytochrome P450 3A4 (*CYP3A4*), and glucose regulated protein 78 (*GRP78*) (136). In addition, BBR effectively reduces the expression of DNMT1/3B and promotes p53-hypomethylation, thus further altering the p53-dependent signaling pathway to hinder the growth of myeloma U266 cells (137, 140).

5.2 Anti-Tumor Epigenetic Regulatory Effects of Ginsenosides

Ginsenosides, derived from saponins of ginseng, have a steroid-like hydrophobic backbone connected to one or more sugar moieties and are generally believed to be the major bioactive constituents of ginseng (141). Ginsenosides are divided into two groups based on their chemical structures, panaxatriol (Re, Rf, Rg1, Rg2, and Rh1) and panaxadiol (Rb1, Rb2, Rb3, Rc, Rj, Rg3, and Rh2) (142) (**Table 6**). Although ginsenosides possess various pharmacological activities, including anti-inflammatory, anti-allergic, anti-fatigue, anti-

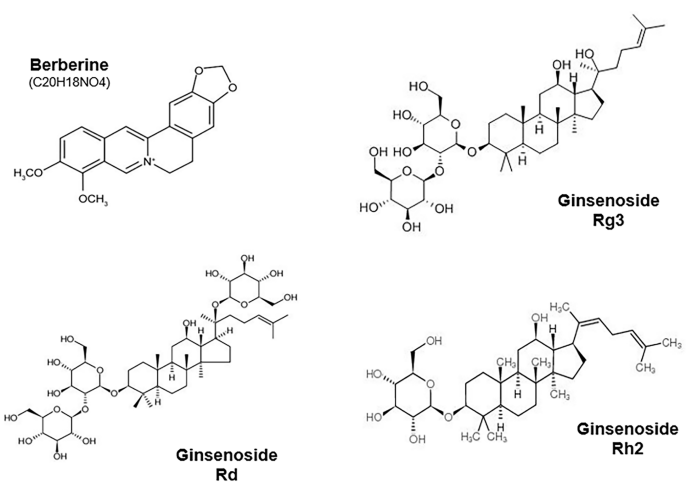

FIGURE 3 | Chemical structure of berberine and Ginsenosides Rh2, Rg3 and Rd.

TABLE 5 | Berberine targets epigenetic enzymes for cancer therapeutics.

Compound	Targets	Tumor types	Ref.
Berberine	EZH2/H3K27me3	Osteosarcoma	(134)
Berberine	Global histone H3/H4 acetylation	Lung cancer	(135)
Berberine	DNMTs	Gastric cancer	(136)
Berberine	DNMT1/DNMT3B	MM	(137)

stress, and anti-cancer properties (152), their basic biological characteristics have not been fully studied. Recent studies have demonstrated that epigenetic mechanisms might be involved in pharmacological effects of ginsenosides (153).

Genome-wide DNA methylation analysis revealed that ginsenoside Rh2 inhibits the growth of breast cancer MCF-7 cells by reducing long interspersed nucleotide element methylation and the expression of hypermethylated genes involved in tumorigenesis (143). Similarly, ginsenoside Rg3 treatment downregulates hypermethylated tRNA methyltransferase 1-like (TRMT1L), proteasome 26S subunit, ATPase 6 (PSMC6), and NADPH oxidase 4 (NOX4), while upregulating hypomethylated ST3 beta-galactoside alpha-2, 3-sialyltransferase 4 (ST3GAL4), RNLS, and KDM5A in breast cancer MCF-7 cells to block tumor growth (154). Ginsenosides also block DNMTs by modulating their target genes. Compound K (the main metabolite of ginseng saponin) suppresses *DNMT1* expression to reduce the proliferation of colorectal cancer (CRC) cells by reactivating the epigenetically silenced *RUNX3* gene (144). Ginsenoside Rg3 treatment decreases the expression of DNMT1/3A/3B and increases the acetylation of histones H3K9/K14 and H4K5/K12/K16 to inhibit the growth of ovarian cancer cells (145). Treatment with 20(s)-ginsenoside Rh2 suppresses the proliferation of K562 and KG1-α leukemia cells by reducing the expression and activity of HDACs, including HDAC1/C2/C6, suggesting that 20(s)-ginsenoside Rh2 acts as an HDACi (155). Interestingly, treatment with ginsenoside Rh2 also suppresses PDZ-binding kinase/T-LAK cell-originated protein kinase (PBK/TOPK), which retards the proliferation of tumor cells through the ERK1/2 signaling pathway (156).

A recent study reported the ability of ginsenosides to suppress cancer by regulating miRNAs (150, 157). The activity of ginsenoside Rh2 against different types of cancer cells is mediated by upregulating miR-146a-5p, miR-21, miR-491, and miR128 (158–160) or by downregulating miR-4295, miR-31, and miR-638 (146, 161–163). In addition, treatment with the ginsenoside Rh2 reduces anti-tumor drug resistance in breast cancer cells by reducing the expression of miR-222, miR-34a, and miR-29a (147). Further, treatment with 20 (S)-ginsenoside Rg3 reverses epithelial–mesenchymal transition in ovarian cancer cells by downregulating DNMT3A-mediated miR-145 (148). Similarly, ginsenoside Rg3 treatment downregulates miR-221 to reduce epithelial–mesenchymal transition in human oral squamous carcinoma cells (149). 20(S)-ginsenoside Rg3-mediated miR-532-3p/miR-324-5p also represses the expression of pyruvate kinase M2 (PMK2), resulting in an anti-tumor effect (164, 165).

Ginsenosides also modulate lncRNAs to hamper the growth of cancer cells (150, 166). Treatment with ginsenoside Rh2 suppresses the lncRNA C3orf67 in breast cancer MCF-7 cells (151). Moreover, ginsenoside Rg3 binds to the promoters of two lncRNAs, regulatory factor X-antisense 1 (RFX-AS1) and syntaxin-binding protein 5-antisense 1 (STXBP5-AS1), to alter DNA methylation, thus inhibiting the growth of breast cancer MCF-7 cells (56) (**Table 6**). Thus, ginsenosides mediate the expression of DNMTs and lncRNAs in tumor growth. In summary, natural compounds and their active components, targeting epigenetic enzymes, have therapeutic potential for cancer treatment (57).

6 CONCLUSIONS AND PERSPECTIVES

Epigenomic alterations mediated by epigenetic regulatory enzymes have a profound effect on many hallmarks of cancer, including malignant self-renewal, differentiation blockade, evasion of cell death, and tissue invasiveness (167). The anticancer roles of inhibitors targeting epigenetic regulatory enzymes provide attractive targets for novel drugs, even if enzymes that selectively regulate the target genes are not well known (168). Some HATis, HDACis, and DNMTis have been approved as anticancer epidrugs. However, the use of most epigenetic regulatory enzyme inhibitors is limited by their poor bioavailability, cytotoxicity, and specificity. Therefore, developing effective drugs that target epigenetic enzymes remains challenging. An increasing number of studies has demonstrated that many natural compounds and their active components target epigenetic enzymes to successfully delay

TABLE 6 | Ginsenosides target epigenetic enzymes against cancers.

Compound	Targets	Tumor types	Ref.
Ginsenosides Rh2	Hyper-methylated genes	Breast cancer	(143)
Ginsenosides CK	DNMT1	Colorectal cancer	(144)
Ginsenosides Rg3	DNMTs	Ovarian cancer	(145)
20(S)-ginsenoside Rh2	HDACs	Leukemia	(146)
Ginsenosides Rh2	MiR-222/MiR-34a/MiR-29a	Breast cancer	(147)
20(S)-ginsenoside Rg3	MiR-145	Ovarian cancer	(148)
Ginsenosides Rg3	MiR-221	Oral squamous carcinoma	(149)
Ginsenosides Rh2	lncRNA C3orf67	Breast cancer	(150)
Ginsenosides Rg3	lncRNA RFX-AS1/STXBP5-AS1	Breast cancer	(151)

cancer progression, suggesting attractive alternatives for anticancer treatments.

AUTHOR CONTRIBUTIONS

YJ, TL, HL, YL, and DL participated in writing, editing, and creating figures. All authors have read and approved the final manuscript.

FUNDING

This research was funded by the National Natural Science Foundation of China (Grant Nos. 82003985 and 81973712). The Science and Technology Research Project of the Jilin Provincial Department of Education (Grant No. JJKH20210995KJ, JJKH20210995KJ), and Jilin Province Science and Technology Development Project in China (Grant No. 20210204013YY).

REFERENCES

1. Waddington CH. The Epigenotype. 1942. *Int J Epidemiol* (2012) 41(1):10–3. doi: 10.1093/ije/dyr184
2. Allis CD, Jenuwein T. The Molecular Hallmarks of Epigenetic Control. *Nat Rev Genet* (2016) 17(8):487–500. doi: 10.1038/nrg.2016.59
3. Miranda Furtado CL, Dos Santos Luciano MC, Silva Santos RD, Furtado GP, Moraes MO, Pessoa C. Epidrugs: Targeting Epigenetic Marks in Cancer Treatment. *Epigenetics* (2019) 14(12):1164–76. doi: 10.1080/15592294.2019.1640546
4. Park JW, Han JW. Targeting Epigenetics for Cancer Therapy. *Arch Pharm Res* (2019) 42(2):159–70. doi: 10.1007/s12272-019-01126-z
5. Cai SF, Levine RL. Genetic and Epigenetic Determinants of AML Pathogenesis. *Semin Hematol* (2019) 56(2):84–9. doi: 10.1053/j.seminhematol.2018.08.001
6. Zhu H, Wei T, Cai Y, Jin J. Small Molecules Targeting the Specific Domains of Histone-Mark Readers in Cancer Therapy. *Molecules* (2020) 25(3):578. doi: 10.3390/molecules25030578
7. Wagner W, Frobel J, Goetzke R. Epigenetic Quality Check - How Good are Your Mesenchymal Stromal Cells? *Epigenomics* (2016) 8(7):889–94. doi: 10.2217/epi-2016-0054
8. Lin CC, Chen YP, Yang WZ, Shen JCK, Yuan HS. Structural Insights Into Cpg-Specific DNA Methylation by Human DNA Methyltransferase 3B. *Nucleic Acids Res* (2020) 48(7):3949–61. doi: 10.1093/nar/gkaa111
9. Xie W, Baylin SB, Easwaran H. DNA Methylation in Senescence, Aging and Cancer. *Oncoscience* (2019) 6(1-2):291–3. doi: 10.18632/oncoscience.476
10. Porcellini E, Laprovitera N, Riefolo M, Ravaioli M, Garajova I, Ferracin M. Epigenetic and Epitranscriptomic Changes in Colorectal Cancer: Diagnostic, Prognostic, and Treatment Implications. *Cancer Lett* (2018) 419:84–95. doi: 10.1016/j.canlet.2018.01.049
11. Baubec T, Colombo DF, Wirbelauer C, Schmidt J, Burger L, Krebs AR, et al. Genomic Profiling of DNA Methyltransferases Reveals a Role for DNMT3B in Genic Methylation. *Nature* (2015) 520(7546):243–7. doi: 10.1038/nature14176
12. Weinberg DN, Papillon-Cavanagh S, Chen H, Yue Y, Chen X, Rajagopalan KN, et al. The Histone Mark H3k36me2 Recruits DNMT3A and Shapes the Intergenic DNA Methylation Landscape. *Nature* (2019) 573(7773):281–6. doi: 10.1038/s41586-019-1534-3
13. Chen X, Pan X, Zhang W, Guo H, Cheng S, He Q, et al. Epigenetic Strategies Synergize With PD-L1/PD-1 Targeted Cancer Immunotherapies to Enhance Antitumor Responses. *Acta Pharm Sin B* (2020) 10(5):723–33. doi: 10.1016/j.apsb.2019.09.006
14. Fuks F, Burgers WA, Godin N, Kasai M, Kouzarides T. Dnmt3a Binds Deacetylases and is Recruited by a Sequence-Specific Repressor to Silence Transcription. *EMBO J* (2001) 20(10):2536–44. doi: 10.1093/emboj/20.10.2536
15. Jurkowska RZ, Rajavelu A, Anspach N, Urbanke C, Jankevicius G, Ragozin S, et al. Oligomerization and Binding of the Dnmt3a DNA Methyltransferase to Parallel DNA Molecules: Heterochromatic Localization and Role of Dnmt3L. *J Biol Chem* (2011) 286(27):24200–7. doi: 10.1074/jbc.M111.254987
16. Holz-Schietinger C, Matje DM, Reich NO. Mutations in DNA Methyltransferase (DNMT3A) Observed in Acute Myeloid Leukemia Patients Disrupt Processive Methylation. *J Biol Chem* (2012) 287(37):30941–51. doi: 10.1074/jbc.M112.366625
17. Ren W, Gao L, Song J. Structural Basis of DNMT1 and DNMT3A-Mediated DNA Methylation. *Genes (Basel)* (2018) 9(12):620. doi: 10.3390/genes9120620
18. Bestor TH. Activation of Mammalian DNA Methyltransferase by Cleavage of a Zn Binding Regulatory Domain. *EMBO J* (1992) 11(7):2611–7. doi: 10.1002/j.1460-2075.1992.tb05326.x
19. Parry A, Rulands S, Reik W. Active Turnover of DNA Methylation During Cell Fate Decisions. *Nat Rev Genet* (2021) 22(1):59–66. doi: 10.1038/s41576-020-00287-8
20. Ito S, Shen L, Dai Q, Wu SC, Collins LB, Swenberg JA, et al. Tet Proteins can Convert 5-Methylcytosine to 5-Formylcytosine and 5-Carboxylcytosine. *Science* (2011) 333(6047):1300–3. doi: 10.1126/science.1210597
21. Tahiliani M, Koh KP, Shen Y, Pastor WA, Bandukwala H, Brudno Y, et al. Conversion of 5-Methylcytosine to 5-Hydroxymethylcytosine in Mammalian DNA by MLL Partner TET1. *Science* (2009) 324(5929):930–5. doi: 10.1126/science.1170116
22. Long HK, Blackledge NP, Klose RJ. ZF-Cxxc Domain-Containing Proteins, Cpg Islands and the Chromatin Connection. *Biochem Soc Trans* (2013) 41(3):727–40. doi: 10.1042/bst20130028
23. Hodges AJ, Hudson NO, Buck-Koehntop BA. Cys2His2 Zinc Finger Methyl-Cpg Binding Proteins: Getting a Handle on Methylated DNA. *J Mol Biol* (2019) 16:S0022–2836(19)30567-4. doi: 10.1016/j.jmb.2019.09.012
24. Moore LD, Le T, Fan G. DNA Methylation and its Basic Function. *Neuropsychopharmacology* (2013) 38(1):23–38. doi: 10.1038/npp.2012.112
25. Biswas S, Rao CM. Epigenetic Tools (the Writers, the Readers and the Erasers) and Their Implications in Cancer Therapy. *Eur J Pharmacol* (2018) 837:8–24. doi: 10.1016/j.ejphar.2018.08.021
26. Du Q, Luu PL, Stirzaker C, Clark SJ. Methyl-Cpg-Binding Domain Proteins: Readers of the Epigenome. *Epigenomics* (2015) 7(6):1051–73. doi: 10.2217/epi.15.39
27. Hendrich B, Tweedie S. The Methyl-Cpg Binding Domain and the Evolving Role of DNA Methylation in Animals. *Trends Genet* (2003) 19(5):269–77. doi: 10.1016/s0168-9525(03)00080-5
28. Xu P, Hu G, Luo C, Liang Z. DNA Methyltransferase Inhibitors: An Updated Patent Review (2012-2015). *Expert Opin Ther Pat* (2016) 26(9):1017–30. doi: 10.1080/13543776.2016.1209488
29. Chan AT, Tao Q, Robertson KD, Flinn IW, Mann RB, Klencke B, et al. Azacitidine Induces Demethylation of the Epstein-Barr Virus Genome in Tumors. *J Clin Oncol* (2004) 22(8):1373–81. doi: 10.1200/jco.2004.04.185
30. Brien GL, Valerio DG, Armstrong SA. Exploiting the Epigenome to Control Cancer-Promoting Gene-Expression Programs. *Cancer Cell* (2016) 29(4):464–76. doi: 10.1016/j.ccell.2016.03.007
31. Thottassery JV, Sambandam V, Allan PW, Maddry JA, Maxuitenko YY, Tiwari K, et al. Novel DNA Methyltransferase-1 (DNMT1) Depleting Anticancer Nucleosides, 4'-Thio-2'-Deoxycytidine and 5-Aza-4'-Thio-2'-Deoxycytidine. *Cancer Chemother Pharmacol* (2014) 74(2):291–302. doi: 10.1007/s00280-014-2503-z
32. Christman JK. 5-Azacytidine and 5-Aza-2'-Deoxycytidine as Inhibitors of DNA Methylation: Mechanistic Studies and Their Implications for Cancer Therapy. *Oncogene* (2002) 21(35):5483–95. doi: 10.1038/sj.onc.1205699

33. Lin RK, Hsu CH, Wang YC. Mithramycin a Inhibits DNA Methyltransferase and Metastasis Potential of Lung Cancer Cells. *Anticancer Drugs* (2007) 18 (10):1157–64. doi: 10.1097/CAD.0b013e3282a215e9
34. Datta J, Ghoshal K, Denny WA, Gamage SA, Brooke DG, Phiasivongsa P, et al. A New Class of Quinoline-Based DNA Hypomethylating Agents Reactivates Tumor Suppressor Genes by Blocking DNA Methyltransferase 1 Activity and Inducing its Degradation. *Cancer Res* (2009) 69(10):4277–85. doi: 10.1158/0008-5472.Can-08-3669
35. Villar-Garea A, Fraga MF, Espada J, Esteller M. Procaine is a DNA-Demethylating Agent With Growth-Inhibitory Effects in Human Cancer Cells. *Cancer Res* (2003) 63(16):4984–9.
36. Zambrano P, Segura-Pacheco B, Perez-Cardenas E, Cetina L, Revilla-Vazquez A, Taja-Chayeb L, et al. A Phase I Study of Hydralazine to Demethylate and Reactivate the Expression of Tumor Suppressor Genes. *BMC Cancer* (2005) 5:44. doi: 10.1186/1471-2407-5-44
37. Isakovic L, Saavedra OM, Llewellyn DB, Claridge S, Zhan L, Bernstein N, et al. Constrained (L-)-s-Adenosyl-L-Homocysteine (SAH) Analogues as DNA Methyltransferase Inhibitors. *Bioorg Med Chem Lett* (2009) 19 (10):2742–6. doi: 10.1016/j.bmcl.2009.03.132
38. Liu B, Ma H, Liu Q, Xiao Y, Pan S, Zhou H, et al. Mir-29b/Sp1/FUT4 Axis Modulates the Malignancy of Leukemia Stem Cells by Regulating Fucosylation *via* Wnt/β-Catenin Pathway in Acute Myeloid Leukemia. *J Exp Clin Cancer Res* (2019) 38(1):200. doi: 10.1186/s13046-019-1179-y
39. Fang MZ, Chen D, Sun Y, Jin Z, Christman JK, Yang CS. Reversal of Hypermethylation and Reactivation of P16ink4a, Rarbeta, and MGMT Genes by Genistein and Other Isoflavones From Soy. *Clin Cancer Res* (2005) 11(19 Pt 1):7033–41. doi: 10.1158/1078-0432.Ccr-05-0406
40. Medina-Franco JL, López-Vallejo F, Kuck D, Lyko F. Natural Products as DNA Methyltransferase Inhibitors: A Computer-Aided Discovery Approach. *Mol Divers* (2011) 15(2):293–304. doi: 10.1007/s11030-010-9262-5
41. Ishiguro K, Kitajima H, Niinuma T, Maruyama R, Nishiyama N, Ohtani H, et al. Dual EZH2 and G9a Inhibition Suppresses Multiple Myeloma Cell Proliferation by Regulating the Interferon Signal and IRF4-MYC Axis. *Cell Death Discov* (2021) 7(1):7. doi: 10.1038/s41420-020-00400-0
42. Cerami E, Gao J, Dogrusoz U, Gross BE, Sumer SO, Aksoy BA, et al. The Cbio Cancer Genomics Portal: An Open Platform for Exploring Multidimensional Cancer Genomics Data. *Cancer Discov* (2012) 2(5):401–4. doi: 10.1158/2159-8290.Cd-12-0095
43. Fernández-Serrano M, Winkler R, Santos JC, Le Pannérer MM, Buschbeck M, Roué G. Histone Modifications and Their Targeting in Lymphoid Malignancies. *Int J Mol Sci* (2021) 23(1):253. doi: 10.3390/ijms23010253
44. Zhong H, Zhou J, An XH, Hua YR, Lai YF, Zhang R, et al. Natural Product-Based Design, Synthesis and Biological Evaluation of 2',3,4,4'-Tetrahydrochalcone Analogues as Antivitiligo Agents. *Bioorg Chem* (2019) 87:523–33. doi: 10.1016/j.bioorg.2019.03.054
45. Morschhauser F, Tilly H, Chaidos A, McKay P, Phillips T, Assouline S, et al. Tazemetostat for Patients With Relapsed or Refractory Follicular Lymphoma: An Open-Label, Single-Arm, Multicentre, Phase 2 Trial. *Lancet Oncol* (2020) 21(11):1433–42. doi: 10.1016/S1470-2045(20)30441-1
46. Fu H, Cheng L, Sa R, Jin Y, Chen L. Combined Tazemetostat and Mapki Enhances Differentiation of Papillary Thyroid Cancer Cells Harbouring BRAFV600E by Synergistically Decreasing Global Trimethylation of H3K27. *J Cell Mol Med* (2020) 24(6):3336–45. doi: 10.1111/jcmm.15007
47. Liu Q, Wang MW. Histone Lysine Methyltransferases as Anti-Cancer Targets for Drug Discovery. *Acta Pharmacol Sin* (2016) 37(10):1273–80. doi: 10.1038/aps.2016.64
48. Dilworth D, Barsyte-Lovejoy D. Targeting Protein Methylation: From Chemical Tools to Precision Medicines. *Cell Mol Life Sci* (2019) 76 (15):2967–85. doi: 10.1007/s00018-019-03147-9
49. Liu W, Deng L, Song Y, Redell M. DOT1L Inhibition Sensitizes MLL-Rearranged AML to Chemotherapy. *PloS One* (2014) 9(5):e98270. doi: 10.1371/journal.pone.0098270
50. Fedoriw A, Rajapurkar SR, O'Brien S, Gerhart SV, Mitchell LH, Adams ND, et al. Anti-Tumor Activity of the Type I PRMT Inhibitor, GSK3368715, Synergizes With PRMT5 Inhibition Through MTAP Loss. *Cancer Cell* (2019) 36(1):100–14.e25. doi: 10.1016/j.ccell.2019.05.014
51. Shen Y, Szewczyk MM, Eram MS, Smil D, Kaniskan H, de Freitas RF, et al. Discovery of a Potent, Selective, and Cell-Active Dual Inhibitor of Protein Arginine Methyltransferase 4 and Protein Arginine Methyltransferase 6. *J Med Chem* (2016) 59(19):9124–39. doi: 10.1021/acs.jmedchem.6b01033
52. Chan-Penebre E, Kuplast KG, Majer CR, Boriack-Sjodin PA, Wigle TJ, Johnston LD, et al. A Selective Inhibitor of PRMT5 With *In Vivo* and *In Vitro* Potency in MCL Models. *Nat Chem Biol* (2015) 11(6):432–7. doi: 10.1038/nchembio.1810
53. Bonday ZQ, Cortez GS, Grogan MJ, Antonysamy S, Weichert K, Bocchinfuso WP, et al. LLY-283, a Potent and Selective Inhibitor of Arginine Methyltransferase 5, PRMT5, With Antitumor Activity. *ACS Med Chem Lett* (2018) 9(7):612–7. doi: 10.1021/acsmedchemlett.8b00014
54. Gerhart SV, Kellner WA, Thompson C, Pappalardi MB, Zhang XP, Montes de Oca R, et al. Activation of the P53-MDM4 Regulatory Axis Defines the Anti-Tumour Response to PRMT5 Inhibition Through Its Role in Regulating Cellular Splicing. *Sci Rep* (2018) 8(1):9711. doi: 10.1038/s41598-018-28002-y
55. Liu K, Liu Y, Lau JL, Min J. Epigenetic Targets and Drug Discovery Part 2: Histone Demethylation and DNA Methylation. *Pharmacol Ther* (2015) 151:121–40. doi: 10.1016/j.pharmthera.2015.04.001
56. Ham J, Jeong D, Park S, Kim HW, Kim H, Kim SJ. Ginsenoside Rg3 and Korean Red Ginseng Extract Epigenetically Regulate the Tumor-Related Long Noncoding RNAs RFX3-AS1 and STXBP5-AS1. *J Ginseng Res* (2019) 43(4):625–34. doi: 10.1016/j.jgr.2019.02.004
57. Song H, Liu D, Dong S, Zeng L, Wu Z, Zhao P, et al. Epitranscriptomics and Epiproteomics in Cancer Drug Resistance: Therapeutic Implications. *Signal Transduct Target Ther* (2020) 5(1):193. doi: 10.1038/s41392-020-00300-w
58. Ohnston G, Ramsey HE, Liu Q, Wang J, Stengel KR, Sampathi S, et al. Nascent Transcript and Single-Cell RNA-Seq Analysis Defines the Mechanism of Action of the LSD1 Inhibitor INCB059872 in Myeloid Leukemia. *Gene* (2020) 752:144758. doi: 10.1016/j.gene.2020.144758
59. Vianello P, Sartori L, Amigoni F. Thieno [3, 2-B] Pyrrole-5-Carboxamides as New Reversible Inhibitors of Histone Lysine Demethylase KDM1A/LSD1. Part 2: Structure-Based Drug Design and Structure–Activity Relationship[J]. *J Med Chem* (2017) 60(5):1693–715. doi: 10.1021/acs.jmedchem.6b01019
60. Bauer TM, Besse B, Martinez-Marti A, Trigo JM, Moreno V, Garrido P, et al. Phase I, Open-Label, Dose-Escalation Study of the Safety, Pharmacokinetics, Pharmacodynamics, and Efficacy of GSK2879552 in Relapsed/Refractory SCLC. *J Thorac Oncol* (2019) 14(10):1828–38. doi: 10.1016/j.jtho.2019.06.021
61. Helin K, Dhanak D. Chromatin Proteins and Modifications as Drug Targets. *Nature* (2013) 502(7472):480–8. doi: 10.1038/nature12751
62. Gupta S, Doyle K, Mosbruger TL, Butterfield A, Weston A, Ast A, et al. Reversible LSD1 Inhibition With HCI-2509 Induces the P53 Gene Expression Signature and Disrupts the MYCN Signature in High-Risk Neuroblastoma Cells. *Oncotarget* (2018) 9(11):9907–24. doi: 10.18632/oncotarget.24035
63. Ciechomska M, Roszkowski L, Maslinski W. DNA Methylation as a Future Therapeutic and Diagnostic Target in Rheumatoid Arthritis. *Cells* (2019) 8 (9):953. doi: 10.3390/cells8090953
64. Singh M, Kumar V, Sehrawat N, Yadav M, Chaudhary M, Upadhyay SK, et al. Current Paradigms in Epigenetic Anticancer Therapeutics and Future Challenges. *Semin Cancer Biol* (2021) 22:S1044–579X(21)00063-8. doi: 10.1016/j.semcancer
65. Yin X, Yang S, Zhang M, Yue Y. The Role and Prospect of JMJD3 in Stem Cells and Cancer. *BioMed Pharmacother* (2019) 118:109384. doi: 10.1016/j.biopha.2019.109384
66. Cao H, Li L, Yang D, Zeng L, Yewei X, Yu B, et al. Recent Progress in Histone Methyltransferase (G9a) Inhibitors as Anticancer Agents. *Eur J Med Chem* (2019) 179:537–46. doi: 10.1016/j.ejmech.2019.06.072
67. Hon GC, Hawkins RD, Ren B. Predictive Chromatin Signatures in the Mammalian Genome. *Hum Mol Genet* (2009) 18(R2):R195–201. doi: 10.1093/hmg/ddp409
68. Vermeulen M, Eberl HC, Matarese F, Marks H, Denissov S, Butter F, et al. Quantitative Interaction Proteomics and Genome-Wide Profiling of Epigenetic Histone Marks and Their Readers. *Cell* (2010) 142(6):967–80. doi: 10.1016/j.cell.2010.08.020

69. Maiques-Diaz A, Somervaille TC. LSD1: Biologic Roles and Therapeutic Targeting. *Epigenomics* (2016) 8(8):1103–16. doi: 10.2217/epi-2016-0009
70. Shi Y, Whetstine JR. Dynamic Regulation of Histone Lysine Methylation by Demethylases. *Mol Cell* (2007) 25(1):1–14. doi: 10.1016/j.molcel.2006.12.010
71. Metzger E, Wissmann M, Yin N, Müller JM, Schneider R, Peters AH, et al. LSD1 Demethylates Repressive Histone Marks to Promote Androgen-Receptor-Dependent Transcription. *Nature* (2005) 437(7057):436–9. doi: 10.1038/nature04020
72. Labbé RM, Holowatyj A, Yang ZQ. Histone Lysine Demethylase (KDM) Subfamily 4: Structures, Functions and Therapeutic Potential. *Am J Transl Res* (2013) 6(1):1–15.
73. Dimitrova E, Turberfield AH, Klose RJ. Histone Demethylases in Chromatin Biology and Beyond. *EMBO Rep* (2015) 16(12):1620–39. doi: 10.15252/embr.201541113
74. Kang JY, Kim JY, Kim KB, Park JW, Cho H, Hahm JY, et al. KDM2B Is a Histone H3K79 Demethylase and Induces Transcriptional Repression *via* Sirtuin-1-Mediated Chromatin Silencing. *FASEB J* (2018) 32(10):5737–50. doi: 10.1096/fj.201800242R
75. Murn J, Shi Y. The Winding Path of Protein Methylation Research: Milestones and New Frontiers. *Nat Rev Mol Cell Biol* (2017) 18(8):517–27. doi: 10.1038/nrm.2017.35
76. Salzberg AC, Harris-Becker A, Popova EY, Keasey N, Loughran TP, Claxton DF, et al. Genome-Wide Mapping of Histone H3k9me2 in Acute Myeloid Leukemia Reveals Large Chromosomal Domains Associated With Massive Gene Silencing and Sites of Genome Instability. *PloS One* (2017) 12(3):e0173723. doi: 10.1371/journal.pone.0173723
77. Chae YC, Kim JY, Park JW, Kim KB, Oh H, Lee KH, et al. FOXO1 Degradation *via* G9a-Mediated Methylation Promotes Cell Proliferation in Colon Cancer. *Nucleic Acids Res* (2019) 47(4):1692–705. doi: 10.1093/nar/gky1230
78. Lee CH, Yu JR, Granat J, Saldaña-Meyer R, Andrade J, LeRoy G, et al. Automethylation of PRC2 Promotes H3K27 Methylation and is Impaired in H3K27M Pediatric Glioma. *Genes Dev* (2019) 33(19-20):1428–40. doi: 10.1101/gad.328773.119
79. Żylicz JJ, Heard E. Molecular Mechanisms of Facultative Heterochromatin Formation: An X-Chromosome Perspective. *Annu Rev Biochem* (2020) 89:255–82. doi: 10.1146/annurev-biochem-062917-012655
80. Zhao Y, Hu Z, Li J, Hu T. EZH2 Exacerbates Breast Cancer by Methylating and Activating STAT3 Directly. *J Cancer* (2021) 12(17):5220–30. doi: 10.7150/jca.50675
81. Park SH, Fong KW, Mong E, Martin MC, Schiltz GE, Yu J. Going Beyond Polycomb: EZH2 Functions in Prostate Cancer. *Oncogene* (2021) 40(39):5788–98. doi: 10.1038/s41388-021-01982-4
82. Li C, Wang Y, Gong Y, Zhang T, Huang J, Tan Z, et al. Finding an Easy Way to Harmonize: A Review of Advances in Clinical Research and Combination Strategies of EZH2 Inhibitors. *Clin Epigenet* (2021) 13(1):62. doi: 10.1186/s13148-021-01045-1
83. Gulati N, Béguelin W, Giulino-Roth L. Enhancer of Zeste Homolog 2 (EZH2) Inhibitors. *Leuk Lymphoma* (2018) 59(7):1574–85. doi: 10.1080/10428194.2018.1430795
84. Chen Y, Liu X, Li Y, Quan C, Zheng L, Huang K. Lung Cancer Therapy Targeting Histone Methylation: Opportunities and Challenges. *Comput Struct Biotechnol J* (2018) 16:211–23. doi: 10.1016/j.csbj.2018.06.001
85. Gsell C, Richly H, Coin F, Naegeli H. A Chromatin Scaffold for DNA Damage Recognition: How Histone Methyltransferases Prime Nucleosomes for Repair of Ultraviolet Light-Induced Lesions. *Nucleic Acids Res* (2020) 48(4):1652–68. doi: 10.1093/nar/gkz1229
86. Nguyen AT, Zhang Y. The Diverse Functions of Dot1 and H3K79 Methylation. *Genes Dev* (2011) 25(13):1345–58. doi: 10.1101/gad.2057811
87. Sarno F, Nebbioso A, Altucci L. DOT1L: A Key Target in Normal Chromatin Remodelling and in Mixed-Lineage Leukaemia Treatment. *Epigenetics* (2020) 15(5):439–53. doi: 10.1080/15592294.2019.1699991
88. Raj U, Kumar H, Gupta S, Varadwaj PK. Novel DOT1L Receptornatural Inhibitors Involved in Mixed Lineage Leukemia: A Virtual Screening, Molecular Docking and Dynamics Simulation Study. *Asian Pac J Cancer Prev* (2015) 16(9):3817–25. doi: 10.7314/apjcp.2015.16.9.3817
89. Dominici C, Sgarioto N, Yu Z, Sesma-Sanz L, Masson JY, Richard S, et al. Synergistic Effects of Type I PRMT and PARP Inhibitors Against Non-Small Cell Lung Cancer Cells. *Clin Epigenet* (2021) 13(1):54. doi: 10.1186/s13148-021-01037-1
90. Drew AE, Moradei O, Jacques SL, Rioux N, Boriack-Sjodin AP, Allain C, et al. Identification of a CARM1 Inhibitor With Potent *In Vitro* and *In Vivo* Activity in Preclinical Models of Multiple Myeloma. *Sci Rep* (2017) 7(1):17993. doi: 10.1038/s41598-017-18446-z
91. Nakayama K, Szewczyk MM, Dela Sena C, Wu H, Dong A, Zeng H, et al. TP-064, a Potent and Selective Small Molecule Inhibitor of PRMT4 for Multiple Myeloma. *Oncotarget* (2018) 9(26):18480–93. doi: 10.18632/oncotarget.24883
92. Schmidt DM, McCafferty DG. Trans-2-Phenylcyclopropylamine Is a Mechanism-Based Inactivator of the Histone Demethylase LSD1. *Biochemistry* (2007) 46(14):4408–16. doi: 10.1021/bi0618621
93. Finley A, Copeland RA. Small Molecule Control of Chromatin Remodeling. *Chem Biol* (2014) 21(9):1196–210. doi: 10.1016/j.chembiol.2014.07.024
94. Yoo J, Jeon YH, Cho HY, Lee SW, Kim GW, Lee DH, et al. Advances in Histone Demethylase KDM3A as a Cancer Therapeutic Target. *Cancers (Basel)* (2020) 12(5):1098. doi: 10.3390/cancers12051098
95. Schnetz MP, Bartels CF, Shastri K, Balasubramanian D, Zentner GE, Balaji R, et al. Genomic Distribution of CHD7 on Chromatin Tracks H3K4 Methylation Patterns. *Genome Res* (2009) 19(4):590–601. doi: 10.1101/gr.086983.108
96. Weaver TM, Morrison EA, Musselman CA. Reading More Than Histones: The Prevalence of Nucleic Acid Binding Among Reader Domains. *Molecules* (2018) 23(10):2614. doi: 10.3390/molecules23102614
97. Ali M, Daze KD, Strongin DE, Rothbart SB, Rincon-Arano H, Allen HF, et al. Molecular Insights Into Inhibition of the Methylated Histone-Plant Homeodomain Complexes by Calixarenes. *J Biol Chem* (2015) 290(38):22919–30. doi: 10.1074/jbc.M115.669333
98. Ren C, Morohashi K, Plotnikov AN, Jakoncic J, Smith SG, Li J, et al. Small-Molecule Modulators of Methyl-Lysine Binding for the CBX7 Chromodomain. *Chem Biol* (2015) 22(2):161–8. doi: 10.1016/j.chembiol.2014.11.021
99. Wang S, Denton KE, Hobbs KF, Weaver T, McFarlane JMB, Connelly KE, et al. Optimization of Ligands Using Focused DNA-Encoded Libraries to Develop a Selective, Cell-Permeable CBX8 Chromodomain Inhibitor. *ACS Chem Biol* (2020) 15(1):112–31. doi: 10.1021/acschembio.9b00654
100. Stuckey JI, Dickson BM, Cheng N, Liu Y, Norris JL, Cholensky SH, et al. A Cellular Chemical Probe Targeting the Chromodomains of Polycomb Repressive Complex 1. *Nat Chem Biol* (2016) 12(3):180–7. doi: 10.1038/nchembio.2007
101. Miller TC, Rutherford TJ, Birchall K, Chugh J, Fiedler M, Bienz M. Competitive Binding of a Benzimidazole to the Histone-Binding Pocket of the Pygo PHD Finger. *ACS Chem Biol* (2014) 9(12):2864–74. doi: 10.1021/cb500585s
102. Milosevich N, Hof F. Chemical Inhibitors of Epigenetic Methyllysine Reader Proteins. *Biochemistry* (2016) 55(11):1570–83. doi: 10.1021/acs.biochem.5b01073
103. Yang XJ, Seto E. Hats and Hdacs: From Structure, Function and Regulation to Novel Strategies for Therapy and Prevention. *Oncogene* (2007) 26(37):5310–8. doi: 10.1038/sj.onc.1210599
104. Ikebe J, Sakuraba S, Kono H. H3 Histone Tail Conformation Within the Nucleosome and the Impact of K14 Acetylation Studied Using Enhanced Sampling Simulation. *PloS Comput Biol* (2016) 12(3):e1004788. doi: 10.1371/journal.pcbi.1004788
105. Su J, Wang F, Cai Y, Jin J. The Functional Analysis of Histone Acetyltransferase MOF in Tumorigenesis. *Int J Mol Sci* (2016) 17(1):99. doi: 10.3390/ijms17010099
106. Gregoretti IV, Lee YM, Goodson HV. Molecular Evolution of the Histone Deacetylase Family: Functional Implications of Phylogenetic Analysis. *J Mol Biol* (2004) 338(1):17–31. doi: 10.1016/j.jmb.2004.02.006
107. Whittle JR, Powell MJ, Popov VM, Shirley LA, Wang C, Pestell RG. Sirtuins, Nuclear Hormone Receptor Acetylation and Transcriptional Regulation. *Trends Endocrinol Metab* (2007) 18(9):356–64. doi: 10.1016/j.tem.2007.07.007
108. Yao Z, Chen Y, Cao W, Shyh-Chang N. Chromatin-Modifying Drugs and Metabolites in Cell Fate Control. *Cell Prolif* (2020) 53(11):e12898. doi: 10.1111/cpr.12898

109. Richters A, Koehler AN. Epigenetic Modulation Using Small Molecules - Targeting Histone Acetyltransferases in Disease. *Curr Med Chem* (2017) 24 (37):4121–50. doi: 10.2174/0929867324666170223153115
110. Gajer JM, Furdas SD, Gründer A, Gothwal M, Heinicke U, Keller K, et al. Histone Acetyltransferase Inhibitors Block Neuroblastoma Cell Growth *In Vivo*. *Oncogenesis* (2015) 4(2):e137. doi: 10.1038/oncsis.2014.51
111. Li Y, Wang F, Chen X, Wang J, Zhao Y, Li Y, et al. Zinc-Dependent Deacetylase (HDAC) Inhibitors With Different Zinc Binding Groups. *Curr Top Med Chem* (2019) 19(3):223–41. doi: 10.2174/1568026619666190122144949
112. Banerjee NS, Moore DW, Broker TR, Chow LT. Vorinostat, a Pan-HDAC Inhibitor, Abrogates Productive HPV-18 DNA Amplification. *Proc Natl Acad Sci USA* (2018) 115(47):E11138–47. doi: 10.1073/pnas.1801156115
113. McDermott J, Jimeno A. Belinostat for the Treatment of Peripheral T-Cell Lymphomas. *Drugs Today (Barc)* (2014) 50(5):337–45. doi: 10.1358/dot.2014.50.5.2138703
114. Eleutherakis-Papaiakovou E, Kanellias N, Kastritis E, Gavriatopoulou M, Terpos E, Dimopoulos MA. Efficacy of Panobinostat for the Treatment of Multiple Myeloma. *J Oncol* (2020) 2020:7131802. doi: 10.1155/2020/7131802
115. Morschhauser F, Flinn IW, Advani R, Sehn LH, Diefenbach C, Kolibaba K, et al. Polatuzumab Vedotin or Pinatuzumab Vedotin Plus Rituximab in Patients With Relapsed or Refractory non-Hodgkin Lymphoma: Final Results From a Phase 2 Randomised Study (ROMULUS). *Lancet Haematol* (2019) 6(5):e254–e65. doi: 10.1016/s2352-3026(19)30026-2
116. Shimony S, Horowitz N, Ribakovsky E, Rozovski U, Avigdor A, Zloto K, et al. Romidepsin Treatment for Relapsed or Refractory Peripheral and Cutaneous T-Cell Lymphoma: Real-Life Data From a National Multicenter Observational Study. *Hematol Oncol* (2019) 37(5):569–77. doi: 10.1002/hon.2691
117. Xu Y, Zhang P, Liu Y. Chidamide Tablets: HDAC Inhibition to Treat Lymphoma. *Drugs Today (Barc)* (2017) 53(3):167–76. doi: 10.1358/dot.2017.53.3.2595452
118. Soukupova J, Bertran E, Peñuelas-Haro I, Urdiroz-Urricelqui U, Borgman M, Kohlhof H, et al. Resminostat Induces Changes in Epithelial Plasticity of Hepatocellular Carcinoma Cells and Sensitizes Them to Sorafenib-Induced Apoptosis. *Oncotarget* (2017) 8(66):110367–79. doi: 10.18632/oncotarget.22775
119. Chifotides HT, Bose P, Verstovsek S. Givinostat: An Emerging Treatment for Polycythemia Vera. *Expert Opin Investig Drugs* (2020) 29(6):525–36. doi: 10.1080/13543784.2020.1761323
120. Child F, Ortiz-Romero PL, Alvarez R, Bagot M, Stadler R, Weichenthal M, et al. Phase II Multicentre Trial of Oral Quisinostat, a Histone Deacetylase Inhibitor, in Patients With Previously Treated Stage IB-IVA Mycosis Fungoides/Sézary Syndrome. *Br J Dermatol* (2016) 175(1):80–8. doi: 10.1111/bjd.14427
121. Trapani D, Esposito A, Criscitiello C, Mazzarella L, Locatelli M, Minchella I, et al. Entinostat for the Treatment of Breast Cancer. *Expert Opin Investig Drugs* (2017) 26(8):965–71. doi: 10.1080/13543784.2017.1353077
122. Batlevi CL, Crump M, Andreadis C, Rizzieri D, Assouline SE, Fox S, et al. A Phase 2 Study of Mocetinostat, a Histone Deacetylase Inhibitor, in Relapsed or Refractory Lymphoma. *Br J Haematol* (2017) 178(3):434–41. doi: 10.1111/bjh.14698
123. Wang J, Kim TH, Ahn MY, Lee J, Jung JH, Choi WS, et al. Sirtinol, a Class III HDAC Inhibitor, Induces Apoptotic and Autophagic Cell Death in MCF-7 Human Breast Cancer Cells. *Int J Oncol* (2012) 41(3):1101–9. doi: 10.3892/ijo.2012.1534
124. Wang YM, Gu ML, Meng FS, Jiao WR, Zhou XX, Yao HP, et al. Histone Acetyltransferase P300/CBP Inhibitor C646 Blocks the Survival and Invasion Pathways of Gastric Cancer Cell Lines. *Int J Oncol* (2017) 51(6):1860–8. doi: 10.3892/ijo.2017.4176
125. Wang T, Cui H, Ma N, Jiang Y. Nicotinamide-Mediated Inhibition of SIRT1 Deacetylase Is Associated With the Viability of Cancer Cells Exposed to Antitumor Agents and Apoptosis. *Oncol Lett* (2013) 6(2):600–4. doi: 10.1038/s41467-019-10324-8
126. Shvedunova M, Akhtar A. Modulation of Cellular Processes by Histone and Non-Histone Protein Acetylation. *Nat Rev Mol Cell Biol* (2022) 18:29168. doi: 10.1038/s41580-021-00441-y
127. Ferri E, Petosa C, McKenna CE. Bromodomains: Structure, Function and Pharmacology of Inhibition. *Biochem Pharmacol* (2016) 106:1–18. doi: 10.1016/j.bcp.2015.12.005
128. Lu P, Shen Y, Yang H, Wang Y, Jiang Z, Yang X, et al. BET Inhibitors RVX-208 and PFI-1 Reactivate HIV-1 From Latency. *Sci Rep* (2017) 7(1):16646. doi: 10.1038/s41598-017-16816-1
129. Leal AS, Williams CR, Royce DB, Pioli PA, Sporn MB, Liby KT. Bromodomain Inhibitors, JQ1 and I-BET 762, as Potential Therapies for Pancreatic Cancer. *Cancer Lett* (2017) 394:76–87. doi: 10.1016/j.canlet.2017.02.021
130. Zhu X, Park S, Lee WK, Cheng SY. Potentiated Anti-Tumor Effects of Beti by Meki in Anaplastic Thyroid Cancer. *Endocr Relat Cancer* (2019) 26(9):739–50. doi: 10.1530/erc-19-0107
131. Gerlach D, Tontsch-Grunt U, Baum A, Popow J, Scharn D, Hofmann MH, et al. The Novel BET Bromodomain Inhibitor BI 894999 Represses Super-Enhancer-Associated Transcription and Synergizes With CDK9 Inhibition in AML. *Oncogene* (2018) 37(20):2687–701. doi: 10.1038/s41388-018-0150-2
132. Theodoulou NH, Bamborough P, Bannister AJ, Becher I, Bit RA, Che KH, et al. Discovery of I-BRD9, a Selective Cell Active Chemical Probe for Bromodomain Containing Protein 9 Inhibition. *J Med Chem* (2016) 59 (4):1425–39. doi: 10.1021/acs.jmedchem.5b00256
133. Martin LJ, Koegl M, Bader G, Cockcroft XL, Fedorov O, Fiegen D, et al. Structure-Based Design of an *In Vivo* Active Selective Brd9 Inhibitor. *J Med Chem* (2016) 59(10):4462–75. doi: 10.1021/acs.jmedchem.5b01865
134. Shahabipour F, Caraglia M, Majeed M, Derosa G, Maffioli P, Sahebkar A. Naturally Occurring Anti-Cancer Agents Targeting EZH2. *Cancer Lett* (2017) 400:325–35. doi: 10.1016/j.canlet.2017.03.020
135. Chen J, Lin X, Park KJ, Lee KR, Park HJ. Identification of Protoberberine Alkaloids as Novel Histone Methyltransferase G9a Inhibitors by Structure-Based Virtual Screening. *J Comput Aided Mol Des* (2018) 32(9):917–28. doi: 10.1007/s10822-018-0156-4
136. Zhang L, Miao XJ, Wang X, Pan HH, Li P, Ren H, et al. Antiproliferation of Berberine Is Mediated by Epigenetic Modification of Constitutive Androstane Receptor (CAR) Metabolic Pathway in Hepatoma Cells. *Sci Rep* (2016) 6:28116. doi: 10.1038/srep28116
137. Qing Y, Hu H, Liu Y, Feng T, Meng W, Jiang L, et al. Berberine Induces Apoptosis in Human Multiple Myeloma Cell Line U266 Through Hypomethylation of P53 Promoter. *Cell Biol Int* (2014) 38(5):563–70. doi: 10.1002/cbin.10206
138. Wang Z, Liu Y, Xue Y, Hu H, Ye J, Li X, et al. Berberine Acts as a Putative Epigenetic Modulator by Affecting the Histone Code. *Toxicol In Vitro* (2016) 36:10–7. doi: 10.1016/j.tiv.2016.06.004
139. Kalaiarasi A, Anusha C, Sankar R, Rajasekaran S, John Marshal J, Muthusamy K, et al. Plant Isoquinoline Alkaloid Berberine Exhibits Chromatin Remodeling by Modulation of Histone Deacetylase to Induce Growth Arrest and Apoptosis in the A549 Cell Line. *J Agric Food Chem* (2016) 64(50):9542–50. doi: 10.1021/acs.jafc.6b04453
140. Liu D, Meng X, Wu D, Qiu Z, Luo H. A Natural Isoquinoline Alkaloid With Antitumor Activity: Studies of the Biological Activities of Berberine. *Front Pharmacol* (2019) 10:9. doi: 10.3389/fphar.2019.00009
141. Shi ZY, Zeng JZ, Wong AST. Chemical Structures and Pharmacological Profiles of Ginseng Saponins. *Molecules* (2019) 24(13):2443. doi: 10.3390/molecules24132443
142. Hu HY, Li KP, Wang XJ, Liu Y, Lu ZG, Dong RH, et al. Set9, NF-κb, and MicroRNA-21 Mediate Berberine-Induced Apoptosis of Human Multiple Myeloma Cells. *Acta Pharmacol Sin* (2013) 34(1):157–66. doi: 10.1038/aps.2012.161
143. Lee H, Lee S, Jeong D, Kim SJ. Ginsenoside Rh2 Epigenetically Regulates Cell-Mediated Immune Pathway to Inhibit Proliferation of MCF-7 Breast Cancer Cells. *J Ginseng Res* (2018) 42(4):455–62. doi: 10.1016/j.jgr.2017.05.003
144. Kang KA, Kim HS, Kim DH, Hyun JW. The Role of a Ginseng Saponin Metabolite as a DNA Methyltransferase Inhibitor in Colorectal Cancer Cells. *Int J Oncol* (2013) 43(1):228–36. doi: 10.3892/ijo.2013.1931
145. Zhao L, Shou H, Chen L, Gao W, Fang C, Zhang P. Effects of Ginsenoside Rg3 on Epigenetic Modification in Ovarian Cancer Cells. *Oncol Rep* (2019) 41(6):3209–18. doi: 10.3892/or.2019.7115

146. Chen Y, Shang H, Zhang S, Zhang X. Ginsenoside Rh2 Inhibits Proliferation and Migration of Medulloblastoma Daoy by Down-Regulation of MicroRNA-31. *J Cell Biochem* (2018) 119(8):6527–34. doi: 10.1002/jcb.26716
147. Jin Y, Huynh DTN, Nguyen TLL, Jeon H, Heo KS. Therapeutic Effects of Ginsenosides on Breast Cancer Growth and Metastasis. *Arch Pharm Res* (2020) 43(8):773–87. doi: 10.1007/s12272-020-01265-8
148. Li J, Lu J, Ye Z, Han X, Zheng X, Hou H, et al. 20(s)-Rg3 Blocked Epithelial-Mesenchymal Transition Through DNMT3A/Mir-145/FSCN1 in Ovarian Cancer. *Oncotarget* (2017) 8(32):53375–86. doi: 10.18632/oncotarget.18482
149. Zheng X, Zhou Y, Chen W, Chen L, Lu J, He F, et al. Ginsenoside 20(s)-Rg3 Prevents PKM2-Targeting Mir-324-5p From H19 Sponging to Antagonize the Warburg Effect in Ovarian Cancer Cells. *Cell Physiol Biochem* (2018) 51 (3):1340–53. doi: 10.1159/000495552
150. Liu TJ, Hu S, Qiu ZD, Liu D. Anti-Tumor Mechanisms Associated With Regulation of Non-Coding RNA by Active Ingredients of Chinese Medicine: A Review. *Front Oncol* (2020) 10:634936. doi: 10.3389/fonc.2020.634936
151. Jeong D, Ham J, Park S, Kim HW, Kim H, Ji HW, et al. Ginsenoside Rh2 Suppresses Breast Cancer Cell Proliferation by Epigenetically Regulating the Long Noncoding RNA C3orf67-AS1. *Am J Chin Med* (2019) 47(7):1643–58. doi: 10.1142/s0192415x19500848
152. Christensen LP. Ginsenosides Chemistry, Biosynthesis, Analysis, and Potential Health Effects. *Adv Food Nutr Res* (2009) 55:1–99. doi: 10.1016/s1043-4526(08)00401-4
153. Wan Q, Ma X, Zhang ZJ, Sun T, Xia F, Zhao G, et al. Ginsenoside Reduces Cognitive Impairment During Chronic Cerebral Hypoperfusion Through Brain-Derived Neurotrophic Factor Regulated by Epigenetic Modulation. *Mol Neurobiol* (2017) 54(4):2889–900. doi: 10.1007/s12035-016-9868-4
154. Ham J, Lee S, Lee H, Jeong D, Park S, Kim SJ. Genome-Wide Methylation Analysis Identifies NOX4 and KDM5A as Key Regulators in Inhibiting Breast Cancer Cell Proliferation by Ginsenoside Rg3. *Am J Chin Med* (2018) 46(6):1333–55. doi: 10.1142/s0192415x18500702
155. Liu ZH, Li J, Xia J, Jiang R, Zuo GW, Li XP, et al. Ginsenoside 20(s)-Rh2 as Potent Natural Histone Deacetylase Inhibitors Suppressing the Growth of Human Leukemia Cells. *Chem Biol Interact* (2015) 242:227–34. doi: 10.1016/j.cbi.2015.10.014
156. Yang J, Yuan D, Xing T, Su H, Zhang S, Wen J, et al. Ginsenoside Rh2 Inhibiting HCT116 Colon Cancer Cell Proliferation Through Blocking PDZ-Binding Kinase/T-LAK Cell-Originated Protein Kinase. *J Ginseng Res* (2016) 40(4):400–8. doi: 10.1016/j.jgr.2016.03.007
157. Ashrafizadeh M, Ahmadi Z, Mohammadinejad R, Farkhondeh T, Samarghandian S. MicroRNAs Mediate the Anti-Tumor and Protective Effects of Ginsenosides. *Nutr Cancer* (2020) 72(8):1264–75. doi: 10.1080/01635581.2019.1675722
158. Chen W, Chu S, Li H, Qiu Y. MicroRNA-146a-5p Enhances Ginsenoside Rh2-Induced Anti-Proliferation and the Apoptosis of the Human Liver Cancer Cell Line Hepg2. *Oncol Lett* (2018) 16(4):5367–74. doi: 10.3892/ol.2018.9235
159. Wang X, Wang Y. Ginsenoside Rh2 Mitigates Pediatric Leukemia Through Suppression of Bcl-2 in Leukemia Cells. *Cell Physiol Biochem* (2015) 37 (2):641–50. doi: 10.1159/000430383
160. Chen Y, Zhang Y, Song W, Zhang Y, Dong X, Tan M. Ginsenoside Rh2 Inhibits Migration of Lung Cancer Cells Under Hypoxia *via* Mir-491. *Anticancer Agents Med Chem* (2019) 19(13):1633–41. doi: 10.2174/1871520619666190704165205
161. Wu N, Wu GC, Hu R, Li M, Feng H. Ginsenoside Rh2 Inhibits Glioma Cell Proliferation by Targeting MicroRNA-128. *Acta Pharmacol Sin* (2011) 32 (3):345–53. doi: 10.1038/aps.2010.220
162. Gao Q, Zheng J. Ginsenoside Rh2 Inhibits Prostate Cancer Cell Growth Through Suppression of MicroRNA-4295 That Activates CDKN1A. *Cell Prolif* (2018) 51(3):e12438. doi: 10.1111/cpr.12438
163. Li M, Zhang D, Cheng J, Liang J, Yu F. Ginsenoside Rh2 Inhibits Proliferation But Promotes Apoptosis and Autophagy by Down-Regulating MicroRNA-638 in Human Retinoblastoma Cells. *Exp Mol Pathol* (2019) 108:17–23. doi: 10.1016/j.yexmp.2019.03.004
164. Zhou Y, Zheng X, Lu J, Chen W, Li X, Zhao L. Ginsenoside 20(s)-Rg3 Inhibits the Warburg Effect *via* Modulating DNMT3A/Mir-532-3p/HK2 Pathway in Ovarian Cancer Cells. *Cell Physiol Biochem* (2018) 45(6):2548–59. doi: 10.1159/000488273
165. Cheng Z, Xing D. Ginsenoside Rg3 Inhibits Growth and Epithelial-Mesenchymal Transition of Human Oral Squamous Carcinoma Cells by Down-Regulating Mir-221. *Eur J Pharmacol* (2019) 853:353–63. doi: 10.1016/j.ejphar.2019.03.040
166. Xiang Y, Guo Z, Zhu P, Chen J, Huang Y. Traditional Chinese Medicine as a Cancer Treatment: Modern Perspectives of Ancient But Advanced Science. *Cancer Med* (2019) 8(5):1958–75. doi: 10.1002/cam4.2108
167. Ahuja N, Sharma AR, Baylin SB. Epigenetic Therapeutics: A New Weapon in the War Against Cancer. *Annu Rev Med* (2016) 67:73–89. doi: 10.1146/annurev-med-111314-035900
168. He X, Li Z, Zhuo XT, Hui Z, Xie T, Ye XY. Novel Selective Histone Deacetylase 6 (Hdac6) Inhibitors: A Patent Review (2016-2019). *Recent Patents Anti-Cancer Drug Discov* (2020) 15(1):32–48. doi: 10.2174/1574892815666200217125419

Conflict of Interest: The authors declare that the research was conducted in the absence of any commercial or financial relationships that could be construed as a potential conflict of interest.

Publisher's Note: All claims expressed in this article are solely those of the authors and do not necessarily represent those of their affiliated organizations, or those of the publisher, the editors and the reviewers. Any product that may be evaluated in this article, or claim that may be made by its manufacturer, is not guaranteed or endorsed by the publisher.

frontiers | Frontiers in Oncology

ORIGINAL RESEARCH
published: 11 April 2022
doi: 10.3389/fonc.2022.844135

MUS81 Inhibition Enhances the Anticancer Efficacy of Talazoparib by Impairing ATR/CHK1 Signaling Pathway in Gastric Cancer

Tao Wang†, Peng Zhang†, Chengguo Li, Weizhen Liu, Qian Shen, Lei Yang, Gengchen Xie, Jie Bai, Ruidong Li, Kaixiong Tao and Yuping Yin**

Department of Gastrointestinal Surgery, Union Hospital, Tongji Medical College, Huazhong University of Science and Technology, Wuhan, China

OPEN ACCESS

Edited by:
Jian-ye Zhang, Guangzhou Medical University, China

Reviewed by:
James William Jacobberger, Case Western Reserve University, United States
Matthew K. Summers, The Ohio State University, United States

***Correspondence:**
Yuping Yin
yinyuping2017@hust.edu.cn
Kaixiong Tao
kaixiongtao@hust.edu.cn

†These authors have contributed equally to this work

Specialty section:
This article was submitted to Cancer Molecular Targets and Therapeutics, a section of the journal Frontiers in Oncology

Received: *27 December 2021*
Accepted: *21 March 2022*
Published: *11 April 2022*

Citation:
Wang T, Zhang P, Li C, Liu W, Shen Q, Yang L, Xie G, Bai J, Li R, Tao K and Yin Y (2022) MUS81 Inhibition Enhances the Anticancer Efficacy of Talazoparib by Impairing ATR/CHK1 Signaling Pathway in Gastric Cancer. Front. Oncol. 12:844135. doi: 10.3389/fonc.2022.844135

MUS81 is a critical endonuclease involved in heterodimer formation with Eme1/Mms4 and an important DNA damage repair regulatory molecule. Our previous study suggested that MUS81 was overexpressed and its high expression was positively correlated with gastric cancer metastasis. However, the therapeutic potential of targeting MUS81 in gastric cancer requires further exploration. Therefore, in this study, the Cancer Genome Atlas (TCGA) data were analyzed and showed that MUS81 is a key regulator of cell cycle distribution and DNA damage repair in gastric cancer. *In vitro* and *in vivo*, MUS81 knockdown significantly enhanced the anticancer effect of the PARP inhibitor talazoparib. Mechanistically, MUS81 inhibition impaired the activation of the ATR/CHK1 cell cycle signaling pathway and promoted gastric cancer cells with talazoparib-induced DNA damage to continue mitosis. Moreover, addition of the bromodomain-containing protein 4 inhibitor AZD5153 increased the anticancer effect of talazoparib *via* MUS81 inhibition in gastric cancer cells, and this combination effect was largely impaired when MUS81 was knocked down. In conclusion, these data suggested that MUS81 regulated ATR/CHK1 activation, a key signaling pathway in the G2M checkpoint, and targeting MUS81 enhanced the antitumor efficacy of talazoparib. Therefore, AZD5153 combined with talazoparib may represent a promising therapeutic strategy for patients with MUS81 proficient gastric cancer.

Keywords: gastric cancer, MUS81, PARP inhibitor, BRD4 inhibitor, DNA damage

INTRODUCTION

Gastric cancer is one of the most prevalent forms of cancers and the third leading cause of cancer-related deaths worldwide (1). For early gastric cancer, radical surgical resection is currently the main treatment. However, among patients newly diagnosed with gastric cancer, 70% of them have advanced gastric cancer, and surgery combined with chemoradiotherapy is the standard treatment

Abbreviations: ATR, ataxia telangiectasia and Rad3-related; BRCA, breast cancer susceptibility gene; CHK1, checkpoint kinase 1; DSB, double-strand break; HR, homologous recombination repair; PARP, poly (ADP-ribose) polymerase; SSB, single-strand break; TCGA, the Cancer Genome Atlas; Xpf, Xeroderma pigmentosum type F/Cockayne syndrome.

(2). Limited by the high heterogeneity of gastric cancer biology and genetics, the effect of traditional chemotherapy regimens for gastric cancer has less than optimal results (3). Therefore, more effective treatment strategies need to be explored.

PARP inhibitors block the single-strand break (SSB) repair pathway by targeting PARP, causing homologous recombination deficiency malignant tumors to be synthetically lethal (4, 5). MUS81 belongs to the Xpf family of structure-specific endonucleases (6). It acts as a DNA replication pressure sensor, regulating the DNA replication forks reactivation, further affecting important DNA damage repair pathways, such as cell non-homologous end joining and homologous recombination repair (HR) (6, 7). Inhibition of MUS81 expression in ovarian cancer, significantly impairs cell HR activity (8, 9). Our previous research showed that MUS81 was overexpressed in gastric cancer cells and might promote gastric cancer cell invasion and metastasis (10). However, the therapeutic value of targeting MUS81 requires further investigation.

In this study, whether MUS81 silencing enhances talazoparib sensitivity, was evaluated in gastric cancer, and the mechanism of MUS81 knockdown sensitizing the anticancer effect of talazoparib was characterized. Furthermore, it was observed that AZD5153 sensitized the anticancer effect of talazoparib in gastric cancer *via* down-regulating the expression of MUS81. This is the first report to show that AZD5153 sensitizes the efficacy of talazoparib in gastric cancer by increasing DNA damage and apoptosis.

MATERIALS AND METHODS

Cell Lines, Cell Culture, and Antibodies

SGC7901 and BGC823 cells were purchased from the National Collection of Authenticated Cell Cultures of China. RPMI-1640 medium (Gibco, USA) containing 10% FBS (Gibco BRL, USA) was used to cultivate cells at 37°C in a 5% CO_2 atmosphere.

The primary antibodies against histone H2AX (γ-H2AX)^{S139} (9718S), ATR (13934S), p-ATR^{T1989} (30632S), CHK1 (2360), p-CHK1^{S317} (12302S), p-Histone H3^{Ser10} (53348S), Ki67 (9449S), and GAPDH (5174S) were obtained from Cell Signaling Technology (MA, USA). Antibodies against cleaved PARP (ab32064) were obtained from Abcam (MA, USA). HRP-conjugated secondary antibodies (SA00001-1 and SA00001-2) and anti-MUS81 antibodies were purchased from Proteintech (Wuhan, China).

Cell Survival Assay

SGC7901 and BGC823 cells (1×10^3 cells/well) were seeded in 96-well plates, and then treated with 0 to 1 μmol/L of talazoparib for 5 d. After drug treatment, the cell proliferation rate was determined using the CellTiter^{TM} AQueous assay (MTS, Promega). Ten microliters of CellTiter 96$^{®}$ AQueous One Solution Reagent was added to each well. After incubating for 1 h at 37°C , the absorbance was read at 490 nm using a microplate reader. The cell proliferation rate was calculated using the following formula: (mean optical density (OD) treated well [−blank])/(mean OD control well [−blank]) × 100. Five technical replicates were prepared for each sample in three separate experiments.

Clonogenic Assay

Cells (1×10^3 cells/well) were seeded into 6-well plates and exposed to different concentrations of talazoparib (0 or 100 nmol/L) for 10 d. Cells fixation and staining were performed as previously described (11). Finally, cell clones in 6-well plates were evaluated by ImageJ. The experiments were carried out three times.

Western Blot Analysis

Western blotting was performed as described previously (12). RIPA buffer (V900854, Sigma, MO, USA) containing phosphatase inhibitors (G2007, Servicebio, Wuhan, China) and protease (B14001, Bimake, TX, USA) was used to lyse cells. Equivalent proteins were separated by 7.5%–12.5% SDS-PAGE. Finally, protein bands were detected using the ECL detection reagent (Thermo Fisher Scientific, USA). The results were analyzed using ImageJ. Experiments were performed three times.

Apoptosis and Cell Cycle Analysis

Cells (2×10^5 cells/well) were seeded into 6-well plates and exposed to DMSO or talazoparib (1 μmol/L) for 3 d. To examine apoptosis, the cells were harvested by trypsinization and washed twice with PBS at 4°C . The cells were resuspended in 100 μL Annexin V binding buffer, and 5 μL 7-AAD and 5 μL allophycocyanin-Annexin V were added. After the cells were incubated for 15 min in the dark at room temperature, 100 μL Annexin V binding buffer was added, and the proportion of apoptotic cells was analyzed by flow cytometry.

Cell cycle detection was performed as described previously (13). These experiments were performed using three biological replicates.

Immunofluorescence Assay

Coverslips were coated with 0.01% poly-L-lysine and exposed to DMSO, talazoparib (0.5 μmol/L), AZD5153 (1 μmol/L), or their combination after the cells were plated. After two days of treatment, immunofluorescence was performed by staining with primary antibodies against γ-H2AX (1:100), p-Histone H3 (1:1600), or p-CHK1 (1:800) as previously described (14). Then, the coverslips were incubated with DAPI and CY3-conjugated secondary antibodies. Finally, coverslips were scanned using a fluorescence microscope (Nikon, Tokyo, Japan). The reproducibility of the results was confirmed by at least three separate experiments.

Cell Transfection and RNA Interference

Two different shRNA sequences were used for MUS81 knockdown. Lentivirus (GeneChem Co. Ltd., China) targeting the sequence of human MUS81 (shRNA #1: 5′-TACCAACAAA CAGCAAGTGGG-3′, shRNA #2: 5′-CACGCGCTTCGTATTT CAGAA-3′) was purchased from GeneChem Co. Ltd. (Shanghai, China). The corresponding control shRNA sequence was 5′-TTCTCCGAACGTGTCACGT-3′. Lentiviral infection was conducted as described previously (15). Stable GC cell lines transfected with scramble shRNA, shRNA #1, or shRNA #2 were selected for 7 d with 4 μg/mL puromycin.

Two specific MUS81 siRNAs were purchased from RiboBio (Guangzhou, China). The negative control siRNA sequence is 5'-GGGUAUCGACGAUUACAAA-3', and the sequences of siRNA #1 and siRNA #2 targeting MUS81 are 5'-TACCAACAAACAGCAAGTGGG-3' and 5'-CACGCGCTTCGTATTTCAGAA-3', respectively. Transient transfection was performed using Lipofectamine 2000 (Thermo Fisher Scientific, USA) and siRNAs for 24 h. Western blotting was used to verify the knockdown effect of MUS81.

In Vivo Experiments

The Institutional Animal Care and Use Committee of Tongji Medical College, Huazhong University of Science and Technology approved all animal experiments in this study. A total of 20 five-week-old BALB/c-null mice were purchased from HFK Biotechnology (Beijing, China). $SGC7901^{shCtrl}$ and $SGC7901^{shMUS81}$ cells were resuspended in PBS to obtain a concentration of 1×10^7 cells/mL, and then each mouse was subcutaneously injected 150 μL of the solution in the right flank. When the tumor volume reached 100 mm^3, the mice were randomly divided into four groups: control, MUS81-knockdown, talazoparib-treated, and MUS81-knockdown plus talazoparib-treated groups (five mice per group). Mice in the talazoparib group was administered talazoparib (0.33 mg/kg) by gavage for 21 consecutive days. The control group was administered the same dose of DMSO and PBS by gavage. After treatment, the mice were sacrificed, tumors were collected and embedded in paraffin, and immunohistochemically stained.

Immunohistochemistry

Immunohistochemistry was performed using an antibody against Ki67 or γ-H2AX at a dilution of 1:200 as previously described (16). A brown signal was defined as a positive reaction in the cells. The results of immunohistochemical staining using a mean score were compared, considering both the intensity of staining and the proportion of tumor cells; the staining intensity score was 3, strong; 2, moderate; 1, weak; and 0, negative. The positive cell frequency was defined as 4 (76%–100%), 3 (51%–75%), 2 (26%–50%), 1 (1%–25%), and 0 (none). Immunohistochemical staining was performed for each component and the final score was obtained *via* multiplying the score of staining intensity and the score of positive cell frequency. Scores 0–7 were defined as negative staining, and 8–12 were defined as positive staining.

Statistical Analyses

Statistical analysis was performed using GraphPad Prism version 9. A *t*-test was performed for intergroup comparisons and data are presented as the mean ± standard deviation (SD). *P* values less than 0.05 were considered significantly different and all tests were two-tailed.

RESULTS

MUS81 Was Highly Expressed and Enriched in DNA Damage Repair Pathways in Gastric Cancer

Using TCGA database, the differential expression of DNA damage repair network-related molecules was analyzed in 18 common malignant tumors; MUS81 was significantly highly expressed in gastric cancer (**Figures 1A, B**). Based on the gene set enrichment analysis in malignant tumors, MUS81 may play a critical role in many signaling pathways, such as the cell cycle regulation and DNA damage response pathways (**Figures 1C, D**). These results suggested that targeting MUS81 is a potential treatment strategy in the clinical treatment of gastric cancer.

MUS81 Knockdown Promoted Apoptosis and Anticancer Efficacy of Talazoparib *In Vitro*

Next, SGC7901 and BGC823 cells were infected with the lentivirus vector (LV)-shMUS81. Western blotting was used to examine MUS81 protein levels in SGC7901 and BGC823 cells infected with LV-shMUS81 and LV-Ctrl. MUS81 protein levels were significantly decreased in MUS81 knockdown cells (**Figure 2A**).

MUS81 is an important DNA damage repair regulatory molecule and MUS81 deficiency impairs cell HR (8, 17). To explore whether down-regulation of MUS81 expression in gastric cancer cells affected the antitumoral efficacy of PARP inhibitors, MTS assay was performed and the data were analyzed to construct the dose-inhibition efficiency curves of the PARP inhibitor talazoparib in different groups. As shown in **Figure 2B**, cell proliferation of the LV-shMUS81 group was significantly decreased compared to that of the LV-Ctrl group in both SGC7901 and BGC823 cells, and the clone formation rate in the LV-shMUS81 group was significantly lower than that in the LV-Ctrl group after talazoparib treatment (71.69% ± 3.61% versus 12.38% ± 2.21% and 65.34% ± 3.22% versus 7.67% ± 1.53%, respectively, $P < 0.01$ for all) (**Figure 2C**).

To further confirm whether the antitumor effect of PARP inhibitors increased by MUS81 knockdown was due to increased apoptosis, flow cytometry was performed to measure the apoptosis rate of gastric cancer cells. Seventy-two hours after talazoparib treatment, a marked increase in apoptotic SGC7901 and BGC823 cells was revealed in the LV-shMUS81 group compared to that in the LV-Ctrl group (39.67% ± 2.08% versus 20.67% ± 1.50% and 48.69% ± 5.51% versus 17.34% ± 2.00%, respectively, $P < 0.01$ for all) (**Figure 2D**). In addition, western blotting also showed that the expression of cleaved PARP, a marker of apoptosis, increased significantly after exposure to talazoparib in the LV-shMUS81 group (**Figure 2E**).

MUS81 Inhibition Pushed Cells Into Mitosis From G2M Checkpoint Arrest Induced by Talazoparib and Increased DNA Damage Caused by Talazoparib in Gastric Cancer Cells

To further investigate the mechanism by which MUS81 knockdown enhanced the sensitivity of SGC7901 and BGC823 cells to talazoparib, flow cytometry was performed for cell cycle analysis. Cell cycle analysis showed that talazoparib treatment induced significant G2M phase arrest in SGC7901 and BGC823 cells (**Figure 3A**). However, after stably transfecting with shMUS81, SGC7901 and BGC823 cells that were arrested by talazoparib in the G2M phase continued to mitosis, and the

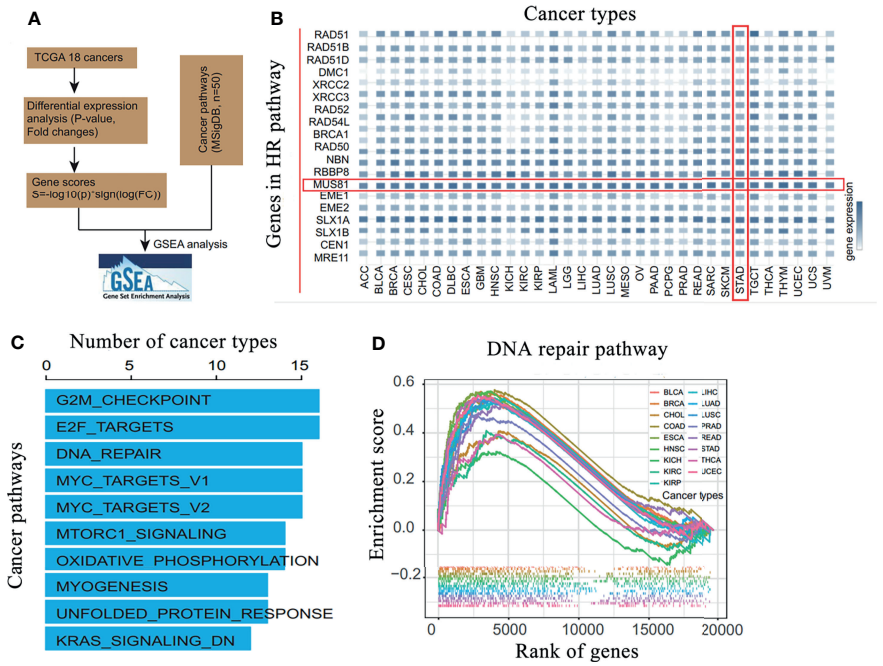

FIGURE 1 | MUS81 is overexpressed in gastric cancer and is enriched in DNA damage repair pathways in malignant tumors. **(A)** Bioinformatics analysis process. **(B)** Analysis of the differential expression of DNA damage and repair-related molecules in 18 common malignant tumors in TCGA database suggests that MUS81 is overexpressed in gastric cancer. **(C)** Gene set enrichment analysis of MUS81-related enrichment signaling pathways in malignant tumors. **(D)** Enrichment of MUS81 in DNA damage repair pathways in malignant tumors.

proportion of G0/G1 phase cells increased significantly (**Figure 3A**). To verify the effect of MUS81 knockdown on cell mitosis, the LV-shMUS81 and LV-Ctrl groups were stained for p-Histone H3 (Ser10), a mitosis marker, following treatment with talazoparib. MUS81 knockdown pushed gastric cancer cells with talazoparib-induced DNA damage into mitosis (**Figure 3B**).

Next, whether MUS81 deficiency impaired cellular DNA repair ability was tested. In this study, a DNA damage model was established using talazoparib. γ-H2AX expression was significantly increased after talazoparib treatment in LV-shMUS81 cells (**Figures 3C, D**). These data indicated that MUS81 knockdown increased talazoparib-induced DNA damage in gastric cancer cells.

MUS81 Deficiency Impaired ATR/CHK1 Activation Induced by Talazoparib in Gastric Cancer

Having observed a defective G2M phase checkpoint in MUS81-deficient cells, whether MUS81 deficiency impaired the DNA damage checkpoint signaling pathway was further examined. Because CHK1 is a key G2/M checkpoint regulator, cells were exposed to talazoparib and CHK1 phosphorylation (Ser317) was examined by immunofluorescence and western blotting. In SGC7901 and BGC823 LV-Ctrl cells, CHK1 phosphorylation (Ser317) significantly increased after treatment with talazoparib. However, relatively reduced CHK1 phosphorylation (Ser317) was observed in response to talazoparib in LV-shMUS81 cells (**Figure 4A**).

CHK1 (Ser317) can be phosphorylated by ATR phosphorylation, and CHK1 phosphorylation prompts cells to enter G2M phase arrest for DNA repair (18–21). Therefore, whether MUS81 deficiency affected ATR activation was examined. Western blotting showed that MUS81 knockdown significantly decreased ATR activation and reduced the CHK1 activation response to talazoparib (**Figures 4B, C**). These results indicated that MUS81 knockdown impaired the G2M phase checkpoint of cells by suppressing ATR/CHK1 signaling.

MUS81 Knockdown Enhanced Anticancer Efficacy of Talazoparib in Gastric Cancer *In Vivo*

To demonstrate that MUS81 knockdown increases the antitumor effect of talazoparib *in vivo*, nude mice bearing MUS81-deficient and parental xenograft gastric cancer were treated daily with and without oral 0.33 mg/kg talazoparib. Talazoparib showed outstanding anticancer effect in the MUS81-deficient gastric cancer model (**Figure 5A**); the antitumor effect was most significant after 21 d of treatment (**Figure 5B**). There was no significant difference in the body weight among the four groups of nude mice (**Figure 5C**).

IHC studies indicated that after treatment with talazoparib, tumor tissues from the MUS81-deficient group showed lower Ki67 expression, suggesting lower proliferation ability compared to that of the parental xenograft group (**Figure 5D**). Furthermore, the expression of γ-H2AX was analyzed. As

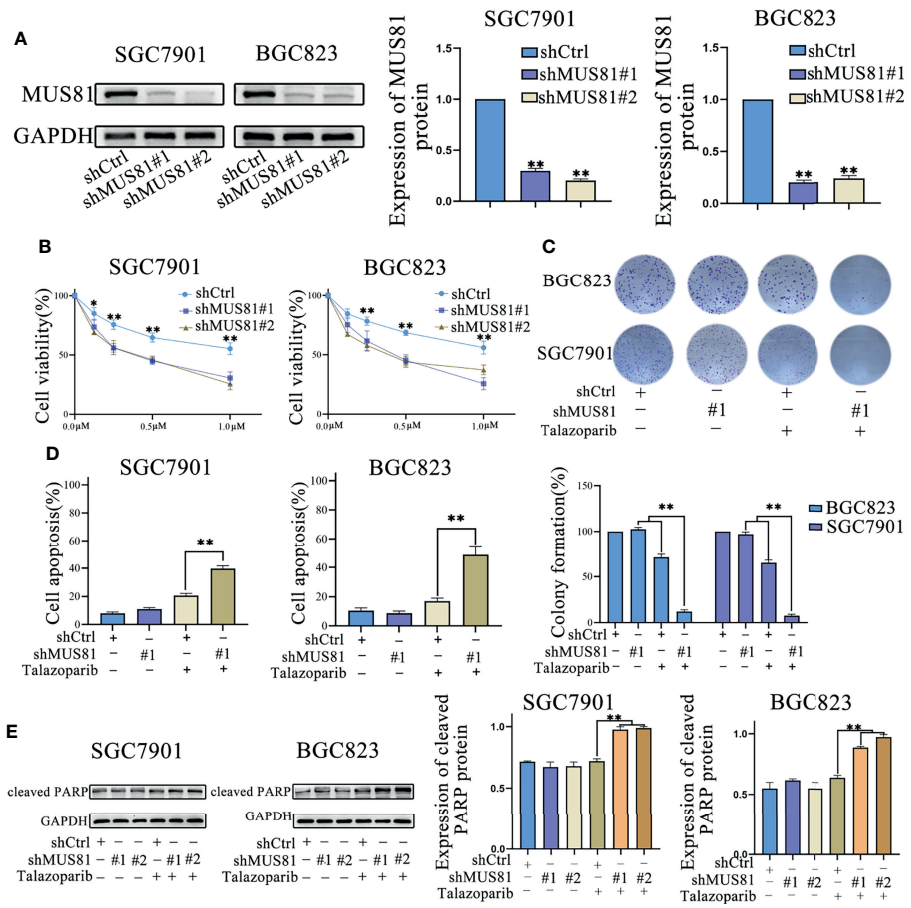

FIGURE 2 | MUS81 knockdown promotes apoptosis and talazoparib anticancer efficacy *in vitro*. **(A)** Western blotting of MUS81 protein expression after transfection with the lentivirus expressing short hairpin RNA (shRNA) targeting the sequence of human MUS81 for 24 h. $^{**}P < 0.01$. **(B, C)** Viability of SGC7901 and BGC823 cells transfected with lentivirus expressing shMUS81 #1, shMUS81 #2 or shCtrl, as determined using MTS and colony formation assays (t-test). $^{*}P < 0.05$. $^{**}P < 0.01$. **(D)** Cells treated with DMSO or talazoparib (1 μmol/L) for 3 d to evaluate apoptosis by flow cytometry (*t*-test). $^{**}P < 0.01$. **(E)** Expression of apoptosis-related proteins in SGC7901 and BGC823 cells treated with DMSO or talazoparib (0.5 μmol/L) for 24 h, as evaluated by western blotting (*t*-test). $^{**}P < 0.01$.

expected, MUS81 knockdown tumor cells showed higher expression of γ-H2AX than control cells in response to talazoparib (**Figure 5D**). Overall, these data represented excellent antitumor efficacy of talazoparib in the MUS81-deficient gastric cancer xenograft model.

AZD5153 Sensitized the Anticancer Effect of Talazoparib in a MUS81-Dependent Manner in Gastric Cancer Cells

Our previous study has shown that the BRD4 inhibitor AZD5153 downregulates MUS81 expression (10). Thus, it was hypothesized that AZD5153 might sensitize the talazoparib antitumor effect in gastric cancer cells by regulating MUS81 expression. To verify the potential synergy between AZD5153 and talazoparib, the effects of monotherapy and combination therapy were assessed in SGC7901 and BGC823 cell lines. MTS data showed that the AZD5153/talazoparib combination was synergistic with a combination index of less than 0.5 in LV-Ctrl cell lines. Interestingly, in the MUS81 knockdown cell line, the AZD5153/talazoparib combination effect was significantly impaired (**Figures 6A, B**).

Next, western blotting showed that AZD5153 significantly reduced MUS81 expression. Furthermore, similar to talazoparib therapy in MUS81 knockdown cells, the AZD5153/talazoparib combination therapy significantly improved the expression of γ-H2AX and cleaved PARP in LV-Ctrl cells (**Figures 6C, D**). These data suggested that the efficacy of AZD5153 sensitized talazoparib in gastric cancer cells may be attributed to its ability to downregulate MUS81. AZD5153/talazoparib combination therapy promoted DNA damage and apoptosis in SGC7901 and BGC823 cells (**Figure 7**).

DISCUSSION

Among DNA damage repair pathways, PARP plays an indispensable role in the repair of DNA SSBs (22, 23). PARP

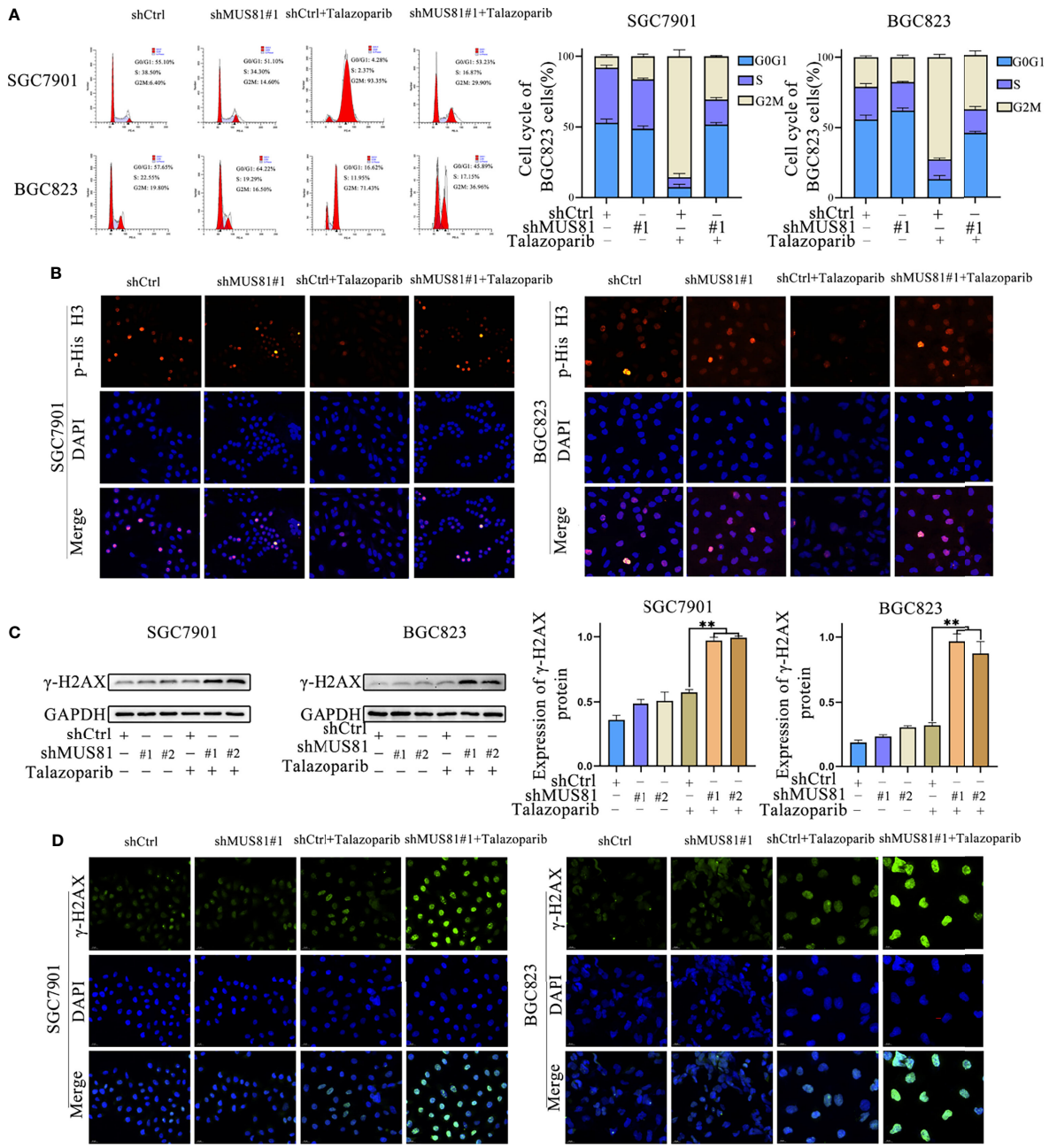

FIGURE 3 | MUS81 inhibition may increase talazoparib-induced DNA damage in gastric cancer cells. **(A)** Cells treated with DMSO or talazoparib (1 μmol/L) for 3 d to evaluate cell cycle distribution by flow cytometry (*t*-test). $^{**}P < 0.01$. **(B)** Immunofluorescence to detect the expression of p-Histone H3 (Ser10) in DMSO or talazoparib-treated (0.5 μmol/L) cells for 2 d. Magnification, 400×. **(C)** Western blot analysis of γ-H2AX expression after treatment with 0.5 μmol/L talazoparib for 24 h (t-test). $^{**}P < 0.01$. **(D)** Immunofluorescence to detect the expression of γ-H2AX in DMSO or talazoparib-treated (0.5 μmol/L) cells for 2 d. Magnification, 400×. $^{**}P < 0.01$.

inhibitors impair SSB repair to cause tumor cells to transform into DNA DSBs in the S phase, which leads to cell death due to mitotic catastrophe or apoptosis in tumors with BRCA1 and BRCA2 mutations as well as an HR deficiency (24). However, in gastric cancer, mutation rates in HRD genes (BRCA1 and BRCA2) are low, and individual PARP inhibitors have limited efficacy (25). Therefore, it is urgent to explore other targets to enhance the antitumor effect of PARP inhibitors and to expand the beneficiary population in gastric cancer. The DNA endonuclease MUS81 is a member of the endonuclear

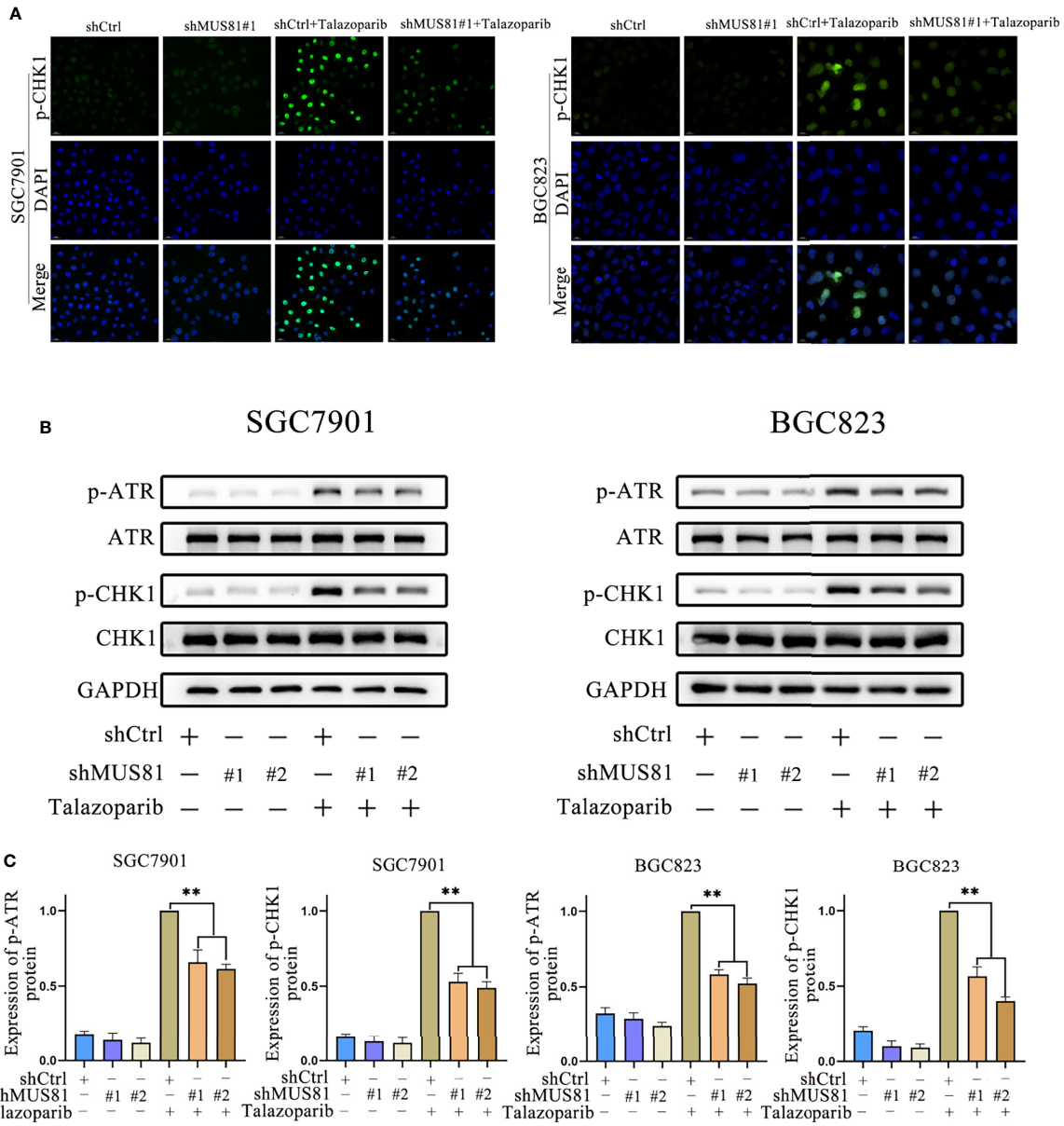

FIGURE 4 | MUS81 deficiency impairs ATR/CHK1 activation induced by talazoparib in gastric cancer. **(A)** Immunofluorescence to detect p-CHK1 expression in talazoparib-treated (0.5 μmol/L) cells for 2 d. Magnification, 400×. **(B, C)** Western blot analysis examining the expression of p-ATR and p-CHK1 after treatment with 0.5 μmol/L talazoparib for 24 h (*t*-test). $^{**}P < 0.01$.

XPF family, which has been implicated in DNA repair *via* HR (7, 26–28). In the present study, MUS81 was involved in DNA damage repair and cell cycle regulation pathways in gastric cancer. MUS81 knockdown enhanced the cytotoxic effects of talazoparib-induced apoptosis in gastric cancer cells.

DNA damage checkpoints mainly include G1-S and G2-M, which regulate whether the cell continues mitosis or performs DNA repair or apoptosis (29, 30). Our research showed that talazoparib causes DNA damage in tumor cells, activates G2-M checkpoints, and leads to G2-M phase arrest. A previous study showed that MUS81 knockdown reverses the G2-M block caused by epirubicin in liver cancer cells (31). The current study also confirmed that MUS81 knockdown reversed G2-M block caused by talazoparib in gastric cancer, which might cause tumor cells to continue mitosis with unrepaired DNA and eventually lead to cell death. This research showed that talazoparib had significant antitumor effects in a MUS81-deficient SGC7901 xenograft model, and there was no significant difference in the body weight among the four groups of nude mice during the treatment.

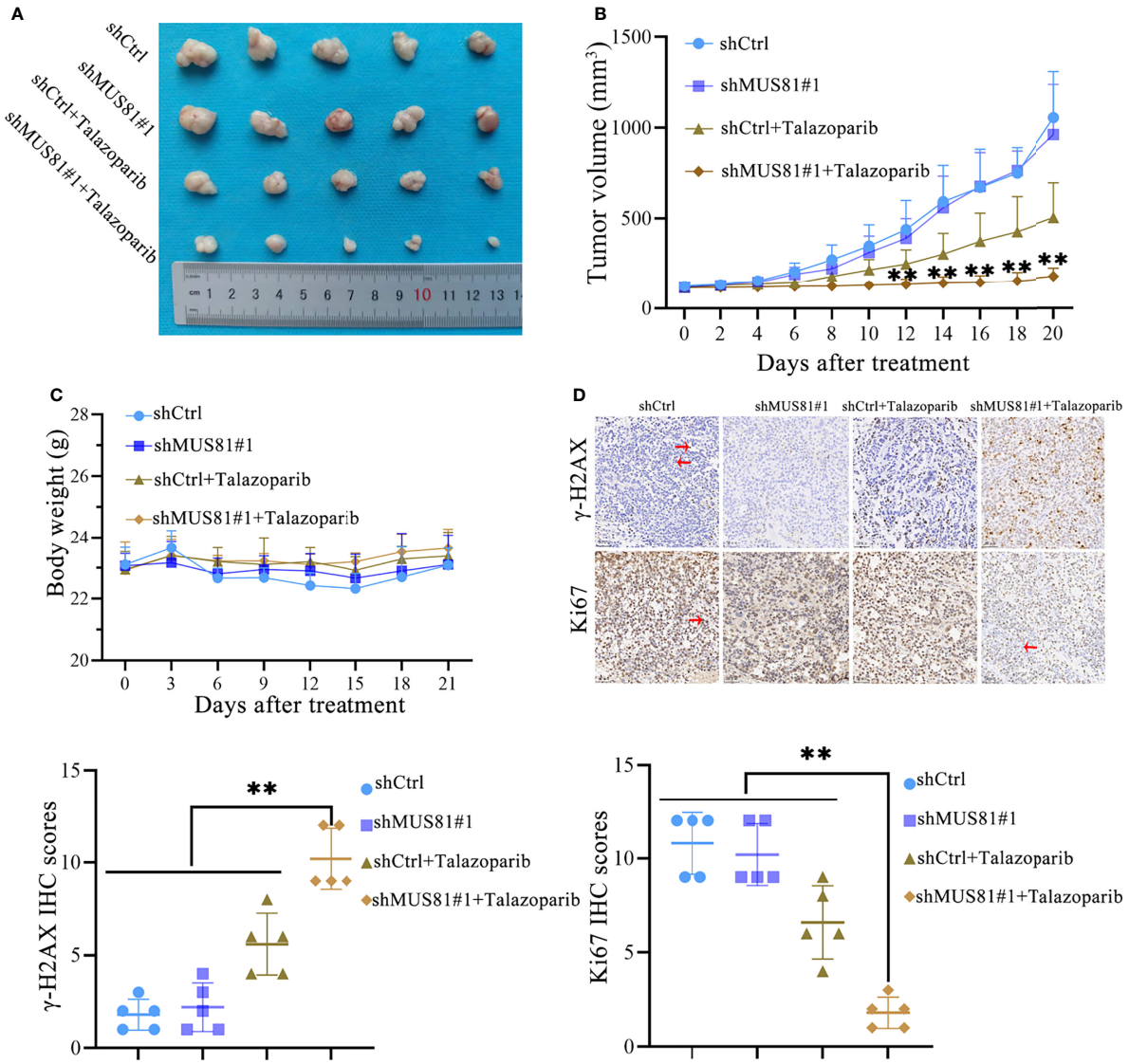

FIGURE 5 | MUS81 knockdown enhances the anticancer efficacy of talazoparib in gastric cancer *in vivo*. **(A, B)** Tumor volume of each group on the indicated days of treatment (*t*-test). $^{**}P < 0.01$. **(C)** Weight of nude mice on indicated days of treatment (*t*-test). **(D)** Representative images of γ-H2AX and Ki-67 immunohistochemistry (*t*-test). Positive expression (→). Negative expression (←). Magnification, 200×. $^{**}P < 0.01$.

In addition, it was observed that MUS81 knockdown reduced the activation of ATR and CHK1 in gastric cancer cells induced by talazoparib. ATR is one of the central regulators that control cellular responses to DNA damage (32, 33). In the G2 phase, activation of the ATR/CHK1 pathway blocks cells from continuing mitosis with damaged DNA (34, 35). Our previous study has shown that the CHK1 inhibitor LY2606368 impairs HR-mediated DNA damage repair, thereby sensitizing the antitumor efficacy of PARP inhibitors (36). Therefore, MUS81 knockdown promoted talazoparib-induced DNA damage by regulating the ATR/CHK1 pathway.

Overall, these findings indicated that sensitivity of gastric cancer to talazoparib relied on MUS81 inactivation. Our previous research has shown that AZD5153, a novel BRD4 inhibitor, downregulates MUS81 expression, and reduces the migration of gastric cancer cells *in vitro* and *in vivo* (10). Therefore, talazoparib combined with AZD5153 was applied to treat gastric cancer. In LV-Ctrl gastric cancer cells, combined MUS81 and AZD5153 treatment achieved the same antitumor effect as MUS81 knockdown combined with talazoparib treatment. Our previous work confirmed that AZD5153 inhibits the expression of sirt5 and impairs the MUS81 transcription function in gastric cancer cells (10); however,

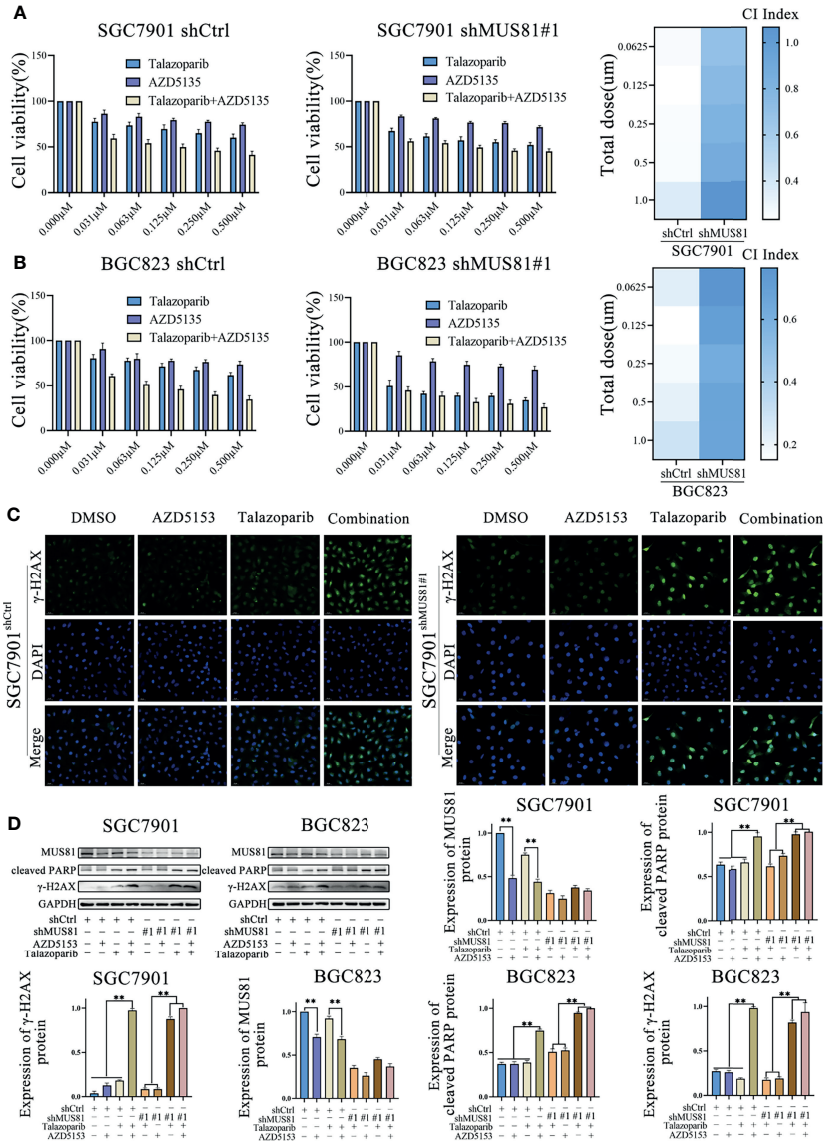

FIGURE 6 | AZD5153 sensitizes the talazoparib anticancer effect in a MUS81-dependent manner in gastric cancer cells. **(A, B)** Viability of cells treated with monotherapy and combination therapy for 5 d, as determined using MTS (*t*-test). At five gradually increasing concentrations (0.0625 μmol/L to 1.000 μmol/L), the mean CI of SGC7901^{shCtrl} cells were 0.26, 0.23, 0.25, 0.26, and 0.36, respectively; the mean CI of SGC7901^{shMU81} cells were 0.69, 0.75, 0.81, 0.87, and 1.07, respectively; the mean CI of BGC823^{shCtrl} cells were 0.23, 0.15, 0.18, 0.21, and 0.29, respectively; the mean CI of BGC823^{shMU81} cells were 0.76, 0.69, 0.62, 0.67, and 0.67, respectively. The difference between shMU81 and shCtrl groups was statistically significant (all $P < 0.01$). **(C)** Immunofluorescence to detect the expression of phosphorylated checkpoint kinase 1 (p-CHK1) in cells treated with DMSO, AZD5153 (1 μmol/L), talazoparib (0.5 μmol/L), or combination therapy for 2 d. Magnification, 400×. **(D)** Western blot analysis examining the expression of MUS81, cleaved PARP, and γ-H2AX in gastric cancer cells after treatment with DMSO, AZD5153 (1 μmol/L), talazoparib (0.5 μmol/L), or combination therapy for 2 d (*t*-test). $^{**}P < 0.01$.

the underlying mechanism by which AZD5153 regulates MUS81 remains to be explored. In future, the combined use of AZD5153 and talazoparib in clinical trials may further verify their efficacy in the treatment of gastric cancer and may improve the prognosis of patients with advanced gastric cancer. However, *in vivo* experiments need to be conducted to examine whether AZD5153 can enhance the lethality of talazoparib to normal cells. Additionally, the combination therapy's therapeutic window remains to be confirmed by further studies.

In conclusion, MUS81 was overexpressed in gastric cancer cells and was closely related to cell cycle regulation and DNA damage repair pathways. Moreover, MUS81 was a key molecule that enhanced the talazoparib antitumor effect in gastric cancer cells. MUS81 targeting markedly induced DNA damage and promoted cell apoptosis after talazoparib treatment by inhibiting ATR/CHK1

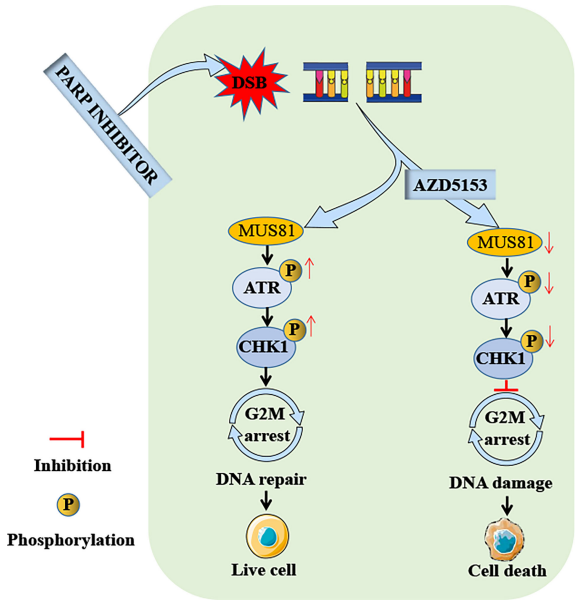

FIGURE 7 | Schema of the antitumor effect of AZD5153 sensitizing gastric cancer cells to talazoparib. AZD5153 inhibits the ATR/CHK1 pathway activated by DNA damage by downregulating MUS81 expression, causing gastric cancer cells to continue mitosis with damaged DNA, ultimately leading to cell death.

pathway activation. Importantly, AZD5153 enhanced the talazoparib antitumor effect in gastric cancer cells by reducing MUS81 expression. Taken together, talazoparib in combination with AZD5153 may be a promising treatment strategy for MUS81 overexpressed gastric cancer.

DATA AVAILABILITY STATEMENT

The datasets presented in this study can be found in online repositories. The names of the repository/repositories and accession number(s) can be found in the article/supplementary material.

ETHICS STATEMENT

The animal study was reviewed and approved by the Institutional Animal Care and Use Committee of Tongji Medical College, Huazhong University of Science and Technology.

AUTHOR CONTRIBUTIONS

TW and PZ conducted the experiments, performed the data analysis and wrote the paper. CL, WL, QS, and LY performed the experiments. GX, JB, and RL analyzed data. YY and KT revised the manuscript and designed the experiment. All authors contributed to the article and approved the submitted version.

FUNDING

This work was supported by the Natural Science Foundation of Hubei Province (No. 2019CFB660, 2019CFB100 and 2021CFB566), the Key Research and Development Program of Hubei Province (No. 2021BCA116) and the National Natural Science Foundation of China (No. 81874184, 82003205, and 82003131).

REFERENCES

1. Bray F, Ferlay J, Soerjomataram I, Siegel RL, Torre LA, Jemal A. Global Cancer Statistics 2018: GLOBOCAN Estimates of Incidence and Mortality Worldwide for 36 Cancers in 185 Countries. *CA Cancer J Clin* (2018) 68 (6):394–424. doi: 10.3322/caac.21492
2. Wagner AD, Syn NL, Moehler M, Grothe W, Yong WP, Tai BC, et al. Chemotherapy for Advanced Gastric Cancer. *Cochrane Database Syst Rev* (2017) 8(8):CD004064. doi: 10.1002/14651858.CD004064.pub4
3. Padmanabhan N, Ushijima T, Tan P. How to Stomach an Epigenetic Insult: The Gastric Cancer Epigenome. *Nat Rev Gastroenterol Hepatol* (2017) 14 (8):467–78. doi: 10.1038/nrgastro.2017.53
4. Negrini S, Gorgoulis VG, Halazonetis TD. Genomic Instability–An Evolving Hallmark of Cancer. *Nat Rev Mol Cell Biol* (2010) 11(3):220–8. doi: 10.1038/nrm2858
5. Pearl LH, Schierz AC, Ward SE, Al-Lazikani B, Pearl FM. Therapeutic Opportunities Within the DNA Damage Response. *Nat Rev Cancer* (2015) 15(3):166–80. doi: 10.1038/nrc3891
6. Ho CK, Mazón G, Lam AF, Symington LS. Mus81 and Yen1 Promote Reciprocal Exchange During Mitotic Recombination to Maintain Genome Integrity in Budding Yeast. *Mol Cell* (2010) 40(6):988–1000. doi: 10.1016/j.molcel.2010.11.016
7. Di Marco S, Hasanova Z, Kanagaraj R, Chappidi N, Altmannova V, Menon S, et al. RECQ5 Helicase Cooperates With MUS81 Endonuclease in Processing Stalled Replication Forks at Common Fragile Sites During Mitosis. *Mol Cell* (2017) 66(5):658–71. doi: 10.1016/j.molcel.2017.05.006
8. Lu R, Xie S, Wang Y, Zheng H, Zhang H, Deng M, et al. MUS81 Participates in the Progression of Serous Ovarian Cancer Associated With Dysfunctional DNA Repair System. *Front Oncol* (2019) 9:1189. doi: 10.3389/fonc.2019.01189
9. Zhong A, Zhang H, Xie S, Deng M, Zheng H, Wang Y, et al. Inhibition of MUS81 Improves the Chemical Sensitivity of Olaparib by Regulating MCM2 in Epithelial Ovarian Cancer. *Oncol Rep* (2018) 39(4):1747–56. doi: 10.3892/or.2018.6229
10. Yin Y, Liu W, Shen Q, Zhang P, Wang L, Tao R, et al. The DNA Endonuclease Mus81 Regulates ZEB1 Expression and Serves as a Target of BET4 Inhibitors in Gastric Cancer. *Mol Cancer Ther* (2019) 18(8):1439–50. doi: 10.1158/1535-7163.MCT-18-0833
11. Huang Y, Zhang J, Hou L, Wang G, Liu H, Zhang R, et al. LncRNA AK023391 Promotes Tumorigenesis and Invasion of Gastric Cancer Through Activation of the PI3K/Akt Signaling Pathway. *J Exp Clin Cancer Res* (2019) 36(1):194. doi: 10.1186/s13046-017-0666-2
12. Nam HJ, Kim HP, Yoon YK, Song SH, Min AR, Han SW, et al. The Irreversible Pan-HER Inhibitor PF00299804 Alone or Combined With Gemcitabine Has an Antitumor Effect in Biliary Tract Cancer Cell Lines. *Invest New Drugs* (2012) 30(6):2148–60. doi: 10.1007/s10637-011-9782-6
13. Zhang J, Wang G, Chu SJ, Zhu JS, Zhang R, Lu WW, et al. Loss of Large Tumor Suppressor 1 Promotes Growth and Metastasis of Gastric Cancer Cells Through Upregulation of the YAP Signaling. *Oncotarget* (2016) 7(13):16180–93. doi: 10.18632/oncotarget.7568
14. Chen X, Li L, Liu F, Hoh J, Kapron CM, Liu J. Cadmium Induces Glomerular Endothelial Cell-Specific Expression of Complement Factor H *via* the -1635

AP-1 Binding Site. *J Immunol* (2019) 202(4):1210–8. doi: 10.4049/jimmunol.1800081
15. Fang Z, Cao B, Liao JM, Deng J, Plummer KD, Liao P, et al. SPIN1 Promotes Tumorigenesis by Blocking the Ul18 (Universal Large Ribosomal Subunit Protein 18)-MDM2-P53 Pathway in Human Cancer. *Elife* (2018) 7:e31275. doi: 10.7554/eLife.31275
16. Jia X, Guo T, Li Z, Zhang M, Feng Y, Dong B, et al. Clinicopathological and Immunomicroenvironment Characteristics of Epstein-Barr Virus-Associated Gastric Cancer in a Chinese Population. *Front Oncol* (2021) 10:586752. doi: 10.3389/fonc.2020.586752
17. Ghamrasni SE, Cardoso R, Li L, Guturi KK, Bjerregaard VA, Liu Y, et al. Rad54 and Mus81 Cooperation Promotes DNA Damage Repair and Restrains Chromosome Missegregation. *Oncogene* (2016) 35(37):4836–45. doi: 10.1038/onc.2016.16
18. Jazayeri A, Falck J, Lukas C, Bartek J, Smith GC, Lukas J, et al. ATM- and Cell Cycle-Dependent Regulation of ATR in Response to DNA Double-Strand Breaks. *Nat Cell Biol* (2006) 8(1):37–45. doi: 10.1038/ncb1337
19. Kozlov SV, Graham ME, Peng C, Chen P, Robinson PJ, Lavin MF. Involvement of Novel Autophosphorylation Sites in ATM Activation. *EMBO J* (2006) 25(15):3504–14. doi: 10.1038/sj.emboj.7601231
20. Nam EA, Zhao R, Glick GG, Bansbach CE, Friedman DB, Cortez D. Thr-1989 Phosphorylation Is a Marker of Active Ataxia Telangiectasia-Mutated and Rad3-Related (ATR) Kinase. *J Biol Chem* (2011) 286(33):28707–14. doi: 10.1074/jbc.M111.248914
21. Liu S, Shiotani B, Lahiri M, Maréchal A, Tse A, Leung CC, et al. ATR Autophosphorylation as a Molecular Switch for Checkpoint Activation. *Mol Cell* (2011) 43(2):192–202. doi: 10.1016/j.molcel.2011.06.019
22. Powell SN, Bindra RS. Targeting the DNA Damage Response for Cancer Therapy. *DNA Repair (Amst)* (2009) 8(9):1153–65. doi: 10.1016/j.dnarep.2009.04.011
23. Pascal JM, Ellenberger T. The Rise and Fall of Poly(ADP-Ribose): An Enzymatic Perspective. *DNA Repair (Amst)* (2015) 32:10–6. doi: 10.1016/j.dnarep.2015.04.008
24. Hoevenaar WHM, Janssen A, Quirindongo AI, Ma H, Klaasen SJ, Teixeira A, et al. Degree and Site of Chromosomal Instability Define Its Oncogenicpotential. *Nat Commun* (2020) 11(1):1501. doi: 10.1038/s41467-020-15279-9
25. Alexandrov LB, Nik-Zainal S, Siu HC, Leung SY, Stratton MR. A Mutational Signature in Gastric Cancer Suggests Therapeutic Strategies. *Nat Commun* (2015) 6:8683. doi: 10.1038/ncomms9683
26. McCabe N, Turner NC, Lord CJ, Kluzek K, Bialkowska A, Swift S, et al. Defificiency in the Repair of DNA Damage by Homologous Recombination and Sensitivity to Poly(ADP-Ribose) Polymerase Inhibition. *Cancer Res* (2006) 66(16):8109–15. doi: 10.1158/0008-5472.CAN-06-0140
27. Kikuchi K, Narita T, Pham VT, Iijima J, Hirota K, Keka IS, et al. Structure-Specific Endonucleases Xpf and Mus81 Play Overlapping But Essential Roles in DNA Repair by Homologous Recombination. *Cancer Res* (2013) 73 (14):4362–71. doi: 10.1158/0008-5472.CAN-12-3154
28. Lai X, Broderick R, Bergoglio V, Zimmer J, Badie S, Niedzwiedz W, et al. MUS81 Nuclease Activity Is Essential for Replication Stress Tolerance and Chromosome Segregation in BRCA2-Deficient Cells. *Nat Commun* (2017) 8:15983. doi: 10.1038/ncomms15983
29. Abroudi A, Samarasinghe S, Kulasiri D. A Comprehensive Complex Systems Approach to the Study and Analysis of Mammalian Cell Cycle Control System in the Presence of DNA Damage Stress. *J Theor Biol* (2017) 429:204–28. doi: 10.1016/j.jtbi.2017.06.018
30. Sancar A, Lindsey-Boltz LA, Unsal-Kaçmaz K, Linn S. Molecular Mechanisms of Mammalian DNA Repair and the DNA Damage Checkpoints. *Annu Rev Biochem* (2004) 73:39–85. doi: 10.1146/annurev.biochem.73.011303.073723
31. Wu F, Chen WJ, Yan L, Tan GQ, Li WT, Zhu XJ, et al. Mus81 Knockdown Improves Chemosensitivity of Hepatocellular Carcinoma Cells by Inducing S-Phase Arrest and Promoting Apoptosis Through CHK1 Pathway. *Cancer Med* (2016) 5(2):370–85. doi: 10.1002/cam4.588
32. Ciccia A, Elledge SJ. The DNA Damage Response: Making It Safe to Play With Knives. *Mol Cell* (2010) 40(2):179–204. doi: 10.1016/j.molcel.2010.09.019
33. Jackson SP, Bartek J. The DNA-Damage Response in Human Biology and Disease. *Nature* (2009) 461(7267):1071–8. doi: 10.1038/nature08467
34. Cortez D, Guntuku S, Qin J, Elledge SJ. ATR and ATRIP: Partners in Checkpoint Signaling. *Science* (2001) 294(5547):1713–6. doi: 10.1126/science.1065521
35. Brown EJ. The ATR-Independent DNA Replication Checkpoint. *Cell Cycle* (2003) 2(3):188–9. doi: 10.4161/cc.2.3.395
36. Yin Y, Shen Q, Zhang P, Tao R, Chang W, Li R, et al. Chk1 Inhibition Potentiates the Therapeutic Efficacy of PARP Inhibitor BMN673 in Gastric Cancer. *Am J Cancer Res* (2017) 7(3):473–83.

Conflict of Interest: The authors declare that the research was conducted in the absence of any commercial or financial relationships that could be construed as a potential conflict of interest.

Publisher's Note: All claims expressed in this article are solely those of the authors and do not necessarily represent those of their affiliated organizations, or those of the publisher, the editors and the reviewers. Any product that may be evaluated in this article, or claim that may be made by its manufacturer, is not guaranteed or endorsed by the publisher.

frontiers | Frontiers in Oncology

ORIGINAL RESEARCH
published: 12 April 2022
doi: 10.3389/fonc.2022.855570

The Histone Deacetylase Inhibitor I13 Induces Differentiation of M2, M3 and M5 Subtypes of Acute Myeloid Leukemia Cells and Leukemic Stem-Like Cells

Xiangyu Ma[1], Mengjie Zhao[1], Zhuo-Xun Wu[2], Jingfang Yao[1], Lei Zhang[1], Jinhong Wang[1], Zhenbo Hu[3], Liuya Wei[1] and Zhe-Sheng Chen[2]**

[1] School of Pharmacy, Weifang Medical University, Weifang, China, [2] Department of Pharmaceutical Sciences, College of Pharmacy and Health Sciences, St. John's University, New York, NY, United States, [3] Laboratory for Stem Cell and Regenerative Medicine, Affiliated Hospital of Weifang Medical University, Weifang, China

OPEN ACCESS

Edited by:
Xiangbing Meng,
The University of Iowa, United States

Reviewed by:
Shibin Cheng,
Brown University, United States
Jianguo Xu,
Hefei University of Technology, China

***Correspondence:**
Liuya Wei
weily@wfmc.edu.cn
Zhe-Sheng Chen
chenz@stjohns.edu

Specialty section:
This article was submitted to Cancer Molecular Targets and Therapeutics, a section of the journal Frontiers in Oncology

Received: *18 January 2022*
Accepted: *14 March 2022*
Published: *12 April 2022*

Citation:
Ma X, Zhao M, Wu Z-X, Yao J, Zhang L, Wang J, Hu Z, Wei L and Chen Z-S (2022) The Histone Deacetylase Inhibitor I13 Induces Differentiation of M2, M3 and M5 Subtypes of Acute Myeloid Leukemia Cells and Leukemic Stem-Like Cells. Front. Oncol. 12:855570. doi: 10.3389/fonc.2022.855570

Acute myeloid leukemia (AML) is a heterogeneous hematologic malignancy characterized by reduced differentiation of myeloid cells and uncontrolled cell proliferation. AML is prone to drug resistance and has a high recurrence rate during treatment with cytarabine-based chemotherapy. Our study aims to explore the cell differentiation effect of a potent histone deacetylase inhibitor (HDACi), I13, and its possible mechanism on AML cell lines (Kasumi-1, KG-1, MOLM-13 and NB4). It has been shown that I13 can significantly inhibit proliferation and colony formation of these AML cells by inducing cell differentiation coupled with cell-cycle exit at G0/G1. Mechanically, I13 presented the property of HDAC inhibition, as assessed by the acetylation of histone H3, which led to the differentiation of Kasumi-1 cells. In addition, the HDAC inhibition of I13 likely dictated the activation of the antigen processing and presentation pathway, which maybe has the potential to promote immune cells to recognize leukemic cells and respond directly against leukemic cells. These results indicated that I13 could induce differentiation of M3 and M5 subtypes of AML cells, M2 subtype AML cells with t(8;21) translocation and leukemic stem-like cells. Therefore, I13 could be an alternative compound which is able to overcome differentiation blocks in AML.

Keywords: acute myeloid leukemia, differentiation therapy, antigen processing and presentation, blockage of differentiation, HDAC inhibitor

INTRODUCTION

Acute myeloid leukemia (AML) is the most common clonal disease in adult acute leukemia and accounts for more deaths than any other leukemia (1). It is characterized by impaired differentiation of myeloid cells and aggregation of immature progenitor cells in the bone marrow. Acute promyelocytic leukemia (APL), the M3 subtype of AML, is one of the most aggressive forms and accounts for 10-15% of AML (2). For the treatment of APL, the combination of all-trans retinoic

acid (ATRA) and arsenic trioxide (ATO) results in myeloid differentiation of the leukemic blasts and yields a 90% disease-free survival rate of 5 years. In addition, AML with (8;21) translocation is associated with 40-80% of M2 subtype of AML and 12-20% of AML in totality (3). Futhermore, AML with mixed-lineage leukemia (MLL) gene rearrangements (MLLr) associated with subtypes M4 and M5 of AML, is found in about 10% of AML patients with poor prognosis (4). Cytarabine (AraC) has been used as the cornerstone of induction therapy/consolidation therapy for non-APL AML. The 5-year survival rate of patients younger than 60 years of age with non-APL AML is about 40%, while only 10- 20% of those older than 60 years has achieved 5-year survival (5). The unsatisfactory outcomes of non-APL AML highlight the continuous need to develop novel therapies. Differentiation therapy with ATRA for APL has introduced a paradigm for success of cell differentiation therapy for AML (6). However, differentiation therapy with ATRA is not effective in non-APL AML.

Histone deacetylase (HDAC) is an epigenetic regulator of histone tail, chromatin conformation, protein-DNA interaction, and transcriptional and post-transcriptional modification (7, 8). HDAC inhibitors have been highlighted as a new category of anticancer drugs that regulate cell proliferation, differentiation and apoptosis through altering the acetylation status of histone and non-histone proteins (9, 10). Some HDAC inhibitors that have been approved in cancer therapy by the United States Food and Drug Administration (FDA) include suberoylanilide hydroxamic acid (SAHA), FK228, LBH58925 and PDX10124. SAHA (11) and FK228 (12) have been approved for the treatment of refractory cutaneous T-cell lymphoma. LBH58925 (13) and PDX10124 (14) have been approved for the treatment of multiple myeloma and peripheral T-cell lymphoma, respectively. This success has encouraged the developments of other HDAC inhibitors.

I13 is an indole-3-butyric acid containing HDAC inhibitor developed in our previous study (15). In the HDAC enzyme inhibitory assay, I13 exhibited IC50 value of 13.9, 49.9, 12.1 and 7.71 nM against HDAC1, 2, 3 and 6 comparing with SAHA (IC50 value of 50.7, 90.4, 164.1 and 169.5 nM, respectively). Moreover, I13 exhibited higher antitumor effects than SAHA in a HepG2 xenograft tumor model, likely by induction of apoptosis (15). In the present study, we evaluated whether I13 has significant activity against APL cells (M3 subtype of AML cells), M2 subtype of AML cells, especially t(8;21), M5 subtype of AML cells with MLLr and stem-like cells by inducing cell differentiation and elucidated the possible mechanism.

MATERIALS AND METHODS

Chemicals

I13 was prepared by our lab. The structure of I13 and SAHA is shown in **Figure 1A**. I13 and SAHA (10 mM) as stock solutions were dissolved in dimethyl sulfoxide (DMSO) and stored at -20°C. They were diluted with RPMI-1640 medium to the desired concentration. The same concentration of DMSO as that of the I13 solution was used as the control. The final concentrations of DMSO did not exceed 0.1% in all cultures, and they had no obvious toxic effect on cells. Fetal bovine serum (FBS) and RPMI-1640 were purchased from Sigma-Aldrich (St. Louis, MO, United States). The cell apoptosis assay was detected by staining solution containing propidium iodide (PI)/RNase and fluorescein isothiocyanate (FITC)-Annexin V (Becton Dickinson San Diego, CA, United States). MTT (3-(4,5-dimethylthiazol-2-yl)-2,5-diphenyltetrazolium bromide) and penicillin-streptomycin were purchased from Solarbio (Beijing, China). FITC anti-human CD11b (cat #301403), PE anti-CD13 (cat #301704 RRID: AB_314180), FITC anti-CD14 (cat #301804, RRID: AB_314186), and PE anti-CD15 (cat #301906, RRID: AB_314198) were obtained from Biolegend Inc. (San Diego, CA, United States). PE anti-human HLA-DR (Cat # FAB4869P) was obtained from R&D SYSTEMS (Minneapolis, MN, USA). Anti-human HLA-DP (Cat #A0906) was purchased from Santa Cruz Biotechnology (Santa Cruz, CA, USA). MethoCult H4100 (cat #04100) was obtained from STEMCELL Technologies (V ancouver, BC, Canada). Monoclonal antibodies against GAPDH (Cat #5174), H3 (Cat #4499), Acetyl-Histone H3

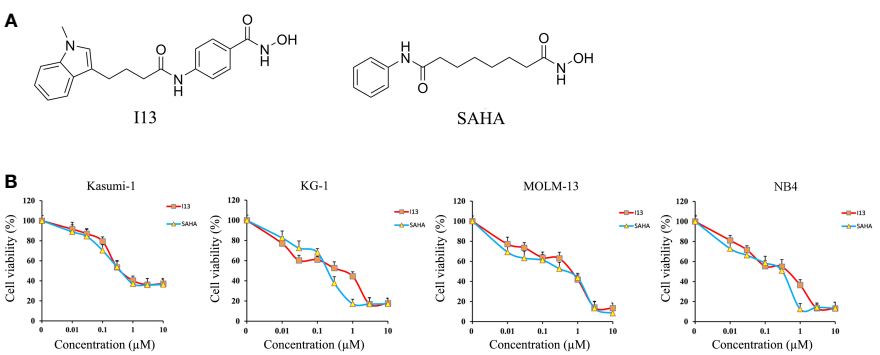

FIGURE 1 | The anti-proliferation effect of I13 on Kasumi-1, KG-1, MOLM-13 and NB4 cells. **(A)** The chemical structure of I13 and SAHA. **(B)** The effect of I13 on the proliferation of AML cells (Kasumi-1, KG-1, MOLM-13 and NB4). Cells were treated with I13 or SAHA (0.01–10 μM) for 72 h and then evaluated by MTT assay. The points represent the mean and error bars represent standard error from three independent triplicate experiments.

(Ac-H3, Cat #8173), CIITA (Cat #3793), and HLA-DRA (Cat #97971) were obtained from Cell Signaling Technology (Beverly, MA, United States). Monoclonal antibodies against HLA-B (Cat #DF7972 RRID: AB_2841362) were obtained from Affinity Biosciences (Affinity Biosciences, OH, USA).

Cell Lines and Cell Culture

NB4 (M3 subtype of AML, APL cell line expressing PML-RARα, DSMZ: ACC 207), Kasumi-1 (M2 subtype of AML with t(8;21) translocation, DSMZ: ACC 220), MOLM-13 (M5 subtype of AML with MLLr, DSMZ: ACC 554) and KG-1 (leukemic stem-like cells established from the bone marrow cells of an AML patient, whose development was blocked at the myeloblast-promyelocyte stage of maturation, DSMZ: ACC 14) cell lines were used. All cells were maintained and cultured in RPMI 1640 medium containing 10% or 20% FBS and 1% penicillin-streptomycin. Cells were incubated at 37°C and 5% CO_2 in a humidified incubator (Thermo scientific, Germany).

Cell Proliferation Assay

MTT assay was performed to evaluate the effect of I13 on cell proliferation. Kasumi-1, KG-1, MOLM-13, and NB4 cell lines were cultured in 96-well plates at approximately 5,000 cells/well for 24 h. Then, the cells were incubated with I13 or SAHA (0.01-10 μM). After treatment for 72 h, 20 μL MTT (4 mg/mL) reagent was added to each well, and the supernatant was centrifuged after incubation for 4 h. Finally, 150 μL DMSO was added to each well, and the absorbance was measured at 570 nm by a microplate reader (Thermo scientific multiskan FC, Germany). The results were expressed as a percentage of cell viability standardized against DMSO-treated control cells.

Colony-Formation Assay

About 5000 cells (Kasumi-1, KG-1, MOLM-13 and NB4 cells) were incubated with specific concentration of I13 in 500 mL of 2.6% methyl-cellulose medium (H4100) containing 10% FBS. After about 15 days, the number of colonies composed of more than 50 cells was calculated under an inverted microscope.

Cell Cycle Analysis

Kasumi-1, KG-1, MOLM-13, and NB4 cells were incubated with varying concentrations of I13 (0.5 μM, 0.45 μM, 0.75 μM, and 0.5 μM, respectively) for 24, 48, or 72 h. These cells were washed with cold PBS and fixed with 70% ethanol at -20°C. Then, these cells were collected and stained with RNase A (100 mg/mL) and PI (50 mg/mL) at room temperature in the dark for 30 min. The percentage of cells in G0/G1, S and G2/M was determined by flow cytometry using the BD Accuri C6 plus flow cytometer (San Jose, CA, USA).

Cell Apoptotic Rate Analysis

Kasumi-1, KG-1, MOLM-13 and NB4 cells were incubated with varying concentrations of I13 (0.25-1.5 μM) and SAHA (0.5-1 μM) for 72 h. Then, the cells were collected, washed with cold PBS, resuspended in 1× binding buffer and stained with FITC Annexin V/PI double labeling. After incubation for 30 min at room temperature in darkness, the apoptotic rate was quantitatively detected by flow cytometry with Cell Quest Software (FACSCalibur, BectonDickinson, United States).

Analysis of Cell Morphology

To analyze cell morphology, Kasumi-1, KG-1, MOLM-13 and NB4 cells were incubated with I13 (0.5 μM, 0.45 μM, 0.75 μM, and 0.5 μM, respectively) for 72 h. The cells were centrifuged, dried naturally, stained with Wright-Giemsa for 10 min, washed with water, and dried. Finally, the slides were created and observed under light microscope.

Analysis of Cell Surface Antigens

Kasumi-1, KG-1, MOLM-13 and NB4 cells were incubated with I13 (0.5 μM, 0.45 μM, 0.75 μM, and 0.5 μM, respectively). After 72 h, the cells were collected and incubated with antibodies at room temperature for 30 min in the dark. Finally, the cell surface antigens were detected by flow cytometry.

Messenger Ribonucleic Acid (mRNA) Sequencing

Kasumi-1 was incubated with 0.5 μM of I13 for 48 h, and the cells were collected for RNA extraction and mRNA sequencing analysis. As described in our previous work (16, 17), the cDNA library was sequenced by Illumina genome analyzer. Levels of gene expression were estimated using fragments per kilobase of exon per million fragments mapped (FPKM) values. Differentially expressed genes (DEGs) were identified with a threshold (corrected p value 0.05 and $\log_2$ (folding change) ≥ 0.58). Gene Set Variation Analysis (GSVA) was conducted to analyze the potential signaling pathways involved. The clusterProfiler package of R software was used to perform the enrichment analysis of DEGs. The pathways with p value of < 0.05 were considered significantly enriched.

Verification of Differentially Expressed Genes by Real-Time PCR Analysis

Kasumi-1 cells were incubated with 0.5 μM of I13 for 72 h. cDNA was synthesized using Primerscript RT reagent kit. Quantitative real-time PCR was performed on an Applied Biosystems 7500 Fast System (Thermo scientific, Germany) and the relative mRNA level of the target gene was measured *via* the 2−ΔΔCT method. Primers were used as follows: forward GAPDH: 5′-TGGGTGTGAACCATGAGAAGT-3′ and reverse GAPDH: 5′-TGAGTCCTTCCACGATACCAA-3′; forward CIITA: 5′- CCTGGAGCTTCTTAACAGCGA-3′ and reverse CIITA: 5′-TGTGTCGGGTTCTGAGTAGAG-3′; forward AML1-ETO: 5′- CACCTACCACAGAGCCATCAAA-3′ and reverse AML1-ETO: 5′- ATCCACAGGTGAAGTCTGGCATT -3′; forward HLA-DRA: 5′- AGTCCCTGTGCTAGGATTTTT CA-3′ and reverse HLA-DRA: 5′- ACATAAACTCGCCTGATT GGTC-3′; forward HLA-B: 5′- CGGAACACACAGATCTACA AGG-3′ and reverse HLA-B: 5′-GATGTAATCCTTGCCGTCG TAG-3′.

Western Blotting Analysis

Cells were lysed with RIPA buffer containing protease inhibitors. The protein lysate was separated by sodium dodecyl sulfate

polyacrylamide gel (SDS-PAGE) and transferred to PVDF membrane. After incubation with 10% skim milk for 90 minutes, the membranes were incubated with specific primary antibodies at 4°C for about 10 h, and then incubated with goat anti-rabbit immunoglobulin G (IgG) antibody at room temperature for 1 h. The protein expression was visualized using the enhanced chemiluminescence reagent detection system (FluorChem Q, Protein Simple, USA).

Statistical Analysis

All data were expressed as the mean ± standard deviation (SD) of at least three repeated and independent experiments. One-way Anova was used for the comparison of each experiment group with the control using the SPSS software. $p < 0.05$ or $p < 0.01$ indicate statistical significance.

RESULTS

I13 Significantly Inhibits Proliferation of Different Subtype of AML Cell Lines

MTT assay was used to detect the inhibitory effect of I13 on Kasumi-1, KG-1, MOLM-13 and NB4 cell lines. **Figure 1B** shows that I13 significantly inhibited the proliferation of Kasumi-1, KG-1, MOLM-13, and NB4 cells. The IC_{50} values for 72 h were 0.52, 0.51, 0.71 and 0.44 μM, respectively. These values were comparable to those of SAHA, which were 0.49, 0.24, 0.53 and 0.31 μM, respectively. This finding revealed that I13 has significant activity against the proliferation of M2, M3 and M5 subtype of AML cells including leukemic stem-like cells.

I13 Remarkably Suppresses Colony-Formation Capacity of AML Cells

The effect of I13 on the colony-formation capacity of Kasumi-1, KG-1, MOLM-13 and NB4 cells was next studied. As shown in **Figures 2A, B**, I13 (0.25-2 μM) remarkably suppressed colony formation capacity of Kasumi-1, KG-1, MOLM-13 and NB4 cells in a concentration-dependent manner. This result indicated that I13 could significantly inhibit the colony-formation capacity of M2, M3, M5 subtype of AML cells even leukemic stem-like cells at a low concentration.

I13 Induces G1/G0 Arrest in AML Cell Lines

The effect of I13 on cell cycle distribution was evaluated in Kasumi-1, KG-1, MOLM-13 and NB4 cells. These cells were incubated with 0.5, 0.45, 0.75 and 0.5 μM I13, respectively for 24, 48 or 72 h. As shown in **Figures 3A, B**, the proportion of G0/G1 phase cells was significantly increased with increasing treatment time in these cells. These results indicated that I13 may induce G0/G1 arrest in these cells.

I13 Induces Less Apoptosis in AML Cells

In order to determine whether the inhibitory effect of I13 is caused by the induction of apoptosis, Kasumi-1, KG-1, MOLM-13 and NB4 cells were treated with indicated concentration of I13 or SAHA for 72 h. It is shown in **Figures 4A, B** that no significant apoptosis was observed in Kasumi-1 and NB4 cells incubated with 0.5 μM I13. Similarly, less signs of apoptosis were found when KG-1 and MOLM-13 cells were treated with I13 under 1.0 and 1.5 μM, respectively. As a comparison, SAHA induced obvious apoptosis of these cells at the comparable concentration. This data suggests that the cell-cycle exit is not related to cell apoptosis in Kasumi-1, KG-1, MOLM-13 and NB4 cells treated with I13 at 0.5, 0.45, 0.75, 0.5 μM, respectively. Hence, these concentrations of I13 will be used to treat these cell lines in a subsequent experiment.

I13 Promotes Differentiation in AML Cells

The above results indicated that I13 inhibits the proliferation of Kasumi-1, KG-1, MOLM-13 and NB4 cells, which is not associated with cell apoptosis. Hence, morphological and surface antigen analysis was performed to determine the differentiation of these cells treated with I13. It can be seen from **Figure 5A**, Kasumi-1, KG-1, MOLM-13 and NB4 cells undergo morphological changes with a decrease in the nuclear to cytoplasmic ratio and increased cell size. In addition, **Figures 5B, C** show that the expression of cell surface antigens CD14 and CD15 (markers of myeloid differentiation) were upregulated in KG-1 cells incubated with 0.45 μM I13. Similarly, 0.5 μM I13 induced differentiation of Kasumi-1 cells with an increasing expression of CD11b, CD13, HLA-DP, and HLA-DRA (major histocompatibility complex class II (MHCII)). In addition, 0.5 and 0.75 μM I13 also induced differentiation of MOLM-13 and NB4 cells, respectively, with increase in expression of CD13 and CD15. Therefore, the result suggests that the G0/G1 arrest of cell cycle induced by I13 may be caused by cell differentiation.

I13 Induces Cell Differentiation Through HDAC inhibition Coupled With Exploiting the Antigen Processing and Presentation Signaling Pathway in Kasumi-1 Cells

To understand the molecular mechanism involved in cell differentiation induced by I13, we performed an overall gene expression analysis of Kasumi-1 cells using mRNA sequencing. The volcanic diagram of Kasumi-1 cells is shown in **Figure 6A**. A total of 65 genes were downregulated and 76 genes were upregulated, indicating that I13 does not affect the mRNA expression of all genes universally. As shown in **Figure 6B**, CIITA, HLA-B, HLA-DP and HLA-DRA were significantly upregulated. These genes were enriched in the antigen processing and presentation signaling pathways by GSVA analysis **Figure 6C**.

Since I13 is a HDAC inhibitor, we tested the HDAC inhibition by examining the level of acetylated histone protein H3 *via* Western blotting analysis. As shown in **Figures 7B, C**, Kasumi-1 cells with I13 treatment displayed significant concentration-dependent increase in the acetylated histone H3. Meanwhile, the same concentration of SAHA did not induce HDAC inhibition. In addition, the transcriptional

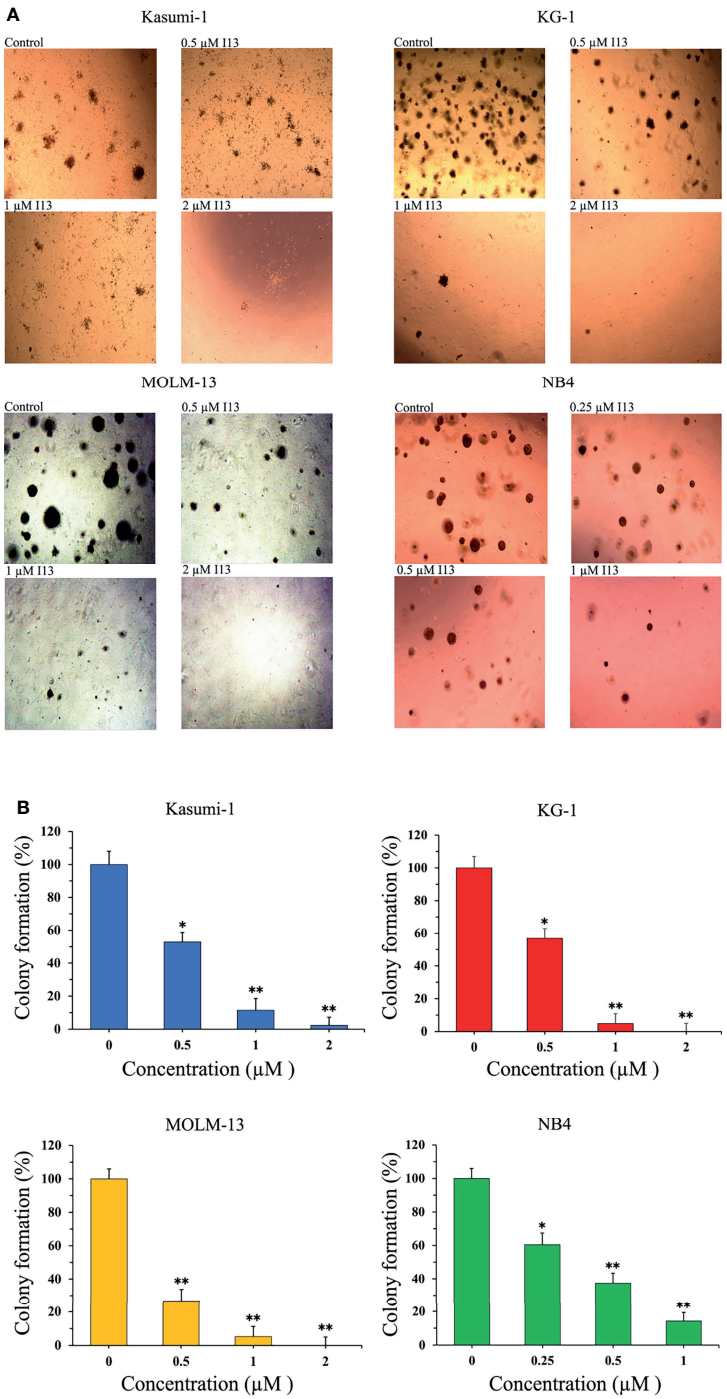

FIGURE 2 | I13 reduced the colony-forming efficiency of Kasumi-1, KG-1, MOLM-13 and NB4 cells. **(A)** Kasumi-1, KG-1, MOLM-13 and NB4 cells were incubated with I13 (0.25–2 μM) for 15 days and examined with light microscopy. **(B)** A bar graph showing the statistical analysis of colony-formation number (*$p < 0.05$ and **$p < 0.01$). The analysis was performed three times.

and protein expression levels of CIITA, HLA-B, and HLA-DRA screened by mRNA sequencing were confirmed by RT-PCR and Western Blotting in Kasumi-1 cells. As shown in **Figures 7A–C**, I13 treatment significantly altered the mRNA and protein expression of CIITA, HLA-B and HLA-DRA. Because AML1-ETO fusion oncoprotein plays important roles in AML with t (8;21) translocation, the expression levels of AML1-ETO mRNA and protein were detected in Kasumi-1 cells. It is

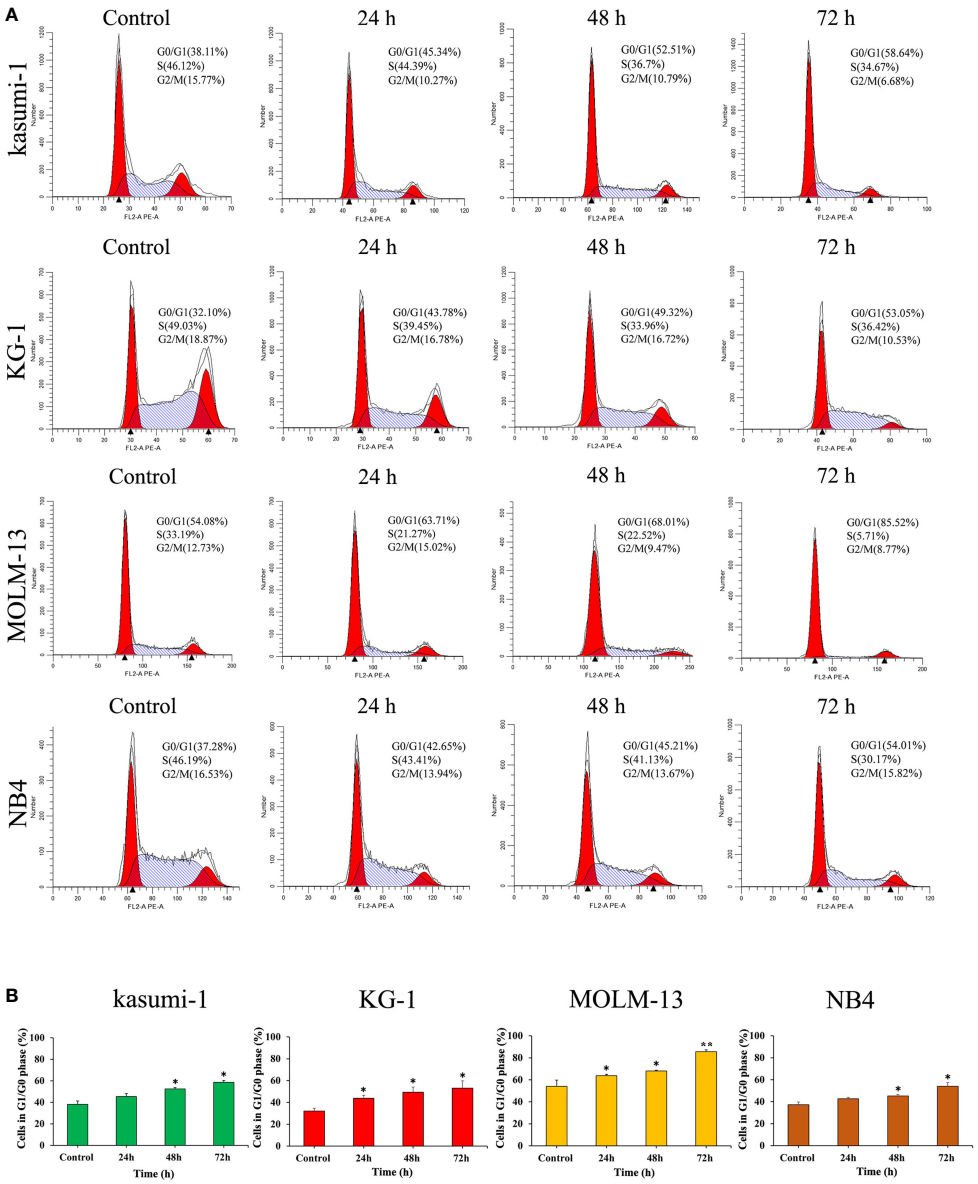

FIGURE 3 | I13 induced the cell-cycle exit in Kasumi-1, KG-1, MOLM-13 and NB4 cells. **(A)** Kasumi-1, KG-1, MOLM-13 and NB4 cells were treated with I13 at concentrations of 0.5, 0.45, 0.75 or 0.5 μM, respectively, for 24, 48, or 72 h, then stained with PI, and detected by flow cytometry. **(B)** A bar graph showing the percentage of cells at G1/G0 phase (*p < 0.05 and **p < 0.01). The analysis was performed three times.

shown that I13 did not alter the transcriptional and protein levels of AML1-ETO.

DISCUSSION

AML, the most common type of acute leukemia in adults, is characterized by the proliferation of precursor myeloid cells with blocked differentiation (18). The use of Ara-C-based chemotherapeutic agents has been the dominant therapeutic approach. The prognosis has improved significantly in recent years, but remains poor particularly in elderly patients because of life-threatening toxicity of the medications (19). Moreover, relapses are still common, and long-term relapse-free survival is poor for most cases of AML leading to treatment failures. Hence, new therapeutic approaches are required. Differentiation therapy with ATRA for APL has dramatically improved the rate of complete remission and the long-term survival of APL patients (20). However, differentiation therapy with ATRA has not been used in non-APL AML. Therefore, the development of new compounds that can effectively induce cell differentiation in non-APL AML is a key area of investigation.

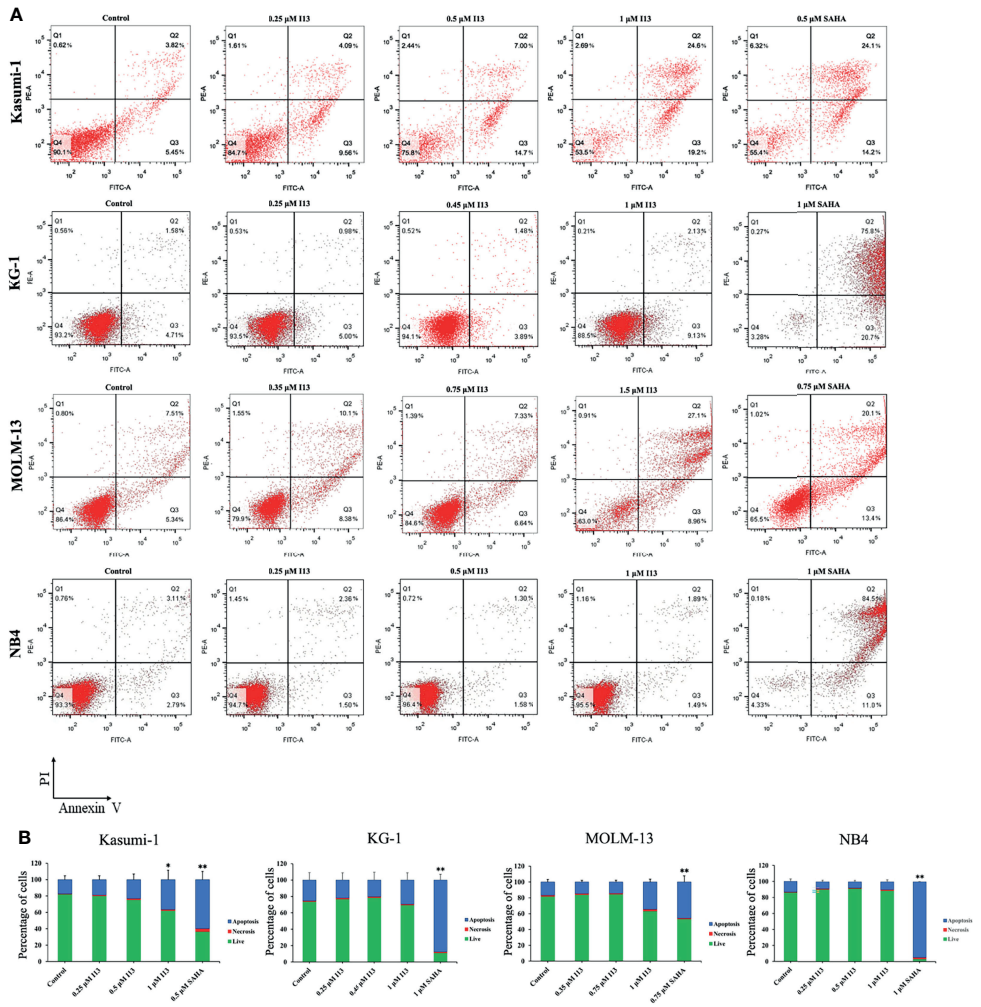

FIGURE 4 | I13 reduced less apoptosis of Kasumi-1, KG-1, MOLM-13 and NB4 cells. **(A)** Kasumi-1, KG-1, MOLM-13 and NB4 cells were treated with I13 (0.25-1.5 μM) or SAHA (0.5, 0.75 or 1 μM) for 72 h. Cells were then stained with Annexin V-FITC/PI and detected by flow cytometry. **(B)** A bar graph showing the statistical analysis of apoptosis (*$p < 0.05$ and **$p < 0.01$). The analysis was carried out three times.

The Histone deacetylase inhibitor (HDACi), I13, has exhibited antitumor activity in xenograft models of human hepatocellular carcinoma by induction of apoptosis (15). In this study, we provided the first demonstration that I13 exhibited differentiation-inducing activity in AML cell lines. It has been shown that I13 could induce the differentiation of Kasumi-1, KG-1, MOLM-13, and NB4 cells, and inhibit cell proliferation and colony formation. Treatment with I13 resulted in G0/G1 phase arrest in these cells and cell line-specific morphological changes, and increased the expression of hematopoietic differentiation antigens, including HLA-B, HLADR, HLADP (MHCII, immune regulation antigens), and monocyte/granulocyte biomarkers such as CD11b, CD13, CD14 or CD15. Taken together, we found that I13 induces cell differentiation and is effective against M2, M3 and M5 subtypes of AML cells including leukemic stem-like cells.

HDACis have been clinically validated as a therapeutic strategy for the treatment of cancers or other diseases (21, 22). Moreover, HDACis have been shown to inhibit cell growth and proliferation through various mechanisms, including cell cycle arrest, induction of cell differentiation and apoptosis *via* the acetylation of histone (23–25). We therefore examined the level of H3 acetylation and found the accumulation of acetylated H3 in a concentration -dependent manner with the I13 treatment. In contrast, the same concentration of SAHA did not exhibit the HDAC inhibitory effect for no alteration of expression of Ac-H3, which suggested the activity of HDAC inhibition of I13 is stronger than that of SAHA in Kasumi-1 cells at comparative treatment concentration. These may suggest that I13 targeted the HDAC, and the effect of HDAC inhibition resulting in the acetylation of histone H3 contributed to the anti-proliferative activities by inducing cell differentiation.

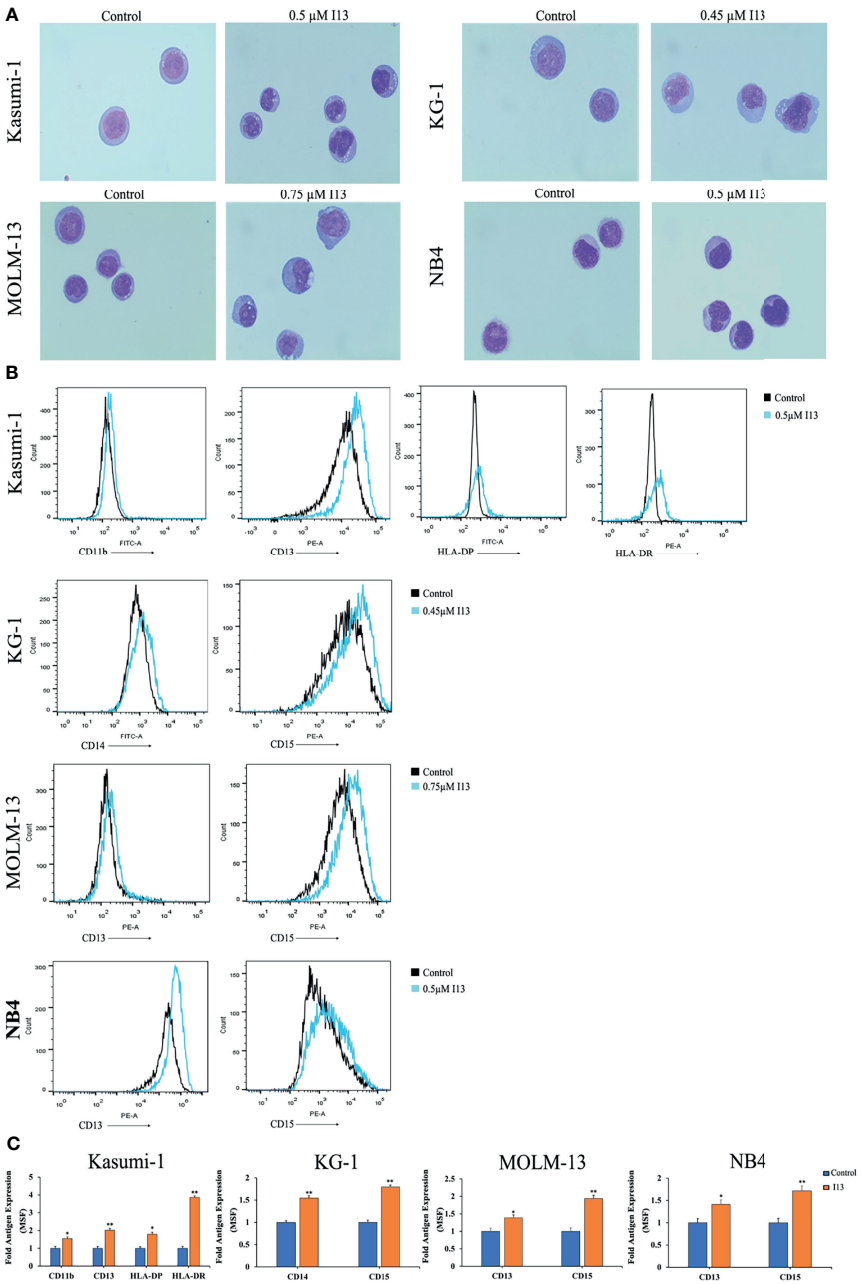

FIGURE 5 | I13 induced cell differentiation of Kasumi-1, KG-1, MOLM-13 and NB4 cells. **(A)** Morphological changes of Kasumi-1, KG-1, MOLM-13 and NB4 cells captured by oil immersion lens (1000×). **(B, C)** The expression of cell surface antigens in Kasumi-1, KG-1, MOLM-13 and NB4 cells treated with 0.5, 0.45, or 0.75 μM I13 for 72 h. **(B)** Mean fluorescence intensity (MFI) of antigens. **(C)** A bar graph showing the statistical analysis of MFI (*$p < 0.05$ and **$p < 0.01$). The analysis was performed three times.

In addition, T cell recognition antigens, also known as HLAs, are present in complex forms of MHC molecules on human cells (26, 27). HLAs play a pivotal role in the interaction of cancer cells with immune cells (28). In this study, we found that I13 could upregulate the expression of HLA-B (HLA class I antigen) in Kasumi-1 cells, indicating the possibility of immunity acquisition in differentiated Kasumi-1 cells. Furthermore, it is shown that the expression of HLA class II antigens are tightly regulated to ensure an immune response directed against malignant cells (29). In addition, evidence indicates that HLA class II antigen expression by tumor cells has a significant impact on their immunogenicity and the deletion of HLA class II eliminated donor T cells' recognition of leukemia (30, 31). Based on these findings, we found that HLA-DRA and CIITA (the HLA trans-activator)

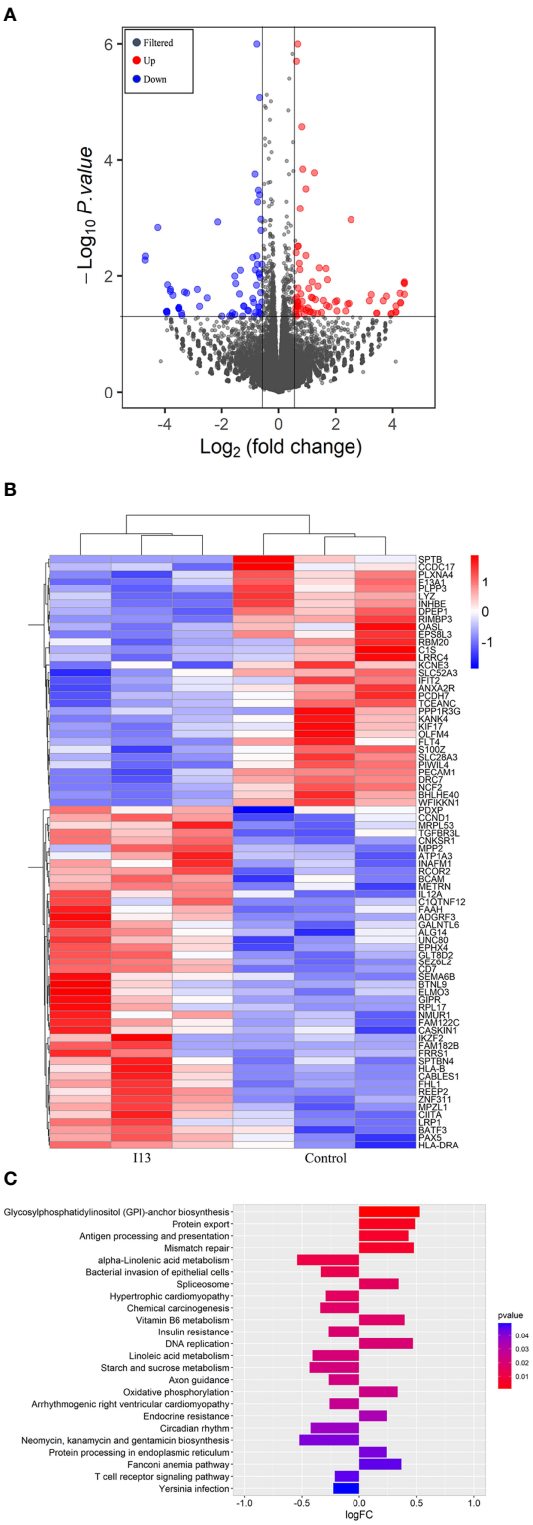

FIGURE 6 | The cell differentiation effect of I13 is associated with antigen-processing and presentation-signaling pathways in Kasumi-1 cells. **(A)** Volcano plots of Kasumi-1 cells. **(B)** Heatmap of differentially expressed genes ($p < 0.05$ and$\log2FC| > 0.58$) according to their p-value. **(C)** The enriched pathways of differentially expressed genes using GSVA analysis. Kasumi-1 cells were incubated with 0.5 μM I13 for 48 h, and then mRNA sequencing was performed. The figures are representative of three independent experiments.

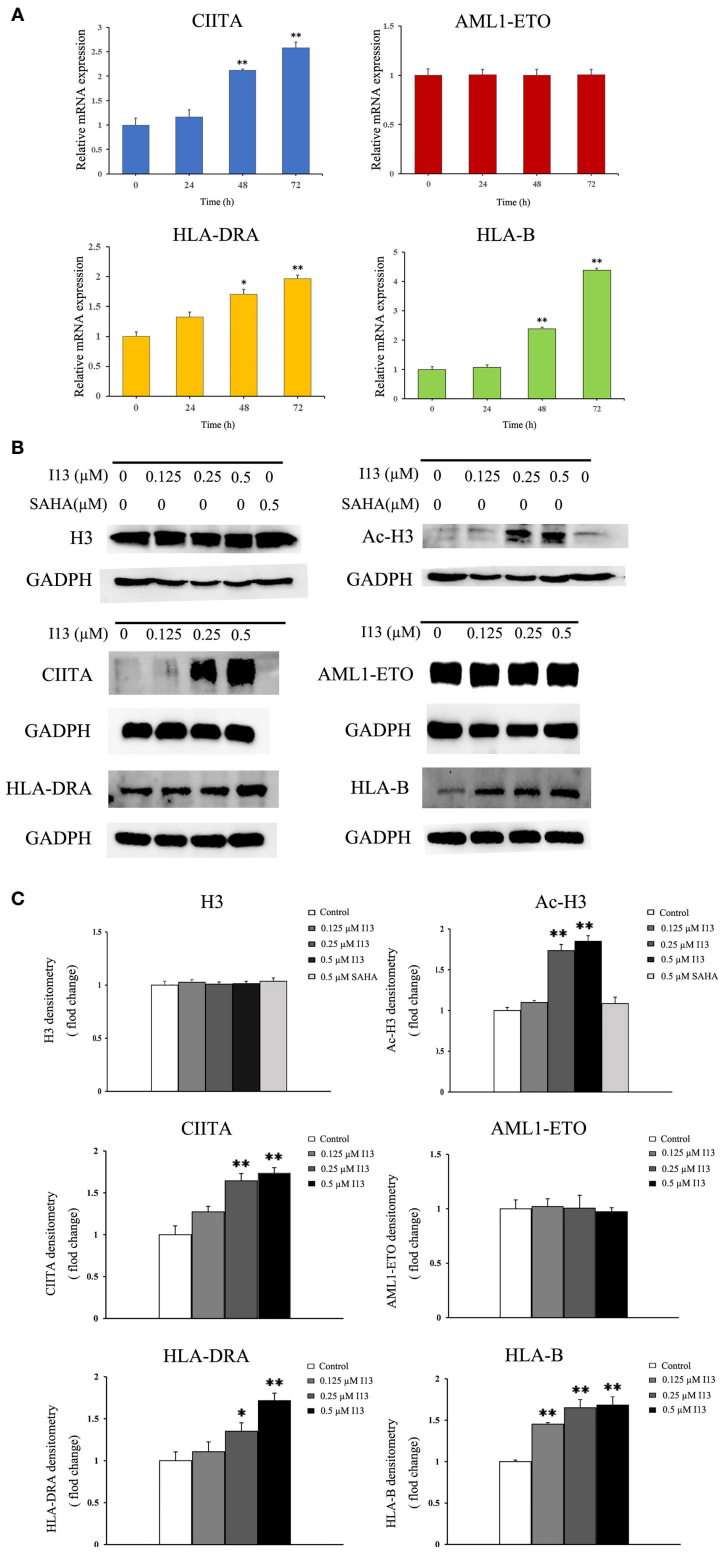

FIGURE 7 | The expression of several genes and proteins related to cell differentiation or enriched in antigen-processing and presentation-signaling pathways in Kasumi-1 cells. **(A)** The mRNA expression of CIITA, AML1-ETO, HLA-DRA and HLA-B *via* real-time PCR **(B)** The protein expression of Ac-H3, H3, CIITA, AML1-ETO, HLA-DRA and HLA-B *via* Western blotting. **(C)** Protein expression was quantified by the software AI600 images. Kasumi-1 cells were treated with I13 (0.5 μM) for 72 h. *$p < 0.05$ and **$p < 0.01$. The analysis was carried out three times.

were significantly upregulated in Kasumi-1 cells treated with I13. It was consistent with the upregulation of CIITA expression, which enhances the expression of HLA class II antigens (32). Therefore, it is suggested that increasing expression levels of HLA-DRA and HLA-DP may increase the acquisition of leukemic cells by immune cells, which potently exert helper function of immune cells. As mentioned above, CIITA, HLA-B, HLA-DP and HLA-DRA were enriched in the antigen processing and presentation signaling pathways. Therefore, I13 activated the antigen processing and presentation signaling pathways, indicating that I13 potently promotes immune cells to have a helper function or display an effector function with HLAs molecules in differentiated leukemic cells. Moreover, it is well known that antigen processing and presentation signaling pathway is a differentiation-related pathway, which denotes the development and differentiation of the hematopoietic cells into various cell types of hematopoietic lineages (33). Our present study showed that I13 treatment induced cell differentiation with morphological changes, increasing the expression of CD11b, CD13, HLA-DP and HLA-DR in Kasumi-1 cells. Further, it was known that cell fate involved in lineage commitment might be dictated by the activity of chromatin remodeling enzymes such as HDACs (34). Hence, the cell differentiation induced by I13 likely originate from the HDAC inhibition activity and subsequent activation of the antigen processing and presentation pathway in Kasumi-1 cells.

It was known that AML1-ETO generated by the t(8;21) translocation plays a central role in AML as a leukemia-promoting oncogene (35). The oncogene controls the leukemic phenotype in t(8;21)-carrying AML (36). We found that there was no significant change in the transcription and protein levels of AML1-ETO in Kasumi-1 cells. Therefore, the differentiation of AML cells induced by I13 was independent of the AML1-ETO gene.

Taken together, we found that I13 is effective against Kasumi-1 cells by inducing cell differentiation *via* presenting property of HDAC inhibition and exploiting the antigen processing and presentation signaling pathway.

In conclusion, I13 had significant anti-proliferative effect not only on M3 and M5 subtypes AML cell lines, but also on AML cells with t(8;21) translocation and leukemic stem-like cells. In addition, I13 can arrest the G0/G1 phase of these cells by inducing cell differentiation. The differentiation of kasumi-1 cells induced by I13 may be associated with the HDAC inhibition coupled with the activation of the antigen processing and presentation pathway. Moreover, I13 may have the potential to promote immune cells to exert a helper function or display an effector function. These findings reveal that I13 could be a potential lead compound for surmounting differentiation blockage in AML.

DATA AVAILABILITY STATEMENT

The datasets presented in this study can be found in online repositories. The names of the repository/repositories and accession number(s) can be found below: https://www.ncbi.nlm.nih.gov/geo; GSE193964.

AUTHOR CONTRIBUTIONS

XM: conceptualization, methodology, and writing-original draft. MZ, ZW, JY, XZ, LZ, and JW: methodology. ZH: supervision. LW: writing- editing and supervision. Z-SC: conceptualization and supervision. All authors contributed to the article and approved the submitted version.

FUNDING

This work was supported by the National Natural Science Foundation of China (No 81700167 to LW), Science and technology support plan for youth innovation in universities of Shandong Province (2019KJM001 to LZ) and Natural Foundation of Shandong Province (Youth Found, ZR2019QH005 to LZ).

REFERENCES

1. Prada-Arismendy J, Arroyave JC, Rothlisberger S. Molecular Biomarkers in Acute Myeloid Leukemia. *Blood Rev* (2017) 31(1):63–76. doi: 10.1016/j.blre.2016.08.005
2. de The H, Chomienne C, Lanotte M, Degos L, Dejean A. The T (15,17) Translocation of Acute Promyelocytic Leukaemia Fuses the Retinoic Acid Receptor Alpha Gene to a Novel Transcribed Locus. *Nature* (1990) 347 (6293):558–61. doi: 10.1038/347558a0
3. Linggi B, Muller-Tidow C, van de Locht L, Hu M, Nip J, Serve H, et al. The T (8,21) Fusion Protein, AML1 ETO, Specifically Represses the Transcription of the P14(ARF) Tumor Suppressor in Acute Myeloid Leukemia. *Nat Med* (2002) 8(7):743–50. doi: 10.1038/nm726
4. Gole B, Wiesmuller L. Leukemogenic Rearrangements at the Mixed Lineage Leukemia Gene (MLL)-Multiple Rather Than a Single Mechanism. *Front Cell Dev Biol* (2015) 3:41. doi: 10.3389/fcell.2015.00041
5. Dohner H, Weisdorf DJ, Bloomfield CD. Acute Myeloid Leukemia. *N Engl J Med* (2015) 373(12):1136–52. doi: 10.1056/NEJMra1406184
6. Wang ZY, Chen Z. Acute Promyelocytic Leukemia: From Highly Fatal to Highly Curable. *Blood* (2008) 111(5):2505–15. doi: 10.1182/blood-2007-07-102798
7. Minucci S, Nervi C, Lo Coco F, Pelicci PG. Histone Deacetylases: A Common Molecular Target for Differentiation Treatment of Acute Myeloid Leukemias? *Oncogene* (2001) 20(24):3110–5. doi: 10.1038/sj.onc.1204336
8. Cheng Y, He C, Wang M, Max X, Mo F, Yang S, et al. Targeting Epigenetic Regulators for Cancer Therapy: Mechanisms and Advances in Clinical Trials. *Signal Transduct Target Ther* (2019) 4:62. doi: 10.1038/s41392-019-0095-0
9. Rosato RR, Almenara JA, Grant S. The Histone Deacetylase Inhibitor MS-275 Promotes Differentiation or Apoptosis in Human Leukemia Cells Through a Process Regulated by Generation of Reactive Oxygen Species and Induction of P21cip1/WAF1 1. *Cancer Res* (2003) 63(13):3637–45.doi: 10.1038/s41467-019-12735-z
10. Manal M, Chandrasekar MJ, Gomathi Priya J, Nanjan MJ. Inhibitors of Histone Deacetylase as Antitumor Agents: A Critical Review. *Bioorg Chem* (2016) 67:18–42. doi: 10.1016/j.bioorg.2016.05.005

11. Richon VM, Emiliani S, Verdin E, Webby Y, Breslow R, Rifkind RA, et al, . A Class of Hybrid Polar Inducers of Transformed Cell Differentiation Inhibits Histone Deacetylases. *Proc Natl Acad Sci USA* (1998) 95(6):3003–7. doi: 10.1073/pnas.95.6.3003
12. Ueda H, Nakajima H, Hori Y, Fujita T, Nishimura M, Goto T, et al. FR901228, a Novel Antitumor Bicyclic Depsipeptide Produced by Chromobacterium Violaceum No. 968. I. Taxonomy, Fermentation, Isolation, Physico-Chemical and Biological Properties, and Antitumor Activity. *J Antibiot (Tokyo)* (1994) 47(3):301–10. doi: 10.7164/antibiotics.47.301
13. Yang L, Xue XW, Zhang YH. Simple and Efficient Synthesis of Belinostat. *Synthetic Commun* (2010) 40(17):2520–4. doi: 10.1080/00397910903277870
14. Neri P, Bahlis NJ, Lonial S. Panobinostat for the Treatment of Multiple Myeloma. *Expert Opin Investig Drugs* (2012) 21(5):733–47. doi: 10.1517/13543784.2012.668883
15. Chen Y, Zhang L, Zhang L, Jiang Q, Zhang L. Discovery of Indole-3-Butyric Acid Derivatives as Potent Histone Deacetylase Inhibitors. *J Enzyme Inhib Med Chem* (2021) 36(1):425–36. doi: 10.1080/14756366.2020.1870457
16. Zhao M, Wang J, Qu M, Zhao Y, Wang H, Ke Y, et al. OGP46 Induces Differentiation of Acute Myeloid Leukemia Cells *via* Different Optimal Signaling Pathways. *Front Cell Dev Biol* (2021) 9:652972. doi: 10.3389/fcell.2021.652972
17. Qu M, Duan Y, Zhao M, Wang Z, Zhao M, Zhao Y, et al. Jiyuan Oridonin A Overcomes Differentiation Blockade in Acute Myeloid Leukemia Cells With MLL Rearrangements *via* Multiple Signaling Pathways. *Front Oncol* (2021) 11:659720. doi: 10.3389/fonc.2021.659720
18. McCulloch EA. Stem Cells in Normal and Leukemic Hemopoiesis (Henry Stratton Lecture, 1982). *Blood* (1983) 62(1):1–13.
19. Yu ZY, Xiao H, Wang LM, Shen X, Jing Y, Wang L, et al. Natural Product Vibsanin A Induces Differentiation of Myeloid Leukemia Cells Through PKC Activation. *Cancer Res* (2016) 76(9):2698–709. doi: 10.1158/0008-5472.CAN-15-1616
20. Chen XJ, Zhang WN, Chen B, Xi WD, Lu Y, Huang JY, et al. Homoharringtonine Deregulates MYC Transcriptional Expression by Directly Binding NF-kappaB Repressing Factor. *Proc Natl Acad Sci USA* (2019) 116(6):2220–5. doi: 10.1073/pnas.1818539116
21. Marson CM. Histone Deacetylase Inhibitors: Design, Structure-Activity Relationships and Therapeutic Implications for Cancer. *Anticancer Agents Med Chem* (2009) 9(6):661–92. doi: 10.2174/187152009788679976
22. Falkenberg KJ, Johnstone RW. Histone Deacetylases and Their Inhibitors in Cancer, Neurological Diseases and Immune Disorders. *Nat Rev Drug Discov* (2014) 13(9):673–91. doi: 10.1038/nrd4360
23. Jenuwein T, Allis CD. Translating the Histone Code. *Science* (2001) 293 (5532):1074–80. doi: 10.1126/science.1063127
24. Marks P, Rifkind RA, Richon VM, Breslow R, Miller T, Kelly WK. Histone Deacetylases and Cancer: Causes and Therapies. *Nat Rev Cancer* (2001) 1 (3):194–202. doi: 10.1038/35106079
25. Minucci S, Pelicci PG. Histone Deacetylase Inhibitors and the Promise of Epigenetic (and More) Treatments for Cancer. *Nat Rev Cancer* (2006) 6 (1):38–51. doi: 10.1038/nrc1779
26. Biernacki MA, Brault M. Bleakley M. T-Cell Receptor-Based Immunotherapy for Hematologic Malignancies. *Cancer J* (2019) 25(3):179–90.doi: 10.1097/PPO.0000000000000378
27. Mussai F, De Santo C, Abu-Dayyeh I, Booth S, Quek L, McEwen–Smith RM, et al. Acute Myeloid Leukemia Creates an Arginase-Dependent Immunosuppressive Microenvironment. *Blood* (2013) 122(5):749–58. doi: 10.1182/blood-2013-01-480129
28. Seliger B, Kloor M, Ferrone S. HLA Class II Antigen-Processing Pathway in Tumors: Molecular Defects and Clinical Relevance. *Oncoimmunology* (2017) 6 (2):e1171447. doi: 10.1080/2162402X.2016.1171447
29. van den Elsen PJ, Holling TM, Kuipers HF, van der Stoep N. Transcriptional Regulation of Antigen Presentation. *Curr Opin Immunol* (2004) 16(1):67–75. doi: 10.1016/j.coi.2003.11.015
30. van den Hoorn T, Paul P, Jongsma ML, Neefjes J. Routes to Manipulate MHC Class II Antigen Presentation. *Curr Opin Immunol* (2011) 23(1):88–95. doi: 10.1016/j.coi.2010.11.002
31. Stevanovic S, van Schie ML, Griffioen M, Falkenburg JH. HLA-Class II Disparity is Necessary for Effective T Cell Mediated Graft-Versus-Leukemia Effects in NOD/scid Mice Engrafted With Human Acute Lymphoblastic Leukemia. *Leukemia* (2013) 27(4):985–7. doi: 10.1038/leu.2012.270
32. Lazzaro B, Anderson AE, Kajdacsy-Balla A, Hessner MJ. Antigenic Characterization of Medullary Carcinoma of the Breast: HLA-DR Expression in Lymph Node Positive Cases. *Appl Immunohistochem Mol Morphol* (2001) 9(3):234–41. doi: 10.1097/00129039-200109000-00007
33. Bug G, Gül H, Schwarz K, Pfeifer H, Kampfmann M, Zheng X, et al. Valproic Acid Stimulates Proliferation and Self-Renewal of Hema-Topoietic Stem Cells. *Cancer Res* (2005) 65(7):2537–41. doi: 10.1158/0008-5472.CAN-04-3011
34. Zardo G, Cimino G, Nervi C. Epigenetic Plasticity of Chromatin in Embryonic and Hematopoietic Stem/Progenitor Cells: Therapeutic Potential of Cell Reprogramming. *Leukemia* (2008) 22(8):1503–18. doi: 10.1038/leu.2008.141
35. De Braekeleer E, Douet-Guilbert N, Morel F, Le Bris MJ, Ferec C, De Braekeleer M. RUNX1 Translocations and Fusion Genes in Malignant Hemopathies. *Future Oncol* (2011) 7(1):77–91. doi: 10.2217/fon.10.158
36. Xu Y, Man N, Karl D, Martinez C, Liu F, Sun J, et al. TAF1 Plays a Critical Role in AML1-ETO Driven Leukemogenesis. *Nat Commun* (2019) 10 (1):4925. doi: 10.1038/s41467-019-12735-z

Conflict of Interest: The authors declare that the research was conducted in the absence of any commercial or financial relationships that could be construed as a potential conflict of interest.

frontiers | Frontiers in Oncology

ORIGINAL RESEARCH
published: 13 April 2022
doi: 10.3389/fonc.2022.889583

Silencing circOMA1 Inhibits Osteosarcoma Progression by Sponging miR-1294 to Regulate c-Myc Expression

Yubo Shi[†], *Yunyun Tian*[†], *Xiangran Sun*, *Yonglong Qiu* and *Yingchun Zhao*[*]

Department of Orthopedics, Renmin Hospital of Wuhan University, Wuhan, China

Background: Several studies have reported that circRNAs have a crucial function in the tumorigenesis of various cancers. However, the expression and function of circOMA1 in osteosarcoma is unknown.

Methods: circOMA1 was identified through bioinformatics analysis. qRT-PCR was used to assess the expressions of circOMA1, miR-1294, and c-Myc in osteosarcoma tissues. Further, we performed functional experiments to explore the biological function of circOMA1 in osteosarcoma. Moreover, a luciferase reporter assay, RNA immunoprecipitation (RIP), and fluorescence *in situ* hybridisation (FISH) assay were performed to demonstrate the association between circOMA1 and miR-1294.

Results: circOMA1 exhibited considerable upregulation in osteosarcoma tissues compared with adjacent normal tissues. Silencing circOMA1 suppressed osteosarcoma progression *in vitro* and *in vivo*. Mechanically, circOMA1 functioned as a sponge of miR-1294 to upregulate c-Myc expression.

Conclusion: circOMA1 played the role of an oncogene in osteosarcoma and promoted osteosarcoma progression by mediating the miR-1294/c-Myc pathway, which might be a new target for treating osteosarcoma.

Keywords: circOMA1, miR-1294, c-Myc, osteosarcoma, progression

OPEN ACCESS

Edited by:
Yan-yan Yan,
Shanxi Datong University, China

Reviewed by:
Yutian Zou,
Sun Yat-sen University Cancer Center (SYSUCC), China
Qiheng Gou,
Sichuan University, China

***Correspondence:**
Yingchun Zhao
zhaoyc1887@163.com

[†]*These authors have contributed equally to this work*

Specialty section:
This article was submitted to Cancer Molecular Targets and Therapeutics, a section of the journal Frontiers in Oncology

Received: *04 March 2022*
Accepted: *21 March 2022*
Published: *13 April 2022*

Citation:
Shi Y, Tian Y, Sun X, Qiu Y and Zhao Y (2022) Silencing circOMA1 Inhibits Osteosarcoma Progression by Sponging miR-1294 to Regulate c-Myc Expression. Front. Oncol. 12:889583. doi: 10.3389/fonc.2022.889583

INTRODUCTION

Osteosarcoma (OS) is a primary malignant bone tumour with an annual incidence of approximately 4 per million (1). OS is characterised by a highly aggressive and metastatic ability and is common in children and adolescents (2). With the rapid development of surgical techniques, neoadjuvant chemotherapy regimens, and immunotherapy techniques, the prognosis of patients with OS has been significantly improved (3–5). However, patients with OS experience chemotherapy resistance, recurrence, and severe adverse immune reactions, affecting their quality of life (6). Therefore, it is essential to study the molecular mechanism of OS pathogenesis and identify new targets to improve early diagnosis and targeted therapy.

Circular RNAs (circRNAs) have a closed-loop structure connected by covalent bonds and are highly abundant, stable, and conserved (7–9). CircRNAs can regulate gene transcription and

splicing, encode or interact with proteins, and play the role of competitive endogenous RNAs (ceRNAs) to sponge miRNAs (10). According to some studies, circRNAs exert an indispensable function in tumorigenesis through sponging miRNAs. For example, circ-0074027 could promote the malignant phenotype of lung cancer through sponging miR-2467-3P to induce RhoA expression (11). In addition, Liu (12) reported 252 differentially expressed circRNAs between normal osteoblasts and osteosarcoma cell lines, which suggested that circRNAs are a new strategy and direction to explore the molecular targets of OS. Under the GSE96964 dataset, we observed that circOMA1 (hsa_circ_0002316) was strongly expressed in OS tissues compared with adjacent normal tissues. To the best of our knowledge, no study has reported the function of circOMA1 in OS. Therefore, the specific function of circOMA1 in developing osteosarcoma needs to be further explored.

In our study, using bioinformatics and molecular biology techniques, we explored the biological functions of circOMA1/miR-1294/c-Myc axis in tumorigenesis and development of OS, aiming to provide new targets and strategies for clinically treating osteosarcoma.

MATERIALS AND METHODS

Tissue Samples

Eighteen paired OS specimens, and adjacent normal tissues were collected and stored at −80°C until further application. This work acquired approval from the Ethics Committee of Renmin Hospital of Wuhan University.

Cell Culture and Transfection

Human osteoblast (hFOB1.19) and OS cell lines were cultured in DMEM with 10% foetal bovine serum (Gibco) at 37°C with 5% CO_2. Short hairpin RNA over circOMA1 (sh-circOMA1) and the negative control shRNA (sh-NC) was obtained from Servicebo (Wuhan, China). miR-1294 mimics and negative control miRNA mimics (miR-NC) were synthesised by GenePharma (Shanghai, China). Lipofectamine (Invitrogen) was used to transfect these RNAs in OS cells per the manufacturer's instructions.

Cell Proliferation and EdU Assay

The transfected cells were cultured for 24, 48, and 72 h. Further, 10 μL CCK-8 solution was added to the 96-well plate, and the optical density (OD) was measured at 450 nm using a microplate reader. Further, a 5-ethynyl-2′-deoxyuridine (EdU) assay was performed to evaluate cell proliferation using Click-iT EdU-488 Kit (Servicebio, Wuhan, China).

Transwell Assay and Wound Healing Assay

In transwell assay, 100 μL matrix gel was added to the upper chamber, and 600 μL DMEM with 10% FBS was added to the lower chamber. Subsequently, the cell suspension was added to the upper chamber and incubated for 2 days. Further, the cells were fixed, stained, and photographed. In the wound healing assay, the transfected cells were seeded in a 6-well plate at a density of 5×10^5 cells per well. When the confluency reached 90%, a pipette tip was used to scratch a wound line. Photographs were taken to record the healing of scratches at different times.

RNase R Treatment

Total RNA was treated with 3 U/mg of RNase R for 20 min. Further, qRT-PCR was performed for detecting the mRNA levels of circOMA1 and OMA1 mRNA.

qRT-PCR

TRIzol reagent (Invitrogen) was used to extract total RNA from tissues or cells. Nano-Drop 2000 spectrophotometer was used to measure the concentration of RNA. cDNA was generated using a cDNA Synthesis Kit (Takara, China). The circRNA miRNA and mRNA levels were quantified using qPCR with SYBR Green (Takara, China), with U6 as the internal control for miRNA and GAPDH for circRNA and mRNA. The primers are listed in **Supplementary Table 1**.

Western Blot

We extracted total proteins from tissues or cells from the lysis solutions (Servicebio, China). Next, the proteins were separated by SDS-PAGE and transferred to a PVDF membrane. Further, the membrane was rinsed with TBST and incubated with primary antibodies, namely, anti-c-Myc (Servicebio, China) and anti-β-actin (Servicebio, China). Subsequently, the membrane was incubated with secondary antibodies, and images were taken.

Luciferase Reporter Assay

The circOMA1 and c-Myc 3′-UTR sequences containing the wild-type or mutant miR-1294 binding sites were amplified by PCR. These sequences were loaded to pmirGLO vectors to construct recombinant plasmids. Further, we co-transfected the recombinant plasmids and miR-1294 mimics or miR-NC to 143B and U2OS. Luciferase activity was measured using Luciferase Assay Kit (Beyotime, China).

RNA Immunoprecipitation (RIP)

According to the standard protocol, the RIP assay was performed using Magna RIP™ RNA-Binding Protein Immunoprecipitation Kit (Milibo, USA). Further, qRT-PCR was performed to detect ircOMA1 and miR-1294 expressions in samples.

Fluorescence *In Situ* Hybridisation (FISH) Assay

CircOMA1 probes and miR-1294 probes were synthesised by Servicebio (Wuhan, China). The cells were incubated with a hybridisation solution containing circOMA1 and miR-1294 probes overnight at 37°C. Confocal images were photographed using a Nikon Eclipse Ti microscope.

Animal Experiments

Briefly, six BALB/c nude mice were classified into two groups, namely, sh-circOMA1 and sh-NC groups. In the sh-circOMA1

group, the 143B cells with a knockdown of circOMA1 were injected in mice, whereas 143B cells transinfected with negative control were subcutaneously injected in the sh-NC group. We measured and recorded the tumour volume every 5 days. After 30 days, the tumours were removed, weighed, and subjected to qRT-PCR.

Bioinformatics Analysis

The circRNA expression profiles of OS were acquired from the GEO database. The interactions between circRNA and miRNA were predicted by Circinteractome and circBank, whereas miRNA–mRNA interactions were estimated using Targetscan, miRDB, and miRTarBase.

Statistical Analysis

We used SPSS 13.0 software for data analysis. ANOVA was performed to evaluate the differences among more than two groups. The student's unpaired t-test was used for unpaired comparisons, and paired t-test was used for paired comparisons. $P < 0.05$ was considered significant.

RESULTS

circOMA1 Is Highly Expressed in OS Tissues and Cells

Through analysing the GSE96964 dataset, it was observed that hsa_circ_0002316 (circOMA1) was highly denoted in OS cell lines (**Figure 1A**). circOMA1 is derived from 2–9 exons of the OMA1 gene on human chromosome 1. Subsequently, Sanger sequencing validated the circular structure of circOMA1 (**Figure 1B**). In addition, the circOMA1 was detected in cDNA with divergent primers but not in gDNA with divergent primers (**Figure 1C**). Similarly, the results revealed that circOMA1 had resistance to RNase R treatment, whereas linear OMA1 levels significantly decreased under RNase R treatment (**Figure 1D**). Furthermore, the expression of circOMA1 in OS tissues and cell lines (MG63, 143B, and U2OS) was assessed. circOMA1 expressions were notably denoted in OS cell lines and clinical samples (**Figures 1E, F**). Moreover, FISH assays demonstrated that circOMA1 was mainly localised in the cytoplasm (**Figure 1G**).

Silencing circOMA1 Expression Inhibited OS Progression *In Vitro*

To investigate the role of circOMA1 in OS, two shRNAs (sh-circOMA1#1 and sh-cirCOMA1#2) were transfected into 143B and U2OS cells. circOMA1 expression was notably downregulated after transfection with sh-circOMA1 in 143B and U2OS cells (**Figure 2A**). However, the level of OMA1 mRNA remained unchanged (**Figure 2B**). CCK-8 assay results demonstrated that the cell viability of both cell lines in the sh-circOMA1 group was significantly inhibited compared with the sh-NC group (**Figure 2C**). Additionally, depletion of circOMA1 could inhibit the proliferation of 143B and U2OS cells (**Figures 2D, E**). Similarly, silencing circOMA1 could impair the migratory and invasive capacity of OS cells (**Figures 2F, G**). Therefore, these data revealed that silencing circOMA1 expression inhibited OS progression *in vitro*. Sh-circOMA1#1 was selected for subsequent study because it had a better silencing efficiency.

circOMA1 Acts as a Sponge for miR-1294

The circRNA–miRNA interactions were predicted using bioinformatics analysis. Three miRNAs might bind to circOMA1 (**Figure 3A**). To investigate the interactions between circOMA1 and its potential targeted miRNAs, the expressions of miR-654-3p, miR-330-3p, and miR-1294 were evaluated in transfected cells (**Figure 3B**). Because miR-1294 was upregulated after the knockdown of circOMA1 in both cells, it was selected for further study. The data indicated that miR-1294 might bind to circOMA1 (**Figure 3C**). Moreover, miR-1294 mimicking lowered the luciferase activity in the wild-type construct but not in the mutant construct (**Figure 3D**). Similarly, the RIP assay revealed that circOMA1 and miR-1294 complex was enriched in the Ago2 group (**Figure 3E**). The FISH assay was used for detecting the co-localization between circOMA1 and miR-1294. The results demonstrated that circOMA1 and miR-1294 were co-localised in the cytoplasm (**Figure 3F**). Additionally, this study identified miR-1294 expression in OS tissues and cell lines. As expected, miRNA expression was decreased in both OS cell lines and tissues (**Figures 3G, H**). The qRT-PCR results revealed that knockdown of circOMA1 resulted in the upregulation of miR-1270 expression in OS cells (**Figure 3I**). Interestingly, miR-1294 expression negatively correlated with circOMA1 (**Figure 3J**). Collectively, these results demonstrated that circOMA1 played the role of a sponge for miR-1294.

Downregulation of miR-1294 Reversed the Anti-Tumorigenic Impact of sh-circOMA1

To investigate the interaction between miR-1294 and circOMA1, OS cells were transfected with sh-circOMA1 and miR-1294 inhibitors. The results showed that miR-1294 expression was notably upregulated in OS cells after transfection with sh-circOMA1, whereas the miR-1294 inhibitor reversed the effect (**Figure 4A**). CCK-8 and colony-forming assay results indicated that mi-1294 inhibitor weakened the impact of sh-circOMA1 on cell viability and proliferation (**Figures 4B, C**). Similarly, sh-circOMA1 remarkably inhibited the invasive and migrant abilities of OS cells, whereas the impact was reversed by a miR-1294 inhibitor (**Figures 4D, E**). Therefore, downregulation of miR-1294 reversed the anti-tumorigenic effect of sh-circOMA1.

circOMA1 Regulates the c-Myc Expression *via* miR-1294

Bioinformatics analysis revealed that FGFR1, c-Myc, and SURF4 were the three candidates for miR-1294 (**Figure 5A**). The expression of c-Myc was notably lowered in OS cells after transfection with miR-1294 mimic (**Figure 5B**). Targetscan database was used for detecting the binding sites between miR-1294 and circOMA1 (**Figure 5C**). Furthermore, the luciferase reporter assay confirmed the direct binding relationship between miR-1294 and c-Myc (**Figure 5D**). The c-Myc expressions in OS

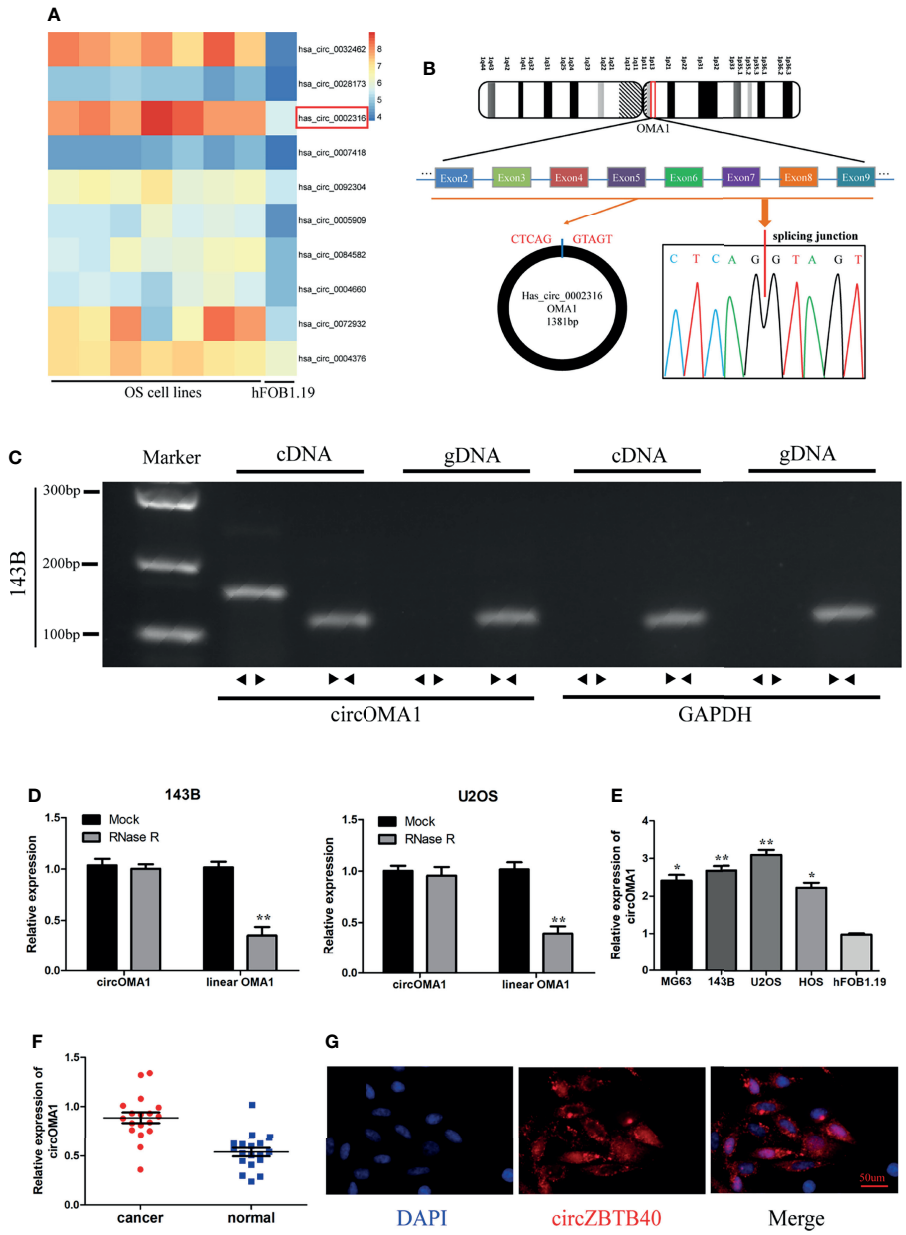

FIGURE 1 | Characterisation and expression of circOMA1 in OS tissues and cell lines. **(A)** The heatmap exhibited DEcircRNAs in GSE96964. **(B)** The back-spliced region of circOMA1 was identified using Sanger sequencing. **(C)** Gel electrophoresis was performed to confirm the presence of circOMA1. **(D)** The expression of circOMA1 was assessed after RNase R treatment. **(E, F)** circOMA1 expression in OS tissues and cell lines. **(G)** We performed a FISH assay for detecting the location of circOMA1 in 143B cells. *$P < 0.05$, **$P < 0.01$.

tissues were examined using qRT-PCR. It was observed that the expression of c-Myc was enhanced in OS tissues (**Figure 5E**). In addition, c-Myc mRNA and protein levels in both cells were downregulated following miR-1294 mimic (**Figures 5F, G**). Interestingly, c-Myc negatively correlated with miR-1294 expression (**Figure 5H**).

To explore whether circOMA1 could regulate c-Myc, the expression of c-Myc was identified after the knockdown of circOMA1. The obtained results indicated that silencing circOMA1 inhibited c-Myc mRNA and protein expressions in 143B and U2OS cells (**Figures 5I, J**). C-Myc exhibited a positive correlation with circOMA1 expression (**Figure 5K**). To further identify whether circOMA1 regulated c-Myc *via* miR-1294, sh-circOMA1 and miR-1294 inhibitor were co-transfected into OS cells. The reductions in the mRNA and protein levels of c-Myc after sh-circOMA1 transfection were reversed by transfection with miR-1294 inhibitor (**Figures 5L, M**). It can be concluded that circOMA1 controlled the c-Myc expression *via* miR-1294.

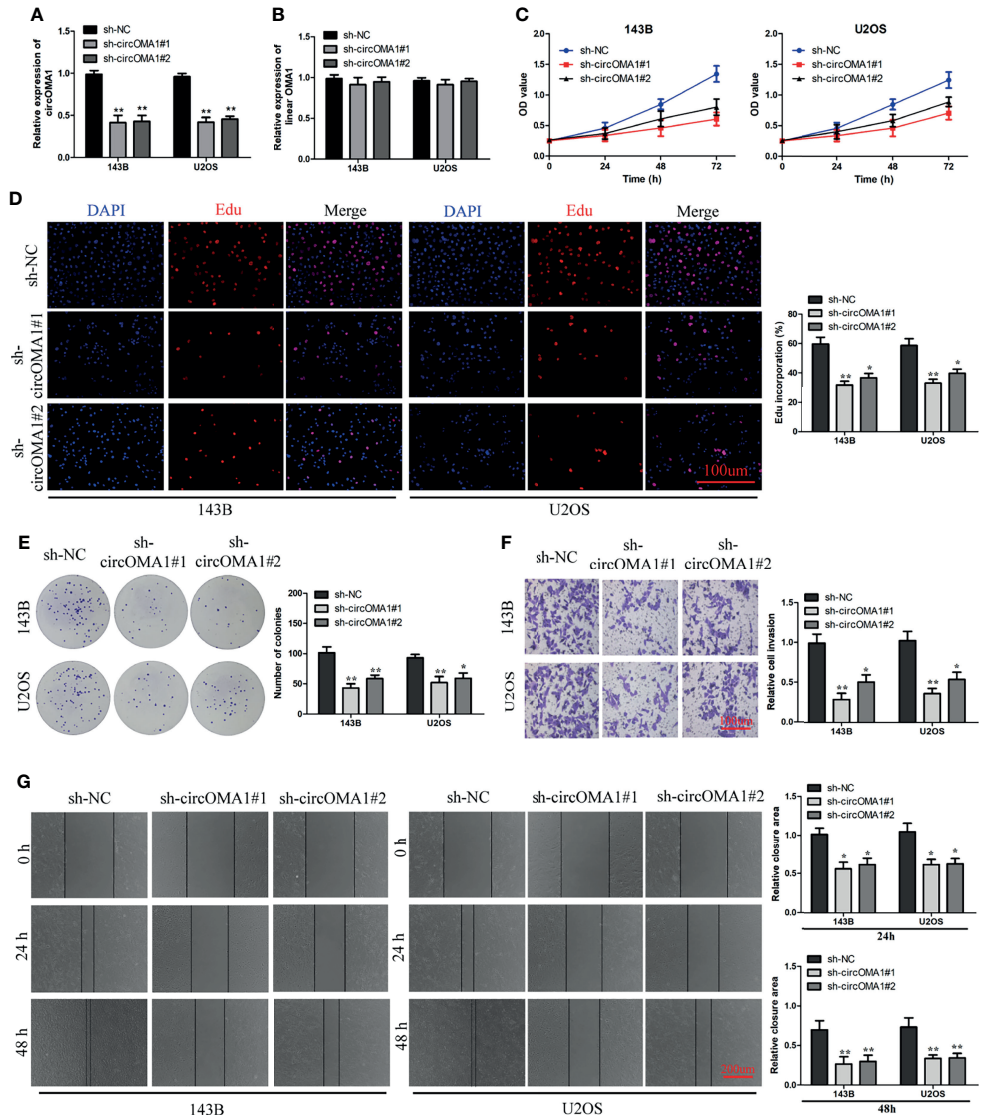

FIGURE 2 | Knockdown of circOMA1 caused inhibition of OS progression. **(A, B)** The mRNA expression of circOMA1 and OMA1 in OS cells after transfection with sh-circOMA1 or sh-NC. **(C)** CCK8 assay was performed to assess cell viability. **(D, E)** Assessment of cell proliferation based on Edu **(D)** and colony formation assays **(E)** in OS cells. **(F)** The invasive ability of transfected cells was assessed using a transwell assay. **(G)** A wound-healing assay was performed to assess the migration of OS cells. $^{*}P < 0.05$, $^{**}P < 0.01$.

Silencing circOMA1 Inhibited OS Growth *In Vivo*

To further explore the impact of circOMA1 on OS cells *in vivo*, 143B cells transfected with sh-circOMA1 or sh-NC were injected subcutaneously in mice. The data indicated that silencing circOMA1 inhibited tumour volume and weight in the sh-circOMA1 group compared to the sh-NC group (**Figures 6A–C**). In addition, immunochemical findings revealed that the expression of the ki-67 protein was lowered in the sh-circOMA1 group (**Figure 6D**). According to qRT-PCR results, circOMA1 and c-Myc were downregulated in the sh-circOMA1 group, whereas miR-1294 expression exhibited upregulation in the sh-circOMA1 group (**Figures 6E–G**). The FISH assay showed that circOMA1 and miR-1294 were co-localised in the cytoplasm (**Figure 6H**).

DISCUSSION

CircRNA is a new type of non-coding RNA with various biological properties different from linear RNAs (13). Due to its unique circular structure, cirRNA has attracted increasing attention in recent years (14). Researchers have used second-generation sequencing and gene chip to screen for differentially expressed circRNAs in various tumours and observed that circRNAs have an

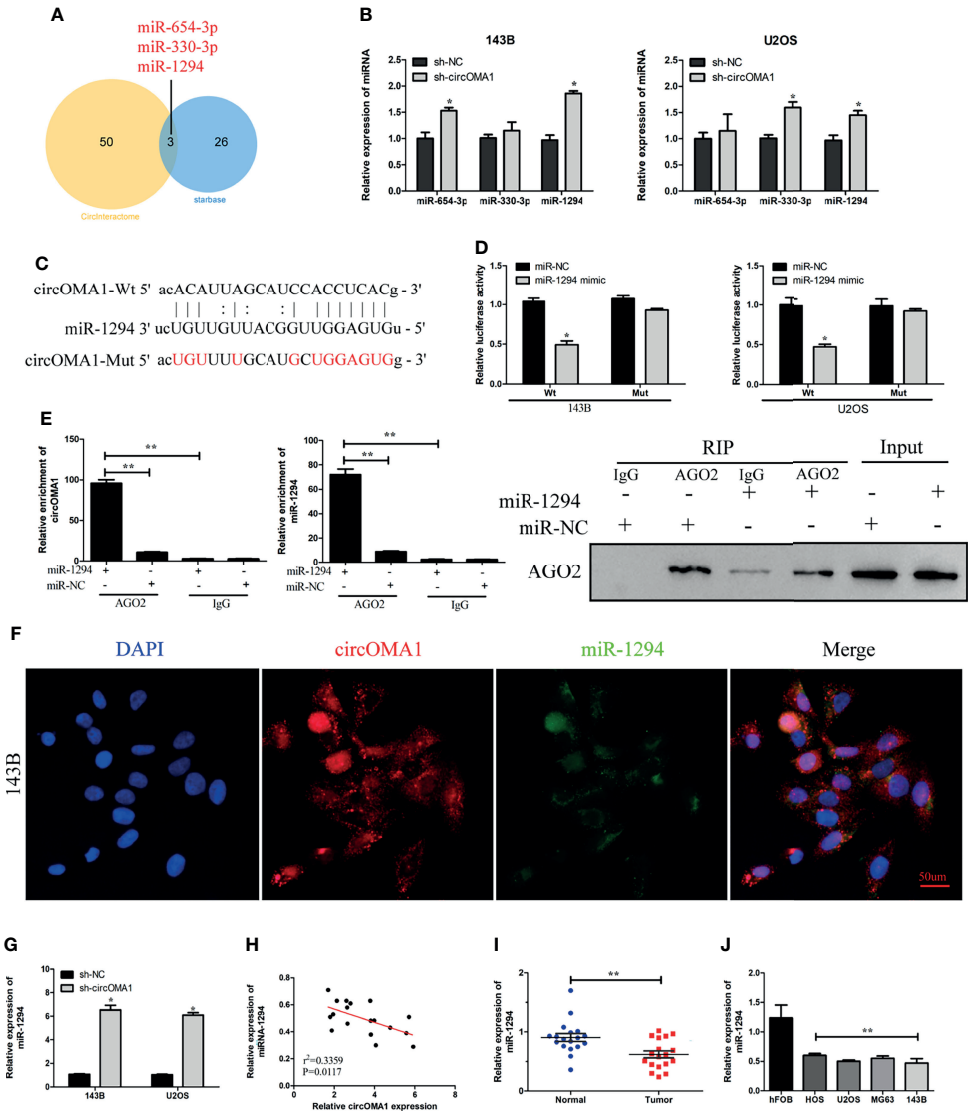

FIGURE 3 | circOMA1 sponged miR-1294 in OS cells. **(A)** The Venn plot demonstrated the overlapping miRNAs screened by Starbase and CircInteractome. **(B)** The expression of three potential miRNAs in transfected cells. **(C)** The binding sites between circOMA1 and miR-1294. **(D)** Luciferase activity could be identified in OS cells after co-transfection. **(E)** The binding between circOMA1 and miR-1294 was verified by RIP assay and immunoblotting. **(F)** The relationship between circZBTB40 and miR-1270 was assessed by the FISH assay. **(G, H)** miR-1270 expression in OS tissues and cell lines. **(I)** MiR-1294 expression was examined in OS cells after the knockdown of circOMA1. **(J)** The relationship between circOMA1 and miR-1294. *$P < 0.05$, **$P < 0.01$.

essential function in tumour proliferation, metastasis, and drug resistance (15–18). For example, has_circ_0018414 accelerated malignant progression of lung adenocarcinoma *via* sponging miR-6807-3P (19). In addition, increasing evidence indicates that circRNA may be involved in tumorigenesis and progression as a tumour suppressor or activator (20–23).

OS is a normal aggressive malignant bone tumour (24). At present, the pathogenesis of OS is still unclear and believed to be complex and multifactorial (25). In addition, current treatment strategies are minimal for patients with early metastasis and recurrence, particularly in children and adolescents (26). Therefore, investigation of the potential mechanism of OS progression at the molecular level is urgently needed. circOMA1 is derived from 2–9 exons of the OMA1 gene on human chromosome 1.

Nevertheless, the biological role of circOMA1 in developing OS is not known. Through the analysis of the GSE96964 dataset, this study discovered that circOMA1 expression was notably upregulated in OS tissues compared with adjacent healthy tissues. It was further verified that circOMA1 was highly denoted in clinical samples of OS and cell lines. In addition, the results suggested that silencing circOMA1 impaired the migratory, invasive, and colony-forming abilities of OS cells. Moreover, animal experiments demonstrated that depletion of circOMA1 inhibited tumour

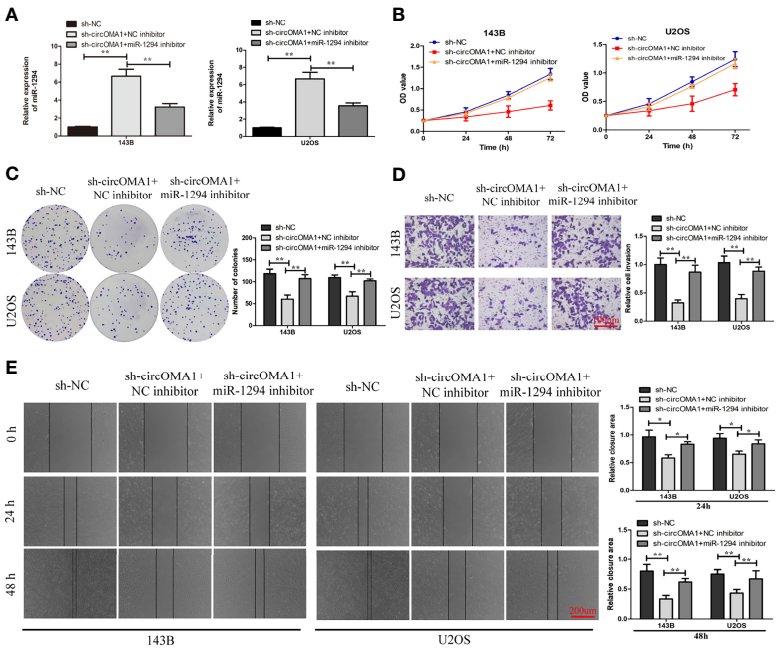

FIGURE 4 | Downregulation of miR-1294 could reverse the anti-tumorigenic impact of sh-circOMA1. **(A)** The mRNA levels of miR-1294 were assessed using qRT-PCR. **(B, C)** CCK-8 and colony-forming assays evaluated the impact of miR-1294 on cell viability and proliferation. **(D, E)** The impact of miR-1294 on cell invasion and migration was detected by transwell and wound healing assays. *$P < 0.05$, **$P < 0.01$.

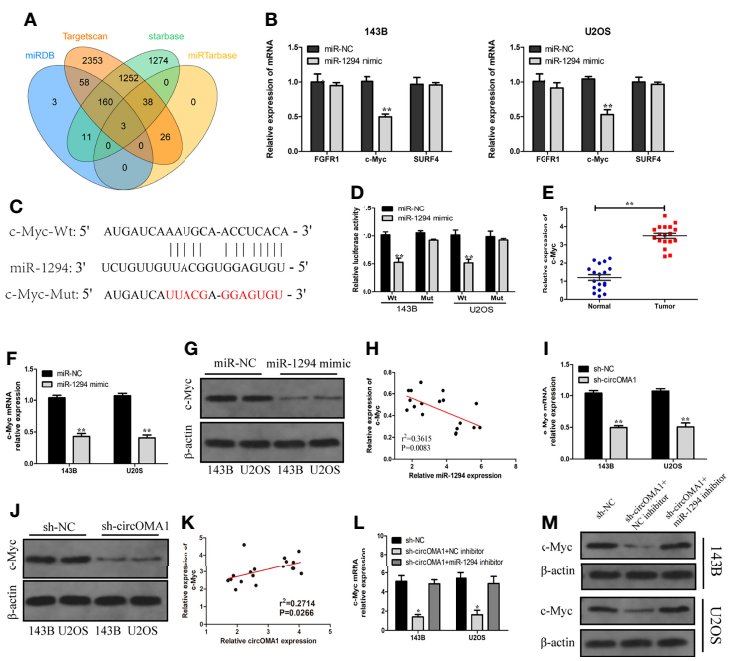

FIGURE 5 | circOMA1 upregulated c-Myc expression *via* sponging miR-1294. **(A)** The intersection of possible target genes predicted by bioinformatics analysis. **(B)** The expressions of the potential target genes were assessed in OS cells after transfection with miR-1294 mimic or miR-NC. **(C)** The binding sites between miR-1294 and c-Myc. **(D)** Luciferase reporter assay confirmed the relationship between miR-1294 and c-Myc. **(E)** The expression of c-Myc in OS tissues. **(F, G)** MiR-1270 mimics decreased c-Myc mRNA and protein levels in OS cells. **(H)** The correlation between miR-1294 and c-Myc. **(I, J)** Sh-circOMA1 decreased c-Myc mRNA and protein levels in OS cells. **(K)** The relationship between circOMA1 and c-Myc. **(L, M)** The mRNA and protein levels of c-Myc in transfected cells. *$P < 0.05$, **$P < 0.01$.

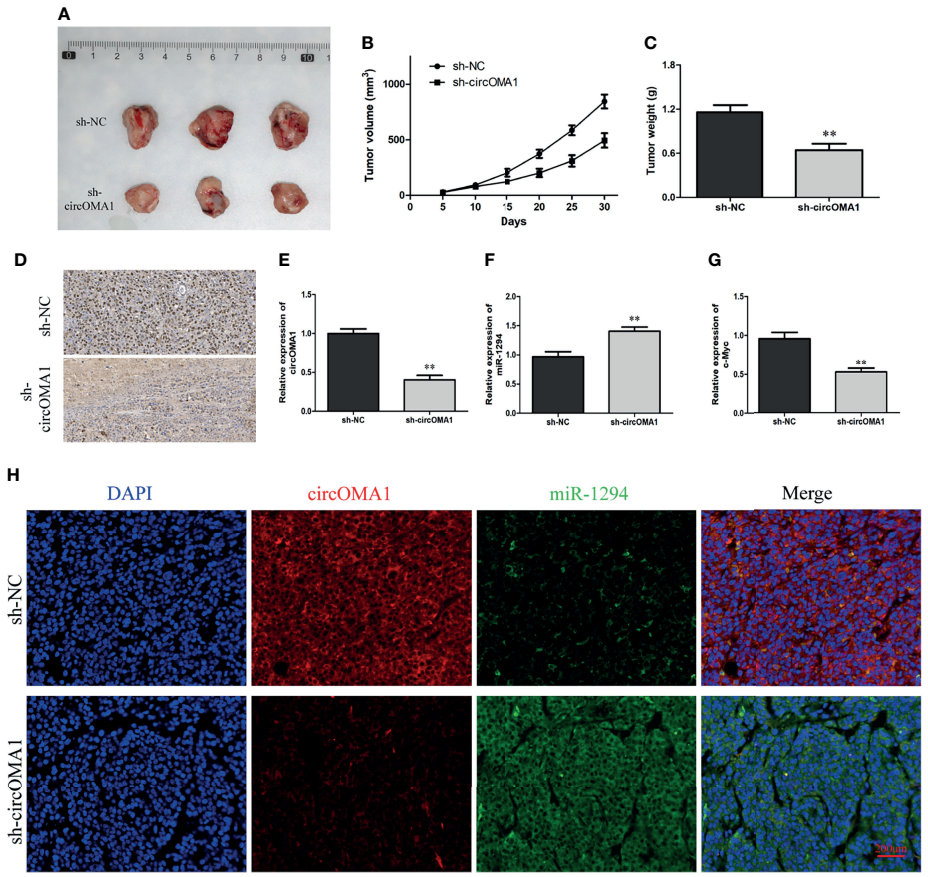

FIGURE 6 | Silencing circOMA1 hindered the growth of tumour *in vivo*. **(A)** The images of tumour masses. **(B, C)** The tumour volume and weight are in two groups. **(D)** Ki-67 staining of tumour tissues. **(E–G)** The mRNA levels of circOMA1, miR-1294, and c-Myc were assessed using qRT-PCR. **(H)** FISH of circOMA1 and miR-1294 in tumors, $^{**}P < 0.01$.

growth. Collectively, these data proved that circOMA1 exhibited a carcinogenic function in developing OS.

Several studies confirmed that circRNAs regulate gene expression *via* sponging miRNA (27, 28). Therefore, we speculated that circOMA1 could modulate OS progression through this mechanism. Through bioinformatics analysis, we observed that miR-1294 might be a target of circOMA1. Further, FISH assay, a luciferase reporter assay, and RIP confirmed that circOMA1 could bind to miR-1294 in OS cells. Importantly, miR-1294 had a negative correlation with circOMA1 expression. These results demonstrated that circOMA1 played the role of a sponge for miR-1294.

C-Myc has been shown to have a vital function in tumorigenesis of various cancers (29, 30). Therefore, we investigated the relationship between cirOMA1, miR-1294, and c-Myc. Through luciferase reporter assay, we confirmed that c-Myc was a target of miR-1294. The finding was consistent with the results obtained by Rong et al., who verified the binding relationship between c-Myc and miR-1294 (31). Besides, the decrease in the mRNA and protein levels of c-Myc following circOMA1 shRNA transfection could be reversed by transfection with miR-1294 inhibitor. In addition, c-Myc expression exhibited a positive relationship with circOMA1, which verified the existence of a circOMA1/miR-1294/c-Myc axis in OS. These results indicated that circOMA1 could regulate the c-Myc expression *via* miR-1294.

In conclusion, this study suggested that circOMA1 played the role of an oncogene in OS and promoted OS progression by mediating the miR-1294/c-Myc pathway, which might be a novel target for OS therapy.

DATA AVAILABILITY STATEMENT

The original contributions presented in the study are included in the article/**Supplementary Material**. Further inquiries can be directed to the corresponding author.

ETHICS STATEMENT

The studies involving human participants were reviewed and approved by Renmin Hospital of Wuhan University.

The patients/participants provided their written informed consent to participate in this study.

AUTHOR CONTRIBUTIONS

YS and YT made contributions to the conception and manuscript drafting of this study. XS and YQ were responsible for data analysis. YZ revised the manuscript. All authors contributed to the article and approved the submitted version.

SUPPLEMENTARY MATERIAL

The Supplementary Material for this article can be found online at: https://www.frontiersin.org/articles/10.3389/fonc.2022.889583/full#supplementary-material

REFERENCES

1. Meltzer PS, Helman LJ. New Horizons in the Treatment of Osteosarcoma. *N Engl J Med* (2021) 385(22):2066–76. doi: 10.1056/NEJMra2103423
2. Yoshida A. Osteosarcoma: Old and New Challenges. *Surg Pathol Clin* (2021) 14(4):567–83. doi: 10.1016/j.path.2021.06.003
3. Hecker-Nolting S, Langer T, Blattmann C, Kager L, Bielack SS. Current Insights Into the Management of Late Chemotherapy Toxicities in Pediatric Osteosarcoma Patients. *Cancer Manag Res* (2021) 13:8989–98. doi: 10.2147/cmar.S287908
4. Ottesen TD, Shultz BN, Munger AM, Sibindi C, Yurter A, Varthi AG, et al. Characteristics, Management, and Outcomes of Patients With Osteosarcoma: An Analysis of Outcomes From the National Cancer Database. *J Am Acad Orthop Surg Glob Res Rev* (2022) 6(2):e22.00009. doi: 10.5435/JAAOSGlobal-D-22-00009
5. Song XJ, Bi MC, Zhu QS, Liu XL. The Emerging Role of lncRNAs in the Regulation of Osteosarcoma Stem Cells. *Eur Rev Med Pharmacol Sci* (2022) 26 (3):966–74. doi: 10.26355/eurrev_202202_28006
6. Meftahpour V, Aghebati-Maleki A, Fotouhi A, Safarzadeh E, Aghebati-Maleki L. Prognostic Significance and Therapeutic Potentials of Immune Checkpoints in Osteosarcoma. *EXCLI J* (2022) 21:250–68. doi: 10.17179/excli2021-4094
7. Huang W, Wu Y, Qiao M, Xie Z, Cen X, Huang X, et al. CircRNA-miRNA Networks in Regulating Bone Disease. *J Cell Physiol* (2022) 237(2):1225–44. doi: 10.1002/jcp.30625
8. Yang G, Wu Y, Wan R, Sang H, Liu H, Huang W. The Role of Non–Coding RNAs in the Regulation, Diagnosis, Prognosis and Treatment of Osteosarcoma (Review). *Int J Oncol* (2021) 59(3):69. doi: 10.3892/ijo.2021.5249
9. Liu J, Yang L, Fu Q, Liu S. Emerging Roles and Potential Biological Value of CircRNA in Osteosarcoma. *Front Oncol* (2020) 10:552236. doi: 10.3389/fonc.2020.552236
10. Li Z, Li X, Xu D, Chen X, Li S, Zhang L, et al. An Update on the Roles of Circular RNAs in Osteosarcoma. *Cell Prolif* (2021) 54(1):e12936. doi: 10.1111/cpr.12936
11. Duan Z, Wei S, Liu Y. Circ_0074027 Contributes to Non-Small Cell Lung Cancer Progression Through Positively Modulating RHOA *via* Sequestering miR-2467-3p. *J Bioenerg Biomembr* (2021) 53(2):223–33. doi: 10.1007/s10863-021-09876-6
12. Liu W, Zhang J, Zou C, Xie X, Wang Y, Wang B, et al. Microarray Expression Profile and Functional Analysis of Circular RNAs in Osteosarcoma. *Cell Physiol Biochem* (2017) 43(3):969–85. doi: 10.1159/000481650
13. Enuka Y, Lauriola M, Feldman ME, Sas-Chen A, Ulitsky I, Yarden Y. Circular RNAs Are Long-Lived and Display Only Minimal Early Alterations in Response to a Growth Factor. *Nucleic Acids Res* (2016) 44(3):1370–83. doi: 10.1093/nar/gkv1367
14. Harrison DJ, Geller DS, Gill JD, Lewis VO, Gorlick R. Current and Future Therapeutic Approaches for Osteosarcoma. *Expert Rev Anticancer Ther* (2018) 18(1):39–50. doi: 10.1080/14737140.2018.1413939
15. Li S, Liu F, Zheng K, Wang W, Qiu E, Pei Y, et al. CircDOCK1 Promotes the Tumorigenesis and Cisplatin Resistance of Osteogenic Sarcoma *via* the miR-339-3p/IGF1R Axis. *Mol Cancer* (2021) 20(1):161. doi: 10.1186/s12943-021-01453-0
16. Lou J, Zhang H, Xu J, Ren T, Huang Y, Tang X, et al. Circusp34 Accelerates Osteosarcoma Malignant Progression by Sponging miR-16-5p. *Cancer Sci* (2022) 113(1):120–31. doi: 10.1111/cas.15147
17. Mao X, Guo S, Gao L, Li G. Circ-XPR1 Promotes Osteosarcoma Proliferation Through Regulating the miR-214-5p/DDX5 Axis. *Hum Cell* (2021) 34(1):122–31. doi: 10.1007/s13577-020-00412-z
18. Qi X, Zhang DH, Wu N, Xiao JH, Wang X, Ma W. ceRNA in Cancer: Possible Functions and Clinical Implications. *J Med Genet* (2015) 52(10):710–8. doi: 10.1136/jmedgenet-2015-103334
19. Yao Y, Zhou Y, Hua Q. circRNA Hsa_Circ_0018414 Inhibits the Progression of LUAD by Sponging miR-6807-3p and Upregulating DKK1. *Mol Ther Nucleic Acids* (2021) 23:783–96. doi: 10.1016/j.omtn.2020.12.031
20. Qin G, Wu X. Circular RNA Hsa_Circ_0032463 Acts as the Tumor Promoter in Osteosarcoma by Regulating the MicroRNA 498/LEF1 Axis. *Mol Cell Biol* (2021) 41(8):e0010021. doi: 10.1128/mcb.00100-21
21. Wang L, Li B, Yi X, Xiao X, Zheng Q, Ma L. Circ_SMAD4 Promotes Gastric Carcinogenesis by Activating Wnt/β-Catenin Pathway. *Cell Prolif* (2021) 54 (3):e12981. doi: 10.1111/cpr.12981
22. Wang Y, Wo Y, Lu T, Sun X, Liu A, Dong Y, et al. Circ-AASDH Functions as the Progression of Early Stage Lung Adenocarcinoma by Targeting miR-140-3p to Activate E2F7 Expression. *Transl Lung Cancer Res* (2021) 10(1):57–70. doi: 10.21037/tlcr-20-1062
23. Wu Y, Xie Z, Chen J, Chen J, Ni W, Ma Y, et al. Circular RNA Circtada2a Promotes Osteosarcoma Progression and Metastasis by Sponging miR-203a-3p and Regulating CREB3 Expression. *Mol Cancer* (2019) 18(1):73. doi: 10.1186/s12943-019-1007-1
24. Anderson ME. Update on Survival in Osteosarcoma. *Orthop Clin North Am* (2016) 47(1):283–92. doi: 10.1016/j.ocl.2015.08.022
25. Zhao X, Wu Q, Gong X, Liu J, Ma Y. Osteosarcoma: A Review of Current and Future Therapeutic Approaches. *BioMed Eng Online* (2021) 20(1):24. doi: 10.1186/s12938-021-00860-0
26. Otoukesh B, Boddouhi B, Moghtadaei M, Kaghazian P, Kaghazian M. Novel Molecular Insights and New Therapeutic Strategies in Osteosarcoma. *Cancer Cell Int* (2018) 18:158. doi: 10.1186/s12935-018-0654-4
27. Wang J, Zhao X, Wang Y, Ren F, Sun D, Yan Y, et al. circRNA-002178 Act as a ceRNA to Promote PDL1/PD1 Expression in Lung Adenocarcinoma. *Cell Death Dis* (2020) 11(1):32. doi: 10.1038/s41419-020-2230-9
28. Zhang C, Zhou H, Yuan K, Xie R, Chen C. Overexpression of Hsa_Circ_0136666 Predicts Poor Prognosis and Initiates Osteosarcoma Tumorigenesis Through miR-593-3p/ZEB2 Pathway. *Aging (Albany NY)* (2020) 12(11):10488–96. doi: 10.18632/aging.103273
29. van Schaijik B, Davis PF, Wickremesekera AC, Tan ST, Itinteang T. Subcellular Localisation of the Stem Cell Markers OCT4, SOX2, NANOG, KLF4 and C-MYC in Cancer: A Review. *J Clin Pathol* (2018) 71(1):88–91. doi: 10.1136/jclinpath-2017-204815
30. Peng Y, Liu J, Wang Z, Cui C, Zhang T, Zhang S, et al. Prostate-Specific Oncogene OTUD6A Promotes Prostatic Tumorigenesis via deubiquitinating and stabilizing c-Myc. *Cell Death Differ* (2022). doi: 10.1038/s41418-022-00960-x
31. Rong Z, Shi S, Tan Z, Xu J, Meng Q, Hua J, et al. Circular RNA CircEYA3 Induces Energy Production to Promote Pancreatic Ductal Adenocarcinoma Progression Through the miR-1294/C-Myc Axis. *Mol Cancer* (2021) 20 (1):106. doi: 10.1186/s12943-021-01400-z

Conflict of Interest: The authors declare that the research was conducted in the absence of any commercial or financial relationships that could be construed as a potential conflict of interest.

this article, or claim that may be made by its manufacturer, is not guaranteed or endorsed by the publisher.

frontiers | Frontiers in Oncology

CASE REPORT
published: 14 April 2022
doi: 10.3389/fonc.2022.877279

Olaparib Combined With Dacomitinib in Osimertinib-Resistant Brain and Leptomeningeal Metastases From Non-Small Cell Lung Cancer: A Case Report and Systematic Review

Hui Zhang[1,2†], Yong Wang[3†], Huaguo Wu[4], Shizhen Zhou[3], Shuo Li[5], Xiangji Meng[3], Rongjie Tao[2] and Jinming Yu[1,6*]*

[1] Tianjin Cancer Institute, Key Laboratory of Cancer Prevention and Therapy, National Clinical Research Center for Cancer, Tianjin Medical University Cancer Institute and Hospital, Tianjin's Clinical Research Center for Cancer, Tianjin Medical University, Tianjin, China, [2] Department of Medical Oncology, Shandong Cancer Hospital and Institute, Shandong First Medical University and Shandong Academy of Medical Science, Jinan, China, [3] Department of Neurosurgery, Shandong Cancer Hospital and Institute, Shandong First Medical University and Shandong Academy of Medical Science, Jinan, China, [4] Department of Head and Neck Surgery, Shandong Cancer Hospital and Institute, Shandong First Medical University and Shandong Academy of Medical Science, Jinan, China, [5] School of Medicine and Life Science, University of Jinan-Shandong Academy of Medical Science, Jinan, China, [6] Department of Radiation Oncology, Shandong Cancer Hospital and Institute, Shandong First Medical University and Shandong Academy of Medical Science, Jinan, China

Lung cancer patients with brain and leptomeningeal metastases usually have poor prognosis. For those patients with EGFR mutations, osimertinib, a third-generation tyrosine kinase inhibitor (TKI), is the first choice of treatment. However, drug resistance to osimertinib frequently occurs; and to date, the available follow-up treatment strategies have limited efficacy. In this case study, we report that treatments with olaparib, a Poly (ADP-ribose) polymerase (PARP) inhibitor, combined with dacomitinib, a second-generation EGFR TKI, benefited a lung cancer patient with osimertinib-resistant brain and leptomeningeal metastases. This 55-year-old male patient was found to have a pL858R mutation on EGFR exon 21 combined with TP53 and ERBB2 mutations after developing drug resistance to osimertinib treatment. Based on the genetic testing results, he was treated with olaparib and dacomitinib, and obtained 6 months of progression-free survival (PFS) and 13 months of overall survival (OS) after the diagnosis of leptomeningeal metastasis. This case report represents the first study applying PARP inhibitor in combination with dacomitinib in the treatment of leptomeningeal metastases after osimertinib resistance.

Keywords: olaparib, dacomitinib, osimertinib-resistant, brain and leptomeningeal metastases, non-small cell lung cancer

OPEN ACCESS

Edited by:
Zhe-Sheng Chen,
St. John's University, United States

Reviewed by:
Zhenguo Liu,
First Affiliated Hospital of Sun Yat-Sen University, China
Longhui Qiu,
University of California, San Francisco, United States

***Correspondence:**
Jinming Yu
sdyujinming@163.com
Rongjie Tao
Drtaorongjie@163.com

†These authors have contributed equally to this work

Specialty section:
This article was submitted to Cancer Molecular Targets and Therapeutics, a section of the journal Frontiers in Oncology

Received: *16 February 2022*
Accepted: *24 March 2022*
Published: *14 April 2022*

Citation:
Zhang H, Wang Y, Wu H, Zhou S, Li S, Meng X, Tao R and Yu J (2022) Olaparib Combined With Dacomitinib in Osimertinib-Resistant Brain and Leptomeningeal Metastases From Non-Small Cell Lung Cancer: A Case Report and Systematic Review. Front. Oncol. 12:877279. doi: 10.3389/fonc.2022.877279

INTRODUCTION

Patients with central nervous system (CNS) metastases from non-small cell lung cancer (NSCLC) usually have very poor prognosis (1, 2). The median survival of patients in this population is usually less than 1 year despite the emerging advancement in treatment options (3–5). It has been reported that in patients with NSCLC, up to 50% would develop brain metastases (BM) during the course of their illness (5) and 3-5% would develop leptomeningeal metastases (LM) (6). The incidence could be higher in those with anaplastic lymphoma kinase (ALK)-rearrangement or epidermal growth factor receptor (EGFR) mutations (7). Currently, a combinational strategy of multidisciplinary therapies involving systemic and intrathecal chemotherapy, radiotherapy, and targeted therapies (such as osimertinib and bevacizumab) is preferred for NSCLC patients with brain and leptomeningeal metastases (2, 8). However, the reported survival time remains unsatisfied and more investigation on treatment strategies is needed.

Osimertinib (AZD9291), a third-generation oral irreversible EGFR tyrosine kinase inhibitor (TKI) (9), has been approved by the United States Food and Drug Administration (FDA) and the European Medicines Agency (EMA) for patients with acquired EGFR T790M mutation (10). In preclinical studies, osimertinib exhibited greater penetration of the mouse blood-brain barrier than gefitinib, rociletinib, or afatinib at clinically relevant doses and showed some effectiveness for treating the first or second-generation EGFR-TKI resistant leptomeningeal metastases from EGFR-mutant lung cancer (11, 12). In clinical studies, osimertinib also showed significant intracranial activity (13, 14). In the most recent prospective phase II study which evaluated the efficacy of osimertinib 160 mg in T790M-positive BM or LM of NSCLC patients who progressed on prior EGFR TKI treatment, the median overall survival was 16.9 months in the BM cohort and 13.3 months in the LM cohort (14).

In spite of the success of osimertinib as a therapy for patients with NSCLC and its potential efficacy for CNS metastases, acquired resistance involving EGFR-dependent or EGFR-independent mechanisms inevitably occurs and hampers its clinical benefits (15). It is estimated that when osimertinib is used as a first-line treatment, resistance develops approximately after 19 months of treatment; and when it is used as a second-line treatment, resistance could occur after 11 months (16). The mechanisms of resistance to osimertinib are complicated, but most of them involved in EGFR exon 20 mutations (C797S, M766Q, S768I, L718 V, and others) leading to disruption of osimertinib binding sites, alternative pathway activation, aberrant downstream signaling and lineage plasticity leading to small cell transformation, such as *MET* and *ERBB2* amplifications, inactivation of *TP53* and/or *RB1*, and so on (15, 16). The good treatment option for patients who develop resistance to osimertinib remains a critical unresolved issue in the field. Current clinical trials are focusing on targeting alternative pathways (resistance mediated by *MET*, *ERBB2*, and C979S mutation) and combination of VEGF inhibitions with EGFR-TKIs (clinical trials: NCT03392246, NCT03784599, NCT04181060, NCT03909334, and so on.) (16, 17).

Poly (ADP-ribose) polymerase 1 (PARP1) is an important DNA repair enzyme of the base excision repair (BER) pathway and represents a critical target in cancer treatments (18). FDA has approved four PARP inhibitors (Olaparib, Rucaparib, Niraparib, and Talazoparib) for treatments of ovarian and breast cancers (19). To date, very few studies have reported their efficacies in lung adenocarcinoma. A pre-clinical study by Lynnette Marcar et al. showed that compared to TKI sensitive cells, TKI (gefitinib and osimertinib) resistant EGFR mutant NSCLC cells were more sensitive to PARP inhibitors, indicating the potential efficacy of PARP inhibitors in treating osimertinib-resistant NSCLC (20). A phase I clinical trial investigating the efficacy of the PARP inhibitor, niraparib, together with osimertinib in treating patients with stage IV EGFR-mutated NSCLC is ongoing (NCT03891615).

In this case study, we report that the treatment using PARP inhibitor olaparib in combination with dacomitinib, a second generation EGFR-TKI, benefited a NSCLC patient with osimertinib-resistant brain and leptomeningeal metastases who had EGFR mutations combined with TP53 and ERBB2 mutations.

CASE PRESENTATION

A 55-year-old male underwent thoracoscopic-assisted small-incision radical resection of lung cancer in October 11, 2017 after diagnosis of lung adenocarcinoma (stage pT1bN0M0, IA) (**Figure 1**). His postoperative regular magnetic resonance imaging (MRI) and computerized tomography (CT) examinations showed no obvious abnormalities. Two years later (on October 12, 2019), the patient started to experience headache, blurred vision, and hearing loss. On October 31, 2019, his brain MRI exam showed multiple brain masses including multiple metastases in the lateral ventricle, right frontal lobe, and cerebellar hemisphere (**Figure 2A**). His genetic testing revealed the L858R mutation in exon 21 of EGFR. His positron emission tomography (PET) CT scan suggested bone metastasis (**Figure S1**). The patient was then treated with osimertinib (80 mg oral administration daily), bevacizumab (7.5mg/kg q3w), and bisphosphonate (4mg q3w). After treatment for 1 month, his symptom of headache almost disappeared, but he developed blurred vision and unstable walking on both feet. On 2020-1-4, the patient complained increased blurred vision and occasional headache. On 2020-4-21, his brain MRI (**Figure 2B**) showed multiple dot-line enhancements (masses) in the cerebellar sulci, suggesting meningeal metastasis. On 2020-4-30, the patient underwent cerebrospinal fluid (CSF) cytology examination and cancer cells were found in the cerebrospinal fluid, which was in line with the characteristics of adenocarcinoma cells (**Figure 2C**). His CSF genetic testing results in May 2020 showed that mutations were EGFR p.L858R, TP53 p.R273C and ERBB2 p.S442L (**Figure 3A**). The patient was then treated with whole brain radiotherapy (40Gy/20 fractions). Between July 2020 and December 2020, the patient was treated with osimertinib (80 mg oral administration daily), anlotinib (12mg d1-14, q3w), pemetrexed (500mg/kg q4w), and temozolomide (300mg d1-5, q4w). Then, the patient experienced less headache. The re-test of the CSF samples showed that the mutations included EGFR

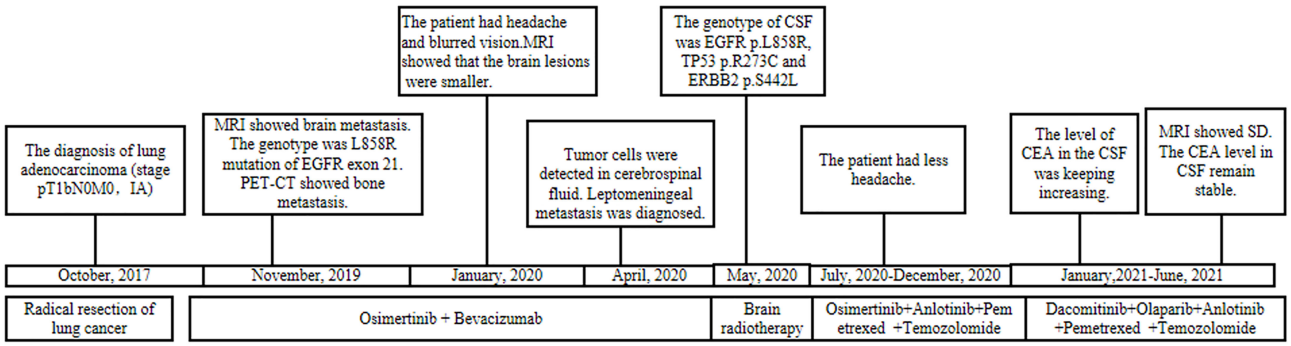

FIGURE 1 | Summary of the diagnosis and treatment process.

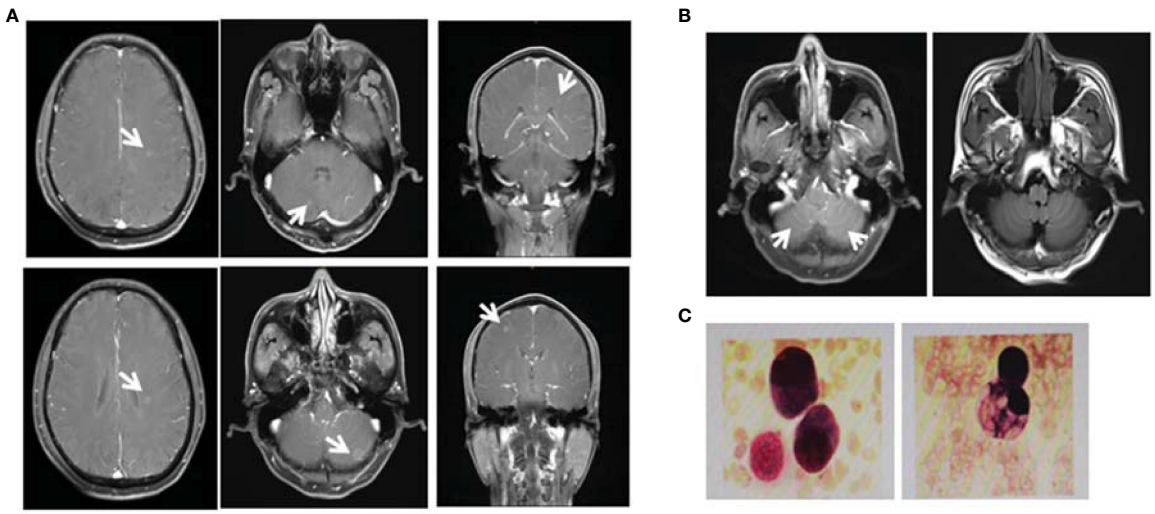

FIGURE 2 | Diagnosis of brain metastases. **(A)** On October 31, 2019, the magnetic resonance imaging (MRI) examination of the patient showed multiple brain masses including multiple metastases in the lateral ventricle, right frontal lobe, and cerebellar hemisphere. Diagnosis of leptomeningeal metastases. **(B)** On April 21, 2020, MRI T1 enhancement and FLARE examination showed that the cerebellar sulci had multiple line-like and spot-like enhancements, suggesting meningeal metastasis. **(C)** On April 30, 2020, retest of the cerebrospinal fluid (CSF) showed the presence of cancer cells with the characteristics of adenocarcinoma cells.

p.L858R, TP53, ERBB2, and others (October 28, 2021). (**Figure 3A**). In January 2021, due to the continued elevated levels of tumor marker carcinoembryonic antigen (CEA) in his CSF (**Figure 3B**) and based on his CSF genetic test results, his treatment was switched to dacomitinib (30mg po qd), olaparib (100mg po bid), anlotinib (8mg po d1-14,q3w), pemetrexed (500mg/m^2, q3w), and temozolomide (200mg/m^2 d1-5, q4w). The patient's condition was stable after adjusting the treatment plan. His level of CEA was stable (**Figure 3B**), and his brain MRI showed no progression of the brain metastasis. The efficacy evaluation during the treatment period is shown in **Figure 4**. In addition, after switching to targeted therapy, the patient no longer experienced obvious headache and dizziness, and his quality of life was significantly improved. Although he had the 2nd degree bone marrow suppression, there was no obvious functional damage of the liver and kidney during the process of treatment. The patient died of cachexia caused by the tumor in June 2021. Based upon, targeted drug therapy helped this patient obtain 6 months of progression-free survival (PFS). After the diagnosis of CNS metastases, although he was no longer sensitive to osimertinib, his overall survival reached 13 months which might be benefited from the treatment of olaparib in combination with dacomitinib.

DISCUSSION

This case represents the first study applying PARP inhibitor combined with dacomitinib for treating CNS metastases from NSCLC after osimertinib resistance. Using this new treatment strategy in combination with other chemotherapeutic drugs and

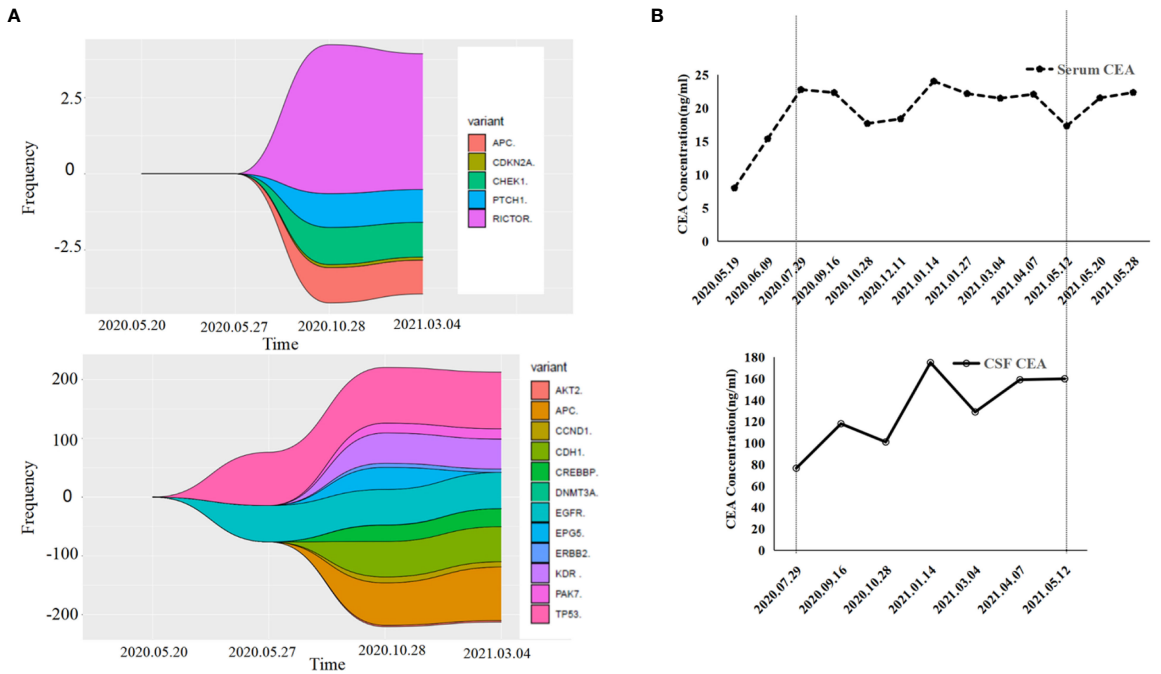

FIGURE 3 | Gene detection diagram and levels of carcinoembryonic antigen (CEA) during treatment. **(A)** Gene detection diagram during the treatment was shown. Different colors represent different genes and different wave widths. The number on the vertical axis represents the mutation frequency (wave width). **(B)** The levels of CEA, including serum CEA and cerebrospinal fluid CEA, were shown.

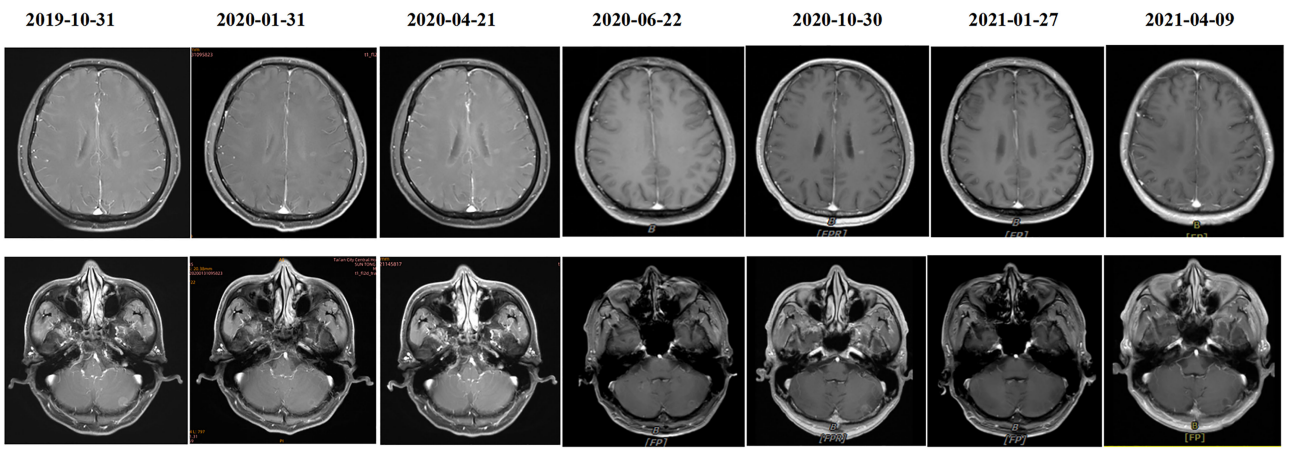

FIGURE 4 | MRI imaging changes at different time points during the treatment process.

radiotherapy, the patient eventually obtained 6 months of progression-free survival and 13 months of overall survival after the diagnosis of leptomeningeal metastasis, which is markedly longer than the median survival reported in previous studies (3, 4, 21).

Unlike a previous case report which showed that dacomitinib, the second-generation TKI, did not benefit a patient who developed mutations after later-line osimertinib treatment (22), the present case with ERBB2 mutations showed a different outcome. This patient also had mutations in TP53, a gene that is essential for DNA repair. Given the effects of PARP inhibitors in DNA repair pathway, this patient was treated with olaparib and seemed to be benefited from this combined targeted therapy.

This case report also highlighted the importance of CSF genetic testing in the diagnoses of CNS metastases. For this

patient, his plasma genetic testing in May 2020 was negative for EGFR mutations; however, his CSF samples were positive and showed mutations in EGFR p.L858R, TP53, and ERBB2, which helped determining his subsequent treatment strategies (dacomitinib and olaparib). This case suggests that CSF genetic testing is necessary for patients who may have CNS metastases. Indeed, CSF-derived cell free DNA holds promise for diagnosis and characterization of CNS tumors or metastases (23). In a study involving 26 lung cancer patients with leptomeningeal metastasis and known EGFR mutations in the primary tumor, mutations in driver genes were detected in 100% (26/26), 84.6% (22/26), and 73.1% (19/26) of samples from CSF cell-free DNA (cfDNA), CSF precipitates, and plasma, respectively (24). Therefore, genetic profiling of CSF samples could help the diagnoses of patients with CNS metastases and improve their treatment outcomes.

For cancer patients, a significant increase in CEA level is often related to meningeal metastases (25). Therefore, CEA levels in CSF samples could be an indicator for the prognosis. In this case, the CEA levels in the CSF samples were notably higher than that in the blood. After targeted therapy, his CEA levels were stable, which was consistent with his MRI test results.

CNS metastases frequently occur in patients with lung cancer; and these patients often have an extremely poor prognosis. Due to the poor penetration of the blood-brain barrier, the first- and second- generation of EGFR-TKIs have low efficacy in the treatment of BM and LM in NSCLC. Although the third generation of EGFR-TKI, osimertinib, has shown increased penetration into the blood-brain barrier and enhanced clinical activity in patients with CNS metastasis, unfortunately, similar to the first- and second- generation of EGFR-TKIs, drug resistance to osimertinib commonly occurs after over 1 year of treatment. As reviewed by Alessandro Leonetti et al., the known mechanisms of resistance to osimertinib include EGFR modifications, activation of bypass signaling pathways mediated by MET, ERBB2, ALK, IGFR1, FGFR, and others, downstream pathway activation, epithelial-to-mesenchymal transition, histologic transformation, oncogenic gene fusions and cell-cycle gene aberrations (15).

Currently, platinum-based chemotherapy remains the standard of care after osimertinib resistance develops. Several early phase clinical trials for overcoming osimertinib resistance in NSCLC patients are ongoing. The strategies in these trials are mainly targeting specific known resistance mechanisms, including MET-inhibitors, MEK inhibitors, or combination of VEGF-inhibition with EGFR-TKIs (16). According to the phase Ib TATTON study involving patients with advanced EGFR-mutant NSCLC, osimertinib with either the MEK1/2 inhibitors (selumetinib or durvalumab), MET-inhibitor (savolitinib), or the PDL1-inhibitor (durvalumab) seemed to be safe and tolerable by patients (26). Currently the phase II clinical trial testing osimertinib plus savolitinib in EGFRm+/MET+ NSCLC patients following prior osimertinib (SAVANNAH) is still ongoing (NCT03778229). In another phase II study recruiting patients with advanced NSCLC who progressed on first-line osimertinib therapy (ORCHARD; NCT03944772), up to 9 experimental modules are tested: including Osimertinib + Savolitinib, Osimertinib + Gefitinib, Osimertinib + Necitumumab, Carboplatin + Pemetrexed + Durvalumab, Osimertinib + Alectinib, Osimertinib + Selpercatinib, Etoposide + Durvalumab + Carboplatin or Cisplatin, Osimertinib + Pemetrexed + Carboplatin or Cisplatin, Osimertinib + Selumetinib. However, the estimated primary completion date is set to be in the year of 2025. Therefore, whether these strategies could be beneficial to NSCLC patients with CNS metastasis and osimertinib resistance remains unclear. Immunotherapy using immune checkpoint inhibitors has been utilized in EGFR-mutated NSCLC patients, though its efficacy seemed to be not as good as in other cancers (27). Currently it is not clear whether immunotherapy has beneficial effects in NSCLC patients with Osimertinib resistance. However, it should be noted that interstitial lung disease-like events could occur when combining checkpoint inhibitors with osimertinib according to the phase Ib TATTON trial which assessed treatment of osimertinib in combination with durvalumab (26).

This case report in the patient with mutations in EGFR pL858R, TP53, and ERBB2 supported that dacomitinib, a second-generation EGFR-TKI, together with olaparib, a PARP inhibitor, may benefit NSCLC patient with CNS metastases after developing osimertinib resistance. The possible mechanisms could be as followed. First, dacomitinib is a selective inhibitor for ERBB2. It has been reported that dacomitinib could suppress the proliferation of Ba/F3 cells expressing T790M in *cis* to different deletions in exon 19 (IC50: 140-330 nmol/L) (28). Since this patient was tested positive for ERBB2 mutation in his CSF samples, dacomitinib might be the most relevant drug and he obtained the beneficial treatment result. Second, as suggested in the *in vitro* and *in vivo* experiments by Lynnette Marcar et al., the PARP inhibitor could increase reactive oxygen species (ROS) production and induce oxidative damage in osimertinib-resistant EGFR mutant NSCLC cells (20). Third, in triple-negative breast cancer, it has been shown that TP53 mutations combined with BRCA1 mutations are very frequent and may be sensitive to PARP inhibitors (29). Therefore, PARP inhibitors may also benefit NSCLC patients with TP53 mutations, which requires further evaluation. Moreover, it is known that P-glycoprotein (P-gp) is one of the proteins expressed naturally on the plasma membrane of endothelial cells in the blood-brain barrier (BBB), that could restrict substrate compounds from entering the brain (30). PARP inhibitors including olaparib, veliparib, and CEP-8983 are P-glycoprotein substrates (31). Therefore, olaparib may help enhance the antagonizing effect of dacomitinib on multidrug resistance, by inhibiting the efflux activity of ABCB1 and ABCG2 transporters (32).

In summary, exploring treatment strategies for patients with acquired osimertinib drug resistance is critical, particularly for patients with CNS metastases. The cerebrospinal fluid genetic testing plays an important role in guiding individualized treatment of patients with CNS metastases, as appropriate targeted treatments could be selected based on testing results. PARP inhibitors, olaparib, combined with EGFR-TKIs, may benefit patients with CNS metastases of NSCLC, and this combination strategy of multiple-target therapy is safe and holds promise for clinical application.

DATA AVAILABILITY STATEMENT

The datasets presented in this study can be found in online repositories. The names of the repository/repositories and accession number(s) can be found in the article/**Supplementary Material**.

ETHICS STATEMENT

The studies involving human participants were reviewed and approved by Ethics Committee of Shandong Cancer Hospital and Institute. The patients/participants provided their written informed consent to participate in this study.

AUTHOR CONTRIBUTIONS

HZ, YW, XM, and SZ collected the clinical and pathological data. HW and HZ wrote the manuscript. JY and RT assisted in revising the manuscript. All authors contributed to the article and approved the submitted version.

FUNDING

This work was supported by funds from the National Natural Sciences Foundation of China (no. 8150111724; to HZ), the Joint Fund for Cancer Prevention and Treatment of Shandong Natural Fund (no. ZR2019LZL015; to HZ), and Wu Jieping Medical Fund (no.320.6750.19088-24; to HZ).

SUPPLEMENTARY MATERIAL

The Supplementary Material for this article can be found online at: https://www.frontiersin.org/articles/10.3389/fonc.2022.877279/full#supplementary-material

REFERENCES

1. Dawe DE, Greenspoon JN, Ellis PM. Brain Metastases in Non-Small-Cell Lung Cancer. *Clin Lung Cancer* (2014) 15(4):249–57. doi: 10.1016/j.cllc.2014.04.008
2. Cheng H, Perez-Soler R. Leptomeningeal Metastases in Non-Small-Cell Lung Cancer. *Lancet Oncol* (2018) 19(1):e43–55. doi: 10.1016/S1470-2045(17)30689-7
3. Morris PG, Reiner AS, Szenberg OR, Clarke JL, Panageas KS, Perez HR, et al. Leptomeningeal Metastasis From Non-Small Cell Lung Cancer: Survival and the Impact of Whole Brain Radiotherapy. *J Thorac Oncol* (2012) 7(2):382–5. doi: 10.1097/JTO.0b013e3182398e4f
4. Wu YL, Zhou L, Lu Y. Intrathecal Chemotherapy as a Treatment for Leptomeningeal Metastasis of Non-Small Cell Lung Cancer: A Pooled Analysis. *Oncol Lett* (2016) 12(2):1301–14. doi: 10.3892/ol.2016.4783
5. Page S, Milner-Watts C, Perna M, Janzic U, Vidal N, Kaudeer N, et al. Systemic Treatment of Brain Metastases in Non-Small Cell Lung Cancer. *Eur J Cancer* (2020) 132:187–98. doi: 10.1016/j.ejca.2020.03.006
6. Remon J, Le Rhun E, Besse B. Leptomeningeal Carcinomatosis in Non-Small Cell Lung Cancer Patients: A Continuing Challenge in the Personalized Treatment Era. *Cancer Treat Rev* (2017) 53:128–37. doi: 10.1016/j.ctrv.2016.12.006
7. Li YS, Jiang BY, Yang JJ, Tu HY, Zhou Q, Guo WB, et al. Leptomeningeal Metastases in Patients With Nsclc With Egfr Mutations. *J Thorac Oncol* (2016) 11(11):1962–9. doi: 10.1016/j.jtho.2016.06.029
8. Mantovani C, Gastino A, Cerrato M, Badellino S, Ricardi U, Levis M. Modern Radiation Therapy for the Management of Brain Metastases From Non-Small Cell Lung Cancer: Current Approaches and Future Directions. *Front Oncol* (2021) 11:772789. doi: 10.3389/fonc.2021.772789
9. Cross DA, Ashton SE, Ghiorghiu S, Eberlein C, Nebhan CA, Spitzler PJ, et al. Azd9291, an Irreversible Egfr Tki, Overcomes T790m-Mediated Resistance to Egfr Inhibitors in Lung Cancer. *Cancer Discov* (2014) 4(9):1046–61. doi: 10.1158/2159-8290.CD-14-0337
10. Odogwu L, Mathieu L, Goldberg KB, Blumenthal GM, Larkins E, Fiero MH, et al. Fda Benefit-Risk Assessment of Osimertinib for the Treatment of Metastatic Non-Small Cell Lung Cancer Harboring Epidermal Growth Factor Receptor T790m Mutation. *Oncologist* (2018) 23(3):353–9. doi: 10.1634/theoncologist.2017-0425
11. Ballard P, Yates JW, Yang Z, Kim DW, Yang JC, Cantarini M, et al. Preclinical Comparison of Osimertinib With Other Egfr-Tkis in Egfr-Mutant Nsclc Brain Metastases Models, and Early Evidence of Clinical Brain Metastases Activity. *Clin Cancer Res* (2016) 22(20):5130–40. doi: 10.1158/1078-0432.CCR-16-0399
12. Nanjo S, Ebi H, Arai S, Takeuchi S, Yamada T, Mochizuki S, et al. High Efficacy of Third Generation Egfr Inhibitor Azd9291 in a Leptomeningeal Carcinomatosis Model With Egfr-Mutant Lung Cancer Cells. *Oncotarget* (2016) 7(4):3847–56. doi: 10.18632/oncotarget.6758
13. Yang JCH, Kim SW, Kim DW, Lee JS, Cho BC, Ahn JS, et al. Osimertinib in Patients With Epidermal Growth Factor Receptor Mutation-Positive Non-Small-Cell Lung Cancer and Leptomeningeal Metastases: The Bloom Study. *J Clin Oncol* (2020) 38(6):538–47. doi: 10.1200/JCO.19.00457
14. Park S, Lee MH, Seong M, Kim ST, Kang JH, Cho BC, et al. A Phase Ii, Multicenter, Two Cohort Study of 160 Mg Osimertinib in Egfr T790m-Positive Non-Small-Cell Lung Cancer Patients With Brain Metastases or Leptomeningeal Disease Who Progressed on Prior Egfr Tki Therapy. *Ann Oncol* (2020) 31(10):1397–404. doi: 10.1016/j.annonc.2020.06.017
15. Leonetti A, Sharma S, Minari R, Perego P, Giovannetti E, Tiseo M. Resistance Mechanisms to Osimertinib in Egfr-Mutated Non-Small Cell Lung Cancer. *Br J Cancer* (2019) 121(9):725–37. doi: 10.1038/s41416-019-0573-8
16. Schmid S, Li JJN, Leighl NB. Mechanisms of Osimertinib Resistance and Emerging Treatment Options. *Lung Cancer* (2020) 147:123–9. doi: 10.1016/j.lungcan.2020.07.014
17. Sequist LV, Han JY, Ahn MJ, Cho BC, Yu H, Kim SW, et al. Osimertinib Plus Savolitinib in Patients With Egfr Mutation-Positive, Met-Amplified, Non-Small-Cell Lung Cancer After Progression on Egfr Tyrosine Kinase Inhibitors: Interim Results From a Multicentre, Open-Label, Phase 1b Study. *Lancet Oncol* (2020) 21(3):373–86. doi: 10.1016/S1470-2045(19)30785-5
18. Chen A. Parp Inhibitors: Its Role in Treatment of Cancer. *Chin J Cancer* (2011) 30(7):463–71. doi: 10.5732/cjc.011.10111
19. Rose M, Burgess JT, O'Byrne K, Richard DJ, Bolderson E. Parp Inhibitors: Clinical Relevance, Mechanisms of Action and Tumor Resistance. *Front Cell Dev Biol* (2020) 8:564601. doi: 10.3389/fcell.2020.564601
20. Marcar L, Bardhan K, Gheorghiu L, Dinkelborg P, Pfaffle H, Liu Q, et al. Acquired Resistance of Egfr-Mutated Lung Cancer to Tyrosine Kinase Inhibitor Treatment Promotes Parp Inhibitor Sensitivity. *Cell Rep* (2019) 27(12):3422–32 e4. doi: 10.1016/j.celrep.2019.05.058
21. Marcinowska-Suchowierska E, Lorenc R, Brzozowski R. [Effect of Long-Term Irradiation of the Skin on Calcium-Phosphate Metabolism and the 25-Oh-D Level in Patients With Chronic Diseases of the Digestive System]. *Przegl Lek* (1988) 45(8):614–9.
22. Li HS, Yang GJ, Wang Y. Case Report: Dacomitinib May Not Benefit Patients Who Develop Rare Compound Mutations After Later-Line Osimertinib Treatment. *Front Oncol* (2021) 11:649843. doi: 10.3389/fonc.2021.649843
23. McEwen AE, Leary SES, Lockwood CM. Beyond the Blood: Csf-Derived Cfdna for Diagnosis and Characterization of Cns Tumors. *Front Cell Dev Biol* (2020) 8:45. doi: 10.3389/fcell.2020.00045

24. Li YS, Jiang BY, Yang JJ, Zhang XC, Zhang Z, Ye JY, et al. Unique Genetic Profiles From Cerebrospinal Fluid Cell-Free DNA in Leptomeningeal Metastases of Egfr-Mutant Non-Small-Cell Lung Cancer: A New Medium of Liquid Biopsy. *Ann Oncol* (2018) 29(4):945–52. doi: 10.1093/annonc/mdy009
25. Kang SJ, Kim KS, Ha YS, Huh SY, Lee JH, Kim JK, et al. Diagnostic Value of Cerebrospinal Fluid Level of Carcinoembryonic Antigen in Patients With Leptomeningeal Carcinomatous Metastasis. *J Clin Neurol* (2010) 6(1):33–7. doi: 10.3988/jcn.2010.6.1.33
26. Oxnard GR, Yang JC, Yu H, Kim SW, Saka H, Horn L, et al. Tatton: A Multi-Arm, Phase Ib Trial of Osimertinib Combined With Selumetinib, Savolitinib, or Durvalumab in Egfr-Mutant Lung Cancer. *Ann Oncol* (2020) 31(4):507–16. doi: 10.1016/j.annonc.2020.01.013
27. Jin R, Zhao J, Xia L, Li Q, Li W, Peng L, et al. Application of Immune Checkpoint Inhibitors in Egfr-Mutant Non-Small-Cell Lung Cancer: From Bed to Bench. *Ther Adv Med Oncol* (2020) 12:1758835920930333. doi: 10.1177/1758835920930333
28. Lavacchi D, Mazzoni F, Giaccone G. Clinical Evaluation of Dacomitinib for the Treatment of Metastatic Non-Small Cell Lung Cancer (Nsclc): Current Perspectives. *Drug Des Devel Ther* (2019) 13:3187–98. doi: 10.2147/DDDT.S194231
29. Na B, Yu X, Withers T, Gilleran J, Yao M, Foo TK, et al. Therapeutic Targeting of Brca1 and Tp53 Mutant Breast Cancer Through Mutant P53 Reactivation. *NPJ Breast Cancer* (2019) 5:14. doi: 10.1038/s41523-019-0110-1
30. Aryal M, Fischer K, Gentile C, Gitto S, Zhang YZ, McDannold N. Effects on P-Glycoprotein Expression After Blood-Brain Barrier Disruption Using Focused Ultrasound and Microbubbles. *PloS One* (2017) 12(1):e0166061. doi: 10.1371/journal.pone.0166061
31. Lawlor D, Martin P, Busschots S, Thery J, O'Leary JJ, Hennessy BT, et al. Parp Inhibitors as P-Glyoprotein Substrates. *J Pharm Sci* (2014) 103(6):1913–20. doi: 10.1002/jps.23952
32. Fan YF, Zhang W, Zeng L, Lei ZN, Cai CY, Gupta P, et al. Dacomitinib Antagonizes Multidrug Resistance (Mdr) in Cancer Cells by Inhibiting the Efflux Activity of Abcb1 and Abcg2 Transporters. *Cancer Lett* (2018) 421:186–98. doi: 10.1016/j.canlet.2018.01.021

Conflict of Interest: The authors declare that the research was conducted in the absence of any commercial or financial relationships that could be construed as a potential conflict of interest.

Publisher's Note: All claims expressed in this article are solely those of the authors and do not necessarily represent those of their affiliated organizations, or those of the publisher, the editors and the reviewers. Any product that may be evaluated in this article, or claim that may be made by its manufacturer, is not guaranteed or endorsed by the publisher.

frontiers | Frontiers in Pharmacology

ORIGINAL RESEARCH
published: 20 April 2022
doi: 10.3389/fphar.2022.860546

Antitumor Effect of Simvastatin in Combination With DNA Methyltransferase Inhibitor on Gastric Cancer *via* GSDME-Mediated Pyroptosis

Ying Xia[1,2,3,4†], *Yong Jin*[1,4†], *Daxiang Cui*[5], *Xia Wu*[6], *Cunfeng Song*[5*], *Weilin Jin*[5,7*] and *Hai Huang*[1,4*]

[1]Center for Clinical Laboratories, The Affiliated Hospital of Guizhou Medical University, Guiyang, China, [2]Department of Pathophysiology, School of Basic Medical Science, Guizhou Medical University, Guiyang, China, [3]Department of Clinical Laboratory, The First Affiliated Hospital of Guizhou University of Traditional Chinese Medicine, Guiyang, China, [4]School of Clinical Laboratory Science, Guizhou Medical University, Guiyang, China, [5]Shanghai Engineering Research Center for Intelligent Diagnosis and Treatment Instrument, Department of Instrument Science and Engineering, School of Electronic Information and Electrical Engineering, Institute of Nano Biomedicine and Engineering, Shanghai Jiao Tong University, Shanghai, China, [6]Guizhou Provincial People's Hospital, Guiyang, China, [7]Institute of Cancer Neuroscience, Medical Frontier Innovation Research Center, The First Hospital of Lanzhou University, The First Clinical Medical College of Lanzhou University, Lanzhou, China

Gasdermin E (GSDME) is one of the executors of pyroptosis, a type of programmed lytic cell death, which can be triggered by caspase-3 activation upon stimulation. Silenced GSDME expression due to promoter hypermethylation is associated with gastric cancer (GC), which is confirmed in the present study by bioinformatics analysis and methylation-specific PCR (MSP) test of GC cell lines and clinical samples. GC cell lines and mouse xenograft models were used to investigate the pyroptosis-inducing effect of the common cholesterol-depleting, drug simvastatin (SIM), allied with upregulating GSDME expression by doxycycline (DOX)- inducible Tet-on system or DNA methyltransferase inhibitor 5-Aza-2′-deoxycytidine (5-Aza-CdR). Cell viability assessment and xenograft tumour growth demonstrated that the tumour inhibition effects of SIM can be enhanced by elevated GSDME expression. Morphological examinations and assays measuring lactate dehydrogenase (LDH) release and caspase-3/GSDME protein cleavage underlined the stimulation of pyroptosis as an important mechanism. Using short hairpin RNA (shRNA) knockdown of caspase-3 or GSDME, and caspase-3-specific inhibitors, we provided evidence of the requirement of caspase-3/GSDME in the pyroptosis process triggered by SIM. We conclude that reactivating GSDME expression and thereby inducing cancer cell-specific pyroptosis could be a potential therapeutic strategy against GC.

Keywords: GSDME, pyroptosis, DNA methyltransferase inhibitor, gastric cancer, simvastatin

OPEN ACCESS

Edited by:
Zhe-Sheng Chen,
St. John's University, United States

Reviewed by:
Bo Hu,
Jiaxing University, China
Hui Qian,
Jiangsu University, China

****Correspondence:***
Cunfeng Song
songcf@sjtu.edu.cn
Weilin Jin
ldyy_jinwl@lzu.edu.cn
Hai Huang
huanghai828@gmc.edu.cn

†These authors have contributed equally to this work

Specialty section:
This article was submitted to Experimental Pharmacology and Drug Discovery, a section of the journal Frontiers in Pharmacology

Received: *09 February 2022*
Accepted: *28 March 2022*
Published: *20 April 2022*

Citation:
Xia Y, Jin Y, Cui D, Wu X, Song C, Jin W and Huang H (2022) Antitumor Effect of Simvastatin in Combination With DNA Methyltransferase Inhibitor on Gastric Cancer via GSDME-Mediated Pyroptosis. Front. Pharmacol. 13:860546. doi: 10.3389/fphar.2022.860546

INTRODUCTION

Gastric cancer (GC) is ranked third in cancer mortality and poses a serious threat to human health (Mattiuzzi and Lippi, 2020). To date, surgery and chemoradiotherapy remain the first-line treatment towards GC, but many patients still suffer from poor prognosis and low 5-year survival rate due to severe adverse effects and acquired drug resistance (Yang et al., 2022). Induction of pyroptosis has been emerging as a novel therapeutic strategy against a variety of malignant tumours including GC (Zhou and Fang, 2019; Tan et al., 2021a; Li et al., 2021; Shao et al., 2021), because of its dual function of cytotoxicity and immunogenicity.

Pyroptosis is a gasdermin (GSDM)-dependent programmed cell death featuring membrane rupture formed by translocated GSDM fragments originated from caspase cleavage (Xia et al., 2020). One important characteristic of pyroptosis is the release of cellular contents such as pro-inflammatory cytokines interleukin-1β (IL-1β) and interleukin-18 (IL-18), which actively regulate the immune profile of the tumour microenvironment (Tan et al., 2021b). Gasdermin D (GSDMD) and gasdermin E (GSDME) are the best-studied pyroptotic effectors in the GSDM family. Their sheared N-terminals perforate cell membrane in a similar manner but differ in the activation cascades (Jorgensen and Miao, 2015; Hou et al., 2021). The anti-tumour action of Cucurbitacin B was found to involve the activation of GSDMD-dependent pyroptosis of non-small cell lung cancer (NSCLC) cells *in vitro* and *in vivo* (Yuan et al., 2021). GSDME, located on chromosome 7p15 and also named deafness autosomal dominant 5 (DFNA5) due to its association with hereditary hearing loss (Van Laer et al., 1998), has been implicated as a putative tumour suppressor (Rogers et al., 2017; Wang et al., 2017). Cleaved by the activated caspase-3, the N-terminal of GSDME (GSDME-N) inserts into the membrane lipids and forms pores to trigger pyroptosis (Wang et al., 2017).

In contrast to the substantial investment of time and resources into developing a new drug from scratch repurposing approved drugs can significantly accelerate the clinical translation of basic research (Pushpakom et al., 2019), as exemplified in the quest for drugs to induce pyroptosis. The histamine 2 antagonist famotidine is found to induce GSDME-, not GSDMD-, mediated cell pyroptosis by activation of NLRP3 inflammasome form, leading to increase Caspase-1 activation and IL-18 release in GC cells (Huang et al., 2021). In recent years, studies and clinical trials exploiting the preventive and therapeutic potential of statin in cancer treatment are flourishing. Statin is a class of HMG-CoA reductase inhibitors and the most commonly prescribed cholesterol-reducing drugs thanks to their safety, efficacy, and low cost (Jiang et al., 2021a). In particular, it was shown that simvastatin (SIM), one of the six statin medicines, elicits its anti-cancer effects through not only lowering of cholesterol content, but also activation of caspase-3 (Deng et al., 2019; Alhakamy et al., 2020; Sun et al., 2020) and consequently apoptosis or pyroptosis (Peng et al., 2020; Xu et al., 2021). Moreover, the SIM-induced pyroptosis is confirmed to be cancer cell-specific in lung cancer, without causing toxicity to normal cells (Wang et al., 2018).

However, the death of tumour cells *via* pyroptosis is often dampened by epigenetic silencing of GSDME, as hypermethylation of GSDME promoter is found in about 52%–65% of primary cancers (Op de Beeck et al., 2011) including colorectal cancer (Kim et al., 2008a; Yokomizo et al., 2012) and GC (Akino et al., 2007). Studies have used hypomethylating agents such as decitabine (DAC) (Fan et al., 2019) or 5-aza-2′-deoxycytidine (5-Aza-CdR) (Kim et al., 2008b) to restore the transcription of the GSDME gene and reinstate the sensitivity of various cancer cells, including GC cells, to chemotherapy (Akino et al., 2007). In this study, using GC cell lines MGC-803 and HGC-27 and mouse xenograft GC models, we aim to seek the optimal antitumor effects of SIM-induced pyroptosis, in tandem with upregulating GSDME gene expression.

MATERIALS AND METHODS

Patient Samples

The surgical specimens of 20 paired GC tissues and adjacent non-cancerous tissues were collected from the Departments of Gastrointestinal Surgery, Affiliated Hospital of Guizhou Medical University. Use of the clinical samples were approved by the Affiliated Hospital of Guizhou Medical University Ethics Committee, approval number: 2020 (106). Written informed consent was acquired from all patients. The clinicopathological characteristics of the patients are shown in **Supplementary Table S1**.

Cell Culture and Reagents

The GC cell lines AGS, MKN45, and HGC-27 were obtained from the Chinese Academy of Sciences (Shanghai, China). The GC cell line MGC-803 was from the Institute of Nano Biomedicine and Engineering, Shanghai Engineering Research Centre (Shanghai, China). The cells were cultured in Dulbecco's modified Eagle's medium (HyClone, Logan, UT, United States) containing 10% foetal bovine serum (FBS, Gibco BRL, Gaithersburg, MD, United States), 100 U/ml penicillin, and 100 mg/ml streptomycin (Invitrogen, Carlsbad, CA, United States). All cells were incubated at 37°C in 5% CO_2. SIM (Cat. HY-17502) and 5-Aza-CdR (Cat. HY-0004) were purchased from MedChemExpress (Shanghai, China). Doxorubicin hydrochloride (DOX, Cat. ST039A) was from Beyotime Biotechnology (Shanghai, China). 3, 3′-Dioctadecyloxacarbocyanine perchlorate (DIO, Cat. 40725ES10) was from YEASEN (Shanghai, China). Caspase-3 inhibitors (Ac-DMPD-CMK [DMPD] and Ac-DMLD-CMK [DMLD]) were courtesy of Professor Li-Juan Cao (China Pharmaceutical University, Nanjing, China). DOX and 5-Aza-CdR were dissolved in phosphate-buffered saline (PBS, Servicebio, Cat. G0002-2L) and stored at −20°C. SIM, DIO, and the caspase-3 inhibitors were dissolved in dimethyl sulfoxide (DMSO, Sigma, Cat. D2650) and stored at −20°C.

Cell Treatment

Cells were seeded in 10 cm-diameter culture plates. Once the cells were 80% confluent, they were treated with certain concentration of SIM or with equal volumes of DMSO as control, for 48 h. For the inhibitor experiments, DMPD (5 μM) or DMLD (5 μM) was added to the cells 6 h before SIM treatment. For the SIM and 5-Aza-CdR combination experiments, MGC-803 and HGC-27 cells were incubated in medium containing 1 μM 5-Aza-CdR, refreshed daily for 72 h (Akino et al., 2007; Yanokura et al., 2020) before treatmen with 5 μM SIM (MGC-803 cells) or 20 μM SIM (HGC-27 cells) in the new medium for another 48 h.

Cell Viability Assay

Cell proliferation was measured by a Cell Counting Kit-8 (CCK8) Assay Kit following manufacturer's instructions (YEASEN, Cat. 40203ES60). The data is presented as the percent (%) of viable cells relative to the control.

Lactate Dehydrogenase Release Assay

Cellular toxicity was detected using an LDH Cytotoxicity Assay kit, following the manufacturer's instructions (Beyotime Biotechnology, Cat. C0017). Cellular membrane integrity was evaluated by the amount of LDH leaking from the damaged cell membrane and presented as fold changes to the control.

Transmission Electron Microscopy (TEM)

MGC-803 cells were treated with SIM (5 μM) and after 48 h incubation, they were harvested and fixed in 2.5% glutaraldehyde in PBS (pH 7.4) at 4°C, and post-fixed with 1.3% osmic tetroxide. Subsequently, the cells were dehydrated in graded alcohols, transferred to propylene oxide, and embedded in epoxy resin. Thereafter, ultrathin sections were stained with uranyl acetate followed by lead citrate. Finally, sections were transferred to copper grids and observed with an 80-kV transmission electron microscope (Wang et al., 2021).

Plasmids Lentivirus Transfection

All plasmids (Tet-on overexpression GSDME plasmid, the plasmids of GSDME-shRNA and caspase 3-shRNA knockdown and their control plasmids) were constructed by Public Protein/Plasmid Library. The procedure for lentivirus transfection has already been described previously (Zhou et al., 2019). For GSDME gene expression induction, 1 μg/ml of DOX was used in the medium for 4 days incubation (Croft et al., 2011). Stable low-expression or over-expression of GSDME in MGC-803 cells and HGC-27 cells were detected by real-time quantitative PCR (RT-qPCR) and Western blotting.

RNA Extraction and Real-Time quantitative PCR

Total RNA was extracted from the frozen tissue or cultured cells with TRIzol (Invitrogen, Cat. 15596018), following the manufacturer's instructions. Expression of the target genes was quantified with reverse transcription and RT-qPCR kits (Takara, Cat. DRR820A), normalized to the housekeeping gene β-actin. The relative gene expression levels were determined by the comparative threshold cycle ($2^{-\Delta\Delta CT}$) method. **Supplementary Table S1** shows the primers used in the RT-qPCR.

Western Blotting

Protein lysates were processed in RIPA-buffer (Beyotime, Cat. P0013C) supplemented with phosphatase inhibitor cocktail (Beyotime, Cat. P1050) and protease inhibitors (Beyotime, Cat. P1010). The protein was quantified by bicinchoninic acid (BCA) analysis (Beyotime, Cat. P0012). The protein extracts (30 μg/lane) were separated on SDS-PAGE gels, followed by electrotransferring onto polyvinylidene fluoride (PVDF) membranes. After blocking with 5% fat-free milk for 2 h at room temperature, the membranes were incubated with primary antibodies and subsequently incubated with secondary antibody. Information regarding the primary antibodies used is listed in **Supplementary Table S3**.

Colony Formation Assay

The cells (5000 cells/well) were seeded into 6-well plates. After overnight incubation, they were subjected to the indicated treatment and then cultured in a fresh medium for 2 weeks. Colonies were fixed in 4% paraformaldehyde and visualized with 0.1% crystalline violet.

Methylation Analyses

The association between GC and other common cancers with the degree of GSDME gene methylation was assessed using DiseaseMeth version 2.0 (http://biobigdata.hrbmu.edu.cn/diseasemeth/, accessed 30 August 2021). The database is used to provide information on abnormal DNA methylation in human diseases, especially cancer, in the most complete collection and annotations to date (Xiong et al., 2017).

Methylation-Specific PCR

The genomic DNA was extracted using a genomic DNA kit (Tiangen Biotech, Beijing, China) to determine the GSDME methylation status by MSP. Briefly, genomic DNA was bisulfite-treated using an EZ DNA Methylation-Gold Kit (Zymo Research, Cat. D5005). Bisulphite-treated DNA was amplified using primers specific for either methylated or unmethylated DNA, designed by Sangon Biotech (Shanghai, China). The methylated DNA-specific (M) and unmethylated DNA-specific (U) primer sequences for GSDME are shown in **Supplementary Table S5**.

Pyroptotic Cell Imaging

To observe the features of pyroptosis, the cells were plated in 24-well plates. The cytomembrane and the nucleus of cells post-treatment were stained with DIO (green fluorescence) and Hoechst 33342 (blue fluorescence), respectively. Fluorescence images were photographed using an inverted fluorescence microscope (Nikon Eclipse Ti, Tokyo, Japan).

In Vivo Experiments

All procedures involving animals were reviewed and approved by the Guizhou Medical University the Animal Care Welfare

Committee (approval number: 2001338). Five-week-old female immunodeficient BALB/c nude mice were purchased from the SLRC Laboratory Animal Center (Shanghai, China). MGC-803 cells w/wo Tet-on system for DOX-indicible GSDME were implanted subcutaneously in the right flanks of the mice to study the antitumor effects of SIM w/wo GSDME overexpression (mouse set 1) and w/wo the auxiliary therapy of 5-Aza-CdR (mouse set 2), respectively. When the tumours reached a volume of approximately 60 mm^3, the mice were randomly divided into four groups (n = 5 each). Groups in set 1 were DOX (-) vehicle control, DOX (+) GSDME overexpression, DOX (-) with SIM, and DOX (+) with SIM, as summarized in **Supplementary Figure S1A**. Groups in set 2 were vehicle control, 5-Aza-CdR, SIM and SIM+5-Aza-CdR group, as illustrated in **Supplementary Figure S1B**. Mice were weighed every 2–3 days. The tumour size was measured with digital callipers every 2 or 3 days. Tumour volume was calculated using the following equation: volume = ($width^2$ × length)/2. In each group, changes in the tumor sites were recorded every 7 days by the camera. The treatment lasted 18 days. At the end of the experiment, blood, tumours, livers, lungs, hearts, spleens, and kidneys of the mice were collected for subsequent experiments. Half of the tumour tissues and main organs were fixed in formalin and were paraffin-embedded for immunohistochemical (IHC) analysis, haematoxylin and eosin (H&E) staining and terminal deoxynucleotidyl transferase dUTP nick end labelling (TUNEL) assay (Roche, Cat. 1215679910). After TUNEL staining, the nucleus was counterstained with DAPI. The TUNEL-positive cells were photographed using an Ortho-Fluorescent Microscope (Nikon, Tokyo, Japan). The remaining tumour tissues were quickly frozen in liquid nitrogen and stored at −80°C for protein and nucleic acid detection. The blood was placed at room temperature for 2 h, centrifuged at 1,000 rpm for 20 min, and the separated serum was frozen at −80°C for subsequent experiments. The serum aspartate transaminase (AST), alanine transaminase (ALT), blood urea nitrogen (BUN), and creatinine (CRE) levels were analysed with an automated biochemical analyser, Chemray 240 (Lei Du Life Scientific and Technical Corporation, Shenzhen, China).

H&E Staining and Immunohistochemical

Xenograft tumour tissues and main organs of the mice as well as human GC tissues and paired adjacent non-cancerous tissues were dewaxed in xylene and rehydrated in a graded alcohol series. Tumour tissue and main organ morphology were observed using H&E staining. IHC was performed using antibodies against Ki67, GSDME, and cleaved (Cl)-caspase-3 using an immunohistochemical test kit (Boster, SA1020). Images were captured using a Nikon E100 upright microscope (Nikon, Tokyo, Japan). The source and dilution of the primary antibodies are listed in **Supplemenatry Table S2**. The mean analyses of integrated optical density (IOD) in IHC staining were calculated with Image-ProPlus6.0 (Media Cybernetics, Silver Spring, MD, United States). Protein expression levels were quantified by IOD in five random visual fields (×40) before calculating the average value. For animal experiments, from each group of mice, tissues of three mice were selected for statistical analysis.

Statistical Analysis

GraphPad Prism 7.04 (GraphPad, San Diego, CA, United States) was used for statistical analysis and graphics. The data are the mean ± SD of at least three independent experiments. Comparisons between two groups were analyzed by Student's t-test. Comparisons between multiple groups were made using one-way analysis of variance (ANOVA), and two-way ANOVA for comparisons between multiple groups with independent variables. A p-value < 0.05 was considered significant.

RESULTS

SIM Activates GSDME-Dependent Pyroptosis in GC Cells

Cell proliferation of the four different GC cell lines was inhibited to various degrees by treatment of SIM from 2.5 to 20 μM for 48 h (**Figure 1A**). Among them, MGC-803 cells were the most sensitive (IC_{50} = 4.623 μM), while HGC-27 cells were the most resistant (IC_{50} = 20.24 μM) to SIM (**Figure 1A**; **Table 1**). Consistently, membrane ballooning, a signature of pyroptosis, was revealed extensively in SIM-treated MGC-803 cells by microscopy, but sparse in HGC-27 cells (**Figure 1B**). The basal expression levels of GSDME protein and mRNA were low or undetectable in AGS and HGC-27 cells (**Figures 1C,D**), whereas the MGC-803 cells had the highest GSDME expression at both mRNA and protein levels. The different abundance of GSDME in the four cell lines displayed a positive correlation with cell sensitivity to SIM, which was not shown in GSDMD expression (**Figures 1C,E**). A dose-dependent increase in the LDH release rates in the culture medium of SIM-treated MGC-803 cells was detected (**Figure 1F**). SIM also induced the cleavage of caspase-3 (Cl-casp3) and GSDME (GSDME-N) in the MGC-803 cells in a dose-dependent manner, but not GSDMD (**Figure 1G**). Therefore, the involvement of GSDMD in SIM-induced pyroptosis is disproved. Treatment of SIM at 5 μM was chosen for all subsequent experiments in MGC-803 cells as the cells would retain half of the viability, plateaued LDH release and significant GSDME-N cleavage, representing an ideal induction of pyroptosis. Further observation of the morphological alterations by TEM showed that SIM-treated cells had typical pyroptosis features including membrane pore formation, membrane leakiness and organelle swelling, and low cytosol density (**Figure 1H**), confirming the microscopy results (**Figure 1B**). Collectively, these data indicate that SIM induces pyroptosis in GC cells by activating GSDME.

SIM-Induced Pyroptosis in GC cells Involves Caspase-3-Mediated Cleavage of GSDME

In MGC-803 cells with stable knock down of caspase-3 (CASP3) or GSDME by lentiviral shRNA (**Figures 2A–D**), SIM-induced

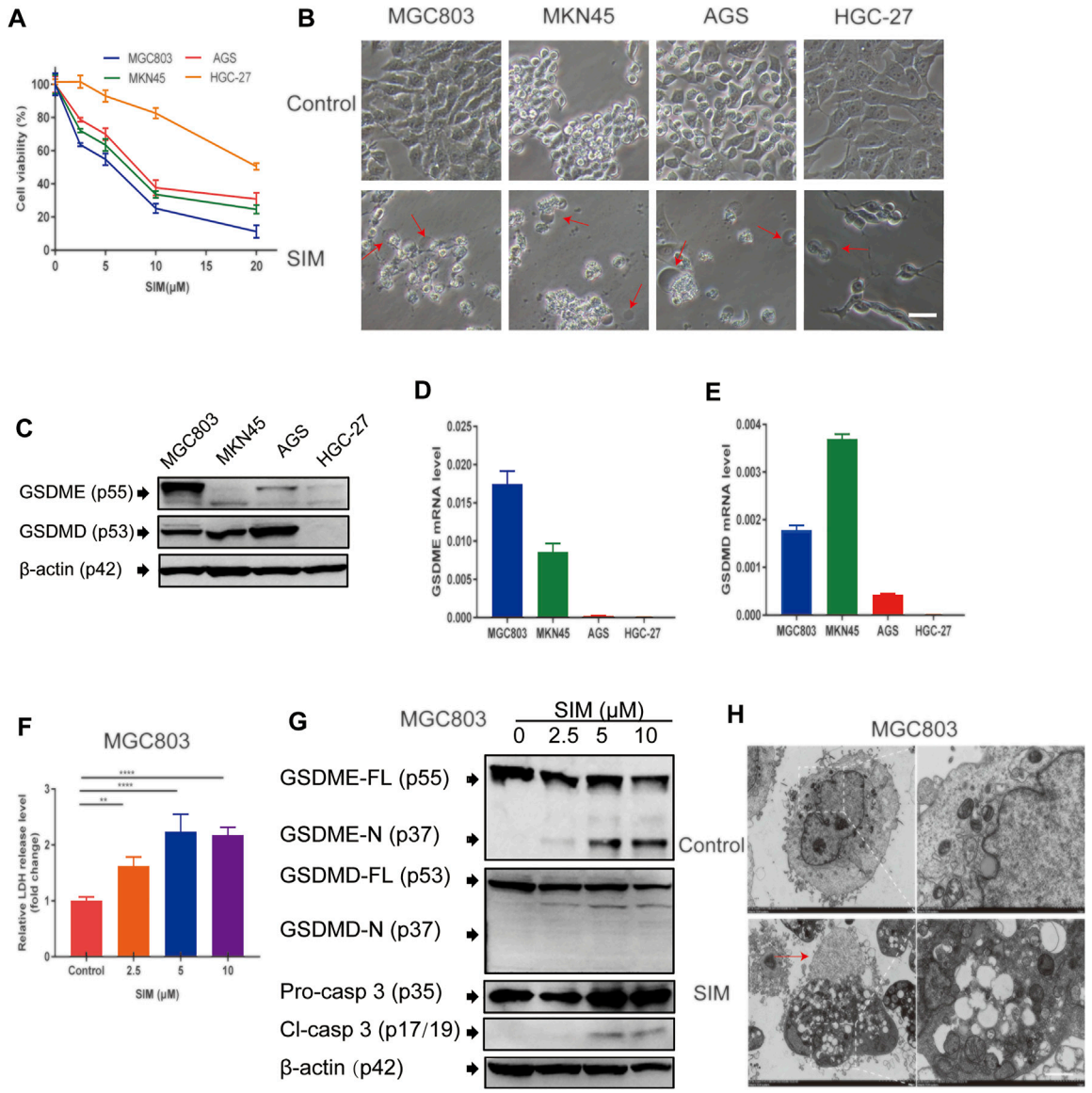

FIGURE 1 | SIM induces GSDME-dependent pyroptosis in GC cells**. (A)** Cell viability of four GC cell lines treated with different doses of SIM for 48 h, detected by CCK8 (n = 3). **(B)** Microscopic imaging of four GC cell lines treated with SIM. Red arrows indicate ballooned cell membrane, a characteristic of pyroptotic cells; scale bar = 50 μm. **(C)** Protein levels of GSDME and GSDMD in four GC cell lines, determined by Western blotting. **(D,E)** The mRNA expression of GSDME and GSDMD gene, detected by RT-qPCR. **(F)** Release of LDH into the culture supernatant, detected by LDH assay kit (n = 4). **(G)** Protein levels of full length (FL) or N-terminal of GSDME and GSDMD, pro-caspase 3 (pro-casp3) and cleaved caspase-3 (Cl-casp3) of SIM-treated MGC-803 cells. **(H)** Electron microscopic images of MGC-803 cells treated with 5 μM SIM for 48 h. Red arrows indicate ballooned cell membrane characteristic of pyroptotic cells; scale bar = 10 μm. Data are shown as mean ± SD or representatives of at least three independent experiments. β-actin was used as an internal control for Western blot. $^{**}p < 0.01$, and $^{****}p < 0.0001$.

TABLE 1 | IC_{50} values of SIM treatment on four GC cell lines.

Cell lines	IC_{50} (μM)	±SD
MGC-803	4.623	0.030
MKN45	6.630	0.026
AGS	8.376	0.033
HGC-27	20.240	0.016

SD, standard deviation.

proliferation inhibition (**Figure 2E**), LDH release (**Figure 2F**), cell swelling (**Figure 2G**), cleavage of GSDME-N and Cl-caspase 3 (**Figure 2H**) were all significantly blunted. Similar blocking effects were observed in the cells treated with caspase-3 inhibitor DMPD or DMLD, 6 h prior to SIM administration (**Figures 2I–K**). DMPD and DMLD bind directly to the catalytic domains of caspase-3 to specifically inhibit the activity of GSDME. The results indicated that caspase-3 and GSDME are necessary for SIM-induced pyroptosis.

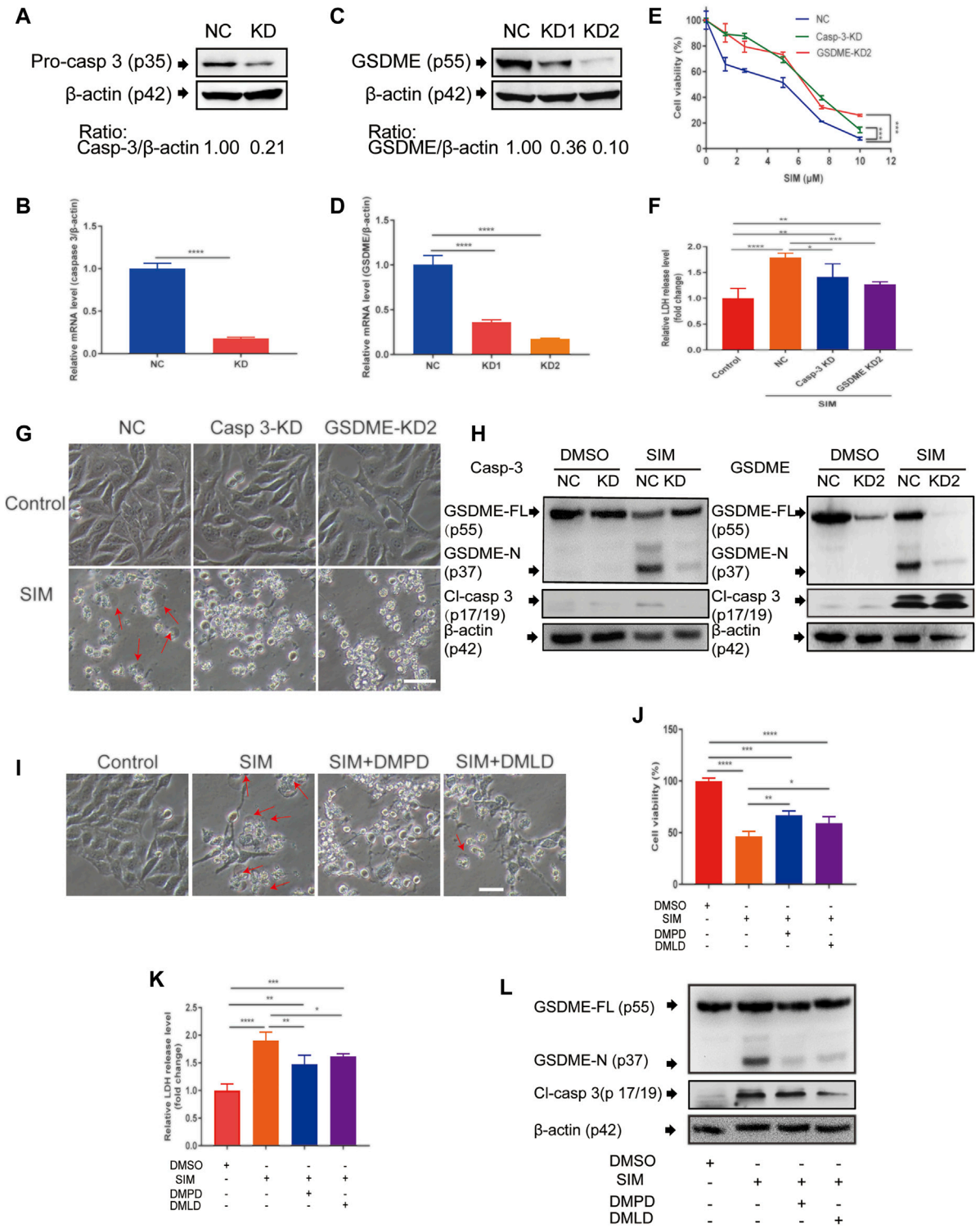

FIGURE 2 | Caspase-3 and GSDME are required in SIM-induced pyroptosis. **(A–D)** Validation of the shRNA knockdown of caspase 3 or GSDME in MGC-803 cells by Western blotting and RT-qPCR. After the treatment of SIM at concentrations ranging from 0 to 10 μM with caspase 3 or GSDME knockdown, scrambled NC as the control, **(E)** cell viability was detected by CCK8 ($n = 3$) and **(F)** release of LDH into the culture supernatant was detected by LDH assay kit ($n = 4$), **(G)** Microscopic imaging of the cells treated with 5 μM SIM for 48 h, w/wo caspase 3 or GSDME knockdown. Red arrows indicate ballooned cell membrane; scale bar = 50 μm ($n = 3$). **(H)** Representative immunoblotting analysis of GSDME and cl-casp3 of the cells treated with 5 μM SIM for 48 h, w/wo caspase 3 or GSDME knockdown. **(I–L)** Microscopic morphology, cell viability, LDH release and protein cleavage of GSDME and caspase-3 of MGC-803 cells treated with 5 μM SIM for 48 h, w/wo the caspase-3 inhibitor Ac-DMPD-CMK (DMPD) or Ac-DMLD-CMKR (DMLD). Data are shown as mean ± SD or representatives of at least three independent experiments. β-actin was used as an internal control for Western blot. $^{*}p < 0.05$, $^{**}p < 0.01$, $^{***}p < 0.001$ and $^{****}p < 0.0001$.

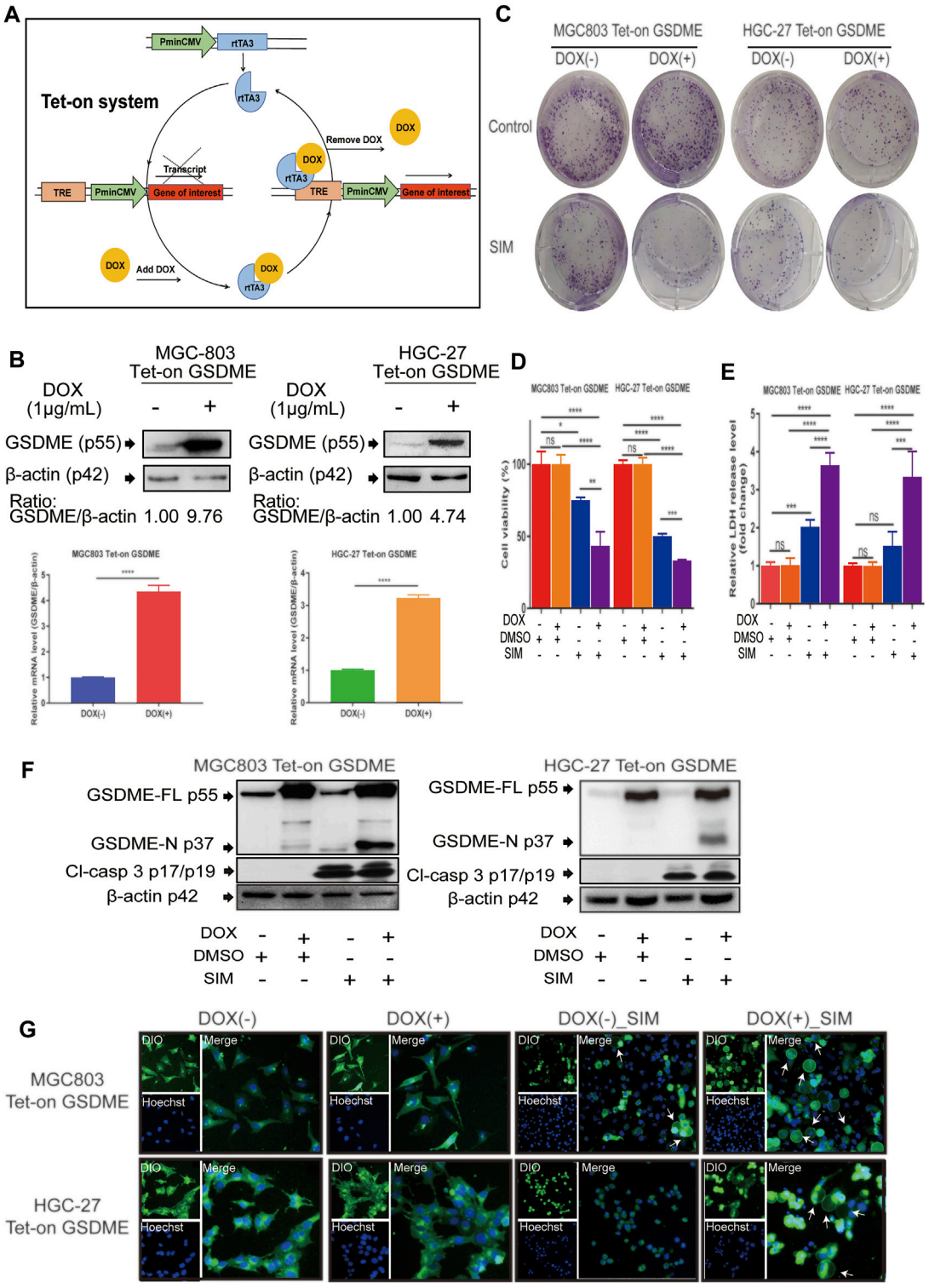

FIGURE 3 | Overexpression of GSDME enhanced SIM-induced cell pyroptosis. **(A)** Schematic representation of the DOX- controlled Tet-on system. **(B)** Validated of GSDME overexpression in MGC-803 or HGC-27 cells by Western blotting and RT-qPCR. Colony formation **(C)**, Cell viability **(D)**, LDH release **(E)** and protein cleavage of GSDME and caspase-3 **(F)** of GSDME-overexpressing MGC-803 and HGC-27 cells treated with SIM for 48 h. **(G)** Fluorescence microscopy imaging of GSDME-overexpressing MGC-803 and HGC-27 cells treated with SIM for 48 h, DIO (green fluorescence) was used to dye cell cytomembrane, and Hoechst 33342 (Blue fluorescence) the cell nucleus. White arrows indicate ballooned cell membrane; scale bar = 50 μm. Data are shown as mean ± SD or representatives of at least three independent experiments. β-actin was used as an internal control for Western blot. $^{*}p < 0.05$, $^{**}p < 0.01$, $^{***}p < 0.001$ and $^{****}p < 0.0001$.

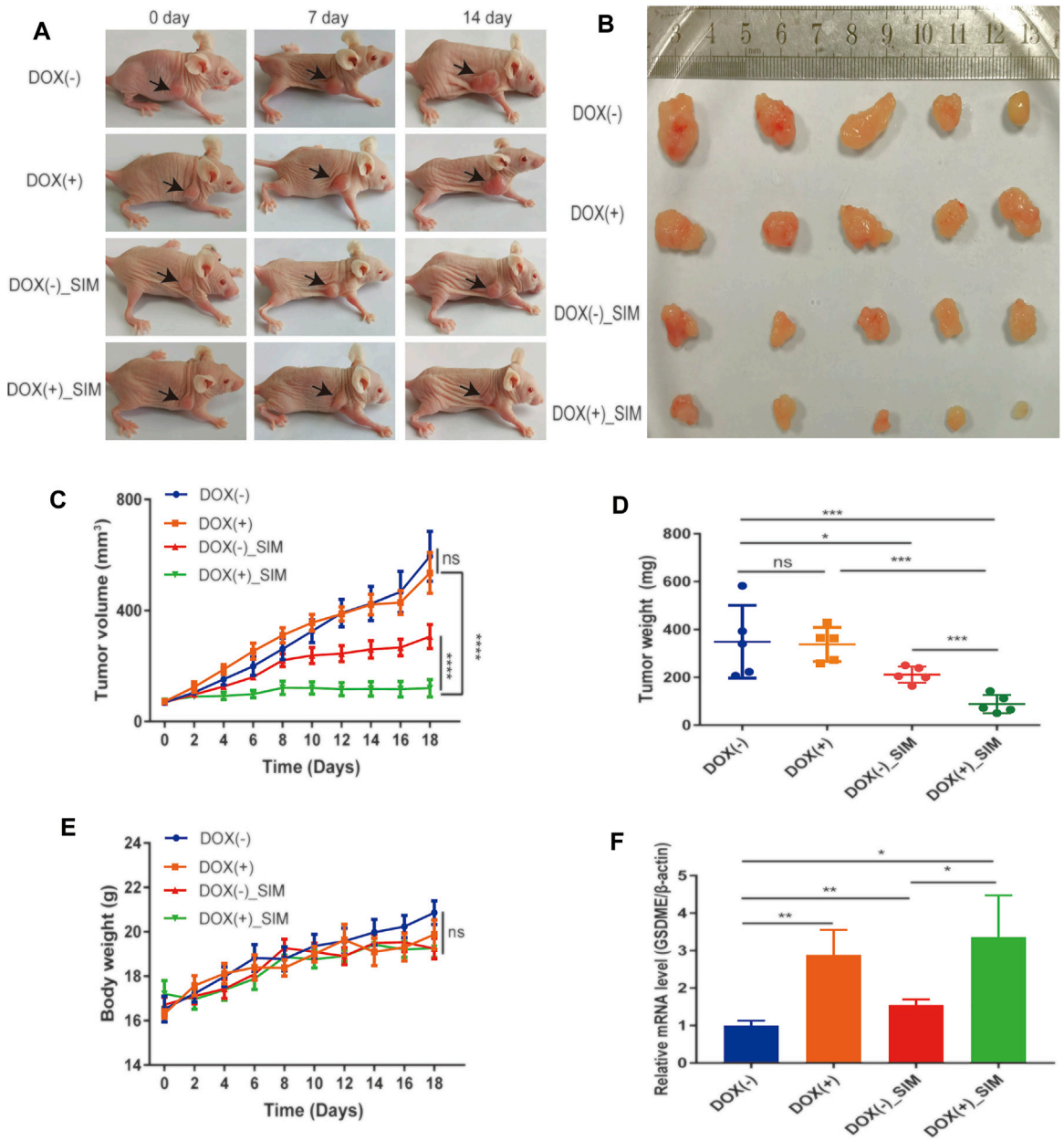

FIGURE 4 | SIM and GSDME overexpression additively inhibit tumour growth in mouse xenografts. **(A)** Photos of mice with xenograft tumours during the treatment. **(B)** Tumours dissected and imaged at the end point of experiment. **(C)** Tumour volumes during the treatment ($n = 5$). **(D)** Tumour weights at the end of the experiment ($n = 5$). **(E)** Average body weight of each group ($n = 5$) **(F)** The of GSDME gene expression in xenograft tumour tissues, detected by RT-qPCR ($n = 3$). $^{*}p < 0.05$, $^{**}p < 0.01$, $^{***}p < 0.001$, $^{****}p < 0.0001$ and $p > 0.05$ not significant (ns).

GSDME Overexpression Enhances SIM-Induced GC Cell Pyroptosis

To manipulate the gene expression of GSDME, we used the doxycycline (DOX)- inducible Tet-on system that allows reversibly switching on or off the GSDME gene by DOX (**Figure 3A**). The efficiency of the system was confirmed by successful induction of GSDME overexpression in MGC-803 and HGC-27 cells upon the addition of DOX to the culture medium (**Figure 3B**). While adding DOX alone had no impact on cell viability and colony formation, it synergistically enhanced the SIM-induced inhibition of proliferation and clonogenicity of these cells (**Figures 3C,D**). Moreover, LDH release (**Figure 3E**), GSDME cleavage (**Figure 3F**) and cell swelling (**Figure 3G**) were augmented with consistency, demonstrating an additive effect of GSDME overexpression on SIM-induced pyroptosis.

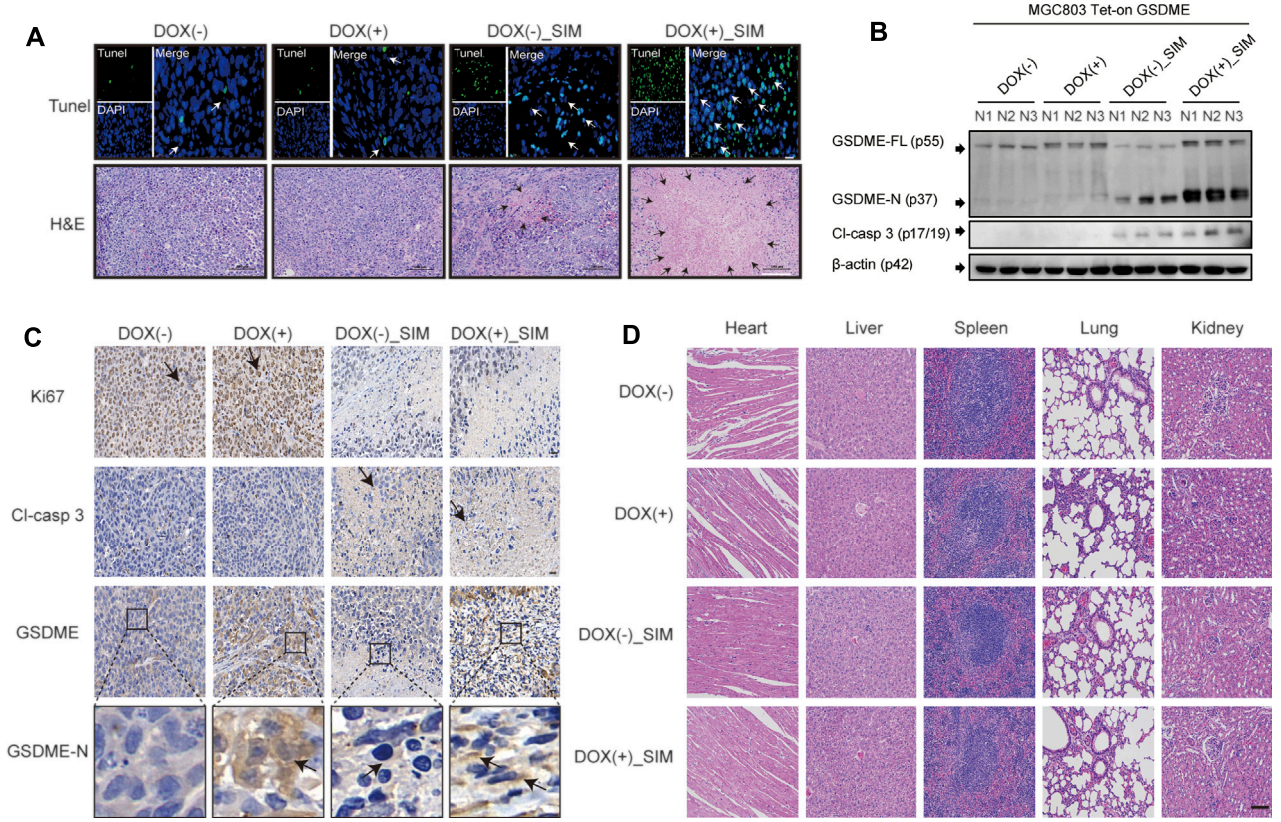

FIGURE 5 | SIM combined with overexpression-GSDME promotes the progression of GC pyroptosis *in vivo*. **(A)** TUNEL and H&E staining images for tumour slices after indicated treatment. White arrows indicate TUNEL positive cells. TUNEL scale bar: 20 μm; the areas of necrosis were indicated by black arrows in the figures. H&E scale bar: 100 μm. **(B)** Protein cleavage of GSDME and caspase-3 in tumour tissues, detected by Western blotting **(C)** Immunohistochemistry (IHC) images of Ki67, Cl-casp3, GSDME and GSDME-N for tumour tissues after indicated treatment; black arrows indicate the IHC staining-positive cells; scale bar: 20 μm. **(D)** HE staining of heart, liver, spleen, lung, and kidney tissues in each group; scale bar = 100 μm.

Combining SIM With GSDME Overexpression Potently Inhibits Tumour Growth *In Vivo*

To examine the *in vivo* GC tumorigenicity under influence of GSDME regulation, we established a xenograft model by injecting the DOX-inducible Tet-on MGC-803 cells into nude mice (**Supplementary Figure S1A**). During the 18-day treatment, the changes at tumour sites of each group were recorded every 7 days (**Figure 4A**). Both SIM group and DOX (+) _SIM group demonstrated significantly inhibited tumour growth (**Figure 4B**) and reduced tumour volume (**Figure 4C**) and tumour weight (**Figure 4D**), but no impact on body weight (**Figure 4E**). Compared to SIM alone, the extent of the inhibition was notably exaggerated when GSDME gene expression was promoted in the xenograft tissues by intake of DOX water by the mice (**Figures 4A–F**), whereas switching on the GSDME gene expression *per se* did not affect tumour development (**Figures 4C–E**). H&E and TUNEL staining indicated that GSDME overexpression combined with SIM induced more intensive DNA fragmentation and ultimately cell death in the tumour (**Figure 5A**), accompanied by decreased Ki67 expression, a cell proliferation marker (**Figure 5C**; **Supplementary Figure S2A**). The increased Cl-caspase-3 and GSDME-N abundance in the SIM group were evidently boosted by GSDME overexpression in DOX (+) SIM group, shown consistently by western blot (**Figure 5B**) and IHC (**Figure 5C**; **Supplementary Figures S2B,C**). Meanwhile, no damage was observed in the heart, spleen, lung, and kidney, compared between all groups (**Figure 5D**). The functionality of the liver and kidney remained intact, as suggested by the healthy serum levels of AST, ALT, BUN, and CRE in all groups ($p > 0.05$) (**Supplementary Table S5**). These *in vivo* data confirmed the previous finding that GSDME overexpression enhanced SIM-induced cell growth inhibition and pyroptosis by activating the caspase-3/GSDME pathway.

GSDME Demethylation Enhances SIM-Induced GC Cell Pyroptosis

The association between some common cancers and GSDME gene methylation was examined using DiseaseMeth version 2.0. Among all the malignancies examined, GC had the highest statistical significance of its positive association with GSDME

TABLE 2 | Association between disease and methylation of GSDME/DFNA5.

Disease name	Gene symbol	Mean methyl disease	Mean methyl normal	*p*-value	Methyl-type
Gastric cancer	GSDME/DFNA5	0.235	0.092	1.62E-12****	hyper-methyl
Breast neoplasms	GSDME/DFNA5	0.54	0.441	1.89E-05****	—
Esophageal cancer esophageal squamous cell carcinoma without metastasis	GSDME/DFNA5	0.392	0.308	3.22E-02*	—
Brain cancer ganglioneuroma	GSDME/DFNA5	0.03	0.022	1.98E-01	—
Lung cancer lung squamous cell carcinoma	GSDME/DFNA5	0.45	0.446	5.14E-01	—

*p < *0.05 and* ****p < *0.0001.*

hypermethylation (p = 1.62E-12, **Table 2**). The heatmap of methylation showed that GC tissues had a significantly higher degree of GSDME methylation than the normal tissues (**Figure 6A**). In the GC tissues, GSDME protein and mRNA levels were downregulated compared with the adjacent normal tissues, as determined by IHC and RT-qPCR (**Figures 6B,C**; **Supplementary Figure S2D**). However, no significant correlation was found between the clinicopathological parameters and GSDME expression levels in GC tissue of 20 patients with GC (**Supplementary Table S1**). MSP revealed partial methylation of GSDME at the promoter region in HGC-27 cells and to a lesser extent in MGC-803 cells (**Figure 6D**), which matched the superior resilience of HGC-27 cells to pyroptosis (**Figure 1**). Treatment of 5-Aza-CdR on MGC-803 and HGC-27 cells demethylated the GSDME gene (**Figure 6D**) and restored its mRNA transcription (**Figure 6E**). Cells pre-treated with 1 μM 5-Aza-CdR for 72 h were more responsive to SIM treatment than SIM alone, demonstrated by cell viability (**Figure 6F**), LDH release (**Figure 6G**), GSDME/caspase-3 cleavage (**Figure 6H**) and cell swelling (**Figure 6I**). These results implied that GSDME demethylation facilitated SIM-induced GC cell proliferation inhibition and pyroptosis.

5-Aza-CdR Amplifies the Antitumor Effects of SIM in a Xenograft Model

Mice bearing GC xenograft was generated by subcutaneous transplantation of MGC-803 cells into nude mice (**Supplementary Figure 1B**). Compared to the vehicle group, both the SIM and SIM+5-Aza-CdR combination group had significantly inhibited tumour growth (**Figures 7A,B**) and reduced tumour volume (**Figure 7C**) and tumour weight (**Figure 7D**). The delay in tumour growth was considerably more pronounced in the combination group compared with the SIM group (**Figures 7A–D**), which mirrored what we observed in the Tet-on GSDME overexpression mouse model. However, rather than continuous and undistinguishable bodyweight gain in all groups, as seen in the previous xenograft experiment, the bodyweight of the mice in the SIM+5-Aza-CdR combination group decreased during treatment and started to catch up at day 15 (**Figure 7E**). Compared with the vehicle, 5-Aza-CdR monotherapy promoted GSDME expression (**Figure 7F**) but did not affect tumour growth (**Figures 7C,D**). Furthermore, compared with the SIM group, the combination group induced more significant caspase-3-dependent cleavage of GSDME (**Figure 7F**). As expected, TUNEL and H&E staining showed more remarkable DNA breakdown and diminished Ki67 staining in tumour tissues, reflecting an increased vulnerability of cancer cells to pyroptosis triggered by the combined therapy (**Figure 8A**) than the SIM monotherapy. In addition to that, there was no detectable damage found in the heart, liver, spleen, lung, and kidney by H&E staining (**Figure 8B**), and the serum concentrations of AST, ALT, BUN, and CRE remained in the normal range throughout all groups (**Supplementary Table S6**). In summary, GSDME demethylation enhanced SIM-induced GC cell proliferation inhibition and pyroptosis by regulating the caspase-3/GSDME pathway, without damage to the main organs.

DISCUSSION

Beyond cardiovascular protection *via* interrupting the biosynthesis of cholesterol, statins merit great attention for their antineoplastic activity (Jiang et al., 2021a), evidenced in multiple clinical observations and experimental investigations. A recent South Korean prospective study pointed out that the use of statins could reduce GC mortality in the general population (Cho et al., 2021). In particular, pleiotropic mechanisms have been proposed to underlie the action of SIM against cancers (Chiu et al., 2011), such as inhibiting tumour cell proliferation, migration and invasion, and promoting apoptosis by simultaneously targeting YAP and β-catenin signalling (Liu et al., 2020). Adding to the extant knowledge, we found that SIM treatment for GC induces pyroptosis by activating caspase-3 to cleave GSDME.

Both GSDMD and GSDME could perforate cell membrane to initiate the pyroptosis process (Yu and He, 2017; Shi et al., 2015). GSDMD is abundantly present in GC cell lines except HGC-27. However, we found that the IC50 value of SIM on CG cells was negatively correlated with the baseline expression level of GSDME, not GSDMD (**Figure 1**; **Table 1**). The signs of pyroptosis including plasma membrane swelling and LDH release in SIM-treated MGC-803 cells were accompanied by the generation of GSDME-N, not GSDMD-N (**Figure 1**). Blocking the caspase-3/GSDME pathway by shRNA knockdown or inhibitors attenuated the SIM-induced pyroptosis, while conversely overexpressing GSDME encouraged GC cells to shift into pyroptotic death.

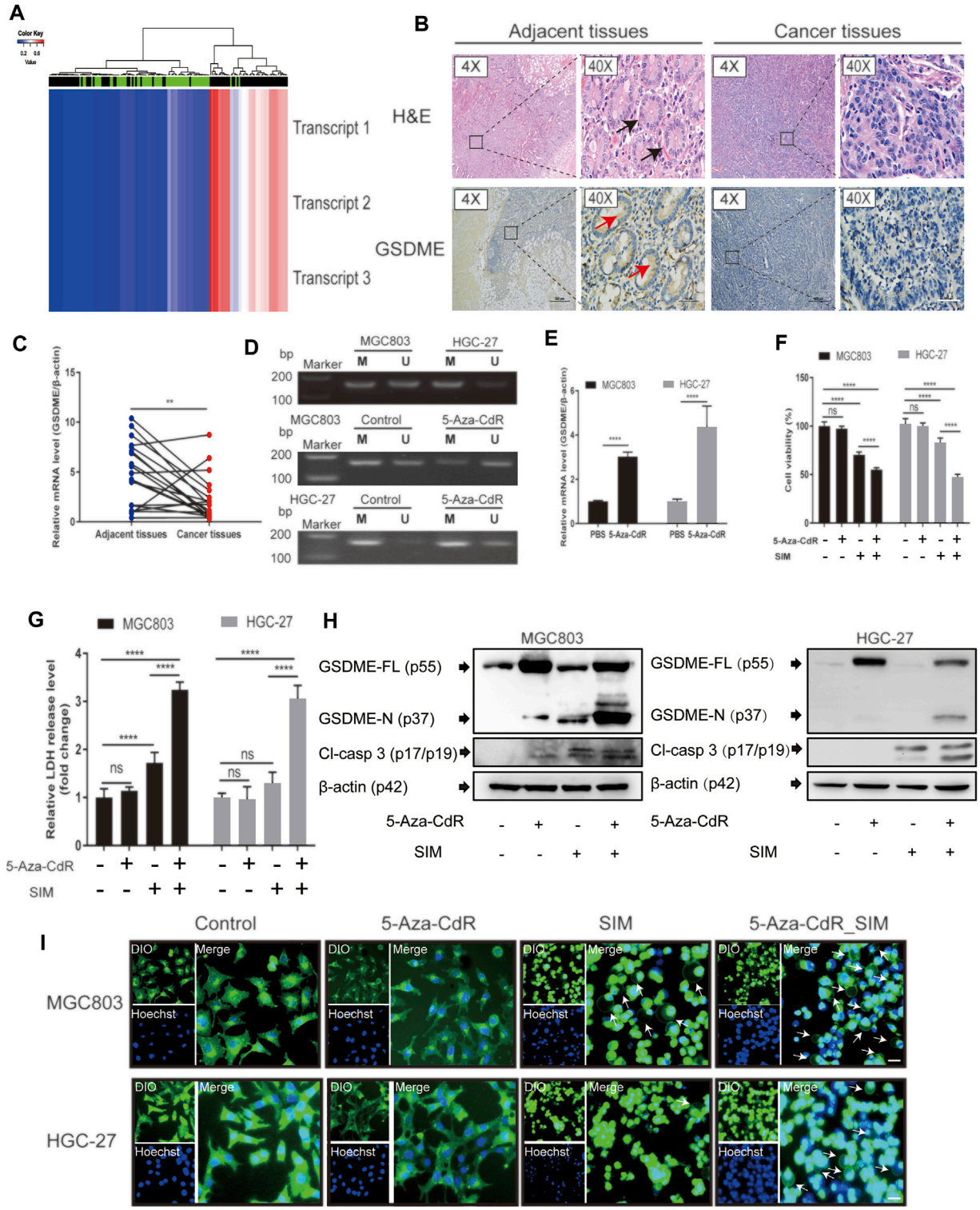

FIGURE 6 | Combination of SIM and 5-Aza-CdR enhances pyroptosis in GC. **(A)** The heatmap of GSDME methylation in GC. The heatmap contains methylation data of 3 transcripts from 141 samples of 27 k arrays. Rows represent transcripts and columns represent samples (green: normal profiles, black: disease profiles). **(B)** GSDME protein levels in human GC tissues and adjacent tissues, detected immunohistochemically using HE staining; black arrows indicate complete gastric gland; red arrows indicate the IHC staining-positive cells; scale bar = 50 μm. **(C)** Relative GSDME mRNA expression in human GC tissues and adjacent normal tissues, determined by RT-qPCR ($n = 20$). **(D)** MSP profiles of GSDME promoter methylation status in MGC-803 and HGC-27 cell before and after a daily dosing of 5-Aza-CdR for 72 h, M, methylated; U, unmethylated. After SIM treatment w/wo 5-Aza-CdR pre-dosing, **(E)** GSDME gene, **(F)** Cell viability, **(G)** LDH release, **(H)** protein cleavage of GSDME and caspase-3, and **(I)** fluorescence microscopy of theMGC-803 and HGC-27 cells examined. Data are shown as mean ± SD or representatives of at least three independent experiments. β-actin was used as an internal control for Western blot. $^{****}p < 0.0001$ and $p > 0.05$; ns, not significant.

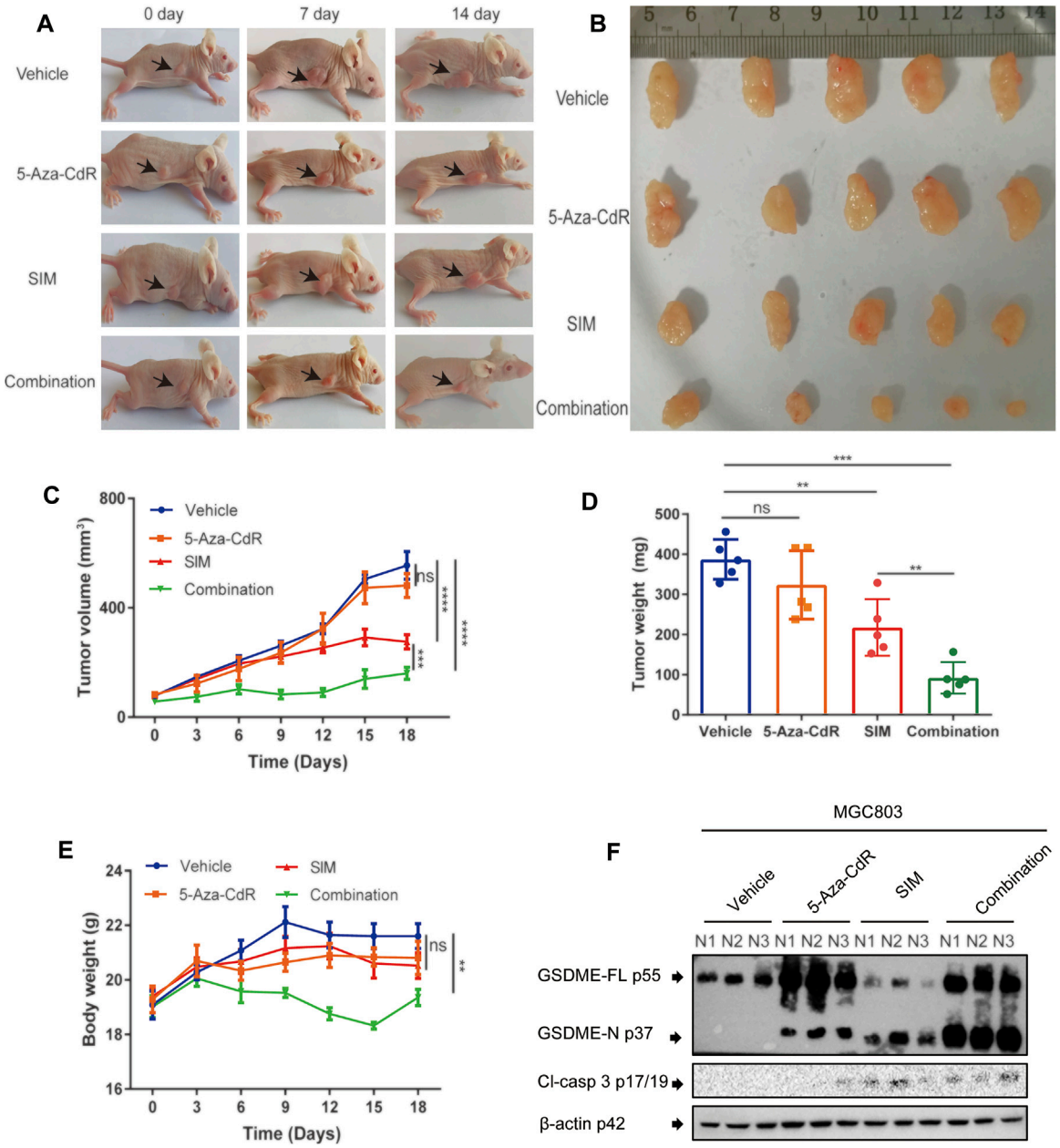

FIGURE 7 | Combination of SIM and 5-Aza-CdR potently inhibits tumour growth *in vivo*. **(A)** Photos of mice with xenograft tumours during the treatment. **(B)** Tumours dissected at the end point of the experiment. **(C)** Tumour volumes during the treatment ($n = 5$). **(D)** Tumour weights at the end of the experiment ($n = 5$). **(E)** Average body weight of each group during the treatment ($n = 5$). **(F)** Protein cleavage of GSDME and caspase-3 in tumour tissues, detected by Western blotting ($n = 3$). Data are shown as mean ± SD or representatives of at least three independent experiments. β-actin was used as an internal control for Western blot. $^{****}p < 0.0001$ and $p > 0.05$ not significant (ns).

These data demonstrate that GSDME, not GSDMD, is responsible for the pyroptosis in GC cells induced by SIM, corroborating the previous reports that GSDMD-dependent pyroptosis occurs mainly in non-cancerous cells (Ding et al., 2021; Han et al., 2021; Shi et al., 2021) and GSDME-dependent pyroptosis in cancer cells (Cai et al., 2021; Li et al., 2021; Shangguan et al., 2021).

Targeting pyroptosis is considered a novel enrichment to our cancer-fighting arsenal (Guo et al., 2021; Yuan et al., 2021) and GSDME is the newly recognized executor of pyroptosis (Xia et al., 2020). It has been reported that dihydroartemisinin (DHA), a conventional drug to kill malaria parasites, can induce pyroptosis of esophageal squamous cell carcinoma (ESCC) cells *via* PKM2 caspase-8/3-GSDME pathway, providing a potential therapeutic

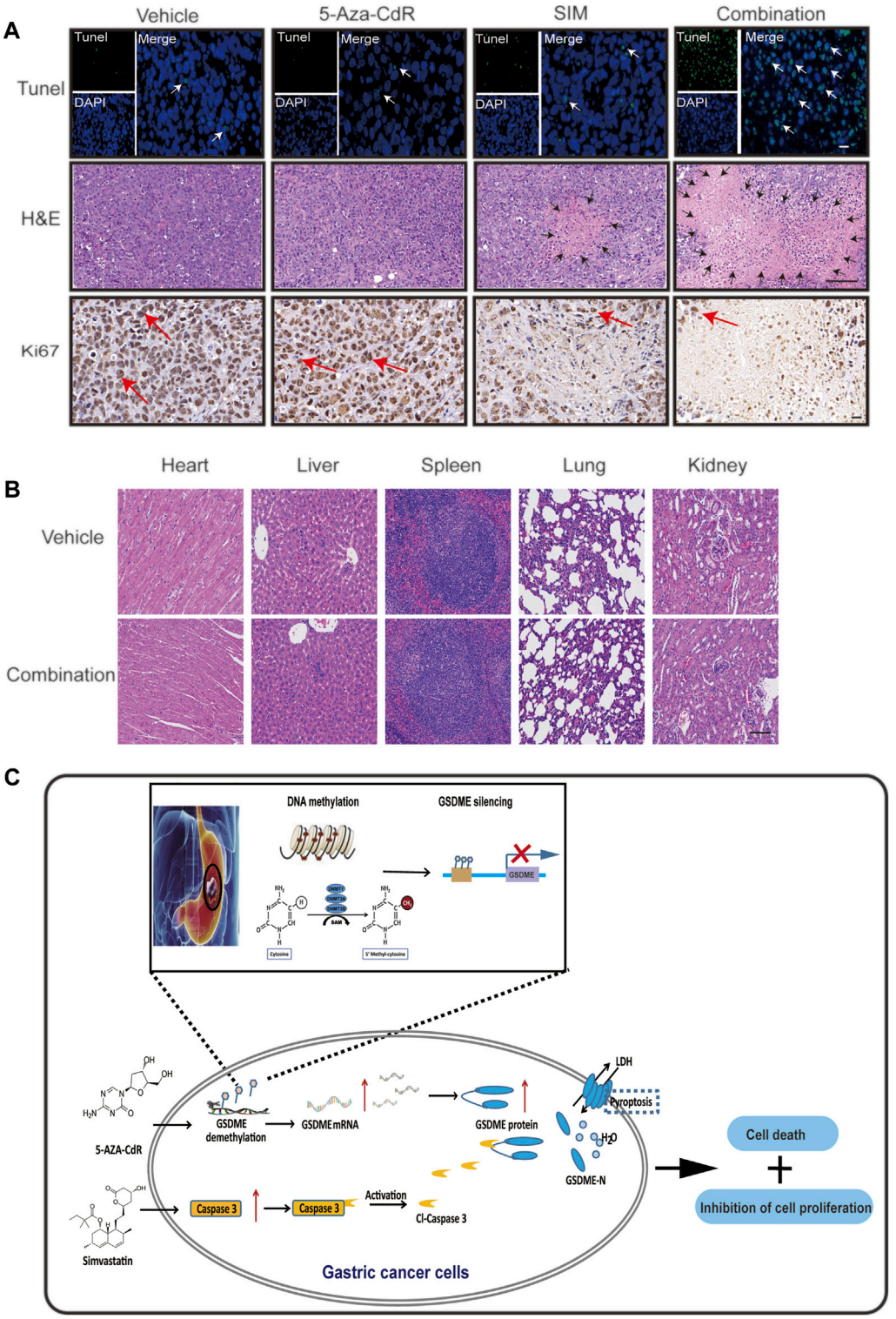

FIGURE 8 | 5-Aza-CdR promotes SIM-induced GC pyroptosis *via* caspase 3/GSDME pathway *in vivo*. **(A)** TUNEL, H&E staining and Ki67 IHC of xenograft tumour slices after indicated treatment. TUNEL scale bar: 20 μm. White arrows: TUNEL positive cells; H&E scale bar: 100 μm. Black arrows: the areas of necrosis; IHC scale bar: 20 μm. Red arrows: Ki67-positive cells. **(B)** HE staining of heart, liver, spleen, lung, and kidney tissues in each group; scale bar: 100 μm. **(C)** Schematic diagram to illustrate the mechanisms underlying the induction of pyroptosis in GC by a combined treatment of SIM with 5-Aza-CdR *via* caspase-3/GSDME activation.

agent for the treatment of ESCC (Jiang et al., 2021b). GSDME-dependent pyroptosis can also be triggered by chemotherapy (paclitaxel, cisplatin, lobaplatin, 5-fluorouracil (5-FU) and doxorubicin) or by targeted molecular drugs in malignant cells (Lu et al., 2018; Xia et al., 2020). As the GSDME gene is often silenced through hypermethylation in GC, either genetic tools or demethylating agents such as 5-Aza-CdR could restore the GSDME expression to facilitate a more efficient SIM therapy, as shown in our xenograft mice. As a potent methyltransferase inhibitor, 5-Aza-CdR is an FDA-approved epigenetic therapy to treat a wide array of cancers by reactivating multiple tumour suppressor genes (Christman, 2002). In our xenograft GC mice, combining SIM with GSDME overexpression demonstrated a tumour-specific targeting, and none of the main organs examined displayed observable damage. Nevertheless, effects of drug discontinuation and long-term administration, and potential adverse effects with a prolonged treatment duration, remain to be clarified by further investigation. Other vital tissues such as muscle and adipose would be included in future research too. In mice treated with both 5-Aza-CdR and SIM, we have seen a weight loss up to 37% to the initial value, which was rebounded promptly after treatment cessation. This side effect may be circumvented by an appropriate extension of the interval of the treatment cycle.

It must be stressed that SIM, the same as other statin medications, can exhibit anti-tumour effects from various aspects, such as metabolic reprogramming (Ni et al., 2021), immune regulation (Yu et al., 2022), and angiogenesis (Wesołowska et al., 2021), etc. that may not necessarily involve GSDME. Although the declined cell viability upon SIM treatment was attenuated significantly with disruption of caspase-3 or GSDME expression or function, the cytotoxicity of SIM was still profound, suggesting contributions of other mechanisms. How these different pathways crosstalk to each other is a burning question awaiting an answer.

In conclusion, SIM exerts an antitumor effect on GC *via* impaired cell proliferation and caspase-3/GSDME-mediated pyroptosis. Restorring GSDME expression by 5-Aza-CdR could be beneficial by sensitising GC cells to SIM.

LIMITATIONS OF THE STUDY

We noticed that SIM increased the transcription of the GSDME gene in MGC-803 cells and in the xenograft (**Figure 4F**; **Supplementary Figure S3**), and had to leave it unaddressed in the present work. Interestingly, statin has been hinted at as a DNA methyltransferase (DNMT) inhibitor. By suppressing DNMT, statins such as lovastatin and simvastatin could upregulate a couple of genes that were silenced by promoter hypermethylation, including BMP2, in colorectal cancer cells and xenograft mice. The outcome of this modulation by statin was a reversal of the malignant cells from the stem-like state into a more differentiated state (Kodach et al., 2011). We may speculate a similar epigenetic mechanism operating in our models.

DATA AVAILABILITY STATEMENT

The original contributions presented in the study are included in the article/**Supplementary Material**, further inquiries can be directed to the corresponding authors.

ETHICS STATEMENT

The studies involving human participants were reviewed and approved by the Affiliated Hospital of Guizhou Medical University Ethics Committee. The patients/participants provided their written informed consent to participate in this study. The animal study was reviewed and approved by the Guizhou Medical University Ethics Committee.

AUTHOR CONTRIBUTIONS

YX and YJ performed the experiment, and was a major contributor in writing the manuscript. YX and XW analyzed and collected the patient data. DXC and CFS supervised the research of animal and provided facilities. HH and WLJ initiated the study. HH, WLJ and CFS revised the manuscript. All authors read and approved the final manuscript.

FUNDING

This study was supported by the research grants from the National Natural Science Foundation of China to HH (Grant No. 81760429 and 82060442), as well as the Research Funds for Guizhou Provincial Innovative Talents Team for 2019 (Grant No. 5610), the Science and Technology Project of Health and Family Planning Commission of Guizhou Province to YX (Grant No. gzwjkj 2018-1-072), the Science and Technology Project of Guizhou University of Traditional Chinese Medicine to YX [Grant No. (2018)101] and the Science and Technology Project of Guiyang City to YX [Grant No. (2019) 9-2].

ACKNOWLEDGMENTS

We thank Professor Li-Juan Cao for the gift of the caspase 3 inhibitors (Ac-DMPD-CMK and Ac-DMLD-CMK). The technical helps from Chang Yang, Hong Du, Wutong Zhou, and Shuqiang Chen are appreciated.

SUPPLEMENTARY MATERIAL

The Supplementary Material for this article can be found online at: https://www.frontiersin.org/articles/10.3389/fphar.2022.860546/full#supplementary-material

REFERENCES

Akino, K., Toyota, M., Suzuki, H., Imai, T., Maruyama, R., Kusano, M., et al. (2007). Identification of DFNA5 as a Target of Epigenetic Inactivation in Gastric Cancer. *Cancer Sci.* 98 (1), 88–95. doi:10.1111/j.1349-7006.2006.00351.x

Alhakamy, N. A., Fahmy, U. A., Ahmed, O. A. A., Caruso, G., Caraci, F., Asfour, H. Z., et al. (2020). Chitosan Coated Microparticles Enhance Simvastatin Colon Targeting and Pro-apoptotic Activity. *Mar. Drugs* 18 (4). doi:10.3390/md18040226

Cai, J., Yi, M., Tan, Y., Li, X., Li, G., Zeng, Z., et al. (2021). Natural Product Triptolide Induces GSDME-Mediated Pyroptosis in Head and Neck Cancer through Suppressing Mitochondrial Hexokinase-Ιι. *J. Exp. Clin. Cancer Res.* 40 (1), 190. doi:10.1186/s13046-021-01995-7

Chiu, H. F., Ho, S. C., Chang, C. C., Wu, T. N., and Yang, C. Y. (2011). Statins Are Associated with a Reduced Risk of Gastric Cancer: a Population-Based Case-Control Study. *Am. J. Gastroenterol.* 106 (12), 2098–2103. doi:10.1038/ajg.2011.277

Cho, M. H., Yoo, T. G., Jeong, S. M., and Shin, D. W. (2021). Association of Aspirin, Metformin, and Statin Use with Gastric Cancer Incidence and Mortality: A Nationwide Cohort Study. *Cancer Prev. Res. (Phila)* 14 (1), 95–104. doi:10.1158/1940-6207.CAPR-20-0123

Christman, J. K. (2002). 5-Azacytidine and 5-Aza-2'-Deoxycytidine as Inhibitors of DNA Methylation: Mechanistic Studies and Their Implications for Cancer Therapy. *Oncogene* 21 (35), 5483–5495. doi:10.1038/sj.onc.1205699

Croft, D. R., Crighton, D., Samuel, M. S., Lourenco, F. C., Munro, J., Wood, J., et al. (2011). p53-mediated Transcriptional Regulation and Activation of the Actin Cytoskeleton Regulatory RhoC to LIMK2 Signaling Pathway Promotes Cell Survival. *Cell Res* 21 (4), 666–682. doi:10.1038/cr.2010.154

Deng, J. L., Zhang, R., Zeng, Y., Zhu, Y. S., and Wang, G. (2019). Statins Induce Cell Apoptosis through a Modulation of AKT/FOXO1 Pathway in Prostate Cancer Cells. *Cancer Manag. Res.* 11, 7231–7242. doi:10.2147/CMAR.S212643

Ding, X., Kambara, H., Guo, R., Kanneganti, A., Acosta-Zaldívar, M., Li, J., et al. (2021). Inflammasome-mediated GSDMD Activation Facilitates Escape of Candida Albicans from Macrophages. *Nat. Commun.* 12 (1), 6699. doi:10.1038/s41467-021-27034-9

Fan, J. X., Deng, R. H., Wang, H., Liu, X. H., Wang, X. N., Qin, R., et al. (2019). Epigenetics-Based Tumor Cells Pyroptosis for Enhancing the Immunological Effect of Chemotherapeutic Nanocarriers. *Nano Lett.* 19 (11), 8049–8058. doi:10.1021/acs.nanolett.9b03245

Guo, J., Zheng, J., Mu, M., Chen, Z., Xu, Z., Zhao, C., et al. (2021). GW4064 Enhances the Chemosensitivity of Colorectal Cancer to Oxaliplatin by Inducing Pyroptosis. *Biochem. Biophys. Res. Commun.* 548, 60–66. doi:10.1016/j.bbrc.2021.02.043

Han, J., Zuo, Z., Shi, X., Zhang, Y., Peng, Z., Xing, Y., et al. (2021). Hirudin Ameliorates Diabetic Nephropathy by Inhibiting Gsdmd-Mediated Pyroptosis. *Cell Biol Toxicol*. doi:10.1007/s10565-021-09622-z

Hou, J., Hsu, J. M., and Hung, M. C. (2021). Molecular Mechanisms and Functions of Pyroptosis in Inflammation and Antitumor Immunity. *Mol. Cel* 81 (22), 4579–4590. doi:10.1016/j.molcel.2021.09.003

Huang, J., Fan, P., Liu, M., Weng, C., Fan, G., Zhang, T., et al. (2021). Famotidine Promotes Inflammation by Triggering Cell Pyroptosis in Gastric Cancer Cells. *BMC Pharmacol. Toxicol.* 22 (1), 62. doi:10.1186/s40360-021-00533-7

Jiang, M., Wu, Y., Qi, L., Li, L., Song, D., Gan, J., et al. (2021). Dihydroartemisinin Mediating PKM2-Caspase-8/3-GSDME axis for Pyroptosis in Esophageal Squamous Cell Carcinoma. *Chemico-Biological Interactions* 350, 109704. doi:10.1016/j.cbi.2021.109704

Jiang, W., Hu, J.-W., He, X.-R., Jin, W.-L., and He, X.-Y. (2021). Statins: a Repurposed Drug to Fight Cancer. *J. Exp. Clin. Cancer Res.* 40 (1), 241. doi:10.1186/s13046-021-02041-2

Jorgensen, I., and Miao, E. A. (2015). Pyroptotic Cell Death Defends against Intracellular Pathogens. *Immunol. Rev.* 265 (1), 130–142. doi:10.1111/imr.12287

Kim, M. S., Chang, X., Yamashita, K., Nagpal, J. K., Baek, J. H., Wu, G., et al. (2008). Aberrant Promoter Methylation and Tumor Suppressive Activity of the DFNA5 Gene in Colorectal Carcinoma. *Oncogene* 27 (25), 3624–3634. doi:10.1038/sj.onc.1211021

Kim, M. S., Lebron, C., Nagpal, J. K., Chae, Y. K., Chang, X., Huang, Y., et al. (2008). Methylation of the DFNA5 Increases Risk of Lymph Node Metastasis in Human Breast Cancer. *Biochem. Biophys. Res. Commun.* 370 (1), 38–43. doi:10.1016/j.bbrc.2008.03.026

Kodach, L. L., Jacobs, R. J., Voorneveld, P. W., Wildenberg, M. E., Verspaget, H. W., van Wezel, T., et al. (2011). Statins Augment the Chemosensitivity of Colorectal Cancer Cells Inducing Epigenetic Reprogramming and Reducing Colorectal Cancer Cell 'stemness' via the Bone Morphogenetic Protein Pathway. *Gut* 60 (11), 1544–1553. doi:10.1136/gut.2011.237495

Li, L., Song, D., Qi, L., Jiang, M., Wu, Y., Gan, J., et al. (2021). Photodynamic Therapy Induces Human Esophageal Carcinoma Cell Pyroptosis by Targeting the PKM2/caspase-8/caspase-3/GSDME axis. *Cancer Lett.* 520, 143–159. doi:10.1016/j.canlet.2021.07.014

Liu, Q., Xia, H., Zhou, S., Tang, Q., Zhou, J., Ren, M., et al. (2020). Simvastatin Inhibits the Malignant Behaviors of Gastric Cancer Cells by Simultaneously Suppressing YAP and β-Catenin Signaling. *Onco Targets Ther.* 13, 2057–2066. doi:10.2147/OTT.S237693

Lu, H., Zhang, S., Wu, J., Chen, M., Cai, M. C., Fu, Y., et al. (2018). Molecular Targeted Therapies Elicit Concurrent Apoptotic and GSDME-dependent Pyroptotic Tumor Cell Death. *Clin. Cancer Res.* 24 (23), 6066–6077. doi:10.1158/1078-0432.CCR-18-1478

Mattiuzzi, C., and Lippi, G. (2020). Cancer Statistics: a Comparison between World Health Organization (WHO) and Global Burden of Disease (GBD). *Eur. J. Public Health* 30 (5), 1026–1027. doi:10.1093/eurpub/ckz216

Ni, W., Mo, H., Liu, Y., Xu, Y., Qin, C., Zhou, Y., et al. (2021). Targeting Cholesterol Biosynthesis Promotes Anti-tumor Immunity by Inhibiting Long Noncoding RNA SNHG29-Mediated YAP Activation. *Mol. Ther.* 29 (10), 2995–3010. doi:10.1016/j.ymthe.2021.05.012

Op de Beeck, K., Van Camp, G., Thys, S., Cools, N., Callebaut, I., Vrijens, K., et al. (2011). The DFNA5 Gene, Responsible for Hearing Loss and Involved in Cancer, Encodes a Novel Apoptosis-Inducing Protein. *Eur. J. Hum. Genet.* 19 (9), 965–973. doi:10.1038/ejhg.2011.63

Peng, Z., Wang, P., Song, W., Yao, Q., Li, Y., Liu, L., et al. (2020). GSDME Enhances Cisplatin Sensitivity to Regress Non-small Cell Lung Carcinoma by Mediating Pyroptosis to Trigger Antitumor Immunocyte Infiltration. *Signal. Transduct Target. Ther.* 5 (1), 159. doi:10.1038/s41392-020-00274-9

Pushpakom, S., Iorio, F., Eyers, P. A., Escott, K. J., Hopper, S., Wells, A., et al. (2019). Drug Repurposing: Progress, Challenges and Recommendations. *Nat. Rev. Drug Discov.* 18 (1), 41–58. doi:10.1038/nrd.2018.168

Rogers, C., Fernandes-Alnemri, T., Mayes, L., Alnemri, D., Cingolani, G., and Alnemri, E. S. (2017). Cleavage of DFNA5 by Caspase-3 during Apoptosis Mediates Progression to Secondary Necrotic/pyroptotic Cell Death. *Nat. Commun.* 8, 14128. doi:10.1038/ncomms14128

Shangguan, F., Zhou, H., Ma, N., Wu, S., Huang, H., Jin, G., et al. (2021). A Novel Mechanism of Cannabidiol in Suppressing Hepatocellular Carcinoma by Inducing GSDME Dependent Pyroptosis. *Front Cel Dev Biol* 9, 697832. doi:10.3389/fcell.2021.697832

Shao, W., Yang, Z., Fu, Y., Zheng, L., Liu, F., Chai, L., et al. (2021). The Pyroptosis-Related Signature Predicts Prognosis and Indicates Immune Microenvironment Infiltration in Gastric Cancer. *Front. Cel Dev Biol* 9, 676485. doi:10.3389/fcell.2021.676485

Shi, H., Gao, Y., Dong, Z., Yang, J. e., Gao, R., Li, X., et al. (2021). GSDMD-mediated Cardiomyocyte Pyroptosis Promotes Myocardial I/R Injury. *Circ. Res.* 129 (3), 383–396. doi:10.1161/circresaha.120.318629

Shi, J., Zhao, Y., Wang, K., Shi, X., Wang, Y., Huang, H., et al. (2015). Cleavage of GSDMD by Inflammatory Caspases Determines Pyroptotic Cell Death. *Nature* 526 (7575), 660–665. doi:10.1038/nature15514

Sun, F. R., Wang, S. L., Wang, M., and Sun, L. M. (2020). Simvastatin Induces Apoptosis of Nasopharyngeal Carcinoma Cells through NF-Kb Signaling Pathway. *Eur. Rev. Med. Pharmacol. Sci.* 24 (12), 6726–6734. doi:10.26355/eurrev_202006_21660

Tan, G., Lin, C., Huang, C., Chen, B., Chen, J., Shi, Y., et al. (2021). Radiosensitivity of Colorectal Cancer and Radiation-Induced Gut Damages Are Regulated by Gasdermin. ***E.*** *Cancer Lett.* 529, 1–10. doi:10.1016/j.canlet.2021.12.034

Tan, Y., Chen, Q., Li, X., Zeng, Z., Xiong, W., Li, G., et al. (2021). Pyroptosis: a New Paradigm of Cell Death for Fighting against Cancer. *J. Exp. Clin. Cancer Res.* 40 (1), 153. doi:10.1186/s13046-021-01959-x

Van Laer, L., Huizing, E. H., Verstreken, M., van Zuijlen, D., Wauters, J. G., Bossuyt, P. J., et al. (1998). Nonsyndromic Hearing Impairment Is Associated with a Mutation in DFNA5. *Nat. Genet.* 20 (2), 194–197. doi:10.1038/2503

Wang, F., Liu, W., Ning, J., Wang, J., Lang, Y., Jin, X., et al. (2018). Simvastatin Suppresses Proliferation and Migration in Non-small Cell Lung Cancer via Pyroptosis. *Int. J. Biol. Sci.* 14 (4), 406–417. doi:10.7150/ijbs.23542

Wang, L., Zhang, C., Hong, Y., Li, X., Li, T., Gao, A., et al. (2021). Integrating Epigenetic Modulators in Nanofibers for Synergistic Gastric Cancer Therapy via Epigenetic Reprogramming. *Nano Lett.* 21 (1), 298–307. doi:10.1021/acs.nanolett.0c03665

Wang, Y., Gao, W., Shi, X., Ding, J., Liu, W., He, H., et al. (2017). Chemotherapy Drugs Induce Pyroptosis through Caspase-3 Cleavage of a Gasdermin. *Nature* 547 (7661), 99–103. doi:10.1038/nature22393

Wesołowska, A., Winiarska, H., Owoc, J., Borowska, M., Domagała, J., Mikołajczak, P. Ł., et al. (2021). Effects of Low-Dose Atorvastatin on the Peripheral Blood Mononuclear Cell Secretion of Angiogenic Factors in Type 2 Diabetes. *Biomolecules* 11 (12). doi:10.3390/biom11121885

Xia, S., Hollingsworth, L. R., and Wu, H. (2020). Mechanism and Regulation of Gasdermin-Mediated Cell Death. *Cold Spring Harb Perspect. Biol.* 12 (3), a036400. doi:10.1101/cshperspect.a036400

Xiong, Y., Wei, Y., Gu, Y., Zhang, S., Lyu, J., Zhang, B., et al. (2017). DiseaseMeth Version 2.0: a Major Expansion and Update of the Human Disease Methylation Database. *Nucleic Acids Res.* 45 (D1), D888–D895. doi:10.1093/nar/gkw1123

Xu, W. F., Zhang, Q., Ding, C. J., Sun, H. Y., Che, Y., Huang, H., et al. (2021). Gasdermin E-Derived Caspase-3 Inhibitors Effectively Protect Mice from Acute Hepatic Failure. *Acta Pharmacol. Sin* 42 (1), 68–76. doi:10.1038/s41401-020-0434-2

Yang, F., Sun, S. Y., Wang, S., Guo, J. T., Liu, X., Ge, N., et al. (2022). Molecular Regulatory Mechanism of Ferroptosis and its Role in Gastrointestinal Oncology: Progress and Updates. *World J. Gastrointest. Oncol.* 14 (1), 1–18. doi:10.4251/wjgo.v14.i1.1

Yanokura, M., Banno, K., and Aoki, D. (2020). MicroRNA-34b E-xpression E-nhances C-hemosensitivity of E-ndometrial C-ancer C-ells to P-aclitaxel. *Int. J. Oncol.* 57 (5), 1145–1156. doi:10.3892/ijo.2020.5127

Yokomizo, K., Harada, Y., Kijima, K., Shinmura, K., Sakata, M., Sakuraba, K., et al. (2012). Methylation of the DFNA5 Gene Is Frequently Detected in Colorectal Cancer. *Anticancer Res.* 32 (4), 1319–1322.

Yu, X., and He, S. (2017). GSDME as an Executioner of Chemotherapy-Induced Cell Death. *Sci. China Life Sci.* 60 (11), 1291–1294. doi:10.1007/s11427-017-9142-2

Yu, Z., Guo, J., Liu, Y., Wang, M., Liu, Z., Gao, Y., et al. (2022). Nano Delivery of Simvastatin Targets Liver Sinusoidal Endothelial Cells to Remodel Tumor Microenvironment for Hepatocellular Carcinoma. *J. Nanobiotechnology* 20 (1), 9. doi:10.1186/s12951-021-01205-8

Yuan, R., Zhao, W., Wang, Q. Q., He, J., Han, S., Gao, H., et al. (2021). Cucurbitacin B Inhibits Non-small Cell Lung Cancer *In Vivo* and *In Vitro* by Triggering TLR4/NLRP3/GSDMD-dependent Pyroptosis. *Pharmacol. Res.* 170, 105748. doi:10.1016/j.phrs.2021.105748

Zhou, C., Zhao, J., Liu, J., Wei, S., Xia, Y., Xia, W., et al. (2019). LncRNA SNHG16 Promotes Epithelial- Mesenchymal Transition via Down-Regulation of DKK3 in Gastric Cancer. *Cancer Biomark* 26 (4), 393–401. doi:10.3233/CBM-190497

Zhou, C. B., and Fang, J. Y. (2019). The Role of Pyroptosis in Gastrointestinal Cancer and Immune Responses to Intestinal Microbial Infection. *Biochim. Biophys. Acta Rev. Cancer* 1872 (1), 1–10. doi:10.1016/j.bbcan.2019.05.001

Conflict of Interest: The authors declare that the research was conducted in the absence of any commercial or financial relationships that could be construed as a potential conflict of interest.

Publisher's Note: All claims expressed in this article are solely those of the authors and do not necessarily represent those of their affiliated organizations, or those of the publisher, the editors and the reviewers. Any product that may be evaluated in this article, or claim that may be made by its manufacturer, is not guaranteed or endorsed by the publisher.

frontiers | Frontiers in Pharmacology

ORIGINAL RESEARCH
published: 26 April 2022
doi: 10.3389/fphar.2022.874235

VRK1 Predicts Poor Prognosis and Promotes Bladder Cancer Growth and Metastasis *In Vitro* and *In Vivo*

Jiacheng Wu[1†], *Tao Li*[2†], *Hao Ji*[1], *Zhi Chen*[3*] and *Baoqian Zhai*[4*]

[1]Department of Urology, The Affiliated Tumor Hospital of Nantong University, Nantong, China, [2]Department of Medical Oncology, The Affiliated Tumor Hospital of Nantong University, Nantong, China, [3]Department of Pathology, The First People's Hospital of Longquanyi District, Chengdu, China, [4]Department of Oncology Radiotherapy, Yancheng No. 1 People's Hospital, Yancheng, China

Bladder cancer (BC) is one of the most common malignant tumors in the urinary system with growing morbidity and diagnostic rate in recent years. Therefore, identifying new molecular biomarkers that inhibit the progression of bladder cancer is needed for developing further therapeutics. This study found a new potential treatment target: vaccinia-related kinase 1 (VRK1) and explored the function and mechanism of VRK1 in the development of bladder cancer. First, TCGA database and tissue microarray analysis showed that VRK1 was significantly upregulated in bladder cancer. Kaplan–Meier survival analysis indicates that the OS and PFS of the VRK1 high expression group were significantly lower than the VRK1 low expression group (p = 0.002, p = 0.005). Cox multi-factor analysis results show that VRK1 expression is an independent risk factor affecting tumor progress. The maximum tumor diameter, staging, and adjuvant chemotherapy also have a certain impact on tumor progression ($p < 0.05$). In internal validation, the column C index is 0.841 (95% CI, 0.803–0.880). In addition, cell functional studies have shown that VRK1 can significantly inhibit the proliferation, migration, and invasiveness of bladder cancer cells. *In vivo*, nude mice transplanted tumors further prove that low VRK1 can significantly inhibit the proliferation capacity of bladder cancer cells. In summary, VRK1 expression is significantly related to the staging, grade, and poor prognosis of patients with bladder cancer. At the same time, *in vivo* and *in vitro* experiments have shown that downregulation of VRK1 can significantly inhibit the proliferation of bladder cancer cells. These findings provide a basis for using VRK1 as a potential therapeutic target for patients with bladder cancer.

Keywords: VRK1, bladder cancer, growth and metastasis, nomogram, TCGA (the cancer genome atlas program), GEO, GSEA

OPEN ACCESS

Edited by:
Zhe-Sheng Chen,
St. John's University, United States

Reviewed by:
Guobing Chen,
Jinan University, China
Yuejiao Zhong,
The Affiliated Hospital of Nanjing University Medical School, China

***Correspondence:**
Baoqian Zhai
baoqzhai2018@163.com
Zhi Chen
459509409@163.com

[†]*These authors have contributed equally to this work*

Specialty section:
This article was submitted to Experimental Pharmacology and Drug Discovery, a section of the journal Frontiers in Pharmacology

Received: *11 February 2022*
Accepted: *09 March 2022*
Published: *26 April 2022*

Citation:
Wu J, Li T, Ji H, Chen Z and Zhai B (2022) VRK1 Predicts Poor Prognosis and Promotes Bladder Cancer Growth and Metastasis In Vitro and In Vivo. Front. Pharmacol. 13:874235. doi: 10.3389/fphar.2022.874235

INTRODUCTION

Bladder cancer (BC) is one of the most common malignant tumors in the urinary system, and is the 11th most common cancer in the world (Torre et al., 20122015). More than 430,000 patients have been diagnosed with bladder cancer (Rajwa et al., 2018) every year, and about 165,000 people will die. Although considerable progress has been made in surgical techniques, its 5-year survival rate remains at a relatively low level (Li et al., 2017; Peng et al., 2017). Postoperative tumor recurrence and progress are the major clinical events affecting the prognosis of these patients (Wang et al., 2019). Recent

research studies show that relative parameters such as postoperative pathological staging of the tumor can predict the survival and prognosis of bladder cancer patients, but the effectiveness is not reliable. Thus, new prognosis indicators and possible targets for bladder cancer are crucial.

VRK1 is a member of the vaccinia-related kinase (VRK) family of serine/threonine protein kinases. It is a Ser–Thr kinase with atypical activity (Campillo-Marcos et al., 2021), and a nucleosome kinase or chromatin kinase (Kang et al., 2007). It can interact directly and stably with different chromatin proteins, and is related to cell cycle entry, apoptosis, and autophagy control (Kim et al., 2012). It regulates a variety of transcription factors, including ATF2 (Sevilla et al., 2004), p53 (Lopez-Borges and Lazo, 2000), and c-Jun (Liu et al., 2017). All of them are highly involved in tumorigenesis. Studies have indicated that VRK1 is highly expressed in many human tumors and affects the prognosis of patients. For example, VRK1 increases the number of G1-arrested cells by reducing cyclin D1 and p-Rb while upregulating p21 and p27. Its consumption downregulates the phosphorylation of CREB to participate in the tumorigenesis and development of liver cancer (Huang et al., 2016). VRK1 relates to poor prognosis of glioma by participating in the PI3K/AKT pathway (Ben et al., 2018); studies have also shown that ginsenoside Rg3 affects DNA damage and causes VRK1 upregulation and P53BP1 foci formation, thereby inhibiting lung cancer cell viability (Liu et al., 2019). VRK1 overexpression can promote breast cancer cell mesenchymal transition (MET) by regulating the transcriptional repressor snail, slug, and twist (Mon et al., 2018). At the same time, there are related research reports on rectal adenocarcinoma (Del Puerto-Nevado et al., 2016) and other tumors. However, there is no relevant research on VRK1 and bladder cancer. Therefore, the purpose of this study is to evaluate the role of VRK1 in the prognosis of bladder cancer. In addition, our research hopes to further explore the specific biological functions of VRK1 in bladder cancer through *in vivo* and *in vitro* experiments.

MATERIALS AND METHODS

Classification of Differentially Expressed Genes in TCGA and GEO Database

We used the GEO query package to download two RNA expression data sets GSE13507 and GSE65635 (containing tumor tissue and normal tissue) from the GEO database (https://www.ncbi.nlm.nih.gov/geo/query/acc.cgi). GEO online GEO2R tool was used to analyze the differential genes. The parameters for screening DEG are selected if the log2FC is greater than 0 and p value is less than 0.02. The data set of differentially expressed genes of bladder cancer is downloaded from the TCGA database (https://tcga-data.nci.nih.gov/), and the parameters for screening DEG are determined if the log2FC is greater than 0 and p value is less than 0.0001 (Diboun et al., 2006; Davis and Meltzer, 2007; Gu et al., 2016). Finally, the intersection of the three data sets is showed in a Venn diagram to obtain the common upregulated differentially expressed genes.

Data Analysis Using the TCGA Database

In order to study the expression of VRK1 in bladder cancer, we used the TCGA database (https://tcga-data.nci.nih.gov/) for analysis. Among them, 414 cases of cancer tissues and 19 paracancerous tissues were included in the study. R 3.6.3 software is used to collect and analyze the data. The expression of VRK1 gene in bladder cancer tissue and paracancerous tissue was compared according to the standard calculation method as described previously.

Gene Enrichment of VRK1

We used gene enrichment methods to further explore the possible signaling pathways VRK1 may participate in the poor prognosis of bladder cancer. GSEA analysis is mainly performed using GSEA software version 2.2.2.0 (Mootha et al., 2003), which uses a predefined gene set from the molecular signature database (MSigDB v5.0) (Subramanian et al., 2005). A gene set is a group of genes that share pathways, functions, chromosomal locations, or other characteristics. In this study, we used all the C sets for GSEA analysis (i.e., C1–C7 sets in MsigDB), and listed the ranking genes based on the score of -log10 of the p value multiplied by the fraction of multiple change of the expression. The gene sets collected according to the minimum and maximum selection criteria were 10 and 500 genes, respectively.

Clinical Data Selection

The clinical data of 101 patients with bladder cancer who underwent surgical resection in the Department of Urology, Nantong Cancer Hospital from May 2013 to May 2015 were selected. Among them, 30 cases of bladder cancer were accompanied by corresponding paracancerous tissues. The inclusion criteria were: ① all patients who were diagnosed with bladder cancer for the first time and only had bladder cancer as tumor diagnosis and surgery; ② clinical staging was stage I–III; ③ postoperative pathology was confirmed to be bladder cancer (urothelial carcinoma); ④ have complete clinical data and follow-up data; ⑤ have no other antitumor therapy before admission (neoadjuvant chemoradiation or other antitumor therapies); and ⑥ good patient compliance. The exclusion criteria were: ① received radiotherapy, chemotherapy, hormone therapy, etc., before surgery; ② combined with other serious diseases, such as severe hypertension; ③ combined with certain acute-stage diseases, such as infection; and ④ refused to follow-up. The age range of the patients included in this study was 34–81 years old, with an average age of (63.0 ± 9.5) years. There are 82 males and 19 females. All samples were collected under the written informed consent of the participants, and the experiment was approved by the Ethics Committee of Nantong Cancer Hospital. Follow-up is carried out by outpatient review or telephone follow-up. The outpatient follow-up was conducted every 3 months in the first year after surgery, every 6 months in the second year, and once a year after 2 years until May 2020. Follow-up examination: cystoscopy, abdominal MRI, CT or color Doppler ultrasound, tumor markers, urinalysis, etc., (additional examinations might be added depending on the patient's condition). Observation indicators: OS is defined as the time from the diagnosis of the

disease to death from any cause or the cut-off time of follow-up. PFS is defined as the time from the beginning of treatment to any follow-up examination that indicates disease progression. At the end of the follow-up, if the subject was still alive but lost to the follow-up, the data from the final cut-off time will be used for statistical analysis.

Cell Source

The five bladder cancer cell lines (J82, SW780, T24, 5637, and UM-UC-3) and a normal human bladder normal epithelial cell (SV-HUC-1) used in this study were mainly purchased from Chinese Academy of Sciences Cell bank, Shanghai.

Tissue Microarray Construction, Immunohistochemistry, and Its Correlation With Survival Prognosis and Clinical Data Parameters

The tissue microarray was constructed by the Department of Pathology, Nantong Cancer Hospital. Hematoxylin–eosin was used to stain the paraffin embedded tissue blocks of 101 cases of bladder cancer. The most typical features were selected and marked at fixed points under the microscope. Each dot array contains less than 160 dots. A 3-micron-thick section was cut from the paraffin embedded tissue block and transferred to a glass slide using tape transfer system for UV cross-linking. IHC staining was performed according to the previously described protocol (Laurberg et al., 2014). Anti-VRK1 antibody [5D1]-N-terminal mouse monoclonal antibody (1:500, abcam ab171933) was used. The tissue sections were examined through two experienced pathologists under double-blind condition. The immunohistochemistry results were scored considering two factors: the proportion of positive cells and the intensity of cell staining. We found that VRK1 is mainly located in the nucleus. The score according to the proportion of positive staining cells: 0 (negative), 1 (< 25%), 2 (25–50%), 3 (51–75%), and 4 (>75%), and staining intensity: 0 (negative or no staining), 1 (weak positive), 2 (central type), and 3 (strong positive). The value obtained by multiplying these two scores is the final score corresponding to each specimen. After calculating the arithmetic mean of these scores, the specimen with a score lower than 6 is finally defined as a low expression of VRK1. According to the expression of VRK1 under immunohistochemistry, the 101 bladder cancer patients included in the study were divided into two groups: high and low expression of VRK1. SPSS software was used to compare the correlation between the expression of VRK1 in these two groups and the survival prognosis and clinical parameters of the patients. Meanwhile, the independent prognostic factors that are meaningful for the prognosis of bladder cancer patients were further screened through uni- and multi-variate analysis.

Reverse Transcription Quantitative PCR Method to Detect the mRNA Encoding VRK1

Take 100 mg sample of both the tumor tissue and paracancerous tissue of the patients included in the study and mill these samples into powder by the liquid nitrogen grinding method. Add 1 ml Trizol lysis solution, and extract the total RNA according to the instructions. The primers are: 5′-CTTCAGAGTCAGTTGGCA GTG-3′, 5′-CTTCAGCTTACGGGTACGAAT-3′; GAPDH is 5′-CAT GGG TGT GAA CCA TGA GAA GTA-3′. Use the reverse transcription kit to reverse transcribe RNA to obtain cDNA. Perform real-time fluorescent quantitative PCR on a fluorescent quantitative PCR machine. Calculate the relative expression of the target molecule's mRNA by the $2^{-\triangle\triangle ct}$ method. Therefore, we obtained the expression of VRK1 in cancer and paracancerous tissue.

In vitro Cytology Experiment Verification

CCK8-Detection Cell Activity

1) Screen five bladder cancer cell lines (J82, SW780, T24, 5637, and UM-UC-3) with high VRK1 expression. Construct VRK1 knockdown bladder cancer cell lines by using small interfering RNA knockdown techniques. Digest the T24 and 5637 cells transfected with these siRNA and the negative control cells separately. Centrifuge at low speed, then resuspend the target cells using complete medium.
2) Use a cell counter to adjust all sample cells to the same number (about $4*10^3$ cells in each well in a 96-well plate). Add 100 uL of culture medium per well.
3) Set up three replicate wells for each experimental group. Set complete medium as the blank control group at the same time. Shake well and then observe the cell distribution under the microscope to ensure that the cells are evenly distributed without accumulation or overlap. Transfer to 37°C, 5% CO_2 cell incubator for overnight culture.
4) After overnight incubation, add CCK-8 reagent to each well, usually 10 ul, and then move it again into a 37°C, 5% CO_2 cell incubator for incubation for 2 h.
5) Determine the absorbance value at 450 nm according to the instruction manual of the microplate reader. Record the OD value, and draw the proliferation curve according to the data.

Cloning Formation Assay

1) Prepare a suspension of the target cells. Adjust the cell density of the stock solution by cell counter. Dilute slowly till the cell density decreased to about 300 cells in each well of the 6-well plate. Cultivate for about 14 days without replacing complete medium.
2) After the incubation, absorb the original medium as much as possible. Add paraformaldehyde (4%) to fix the cells for about 20 min.
3) Rinse with pre-cooled PBS (1x) 2–3 times. After the last PBS buffer rinsing, add crystal violet staining solution (0.1%) for about 30 min to stain the cell.
4) Use pre-cooled PBS (1x) to wash 2–3 times to wash off the excess crystal violet staining solution as much as possible and calculate the number of clone groups.

Transwell Migration Experiment

1) Digest the selected target cells, centrifuge, and then resuspend the target cells with PBS (1x) to wash. Centrifuge and then remove the upper layer of the liquid. Resuspend the cells with serum-free medium.

2) Take the serum-free minimal medium cell stock solution for cell count. Adjust the cell density with serum-free minimal medium to reach the target cell number, about $3*10^5$.
3) Put 500 ml of complete culture (containing 10% fetal bovine serum) in the lower chamber of the sterile 24-well plate. Put the small chamber into the corresponding 24-well plate.
4) Add the cell suspension stock solution to the upper chamber of the 24-well plate; the volume is about 200 ul. Shake slightly. Incubate in cell incubator for 24 h.
5) After incubation, add about 600 ml 4% paraformaldehyde dropwise to the blank wells. Rinse the small chamber with PBS and put it back in for fixation for 20 min.
6) Generally, use PBS to rinse slowly after the fixation. After letting it air dry for a proper amount of time, stain with crystal violet staining solution (0.1%) for 30 min.
7) Gently take out the small chamber and wash it with PBS 2–3 times. Then, use a cotton swab to clean the cells that have not migrated in the upper small chamber. After drying, observe and take pictures with a microscope.

Transwell Invasion Experiment

Transwell Chamber Preparation

i) Matrigel-Free Transwell Cell Preparation
   ① Coating basement membrane: Coat the upper chamber surface of the bottom membrane of the Transwell chamber with 50 mg/L Matrigel 1:8 dilution. Air-dry at 4°C.

Preparation of Cell Suspension

   ① Before preparing the cell suspension, the cells can be de-serum–starved for 12–24 h to further remove the influence of the serum, but this step is not necessary.
   ② Digest the cells: centrifuge and discard the culture medium after terminating the digestion. Wash 1–2 times with PBS, and resuspend in serum-free medium containing BSA. Adjust the cell density to $1–10 \times 10^5$.

Inoculation of the Cells

   ① Take 200 μl of cell suspension into the Transwell chamber.
   ② Generally, 500 μl of medium containing FBS is added to the lower chamber of the 24-well plate. Please refer to the instructions for details. Special attention should be paid to the fact that there are often bubbles between the lower culture medium and the chamber. Once bubbles are generated, the chemotaxis of the lower culture medium is weakened or even disappeared. Pay special attention when planting plates. Lift the chamber to remove air bubbles, and then put the chamber into the culture plate.
   ③ Cultivate cells: conventionally culture for 12–48 h (mainly depending on the invasiveness of the cancer cells). In addition to the invasiveness of cells, when selecting the incubation time, the influence of each process on the number of cells cannot be ignored.

"Adherent" Cell Count

   ① By staining the cells, the cells can be counted under the microscope.
   ② Wipe off the Matrigel and the cells in the upper chamber with a cotton swab.
   ③ Dyeing: The commonly used dyeing methods include crystal violet dyeing.

Western Blot Detection

1) Electrophoresis process: Choose a constant voltage of 80 V for the upper layer of compression gel. After the protein sample runs to the lower layer of the separation gel and the protein marker layer can be observed with the naked eye, change the voltage to 120–150 V. End the electrophoresis when the sample runs to a distance of about 0.5 cm from the bottom edge of the separation gel.
2) Transfer: Pour the 1x transfer membrane solution prepared 1 day in advance from the refrigerator into the iron pan used in the operation. Immerse the required PVDF membrane in methanol to activate (about 15–30 s) in advance, and then transfer the PVDF membrane so that it is completely immersed in ddH_2O for depolarization. Place the PVDF membrane in the pre-cooled transfer buffer. Soak the black sponge pad and filter paper larger than the size of the PVDF membrane into the transfer fluid (1x) in advance. Gently lift one end of the short glass plate to leave the gel, and then cut out the upper layer glue and the excess part of the lower layer glue and move the gel to the black side of the transfer membrane clamp. The black side of the transfer membrane is the bottom and the white side is the top. It is placed layer by layer in the order of sponge pad, two layers of filter paper, gel, PVDF membrane, two layers of filter paper, sponge pad, etc., from bottom to top. Slowly clamp the transfer membrane and immerse into the electrophoresis tank containing the transfer buffer. It must be ensured that a suitable ice box has been placed outside the transfer tank. Add the transfer buffer to the silver wire on the upper edge of the transfer membrane clamp. Tighten the lid and put it in an ice–water mixed bath and turn on the power. Generally, the transfer uses a constant current of 300 mA for 90 min.
3) Blocking: After transfer time, immerse the PVDF membrane faceup in the pre-prepared skimmed milk blocking solution (5%), and place it in a room temperature slow-speed shaker for about 2 h.
4) Incubate the primary antibody: Prepare the wet box and the incubation tank. Dilute with the special primary antibody diluent according to the instructions of the primary antibody. Put it into the corresponding incubation tank. Wash the completely blocked PVDF membrane using TBST (1x) 2–3 times. Use filter paper to remove excess liquid. Completely soak the membrane containing the target protein facedown in the primary antibody incubation solution. Put it in the refrigerator at 4° overnight.
5) Wash the membrane: Take out the wet box from the refrigerator and let it stand for 20–30 min at room temperature. Recover the primary antibody and note the relevant information of the antibody. Put the membrane faceup in TBST (1x) to wash 3–4 times with gentle but quick shaking for cleaning. Each cleaning period should last for about 4–5 min.

6) Incubate the secondary antibody: Following the instructions of the secondary antibody, use TBST (1x) to dilute the corresponding secondary antibody to the corresponding concentration. Use filter paper to absorb the excess solution on the membrane. Turn the membrane containing the target protein facedown to ensure that it is completely immersed in the secondary antibody. Normally, it should be incubated at room temperature for about 2 h.
7) Wash the membrane again: After secondary antibody incubation, place the membrane containing the target protein faceup. Wash it in TBST (1x) 3–4 times, with gentle but quick shaking for cleaning. Each cleaning period should last for about 20 min. Soak the membrane in the last cleaning solution to prepare for Chemiluminescent.
8) Chemiluminescent: Fully mix ECL developer A and B at equal volume. Add sufficient amount of mixed liquid on the front of the membrane. Perform the chemiluminesent according to the instructions of the instrument and save the picture.

In Vivo Nude Mice Experimental

For animal experiments, male NOD-SCID nude mice, 6–7 weeks old (weight 18–20 g), were purchased from the Animal Center of the Chinese Academy of Sciences. All mice are raised in the SPF animal room of the Key Laboratory of the Ministry of Health in accordance with the NIH animal experiment guidelines in the United States. In this project, we used a total of eight animals, with four animals in each group. 1) T24 bladder tumor cell lines (shVRK1-NC and shVRK1-2) at exponential growth phase were selected. Cell line was digested using Trypsin and neutralized with complete medium. Transfer it to a 50 ml sterile centrifuge tube with a pipette, centrifuge at 1000 rpm for 5 min, and then discard the supernatant. Mix the cells thoroughly with appropriate complete medium and count the cells. 2) Dilute the cells to 5×10^7/ml, according to the calculated cell concentration. 3) Randomly divide the mice into an experimental group and a control group: each nude mouse is subcutaneously injected into the lower abdominal wall under the axillary region with 100 μL of 5 × 106 cells per mice with a syringe. 4) After 1 week of subcutaneous injection, measure the tumor on the abdominal wall of nude mice every 2–3 days to calculate the volume of the tumor (cm3) = width (cm) x width (cm) x length (cm)/2; 5). After 6 weeks, the nude mice of the experimental group and the control group were sacrificed using cervical dislocation. The tumors formed under the skin were collected, the size and weight were measured, and the relationship between the growth of tumor tissue and the proliferation ability of bladder cancer cells in the body were analyzed, followed by the follow-up immunohistochemistry experiment.

Statistical Analysis

Use software R (version 3.6.3) for statistical analysis and visualization; R package: DESeq2 (version 1.26.0) (Love MI et al., 2014) for data download; limma package (version 3.42.2) for difference analysis. Use the ggplot2 package (version 3.3.3) for image visualization. Through gene set enrichment analysis (GSEA), use R package: mainly clusterProfiler package (3.14.3 version) (for GSEA analysis) to explore the possible cellular mechanism of VRK1. Use SPSS version 22.0 (IBM) software for statistical analysis. The chi-square test was used to compare and analyze the clinicopathological conditions of the two groups of patients. The Kaplan–Meier method was used to evaluate the survival of patients, and the log rank statistical method was used for significance testing. The Cox proportional hazard regression model is used to clarify the independent prognostic factors that are meaningful for the prognosis of bladder cancer patients. On this basis, the R language is used to draw a nomogram to construct a predictive model: nomogram drawing is composed of survival and rms software packages in R. The main steps for creating a nomogram model are as follows: 1) Select a research model: According to the research data and corresponding results, different models can be selected for the nomogram. This study is the survival analysis of 101 patients with bladder cancer undergoing surgical resection, so COX risk ratio model is ideal. 2) Selection of predictors: The COX risk ratio model can be used to obtain the independent risk factors and risk ratios (HR) of 101 bladder cancer patients undergoing surgical resection. R gives the impact score of each risk factor according to the degree of contribution of different risk factors to the result, and finally obtains the corresponding survival rate of the individual patient based on the total score. The difference was statistically significant with $p < 0.05$.

RESULTS

Selection of Differentially Expressed Genes, Their Expression in the TCGA Database, and Using GSEA, GO, and KEGG for Gene Enrichment Analysis

We used the GEO query package to download two RNA expression data sets GSE13507 and GSE65635 (containing tumor tissue and normal tissue) from the GEO database (https://www.ncbi.nlm.nih.gov/geo/query/acc.cgi). We used the GEO online GEO2R tool to analyze the differential genes. The parameters for screening DEG were selected if the log2FC is greater than 0 and p value is less than 0.02. Then, the data set of differentially expressed genes for bladder cancer from the TCGA database was downloaded (https://tcga-data.nci.nih.gov/). The parameters for screening DEG were selected if the log2FC is greater than 0 and p value is less than 0.0001 (**Figure 1A**). The differentially expressed gene is screened and confirmed to be VRK1. In order to confirm the expression level of VRK1 in bladder cancer tissues, we used the TCGA database (https://tcga-data.nci.nih.gov/) to search and analyze the mRNA expression level of VRK1. Meanwhile, we found that compared with the paracancerous tissues in the TCGA database, the mRNA expression of VRK1 in tumor tissues is upregulated (**Figures 1B,C**).

In order to further explore the possible role of the differentially expressed genes screened in bladder cancer, we first predicted the possible related molecular mechanisms through GSEA. We found that VRK1 may participate in DNA repair, cell cycle checkpoints, NOTCH signaling pathways, WNT signal pathway, and the

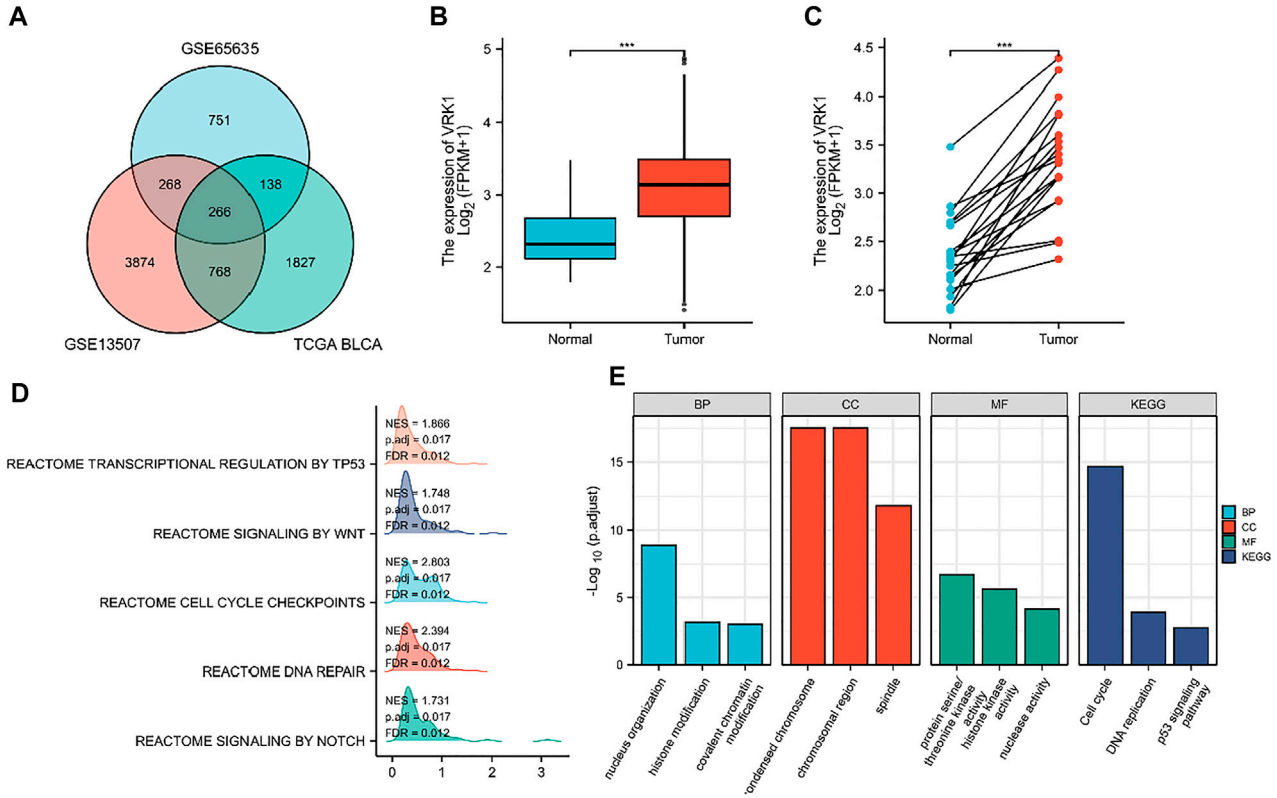

FIGURE 1 | Differentially expressed genes (DEGs) and their expression in the TCGA database and gene enrichment analysis results of VRK1. **(A)** Venn diagrams of upregulated genes in three data sets. **(B)** VRK1 in unmatched bladder cancer tissues (n = 414) and paracancerous tissues (n = 19) in the TCGA database is highly expressed in tumor tissues. **(C)** VRK1 in the matched bladder cancer tissues (n = 19) and paracancerous tissues (n = 19) in the TCGA database is highly expressed in tumor tissues. **(D)** GSEA analysis results for VRK1. **(E)** Functional analysis results of GO and KEGG. Note: ***<0.001, the difference is statistically significant.

transcription and regulation of TP53 to affect the biological process of bladder cancer, leading to different prognosis of bladder cancer (**Figure 1D**). We also used Metascape for online functional analysis. The differential genes were added to Metascape for functional analysis of GO and KEGG. GO-BP analysis showed that nucleus organization, histone modification, and covalent chromatin modification are possible cytological behaviors involved. GO-CC analysis found that condensed chromosome, chromosomal region, and spindle are possible sites involved. GO-MF analysis found that protein serine/threonine kinase activity, histone kinase activity, and nuclease activity are the molecular functions that may be affected. KEGG analysis found that cell cycle, DNA replication, and p53 signaling pathway are signaling pathways that may be affected (**Figure 1E**).

Expression of VRK1 in Bladder Cancer Tissue and VRK1 Knockdown can Significantly Inhibit the Proliferation and Clonal Formation Assay of Bladder Cancer Cells

The tumor tissues and paracancerous tissues of the patients included in the study were taken to compare the VRK1 expression. Using reverse transcription quantitative PCR (**Figure 2A**) and Western blotting (**Figure 2B**), we found that VRK1 expression in cancer tissues is higher than that in adjacent tissues ($p < 0.05$). The Human Protein Atlas (https://www.proteinatlas.org/) database indicates that VRK1 has a higher expression in cancerous tissues than in paracancerous tissues. Moreover, the gene is mainly located in the nucleus, with a small amount expressed in the cytoplasm (**Figure 2C**). We used immunohistochemistry to check the expression of VRK1 in the pathological tissues studied in this project. We found that VRK1 is also mainly expressed in the nucleus (**Figure 2D**), which is consistent with the expression in the database. Moreover, VRK1 was low expressed in 43 bladder cancer tissue samples (42.6%), and highly expressed in 58 bladder cancer tissue samples (57.4%).

The aforementioned results indicate that VRK1 is highly expressed in bladder cancer tissues. Therefore, in order to study the specific biological function of this gene in bladder cancer, it is planned to use bladder cancer cell lines for further functional research. qRT-PCR was used to detect the expression level of VRK1 in 5 bladder cancer cell lines (J82, SW780, T24, 5637, and UM-UC-3) and a normal human bladder normal epithelial cell (SV-HUC-1). The results of fluorescence qPCR and Western blot showed that the expression levels of VRK1 in various bladder cancer cell lines are quite different, with the highest expression levels in T24 and 5637

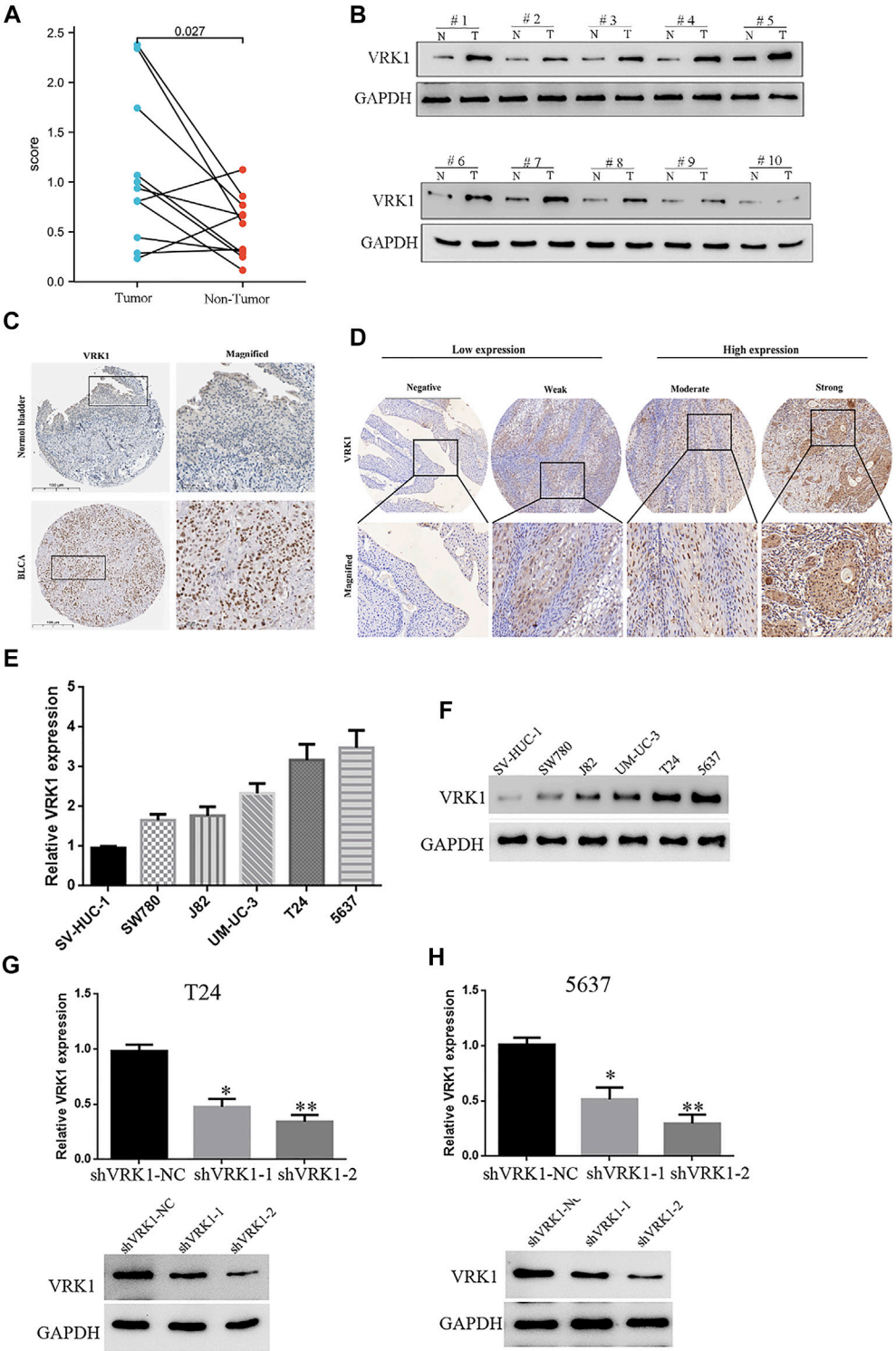

FIGURE 2 | High expression of VRK1 in bladder cancer tissues and bladder cancer cell lines. **(A)** Reverse transcription quantitative PCR showed that the expression of VRK1 in cancer tissues was higher than that in paracancerous tissues at the mRNA level ($p < 0.05$). **(B)** Western blot experiments showed that the expression of VRK1 in cancer tissues was higher than that in paracancerous tissues at the protein level ($p < 0.05$). **(C)** In The Human Protein Atlas database, VRK1 is higher expressed in cancerous tissues than in paracancerous tissues, and is mainly expressed in the nucleus. **(D)** Immunohistochemistry showed that VRK1 was mainly expressed in the nucleus. **(E)** Fluorescence qPCR to detect the expression of VRK1 in bladder cancer cell lines and normal human bladder normal epithelial cells. The experiments were repeated three times. **(F)** Western blot to detect the expression of VRK1 in bladder cancer cell lines and normal human bladder normal epithelial cells. **(G,H)** Fluorescence qPCR and Western blot to detect the expression in bladder cancer T24 and 5637 cells after knocking down VRK1, $*p < 0.05$, $**p < 0.01$.

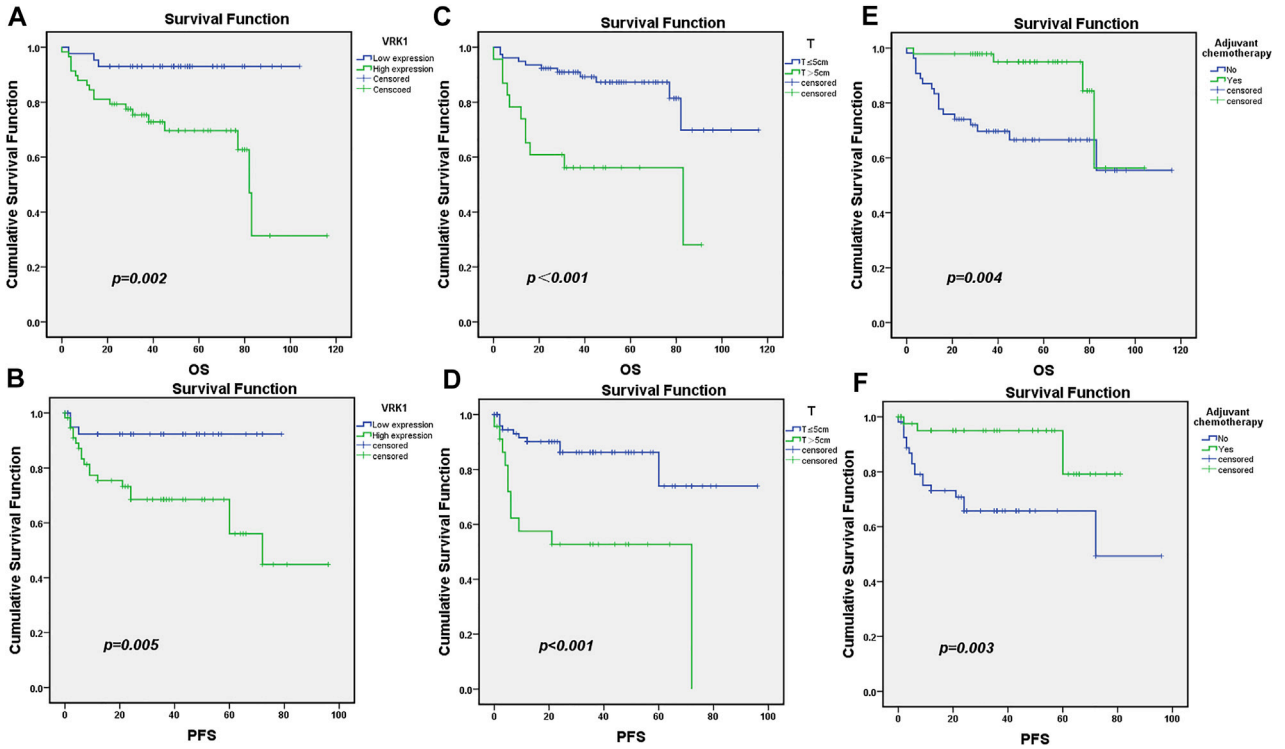

FIGURE 3 | Survival and prognosis of patients included in the study. **(A,B)**: OS and PFS of patients in the VRK1 low expression group are better than those in the VRK1 high expression group. **(C,D)**: OS and PFS of patients with tumor diameter ≤5 cm are better than those in the group with tumor diameter >5 cm. **(E,F)**: OS and PFS of patients that have undergone adjuvant chemotherapy are better than those of those who have not undergone adjuvant chemotherapy.

cells, followed by UM-UC-3, J82, and SW780 cells (**Figures 2E,F**). Therefore, in the follow-up cell function research, we selected VRK1 highly expressing T24 and 5637 cells as the research objects to conduct in-depth cell function and molecular mechanism research. First, we constructed two lentiviral-mediated RNA interference vectors targeting VRK1 gene (shVRK1-1 and shVRK1-2) and shVRK1-control (shVRK1-NC) in T24 and 5637 cells, respectively, and then detected knockdown by fluorescent qPCR and Western blot. The results suggested: compared with the blank control group (shVRK1-NC), shVRK1-1 and shVRK1-2 can significantly knockdown the expression level of VRK1 in bladder cancer cells after transfection, and shVRK1-2 has a higher knockdown efficiency (**Figures 2G,H**). The aforementioned results indicate that the bladder cancer cell line with VRK1 knockdown is successfully constructed, providing experimental materials for subsequent functional studies.

Survival and Prognosis of Patients Included in This Study

All patients were followed up for 5 years. A total of 79 patients survived, with a survival rate of 78.2%, and 22 patients died, with a mortality rate of 21.8%. Kaplan–Meier survival analysis results showed that the OS and PFS of patients in the VRK1 high expression group were significantly lower than those in the VRK1 low expression group (p = 0.002, p = 0.005) (**Figures 3A,B**). Meanwhile, further stratified analysis also reveals that patients with tumor diameters ≤5 cm and undergoing adjuvant chemotherapy had better OS and PFS (**Figures 3C–F**).

Relationship Between VRK1 and Clinicopathological Data of Patients With Bladder Cancer

Among the 101 bladder cancer patients included, 43 cases (42.6%) were in the VRK1 low expression group, and 58 cases (57.4%) were in the VRK1 high expression group. The difference between two groups of patients in terms of gender, age, recurrence, surgical methods, adjuvant chemotherapy, invasion of the bladder triangle, tumor invasion, vascular tumor thrombus, T stage, grade, lymph node metastasis, and presence or absence of distant metastasis was not statistically significant ($p > 0.05$), but the difference in tumor size was statistically significant ($p < 0.05$) (**Table 1**). This also provides some reference for our follow-up experiments to explore the role of VRK1 in the tumorigenesis and development of bladder cancer.

Results of Univariate Analysis and Multi-Factor Analysis

In order to further determine the risk factors associated with OS in patients with bladder cancer, we conducted univariate and

TABLE 1 | Relationship between the expression of VRK1 and clinicopathological data.

Variable	Total	Low expression	High expression	p
	n (%)	n (%)	n (%)	
Gender				
Male	82 (81.2)	37 (36.6)	45 (44.6)	0.282
Female	19 (18.8)	6 (5.9)	13 (12.9)	
Age				
≤65	56 (55.4)	21 (20.8)	35 (34.7)	0.250
> 65	45 (44.6)	22 (21.8)	23 (22.8)	
Recurrence				
Yes	23 (22.8)	11 (10.9)	12 (11.9)	0.562
No	78 (77.2)	32 (31.7)	46 (45.5)	
Tumor size (cm)				
≤5	78 (77.2)	38 (37.6)	40 (39.6)	0.021[a]
> 5	23 (22.8)	5 (5.0)	18 (17.8)	
Operation mode				
Transurethral resection	50 (49.5)	23 (22.8)	27 (26.7)	0.491
Radical cystectomy	51 (50.5)	20 (19.8)	31 (30.7)	
Adjuvant chemotherapy				
Yes	47 (46.5)	24 (23.8)	23 (22.8)	0.107
No	54 (53.5)	19 (18.8)	35 (34.7)	
Bladder triangle involvement				
Yes	36 (35.6)	15 (14.9)	21 (20.8)	0.891
No	65 (64.4)	28 (27.7)	37 (36.6)	
External invasion				
Yes	13 (12.9)	6 (5.9)	78 (6.9)	0.780
No	88 (87.1)	37 (36.6)	51 (50.5)	
Vascular tumor thrombus				
Yes	2 (2.0)	0 (0.0)	2 (2.0)	0.219
No	99 (98.0)	43 (42.6)	56 (55.4)	
T stage				
T1	22 (21.8)	9 (8.9)	13 (12.9)	0.858
T2+T3	79 (78.2)	34 (33.7)	45 (44.6)	
Grade				
G1+G2	53 (52.5)	26 (25.7)	27 (26.7)	0.166
G3	48 (47.5)	17 (16.8)	31 (30.7)	
Lymph node metastasis				
Yes	32 (31.7)	14 (13.9)	18 (17.8)	0.871
No	69 (68.3)	29 (28.7)	40 (39.6)	
Other site metastasis				
Yes	10 (9.9)	3 (3.0)	7 (6.9)	0.397
No	91 (90.1)	40 (39.6)	51 (50.5)	

[a]*<0.05, the difference is statistically significant.*

multivariate analysis to confirm whether VRK1 is an independent risk factor for poor prognosis. Univariate analysis showed that the maximum pathological diameter of the tumor, whether adjuvant chemotherapy, the presence or absence of vascular tumor thrombus, T stage, and VRK1 expression are factors that affect the patient's OS ($p < 0.05$). The results of Cox multivariate analysis showed that the expression of VRK1 is an independent risk factor affecting tumor progression. The pathological maximum diameter, staging, and adjuvant chemotherapy also have a certain impact on tumor progression ($p < 0.05$) (**Table 2**).

Nomogram Construction

Predicting the 2-, 4-, and 6-year survival rates of patients with bladder cancer has a certain guiding effect to improve the prognosis of patients with poor prognostic characteristics in the clinical practice. Compared with the nomogram constructed using a single prognostic factor, the nomogram constructed by a combined model might be the bettter nomogram for predicting short-term survival rates (2, 4, and 6 years). We constructed a nomogram based on Cox regression analysis. The model successfully included 4 independent prognostic factors, including tumor diameter, adjuvant chemotherapy, T stage, and VRK1 expression. Predictive models were contracted with internal validation. In internal validation, the nomogram C-index was 0.841 (95% CI, 0.803–0.880) (**Figure 4**). Therefore, the prediction model has better accuracy.

Knockdown of VRK1 Significantly Inhibits the Invasion and Migration of Bladder Cancer Cells

The results showed that compared with the blank control group (shVRK1-NC), shVRK1-1 and shVRK1-2 began to significantly

TABLE 2 | Univariate analysis and multivariate analysis of clinical factors on 101 patients with OS.

Variable	Univariate analysis			Multivariate analysis		
	HR	(95%CI)	p	HR	(95%CI)	P
Gender						
Male	1.019	(0.344–3.021)	0.972			
Female	1					
Age						
≤65	1	(0.953–5.427)	0.064			
> 65	2.274					
Recurrence						
Yes	0.896	(0.332–2.417)	0.829			
No	1					
Tumor size (cm)						
≤5	1	(1.834–9.875)	0.001[a]	1	(1.182–6.719)	0.019[a]
> 5	4.256			2.818		
Operation mode						
Transurethral resection	1	(0.704–4.075)	0.240			
Radical cystectomy	1.693					
Adjuvant chemotherapy						
Yes	0.230	(0.078–0.684)	0.008[a]	0.275	(0.088–0.858)	0.026[a]
No	1			1		
Bladder triangle involvement						
Yes	2.271	(0.965–5.347)	0.060			
No	1					
External invasion						
Yes	1.469	(0.493–4.374)	0.490			
No	1					
Vascular tumor thrombus						
Yes	11.994	(2.633–54.642)	0.001[a]			
No	1					
T stage						
T1	1	(1.164–78.517)	0.036[a]	1	(1.241–147.896)	0.033[a]
T2+T3	9.561			13.547		
Grade						
G1+G2	1	(0.792–4.527)	0.151			
G3	1.893					
Lymph node metastasis						
Yes	0.949	(0.383–2.347)	0.909			
No	1					
Other site metastasis						
Yes	2.319	(0.779–6.897)	0.131			
No	1					
Expression of VRK1						
Low expression	1	(1.672–19.238)	0.005[a]	1	(1.114–13.338)	0.033[a]
High expression	5.671			3.854		

Note: [a]<0.05, the difference is statistically significant.

inhibit cell proliferation at 48 h. The inhibition phenomenon is particularly significant when cultured to 72 h (**Figure 5A**). The results of the clone formation assay showed that compared with the blank control group (shVRK1-NC), shVRK1-1 and shVRK1-2 could significantly inhibit the number of T24 and 5637 clones (**Figure 5B**). This indicates that knocking down VRK1 can significantly inhibit the proliferation of bladder cells (T24 and 5637).

In order to further study the role of VRK1 in the invasion and migration of bladder cancer cells, Transwell was used to detect the invasion and migration ability of T24 and 5637 cells after knocking down VRK1. The test results showed that compared with the blank control group (shVRK1-NC), knocking down VRK1 (shVRK1-1 and shVRK1-2) can significantly inhibit the invasion and migration of T24 and 5637 cells (**Figure 5C**).

Knockdown of VRK1 Significantly Inhibits the Expression of Proliferation- and Invasion-Related Molecules in Bladder Cancer Cells

The aforementioned results indicate that knockdown of VRK1 can significantly inhibit the proliferation and invasion of bladder cancer cells. To further detect whether knockdown of VRK1 affects the proliferation- (Ki-67, PCNA, and p21) and invasion-(E-cadherin, N-cadherin, vimentin, and fibronectin) related molecules of bladder cancer T24 cells, Western blot was

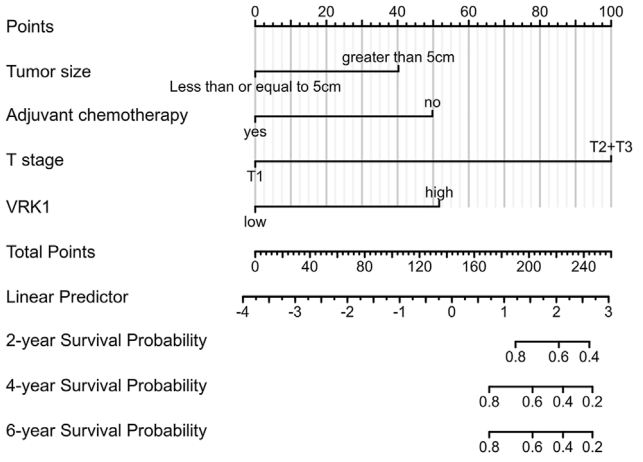

FIGURE 4 | Nomogram predicts the overall survival of bladder cancer patients. For each patient, draw four lines up to determine the points received from the four predictors in the nomogram. The sum of these points is on the "Total Points" axis. Then, draw a line down to determine the probability of 2-, 4-, and 6-year overall survival for bladder cancer. * The C-index is 0.841 (95% CI is 0.803–0.880).

performed. Results suggested that compared with the blank control group (shVRK1-NC), knocking down VRK1 can significantly affect the expression of proliferating cell nuclear antigen Ki-67 and PCNA, and promote the expression of cell cycle inhibitory protein p21 (**Figure 6A**). In addition, knocking down VRK1 can significantly promote the expression of E-cadherin and inhibit the expression of N-cadherin, vimentin, and fibronectin (**Figure 6C**). The abovementioned results indicate that knocking down VRK1 can significantly inhibit the expression of proliferation and invasion-related molecules in T24 cells. Moreover, we found that VRK1 gene was positively correlated with Ki-67 (MKI67), PCNA, N-cadherin (CDH2), and Fibronectin (FN1), and negatively correlated with P21(CDKN1A) in TCGA database (**Figures 6B,D**).

Knockdown of VRK1 Significantly Inhibits the Proliferation of Bladder Cancer Cells *in vivo*

In order to further study the effect of knocking down VRK1 on the proliferation of bladder cancer cells *in vivo*, the shVRK1-NC and shVRK1-2 bladder cancer T24 cells transfected with lentivirus were collected, and then injected into nude mice under the skin. The growth of tumor-bearing tissues was observed and recorded. After 30 days, the nude mice were sacrificed, and the tumor-bearing tissue was taken out for photographing and measurement. The results manifest that compared with the blank control group (shVRK1-NC), knocking down VRK1-2 can significantly inhibit the growth of bladder cancer cell T24 *in vivo* (**Figures 7A,B**). Then, the stripped tumor-bearing tissue was weighed, and the results imply that compared with the blank control group (shVRK1-NC), the proliferation ability of bladder cancer cell T24 *in vivo* was significantly reduced after knocking down VRK1-2 (**Figure 7C**). The aforementioned results show that knocking down VRK1 significantly inhibits the proliferation of bladder cancer cells *in vivo*.

In order to further detect the expression of VRK1 and proliferation-related proteins in tumor-bearing tissues, after fixing the tumor-bearing tissues, immunohistochemistry was used to detect the expression of VRK1 and Ki-67 proteins in the tumor-bearing tissues. The results suggest, compared with the blank control group (shVRK1-NC) tumor-bearing tissue, the expression of VRK1 in the tumor-bearing tissue of the knockdown group (shVRK1-2) was significantly reduced. Similarly, compared with the blank control group (shVRK1-NC) tumor-bearing tissue, the expression level of Ki-67 in the knockdown group (shVRK1-2) tumor-bearing tissue was significantly reduced (**Figures 7D,E**).

DISCUSSION

In this study, we first screened the differential genes of bladder cancer from GEO and TCGA data, and screened the differentially expressed molecules VRK1 from the differential genes. Further data analysis found that the expression differences of VRK1 is not only in between the cancer and paracancerous tissues as described in the database but also in the clinical data we included, which related to the prognosis of patients. The expression level of VRK is an independent risk factor for the prognosis of bladder cancer. We found that patients with low expression of the VRK1 molecule have a better prognosis. Then, we verified from the cytology and the nude mouse level that the reduction of VRK1 expression can inhibit the proliferation and invasion of bladder cancer cells. These results also consistently reflect the potential importance of using VRK1 to assess the prognosis of bladder cancer.

At the beginning of this study, we downloaded two RNA expression data sets GSE13507 and GSE65635 (containing tumor tissue and normal tissue) through GEO database (https://www.ncbi.nlm.nih.gov/geo/query/acc.cgi) *via* GEO query pack. The GEO online GEO2R tool was used to analyze the differential genes, using log2FC greater than 0 and p value less than 0.02 as the parameters to determine the screening DEG. Then, the data set of differentially expressed genes for bladder cancer was downloaded from the TCGA database (https://tcga-data.nci.nih.gov/), and the parameters for screening DEG according to $\log_2$FC greater than 0 and p value less than 0.0001 were determined. Finally, the intersection of the three data sets is mapped in a Venn diagram to obtain the common upregulated differentially expressed genes. Thus, we determined our research molecule VRK1, and verified in the TCGA database that the expression of VRK1 in cancer tissues is higher than that in paracancerous tissues. The current clinical treatment of bladder cancer is now in the era of immunotherapy, and previous analysis has shown that tumor infiltrating lymphocytes are an independent predictor of the sentinel lymph node status and survival rate in cancer patients (Azimi et al., 2012). We also used the established computing resource

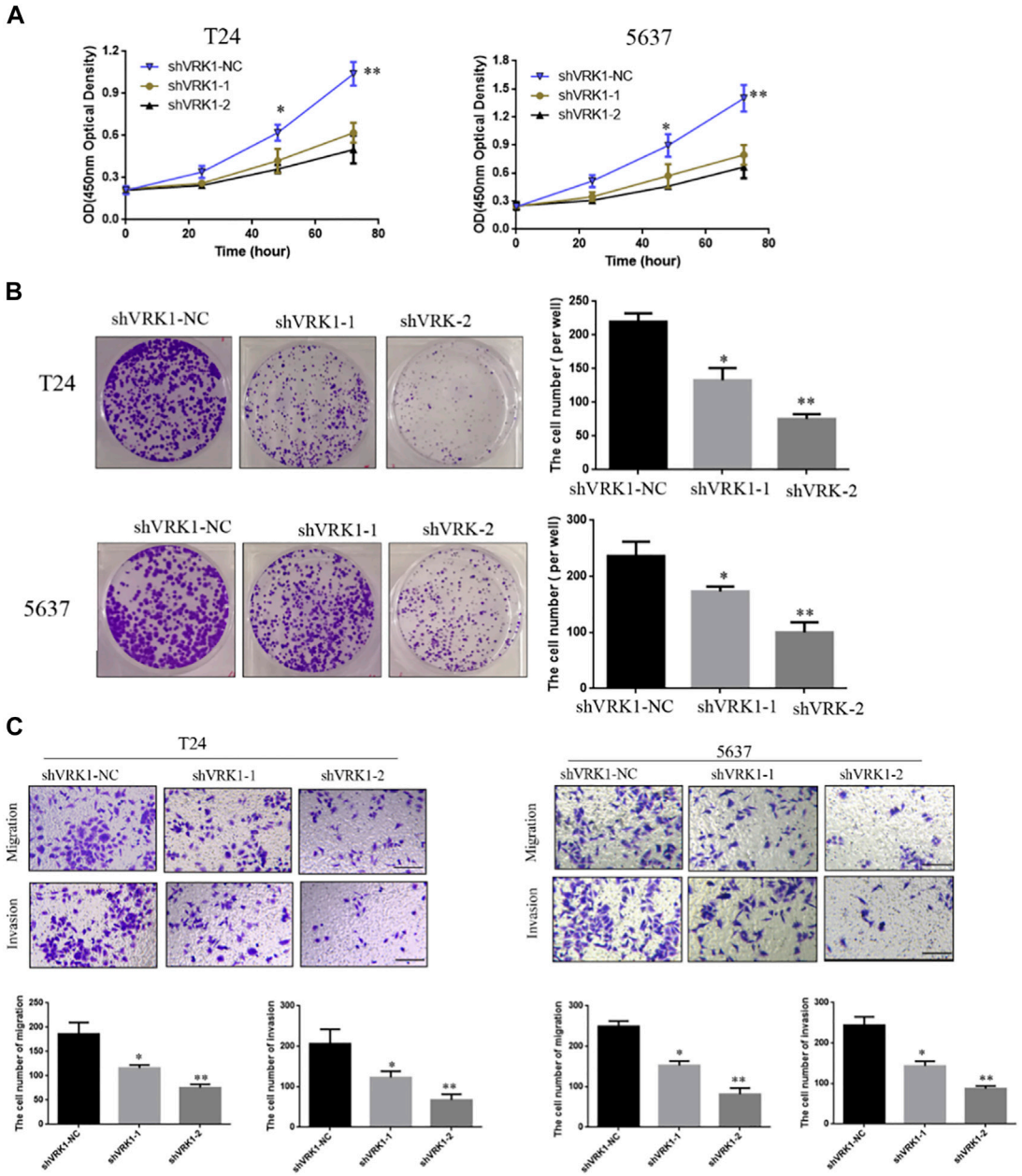

FIGURE 5 | Knockout of VRK1 inhibited the proliferation, clonal capacity, migration, and invasion of bladder cancer T24 and 5637 cells. **(A)** CCK-8 detects the effect of knocking down VRK1 on the proliferation of bladder cancer T24 and 5637 cells. **(B)** Clone formation assay: The effect of knocking down VRK1 on the cloning ability of bladder cancer T24 and 5637 cells. **(C)** The effect of knocking down VRK1 on the migration and invasion of bladder cancer T24 and 5637 cells. $^{*}p < 0.05$, $^{**}p < 0.01$; the scale is 100 μm.

(CIBERSORT) (http://cibersort.stanford.edu/) to explore the gene expression profile of the downloaded sample (Gentles et al., 2015; Ali et al., 2016; Bense et al., 2017). A total of 24 types of TIIC immune response in bladder cancer are detected to evaluate their correlation with survival and molecular subgroups. We tried to find out whether the expression of VRK1 is related to the immune infiltration of bladder cancer. We were surprised to find that pDC, NK cells, Th2 cells, Tgd, T-helper cells, NK CD56 bright cells, and mast cells are the main immune cells affected by the expression of VRK1 ($p < 0.001$). Therefore, the expression of VRK1 may also have a certain relationship with the immune infiltration of bladder cancer (**Supplementary Figure S1**). We used the string database to analyze related genes that interact with VRK1 from the perspectives of protein–protein, protein–DNA and genetic interactions, pathways, physiological and biochemical reactions, gene and protein expression, protein domains, and phenotype screening to construct a protein–protein interaction (PPI) network. Based on the

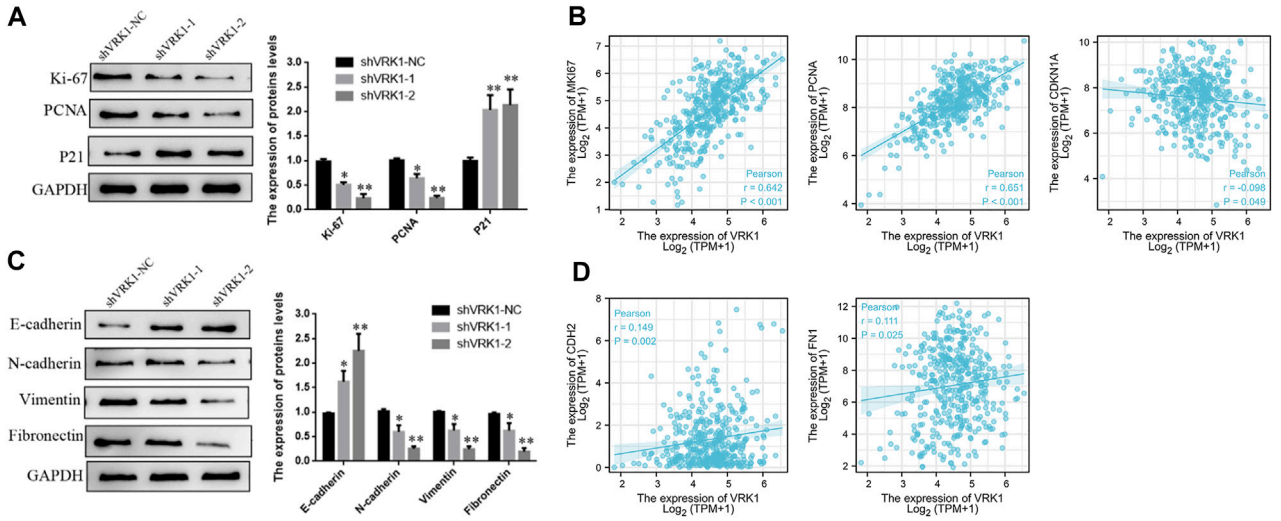

FIGURE 6 | Knockdown of VRK1 inhibited proliferation and invasion in BLCA cells. **(A)** A significant reduction of Ki-67 and PCNA but increase P21 was detected in shVRK1 cells compared to shNC cells by Western blotting. GAPDH was used as an internal control. Data are presented as means ± SD of three independent experiments. **(B)** The correlation between VRK1 and Ki67, PCNA, P21 (CDNK1A) at the mRNA level was detected in the TCGA database **(C)** A significant reduction of N-cadherin, vimentin and Fibronectin but increase E-cadherin was detected in shVRK1 cells compared to shNC cells by Western blotting. GAPDH was used as an internal control. Data are presented as means ± SD of three independent experiments. **(B,D)** The correlation between VRK1 and N-cadherin (CDH2) and Fibronectin (FN1) at the mRNA level was detected in the TCGA database $^{*}p < 0.05$, $^{**}p < 0.01$.

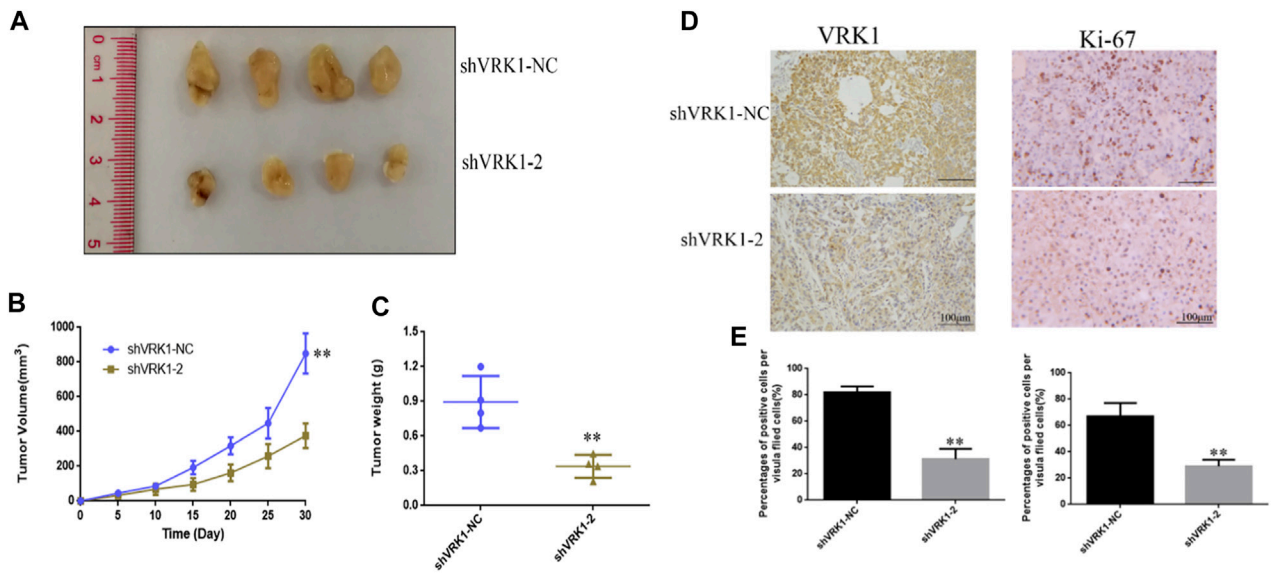

FIGURE 7 | Knockdown of VRK1 significantly inhibits the proliferation of bladder cancer cells *in vivo*. **(A)** Pictures after stripping the tumor-bearing tissue from nude mice. **(B)** Measure the tumor-bearing tissue every 5 days. **(C)** Weigh the tumor-bearing tissue. **(D,E)** Immunohistochemistry to detect the expression of VRK1 and Ki-67 in tumor-bearing tissues. $^{*}p < 0.05$, $^{**}p < 0.01$.

strength of the interaction, we selected the top 100 genes from this database (**Supplementary Figure S2**). We also used GSEA to predict possible related molecular mechanisms. We found that VRK1 may affect the biological processes of bladder cancer by participating in DNA repair, cell cycle checkpoints, NOTCH signaling pathway, WNT signaling pathway, and transcription and regulation of TP53, eventually leading to different prognosis of bladder cancer. We also used Metascape for online functional analysis. The differential genes were added to Metascape for functional analysis of GO and KEGG. GO-BP analysis found

that nucleus organization, histone modification, and covalent chromatin modification are possible cytological behaviors involved. GO-CC analysis found that condensed chromosome, chromosomal region, and spindle are possible sites involved. GO-MF analysis found that protein serine/threonine kinase activity, histone kinase activity, and nuclease activity are the molecular functions that may be affected. KEGG analysis found that cell cycle, DNA replication, and p53 signaling pathway may be affected. Studies have found that VRK1 has regulatory effects on transcription factors such as p53 (Yokobori et al., 2020), ATF2 (Sevilla et al., 2004), CREB (Kim et al., 2014), c-Jun (Martín-Doncel et al., 2019), and p300 acetyltransferase (Valbuena et al., 2008). Moreover, these transcription factors have a regulatory effect on both the progression and evolution of tumors.

Studies have also pointed out that VRK1 promotes cisplatin resistance by upregulating c-MYC through c-Jun activation and serves as a therapeutic target for esophageal squamous cell carcinoma (Liu et al., 2017). The mutual influence of VRK1 and NOTCH pathways is related to the prognosis of laryngeal cancer (de Miguel-Luken et al., 2016). VRK1 may provide new potential biomarkers for improving the prognosis and treatment of Wilms tumor (WT) patients by showing the WNT signaling pathway (Liu et al., 2021). At the same time, the WNT pathway is also a crucial pathway for regulating epithelial mesenchymal EMT. VRK1 is a member of the VRK family, which also includes VRK2 and VRK3. These members have also been reported to be mostly related to the poor prognosis of tumors. For example, VRK1 is highly expressed in many human tumors and affects the prognosis of patients. For example, the consumption of VRK1 can delay cell cycle progression and reduce the proliferation of liver cancer cells, that is, the high expression of VRK1 contributes to the cell proliferation and survival of hepatocellular carcinoma (Huang et al., 2016). VRK2 regulates tumor cell invasion through the over-activation of NFAT1 and the expression of cyclooxygenase 2 (Vázquez-Cedeira and Lazo, 2012). VRK3 is involved in the cell cycle regulation, DNA repair, and neuronal differentiation of diffuse pontine gliomas, which are the essential genes for tumor cell survival (Silva-Evangelista et al., 2019). These mature research studies also provide better help for follow-up research on the role of VRK1 in bladder cancer.

The key factors in predicting outcomes and discovering the biological mechanisms leading to poor prognosis are two important parts in cancer research (Quan et al., 2015). We verified the bladder cancer tissue of the patients we included in the study by reverse transcription qPCR, and found that the expression of VRK1 in cancer tissues was significantly higher than that in paracancerous tissues. The immunohistochemistry results also confirmed that VRK1 is highly expressed in bladder cancer tissues and mainly expressed in the nucleus. These results are also consistent with the expression of VRK1 in the database. We further analyzed the expression of VRK1 with the patient's prognosis and clinical parameters. The results reveal that the OS and PFS of patients in the VRK1 high expression group were significantly lower than those in the VRK1 low expression group ($p < 0.05$), which was also comparable to the immunohistochemistry results that patients with high VRK1 expression had worse tumor differentiation than patients with low VRK1 expression. In the analysis of clinical data, among 101 bladder cancer patients included, 43 cases (42.6%) were in the VRK1 low expression group, and 58 cases (57.4%) were in the VRK1 high expression group. The difference in tumor size between the two groups of patients was statistically significant ($p < 0.05$). This also provides some reference for our follow-up experiments to explore the role of VRK1 in the biological process of the tumorigenesis and development of bladder cancer. Further COX regression analysis indicated that the expression of VRK1 is an independent risk factor affecting tumor progression. The pathological maximum diameter, staging, and adjuvant chemotherapy also have a certain impact on tumor progression ($p < 0.05$). Based on the results of Cox regression analysis, we constructed a nomogram through a combined model and conducted internal verification, so as to have a more accurate judgment on the prediction of the 2-, 4-, and 6-year survival rate of bladder cancer patients. This is useful for the development of clinical practice. In internal verification, the C-index of the nomogram is 0.841 (95% CI is 0.803–0.880), so this prediction model also has good accuracy. Our analysis of health information and clinical data have reflected that the high expression of VRK1 is related to the poor prognosis of patients with bladder cancer, which has also aroused our interest in further research and exploration at the level of cytology and nude mice.

At the cytological level, we first used qRT-PCR to detect the expression level of VRK1 in five bladder cancer cell lines (J82, SW780, T24, 5637, and UM-UC-3) and a normal human bladder normal epithelial cell (SV-HUC- 1). The T24 and 5637 cells with high expression of VRK1 were selected as the research objects through fluorescence qPCR and Western blot. We constructed VRK knockdown cell line through lentivirus-mediated RNA interference vector for subsequent functional studies. Both CCK-8 and clone formation assay showed that knocking down VRK1 can significantly inhibit the proliferation of bladder cells (T24 and 5637). Transwell experiment results show that knocking down VRK1 can also significantly inhibit the invasion and migration ability of T24 and 5637 cells. To our surprise, further experimental studies found that knocking down VRK1 can significantly affect the expression of proliferating cell nuclear antigen Ki-67 and PNCA and promote the expression of cell cycle inhibitory protein p21. This is also consistent with the study reported by Huang et al. (2016) that the low expression of VRK1 in hepatocellular carcinoma can stabilize p53, thereby promoting the expression of P21, causing necessary cell cycle arrest and leading to a better prognosis. Knockdown of VRK1 can significantly promote the expression of E-cadherin and inhibit the expression of N-cadherin, vimentin, and fibronectin. This is also consistent with the abovementioned prediction and analysis results of GSEA that VRK1 may participate in the proliferation and metastasis of bladder cancer through certain pathways. The results of *in vitro* cytology experiments all show that VRK1 exhibits a kind of "oncogene" performance in bladder cancer cell lines. In order to better study the possible mechanism of VRK1 in the biology of bladder cancer, we conducted *in vivo* experiments.

We collected shVRK1-NC and shVRK1-2 T24 bladder cancer cells transfected with lentivirus, and then injected them under the skin of nude mice to observe and record the growth of tumor-bearing tissues. By comparing the weight of tumor-bearing tissues, we found that VRK1 knockdown can significantly inhibit the proliferation of bladder cancer cells in the body. Further immunohistochemistry results of tumor-bearing tissues suggested that the expression of VRK1 in tumor-bearing tissues of the knockdown group (shVRK1-2) was significantly lower than that of the blank control group (shVRK1-NC). Compared with the blank control group (shVRK1-NC), the expression level of Ki-67 in the knockdown group (shVRK1-2) tumor-bearing tissue was significantly reduced. *In vivo* experimental results also indicate that VRK1 has the expression status of "oncogenes" in the bladder cancer tissue.

CONCLUSION

Our research results range from bioinformatics data analysis to patient clinical data comparison and from *in vitro* cytology experiments to *in vivo* nude mouse experiments. All research results consistently reflect the positive relationship between low VRK1 expression and better prognosis of bladder cancer. Therefore, further research is necessary to clarify more specific molecular mechanisms, which will also be helpful for the development of new drug candidates for targeted therapies for bladder cancer.

DATA AVAILABILITY STATEMENT

The datasets presented in this study can be found in online repositories. The names of the repository/repositories and accession number(s) can be found in the article/**Supplementary Material**.

ETHICS STATEMENT

The studies involving human participants were reviewed and approved by the Ethics Committee of the Tumor Hospital Affiliated to Nantong University. Written informed consent for participation was not required for this study in accordance with the national legislation and the institutional requirements. The animal study was reviewed and approved by the Ethics Committee of the Tumor Hospital Affiliated to Nantong University.

AUTHOR CONTRIBUTIONS

JCW, TL, and BQZ developed the project. JCW, HJ, and BQZ performed experiments and wrote the manuscript. TL and ZC supervised the work. All authors contributed to the article and approved the submitted version.

FUNDING

This work was supported financially by grants from the Nantong science and technology plan fund (MS22019010), youth fund of Nantong Health Commission (QA2020023), the Nantong Science and Technology Bureau (MS12020046), the general project of Nantong Municipal Health Commission (MA2021021), and clinical medicine program of Nantong University (Youth Program—2019LQ013, 2019LQ011).

SUPPLEMENTARY MATERIAL

The Supplementary Material for this article can be found online at: https://www.frontiersin.org/articles/10.3389/fphar.2022.874235/full#supplementary-material

REFERENCES

Ali, H. R., Chlon, L., Pharoah, P. D., Markowetz, F., and Caldas, C. (2016). Patterns of Immune Infiltration in Breast Cancer and Their Clinical Implications: A Gene-Expression-Based Retrospective Study. *Plos Med.* 13 (12), e1002194. doi:10.1371/journal.pmed.1002194

Azimi, F., Scolyer, R. A., Rumcheva, P., Moncrieff, M., Murali, R., McCarthy, S. W., et al. (2012). Tumor-infiltrating Lymphocyte Grade Is an Independent Predictor of sentinel Lymph Node Status and Survival in Patients with Cutaneous Melanoma. *J. Clin. Oncol.* 30 (21), 2678–2683. doi:10.1200/JCO.2011.37.8539

Ben, Z., Gong, L., and Qiu, Y. (2018). High Expression of VRK1 Is Related to Poor Prognosis in Glioma. *Pathol. Res. Pract.* 214 (1), 112–118. doi:10.1016/j.prp.2017.10.014

Bense, R. D., Sotiriou, C., Piccart-Gebhart, M. J., Haanen, J. B. A. G., van Vugt, M. A. T. M., de Vries, E. G. E., et al. (2017). Relevance of Tumor-Infiltrating Immune Cell Composition and Functionality for Disease Outcome in Breast Cancer. *J. Natl. Cancer Inst.* 109 (1). doi:10.1093/jnci/djw192

Campillo-Marcos, I., García-González, R., Navarro-Carrasco, E., and Lazo, P. A. (2021). The Human VRK1 Chromatin Kinase in Cancer Biology. *Cancer Lett.* 503, 117–128. doi:10.1016/j.canlet.2020.12.032

Davis, S., and Meltzer, P. S. (2007). GEOquery: a Bridge between the Gene Expression Omnibus (GEO) and BioConductor. *Bioinformatics* 23 (14), 1846–1847. doi:10.1093/bioinformatics/btm254

de Miguel-Luken, M. J., Chaves-Conde, M., and Carnero, A. (2016). A Genetic View of Laryngeal Cancer Heterogeneity. *Cell Cycle* 15 (9), 1202–1212. doi:10.1080/15384101.2016.1156275

Del Puerto-Nevado, L., Marin-Arango, J. P., Fernandez-Aceñero, M. J., Arroyo-Manzano, D., Martinez-Useros, J., Borrero-Palacios, A., et al. (2016). Predictive Value of Vrk 1 and 2 for Rectal Adenocarcinoma Response to Neoadjuvant Chemoradiation Therapy: a Retrospective Observational Cohort Study. *BMC Cancer* 16, 519. doi:10.1186/s12885-016-2574-9

Diboun, I., Wernisch, L., Orengo, C. A., and Koltzenburg, M. (2006). Microarray Analysis after RNA Amplification Can Detect Pronounced Differences in Gene Expression Using Limma. *BMC Genomics* 7, 252. doi:10.1186/1471-2164-7-252

Gentles, A. J., Newman, A. M., Liu, C. L., Bratman, S. V., Feng, W., Kim, D., et al. (2015). The Prognostic Landscape of Genes and Infiltrating Immune Cells across Human Cancers. *Nat. Med.* 21 (8), 938–945. doi:10.1038/nm.3909

Gu, Z., Eils, R., and Schlesner, M. (2016). Complex Heatmaps Reveal Patterns and Correlations in Multidimensional Genomic Data. *Bioinformatics* 32 (18), 2847–2849. doi:10.1093/bioinformatics/btw313

Huang, W., Cui, X., Chen, Y., Shao, M., Shao, X., Shen, Y., et al. (2016). High VRK1 Expression Contributes to Cell Proliferation and Survival in Hepatocellular Carcinoma. *Pathol. Res. Pract.* 212 (3), 171–178. doi:10.1016/j.prp.2015.11.015

Kang, T. H., Park, D. Y., Choi, Y. H., Kim, K. J., Yoon, H. S., and Kim, K. T. (2007). Mitotic Histone H3 Phosphorylation by Vaccinia-Related Kinase 1 in Mammalian Cells. *Mol. Cel Biol* 27 (24), 8533–8546. doi:10.1128/MCB.00018-07

Kim, W., Chakraborty, G., Kim, S., Shin, J., Park, C. H., Jeong, M. W., et al. (2012). Macro Histone H2A1.2 (macroH2A1) Protein Suppresses Mitotic Kinase VRK1 during Interphase. *J. Biol. Chem.* 287 (8), 5278–5289. doi:10.1074/jbc.M111.281709

Kim, Y. S., Kim, S. H., Shin, J., Harikishore, A., Lim, J. K., Jung, Y., et al. (2014). Luteolin Suppresses Cancer Cell Proliferation by Targeting Vaccinia-Related Kinase 1. *PLoS One* 9 (10), e109655. doi:10.1371/journal.pone.0109655

Laurberg, J. R., Jensen, J. B., Schepeler, T., Borre, M., Ørntoft, T. F., and Dyrskjøt, L. (2014). High Expression of GEM and EDNRA Is Associated with Metastasis and Poor Outcome in Patients with Advanced Bladder Cancer. *BMC Cancer* 14, 638. doi:10.1186/1471-2407-14-638

Li, B., Xie, F., Zheng, F. X., Jiang, G. S., Zeng, F. Q., and Xiao, X. Y. (2017). Overexpression of CircRNA BCRC4 Regulates Cell Apoptosis and MicroRNA-101/EZH2 Signaling in Bladder Cancer. *J. Huazhong Univ. Sci. Technolog Med. Sci.* 37 (6), 886–890. doi:10.1007/s11596-017-1822-9

Liu, H., Zhang, M., Shi, M., Zhang, T., Zhang, Z., Cui, Q., et al. (2021). A Survival-Related Competitive Endogenous RNA Network of Prognostic lncRNAs, miRNAs, and mRNAs in Wilms Tumor. *Front. Oncol.* 11, 608433. doi:10.3389/fonc.2021.608433

Liu, T., Zuo, L., Guo, D., Chai, X., Xu, J., Cui, Z., et al. (2019). Ginsenoside Rg3 Regulates DNA Damage in Non-small Cell Lung Cancer Cells by Activating VRK1/P53BP1 Pathway. *Biomed. Pharmacother.* 120, 109483. doi:10.1016/j.biopha.2019.109483

Liu, Z. C., Cao, K., Xiao, Z. H., Qiao, L., Wang, X. Q., Shang, B., et al. (2017). VRK1 Promotes Cisplatin Resistance by Up-Regulating C-MYC via C-Jun Activation and Serves as a Therapeutic Target in Esophageal Squamous Cell Carcinoma. *Oncotarget* 8 (39), 65642–65658. doi:10.18632/oncotarget.20020

Lopez-Borges, S., and Lazo, P. A. (2000). The Human Vaccinia-Related Kinase 1 (VRK1) Phosphorylates Threonine-18 within the Mdm-2 Binding Site of the P53 Tumour Suppressor Protein. *Oncogene* 19 (32), 3656–3664. doi:10.1038/sj.onc.1203709

Martín-Doncel, E., Rojas, A. M., Cantarero, L., and Lazo, P. A. (2019). VRK1 Functional Insufficiency Due to Alterations in Protein Stability or Kinase Activity of Human VRK1 Pathogenic Variants Implicated in Neuromotor Syndromes. *Sci. Rep.* 9 (1), 13381. doi:10.1038/s41598-019-49821-7

Mon, A. M., MacKinnon, A. C., Jr., and Traktman, P. (2018). Overexpression of the VRK1 Kinase, Which Is Associated with Breast Cancer, Induces a Mesenchymal to Epithelial Transition in Mammary Epithelial Cells. *PLoS One* 13 (9), e0203397. doi:10.1371/journal.pone.0203397

Mootha, V. K., Lindgren, C. M., Eriksson, K. F., Subramanian, A., Sihag, S., Lehar, J., et al. (2003). PGC-1alpha-responsive Genes Involved in Oxidative Phosphorylation Are Coordinately Downregulated in Human Diabetes. *Nat. Genet.* 34 (3), 267–273. doi:10.1038/ng1180

Peng, D., Gong, Y. Q., Hao, H., He, Z. S., Li, X. S., Zhang, C. J., et al. (2017). Preoperative Prognostic Nutritional Index Is a Significant Predictor of Survival with Bladder Cancer after Radical Cystectomy: a Retrospective Study. *BMC Cancer* 17 (1), 391. doi:10.1186/s12885-017-3372-8

Quan, Y., Xu, M., Cui, P., Ye, M., Zhuang, B., and Min, Z. (2015). Grainyhead-like 2 Promotes Tumor Growth and Is Associated with Poor Prognosis in Colorectal Cancer. *J. Cancer* 6 (4), 342–350. doi:10.7150/jca.10969

Rajwa, P., Życzkowski, M., Paradysz, A., Bujak, K., and Bryniarski, P. (2018). Evaluation of the Prognostic Value of LMR, PLR, NLR, and dNLR in Urothelial Bladder Cancer Patients Treated with Radical Cystectomy. *Eur. Rev. Med. Pharmacol. Sci.* 22 (10), 3027–3037. doi:10.26355/eurrev_201805_15060

Sevilla, A., Santos, C. R., Vega, F. M., and Lazo, P. A. (2004). Human Vaccinia-Related Kinase 1 (VRK1) Activates the ATF2 Transcriptional Activity by Novel Phosphorylation on Thr-73 and Ser-62 and Cooperates with JNK. *J. Biol. Chem.* 279 (26), 27458–27465. doi:10.1074/jbc.M401009200

Silva-Evangelista, C., Barret, E., Ménez, V., Merlevede, J., Kergrohen, T., Saccasyn, A., et al. (2019). A Kinome-wide shRNA Screen Uncovers Vaccinia-Related Kinase 3 (VRK3) as an Essential Gene for Diffuse Intrinsic Pontine Glioma Survival. *Oncogene* 38 (38), 6479–6490. doi:10.1038/s41388-019-0884-5

Subramanian, A., Tamayo, P., Mootha, V. K., Mukherjee, S., Ebert, B. L., Gillette, M. A., et al. (2005). Gene Set Enrichment Analysis: a Knowledge-Based Approach for Interpreting Genome-wide Expression Profiles. *Proc. Natl. Acad. Sci. U S A.* 102 (43), 15545–15550. doi:10.1073/pnas.0506580102

Torre, L. A., Bray, F., Siegel, R. L., Ferlay, J., Lortet-Tieulent, J., and Jemal, A. (20122015). Global Cancer Statistics, 2012. *CA Cancer J. Clin.* 65 (2), 87–108. doi:10.3322/caac.21262

Valbuena, A., Blanco, S., Vega, F. M., and Lazo, P. A. (2008). The C/H3 Domain of P300 Is Required to Protect VRK1 and VRK2 from Their Downregulation Induced by P53. *PLoS One* 3 (7), e2649. doi:10.1371/journal.pone.0002649

Vázquez-Cedeira, M., and Lazo, P. A. (2012). Human VRK2 (Vaccinia-related Kinase 2) Modulates Tumor Cell Invasion by Hyperactivation of NFAT1 and Expression of Cyclooxygenase-2. *J. Biol. Chem.* 287 (51), 42739–42750. doi:10.1074/jbc.M112.404285

Wang, Q. H., Ji, J. L., Li, H., He, P. L., Song, L. X., Zhao, Y., et al. (2019). Preoperative Lymphocyte-To-Monocyte Ratio Predicts Prognosis in Patients with Stage T1 Non-muscle Invasive Bladder Cancer. *Zhongguo Yi Xue Ke Xue Yuan Xue Bao* 41 (5), 622–629. doi:10.3881/j.issn.1000-503X.11227

Wang, Y., and Zheng, T. (2014). Screening of Hub Genes and Pathways in Colorectal Cancer with Microarray Technology. *Pathol. Oncol. Res.* 20 (3), 611–618. doi:10.1007/s12253-013-9739-5

Yokobori, K., Miyauchi, Y., Williams, J. G., and Negishi, M. (2020). Phosphorylation of Vaccinia-Related Kinase 1 at Threonine 386 Transduces Glucose Stress Signal in Human Liver Cells. *Biosci. Rep.* 40 (4). doi:10.1042/BSR20200498

Conflict of Interest: The authors declare that the research was conducted in the absence of any commercial or financial relationships that could be construed as a potential conflict of interest.

Publisher's Note: All claims expressed in this article are solely those of the authors and do not necessarily represent those of their affiliated organizations, or those of the publisher, the editors, and the reviewers. Any product that may be evaluated in this article, or claim that may be made by its manufacturer, is not guaranteed or endorsed by the publisher.

frontiers in Oncology

REVIEW
published: 27 April 2022
doi: 10.3389/fonc.2022.859455

Dual-Targeted Therapy Circumvents Non-Genetic Drug Resistance to Targeted Therapy

Wei Wang[1], *Yue Sun*[1], *Xiaobo Liu*[1], *Shaji K. Kumar*[2], *Fengyan Jin*[3*†] *and Yun Dai*[1*†]

[1] Laboratory of Cancer Precision Medicine, The First Hospital of Jilin University, Changchun, China, [2] Division of Hematology, Mayo Clinic College of Medicine, Rochester, MN, United States, [3] Department of Hematology, The First Hospital of Jilin University, Changchun, China

OPEN ACCESS

Edited by:
Yunkai Zhang,
Vanderbilt University Medical Center, United States

Reviewed by:
Albrecht Reichle, University Medical Center Regensburg, Germany
Mohane S. Coumar, Pondicherry University, India

***Correspondence:**
Yun Dai
daiyun@jlu.edu.cn;
daiyun62@hotmail.com
Fengyan Jin
fengyanjin@jlu.edu.cn

†ORCID:
Yun Dai
orcid.org/0000-0003-2285-0818
Fengyan Jin
orcid.org/0000-0003-2288-556X

Specialty section:
This article was submitted to Cancer Molecular Targets and Therapeutics, a section of the journal Frontiers in Oncology

Received: *21 January 2022*
Accepted: *14 March 2022*
Published: *27 April 2022*

Citation:
Wang W, Sun Y, Liu X, Kumar SK, Jin F and Dai Y (2022) Dual-Targeted Therapy Circumvents Non-Genetic Drug Resistance to Targeted Therapy. Front. Oncol. 12:859455. doi: 10.3389/fonc.2022.859455

The introduction of various targeted agents into the armamentarium of cancer treatment has revolutionized the standard care of patients with cancer. However, like conventional chemotherapy, drug resistance, either preexisting (primary or intrinsic resistance) or developed following treatment (secondary or acquired resistance), remains the Achilles heel of all targeted agents with no exception, *via* either genetic or non-genetic mechanisms. In the latter, emerging evidence supports the notion that intracellular signaling pathways for tumor cell survival act as a mutually interdependent network *via* extensive cross-talks and feedback loops. Thus, dysregulations of multiple signaling pathways usually join forces to drive oncogenesis, tumor progression, invasion, metastasis, and drug resistance, thereby providing a basis for so-called "bypass" mechanisms underlying non-genetic resistance in response to targeted agents. In this context, simultaneous interruption of two or more related targets or pathways (an approach called dual-targeted therapy, DTT), *via* either linear or parallel inhibition, is required to deal with such a form of drug resistance to targeted agents that specifically inhibit a single oncoprotein or oncogenic pathway. Together, while most types of tumor cells are often addicted to two or more targets or pathways or can switch their dependency between them, DTT targeting either intrinsically activated or drug-induced compensatory targets/pathways would efficiently overcome drug resistance caused by non-genetic events, with a great opportunity that those resistant cells might be particularly more vulnerable. In this review article, we discuss, with our experience, diverse mechanisms for non-genetic resistance to targeted agents and the rationales to circumvent them in the treatment of cancer, emphasizing hematologic malignancies.

Keywords: targeted agent, non-genetic mechanism, dual-targeted therapy, parallel inhibition, drug resistance, cancer, linear inhibition, hematologic malignancy

INTRODUCTION

Targeted therapy refers to the treatment specifically targeting a protein (oncoprotein in most cases) or dysregulated pathway that drives oncogenesis. Imatinib mesylate (Gleevec), a tyrosine kinase inhibitor (TKI) targeting BCR-ABL fusion oncoprotein for treating Ph+ chronic myelogenous leukemia (CML) (1), is considered as the first targeted agent for this approach. Another prototypic

targeted agent is all-trans retinoic acid (ATRA), which acts to override the differentiation block mediated by PML-RARα fusion protein due to t(15;17) translocation in promyelocytic leukemia (PML) cells, resulting in the high efficacy of ATRA in treatment of PML (2). These successes have ignited enthusiasm to identify numerous novel molecular targets and develop a tremendous number of the first-in-class or best-in-class agents selectively against these targets. In consequence, we have witnessed an explosive increase in the number of targeted agents approved for the treatment of various cancer types, including both hematologic malignancies and solid tumors. The introduction of targeted therapy into the armamentarium for cancer treatment has initiated an era of precision medicine, which has been advanced with astonishing speed afterwards (3).

The notion of resistance to targeted agents is intimately associated with the concept of oncogene addiction (4), one of cancer hallmarks initially described in 2000 and subsequently updated and expanded (5–7). Although the mechanism by which oncogene addiction occurs remains to be elucidated with certainty, one concept holds that the genes responsible for malignant transformation may have certain lethal effects that must be overridden in order for transformed cells to survive (4). For example, c-Myc, a well-described oncogene that promotes cell proliferation, may exert a pro-apoptotic action in some circumstances. Under these conditions, over-expression of the anti-apoptotic gene Bcl-2 is required for survival of c-Myc-driven transformed cells (8). Then, such cells become dependent on Bcl-2 and thus susceptible to strategies targeting Bcl-2. In addition, transformed cells are equipped with powerful anti-stress properties to adapt not only intracellular stresses (e.g., oxidative, replicative, metabolic, etc.) during oncogenesis but also various extracellular insults (e.g., hypoxic, inflammatory, etc.) in tumor microenvironment, both of which must be overcome in order to preserve their survival and proliferative advantages over their normal counterparts (6). Moreover, oncogene addiction is dynamic due to clonal selection or evolution under therapeutic pressure, an event stemmed from tumor heterogeneity (9–11). It is common that new genetic alterations (e.g., point mutations) of either primary targeted oncogene or other related oncogenes occur during treatment with targeted agents, thus conferring resistance to those agents *via* such a genetic mechanism involving the change of addicting oncogene (named *de novo* mutation). Even more problematically, only a few types of cancer are addicted to only one oncogene for transformation and tumor cell survival, while the vast majority of malignancies rely on multiple alterations involving oncogenic and non-oncogenic proteins or pathways (12). Thus, the mechanisms of drug resistance are often multifaceted and highly heterogeneous at intratumoral or intercellular levels, as well as from genetic and non-genetic point of view (11, 13, 14). Of note, in addition to the well-recognized genetic mechanism, non-genetic mechanisms of drug resistance have been emerging as a much broader (not only for TKIs but also for non-TKI targeted agents) and more complicated challenge in cancer treatment.

In this review, we do not intend to provide a comprehensive overview of current understanding of overall mechanisms for resistance to targeted agents or strategies to circumvent them; a number of reviews dealing with these subjects have been published (9, 10, 12–15). Instead, we aim to focus on the non-genetic mechanisms by which tumor cells escape the lethal effects of targeted agents, and how rational strategies can be designed to solve this problem, with our experience.

THE ORIGIN OF DRUG RESISTANCE - INTRINSIC VERSUS ACQUIRED

As in the case of more conventional chemotherapeutic agents, resistance to targeted agents may be either intrinsic or acquired (**Figure 1**) (16). During targeted therapy, most patients carrying the driver genetic alterations (e.g., EGFR mutations in non-small cell lung cancer (NSCLC) and fusion protein BCR/ABL in CML) would respond to corresponding targeted agents thus be benefited, while some patients do not respond well and thus are considered to experience primary or intrinsic resistance. However, only a few diseases like CML are addicted to single

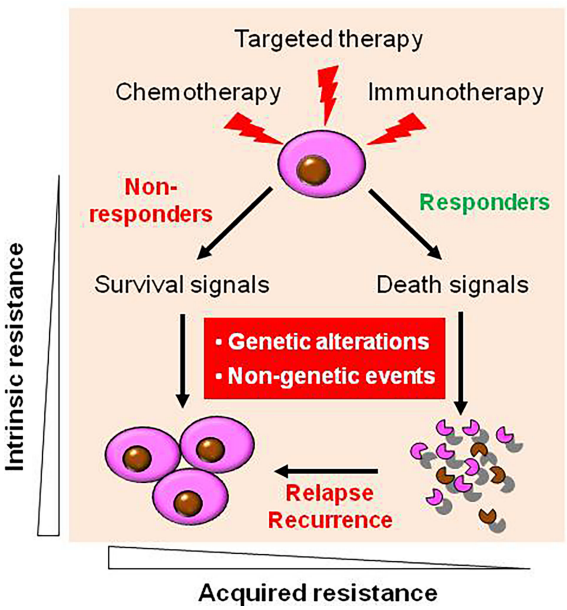

FIGURE 1 | Diverse types of drug resistance to targeted therapy. During targeted therapy as well as conventional chemotherapy and novel immunotherapy, most patients carrying the driver genetic alterations respond to corresponding targeted agents, who are known as responders, while some patients who do not respond well, who are known as non-responder, due to intrinsic (primary) resistance. However, virtually all responders will eventually relapse and become resistant to agents targeting the original oncoproteins (as well as other targeted agents in most cases) due to acquired (secondary) resistance. Mechanistically, both intrinsic and acquired resistance stem from either genetic (e.g., *de novo* mutations) or non-genetic mechanisms, or both.

oncogene (e.g., BCR-ABL), most cancer types rely on multiple oncogenic alterations, with only partial dependency upon an individual target or pathway. Patients with NSCLC expressing certain activating EGFR mutations are much more likely to respond to EGFR inhibitors (17), and thus such tumors appear to be particularly addicted to EGFR signaling for survival. Unfortunately, some patients with NSCLC carrying EGFR mutations do not respond to EGFR inhibitors, suggesting EGFR mutation-independent mechanisms such as co-occurrence of KRAS mutations (18). Similarly, patients with colon cancer carrying KRAS mutations are unlikely to respond to TKIs directed against EGFR (19). A likely explanation for this phenomenon is that activation of the Ras/Raf/MEK/ERK pathway, which lies downstream of EGFR may bypass the addiction to EGFR activation. This may also apply to the case of the PTEN/PI3K/AKT/mTOR pathway, which is activated downstream of EGFR (20, 21). The development or pre-existence of PTEN mutations may, as in the case of mutant RAS, relieve transformed cells from their dependency on EGFR signaling. In this context, interventions capable of interrupting the PTEN/PI3K/AKT pathway (e.g., by PI3K inhibitors) have been shown to be effective in this setting (22). While the mechanisms underlying this phenomenon remain to be fully elucidated, one speculative possibility is that for reasons not yet understood, the activating mutations do not require or induce activation of "orthogonal" protective pathways (4). Alternatively, in the case of KRAS mutation that is commonly considered "undruggable" (11, 23), the activation of wild-type RAS by multiple receptor tyrosine kinases (RTKs) can confer resistance to mutated-KRAS (e.g., KRAS-G12C) inhibitors (in addition to *de novo* KRAS mutations) (24), suggesting a role of "horizontal" protective pathways (4). Consequently, inhibition of such activated compensatory signaling pathways in a linear or parallel manner may render interruption of the mutant RTK particularly lethal. More importantly, it should be kept in mind that although TKIs display significant activity in patients carrying oncogenic mutations, these targeted agents are not curative, and patients ultimately die of their disease. This raises a possibility that even in the case of susceptible disease with oncogenic mutations, interrupting complementary survival signaling pathways in combination with TKIs may improve patient outcome further.

Virtually all of patients who initially respond to targeted agents eventually develop acquired resistance to these agents, with no exception thus far. Such resistance may stem from *de novo* mutations in oncoprotein that prevent drug binding to their active sites (e.g., ATP-binding site in most cases) (25). The classic example is the development of point mutations (e.g., T315I or T790M) in the ATP binding pocket of BCR/ABL or EGFR, thereby conferring resistance to TKIs by preventing their binding to targets (26). Thus, *de novo* mutation represents a primary genetic mechanism for acquired TKI resistance (1). Furthermore, such new genetic alterations are not necessary to occur only in original targets, but also involve other oncoproteins (27). For example, acquired RET fusion proteins (e.g., CCDC6-RET fusion) in NSCLC cells bearing both primary and acquired EGFR mutations (e.g., del19 and L858R/T790M) confer resistance to both first- and second-generation TKIs (e.g., AZD9291/osimertinib) (18, 28). Similar phenomenon has also been observed in the case of acquired resistance to FGFR inhibitors in different cancer types bearing FGFR mutations or fusions (29). Both *de novo* FGFR gatekeeper mutations and activation of alternate RTKs account for acquired resistance to FGFR inhibitors. However, the distinction between acquired versus intrinsic resistance may be blurred in view of evidence that resistant cells carrying "*de novo*" mutations may pre-exist, while they remain dormant (like leukemic stem cells, LSCs) but expand after leukemic blasts carrying primary targets (e.g., BCR-ABL) are selectively eliminated by targeted therapy and eventually become dominant, a process known as clonal selection or evolution (11). A main strategy to overcome such mechanisms of drug resistance, either intrinsic or acquired, is to develop new-generation of TKIs active against mutant oncoproteins (26). However, although second- and third-generation TKIs are active to bind to and target these mutants, other *de novo* mutations (e.g., gatekeeper mutations such as T315I in BCR-ABL, which cannot be effectively targeted thus far) confer resistance to these next-generation TKIs again (26). Almost identical phenomena have been observed in the case of solid tumors, such as TKIs targeting activating EGFR mutations and EML4-ALK fusion protein in NSCLC (12). Another potentially promising strategy directed against either intrinsic or acquired mechanisms of resistance involves inhibition of critical pathways downstream of the original target (termed linear inhibition; see below). For example, because many kinases, including Aurora kinase A and Polo-like kinase 1 (PLK-1), operate downstream of BCR/ABL, inhibitors of Aurora kinases or PLK-1 may bypass the resistant barrier (e.g., T315I gatekeeper mutation of BCR/ABL) to induce apoptosis in imatinib mesylate-resistant cells (30–32). The advantage of such a strategy is that inhibiting such a downstream target or pathway eliminates the need to circumvent the primary resistance mechanism (e.g., *de novo* mutation), whatever its origin (intrinsic or acquired).

Similar mechanisms may also apply to immunotherapy such as monoclonal antibodies (MoAbs) targeting cell surface receptors like HER2 in breast cancer and CD20 in lymphoma. For example, in the case of MoAbs (e.g., the HER2 MoAb trastuzumab), resistance can be acquired *via* genetic alterations in the receptor (e.g., the presence of its mutant forms that do not bind to the MoAb), competition with endogenous ligands, activation of parallel or downstream pathways, or other immunological mechanisms (10, 33).

THE NATURE OF RESISTANCE - GENETIC VS NON-GENETIC

Mechanistically, drug resistance to targeted agents, either intrinsic or acquired, can be divided into genetic (target-dependent) versus non-genetic (target-independent) (**Figure 1**) (34). In this classification, the former is primarily related to

oncogene addiction, while the latter often reflects the ability of transformed cells to escape or adapt to the lethal actions of targeted agents due to acquisition of the perturbations that protect tumor cells from lethality of targeted agents, a "bypass" mechanism (12, 27). For the genetic mechanism, the development of *de novo* mutations that prevent binding of a targeted agent to its target of interest represents a primary resistance mechanism as discussed above (35). Other mechanisms also involve addiction to multiple targets/pathways and pharmacokinetic reasons preventing achievement of effective plasma concentrations (36). For the non-genetic mechanism, replacement or substitution of tumor cell dependency often involves the activation of a complementary pathway, an event capable of transmitting alternative signals sufficient to survive from the lethal consequences of interrupting the primary pathway by a targeted agent (10).

A typical example is that the lethal consequences of blocking the Ras/Raf/MEK/ERK pathway (e.g., by BRAF inhibitors) can be compromised by the activation of the PI3K/AKT pathway in tumor cells (20, 21). Alternatively, up-regulation of anti-apoptotic proteins or down-regulation of their pro-apoptotic counterparts can abrogate the lethality of various targeted agents (especially including most TKIs) (37, 38). In general, such a non-genetic form of resistance involves a fundamental change that makes neoplastic cells no longer dependent upon primary oncogenic signals, which originally drive transformation, for their survival. Thus, the strategies to overcome drug resistance *via* increasing the degree or duration of target inhibition by pharmacokinetic means (36) or developing more potent next-generation agents are most likely to fail in this circumstance. Since tumor cells has developed, in response to a targeted agent, such a non-genetic mechanism that makes them independent of their oncogenic drivers for survival, the identification of alternative targets responsible for or involved in this form of resistance and the development of fundamentally different approaches are required to prime resistant tumor cells for death.

In this context, dysregulation of the apoptosis-regulatory machinery mediated by the Bcl-2 family represents a universal non-genetic mechanism for drug resistance to targeted agents. It has been well documented that the Bcl-2 family of pro- and anti-apoptotic proteins is ultimately responsible for determining the fate of tumor cells. Anti-apoptotic proteins (e.g., Bcl-2, Bcl-xL, Mcl-1, and A1) are often multi-domain proteins that promote cell survival either directly by preserving mitochondrial integrity, or indirectly by binding to and blocking the activity of pro-apoptotic proteins (an event known as neutralization) (37, 38). The pro-apoptotic proteins include multi-domain (e.g., Bak and Bax) and BH3-only proteins (e.g., Bim, Bid, Bik, Bad, Puma, Noxa, and Hrk) (37). Based on their mechanisms of action, these pro-apoptotic proteins can be further subdivided into activator (e.g., Bim, Bid, and Puma), which directly triggers mitochondrial injury, and sensitizer (e.g., Bad), which antagonize the functions of anti-apoptotic proteins (39). The lethal actions of various targeted agents that disrupt oncogenic signaling pathways are considered to be integrated at the level of pro- and anti-apoptotic proteins (40). For example, the intracellular levels and disposition of Bim and Bad is regulated *via* their phosphorylation by multiple upstream kinases involving major signaling pathways, particularly Ras/Raf/MEK/ERK and PI3K/AKT/mTOR (20, 41). Thus, simultaneous interruption of these pathways results in accumulation of Bad and Bim in tumor cells and thus enhances lethality (42). On the other hand, co-administration of Bcl-2 inhibitors can circumvent resistance to targeted agents due to increased expression of anti-apoptotic proteins (43). An alternative strategy is to bypass the barrier of the intrinsic, mitochondrial apoptotic pathway (due to up-regulation of anti-apoptotic proteins or down-regulation of pro-apoptotic proteins) by triggering the extrinsic apoptotic cascade *via* up-regulating and activating death receptors (44–46). Moreover, in addition to apoptosis, multiple other forms of programmed cell death (PCD e.g., necroptosis, ferroptosis, pyroptosis, etc.) with almost entirely distinctive mechanisms have been identified (47, 48), which may provide much more choices to develop therapeutic approaches, particularly for enhancing apoptosis and overcoming the resistance to apoptosis based on these unique mechanisms.

Another common non-genetic mechanism is related to autophagy, a term literally meaning "self-eating". Autophagy is a process in which cellular constituents are catabolized in the lysosome, which provides a source of energy to maintain critical cellular functions (49, 50). Autophagy thus functions as a cytoprotective mechanism to protect cells from environmental insults as well as anti-cancer treatment (particularly targeted therapy) (50). Under conditions in which autophagy protects cells from the lethal effects of targeted agents, co-administration of autophagy antagonists may dramatically increase the lethality of targeted agents (51). However, autophagy can also contribute to cell death under other circumstances. Instead of simply inhibiting autophagy, targeting the key step (e.g., cargo-loading mediated by SQSTM1/p62) leads to "inefficient" autophagy, which may more selectively kill malignant cells (52). While it could be a challenge to develop small molecule inhibitors for this kind of autophagy adaptor proteins, nanocarriers may represent an alternative and promising approach to deliver siRNA and shRNA specifically targeting molecular components that regulate autophagy (e.g., Beclin-1, LC3-II, ATGs, or even SQSTM1/p62) (53).

THE DTT STRATEGY TO OVERCOME RESISTANCE - LINEAR VS PARALLEL INHIBITION

Despite the diversity for the nature of resistance, it is certain that strategies will have to be tailored specifically to the mechanism(s) responsible for resistance. For example, improving drug pharmacokinetics through optimizing drug doses or schedules as well as ameliorating drug design (36, 54), or developing next-generation agents capable of inhibiting mutants resistant to first-generation inhibitors (55), is capable of overcoming target-dependent (genetic) resistance, but most likely not going to work for target-independent (non-genetic) resistance. For the latter, emerging evidence supports that dual-targeted therapy

(DTT), which is here defined as inhibition of two or more survival-related targets or signaling pathways, represents a promising strategy, for target-dependent and particularly target-independent forms of resistance (55). In general, inhibition of multiple targets *via* DTT includes at least two ways - parallel versus linear inhibition.

Parallel Inhibition

DTT that simultaneously inhibits two or more complementary oncogenic pathways, which cooperate to maintain transformed cell survival or confer resistance (intrinsic or acquired), may be effective when targeting either single pathway is no longer capable of triggering cell death. This kind of DTT is considered a parallel inhibition approach to overcome resistance to primary targeted agents (56). A classic example of such an approach involves the Ras/Raf/MEK/ERK and PI3K/AKT/mTOR pathways (21), both of which prevent cell death by promoting phosphorylation, at different amino acid residues, and subsequent degradation of pro-death proteins (e.g., Bim and Bad). In this context, several studies have demonstrated that regimens combining PI3K or AKT inhibitors and MEK1/2 inhibitors potently induce cell death in both solid tumor and hematologic malignancies (20, 22, 40, 57). Another example is to combine the second-generation EGFR TKI osimertinib, which is active against the most important *de novo* mutation T790M that confers resistance to first-generation EGFR TKIs, with RET inhibition to overcome resistance to osimertinib due to acquired RET fusion in NSCLC (28). Similarly, simultaneous inhibition of canonical and non-canonical NF-κB pathways can also potentiate lethality in drug-sensitive and -resistant cells (58). Moreover, a DTT approach, known as dual targeting of epigenetic therapy that combines a DNMT inhibitor with a HDAC inhibitor to simultaneously target two epigenetic mechanisms (e.g., DNA methylation and histone acetylation, respectively), has already been used to treat several myeloid malignancies (59). This approach may be extended to include agents targeting other epigenetic mechanisms (e.g., histone methylation) as well (60). Notably, as these therapeutics primarily target epigenetic modifications of DNA or histones involving the transcription-regulatory machinery, they would theoretically influence numerous downstream targets with various functions and signaling pathways. Thus, they could be good candidates suitable for the development of the DTT regimens. However, the caution needs to be taken that they may also increase the incidence of adverse effects due to the diversity of their targets.

Numerous links have been found between the cell cycle- and survival-regulatory machineries. For example, the Ras/Raf/MEK/ERK pathway has been implicated in the regulation of G2/M progression and in the disposition of cyclin D1, which is involved in the progression from G0/G1 into cell cycle (61). A DTT strategy targeting the cell cycle and survival signaling pathways involves inhibition of cell cycle checkpoints, most notably Chk1 or Wee1. Chk1 and Wee1 are key components of the DNA damage response (DDR), which trigger cell cycle arrest in cells subjected to genotoxic insults, allowing repair to occur if the damage is fixable, or apoptosis if it is not (62–64). This "self-checking" mechanism may be particularly important in maintaining survival of tumor cells harboring driver oncogenic mutations (64–66). Thus, Chk1 has been an attractive target for therapeutic intervention because it is involved in virtually all DNA damage checkpoints, and may also contribute to cell survival in a more direct manner (67). Most strategies involving the inhibitors of Chk1 or Wee1, as well as many other key components of various DDR pathways, have been combining them with various DNA-damaging agents (68). In this area, an elegant review article recently published has provided an overview of the advances and current status for the development of agents targeting DDR in various types of cancer (69). However, we observed that Chk1 inhibition triggers a compensatory activation of the Ras/Raf/MEK/ERK pathway in both hematologic malignancies and solid tumors, which may limit the lethal effect of Chk1 inhibitors (70, 71). Notably, abrogation of this signaling pathway at downstream sites (e.g., by MEK1/2 inhibitors) or more upstream sites (e.g., by farnesyltransferase or Src inhibitors) dramatically increases Chk1 inhibitor lethality (70–76). This phenomenon has been specifically attributed to potentiation of Chk1 inhibitor-mediated DNA damage (77), as well as up-regulation of the pro-apoptotic protein Bim, due to prevention of its phosphorylation and degradation *via* the ubiquitin-proteasome system (UPS) (78, 79). Such observations raise a possibility that in transformed cells, disruption of cell cycle checkpoints, which are often dysregulated in neoplasia, triggers a compensatory activation of the Ras/Raf/MEK/ERK pathway allowing them to survive, though the link between them remains unknown. Consequently, a DTT approach *via* parallel inhibition of these two critical survival pathways can lower the threshold for DNA damage-induced cell death (**Figure 2**), thus improving the anti-tumor activity of Chk1 inhibitors alone or in combination with conventional DNA-damaging agents (80, 81).

As a key family of anti-apoptotic proteins, Bcl-2 or its relatives (e.g., Bcl-xL and Mcl-1) are highly expressed in various types of cancer, particularly hematologic malignancies (e.g., lymphoma, leukemia, and multiple myeloma/MM), therefore representing one of the most attractive therapeutic targets (37, 38). However, it has taken a long time to develop the Bcl-2 inhibitor venetoclax (formerly ABT-199), which has been approved for the treatment of CLL and AML (82). One potential hurdle stems from a phenomenon that pro-apoptotic BH3-only proteins (e.g., Bim) released from one anti-apoptotic protein (e.g., Bcl-2) would bind to another anti-apoptotic protein (e.g., Mcl-1), thus disabling the lethal action of agents (e.g., Bcl-2 inhibitors) targeting only one arm of the apoptosis-regulatory machinery (83). Consequently, the activity of Bcl-2 inhibitors is inversely related to expression of Mcl-1 in tumor cells (83, 84). A corollary of this notion is that agents or interventions capable of down-regulating or inhibiting Mcl-1 could increase the activity of Bcl-2 inhibitors (85–87). Indeed, multiple such agents have been demonstrated to synergistically interact with Bcl-2 inhibitors in various hematologic malignancies. For example, CDK inhibitors that target transcription-regulatory CDKs (e.g.,

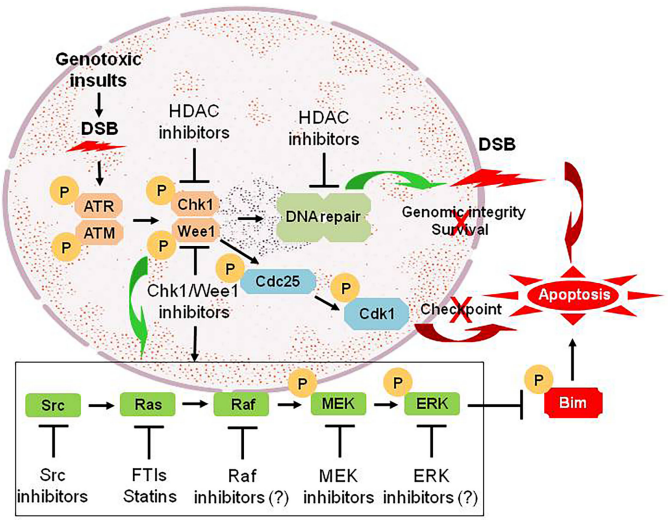

FIGURE 2 | An example for the DTT approach *via* parallel inhibition. As DNA damage checkpoint and the Ras/Raf/MEK/ERK pathway represent two separate mechanisms for maintaining genomic integrity and survival of tumor cells under intracellular and extracellular stresses (e.g., genotoxic insults caused by conventional DNA-damaging chemotherapeutics). Treatment with Chk1 (or Wee1) inhibitors promotes DNA damage by abrogating checkpoints *via* Cdc25-mediated dephosphorylation of Cdk1 at inhibitory sites, an effect that could be potentiated by HDAC inhibitors *via* down-regulation of multiple genes involving DNA damage checkpoint and repair (linear inhibition). However, they also triggers activation of the Ras/Raf/MEK/ERK pathway *via* a not-yet-defined crosstalk between these two pathways, which most likely accounts for non-genetic resistance to Chk1 (or Wee1) inhibitors. Thus, a DTT approach *via* parallel inhibition of both DNA damage checkpoint (pathway #1) and its complementary Ras/Raf/MEK/ERK signaling cascade (pathway #2; e.g., by inhibitors of Src, Ras, Raf, MEK, and ERK, which act to prevent phosphorylation and degradation of pro-apoptotic proteins such as Bim, thus priming tumor cells for death induced by targeted agents like Chk1/Wee1 inhibitors), leads to unfixable DNA damage and thus triggers robust apoptosis. DSB, double-stranded break; P, phosphorylation.

CDK9 and CDK7) and thus down-regulate Mcl-1 by disrupting the transcriptional regulatory apparatus (e.g., P-TEFb) *via* inhibiting the phosphorylation of the carboxy-terminal domain (CTD) of RNA Pol II (88–90). Analogous phenomenon has also found in the case of Mcl-1 down-regulation by B-Raf or MEK1/2 inhibitors (86, 91), or Bcl-xL down-regulation by PI3K/AKT inhibitors (92). An alternative approach is to up-regulate pro-apoptotic proteins (e.g., Bim) that prime tumor cells (e.g., by pre-occupying or saturating anti-apoptotic proteins) for death induced by Bcl-2 inhibitors (93). For example, HDAC inhibitors can up-regulate Bim in transformed cells (94), thus potentiating the activity of Bcl-2 inhibitors (95). Similarly, MEK1/2 and proteasome inhibitors prevent phosphorylation and following UPS-mediated degradation of Bim, thereby synergistically interacting with Bcl-2 inhibitors in hematologic malignancies (e.g., MM and lymphoma) (43, 96, 97).

Because the majority of targeted agents have multiple targets, attempts to understand the basis for interactions between them have been hindered by their complexity. Nevertheless, due to a variety of factors (e.g., the development of resistance or the presence or emergence of compensatory survival pathways), the need to interrupt two or more such pathways to achieve meaningful clinical benefits is now generally acknowledged. In addition, up-regulated expression of targeted oncogenic proteins also contributes to acquired resistance as observed in the case of mutant RTK-driven malignancies (1). Conventional strategies to circumvent this mechanism of acquired resistance include increasing drug doses, optimizing dosing schedules, or developing more potent next-generation kinase inhibitors active against mutant oncoproteins (55). However, these approaches may not be efficient enough, at least in certain circumstances, to overcome such a target-dependent mechanism of resistance. In this scenario, DTT combining targeted agents with inhibitors of other relevant targets/pathways *via* parallel inhibition provide an alternative, probably more effective, strategy to circumvent this resistance mechanism.

Linear Inhibition

An alternative approach for overcoming resistance is to inhibit multiple targets involving two or more "orthogonal" pathways. In the other words, it attacks critical targets downstream of the primary target or its *de novo* mutant form, therefore circumventing target-independent (non-genetic) resistance (56). Such a DTT approach can be considered a "linear inhibition" strategy, which either improves the anti-tumor efficacy of targeted therapy (e.g., TKIs) or more importantly, overcomes its acquired resistance *via* a bypass mechanism. Linear inhibition often refers to blockade of a single pathway at two or more separate sites. For example, DTT can lower the threshold for cell death triggered by the primary targeted agent by inhibiting additional survival- or proliferation-regulatory pathways. In this case, dual inhibition of the driver oncogene and its downstream target (e.g., anti-apoptotic proteins of the Bcl-2 family), which is required for survival of tumor cells under oncogene-related stress (e.g., oxidative, replicative, metabolic,

etc.) or in response to inhibition of the primary target, could yield a synergistic effect in both sensitive and resistant cells (98).

Clinical observations have shed light on the reciprocal nature of resistance versus sensitivity to targeted agents in a linear manner. For example, CML with overexpression and activation of other kinases (e.g., the Src family kinases such as Lyn, Hck, and Fyn) at downstream signaling cascade of BCR-ABL signaling are likely resistant to TKIs directed against BCR-ABL (99). Furthermore, these Src family kinases can phosphorylate BCR-ABL to alter its oncogenicity, a positive feedback to amplify this oncogenic signal. Thus, increased expression and activity of the downstream kinases of targeted oncoproteins may play an important role in determining the clinical response to TKIs and patient outcome. This may provide an explanation for the fact that multi-kinase inhibitors often display better activity against TKI-sensitive and -resistant tumor cells than those targeting only one kinase. For example, dasatinib, a dual-specific TKI targeting both BCR-ABL and the Src family kinases (e.g., Lyn) (26) is active against both imatinib-sensitive and -resistant CML *via* target-dependent or -independent mechanisms (99). In the latter, Lyn up-regulation and activation are associated with expression of Bcl-2, which is often silenced in BCR-ABL-positive CML cells, which in turn confers imatinib resistance (100). Thus, Bcl-2 inhibitors are able to overcome this form of imatinib resistance, suggesting a shift of oncogene addiction from BCR-ABL to Bcl-2 in these imatinib-resistant CML cells. Because Bcl-2 is a crucial survival factor for CML stem cells that are not addicted to BCR-ABL (26, 101), the most important factor for disease recurrence and TKI resistance (102), DTT targeting both RTK (e.g., BCR-ABL) and Bcl-2 thus represents a rational approach to circumvent acquired TKI resistance (100, 101). Other examples include simultaneous inhibition of PI3K and AKT or mTOR (103), inhibition of BCR/ABL and its downstream targets (e.g., Aurora kinase A and PLK-1) (30, 31), EGFR and MEK1/2 inhibitors (20), etc.

HDAC inhibitors, a class of epigenetic therapeutics, are truly pleiotropic agents that exert their anti-tumor activity through diverse mechanisms, including up-regulation of death receptors, generation of reactive oxygen species (ROS), disruption of multiple cell cycle checkpoints and DNA repair processes, down-regulation of survival-related proteins, and induction of pro-apoptotic proteins, among many others (104–106). Based on their multifaceted functions, it is not surprising that HDAC inhibitors have been shown to interact synergistically with multiple targeted agents as well as more conventional therapeutics, therefore representing an ideal candidate for the development of DTT (parallel or linear inhibition) (106, 107). A prototypical example for linear inhibition is activation of the NF-κB pathway as a compensatory response to HDAC inhibition. HDACs are responsible for deacetylation of multiple histones (primarily involving transcriptional regulation of gene expression) as well as numerous non-histone proteins involving cell cycle, DDR, DNA repair, cellular signaling, apoptosis, autophagy, RNA processing and stability, protein folding and aggregation, etc. (108). In this case, HDAC has also been named as lysine (K) deacetylase (KDAC). Among multiple proteins involved in cell survival decisions (105, 109), one such protein is RelA/p65, the most abundant component of the canonical NF-κB pathway, which plays an important role in drug resistance (acquired in particular) involving both solid tumor and hematologic malignancies (110, 111). Under basal conditions, RelA is bound by IκBα and sequestered in the cytoplasm, thus keeping the NF-κB pathway inactivated. Upon stimulation (e.g., by TNF-α), the activation of the IKK complex (consisting of IKKα/IKK1, IKKβ/IKK2, and IKKγ/NEMO) results in IKKβ phosphorylation (activation), which in turn phosphorylates IκBα and leads to its degradation *via* the UPS (112). This unleashes RelA, which then translocates into the nucleus where it is acetylated by histone (or lysine) acetyltransferases (HATs or KATs) and exerts its role as a transcription factor. RelA is then deacetylated by nuclear HDACs (e.g., HDAC1-3), an event required for binding of *de novo* synthesized IκBα and thus its nuclear export (113), as RelA itself lacks a nuclear export sequence. This process accounts for terminating NF-κB signal, thus making NF-κB activation as a short-term and reversible response in the case of TNF-α. However, hyperacetylation of RelA due to failure of its deacetylation (e.g., by HDAC inhibitors) leads to sustained NF-κB activation as observed in leukemic cells exposed to HDAC inhibitors (114), which in turn limits anti-tumor activity of HDAC inhibitors (115). Moreover, exposure to HDAC inhibitors also increases RelA phosphorylation (e.g., S365), an event mediated by IKKβ, which promotes its nuclear entry and susceptibility for acetylation by HATs (116). Notably, disruption of such compensatory NF-κB activation at either upstream (e.g., by IKK inhibitors that block phosphorylation of both IκBα and RelA) or downstream sites (e.g., by proteasome inhibitors that prevent IκBα degradation) interferes with RelA acetylation and nuclear import, resulting in down-regulation of NF-κB-dependent genes such as XIAP, cIAP1/2, Bcl-xL, and SOD2 (115–119). This intervention markedly increases the lethal action of HDAC inhibitors, suggesting another linear inhibition-based DTT approach (**Figure 3**). One of the examples for this approach is the combination of the HDAC inhibitor panobinostat and the proteasome inhibitor bortezomib, which has been approved to treat relapsed and refractory MM that are resistant to front-line therapy in virtually all cases. Similar phenomenon has also been observed in other hematologic malignancies (e.g., CLL and AML) when either pan-HDAC or class I HDAC inhibitors are utilized) (120, 121).

It is worth noting that DTT may be particularly appropriate when inhibition of a single component of the targeting pathway is incomplete and insufficient to trigger cell death. In this case, simultaneous interruption of this pathway at a second, downstream site may reduce survival signals below the threshold necessary to support survival. However, interruption of such a pathway at both upstream and downstream sites may be redundant, and could, at least theoretically, be counterproductive. For example, the lethal consequence of interruption of an upstream node may depend upon signaling imbalances stemming from activation of downstream targets. Thus, interruption of such conflicting signals could instead potentially attenuate the lethal consequences.

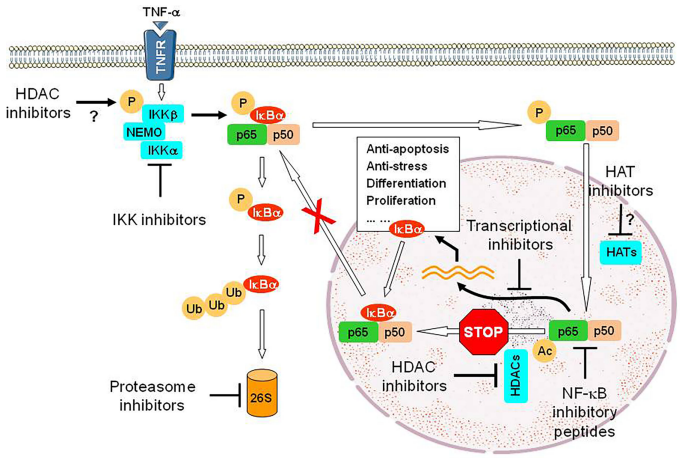

FIGURE 3 | An example for the DTT approach *via* linear inhibition. While HDAC inhibitors exhibit anti-tumor activity *via* multiple mechanisms of action, exposure to HDAC inhibitors however activates the NF-κB pathway *via* post-translational modifications of RelA/p65, a major component of this critical survival pathway, including phosphorylation mediated by IKKβ (the mechanism for IKK activation by HDAC inhibitors remains unclear) and then acetylation mediated by HATs, but failure of its deacetylation due to inhibition of nuclear HDACs (e.g., HDAC1-3). Hyperacetylation of RelA/p65 prevents its nuclear export *via* binding of *de novo* synthesized IκBα, a downstream gene of NF-κB, resulting in sustained activation of NF-κB signal and therefore counteracting the lethal action of HDAC inhibitors. Thus, a DTT approach *via* linear inhibition of this non-genetic survival pathway at multiple sites can eliminate such an "off-target" effect of HDAC inhibitors and improve their efficacy as anti-tumor epigenetic therapy, though HDAC inhibitors often display limited single-agent activity. Disruption of these sites could involve IKK inhibitors that block phosphorylation of both IκBα and RelA/p65 (preventing IκBα degradation *via* the UPS and subsequent RelA/p65 entering into the nucleus), proteasome inhibitors that block proteasomal degradation of IκBα, (thus sequestering RelA/p65 in the cytoplasm), transcriptional inhibitors (e.g., inhibitors of CDK7 and CDK9) that block the expression of NF-κB-dependent genes), inhibitory peptides directly targeting RelA/p65 or its partner p50, and probably HAT inhibitors that block acetylation of RelA/p65. P, phosphorylation; Ub, ubiquitination; Ac, acetylation; 26S, 26S proteasome.

CONCLUSION AND FUTURE DIRECTIONS

To date, the bulk of evidence suggests that targeting a single oncogenic target or pathway would most likely be insufficient to achieve meaningful clinical responses and long-term survival of patients with most cancer types, despite a few exceptions (e.g., BCR/ABL inhibitors in CML and EGFR or ALK inhibitors in NSCLC). Diverse DTT approaches combining a targeted agent with another targeted agent, chemotherapy, or immunotherapy have been required for effective treatment and even cures of cancer (56), including hematologic malignancies such as diffuse large B-cell lymphoma (DLBCL), Hodgkin's lymphoma, acute myeloid and lymphoid leukemia, and MM. Although it seems logic that targeted agents may have the capacity to enhance the activity of conventional cytotoxic agents, results with this strategy have not yet realized their potential. On the other hand, the rational combination of targeted agents, particularly those targeting complementary survival signaling or cell cycle regulatory pathways, in a parallel or linear inhibition manner, represents another promising DTT approach (**Table 1**). The notion of targeting two or more survival pathways specifically implicated in transformation offers the prospect of personalized therapy and the potential for therapeutic selectivity.

According to our and others' experience, optimization of a DTT approach requires addressing a number of unanswered questions. Among them, a key question is whether a targeted agent should have single agent activity in a particular disease in order to be of benefit in a DTT regimen. It is conceivable, although not formally proven yet, that a targeted agent inactive alone may also be able to potentiate the activity of another targeted agent if it disables a critical compensatory pathway. For example, while the HDAC inhibitor panobinostat does not show single agent activity in MM, it however enhances the efficacy of the proteasome inhibitor bortezomib in this setting, a DTT regimen approved to treat relapsed MM. Another key question is what a role of targeted agents that disrupts so-called "orthogonal" pathways downstream of driver oncogenes should play in the DTT strategies. They may ameliorate the otherwise lethal effects of oxidative, proteotoxic, DNA damage-related and other forms of stress due to the activation of oncogenes such as RAS and c-Myc. Although such inhibitors may not be as specific as those directly targeting oncoproteins that drive transformation (e.g., BCR/ABL in CML, FLT3 mutations in AML, and EGFR mutation or EML4-ALK fusion protein in NSCLC), they may disrupt the mechanisms required for maintaining survival of transformed cells and thus play an important adjunctive role in various DTT approaches. Notably, unlike in the case of TKIs, the mechanisms for drug resistance (either intrinsic or acquired) to non-TKI agents (e.g., proteasome inhibitors and IMiDs, the frontline therapy in MM treatment) remain largely unclear, most likely involving diverse and even more complicated non-genetic mechanisms (162, 163), although multiple DTT regimens (with undefined mechanisms for synergism) have already be successfully used in clinical practice.

TABLE 1 | Dual-targeted therapy (DDT) in hematologic malignancies and other cancers.

DDT strategy	Targeting pathway	MOA	Cancer type	Refs
Chk1/Wee1 inhibitor-based combinations				
Chk1 inhibitors + MEK inhibitors, FTIs, or Src inhibitors	DNA damage checkpoint & Ras/Raf/MEK/ERK pathway	Prevention of Bim phosphorylation and degradation; promotion of DNA damage; targeting myeloma stem cells; anti-angiogenesis; disrupting Ras farnesylation; activation of SEK1/JNK pathway	AML, MM, glioblastoma, breast, prostate	(70–78, 122–127)
Chk1 or Wee1 inhibitors + HDAC inhibitors	Epigenetic regulation & DNA damage checkpoints	DDR inhibition; disruption of DNA replication	AML	(63, 64)
Chk1 inhibitors + PARP1 inhibitors	DNA damage checkpoints & DNA repair	Potentiation of DNA damage	Breast, ovarian	(69, 128, 129)
HDAC inhibitor-based combinations				
HDAC inhibitors + DNMT inhibitors	DNA methylation & histone acetylation	Dual inhibition of HDACs and DNMTs; targeting CSCs	AML (approved), breast	(130, 131)
HDAC inhibitors + NAE inhibitors	DNA damage checkpoint & NEDD8	NF-κB inhibition; Bim up-regulation; inhibition of DNA repair	AML	(79)
HDAC inhibitors + TRAIL	Epigenetic regulation & extrinsic apoptotic cascade	Upregulation of DR4 and DR5	AML	(44, 132)
HDAC inhibitors + TKIs	Epigenetic regulation & oncogenic signaling	Disruption of chaperone function; overcoming TKI resistance	AML, CML, lung	(133–138)
HDAC inhibitors + Aurora kinase inhibitors	Epigenetic regulation & cell cycle	Potentiation of aurora kinase inhibition; overcoming TKI resistance	CML, kidney	(30, 139)
HDAC inhibitors + CDK inhibitors	Epigenetic regulation & cell cycle	Downregulation of Mcl-1 and $p21^{CIP1}$ *via* inhibition of RNA Pol II	AML	(140, 141)
HDAC inhibitors + IKK inhibitors	Epigenetic regulation & NF-κB pathway	Prevention of NF-κB activation by blocking RelA acetylation	AML, MM	(115, 116)
HDAC inhibitors + Bcl-2 antagonists	Epigenetic regulation & apoptosis-regulatory pathway	Up-regulation and reactivation of Bim; autophagy inhibition	AML, MM	(51, 82, 95)
HDAC inhibitors + HSP90 antagonists	Epigenetic regulation & HSP90	$p21^{CIP1}$ upregulation; Mcl-1 downregulation; inhibition of Bcr/Abl and its downstream STAT5	AML, CML	(142, 143)
HDAC inhibitors + IAP antagonists	Non-canonical NF-κB pathway & extrinsic apoptotic cascade	NF-κB inhibition; caspase 8 activation	MM	(46)
HDAC inhibitors + MLL-menin antagonists	DNA damage checkpoint & MLL-menin interaction	Disruption of DNA damage checkpoint and DNA repair	AML	(144)
Proteasome inhibitor-based combinations				
Proteasome inhibitors + HDAC inhibitors	UPS & epigenetic regulation	NF-κB inhibition; aggresome disruption; ER stress; Bim upregulation; ROS	MM (approved), CLL, ALL pancreatic cancer	(119–121, 145–148)
Proteasome inhibitors + CDK inhibitors	UPS & cell cycle	Bim upregulation; SAPK/JNK activation; NF-κB inhibition; Induction of ER stress	CML, AML, MM	(117, 149–151)
Proteasome inhibitors + Bcl-2 antagonists	UPS & apoptosis-regulatory pathway	Mcl-1 downregulation; SAPK/JNK activation; BAK activation; ROS	MM, MCL, DLBCL,CLL	(43, 96, 152, 153)
Proteasome inhibitors + IAP antagonist	UPS & cIAPs	Inhibition of canonical and non-canonical NF-κB pathways; Bcl-xL downregulation	MM	(58)
Proteasome inhibitors + XPO-1 inhibitor	UPS & NF-κB pathway	Nuclear localization of IκBα; overcome drug resistance	MM (approved)	(154, 155)
Bcl-2 antagonist-based combinations				
Bcl-2 antagonists + MEK inhibitors	Apoptosis-regulatory pathway & Ras/Raf/MEK/ERK pathway	Downregulation of Mcl-1	AML,	(86)

(Continued)

TABLE 1 | Continued

DDT strategy	Targeting pathway	MOA	Cancer type	Refs
Bcl-2 antagonists + CDK inhibitors	Apoptosis- or autophagy-regulatory pathways & transcription-regulatory machinery	Mcl-1 downregulation by RNA Pol II inhibition; down-regulation of SQSTM1/p62 (inefficient autophagy); up-regulation of pro-apoptotic BH3-only proteins; BAK/BAX activation; ROS; JNK activation	AML, MM	(51, 85, 87, 89, 90, 97, 156)
Bcl-2 inhibitors + sorafenib	Apoptosis-regulatory pathways & oncogenic signaling	Mcl-1 downregulation; Bim upregulation	AML	(157)
Bcl-2 inhibitors + TKIs	Apoptosis-regulatory pathways & oncogenic signaling	Overcoming TKI resistance; Lyn inhibition; targeting CSCs	CML, Ph+ ALL	(100, 101, 158)
MEK inhibitor-based combinations				
MEK inhibitors + TKI	Ras/Raf/MEK/ERK pathway & Bcr/Abl	Co-inhibition of Bcr/Abl downstream signals	CML	(159)
MEK inhibitors + AKT/mTOR inhibitors	Ras/Raf/MEK/ERK pathway & P13K/AKT/mTOR pathway	Prevention of feedback ERK activation; prevention of BAD degradation; Bim upregulation	AML, Prostate cancer, breast cancer, melanoma, colon cancer, glioblastoma	(20, 22, 41, 57)
MEK inhibitors + proteasome inhibitors	Ras/Raf/MEK/ERK pathway & UPS	ERK inhibition; RANKL inhibition	MM	(160)
MEK inhibitors + sorafenib	Ras/Raf/MEK/ERK pathway	Bim upregulation; Mcl-1 downregulation	DLBCL	(161)

MOA, mechanism of action; DDR, DNA damage response; HDAC, histone deacetylase; DNMT, DNA methyltransferase; CDK, cyclin-dependent kinase; NAE, NEDD8 activating enzyme; TKI, tyrosine kinase inhibitor; CSC, cancer stem cell; AML, acute myeloid leukemia, CML, chronic myeloid leukemia; MM, multiple myeloma, MCL, mantle cell lymphoma; DLBCL, diffuse large B-cell lymphoma; CLL, chronic lymphocytic leukemia; ALL, acute lymphoblastic leukemia.

The bulk of attention in this area of DTT has focused on the simultaneous interruption of two complementary survival pathways to achieve enhanced efficacy of targeted therapy thus far. However, some of the successful DTT approaches have involved more than two agents e.g., R-CHOP in DLBCL and several triplet regimens in MM. In this case, emerging evidence suggests that simultaneous interruption of more than two pathways may be required for maximal cell killing of transformed cells, or in the other words, to reduce the size of minimal residue disease (MRD), a main cause for disease recurrence (15). A future paradigm for such a DTT approach may combine targeted agents with more than two separate but somehow complementary mechanisms of action involving both linear and parallel inhibition, such as an inhibitor directly targeting oncoprotein (e.g., TKI) in conjunction with an inhibitor targeting potential compensatory survival pathway (parallel inhibition) and an inhibitor of an "orthogonal" pathway (linear inhibition).

Last, a curative approach may ultimately depend upon the eradication of both tumor cells (e.g., leukemic blasts) and cancer stem cells (CSCs e.g., leukemia-initiating cells) (164). Notably, CSCs seem not to addict to the oncogenic target or pathway for transformation (e.g., BCR/ABL for CML blasts but not CSCs) (165) but depend upon their unique survival pathways (166, 167). Indeed, a DTT approach combining inhibitors of such pathways for CSC survival and maintenance with agents targeting oncoproteins directly implicated in oncogenesis may yield results superior to those obtained with either agent alone or may overcome both genetic and non-genetic resistance (164, 167). A logical extension of this DTT approach would be to incorporate inhibitors of CSC-related pathways into the multi-agent regimens targeting two or more pathways described above. It is also worth mentioning that although resistance (either intrinsic or acquired) to immunotherapy (particularly immune checkpoint inhibitors such as PD-1 and PD-L1 MoAbs) has its unique mechanisms (e.g., those related to immune response and its regulatory machineries) (168), the principle of diverse resistance mechanisms and DTT approaches discussed above may also be implicated in this novel type of "targeted" therapy. Non-genetic mechanisms may also contribute to resistance to novel forms of targeted agents (e.g., PROTACs that act to degrade, rather than inhibit, targeted proteins) (169). In addition, with recent applications of single-cell sequencing techniques, dissection of intratumoral heterogeneity has helped identify distinctive targets and pathways in different clusters (clones) of tumor cells within the same tumor (170, 171). On the one hand, this could explain why many agents targeting a single oncoprotein (even though it drives malignant transformation or oncogenesis) presumably existed in dominant clones are not sufficient enough to kill the meaningful number of tumor cells. On the other hand, it provides a great opportunity for developing the DTT approaches that target multiple oncoproteins or survival pathways existed in different clones to achieve maximal killing of tumor cells. Given the large number of agents capable of inhibiting numerous targets currently available, DTT (linear or parallel inhibition, or both) may offer a chance of achieving the best response and long-lasting remissions or even cures of some cancer types, especially hematologic malignancies, otherwise considered fatal. Future progress in this effort is awaited with considerable anticipation.

AUTHOR CONTRIBUTIONS

YD and FJ conceptualized, wrote, edited, and revised the manuscript. YD and WW gathered and analyzed the literatures, and prepared the figures. YS and XL contributed to literature search and collection. SKK contributed to writing, editing, and revising the manuscript. All authors contributed to the article and approved the submitted version.

FUNDING

This work was supported by the National Natural Science Foundation of China (Nos. 81471165, 81670190, 81671108, 81670189, and 81870160), the Natural Science Foundation of the Jilin Province (Nos. 20190201042JC and 20190201163JC), Science and Technology Development Program of the Jilin Province (No. 20210509010RQ), and Interdisciplinary Integration and Innovation Project of JLU.

REFERENCES

1. Braun TP, Eide CA, Druker BJ. Response and Resistance to BCR-ABL1-Targeted Therapies. *Cancer Cell* (2020) 37:530–42. doi: 10.1016/j.ccell.2020.03.006
2. de The H. Differentiation Therapy Revisited. *Nat Rev Cancer* (2018) 18:117–27. doi: 10.1038/nrc.2017.103
3. Bedard PL, Hyman DM, Davids MS, Siu LL. Small Molecules, Big Impact: 20 Years of Targeted Therapy in Oncology. *Lancet* (2020) 395:1078–88. doi: 10.1016/S0140-6736(20)30164-1
4. Orlando E, Aebersold DM, Medová M, Zimmer Y. Oncogene Addiction as a Foundation of Targeted Cancer Therapy: The Paradigm of the MET Receptor Tyrosine Kinase. *Cancer Lett* (2019) 443:189–202. doi: 10.1016/j.canlet.2018.12.001
5. Hanahan D, Weinberg RA. The Hallmarks of Cancer. *Cell* (2000) 100:57–70. doi: 10.1016/s0092-8674(00)81683-9
6. Luo J, Solimini NL, Elledge SJ. Principles of Cancer Therapy: Oncogene and Non-Oncogene Addiction. *Cell* (2009) 136:823–37. doi: 10.1016/j.cell.2009.02.024
7. Hanahan D. Hallmarks of Cancer: New Dimensions. *Cancer Discov* (2022) 12:31–46. doi: 10.1158/2159-8290.CD-21-1059
8. Vaux DL, Cory S, Adams JM. Bcl-2 Gene Promotes Haemopoietic Cell Survival and Cooperates With C-Myc to Immortalize Pre-B Cells. *Nature* (1988) 335:440–2. doi: 10.1038/335440a0
9. Lim Z-F, Ma PC. Emerging Insights of Tumor Heterogeneity and Drug Resistance Mechanisms in Lung Cancer Targeted Therapy. *J Hematol Oncol* (2019) 12:134. doi: 10.1186/s13045-019-0818-2
10. Aleksakhina SN, Kashyap A, Imyanitov EN. Mechanisms of Acquired Tumor Drug Resistance. *Biochim Biophys Acta Rev Cancer* (2019) 1872:188310. doi: 10.1016/j.bbcan.2019.188310
11. Michael JV, Goldfinger LE. Concepts and Advances in Cancer Therapeutic Vulnerabilities in RAS Membrane Targeting. *Semin Cancer Biol* (2019) 54:121–30. doi: 10.1016/j.semcancer.2017.11.021
12. Lovly CM, Shaw AT. Molecular Pathways: Resistance to Kinase Inhibitors and Implications for Therapeutic Strategies. *Clin Cancer Res* (2014) 20:2249–56. doi: 10.1158/1078-0432.CCR-13-1610
13. Holohan C, Van Schaeybroeck S, Longley DB, Johnston PG. Cancer Drug Resistance: An Evolving Paradigm. *Nat Rev Cancer* (2013) 13:714–26. doi: 10.1038/nrc3599
14. Chatterjee N, Bivona TG. Polytherapy and Targeted Cancer Drug Resistance. *Trends Cancer* (2019) 5:170–82. doi: 10.1016/j.trecan.2019.02.003
15. Vasan N, Baselga J, David M, Hyman DM. A View on Drug Resistance in Cancer. *Nature* (2019) 575:299–309. doi: 10.1038/s41586-019-1730-1
16. Wang X, Zhang H, Chen X. Drug Resistance and Combating Drug Resistance in Cancer. *Cancer Drug Resist* (2019) 2:141–60. doi: 10.20517/cdr.2019.10
17. Sharma SV, Bell DW, Settleman J, Haber DA. Epidermal Growth Factor Receptor Mutations in Lung Cancer. *Nat Rev Cancer* (2007) 7:169–81. doi: 10.1038/nrc2088
18. Oxnard GR, Hu Y, Mileham KF, Husain H, Costa DB, Tracy P, et al. Assessment of Resistance Mechanisms and Clinical Implications in Patients With EGFR T790M-Positive Lung Cancer and Acquired Resistance to Osimertinib. *JAMA Oncol* (2018) 4:1527–34. doi: 10.1001/jamaoncol.2018.2969
19. Raponi M, Winkler H, Dracopoli NC. KRAS Mutations Predict Response to EGFR Inhibitors. *Curr Opin Pharmacol* (2008) 8:413–8. doi: 10.1016/j.coph.2008.06.006
20. She QB, Solit DB, Ye Q, O'Reilly KE, Lobo J, Rosen N. The BAD Protein Integrates Survival Signaling by EGFR/MAPK and PI3K/Akt Kinase Pathways in PTEN-Deficient Tumor Cells. *Cancer Cell* (2005) 8:287–97. doi: 10.1016/j.ccr.2005.09.006
21. Fruman DA, Rommel C. PI3K and Cancer: Lessons, Challenges and Opportunities. *Nat Rev Drug Discov* (2014) 13:140–56. doi: 10.1038/nrd4204
22. Kinkade CW, Castillo-Martin M, Puzio-Kuter A, Yan J, Foster TH, Gao H, et al. Targeting AKT/mTOR and ERK MAPK Signaling Inhibits Hormone-Refractory Prostate Cancer in a Preclinical Mouse Model. *J Clin Invest* (2008) 118:3051–64. doi: 10.1172/JCI34764
23. Timar J, Kashofer K. Molecular Epidemiology and Diagnostics of KRAS Mutations in Human Cancer. *Cancer Metastasis Rev* (2020) 39:1029–38. doi: 10.1007/s10555-020-09915-5
24. Awad MM, Liu S, Rybkin II, Arbour KC, Dilly J, Zhu VW, et al. Acquired Resistance to KRASG12C Inhibition in Cancer. *N Engl J Med* (2021) 384:2382–93. doi: 10.1056/NEJMoa2105281
25. Gottesman MM, Lavi O, Hall MD, Gillet J-P. Toward a Better Understanding of the Complexity of Cancer Drug Resistance. *Annu Rev Pharmacol Toxicol* (2016) 56:20.1–20.18. doi: 10.1146/annurev-pharmtox-010715-103111
26. Jabbour E, Kantarjian H. Chronic Myeloid Leukemia: 2020 Update on Diagnosis, Therapy and Monitoring. *Am J Hematol* (2020) 95:691–709. doi: 10.1002/ajh.25792
27. Shaikh M, Shinde Y, Pawara P, Noolvi M, Surana S, Ahmad I, et al. Emerging Approaches to Overcome Acquired Drug Resistance Obstacles to Osimertinib in Non-Small-Cell Lung Cancer. *J Med Chem* (2022) 65:1008-46.. doi: 10.1021/acs.jmedchem.1c00876
28. Piotrowska Z, Isozaki H, Lennerz JK, Gainor JF, Lennes IF, Zhu VW, et al. Landscape of Acquired Resistance to Osimertinib in EGFR-Mutant NSCLC and Clinical Validation of Combined EGFR and RET Inhibition With Osimertinib and BLU-667 for Acquired RET Fusion. *Cancer Discov* (2018) 8:1529–39. doi: 10.1158/2159-8290.CD-18-1022
29. Lau DK, Jenkins L, Weickhardt A. Mechanisms of Acquired Resistance to Fibroblast Growth Factor Receptor Targeted Therapy. *Cancer Drug Resist* (2019) 2:568–79. doi: 10.20517/cdr.2019.42
30. Dai Y, Chen S, Venditti CA, Pei X-Y, Nguyen TK, Dent P, et al. Vorinostat Synergistically Potentiates MK-0457 Lethality in Chronic Myelogenous Leukemia Cells Sensitive and Resistant to Imatinib Mesylate. *Blood* (2008) 112:793–804. doi: 10.1182/blood-2007-10-116376
31. Gleixner KV, Ferenc V, Peter B, Gruze A, Meyer RA, Hadzijusufovic E, et al. Polo-Like Kinase 1 (Plk1) as a Novel Drug Target in Chronic Myeloid Leukemia: Overriding Imatinib Resistance With the Plk1 Inhibitor BI 2536. *Cancer Res* (2010) 70:1513–23. doi: 10.1158/0008-5472.CAN-09-2181
32. Giles FJ, Swords RT, Nagler A, Hochhaus A, Ottmann OG, DA Rizzieri DA, et al. MK-0457, an Aurora Kinase and BCR–ABL Inhibitor, is Active in Patients With BCR–ABL T315I Leukemia. *Leukemia* (2013) 27:113–7. doi: 10.1038/leu.2012.186
33. Choong GM, Cullen GD, O'Sullivan CC. Evolving Standards of Care and New Challenges in the Management of HER2-Positive Breast Cancer. *CA Cancer J Clin* (2020) 70:355–74. doi: 10.3322/caac.21634
34. Ma L, Shan Y, Bai R, Xue L, Eide CA, Ou J, et al. A Therapeutically Targetable Mechanism of BCR-ABL Independent Imatinib Resistance in Chronic Myeloid Leukemia. *Sci Transl Med* (2014) 6:252ra121. doi: 10.1126/scitranslmed.3009073
35. Marusyk A, Janiszewska M, Polyak K. Intratumor Heterogeneity: The Rosetta Stone of Therapy Resistance. *Cancer Cell* (2020) 37:471–84. doi: 10.1016/j.ccell.2020.03.007

36. Laramy JK, Kim M, Parrish KE, Sarkaria JN, Elmquist WF. Pharmacokinetic Assessment of Cooperative Efflux of the Multitargeted Kinase Inhibitor Ponatinib Across the Blood-Brain Barrier. *J Pharmacol Exp Ther* (2018) 365:249–61. doi: 10.1124/jpet.117.246116
37. Basu A. The Interplay Between Apoptosis and Cellular Senescence: Bcl-2 Family Proteins as Targets for Cancer Therapy. *Pharmacol Ther* (2022) 230:107943.. doi: 10.1016/j.pharmthera.2021.107943
38. Wang H, Guo M, Wei H, Chen Y. Targeting MCL-1 in Cancer: Current Status and Perspectives. *J Hematol Oncol* (2021) 14:67. doi: 10.1186/s13045-021-01079-1
39. Green DR. At the Gates of Death. *Cancer Cell* (2006) 9:328–30. doi: 10.1016/j.ccr.2006.05.004
40. Watanabe D, Nogami A, Okada K, Akiyama H, Umezawa Y, Miura O. FLT3-ITD Activates RSK1 to Enhance Proliferation and Survival of AML Cells by Activating Mtorc1 and Eif4b Cooperatively With PIM or PI3K and by Inhibiting Bad and BIM. *Cancers (Basel)* (2019) 11:1827. doi: 10.3390/cancers11121827
41. Carracedo A, Ma L, Teruya-Feldstein J, Rojo F, Salmena L, Alimonti A, et al. Inhibition of Mtorc1 Leads to MAPK Pathway Activation Through a PI3K-Dependent Feedback Loop in Human Cancer. *J Clin Invest* (2008) 118:3065–74. doi: 10.1172/JCI34739
42. Han Z, Liang J, Li Y, He J. Drugs and Clinical Approaches Targeting the Antiapoptotic Protein: A Review. *BioMed Res Int* (2019) 2019:1212369. doi: 10.1155/2019/1212369
43. Pei XY, Dai Y, Grant S. The Proteasome Inhibitor Bortezomib Promotes Mitochondrial Injury and Apoptosis Induced by the Small Molecule Bcl-2 Inhibitor HA14-1 in Multiple Myeloma Cells. *Leukemia* (2003) 17:2036–45. doi: 10.1038/sj.leu.2403109
44. Insinga A, Monestiroli S, Ronzoni S, Gelmetti V, Marchesi F, Viale A, et al. Inhibitors of Histone Deacetylases Induce Tumor-Selective Apoptosis Through Activation of the Death Receptor Pathway. *Nat Med* (2005) 11:71–6. doi: 10.1038/nm1160
45. Dai Y, Dent P, Grant S. Tumor Necrosis Factor-Related Apoptosis-Inducing Ligand (TRAIL) Promotes Mitochondrial Dysfunction and Apoptosis Induced by 7-Hydroxystaurosporine and Mitogen-Activated Protein Kinase Kinase Inhibitors in Human Leukemia Cells That Ectopically Express Bcl-2 and Bcl-xL. *Mol Pharmacol* (2003) 64:1402–9. doi: 10.1124/mol.64.6.1402
46. Zhou L, Zhang Y, Meads MB, Dai Y, Ning Y, Hu X, et al. LCL161 Interacts Synergystically With Panobinostat in Multiple Myeloma Cells Through non-Canonical NF-κB- and Caspase-8-Dependent Mechanisms. *Blood Adv* (2021) 5:3776–88. doi: 10.1182/bloodadvances.2020003597
47. Chen X, Zeh HJ, Kang R, Kroemer G, Tang D. Cell Death in Pancreatic Cancer: From Pathogenesis to Therapy. *Nat Rev Gastroenterol Hepatol* (2021) 18:804–23. doi: 10.1038/s41575-021-00486-6
48. Ye L, Jin F, Kumar SK, Dai Y. The Mechanisms and Therapeutic Targets of Ferroptosis in Cancer. *Expert Opin Ther Targets* (2021) 25:965–86. doi: 10.1080/14728222.2021.2011206
49. Zhao YG, Codogno P, Zhang H. Machinery, Regulation and Pathophysiological Implications of Autophagosome Maturation. *Nat Rev Mol Cell Biol* (2021) 22:733–50. doi: 10.1038/s41580-021-00392-4
50. Dai Y, Grant S. BCL2L11/Bim as a Dual-Agent Regulating Autophagy and Apoptosis in Drug Resistance. *Autophagy* (2015) 11:416–8. doi: 10.1080/15548627.2014.998892
51. Chen S, Zhang Y, Zhou L, Leng Y, Lin H, Kmieciak M, et al. A Bim-Targeting Strategy Overcomes Adaptive Bortezomib-Resistance in Multiple Myeloma Through a Novel Link Between Autophagy and Apoptosis. *Blood* (2014) 124:2687–97. doi: 10.1182/blood-2014-03-564534
52. Chen S, Zhou L, Zhang Y, Leng Y, Pei X-Y, Lin H, et al. Targeting SQSTM1/p62 Induces Cargo-Loading Failure and Converts Autophagy to Apoptosis *Via* NBK/Bik. *Mol Cell Biol* (2014) 34:3435–49. doi: 10.1128/MCB.01383-13
53. Paskeh MDA, Entezari M, Clark C, Zabolian A, Ranjbar E, Farahani MV, et al. Targeted Regulation of Autophagy Using Nanoparticles: New Insight Into Cancer Therapy. *Biochim Biophys Acta Mol Basis Dis* (2021) 1868:166326. doi: 10.1016/j.bbadis.2021.166326
54. Ward RA, Fawell S, Floc'h N, Flemington V, McKerrecher D, Smith PD. Challenges and Opportunities in Cancer Drug Resistance. *Chem Rev* (2021) 121:3297–351. doi: 10.1021/acs.chemrev.0c00383
55. Cree IA, Charlton P. Molecular Chess? Hallmarks of Anti-Cancer Drug Resistance. *BMC Cancer* (2017) 17:10. doi: 10.1186/s12885-016-2999-1
56. Sabnis AJ, Bivona TG. Principles of Resistance to Targeted Cancer Therapy: Lessons From Basic and Translational Cancer Biology. *Trends Mol Med* (2019) 25:185–97. doi: 10.1016/j.molmed.2018.12.009
57. Rahmani M, Anderson A, Habibi JR, Crabtree TR, Mayo M, Harada H, et al. The BH3-Only Protein Bim Plays a Critical Role in Leukemia Cell Death Triggered by Concomitant Inhibition of the PI3K/Akt and MEK/ERK1/2 Pathways. *Blood* (2009) 114:4507–16. doi: 10.1182/blood-2008-09-177881
58. Zhou L, Zhang Y, Leng Y, Dai Y, Kmieciak M, Kramer L, et al. The IAP Antagonist Birinapant Potentiates Bortezomib Anti-Myeloma Activity *In Vitro* and *In Vivo*. *J Hematol Oncol* (2019) 12:25. doi: 10.1186/s13045-019-0713-x
59. Yang T, Liu X, Kumar SK, Jin F, Dai Y. Decoding DNA Methylation in Epigenetics of Multiple Myeloma. *Blood Rev* (2022) 51:100872. doi: 10.1016/j.blre.2021.100872
60. Yang C, Zhang J, Ma Y, Wu C, Cui W, Wang L. Histone Methyltransferase and Drug Resistance in Cancers. *J Exp Clin Cancer Res* (2020) 39:173. doi: 10.1186/s13046-020-01682-z
61. Wu PK, Becker A, Park JI. Growth Inhibitory Signaling of the Raf/MEK/ERK Pathway. *Int J Mol Sci* (2020) 21:5436. doi: 10.3390/ijms21155436
62. Dai Y, Pei XY, Rahmani M, Conrad DH, Dent P, Grant S. Interruption of the NF-kappaB Pathway by Bay 11-7082 Promotes UCN-01-Mediated Mitochondrial Dysfunction and Apoptosis in Human Multiple Myeloma Cells. *Blood* (2004) 103:2761–70. doi: 10.1182/blood-2003-09-3037
63. Dai Y, Chen S, Kmieciak M, Zhou L, Lin H, Pei XY, et al. The Novel Chk1 Inhibitor MK-8776 Sensitizes Human Leukemia Cells to HDAC Inhibitors by Targeting the Intra-S Checkpoint and DNA Replication and Repair. *Mol Cancer Ther* (2013) 12:878–89. doi: 10.1158/1535-7163.MCT-12-0902
64. Zhou L, Zhang Y, Chen S, Kmieciak M, Leng Y, Lin H, et al. A Regimen Combining the Wee1 Inhibitor AZD1775 With HDAC Inhibitors Targets Human Acute Myeloid Leukemia Cells Harboring Various Genetic Mutations. *Leukemia* (2015) 29:807–18. doi: 10.1038/leu.2014.296
65. Sirbu BM, Cortez D. DNA Damage Response: Three Levels of DNA Repair Regulation. *Cold Spring Harb Perspect Biol* (2013) 5:a012724. doi: 10.1101/cshperspect.a012724
66. Jia R, Kutzner L, Koren A, Runggatscher K, Májek P, Müller AC, et al. High-Throughput Drug Screening Identifies the ATR-CHK1 Pathway as a Therapeutic Vulnerability of CALR Mutated Hematopoietic Cells. *Blood Cancer J* (2021) 11:137. doi: 10.1038/s41408-021-00531-2
67. Mull BB, Livingston JA, Patel N, Bui T, Hunt KK, Keyomarsi K. Specific, Reversible G1 Arrest by UCN-01 *In Vivo* Provides Cytostatic Protection of Normal Cells Against Cytotoxic Chemotherapy in Breast Cancer. *Br J Cancer* (2020) 122:812–22. doi: 10.1038/s41416-019-0707-z
68. Klomp JE, Lee YS, Goodwin CM, Papke B, Klomp JA, Waters AM, et al. CHK1 Protects Oncogenic KRAS-Expressing Cells From DNA Damage and Is a Target for Pancreatic Cancer Treatment. *Cell Rep* (2021) 37:110060. doi: 10.1016/j.celrep.2021.110060
69. Chang HR, Jung E, Cho S, Jeon Y-J, Kim Y. Targeting non-Oncogene Addiction for Cancer Therapy. *Biomolecules* (2021) 11:129. doi: 10.3390/biom11020129
70. Dai Y, Yu C, Singh V, Tang L, Wang Z, McInistry R, et al. Pharmacological Inhibitors of the Mitogen-Activated Protein Kinase (MAPK) Kinase/MAPK Cascade Interact Synergistically With UCN-01 to Induce Mitochondrial Dysfunction and Apoptosis in Human Leukemia Cells. *Cancer Res* (2001) 61:5106–15.
71. Dai Y, Landowski TH, Rosen ST, Dent P, Grant S. Combined Treatment With the Checkpoint Abrogator UCN-01 and MEK1/2 Inhibitors Potently Induces Apoptosis in Drug-Sensitive and -Resistant Myeloma Cells Through an IL-6-Independent Mechanism. *Blood* (2002) 100:3333–43. doi: 10.1182/blood-2002-03-0940
72. Dai Y, Rahmani M, Pei XY, Khanna P, Han SI, Mitchell C, et al. Farnesyltransferase Inhibitors Interact Synergistically With the Chk1 Inhibitor UCN-01 to Induce Apoptosis in Human Leukemia Cells Through Interruption of Both Akt and MEK/ERK Pathways and Activation of SEK1/JNK. *Blood* (2005) 105:1706–16. doi: 10.1182/blood-2004-07-2767

73. Pei XY, Dai Y, Rahmani M, Li W, Dent P, Grant S. The Farnesyltransferase Inhibitor L744832 Potentiates UCN-01-Induced Apoptosis in Human Multiple Myeloma Cells. *Clin Cancer Res* (2005) 11:4589–600. doi: 10.1158/1078-0432.CCR-04-2346
74. Dai Y, Khanna P, Chen S, Pei XY, Dent P, Grant S. Statins Synergistically Potentiate 7-Hydroxystaurosporine (UCN-01) Lethality in Human Leukemia and Myeloma Cells by Disrupting Ras Farnesylation and Activation. *Blood* (2007) 109:4415–23. doi: 10.1182/blood-2006-09-047076
75. Dai Y, Chen S, Shah R, Pei X-Y, Wang L, Almenara JA, et al. Disruption of Src Function Potentiates Chk1 Inhibitor-Induced Apoptosis in Human Multiple Myeloma Cells *In Vitro* and *In Vivo*. *Blood* (2011) 117:1947–57. doi: 10.1182/blood-2010-06-291146
76. Pei X-Y, Dai Y, Youssefian LE, Chen S, Bodie WW, Takabatake Y, et al. Cytokinetically Quiescent (G0/G1) Human Multiple Myeloma Cells are Susceptible to Simultaneous Inhibition of Chk1 and MEK1/2. *Blood* (2011) 118:5189–200. doi: 10.1182/blood-2011-02-339432
77. Dai Y, Chen S, Pei X-Y, Almenara JA, Kramer LB, Venditti CA, et al. Interruption of the Ras/MEK/ERK Signaling Cascade Enhances Chk1 Inhibitor-Induced DNA Damage *In Vitro* and *In Vivo* in Human Multiple Myeloma Cells. *Blood* (2008) 112:2439–49. doi: 10.1182/blood-2008-05-159392
78. Pei XY, Dai Y, Tenorio S, Lu J, Harada H, Dent P, et al. MEK1/2 Inhibitors Potentiate UCN-01 Lethality in Human Multiple Myeloma Cells Through a Bim-Dependent Mechanism. *Blood* (2007) 110:2092–101. doi: 10.1182/blood-2007-04-083204
79. Zhou L, Chen S, Zhang Y, Kmieciak M, Leng Y, Li L, et al. The NAE Inhibitor Pevonedistat Interacts With the HDAC Inhibitor Belinostat to Target AML Cells by Disrupting the DDR. *Blood* (2016) 127:2219–30. doi: 10.1182/blood-2015-06-653717
80. Dai Y, Grant S. Molecular Pathways Feature: New Insights Into Checkpoint Kinase 1 in the DNA Damage Response Signaling Network. *Clin Cancer Res* (2010) 16:376–83. doi: 10.1158/1078-0432.CCR-09-1029
81. Dent P, Tang Y, Yacoub A, Dai Y, Fisher PB, Grant S. CHK1 Inhibitors in Combination Chemotherapy: Thinking Beyond the Cell Cycle. *Mol Interv* (2011) 11:133–40. doi: 10.1124/mi.11.2.11
82. Chen K, Yang Q, Zha J, Deng M, Zhou Y, Fu G, et al. Preclinical Evaluation of a Regimen Combining Chidamide and ABT-199 in Acute Myeloid Leukemia. *Cell Death Dis* (2020) 11:778. doi: 10.1038/s41419-020-02972-2
83. Dai Y, Grant S. Targeting Multiple Arms of the Apoptotic Regulatory Machinery. *Cancer Res* (2007) 67:2908–11. doi: 10.1158/0008-5472.CAN-07-0082
84. Deng J, Carlson N, Takeyama K, Cin PD, Shipp M, Letai A. BH3 Profiling Identifies Three Distinct Classes of Apoptotic Blocks to Predict Response to ABT-737 and Conventional Chemotherapeutic Agents. *Cancer Cell* (2007) 12:171–85. doi: 10.1016/j.ccr.2007.07.001
85. Chen S, Dai Y, Harada H, Dent P, Grant S. Mcl-1 Down-Regulation Potentiates ABT-737 Lethality by Cooperatively Inducing Bak Activation and Bax Translocation. *Cancer Res* (2007) 67(2):782–91. doi: 10.1158/0008-5472.CAN-06-3964
86. Konopleva M, Contractor R, Tsao T, Samudio I, Ruvolo PP, Kitada S, et al. Mechanisms of Apoptosis Sensitivity and Resistance to the BH3 Mimetic ABT-737 in Acute Myeloid Leukemia. *Cancer Cell* (2006) 10:375–88. doi: 10.1016/j.ccr.2006.10.006
87. Lin X, Morgan-Lappe S, Huang X, Li L, Zakula DM, Vernetti LA, et al. 'Seed' Analysis of Off-Target siRNAs Reveals an Essential Role of Mcl-1 in Resistance to the Small-Molecule Bcl-2/Bcl-XL Inhibitor ABT-737. *Oncogene* (2007) 26:3972–9. doi: 10.1038/sj.onc.1210166
88. Dai Y, Jin F, Wu W, Kumar SK. Cell Cycle Regulation and Hematologic Malignancies. *Blood Sci* (2019) 1:34–43. doi: 10.1097/BS9.0000000000000009
89. Zhou L, Zhang Y, Sampath D, Leverson J, Dai Y, Kmieciak M, et al. Flavopiridol Enhances ABT-199 Sensitivity in Unfavourable-Risk Multiple Myeloma Cells *In Vitro* and *In Vivo*. *Br J Cancer* (2018) 118:388–97. doi: 10.1038/bjc.2017.432
90. Zhang Y, Zhou L, Bandyopadhyay D, Sharma K, Allen AJ, Kmieciak M, et al. The Covalent CDK7 Inhibitor THZ1 Potently Induces Apoptosis in Multiple Myeloma Cells *In Vitro* and *In Vivo*. *Clin Cancer Res* (2019) 25:6195–205. doi: 10.1158/1078-0432.CCR-18-3788
91. Rahmani M, Davis EM, Bauer C, Dent P, Grant S. Apoptosis Induced by the Kinase Inhibitor BAY 43-9006 in Human Leukemia Cells Involves Down-Regulation of Mcl-1 Through Inhibition of Translation. *J Biol Chem* (2005) 280:35217–27. doi: 10.1074/jbc.M506551200
92. Qian J, Zou Y, Rahman JSM, Lu B, Massion PP. Synergy Between Phosphatidylinositol 3-Kinase/Akt Pathway and Bcl-xL in the Control of Apoptosis in Adenocarcinoma Cells of the Lung. *Mol Cancer Ther* (2009) 8:101–9. doi: 10.1158/1535-7163.MCT-08-0973
93. Potter DS, Letai A. To Prime, or Not to Prime: That is the Question. *Cold Spring Harb Symp Quant Biol* (2016) 81:131–40. doi: 10.1101/sqb.2016.81.030841
94. Zhao Y, Tan J, Zhuang L, Jiang X, Liu ET, Yu Q, et al. Inhibitors of Histone Deacetylases Target the Rb-E2F1 Pathway for Apoptosis Induction Through Activation of Proapoptotic Protein Bim. *Proc Natl Acad Sci USA* (2005) 102:16090–5. doi: 10.1073/pnas.0505585102
95. Chen S, Dai Y, Pei X-Y, Grant S. Bim Upregulation by Histone Deacetylase Inhibitors Mediates Interactions With the Bcl-2 Antagonist ABT-737: Evidence for Distinct Roles for Bcl-2, Bcl-Xl, and Mcl-1. *Mol Cell Biol* (2009) 29:6149–69. doi: 10.1128/MCB.01481-08
96. Paoluzzi L, Gonen M, Bhagat G, Furman RR, Gardner JR, Scotto L, et al. The BH3-Only Mimetic ABT-737 Synergizes the Antineoplastic Activity of Proteasome Inhibitors in Lymphoid Malignancies. *Blood* (2008) 112:2906–16. doi: 10.1182/blood-2007-12-130781
97. Chen S, Dai Y, Pei XY, Myers J, Wang L, Kramer LB, et al. CDK Inhibitors Up-Regulate BH3-Only Proteins to Sensitize Human Myeloma Cells to BH3 Mimetic Therapies. *Cancer Res* (2012) 72:4225–37. doi: 10.1158/0008-5472.CAN-12-1118
98. Dai Y, Grant S. Chapter 10: Rational Combination of Targeted Agents to Overcome Cancer Cell Resistance. In: Gioeli D, editor. *Targeted Therapies: Mechanisms of Resistance, Molecular and Translational Medicine*. New York, NY: Springer Science+Business Media, LLC. (2011). doi: 10.1007/978-1-60761-478-4_10
99. Wu J, Meng F, Kong L-Y, Peng Z, Ying Y, Bornmann WG, et al. Association Between Imatinib-Resistant BCR-ABL Mutation-Negative Leukemia and Persistent Activation of LYN Kinase. *J Natl Cancer Inst* (2008) 100:926–39. doi: 10.1093/jnci/djn188
100. Dai Y, Rahmani M, Corey SJ, Dent P, Grant S. A Bcr/Abl-Independent, Lyn-Dependent Form of Imatinib Mesylate (STI-571) Resistance Is Associated With Altered Expression of Bcl-2. *J Biol Chem* (2004) 279:34227–39. doi: 10.1074/jbc.M402290200
101. Carter BZ, Mak PY, Mu H, Zhou H, Mak DH, Schober W, et al. Combined Targeting of BCL-2 and BCR-ABL Tyrosine Kinase Eradicates Chronic Myeloid Leukemia Stem Cells. *Sci Transl Med* (2016) 8:355ra117. doi: 10.1126/scitranslmed.aag1180
102. Shibue T, Weinberg RA. EMT, CSCs, and Drug Resistance: The Mechanistic Link and Clinical Implications. *Nat Rev Clin Oncol* (2017) 14:611–29. doi: 10.1038/nrclinonc.2017.44
103. Bhatt AP, Bhende PM, Sin S-H, Roy D, Dittmer DP, Damania B, et al. Dual Inhibition of PI3K and mTOR Inhibits Autocrine and Paracrine Proliferative Loops in PI3K/Akt/mTOR-Addicted Lymphomas. *Blood* (2010) 115:4455–63. doi: 10.1182/blood-2009-10-251082
104. Bose P, Dai Y, Grant S. Histone Deacetylase Inhibitor (HDACI) Mechanisms of Action: Emerging Insights. *Pharmacol Ther* (2014) 143:323–36. doi: 10.1016/j.pharmthera.2014.04.004
105. Dai Y, Bose P, Grant S. Chapter 16 – Cell-Cycle Regulation and Hematologic Disorders. In: Kaushansky K, et al, editors. *Williams Hematology*, *9th Edition*. New York, NY: McGraw-Hill Education. (2015).
106. Jenke R, Reßing N, Hansen FK, Aigner A, Büch T. Anticancer Therapy With HDAC Inhibitors: Mechanism-Based Combination Strategies and Future Perspectives. *Cancers (Basel)* (2021) 13:634. doi: 10.3390/cancers13040634
107. Grant S, Dai Y. Histone Deacetylase Inhibitors and Rational Combination Therapies. *Adv Cancer Res* (2012) 116:199–37. doi: 10.1016/B978-0-12-394387-3.00006-9
108. Narita T, Weinert BT, Choudhary C. Functions and Mechanisms of Non-Histone Protein Acetylation. *Nat Rev Mol Cell Biol* (2019) 20:156–74. doi: 10.1038/s41580-018-0081-3
109. Nebbioso A, Carafa V, Conte M, Tambaro FP, Abbondanza C, Martens J, et al. C-Myc Modulation and Acetylation Is a Key HDAC Inhibitor Target in

Cancer. *Clin Cancer Res* (2017) 23:2542–55. doi: 10.1158/1078-0432.CCR-15-2388

110. Xia Y, Shen S, Verma IM. NF-κB, an Active Player in Human Cancers. *Cancer Immunol Res* (2014) 2:823–30. doi: 10.1158/2326-6066.CIR-14-0112
111. Lantermann AB, Chen D, McCutcheon K, Hoffman K, Frias E, Ruddy D, et al. Inhibition of Casein Kinase 1 Alpha Prevents Acquired Drug Resistance to Erlotinib in EGFR-Mutant Non-Small Cell Lung Cancer. *Cancer Res* (2015) 75:4937–48. doi: 10.1158/0008-5472.CAN-15-1113
112. Juvekar A, Manna S, Ramaswami S, Chang T-P, Vu H-Y, Ghosh CC, et al. Bortezomib Induces Nuclear Translocation of IκBα Resulting in Gene-Specific Suppression of NF-κB–Dependent Transcription and Induction of Apoptosis in CTCL. *Mol Cancer Res* (2011) 9:183–94. doi: 10.1158/1541-7786.MCR-10-0368
113. Chen LF, Greene WC. Regulation of Distinct Biological Activities of the NF-kappaB Transcription Factor Complex by Acetylation. *J Mol Med (Berl)* (2003) 81:549–57. doi: 10.1007/s00109-003-0469-0
114. Dai Y, Rahmani M, Grant S. An Intact NF-kappaB Pathway is Required for Histone Deacetylase Inhibitor-Induced G1 Arrest and Maturation in U937 Human Myeloid Leukemia Cells. *Cell Cycle* (2003) 2:467–72. doi: 10.4161/cc.2.5.465
115. Dai Y, Rahmani M, Dent P, Grant S. Blockade of Histone Deacetylase Inhibitor-Induced RelA/p65 Acetylation and NF-kappaB Activation Potentiates Apoptosis in Leukemia Cells Through a Process Mediated by Oxidative Damage, XIAP Downregulation, and C-Jun N-Terminal Kinase 1 Activation. *Mol Cell Biol* (2005) 25:5429–44. doi: 10.1128/mcb.25.13.5429-5444.2005
116. Dai Y, Chen S, Wang L, Pei XY, Funk VL, Kramer LB, et al. Disruption of IKK-Mediated RelA Serine 536 Phosphorylation Sensitizes Human Multiple Myeloma Cells to HDAC Inhibitors. *J Biol Chem* (2011) 286:34036–50. doi: 10.1074/jbc.M111.284216
117. Dai Y, Rahmani M, Grant S. Proteasome Inhibitors Potentiate Leukemic Cell Apoptosis Induced by the Cyclin-Dependent Kinase Inhibitor Flavopiridol Through a SAPK/JNK- and NF-KappaB-Dependent Process. *Oncogene* (2003) 22:7108–22. doi: 10.1038/sj.onc.1206863
118. Dai Y, Guzman M, Chen S, Yeung S-K, Dent P, Jordan CT, et al. The NF (Nuclear Factor)-kB Inhibitor Parthenolide Interacts With Histone Deacetylase Inhibitors to Induce MKK7/JNK1-Dependent Apoptosis in Human Acute Myeloid Leukaemia Cells. *Br J Haematol* (2010) 151:70–83. doi: 10.1111/j.1365-2141.2010.08319.x
119. Pei XY, Dai Y, Grant S. Synergistic Induction of Oxidative Injury and Apoptosis in Human Multiple Myeloma Cells by the Proteasome Inhibitor Bortezomib and Histone Deacetylase Inhibitors. *Clin Cancer Res* (2004) 10:3839–52. doi: 10.1158/1078-0432.CCR-03-0561
120. Dai Y, Chen S, Kramer LB, Funk VL, Dent P, Grant S. Interactions Between Bortezomib and Romidepsin and Belinostat in Chronic Lymphocytic Leukemia Cells. *Clin Cancer Res* (2008) 14:549–58. doi: 10.1158/1078-0432.CCR-07-1934
121. Dai Y, Chen S, Wang L, Pei X-Y, Kramer LB, Dent P, et al. Bortezomib Interacts Synergistically With Belinostat in Human AML and ALL Cells in Association With Perturbation in NF-κB and Bim. *Br J Haematol* (2011) 153:222–35. doi: 10.1111/j.1365-2141.2011.08591.x
122. Pei X-Y, Dai Y, Felthousen J, Chen S, Takabatake Y, Liang L, et al. Circumvention of Mcl-1-Dependent Drug Resistance by Simultaneous Chk1 and MEK1/2 Inhibition in Human Multiple Myeloma Cells. *PloS One* (2014) 9:e89064. doi: 10.1371/journal.pone.0089064
123. Tang Y, Dai Y, Grant S, Dent P. Enhancing CHK1 Inhibitor Lethality in Glioblastoma. *Cancer Biol Ther* (2012) 13:379–88. doi: 10.4161/cbt.19240
124. Mitchell C, Hamed HA, Cruickshanks N, Tang Y, Bareford MD, Hubbard N, et al. Simultaneous Exposure of Transformed Cells to SRC Family Inhibitors and CHK1 Inhibitors Causes Cell Death. *Cancer Biol Ther* (2011) 12:215–28. doi: 10.4161/cbt.12.3.16218
125. Hamed H, Hawkins W, Mitchell C, Gilfor D, Zhang G, Pei XY, et al. Transient Exposure of Carcinoma Cells to RAS/MEK Inhibitors and UCN-01 Causes Cell Death *In Vitro* and *In Vivo*. *Mol Cancer Ther* (2008) 7:616–29. doi: 10.1158/1535-7163.MCT-07-2376
126. Pei X-Y, Li W, Dai Y, Dent P, Grant S. Dissecting the Roles of Chk1/cdc2 and MEK1/2/ERK1/2 in Relation to UCN-01-Induced Apoptosis in Human Multiple Myeloma Cells. *Mol Pharmacol* (2006) 70:1965–73. doi: 10.1124/mol.106.028373
127. Hawkins W, Mitchell C, McKinstry R, Gilfor D, Starkey J, Dai Y, et al. Transient Exposure of Mammary Tumors to PD184352 and UCN-01 Causes Tumor Cell Death *In Vivo* and Prolonged Suppression of Tumor Regrowth. *Cancer Biol Ther* (2005) 4:1275–84. doi: 10.4161/cbt.4.11.2286
128. Booth L, Cruickshanks N, Ridder T, Dai Y, Grant S, Dent P. PARP and CHK Inhibitors Interact to Cause DNA Damage and Cell Death in Mammary Carcinoma Cells. *Cancer Biol Ther* (2013) 14:458–65. doi: 10.4161/cbt.24424
129. Tang Y, Hamed HA, Poklepovic A, Dai Y, Grant S, Dent P. Poly(ADP-Ribose) Polymerase 1 Modulates the Lethality of CHK1 Inhibitors in Mammary Tumors. *Mol Pharmacol* (2012) 82:322–32. doi: 10.1124/mol.112.078907
130. Pathania R, Ramachandran S, Mariappan G, Thakur P, Shi H, Choi J-H, et al. Combined Inhibition of DNMT and HDAC Blocks the Tumorigenicity of Cancer Stem-Like Cells and Attenuates Mammary Tumor Growth. *Cancer Res* (2016) 76:3224–35. doi: 10.1158/0008-5472.CAN-15-2249
131. Blagitko-Dorfs N, Schlosser P, Greve G, Pfeifer D, Meier R, Baude A, et al. Combination Treatment of Acute Myeloid Leukemia Cells With DNMT and HDAC Inhibitors: Predominant Synergistic Gene Downregulation Associated With Gene Body Demethylation. *Leukemia* (2019) 33:945–56. doi: 10.1038/s41375-018-0293-8
132. Rosato RR, Almenara JA, Dai Y, Grant S. Simultaneous Activation of the Intrinsic and Extrinsic Pathways by Histone Deacetylase (HDAC) Inhibitors and Tumor Necrosis Factor-Related Apoptosis-Inducing Ligand (TRAIL) Synergistically Induces Mitochondrial Damage and Apoptosis in Human Leukemia Cells. *Mol Cancer Ther* (2003) 2:1273–84.
133. Workman P, Burrows F, Neckers L, Rosen N. Drugging the Cancer Chaperone HSP90: Combinatorial Therapeutic Exploitation of Oncogene Addiction and Tumor Stress. *Ann N Y Acad Sci* (2007) 1113:202–16. doi: 10.1196/annals.1391.012
134. Yu C, Rahmani M, Almenara J, Subler M, Krystal G, Conrad C, et al. Histone Deacetylase Inhibitors Promote STI571-Mediated Apoptosis in STI571-Sensitive and -Resistant Bcr/Abl+ Human Myeloid Leukemia Cells. *Cancer Res* (2003) 63:2118–26.
135. Fiskus W, Pranpat M, Balasis M, Bali P, Estrella V, Kumaraswamy S, et al. Cotreatment With Vorinostat (Suberoylanilide Hydroxamic Acid) Enhances Activity of Dasatinib (BMS-354825) Against Imatinib Mesylate-Sensitive or Imatinib Mesylate-Resistant Chronic Myelogenous Leukemia Cells. *Clin Cancer Res* (2006) 12:5869–78. doi: 10.1158/1078-0432.CCR-06-0980
136. Bali P, George P, Cohen P, Tao J, Guo F, Sigua C, et al. Superior Activity of the Combination of Histone Deacetylase Inhibitor LAQ824 and the FLT-3 Kinase Inhibitor PKC412 Against Human Acute Myelogenous Leukemia Cells With Mutant FLT-3. *Clin Cancer Res* (2004) 10:4991–7. doi: 10.1158/1078-0432.CCR-04-0210
137. Witta SE, Gemmill RM, Hirsch FR, Coldren CD, Hedman K, Ravdel L, et al. Restoring E-Cadherin Expression Increases Sensitivity to Epidermal Growth Factor Receptor Inhibitors in Lung Cancer Cell Lines. *Cancer Res* (2006) 66:944–50. doi: 10.1158/0008-5472.CAN-05-1988
138. Nguyen T, Dai Y, Attkisson E, Kramer L, Jordan N, Nguyen N, et al. HDAC Inhibitors Potentiate the Activity of the BCR/ABL Kinase Inhibitor KW-2449 in Imatinib-Sensitive or -Resistant BCR/ABL+ Leukemia Cells *In Vitro* and *In Vivo*. *Clin Cancer Res* (2011) 17:3219–32. doi: 10.1158/1078-0432.CCR-11-0234
139. Cha TL, Chuang MJ, Wu ST, Sun G-H, Chang S-Y, Yu D-S, et al. Dual Degradation of Aurora A and B Kinases by the Histone Deacetylase Inhibitor LBH589 Induces G2-M Arrest and Apoptosis of Renal Cancer Cells. *Clin Cancer Res* (2009) 15:840–50. doi: 10.1158/1078-0432.CCR-08-1918
140. Almenara J, Rosato R, Grant S. Synergistic Induction of Mitochondrial Damage and Apoptosis in Human Leukemia Cells by Flavopiridol and the Histone Deacetylase Inhibitor Suberoylanilide Hydroxamic Acid (SAHA). *Leukemia* (2002) 16:1331–43. doi: 10.1038/sj.leu.2402535
141. Grant S, Kolla S, Sirulnik A, Shapiro G, Supko J, Cooper B, et al. Phase I Trial of Vorinostat (SAHA) in Combinatin With Alvocidib (Flavopiridol) in Patients With Refractory, Relapsed, or (Selected) Poor-Prognosis AML or Refractory Anemia With Excess Blasts-2 (RAEB-2). *Blood* (2008) 112:2986. doi: 10.1182/blood.V112.11.2986.2986
142. Rahmani M, Yu C, Dai Y, Reese E, Ahmed W, Dent P, et al. Coadministration of the Heat Shock Protein 90 Antagonist 17-

Allylamino- 17-Demethoxygeldanamycin With Suberoylanilide Hydroxamic Acid or Sodium Butyrate Synergistically Induces Apoptosis in Human Leukemia Cells. *Cancer Res* (2003) 63:8420–7.
143. Rahmani M, Reese E, Dai Y, Bauer C, Kramer LB, Huang M, et al. Cotreatment With Suberanoylanilide Hydroxamic Acid and 17-Allylamino 17-Demethoxygeldanamycin Synergistically Induces Apoptosis in Bcr-Abl+ Cells Sensitive and Resistant to STI571 (Imatinib Mesylate) in Association With Down-Regulation of Bcr-Abl, Abrogation of Signal Transducer and Activator of Transcription 5 Activity, and Bax Conformational Change. *Mol Pharmacol* (2005) 67:1166–76. doi: 10.1124/mol.104.007831
144. Ye J, Zha J, Shi Y, Li Y, Yuan D, Chen Q, et al. Co-Inhibition of HDAC and MLL-Menin Interaction Targets MLL-Rearranged Acute Myeloid Leukemia Cells *Via* Disruption of DNA Damage Checkpoint and DNA Repair. *Clin Epigenetics* (2019) 11:137. doi: 10.1186/s13148-019-0723-0
145. Mitsiades CS, Mitsiades NS, McMullan CJ, Poulaki V, Shringarpure R, Hideshima T, et al. Transcriptional Signature of Histone Deacetylase Inhibition in Multiple Myeloma: Biological and Clinical Implications. *Proc Natl Acad Sci USA* (2004) 101:540–5. doi: 10.1073/pnas.2536759100
146. Badros A, Burger AM, Philip S, Niesvizky R, Kolla SS, Goloubeva O, et al. Phase I Study of Vorinostat in Combination With Bortezomib for Relapsed and Refractory Multiple Myeloma. *Clin Cancer Res* (2009) 15:5250–7. doi: 10.1158/1078-0432.CCR-08-2850
147. Bali P, Pranpat M, Bradner J, Balasis M, Fiskus W, Guo F, et al. Inhibition of Histone Deacetylase 6 Acetylates and Disrupts the Chaperone Function of Heat Shock Protein 90: A Novel Basis of Antileukemia Activity of Histone Deacetylase Inhibitors. *J Biol Chem* (2005) 280:26729–34. doi: 10.1074/jbc.C500186200
148. Nawrocki ST, Carew JS, Dunner KJr., Boise LH, Paul J, Chiao PJ, et al. Bortezomib Inhibits PKR-Like Endoplasmic Reticulum (ER) Kinase and Induces Apoptosis *Via* ER Stress in Human Pancreatic Cancer Cells. *Cancer Res* (2005) 65:11510–9. doi: 10.1158/0008-5472.CAN-05-2394
149. Dai Y, Rahmani M, Pei XY, Dent P, Grant S. Bortezomib and Flavopiridol Interact Synergistically to Induce Apoptosis in Chronic Myeloid Leukemia Cells Resistant to Imatinib Mesylate Through Both Bcr/Abl-Dependent and -Independent Mechanisms. *Blood* (2004) 104:509–18. doi: 10.1182/blood-2003-12-4121
150. Holkova B, Perkins EB, Ramakrishnan V, Tombes MB, Shrader E, Talreja N, et al. Phase I Trial of Bortezomib (PS-341; NSC 681239) and Alvocidib (Flavopiridol; NSC 649890) in Patients With Recurrent or Refractory B-Cell Neoplasms. *Clin Cancer Res* (2011) 17:3388–97. doi: 10.1158/1078-0432.CCR-10-2876
151. Holkova B, Kmieciak M, Perkins EB, Bose P, Baz RC, Roodman GD, et al. Phase I Trial of Bortezomib (PS-341; NSC 681239) and "Nonhybrid" (Bolus) Infusion Schedule of Alvocidib (Flavopiridol; NSC 649890) in Patients With Recurrent or Refractory Indolent B-Cell Neoplasms. *Clin Cancer Res* (2014) 20:5652–62. doi: 10.1158/1078-0432.CCR-14-0805
152. Perez-Galan P, Roue G, Villamor N, Campo E, Colomer D. The BH3-Mimetic GX15–070 Synergizes With Bortezomib in Mantle Cell Lymphoma by Enhancing Noxa-Mediated Activation of Bak. *Blood* (2007) 109:4441–9. doi: 10.1182/blood-2006-07-034173
153. Trudel S, Li ZH, Rauw J, Tiedemann RE, Wen XY, Stewart AK. Preclinical Studies of the Pan-Bcl Inhibitor Obatoclax (GX015–070) in Multiple Myeloma. *Blood* (2007) 109:5430–8. doi: 10.1182/blood-2006-10-047951
154. Turner JG, Kashyap T, Dawson JL, Gomez J, Bauer AA, Grant S, et al. XPO1 Inhibitor Combination Therapy With Bortezomib or Carfilzomib Induces Nuclear Localization of IκBα and Overcomes Acquired Proteasome Inhibitor Resistance in Human Multiple Myeloma. *Oncotarget* (2016) 7:78896–909. doi: 10.18632/oncotarget.12969
155. Turner JG, Dawson JL, Grant S, Shain KH, Dalton WS, Dai Y, et al. Treatment of Acquired Drug Resistance in Multiple Myeloma by Combination Therapy With XPO1 and Topoisomerase II Inhibitors. *J Hematol Oncol* (2016) 9:73. doi: 10.1186/s13045-016-0304-z
156. Zhang Y, Zhou L, Leng Y, Dai Y, Orlowski R, Grant S. Positive Transcription Elongation Factor B (P-TEFb) is a Therapeutic Target in Human Multiple Myeloma. *Oncotarget* (2017) 8:59476–9. doi: 10.18632/oncotarget.19761
157. Zhang W, Konopleva M, Ruvolo VR, McQueen T, Evans RL, Bornmann WG, et al. Sorafenib Induces Apoptosis of AML Cells *Via* Bim-Mediated Activation of the Intrinsic Apoptotic Pathway. *Leukemia* (2008) 22:808–18. doi: 10.1038/sj.leu.2405098
158. Massimino M, Tirrò E, Stella S, Pennisi MS, Vitale SR, Puma A, et al. Targeting BCL-2 as a Therapeutic Strategy for Primary P210 BCR-ABL1-Positive B-ALL Cells. *In Vivo* (2020) 34:511–6. doi: 10.21873/invivo.11802
159. Yu C, Krystal G, Varticovksi L, McKinstry R, Rahmani M, Dent P, et al. Pharmacologic Mitogen-Activated Protein/Extracellular Signal-Regulated Kinase Kinase/Mitogen-Activated Protein Kinase Inhibitors Interact Synergistically With STI571 to Induce Apoptosis in Bcr/Abl-Expressing Human Leukemia Cells. *Cancer Res* (2002) 62:188–99.
160. Tai YT, Fulciniti M, Hideshima T, Song W, Leiba M, Li X-F, et al. Targeting MEK Induces Myeloma Cell Cytotoxicity and Inhibits Osteoclastogenesis. *Blood* (2007) 110:1656–63. doi: 10.1182/blood-2007-03-081240
161. Nguyen TK, Jordan N, Friedberg J, Fisher RI, Dent P, Grant S. Inhibition of MEK/ERK1/2 Sensitizes Lymphoma Cells to Sorafenib-Induced Apoptosis. *Leuk Res* (2010) 34:379–86. doi: 10.1016/j.leukres.2009.07.013
162. Jin F, Li W, Turner JG, Dai Y. Novel Mechanisms of Action for Immunomodulatory Drugs (IMiDs) Against Multiple Myeloma: From a Tragedy to a Therapy. *Int J Hematol Ther* (2015) 2:1–6. doi: 10.15436/2381-1404.15.008
163. Davis LN, Sherbenou DW. Emerging Therapeutic Strategies to Overcome Drug Resistance in Multiple Myeloma. *Cancers (Basel)* (2021) 13:1686. doi: 10.3390/cancers13071686
164. Jones CL, Stevens BM, D'Alessandro A, Reisz JA, Culp-Hill R, Nemkov T, et al. Inhibition of Amino Acid Metabolism Selectively Targets Human Leukemia Stem Cells. *Cancer Cell* (2018) 34:724–40.e4. doi: 10.1016/j.ccell.2018.10.005
165. Perl A, Carroll M. BCR-ABL Kinase is Dead; Long Live the CML Stem Cell. *J Clin Invest* (2011) 121:22–5. doi: 10.1172/JCI43605
166. Tanaka Y, Takeda R, Fukushima T, Mikami K, Tsuchiya S, Tamura M, et al. Eliminating Chronic Myeloid Leukemia Stem Cells by IRAK1/4 Inhibitors. *Nat Commun* (2022) 13:271. doi: 10.1038/s41467-021-27928-8
167. Zhou J, Wang S, Nie D, Lai P, Li Y, Li Y, et al. Super-Enhancer Landscape Reveals Leukemia Stem Cell Reliance on X-Box Binding Protein 1 as a Therapeutic Vulnerability. *Sci Trans Med* (2021) 13:eabh3462. doi: 10.1126/scitranslmed.abh3462
168. Fujiwara Y, Mittra A, Naqash AR, Takebe N. A Review of Mechanisms of Resistance to Immune Checkpoint Inhibitors and Potential Strategies for Therapy. *Cancer Drug Resist* (2020) 3:252–75. doi: 10.20517/cdr.2020.11
169. Zhang L, Riley-Gillis B, Vijay P, Shen Y. Acquired Resistance to BET-PROTACs (Proteolysis-Targeting Chimeras) Caused by Genomic Alterations in Core Components of E3 Ligase Complexes. *Mol Cancer Ther* (2019) 18:1302–11. doi: 10.1158/1535-7163.MCT-18-1129
170. Contreras-Trujillo H, Eerdeng J, Akre S, Jiang D, Contreras J, Gala B, et al. Deciphering Intratumoral Heterogeneity Using Integrated Clonal Tracking and Single-Cell Transcriptome Analyses. *Nat Commun* (2021) 12:6522. doi: 10.1038/s41467-021-26771-1
171. Hinohara K, Polyak K. Intratumoral Heterogeneity: More Than Just Mutations. *Trends Cell Biol* (2019) 29:569–79. doi: 10.1016/j.tcb.2019.03.003

Conflict of Interest: The authors declare that the research was conducted in the absence of any commercial or financial relationships that could be construed as a potential conflict of interest.

frontiers | Frontiers in Oncology

MINI REVIEW
published: 28 April 2022
doi: 10.3389/fonc.2022.843598

Transfer RNA-Derived Small RNAs: Novel Regulators and Biomarkers of Cancers

Bi-Fei Fu and Chao-Yang Xu *

Department of Breast and Thyroid Surgery, Affiliated Jinhua Hospital, Zhejiang University School of Medicine, Jinhua, China

Transfer RNA-derived small RNAs (tsRNAs) are conventional non-coding RNAs (ncRNAs) with a length between18 and 40 nucleotides (nt) playing a crucial role in treating various human diseases including tumours. Nowadays, with the use of high-throughput sequencing technologies, it has been proven that certain tsRNAs are dysregulated in multiple tumour tissues as well as in the blood serum of cancer patients. Meanwhile, data retrieved from the literature show that tsRNAs are correlated with the regulation of the hallmarks of cancer, modification of tumour microenvironment, and modulation of drug resistance. On the other side, the emerging role of tsRNAs as biomarkers for cancer diagnosis and prognosis is promising. In this review, we focus on the specific characteristics and biological functions of tsRNAs with a focus on their impact on various tumours and discuss the possibility of tsRNAs as novel potential biomarkers for cancer diagnosis and prognosis.

Keywords: tsRNAs, human carcinoma, biomarker, carcinogenesis, diagnosis

OPEN ACCESS

Edited by:
Jian-ye Zhang,
Guangzhou Medical University, China

Reviewed by:
Christos K. Kontos,
National and Kapodistrian University of Athens, Greece

***Correspondence:**
Chao-Yang Xu
xuchaoyang@zju.edu.cn

Specialty section:
This article was submitted to Cancer Molecular Targets and Therapeutics, a section of the journal Frontiers in Oncology

Received: *26 December 2021*
Accepted: *06 April 2022*
Published: *28 April 2022*

Citation:
Fu B-F and Xu C-Y (2022) Transfer RNA-Derived Small RNAs: Novel Regulators and Biomarkers of Cancers. Front. Oncol. 12:843598. doi: 10.3389/fonc.2022.843598

INTRODUCTION

Non-coding RNAs (ncRNAs) that exist widely in cells are not translated into proteins and can be roughly divided into two categories: small ncRNAs (sncRNAs) and long ncRNAs (lncRNAs) (1). Recent sequencing data reveal that ncRNA transcripts are four times than protein-coding RNA transcripts in human cells (2, 3). However, the majority of ncRNAs and their functions in mammals are underappreciated (4). LncRNAs are longer than 200 nt and include the most nuclear ncRNAs (5). SncRNAs are up to 200 nt in length and mainly include small interfering RNAs (siRNAs), microRNAs (miRNAs), PIWI-interacting RNAs (piRNAs), and small nucleolar RNAs (snoRNAs) (6–8). These sncRNAs have been extensively studied in the past two decades and exert complex roles in biological processes, such as inhibition of translation, metabolic modulation and others (9–11). In this review, we will focus on an emerging functional sncRNA called transfer RNA-derived small RNAs (tsRNAs).

Transfer RNAs (tRNAs) are a group of classic sncRNAs, which transport amino acids to messenger RNAs (mRNAs) during the process of translation (12). The typical two-dimensional configuration of mature tRNAs has a stem-loop structure. As it has been reported in previous studies, from the 5' to 3' end the stem-loop constructions compose the acceptor stem, the D-loop, the anti-codon loop, the variable loop and the TψC loop (13). Recent data have unveiled the role of

tRNAs' posttranscriptional modifications to dysregulation of certain genes resulting in the development of different human diseases (14, 15).

As a novel group of sncRNAs derived from tRNAs, transfer RNA-derived small RNAs (tsRNAs) are produced by specific nucleases (16). They cut specific sites of the precursor or mature tRNAs, when found under stress, infection, tumorigenesis, and other specific conditions, which are barely connected with parental tRNA abundance (17–20). Recently, multiple tsRNAs have been discovered in various tumour cells (21). Meanwhile, emerging evidence has suggested that tsRNAs play a critical role in regulating cancer hallmarks, modifying tumour microenvironment, and modulating drug resistance by involving multiple biological processes, such as inhibition of mRNA translation, promotion of ribosome biogenesis, and regulation of epigenetic processes (22–26). Moreover, these findings highlight that tsRNAs can potentially be considered as biomarkers for cancer diagnosis and prognosis (27–29).

Herein, we provide a comprehensive summary of the tsRNAs' characteristics. Furthermore, we discuss the dysregulations and functions of tsRNAs in numerous cancers and explore the possibility of tsRNAs as diagnostic and prognostic biomarkers for cancers.

BIOGENESIS AND CHARACTERISTICS OF TSRNAS

tsRNAs are conventional sncRNAs that can be classified into two major subtypes: tRNA-related small RNA fragments (tRFs) with a length of 18-30 nt and tRNA halves with a length of 30-40 nt (**Figure 1A**). tsRNAs were initially classified as degradation debris of tRNAs during biological processes and were closely related to parental tRNA abundance. However, accumulating evidence indicates that tsRNAs are enzyme-digested products of

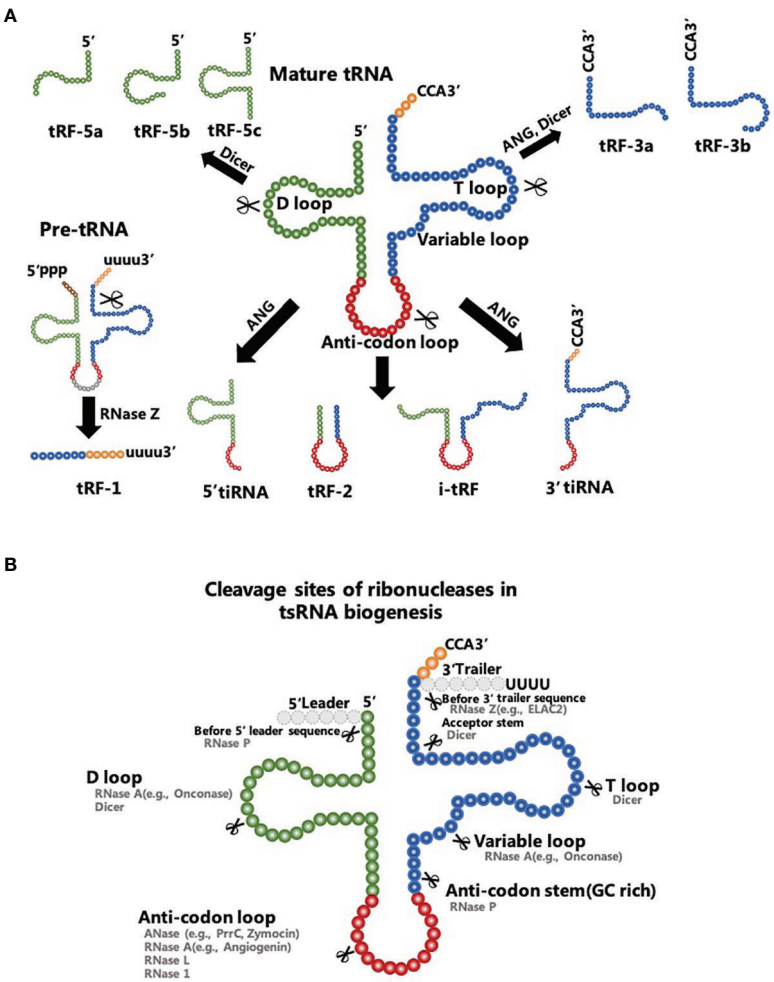

FIGURE 1 | Biogenesis and characteristics of tsRNAs. **(A)** tRF-1s are products of the RNase Z clipping off the 3'-end of precursor tRNAs. tRF-5s are generated from the 5'-tail of mature tRNAs to the D-loop or the sequence between the D-loop and the anti-codon loop of a mature tRNA. tRF-3s are derived from the TψC loop to the 3' end of mature tRNAs. tRF-2s comprise the sequence straddling the anti-codon loop of mature tRNAs. i-tRFs comprise the anti-codon loop of mature tRNAs and sections of the D-loop and T-loop. **(B)** Ribonucleases in tsRNA biogenesis include Dicer, RNase P, RNase 1 and others with their known cleavage sites.

exact nucleases that cut into concrete sites of precursor or mature tRNAs under specific conditions, such as stress, infection, neurodegeneration, and tumorigenesis (30–33). In addition, authors report that tsRNAs have various types of RNA modifications, including methylation modification, modification of the 5'-hydroxyl terminal and 2', 3'-cyclic phosphorylation modification (34). These modifications have been proposed to depend on their precursor tRNAs and the type of enzymatic processing (35). Thus tsRNAs are not considered random tRNA degradation byproducts, but a cluster of functional molecules with high stability and inherent conservation (35, 36). Interestingly, data reveal the pivotal role of all these types of regulatory tsRNAs in post-transcriptional regulation in cancer cells (37, 38).

Five classes of tRFs are known and they are tRF-1s, tRF-2s, tRF-3s, tRF-5s, and i-tRFs (39). Besides the fact that the tRF-1s are products of the ribonuclease Z (RNase Z) clipping off the 3'-end of precursor tRNAs (40), other tRFs have proven to be enzyme-digested products of mature tRNAs (41). Dicer, angiogenin (ANG), and other particular ribonucleases participate in the digesting processes of these mature tRNAs (**Figure 1B**). A tRF-5s is generated from the 5'-tail of a mature tRNA to the D-loop (tRF-5a) or the sequence between the D-loop and the anti-codon loop (tRF-5b and tRF-5c) of a mature tRNA. tRF-5s are typically produced by Dicer and ANG cleavage into the different termination site between 5' end and the anti-codon loop. tRF-3s that mainly contain tRF-3a and tRF-3b are derived from the TψC loop to the 3' end of mature tRNAs. Dicer is the main ribonuclease cutting into the TψC loop to produce tRF-3s. In that sense, tRF-2s comprise the sequence straddling the anti-codon loop of mature tRNAs with variable lengths. Alternatively, i-tRFs comprise the anti-codon loop of mature tRNAs and sections of the D-loop and T-loop. The specific mechanism of tRF-2s/i-tRFs production remains unclear (42).

tRNA halves, as the name suggests, are derived from the 5′ end of mature tRNAs to the terminus of the anti-codon loop (5′-tRNA halves) or start at the anti-codon loop and proceed to the 3' end of mature tRNAs (3′-tRNA halves). Findings retrieved from the literature indicate that these tsRNAs are mainly involved in hypoxic conditions, nutritional deficiency, heat shock, and other conditions of stress (43). Therefore, tRNA halves are universally called tRNA-derived stress-induced RNAs (tiRNAs) that act as effectors of cellular stress responses (44). tiRNAs are known to be produced by ANG which knockdown considerably reduces the level of tiRNAs in human U2OS cells (45). In a recent study, Su et al. found that production of certain tiRNAs was dependent on RNase L cleavage and hence ANG was not the only ribonuclease to produce tiRNAs (46). Interestingly, the other type of tRNA halves known as the sex hormone-dependent tRNA-derived RNAs (SHOT-RNAs) are not induced by various stress stimuli, but they are highly expressed in hormone receptor-positive breast and prostate cancer cells (47). Therefore, SHOT-RNAs represent a separated category of tRNA halves with distinct specificity of expression (48).

tsRNA biogenesis is regulated by tRNA modifications. It has been reported that two (cytosine-5) RNA methyltransferases, DNMT2 and NSUN2, add 5-methylcytosine (m^5C) modification to particular tRNAs. Thus they protect tRNAs from cleavage into tsRNAs in mice (49). The tRNA methyltransferase 10 homolog A (TRMT10A) was also found to mediate N1-methylguanine (m^1G) modification to several tRNAs and decrease tsRNA's production (50). In addition, the queuine tRNA-ribosylthansferase catalytic subunit 1 (QTRT1)-dependent addition of queuosine (Q) modification to several tRNAs increases tRNA stability in HEK293T cells (51). Moreover, 2'-O-methylation modification of the C34 residue in the $tRNA^{Met}$ can inhibit tRNA degradation by ANG and decrease tsRNA production (52). Except for preventing tsRNA biogenesis, some tRNA modifications have promoted tRNA cleavage into tsRNAs (35). For example, pseudouridylate synthase 7 homolog (PUS7)-dependent addition of pseudouridine (Ψ) modification to several tRNAs promotes tsRNA biogenesis in stem cells (53). A recent study demonstrated that the knockout of ALKBH1 or ALKBH3 genes increases N1-methyladenine (m^1A) modification in several tRNAs and lowers the abundance of tsRNAs in human 293T cells (54). In another study, the 5-methoxycarbonylmethyl-2-thiouridine (mcm^5s^2U) modification at position 34 (wobble position) was found to promote efficient cleavage of substrate tRNAs into yeast tsRNAs (55). In this regard, it is of great importance to mention that tRNA modification not only correlates to tsRNA biogenesis but is also associated with changes in tsRNA functions. The last occurs due to the abovementioned modifications, which have posed challenges for tsRNA library preparation and the conduction of studies concerning the mechanism of tsRNAs.

To date, the next-generation sequencing data allowed a deeper analysis of the obtained evidence, researchers have made remarkable progress in terms of the biogenesis and classification of tsRNAs. Meanwhile, online databases like tsRBase and OncotRF providing validated tsRNAs are emerging (56, 57) (**Table 1**). The last is a result of the fact that important biological processes have been demonstrated to be

TABLE 1 | tsRNA databases.

Database	Description	URL link
tRFdb	A relational database of tRFs	http://genome.bioch.virginia.edu/trfdb/
MINTbase	A database for interaction of mitochondrial and tRFs	http://cm.jefferson.edu/MINTbase/
tRFexplorer	A database shows tRFs expression profile in each TCGA tumor type	https://trfexplorer.cloud/
tRF2Cancer	A database identifies tRFs from sequencing datasets in various cancers	http://rna.sysu.edu.cn/tRFfinder/
OncotRF	A database provides the comprehensive tRF information related to various cancers	http://bioinformatics.zju.edu.cn/OncotRF
tsRBase	A comprehensive database for tsRNA expression and function	http://www.tsrbase.org/search.php

strongly correlated with tsRNAs, which has drawn broad attention, especially in cancer studies.

BIOLOGICAL PROCESSES CORRELATED WITH TSRNAS

The biological processes correlated with tsRNAs involve multiple pathways such as inhibition of mRNA translation, promotion of ribosome biogenesis, and regulation of epigenetic processes (17). **Figure 2** comprehensively summarizes the three main tsRNA-associated molecular mechanisms (**Figure 2**).

Inhibition of mRNA Translation

tsRNAs are thought to inhibit mRNA translation by either regulating mRNA stability or interfering with translation initiation and elongation (19). Unlike other sncRNAs, tsRNAs regulate mRNA stability by either canonical miRNA pathway, binding to Argonaute 2 (Ago2) protein or non-canonical miRNA pathway, incorporating into other Argonaute (Ago) family proteins (58, 59). For example, CU1276 was considered as a type of tRFs in human germinal centre B cells and was a DICER1-mediated cleavage production of tRNA-Gly. This specific tRFs repressed replication protein A1 (RPA1) protein by complementarily targeting the 3'UTR of its mRNA, thus

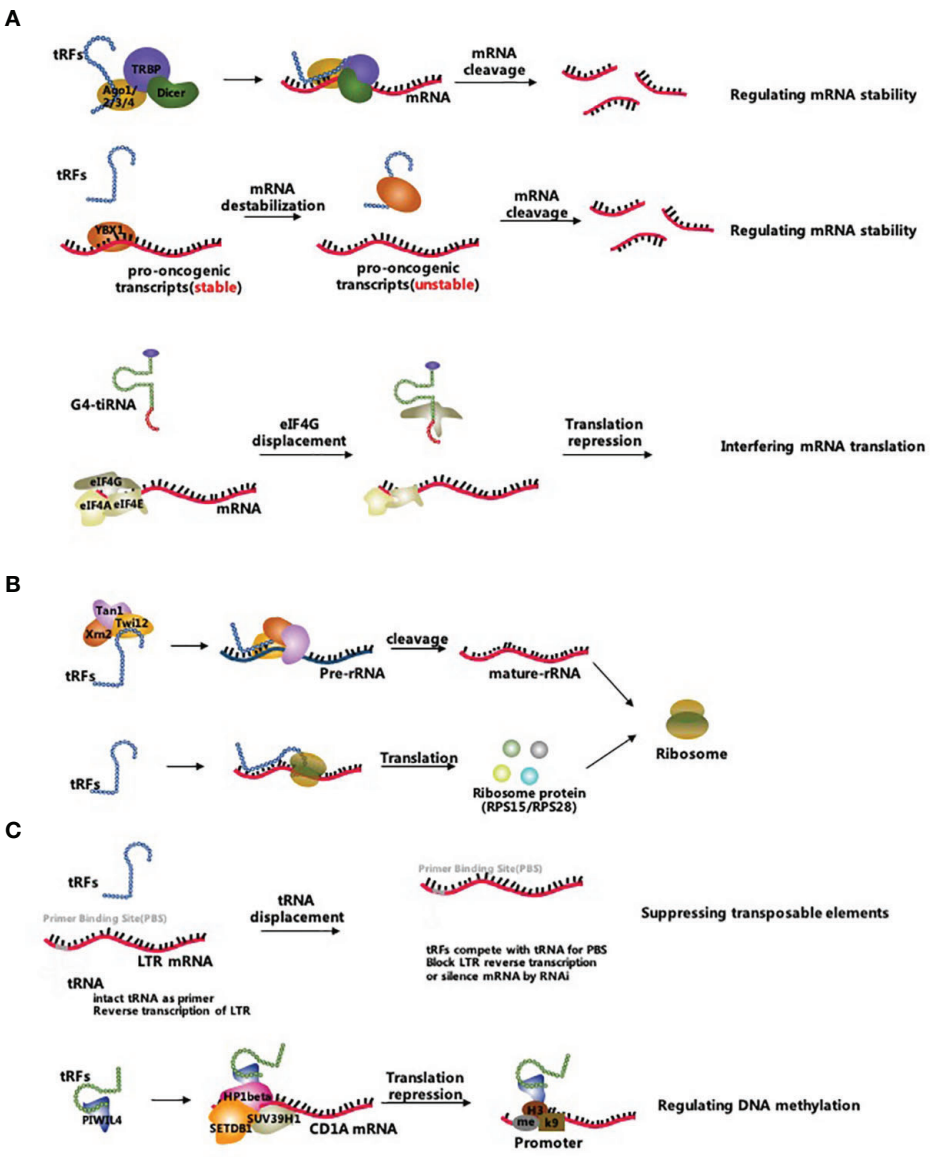

FIGURE 2 | Biological functions of tsRNAs. **(A)** tsRNAs inhibit mRNA translation by reducing mRNA stability and interfering mRNA translation; **(B)** tsRNAs promote ribosome biogenesis by regulating rRNAs and ribosomal proteins; **(C)** tsRNAs regulate epigenetic processes by suppressing transposable elements and targeting the DNA methylation.

suppressing proliferation. More specifically, CU1276 incorporated into silencing complexes with each of the four Argonautes *via* analysis of coprecipitated RNA using an Ago-reactive antibody in human kidney 293 cells (60). A study conducted on colorectal cancer cells showcased that a tRF derived from $tRNA^{Leu}$ functions as miRNAs and inhibits the Notch pathway by interacting with the 3'UTR of Notch ligand jagged 2 (JAG2) mRNA, and suppresses cancer stem-like cells in colorectal cancer progress (61). Li et al. found that some ANG-dependent tRF-3s cleaved the target mRNA by guiding the Ago2 protein, which was similar to the miRNA induced silencing complex (62). Concerning the miRNA-like gene silencing pathway, Haussecker et al. found that some tRFs regulated mRNA stability *via* binding to Ago proteins except for the Ago2 protein forming in this way tRF-induced silencing complexes (63). Subsequent reports indicated that these tRF-induced silencing complexes probably targeted the coding regions, 3'UTRs and 5'UTRs of mature mRNAs (64–66). Furthermore, tRFs mainly derived from tRNA-Glu, tRNA-Asp, tRNA-Gly, and tRNA-Tyr were demonstrated to competitively bind to Y-box-binding protein 1 (YBX1), which enabled the displacement of multiple oncogenic transcripts from the YBX1 protein in breast cancer cells. Subsequently, this led to a reduction in the stability of oncogenic transcripts and inhibited the progress of breast cancer cells (67).

A considerable body of evidence has shown that tsRNAs inhibited translation by interfering with translation initiation and elongation. Specifically, Lyons et al. identified that G-quadruplex (G4) structures containing tiRNAs (G4-tiRNAs) displaced eIF4G, impaired the assembly of 40S ribosomal subunit and ultimately inhibited the translation initiation (68, 69). Moreover, Gebetsberger et al. demonstrated that a tRF-5s derived from tRNA-Val acted as a translation elongation brake for the polysome assembly in *Haloferax volcanii*, which bound the small ribosomal subunit and repressed the consequent protein biosynthesis (70).

Briefly, the piled-up evidence proposes that some tsRNAs probably weaken protein biosynthesis by inhibiting translation processes. Further efforts are needed to explore the regulatory networks between mRNA targets and tsRNAs.

Promotion of the Ribosome Biogenesis

Recent studies proved that some tsRNAs promoted ribosome biogenesis *via* the regulation of ribosomal RNAs (rRNAs) and ribosomal proteins (22). An example of the last assertion is the tRF-3s in *Protozoa* that was shown to recruit the *Tetrahymena* Piwi 12 (Twi12), exoribonuclease 2 (Xrn2) and Twi-associated novel 1 (Tan1) proteins to compose the pre-rRNA splicing complex Twi12/Xrn2/Tan1 (TXT), which processed the precursor rRNAs to mature rRNAs (71, 72). However, whether tRFs promoted rRNA production in higher-level classified living organisms is still unknown. Additionally, a group of tRF-3s derived from $tRNA^{Leu}$ was shown to bind RPS28 or RPS15 mRNAs to promote ribosomal protein translation (22, 73). Yet, the available evidence is insufficient to indicate the extent of the relation of tiRNAs to ribosome biogenesis. In conclusion, the regulatory pathways of tsRNAs role in ribosome biogenesis are the focus for future studies.

Regulation of Epigenetic Processes

tsRNAs have gradually emerged as a novel epigenetic factor. On one hand, tsRNAs act as epigenetic regulators that maintain the genome's stability by targeting and suppressing transposable elements (23). Studies have shown that some tRF-3s silenced the LTR-retrotransposons by blocking reverse transcription and by post-transcriptional silencing (74, 75). Furthermore, abundant tiRNAs in the mature sperm altered the transcriptome of mouse embryos without changing the DNA methylation status. The observed phenomenon indicated that tiRNAs acted as epigenetic factors in the mature sperm but also affected the next-generation phenotyping (76–78). On the other hand, tsRNAs regulated the epigenetic processes *via* targeting DNA methylation and histone modifications (79). Data have revealed that tRF-5s derived from tRNA-Glu was combined with Piwi-like protein 4 (PIWIL4) thus recruiting the SET domain bifurcated histone lysine methyltransferase 1 (SETDB1), SUV39H1 histone lysine methyltransferase (SUV39H1), and heterochromatin protein 1β (HP1β) proteins leading to the methylation of the promoter region and inhibition of CD1A expression in monocytes (80, 81). These findings suggest that a new chapter has been unfolded regarding the tsRNA-related epigenetic regulations, but yet there is a shortage of knowledge concerning the precise functions of tsRNAs in the epigenetic control, which eventually will be determined on a case-by-case basis.

The Role of tsRNAs in Cancer Development and Promotion

The functions of tsRNAs have drawn broad attention across the scientific world concerning cancers. So far, numerous studies have demonstrated that tsRNAs have pivotal functions in regulating proliferation, apoptosis, and migration of cancer cells, modifying tumour microenvironment, and modulating cancer drug resistance (29). Moreover, recent clinical research has revealed that tsRNAs were commonly detected in the serum samples from tumour patients (82). Therefore, tsRNAs have great potential to serve as novel biomarkers for various types of cancers, such as breast, lung, colorectal, ovarian and other types (**Table 2**).

Dysregulations of tsRNAs in Cancers

The first abnormally expressed tsRNA (tRF-1001) was found in various cancer cells (40) and since then the number of dysregulated tsRNAs have increased. The role of tsRNA in oncology research was revisited and many entered clinical trials. In that sense, Fabris and colleagues reported a significant downregulation of ts-53 and ts-101 in chronic lymphocytic leukaemia (CLL) (110). Similarly, Maute et al. observed that some tRF-3s were also downregulated in germinal centre-derived lymphomas (60). tDR-7816 was distinctly downregulated in breast cancer cells (118, 119). However, in cancer tissues from non-small cell lung cancer (NSCLC), the tRF-Leu-CAG was significantly upregulated, while the serum level of tRF-Leu-CAG was positively correlated to cancer stages (100). Likewise, Papadimitriou et al. reported a significant elevation of the tRF-Lys-

TABLE 2 | Summary of cancer-associated tsRNAs.

Cancer	tsRNAs	Effect	Mechanism	Clinical Value	References
Breast cancer	$tRF^{Glu\text{-}YTC}$ $tRF^{Asp\text{-}GTC}$ $tRF^{Gly\text{-}TCC}$	Tumor suppressor	Displace oncogenic transcripts from YBX1 and then suppress cell proliferation	Need to be further studied	(67)
	$tiRNA^{Asp\text{-}GUC}$ $tiRNA^{His\text{-}GUG}$ $tiRNA^{Lys\text{-}CUU}$	Tumor promoter	Involvement in cell proliferation	Potential biomarker for ER^+ patient	(47)
	ts-112	Tumor promoter	Target RUNX1 and promote tumor-related activities	Need to be further studied	(83)
	$tRF^{Lys\text{-}CTT\text{-}010}$	Tumor promoter	Interact with G6PC and then promote cell proliferation	Need to be further studied	(84)
	tRF-Arg-CCT-017, tRF-Gly-CCC001, tiRNA-Phe-GAA-003	Unknown	Unknown	Diagnostic and prognosis biomarker	(85)
	tRF-31-87R8WP9I1EWJ0	Unknown	Unknown	Diagnostic and prognosis biomarker	(86)
	tDR-000620	Unknown	Unknown	Diagnostic biomarker	(87)
	tRF3E	Tumor suppressor	Interact with nucleolin and repress the translation of P 53	Diagnostic biomarker	(88)
	tRF-30-JZOYJE22RR33 ,tRF-27-ZDXPHO53KSN	Unknown	Unknown	Prognostic biomarker	(89)
Gastric cancer	tiRNA-5034-GluTTC-2	Unknown	Unknown	Diagnostic biomarker	(90)
	tRF-Glu-TTC-027	Tumor suppressor	Regulate progression via MAPK pathway	Potential target for clinical therapy	(91)
	tRF-19-3L7L73JD	Tumor suppressor	Inhibit proliferation and Promote apoptosis	Diagnostic biomarker	(92)
	tRF-33-P4R8YP9LON4VDP	Tumor suppressor	Inhibit proliferation and migration	Diagnostic biomarker	(93)
	tRF-24-V29K9UV3IU	Tumor suppressor	Inhibit proliferation and migration by regulating the Wnt pathway	Potential target for clinical therapy	(94)
Colorectal cancer	tRF-24-NMEH623K25, tRF-30- XSXMSL73VL4Y, tRF-29-QU7BPN6ISBJO, tRF-27- Q99P9P9NH5N	Tumor promoter	Regulate the progression of colon cancer via cGMP-PKG signaling pathway	Diagnostic biomarker	(95)
	tRF/miR-1280	Tumor suppressor	Suppress stem cell-like cells and metastasis	Potential diagnostic marker	(61)
	$tiRNA^{His\text{-}GTG}$	Tumor promoter	Regulate LATS2 and promote progression	Need to be further studied	(26)
	50-tiRNA-Val, 50-tiRNA-Cys, 50-tiRNA-Ala	Tumor promoter	Promote migration and invasion	Potential target for diagnosis	(96)
	tRF-20-M0NK5Y93	Tumor suppressor	Inhibit metastasis by targeting Claudin-1	Need to be further studied	(97)
Prostate cancer	tRF-1001	Tumor promoter	ELAC2 dependent production and promote proliferation	Need to be further studied	(40)
	$tiRNA^{Asp\text{-}GUC}$ $tiRNA^{His\text{-}GUG}$ $tiRNA^{Lys\text{-}CUU}$	Tumor promoter	Involvement in cell proliferation	Potential diagnostic marker	(47)
	tRF-544 tRF-315	Tumor promoter	Target GADD45A and protect cancer cells from apoptosis	Prognostic biomarker for recurrence	(98, 99)
Lung cancer	$tRF^{Leu\text{-}CAG}$	Tumor promoter	Regulate AURKA and increase proliferative ability of cancer	Potential diagnostic marker	(100)
	ts-46 ts-47	Tumor suppressor	Interfere with S1P pathway and inhibit cancer progress	Need to be further studied	(17)
	ts-3676 ts-4521	Tumor suppressor	Interact with PIWI proteins and inhibit cancer progression	Need to be further studied	(101)
Hepatocellular cancer	tRNA-ValTAC-3, tRNA-GlyTCC-5, tRNA-ValAAC-5, tRNA-GluCTC-5	Unknown	Unknown	Diagnostic biomarker	(102)
	tRF^{Gly}	Tumor promoter	Promote cell migration by targeting NDFIP2	Potential therapeutic target	(103)
Ovarian cancer	tRF-03357	Tumor promoter	Promote proliferation by targeting HMBOX1	Potential diagnostic marker	(104)
	tRF-03358	Unknown	Unknown	Diagnostic biomarker	(105)
Pancreatic cancer	tRF-3-Leu-AAG-1-1, tRF-3-Gln-CTG-1-1, tRF-3-AlaCGC-1-1	Tumor promoter	Target cancer-related pathways	Diagnostic biomarker	(106)
	tRF-Pro-CGG	Tumor suppressor	inhibits the metastasis of pancreatic cancer	Diagnostic biomarker	(85)

(Continued)

TABLE 2 | Continued

Cancer	tsRNAs	Effect	Mechanism	Clinical Value	References
Leukemia	i-tRF-Phe^{GAA}	Unknown	Unknown	Biomarker for prognosis	(107)
	i-tRF-Gly^{GCC}	Unknown	Unknown	Prognostic biomarker	(108)
	i-tRF-Gly^{CCC}	Unknown	Unknown	Diagnostic and prognostic biomarker	(109)
	ts-101, ts-53, ts-44	Tumor suppressor	Target TCL1 and suppress progression	Need to be further studied	(110)
	tRF-Leu$^{AAG/TAG}$	Unknown	Unknown	Prognostic biomarker	(111)
Renal cell carcinoma	tRF$^{Val\text{-}AAC}$	Tumor suppressor	Act in a tumor-suppressive manner	Prognostic biomarker	(112, 113)
	tiRNA$^{Leu\text{-}CAG}$-5				
	tiRNA$^{Arg\text{-}CCT}$-5				
	tiRNA$^{Glu\text{-}CTC}$-5				
	tiRNA$^{Lys\text{-}TTT}$-5				
Osteosarcoma	tiRNA^{Ala}	Tumor promoter	Trigger assembly of stress granules	Need to be further studied	(114)
	tiRNA^{Cys}				
B cell lymphoma	CU1276/tRF-3018	Tumor suppressor	Associate with Ago proteins and suppress proliferation		(60)
Bladder cancer	5′-tRF-Lys-CTT	Unknown	Unknown	Diagnostic and prognosis biomarker	(115)
Papillary thyroid cancer	tRF-39-0VL8K87SIRMM12E2, tRF-38-0VL8K87SIRMM12V tRF-34-YSV4V47Q2WW1J1, tRF27-PIR8YP9LON3	Unknown	Unknown	Diagnostic biomarker	(116)
Oral squamous cell carcinoma	tRF-20-S998LO9	Unknown	Unknown	Prognosis biomarker	(117)

CTT in bladder tumors and a positive association with clinical prognosis (115). Interestingly, data demonstrated diverse expression of three different tRF-5s in the testicular germinoma (120). As a result, data suggested that deregulation of tsRNAs turned to be a key factor in the progress of cancers thus introducing the tsRNAs as cancer biomarkers in the medical practice.

The Role of tsRNAs in the Regulation of Cancer Hallmarks

Cell proliferation, apoptosis, and migration are well-known hallmarks of cancers and determinants of the prognosis of cancer patients. tRF-1001 derived from the pre-tRNA^{Ser} was the first tsRNA found to promote the proliferation of prostate cancer cells (40). Moreover, Lee et al. found that the knockdown of tRF-1001 impaired cell proliferation and resulted in the accumulation of cells in interphase with phenotypes reversed by transfecting cells with the synthetic tRF-1001 oligoribonucleotide. In another study, SHOT-RNAs were significantly upregulated in hormone receptor-positive prostate and breast carcinoma cells, and the proliferation of cancer cells was distinctly decreased when transfecting cancer cells with SHOT-RNA-targeted siRNAs (47). These observations suggested that SHOT-RNAs probably stimulated cell proliferation in hormone receptor-positive prostate and breast carcinoma cells. Regarding ovarian cancer cells, Zhang et al. found that tRF-03357 was upregulated and that this tsRNA promoted the proliferation of ovarian cancer cells *via* downregulation of the Homeobox-containing protein 1 (HMBOX1) transcription factor (104). On the other hand, the expression of HMBOX1 in high-grade serous ovarian cancer cells was significantly lower than that in normal ovarian cells. However, the specific pathway involved in tRF-03357 regulating HMBOX1 and other tRFs that modulated the progression of ovarian cancer required further investigation. Contrary to tRF-03357, a tRF-5s derived from tRNA-Glu has been elucidated to target the breast cancer anti-estrogen resistance protein 3 (BCAR3) and hence to inhibit the proliferation of ovarian carcinoma cells (121). Zhou and colleagues demonstrated that the decrease in the expression of BCAR3 and the increase of tRF suppressed the proliferation of ovarian cancer cells. The authors further confirmed that the same tRF bound directly to the 3'UTR of BCAR3 mRNA, which then resulted in downregulation of the BCAR3 protein. Furthermore, previous studies have suggested that tRF-Leu-CAG affected the proliferation of lung carcinoma cells by targeting the Aurora Kinase A (AURKA) protein, which participated in the control of cell cycle and the regulation of the cell division (100, 122). Even more, a recent study showed that tsRNA-5001a was significantly upregulated in lung adenocarcinoma tissues and the overexpression of tsRNA-5001a significantly promoted cell proliferation (123). Hu et al. discovered that tsRNA-5001a promoted cancer cell proliferation by targeting the growth arrest and DNA damage inducible gamma (GADD45G) and downregulating its expression (123). GADD45G is widely known for its antitumor function (124). However, the relationship between tRFs and other DNA repair genes similar to GADD45G in lung adenocarcinoma patients needs to be further explored. In this regard, Maute et al. demonstrated that CU1276, as one of the representatives of tRF-3s, inhibited the proliferation of B cell

lymphoma *via* the RPA1-dependent pathway (60, 125). Additionally, Shen et al. found that levels of tRF-33-P4R8YP9LON4VDP were significantly downregulated in plasma samples of gastric patients and that this tsRNA inhibited the proliferation of gastric carcinoma cells (93).

Cell apoptosis, also known as programmed cell death, is an important hallmark of cancer cells (126). Recently, it has been suggested that tRF-315 targeted the growth arrest and DNA damage inducible alpha (GADD45A) gene known for being a tumour suppressor, which then regulated the cell cycle, and finally protected the prostate cancer cells from apoptosis (99). Furthermore, 5'-tiRNA-His targeted the large tumour suppressor kinase 2 (LATS2) protein to turn off the downstream signalling pathway and finally upregulated the anti-apoptotic-related genes (26). Alternatively, Elbarbary et al. found that 5'-half-tRNA (Glu), working as sgRNA, stimulated tRNA 3' processing endoribonuclease (tRNase Z) to cleave the target protein phosphatase 1F (PPM1F) mRNA and thus affected the apoptosis of human kidney 293 cells *via* suppressing the expression of the PPM1F protein (127). These data are an indication that various tsRNAs are negatively connected with the apoptosis of cancer cells. On the contrary, in breast carcinoma, 5′-tiRNA-Val was shown to alter the colony formation. Another study confirmed that 5′-tiRNA-Val targeted the Frizzled-3 (FZD3) protein, attenuating the Wnt/β-catenin pathway, and finally promoting the apoptosis of cancer cells (118).

Cell migration is also the main trait of malignant tumours and indicates the degree of cancer progression (128). Retrieved data from clinical trial research link distant metastasis with significant tRFs dysregulations in uveal melanoma (129). Further, Birch et al. found that these dysregulated tRFs affected the retrotransposon activity and probably played a pivotal role in cancer cell migration (130). Even more, a tRF derived from $tRNA^{Leu}$ was determined as an inhibitor of migration by preventing the premetastatic niche (PMN) formation in colorectal cancer cells (131). The endothelial–mesenchymal transition (EMT) is a critical factor for the regulation of the cancer cells' migration (132). Recently, it has been demonstrated that tRFs derived from tRNA-Gly targeted the EMT-related proteins and regulated the migration of hepatocellular carcinoma (103). Regarding other malignancies, tsRNAs were shown to regulate the migration of cancer cells. Specifically, tRF-3019a was found to promote the migration of gastric cancer cells *via* targeting tumour suppressors, while tRF-17-79MP9PP inhibited the migration of breast cancer cells *via* regulating the thrombospondin 1 (THBS1)-mediated transforming growth factor beta 1 (TGF-β1)/SMAD family member 3 (smad3) signalling pathway (133, 134).

The Role of tsRNAs in Modifying the Tumour Microenvironment

The tumour microenvironment (TME) consists of tumour cells, cancer stem cells, as well as of tumour stromal cells including endothelial cells, fibroblasts, and immune cells, in addition to non-cellular components of the extracellular matrix (135). In recent years, it has been demonstrated that tsRNAs orchestrated the tumour processes by modifying the TME (136). On the one hand, accumulating evidence has shown that exosomes produced by tumour cells possess multiple tRFs that modify the TME (137). For example, exosomes in oral squamous cell carcinoma (OSCC) were shown to contain multiple tsRNAs that are involved in transforming TME to conditions favourable for cancer progression (25). However, the mechanism through which this favourable environment for OSCC growth and metastasis is promoted by tsRNAs remains unknown and needs further studies. Interestingly, exosomal tsRNAs derived from tRNA-Val, tRNA-Gly, and tRNA-Glu were shown to participate in the modulation of TME in hepatic carcinoma (137). Regardless of the above-discussed, the specific biological functions of exosome-derived tRFs in tumour regulation remain to be further investigated. On the other hand, recent studies have drawn increasing attention to cancer stem cells (CSCs) as important components of the TME, while they are involved in numerous tumour biological processes (138, 139). Meanwhile, data indicated that some tRFs have modified the TME by regulating the CSC functions (140). Huang and colleagues reported that tRFs derived from $tRNA^{Leu}$ were found to suppress CSC functions *via* the inactivation of Notch signaling in colorectal cancer cells (61). Recently it has been found that dysregulation of tRF-mediated translational regulatory circuitry impaired the stem cells growth, which was commonly associated with aggressive characteristics of human myelodysplastic syndromes (53). In summary, TME were modified by tsRNAs, but the underlying molecular mechanisms of tsRNAs that regulated the TME remained yet not fully understood. Hence, our suggestion for future studies is that the focus should be on the elucidation of these mechanisms.

The Role of tsRNAs in the Modulation of Tumour Drug Resistance

Drug resistance is considered a vital factor determining the efficacy of anti-cancer therapies. Emerging evidence showed that some tsRNAs modulated the drug resistance of multiple tumours (24). For example, Cui et al. found that the upregulated tDR-0009 and tDR-7336 sustained the interleukin-6 reactivity and finally participated in multidrug resistance by activating downstream pathways in triple-negative breast cancer cells (141). Meanwhile, another study showed that tRF-30-JZOYJE22RR33 and tRF-27-ZDXPHO53KSN orchestrated trastuzumab resistance in HER2-positive breast cancer cells (89). Sun et al. studied the expression levels of tRFs in trastuzumab-sensitive and resistant breast cancer cell lines. The authors revealed the effect of tRFs on clinical trastuzumab efficacy using the Cox regression analysis. The obtained results highlight the need for further studies that aim at the accumulation of more data that will clarify the role of tRFs in the pathways that regulate the HER2-positive breast cancer drug resistance toward trastuzumab. In addition, other studies showcased that some downregulated tsRNAs were involved in the chemoresistance of lung cancer cells *via* integrin-linked kinase (ILK) signalling, phosphatase and tensin homolog (PTEN) signalling, and other

pathways involved in the regulation of chemo-resistance (17, 142). Therefore, with the accumulating evidence on the role of tsRNA in tumour drug resistance, the clinical efficacy of anti-cancer drugs and the prognosis of cancer patients can progress to a new phase.

The Role of tsRNAs as Biomarkers for Cancer Diagnosis and Prognosis

Multiple ncRNAs have been regarded as potential biomarkers for cancer diagnosis and prognosis (143, 144). Recent studies have further proposed tsRNAs as novel tumour biomarkers (**Table 2**). On one hand, some tsRNAs have demonstrated dysregulations in cancer tissues and serum samples. Hence, these tsRNAs were demonstrated as potential biomarkers for cancer diagnosis. For example, tRFs derived from tRNA-Met and tRNA-Val have been significantly elevated in the serum of pancreatic ductal adenocarcinoma (PDAC) patients as supposed by Xue and colleagues (82). Moreover, Li et al. found that the expression of tRF-Pro-CGG was significantly downregulated in PDAC than this in normal pancreatic tissues, which was further associated with the TNM stage of patients. Thus, tRF-Pro-CGG has been considered as a biomarker for PDAC diagnosis and therapy (85). Similarly, tRFs derived from $tRNA^{Leu}$ were significantly elevated in NSCLC tissues and serum samples, and therefore they were regarded as a potential biomarker for NSCLC diagnosis (100). In respect of tRFs in lung cancer, such as ts-46, ts-47, ts-3676 and ts-4521, they have been demonstrated as tumour suppressors based on recent reports as to the mechanism (17, 101). However, the clinical value of these tRFs needs to be clarified based on the registered clinical samples. Multiple investigations revealed that some tsRNAs derived from tRNA-Glu, tRNA-Gly, tRNA-Leu, and tRNA-Ser were significantly dysregulated in breast cancer serum samples (145). In another example of the Triple-negative breast cancer, the expression of tDR-000620 was strongly correlated with age, node status and local recurrence as proposed by Feng et al. In this study, the multivariate Cox regression demonstrated that the low expression of tDR-000620 was an adverse predictive factor for recurrence-free survival (87). Equally important were the findings of Huang et al. who found that tRF-31-U5YKFN8DYDZDD was highly upregulated in serum samples of gastric cancer (GC) patients (146). All these results denoted that circulating tsRNAs could be a potential non-invasive indicator of a cancer diagnosis. On the other hand, these abnormally expressed tsRNAs were established as prognostic models for cancer treatments. For instance, tRF-30-JZOYJE22RR33 and tRF-27-ZDXPHO53KSN were demonstrated to shorten the progression-free survival (PFS) of trastuzumab-resistant breast carcinoma patients (89). Subsequently, data proved that these tRFs were likely to act as biomarkers for the prognosis of trastuzumab-resistant breast carcinoma patients (89). Additionally, another study demonstrated that tRFs derived from tRNA-Lys were associated with a higher risk for progression and poor clinical survival in bladder carcinoma (115). Thus, these data established a prognostic model for bladder cancer based on the expression levels of specific tsRNA. Recently, researchers have also discovered multiple tsRNA signatures in gastric cancer, papillary thyroid cancer, and other malignancies (38, 91, 93). The literature research on this matter highlighted the need for a broader validation of tsRNAs as sensitive biomarkers for cancer diagnosis and prognosis.

SUMMARY AND PERSPECTIVES

tsRNAs are a group of conventional small ncRNAs and play complicated roles in most malignancies. Their biological roles include regulation of cancer hallmarks, modification of TME, and modulation of drug resistance. Biofluid screening of miRNAs in clinical practice demonstrated that specific tsRNAs were upregulated in the biofluids of solid and blood malignancies (62, 147). Therefore, the biological functions of multiple tsRNAs in cancers have been widely studied. What is the most important from the aforementioned studies is that these functional tsRNAs potentially serve as novel biomarkers for cancer diagnosis and prognosis. However, for a deeper understanding of the tsRNA-related regulatory networks, further investigation is needed.

Our literature research showed that in the first place, the databases of tsRNAs, especially of tsRNAs in multiple tumours, should be perfected. Recently, biomedical investigations on tsRNAs in multiple cancers have been extensively driven by big data. Thus, OncotRF, tRFdb, and other tsRNA-related databases have been expansively applied in oncological research. However, there is no consensus among the existing databases in terms of the standardized terminology of tsRNAs (57, 148–150). Consequently, the big data analytics for tsRNAs in multiple tumours is yet inefficient. Moreover, current studies have shown that tsRNAs are dysregulated in neoplasm tissues and serum samples of tumour patients. However, our knowledge concerning the upstream regulatory mechanism causing the abnormal expression of tsRNAs and the biological functions of tsRNAs in multiple tumours remains at a relatively superficial level. It is unknown whether the tsRNA dysregulation triggers the progress of tumours. Therefore, it is compulsory to identify the concrete molecular mechanisms of tsRNAs in regulating multiple tumours. Lately, enormous efforts were invested in the exploration of the mechanisms of tsRNAs in cancer cells. To advance clinical application of tsRNAs, future studies should focus on collecting patient samples with warranty of safety and efficacy, such as body fluids and tumour tissues. As it has already been reported, both tsRNAs and their precursor tRNAs contain various modifications (35, 36, 151). Interestingly, the modification status of tRNA can change the endonuclease activity and thus affect the tRNA cleavage process. However, the determination of exactly which tRNA modification affects tsRNA production in cancer progression as well as the potential relationship of tsRNA modification with their functions in tumours needs further investigation. Therefore, it is necessary to establish the localization and detection techniques for examining multiple RNA modifications of tsRNAs in various tumours. Based on detection techniques, the potential future research would focus on investigating upstream regulatory factors of tRNA modifications and endonuclease activity in tumours. Finally, diverse chemotherapies encounter drug

resistance, which leads to the necessity of more targeted treatments. Moreover, the advent of RNA therapies bodes for the development of therapeutic approaches involving small RNAs. Thus, some tsRNAs, which are biologically correlated with tumour initiation and progression, are expected to become biomarkers for cancer diagnosis and prognosis. It is worth mentioning that tsRNAs can be encapsulated in exosomes and liquid biopsies based on exosomes can be a potential approach for molecular diagnosis in cancers. For example, some tRFs delivered *via* plasma exosomes served as a novel diagnostic biomarker in the liver cancer (102). These tRFs allow us to understand the pathological conditions of cancer patients by detecting specific tsRNAs encapsulated in exosomes. Moreover, engineered exosomes can load therapeutic miRNAs and anti-tumour drugs (152). Thus, therapeutic tsRNAs are likely to be another potential anti-tumour molecule loaded in engineered exosomes.

Given the abovementioned challenges, most tsRNA-related research on tumours has yet to be profound. Therefore, with the application of novel sequencing techniques and bioinformatics methods, such as photoactivatable-ribonucleoside-enhanced crosslinking and immunoprecipitation (PAR-CLIP) and cross-linking ligation and sequencing of hybrids (CLASH), more in-depth studies of tsRNAs in multiple tumours can provide a brand new insight into tumour cell biology for the establishment of solid foundations for further clinical applications of tsRNAs.

AUTHOR CONTRIBUTIONS

C-YX provided direction and guidance throughout the preparation of this manuscript. B-FF wrote and edited the manuscript. B-FF generated the figures and made significant revisions to the manuscript. All authors have read and approved the final version of the manuscript.

FUNDING

This study was supported by Jinhua central hospital basic research projects of Zhejiang China(Grant No: JY2021-6-05) and Zhejiang non-profit technology applied research projects of China (Grant No: LGF20H160017).

REFERENCES

1. Wei JW, Huang K, Yang C, Kang CS. Non-Coding RNAs as Regulators in Epigenetics (Review). *Oncol Rep* (2017) 37:3–9. doi: 10.3892/or.2016.5236
2. Pennisi E. GenomicsENCODE Project Writes Eulogy for Junk DNA. *Science* (2012) 337:1159, 1161. doi: 10.1126/science.337.6099.1159
3. Isakova A, Neff N, Quake SR. Single-Cell Quantification of a Broad RNA Spectrum Reveals Unique Noncoding Patterns Associated With Cell Types and States. *Proc Natl Acad Sci USA* (2021) 118. doi: 10.1073/pnas.2113568118
4. Fu Y, Lee I, Lee YS, Bao X. Small Non-Coding Transfer RNA-Derived RNA Fragments (tRFs): Their Biogenesis, Function and Implication in Human Diseases. *Genomics Inform* (2015) 13:94–101. doi: 10.5808/GI.2015.13.4.94
5. Statello L, Guo CJ, Chen LL, Huarte M. Gene Regulation by Long non-Coding RNAs and its Biological Functions. *Nat Rev Mol Cell Biol* (2021) 22:96–118. doi: 10.1038/s41580-020-00315-9
6. Zaratiegui M, Irvine DV, Martienssen RA. Noncoding RNAs and Gene Silencing. *Cell* (2007) 128:763–76. doi: 10.1016/j.cell.2007.02.016
7. Ponting CP, Oliver PL, Reik W. Evolution and Functions of Long Noncoding RNAs. *Cell* (2009) 136:629–41. doi: 10.1016/j.cell.2009.02.006
8. Hombach S, Kretz M. Non-Coding RNAs: Classification, Biology and Functioning. *Adv Exp Med Biol* (2016) 937:3–17. doi: 10.1007/978-3-319-42059-2_1
9. Huntzinger E, Izaurralde E. Gene Silencing by microRNAs: Contributions of Translational Repression and mRNA Decay. *Nat Rev Genet* (2011) 12:99–110. doi: 10.1038/nrg2936
10. Carvalho Barbosa C, Calhoun SH, Wieden HJ. Non-Coding RNAs: What are We Missing? *Biochem Cell Biol* (2020) 98:23–30. doi: 10.1139/bcb-2019-0037
11. Machado IF, Teodoro JS, Palmeira CM, Rolo AP. miR-378a: A New Emerging microRNA in Metabolism. *Cell Mol Life Sci* (2020) 77:1947–58. doi: 10.1007/s00018-019-03375-z
12. Fu XD. Non-Coding RNA: A New Frontier in Regulatory Biology. *Natl Sci Rev* (2014) 1:190–204. doi: 10.1093/nsr/nwu008
13. Berg MD, Brandl CJ. Transfer RNAs: Diversity in Form and Function. *RNA Biol* (2021) 18:316–39. doi: 10.1080/15476286.2020.1809197
14. Wei FY, Tomizawa K. tRNA Modifications and Islet Function. *Diabetes Obes Metab* (2018) 20 Suppl 2:20–7. doi: 10.1111/dom.13405
15. Yanas A, Liu KF. RNA Modifications and the Link to Human Disease. *Methods Enzymol* (2019) 626:133–46. doi: 10.1016/bs.mie.2019.08.003
16. Zhang Y, Deng Q, Tu L, Lv D, Liu D. Trnaderived Small RNAs: A Novel Class of Small RNAs in Human Hypertrophic Scar Fibroblasts. *Int J Mol Med* (2020) 45:115–30. doi: 10.3892/ijmm.2019.4411
17. Balatti V, Nigita G, Veneziano D, Drusco A, Stein GS, Messier TL, et al. tsRNA Signatures in Cancer. *Proc Natl Acad Sci USA* (2017) 114:8071–6. doi: 10.1073/pnas.1706908114
18. Li S, Xu Z, Sheng J. tRNA-Derived Small RNA: A Novel Regulatory Small Non-Coding RNA. *Genes (Basel)* (2018) 9:246. doi: 10.3390/genes9050246
19. Shen Y, Yu X, Zhu L, Li T, Yan Z, Guo J. Transfer RNA-Derived Fragments and tRNA Halves: Biogenesis, Biological Functions and Their Roles in Diseases. *J Mol Med (Berl)* (2018) 96:1167–76. doi: 10.1007/s00109-018-1693-y
20. Cho H, Lee W, Kim GW, Lee SH, Moon JS, Kim M, et al. Regulation of La/SSB-Dependent Viral Gene Expression by pre-tRNA 3' Trailer-Derived tRNA Fragments. *Nucleic Acids Res* (2019) 47:9888–901. doi: 10.1093/nar/gkz732
21. Xiao L, Wang J, Ju S, Cui M, Jing R. Disorders and Roles of tsRNA, snoRNA, snRNA and piRNA in Cancer. *J Med Genet* (2022). doi: 10.1136/jmedgenet-2021-108327
22. Kim HK, Fuchs G, Wang S, Wei W, Zhang Y, Park H, et al. A Transfer-RNA-Derived Small RNA Regulates Ribosome Biogenesis. *Nature* (2017) 552:57–62. doi: 10.1038/nature25005
23. Park J, Ahn SH, Shin MG, Kim HK, Chang S. tRNA-Derived Small RNAs: Novel Epigenetic Regulators. *Cancers (Basel)* (2020) 12:2773. doi: 10.3390/cancers12102773
24. Zhang Y, Qian H, He J, Gao W. Mechanisms of tRNA-Derived Fragments and tRNA Halves in Cancer Treatment Resistance. *biomark Res* (2020) 8:52. doi: 10.1186/s40364-020-00233-0
25. Lu Y, Zheng Z, Yuan Y, Pathak JL, Yang X, Wang L, et al. The Emerging Role of Exosomes in Oral Squamous Cell Carcinoma. *Front Cell Dev Biol* (2021) 9:628103. doi: 10.3389/fcell.2021.628103
26. Tao EW, Wang HL, Cheng WY, Liu QQ, Chen YX, Gao QY. A Specific tRNA Half, 5'tirna-His-GTG, Responds to Hypoxia *via* the HIF1alpha/ANG Axis and Promotes Colorectal Cancer Progression by Regulating LATS2. *J Exp Clin Cancer Res* (2021) 40:67. doi: 10.1186/s13046-021-01836-7

27. Jia Y, Tan W, Zhou Y. Transfer RNA-Derived Small RNAs: Potential Applications as Novel Biomarkers for Disease Diagnosis and Prognosis. *Ann Transl Med* (2020) 8:1092. doi: 10.21037/atm-20-2797
28. Kim HK, Yeom JH, Kay MA. Transfer RNA-Derived Small RNAs: Another Layer of Gene Regulation and Novel Targets for Disease Therapeutics. *Mol Ther* (2020) 28:2340–57. doi: 10.1016/j.ymthe.2020.09.013
29. Li X, Liu X, Zhao D, Cui W, Wu Y, Zhang C, et al. tRNA-Derived Small RNAs: Novel Regulators of Cancer Hallmarks and Targets of Clinical Application. *Cell Death Discovery* (2021) 7:249. doi: 10.1038/s41420-021-00647-1
30. Taxis TM, Bauermann FV, Ridpath JF, Casas E. Analysis of tRNA Halves (tsRNAs) in Serum From Cattle Challenged With Bovine Viral Diarrhea Virus. *Genet Mol Biol* (2019) 42:374–9. doi: 10.1590/1678-4685-gmb-2018-0019
31. Drino A, Oberbauer V, Troger C, Janisiw E, Anrather D, Hartl M, et al. Production and Purification of Endogenously Modified tRNA-Derived Small RNAs. *RNA Biol* (2020) 17:1104–15. doi: 10.1080/15476286.2020.1733798
32. Ma Z, Zhou J, Shao Y, Jafari FA, Qi P, Li Y. Biochemical Properties and Progress in Cancers of tRNA-Derived Fragments. *J Cell Biochem* (2020) 121:2058–63. doi: 10.1002/jcb.29492
33. Qin C, Xu PP, Zhang X, Zhang C, Liu CB, Yang DG, et al. Pathological Significance of tRNA-Derived Small RNAs in Neurological Disorders. *Neural Regener Res* (2020) 15:212–21. doi: 10.4103/1673-5374.265560
34. Oberbauer V, Schaefer MR. tRNA-Derived Small RNAs: Biogenesis, Modification, Function and Potential Impact on Human Disease Development. *Genes (Basel)* (2018) 9:607. doi: 10.3390/genes9120607
35. Chen Q, Zhang X, Shi J, Yan M, Zhou T. Origins and Evolving Functionalities of tRNA-Derived Small RNAs. *Trends Biochem Sci* (2021) 46:790–804. doi: 10.1016/j.tibs.2021.05.001
36. Zhang X, Cozen AE, Liu Y, Chen Q, Lowe TM. Small RNA Modifications: Integral to Function and Disease. *Trends Mol Med* (2016) 22:1025–34. doi: 10.1016/j.molmed.2016.10.009
37. Zhou J, Wan F, Wang Y, Long J, Zhu X. Small RNA Sequencing Reveals a Novel tsRNA-26576 Mediating Tumorigenesis of Breast Cancer. *Cancer Manag Res* (2019) 11:3945–56. doi: 10.2147/CMAR.S199281
38. Zhu Y, Chen S, Ling Z, Winnicki A, Xu L, Xu S, et al. Comprehensive Analysis of a tRNA-Derived Small RNA in Colorectal Cancer. *Front Oncol* (2021) 11:701440. doi: 10.3389/fonc.2021.701440
39. Xie Y, Yao L, Yu X, Ruan Y, Li Z, Guo J. Action Mechanisms and Research Methods of tRNA-Derived Small RNAs. *Signal Transduct Target Ther* (2020) 5:109. doi: 10.1038/s41392-020-00217-4
40. Lee YS, Shibata Y, Malhotra A, Dutta A. A Novel Class of Small RNAs: tRNA-Derived RNA Fragments (tRFs). *Genes Dev* (2009) 23:2639–49. doi: 10.1101/gad.1837609
41. Yuan Y, Li J, He Z, Fan X, Mao X, Yang M, et al. tRNA-Derived Fragments as New Hallmarks of Aging and Age-Related Diseases. *Aging Dis* (2021) 12:1304–22. doi: 10.14336/AD.2021.0115
42. Yu X, Xie Y, Zhang S, Song X, Xiao B, Yan Z. tRNA-Derived Fragments: Mechanisms Underlying Their Regulation of Gene Expression and Potential Applications as Therapeutic Targets in Cancers and Virus Infections. *Theranostics* (2021) 11:461–9. doi: 10.7150/thno.51963
43. Jiang P, Yan F. tiRNAs & tRFs Biogenesis and Regulation of Diseases: A Review. *Curr Med Chem* (2019) 26:5849–61. doi: 10.2174/0929867326666190124123831
44. Tao EW, Cheng WY, Li WL, Yu J, Gao QY. tiRNAs: A Novel Class of Small Noncoding RNAs That Helps Cells Respond to Stressors and Plays Roles in Cancer Progression. *J Cell Physiol* (2020) 235:683–90. doi: 10.1002/jcp.29057
45. Yamasaki S, Ivanov P, Hu GF, Anderson P. Angiogenin Cleaves tRNA and Promotes Stress-Induced Translational Repression. *J Cell Biol* (2009) 185:35–42. doi: 10.1083/jcb.200811106
46. Su Z, Kuscu C, Malik A, Shibata E, Dutta A. Angiogenin Generates Specific Stress-Induced tRNA Halves and is Not Involved in tRF-3-Mediated Gene Silencing. *J Biol Chem* (2019) 294:16930–41. doi: 10.1074/jbc.RA119.009272
47. Honda S, Loher P, Shigematsu M, Palazzo JP, Suzuki R, Imoto I, et al. Sex Hormone-Dependent tRNA Halves Enhance Cell Proliferation in Breast and Prostate Cancers. *Proc Natl Acad Sci USA* (2015) 112:E3816–3825. doi: 10.1073/pnas.1510077112
48. Honda S, Kirino Y. SHOT-RNAs: A Novel Class of tRNA-Derived Functional RNAs Expressed in Hormone-Dependent Cancers. *Mol Cell Oncol* (2016) 3:e1079672. doi: 10.1080/23723556.2015.1079672
49. Zhang Y, Zhang X, Shi J, Tuorto F, Li X, Liu Y, et al. Dnmt2 Mediates Intergenerational Transmission of Paternally Acquired Metabolic Disorders Through Sperm Small non-Coding RNAs. *Nat Cell Biol* (2018) 20:535–40. doi: 10.1038/s41556-018-0087-2
50. Ontiveros RJ, Shen H, Stoute J, Yanas A, Cui Y, Zhang Y, et al. Coordination of mRNA and tRNA Methylations by TRMT10A. *Proc Natl Acad Sci USA* (2020) 117:7782–91. doi: 10.1073/pnas.1913448117
51. Zhang J, Lu R, Zhang Y, Matuszek Z, Zhang W, Xia Y, et al. tRNA Queuosine Modification Enzyme Modulates the Growth and Microbiome Recruitment to Breast Tumors. *Cancers (Basel)* (2020) 12:628. doi: 10.21203/rs.2.21087/v1
52. Dimitrova DG, Teysset L, Carre C. RNA 2'-O-Methylation (Nm) Modification in Human Diseases. *Genes (Basel)* (2019) 10:117. doi: 10.3390/genes10020117
53. Guzzi N, Ciesla M, Ngoc PCT, Lang S, Arora S, Dimitriou M, et al. Pseudouridylation of tRNA-Derived Fragments Steers Translational Control in Stem Cells. *Cell* (2018) 173:1204–16:e1226. doi: 10.1016/j.cell.2018.03.008
54. Kawarada L, Suzuki T, Ohira T, Hirata S, Miyauchi K, Suzuki T. ALKBH1 is an RNA Dioxygenase Responsible for Cytoplasmic and Mitochondrial tRNA Modifications. *Nucleic Acids Res* (2017) 45:7401–15. doi: 10.1093/nar/gkx354
55. Zong T, Yang Y, Zhao H, Li L, Liu M, Fu X, et al. tsRNAs: Novel Small Molecules From Cell Function and Regulatory Mechanism to Therapeutic Targets. *Cell Prolif* (2021) 54:e12977. doi: 10.1111/cpr.12977
56. Kumar P, Mudunuri SB, Anaya J, Dutta A. Trfdb: A Database for Transfer RNA Fragments. *Nucleic Acids Res* (2015) 43:D141–145. doi: 10.1093/nar/gku1138
57. Yao D, Sun X, Zhou L, Amanullah M, Pan X, Liu Y, et al. OncotRF: An Online Resource for Exploration of tRNA-Derived Fragments in Human Cancers. *RNA Biol* (2020) 17:1081–91. doi: 10.1080/15476286.2020.1776506
58. Kuscu C, Kumar P, Kiran M, Su Z, Malik A, Dutta A. tRNA Fragments (tRFs) Guide Ago to Regulate Gene Expression Post-Transcriptionally in a Dicer-Independent Manner. *RNA* (2018) 24:1093–105. doi: 10.1261/rna.066126.118
59. Zhou Y, Peng H, Cui Q, Zhou Y. Trftar: Prediction of tRF-Target Gene Interactions *via* Systemic Re-Analysis of Argonaute CLIP-Seq Datasets. *Methods* (2021) 187:57–67. doi: 10.1016/j.ymeth.2020.10.006
60. Maute RL, Schneider C, Sumazin P, Holmes A, Califano A, Basso K, et al. tRNA-Derived microRNA Modulates Proliferation and the DNA Damage Response and is Down-Regulated in B Cell Lymphoma. *Proc Natl Acad Sci USA* (2013) 110:1404–9. doi: 10.1073/pnas.1206761110
61. Huang B, Yang H, Cheng X, Wang D, Fu S, Shen W, et al. tRF/miR-1280 Suppresses Stem Cell-Like Cells and Metastasis in Colorectal Cancer. *Cancer Res* (2017) 77:3194–206. doi: 10.1158/0008-5472.CAN-16-3146
62. Li Z, Ender C, Meister G, Moore PS, Chang Y, John B. Extensive Terminal and Asymmetric Processing of Small RNAs From rRNAs, snoRNAs, snRNAs, and tRNAs. *Nucleic Acids Res* (2012) 40:6787–99. doi: 10.1093/nar/gks307
63. Haussecker D, Huang Y, Lau A, Parameswaran P, Fire AZ, Kay MA. Human tRNA-Derived Small RNAs in the Global Regulation of RNA Silencing. *RNA* (2010) 16:673–95. doi: 10.1261/rna.2000810
64. Zhong F, Hu Z, Jiang K, Lei B, Wu Z, Yuan G, et al. Complement C3 Activation Regulates the Production of tRNA-Derived Fragments Gly-tRFs and Promotes Alcohol-Induced Liver Injury and Steatosis. *Cell Res* (2019) 29:548–61. doi: 10.1038/s41422-019-0175-2
65. Choi EJ, Ren J, Zhang K, Wu W, Lee YS, Lee I, et al. The Importance of AGO 1 and 4 in Post-Transcriptional Gene Regulatory Function of Trf5-GluCTC, an Respiratory Syncytial Virus-Induced tRNA-Derived RNA Fragment. *Int J Mol Sci* (2020) 21:8766. doi: 10.3390/ijms21228766
66. Green JA, Ansari MY, Ball HC, Haqqi TM. tRNA-Derived Fragments (tRFs) Regulate Post-Transcriptional Gene Expression *via* AGO-Dependent Mechanism in IL-1beta Stimulated Chondrocytes. *Osteoarthritis Cartilage* (2020) 28:1102–10. doi: 10.1016/j.joca.2020.04.014
67. Goodarzi H, Liu X, Nguyen HC, Zhang S, Fish L, Tavazoie SF. Endogenous tRNA-Derived Fragments Suppress Breast Cancer Progression *via* YBX1 Displacement. *Cell* (2015) 161:790–802. doi: 10.1016/j.cell.2015.02.053

68. Lyons SM, Gudanis D, Coyne SM, Gdaniec Z, Ivanov P. Identification of Functional Tetramolecular RNA G-Quadruplexes Derived From Transfer RNAs. *Nat Commun* (2017) 8:1127. doi: 10.1038/s41467-017-01278-w
69. Lyons SM, Kharel P, Akiyama Y, Ojha S, Dave D, Tsvetkov V, et al. Eif4g has Intrinsic G-Quadruplex Binding Activity That is Required for tiRNA Function. *Nucleic Acids Res* (2020) 48:6223–33. doi: 10.1093/nar/gkaa336
70. Gebetsberger J, Wyss L, Mleczko AM, Reuther J, Polacek N. A tRNA-Derived Fragment Competes With mRNA for Ribosome Binding and Regulates Translation During Stress. *RNA Biol* (2017) 14:1364–73. doi: 10.1080/15476286.2016.1257470
71. Couvillion MT, Sachidanandam R, Collins K. A Growth-Essential Tetrahymena Piwi Protein Carries tRNA Fragment Cargo. *Genes Dev* (2010) 24:2742–7. doi: 10.1101/gad.1996210
72. Couvillion MT, Bounova G, Purdom E, Speed TP, Collins K. A Tetrahymena Piwi Bound to Mature tRNA 3' Fragments Activates the Exonuclease Xrn2 for RNA Processing in the Nucleus. *Mol Cell* (2012) 48:509–20. doi: 10.1016/j.molcel.2012.09.010
73. Kim HK, Xu J, Chu K, Park H, Jang H, Li P, et al. A tRNA-Derived Small RNA Regulates Ribosomal Protein S28 Protein Levels After Translation Initiation in Humans and Mice. *Cell Rep* (2019) 29:3816–3824.e3814. doi: 10.1016/j.celrep.2019.11.062
74. Watanabe T, Tomizawa S, Mitsuya K, Totoki Y, Yamamoto Y, Kuramochi-Miyagawa S, et al. Role for piRNAs and Noncoding RNA in*De Novo* DNA Methylation of the Imprinted Mouse Rasgrf1 Locus. *Science* (2011) 332:848–52. doi: 10.1126/science.1203919
75. Schorn AJ, Gutbrod MJ, Leblanc C, Martienssen R. LTR-Retrotransposon Control by tRNA-Derived Small RNAs. *Cell* (2017) 170:61–71.e11. doi: 10.1016/j.cell.2017.06.013
76. Peng H, Shi J, Zhang Y, Zhang H, Liao S, Li W, et al. A Novel Class of tRNA-Derived Small RNAs Extremely Enriched in Mature Mouse Sperm. *Cell Res* (2012) 22:1609–12. doi: 10.1038/cr.2012.141
77. Chen Q, Yan M, Cao Z, Li X, Zhang Y, Shi J, et al. Sperm tsRNAs Contribute to Intergenerational Inheritance of an Acquired Metabolic Disorder. *Science* (2016) 351:397–400. doi: 10.1126/science.aad7977
78. Sharma U, Conine CC, Shea JM, Boskovic A, Derr AG, Bing XY, et al. Biogenesis and Function of tRNA Fragments During Sperm Maturation and Fertilization in Mammals. *Science* (2016) 351:391–6. doi: 10.1126/science.aad6780
79. Zhang Y, Shi J, Chen Q. tsRNAs: New Players in Mammalian Retrotransposon Control. *Cell Res* (2017) 27:1307–8. doi: 10.1038/cr.2017.109
80. Siomi MC, Sato K, Pezic D, Aravin AA. PIWI-Interacting Small RNAs: The Vanguard of Genome Defence. *Nat Rev Mol Cell Biol* (2011) 12:246–58. doi: 10.1038/nrm3089
81. Zhang X, He X, Liu C, Liu J, Hu Q, Pan T, et al. IL-4 Inhibits the Biogenesis of an Epigenetically Suppressive PIWI-Interacting RNA To Upregulate CD1a Molecules on Monocytes/Dendritic Cells. *J Immunol* (2016) 196:1591–603. doi: 10.4049/jimmunol.1500805
82. Xue M, Shi M, Xie J, Zhang J, Jiang L, Deng X, et al. Serum tRNA-Derived Small RNAs as Potential Novel Diagnostic Biomarkers for Pancreatic Ductal Adenocarcinoma. *Am J Cancer Res* (2021) 11:837–48. doi: 10.21203/rs.3.rs-63978/v1
83. Farina NH, Scalia S, Adams CE, Hong D, Fritz AJ, Messier TL, et al. Identification of tRNA-Derived Small RNA (tsRNA) Responsive to the Tumor Suppressor, RUNX1, in Breast Cancer. *J Cell Physiol* (2020) 235:5318–27. doi: 10.1002/jcp.29419
84. Zhu P, Lu J, Zhi X, Zhou Y, Wang X, Wang C, et al. tRNA-Derived Fragment Trflys-CTT-010 Promotes Triple-Negative Breast Cancer Progression by Regulating Glucose Metabolism *via* G6PC. *Carcinogenesis* (2021) 42:1196–207. doi: 10.1093/carcin/bgab058
85. Li J, Jin L, Gao Y, Gao P, Ma L, Zhu B, et al. Low Expression of tRF-Pro-CGG Predicts Poor Prognosis in Pancreatic Ductal Adenocarcinoma. *J Clin Lab Anal* (2021) 35:e23742. doi: 10.1002/jcla.23742
86. Wang J, Ma G, Ge H, Han X, Mao X, Wang X, et al. Circulating tRNA-Derived Small RNAs (tsRNAs) Signature for the Diagnosis and Prognosis of Breast Cancer. *NPJ Breast Cancer* (2021) 7:4. doi: 10.1038/s41523-020-00211-7
87. Feng W, Li Y, Chu J, Li J, Zhang Y, Ding X, et al. Identification of tRNA-Derived Small Noncoding RNAs as Potential Biomarkers for Prediction of Recurrence in Triple-Negative Breast Cancer. *Cancer Med* (2018) 7:5130–44. doi: 10.1002/cam4.1761
88. Falconi M, Giangrossi M, Zabaleta ME, Wang J, Gambini V, Tilio M, et al. A Novel 3'-tRNA(Glu)-Derived Fragment Acts as a Tumor Suppressor in Breast Cancer by Targeting Nucleolin. *FASEB J* (2019) 33:13228–40. doi: 10.1096/fj.201900382RR
89. Sun C, Yang F, Zhang Y, Chu J, Wang J, Wang Y, et al. tRNA-Derived Fragments as Novel Predictive Biomarkers for Trastuzumab-Resistant Breast Cancer. *Cell Physiol Biochem* (2018) 49:419–31. doi: 10.1159/000492977
90. Zhu L, Li T, Shen Y, Yu X, Xiao B, Guo J. Using tRNA Halves as Novel Biomarkers for the Diagnosis of Gastric Cancer. *Cancer biomark* (2019) 25:169–76. doi: 10.3233/CBM-182184
91. Xu W, Zhou B, Wang J, Tang L, Hu Q, Wang J, et al. tRNA-Derived Fragment tRF-Glu-TTC-027 Regulates the Progression of Gastric Carcinoma *via* MAPK Signaling Pathway. *Front Oncol* (2021) 11:733763. doi: 10.3389/fonc.2021.733763
92. Shen Y, Xie Y, Yu X, Zhang S, Wen Q, Ye G, et al. Clinical Diagnostic Values of Transfer RNA-Derived Fragment tRF-19-3L7L73JD and its Effects on the Growth of Gastric Cancer Cells. *J Cancer* (2021) 12:3230–8. doi: 10.7150/jca.51567
93. Shen Y, Yu X, Ruan Y, Li Z, Xie Y, Yan Z, et al. Global Profile of tRNA-Derived Small RNAs in Gastric Cancer Patient Plasma and Identification of tRF-33-P4R8YP9LON4VDP as a New Tumor Suppressor. *Int J Med Sci* (2021) 18:1570–9. doi: 10.7150/ijms.53220
94. Dong X, Fan X, He X, Chen S, Huang W, Gao J, et al. Comprehensively Identifying the Key tRNA-Derived Fragments and Investigating Their Function in Gastric Cancer Processes. *Onco Targets Ther* (2020) 13:10931–43. doi: 10.2147/OTT.S266130
95. Xiong W, Wang X, Cai X, Xiong W, Liu Y, Li C, et al. Identification of Trnaderived Fragments in Colon Cancer by Comprehensive Small RNA Sequencing. *Oncol Rep* (2019) 42:735–44. doi: 10.3892/or.2019.7178
96. Li S, Shi X, Chen M, Xu N, Sun D, Bai R, et al. Angiogenin Promotes Colorectal Cancer Metastasis *via* tiRNA Production. *Int J Cancer* (2019) 145:1395–407. doi: 10.1002/ijc.32245
97. Luan N, Chen Y, Li Q, Mu Y, Zhou Q, Ye X, et al. TRF-20-M0NK5Y93 Suppresses the Metastasis of Colon Cancer Cells by Impairing the Epithelial-to-Mesenchymal Transition Through Targeting Claudin-1. *Am J Transl Res* (2021) 13:124–42.
98. Olvedy M, Scaravilli M, Hoogstrate Y, Visakorpi T, Jenster G, Martens-Uzunova ES. A Comprehensive Repertoire of tRNA-Derived Fragments in Prostate Cancer. *Oncotarget* (2016) 7:24766–77. doi: 10.18632/oncotarget.8293
99. Yang C, Lee M, Song G, Lim W. tRNA(Lys)-Derived Fragment Alleviates Cisplatin-Induced Apoptosis in Prostate Cancer Cells. *Pharmaceutics* (2021) 13:55. doi: 10.3390/pharmaceutics13010055
100. Shao Y, Sun Q, Liu X, Wang P, Wu R, Ma Z. tRF-Leu-CAG Promotes Cell Proliferation and Cell Cycle in non-Small Cell Lung Cancer. *Chem Biol Drug Des* (2017) 90:730–8. doi: 10.1111/cbdd.12994
101. Pekarsky Y, Balatti V, Palamarchuk A, Rizzotto L, Veneziano D, Nigita G, et al. Dysregulation of a Family of Short Noncoding RNAs, tsRNAs, in Human Cancer. *Proc Natl Acad Sci USA* (2016) 113:5071–6. doi: 10.1073/pnas.1604266113
102. Zhu L, Li J, Gong Y, Wu Q, Tan S, Sun D, et al. Exosomal tRNA-Derived Small RNA as a Promising Biomarker for Cancer Diagnosis. *Mol Cancer* (2019) 18:74. doi: 10.1186/s12943-019-1000-8
103. Zhou Y, Hu J, Liu L, Yan M, Zhang Q, Song X, et al. Gly-tRF Enhances LCSC-Like Properties and Promotes HCC Cells Migration by Targeting NDFIP2. *Cancer Cell Int* (2021) 21:502. doi: 10.1186/s12935-021-02102-8
104. Zhang M, Li F, Wang J, He W, Li Y, Li H, et al. tRNA-Derived Fragment tRF-03357 Promotes Cell Proliferation, Migration and Invasion in High-Grade Serous Ovarian Cancer. *Onco Targets Ther* (2019) 12:6371–83. doi: 10.2147/OTT.S206861
105. Peng EY, Shu Y, Wu Y, Zeng F, Tan S, Deng Y, et al. Presence and Diagnostic Value of Circulating tsncRNA for Ovarian Tumor. *Mol Cancer* (2018) 17:163. doi: 10.1186/s12943-018-0910-1

106. Wang BG, Yan LR, Xu Q, Zhong XP. The Role of Transfer RNA-Derived Small RNAs (tsRNAs) in Digestive System Tumors. *J Cancer* (2020) 11:7237–45. doi: 10.7150/jca.46055
107. Karousi P, Adamopoulos PG, Papageorgiou SG, Pappa V, Scorilas A, Kontos CK. A Novel, Mitochondrial, Internal tRNA-Derived RNA Fragment Possesses Clinical Utility as a Molecular Prognostic Biomarker in Chronic Lymphocytic Leukemia. *Clin Biochem* (2020) 85:20–6. doi: 10.1016/j.clinbiochem.2020.07.005
108. Karousi P, Katsaraki K, Papageorgiou SG, Pappa V, Scorilas A, Kontos CK. Identification of a Novel tRNA-Derived RNA Fragment Exhibiting High Prognostic Potential in Chronic Lymphocytic Leukemia. *Hematol Oncol* (2019) 37:498–504. doi: 10.1002/hon.2616
109. Katsaraki K, Artemaki PI, Papageorgiou SG, Pappa V, Scorilas A, Kontos CK. Identification of a Novel, Internal tRNA-Derived RNA Fragment as a New Prognostic and Screening Biomarker in Chronic Lymphocytic Leukemia, Using an Innovative Quantitative Real-Time PCR Assay. *Leuk Res* (2019) 87:106234. doi: 10.1016/j.leukres.2019.106234
110. Fabris L, Juracek J, Calin G. Non-Coding RNAs as Cancer Hallmarks in Chronic Lymphocytic Leukemia. *Int J Mol Sci* (2020) 21:6720. doi: 10.3390/ijms21186720
111. Katsaraki K, Adamopoulos PG, Papageorgiou SG, Pappa V, Scorilas A, Kontos CK. A 3' tRNA-Derived Fragment Produced by tRNA(LeuAAG) and tRNA(LeuTAG) is Associated With Poor Prognosis in B-Cell Chronic Lymphocytic Leukemia, Independently of Classical Prognostic Factors. *Eur J Haematol* (2021) 106:821–30. doi: 10.1111/ejh.13613
112. Nientiedt M, Deng M, Schmidt D, Perner S, Muller SC, Ellinger J. Identification of Aberrant tRNA-Halves Expression Patterns in Clear Cell Renal Cell Carcinoma. *Sci Rep* (2016) 6:37158. doi: 10.1038/srep37158
113. Zhao C, Tolkach Y, Schmidt D, Kristiansen G, Muller SC, Ellinger J. 5'-tRNA Halves are Dysregulated in Clear Cell Renal Cell Carcinoma. *J Urol* (2018) 199:378–83. doi: 10.1016/j.juro.2017.07.082
114. Ivanov P, Emara MM, Villen J, Gygi SP, Anderson P. Angiogenin-Induced tRNA Fragments Inhibit Translation Initiation. *Mol Cell* (2011) 43:613–23. doi: 10.1016/j.molcel.2011.06.022
115. Papadimitriou MA, Avgeris M, Levis P, Papasotiriou EC, Kotronopoulos G, Stravodimos K, et al. tRNA-Derived Fragments (tRFs) in Bladder Cancer: Increased 5'-tRF-LysCTT Results in Disease Early Progression and Patients' Poor Treatment Outcome. *Cancers (Basel)* (2020) 12:3661. doi: 10.3390/cancers12123661
116. Shan S, Wang Y, Zhu C. A Comprehensive Expression Profile of tRNA-Derived Fragments in Papillary Thyroid Cancer. *J Clin Lab Anal* (2021) 35: e23664. doi: 10.1002/jcla.23664
117. Gu X, Wang L, Coates PJ, Boldrup L, Fahraeus R, Wilms T, et al. Transfer-RNA-Derived Fragments Are Potential Prognostic Factors in Patients With Squamous Cell Carcinoma of the Head and Neck. *Genes (Basel)* (2020) 11:1344. doi: 10.3390/genes11111344
118. Mo D, Jiang P, Yang Y, Mao X, Tan X, Tang X, et al. A tRNA Fragment, 5'-tiRNA(Val), Suppresses the Wnt/beta-Catenin Signaling Pathway by Targeting FZD3 in Breast Cancer. *Cancer Lett* (2019) 457:60–73. doi: 10.1016/j.canlet.2019.05.007
119. Huang Y, Ge H, Zheng M, Cui Y, Fu Z, Wu X, et al. Serum tRNA-Derived Fragments (tRFs) as Potential Candidates for Diagnosis of Nontriple Negative Breast Cancer. *J Cell Physiol* (2020) 235:2809–24. doi: 10.1002/jcp.29185
120. Rounge TB, Furu K, Skotheim RI, Haugen TB, Grotmol T, Enerly E. Profiling of the Small RNA Populations in Human Testicular Germ Cell Tumors Shows Global Loss of piRNAs. *Mol Cancer* (2015) 14:153. doi: 10.1186/s12943-015-0411-4
121. Zhou K, Diebel KW, Holy J, Skildum A, Odean E, Hicks DA, et al. A tRNA Fragment, Trf5-Glu, Regulates BCAR3 Expression and Proliferation in Ovarian Cancer Cells. *Oncotarget* (2017) 8:95377–91. doi: 10.18632/oncotarget.20709
122. Ma ZL, Zhang BJ, Wang DT, Li X, Wei JL, Zhao BT, et al. Tanshinones Suppress AURKA Through Up-Regulation of miR-32 Expression in non-Small Cell Lung Cancer. *Oncotarget* (2015) 6:20111–20. doi: 10.18632/oncotarget.3933
123. Hu F, Niu Y, Mao X, Cui J, Wu X, Simone CB2nd, et al. tsRNA-5001a Promotes Proliferation of Lung Adenocarcinoma Cells and is Associated With Postoperative Recurrence in Lung Adenocarcinoma Patients. *Transl Lung Cancer Res* (2021) 10:3957–72. doi: 10.21037/tlcr-21-829
124. Tamura RE, De Vasconcellos JF, Sarkar D, Libermann TA, Fisher PB, Zerbini LF. GADD45 Proteins: Central Players in Tumorigenesis. *Curr Mol Med* (2012) 12:634–51. doi: 10.2174/156652412800619978
125. Haring SJ, Mason AC, Binz SK, Wold MS. Cellular Functions of Human RPA1. Multiple Roles of Domains in Replication, Repair, and Checkpoints. *J Biol Chem* (2008) 283:19095–111. doi: 10.1074/jbc.M800881200
126. Hanahan D, Weinberg RA. Hallmarks of Cancer: The Next Generation. *Cell* (2011) 144:646–74. doi: 10.1016/j.cell.2011.02.013
127. Elbarbary RA, Takaku H, Uchiumi N, Tamiya H, Abe M, Takahashi M, et al. Modulation of Gene Expression by Human Cytosolic Trnase Z(L) Through 5'-half-tRNA. *PloS One* (2009) 4:e5908. doi: 10.1371/journal.pone.0005908
128. Fares J, Fares MY, Khachfe HH, Salhab HA, Fares Y. Molecular Principles of Metastasis: A Hallmark of Cancer Revisited. *Signal Transduct Target Ther* (2020) 5:28. doi: 10.1038/s41392-020-0134-x
129. Londin E, Magee R, Shields CL, Lally SE, Sato T, Rigoutsos I. IsomiRs and tRNA-Derived Fragments are Associated With Metastasis and Patient Survival in Uveal Melanoma. *Pigment Cell Melanoma Res* (2020) 33:52–62. doi: 10.1111/pcmr.12810
130. Birch J, Clarke CJ, Campbell AD, Campbell K, Mitchell L, Liko D, et al. The Initiator Methionine tRNA Drives Cell Migration and Invasion Leading to Increased Metastatic Potential in Melanoma. *Biol Open* (2016) 5:1371–9. doi: 10.1242/bio.019075
131. Peinado H, Zhang H, Matei IR, Costa-Silva B, Hoshino A, Rodrigues G, et al. Pre-Metastatic Niches: Organ-Specific Homes for Metastases. *Nat Rev Cancer* (2017) 17:302–17. doi: 10.1038/nrc.2017.6
132. Pastushenko I, Blanpain C. EMT Transition States During Tumor Progression and Metastasis. *Trends Cell Biol* (2019) 29:212–26. doi: 10.1016/j.tcb.2018.12.001
133. Zhang F, Shi J, Wu Z, Gao P, Zhang W, Qu B, et al. A 3'-tRNA-Derived Fragment Enhances Cell Proliferation, Migration and Invasion in Gastric Cancer by Targeting FBXO47. *Arch Biochem Biophys* (2020) 690:108467. doi: 10.1016/j.abb.2020.108467
134. Mo D, He F, Zheng J, Chen H, Tang L, Yan F. tRNA-Derived Fragment tRF-17-79mp9pp Attenuates Cell Invasion and Migration *via* THBS1/TGF-Beta1/Smad3 Axis in Breast Cancer. *Front Oncol* (2021) 11:656078. doi: 10.3389/fonc.2021.656078
135. Hinshaw DC, Shevde LA. The Tumor Microenvironment Innately Modulates Cancer Progression. *Cancer Res* (2019) 79:4557–66. doi: 10.1158/0008-5472.CAN-18-3962
136. Slack FJ, Chinnaiyan AM. The Role of Non-Coding RNAs in Oncology. *Cell* (2019) 179:1033–55. doi: 10.1016/j.cell.2019.10.017
137. Chen Q, Li Y, Liu Y, Xu W, Zhu X. Exosomal Non-Coding RNAs-Mediated Crosstalk in the Tumor Microenvironment. *Front Cell Dev Biol* (2021) 9:646864. doi: 10.3389/fcell.2021.646864
138. Clara JA, Monge C, Yang Y, Takebe N. Targeting Signalling Pathways and the Immune Microenvironment of Cancer Stem Cells - a Clinical Update. *Nat Rev Clin Oncol* (2020) 17:204–32. doi: 10.1038/s41571-019-0293-2
139. Sistigu A, Musella M, Galassi C, Vitale I, De Maria R. Tuning Cancer Fate: Tumor Microenvironment's Role in Cancer Stem Cell Quiescence and Reawakening. *Front Immunol* (2020) 11:2166. doi: 10.3389/fimmu.2020.02166
140. Guzzi N, Bellodi C. Novel Insights Into the Emerging Roles of tRNA-Derived Fragments in Mammalian Development. *RNA Biol* (2020) 17:1214–22. doi: 10.1080/15476286.2020.1732694
141. Cui Y, Huang Y, Wu X, Zheng M, Xia Y, Fu Z, et al. Hypoxia-Induced tRNA-Derived Fragments, Novel Regulatory Factor for Doxorubicin Resistance in Triple-Negative Breast Cancer. *J Cell Physiol* (2019) 234:8740–51. doi: 10.1002/jcp.27533
142. Jia Z. Role of Integrin-Linked Kinase in Drug Resistance of Lung Cancer. *Onco Targets Ther* (2015) 8:1561–5. doi: 10.2147/OTT.S81447
143. Saw PE, Xu X, Chen J, Song EW. Non-Coding RNAs: The New Central Dogma of Cancer Biology. *Sci China Life Sci* (2021) 64:22–50. doi: 10.1007/s11427-020-1700-9
144. Wei G, Zhu J, Hu HB, Liu JQ. Circular RNAs: Promising Biomarkers for Cancer Diagnosis and Prognosis. *Gene* (2021) 771:145365. doi: 10.1016/j.gene.2020.145365
145. Wang J, Ma G, Li M, Han X, Xu J, Liang M, et al. Plasma tRNA Fragments Derived From 5' Ends as Novel Diagnostic Biomarkers for Early-Stage Breast

Cancer. *Mol Ther Nucleic Acids* (2020) 21:954–64. doi: 10.1016/j.omtn.2020.07.026
146. Huang Y, Zhang H, Gu X, Qin S, Zheng M, Shi X, et al. Elucidating the Role of Serum tRF-31-U5YKFN8DYDZDD as a Novel Diagnostic Biomarker in Gastric Cancer (Gc). *Front Oncol* (2021) 11:723753. doi: 10.3389/fonc.2021.723753
147. Zhang S, Sun L, Kragler F. The Phloem-Delivered RNA Pool Contains Small Noncoding RNAs and Interferes With Translation. *Plant Physiol* (2009) 150:378–87. doi: 10.1104/pp.108.134767
148. Xu WL, Yang Y, Wang YD, Qu LH, Zheng LL. Computational Approaches to tRNA-Derived Small RNAs. *Noncoding RNA* (2017) 3:2. doi: 10.3390/ncrna3010002
149. Saleembhasha A, Mishra S. Novel Molecules lncRNAs, tRFs and circRNAs Deciphered From Next-Generation Sequencing/RNA Sequencing: Computational Databases and Tools. *Brief Funct Genomics* (2018) 17:15–25. doi: 10.1093/bfgp/elx013
150. Li N, Shan N, Lu L, Wang Z. Trftarget: A Database for Transfer RNA-Derived Fragment Targets. *Nucleic Acids Res* (2021) 49:D254–60. doi: 10.1093/nar/gkaa831
151. Zhang X, Trebak F, Souza LAC, Shi J, Zhou T, Kehoe PG, et al. Small RNA Modifications in Alzheimer's Disease. *Neurobiol Dis* (2020) 145:105058. doi: 10.1016/j.nbd.2020.105058
152. Liang G, Zhu Y, Ali DJ, Tian T, Xu H, Si K, et al. Engineered Exosomes for Targeted Co-Delivery of miR-21 Inhibitor and Chemotherapeutics to Reverse Drug Resistance in Colon Cancer. *J Nanobiotechnol* (2020) 18:10. doi: 10.1186/s12951-019-0563-2

Conflict of Interest: The authors declare that the research was conducted in the absence of any commercial or financial relationships that could be construed as a potential conflict of interest.

Publisher's Note: All claims expressed in this article are solely those of the authors and do not necessarily represent those of their affiliated organizations, or those of the publisher, the editors and the reviewers. Any product that may be evaluated in this article, or claim that may be made by its manufacturer, is not guaranteed or endorsed by the publisher.

frontiers | Frontiers in Oncology

ORIGINAL RESEARCH
published: 04 May 2022
doi: 10.3389/fonc.2022.856424

Targeting a Tumor-Specific Epitope on Podocalyxin Increases Survival in Human Tumor Preclinical Models

Diana Canals Hernaez[1], Michael R. Hughes[1], Yicong Li[1], Ilaria Mainero Rocca[2], Pamela Dean[3], Julyanne Brassard[1], Erin M. Bell[3], Ismael Samudio[4], Anne-Marie Mes-Masson[5], Yoshiki Narimatsu[6], Henrik Clausen[6], Ola Blixt[2], Calvin D. Roskelley[3] and Kelly M. McNagny[1]**

[1] The Biomedical Research Centre and School of Biomedical Engineering, University of British Columbia, Vancouver, BC, Canada, [2] Department of Biotechnology and Biomedicine, Technical University of Denmark, Lyngby, Denmark, [3] Department of Cellular and Physiological Sciences, University of British Columbia, Vancouver, BC, Canada, [4] Centre for Drug Research and Development, Vancouver, BC, Canada, [5] Department of Medicine,Institut du Cancer de Montreal, Montreal, QC, Canada, [6] Copenhagen Center for Glycomics, Department of Cellular and Molecular Medicine (ICMM), University of Copenhagen, Copenhagen, Denmark

OPEN ACCESS

Edited by:
Yan-yan Yan,
Shanxi Datong University, China

Reviewed by:
Behjatolah Monzavi-Karbassi,
University of Arkansas for Medical Sciences, United States
Luciana N. S. Andrade,
University of São Paulo, Brazil

***Correspondence:**
Kelly M. McNagny
kelly@brc.ubc.ca
Calvin D. Roskelley
calvin.roskelley@ubc.ca

Specialty section:
This article was submitted to Cancer Molecular Targets and Therapeutics, a section of the journal Frontiers in Oncology

Received: 17 January 2022
Accepted: 04 April 2022
Published: 04 May 2022

Citation:
Canals Hernaez D, Hughes MR, Li Y, Mainero Rocca I, Dean P, Brassard J, Bell EM, Samudio I, Mes-Masson A-M, Narimatsu Y, Clausen H, Blixt O, Roskelley CD and McNagny KM (2022) Targeting a Tumor-Specific Epitope on Podocalyxin Increases Survival in Human Tumor Preclinical Models. Front. Oncol. 12:856424. doi: 10.3389/fonc.2022.856424

Podocalyxin (Podxl) is a CD34-related cell surface sialomucin that is normally highly expressed by adult vascular endothelia and kidney podocytes where it plays a key role in blocking adhesion. Importantly, it is also frequently upregulated on a wide array of human tumors and its expression often correlates with poor prognosis. We previously showed that, in xenograft studies, Podxl plays a key role in metastatic disease by making tumor initiating cells more mobile and invasive. Recently, we developed a novel antibody, PODO447, which shows exquisite specificity for a tumor-restricted glycoform of Podxl but does not react with Podxl expressed by normal adult tissue. Here we utilized an array of glycosylation defective cell lines to further define the PODO447 reactive epitope and reveal it as an O-linked core 1 glycan presented in the context of the Podxl peptide backbone. Further, we show that when coupled to monomethyl auristatin E (MMAE) toxic payload, PODO447 functions as a highly specific and effective antibody drug conjugate (ADC) in killing ovarian, pancreatic, glioblastoma and leukemia cell lines *in vitro*. Finally, we demonstrate PODO447-ADCs are highly effective in targeting human pancreatic and ovarian tumors in xenografted NSG and Nude mouse models. These data reveal PODO447-ADCs as exquisitely tumor-specific and highly efficacious immunotherapeutic reagents for the targeting of human tumors. Thus, PODO447 exhibits the appropriate characteristics for further development as a targeted clinical immunotherapy.

Keywords: podocalyxin, antibody-drug conjugate, PODO447, tumor-specific, glycoepitope

Abbreviations: Ab(s), antibodies; ADC, antibody drug conjugate; AML, acute myeloid leukemia; HGS, high grade serous; KI, knock-in; KO, knockout; NK, natural killer cells; NSG, NOD.Cg-Prkdcscid Il2rgtmWji/SzJ; Podxl, podocalyxin; RSV, respiratory syncytial virus; T, T-antigen.

INTRODUCTION

Despite dramatic improvements in early detection, diagnosis and treatment, cancer remains one of the leading causes of death worldwide with an estimated 10 million deaths in 2020 (1). Importantly, over 90% of these cancer-related deaths are the result of metastatic disease which remains the most difficult to treat. This is largely due to its diffuse nature and the paucity of effective immuno- and chemotherapeutic agents with the appropriate selectivity for targeting tumor cells while sparing normal healthy tissue (2).

Podocalyxin (Podxl), a member of the CD34-family of sialomucins (3), is normally expressed by embryonic (ES) and induced pluripotent (iPS) stem cells, early hematopoietic progenitor, adult vascular endothelia and kidney podocytes (4–11). Podxl plays an essential role in murine and human development and null mutations lead to perinatal lethality (4, 12, 13). Functionally, we and others have shown that this molecule is targeted to the apical domain of cells where it plays a key role in blocking adhesion, opening luminal structures and enhancing cell mobility and invasiveness (8, 14).

Importantly, in addition to its normal tissue expression pattern, Podxl is also aberrantly expressed by a wide variety of human tumors and its expression is consistently an indicator of poor prognosis (10, 15–25). Recent gene silencing and xenograft studies reveal an essential role for Podxl in disease progression through enhancing the mobility and invasiveness of tumor cells and promoting formation of distal metastasis (16, 26–28). Accordingly, Podxl has garnered increasing attention as a target for immunotherapy and we previously identified a core protein binding antibody (PODO83/PODOC1) that slows primary tumor growth and blocks metastatic disease (16). Nevertheless, further development of Podxl core protein-binding antibodies as cancer immunotherapeutics has been hampered by concerns over possible toxicity to normal vascular and renal tissue where Podxl is abundantly expressed in healthy adults.

The 53 kDa Podxl core protein undergoes extensive, tissue-specific N- and O-linked glycosylation leading to a mature protein with an apparent molecular weight of 150-200 kDa (8, 10, 14). Since glycosylation processes are frequently altered in cancer (29–31), we recently engaged in an antibody development campaign to identify antibodies that would recognize tumor specific glycoepitopes on Podxl but not react with Podxl expressed by normal tissue (32). One resultant antibody, PODO447, exhibits exquisite specificity for a tumor glycoform of Podxl but lacks reactivity with normal adult human tissue. Furthermore, in a tissue microarray (TMA) screen we showed that this epitope is expressed by over 60% of high grade serous (HGS) ovarian tumors (32). Thus, this antibody exhibits the appropriate specificity and distribution for further development as a therapeutic, particularly for highly metastatic disease.

In the current work, we evaluate the ability of PODO447 to serve as the targeting arm for therapeutic drug delivery in ADC assays. We find that although this antibody lacks inherent Podxl function blocking activity, it is highly effective in killing a variety of tumor cells *in vitro* as an ADC. Moreover, we find that PODO447-ADC shows potent efficacy against human tumor cell lines in two different mouse xenograft models. Finally, using a cell-based glycan array we reveal the PODO447-reactive epitope to be a core 1 O-glycan in the context of the Podxl polypeptide. In aggregate, these data reveal PODO447-ADC as a highly specific and efficacious immunotherapeutic agent and highlight its promise for treating high grade human tumors.

MATERIALS AND METHODS

Cell Culture

HEK-293 WT, HUVEC, SKOV3, A-172, MIA PaCa-2, THP-1 and MDA-MB-231 cells were obtained from the American Tissue Culture Collection (ATCC). Glycosylation-mutant HEK-293 cells (33, 34) and patient tumor-derived epithelial high grade serous ovarian OV3331 and TOV3133D cancer cell lines (35, 36) were previously described. ONS-76 medulloblastoma cell line was generously provided by Dr. Sorensen from the University of British Columbia. PODO447-positive and PODO447-negative CFPAC-1 cells were generated by sorting parental pancreatic CFPAC-1 cells (metastatic tumor-derived) with or without PODO447 expression. HEK-293 WT and isogenic cells were grown in DMEM (Gibco, #11965-092) supplemented with 10% FBS and 2mM GlutaMAX (Gibco, #35050061). CFPAC-1 cells were grown in IMDM (Gibco, #12440053) supplemented with 10% FBS. MIA PaCa-2, A-172, and MDA-MB-231 cells were grown in DMEM (Gibco, #11965-092) supplemented with 10% FBS and 10 U/ml penicillin and streptomycin (P/S) (Gibco, #15140-122). Human umbilical vein endothelial (HUVEC) cells were harvested from donor umbilical cords (Human Ethics no. H10-00643), grown in Endothelial Cell Growth Medium-2 Bulletkit™ (LONZA, #CC-3162), and used between passages 2 and 8. Human ovarian cancer SKOV3 cells were grown in DMEM F-12 with 15 mM HEPES (Sigma, #D6421) supplemented with 10% FBS, 0.2 mM L-glutamine (Gibco, #25030-081) and 10 U/ml P/S. OV3331 and TOV3133D cells were grown in complete OSE medium (36). ONS-76 cells were grown in RPMI (Gibco, #11875093) supplemented with 10% FBS. All cell lines were maintained at 37°C, 5% CO_2 and high humidity.

Flow Cytometry

Cells were washed 1X with Ca^{2+}- and Mg^{2+}-free HBSS (Gibco, #14170-112), incubated for 1-2 min at 37°C in a 0.25% trypsin solution, quenched with complete growth media, then centrifuged for 4 min at 394*g*, washed 2X with FACS buffer (PBS, 2 mM EDTA, 5% FBS, 0.05% sodium azide) and transferred to a 96 well 'v' bottom plate. Cells were resuspended in 100 µl blocking buffer (FACS buffer, 1 µg/ml of anti-CD16/CD32 (clone 2.4G), 2% rat serum) for 20 min at 4°C in the dark, then spun at 394*g* for 4 min and incubated in 100 µl primary antibody (Ab) solution for 30 min at 4°C in the dark. Rabbit-PODO83 (16) (2 µg/ml); and either rabbit or chimeric PODO447 (32) (5 µg/ml) were used to detect Podxl. Biotinylated pan-lectenz lectin (1 µg/ml, Lectenz-Bio #SK0501B) was used to detect sialylated complex glycans. 3C9 (37), 5F4 (38) and TKH2 (39) antibodies were used to detect core

1, Tn and STn glycostructures, respectively. Wisteria Floribunda lectin (WFA, 0.25 μg/ml, Vector Laboratories, #B-1355-2) was used to detect α/β N-acetylgalactosamine (α/β-GalNAc). Erythrina Cristagalli lectin (ECL, 1 μg/ml, Vector Laboratories, #B-1145-5) was used to detect galactose, lactose and N-acetylgalactosamine. Peanut agglutinin (PNA, 5μg/ml, Vector Laboratories #B1075-5; ThermoFisher #L32459) was used to detect T-antigen. Rabbit-IgG (5 μg/ml, Vector Laboratories, #I-1000-5) and mouse/human-chimeric palivizumab (5 μg/ml, National Research Council, NRC) were used as isotype controls. Next, cells were washed 3X with FACS buffer and resuspended in 100 μl of secondary Ab solution (Alexa Fluor 647 (AF647) donkey-anti-rabbit (2 μg/ml, Invitrogen, #A31573); AF647 goat-anti-human (2 μg/ml, Jackson ImmunoResearch Laboratories, #109-605-098); Brilliant Violet 450 (BV450) Streptavidin (2 μg/ml)) for 30 min at 4°C in the dark. Cells were washed 2X with FACS buffer and resuspended in FACS buffer containing propidium iodide (PI) (0.5 μg/ml, Life Technologies, #P3566). High-throughput flow cytometry data was acquired using an SA3800 spectral analyzer. The remaining flow cytometry data was acquired using a BD LSRII and analyzed using FlowJo™ software (BD Biosciences, Ashland).

In Vitro Antibody Internalization

Sub-confluent cells were harvested and plated in 50 μl per well at the following concentrations: MIA PaCa-2 (8 x 10^3 cells/well), A-172 (8 x 10^3 cells/well) and SKOV3 (1 x 10^4 cells/well). Cells were then incubated overnight at 37°C, in 5% CO_2. On day 1, coupling of the antibodies was performed by incubation of biotinylated PODO447 or palivizumab control mAb (40) with pHrodo™ Red Avidin (ThermoFisher, #P35362) at 1:1 molar ratio for 30 min at 4°C. Next, 50 μl of cold pHrodo™-mAb mix was added to the cells and the plate was placed in the Incucyte®. The Incucyte® ZOOM software was set in "standard" mode with the phase and red channels selected and set to scan every 10 min for 24 hours. The rate of antibody internalization was evaluated through increased fluorescent area, reported as total internalization area (μm^2/well). Average internalization was calculated, and statistical analyses was performed using two-way ANOVA in GraphPad Prism software.

In Vitro Antibody Cytotoxicity

Cells were plated on 96-well plates in 100μl culture medium and allowed to adhere overnight. SKOV3, MIA PaCa-2, A-172, THP-1 and HUVEC were seeded at 2.5 x 10^3 cells per well; OV3331, TOV3133D and ONS-76 were seeded at 5 x 10^3 cells per well. On day 1, a 5X stock solution of each mAb/ADC concentration to be tested was prepared in a stepwise 1:3 serial dilution series in cell culture medium, and 25μl of each dilution was added to cells in triplicate. Treated cells were cultured at 37°C, 5% CO_2 and high humidity for 144 h. On day 6, thiazolyl blue tetrazolium bromide (MTT) assays were used to determine relative cytotoxicity. Briefly, 100μl of MTT (1mg/ml, Thermo Fisher Scientific, #AC158990010) was added to the cells and left to incubate for 3 h at 37°C. Next, MTT media was removed and 50μl of DMSO was added to the cells and allowed to incubate for 15 min at RT, protected from light and with mild shaking. Absorbance was then read at 570nm. Percent viability was calculated as [1-(absorbance of treated samples/average absorbance of control samples)] x 100. Average relative cytotoxicity was calculated, and statistical analyses were performed using two-way ANOVA (GraphPad Prism software).

Antibody-Dependent Cell-Mediated Cytotoxicity Assay

A-172 (2x10^6) cells were stained with 10μM CellTrace™ Far Red (Invitrogen™, #C34572) for 30 min at 37°C. Next, cells were washed 2X and seeded at 2 x 10^3 cells per well on a 96-well plate and allowed to adhere. 16 h after seeding A-172 labelled cells were incubated with 2.5, 0.5, or 0.1 μg/ml of PODO447, and 2.5 μg/ml of control human IgG1 for 15 min at RT. Next, antibody-labelled A-172 cells were co-cultured with human PBMCs at a 7:1 and 3:1 ratio for 1 h at 37°C, 5% CO_2. Cells were then harvested and stained with 1 μg/ml of PI for 5 min at RT. Cell viability was assessed *via* flow cytometry using a BD LSRFortessa™ X-20 and analyzed using FlowJo™ software (BD Biosciences, Ashland).

ADC Linker Stability Assay

Human cord blood CD34+ cells (1x10^6 cells/well, STEMCELL Technologies, # 70008.2) were seeded in 200 μL of complete growth medium [X-Vivo™ 15 (Lonza, #BE02-060F), rhIL-3 (20 ng/mL, Peprotech, #200-03), rhIL-6 (20 ng/mL, Peprotech, #200-06), rhSCF (100 ng/mL, Peprotech, #AF-300-07) and rhFlt-3L (100 ng/mL, Peprotech, #300-19)] in round-bottom 96-well plates and cultured at 37°C in 5% CO_2. On day 3, cells were washed 2X with X-Vivo™ 15 medium and incubated in X-Vivo™ 15 medium supplemented with rhSCF (50 ng/mL), rhFlt-3L (100 ng/mL), rh-IL3 (5 ng/mL), rhGM-CSF (5 ng/mL, Peprotech, #300-03) rhG-CSF (5 ng/mL, Peprotech, #300-23) at 37°C in 5% CO_2 for 4 days. On day 7, cells were then washed 2X and incubated in X-Vivo™ 15 medium supplemented with rhIL-3 (5 ng/mL) and rhG-CSF (30 ng/mL) for an additional 4 days. On day 11, cells were washed 2X and cultured in X-Vivo™ 15 medium supplemented with rhG-CSF (30 ng/mL) and either PODO447- or palivizumab-Vedotin at concentrations ranging from 0.01 – 10 μg/mL for an additional 6 days. On day 17, cells were harvested and prepared for flow cytometric analysis, as follows. Cells were blocked with 10% FBS and 20 μg/mL human IgG at 4°C for 10 minutes. Following blocking, cells were stained with anti-CD66b antibody (Biolegend, #305106) and DAPI (Biolegend, #422801) at 4°C for 20 minutes. Cells were then washed 2X and resuspended in FACS buffer. Flow cytometry data was acquired using a Beckman Coulter CytoFlex and analyzed using FlowJo™ software (BD Biosciences, Ashland) This assay was performed by ReachBio Research Labs, Seattle, USA (www.reachbio.com). The effect of ADCs on neutrophil differentiation is represented by percentage of CD66b+ cells within the viable cell population.

Mice

Tumor model animal experiments were carried out using 6-12-week-old female NOD.Cg-*Prkdc*^{scid}*Il2rg*^{tm1Wjl}/SzJ (NSG) and NU/J (nude) mice obtained from Jackson's Laboratories

(#005557 and #002019, respectively). Animals were bred in a specific, pathogen-free facility and all experiments were carried out under approved University of British Columbia Animal Care committee protocols (ACC protocol #A16-0007 and A20-0042) based on the recommendations of the Canadian Council on Animal Care.

Pre-Clinical *In Vivo* Xenograft Models to Assess PODO447-ADC Efficacy

MIA PaCa-2 ($1x10^6$) or OV3331 ($1x10^6$) cells were injected subcutaneously into the right flank of NSG or nude mice. Tumor dimensions were measured twice a week and tumor volumes (cm^3) were calculated by [(length x $width^2$)/2]. Once tumors reached $0.15cm^3$, mice were treated with either PODO447- or palivizumab-Vedotin at concentrations ranging from 4 – 2 mg/kg. ADC treatments were administered intravenously every 4 days. Average tumor volume over time was calculated, and statistical analysis was performed using two-way ANOVA test in GraphPad Prism software. Endpoints for survival analyses included animals with tumors exceeding 1 cm^3 or any animals with signs of morbidity reaching a humane endpoint regardless of tumor size. Survival Kaplan-Meier curves were calculated, and statistical analysis was performed using a Log-rank (Mantel-Cox) test in GraphPad Prism software.

Immunohistochemistry

Tumor slides were stained with either rabbit-PODO83 (5 µg/ml), Rbt/Hu-chimeric PODO447 (1 µg/ml), Mo/Hu-chimeric pavilizumab control (1 µg/ml) or rabbit IgG control (5 µg/ml, Vector laboratories, #I-1000-5). Briefly, slides were deparaffinized and rehydrated in 100% xylene (3X, 5 min), 100% ethanol (2X, 3 min), 95% ethanol (1X, 3 min), 70% ethanol (1X, 3 min) and distilled water (1X, 3 min). Antigen retrieval was performed by heating slides in citrate buffer at 90°C for 40 min. Slides were washed in PBS (3X, 5min), incubated for 30 min in blocking solution (PBS, 5% donkey serum, 0.5% BSA, 0.3% Triton X-100), and incubated in primary Ab solution overnight at 4°C. Slides were then washed with TBST (3X, 15 min), incubated with either anti-rabbit-BIOT (2 µg/ml, SouthernBiotech, #6440-06) or anti-human-BIOT (2 µg/ml, Jackson ImmunoResearch, #209-065-098) in blocking solution for 30 min at RT, and washed again with TBST (4X, 15 min). Endogenous peroxidase was blocked with 3% hydrogen peroxide in methanol for 40 min at RT prior to rinsing 3X with PBS. Signal was amplified using Vectastain® Elite® ABC HRP Kit (Vector Laboratories, #PK-6100) according to manufacturer's instructions, and then washed with PBS (3X, 5min). Signal was visualized using a DAB peroxidase (HRP) Substrate Kit (Vector Laboratories, #SK-4100) following the manufacturer's recommendations. Each slide was incubated with DAB solution for 30-40 sec until strong signal appeared, then the reaction was stopped by dilution with PBS. Slides were counterstained with Harris Hematoxylin (2.5 min, Fisher HealthCare™ PROTOCOL™, #23-245651), rinsed 1X with distilled water (30 sec), incubated with differentiator solution (30 sec, 1% HCl in 70% EtOH) and rinsed with distilled water (30 sec). Staining was fixed in Bluing Solution (0.1% sodium bicarbonate) for 30 sec and rinsed in distilled water (1X, 30 sec) prior to dehydration in graded alcohols and xylene. Slides were mounted using Permount solution (Fisher Scientific, #SP15100) and subsequently analyzed for Podxl staining.

RESULTS

PODO447 Binds to a Core 1 Glycostructure on Podxl

Previously we showed that PODO447 exhibits high affinity for tumor-specific glycoepitopes using a well-characterized printed glycan array (32, 41). One limitation of these arrays, however, is that they present glycostructures in isolation and not in the context of their normal attachment to proteins or lipids (41). Thus, while they provide guidance on the types of carbohydrate structures antibodies detect, they lack the full antigenic context for determining their true specificity. Accordingly, to gain further insight into PODO447's specificity in a natural context, we probed its reactivity against a cell-based glycan array composed of isogenic HEK-293 cells, which express endogenous Podxl, with a combination of knockout (KO) and knock-in (KI) glycosyltransferase genes that control the loss or gain of core 1 and core 2 O-glycosylation (33). First, we verified that the glycoengineered HEK-293 cells correctly displayed the predicted O-glycoforms using a variety of lectins and monoclonal antibodies (mAbs) (**Supplementary Figure 1**). Next, we probed this cell array with PODO447. In contrast to the printed array, PODO447 failed to recognize LacDiNAc glycostructures on HEK-293 cells and, instead, exhibited selective binding for core 1 O-glycans as demonstrated by the lack of Ab recognition after the loss of core 1 structures (Tn, KO C1GALT1), and increased Ab binding after the loss of core 2 O-glycans (T/ST/dST, KO GCNT1) (**Figure 1A**). Additionally, loss of α6 (KO ST6GALNACT2/3/4) and α3 (KO ST3GAL1/2) sialylation increased Ab binding suggesting that sialylation, although tolerated, is dispensable for PODO447 binding. Lastly, we also tested PODO447 recognition of cancer-associated STn (KI ST6GALNAC1/KO COSMC) and core 3 O-glycans (KI B3GNT3/KO COSMC) and observed no Ab binding to either of these structures. From these data, we conclude that PODO447 binds preferentially to a non-sialylated core 1 O-glycan, also known as T-antigen (T), a glycomotif that has been previously reported as a cancer-associated glycan epitope (42). Importantly, PODO447 recognizes T-antigen only in the context of the Podxl backbone since PODO447 fails to bind to PODXL-KO HEK-293 cells (**Figure 1A**).

To further validate the contribution of Podxl's peptide backbone to the PODO447 epitope, we evaluated the binding of PODO447, PODO83 and peanut agglutinin (PNA) to SKOV3 wild type (WT) and Podxl knock-out (PODXL-KO) cells. The Podxl core protein-binding Ab, PODO83 (32), served as a control for ablation of protein expression, while PNA served as a control for T-antigen expression by all cell surface proteins. We

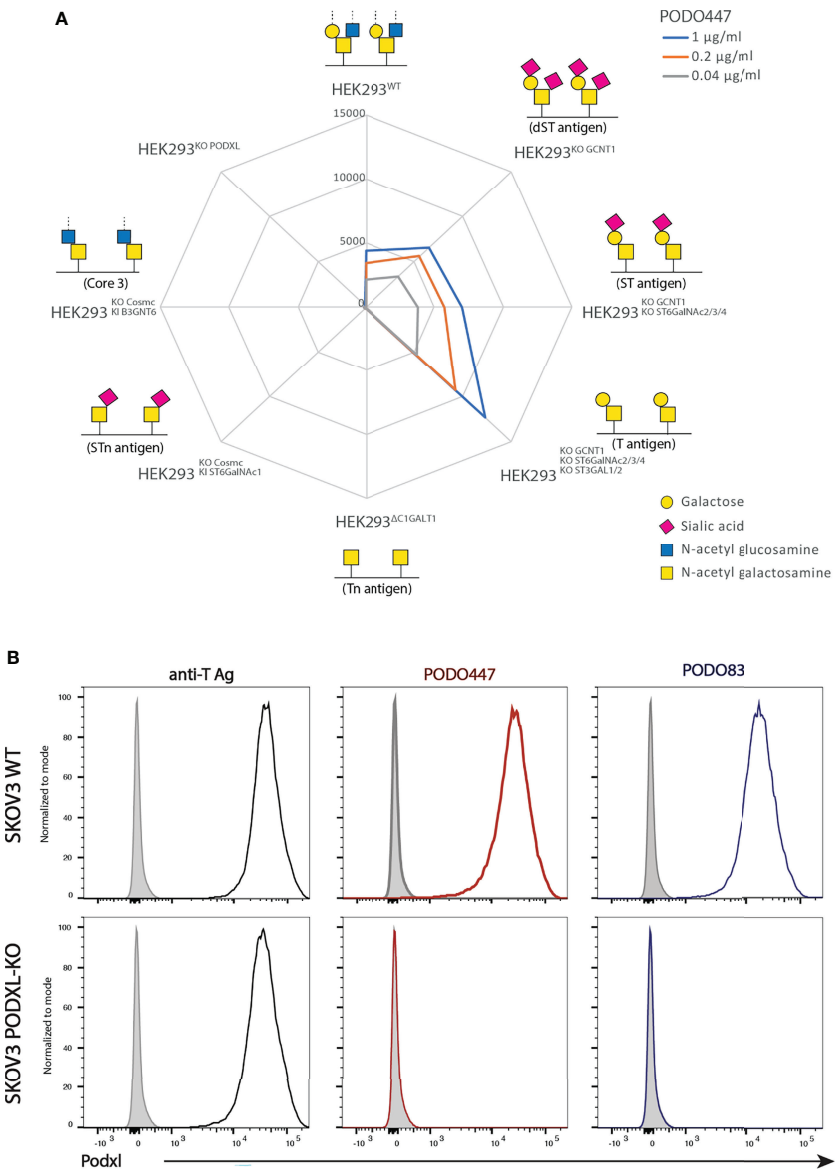

FIGURE 1 | PODO447 binds to a core 1 O-glycan structure on Podxl. **(A)** Isogenic HEK-293 cells bearing mutations in glycosyl transferases were stained with various concentrations of PODO447 and evaluated by flow cytometry. Mean Fluorescence Intensity (MFI) results are summarized in the "spiderweb plot". **(B)** Flow cytometric anti-core 1 PNA lectin (black lines), PODO447 (red lines) and PODO83 (blue lines) binding profiles of SKOV3 WT and SKOV3 PODXL-KO cells.

found that PNA bound both SKOV3 WT and SKOV3 PODXL-KO cells suggesting a wide array of T-antigen epitopes are expressed on these cell lines (**Figure 1B**). Conversely, PODO447 and PODO83 Abs reacted exclusively with WT but not PODXL-KO cells, confirming the specificity of these Abs for epitopes linked to the Podxl core protein. In addition, we further validated the contribution of the T-antigen to the PODO447 epitope using the human pancreatic CFPAC-1 cell line. This cell line shows heterogeneous expression of the PODO447 epitope (low to high) and a linear correlation between PODO447 and PNA staining. This was further validated by sorting this line into PODO447-positive and -negative CFPAC-1 cell subclones which, correspondingly, showed high and low PNA staining, respectively (**Supplementary Figure 2**). In summary, these experiments suggest that PODO447 specifically binds a glycopeptide epitope consisting of the core 1 O-glycan in the context of the Podxl polypeptide but does not recognize general core 1 glycans decorating other proteins.

PODO447 Lacks a Direct Effect on Cell Viability

Prompted by previous reports of anti-Podxl Abs with cytotoxic activity against undifferentiated human embryonic stem cells (43), and our own data showing PODO83 blocks metastasis *in*

vivo (16), we investigated whether PODO447 binding exhibits any effects on cell viability. We performed a long-term (144h) *in vitro* exposure assay using unconjugated PODO447 or palivizumab, an Ab specific for the F protein of the respiratory syncytial virus (RSV) that served as a control. We used normal human endothelia (HUVEC) cells and an array of human cancer cell lines, including pancreatic (MIA PaCa-2), glioblastoma (A-172) and acute monocytic leukemia (THP-1, AML) lines (**Figures 2A–D**). Unconjugated PODO447 had no effect on cell viability at any concentration, suggesting that binding of this antibody does not block pathways critical for cancer cell survival and proliferation *in vitro*.

PODO447 Induces Cellular Toxicity *Via* ADCC

We next evaluated if binding of PODO447 induces antibody-dependent cell-mediated cytotoxicity (ADCC). We first incubated A-172 cells with 0.1, 0.5 and 2.5 μg/ml of PODO447 or 2.5 μg/ml of palivizumab control antibody. Next, we co-cultured the antibody-bound cells with human peripheral blood mononuclear cells (PBMCs) at 7:1 and 3.5:1 ratio of effector (PBMCs) to target (A-172) cells and assessed A-172 cell viability by flow cytometry. We found that PODO447 induced a modest, dose-dependent, level of ADCC activity on A-172 cells at both effector to target cell ratios (**Figure 2E**). From these results we conclude that unconjugated PODO447 can affect tumor cell viability *via* ADCC.

Evaluation of PODO447 Antibody-Drug Conjugates

Since unconjugated PODO447 did not directly affect cancer cell survival and only showed a low level of ADCC activity, we next investigated the potential use of PODO447 as the targeting arm for an ADC. We selected monomethyl auristatin E (MMAE) as the toxic payload since it is a well-studied tubulin polymerization inhibitor that, when internalized into cells, exhibits potent and

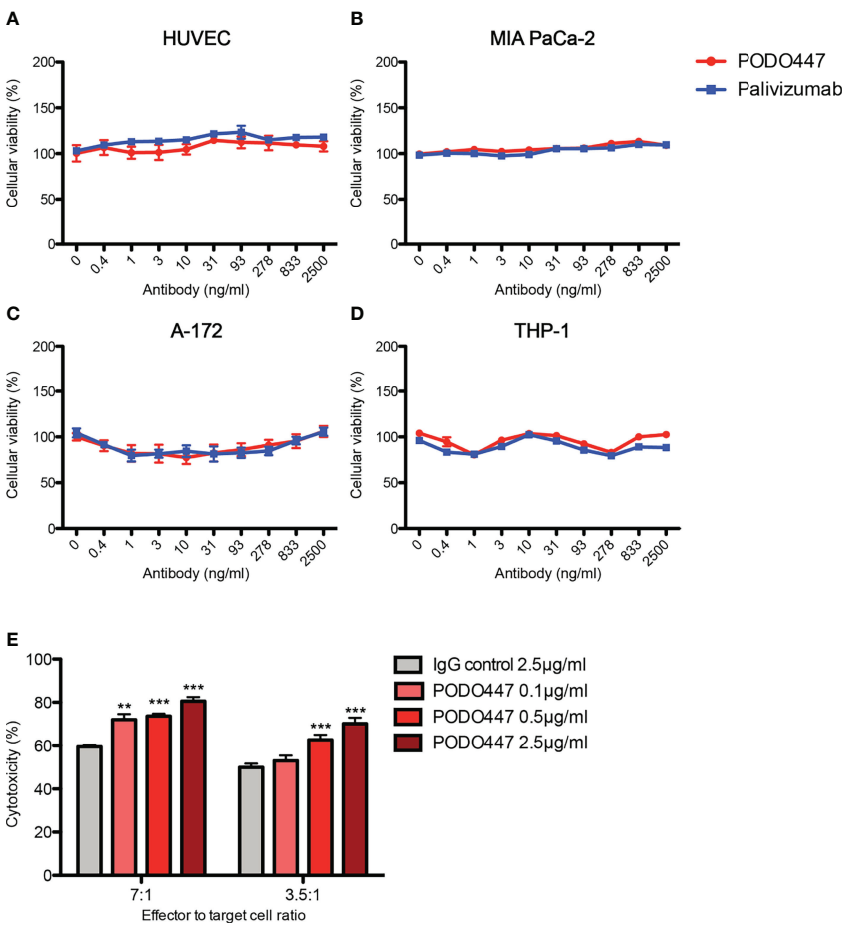

FIGURE 2 | Unconjugated PODO447 lacks inherent cytotoxic activity but induces ADCC. Cytotoxic effect of unconjugated PODO447 and palivizumab control Abs on **(A)** human umbilical vein endothelial cells (HUVEC), **(B)** pancreatic ductal adenocarcinoma (MIA PaCa-2), **(C)** glioblastoma (A-172) and **(D)** acute monocytic leukemia (THP-1) cell lines as determined by MTT assay; and **(E)** antibody-dependent cellular cytotoxicity induced by PODO447 in A-172 cells after 1 hr co-incubation with human PBMCs at a 7:1 and 3.5 ratio of effector (PBMCs) to target (A-172) cells. ADCC-induced cellular toxicity was determined by flow cytometry. $^{**}p < 0.01$, $^{***}p < 0.001$.

broad anti-tumor activity (44). MMAE was conjugated to either PODO447 or palivizumab control. Coupling was accomplished using a valine-citrulline (val-cit) proteolytically cleavable linker, resulting in "Vedotin" (Val-Cit-PABC-MMAE)-ADCs (**Figure 3A**). Linker stability was independently assessed by ReachBio Research Labs (RRL, www.reachbio.com) using an *in vitro* neutrophil differentiation killing assay, where extracellular proteolysis of the cleavable linker results in neutrophil cytotoxicity (45). RRL found that PODO447-ADC behaved very similarly to palivizumab control-ADC in the presence of neutrophils (**Supplementary Figure 3A**), thus suggesting both antibodies induce similar low levels of off-target toxicity as a result of non-specific extracellular cleavage.

Since these ADCs are dependent on internalization into acid compartments for cleavage and toxicity, we first tracked the ability of membrane-bound PODO447 to be internalized by tumor cells. Biotinylated PODO447 or palivizumab control Ab were conjugated to pHrodo™ Red Avidin (Invitrogen™), a pH sensitive dye that becomes fluorescent in acidic intracellular environments. Importantly, neither MMAE nor biotin conjugation altered the binding profile of PODO447 (**Supplementary Figures 3B, C**). We monitored antibody internalization by SKOV3, A-172 and MIA PaCa-2 cultures over 24 hours (**Figure 3B**) and found that PODO447 was robustly internalized by all cell lines tested. In contrast, palivizumab control Ab exhibited negligible background

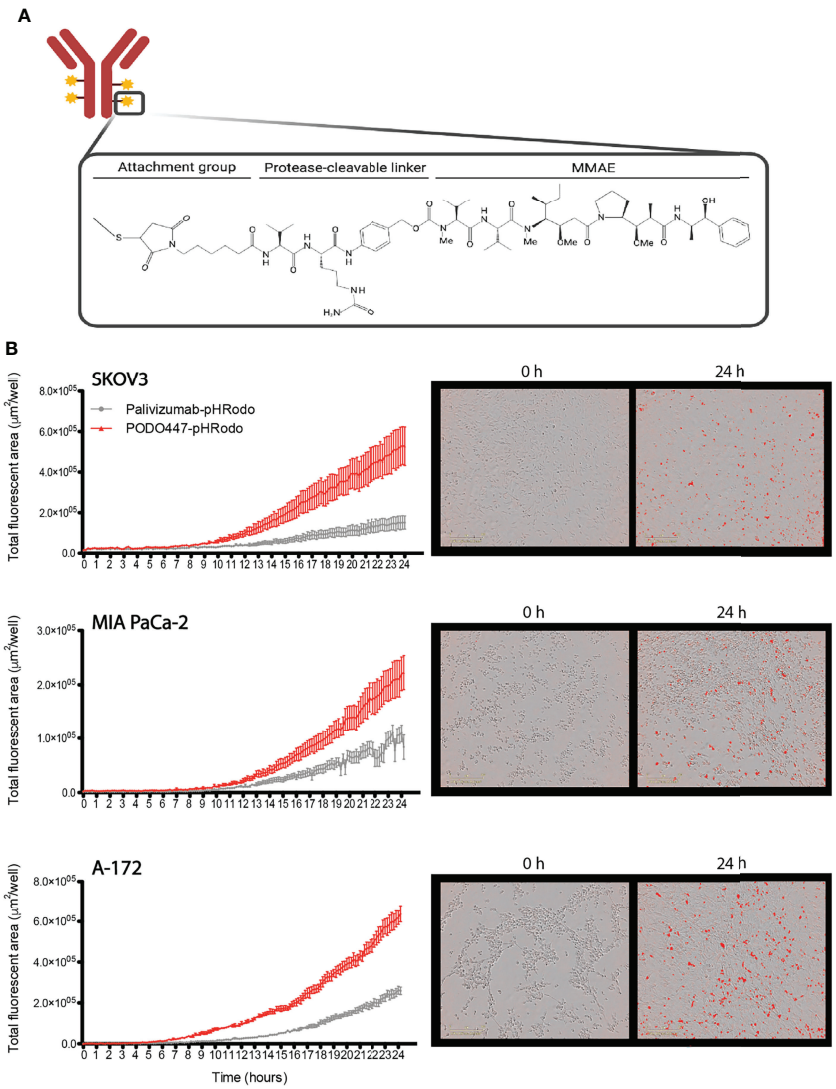

FIGURE 3 | PODO447 internalization on cancer cells. **(A)** Representative image of mAb-Vedotin structure (created with Biorender.com). **(B)** Internalization of PODO447- and palivizumab-pHRodo conjugates on SKOV3 ($P < 0.001$), MIA PaCa-2 ($P < 0.001$), and A-172 ($P < 0.001$) cells. Left graphs show internalization over 24h as determined by Incucyte® evaluation of the increase of total fluorescent area per well. Pictures on the right are representative images of PODO447 internalization at 0- and 24-h timepoints.

internalization. Thus, PODO447-ADC is competent to deliver a cytotoxic payload to the intracellular compartment of Podxl-expressing tumor cells (**Figure 3B**).

To evaluate PODO447-ADC cytotoxic activity, we selected a panel of Podxl-expressing human cancer cell lines, including SKOV3 (ovarian, ascites-derived), MIA PaCa-2 (pancreatic, primary tumor-derived), A-172 (glioblastoma, primary tumor-derived), ONS-76 (medulloblastoma, primary tumor-derived), THP-1 (acute monocytic leukemia), and patient tumor-derived TOV3133D and OV3331 [ovarian, primary solid tumor- and ascites-derived, respectively (35, 36)] (**Figure 4A**; **Supplementary Figure 4**). Cells were treated with serial dilutions of PODO447- or palivizumab-ADC for 6 days and then evaluated for cell viability. Although we saw a significant but modest toxicity (~40%) on ONS-76 cells at 2500 ng/ml, we observed potent cytotoxicity against THP-1 and A-172 cells with an IC_{50} of 31 ng/ml and 93 ng/ml, respectively, and over 90% cytotoxicity at 278 ng/ml and higher PODO447-Vedotin doses. While the cytotoxic effect of PODO447-ADC on TOV3133D cells was modest (IC_{50} of 833 ng/ml), we observed a potent cytotoxic effect in OV3331 cells with an IC_{50} of 278 ng/ml and 80% cytotoxicity at 833 ng/ml. In contrast, no significant toxicity was observed against any cell lines treated with control palivizumab-ADC. Importantly, PODO447-ADC treatment of HUVEC cells, which express the Podxl core protein but not the PODO447 epitope, led to no significant toxicity. In summary, these data suggest that PODO447-ADC exhibits specific toxicity against a broad array of Podxl-expressing tumor cell lines and is well tolerated by cells expressing the native Podxl polypeptide but lacking the tumor-specific PODO447 glycoepitope.

To further confirm that PODO447-ADC cytotoxicity is linked to binding of the PODO447 epitope in the context of the Podxl core protein, we assessed *in vitro* killing of WT and PODXL-KO SKOV3 and MIA PaCa-2 cell lines (32) (**Figure 4B**). PODO447-ADC led to a 3-fold reduction in the viability of SKOV3 WT cells and an 8-fold reduction in the viability of MIA PaCa-2 WT cells compared to control ADC-treated cells. In both cell types, this cytotoxic effect was highly specific as we did not observe a reduction in cell viability of palivizumab-ADC treated cells, or in PODXL-KO control cells treated with PODO447-ADC (**Figure 4B**). We conclude that PODO447 is effective in delivering toxic payloads to tumor cells expressing an appropriately glycosylated form of Podxl.

PODO447-ADC Leads to Regression of Xenografted Human Ovarian and Pancreatic Tumors

To further evaluate the anti-tumor activity of PODO447-ADC, we next evaluated its efficacy against human tumors xenografted into immunocompromised NOD.Cg-*Prkdc*^{scid} *Il2rgtm*^{Wji}/SzJ (NSG) mice. These mice bear mutations in genes essential for the development of T, B and natural killer (NK) cells, rendering them unable to reject xenografts and are, thus, a widely used model to evaluate human tumor growth and anti-tumor therapeutics. Mice were injected subcutaneously with MIA PaCa-2 cells, which have previously been shown to grow rapidly in immunocompromised mice (46). Once tumors reached a size of 0.15 cm^3, we began bi-weekly intravenous administration of PODO447-ADC at a dose of 4 mg/kg (**Figure 5A**). In order to monitor off-target toxicity, we used palivizumab-ADC as our control treatment. We found that four doses of PODO447-ADC led to complete tumor regression and significantly increased survival of these mice compared to control animals treated with palivizumab-ADC which exhibited only a minor and transient dip in tumor growth at the time of injection likely due to a low level of non-specific toxin uptake by tumors (**Figure 5A**, PODO447-ADC-treated median survival > 78 days *vs.* control-ADC-treated = 46 days, $\chi^2 = 20.69$). Similar results were obtained at a 2 mg/kg dose of PODO447-ADC, which also led to a dramatic increase in the length of survival of tumor bearing mice (PODO447-ADC-treated median survival > 56 days *vs.* control-ADC-treated = 43 days, $\chi^2 = 22.61$). In addition, to further evaluate the effects of ADC treatment on the PODO447 epitope and PODXL core protein expression *in vivo*, we isolated similar sized tumors from all treatment groups and evaluated them histologically for PODO447 or PODO83 (core protein) epitope expression. While virtually all cells of the palivizumab-ADC-treated tumors continued to express the PODO447 and PODO83 epitopes, in PODO447-ADC treated animals these epitopes were virtually absent in the 4 mg/kg treatment group and restricted to a core population of the cells in the center of tumors in the 2mg/kg cohort, possibly reflecting lower exposure of these core tumor cells to the ADC (**Supplementary Figure 5**). This intriguing result suggests that tumors that survive PODO447-ADC treatment do so by downregulating Podxl protein expression rather than simply altering the expression of the glycoepitope. Moreover, the much slower growth of PODO447-ADC treated tumors is consistent with our previous studies where shRNA-mediated dampening of Podxl expression in breast cancer cells suppressed tumor growth in mouse xenografts (16).

Because PODO447 recognizes the majority of high grade serous (HGS) ovarian carcinomas (32), we performed a similar experiment with the patient-derived HGS ovarian carcinoma line OV3331 (36). Again, bi-weekly intravenous injections of PODO447-ADC at 3 mg/kg dose, for a total of four doses, led to tumor regression and a striking increase in survival compared to control-ADC-treated group (**Figure 5B**, PODO447-ADC-treated median survival = 167 days *vs.* control-ADC-treated = 82 days, $\chi^2 = 5.70$). Importantly, there were no signs of adverse events or weight loss in any of the treatment groups. Thus, PODO447-ADC has a potent anti-tumor effect *in vivo* suggesting that PODO447-based therapeutics could prove beneficial for patients with Podxl-positive tumors.

Enhanced PODO447-ADC Efficacy at Lower Doses in Animals With Functional B and NK Cells

Despite genetic differences, previous studies have noted that the efficacy of therapeutic Abs and ADCs and the level of off-target cytotoxicity varies widely depending on the degree of immunocompetence of the mouse model (47). Accordingly, we examined the effectiveness of PODO447-ADC in a second human tumor xenograft model. Specifically, we chose Nude mice, which bear a spontaneous chromosomal deletion of the *Foxn1* gene

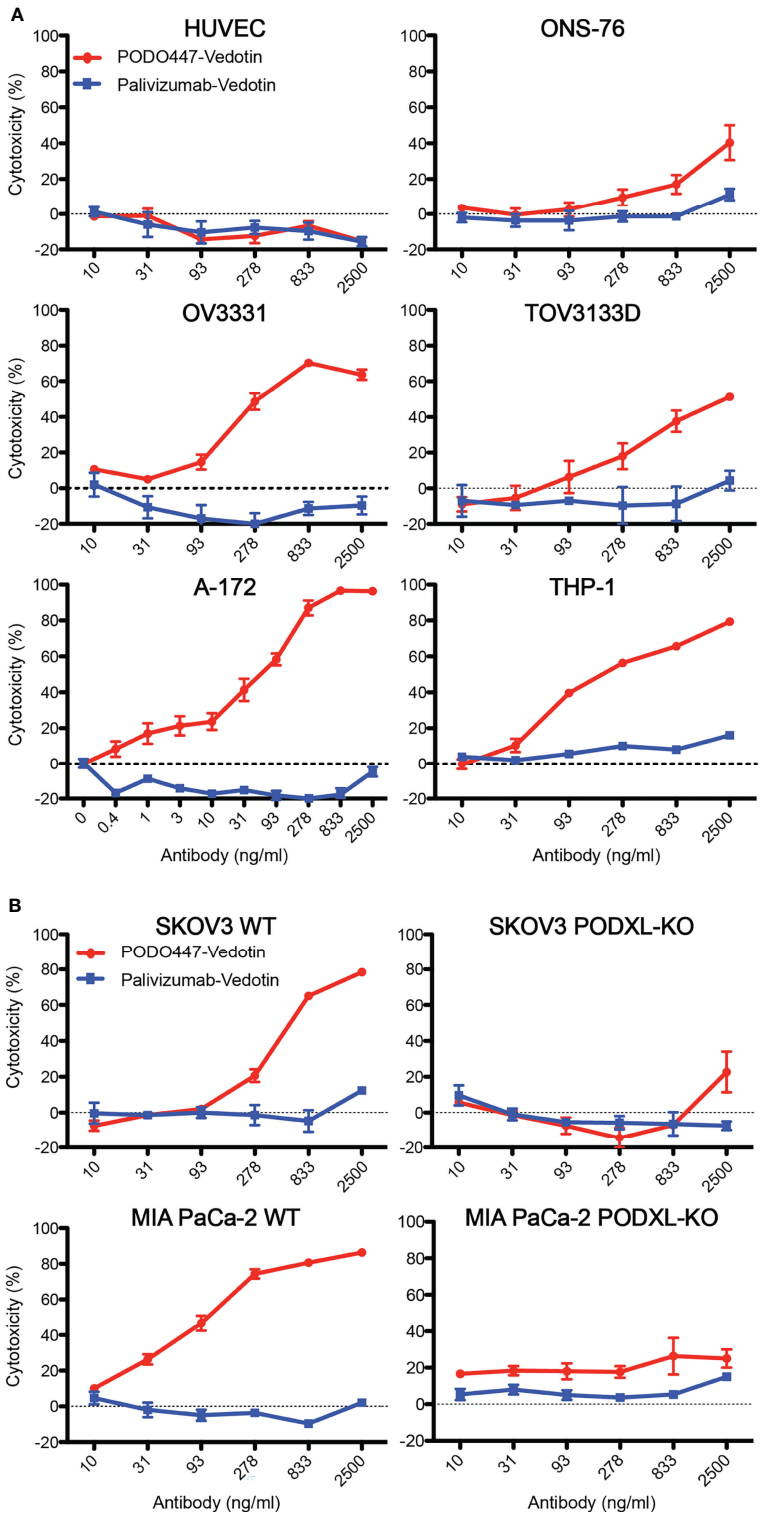

FIGURE 4 | *In vitro* cytotoxicity and selectivity of PODO447-Vedotin. Cytotoxic effect of PODO447- and palivizumab-Vedotin conjugates on **(A)** HUVEC (ns), ONS-76 ($P < 0.001$), OV3331 ($P < 0.001$), TOV3133D ($P < 0.001$), A-172 ($P < 0.001$), THP-1 ($P < 0.001$) and **(B)** SKOV3 ($P < 0.001$) and MIA PaCa-2 ($P < 0.001$) WT and PODXL-KO (ns) cells. Cells were assessed for viability by MTT assay after 144 h of continuous exposure. Horizontal line at 0% cytotoxicity is representative of untreated parental growth rate.

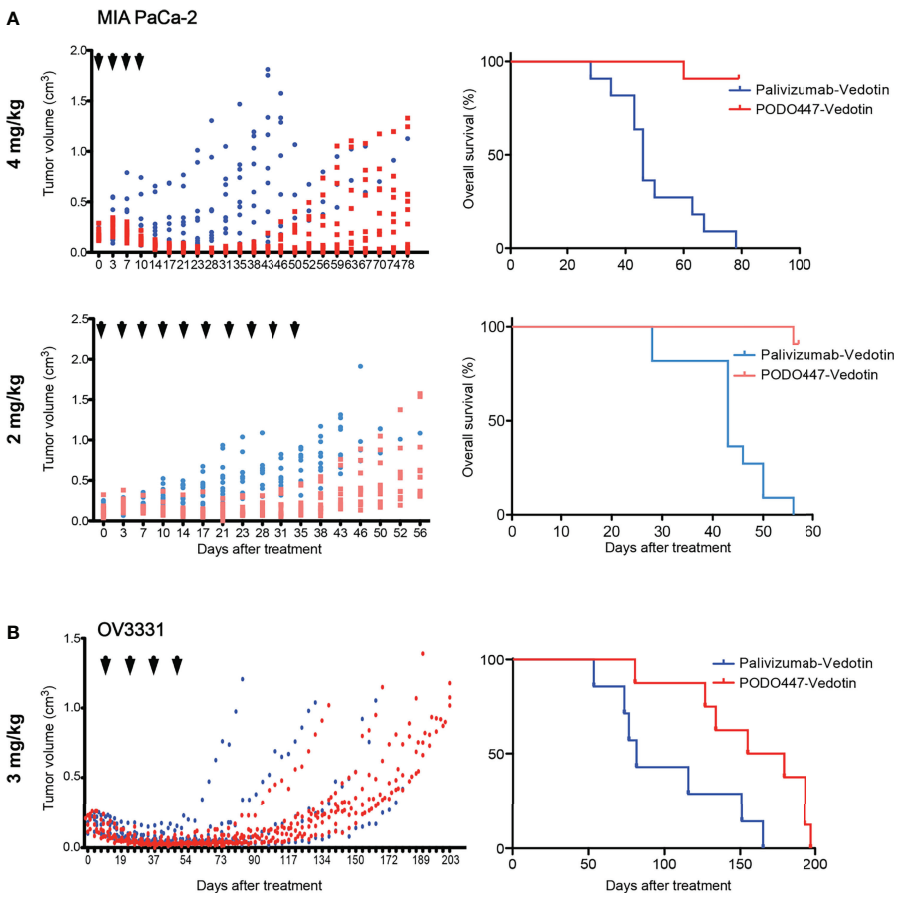

FIGURE 5 | Therapeutic effect of PODO447 on pancreatic and ovarian tumor-bearing NSG mice. Assessment of PODO447- (blue) and palivizumab-ADC (red) *in vivo* therapeutic effect. Once cancer cells injected subcutaneously into the flank of NSG mice became palpable (approximately 0.1 cm^3) mice were injected with ADCs. Graphs show therapeutic effect on tumor growth (left panel) and overall survival (right panel). **(A)** MIA PaCa-2 tumors treated at 4mg/kg/injection (left $P < 0.001$; right $P < 0.0001$) and 2mg/kg/injection (left $P < 0.001$; right $P < 0.0001$), **(B)** OV3331 patient-derived tumors treated at 3mg/kg/injection (left ns; right $P < 0.05$). ADCs were administered i.v. according to the treatment schedule indicated by the arrowheads. Data in **(A)** is from two independent experiments with $n = 5$-6 mice per group. Data in **(B)** is from two independent experiments with $n = 4$-5 mice per group.

essential for the development of an appropriate thymic niche for T cell development. As a result, these mice are severely depleted of T cells but remain competent for the production of B and NK cells. Once again, we observed a strong therapeutic effect at similar doses of PODO447-ADC confirming our previous results. Treatment with PODO447-ADC at 4mg/kg/dose resulted in complete short-term tumor regression in all mice, and long-term regression in 4 out of 7 mice (no tumor relapse present at 100 days, **Figure 6A**, PODO447-ADC-treated median survival > 93 days *vs.* control-ADC-treated = 35 days, $\chi^2 = 5.22$). In contrast, control ADC at 4mg/kg had no significant effect on tumor burden, nor did it induce a transient dip in tumor growth. Additionally, we tested PODO447-ADC at 2 mg/kg/dose. While we observed a trend toward tumor regression in mice treated with PODO447-ADC compared to control, this did not reach statistical significance likely due to half of the control-treated mice reaching their humane endpoint very early (**Figure 6B**). Nevertheless, we found that treatment with 2 mg/kg of PODO447-ADC significantly increased OS and resulted in complete remission in 1 out of 4 mice as assessed at 125 days after initial treatment (**Figure 6B**, PODO447-ADC-treated median survival > 43 days *vs.* control-ADC-treated = 30.5 days, $\chi^2 = 6.80$). One intriguing explanation for this subtle difference between Nude and NSG mouse models is that Nude, but not NSG mice, have functional antibody secreting B cells and relatively normal levels of endogenous immunoglobulin in their serum which would be predicted to block non-specific antibody binding by tumor cells. Regardless, the data suggest that in two different xenograft models PODO447-ADC exhibits effective tumor killing at clinically relevant immunotherapeutic Ab doses.

DISCUSSION

Although novel immunotherapeutics (antibody- and cell-based) are providing an ever-increasing array of approaches to cancer treatments, several barriers continue to limit their broad-spectrum

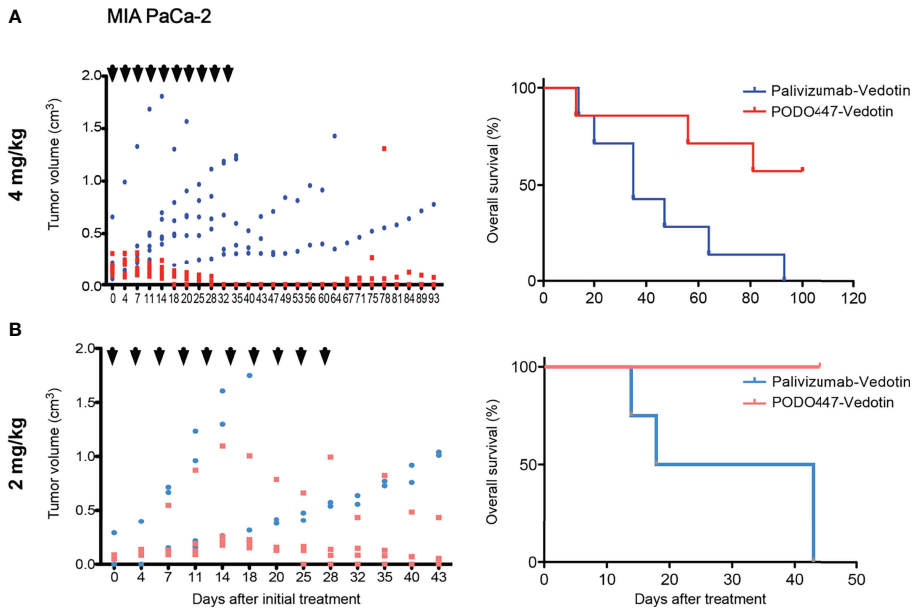

FIGURE 6 | PODO447 therapeutic effect on pancreatic tumor bearing Nude mice with intact B and NK cell activity. PODO447- and palivizumab-ADC therapeutic effect on MIA PaCa-2 tumor growth (left panel) and overall survival (right panel) of tumor-bearing nude mice. Mice were treated with ADCs at **(A)** 4 mg/kg/injection (left $P < 0.01$; right $P < 0.05$) and **(B)** 2mg/kg/injection (left ns; right $P < 0.001$) following the treatment schedule indicated by the arrowheads. Data in **(A)** is from two independent experiments with $n = 3$-4 mice per group. Data in **(B)** is from one experiment with $n = 4$ mice per group.

use, including failure to effectively target late-stage metastatic disease and safety concerns over targeting normal healthy tissues expressing reactive antigenic epitopes (toxicity). Accordingly, there has been a sustained effort to identify rare tumor-specific antigens expressed by a wide range of cancers that can effectively target molecules critical to late-stage disease progression. We find that the PODO447 Ab fulfills these key criteria.

In previous work, we and others have shown that the Podxl core protein is expressed by a wide variety of cancers and is consistently linked to poor outcome (10, 14–17, 32, 48). Although the new PODO447 Ab does not bind to all Podxl-expressing tumors, it does detect many including the majority of high grade serous ovarian tumors, highlighting its therapeutic potential (32). Here we developed this concept further and showed that, when used as the targeting arm of an ADC, PODO447 is highly effective at killing a range of tumor types including human glioblastoma, acute myelomonocytic leukemia, ovarian and pancreatic lines while sparing normal tissue as exemplified by the lack of cytotoxicity on HUVEC cells. Thus, PODO447-ADC could potentially be developed as a broad-spectrum immunotherapeutic to human cancers.

Our previous survey of normal human tissue revealed PODO447 to be exquisitely tumor-specific and lack reactivity with normal kidney podocytes or vascular endothelia, which abundantly express the Podxl core protein (32). This conclusion is further supported by the glycoepitope mapping data presented here, which shows that the PODO447 Ab selectively reacts with a cancer-associated core 1 O-glycostructure in the context of the Podxl polypeptide. *A priori*, this alleviates concerns regarding toxicity of this Ab on normal healthy tissue expressing Podxl and this is further supported by our data showing that PODO447-ADC fails to exhibit any substantial toxicity against normal HUVECs or against human cell lines where the Podxl gene has been inactivated, while simultaneously exhibiting dose-dependent killing of a broad spectrum of Podxl-positive tumor targets at clinically relevant concentrations *in vitro*. Finally, we provide key proof-of-concept data that PODO447-ADCs are effective *in vivo* and provide long-term tumor clearance in two immunodeficient animal models.

The finding that the residual tumors that survive PODO447-ADC treatment have downregulated not only the PODO447 epitope but also expression of the Podxl core protein is noteworthy and encouraging for several reason. First, it suggests that it may be difficult for PODO447+ human tumors to "escape" antibody treatment by simply altering the pattern of PODO447 glycosylation, a general concern for therapeutic strategies targeting these post-translational modifications. Secondly, it suggests that the enzymes that generate the PODO447 glycoepitope may be playing an important functional role for tumor behavior that is difficult to modify. Lastly, it is consistent with previous studies showing that ablation of Podxl in tumor lines cripples the ability of these cells to form tumors in xenografted mice, particularly during the metastatic phase of the disease (16, 27). Indeed, these reports highlight a critical role for Podxl in the subset of tumor cells responsible for tumorsphere formation *in vitro* and for colonization and establishment of tumors in specific niches *in vivo*, two key properties of tumor initiating cells (TIC). Thus, even in tumors where a minor subset of cells express Podxl, these data suggest that targeting this Podxl-expressing TIC population could target cells

with the highest potential for the establishment of distal metastasis. Accordingly, targeting these cells could well have an outsized effect on disease progression. It will now be important to determine whether the PODO447 glycoepitope shows even greater specificity for tumor cells with TIC potential,

Notably, there is an ever-expanding array of antibody-based immunotherapeutic platforms gaining traction in treatment of neoplastic disease. Although our analyses here was limited to the use of PODO447 as an ADC, given its unusual tumor specificity, it holds equal promise for development as a radio-immunotherapeutic reagent for tumor imaging and killing, a bi-specific antibody for recruitment of T cells to tumors, or as a targeting arm for chimeric antigen receptor (CAR-T)-based therapeutic. Indeed, preliminary data suggest PODO447 is suitable for several of these additional applications (in preparation) and highlight the importance of antibodies with this rare specificity for future development.

DATA AVAILABILITY STATEMENT

The original contributions presented in the study are included in the article/**Supplementary Material**. Further inquiries can be directed to the corresponding authors.

ETHICS STATEMENT

All animal experiments were carried out under approved University of British Columbia Animal Care committee protocols (ACC protocol #A16-0007 and A20-0042) based on the recommendations of the Canadian Council on Animal Care. This study was performed in consideration with the Tri-Council Policy Statement of Ethical Conduct for Research involving Humans (TCPS 2).

AUTHOR CONTRIBUTIONS

DCH designed and performed most experiments, analyzed and interpreted data, and was the primary author of this manuscript. MRH assisted with experimental design. YL assisted in flow cytometry and cytotoxicity assays. IMR provided the HEK-293-based glycan array data. PD created the SKOV3 and MIA PaCa-2 *PODXL-KO* cell lines and assisted in flow cytometry assays. JB provided the CFPAC-1 flow cytometry data. EMB created the CFPAC-1 sub-clones. IS provided the A172 ADCC data. AM provided and characterized the patient-derived ovarian carcinoma cell lines. HC, YN, and OB assisted with the glycan array experiments and analysis. CDR and KMM were key contributors to the experimental concept and design. All authors contributed to the article and approved the submitted version.

FUNDING

This research was supported by the Canadian Institutes of Health Research (Grant Number: PJT-166180), the Canadian Cancer Research Institute (Grant number: 704344), the Danish National Research Foundation (Grant number: DNRF107), and European Union's Horizon 2020 Research and Innovation Programme under the Marie Skłodowska-Curie grant agreement synBIOcarb (No. 814029).

ACKNOWLEDGMENTS

We are grateful to all the members of the CDRD Biologics Division for assisting in the development and validation of the anti-Podxl Abs, Dr. Emer Clarke at ReachBio Research Labs (www.reachbio.com) for providing the linker stability assay, Tate Goodman and Alannah Wilson for their technical contributions characterizing the PODXL-KO cell lines, Prof. Poul Sorensen for providing us with cell lines and The Biomedical Research Centre core members R. Dhesi (safety), M. Williams and B. Silva (Abs).

SUPPLEMENTARY MATERIAL

The Supplementary Material for this article can be found online at: https://www.frontiersin.org/articles/10.3389/fonc.2022.856424/full#supplementary-material

Supplementary Figure 1 | Validation of HEK-293 isogenic library O-glycoform expression. Bar graphs summarizing flow cytometric binding of **(A)** anti-Tn (5F4), **(B)** anti-core 1 (3C9), and **(C)** anti-STn (TKH2) antibodies; and **(D)** anti-pan-specific sialoglycan (Pan-Lectenz), **(E)** anti-GalNAc (*Wisteria floribunda*, WFA), and **(F)** anti-Gal, -GalNAc and -Lactose (*Erythrina cristagalli* lectin, ECL) binding lectins to HEK-293 WT and isogenic cells expressing dST (HEK-293 KO GCNT1), ST (HEK-293 KO GCNT1/ST6GALNAC2/3/4), T (HEK-293 KO GCNT1/ST6GALNAC2/3/4/ ST3GAL1/2), Tn (HEK-293 KO C1GALT1), STn (HEK-293 KO COSMC/KI ST6GALNAC1), Core 3 (HEK-293 KO COSMC/KI B3GNT6), and lacking expression of LacDiNAc (ΔLacDiNAc, HEK-293 KO B4GALT1/2/3/4).

Supplementary Figure 2 | PODO447 recognizes a T-antigen epitope on the Podxl core protein. Flow cytometric binding profiles of CFPAC-1 parental, PODO447-positive and PODO447-negative subclones co-stained with anti-core 1 PNA lectin and either PODO83 or PODO447.

Supplementary Figure 3 | Validation of linker stability and biotin/MMAE conjugation. **(A)** Cytotoxic effect of PODO447- and palivizumab-Vedotin on neutrophil differentiation represented by the percentage of viable CD66b+ cells as assessed by flow cytometry after 144 h of continuous exposure. Comparison by flow cytometry of **(B)** unconjugated or biotinylated PODO447 binding profile to SKOV3 parental cells; and **(C)** unconjugated or MMAE-conjugated PODO447 binding profile to SKOV3 Podxl KO cells re-expressing the full-length Podxl protein.

Supplementary Figure 4 | PODO83 and PODO447 binding profile of tumor and normal cells. Flow cytometric PODO83 (blue lines) and PODO447 (red lines) binding profiles of Podxl-positive normal (HUVEC), glioblastoma (A-172), medulloblastoma (ONS-76), acute monocytic leukemia (THP-1), patient tumor-derived high grade serous ovarian carcinoma (OV3331, TOV3133D), ovarian (SKOV3) and pancreatic (MIA PaCa-2) cells lines.

Supplementary Figure 5 | PODO83 and PODO447 staining of ADC-treated tumors. Tumor sections from PODO447- or palivizumab-Vedotin treated animals at 2 and 4 mg/kg doses stained with either PODO447, PODO83 (core protein), palivizumab control or rabbit IgG control antibody.

REFERENCES

1. Sung H, Ferlay J, Siegel RL, Laversanne M, Soerjomataram I, Jemal A, et al. Global Cancer Statistics 2020: GLOBOCAN Estimates of Incidence and Mortality Worldwide for 36 Cancers in 185 Countries. *CA: A Cancer J Clin* (2021) 71:209–49. doi: 10.3322/caac.21660
2. Dillekås H, Rogers MS, Straume O. Are 90% of Deaths From Cancer Caused by Metastases? *Cancer Med* (2019) 8:5574–6. doi: 10.1002/cam4.2474
3. Doyonnas R, Nielsen JS, Chelliah S, Drew E, Hara T, Miyajima A, et al. Podocalyxin Is a CD34-Related Marker of Murine Hematopoietic Stem Cells and Embryonic Erythroid Cells. *Blood* (2005) 105:4170–8. doi: 10.1182/blood-2004-10-4077
4. Doyonnas R, Kershaw DB, Duhme C, Merkens H, Chelliah S, Graf T, et al. Anuria, Omphalocele, and Perinatal Lethality in Mice Lacking the Cd34-Related Protein Podocalyxin. *J Exp Med* (2001) 194:13–28. doi: 10.1084/jem.194.1.13
5. Kerjaschki D, Sharkey DJ, Farquhar MG. Identification and Characterization of Podocalyxin–The Major Sialoprotein of the Renal Glomerular Epithelial Cell. *J Cell Biol* (1984) 98:1591–6. doi: 10.5772/24274
6. McNagny KM, Pettersson I, Rossi F, Flamme I, Shevchenko A, Mann M, et al. Thrombomucin, a Novel Cell Surface Protein That Defines Thrombocytes and Multipotent Hematopoietic Progenitors. *J Cell Biol* (1997) 138:1395–407. doi: 10.1083/jcb.138.6.1395
7. Schopperle WM, DeWolf WC. The TRA-1-60 and TRA-1-81 Human Pluripotent Stem Cell Markers Are Expressed on Podocalyxin in Embryonal Carcinoma. *Stem Cells* (2006) 25:723–30. doi: 10.1634/stemcells.2005-0597
8. Nielsen JS, McNagny KM. Novel Functions of the CD34 Family. *J Cell Sci* (2008) 121:3683–92. doi: 10.1242/jcs.037507
9. Cait J, Hughes MR, Zeglinski MR, Chan AW, Osterhof S, Scott RW, et al. Podocalyxin Is Required for Maintaining Blood–Brain Barrier Function During Acute Inflammation. *PNAS* (2019) 116:4518–27. doi: 10.1073/pnas.1814766116
10. McNagny KM, Roskelley CD, DeBruin EJ, Cipollone J. Podocalyxin in the Diagnosis and Treatment of Cancer. (2012).
11. Graf T, McNagny K, Brady G, Frampton J. Chicken "Erythroid" Cells Transformed by the Gag-Myb-Ets-Encoding E26 Leukemia Virus Are Multipotent. *Cell* (1992) 70:201–13. doi: 10.1016/0092-8674(92)90096-u
12. Strilic B, Kucera T, Eglinger J, Hughes MR, McNagny KM, Tsukita S, et al. The Molecular Basis of Vascular Lumen Formation in the Developing Mouse Aorta. *Dev Cell* (2009) 17:505–15. doi: 10.1016/j.devcel.2009.08.011
13. Kang HG, Lee M, Lee KB, Hughes M, Kwon BS, Lee S, et al. Loss of Podocalyxin Causes a Novel Syndromic Type of Congenital Nephrotic Syndrome. *Exp Mol Med* (2017) 49:e414. doi: 10.1038/emm.2017.227
14. Nielsen JS, McNagny KM. The Role of Podocalyxin in Health and Disease. *J Am Soc Nephrol* (2009) 20:1669–76. doi: 10.1681/ASN.2008070782
15. Somasiri A, Nielsen JS, Makretsov N, McCoy ML, Prentice L, Gilks CB, et al. Overexpression of the Anti-Adhesin Podocalyxin Is an Independent Predictor of Breast Cancer Progression. *Cancer Res* (2004) 64:5068–73. doi: 10.1158/0008-5472.CAN-04-0240
16. Snyder KA, Hughes MR, Hedberg B, Brandon J, Hernaez DC, Bergqvist P, et al. Podocalyxin Enhances Breast Tumor Growth and Metastasis and Is a Target for Monoclonal Antibody Therapy. *Breast Cancer Res* (2015) 17:1–14. doi: 10.1186/s13058-015-0562-7
17. Cipollone JA, Graves ML, Köbel M, Kalloger SE, Poon T, Gilks CB, et al. The Anti-Adhesive Mucin Podocalyxin may Help Initiate the Transperitoneal Metastasis of High Grade Serous Ovarian Carcinoma. *Clin Exp Metastasis* (2012) 29:239–52. doi: 10.1007/s10585-011-9446-0
18. Itai S, Yamada S, Kaneko MK, Harada H, Kato Y. Immunohistochemical Analysis Using Antipodocalyxin Monoclonal Antibody PcMab-47 Demonstrates Podocalyxin Expression in Oral Squamous Cell Carcinomas. *Monoclonal Antibodies Immunodiagnosis Immunother* (2017) 36:220–3. doi: 10.1089/mab.2017.0030
19. Dallas MR, Chen SH, Streppel MM, Sharma S, Maitra A, Konstantopoulos K. Sialofucosylated Podocalyxin Is a Functional E- and L-Selectin Ligand Expressed by Metastatic Pancreatic Cancer Cells. *AJP: Cell Physiol* (2012) 303:C616–24. doi: 10.1152/ajpcell.00149.2012
20. Hsu PD, Lander ES, Zhang F. Development and Applications of CRISPR-Cas9 for Genome Engineering. *Cell* (2014) 157:1262–78. doi: 10.1016/j.cell.2014.05.010
21. Wu H, Yang L, Liao D, Chen Y, Wang W, Fang J. Podocalyxin Regulates Astrocytoma Cell Invasion and Survival Against Temozolomide. *Exp Ther Med* (2013) 5:1025–9. doi: 10.3892/etm.2013.957
22. Favreau AJ, Cross EL, Sathyanarayana P. miR-199b-5p Directly Targets PODXL and DDR1 and Decreased Levels of miR-199b-5p Correlate With Elevated Expressions of PODXL and DDR1 in Acute Myeloid Leukemia. *Am J Hematol* (2012) 87:442–6. doi: 10.1002/ajh.23129
23. Zhou Y, Zhang L, Pan H, Wang B, Yan F, Fang X, et al. Bmi1 Essentially Mediates Podocalyxin-Enhanced Cisplatin Chemoresistance in Oral Tongue Squamous Cell Carcinoma. *PloS One* (2015) 10:e0123208. doi: 10.1371/journal.pone.0123208
24. Wang J, Zhao Y, Qi R, Zhu X, Huang C, Cheng S, et al. Prognostic Role of Podocalyxin-Like Protein Expression in Various Cancers: A Systematic Review and Meta-Analysis. *Oncotarget* (2016) 8:52457–64. doi: 10.18632/oncotarget.14199
25. He S, Du W, Li M, Yan M, Zheng F. PODXL Might be a New Prognostic Biomarker in Various Cancers: A Meta-Analysis and Sequential Verification With TCGA Datasets. *BMC Cancer* (2020) 20:5068. doi: 10.1186/s12885-020-07108-5
26. Wong BS, Shea DJ, Mistriotis P, Tuntithavornwat S, Law RA, Bieber JM, et al. A Direct Podocalyxin–Dynamin-2 Interaction Regulates Cytoskeletal Dynamics to Promote Migration and Metastasis in Pancreatic Cancer Cells. *Cancer Res* (2019) 79:2878–91. doi: 10.1158/0008-5472.CAN-18-3369
27. Fröse J, Chen MB, Hebron KE, Reinhardt F, Hajal C, Zijlstra A, et al. Epithelial-Mesenchymal Transition Induces Podocalyxin to Promote Extravasation *via* Ezrin Signaling. *Cell Rep* (2018) 24:962–72. doi: 10.1016/j.celrep.2018.06.092
28. Graves ML, Cipollone JA, Austin P, Bell EM, Nielsen JS, Gilks CB, et al. The Cell Surface Mucin Podocalyxin Regulates Collective Breast Tumor Budding. *Breast Cancer Res* (2016) 18:11. doi: 10.1186/s13058-015-0670-4
29. Peixoto A, Relvas-Santos M, Azevedo R, Santos LL, Ferreira JA. Protein Glycosylation and Tumor Microenvironment Alterations Driving Cancer Hallmarks. *Front Oncol* (2019) 9:380. doi: 10.3389/fonc.2019.00380
30. Pinho SS, Reis CA. Glycosylation in Cancer: Mechanisms and Clinical Implications. *Nat Rev Cancer* (2015) 15:540–56. doi: 10.1038/nrc3982
31. Pearce OMT, Laubli H. Sialic Acids in Cancer Biology and Immunity. *Glycobiology* (2016) 26:111–28. doi: 10.1093/glycob/cwv097
32. Canals Hernaez D, Hughes MR, Dean P, Bergqvist P, Samudio I, Blixt O, et al. PODO447: A Novel Antibody to a Tumor-Restricted Epitope on the Cancer Antigen Podocalyxin. *J ImmunoTher Cancer* (2020) 8:1–11. doi: 10.1136/jitc-2020-001128
33. Narimatsu Y, Joshi HJ, Nason R, Van Coillie J, Karlsson R, Sun L, et al. An Atlas of Human Glycosylation Pathways Enables Display of the Human Glycome by Gene Engineered Cells. *Mol Cell* (2019) 75:394–407.e5. doi: 10.1016/j.molcel.2019.05.017
34. Büll C, Joshi HJ, Clausen H, Narimatsu Y. Cell-Based Glycan Arrays-A Practical Guide to Dissect the Human Glycome. *STAR Protoc* (2020) 1:100017. doi: 10.1016/j.xpro.2020.100017
35. Létourneau IJ, Quinn MC, Wang L-L, Portelance L, Caceres KY, Cyr L, et al. Derivation and Characterization of Matched Cell Lines From Primary and Recurrent Serous Ovarian Cancer. *BMC Cancer* (2012) 12:379. doi: 10.1186/1471-2407-12-379
36. Sauriol A, Simeone K, Portelance L, Meunier L, Leclerc-Desaulniers K, de Ladurantaye M, et al. Modeling the Diversity of Epithelial Ovarian Cancer Through Ten Novel Well Characterized Cell Lines Covering Multiple Subtypes of the Disease. *Cancers* (2020) 12:2222. doi: 10.3390/cancers12082222
37. Zen K, Notarfrancesco K, Oorschot V, Slot JW, Fisher AB, Shuman H. Generation and Characterization of Monoclonal Antibodies to Alveolar Type II Cell Lamellar Body Membrane. *Am J Physiol* (1998) 275:L172–83. doi: 10.1152/ajplung.1998.275.1.L172
38. Thurnher M, Clausen H, Sharon N, Berger EG. Use of O-Glycosylation-Defective Human Lymphoid Cell Lines and Flow Cytometry to Delineate the Specificity of Moluccella Laevis Lectin and Monoclonal Antibody 5F4 for the Tn Antigen (GalNAc Alpha 1-O-Ser/Thr). *Immunol Lett* (1993) 36:239–43. doi: 10.1016/0165-2478(93)90095-j
39. Steentoft C, Yang Z, Wang S, Ju T, Vester-Christensen MB, Festari MF, et al. A Validated Collection of Mouse Monoclonal Antibodies to Human

Glycosyltransferases Functioning in Mucin-Type O-Glycosylation. *Glycobiology* (2019) 29:645–56. doi: 10.1093/glycob/cwz041
40. Resch B. Product Review on the Monoclonal Antibody Palivizumab for Prevention of Respiratory Syncytial Virus Infection. *Hum Vaccines Immunotherapeutics* (2017) 13:2138–49. doi: 10.1080/21645515.2017.1337614
41. Blixt O, Head S, Mondala T, Scanlan C, Huflejt ME, Alvarez R, et al. Printed Covalent Glycan Array for Ligand Profiling of Diverse Glycan Binding Proteins. *PNAS* (2004) 101:17033–8. doi: 10.1073/pnas.0407902101
42. Gao T, Wen T, Ge Y, Liu J, Yang L, Jiang Y, et al. Disruption of Core 1-Mediated O-Glycosylation Oppositely Regulates CD44 Expression in Human Colon Cancer Cells and Tumor-Derived Exosomes. *Biochem Biophys Res Commun* (2020) 521:514–20. doi: 10.1016/j.bbrc.2019.10.149
43. Kang L, Yao C, Khodadadi-Jamayran A, Xu W, Zhang R, Banerjee NS, et al. The Universal 3d3 Antibody of Human PODXL Is Pluripotent Cytotoxic, and Identifies a Residual Population After Extended Differentiation of Pluripotent Stem Cells. *Stem Cells Dev* (2016) 25:556–68. doi: 10.1089/scd.2015.0321
44. Doronina SO, Toki BE, Torgov MY, Mendelsohn BA, Cerveny CG, Chace DF, et al. Development of Potent Monoclonal Antibody Auristatin Conjugates for Cancer Therapy. *Nat Biotechnol* (2003) 21:778–84. doi: 10.1038/nbt832
45. Zhao H, Gulesserian S, Malinao MC, Ganesan SK, Song J, Chang MS, et al. A Potential Mechanism for ADC-Induced Neutropenia: Role of Neutrophils in Their Own Demise. *Mol Cancer Ther* (2017) 16:1866–76. doi: 10.1158/1535-7163.MCT-17-0133
46. Baylot V, Andrieu C, Katsogiannou M, Taieb D, Garcia S, Giusiano S, et al. OGX-427 Inhibits Tumor Progression and Enhances Gemcitabine Chemotherapy in Pancreatic Cancer. *Cell Death Dis* (2011) 2:e221–1. doi: 10.1038/cddis.2011.104
47. Li F, Ulrich ML, Shih VF-S, Cochran JH, Hunter JH, Westendorf L, et al. Mouse Strains Influence Clearance and Efficacy of Antibody and Antibody–Drug Conjugate *Via* Fc–Fcγr Interaction. *Mol Cancer Ther* (2019) 18:780–7. doi: 10.1158/1535-7163.MCT-18-0977
48. Le Tran N, Wang Y, Nie G. Podocalyxin in Normal Tissue and Epithelial Cancer. *Cancers* (2021) 13:1–18. doi: 10.3390/cancers13122863

Conflict of Interest: The authors DC, MH, PD, IS, OB, KM, CR are inventors of a pending patent application on PODO447 and methods of using the same (US20180296673A1). MH, KM and CR are inventors of a pending patent application on PODO83 and methods of using the same (US20190367606A1). KM and CR possess an awarded patent on podocalyxin as a prognostic marker in cancer (US9309323B2).

The remaining authors declare that the research was conducted in the absence of any commercial or financial relationships that could be construed as a potential conflict of interest.

Publisher's Note: All claims expressed in this article are solely those of the authors and do not necessarily represent those of their affiliated organizations, or those of the publisher, the editors and the reviewers. Any product that may be evaluated in this article, or claim that may be made by its manufacturer, is not guaranteed or endorsed by the publisher.

frontiers | Frontiers in Oncology

ORIGINAL RESEARCH
published: 11 May 2022
doi: 10.3389/fonc.2022.887294

RRM2 Mediates the Anti-Tumor Effect of the Natural Product Pectolinarigenin on Glioblastoma Through Promoting CDK1 Protein Degradation by Increasing Autophagic Flux

Haiping Jiang[1,2,3], Dongzhi Zhang[1,2,3,4], Karpov Denis Aleksandrovich[1,2,3,5], Junyi Ye[1,2,3], Lixiang Wang[1,2,3], Xiaofeng Chen[1,2,3], Ming Gao[1,2,3], Xinzhuang Wang[1,2,3], Tao Yan[1,2,3], He Yang[1,2,3], Enzhou Lu[1,2,3], Wenwu Liu[1,2,3], Cheng Zhang[6], Jianing Wu[7], Penglei Yao[7], Zhenying Sun[7], Xuan Rong[7], Sokhatskii Andrei Timofeevich[1,2,3,5], Safin Shamil Mahmutovich[5], Zhixing Zheng[1,2,3], Xin Chen[1,2,3] and Shiguang Zhao[1,2,3,7*]*

[1] Department of Neurosurgery, The First Affiliated Hospital of Harbin Medical University, Harbin, China, [2] Department of Neurosurgery, Key Colleges and Universities Laboratory of Neurosurgery in Heilongjiang Province, Harbin, China, [3] Institute of Neuroscience, Sino-Russian Medical Research Center, Harbin Medical University, Harbin, China, [4] Department of Neurosurgery, The Affiliated Cancer Hospital of Harbin Medical University, Harbin, China, [5] Department of Neurosurgery and Medical Rehabilitation, Bashkir State Medical University, Ufa, Russia, [6] Department of Undergraduate, Suffolk University, Boston, MA, United States, [7] Department of Neurosurgery, Shenzhen University General Hospital, Shenzhen, China

The natural product pectolinarigenin exerts anti-inflammatory activity and anti-tumor effects, and exhibits different biological functions, particularly in autophagy and cell cycle regulation. However, the antineoplastic effect of pectolinarigenin on glioblastoma (GBM) remains unclear. In the present study, we found that pectolinarigenin inhibits glioblastoma proliferation, increases autophagic flux, and induces cell cycle arrest by inhibiting ribonucleotide reductase subunit M2 (RRM2), which can be reversed by RRM2 overexpression plasmid. Additionally, pectolinarigenin promoted RRM2 protein degradation *via* autolysosome-dependent pathway by increasing autophagic flow. RRM2 knockdown promoted the degradation of CDK1 protein through autolysosome-dependent pathway by increasing autophagic flow, thereby inhibiting the proliferation of glioblastoma by inducing G2/M phase cell cycle arrest. Clinical data analysis revealed that RRM2 expression in glioma patients was inversely correlated with the overall survival. Collectively, pectolinarigenin promoted the degradation of CDK1 protein dependent on autolysosomal pathway through increasing autophagic flux by inhibiting RRM2, thereby inhibiting the proliferation of glioblastoma cells by inducing G2/M phase cell cycle arrest, and RRM2 may be a potential therapeutic target and a prognosis and predictive biomarker in GBM patients.

Keywords: pectolinarigenin, glioblastoma, RRM2, CDK1, autophagic flux

OPEN ACCESS

Edited by:
Yunkai Zhang,
Vanderbilt University Medical Center, United States

Reviewed by:
Hongmei Cui,
Lanzhou University, China
Qingbin Cui,
University of Toledo, United States

****Correspondence:***
Shiguang Zhao
guangsz@hotmail.com
Xin Chen
chenxin_tracy@yeah.net

Specialty section:
This article was submitted to Cancer Molecular Targets and Therapeutics, a section of the journal Frontiers in Oncology

Received: *01 March 2022*
Accepted: *13 April 2022*
Published: *11 May 2022*

Citation:
Jiang H, Zhang D, Aleksandrovich KD, Ye J, Wang L, Chen X, Gao M, Wang X, Yan T, Yang H, Lu E, Liu W, Zhang C, Wu J, Yao P, Sun Z, Rong X, Timofeevich SA, Mahmutovich SS, Zheng Z, Chen X and Zhao S (2022) RRM2 Mediates the Anti-Tumor Effect of the Natural Product Pectolinarigenin on Glioblastoma Through Promoting CDK1 Protein Degradation by Increasing Autophagic Flux. Front. Oncol. 12:887294. doi: 10.3389/fonc.2022.887294

INTRODUCTION

Glioblastoma (World Health Organization grade IV), the most malignant form of intracranial tumor found in adults, accounting for 54% of all gliomas, is incurable due to its high proliferation ability, high invasiveness, resistance to various therapies, and high rate of postoperative recurrence (1). Despite improvements in patients outcomes with the combined radiotherapy and temozolomide regimen since 2005, the median survival duration after the initial diagnosis remains at 15 months with a 5-year survival rate of 7.2% (2). Thus, effective therapeutic approaches for patients with GBM are urgently needed.

Pectolinarigenin (PECT), a dual inhibitor of cyclooxygenase-2/5-lipoxygenase, which is abundantly present in and can be extracted from the Chinese herbal plant *Chromolaena odorata*, has been proven to have numerous pharmacological characteristics, including, anti-inflammatory, anticancer, and anti-allergy activities (3). A previous study also reported that the cancer-specific cytotoxic activity of PECT was mainly attributable to the suppression of proliferative cell cycle, the induction of apoptosis, and the regulation of autophagy (4). However, the benefits of PECT in GBM treatment is not known.

Ribonucleotide reductase subunit M2 (RRM2) encodes the catalytic subunit of ribonucleotide reductase (RNR), which is a hetero-tetramer consisting of two RRM1 and two RRM2 subunits and is involved in regulating DNA synthesis and modifying proteins (5), and is a rate-limiting molecule during the conversion of ribonucleoside triphosphates into dNTPs in the G2 phase of cell cycle (6) and shows elevated levels in some cancers (7, 8). Recent studies demonstrated that overexpression of RRM2 is essential for the cellular response to abnormal dNTP levels, which leads to malignant biological phenotypes such as angiogenesis, epithelial to mesenchymal transition, relapse and drug- or radio-resistance (5, 8). In precision medicine for tumors, targeting of RRM2 has emerged as a therapeutic method for some cancers as it inhibits proliferative cell cycle and regulates autophagy pathways to suppress tumor progress (9). Autophagy is a cellular catabolic process that maintains normal cellular physiological functions by degrading and/or recycling intracellular macromolecules and dysfunctional organelles (10). Moreover, autophagy activation is essential for promoting tumor cell survival and malignant transformation. However, excessive activation or inhibition of autophagy can suppress tumor proliferation and induce cell cycle arrest, and some autophagy genes are involved in cell cycle regulation (11, 12). For example, p62 depletion has been shown to induce cell cycle arrest by promoting cyclin-dependent kinase 1 (CDK1) degradation in human breast cancer (13). In contrast, autophagy related 7 (Atg7) -deficient cells fail to induce p21 expression, thereby impairing p53-mediated cell cycle arrest (14). Although RRM2 is involved in regulating autophagy pathway and cell cycle arrest, it is unclear whether the two biological phenomena are played a role in the anti-tumor effect of PECT on GBM. In this study, we investigate how RRM2 mediates the anti-tumor effect of PECT on GBM *via* reducing CDK1 protein expression and examined the functional significance of autophagy and cell cycle in GBM treatment.

MATERIALS AND METHODS

Patients and Specimens

Normal human brain specimens (n = 6) and fresh glioma specimens (n = 19) were obtained from the Department of Neurosurgery, First Affiliated Hospital of Harbin Medical University. The study protocol was approved by the Clinical Research Ethics Committee of Harbin Medical University. All patients provided written informed consent, and the study was conducted in accordance with the Declaration of Helsinki.

Cell Lines and Chemical Reagents

The U251, U87, and HUVEC cell lines were provided by the China Infrastructure of Cell Line Resource (National Science and Technology Infrastructure) and cultured in Dulbecco's Modified Eagle medium (RNBK0465, Sigma-Aldrich, St. Louis, MO, USA) supplemented with 10% fetal bovine serum (AllBio Science, Taichung, Taiwan). MG132, chloroquine (CQ), and PECT were from MedChemExpress (Monmouth Junction, NJ, USA).

MTT Assay and Clone Formation Assay

The cells were added to a 96-well plate at a density of 5,000 cells/well. At different time points, 10 μL of 3-(4,5-dimethylthiazol-2-yl)-2,5-diphenyl-2H-tetrazolium bromide (MTT; cat# HY-15924, MedChemExpress) dye was added to each well and incubated for 4 h. Finally, we replaced the medium with 150 μL of dimethyl sulfoxide and measured the cell viability (Infinite M200 PRO; Tecan Trading AG, Männedorf, Switzerland). The GBM cells were centrifuged and evenly inoculated into a six-well plate at a density of 800 cells/well. After 14 days of culture at distinct concentrations of PECT, the colonies were measured using the ChemiDoc™ MP imaging software (Bio-Rad Laboratories, Inc., CA, USA).

Immunofluorescence Analysis

After fixation, permeabilization, and sealing, the treated cells and paraffin-embedded glioma tissue sections were incubated with primary antibody and fluorescent secondary antibody, and images were observed with a fluorescence microscope (Lionheart FX; BioTek, Beijing, China). The following primary antibodies were used: CDK1 (BF0091, 1:500, Affinity, USA), p62 (A19700, 1:100, Abclonal, Wuhan, China), LAMP2 (66301-1-lg, 1:100, Proteintech, Hubei, China), Ki67 (A2094, 1:100, Abclonal, Wuhan, China).

Cell Transfection

GBM cells were interfered with siRNA, plasmid, and lentiviruses. The siRNA-NC/RRM2 and RRM2 overexpression plasmid pEnter-NC/RRM2 were from Miaolingbio (Wuhan, China) and lentiviruses were from GeneChem (Shanghai, China). The sequences of siRNA-NC/RRM2 and LV-shNC/LV-shRRM2 are shown in **Table 1**.

Transmission Electron Microscopy

U251 cells were first fixed with 2.5% glutaraldehyde at 4°C, and post-fixed with 1% osmium tetroxide. The immobilized cells were then dehydrated in increasing concentrations of

ethanol and acetone. Finally, Transmission Electron Microscopy (TEM) was used to observe autophagic vesicles.

Western Blot Analysis

For Western Blot (WB) analysis, the tissues and treated cells were first extracted and lysed. After separating the proteins using 12.5% sodium dodecyl sulfate-polyacrylamide gel electrophoresis, they were transferred to a polyvinylidene fluoride membrane, which was blocked and then incubated with primary antibodies and fluorescent-dye conjugated secondary antibodies. Protein bands were imaged using a ChemiDoc™ MP Imaging System (Bio-Rad, Hercules, CA, USA). The following primary antibodies were used: RRM2 (BS7520, 1:1,000, BioWorld, Nanjing, China); LAMP2 (66301-1-lg, 1:1,000, Proteintech, Hubei, China); LC3B (83506S, 1:1,000, Cell Signaling Technology, USA); CCNA2 (A7632, 1:1,000), CCNB1 (A2056, 1:1,000), CDK1 (A0220, 1:1,000) and p62 (A19700, 1:1,000) were purchased from Abclonal (Wuhan, China).

Flow Cytometric Analysis

The treated cells were first digested with 0.25% trysin, centrifuged, and then fixed with 70% ethyl alcohol at 4°C. The next day, the digested cells were stained using a cell cycle analysis kit (P0010, Beyotime, Shanghai, China). Finally, a flow cytometer (Agilent NovoCyte, China) was used to measure the cell cycle distribution.

RFP-GFP-LC3 Lentivirus Transfection and Fluorescence Imaging

After treatment under different conditions, U251 cells transfected with RFP-GFP-LC3 lentivirus were fixed and used to measure autophagy flux. The fluorescence intensity was analyzed using a FluoView FV300 confocal microscope (Olympus Corporation, Tokyo, Japan).

Quantitative Real-Time Polymerase Chain Reaction Assay

Total RNA was extracted from the clinical samples or treated cells using TRIzol (Sigma-Aldrich), and then one microgram of total RNA was reverse-transcribed into cDNA using a ReverTra Ace qPCR RT Kit (Toyobo, Osaka, Japan). Quantitative Real-Time Polymerase Chain Reaction (qRT-PCR) was performed on triplicate samples in a reaction mixture of SYBR Green (Roche, Basel, Switzerland) with a Gene Amp PCR System 9700 (Thermo Fisher Scientific, Waltham, MA, USA). The data were normalized to glyceraldehyde 3-phosphate dehydrogenase (GAPDH) using the ΔΔCt method. The primer sequences for GAPDH, RRM2 and CDK1 are shown in **Table 1**.

Co-Immunoprecipitation

First, the primary antibody was added to Protein A/G Plus-Agarose and incubated at 4°C for 2 h, and then the cell protein lysates were added and incubated at 4°C overnight. We next separated the magnetic beads, collected the supernatant, and performed WB.

Liquid Chromatography-Mass Spectrometry

Each tumor bearing mice brain tissue sample was mixed with methanol (containing 5 μg/mL 2-chloro-L-phenylalanine as an internal standard) and mixed with a vortex mixer for homogenization. The samples were centrifuged and transferred to sampler vial. An in-house quality control (QC) sample was prepared by mixing equal amounts of each sample. We performed Liquid Chromatography-Mass Spectrometry (LC-MS) analysis of the QC samples. The raw data was converted to a common format, and the degree of aggregation of QC samples was assessed using the principal component analysis modeling method and PCA modeling method was used to check the aggregation degree of QC simples.

In Vivo Studies

BALB/c nude mice were purchased from Beijing Vital River Laboratory Animal Technology Co., Ltd. (Beijing, China). For each mouse, 5×10^6 U251 cells were subcutaneously implanted into the right flank, or 1×10^6 U251 cells were implanted into the brain. The mice were randomly divided into control and PECT groups (six mices per group). PECT (25mg/kg every other day, prepared as a 150 mM stock solution in DMSO and stored at -20°C) diluted with 100 μL PBS was administered intraperitoneally for 3 weeks, whereas the control group treated with the same amount of DMSO diluted with 100 μL PBS. Additionally, 1×10^6 U251 cells transfected with LV-shNC or LV-shRRM2 per mice were implanted into the brain. All animal study protocols were approved by the Animal Experiments Ethics Committee of Harbin Medical University and the study was conducted in accordance with the Declaration of Helsinki.

TABLE 1 | Sequences of siRNA, primers, and lentiviruses.

siRNA sequences	
si-NC	5′UUCUCCGAACGUGUCACGUTT3′
RRM2-si RNA1	5′GGCUCAGCUUGGUCGACAA3′, 5′UUGUCGACCAAGCUGAGCC3′
RRM2-si RNA2	5′GGAGAGAGUAAGAGAAAUATT3′
RRM2-si RNA3	5′GAAGAGAGUAGGCGAGUAUTT3′
Primer sequences	
GAPDH	F-5′CACCCACTCCTCCACCTTTGA3′, R-5′ACCACCCTGTTGCTGTAGCCA3′
CDK1	F-5′AAACTACAGGTCAAGTGGTAGCC3′, R-5′TCCTGCATAAGCACATCCTGA3′
RRM2	F-5′TGCCATTGAAACGATGCCTT 3′, R-5′ACTGCAGCAAAGGCTACAAC 3′
Lentivirus sequences	
LV-shNC	5′ TTCTCCGAACGTGTCACGT 3′
LV-shRRM2 1	5′ccCATTTGACTTTATGGAGAA3′
LV-shRRM2 2	5′ gcTCAAGAAACGAGGACTGA3′
LV-shRRM2 3	5′ gcAGATGTATAAGAAGGCAGA3′

Hematoxylin and Eosin Staining and Immunohistochemical Staining

After dehydration and paraffin embedding, the mice brain tumor and organ sections were stained with Hematoxylin and Eosin (H&E). For Immunohistochemical (IHC) assay, tumors were first formalin-fixed, paraffin-embedded, and sliced, and then the sample sections were immunostained with primary antibodies and an anti-mouse/rabbit secondary antibody.

RNA-Sequencing and Bioinformatics Analyses

We used DESeq2 or edgeR to analyze differences in expression and identify enriched functional terms and pathways (*via* Gene Ontology [GO] and Kyoto Encyclopedia of Genes and Genomes [KEGG]). The clinical information and mRNA sequencing data of the 1,038 patients with glioma were obtained from the Chinese Glioma Genome Atlas (CGGA) database http://www.cgga.org.cn/index.jsp, which included data from 625 low-grade glioma (LGG), 388 GBM, and 20 non-glioma patients. OS was determined among 592 LGG and 374 GBM cases, and the median was used as the demarcation point.

Statistical Analysis

Differences between two groups and multiple groups were estimated using Student *t*-test and one-way analysis of variance, respectively. The statistical significance of OS between different groups was evaluated by log-rank test. All statistical analyses were carried using GraphPad Prism version 7.0 software (GraphPad, Inc., San Diego, CA, USA), and a value of $p < 0.05$ was considered to indicate statistically significant results.

RESULTS

PECT Suppresses GBM Cells Proliferation *In Vitro* and *In Vivo*

The 2D structure of PECT is presented in **Figure 1A**. Firstly, human GBM cells U87 and U251, and human normal cell HUVEC were used to verify the anti-proliferation effect of PECT. MTT results showed that PECT inhibited GBM cells proliferation in dose- and time-dependent manners, but not that of HUVECs. The half-maximal inhibitory concentration (IC_{50}) values of PECT for 48 h among U87 and U251 cells were 21.17 and 21.00 μM, respectively (**Figure 1B**). Therefore, the drug concentration closest to IC_{50} of 20 μM was selected for follow-up experiments. Subsequently, we used clonogenic assays to verify the sensitivity of GBM cells to PECT and founded that PECT can prevent the tumor sphere formation in a dose-dependent manner (**Figure 1C**). Additionally, PECT inhibited GBM cells proliferation as shown using ki67 staining (**Figure 1D**). Therefore, PECT inhibited GBM cells proliferation and can be administered safely *in vitro*.

The mice accepted the treatment of PECT showed a much smaller brain tumor size than another (**Figure 1E**) and had a significantly prolonged lifespan (**Figure 1F**). In addition, we performed LC-MS assays to detect the concentration of PECT in gliomas and found that PECT can penetrate the blood-brain barrier (BBB) (**Figures 1G, H**, **Figure S1**), which was consistent with the outcomes described in the traditional Chinese medicine systems pharmacology database and analysis platform (TCMSP) (http://lsp.nwu.edu.cn/tcmsp.php) (**Table S1**) (15). These data indicate that PECT had an anti-tumor effect on GBM *in vivo*.

PECT Downregulates RRM2 Expression and Increased Autophagy Flux *In Vitro*

To determine the mechanism of the anti-tumor effect of PECT on GBM, we screened differentially expressed genes (DEGs) using RNA-Sequencing (RNA-Seq) analysis after PECT treatment, and detected 1,279 DEGs (662 upregulated genes and 617 downregulated genes, |log2 fold-change|>1.0, $p<0.05$), the top 50 of which are shown in **Figure 1I**. The functional annotation analysis of the DEGs using GO. DNA replication and cell cycle regulation were the mainly GO terms (p.adjust <0.05) (**Figure 1J**). In addition, KEGG enrichment pathway (*p*.adjust <0.05) analysis revealed that the DNA replication, cell cycle, lysosomal, and proteasome pathways were the major signs pathways influenced by PECT (**Figure 1K**). Among the top 50 of DEGs, RRM2 was closely correlated with DNA replication, cell cycle, lysosomal and proteasome pathways, so we hypothesized that RRM2 may be a key target gene for the anti-tumor effect of PECT on GBM. To verify the changes of RRM2 expression, we exposed GBM cells to PECT for 48 h and founded that RRM2 mRNA and protein expression gradually decreased with increasing PECT concentrations (**Figures 2A, B**).

Next, we investigated whether PECT regulates autophagy in GBM cells. TEM results revealed that autophagic vacuoles gradually increased after adding PECT to U251 cells from 0 h to 48 h (**Figure 2C**); simultaneously, LC3B-II and LAMP2 protein expression increased and p62 protein expression decreased (**Figure 2E**), indicating that PECT increased autophagic vacuoles in GBM cells by increasing autophagic flux. Further, we performed a RFP-GFP-LC3 transfection assay on U251 cells to re-confirm the above results, and found that both free red puncta (autolysosomes) and yellow puncta (autophagosomes) increased in the merged sections of U251 cells treated with PECT in a time-dependent manner, and the red puncta increased more (**Figure 2D**), validating the increase of autophagic flux.

Subsequently, we investigated whether the autolysosome was involved in RRM2 degradation. chloroquine (CQ), a late-stage autophagy inhibitor, of which low dose that can partially inhibit pH value increase and block protein degradation in the autolysosome, but has no effect on cell activity (16), was used. The results showed that 2 μM CQ did not affect the cell viability of GBM (**Figure S2**), but increased p62 and LC3B-II protein expression, indicating inhibition of autophagic flux (**Figure 2F**). Therefore, 2 μM CQ was selected. An increased number of yellow puncta but a decreased number of free red puncta was observed in the merged sections of the PECT+CQ-treated groups compared to the PECT-treated groups (**Figure 2G**); simultaneously, the reduction of the p62 and RRM2 protein expression was partially recovered, but the LC3B-II protein expression further increased (**Figure 2F**), indicating that CQ

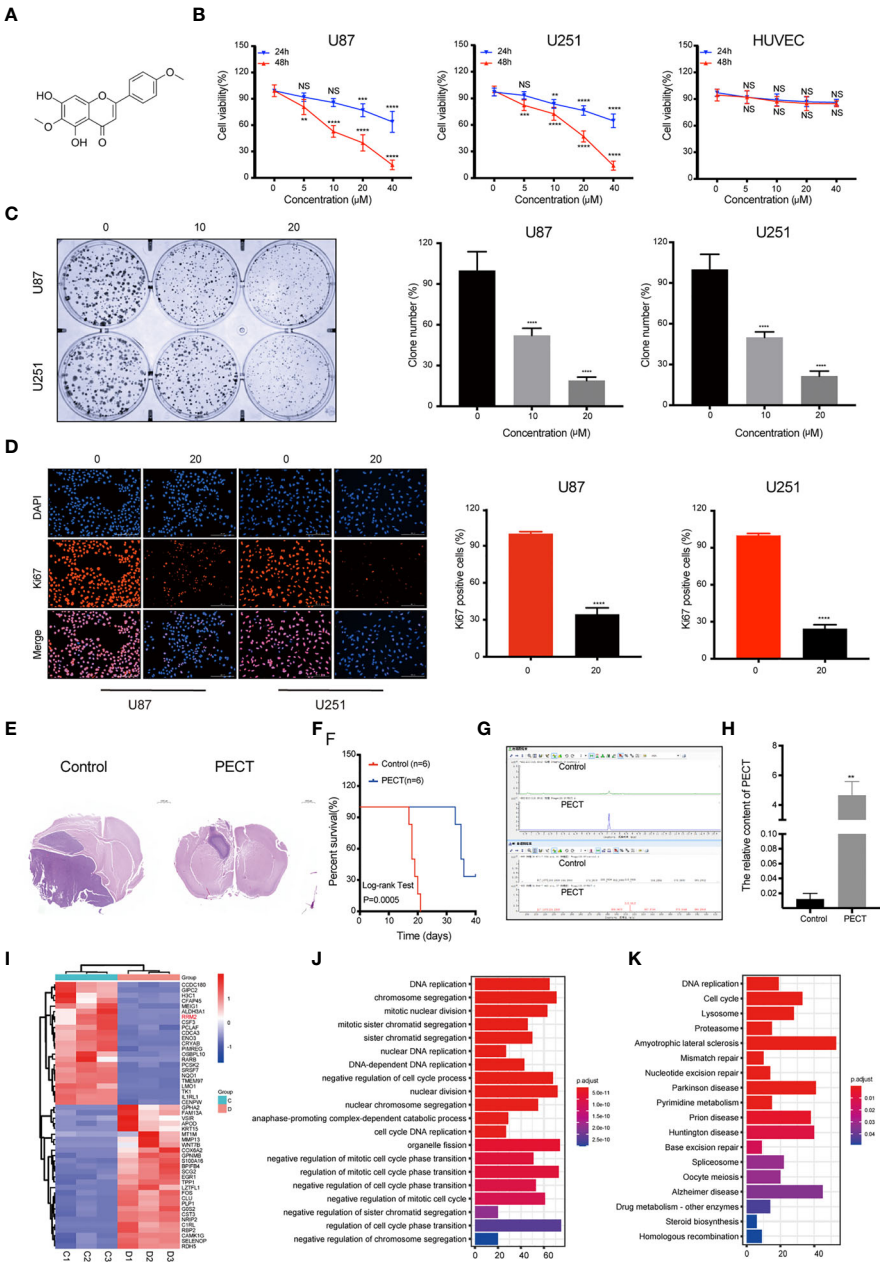

FIGURE 1 | PECT inhibits GBM cells proliferation both *in vitro* and *in vivo*, and RNA-sequencing analysis. **(A)** Structure of PECT. **(B)** After exposuring to different concentrations of PECT for 24 or 48 h, cell viability of U87, U251 and HUVECs cells was assessed using MTT. **(C)** Representative images of colony formation on U87 and 251 cells treated with PECT for different concentrations. **(D)** After U87 and U251 cells were cultured with or without PECT (20 μM, 48 h), Ki67 staining was observed by fluorescence microscopy. Scale bar: 200 μm. **(E)** H&E images of brain sections of mice orthotopically xenografted tumor with U251 cells treated with PECT. Scale bar: 1000 μm. **(F)** Kaplan-Meier survival curve of mice orthotopically xenografted tumor with U251 cells treated with PECT. **(G, H)** LC-MS analysis of PECT content in the tumor bearing mice brain homogenate samples. **(I)** Heatmap of top 50 up- or down-regulated DEGs after PECT treatment. C1-3: control group, D1-3: PECT-treated group. **(J)** GO and **(K)** KEGG analysis of DEGs. The data are presented as the mean ± SD (n=3). NS, non-significant. $^{**}P < 0.01$, $^{***}P < 0.001$, $^{****}P < 0.0001$.

blocked the autophagic flux induced by PECT and inhibited RRM2 protein degradation. As expected, immunofluorescence assay of LAMP2 [a lysosomal membrane marker that is involved in autophagy and critical for some proteins degradation in lysosomes (17)] and RRM2 showed that PECT treatment resulted in more LAMP2 protein expression but less RRM2 protein expression in U251 cells, and increased the cytoplasmic co-localization of LAMP2 and RRM2 (**Figure 2H**), further indicating that RRM2 depends on autolysosome pathway degradation.

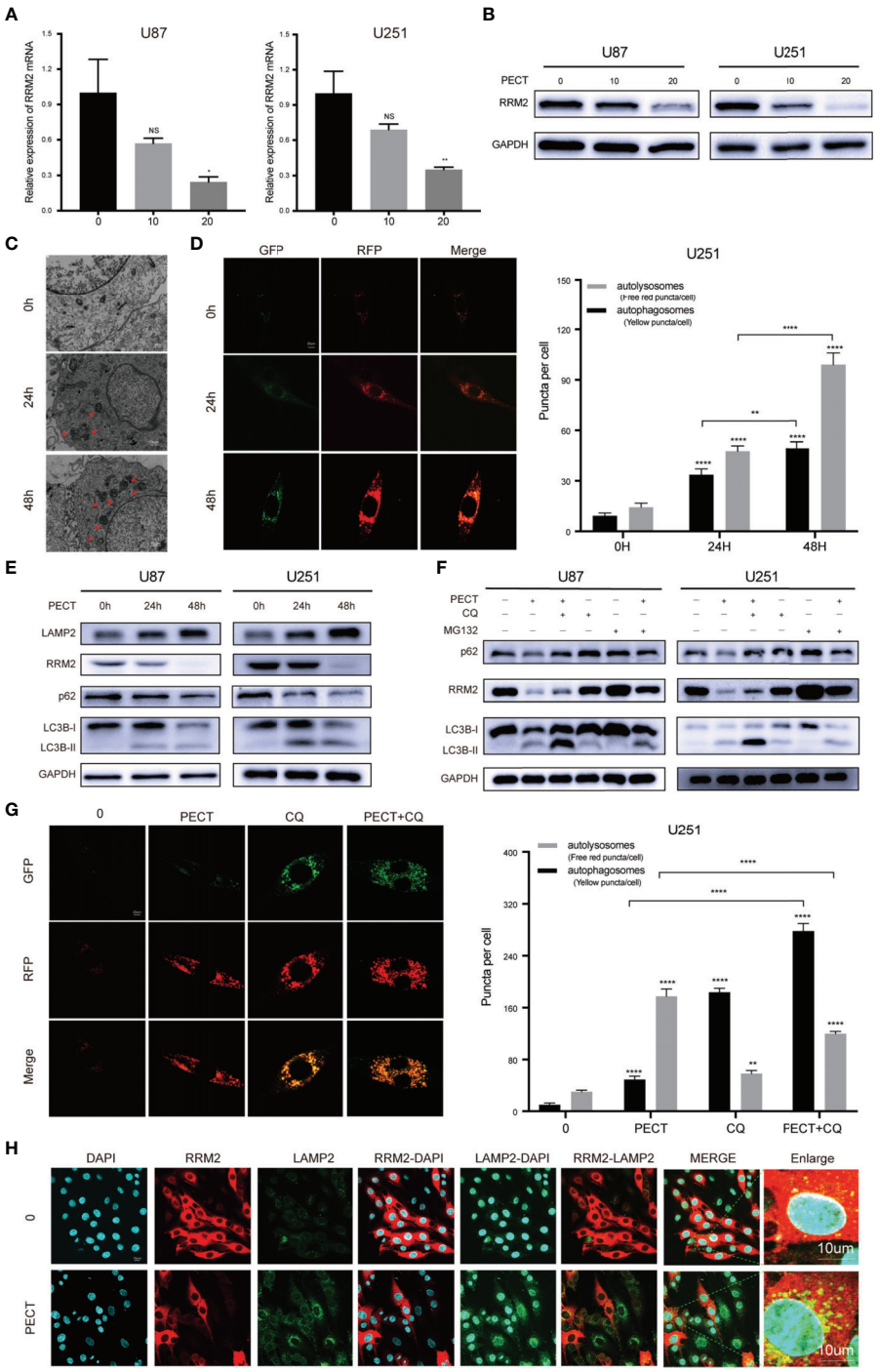

FIGURE 2 | PECT downregulates RRM2 expression and increases autophagy flux *in vitro*. **(A, B)** After culturing U87 and U251 cells with different concentrations of PECT for 48h, RRM2 mRNA and protein expression were examined by qRT-PCR and western blot assay, respectively. **(C)** TEM images of U251 cells exposed to PECT (20 μM) for 0h, 24h, and 48 h. Autophagic vacuole (red arrows). Scale bar: 10 μm. **(D)** After U251 cells cultured with PECT (20 μM) for 0h, 24h, and 48 h, autophagic flux was analyzed using the RFP-GFP-LC3 construct. Scale bar: 20 μm. **(E)** Western blot analysis of RRM2, p62, LC3B and LAMP2 protein expression in U87 and U251 cells cultured with PECT (20 μM) for 0h, 24h, and 48 h. **(F)** Western blot analysis of RRM2, p62 and LC3B protein expression in U87 and U251 cells cultured with PECT (20 μM, 48 h) or CQ (2 μM, 2 h) or MG132 (2 μM, 3 h). **(G)** After U251 cells cultured with PECT (20 μM, 48h) or CQ (2 μM, 2h), autophagic flux was analyzed using the RFP-GFP-LC3 construct. Scale bar: 20 μm. **(H)** Immunofluorescence analysis of RRM2 (red) and LAMP2 (green) in U251 cells treated with or without PECT(20 μM, 48 h). The nuclei were stained with DAPI. Scale bar: 10 μm. The data are presented as the mean ± SD (n=3). NS, non-significant. $^{*}P < 0.05$, $^{**}P < 0.01$, $^{****}P < 0.0001$.

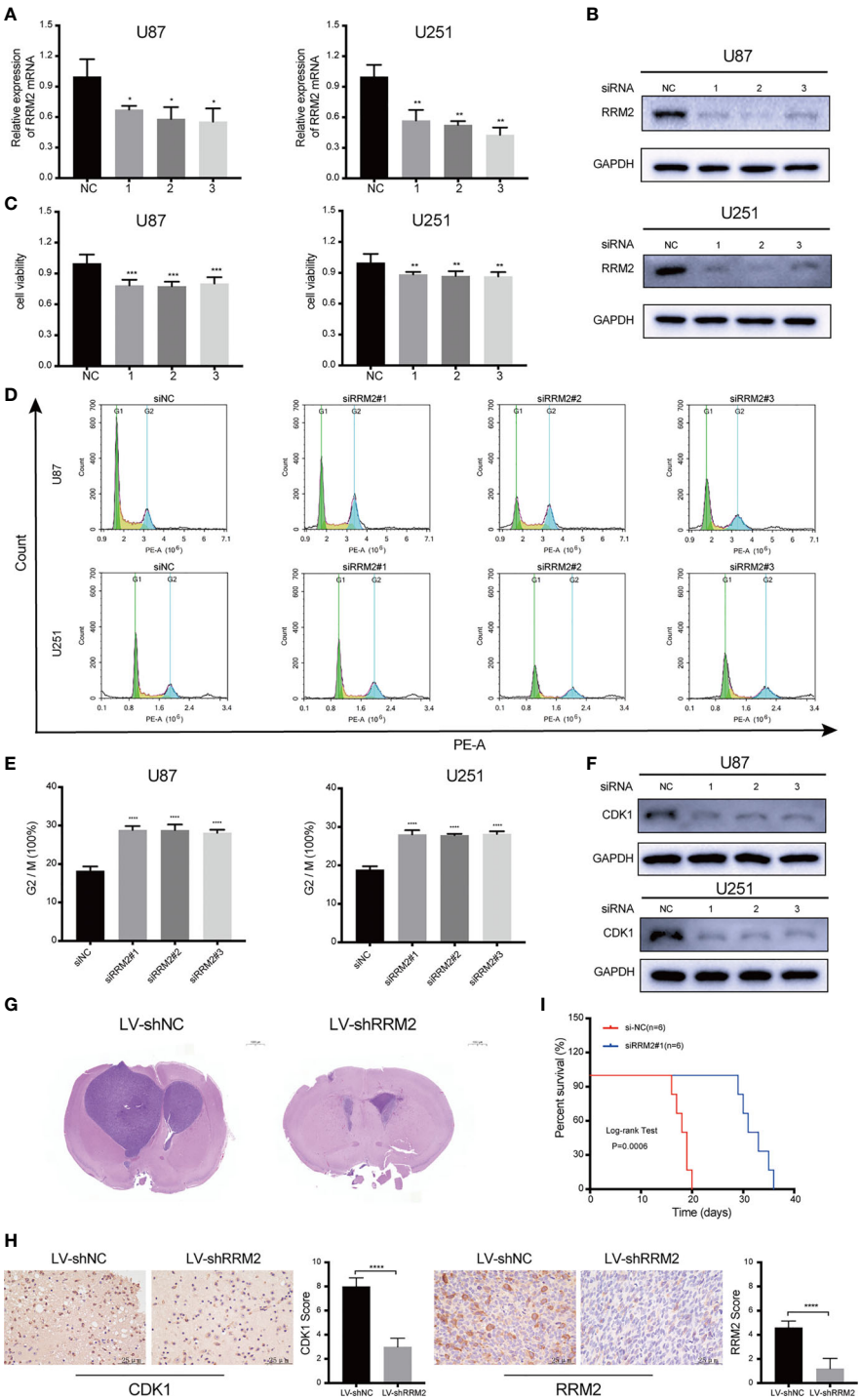

FIGURE 3 | RRM2 knockdown inhibits GBM proliferation and induces cell cycle arrest both *in vitro* and *in vivo*. After transfecting U87 and U251 cells with RRM2 siRNA for 48h, **(A)** RRM2 mRNA expression was examined by qRT-PCR, **(B)** RRM2 protein expression was analyzed by western blot assay, **(C)** cells viability were assessed using MTT, **(D, E)** cells cycle distribution were analyzed using flow cytometry. (green: G0-G1, yellow: S, and blue: G2-M). **(F)** CDK1 protein expression was analyzed by western blot assay. **(G)** H&E images of brain sections of mice orthotopically xenografted with U251 cells transfected with LV-shNC and LV-shRRM2. Scale bar: 1000 μm. **(H)** IHC staining of CDK1 and RRM2 in consecutive brain sections of mice orthotopically xenografted with U251 cells transfected with LV-shNC and LV-shRRM2. Scale bar: 25 μm. **(I)** The survival time of nude mice orthotopically xenografted with U251 cells transfected with LV-shNC and LV-shRRM2. The data are presented as the mean ± SD (n=3). $^{*}P < 0.05$, $^{**}P < 0.01$, $^{***}P < 0.001$, $^{****}P < 0.0001$.

Additionally, we verified that the proteasome is also involed in RRM2 protein degradation, which can be partly reversed by the proteasome inhibitor MG132 (**Figure 2F**).

Overall, our *in vitro* data confirmed that PECT treatment can increase autophagy flux in GBM cells, and RRM2 protein reduction after PECT treatment is not only dependent on transcriptional inhibition but also proteasomal and autolysosomal degradation.

RRM2 Knockdown Inhibits GBM Proliferation and Induces Cell Cycle Arrest *In Vitro* and *In Vivo*

To assess the effect of RRM2 on GBM, we used siRNA to interfere with RRM2 expression in GBM cells. The siRNA efficiency was shown in **Figure 3A**; similarly, RRM2 knockdown not only decreased RRM2 protein expression (**Figure 3B**) but also suppressed GBM cells viability (**Figure 3C**). Moreover, we founded that the proportion of G2/M phase cells increased (**Figures 3D, E**) and CDK1 protein expression was decrease with RRM2 knockdown (**Figure 3F**), but CCNA2 and CCNB1 protein expression no change (**Figure S3**). In addition, we founded that the expression of CDK1 mRNA was also not change (**Figure S4**). These results demonstrated that G2/M cell cycle arrest is caused by the decrease of CDK1 protein, which is consistent with previous reports (18, 19).

Subsequently, RRM2 knockdown was induced by RRM2 lentivirus in U251 cells. After testing the transfection efficiency (**Figure S5**), lentivirus-treated cells were implanted into the brains of 5-week-old nude mice. Mice treated with RRM2 lentivirus showed much smaller tumor volumes compared to controls (**Figure 3G**) and exhibited significantly prolonged survival time (**Figure 3I**). IHC analysis showed that compared with the LV-shNC group, the protein expression of CDK1 and RRM2 decreased in LV-shRRM2 group (**Figure 3H**).

Taken together, our results revealed that RRM2 knockdown could induce G2/M phase cell cycle arrest by reducing the level of CDK1 protein and inhibit GBM cells proliferation *in vitro* and *in vivo*.

RRM2 Knockdown Induces Cell Cycle Arrest in GBM *via* Promoting CDK1 Protein Degradation by Increasing Autophagic Flux *In Vitro*

Firstly, we founded that RRM2 knockdown can promote the autophagic vacuoles accumulated in U251 cells (**Figure 4A**). Simultaneously, a RFP-GFP-LC3 transfection assay revealed that both free red puncta and yellow puncta increased in the merged sections of si-RRM2#1 U251 cells compared with that in si-NC U251 cells, but the free red puncta increased more (**Figure 4B**), indicating the autophagic flux increased.

Subsequently, we sought to determine whether autophagy is required for RRM2-mediated cell cycle progression. The data showed that RRM2 knockdown promoted G2/M phase cell cycle arrest, while this effect was reversed by CQ, an inhibitor of autophagic flux that prevents autophagosome-lysosome fusion and lysosomal protein degradation (**Figures 4C, D**). Interestingly, the change in CDK1 protein level was consistent with the cell cycle distribution (**Figure 4E**). These data indicate that the blockage of G2/M phase cell cycle induced by RRM2 knockdown is dependent on the function of RRM2 in autophagy.

To further investigate the mechanism regarding whether the degradation of CDK1 protein depends on the autolysosomal pathway during RRM2 knockdown, we performed Co-Immunoprecipitation (Co-IP) assays to analyze the interaction between CDK1 and p62, an adapter protein, is required for some protein degradation through the autolysosome pathway (20). As shown in **Figure 4F**, p62 was able to interact with CDK1. Additionally, immunofluorescence analysis showed that CDK1 could co-localize with p62 in U251 cell, but the co-localization of p62 with CDK1 decreased after RRM2 knockdown (**Figure 4G**). Thus, our results demonstrated that RRM2 knockdown induced cell cycle arrest in GBM *via* promoting CDK1 protein degradation by increasing autophagic flux *in vitro*.

PECT Inhibits GBM Proliferation, Promotes Cell Cycle Arrest, and Increases Autophagic Flux by Decreasing RRM2 Expression *In Vitro*

To verify whether RRM2 mediates the anti-tumor effect of PECT on GBM, we overexpressed RRM2 and exposed them to PECT, and founded that GBM cells viability (**Figure 5A**) were partially rescued with RRM2 expression upregulation (**Figures 5B, C**). Similarly, the increased proportion of G2/M phase GBM cells (**Figures 5D, E**) and the downregulation of p62 and CDK1 protein and upregulation of LAMP2 and LC3B-II protein caused by PECT were partially recovered with RRM2 expression upregulation (**Figure 5F**). Overall, our results showd that PECT can inhibit GBM proliferation and promote G2/M phase cell cycle arrest as well as increase autophagic flux by decreasing RRM2 expression *in vitro*.

PECT Inhibits GBM Proliferation *In Vivo*

In vivo, our results showed that PECT suppressed tumor proliferation, accompanied by reducing tumor weight (**Figures 6A, B**) and tumor weight/mouse weight (**Figure 6C**), and downregulating RRM2 mRNA (**Figure 6D**) and protein (**Figure 6E**) expression compared to that in controls. However, the body weight of mice in each group did not differ significantly (**Figure 6F**). Moreover, we founded that PECT itself did not induce additional toxicities by evaluating morphological changes in tissues in all groups (**Figure 6G**). IHC results showed that compared with the control group, the protein expression of LC3B and LAMP2 increased while that of Ki67, RRM2, p62, and CDK1 decreased in xenograft tumors administered with PECT (**Figure 6H**). Taken together, PECT exerts an anti-tumor effect in GBM and can be safely administered *in vivo*.

RRM2 Is Increased in GBM Tissues and Inversely Correlated With the Prognosis of Glioma Patients

To verify the clinical significance of RRM2 in glioma patients, firstly, we performed IHC staining analysis, and founded that

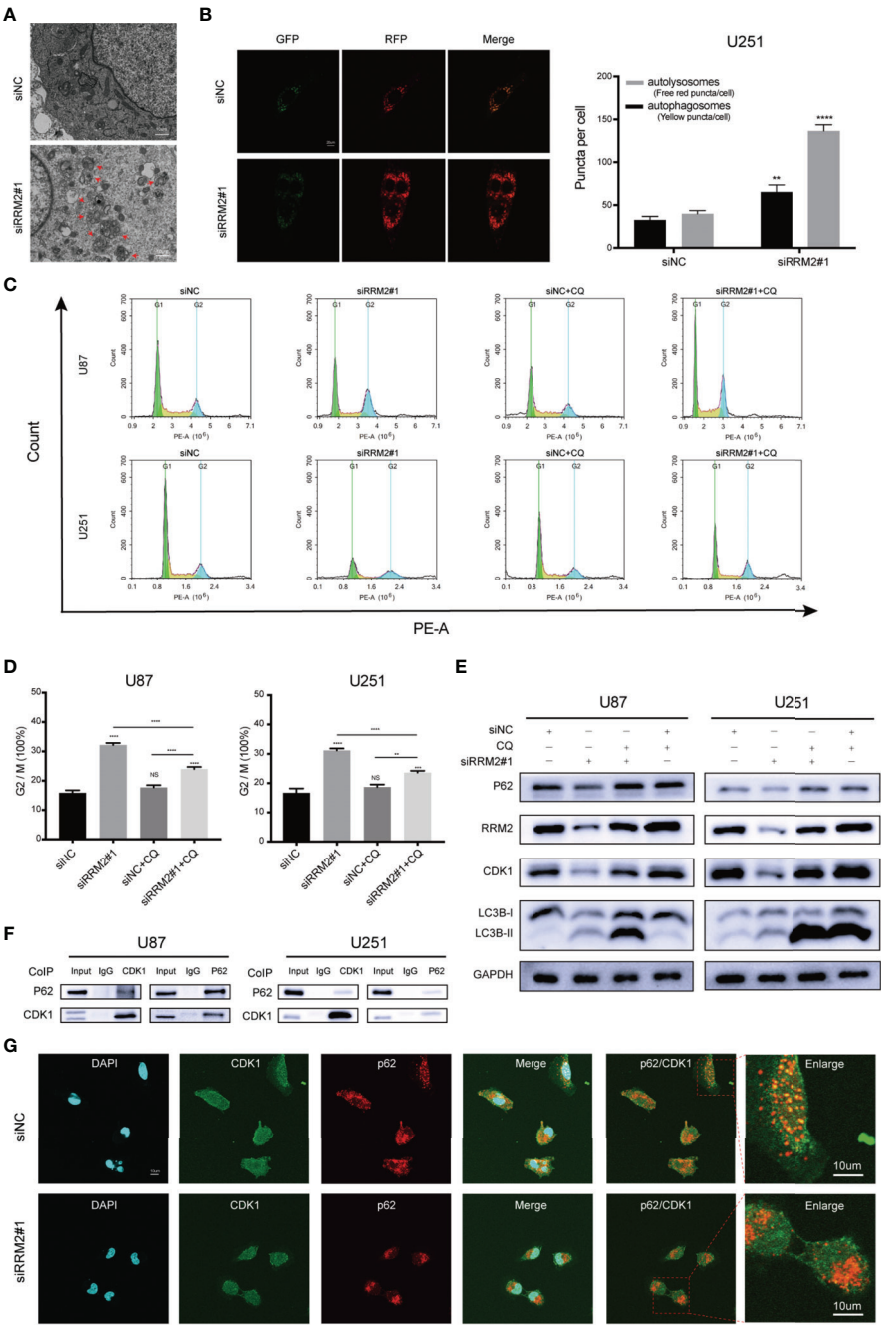

FIGURE 4 | RRM2 knockdown induces cell cycle arrest in GBM *via* promoting CDK1 protein degradation by increasing autophagic flux *in vitro*. **(A)** TEM images of U251 cells transfected with RRM2 siRNA for 48h. Autophagic vacuole (red arrows). Scale bar: 10 μm. **(B)** U251 cells transfected with RRM2 siRNA for 48h, autophagic flux was analyzed using the RFP-GFP-LC3 construct. Scale bar: 20 μm. **(C, D)** After U87 and U251 cells transfected with RRM2 siRNA for 48 h or cultured with CQ (2 μM, 2 h), cells cycle distribution were analyzed using flow cytometry. (green: G0-G1, yellow: S, and blue: G2-M). **(E)** After U87 and U251 cells transfected with RRM2 siRNA for 48 h or cultured with CQ (2 μM, 2 h), CDK1, RRM2, p62 and LC3B proteins expression were analyzed by western blot assay. **(F)** Total protein lysates of U87 or U251 cells were prepared for Co-IP using CDK1 or p62 antibody. **(G)** Immunofluorescence assay of the co-localization of p62 (red) and CDK1 (green) in U251 cells after transfection with RRM2 siRNA for 48 h. Scale bar: 10 μm. The data are presented as the mean ± SD (n=3). NS, non-significant. $^{**}P < 0.01$, $^{***}P < 0.001$, $^{****}P < 0.0001$.

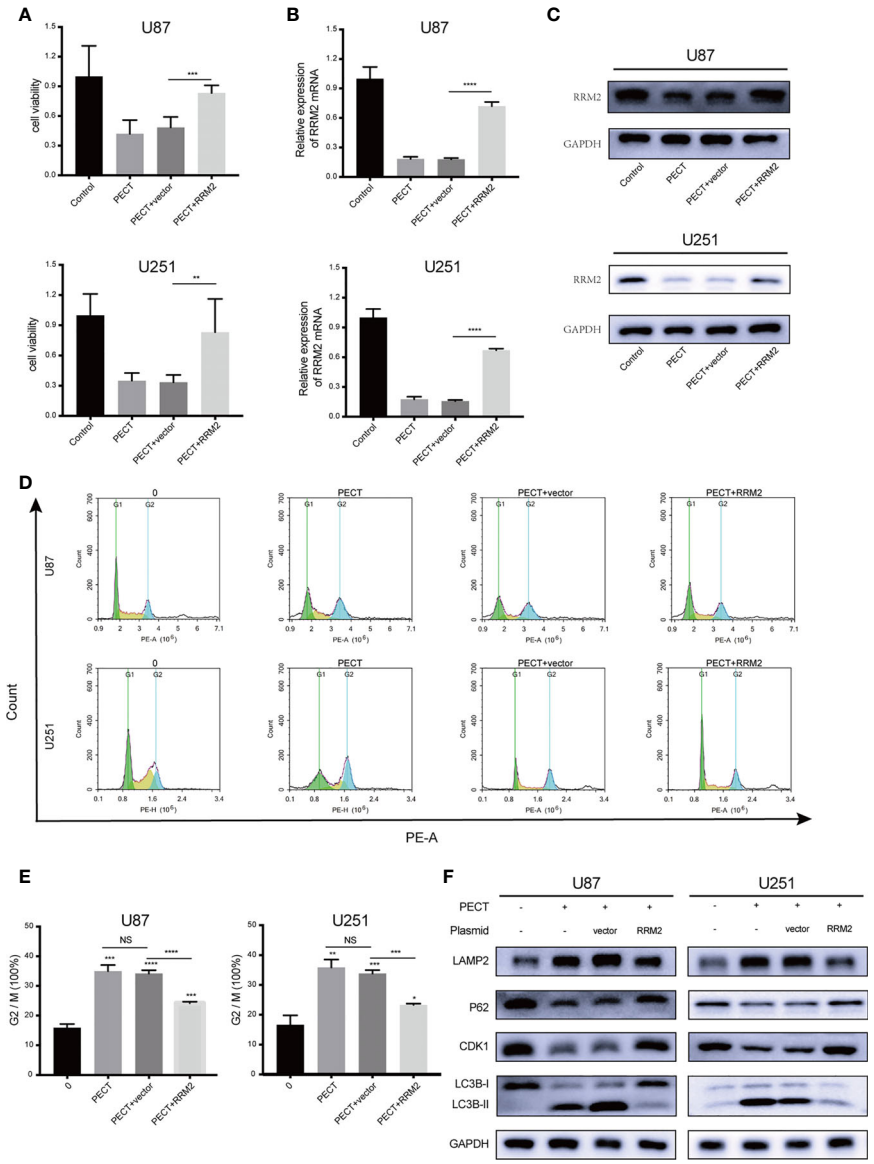

FIGURE 5 | PECT inhibits GBM proliferation, promotes cell cycle arrest, and increases autophagic flux by decreasing RRM2 expression *in vitro*. After U87 and U251 cells transfected with RRM2 overexpression plasmid or cultured with PECT (20 μM, 48 h), **(A)** cells viability were assessed using MTT, **(B)** RRM2 mRNA expression was examined by qRT-PCR, **(C)** RRM2 protein expression was analyzed by western blot assay, **(D, E)** cells cycle distribution were analyzed using flow cytometry. (green: G0-G1, yellow: S, and blue: G2-M). **(F)** CDK1, p62, LAMP2 and LC3B protein expression were analyzed by western blot assay. Vector and RRM2 represent negative control plasmid and RRM2 overexpression plasmid, respectively. The data are presented as the mean ± SD (n=3). NS: non-significant. $^{*}P < 0.05$, $^{**}P < 0.01$, $^{***}P < 0.001$, $^{****}P < 0.0001$.

compared with normal human brain tissues, RRM2, CDK1, and p62 protein expression had increase in distinct grades of glioma, especially in GBM tissues (**Figure 7A**). Additionally, according to the CGGA data and qRT-PCR results, compared with non-tumor brain tissues, RRM2 mRNA expressions gradually increased with increasing the degree of glioma malignancy (**Figure 7B**). WB analysis revealed that RRM2 and CDK1 protein expression in human GBM tissue was higher than that in LGG and normal human brain tissues, but no significant difference between LGG and normal human brain tissues, indicating that RRM2 may be a predictive marker of GBM (**Figures 7C, D**).

We confirmed that p62 can directly interact with CDK1 and is an adapter for the degradation of CDK1 protein in autolysosome *in vitro*. Therefore, we performed immunofluorescence staining, and founded that p62 and CDK1 protein are co-located in the lesional cells from human GBM cases, which indicated that p62 and CDK1 protein could interact directly *in vivo* (**Figure 7E**). More importantly, we examined the clinical data of patients with glioma in the CGGA database and revealed that RRM2

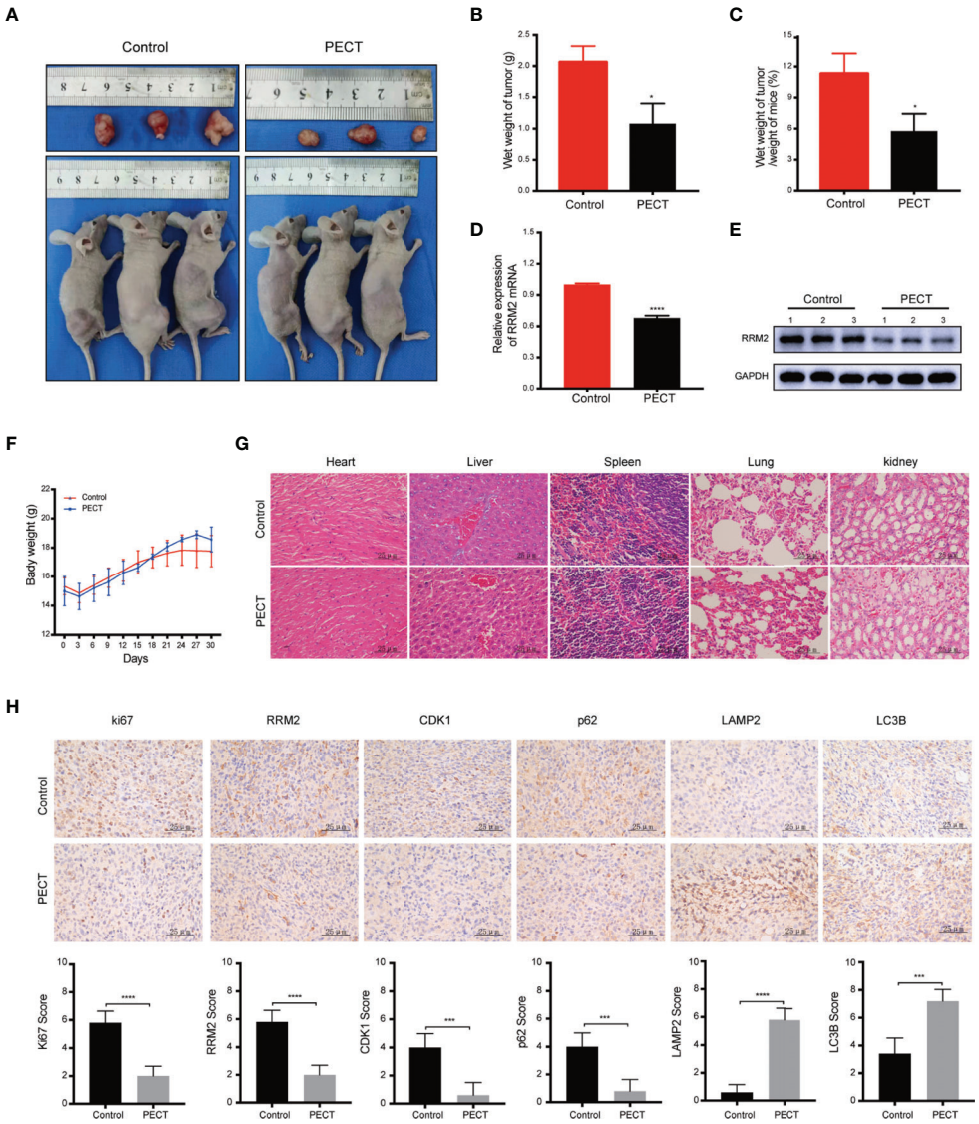

FIGURE 6 | PECT inhibits GBM proliferation *in vivo*. **(A)** Dissected images of mices and tumors, **(B)** tumor wet weight and **(C)** wet weight of tumor/weight of mice between the control and PECT groups. **(D, E)** RRM2 mRNA and protein expressions in mouse tumors with or without PECT treatment. **(F)** Body weight changes in the mouse models. **(G)** Representative images of H&E staining of the organs from mice with or without PECT treatment. Scale bar: 25 μm. **(H)** IHC staining for Ki67, RRM2, CDK1, p62, LAMP2, and LC3B in xenograft tumors between the control and PECT groups. Scale bar: 25 μm. The data are presented as the mean ± SD (n=3). $^{*}P < 0.05$, $^{***}P < 0.001$, $^{****}P < 0.0001$.

expression was inversely correlated with the OS time, indicating that RRM2 may be a prognosis marker of GBM (**Figure 7F**).

DISCUSSION

Chemotherapy is one of the conventional treatments for GBM. However, the existing chemotherapeutic drugs are insufficient to provide a survival period of more than 15 months to GBM patients (21, 22). Nearly a third of the drugs used in clinical care, currently, to treat cancer, come from natural products or its derivatives (23), indicating an attractive prospect for the development of natural products as a novel GBM therapy. PECT, a natural flavonoid, has demonstrated several anticancer activities, including autophagy and G2/M phase cell cycle arrest induction, cell proliferation, and migration inhibition (3, 24, 25). In the present study, we demonstrated for the first time that PECT can suppress GBM proliferation both *in vitro* and *in vivo*. More importantly, PECT significantly suppressed GBM cells, but not HUVECs, proliferation and did not caused morphological changes in organ tissues, indicating that PECT can inhibit tumor growth and can be safely administered *in vitro* and *in vivo*. Effective drugs for treating GBM are currently limited; one of the major limitations to drug development is that therapeutic agents

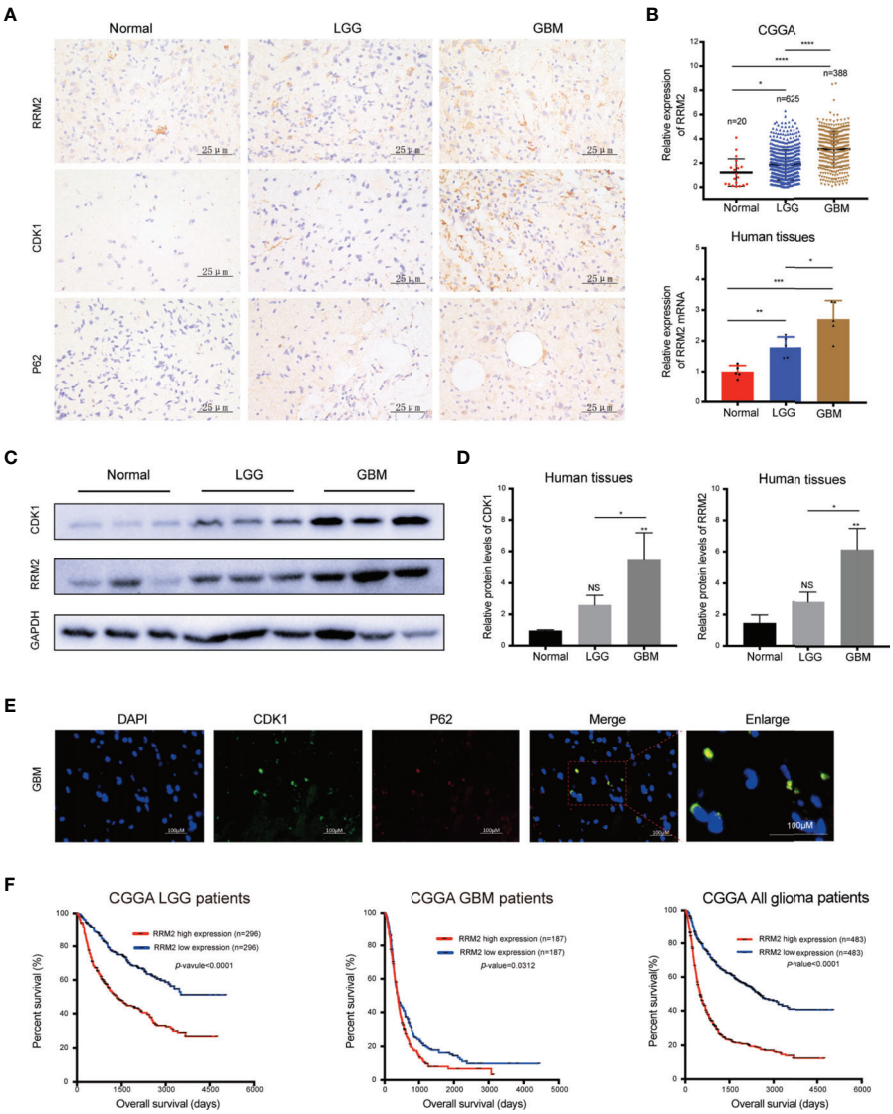

FIGURE 7 | RRM2 is increased in GBM tissues and inversely correlated with the prognosis of glioma patients. **(A)** IHC analysis of RRM2, CDK1, and p62 in sections obtained from primary glioma sample tissues and normal human brain sample tissues. **(B)** Analysis of RRM2 mRNA expression in GBM samples compared to normal human brain samples and LGG samples according to the CGGA data and qRT-PCR results. **(C, D)** WB analysis of RRM2 and CDK1 in GBM sample tissues compared to normal human brain sample tissues and LGG sample tissues. **(E)** Immunofluorescence double-staining analysis showing co-localization of p62 and CDK1 in the same lesional cells in human GBM cases. **(F)** OS curves of patients with glioma according to the median of RRM2. The data are presented as the mean ± SD (n=3). NS, non-significant. $^{*}P < 0.05$, $^{**}P < 0.01$, $^{***}P < 0.001$, $^{****}P < 0.0001$.

must possess the ability to cross BBB (26). Our results revealed that PECT can not only cross BBB, but also suppress the growth of intracranial GBM in nude mice and prolonged their effective survival time. However, the underlying molecular mechanism of the antineoplastic effect of PECT on GBM remains unclear.

We performed RNA-Seq analysis and found PECT treatment could inhibit the expression of RRM2 in U251 cells and affect the signal pathways such as DNA replication, cell cycle, lysosomal, and proteasome. In addition, qRT-PCR and western blotting assays further verified that PECT could reduce the expression of RRM2 mRNA and protein in GBM cells. RRM2 is the catalytic subunit of heterodimeric tetramer RNR and catalyzes *de novo* formation of dNTPs (27). The level of RRM2 changes continuously during the cell cycle to maintain the balance between dNTP production and DNA synthesis. Multiple cancers, such as melanoma, colorectal cancer, prostate cancer, liver cancer, breast cancer, glioma, and ovarian cancer, benefit from therapy targetting RRM2 (5, 28, 29). Sun and coworkers have shown that silencing RRM2 can induce G2/M phase cell cycle arrest of U87 cells (30). Chen et al. reported that RRM2 knockdown can reverse the resistance of human lung squamous carcinoma cells to gemcitabine by inducing autophagy (31). Our

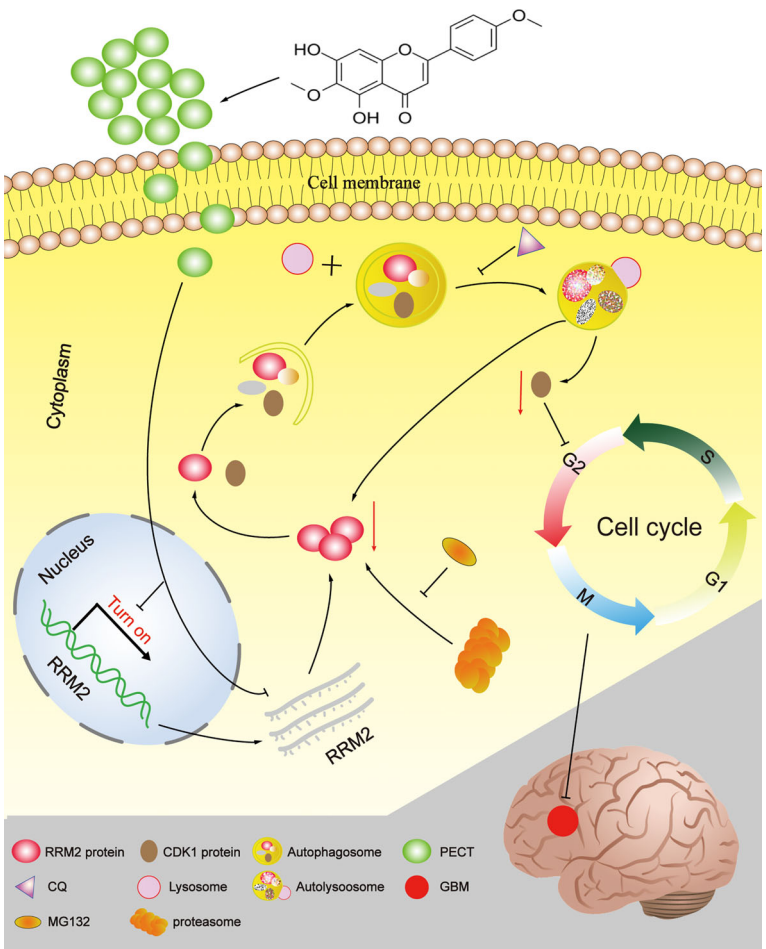

FIGURE 8 | The schematic diagram of RRM2 mediates the anti-tumor effect of PECT on GBM.

results showed that PECT can induce G2/M phase cell cycle arrest and increase autophagic flux of glioblastoma cells by inhibting RRM2 expression, which can be reversed by RRM2 overexpression plasmid.

Additionally, we found that PECT could inhibit RRM2 transcription and promote RRM2 protein degradation through a proteasome-dependent pathway, consistent with previous report. Such as RRM2 is ubiquitinated by APC/CCDH1 or cyclin F, and then degraded through the proteasome-dependent pathway (32, 33). Transcription factors, including Sp1, AP-2, BRCA, E2F1 and MYBL2, bind to the DNA sequence in the promoter region of *RRM2* and regulate their expression in response to DNA damage in cancer cells (34, 35). We did not thoroughly explore the effect of PECT on RRM2 transcription suppression and proteasome degradation, which will be verified in furture studies. However, we found that in addition to transcriptional suppression and proteasome-dependent degradation, RRM2 protein also depend on autophagy-lysosome pathway degradation. It was reported that excessive activation of autophagy could result in type II programmed cell death, which differs from necrosis and apoptosis (36). Additionally, the dual role of autophagy in response to anticancer therapy is well-known. Although there was some controversy regarding whether autophagy should be turned on or off to treat cancer (12), at least in this context, our data confirmed that RRM2 downregulation mediates the anti-proliferation effect of PECT on GBM, which depended on the increase of autophagic flux. Because PECT inhibited RRM2 expression, which can be inhibited by autophagy inhibitor CQ. In addition, immunofluorescence assay showed that RRM2 can co-localize with LAMP2 in U251 cells, while PECT treatment can increase the intracellular co-localization of LAMP2 and RRM2, and decrease the RRM2 protein expression. Thus, these further demonstrated that PECT could promote RRM2 protein degradation by autolysosome-dependent pathway in GBM.

In proliferating cells, RRM2 overexpression is regulated in a G2/M phase cell cycle-dependent manner (37, 38). Additionally, RRM2 downregulation has been demonstrated to promote autophagy-dependent cell death by decreasing intracellular dNTP levels (31). Reduction in RNR activity could suppress DNA replication and damage repair, resulting in cell cycle arrest (9, 39), and Autophagy has played a role in various cellular processes like DNA damage repair and cell cycle regulation (11, 40, 41). However, the effect of autophagy as a multifunctional

regulator on cell cycle progression in GBM remains unclear. In the present study, we confirmed that RRM2 knockdown can induce G2/M phase cell cycle arreste by decreasing CDK1 protein expression, which can be reversed by the inhibition of autophagy. CDK1, an essential kinase regulating cell cycle progression, is upregulated in multiple cancers. CDK1 depletion promote cell-cycle arrest and ultimately inhibit tumor cell proliferation (42–44). Additionally, p62 is an adapter that is widely involved in protein interactions. Our results demonstrated that CDK1 can interact with p62, which provided a basis for autophagy to degrade CDK1. Simultaneously, immunofluorescence assay showed that CDK1 can co-localize with p62 in U251 cells, and RRM2 knockdown can decrease the intracellular co-localization of CDK1 and p62, and decrease the CDK1 protein expression. These data indicated that autophagy is required for RRM2 to inhibit GBM cell proliferation through inducing G2/M phase cell cycle arrest by promoting CDK1 protein degradation, which supported by previous studies that p62-HDAC6 promoted CDK1 degradation through an autophagy-lysosome pathway in breast cancer (13). However, the exact binding site at which CDK1 binds p62 was not identified.

Clinical data revealed that RRM2 is increased in GBM tissues and inversely correlated with glioma sufferers OS time, which suggests RRM2 as a potential therapeutic target, as well as a prognosis and predictive biomarker. Additionally, we found that p62 and CDK1 protein were co-located in the lesional cells from human GBM cases, indicating that autophagy and cell cycle may be related to the occurrence and development of GBM, which may play a certain role for GBM clinical research. We also demonstrated that PECT or RRM2 knockdown was involved in regulating GBM cells migration, and PECT could directly bind to RRM2, and promote CDK1 protein degradation through proteasomal pathway, although the corresponding molecular mechanisms remain to be determined.

CONCLUSIONS

In summary, Our study provides a novel insight into the mechanisms by which PECT promoted the degradation of CDK1 protein dependent on autolysosomal pathway through increasing autophagic flow by inhibiting RRM2 (**Figure 8**). Additionally, RRM2 may be a potential therapeutic target and a prognosis and predictive biomarker in GBM patients, and manipulation of RRM2-mediated autophagy offers promising clinical therapeutic directions for GBM. However, the precise molecular mechanism of RRM2 to regulate autophagy in GBM should be further addressed in the future.

DATA AVAILABILITY STATEMENT

The original contributions presented in the study are included in the article/**Supplementary Material**. Further inquiries can be directed to the corresponding authors.

ETHICS STATEMENT

The study protocol was approved by the Clinical Research Ethics Committee of Harbin Medical University. All patients provided written informed consent, and the study was conducted in accordance with the Declaration of Helsinki. The patients/participants provided their written informed consent to participate in this study. All animal study protocols were approved by the Animal Experiments Ethics Committee of Harbin Medical University and the study was conducted in accordance with the Declaration of Helsinki.

AUTHOR CONTRIBUTIONS

HJ designed, conceived, planned, implemented the experiment, and wrote the original draft. LW, HY and EL assisted in collecting clinical samples. TY assisted in imaging. JY, XW and MG provided experimental guidance, and DZ assisted in completing experiments. KD, WL, CZ, JW, PY, ZS, XR, SA and SS participated in the investigation. XiaoC and ZZ provided financial sponsorship. XinC and SZ supervised and funded the research. All authors contributed to the article and approved the submitted version.

FUNDING

This work was funded by the Natural Science Foundation of China grants (81972363), Research Fund for the Postdoctoral Science Foundation of China (2019M661303), and Heilongjiang Province Postdoctoral Fund (LBH-Z19076).

ACKNOWLEDGMENTS

We would like to thank Editage (www.editage.cn) for English language editing.

SUPPLEMENTARY MATERIAL

The Supplementary Material for this article can be found online at: https://www.frontiersin.org/articles/10.3389/fonc.2022.887294/full#supplementary-material

Supplementary Figure 1 | LC-MS of PECT content using Principal component analysis (PCA).

Supplementary Figure 2 | The cytotoxicity effect of chloroquine on U87 and U251 cells analyzed using MTT assays

Supplementary Figure 3 | CCNA2 and CCNB1 protein expression no change after RRM2 was silenced.

Supplementary Figure 4 | CDK1 mRNA expression no change after RRM2 was silenced.

Supplementary Figure 5 | The transfection efficiency of RRM2 lentivirus in U251 cells.

REFERENCES

1. Li Y, Zhang ZX, Huang GH, Xiang Y, Yang L, Pei YC, et al. A Systematic Review of Multifocal and Multicentric Glioblastoma. *J Clin Neurosci* (2021) 83:71–6. doi: 10.1016/j.jocn.2020.11.025
2. De Waele J, Verhezen T, van der Heijden S, Berneman ZN, Peeters M, Lardon F, et al. A Systematic Review on Poly(I:C) and Poly-ICLC in Glioblastoma: Adjuvants Coordinating the Unlocking of Immunotherapy. *J Exp Clin Cancer Res* (2021) 40:213. doi: 10.1186/s13046-021-02017-2
3. Liu S, Zhang J, Yang H, Zhang Q, Chen M. Pectolinarigenin Flavonoid Exhibits Selective Anti-Proliferative Activity in Cisplatin-Resistant Hepatocellular Carcinoma, Autophagy Activation, Inhibiting Cell Migration and Invasion, G2/M Phase Cell Cycle Arrest and Targeting ERK1/2 MAP Kinases. *J BUON* (2020) 25:415–20.
4. Lee HJ, Saralamma VVG, Kim SM, Ha SE, Raha S, Lee WS, et al. Pectolinarigenin Induced Cell Cycle Arrest, Autophagy, and Apoptosis in Gastric Cancer Cell *via* PI3K/AKT/mTOR Signaling Pathway. *Nutrients* (2018) 10(8):1043. doi: 10.3390/nu10081043
5. Zhan Y, Jiang L, Jin X, Ying S, Wu Z, Wang L, et al. Inhibiting RRM2 to Enhance the Anticancer Activity of Chemotherapy. *BioMed Pharmacother* (2021) 133:110996. doi: 10.1016/j.biopha.2020.110996
6. Engstrom Y, Eriksson S, Jildevik I, Skog S, Thelander L, Tribukait B. Cell Cycle-Dependent Expression of Mammalian Ribonucleotide Reductase. Differential Regulation of the Two Subunits. *J Biol Chem* (1985) 260:9114–6. doi: 10.1016/S0021-9258(17)39337-7
7. Liu Q, Guo L, Qi H, Lou M, Wang R, Hai B, et al. A MYBL2 Complex for RRM2 Transactivation and the Synthetic Effect of MYBL2 Knockdown With WEE1 Inhibition Against Colorectal Cancer. *Cell Death Dis* (2021) 12:683. doi: 10.1038/s41419-021-03969-1
8. Li S, Mai H, Zhu Y, Li G, Sun J, Li G, et al. MicroRNA-4500 Inhibits Migration, Invasion, and Angiogenesis of Breast Cancer Cells *via* RRM2-Dependent MAPK Signaling Pathway. *Mol Ther Nucleic Acids* (2020) 21:278–89. doi: 10.1016/j.omtn.2020.04.018
9. Li ZN, Shu Y, Chen CG, Li XQ, Li MY, Zhao XH, et al. Acquired Tamoxifen Resistance is Surmounted by GW8510 Through Ribonucleotide Reductase M2 Downregulation-Mediated Autophagy Induction. *Biochem Biophys Res Commun* (2020) 528:554–60. doi: 10.1016/j.bbrc.2020.05.149
10. Li X, He S, Ma B. Autophagy and Autophagy-Related Proteins in Cancer. *Mol Cancer* (2020) 19:12. doi: 10.1186/s12943-020-1138-4
11. Li H, Peng X, Wang Y, Cao S, Xiong L, Fan J, et al. Atg5-Mediated Autophagy Deficiency in Proximal Tubules Promotes Cell Cycle G2/M Arrest and Renal Fibrosis. *Autophagy* (2016) 12:1472–86. doi: 10.1080/15548627.2016.1190071
12. Lim SM, Mohamad Hanif EA, Chin SF. Is Targeting Autophagy Mechanism in Cancer a Good Approach? The Possible Double-Edge Sword Effect. *Cell Biosci* (2021) 11:56. doi: 10.1186/s13578-021-00570-z
13. Galindo-Moreno M, Giraldez S, Saez C, Japon MA, Tortolero M, Romero F. Both P62/SQSTM1-HDAC6-Dependent Autophagy and the Aggresome Pathway Mediate CDK1 Degradation in Human Breast Cancer. *Sci Rep* (2017) 7:10078. doi: 10.1038/s41598-017-10506-8
14. Lee IH, Kawai Y, Fergusson MM, Rovira II, Bishop AJ, Motoyama N, et al. Atg7 Modulates P53 Activity to Regulate Cell Cycle and Survival During Metabolic Stress. *Science* (2012) 336:225–8. doi: 10.1126/science.1218395
15. Ru J, Li P, Wang J, Zhou W, Li B, Huang C, et al. TCMSP: A Database of Systems Pharmacology for Drug Discovery From Herbal Medicines. *J Cheminform* (2014) 6:13. doi: 10.1186/1758-2946-6-13
16. Bi Y, Shen C, Li C, Liu Y, Gao D, Shi C, et al. Inhibition of Autophagy Induced by Quercetin at a Late Stage Enhances Cytotoxic Effects on Glioma Cells. *Tumour Biol* (2016) 37:3549–60. doi: 10.1007/s13277-015-4125-4
17. Yamamoto K, Venida A, Yano J, Biancur DE, Kakiuchi M, Gupta S, et al. Autophagy Promotes Immune Evasion of Pancreatic Cancer by Degrading MHC-I. *Nature* (2020) 581:100–5. doi: 10.1038/s41586-020-2229-5
18. Sunada S, Saito H, Zhang D, Xu Z, Miki Y. CDK1 Inhibitor Controls G2/M Phase Transition and Reverses DNA Damage Sensitivity. *Biochem Biophys Res Commun* (2021) 550:56–61. doi: 10.1016/j.bbrc.2021.02.117
19. Xu G, Yan X, Hu Z, Zheng L, Ding K, Zhang Y, et al. Glucocappasalin Induces G2/M-Phase Arrest, Apoptosis, and Autophagy Pathways by Targeting CDK1 and PLK1 in Cervical Carcinoma Cells. *Front Pharmacol* (2021) 12:671138. doi: 10.3389/fphar.2021.671138
20. Zhou C, Liang Y, Zhou L, Yan Y, Liu N, Zhang R, et al. TSPAN1 Promotes Autophagy Flux and Mediates Cooperation Between WNT-CTNNB1 Signaling and Autophagy *via* the MIR454-FAM83A-TSPAN1 Axis in Pancreatic Cancer. *Autophagy* (2021) 17:3175–95. doi: 10.1080/15548627.2020.1826689
21. Qazi MA, Vora P, Venugopal C, Sidhu SS, Moffat J, Swanton C, et al. Intratumoral Heterogeneity: Pathways to Treatment Resistance and Relapse in Human Glioblastoma. *Ann Oncol* (2017) 28:1448–56. doi: 10.1093/annonc/mdx169
22. Lim M, Xia Y, Bettegowda C, Weller M. Current State of Immunotherapy for Glioblastoma. *Nat Rev Clin Oncol* (2018) 15:422–42. doi: 10.1038/s41571-018-0003-5
23. Mann J. Natural Products in Cancer Chemotherapy: Past, Present and Future. *Nat Rev Cancer* (2002) 2:143–8. doi: 10.1038/nrc723
24. Bonesi M, Tundis R, Deguin B, Loizzo MR, Menichini F, Tillequin F, et al. *In Vitro* Biological Evaluation of Novel 7-O-Dialkylaminoalkyl Cytotoxic Pectolinarigenin Derivatives Against a Panel of Human Cancer Cell Lines. *Bioorg Med Chem Lett* (2008) 18:5431–4. doi: 10.1016/j.bmcl.2008.09.037
25. Wu T, Dong X, Yu D, Shen Z, Yu J, Yan S. Natural Product Pectolinarigenin Inhibits Proliferation, Induces Apoptosis, and Causes G2/M Phase Arrest of HCC *via* PI3K/AKT/mTOR/ERK Signaling Pathway. *Onco Targets Ther* (2018) 11:8633–42. doi: 10.2147/OTT.S186186
26. Arvanitis CD, Ferraro GB, Jain RK. The Blood-Brain Barrier and Blood-Tumour Barrier in Brain Tumours and Metastases. *Nat Rev Cancer* (2020) 20:26–41. doi: 10.1038/s41568-019-0205-x
27. Rahman MA, Amin AR, Wang D, Koenig L, Nannapaneni S, Chen Z, et al. RRM2 Regulates Bcl-2 in Head and Neck and Lung Cancers: A Potential Target for Cancer Therapy. *Clin Cancer Res* (2013) 19:3416–28. doi: 10.1158/1078-0432.CCR-13-0073
28. Lee Y, Vassilakos A, Feng N, Lam V, Xie H, Wang M, et al. GTI-2040, an Antisense Agent Targeting the Small Subunit Component (R2) of Human Ribonucleotide Reductase, Shows Potent Antitumor Activity Against a Variety of Tumors. *Cancer Res* (2003) 63:2802–11.
29. Shao J, Liu X, Zhu L, Yen Y. Targeting Ribonucleotide Reductase for Cancer Therapy. *Expert Opin Ther Targets* (2013) 17:1423–37. doi: 10.1517/14728222.2013.840293
30. Sun H, Yang B, Zhang H, Song J, Zhang Y, Xing J, et al. RRM2 is a Potential Prognostic Biomarker With Functional Significance in Glioma. *Int J Biol Sci* (2019) 15:533–43. doi: 10.7150/ijbs.30114
31. Chen P, Wu JN, Shu Y, Jiang HG, Zhao XH, Qian H, et al. Gemcitabine Resistance Mediated by Ribonucleotide Reductase M2 in Lung Squamous Cell Carcinoma is Reversed by GW8510 Through Autophagy Induction. *Clin Sci (Lond)* (2018) 132:1417–33. doi: 10.1042/CS20180010
32. Chabes AL, Pfleger CM, Kirschner MW, Thelander L. Mouse Ribonucleotide Reductase R2 Protein: A New Target for Anaphase-Promoting Complex-Cdh1-Mediated Proteolysis. *Proc Natl Acad Sci USA* (2003) 100:3925–9. doi: 10.1073/pnas.0330774100
33. D'Angiolella V, Donato V, Forrester FM, Jeong YT, Pellacani C, Kudo Y, et al. Cyclin F-Mediated Degradation of Ribonucleotide Reductase M2 Controls Genome Integrity and DNA Repair. *Cell* (2012) 149:1023–34. doi: 10.1016/j.cell.2012.03.043
34. Fang Z, Gong C, Liu H, Zhang X, Mei L, Song M, et al. E2F1 Promote the Aggressiveness of Human Colorectal Cancer by Activating the Ribonucleotide Reductase Small Subunit M2. *Biochem Biophys Res Commun* (2015) 464:407–15. doi: 10.1016/j.bbrc.2015.06.103
35. Gong C, Liu H, Song R, Zhong T, Lou M, Wang T, et al. ATR-CHK1-E2F3 Signaling Transactivates Human Ribonucleotide Reductase Small Subunit M2 for DNA Repair Induced by the Chemical Carcinogen MNNG. *Biochim Biophys Acta* (2016) 1859:612–26. doi: 10.1016/j.bbagrm.2016.02.012
36. Talukdar S, Pradhan AK, Bhoopathi P, Shen XN, August LA, Windle JJ, et al. MDA-9/Syntenin Regulates Protective Autophagy in Anoikis-Resistant Glioma Stem Cells. *Proc Natl Acad Sci USA* (2018) 115:5768–73. doi: 10.1073/pnas.1721650115
37. Chen CW, Li Y, Hu S, Zhou W, Meng Y, Li Z, et al. DHS (Trans-4,4'-Dihydroxystilbene) Suppresses DNA Replication and Tumor Growth by Inhibiting RRM2 (Ribonucleotide Reductase Regulatory Subunit M2). *Oncogene* (2019) 38:2364–79. doi: 10.1038/s41388-018-0584-6

38. Shu Z, Li Z, Huang H, Chen Y, Fan J, Yu L, et al. Cell-Cycle-Dependent Phosphorylation of RRM1 Ensures Efficient DNA Replication and Regulates Cancer Vulnerability to ATR Inhibition. *Oncogene* (2020) 39:5721–33. doi: 10.1038/s41388-020-01403-y
39. Gandhi M, Gross M, Holler JM, Coggins SA, Patil N, Leupold JH, et al. The lncRNA lincNMR Regulates Nucleotide Metabolism *via* a YBX1 - RRM2 Axis in Cancer. *Nat Commun* (2020) 11:3214. doi: 10.1038/s41467-020-17007-9
40. Pathania AS, Guru SK, Kumar S, Kumar A, Ahmad M, Bhushan S, et al. Interplay Between Cell Cycle and Autophagy Induced by Boswellic Acid Analog. *Sci Rep* (2016) 6:33146. doi: 10.1038/srep33146
41. Lin TY, Chan HH, Chen SH, Sarvagalla S, Chen PS, Coumar MS, et al. BIRC5/Survivin is a Novel ATG12-ATG5 Conjugate Interactor and an Autophagy-Induced DNA Damage Suppressor in Human Cancer and Mouse Embryonic Fibroblast Cells. *Autophagy* (2020) 16:1296–313. doi: 10.1080/15548627.2019.1671643
42. Gan H, Qi M, Chan C, Leung P, Ye G, Lei Y, et al. Digitoxin Inhibits HeLa Cell Growth Through the Induction of G2/M Cell Cycle Arrest and Apoptosis *In Vitro* and *In Vivo*. *Int J Oncol* (2020) 57:562–73. doi: 10.3892/ijo.2020.5070
43. Pack LR, Daigh LH, Meyer T. Putting the Brakes on the Cell Cycle: Mechanisms of Cellular Growth Arrest. *Curr Opin Cell Biol* (2019) 60:106–13. doi: 10.1016/j.ceb.2019.05.005
44. Roskoski R Jr. Cyclin-Dependent Protein Serine/Threonine Kinase Inhibitors as Anticancer Drugs. *Pharmacol Res* (2019) 139:471–88. doi: 10.1016/j.phrs.2018.11.035

Conflict of Interest: The authors declare that the research was conducted in the absence of any commercial or financial relationships that could be construed as a potential conflict of interest.

Publisher's Note: All claims expressed in this article are solely those of the authors and do not necessarily represent those of their affiliated organizations, or those of the publisher, the editors and the reviewers. Any product that may be evaluated in this article, or claim that may be made by its manufacturer, is not guaranteed or endorsed by the publisher.

frontiers | Frontiers in Oncology

ORIGINAL RESEARCH
published: 12 May 2022
doi: 10.3389/fonc.2022.857927

Development of Novel CD47-Specific ADCs Possessing High Potency Against Non-Small Cell Lung Cancer *in vitro* and *in vivo*

Zu-Chian Chiang[1,2,3], Shubin Fang[2†], Yang-kun Shen[1], Dongya Cui[1], Huanjiao Weng[2], Dawei Wang[1], Yuxiang Zhao[1], Jizhen Lin[2,4] and Qi Chen[1*]*

[1] Fujian Key Laboratory of Innate Immune Biology, Biomedical Research Center of South China, College of Life Science, Fujian Normal University, Fuzhou, China, [2] The Cancer Center, Union Hospital, Fujian Medical University, Fuzhou, China, [3] College of Photonic and Electronic Engineering, Fujian Normal University, Fuzhou, China, [4] The Department of Otolaryngology, Head and Neck Surgery, University of Minnesota Medical School, Minneapolis, MN, United States

Targeted therapies hold promise for efficiently and accurately delivering cytotoxic drugs directly to tumor tissue to exert anticancer effects. CD47 is a membrane protein expressed in a variety of malignant tumors and hematopoietic cells, which plays a key role in immune escape and tumor progression. Although CD47 immunocheckpoint therapy has been developed in recent years, many patients cannot benefit from it because of its low efficiency. To strengthen and extend the therapeutic efficacy of anti-CD47 monoclonal antibody (mAb), we used the newly developed 7DC2 and 7DC4 mAbs as the targeting payload adaptor and VCMMAE as the toxin payload to construct novel CD47-specific immunotoxin (7DC-VCMMAE) by engineering cysteine residues. These CD47-specific ADCs have the better cell penetration, excellent DAR, similar payload distribution and good antigen-binding affinity. *In vitro*, 7DC-VCMMAE treatment induced death of non-small cell lung cancer (NSCLC) cell lines 95D and SPC-A1, but not A549 that express low levels of CD47 on the cell membrane. This finding suggests that 7DC-VCMMAE may possess greater therapeutic effect on NSCLC tumors expressing a high level of CD47 antigen; however, 7DC-VCMMAE treatment also promoted phagocytosis of A549 cells by macrophages. *In vivo*, 7DC-VCMMAE treatment had remarkable antitumor effects in a NSCLC cell line-derived xenograft (CDX) mouse model based on nonobese diabetic/severe combined immunodeficient (NOD/SCID). In summary, this study combined VCMMAE with anti-CD47 mAbs, emphasizing a novel and promising immunotherapy method for direct killing of NSCLC, which provides a valuable new way to meet the needs of the cancer therapy field.

Keywords: immunotoxin, antibody-drug conjugates, CD47 antigen, non-small cell lung cancer, macrophage, phagocytosis, targeted therapy

OPEN ACCESS

Edited by:
Yan-yan Yan,
Shanxi Datong University, China

Reviewed by:
Helmout Modjathedi,
Kingston University, United Kingdom
Frank Momburg,
German Cancer Research Center (DKFZ), Germany

****Correspondence:***
Jizhen Lin
linjizhen@fjmu.edu.cn
Qi Chen
chenqi@fjnu.edu.cn

[†]These authors share first authorship

Specialty section:
This article was submitted to Cancer Molecular Targets and Therapeutics, a section of the journal Frontiers in Oncology

Received: *19 January 2022*
Accepted: *13 April 2022*
Published: *12 May 2022*

Citation:
Chiang Z-C, Fang S, Shen Y-k, Cui D, Weng H, Wang D, Zhao Y, Lin J and Chen Q (2022) Development of Novel CD47-Specific ADCs Possessing High Potency Against Non-Small Cell Lung Cancer in vitro and in vivo. Front. Oncol. 12:857927. doi: 10.3389/fonc.2022.857927

INTRODUCTION

Lung cancer is the leading cause of cancer mortality worldwide, with approximately 2.5 million new cases and 1.5 million deaths per year (1). Non-small cell lung cancer (NSCLC) accounts for approximately 85% of all lung cancer cases. The 5-year overall survival (OS) rate of NSCLC is less than 21% (2, 3). Antibody and chemotherapy treatments, as well as the development of tyrosine kinase inhibitors (TKIs), have improved the response rate and OS in patients with NSCLC (4, 5), but fewer than 20% of patients receive TKIs. Thus, the prognosis for advanced NSCLC remains poor (6, 7). Approximately 45% of lung cancers are classified as "cold tumors" with little or no infiltration of immune cells, which greatly reduces the efficacy of immunotherapy. Immune checkpoint inhibitors, such as anti-PD-1 antibodies, have only a 25% efficacy in advanced NSCLC. Therefore, there is a significant need for more effective therapeutics for NSCLC, particularly those that can target cold tumors.

Tumor-associated macrophages (TAMs) have been investigated as a potential immunotherapeutic strategy (8) because they promote the activation of immune cells and clearance of tumor cells through phagocytosis (9). Cluster of differentiation 47 (CD47) is a transmembrane glycoprotein with numerous functions (10), including acting as a "don't-eat-me" signal to prevent phagocytosis (11). CD47 expression is widely distributed in hematopoietic cells and protects normal cells from phagocytosis by binding to an immunoglobulin-like cell surface receptor on macrophages, the signal regulatory protein alpha (SIRPα) (12, 13). Tumor cells, such as esophageal squamous cell carcinoma, also express CD47 (14, 15), which allows evasion of host immune surveillance and protection against phagocytosis (16–18). Overexpression of CD47 has been described in various malignancies, including leukemia (19, 20), lymphoma (21), multiple myeloma (22) and solid tumors, such as breast (23), colon (24), hepatocellular carcinoma (25), melanoma (26), and small cell lung cancer (27). CD47 is also highly expressed in NSCLC cells (28, 29) and primary NSCLC tumors, and promotes the invasion and metastasis of NSCLC (30). Therefore, targeting CD47 may provide a new option for targeting therapeutics to NSCLC.

Some studies have examined the potential of CD47 as an anti-cancer therapeutic target to prevent immune evasion of tumor cells (28); however, the CD47-targeted therapies tested thus far have shown low efficacy and limited benefit. Immunotherapeutic efficacy is related to the degree of infiltration of immune cells into the tumor tissue; for cold tumors, new therapeutic approaches are needed, which do not depend on immune cell infiltration. We hypothesized that CD47-targeted therapy could be improved through the development of anti-CD47 antibody-drug conjugates (ADCs). ADCs are one of the fastest developing classes of anticancer drugs; in recent years, they have been shown to efficiently and accurately deliver cytotoxic drugs directly to tumor tissue to exert anticancer effects and reduce systemic exposure and toxicity (31–33). ADCs comprise a monoclonal antibody (mAb) conjugated to small cytotoxic drugs *via* a chemical linker; the mAb delivers the drug to cancer cells that express the specific cell surface target antigen. Internalization of the mAb and release of the cytotoxic payload kills the cancer cell, though some studies have demonstrated that non-internalized ADC products can release the cytotoxic drug into the tumor microenvironment to elicit a potent therapeutic effect (34). Since 2000, ADC drugs have attracted more and more attention from the pharmaceutical industry. So far, more than 100 ADC drugs are undergoing development and 5 ADCs drugs have been approved by FDA. There are at least 5 VC-linked MMAE (VCMMAE) ADC drugs developed globally (35). Recently, an ADC drug targeting CD47 has emerged by using Sulfo-SMCC linker to make non-cleavable ADC, namely anti-CD47-DM1 (36). However, peptide-based linkers are stable in unsuitable pH condition and different serum protease inhibitors; therefore, these peptide linkers are stable in the systemic circulation and only unleash the drug in the target cells (37). Valine citrulline (V-C) is the most commonly used peptide linker in current clinical research. One example of successful use of the V-C linker in ADC design is the Adcetris® for targeting CD30 that has been approved by FDA (38).

In this study, we developed CD47-specific ADCs *via* V-C linker as a new targeted therapy for NSCLC. Firstly, the spleen cells of mice sensitized by CD47 antigen were collected and sequenced on a large scale, and the phage display technology was used to screen the anti-CD47 antibody with high affinity and specificity. Then, we established CD47-targeted ADCs as a specific targeted drug. Through further identification and characterization, the specific-CD47 ADC drug was described. Finally, the killing effect and phagocytosis induction effect on NSCLC *in vitro* were evaluated, and the antitumor efficacies on NSCLC *in vivo* were confirmed by NSCLC cell-derived xenograft (CDX) mouse model, using NOD/SCID mice to mimic the cold tumor environment.

MATERIALS AND METHODS

Chemicals and Reagents

Ammonium sulfate, sodium phosphate, sodium chloride, Tris (2-carboxyethyl) phosphine (TCEP), N-acetylcysteine (NAC), isopropyl alcohol (IPA), dimethyl sulfoxide (DMSO), 2-mercaptoethanol (2-ME), ethylenediaminetetraacetic acid (EDTA), phosphate buffered saline (PBS), and TWEEN® 20 were purchased from Sigma-Aldrich. Centrifugal filter tubes (Amicon-30 kDa) were purchased from Merck Millipore. Maleimidocaproyl-valine-citrulline-monomethyl auristatin E (VCMMAE) was obtained from MedChem Express. Lithium Dodecyl Sulfate (LDS) sample loading buffer (4X) and 12% acrylamide of PAGE gel were purchased from Thermo Fisher Scientific. Grener F 96-well immunoplates were purchased from Sigma-Aldrich.

Abbreviations: ADCs, antibody-drug conjugates; CD47, cluster of differentiation 47; CDX, cell line-derived xenograft; DAR, drug-to-antibody ratio; EC_{50}, half-maximal effective concentration; IC_{50}, half-maximal inhibitory concentration; LDS, lithium dodecyl sulfate; NOD/SCID, nonobese diabetic/severe combined immunodeficient; NSCLC, non-small cell lung cancer; NIRF, near-infrared fluorescence; TCEP, Tris(2-carboxyethyl)phosphine; VCMMAE, Valine-citrulline-monomethyl auristatin E.

Isolation of Mouse Anti-Human CD47 Monoclonal Antibodies from B Cells of Immunized Mice

To isolate CD47 specific monoclonal antibodies, 2 x 10^7 the mouse lymphocytes were collected from the spleen of 3 mice immunized with the human CD47 antigen. All B cells were collected and pooled from the mouse spleens. A mouse single strand fragment variable (scFv) library with high-quality was constructed by using approximate 10^7 the mouse lymphocytes following the method described previously (39, 40). Specifically, the total RNA of the B cells was extracted by conventional Trizol reagent (41), the immune scFv library (containing approximate 10 million different antibodies) were constructed and displayed by phage. The human CD47 antigen was used to screen specifically bound antibodies and isolated from the library through three consecutive enrichment steps. The ability of clones produced by these enrichment steps to bind human CD47 was tested by ELISA. Two clones, namely 7DC2 and 7DC4, were selected. The specific chimeric CD47 binding antibodies containing the mouse Fab plus human IgG1 Fc fragment were constructed, and were expressed, purified and used for later toxin conjugation and further analyses.

Preparation of the New Anti-CD47 Antibodies, 7DC2 and 7DC4

Expi293 (Gibco), a high-yield transient expression system based on suspension-adapted Human Embryonic Kidney (HEK) cells, was used as a production host for 7DC monoclonal antibody expression. OPM-293 CD03 medium (Shanghai OPM Biosciences) is a chemically defined, serum-free, protein-free medium for growth and transfection of Expi293 cells. OPM-293 CD03 medium was supplemented with 2 mM L-glutamine (Gibco) before use. Expi293 cells were incubated in a 37°C incubator with 80% relative humidity and 5% CO_2 on an orbital shaker platform (Thermo fisher). Glucose (SINOPHARM) and OPM-CHO PFF05 (Shanghai OPM Biosciences) were added as feed.

After thawing, Expi293 cells were subcultured to 0.3×10^6 - 0.5×10^6 cells/mL every 4-5 days in suspension in a 125 mL shaker flask containing 30 mL OPM-293 CD03 medium. Before transfection, 20 μg light chain plasmids and 10 μg heavy chain plasmids (endotoxin-free) were mixed with PEI transfection reagent, and then the DNA-PEI complexes were added to transfect cells in the shaker flask. Feed medium was added every 2 days after transfection. 300 g/L glucose was added once daily to achieve a residual glucose concentration of 1 g/L. Glucose concentration was determined using a Glucose Assay Kit (Shanghai Rongsheng bio). When the viability was lower than 75%, cell cultures were harvested.

Flow Cytometry

Lung cancer cell lines SPC-A-1 (FH0082, Shanghai Fuheng Biological Technology Co., Ltd.), A549 (CL-0016, Procell Life Science&Technology Co., Ltd.), and 95D (CL-0011, Procell Life Science&Technology Co., Ltd.) (1×10^6), authenticated by STR and Amelogenin analysis (hppt://web.expasy.org/cellosaurus-str-search) were placed in a 1.5 ml centrifuge tube, centrifuged at 1,200 rpm/min for 5 minutes, and the supernatant was discarded. Cells were suspended in 100 μl FACS buffer and 1 μl of anti-human CD47 antibody with PE fluorescence (clone: CC2C6, BioLegend, Inc.) was added, followed by incubation for 30 min at 25°C. After staining, the cells were washed twice with flow buffer (PBS + 2% FBS). Antibodies with PE fluorescence not bound to cells were removed by centrifuging at 1,200 rpm/min for 5 minutes to discard the supernatant. The cells were resuspended in 300 μl of flow buffer and the fluorescence intensity was analyzed using a FACSymphony™A5 (BD Biosciences).

Antibodies (7DC) and ADCs (7DC-VCMMAE) we developed also were used to check the CD47 expressions of three cancer cell lines. The cells (1×10^6) were firstly incubated by 2 μg of 7DC2, 7DC4, 7DC2-VCMMAE and 7DC4-VCMMAE for 30 min, respectively. After washing, a Goat anti-Human IgG Fc secondary antibody labeled PE (eBioscience™, Invitrogen) was added and incubated for 30 min. They were washed again and centrifuged, and the supernatant was discarded. The secondary Antibody labeled with PE was used to directly bind with the cells without 7DC or 7DC-VCMMAE as a negative control. Their Mean Fluorescence Intensity (MFI) was analyzed as described above.

Internalization Assay for 7DC2 and 7DC4

SPC-A-1 cells were suspended at 2×10^5 cells per mL and treated with 7DC2 and 7DC4, labelled with Fluor-488 (LinKine™ AbFluor 488 Labeling Kit, Abbkine) according to the manufacturer's protocol, at the concentration of 5 μg/mL in complete medium. After 4-hour incubation at 37°C with 5% CO_2, the cells were washed once in PBS (pH 7.4) to remove unbound antibodies. DAPI was used to stain the nucleus and antibody-free Fluor-488 as a negative control. Cells were washed again and subsequently imaged with confocal microscopy. Fluorescence images were acquired with a Zeiss Axio Observer Z1 microscope with laser scanning unit LSM 780 fitted with a Axio Cam MRm camera.

Development of the New ADCs, 7DC2-VCMMAE and 7DC4-VCMMAE

After identification of the CD47-specific mAb, 7DC, CD47-specific ADCs (7DC2-VCMMAE and 7DC4-VCMMAE) were established in a series of chemical reactions, as illustrated in **Scheme 1**. MMAE with maleimide-modified VC was conjugated to the 7DC2 and 7DC4 monoclonal antibody by Michael addition to form 7DC2-VCMMAE and 7DC4-VCMMAE, respectively. The pH 6.8 conjugation buffer solution contained 50 mM sodium phosphate, 50 mM sodium chloride and 2 mM EDTA. The 7DC2 and 7DC4 solution were incubated with conjugation buffer solution respectively, and were filtered by using Amicon-30 kDa. 13.5 μM of 7DC2 and 7DC4 were used in a reduction reaction with excess Tris (2-carboxyethyl) phosphine (TECP, Sigma-Aldrich) at 30°C for 2 hours to create free sulfhydryl groups.

The samples were then conjugated with 10.8 equivalents of VCMMAE dissolved in DMSO at 30°C to achieve high drug-to-

antibody ratio (DAR) and drug distributions. The reaction time was controlled for 12 hours. After reaction quenching, the unreacted VCMMAE and side-products were removed by Amicon-30 kDa using 10.8 equivalents of N-Acetylcysteine (NAC). Finally, Amicon-30 kDa was used again to purify the products; finished products were stored at 4°C for later analysis and application in experiments.

UV-VIS Photo-Profiling

UV-VIS photo-profiling was employed to rapidly confirm successful preparation of ADCs. Nanodrop 2000 spectrophotometers were used to measure the UV-VIS photo-profile of ADCs. The maximum absorption wavelengths of the samples were selected at 280 nm and 248 nm to detect the spectral changes before and after antibody conjugation with VCMMAE. Two microliters of each sample (7DC2, 7DC4, 7DC2-VCMMAE, and 7DC4-VCMMAE) was taken for UV-VIS photo-profiling under the above described conditions.

LDS-PAGE Analysis of ADCs

Polyacrylamide gel electrophoresis (PAGE) of 7CD2, 7DC2-VCMMAE, 7CD4, and 7DC4-VCMMAE was conducted under reducing and non-reducing conditions. Lithium dodecyl sulfate (LDS) sample loading buffer (4X) and working solution, containing 106 mM Tris HCl, 141 mM Tris base, 2% LDS, 10% glycerol, 0.51 mM EDTA, 0.22 mM G250 Coomassie Blue, and 0.175 mM phenol red, pH 8.5 with and without 2-mercaptoethanol (2-ME), were used to run the samples. Samples (approximately 4 µg of protein per sample) were denatured at 95°C for 15 minutes. The mixtures were loaded

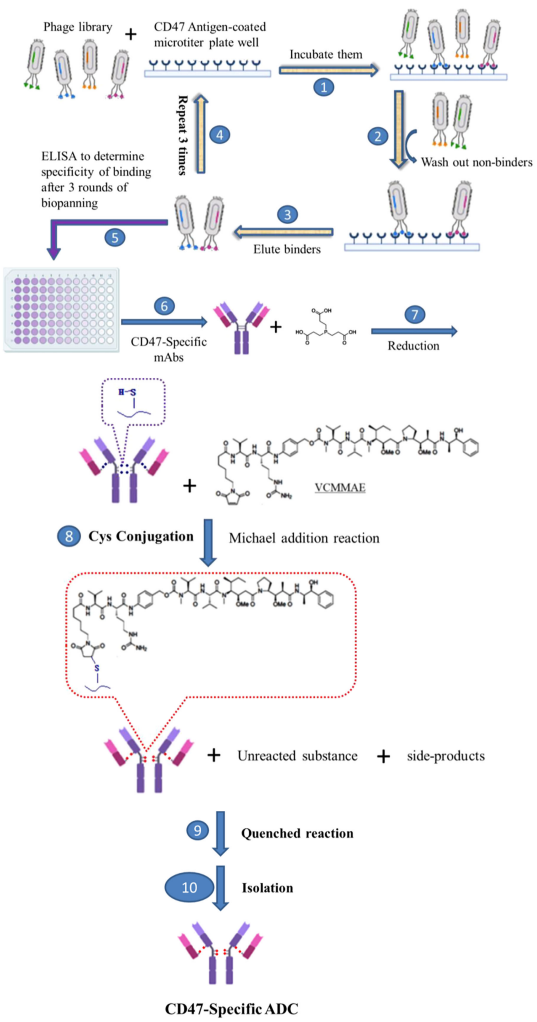

SCHEME 1 | Development of novel CD47-specific ADCs. The specific CD47 mAb, 7DC, was discovered by phage display shown in steps 1. incubating them, 2. washing out non-binders, 3. eluting binders, 4. repeating steps from 1 to 3 for 3 rounds, 5. determining specific of binding by ELISA and 6. making CD47-specific mAbs. CD47-specific ADCs, 7DC2-VCMMAE and 7DC4-VCMMAE, were established by conjugating the small molecule cytotoxic drug, VCMMAE, to the IgG linker region through a series of chemical reactions, as shown in steps 7. reducing the disulfide bonds of CD47-specific mAb to make free sulfhydryl groups, 8. Cys conjugation by Michael addition reaction, 9. quenched reaction, 10. isolation of CD47-specific ADC.

on a 12% polyacrylamide gel and then were separated at 150 V/160 mA for approximately 1 hour. After electrophoresis, the gel was stained with InstantBlue™ solution (Bio-Rad, Hercules, CA), then destained overnight in ultrapure water. Gel images were captured by a Gel Doc™ XR+ (BIO-RAD).

Binding Affinities of the ADCs Determined by ELISA

The half-maximal effective concentrations (EC_{50} values) of 7CD2, 7DC2-VCMMAE, 7CD4, and 7DC4-VCMMAE were determined by titrating IgG antibodies on immobilized CD47/ECD (Gln 19 - Pro 139, His Tag, ACROBiosystems) is expressed from human 293 cells (HEK293). It contains AA (Accession # NP_942088). with ELISA. In brief, CD47/ECD antigen (0.2 μg per well) in PBS buffer (pH 7.4) was coated on Grener F 96-well immunoplates for 16 hours at 4°C, and then the wells were blocked with 2% BSA in PBST (phosphate-buffered saline with 0.05% Tween-20) for 1.5 hours. Samples in PBST with 0.5% BSA were prepared at 11 concentrations by performing two-fold serial dilutions. After blocking, 100 μl of each diluted sample was added to each well and incubated for 1 hour with gentle shaking. The plate was washed with 300 μl of PBST 4 times, and then 100 μl of horseradish peroxidase/anti-human IgG antibody conjugate (1000X dilution) in PBST with 0.5% BSA was added and incubated for 1 hour at room temperature. After washing 4 times with PBST buffer and twice with PBS, the samples were treated with 3,3',5,5'-tetramethylbenzidine peroxidase substrate for 3 minutes, quenched with 1.0 M HCl, and measured at 450 nm with an ELISA reader. The EC_{50} (ng/ml) was calculated by ED_{50} Plus v1.0 software.

HIC-HPLC Analysis

Characterization of DAR and drug distribution was accomplished by using hydrophobic interaction chromatography-high performance liquid chromatography (HIC-HPLC). A TSKgel Butyl-NPR column (Tosoh Bioscience) column with 2.5 μm particles and 4.6 mm ID × 3.5 cm lengths was employed.

Mobile phase A, an aqueous solution of 1.8 M ammonium sulfate with 25 mM sodium phosphate at pH 7, and mobile phase B, a mixture of 75% (v/v) aqueous solution of 25 mM sodium phosphate at pH 7 with 25% (v/v) isopropyl alcohol, were generated to elute the samples. The analytical method was established by the linear gradient from 100% buffer A to 100% buffer B for 12 minutes, a flow rate at 1 mL/min and the temperature at 25°C. The samples were monitored by a UV detector at 248 nm.

The DAR of the samples was calculated by

$$DAR = \sum n \times A_n / \sum A_n \quad (1)$$

Where n denotes the number of drugs attached to the antibody (DAR species) and A_n denotes the area under each DAR species peak cluster.

Cell Culture and Cytotoxicity Assays

Human lung cancer cell lines (95D, A549, and SPC-A-1) were grown in RPMI 1640 and DMEM media (HyClone) supplemented with 10% fetal bovine serum at 37°C in a humidified atmosphere containing 5% carbon dioxide. 95D, SPC-A-1, and A549 cells were seeded at densities of 2×10^4 cells/well in 96-well plates. After cell attachment to the well, 5-fold serial dilutions of the anti-CD47 antibodies (7DC) and ADCs (7DC-VCMMAE) were added, and the cells were incubated at 37°C for 2 to 3 days. To evaluate cytotoxic activity, relative cell viability was measured using the WST-1 colorimetric assay (Roche) following the manufacturer's instructions.

In Vitro Phagocytosis Assay

To demonstrate the phagocytosis induction effect of CD47-specific ADCs *in vitro*, Raw 264.7 macrophages were co-cultured with A549, SPC-A-1, or 95D cancer cells. The phagocytosis phenomenon can be directly observed and compared through the fluorescence imaging method according to the method of Willingham et al. (28) and slightly modified. In brief, 1×10^5 macrophages were plated per well in a 6-well tissue culture plate. The cancer cells were labeled with CFDA SE according to the manufacturer's protocol. Macrophages were incubated in serum-free medium for 2 hours before the addition of 2×10^5 CFDA SE-labeled the cancer cells. Anti-CD47 antibodies and the ADCs were added and incubated at 40 nM for 2.5 hours at 37°C. Macrophages were repeatedly washed and subsequently imaged with an inverted microscope.

In Vivo Tumor Xenograft Studies

95D cells, a human highly metastatic lung cancer cell line, were grown in RPMI 1640 medium (Gibco) as described above. All mouse experiments were conducted according to guidelines and experimental protocols approved by the Institutional Animal Care and Utilization Committee (IACUC) of Fujian Normal University (Protocol ID: 20200010). The 95D cell line-derived xenograft model (NSCLC CDX- model) was established by subcutaneously inoculating 1×10^6 cells into the right flank of 6-week-old female NOD.CB17-Prkdcscid/NcrCrlBltw NOD/SCID mice (WSSYDW). When the tumors reached suitable tumor size 14 days after inoculation, the mice were randomly assigned into six groups (four mice per group): 7DC2 (20 mg/kg), 7DC4 (20 mg/kg), 7DC2-VCMMAE (20 mg/kg), 7DC4-VCMMAE (20 mg/kg), free VCMMAE (0.1755 mg/kg), and PBS (200 μl). All groups' mice were administered without anesthesia. The 95D tumor-bearing mice were treated once a week for a total of three doses for each group through intraperitoneal injection. Tumor size and weight change in mice were recorded twice a week. Tumor volume was calculated by using the ellipsoid formula: length × width × height × 0.523. Survival probability over time was evaluated by the Kaplan-Meier method; mice with tumor of the size above 200 mm^3 were considered treatment failures and were removed from the surviving population when calculating the Kaplan-Meier curves. Thus, "survival" in this study was defined as mice that were alive and with tumor burden less than 200 mm^3.

Serum Biochemical Analysis

8-week-old female NOD/SCID mice were intraperitoneally injected with 20 mg/kg of 7DC2, 7DC4, 7DC2-VCMMAE, or 7DC4-VCMMAE; 133.5 nmole/kg of VCMMAE; or 10 ml/kg of

PBS once a week for a total of three doses. Blood samples were collected and assayed for alanine transaminase (ALT), alkaline phosphatase (ALP), creatinine (CRE), and blood urea nitrogen (BUN) using Mindray BS-800 (Mindray) according to manufacturer's instructions.

DyLight 680 Conjugation, *in vivo* Optical Imaging, and *ex vivo* NIRF Imaging

The interchain disulfide bond of 7DC2 and 7DC4 were reduced by excess of TCEP at 30°C for 2 hours to produce free sulfhydryl groups. The samples were then conjugated with 10.8 equivalents of DyLight 680 (Thermo Scientific) at 30°C for 4 hours. Unreacted DyLight 680 was removed by using Dye Removal Column kit (Pierce) and conjugation efficiency was determined using Nanodrop (Thermo Scientific) to calculate the molar ratio of DyLight 680 to protein.

Mice bearing 95D tumors were intraperitoneally injected with 0.5 nmol of 7DC2-DyLight 680 or 7DC4-DyLight 680 (100 µL per injection; 3 mg/kg) or 1 nmol of free DyLight680 as a control group. For *in vivo* optical imaging, NIRF images were obtained at 24 hours using a small-animal IVIS imaging system (IVIS-Spectrum, Xenogen) with excitation and emission wavelengths of 675 and 720 nm. Fluorescence emission was normalized to photons per second per centimeter squared per steradian (p/s/cm2/sr). For *ex vivo* NIRF imaging, the mice were euthanized 24 hours after injection, and blood and organs were collected. NIRF images were acquired for each tissue as described above.

Statistical Analysis

Data are expressed as mean ± SD and n ≥ 4 as indicated. Differences between two groups were analyzed by two-tailed Student's t-test, and data set comparisons with P values of < 0.05 were considered statistically significant.

RESULTS

CD47 Overexpression in Lung Cancer Cell Lines

SPC-A-1, A549, and 95D are human lung cancer cell lines with differences in aggressiveness, metastasis, drug resistance, and CD47 expression levels. To quantify CD47 expression at the cell surface, the three cell lines were incubated with anti-CD47 antibody labelled with phycoerythrin (PE) and flow cytometry was used to detect cell membrane CD47. All cells expressed CD47 protein on the cell membrane but at distinctly different levels (**Figure 1A**). CD47 overexpression was greatest in 95D cells, followed by SPC-A-1 and A549 cells (**Figure 1A** and **Table 1**). SPC-A-1 and 95D cells expressed approximately 2- to 3-fold more CD47 on the cell surface than A549 cells.

In addition, three lung cancer cells were treated with 7DC2, 7DC4, 7DC2-VCMMAE, or 7DC4-VCMMAE and followed by staining with the anti-Human IgG Fc secondary antibody labeled with PE (**Figure 1B** and **Supplementary Table S1**). As a result, we found that the fluorescence intensity showed in the order of 95D > SPC-A-1 > A549 (**Figure 1B**; **Supplementary Table S1**).

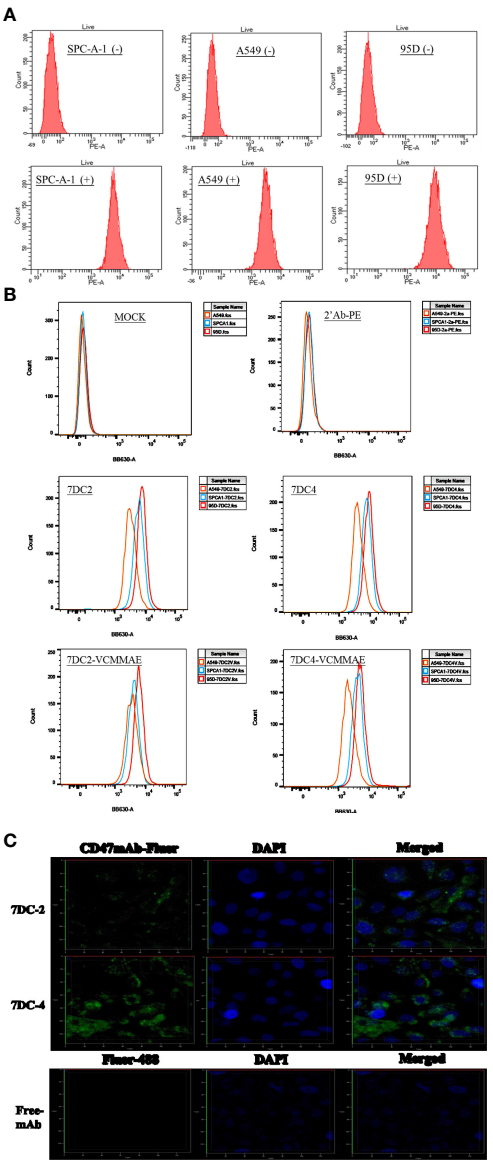

FIGURE 1 | Characterization of CD47-overexpressing cancer cells and anti-CD47 antibodies. **(A)** Flow cytometry showing that CD47-positive human lung cancer cell lines A549, SPC-A-1, and 95D express different amounts of CD47 on their surfaces, stained by using anti-human CD47 antibody with PE fluorescence (clone: CC2C6). **(B)** Flow cytometry showing that the strength of CD47-expressed cell surface of three lung cancer cells were in the order of A549 < SPC-A-1 < 95D, stained by using 7DC2, 7DC4, 7DC4-VCMMAE, or 7DC4-VCMMAE and the anti-Human IgG Fc secondary antibody labeled with PE, respectively. **(C)** Confocal fluorescence images confirming that the anti-CD47 mAbs, 7DC2 and 7DC4, are internalized by SPC-A-1 lung cancer cells (green, Fluro-488-labelled mAbs; blue, DAPI nuclear staining).

In other words, the expression of CD47 on the cell membrane of three lung cancer cells is in the order of 95D > SPC-A-1 > A549. This result is consistent with that in **Figure 1A** and **Table 1**. Additionally, in the absence of 7DC or 7DC-VCMME, the anti-Human IgG Fc secondary antibody labeled PE does not interact

TABLE 1 | Cell surface expression of CD47 on different lung cancer cell lines.

Population (Live Cells)	MFI (Mean)	MFI (Medium)
A549 (-)	44.4	41
A549 (+)	3058	2765
SPC-A-1 (-)	33.9	33
SPC-A-1 (+)	6126	5517
95D (-)	51.5	45
95D (+)	9456	8182

(+) indicates cells incubated with anti-CD47 antibody labeled with PE-A; (-) represents cells only (control). Events (Cell count) were 5000 cells per group for calculating. The colored values (mean fluorescence intensity, MFI).

with cells, so the fluorescence intensity of those cells does not change.

Internalization of CD47-Specific mAbs

Antibodies used for constructing ADCs must be able to enter tumor cells to deliver their cytotoxic payload. Using phage display screening of an internal antibody library, we identified 7DC2 and 7DC4 mAbs as two candidates that recognize different antigenic epitopes on the CD47 antigen. We examined whether the two mAbs are internalized into SPC-A-1 cells (moderate overexpression of cell surface CD47) after binding to CD47. 7DC2 and 7DC4 mAbs were labeled with Fluro-488 and incubated with SPC-A-1 cells. Confocal microscopy revealed fluorescence signals on the cell membrane and within the cell, suggesting that both 7DC2 and 7DC4 are able to enter the cell after binding to cell surface CD47 (**Figure 1C**).

Rapid Identification of VCMMAE Binding to CD47 mAbs

We next identified cytotoxic small molecules that could successfully bind to our two candidate antibodies. We used UV-VIS spectrophotometry to rapidly screen conjugates based on the difference in optical properties between antibodies and cytotoxic drugs, resulting in a UV-VIS photo-profile (spectrogram) of the ADC.

We found that the conjugation of either 7DC2 or 7DC4 mAb with valine-citrulline-monomethyl auristatin E (VCMMAE) led to a significant change in the UV-VIS photo-profile in the spectral range from 248 nm to 280 nm (**Figure 2A**). The absorption values of 7DC4 and 7DC2 mAbs at 248 nm and 280 nm were 0.109 and 0.266, and 0.094 and 0.26, respectively. After the binding reaction, the values were 0.230 and 0.272, and 0.229 and 0.266, respectively (**Figure 2A**). Thus, the absorbance ratio of VCMMAE at 248 nm and 280 nm increased from 0.36 - 0.41 to 0.85 - 0.86, indicating successful bonding with 7DC2 or 7DC4 to form the ADCs 7DC2-VCMMAE and 7DC4-VCMMAE.

Confirmation of ADC Formation by LDS-PAGE

We used LDS-PAGE to confirm the successful production of 7DC2-VCMMAE and 7DC4-VCMMAE; the different molecular weights of 7DC2, 7DC4, 7DC2-VCMMAE, and 7DC4-VCMMAE under reducing and non-reducing conditions are

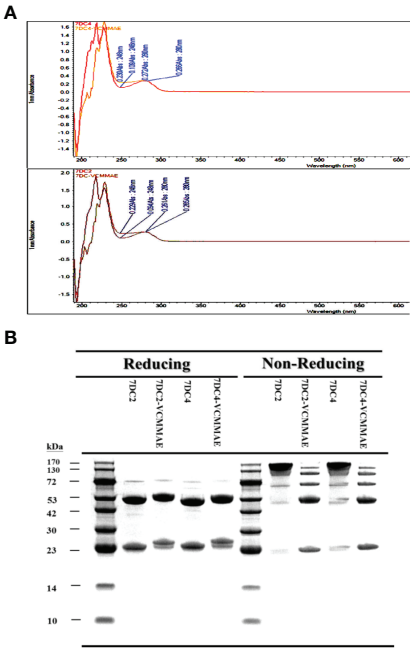

FIGURE 2 | Characterization of 7DC2-VCMMAE and 7DC4-VCMMAE. **(A)** UV-VIS photo-profiles of both ADCs. After the conjugation of 7DC2 or 7DC4 mAbs with VCMMAE, their UV-VIS photo-profiles changed from a hill to flat appearance and in spectral ranges from 248 nm to 280 nm. **(B)** LDS-PAGE images of both ADCs under non-reducing and reducing conditions, confirming that both ADCs were successfully generated by Michael addition (see **Scheme 1**).

displayed in **Figure 2B**. An antibody is composed of two heavy chains and two light chains linked by four disulfide bonds. After reducing the disulfide bonds to free-sulfhydryl groups with 2-mercaptoethanol (2-ME), the antibody and ADC appeared as two main molecular bands: the lower band indicates the light chain and the higher band indicates the heavy chain (**Figure 2B**). The light chain of 7DC4 mAb had a slightly higher molecular weight than that of 7DC2 mAb, while the heavy chain of 7DC4 mAb had a slightly lower molecular weight than that of 7DC2 mAb. This may be caused by differences in glycosylation. When VCMMAE was bonded to either 7DC2 or 7DC4 mAb, the molecular weight of both the heavy and light chain increased significantly, with both bands shifting upwards.

Under non-reducing conditions (**Figure 2B**), both 7DC2 and 7DC4 mAbs displayed a main band of about 150 kDa, while 7DC2-VCMMAE and 7DC4-VCMMAE clearly showed five bands with molecular weights of about 25, 50, 75, 100 and 125 kDa. The band at 150 kDa almost disappeared, indicating that all four disulfide bonds were reduced to free-sulfhydryl groups so that VCMMAE could bind to the antibody through Michael addition to make special 8 DAR. When free-sulfhydryl groups reacted with VCMMAE, the molecular weight increased and each band shifted to a higher position. This result further demonstrated that VCMMAE was successfully bonded to 7DC2 and 7DC4 mAbs.

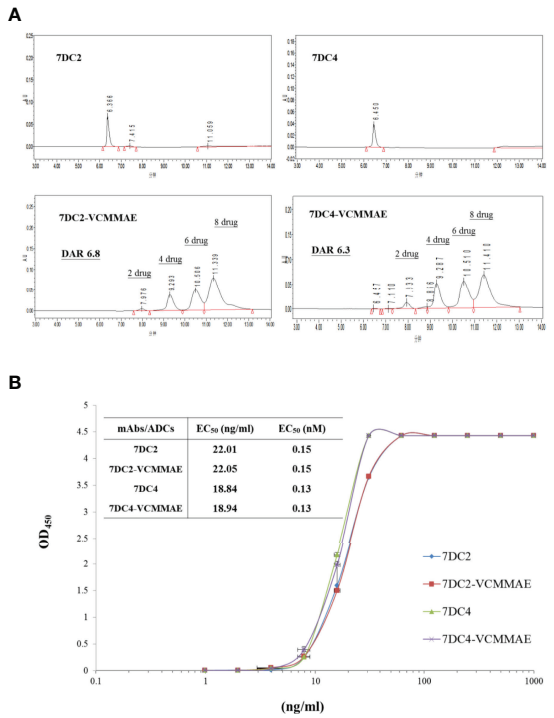

FIGURE 3 | Drug-antibody ratio and drug distribution in 7DC2-VCMMAE and 7DC4-VCMMAE. **(A)** Representative HIC-HPLC chromatograms of both ADCs show similar DAR and drug distributions. **(B)** The EC_{50} values of the graded dose-response curve of both ADCs show similar antigen binding affinities (n = 3).

Drug-to-Antibody Ratio and Distribution of 7DC-VCMMAE

One of the key factors affecting antitumor efficacy of ADCs is the DAR and distribution of payload binding to given concentration of antibody. We used HIC-HPLC to evaluate the characteristics of 7DC2, 7DC4, 7DC2-VCMMAE, and 7DC4-VCMMAE (**Figure 3A**). 7DC2 or 7DC4 showed only a single absorption peak, demonstrating the purity and structural integrity of the antibodies, although a small number of antibodies did not contain four complete disulfide bonds (See **Figure 2B**, non-reducing conditions). We speculated that non-covalent bonds such as hydrogen bonds and hydrophobic bonds are formed in addition to disulfide bonds to stabilize the 3D structure of the antibody. The absorption peaks of 7DC2 and 7DC4 were displayed at the retention times 6.366 and 6.450 (min), respectively. This result indicates that these two antibodies have similar hydrophilic properties, although they have different amino acid sequences and different glycosylation sites.

The chromatogram of 7DC2-VCMMAE showed four absorption peaks at the retention times of 7.976, 9.293, 10.506, and 11.339 (min), but the absorption peak of the 7DC2 antibody (at retention time 6.366 min) was almost undetectable. Thus, all of 7DC2 reacted with VCMMAE but with a different distribution of the drug payload, labeled as 2, 4, 6, and 8 in **Figure 4A**. 7DC4-VCMMAE also exhibited four absorption peaks at the retention times 7.933, 9.287, 10.510, and 11.410 (min), and again, the 7DC4 antibody absorption peak (at retention time 6.450 min) was nearly absent. The drug distribution of 7DC4-VCMMAE was similar to that of 7DC2-VCMMAE, but with slightly different area ratios. Each drug distribution peak for 7DC2-VCMMAE had higher area ratios compared with those of 7DC4-VCMMAE. Therefore, the DAR of 7DC2-VCMMAE was slightly higher than that of 7DC4-VCMMAE (6.8 and 6.3, respectively).

Antigen Binding Affinity of 7DC-VCMMAE

Another factor affecting the therapeutic efficacy of ADCs is antigen binding affinity, which depends on the structure of the antibody itself and whether its conformation changes after binding of the cytotoxic payload to form an ADC. ELISA was used to assess the binding affinity and EC_{50} of the ADCs to the CD47 antigen. The EC_{50} value and the graded dose-response curves of 7DC2 mAb, 7DC4 mAb, 7DC2-VCMMAE, and 7DC4-VCMMAE are shown in **Figure 3B**.

The EC_{50} values of 7DC2 and 7DC4 mAb binding to CD47 antigen were 0.15 nM (22.01 ng/ml) and 0.13 nM (18.84 ng/ml), respectively. Compared with 7DC4 mAb, the binding affinity of 7DC2 mAb was slightly but not significantly lower than that of 7DC4 mAb. The EC_{50} values of ADCs 7DC2-VCMMAE or 7DC4-

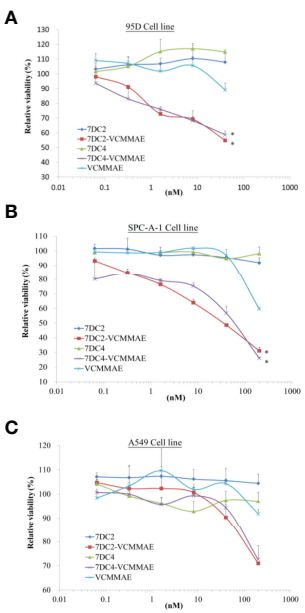

FIGURE 4 | Cytotoxic activity of 7DC2 VCMMAE and 7DC4 VCMMAE in lung cancer cell lines. Three different lung cancer cell lines, **(A)** 95D, **(B)** SPC-A-1, and **(C)** A549, were treated with the indicated concentrations of 7DC2 VCMMAE or 7DC4 VCMMAE. Both ADCs induced significant cell death in 95D and SPC-A-1 cells, but showed lower efficacy in A549 cells. All experiments were performed in three replicates. * indicates $P < 0.05$.

VCMMAE were almost the same as those of the mAbs, at 0.15 nM (22.05 ng/ml) and 0.13 nM (18.94 ng/ml), respectively. Thus, binding of VCMMAE to form the ADC did not change the CD47 antigen binding affinity of either antibody.

Cytotoxic Activity of 7DC-VCMMAE ADCs *In Vitro*

We used 95D, SPC-A-1, and A549 human lung cancer cell lines, each of which express different concentrations of cell surface CD47 antigens (see **Figure 1A**), to evaluate the cytotoxic effect of 7DC2-VCMMAE and 7DC4-VCMMAE *in vitro*, measured as the relative viability rate (**Figure 4**). 95D is a highly metastatic lung cancer cell line with high expression of CD47 glycoprotein. In a dose-response experiment, we treated 95D cells with 7DC2 mAb, 7DC4 mAb, VCMMAE, 7DC2-VCMMAE, or 7DC4-VCMMAE at 40, 8, 1.6, 0.32, and 0.064 nM. In the 7DC2 and 7DC4 mAb negative control groups, relative cell viability rates were almost the same regardless of mAb the concentration, indicating no cytotoxic activity (**Figure 4A**). In VCMMAE group, there was almost no difference in the relative cell viability rate up to 8 nM, which then dropped to 90% at a VCMMAE concentration of 40 nM. By contrast, the relative cell viability rates of 95D decreased with increasing concentrations of either 7DC2-VCMMAE or 7DC4-VCMMAE, reaching approximately 50% at the 40 nM concentration. The IC_{50} of both 7DC2-VCMMAE and 7DC4-VCMMAE was approximately 40 nM.

SPC-A-1 is a human lung adenocarcinoma cell with moderate expression of CD47 glycoprotein; thus, we increased our dose-response concentrations to a maximum of 200 nM (**Figure 4B**). As with 95D cells, a high concentration of 7DC2 or 7DC4 mAb did not affect the relative cell viability rate of SPC-A-1 cells, whereas the relative cell viability rate decreased sharply to approximately 60% with 200 nM VCMMAE treatment. The relative cell viability rate fell further to approximately 20% with 200 nM of either 7DC2-VCMMAE or 7DC4-VCMMAE.

The cell surface expression of CD47 on A549 cells is approximately half of that on SPC-A-1 cells. A549 cultured with 200 nM 7DC2-VCMMAE or 7DC4-VCMMAE had a relative cell viability rate of only about 70% (**Figure 4C**). Together, these results suggest that the 7DC-VCMMAE ADCs have an excellently targeted therapeutic effect, particularly in cancer cells that express high levels of surface CD47 antigen.

Phagocytosis of Targeted CD47 on NSCLC Cells

Next, we investigated whether the new ADCs are able to induce cancer cell phagocytosis by macrophages. In this experiment, cancer cells were co-cultured with macrophages prior to ADC treatment, but we found that even after 2.5 hours of co-culture, 95D or SPC-A-1 cells failed to adhere to the culture plate and remained suspended in the media. Only A549 cells attached to the culture plate with macrophages. Therefore, A549 cancer cells were chosen to evaluate the phagocytosis induction effect of the new ADCs *in vitro*.

The effects of 7DC2, 7DC4, 7DC2-VCMMAE, and 7DC4-VCMMAE on macrophage-mediated phagocytosis of A549 cells labeled with CFDA SE (green) were observed by fluorescence microscopy. A549 cells were co-cultured with macrophages for 2.5 hours. The images in **Figure 5A** show that the labeled A549 cells have a circular cell morphology under light and fluorescence microscopy (green), whereas the unlabeled, migrating macrophages show extended filopodia and appear elongated under light microscopy. Co-cultures treated with media (blank) or VCMMAE showed a similarly small number of fluorescent A549 cells, indicating that the macrophages phagocytized A549 cells, but the low concentration of 40 nM VCMMAE had no additional cytotoxic killing effect. In the presence of 7DC2 or 7DC4 mAbs, phagocytosis was increased as the mAbs bound to CD47 on the surface of A549 cells and effectively inhibited the "don't eat me" signal.

Interestingly, treatment with 40 nM of 7DC2-VCMMAE or 7DC4-VCMMAE significantly induced the phagocytosis of A549 cells. We speculate that 7DC2-VCMMAE and 7DC4-VCMMAE bind to CD47 on the A549 cell membrane and inhibit the "don't eat me" signal, and that internalization of the VCMMAE payload causes cell damage that enhances macrophage recognition, thus greatly increasing phagocytosis. We also noted that macrophages treated with 40 mM of 7DC2, 7DC4, VCMMAE, 7DC2-VCMMAE, or 7DC4-VCMMAE appeared more slender compared with untreated cells (**Figure 5B**), suggesting activation of macrophages under these conditions.

Antitumor Efficacy of ADC *In Vivo*

To parallel our *in vitro* studies in human lung cancer cell lines, we evaluated the antitumor efficacy of our new ADCs *in vivo* using 95D cell line-derived xenografts (CDX) in an immunodeficient NOD/SCID mouse model. 95D cancer cells were implanted into NOD/SCID mice (day -14) and allowed grow for 14 days. Mice were then treated with 20 mg/kg 7DC2, 7DC4, 7DC2-VCMMAE, 7DC4-VCMMAE, or 0.1755 mg/kg free VCMMAE, and 200 µl PBS on days 0, 7, and 14, and xenograft tissues were harvested on day 21. 7DC2-VCMMAE or 7DC4-VCMMAE treatment almost completely eradicated the xenograft 95D tumor, with no signs of toxicity. 7DC2-VCMMAE was more effective than 7DC4-VCMMAE, and both ADCs were significantly more effective than the two 7DC mAbs or VCMMAE alone (**Figures 6A, B**). Representative images of the mice bearing 95D tumors and endpoint tumors harvested from xenograft models are shown in **Supplementary Figure S1** and **Figure 6B**.

Mice treated with 7DC2-VCMMAE and 7DC4-VCMMAE had higher survival rates, with significantly more mice surviving to the study endpoint (day 21), as shown in **Figure 6C**. All mice treated with 7DC2-VCMMAE survived, with treatment almost completely eradicating the xenograft tumors (**Figure 6B**). These results indicated that 7DC2-VCMMAE is more stable and effective than 7DC4-VCMMAE in targeting the xenograft tumors *in vivo*.

Bio-Distribution of 7DC2-VCMMAE and 7DC4-VCMMAE

To further assess the targeting efficacy of 7DC2-VCMMAEand 7DC4-VCMMAE *in vivo*, we examined the bio-distribution of 7DC2-VCMMAE and 7DC4-VCMMAE in which VCMMAE was replaced with the small molecule fluorescent marker Dylight680 to form 7DC2-Dylight680 and 7DC4-Dylight680.

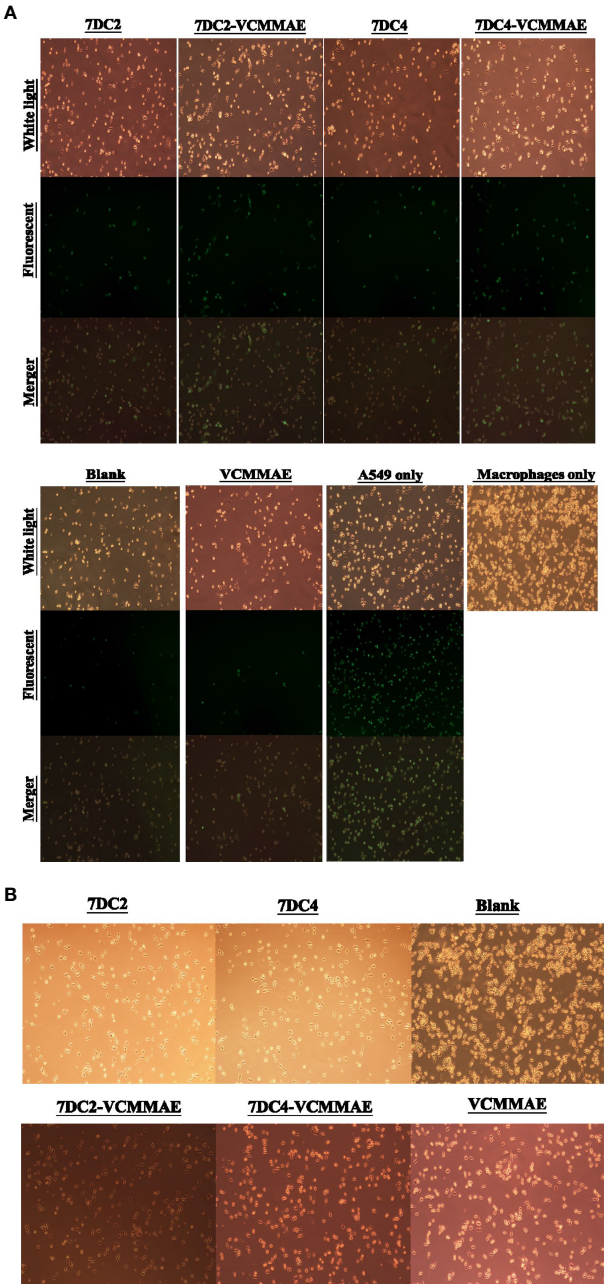

FIGURE 5 | ADC targeting of CD47 induces phagocytosis of NSCLC cells. **(A)** Images of fluorescently labelled A549 cancer cell phagocytosis by macrophages. 7DC2-VCMMAE and 7DC4-VCMMAE elicit macrophage-mediated phagocytosis of A549 cancer cells through targeting CD47, supporting the idea that the ADCs inhibit the "don't eat me" CD47 signal, increasing its antigenicity and promoting recognition by macrophages. **(B)** Cell morphology images of macrophages treated with 40 mM 7DC2 mAb, 7DC4 mAb, VCMMAE, 7DC2-VCMMAE, or 7DC4-VCMMAE, showing a shift to a more slender cell morphology suggesting macrophage activation compared with the blank group.

The results of *in vivo* fluorescence imaging and *ex vivo* biodistribution measurements are shown in **Figure 7**.

One hour after injection of free DyLight680 into mice, the fluorescent signal was distributed across a large area. After 24 hours, the fluorescent signal had completely disappeared, as free DyLight680 was degraded or metabolized. In contrast, both 7DC2-DyLight680 and 7DC4-DyLight680 fluorescent signals were localized at tumor sites 24 hours after administration (**Figure 7A**). Thus, we concluded that 7DC2-VCMMAE and 7DC4-VCMMAE likely localize to the 95D xenografts within one day after administration in our CDX NOD/SCID mouse model. Notably, a greater signal at the tumor site was seen with

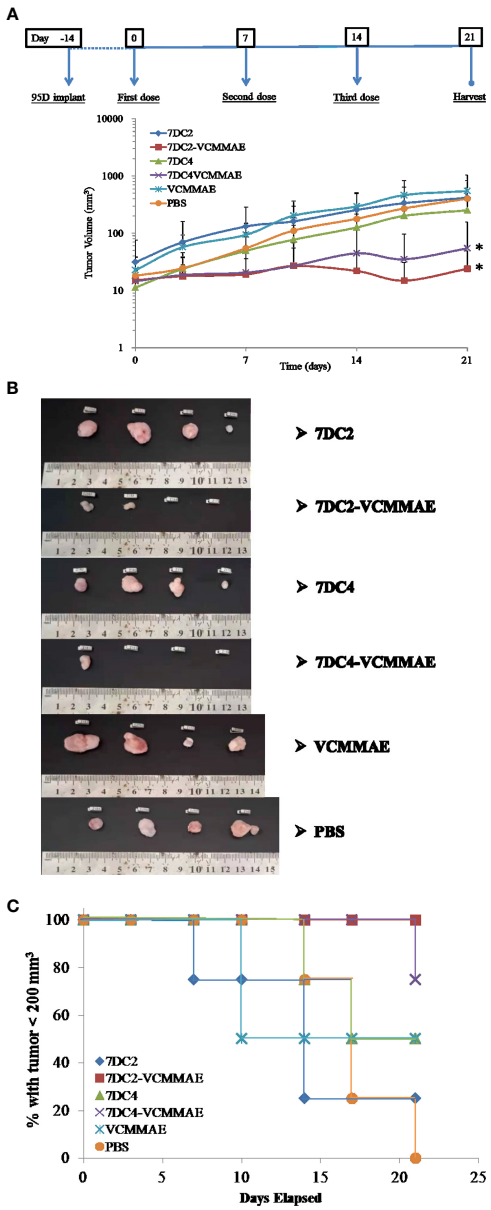

FIGURE 6 | *In vivo* antitumor efficacy of the ADCs in a lung cancer cell-derived xenograft mouse model. **(A)** Changes in tumor size over time in xenograft mouse models bearing 95D tumors. Mice were randomly assigned into 6 groups and treated with 20 mg/kg of 7DC2-VCMMAE, 7DC4-VCMMAE, 7DC2, or 7DC4; 0.1755 mg/kg VCMMAE; or 200 µl PBS on day 0, 7, and 14. **(B)** Excised tumor tissues from each group mice on day 21 indicated greater antitumor efficacy of 7DC2-VCMMAE compared with 7DC4-VCMMAE. **(C)** Kaplan-Meier survival curves for the six treatment groups (defined by tumor size below 200 mm^3, see methods). Mean values and standard deviations of all experiments are calculated from four independent measurements. * indicates $P < 0.05$.

7DC2-DyLight680 compared to 7DC4-DyLight680 (**Figure 7A**), further suggesting that 7DC2-VCMMAE is more stable and specific than 7DC4-VCMMAE in targeting CD47-expressing tumor tissues in mice.

In addition, we performed *ex vivo* NIRF imaging of organs harvested from the 95D tumor-bearing mice, as shown in **Figure 7B** and **Supplementary Figure S2**. One day after intraperitoneal injection of either 7DC2-VCMMAE or 7DC4-VCMMAE, fluorescent signals were detectable in the stomach tissue of mice in each group. No signals were detected in blood, heart, and bone, indicating that neither 7DC4-VCMMAE nor 7DC2-VCMMAE affects the hematopoietic system. The off-target distribution in liver and spleen was greater for 7DC4-DyLight680 than 7DC2-DyLight680, and 7DC4-DyLight680 only was detected in lung. 7DC4-DyLight680 and 7DC2-DyLight680 distribution to the intestine was observed, with greater signals from 7DC2-DyLight680 than 7DC4-DyLight680. Because the fluorescent signal in the intestine was probably produced by metabolites, these results indicate a faster metabolism and excretion rate of 7DC2-VCMMAE than 7DC4-VCMMAE.

Taken together, quantitative *ex vivo* measurement of bio-distribution showed that 7DC2-DyLight680 targeted the 95D tumor with high local concentration and low off-target distribution (**Figure 7B** and **Supplementary Figure S2**), which may underlie the observed higher antitumor potency of 7DC2-VCMMAE (**Figure 6**). Conversely, the higher off-target distribution of 7DC4-DyLight680 could explain the lower stability and specificity of 7DC4-MMAE in our xenograft model (**Figure 7**).

In vivo Biosafety Analysis

We assessed serum biochemical markers and weight changes to evaluate the impact of drug off-target distribution and biological safety of the 7DC4-VCMMAE and 7DC2-VCMMAE ADCs. Though our bio-distribution analysis indicated that 7DC4 or 7DC2 localized to the liver (**Figure 7B** and **Supplementary Figure S2**), no biomarkers indicated hepatotoxicity, and there was also no signal of nephrotoxicity (**Table 2**). Body weight of mice in 7DC4-VCMMAE group decreased slightly after the first administration, but no significant change in body weight was noted in the other treatment groups (**Supplementary Figure S3**). Although both 7DC4 and 7DC2 distribute to the stomach after administration, 7DC2-VCMMAE and 7DC4-VCMMAE did not appear to cause gastric toxicity that would affect appetite or food consumption leading to weight loss. Therefore, the novel ADCs appear to be safe and tolerable in mice.

DISCUSSION

In this study, we developed and evaluated the efficacy and safety of first VC linker- based CD47-targeted ADCs with translational potential for the treatment of NSCLC. We clearly analyze, identify and describe the physicochemical properties and development process of our VC linker-based CD47-targeted ADCs, although anti-CD47-DM1 based on Sulfo-SMCC linker for treating triple-negative breast cancers was reported by Si, et al., in August 2021 (36). Additionally, larger precipitation would be occurred during constructing SMCC linker-based ADC according to the research report of Chiang, et al., in 2020, which greatly increased the

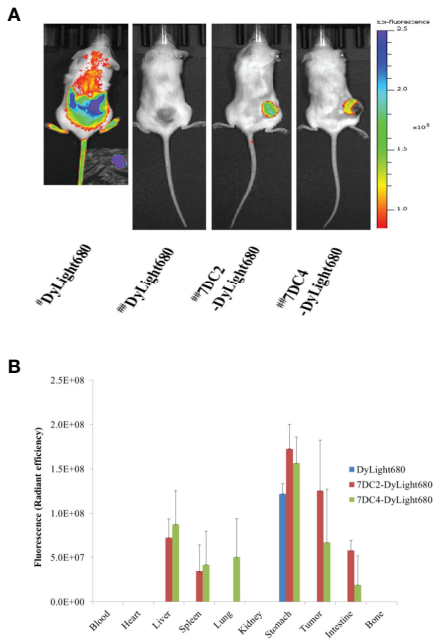

FIGURE 7 | Bio-distribution of 7DC2-VCMMAE and 7DC4-VCMMAE in xenograft models. **(A)** *In vivo* fluorescence imaging of Dylight680, 7DC2-Dylight680, and 7DC4-Dylight680 in mice. # Indicates bio-distribution of the fluorescent marker 1 hour after injection; ## indicates distribution after 24 hours. **(B)** *Ex vivo* bio-distribution of Dylight680, 7DC2-Dylight680, and 7DC4-Dylight680 in the indicated organs or tumor tissue from 95D tumor-bearing mice at 24 hours post-injection (3 mg/kg) determined *ex vivo* with IVIS (see **Supplementary Figure S2**). The mean values and standard deviations are calculated from three independent measurements.

production cost (42). And it cannot improve the drug loading of the antibody due to the steric effect, so its efficacy in cancer cells killing is less than the VC linker-based ADC (42). Furthermore, we demonstrated that 7DC2-VCMMAE has a great antitumor efficacy and specificity and both ADCs appear to be safe and tolerable in a xenograft mouse model of lung cancer.

SGN-35 (brentuximab vedotin, Adcetris®) has been approved by FDA in 2011, which is a VC linker-based ADC targeting CD30, having 4 DAR and possessing good tolerance in clinical use (38). It is aimed at non-solid tumors (Hodgkin's lymphoma and anaplastic large-cell lymphoma), so it cannot achieve the localized effect and cause freer SGN35 to excurse in the blood. However, our 7DC-VCMMAE targets at solid tumors that can attract more ADCs from the blood into tumor tissues and localize the acting range of ADCs. Our studies suggest that the maximum tolerated dose (MTD) of 7DC-VCMMAE may be greatly increased. Additionally, solid tumors are usually more refractory than non-solid tumors, so higher doses are required. When the DAR of ADC is increased, the usage of ADC can be reduced and its targeted anti-tumor efficacy and safety can all be improved. Animal experiments for treating solid tumor model, usually show that the best anti-tumor dose is 30 mg/kg for CDX-mice model (Kuo, et al., 2019, MABS) (43); however, 7DC-VCMMAE at 20 mg/kg for CDX-model mice show quite good anti-tumor effects.

Both 7DC2 and 7DC4 were able to penetrate lung cancer cells and had similar chemical and physical properties, such as affinity and hydrophobicity, yet we observed differences in their efficacy and specificity in our xenograft mouse model of lung cancer. LDS-PAGE indicated differences in the molecular weights of the two IgG1s, with the 7DC2-light chain molecular weight less than that of the 7DC4-light chain, and the 7DC2-heavy chain molecular weight more than that of the 7DC4-heavy chain (**Figure 2B**). Sequence differences between 7DC2 and 7DC4 may also alter their epitopes and glycosylation sites (**Supplementary Figure S4**), which could underlie observed differences in the stability and accuracy of each ADC *in vivo*.

We found that 7DC2-VCMMAE and 7DC4-VCMMAE have greater cytotoxic effects against 95D and SPC-A1 cells compared to A549 cells. This may be due to the lower expression of CD47 on the A549 cell membrane, suggesting that 7DC-VCMMAE may have a greater therapeutic effect for tumors that express high levels of CD47 antigen. Additionally, we found that VCMMAE alone at a concentration of less than 200 nM does not effectively kill the cancer cells, likely because it is unable to specifically enter the cancer cells. Conjugation of VCMMAE to our 7DC antibodies at a high DAR allowed the drug to specifically enter the cancer cells and kill them at a lower effective concentration. Furthermore, our study suggests that the new ADCs have a two-pronged anti-cancer effect, as our cell phagocytosis experiments found that both ADCs have the ability to promote macrophage-mediated phagocytosis of A549 cancer cells, and 7DC2-VCMMAE seems to have a greater effect than 7DC4-VCMMAE.

A549 cancer cells can synthesize lecithin containing a high concentration of unsaturated fatty acids, the building blocks of phospholipids. Phospholipid is one of the main components of cell membranes and plays an important role in the division of organelles, protein storage in cell signal transduction, cell adhesion, and cell cycle regulation (44). Furthermore, phospholipids are involved in tumor cell proliferation, migration, adhesion, apoptosis, signal transduction, cell cycle regulation, and other activities (44). We speculate that alterations in phospholipid synthesis may be one of the reasons why A549 is relatively insensitive to 7DC-VCMMAE, as ADCs depend on cell membrane receptor-mediated endocytosis to enter the tumor cell. Another possibility is that autophagy of A549 cells treated with ADCs may decrease the cytotoxic efficacy of the ADCs. For tumor cells such as A549, the ability of CD47-specific ADCs to stimulate phagocytosis may overcome the limitation of insufficient cytotoxicity.

TABLE 2 | Serum biomarkers of toxicity of ADC 7DC2-VCMMAE in mice*.

	ALT(U/L)	ALP(U/L)	BUN(mg/dL)	CRE(mg/dL)
7DC2	26.75 ± 5.80	88.00 ± 8.04	7.67 ± 0.81	10.73 ± 1.43
7DC2-VCMMAE	25.00 ± 2.45	104.50 ± 25.04	7.55 ± 0.94	15.15 ± 1.10
7DC4	43.75 ± 15.26	85.75 ± 4.50	7.36 ± 0.61	10.85 ± 3.80
7DC4-VCMMAE	22.75 ± 2.87	82.50 ± 5.26	7.60 ± 1.06	15.40 ± 2.51
VCMMAE	26.75 ± 2.87	72.00 ± 11.69	7.57 ± 0.59	14.00 ± 4.82
PBS	29.25 ± 4.99	72.25 ± 4.57	7.81 ± 0.34	10.03 ± 3.71

**Mean ± SD for n = 4 mice.*
ALT, alanine aminotransferase; ALP, alkaline phosphatase; BUN, blood urea nitrogen; CRE, creatinine.

For targeted therapy *in vivo*, we confirmed that 7DC-VCMMAE can effectively inhibit tumor growth, consistent with the results of our *in vitro* cytotoxicity experiments. Furthermore, 7DC2-VCMMAE was more effective than 7DC4-CVMMAE in the xenograft tumor models (**Figure 6**). The survival rate of mice in the 7DC4-CVMMAE group was lower than that of mice in the 7DC2-VCMMAE group, likely due to differences in stability and specificity between the two targeting antibodies. Bio-distribution analysis showed that 7DC2-VCMMAE was more stable and targeted tumor tissue with greater specificity *in vivo* compared to 7DC4-VCMMAE. While safety and tolerability signals were similar for both ADCs, we conclude that 7DC2-VCMMAE has good potential for further development as a novel therapeutic for NSCLC.

DATA AVAILABILITY STATEMENT

The original contributions presented in the study are included in the article/**Supplementary Material**. Further inquiries can be directed to the corresponding authors.

ETHICS STATEMENT

All mouse experiments were conducted according to guidelines and experimental protocols approved by the Institutional Animal Care and Utilization Committee (IACUC) of Fujian Normal University (Protocol ID: 20200010).

AUTHOR CONTRIBUTIONS

Data curation: Z-CC. Formal analysis: Z-CC. Investigation: Z-CC. Resources: SF, Y-KS, HW, DW, YZ. Validation: QC, JL. Writing – original draft: Z-CC. Writing – review and editing: JL, QC. FACS data curation: DC. All authors contributed to the article and approved the submitted version.

FUNDING

This work was supported by the Strait Postdoctoral Exchange Funding Program, Fujian Province, China (Grant no. 2019A001).

ACKNOWLEDGMENTS

We are thankful to Chuangfang Company for providing the antibody screening platform, and Fujian Normal University Hospital for providing serum biochemical safety testing services.

SUPPLEMENTARY MATERIAL

The Supplementary Material for this article can be found online at: https://www.frontiersin.org/articles/10.3389/fonc.2022.857927/full#supplementary-material

Supplementary Figure 1 | Tolerance of the mice to 7DC2-VCMMAE or 7DC4-VCMMAE treatment. 95D cancer cells were implanted into NOD/SCID mice (day -14) and allowed grow for 14 days. The mice treated with 20 mg/kg 7DC2, 7DC4, 7DC2-VCMMAE, 7DC4-VCMMAE, or 0.1755 mg/kg free VCMMAE, and 200 µl PBS on days 0, 7, and 14, and xenograft tissues were harvested on day 21. The images showed live mice, anesthesia, bearing 95D tumors on day 21, before harvesting tumors.

Supplementary Figure 2 | *Ex vivo* NIRF imaging of organs from 95D tumor-bearing mice. Representative images of organs from 95D tumor-bearing mice 24 hours after intraperitoneal injection of DyLight 680, 7DC2-DyLight680, or 7DC4-DyLight680. 1. Blood, 2. Heart, 3. Liver, 4. Spleen, 5. Lung, 6. Kidney, 7. Stomach, 8. Tumor, 9. Intestine, 10. Bone.

Supplementary Figure 3 | Body weight changes after administration of ADC to assess biosafety. There were no significant changes in the body weight of mice in any of the treatment groups, with the exception of a small decrease on day 3 in mice treated with 7DC4-VCMMAE that resolved by day 7, indicated by the asterisk ($P<0.05$).

Supplementary Figure 4 | Alignment and predicted N-glycan patterns of 7DC2 and 7DC4. 7DC2 and 7DC4 have slightly different amino sequences in the heavy and light chains, and 7DC4 has a glycosylation site indicated by a blue box, within its heavy chain variable region. Asterisks indicate overlapping residues within the two sequences.

Supplementary Table 1 | Cell Surface Expression of CD47 on Different Lung Cancer Cell Lines. The CD47 molecules on the cell membranes of A549, SPC-A-1 and 95D cells were bound to 7DC and 7DC-VCMMAE, respectively, and then interacted with the goat anti-Human IgG Fc Secondary Antibody labeled with PE. Mean Fluorescence Intensity (MFI) obtained by using flow cytometry was employed to compare the expression of CD47 differently in three cancer cell lines with different properties. Events (Cell count) were 5000 cells per group for calculating.

REFERENCES

1. Ferlay J, Colombet M, Soerjomataram I, Mathers C, Parkin DM, Piñeros M, et al. Estimating the Global Cancer Incidence and Mortality in 2018: GLOBOCAN Sources and Methods. *Int J Canc* (2019) 144(8):1941–53. doi: 10.1002/ijc.31937
2. Lu T, Yang X, Huang Y, Zhao M, Li M, Ma K, et al. Trends in the Incidence, Treatment, and Survival of Patients With Lung Cancer in the Last Four Decades. *Canc Manage Res* (2019) 11:943–53. doi: 10.2147/CMAR.S187317
3. Bender E. Epidemiology: The Dominant Malignancy. *Nature.* (2014) 513:S2–3. doi: 10.1038/513S2a
4. Gandhi L, Rodríguez-Abreu D, Gadgeel S, Esteban E, Felip E, De-Angelis F, et al. Pembrolizumab Plus Chemotherapy in Metastatic Non-Small-Cell Lung Cancer. *N Engl J Med* (2018) 378:2078–92. doi: 10.1056/NEJMoa1801005
5. Uchibori K, Inase N, Araki M, Kamada M, Sato S, Okuno Y, et al. Brigatinib Combined With Anti-EGFR Antibody Overcomes Osimertinib Resistance in EGFR Mutated Non-Small-Cell Lung Cancer. *Nat Commun* (2017) 8:14768. doi: 10.1038/ncomms14768
6. Ettinger DS, Wood DE, Aisner DL, Akerley W, Bauman J, Chirieac LR, et al. Non-Small Cell Lung Cancer, Version 5.2017, NCCN Clinical Practice Guidelines in Oncology. *J Natl Compr Canc Netw* (2017) 15:504–35. doi: 10.6004/jnccn.2017.0050
7. Novello S, Barlesi F, Califano R, Cufer T, Ekman S, Levra MG, et al. Metastatic Non-Small-Cell Lung Cancer: ESMO Clinical Practice Guidelines for Diagnosis, Treatment and Follow-Up. *Ann Oncol* (2016) 27:v1–27. doi: 10.1093/annonc/mdw326
8. Jaiswal S, Chao MP, Majeti R, Weissman IL. Macrophages as Mediators of Tumor Immunosurveillance. Trends. *Immunol* (2010) 31:212–9. doi: 10.1016/j.it.2010.04.001
9. Tong B, Wang M. CD47 is a Novel Potent Immunotherapy Target in Human Malignancies: Current Studies and Future Promises. *Future Oncol (Lond Engl)* (2018) 14:2179–88. doi: 10.2217/fon-2018-0035
10. Brown EJ, Frazier WA. Integrin-Associated Protein (CD47) and its Ligands. *Trend Cell Biol* (2001) 11:130–5. doi: 10.1016/S0962-8924(00)01906-1

11. Horrigan SK, Iorns E, Williams SR, Perfito N, Errington TM. Replication Study: The CD47-Signal Regulatory Protein Alpha (SIRPA) Interaction is a Therapeutic Target for Human Solid Tumors. *eLife* (2017) 6:6662–7. doi: 10.7554/eLife.18173
12. Baccelli I, Schneeweiss A, Riethdorf S, Stenzinger A, Schillert A, Vogel V, et al. Identification of a Population of Blood Circulating Tumor Cells From Breast Cancer Patients That Initiates Metastasis in a Xenograft Assay. *Nat Biotechnol* (2013) 31:539–44. doi: 10.1038/nbt.2576
13. Tsai RK, Discher DE. Inhibition of "Self "Engulfment Through Deactivation of Myosin-II at the Phagocytic Synapse Between Human Cells. *J Cell Biol* (2008) 180:989–1003. doi: 10.1083/jcb.200708043
14. Zhao CL, Yu S, Wang SH, Li SG, Wang ZJ, Han SN. Characterization of Cluster of Differentiation 47 Expression and its Potential as a Therapeutic Target in Esophageal Squamous Cell Cancer. *Oncol Lett* (2018) 15:2017–23. doi: 10.3892/ol.2017.7447
15. Kaur S, Martin-Manso G, Pendrak ML, Garfield SH, Isenberg JS, Roberts DD. Thrombospondin-1 Inhibits VEGF Receptor-2 Signaling by Disrupting its Association With CD47. *J Biol Chem* (2010) 285:38923–32. doi: 10.1074/jbc.M110.172304
16. Vonderheide RH. CD47 Blockade as Another Immune Checkpoint Therapy for Cancer. *Nat Med* (2015) 21:1122–3. doi: 10.1038/nm.3965
17. Piccione EC, Juarez S, Tseng S, Liu J, Stafford M, Narayanan C, et al. SIRPa Antibody Fusion Proteins Selectively Bind and Eliminate Dual Antigenexpressing Tumor Cells. *Clin Cancer Res* (2016) 22:5109–19. doi: 10.1158/1078-0432.CCR-15-2503
18. Rodriguez PL, Harada T, Christian DA, Pantano DA, Tsai RK, Discher DE. Minimal "Self " Peptides That Inhibit Phagocytic Clearance and Enhance Delivery of Nanoparticles. *Science* (2013) 339:971–5. doi: 10.1126/science.1229568
19. Majeti R, Chao MP, Alizadeh AA, Pang WW, Jaiswal S, Gibbs KDJr., et al. CD47 is an Adverse Prognostic Factor and Therapeutic Antibody Target on Human Acute Myeloid Leukemia Stem Cells. *Cell* (2009) 138:286–99. doi: 10.1016/j.cell.2009.05.045
20. Chao MP, Alizadeh AA, Tang C, Jan M, Weissman-Tsukamoto R, Zhao F, et al. Therapeutic Antibody Targeting of CD47 Eliminates Human Acute Lymphoblastic Leukemia. *Cancer Res* (2011) 71:1374–84. doi: 10.1158/0008-5472.CAN-10-2238
21. Chao MP, Tang C, Pachynski RK, Chin R, Majeti R, Weissman IL. Extranodal Dissemination of Non-Hodgkin Lymphoma Requires CD47 and Is Inhibited by Anti-CD47 Antibody Therapy. *Blood* (2011) 118:4890–901. doi: 10.1182/blood-2011-02-338020
22. Kim D, Wang J, Willingham SB, Martin R, Wernig G, Weissman IL. Anti-CD47 Antibodies Promote Phagocytosis and Inhibit the Growth of Human Myeloma Cells. *Leukemia.* (2012) 26:2538–45. doi: 10.1038/leu.2012.141
23. Zhang H, Lu H, Xiang L, Bullen JW, Zhang C, Samanta D, et al. HIF-1 Regulates CD47 Expression in Breast Cancer Cells to Promote Evasion of Phagocytosis and Maintenance of Cancer Stem Cells. *Proc Natl AcadSci USA* (2015) 112:E6215–23. doi: 10.1073/pnas.1520032112
24. Steinert G, Schölch S, Niemietz T, Iwata N, García SA, Behrens B, et al. Immune Escape and Survival Mechanisms in Circulating Tumor Cells of Colorectal Cancer. *Cancer Res* (2014) 74:1694–704. doi: 10.1158/0008-5472.CAN-13-1885
25. Lee TK, Cheung VC, Lu P, Lau EY, Ma S, Tang KH, et al. Blockade of CD47-Mediated Cathepsin S/protease-Activated Receptor 2 Signaling Provides a Therapeutic Target for Hepatocellular Carcinoma. *Hepatology* (2014) 60:179–91. doi: 10.1002/hep.27070
26. Wang Y, Xu Z, Guo S, Zhang L, Sharma A, Robertson GP, et al. Intravenous Delivery of siRNA Targeting CD47 Effectively Inhibits Melanoma Tumor Growth and Lung Metastasis. *MolTher* (2013) 21:1919–29. doi: 10.1038/mt.2013.135
27. Weiskopf K, Jahchan NS, Schnorr PJ, Cristea S, Ring AM, Maute RL, et al. CD47-Blocking Immunotherapies Stimulate Macrophage-Mediated Destruction of Small-Cell Lung Cancer. *J Clin Invest* (2016) 126:2610–20. doi: 10.1172/JCI81603
28. Willingham SB, Volkmer JP, Gentles AJ, Sahoo D, Dalerba P, Mitra SS, et al. The CD47-Signal Regulatory Protein Alpha (SIRPa) Interaction Is a Therapeutic Target for Human Solid Tumors. *Proc Natl Acad Sci USA* (2012) 109:6662–7. doi: 10.1073/pnas.1121623109
29. Fei F, Li X, Xu L, Li D, Zhang Z, Guo X, et al. CD147-CD98hc Complex Contributes to Poor Prognosis of non-Small Cell Lung Cancer Patients Through Promoting Cell Proliferation *via* the PI3K/Akt Signaling Pathway. *Ann Surg Oncol* (2014) 21:4359–68. doi: 10.1245/s10434-014-3816-1
30. Zhao H, Wang J, Kong X, Li E, Liu Y, Du X, et al. CD47 Promotes Tumor Invasion and Metastasis in Non-Small Cell Lung Cancer. *Sci Rep* (2016) 6:29719. doi: 10.1038/srep29719
31. Baudino TA. Targeted Cancer Therapy: The Next Generation of Cancer Treatment. *Curr Drug Discov Technol* (2015) 12:3–20. doi: 10.2174/1570163812666150602144310
32. Diamantisl N, Banerji U. Antibody-Drug Conjugates: An Emerging Class of Cancer Treatment. *Br J Canc* (2016) 114:362–7. doi: 10.1038/bjc.2015.435
33. Perez HL, Cardarelli PM, Deshpande S, Gangwar S, Schroeder GM, Vite GD, et al. Antibody-Drug Conjugates: Current Status and Future Directions. *Drug Discov Today* (2014) 9:869–81. doi: 10.1016/j.drudis.2013.11.004
34. Casi G, Neri D. Noninternalizing Targeted Cytotoxics for Cancer Therapy. *Mol Pharm* (2015) 12:1880–4. doi: 10.1021/mp500798y
35. Kommineni N, Pandi P, Abraham NC, Domb J, Khan W. Antibody Drug Conjugates: Development, Characterization, and Regulatory Considerations. *Polym Adv Technol* (2019) 31(6):1177–93. doi: 10.1002/pat.4789
36. Si Y, Zhang Y, Guan JS, Ngo HG, Totoro A, Singh AP, et al. Anti-CD47 Monoclonal Antibody-Drug Conjugate: A Targeted Therapy to Treat Triple-Negative Breast Cancers. *Vaccines* (2021) 9(882):1–14. doi: 10.3390/vaccines9080882
37. Dubowchik GM, Firestone RA, Padilla L, Willner D, Hofstead SJ, Mosure K, et al. Cathepsin B-Labile Dipeptide Linkers for Lysosomal Release of Doxorubicin From Internalizing Immunoconjugates: Model Studies of Enzymatic Drug Release and Antigen-Specifific *In Vitro* Anticancer Activity. *Bioconjug Chem* (2002) 13:855–69. doi: 10.1021/bc025536j
38. Younes A, Bartlett NL, Leonard JP, Kennedy DA, Lynch CM, Sievers EL, et al. Brentuximab Vedotin (SGN-35) for Relapsed CD30-Positive Lymphomas. *N Engl J Med* (2010) 363:1812–21. doi: 10.1056/NEJMoa1002965
39. Ivanova PT, Cerda BA, Horn DM, Cohen JS, McLafferty FW, Brown HA. Electrospray Ionization Mass Spectrometry Analysis of Changes in Phospholipids in RBL 2H3 Mastocytoma Cells During Degranulation. *Proc Natl Acad Sci* (2001) 98(13):7152–7. doi: 10.1073/pnas.131195098
40. Frenzel A, Kugler J, Wilke S, Schirrmann T, Hust M. Construction of Human Antibody Gene Libraries and Selection of Antibodies by Phage Display. In: M Steinitz, editor. *Human Monoclonal Antibodies: Methods and Protocols, Methods in Molecular Biology*. Braunschweig, Germany: Springer Science (2014). p. 215–43. doi: 10.1007/978-1-62703-586-6_12
41. Smith GP. Filamentous Fusion Phage: Novel Expression Vectors That Display Cloned Antigens on the Virion Surface. *Sci* (1985) 228:1315–7. doi: 10.1126/science.4001944
42. Chiang ZC, Chiu YK, Lee CC, Hsu NS, Tsou YL, Chen HS, et al. Preparation and Characterization of Antibody-Drug Conjugates Acting on HER2-Positive Cancer Cells. *PloS One* (2020) 15(9):1–15. doi: 10.1371/journal.pone.0239813
43. Kuo WY, Hsu HJ, Wu CY, Chen HS, Chou YC, Tsou YL, et al. Antibody-Drug Conjugates With HER2-Targeting Antibodies From Synthetic Antibody Libraries are Highly Potent Against HER2-Positive Human Gastric Tumor in Xenograft Models. *MABS* (2019) 11:153–65. doi: 10.1080/19420862.2018.1541370
44. Gautam A, Donohue D, Hoke A, Miller SA, Srinivasan S, Sowe B, et al. Investigating Gene Expression Profiles of Whole Blood and Peripheral Blood Mononuclear Cells Using Multiple Collection and Processing Methods. *PloS One* (2019) 14:e0225137. doi: 10.1371/journal.pone.0225137

Conflict of Interest: The authors declare that the research was conducted in the absence of any commercial or financial relationships that could be construed as a potential conflict of interest.

Publisher's Note: All claims expressed in this article are solely those of the authors and do not necessarily represent those of their affiliated organizations, or those of the publisher, the editors and the reviewers. Any product that may be evaluated in this article, or claim that may be made by its manufacturer, is not guaranteed or endorsed by the publisher.

frontiers | Frontiers in Oncology

ORIGINAL RESEARCH
published: 23 May 2022
doi: 10.3389/fonc.2022.894842

Discovery of Novel Tetrahydro-β-carboline Containing Aminopeptidase N Inhibitors as Cancer Chemosensitizers

Xiaoyan Xing[1†], Fahui Li[2†], Yajie Hu[2†], Lin Zhang[2], Qian Hui[2], Hongyu Qin[2], Qixiao Jiang[3], Wenyan Jiang[2], Chunyan Fang[1] and Lei Zhang[2*]*

[1] Department of Pharmacology, School of Pharmacy, Weifang Medical University, Weifang, China, [2] Department of Medicinal Chemistry, School of Pharmacy, Weifang Medical University, Weifang, China, [3] Department of Toxicology, School of Public Health, Qingdao University, Qingdao, China

OPEN ACCESS

Edited by:
Jian-ye Zhang,
Guangzhou Medical University, China

Reviewed by:
Ashraf K. El-Damasy,
Mansoura University, Egypt
Yingjie Zhang,
Shandong University, China

****Correspondence:***
Chunyan Fang
13853660344@163.com
Lei Zhang
leizhangchemical@gmail.com

[†]These authors have contributed equally to this work

Specialty section:
This article was submitted to Cancer Molecular Targets and Therapeutics, a section of the journal Frontiers in Oncology

Received: *12 March 2022*
Accepted: *25 April 2022*
Published: *23 May 2022*

Citation:
Xing X, Li F, Hu Y, Zhang L, Hui Q, Qin H, Jiang Q, Jiang W, Fang C and Zhang L (2022) Discovery of Novel Tetrahydro-β-carboline Containing Aminopeptidase N Inhibitors as Cancer Chemosensitizers. Front. Oncol. 12:894842. doi: 10.3389/fonc.2022.894842

Aminopeptidase N (APN, CD13) is closely associated with the development and progression of cancer. Previous studies suggested APN as a biomarker for cancer stem cells. APN inhibitors have been intensively evaluated as chemosensitizers for cancer treatments. In the present study, tetrahydro-β-carboline scaffold was introduced to the structure of APN inhibitors. The synthesized compounds showed potent enzyme inhibitory activities compared with Bestatin, an approved APN inhibitor, in cell-based enzymatic assay. In combination with chemotherapeutic drugs, representative APN inhibitor molecules **D12**, **D14** and **D16** significantly improved the antiproliferative potency of anticancer drugs in the *in vitro* tests. Further mechanistic studies revealed that the anticancer effects of these drug combinations are correlated with decreased APN expression, increased ROS level, and induction of cell apoptosis. The spheroid-formation assay and colony-formation assay results showed effectiveness of Paclitaxel-APN inhibitor combination against breast cancer stem cell growth. The combined drug treatment led to reduced mRNA expression of OCT-4, SOX-2 and Nanog in the cancer stem cells tested, suggesting the reduced stemness of the cells. In the *in vivo* study, the selected APN inhibitors, especially **D12**, exhibited improved anticancer activity in combination with Paclitaxel compared with Bestatin. Collectively, potent APN inhibitors were discovered, which could be used as lead compounds for tumor chemo-sensitization and cancer stem cell-based therapies.

Keywords: aminopeptidase N, inhibitor, cancer, chemosensitizer, tetrahydro-β-carboline

INTRODUCTION

Aminopeptidase N (APN, also known as CD13) is a widely expressed type II membrane bound metalloprotease (1). It plays important roles in various cellular processes including cell migration, survival (2), viral uptake (3), angiogenesis (4), and autophagy (5). Overexpression of APN have been demonstrated in various cancers such as breast (6), ovarian (7), colorectal (8) and hepatocellular

carcinoma (9). It is reported that the serum level of APN is correlated with tumor size, lymph node metastasis, and tumor metastasis (10). Therefore, serum APN expression and activity could be utilized as diagnostic and prognostic biomarkers for different types of cancers.

Inhibition of APN has been intensively evaluated for the treatment of cancers (11). A number of APN inhibitors have been designed and synthesized for targeting various cancer cellular events, including cell migration, cell growth and tumor angiogenesis (12). According to the chemical structures, different kinds of APN inhibitors have been developed, such as antibodies, peptides, and nonpeptide small molecules (13). Bestatin, a natural product extracted from *Streptomyces olivoreticuli*, is an approved APN inhibitor (14).

Overexpression of APN played important roles in the resistance to anticancer agents, anti-apoptosis of cancer cells, as well as relapse of cancers (5, 15). APN inhibitors, such as Bestatin, have been extensively studied for their abilities in enhancing radiation sensitivity and chemo-sensitivity in different types of cancers (16, 17). Moreover, APN has been identified as a functional marker for cancer stem cells (CSCs) in human cancers (18). Inhibition of APN suppressed the self-renewal and tumor-initiative abilities of CSCs (19). It is indicated that APN is a novel therapeutic target for the treatment of cancer in combination with traditional chemotherapy. Development of APN inhibitors for the enhancement of chemotherapy sensitivity could be a new strategy in cancer treatment.

In our previous work, indoline-2,3-dione containing APN inhibitors have been developed with anticancer activities (20, 21). However, further development of these compounds was terminated due to lack of *in vivo* potency. To develop novel APN inhibitors as chemosensitizers, structural modification was performed on the existing compounds. Generally, a zinc binding group is needed for the chelation of zinc ion, which leads to the binding of inhibitors to the active site of APN. Fragments with various sizes and physicochemical properties were used to occupy different binding pockets in the active site. A linker is used to connect the former pharmacophores. To improve the binding affinity of target molecules in the active site, tetrahydro-β-carboline was utilized as a core fragment in the design of novel APN inhibitors (**Figure 1**). Substitutions were introduced by condensing different benzoyl chlorides to the *N1*-position in the carboline ring, and hydroxamic acid group with different linkers was introduced to *N8*-position as zinc binding group. Short linkers are usually selected in the design of APN inhibitors. In the present study, the contribution of both fatty acid and aromatic linkers was evaluated in the designed APN inhibitors. The synthesized molecules were evaluated using the enzymatic inhibition screening, *in vitro* antiproliferative test, breast CSC- based study and *in vivo* anticancer test.

Chemistry

The synthesis of target compounds was described in **Scheme 1**. The target molecules were prepared by utilizing commercially available 2,3,4,9-tetrahydro-1H-pyrido[3,4-b]indole (**A1**) as the starting material. Firstly, compound **A1** was condensed with substituted benzoyl chlorides to obtain intermediate **B1**-**B17**. Secondly, key intermediate **C1**-**C29** were obtained by coupling of intermediate **B1**-**B17** with methyl bromoacetate or methyl 4-(bromomethyl) benzoate. At last, target molecules **D1**-**D29** were synthesized by treatment of intermediate **C1**-**C29** with NH_2OK in methanol.

RESULTS AND DISCUSSIONS

Enzyme Inhibitory Activity of Synthesized Molecules

The substituted carboline structures are widely utilized in the design of anticancer molecules, such as histone deacetylase

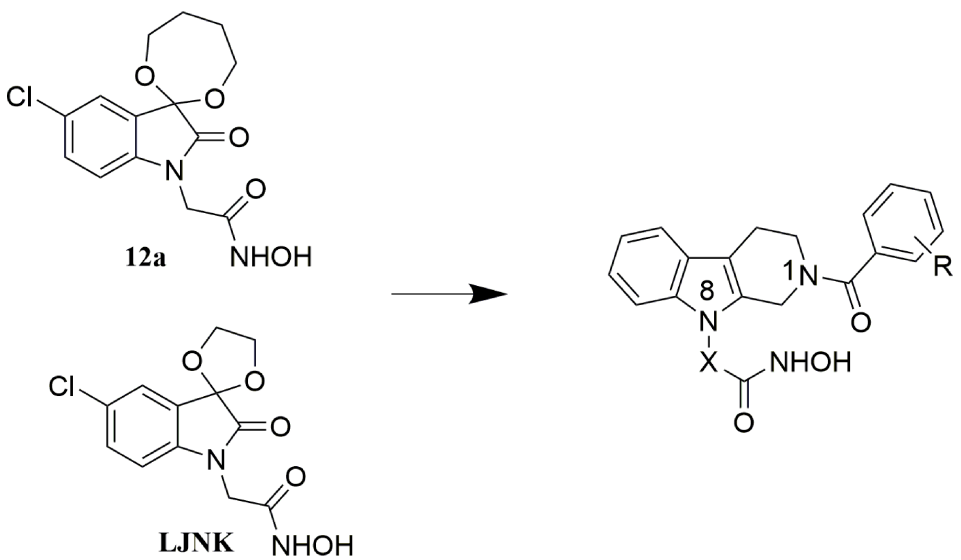

FIGURE 1 | Design of tetrahydro-β-carboline containing APN inhibitors (X = -CH_2-, -$CH_2C_6H_4$-).

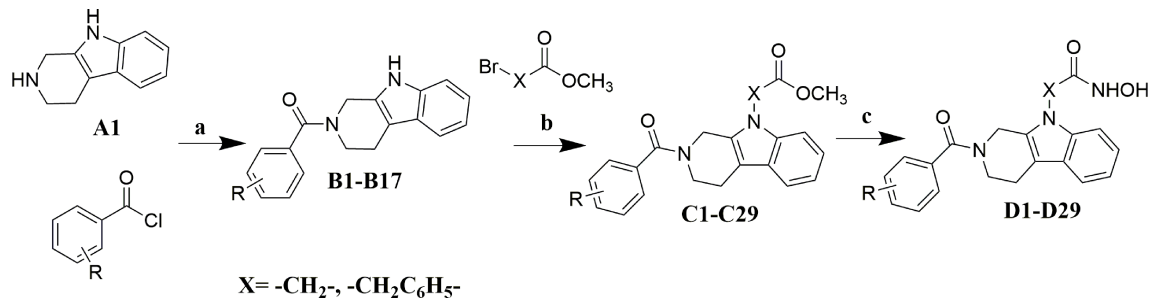

SCHEME 1 | Reagents and conditions: **(A)** Et_3N, DCM, 0°C; **(B)** Cs_2CO_3, DMF, 0°C; **(C)** NH_2OK, MeOH, rt.

(HDAC6) inhibitors (22), kinesin spindle protein inhibitors, breast cancer resistance protein (ABCG2) inhibitors (23), phosphodiesterase 5 inhibitors (24), transforming growth factor beta (TGFβ) signaling pathway inhibitors (25), and bromodomain and extra terminal proteins (BET) inhibitors (26). The carboline moiety played important roles in the site occupation and hydrophobic interaction of the ligand-receptor complexes. On the other hand, the hydrophobic pocket in the active site of APN requires hydrophobic and bulky fragments for efficient binding. Therefore, in the current study, the tetrahydro-*β*-carboline scaffold was utilized for the occupation of target compounds to the hydrophobic pocket of APN.

In the enzyme inhibitory assay, K562-CD13 monoclonal cells were used as APN enzyme source as described in our previous work (27). The derived target molecules were firstly screened at the concentration of 30 μM; then, compounds with inhibitory rate higher than 55% were further investigated for the IC_{50} value (**Table 1** and **Figures 2A, B**). Notably, molecules with a short linker (CH_2) between hydroxamic acid group and tetrahydro-*β*-carboline group exhibited better inhibitory activities than

TABLE 1 | Structures and enzyme inhibitory activities of the derived APN inhibitors.

Compound	X	R	Inhibitory rate (%)[a]	IC_{50} (μM)[a]
D1	CH_2	-CF_3(p)	35.0±1.51	ND
D2	$CH_2C_6H_4$	-CF_3(p)	13.3±3.25	ND
D3	CH_2	-H	74.4±6.42	6.24±0.43
D4	$CH_2C_6H_4$	-H	19.4±4.53	ND
D5	CH_2	-CF_3(o)	62.9±8.72	14.9±1.03
D6	$CH_2C_6H_4$	-CF_3(o)	15.3±3.66	ND
D7	$CH_2C_6H_4$	-OCH_3(o)	17.9±0.84	ND
D8	CH_2	-OCH_3(p)	56.7±0.42	25.0±3.32
D9	$CH_2C_6H_4$	-OCH_3(p)	24.0±0.25	ND
D10	CH_2	-F(p)	42.5±1.42	ND
D11	$CH_2C_6H_4$	-F(p)	35.0±4.57	ND
D12	CH_2	-F(m)	74.9±4.35	8.92±0.38
D13	$CH_2C_6H_4$	-F(m)	13.2±0.40	ND
D14	CH_2	-F(o)	74.3±6.16	7.74±0.33
D15	$CH_2C_6H_4$	-F(o)	28.7±2.75	ND
D16	CH_2	-CH_3(o)	74.5±4.66	7.9±0.27
D17	$CH_2C_6H_4$	-CH_3(o)	23.6±4.51	ND
D18	CH_2	-CH_2CH_3(p)	53.2±2.08	ND
D19	$CH_2C_6H_4$	-CH_2CH_3(p)	19.5±4.22	ND
D20	$CH_2C_6H_4$	-Cl(o)	19.1±4.17	ND
D21	CH_2	-Br(m)	78.2±5.43	7.82±1.05
D22	$CH_2C_6H_4$	-Br(m)	19.2±3.70	ND
D23	$CH_2C_6H_4$	-2,4-2F	65.0±5.97	49.74±9.29
D24	CH_2	-3,5-2F	71.3±4.25	7.13±0.13
D25	$CH_2C_6H_4$	-3,5-2F	27.9±5.85	ND
D26	CH_2	-(CH_2)$_2$$CH_3$(p)	53.1±7.31	ND
D27	$CH_2C_6H_4$	-(CH_2)$_2$$CH_3$(p)	20.4±5.78	ND
D28	CH_2	-2,5-2F	78.0±3.95	4.85±0.55
D29	CH_2	-2-Cl-6-F	60.0±4.95	9.23±0.67
Bestatin			53.9±0.77	18.33±1.68

[a]*Each value is the mean of at least three experiments.*
ND, Not determined.

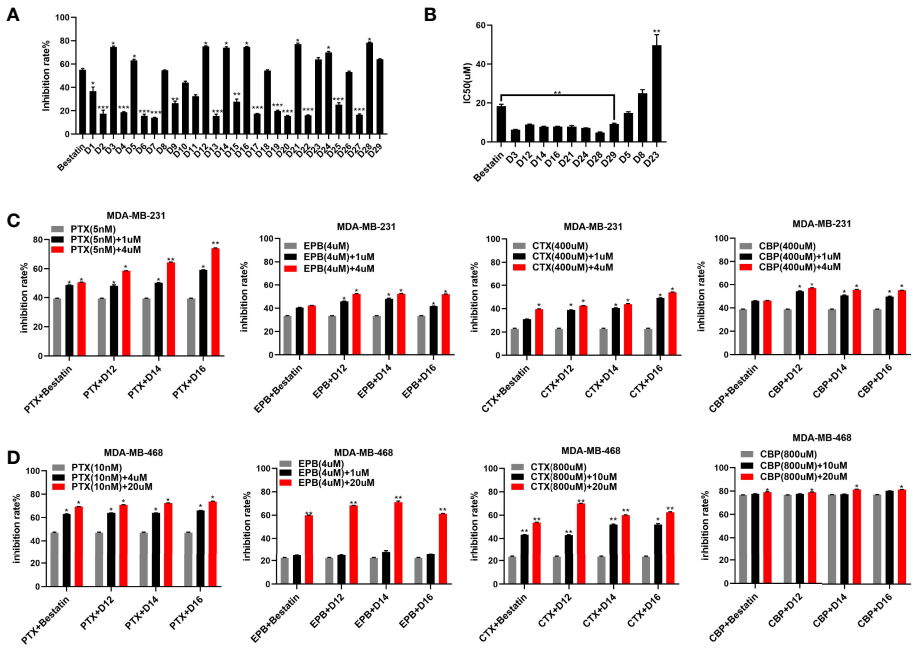

FIGURE 2 | Enzyme inhibitory and antiproliferative activities of the derived APN inhibitors. a: APN enzyme inhibitory rates **(A)** of the synthesized compounds; **(B)** IC_{50} values of selected compounds; **(C)** antiproliferative activities of representative compounds in combination with chemotherapeutic drugs against MDA-MB-231 cells; **(D)** antiproliferative activities of representative compounds in combination with chemotherapeutic drugs against MDA-MB-468 cells; *P ≤ 0.05, **P ≤ 0.01, ***P ≤ 0.001.

compounds with an aromatic linker ($CH_2C_6H_4$). Several compounds exhibited increased activity compared with Bestatin (IC_{50} value 18.33 μM), such as **D3** (IC_{50} value 6.24 μM), **D14** (IC_{50} value 7.74 μM), **D16** (IC_{50} value 7.90 μM), **D21** (IC_{50} value 7.82 μM), **D24** (IC_{50} value 7.13 μM), and **D28** (IC_{50} value 4.85 μM). Comparing with **D3**, introduction of R groups by para substitution on the phenyl ring led to decreased activity as revealed in **Table 1**. Nevertheless, the fluorine substitution on the ortho and meta positions can maintain the inhibitory potency, as seen in **D12**, **D14**, **D24** and **D28**. From the present structure activity relationship analysis, substitution on the ortho position of the phenyl ring could be beneficial to the inhibitory activity, and further structural modification could be performed by targeting this site.

Tumor Chemo-Sensitization Ability of Selected APN Inhibitors

APN has been revealed to be overexpressed in breast cancer and the APN expression is correlated with resistance to anticancer drugs, such as doxorubicin (EPB), in breast cancer cells (6, 28). The combination of APN inhibitor and paclitaxel (PTX), has been employed for the treatment of human breast cancer. In the current study, molecules with good APN inhibitory potency (**D12**, **D14** and **D16)** were selected and used in combination with several chemotherapeutic drugs, such as PTX, EPB, cyclophosphamide (CTX) and carboplatin (CBP) to investigate its inhibitory effect on breast cancer. Human triple negative breast cancer cell (TNBC) lines MDA-MB-231 and MDA-MB-468 were utilized in the *in vitro* studies. The results revealed that the tested compounds improve the antiproliferative activities of chemotherapeutic drugs against both cell lines with superior potency than the approved APN inhibitor Bestatin (**Figures 2C, D**). It was also observed that the synthesized molecules enhanced chemotherapeutic drug sensitivity in a dose dependent manner. Therefore, further analysis was performed to examine the synergistic effects of the derived APN inhibitors and chemotherapeutic drugs.

APN Expression, ROS Level, and Apoptosis Analysis

PTX exhibited the highest inhibitory potency against both cell lines among the tested chemotherapeutic drugs. Moreover, APN inhibitor-induced chemo-sensitization had been frequently reported for PTX (17, 29). Therefore, the combination of PTX-APN inhibitor was selected in the subsequent studies. Enhanced APN expression was detected after treatment with the PTX relative to the untreated control, suggesting that PTX treatment up-regulated APN expression in both MDA-MB-231 and MDA-MB-468 cells (**Figure 3A**). Treatment with **D12**, **D14**, **D16** or Bestatin in combination with PTX decreased APN expression in both cell lines compared with paclitaxel treatment alone. Compared to the control group, increased ROS levels were observed in both breast cancer cell lines following PTX treatment (**Figure 3B**). Co-treatment with selected APN inhibitors resulted in further increase of intracellular ROS levels than PTX treatment alone. The apoptotic results revealed that treatment of the tested breast

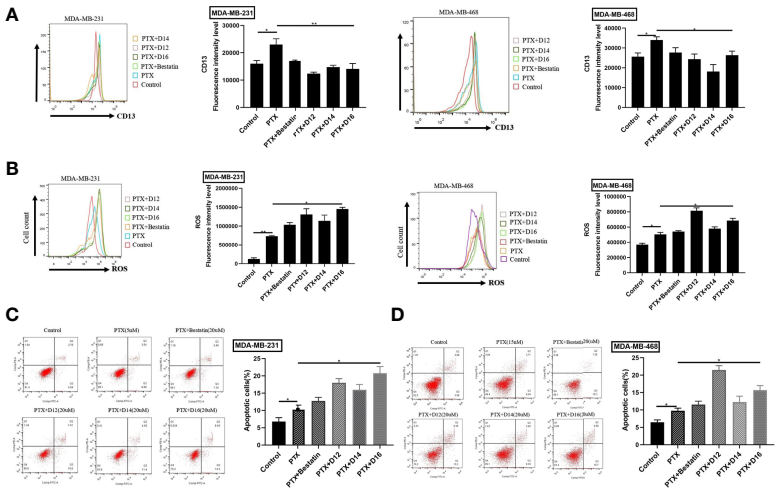

FIGURE 3 | Combination of APN inhibitors with PTX decreased the expression CD13 (APN), increased ROS level, and promoted cell apoptosis. **(A)** CD13 (APN) expression regulated by various PTX-APN inhibitor combinations; **(B)** ROS level monitored by various PTX-APN inhibitor combinations; **(C)** MDA-MB-231 cell apoptosis induced by different PTX-APN inhibitor combinations; **(D)** MDA-MB-468 cell apoptosis induced by different PTX-APN inhibitor combinations; *P ≤ 0.05, **P ≤ 0.01.

cancer cell lines with APN inhibitors promoted the apoptosis-inducing effect of PTX (**Figures 3C, D**). Compared with Bestatin, the synthesized compounds **D12**, **D14** and **D16** in combination with PTX treatment induced higher apoptotic rate. These results suggested that the selected APN inhibitors can sensitize TNBC cells to PTX by decreasing APN expression, increasing ROS level and induction of apoptosis.

Cancer Stemness Inhibitory Test

Cancer stem cells (CSCs) play an important role in the resistance of cancer cells to chemotherapeutic drugs. APN has been reported to be a therapeutic target in human cancer stem cells (18). Therefore, the CSC based test was performed in the present study. Colony-formation assay and spheroid-formation assay are two commonly used methods to assess the capacity of CSCs *in vitro*. In the spheroid-formation assay, MDA-MB-231 and MDA-MB-468 cells were dispersed into single cells, inoculated into low-adherence 6-well plates, and added with stem cell sphere medium. The stem cell spheres became visible after 5-6 days incubation. Stem cell sphere medium was added with 1nM of PTX in combination with 1 μM of **D12**, **D14**, **D16** or Bestatin. After 7 days of incubation, significant decrease in the number of tumor spheres formed in both MDA-MB-231 and MDA-MB-468 cells was observed in the drug combination groups comparing with the control and PTX alone groups (**Figures 4A, B**).To evaluate the effect of PTX in combination with APN inhibitors on the colony formation ability of TNBC cells, MDA-MB-231 and MDA-MB-468 cells were inoculated with 3000 cells per well in a 6-well plate. After treating with 0.2 nM of PTX combined with 1μM of various APN inhibitors for 14 days, the drug combination groups exhibited reduced number of colonies compared with the control and single PTX treatment groups (**Figures 4C, D**). It is known that mRNA levels of the stem cell biomarkers OCT-4, SOX-2 and Nanog are associated with the characteristics of TNBC stem cells (30). Therefore, RT-PCR was performed on the TNBC cells to detect the mRNA levels of these markers. The result showed that the mRNA expression levels of OCT-4, SOX-2 and Nanog in the TNBC stem cell spheres significantly decreased in the combined treatment groups compared with the control and single PTX groups (**Figures 4E, F**). These results suggested that the synthesized APN inhibitors (**D12**, **D14**, **D16**) could inhibit the stemness of TNBC cells when combined with PTX, with a higher potency than Bestatin.

In vivo Anticancer Study

To evaluate the *in vivo* anticancer potency of the combination of PTX-APN inhibitor, cancer xenograft model was established by inoculation of luciferase- expressing MDA-MB-231 cells to female nude mice. About 1×10^7 MDA-MB-231 cells were injected subcutaneously into the right fat pad of the fourth mammary gland of the mice. The tumor growth status of mice in each group was observed with a small animal imaging device. Significant tumor size variations were observed among different groups (**Figures 5A, B**). Bestatin and the APN inhibitors (**D12**, **D14**, **D16**) improved the anticancer effect of PTX compared with the single PTX administration group (**Figure 5C**). Among the tested molecules, compound **D12** in combination with PTX showed the best performance with the smallest tumor size, with an inhibitory rate of 54.02% compared with **D14** (inhibitory rate of 31.32%), **D16** (inhibitory rate of 14.15%) and Bestatin (inhibitory rate of 10.63%). It was also observed that the tested compounds inhibit the tumor growth without causing the loss in body weight (**Figure 5D**). Moreover, no clear signs of toxicity in liver and spleen were detected in the sacrificed mice. These results demonstrated that the derived APN inhibitors (especially **D12**)

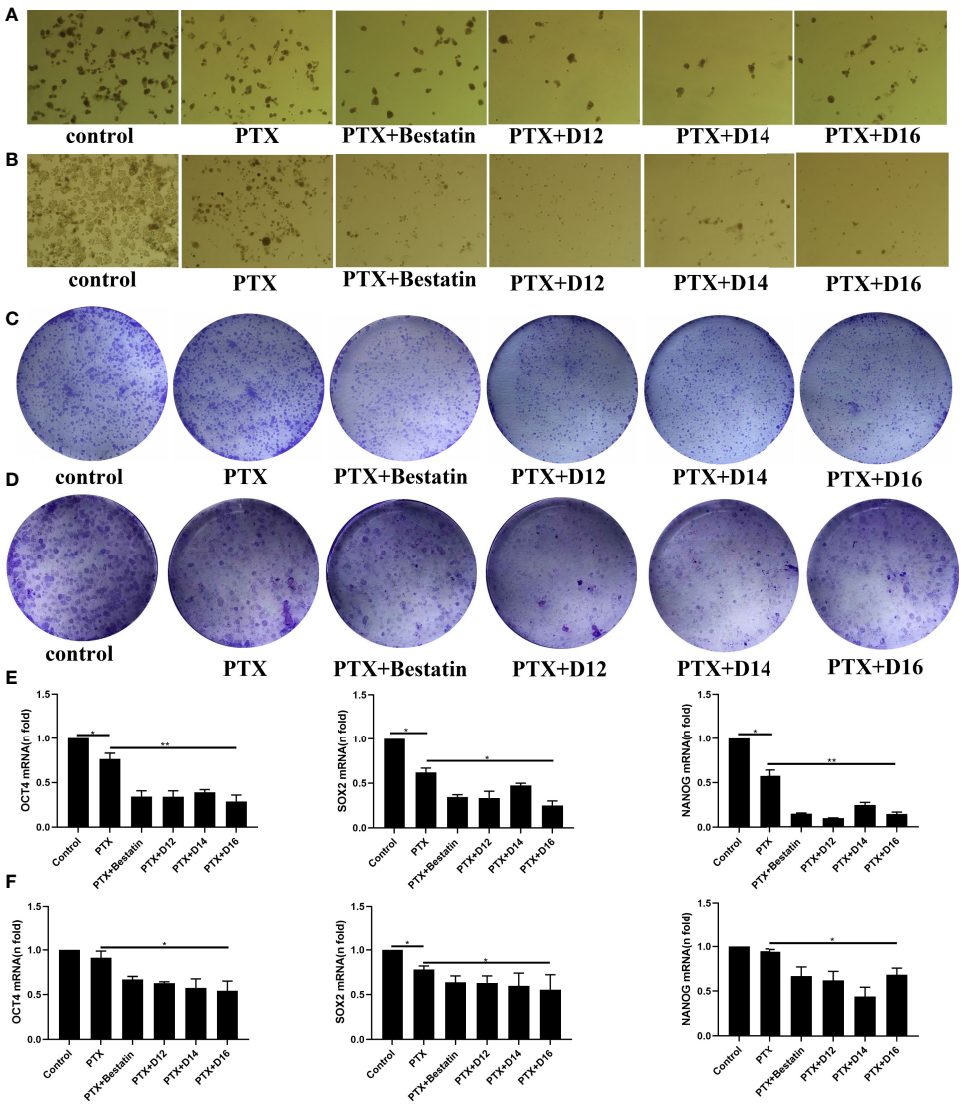

FIGURE 4 | Effects of PTX-APN inhibitor combinations on spheroid and colony formation of tested TNBC cells, and on mRNA expression levels of OCT-4, SOX-2 and Nanog in the tested TNBC stem cells. **(A)** MDA-MB-231 cell spheroid formation affected by different PTX-APN inhibitor combinations; **(B)** MDA-MB-468 cell spheroid formation affected by different PTX-APN inhibitor combinations; **(C)** MDA-MB-231 cell colony formation affected by different PTX-APN inhibitor combinations; **(D)** MDA-MB-468 cell colony formation affected by different PTX-APN inhibitor combinations; **(E)** regulation of mRNA expression levels of OCT-4, SOX-2 and Nanog by different PTX-APN inhibitor combinations in MDA-MB-231 cells; **(F)** regulation of mRNA expression levels of OCT-4, SOX-2 and Nanog by different PTX-APN inhibitor combinations in MDA-MB-468 cells; *P ≤ 0.05, **P ≤ 0.01.

enhanced the anticancer effect of chemotherapeutic drug (PTX) compared with Bestatin in the *in vivo* animal model.

CONCLUSION

Chemotherapy is the standard treatment for various types of cancers, such as TNBC. However, adverse effects and development of multidrug resistance has led to the search for new drugs or combinatory drug regimens for cancer therapy. APN inhibitors have been investigated as chemosensitizers and used to enhance the efficacy of standard chemotherapy. In order to develop potent chemosensitizers for the cancer treatment, novel APN inhibitors with tetrahydro-β-carboline structure were designed and synthesized in the present study. The chemosensitization potential of the derived molecules was evaluated.

Based on the enzymatic assay, the synthesized compounds inhibit the bioactivity of APN with various potency. Several molecules with high enzyme inhibitory activities were selected for further anticancer analysis. In the *in vitro* study, compound **D12**, **D14** and **D16** synergistically improved the antiproliferative activity of chemotherapeutic drugs, such as PTX, EPB, CTX and CBP. PTX, with the highest inhibitory potency against the tested MDA-MB-231 and MDA-MB-468 cells, were evaluated in

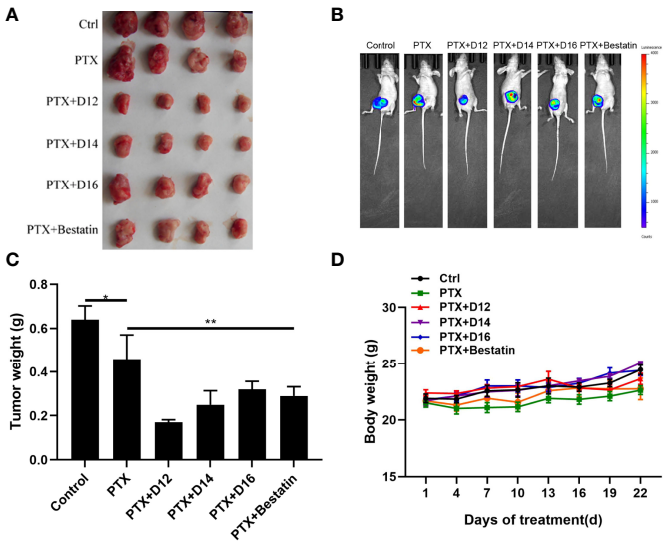

FIGURE 5 | *In vivo* anticancer effects of the PTX-APN inhibitor combinations. **(A)** Dissected tumor tissues taken from mice after administration of various drug combinations; **(B)** representative *in vivo* imaging of tumors; **(C)** Tumor weight plot of different administration groups; **(D)** mice body weight plot of different administration groups; Data were taken as mean ± SEM (n = 4), *P ≤ 0.05, **P ≤ 0.01.

combination with representative APN inhibitors. It is revealed that the addition of APN inhibitors decreases APN expression level, enhances intracellular ROS production, and improves apoptotic rate in the TNBC cells. The subsequent TNBC stem cell-based studies showed that introduction of APN inhibitors (**D12**, **D14** and **D16**) decreased the tumor sphere and colony formation abilities in the stem cells. The mRNA expression of stem cell markers OCT-4, SOX-2 and Nanog were decreased by combination of derived APN inhibitors to PTX. In the *in vivo* nude mouse model, the selected APN inhibitors, especially **D12**, improved the anticancer activity of PTX, as suggested by the observed smaller tumor size. Collectively, potent APN inhibitors were discovered, which can be used as lead compounds for the development of chemo-sensitizers in cancer treatment.

MATERIALS AND METHODS

All commercially available starting materials, reagents and solvents were used without further purification. All reactions were monitored by TLC with 0.25 mm silica gel plates (60GF-254). UV light and ferric chloride were used to visualize the spots. ^{1}H NMR and ^{13}C NMR spectra were recorded on a Bruker DRX spectrometer at 500 MHz, using TMS as an internal standard. High-resolution mass spectra was performed in Weifang Medical University. A Thermo UltiMate 3000 High performance liquid chromatograph was used to measure the purity of the derived molecules, and all the target compounds achieved > 95% purity.

Preparation of **B1** and its analogues: Derivatives **B2-B17** were prepared as described for **B1** (see below).

(1,3,4,9-tetrahydro-2*H*-pyrido[3,4-*b*]indol-2-yl)(4-(trifluoromethyl) phenyl)methanone(**B1**).

To a solution of **A1** (0.50 g, 2.9 mmol) in DCM 4-(trifluoromethyl)-benzoylchlorid (0.73 g, 3.5 mmol) and the followed Et_3N (0.88 g, 8.7 mmol) were added dropwise at 0°C, and the mixture was stirred for 4 h. Then, the solvent was evaporated with the residue being taken up in EtOAc. The EtOAc solution was washed with saturated citric acid, $NaHCO_3$ and saturated brine solution, dried over $MgSO_4$, and evaporated under vacuum. The desired compound **B1** (0.87 g, 87%) was derived by crystallization in EtOAc as white powder. HRMS m/z: 345.12012$[M+H]^+$. ^{1}H-NMR (400 MHz, DMSO). δ 10.93 (s, 1H), 7.86 (d, *J* = 8.0 Hz, 2H), 7.70 (d, *J* = 8.0 Hz, 2H), 7.40 (d, *J* = 8.0 Hz, 1H), 7.35-7.25 (m, 1H), 7.08-7.04 (m, 1H), 7.00-6.96 (m, 1H), 4.86-4.55 (m, 2H), 4.02-3,60 (m, 2H), 2.82-2.75 (m, 2H).

Phenyl(1,3,4,9-tetrahydro-2*H*-pyrido[3,4-*b*]indol-2-yl) methanone (**B2**).

HRMS m/z: 277.13254$[M+H]^+$. ^{1}H-NMR (400 MHz, DMSO). δ 10.94 (s, 1H), 7.48 (d, *J* = 4.0 Hz, 4H), 7.40 (d, *J* = 8.0 Hz, 1H), 7.34-7.26 (m, 1H), 7.05-7.04 (m, 1H), 6.99-6.96 (m, 1H), 4.83-4.60 (m, 2H), 3.99-3,63 (m, 2H), 2.75 (s, 2H).

(1,3,4,9-tetrahydro-2*H*-pyrido[3,4-*b*]indol-2-yl)(2-(trifluoromethyl)phenyl)methanone (**B3**).

HRMS m/z: 345.11850$[M+H]^+$. ^{1}H-NMR (400 MHz, DMSO).δ 10.54 (s, 1H), 7.90-7.86 (m, 1H), 7.83-7.77 (m, 1H), 7.72-7.68 (m, 1H), 7.55-7.49 (m, 1H), 7.41-7.23 (m, 2H), 7.08-7.01 (m, 1H), 6.99-6.95 (m, 1H), 4.87 (dd, *J* = 94.0, 16.8 Hz, 1H), 4.41-4.22 (m, 1H), 3.47-3.42 (m, 2H), 2.81-2.62 (m, 2H).

(2-methoxyphenyl)(1,3,4,9-tetrahydro-2*H*-pyrido[3,4-*b*]indol-2-yl)methanone (**B4**).

HRMS m/z: 307.14319[M+H]$^+$. ^{1}H-NMR (400 MHz, DMSO). δ 10.61 (s, 1H), 7.46-7.32 (m, 3H), 7.25-7.20 (m, 1H), 7.18-6.95 (m, 3H), 4.84-4.37 (m, 2H), 3.80 (s, 2H), 3.72 (s, 1H), 3.50-3.45 (m, 2H), 2.79-2.62 (m, 2H).

(4-methoxyphenyl)(1,3,4,9-tetrahydro-2*H*-pyrido[3,4-*b*]indol-2-yl)methanone (**B5**).

HRMS m/z: 307.14322[M+H]$^+$. ^{1}H-NMR (400 MHz, DMSO). δ 10.84 (s, 1H), 7.46-7.45 (m, 2H), 7.44-7.39 (m, 1H), 7.30 (d, *J* = 8.0 Hz, 1H), 4.74 (s, 2H), 3.89-3.72 (m, 5H), 2.79-2.76 (m, 2H).

(4-fluorophenyl)(1,3,4,9-tetrahydro-2*H*-pyrido[3,4-*b*]indol-2-yl)methanone (**B6**).

HRMS m/z: 295.12253[M+H]$^+$. ^{1}H-NMR (400 MHz, DMSO). δ 10.94 (s, 1H), 7.57-7.53 (m, 2H), 7.40 (d, *J* = 8.0 Hz, 1H), 7.34-7.30 (m, 3H), 7.07-7.03 (m, 1H), 6.99-6.96 (m, 1H), 4.82-4.61 (m, 2H), 3.98-3.63 (m, 2H), 2.77 (s, 2H).

(3-fluorophenyl)(1,3,4,9-tetrahydro-2*H*-pyrido[3,4-*b*]indol-2-yl)methanone (**B7**).

HRMS m/z: 295.12314[M+H]$^+$. ^{1}H-NMR (400 MHz, DMSO). δ 10.92 (s, 1H), 7.57-7.51 (m, 1H), 7.41-7.39 (m, 1H), 7.36-7.30 (m, 4H), 7.07-7.04 (m, 1H), 6.99-6.96 (m, 1H), 4.83-4.59 (m, 2H), 3.99-3.62 (m, 2H), 2.75 (s, 2H).

(2-fluorophenyl)(1,3,4,9-tetrahydro-2*H*-pyrido[3,4-*b*]indol-2-yl)methanone (**B8**).

HRMS m/z: 295.12253[M+H]$^+$. ^{1}H-NMR (400 MHz, DMSO). δ 10.96 (s, 1H), 7.58-7.53 (m, 1H), 7.49-7.25 (m, 5H), 7.07-7.04 (m, 1H), 6.99-6.96 (m, 1H), 4.89-4.50 (m, 2H), 4.03-3.56 (m, 2H), 2.82-2.69 (m, 2H).

(1,3,4,9-tetrahydro-2*H*-pyrido[3,4-*b*]indol-2-yl)(o-tolyl)methanone (**B9**).

HRMS m/z: 291.14819[M+H]$^+$. ^{1}H-NMR (400 MHz, DMSO). δ 10.94 (s, 1H), 7.43-7.17 (m, 6H), 7.07-7.01 (m, 1H), 6.99-6.95 (m, 1H), 4.90 (d, *J* = 72.0 Hz, 2H), 4.40-4.24 (m, 2H), 3.82-3.47 (m, 2H), 2.82-2.63 (m, 2H), 2.27 (s, 2H), 2.15 (s, 1H).

(4-ethylphenyl)(1,3,4,9-tetrahydro-2*H*-pyrido[3,4-*b*]indol-2-yl)methanone (**B10**).

HRMS m/z: 305.16403[M+H]$^+$. ^{1}H-NMR (400 MHz, DMSO). δ 10.90 (s, 1H), 7.41-7.38 (m, 3H), 7.33-7.31 (m, 3H), 7.06-7.03 (m, 1H), 6.99-6.95 (m, 1H), 4.80-4.64 (m, 2H), 3.97-3.65 (m, 2H), 2.77 (s, 2H), 2.67 (q, *J* = 7.6 Hz, 2H),1.22 (t, *J* = 8.0 Hz, 3H).

(2-chlorophenyl)(1,3,4,9-tetrahydro-2*H*-pyrido[3,4-*b*]indol-2-yl)methanone (**B11**).

HRMS m/z: 311.09207[M+H]$^+$. ^{1}H-NMR (400 MHz, DMSO). δ 10.94 (s, 1H), 7.59-7.57 (m, 1H), 7.55-7.24 (m, 5H), 7.07-7.04 (m, 1H), 6.99-6.95 (m, 1H), 4.94-4.39 (m, 2H), 4.13-3.49 (m, 2H), 2.82-2.68 (m, 2H).

(3-bromophenyl)(1,3,4,9-tetrahydro-2*H*-pyrido[3,4-*b*]indol-2-yl)methanone (**B12**).

HRMS m/z: 353.02856[M+H]$^+$. ^{1}H-NMR (400 MHz, DMSO). δ 10.92 (s, 1H), 7.71-7.70 (m, 1H), 7.69 (s, 1H), 7.66-7.41 (m, 3H), 7.39-7.26 (m, 1H), 7.07-7.03 (m, 1H), 6.99-6.95 (m, 1H), 4.83-4.59 (m, 2H), 3.98-3.62 (m, 2H), 2.75 (s, 2H).

(2,4-difluorophenyl)(1,3,4,9-tetrahydro-2*H*-pyrido[3,4-*b*]indol-2-yl)methanone (**B13**).

HRMS m/z: 313.11172[M+H]$^+$. ^{1}H-NMR (400 MHz, DMSO). δ 10.93 (s, 1H), 7.58-7.50 (m, 1H), 7.44-7.19 (m, 4H), 7.08-7.02 (m, 1H), 6.99-6.95 (m, 1H), 4.87-4.50 (m, 2H), 4.02-3.56 (m, 2H), 2.81-2.69 (m, 2H).

(3,5-difluorophenyl)(1,3,4,9-tetrahydro-2*H*-pyrido[3,4-*b*]indol-2-yl)methanone (**B14**).

HRMS m/z: 313.11337[M+H]$^+$. ^{1}H-NMR (400 MHz, DMSO). δ 10.93 (s, 1H), 7.44-7.26 (m, 5H), 7.08-7.02 (m, 1H), 6.99-6.96 (m, 1H), 4.83-4.59 (m, 2H), 3.98-3.59 (m, 2H), 2.80-2.75 (m, 2H).

(4-propylphenyl)(1,3,4,9-tetrahydro-2*H*-pyrido[3,4-*b*]indol-2-yl)methanone (**B15**).

HRMS m/z: 319.17862[M+H]$^+$. ^{1}H-NMR (400 MHz, DMSO). δ 10.94 (s, 1H), 7.41-7.37 (m, 3H), 7.31-7.29 (m, 3H), 7.06-7.03 (m, 1H), 6.99-6.95 (m, 1H), 4.81-4.62 (m, 2H), 3.97-3.33 (m, 2H), 2.76 (s, 2H), 2.61 (t, *J* = 8.0 Hz, 2H), 1.67-1.85 (m, 2H), 0.93 (t, *J* = 4.0 Hz, 3H).

(2,5-difluorophenyl)(1,3,4,9-tetrahydro-2*H*-pyrido[3,4-*b*]indol-2-yl)methanone (**B16**).

HRMS m/z: 313.11273[M+H]$^+$. ^{1}H-NMR (400 MHz, DMSO). δ 10.97 (s, 1H), 7.43-7.38 (m, 4H), 7.35-7.27 (m, 1H), 7.08-7.03 (m, 1H), 7.00-6.96 (m, 1H), 4.88-4.52 (m, 2H), 4.04-3.57 (m, 2H), 2.76 (s, 2H), 2.82-2.71 (m, 2H).

(2-chloro-6-fluorophenyl)(1,3,4,9-tetrahydro-2*H*-pyrido[3,4-*b*]indol-2-yl)methanone (**B17**).

HRMS m/z: 329.08441[M+H]$^+$. ^{1}H-NMR (400 MHz, DMSO). δ 10.61 (s, 1H), 7.59-7.52 (m, 1H), 7.49-7.27 (m, 4H), 7.09-7.03 (m, 1H), 7.00-6.96 (m, 1H), 4.94-4.45 (m, 2H), 4.11-3.55 (m, 2H), 2.83-2.69 (m, 2H).

Preparation of **C1** and its analogues: Derivatives **C2-C29** were prepared as described for **C1** (see below).

Methyl 2-(2-(4-(trifluoromethyl)benzoyl)-1,2,3,4-tetrahydro-9*H*-pyrido[3,4-*b*]indol-9- yl)acetate (**C1**).

The solution of Cs_2CO_3 (1.17 g, 3.6 mmol) and **B1** (0.40 g, 1.2 mmol) in DMF was firstly stirred under Ar_2 and 0°C. After 30 min, methyl bromoacetate was added. The reaction solution was stirred at room temperature for 4 h. Then, the solvent was evaporated under vacuum. The residue was extracted with EtOAc (30 mL), washed with saturated $NaHCO_3$ (3×30 mL), saturated brine solution (3×30 mL), dried over $MgSO_4$, and evaporated under vacuum. The desired compound **C1** (0.33 g, 66%) was derived by crystallization in EtOAc as powder. HRMS m/z: 417.14145[M+H]$^+$. ^{1}H-NMR (400 MHz, DMSO). δ 7.87 (d, *J* = 8.0 Hz, 2H), 7.73-7.65 (m, 2H), 7.46-7.37 (m, 2H), 7.14-7.11 (m, 1H), 7.07-7.03 (m, 1H), 5.15-4.93 (m, 2H), 4.83-4.54 (m, 2H), 4.00-3.50 (m, 2H), 3.71 (s, 3H), 2.78 (s, 2H).

Methyl 4-((2-(4-(trifluoromethyl)benzoyl)-1,2,3,4-tetrahydro-9*H*-pyrido[3,4-*b*]indol- 9-yl)methyl)benzoate (**C2**).

HRMS m/z: 493.17252[M+H]$^+$. ^{1}H-NMR (400 MHz, DMSO). δ 7.92 (d, *J* = 8.0 Hz, 1H), 7.86 (d, *J* = 8.0 Hz, 1H), 7.74-7.57 (m, 3H), 7.50-7.45 (m, 3H), 7.22-6.84 (m, 4H), 5.56-5.32 (m, 2H), 4.80-4.44 (m, 2H), 4.00 (s, 1H), 3.83 (s, 3H), 3.59 (s, 1H), 2.87-2.81 (m, 2H).

Methyl 2-(2-benzoyl-1,2,3,4-tetrahydro-9*H*-pyrido[3,4-*b*]indol-9-yl)acetate (**C3**).

HRMS m/z: 349.15399[M+H]$^+$. ^{1}H-NMR (400 MHz, DMSO). δ 7.50-7.40 (m, 7H), 7.14-7.11 (m, 1H), 7.07-7.04 (m, 1H), 5.15-4.92 (m, 2H), 4.80-4.60 (m, 2H), 3.98-3.51 (m, 5H), 2.80 (s, 2H).

Methyl 2-(2-benzoyl-1,2,3,4-tetrahydro-9*H*-pyrido[3,4-*b*]indol-9-yl)acetate (**C4**).

HRMS m/z: 425.18454[M+H]$^+$. ^{1}H-NMR (400 MHz, DMSO). δ 7.91-7.49 (m, 2H), 7.47-7.44 (m, 5H), 7.22 (s, 3H), 7.11 (t, *J* = 8.0 Hz, 1H), 7.05 (t, *J* = 8.0 Hz, 1H), 6.92 (s, 1H), 5.55-5.29 (m, 2H), 4.77-4.49 (m, 2H), 4.97-4.62 (m, 2H), 3.83 (s, 3H), 2.81 (s, 2H).

Methyl 2-(2-(2-(trifluoromethyl)benzoyl)-1,2,3,4-tetrahydro-9*H*-pyrido[3,4-*b*]indol-9- yl)acetate (**C5**).

HRMS m/z: 417.13935[M+H]$^+$. ^{1}H-NMR (400 MHz, DMSO). δ 7.86-7.67 (m, 3H), 7.58-7.56 (m, 1H), 7.48-7.33 (m, 2H), 7.14-7.10 (m, 1H), 7.09-7.03 (m, 1H), 5.15-4.67 (m, 4H), 4.38-3.86 (m, 1H), 3.72 (s, 2H), 3.49-3.36 (m, 2H), 2.83-2.61 (m, 2H).

Methyl 4-((2-(2-(trifluoromethyl)benzoyl)-1,2,3,4-tetrahydro-9*H*-pyrido[3,4-*b*]indol- 9-yl)methyl)benzoate (**C6**).

HRMS m/z: 493.17227[M+H]$^+$. ^{1}H-NMR (400 MHz, DMSO). δ 7.91-7.85 (m, 2H), 7.79-7.67 (m, 2H), 7.57-7.32 (m, 4H), 7.21 (d, *J* = 8.0 Hz, 1H), 7.12 (d, *J* = 8.0 Hz, 1H), 7.07-7.03 (m, 1H), 6.85 (d, *J* = 8.0 Hz, 1H), 5.57-5.35 (m, 2H), 5.07 (dd, *J* = 64.0, 16.0 Hz, 1H), 4.69-4.35 (m, 2H), 4.07-3.88 (m, 2H), 3.83 (s, 2H), 3.47-3.40 (m, 2H), 2.73-2.67 (m, 2H).

Methyl 4-((2-(2-methoxybenzoyl)-1,2,3,4-tetrahydro-9*H*-pyrido[3,4-*b*]indol-9-yl) methyl)benzoate (**C7**).

HRMS m/z: 455.19534[M+H]$^+$. ^{1}H-NMR (400 MHz, DMSO). δ 7.94-7.73 (m, 2H), 7.50-7.21 (m, 5H), 7.14-7.00 (m, 4H), 6.93-6.81 (m, 1H), 5.55-5.21 (m, 2H), 4.83-4.32 (m, 2H), 4.23-4.16 (m, 1H), 3.86-3.62 (m, 6H), 3.46 (d, *J* = 8.0 Hz, 1H), 2.80-2.69 (m, 2H).

methyl 2-(2-(4-methoxybenzoyl)-1,2,3,4-tetrahydro-9*H*-pyrido[3,4-*b*]indol-9-yl) acetate (**C8**).

HRMS m/z: 379.16446[M+H]$^+$. ^{1}H-NMR (400 MHz, DMSO). δ 7.45 (d, *J* = 8.0 Hz, 2H), 7.39 (d, *J* = 8.0 Hz, 1H), 7.13-7.12 (m, 1H), 7.06-7.01 (m, 2H), 5.08 (s, 2H), 4.72 (s, 2H), 3.82 (s, 3H), 3.66 (s, 2H), 2.81 (s, 2H).

Methyl 4-((2-(4-methoxybenzoyl)-1,2,3,4-tetrahydro-9*H*-pyrido[3,4-*b*]indol-9-yl) methyl)benzoate (**C9**).

HRMS m/z: 455.19592[M+H]$^+$. ^{1}H-NMR (400 MHz, DMSO). δ 7.87 (s, 2H), 7.50-7.40 (m, 4H), 7.13-6.98 (m, 6H), 5.51 (s, 2H), 4.68 (s, 2H), 3.83 (s, 3H), 3.80-3.79 (m, 5H), 2.84-2.83 (m, 2H).

Methyl 2-(2-(4-fluorobenzoyl)-1,2,3,4-tetrahydro-9*H*-pyrido[3,4-*b*]indol-9-yl)acetate (**C10**).

HRMS m/z: 367.14304[M+H]$^+$. ^{1}H-NMR (400 MHz, DMSO). δ 7.56 (s, 2H), 7.46-7.40 (m, 2H), 7.32 (t, *J* = 8.0 Hz, 2H), 7.14-7.10 (m, 1H), 7.07-7.03 (m, 1H), 5.15-4.94 (m, 2H), 4.78-4.60 (m, 2H), 3.95-3.62 (m, 5H), 2.80 (s, 2H).

Methyl 4-((2-(4-fluorobenzoyl)-1,2,3,4-tetrahydro-9*H*-pyrido[3,4-*b*]indol-9-yl)methyl) benzoate (**C11**).

HRMS m/z: 465.15723[M+Na]$^+$. ^{1}H-NMR (400 MHz, DMSO). δ 7.91-7.75 (m, 2H), 7.55 (s, 1H), 7.50-7.45 (m, 2H),7.31-7.20 (m, 2H), 7.13-7.04 (m, 4H), 6.92 (s, 1H), 5.55-5.32 (m, 2H), 4.76-4.48 (m, 2H), 3.95 (s, 1H), 3.83 (s, 3H), 3.62 (s, 1H), 2.82 (s, 2H).

Methyl 2-(2-(3-fluorobenzoyl)-1,2,3,4-tetrahydro-9*H*-pyrido[3,4-*b*]indol-9-yl)acetate (**C12**).

HRMS m/z: 367.14236[M+H]$^+$. ^{1}H-NMR (400 MHz, DMSO). δ 7.54 (d, *J* = 8.0 Hz, 1H), 7.45 (d, *J* = 8.0 Hz, 1H), 7.41-7.32 (m, 4H), 7.14-7.10 (m, 1H), 7.07-7.03 (m, 1H), 5.13-4.92 (m, 2H), 4.80-4.56 (m, 2H), 3.97-3.52 (m, 5H), 2.79 (s, 2H).

Methyl 4-((2-(3-fluorobenzoyl)-1,2,3,4-tetrahydro-9*H*-pyrido[3,4-*b*]indol-9-yl)methyl) benzoate (**C13**).

HRMS m/z: 443.17584[M+H]$^+$. ^{1}H-NMR (400 MHz, DMSO). δ 7.93-7.73 (m, 2H), 7.55-7.32 (m, 5H), 7.21-7.04 (m, 4H), 6.92 (s, 1H), 5.56-5.31 (m, 2H), 4.77-4.47 (m, 2H), 3.96 (s, 1H), 3.83 (s, 3H), 3.60 (s, 1H), 2.81 (s, 2H).

Methyl 2-(2-(2-fluorobenzoyl)-1,2,3,4-tetrahydro-9*H*-pyrido[3,4-*b*]indol-9-yl)acetate (**C14**).

HRMS m/z: 367.14447[M+H]$^+$. ^{1}H-NMR (400 MHz, DMSO). δ 7.55 (d, *J* = 8.0 Hz, 1H), 7.46 (d, *J* = 8.0 Hz, 1H), 7.41-7.34 (m, 4H), 7.14-7.11 (m, 1H), 7.07-7.04 (m, 1H), 5.16-4.94 (m, 2H), 4.81-4.57 (m, 2H), 3.97-3.53 (m, 5H), 2.79 (s, 2H).

Methyl 4-((2-(2-fluorobenzoyl)-1,2,3,4-tetrahydro-9*H*-pyrido[3,4-*b*]indol-9-yl)methyl) benzoate (**C15**).

HRMS m/z: 443.17517[M+H]$^+$. ^{1}H-NMR (400 MHz, DMSO). δ 7.93-7.75 (m, 2H), 7.57-7.45 (m, 3H), 7.34-7.32 (m, 2H), 7.22-7.04 (m, 4H), 6.93 (s, 1H), 5.56-5.32 (m, 2H), 4.77-4.47 (m, 2H), 3.97 (s, 1H), 3.83 (s, 3H), 3.61 (s, 1H), 2.81 (s, 2H).

Methyl 2-(2-(2-methylbenzoyl)-1,2,3,4-tetrahydro-9*H*-pyrido[3,4-*b*]indol-9-yl)acetate (**C16**).

HRMS m/z: 363.16928[M+H]$^+$. ^{1}H-NMR (400 MHz, DMSO). δ 7.48-7.23 (m, 6H), 7.15-7.10 (m, 1H), 7.09-7.02 (m, 1H), 5.15-4.28 (m, 2H), 5.01-4.72 (m, 2H), 3.72-3.47 (m, 5H), 2.82-2.66 (m, 2H), 2.09 (s, 3H).

Methyl 4-((2-(2-methylbenzoyl)-1,2,3,4-tetrahydro-9*H*-pyrido[3,4-*b*]indol-9-yl) methyl)benzoate (**C17**).

HRMS m/z: 439.20081[M+H]$^+$. ^{1}H-NMR (400 MHz, DMSO). δ 7.91-7.73 (m, 2H), 7.51-7.45 (m, 2H), 7.37-7.21 (m, 4H), 7.15-6.85 (m, 4H), 5.56-5.17 (m, 2H), 5.01-4.13 (m, 2H), 3.88 (s, 1H), 3.84 (t, *J* = 4.0 Hz, 2H), 3.75-3.47 (m, 2H), 2.84-2.69 (m, 2H), 2.22 (s, 2H), 1.19-1.16 (m, 1H).

Methyl 2-(2-(4-ethylbenzoyl)-1,2,3,4-tetrahydro-9*H*-pyrido[3,4-*b*]indol-9-yl)acetate (**C18**).

HRMS m/z: 377.18558[M+H]$^+$. ^{1}H-NMR (400 MHz, DMSO). δ 7.45 (d, *J* = 8.0 Hz, 1H), 7.40 (d, *J* = 8.0 Hz, 2H), 7.32 (d, *J* = 8.0 Hz, 2H), 7.13-7.10 (m, 1H), 7.07-7.03 (m, 1H), 5.13-4.96 (m, 2H), 4.95-4.76 (m, 2H), 3.70-3.64 (m, 5H), 2.79 (s, 2H), 2.69 (q, *J* = 7.6 Hz, 2H), 1.22 (t, *J* = 8.0 Hz, 3H).

Methyl 4-((2-(4-ethylbenzoyl)-1,2,3,4-tetrahydro-9*H*-pyrido[3,4-*b*]indol-9-yl)methyl) benzoate (**C19**).

HRMS m/z: 453.21667[M+H]$^+$. ^{1}H-NMR (400 MHz, DMSO). δ 7.91-7.76 (m, 2H), 7.50-7.45 (m, 2H), 7.38-7.20 (m, 4H), 7.14-

6.90 (m, 4H), 5.55-5.32 (m, 2H), 4.75-4.55 (m, 2H), 3.95-3.65 (m, 5H), 2.82 (s, 2H), 2.65 (s, 2H), 1.20 (s, 3H).

Methyl 4-((2-(2-chlorobenzoyl)-1,2,3,4-tetrahydro-9*H*-pyrido[3,4-*b*]indol-9-yl)methyl) benzoate (**C20**).

HRMS m/z: 481.12839$[M+H]^+$. ^{1}H-NMR (400 MHz, DMSO). δ 7.94-7.73 (m, 2H), 7.58 (d, *J* = 8.0 Hz, 1H), 7.49-7.43 (m, 4H), 7.28-6.90 (m, 5H), 5.57 (s, 2H), 5.37-4.18 (m, 3H), 3.88 (s, 1H), 3.83 (s, 2H), 3.49-3.46 (m, 2H), 2.85-2.73 (m, 2H).

Methyl 2-(2-(2-bromobenzoyl)-1,2,3,4-tetrahydro-9*H*-pyrido[3,4-*b*]indol-9-yl)acetate (**C21**).

HRMS m/z: 449.04633$[M+Na]^+$. ^{1}H-NMR (400 MHz, DMSO). δ 7.72-7.61 (m, 2H), 7.49-7.40 (m, 4H), 7.14-7.10 (m, 1H), 7.07-7.03 (m, 1H), 5.15-4.94 (m, 2H), 4.80-4.56 (m, 2H), 3.96-3.54 (m, 5H), 2.78 (s, 2H).

methyl 4-((2-(3-bromobenzoyl)-1,2,3,4-tetrahydro-9*H*-pyrido[3,4-*b*]indol-9-yl)methyl) benzoate (**C22**).

HRMS m/z: 503.09595$[M+H]^+$. ^{1}H-NMR (400 MHz, DMSO). δ 7.93-7.65 (m, 3H), 7.53-7.45 (m, 4H), 7.25-7.19 (m, 2H), 7.13-7.10 (m, 1H), 7.05 (d, *J* = 8.0 Hz, 1H), 6.95 (s, 1H), 5.56-5.31 (m, 2H), 4.76-4.47 (m, 2H), 3.95-3.60 (m, 5H), 2.81 (s, 2H).

Methyl 4-((2-(2,4-difluorobenzoyl)-1,2,3,4-tetrahydro-9*H*-pyrido[3,4-*b*]indol-9-yl) methyl)benzoate (**C23**).

HRMS m/z: 461.16650$[M+H]^+$. ^{1}H-NMR (400 MHz, DMSO). δ 7.93-7.75 (m, 2H), 7.58-7.40 (m, 3H), 7.31 (q, *J* = 8.0 Hz, 1H), 7.24-7.20 (m, 2H), 7.14-7.03 (m, 2H), 6.98-6.92 (m, 1H), 5.55-5.35 (m, 2H), 4.81-4.36 (m, 2H), 3.99 (s, 1H), 3.85 (s, 1H), 3.82 (s, 2H), 3.58-3.55 (m, 1H), 2.84-2.76 (m, 2H).

Methyl 2-(2-(3,5-difluorobenzoyl)-1,2,3,4-tetrahydro-9*H*-pyrido[3,4-*b*]indol-9-yl) acetate (**C24**).

HRMS m/z: 385.13513$[M+H5]^+$. ^{1}H-NMR (400 MHz, DMSO). δ 7.46-7.40 (m, 3H), 7.35-7.26 (m, 2H), 7.18-7.10 (m, 1H), 7.07-7.03 (m, 1H), 5.15-4.96 (m, 2H), 4.80-4.55 (m, 2H), 3.96-3.56 (m, 5H), 2.78 (s, 2H).

Methyl 4-((2-(3,5-difluorobenzoyl)-1,2,3,4-tetrahydro-9*H*-pyrido[3,4-*b*]indol-9-yl) methyl)benzoate (**C25**).

HRMS m/z: 461.16635$[M+H]^+$. ^{1}H-NMR (400 MHz, DMSO). δ 7.93-7.74 (m, 2H), 7.50-7.38 (m, 2H), 7.25-6.94 (m, 7H), 5.56-5.34 (m, 2H), 4.76-4.43 (m, 2H), 3.95 (s, 1H), 3.83 (s, 3H), 3.59 (s, 1H), 2.80 (s, 2H).

Methyl 2-(2-(4-propylbenzoyl)-1,2,3,4-tetrahydro-9H-pyrido[3,4-b]indol-9-yl)acetate (**C26**).

HRMS m/z: 391.20087$[M+H]^+$. ^{1}H-NMR (400 MHz, DMSO). δ 7.46-7.39 (m, 4H), 7.31-7.29 (m, 2H), 7.13-7.10 (m, 1H), 7.06-7.03 (m, 1H), 5.13-4.95 (m, 2H), 4.87-4.77 (m, 2H), 3.91-3.52 (m, 5H), 2.79 (s, 2H), 2.63-2.60 (m, 2H), 1.67-1.58 (m, 2H), 0.92 (t, *J* = 4.0 Hz, 3H).

Methyl 4-((2-(4-propylbenzoyl)-1,2,3,4-tetrahydro-9*H*-pyrido[3,4-*b*]indol-9-yl) methyl)benzoate (**C27**).

HRMS m/z: 467.23260$[M+H]^+$. ^{1}H-NMR (400 MHz, DMSO). δ 7.91-7.76 (m, 2H), 7.47 (dd, *J* = 8.0, 7.6 Hz, 2H), 7.37-7.20 (m, 4H), 7.13-7.03 (m, 3H), 6.88 (s, 1H), 5.55-5.31 (m, 2H), 4.74-4.54 (m, 2H), 3.95 (s, 1H), 3.83 (s, 3H), 3.64 (s, 1H), 2.82 (s, 2H), 2.60 (s, 2H), 1.60 (s, 2H), 0.90 (s, 3H).

Methyl 2-(2-(2,5-difluorobenzoyl)-1,2,3,4-tetrahydro-9*H*-pyrido[3,4-*b*]indol-9-yl) acetate (**C28**).

HRMS m/z: 385.13501$[M+H5]^+$. ^{1}H-NMR (400 MHz, DMSO). δ 7.46-7.29 (m, 5H), 7.14-7.09 (m, 1H), 7.07-7.03 (m, 1H), 5.15-4.96 (m, 2H), 4.85-4.48 (m, 2H), 4.01-3.71 (m, 3H), 3.59-3.53 (m, 2H), 2.82-2.74 (m, 2H).

Methyl 2-(2-(2-chloro-6-fluorobenzoyl)-1,2,3,4-tetrahydro-9*H*-pyrido[3,4-*b*]indol-9- yl)acetate (**C29**).

HRMS m/z: 401.10547$[M+H5]^+$. ^{1}H-NMR (400 MHz, DMSO). δ 7.58-7.35 (m, 5H), 7.15-7.09 (m, 1H), 7.07-7.03 (m, 1H), 5.16-4.43 (m, 2H), 4.97-4.84 (m, 2H), 4.07-3.72 (m, 3H), 3.57-3.52 (m, 2H), 2.84-2.70 (m, 2H).

Preparation of **D1**and its' analogues: **D2-D29**

N-hydroxy-2-(2-(4-(trifluoromethyl)benzoyl)-1,2,3,4-tetrahydro-9*H*-pyrido[3,4-*b*]indol-9-yl)acetamide (**D1**).

Compound **C1** (0.14 g, 0.6 mmol) was dissolved in 14 mL of NH_2OK methanol solution. After 2 h of stiring, the solvent was evaporated under vacuum. The residue was acidified with saturated citric acid, and then extracted with EtOAc for 3 times. The organic layers were combined, washed with brine and dried over $MgSO_4$. The desired compound **D1** (0.33 g, 54%) was derived by crystallization in EtOAc as white powder. Purity of 98.51%. HRMS (AP-ESI) m/z calcd for $C_{21}H_{18}F_3N_3O_3$ $[M+H]^+$ 417.13003, found: 418.13672$[M+H]^+$. ^{1}H-NMR (400 MHz, DMSO). δ 10.91 (d, *J* = 60.28 Hz, 1H), 9.02 (d, *J* = 46.6 Hz, 1H), 7.87 (d, *J* = 7.6 Hz, 2H), 7.72 (d, *J* = 7.6 Hz, 2H), 7.45-7.34 (m, 2H), 7.13 (t, *J* = 8.0 Hz, 1H), 7.03 (t, *J* = 8.0 Hz, 1H), 5.06-4.81 (m, 2H), 4.71-4.47 (m, 2H), 4.00-3.58 (m, 2H), 2.78 (s, 2H). ^{13}C-NMR (400 MHz, DMSO). δ 169.26, 164.80, 137.52, 132.47, 128.12, 126.73, 126.14, 123.16, 121.54, 119.60, 118.22, 115.33, 109.91, 107.50, 45.78, 44.13, 21.92 ppm. HPLC (λ = 210 nm): $t_{R\ =}$ 15.343 $_{min}$ (CH_3CN/H_2O, 45:55).

N-hydroxy-4-((2-(4-(trifluoromethyl)benzoyl)-1,2,3,4-tetrahydro-9*H*-pyrido[3,4-*b*]indol-9-yl)methyl)benzamide (**D2**).

Purity of 96.32%. HRMS (AP-ESI) m/z calcd for $C_{27}H_{22}F_3N_3O_3$ $[M+H]^+$ 493.16133, found: 494.16742$[M+H]^+$. ^{1}H-NMR (400 MHz, DMSO). δ 11.28 (s, 1H), 9.07 (s, 1H), 7.87-7.60 (m, 5H), 7.58-7.39 (m, 3H), 7.15-6.82 (m, 4H), 5.51-5.25 (m, 2H), 4.83-4.54 (m, 2H), 4.02-3.59 (m, 2H), 2.87-2.81 (m, 2H). ^{13}C-NMR (400 MHz, DMSO). δ 169.29, 164.33, 141.75, 140.72, 137.06, 132.29, 131.78, 130.09, 128.13, 127.85, 126.75 (d, *J* = 12.6 Hz), 126.43, 126.08, 121.83, 119.66, 118.43, 110.25, 107.83, 60.23, 46.17, 45.73, 21.95 ppm HPLC (λ = 210 nm): $t_{R\ =}$ 15.497 $_{min}$ (CH_3CN/H_2O, 45:55).

2-(2-benzoyl-1,2,3,4-tetrahydro-9*H*-pyrido[3,4-*b*]indol-9-yl)-*N*-hydroxyacetamide (**D3**).

Purity of 95.50%. HRMS (AP-ESI) m/z calcd for $C_{20}H_{19}N_3O_3$ $[M+H]^+$ 349.14264, found: 350.14944$[M+H]^+$. ^{1}H-NMR (400 MHz, DMSO). δ 10.96 (s, 1H), 9.03 (s, 1H), 7.49-7.40 (m, 7H), 7.12 (t, *J* = 7.6 Hz, 1H), 7.03 (t, *J* = 7.2 Hz, 1H), 5.04-4.70 (m, 4H), 3.97-3.62 (m, 2H), 2.78 (s, 2H). ^{13}C-NMR (400 MHz, DMSO). δ 168.76, 164.80, 137.28, 132.74, 13018,

129.03, 127.22, 126.76, 121.49, 119.57, 118.21, 109.88, 107.42, 45.92, 44.10, 22.03 ppm. HPLC (λ = 210 nm): $t_{R\ =}$ 14.070 $_{min}$ (CH_3CN/H_2O, 45:55).

4-((2-benzoyl-1,2,3,4-tetrahydro-9*H*-pyrido[3,4-*b*]indol-9-yl) methyl)-*N*-hydroxybenzamide (**D4**).

Purity of 97.87%. HRMS (AP-ESI) m/z calcd for $C_{26}H_{23}N_3O_3$ $[M+H]^+$ 425.17394, found: 426.1805$[M+H]^+$. ^{1}H-NMR (400 MHz, DMSO). δ 11.15 (s, 1H), 9.02 (s, 1H), 7.68-7.29 (m, 9H), 7.14-6.85 (m, 4H), 5.50-5.22 (m, 2H), 4.79-4.56 (m, 2H), 3.98-3.63 (m, 2H), 2.81 (m, 2H). ^{13}C-NMR (400 MHz, DMSO). δ 170.69, 164.34, 141.78, 137.04, 136.62, 132.20 (d, *J* = 28.1 Hz), 130.15, 129.00, 127.76, 127.20, 126.83, 126.72, 121.79, 119.63, 118.43, 110.21, 46.14, 45.79, 22.04 ppm. HPLC (λ = 210 nm): $t_{R\ =}$ 15.087 $_{min}$ (CH_3CN/H_2O, 45:55).

N-hydroxy-2-(2-(2-(trifluoromethyl)benzoyl)-1,2,3,4-tetrahydro-9*H*-pyrido[3,4-*b*]indol-9-yl)acetamide (**D5**).

Purity of 99.27%. HRMS (AP-ESI) m/z calcd for $C_{21}H_{18}F_3N_3O_3$ $[M+H]^+$ 417.13003, found: 418.13388$[M+H]^+$. ^{1}H-NMR (400 MHz, DMSO). δ 10.99 (s, 1H), 9.09 (s, 1H), 7.88 (d, *J* = 8.0 Hz, 1H), 7.80 (t, *J* = 8.0 Hz, 1H), 7.74-7.67 (m, 1H), 7.58-7.57 (m, 1H), 7.47-7.33 (m, 2H), 7.12(q, *J* = 8.0 Hz, 1H), 7.03 (t, *J* = 8.0 Hz, 1H), 5.15-5.06 (m, 1H), 4.78-4.72 (m, 2H), 4.60-4.14 (m, 1H), 3.86-3.38 (m, 2H), 2.82-2.60 (m, 2H). ^{13}C-NMR (400 MHz, DMSO). δ 167.62, 164.75, 137.29, 135.43, 133.47 (d, *J* = 14.9 Hz), 132.19, 130.08 (d, *J* = 13.2 Hz), 127.76 (d, *J* = 12.1 Hz), 127.12 (d, *J* = 3.4 Hz), 126.65, 125.85-125.55 (m), 122.93, 121.54, 119.58, 118.27 (d, *J* = 11.6 Hz), 109.93, 107.20, 60.24, 45.31, 44.13, 21.46 ppm. HPLC (λ = 210 nm): $t_{R\ =}$ 14.690 $_{min}$ (CH_3CN/H_2O, 45:55).

N-hydroxy-4-((2-(2-(trifluoromethyl)benzoyl)-1,2,3,4-tetrahydro-9*H*-pyrido[3,4-*b*]indol-9-yl)methyl)benzamide (**D6**).

Purity of 97.92%. HRMS (AP-ESI) m/z calcd for $C_{27}H_{22}F_3N_3O_3$ $[M+H]^+$ 493.16133, found: 494.16602$[M+H]^+$. ^{1}H-NMR (400 MHz, DMSO). δ 11.18 (s, 1H), 9.05 (d, *J* = 9.6 Hz, 1H), 7.88-7.71 (m, 4H), 7.69-7.52 (m, 2H), 7.48-7.32 (m, 2H), 7.16-6.78 (m, 4H), 5.52-4.36 (m, 4H), 4.21-3.41 (m, 2H), 2.85-2.63 (m, 2H). ^{13}C-NMR (400 MHz, DMSO). δ 167.59, 164.40, 141.54 (d, *J* = 24.0 Hz), 137.06 (d, *J* = 5.0 Hz), 135.01 (d, *J* = 35.6 Hz), 133.38 (d, *J* = 24.5 Hz), 132.17 (d, *J* = 35.0 Hz), 131.40 (d, *J* = 20.0 Hz), 129.99(d, *J* = 32.3 Hz), 127.82 (d, *J* = 5.4 Hz), 127.46 (d, *J* = 25.4 Hz), 127.11 (d, *J* = 4.3 Hz), 126.88, 126.63(d, *J* = 5.2 Hz), 126.40, 125.87-125.55 (m), 121.84, 119.63 (d, *J* = 5.8 Hz), 118.46 (d, *J* = 7.5 Hz), 110.18 (d, *J* = 15.1 Hz), 108.1, 107.66, 60.23, 46.08 (d, *J* = 17.8 Hz), 45.06 (d, *J* = 34.0 Hz), 21.19 (d, *J* = 59.0 Hz) ppm. HPLC (λ = 210 nm): $t_{R\ =}$ 16.023 $_{min}$ (CH_3CN/H_2O, 45:55).

N-hydroxy-4-((2-(2-methoxybenzoyl)-1,2,3,4-tetrahydro-9*H*-pyrido[3,4-*b*]indol-9-yl)methyl)benzamide (**D7**).

Purity of 98.27%. HRMS (AP-ESI) m/z calcd for $C_{27}H_{25}N_3O_4$ $[M+H]^+$ 455.18451, found: 456.19095$[M+H]^+$. ^{1}H-NMR (400 MHz, DMSO). δ 11.15 (s, 1H), 9.01 (s, 1H), 7.70-7.54 (m, 2H), 7.50-7.30 (m, 3H), 7.22 (d, *J* = 8.0 Hz, 1H), 7.16-7.01 (m, 5H), 6.97-6.85 (m, 1H), 5.49-5.19 (m, 1H), 4.85-4.28 (m, 2H), 4.15-3.62 (m, 2H), 3.80-3.62 (m, 3H), 3.47 (d, *J* = 8.0 Hz, 2H), 2.80-2.69 (m, 2H). ^{13}C-NMR (400 MHz, DMSO). δ 167.87 (d, *J* = 37.5 Hz), 164.28 (d, *J* = 26.1 Hz), 155.29 (d, *J* = 34.8 Hz), 141.54 (d, *J* = 47.9 Hz), 137.02 (d, *J* = 7.6 Hz), 132.26 (d, *J* = 22.1 Hz), 132.03, 130.91, 128.05, 127.80, 126.92, 126.68 (d, *J* = 6.0 Hz), 126.26, 121.74, 121.16, 119.58, 118.41, 111.89, 110.15 (d, *J* = 5.9 Hz), 108.46, 107.93, 60.24, 55.92, 46.17, 44.95, 21.58 ppm. HPLC (λ = 210 nm): $t_{R\ =}$ 14.790 $_{min}$ (CH_3CN/H_2O, 45:55).

N-hydroxy-2-(2-(2-methoxybenzoyl)-1,2,3,4-tetrahydro-9*H*-pyrido[3,4-*b*]indol-9-yl) acetamide (**D8**).

Purity of 98.39%. HRMS (AP-ESI) m/z calcd for $C_{21}H_{21}N_3O_4$ $[M+H]^+$ 379.15321, found: 380.15985$[M+H]^+$. ^{1}H-NMR (400 MHz, DMSO). δ 10.92 (s, 1H), 9.02 (s, 1H), 7.47-7.43 (m, 3H), 7.38-7.31 (m, 1H), 7.12(t, *J* = 7.6 Hz, 1H), 7.05-7.01 (m, 3H), 4.83-4.65 (m, 4H), 3.82 (s, 3H), 3.73 (s, 2H), 2.80 (s, 2H). ^{13}C-NMR (400 MHz, DMSO). δ 170.53, 164.69, 160.83, 140.43, 137.22, 134.46, 132.92, 129.43, 128.58, 126.78, 123.40, 121.46, 119.55, 118.21, 114.23, 109.85, 107.74, 60.23, 55.74, 44.09, 21.87, 14.53 ppm. HPLC (λ = 210 nm): $t_{R\ =}$ 13.877 $_{min}$ (CH_3CN/H_2O, 45:55).

N-hydroxy-4-((2-(4-methoxybenzoyl)-1,2,3,4-tetrahydro-9*H*-pyrido[3,4-*b*]indol-9-yl)methyl)benzamide (**D9**).

Purity of 95.09%. HRMS (AP-ESI) m/z calcd for $C_{27}H_{25}N_3O_4$ $[M+H]^+$ 455.18451, 456.19104$[M+H]^+$. ^{1}H-NMR (400 MHz, DMSO). δ 11.15 (s, 1H), 9.01 (s, 1H), 7.65 (s, 2H), 7.50-7.43 (m, 4H), 7.15-6.99 (m, 6H), 5.45 (s, 2H), 4.72 (s, 2H), 3.81-3.73 (m, 5H), 2.83 (m, 2H). ^{13}C-NMR (400 MHz, DMSO). δ 171.74, 164.36, 160.79, 141.68, 137.03, 132.25, 129.35, 128.40, 127.74, 126.75, 121.77, 119.62, 118.43, 114.17, 110.19, 108.11, 55.71, 46.11, 44.52, 21.95 ppm. HPLC (λ = 210 nm): $t_{R\ =}$ 14.917 $_{min}$ (CH_3CN/H_2O, 45:55).

2-(2-(4-fluorobenzoyl)-1,2,3,4-tetrahydro-9*H*-pyrido[3,4-*b*] indol-9-yl)-*N*-hydroxyacetamide (**D10**).

Purity of 95.65%. HRMS (AP-ESI) m/z calcd for $C_{20}H_{18}FN_3O_3$ $[M+H]^+$ 367.13322, found: 368.13782$[M+H]^+$. ^{1}H-NMR (400 MHz, DMSO). δ 10.98 (s, 1H), 9.08 (s, 1H), 7.58-7.56 (m, 2H), 7.45-7.40 (m, 2H), 7.34-7.32 (m, 2H), 7.12 (t, *J* = 7.6 Hz, 1H), 7.05-7.02 (m, 1H), 5.05-4.87 (m, 2H), 4.76-4.48 (m, 2H), 3.96-3.62 (m, 2H), 2.79 (s, 2H). ^{13}C-NMR (400 MHz, DMSO). δ 169.76, 164.56 (d, *J* = 36.6 Hz), 161.92, 137.22, 133.07, 129.93, 126.75, 121.51, 119.58, 118.22, 115.99 (d, *J* = 21.7 Hz), 109.87, 107.45.96, 44.10, 21.98 ppm. HPLC (λ = 210 nm): $t_{R\ =}$ 14.390 $_{min}$ (CH_3CN/H_2O, 45:55).

4-((2-(4-fluorobenzoyl)-1,2,3,4-tetrahydro-9*H*-pyrido[3,4-*b*] indol-9-yl)methyl)-*N*-hydroxybenzamide(**D11**).

Purity of 98.60%. HRMS (AP-ESI) m/z calcd for $C_{26}H_{22}FN_3O_3$ $[M+H]^+$ 443.16452, found: 444.16885$[M+H]^+$. ^{1}H-NMR (400 MHz, DMSO). δ 11.18 (s, 1H), 9.04 (s, 1H), 7.69-7.55 (m, 3H), 7.49-7.31 (m, 4H), 7.13-7.03 (m, 3H), 9.04 (s, 2H), 5.50-5.25 (m, 2H), 4.78-4.57 (m, 2H), 3.97-3.63 (m, 2H), 2.82 (s, 2H). ^{13}C-NMR (400 MHz, DMSO). δ 169.79, 164.33, 161.87, 141.76, 137.05, 132.63 (d, *J* = 67.1 Hz), 132.00, 129.88 (d, *J* = 8.5 Hz), 127.77, 126.79, 126.71, 121.81, 119.64, 118.43, 115.96 (d, *J* = 21.4 Hz), 110.21, 107.92, 60.24, 46.12, 21.62 (d, *J* = 76.9 Hz), 14.56 ppm. HPLC (λ = 210 nm): $t_{R\ =}$ 15.263 $_{min}$ (CH_3CN/H_2O, 45:55).

2-(2-(3-fluorobenzoyl)-1,2,3,4-tetrahydro-9*H*-pyrido[3,4-*b*]indol-9-yl)-*N*-hydroxyacetamide (**D12**).

Purity of 97.51%. HRMS (AP-ESI) m/z calcd for $C_{20}H_{18}FN_3O_3$ $[M+H]^+$ 367.13322, found: 368.13693$[M+H]^+$. ^{1}H-NMR (400 MHz, DMSO). δ 10.95 (s, 1H), 9.04 (s, 1H), 7.54 (s, 1H), 7.45-7.32 (m, 5H), 7.12 (t, *J* = 7.2, 1H), 7.05-7.02 (m, 1H), 5.05-4.46 (m, 4H), 3.97-3.60(m, 2H), 2.78 (s, 2H). ^{13}C-NMR (400 MHz, DMSO). δ 169.12, 164.73, 162.39 (d, *J* = 245.2 Hz), 139.06, 137.23, 132.52, 131.31, 126.73, 123.25, 121.51, 119.58, 118.23, 117.04 (d, *J* = 19.46 Hz), 114.30 (d, *J* = 22.17 Hz), 109.86, 107.44, 45.78, 44.10, 21.92 ppm. HPLC (λ = 210 nm): $t_{R\ =}$ 14.407 $_{min}$ (CH_3CN/H_2O, 45:55).

4-((2-(3-fluorobenzoyl)-1,2,3,4-tetrahydro-9*H*-pyrido[3,4-*b*]indol-9-yl)methyl)-*N*-hydroxybenzamide(**D13**).

Purity of 96.92%. HRMS (AP-ESI) m/z calcd for $C_{26}H_{22}FN_3O_3$ $[M+H]^+$ 443.16452, found: 444.17139$[M+H]^+$. ^{1}H-NMR (400 MHz, DMSO).δ 11.15 (s, 1H), 9.01 (s, 1H), 7.69-7.55 (m, 3H), 7.53-7.45 (m, 2H), 7.34-7.20 (m, 3H), 7.19-7.03 (m, 2H), 6.88 (s, 2H), 5.50-5.24 (m, 2H), 4.79-4.54 (m, 2H), 3.98-3.61 (m, 2H), 2.81 (s, 2H). ^{13}C-NMR (400 MHz, DMSO). δ 169.14, 164.38, 162.35 (d, *J* = 246.2 Hz), 141.78, 138.90, 137.04, 132.31, 131.85, 131.29, 127.76, 126.84, 126.69, 123.26, 121.81, 119.63, 118.45, 117.03 (d, *J* = 21.0 Hz), 114.28 (d, *J* = 23.2 Hz), 110.21, 107.92, 60.24, 45.93 (d, *J* = 41.3 Hz), 21.60 (d, *J* = 71.3 Hz), 14.56 ppm. HPLC (λ = 210 nm): $t_{R\ =}$ 15.183 $_{min}$ (CH_3CN/H_2O, 45:55).

2-(2-(2-fluorobenzoyl)-1,2,3,4-tetrahydro-9*H*-pyrido[3,4-*b*]indol-9-yl)-*N*-hydroxyacetamide (**D14**).

Purity of 98.35%. HRMS (AP-ESI) m/z calcd for $C_{20}H_{18}FN_3O_3$ $[M+H]^+$ 367.13322, found: HRMS m/z: 368.13776$[M+H]^+$. ^{1}H-NMR (400 MHz, DMSO). δ 10.87 (d, *J* =63.3 Hz, 1H), 8.99 (d, *J* = 48.9 Hz, 1H), 7.58-7.28 (m, 6H), 7.14-7.09 (m, 1H), 7.05-7.01 (m, 1H), 5.04-4.44 (m, 4H), 4.00-3.54 (m, 2H), 2.81 (s, 2H). ^{13}C-NMR (400 MHz, DMSO). δ 165.55, 164.74, 158.19 (d, *J* = 245.3 Hz), 137.25, 132.40, 132.01 (d, *J* = 8.2 Hz), 129.17, 126.64, 125.53 (d, *J* = 3.0 Hz), 124.86 (d, *J* = 18.1 Hz), 121.52, 119.58, 118.20, 116.38 (d, *J* = 21.0 Hz), 109.93, 107.28, 45.32, 44.13, 21.93 ppm. HPLC (λ = 210 nm): $t_{R\ =}$ 14.300 $_{min}$ (CH_3CN/H_2O, 45:55).

4-((2-(2-fluorobenzoyl)-1,2,3,4-tetrahydro-9*H*-pyrido[3,4-*b*]indol-9-yl)methyl)-*N*-hydroxybenzamide (**D15**).

Purity of 98.13%. HRMS (AP-ESI) m/z calcd for $C_{26}H_{22}FN_3O_3$ $[M+H]^+$ 443.16452, found: 444.16870$[M+H]^+$. ^{1}H-NMR (400 MHz, DMSO). δ 11.17 (s, 1H), 9.04 (d, *J* = 13.6 Hz, 1H), 7.70-7.52 (m, 3H), 7.51-7.31 (m, 4H), 7.26-6.83 (m, 5H), 5.50-5.24 (m, 2H), 4.86-4.43 (m, 2H), 4.04-3.55 (m, 2H), 2.84-2.75 (m, 2H). ^{13}C-NMR (400 MHz, DMSO). δ 165.58, 164.40, 158.18 (d, *J* = 244.2 Hz), 141.54 (d, *J* =41.4 Hz), 137.06, 132.36, 132.03 (d, *J* = 8.0 Hz), 131.74, 128.98 (d, *J* = 30.4 Hz), 127.73 (d, *J* = 15.9 Hz), 126.90, 126.56 (d, *J* = 15.6 Hz), 125.52-124.65 (m), 121.84, 119.65, 118.47 (d, *J* = 8.1 Hz), 116.38 (d, *J* = 21.0 Hz), 110.20 (d, *J* = 8.7 Hz), 108.50, 107.76, 60.24, 46.12 (d, *J* = 14.4 Hz), 44.92 (d, *J* = 70.6 Hz), 21.52(d, *J* = 89.7 Hz) ppm. HPLC (λ = 210 nm): $t_{R\ =}$ 15.110 $_{min}$ (CH_3CN/H_2O, 45:55).

N-hydroxy-2-(2-(2-methylbenzoyl)-1,2,3,4-tetrahydro-9*H*-pyrido[3,4-*b*]indol-9-yl)acetamide (**D16**).

Purity of 95.42%. HRMS (AP-ESI) m/z calcd for $C_{21}H_{21}N_3O_3$ $[M+H]^+$ 363.15829, found: 364.16382$[M+H]^+$. ^{1}H NMR (400 MHz, DMSO). δ 10.90 (d, *J* = 71.4 Hz, 1H), 9.02 (d, *J* = 54.2 Hz, 1H), 7.47-7.16 (m, 6H), 7.14-7.11 (m, 1H), 7.05-7.01 (m, 1H), 5.11-4.71 (m, 3H), 4.51-4.39 (m, 1H), 3.73-3.47 (m, 2H), 2.82-2.66 (m, 2H), 2.25-2.13 (m, 3H). ^{13}C-NMR (400 MHz, DMSO). δ 170.08, 164.75, 137.20 (d, *J* = 11.8 Hz), 134.22, 132.70, 130.73, 129.23, 126.70, 126.41, 125.95, 121.48, 119.55, 118.19, 109.91, 107.26, 44.85, 44.13, 21.92, 21.20, 19.06 ppm. HPLC (λ = 210 nm): $t_{R\ =}$ 14. 923 min (CH_3CN/H_2O, 45:55).

N-hydroxy-4-((2-(2-methylbenzoyl)-1,2,3,4-tetrahydro-9*H*-pyrido[3,4-*b*]indol-9-yl) methyl)benzamide (**D17**).

Purity of 95.30%. HRMS (AP-ESI) m/z calcd for $C_{27}H_{25}N_3O_3$ $[M+H]^+$ 439.18959, found: 440.19635$[M+H]^+$. ^{1}H-NMR (400 MHz, DMSO). δ 11.20 (s, 1H), 9.03 (d, *J* = 9.2 Hz, 1H), 7.71-7.56 (m, 2H), 7.51-7.44 (m, 2H), 7.37-7.22 (m, 3H), 7.20-7.00 (m, 3H), 6.80-6.78 (d, *J* = 8.0 HZ, 2H), 5.51-5.02 (m, 3H), 4.98 -4.20 (m, 2H), 3.74-3.48 (m, 2H), 2.84-2.68 (m, 2H), 2.23 (s, 2H). ^{13}C-NMR (400 MHz, DMSO). δ 170.10, 164.38, 141.52 (d, *J* = 53.3 H), 137.03 (d, *J* = 4.4 Hz), 136.68, 133.92 (d, *J* = 62.5 Hz), 132.33, 132.04 (d, *J* = 5.3 HZ), 130.63 (d, *J* = 16.1 HZ), 129.11 (d, *J* = 26.9 HZ), 127.73 (d, *J* = 14.4 HZ), 126.78 (d, *J* = 18.4 Hz), 126.37 (d, *J* = 7.1 Hz), 125.75 (d, *J* = 46.3 Hz), 121.82 (d, *J* = 7.1 Hz), 119.61, 118.46 (d, *J* = 11.4 Hz), 110.18 (d, *J* = 7. Hz), 108.48, 107.71, 46.09 (d, *J* = 17.7 Hz), 44.81, 44.42, 21.53 (d, *J* = 83.4 Hz), 18.84 (d, *J* = 41.1 Hz) ppm. HPLC (λ = 210 nm): $t_{R\ =}$ 15.820 $_{min}$ (CH_3CN/H_2O, 45:55).

2-(2-(4-ethylbenzoyl)-1,2,3,4-tetrahydro-9*H*-pyrido[3,4-*b*]indol-9-yl)-*N*-hydroxyacetamide (**D18**).

Purity of 97.92%. HRMS (AP-ESI) m/z calcd for $C_{22}H_{23}N_3O_3$ $[M+H]^+$ 377.17394, found: 378.18045$[M+H]^+$. ^{1}H-NMR (400 MHz, DMSO). δ 10.96 (s, 1H), 9.06 (s, 1H), 7.45-7.41 (m, 4H), 7.34-7.32 (d, *J* = 7.6 Hz, 2H), 7.14-7.11 (m, 1H), 7.06-7.02 (m, 1H), 5.04-4.70 (m, 4H), 3.95-3.64 (m, 2H), 2.79 (s, 2H), 2.68 (dd, *J* = 15.2, 7.6 Hz, 2H), 1.23 (t, *J* = 7.6 Hz, 3H). ^{13}C-NMR (400 MHz, DMSO). δ 170.74, 164.72, 146.06, 137.23, 134.03, 132.81, 128.32, 127.47, 126.77, 121.47, 119.56, 118.21, 109.87, 107.45.90, 44.10, 28.49, 22.04, 15.87 ppm. HPLC (λ = 210 nm): $t_{R\ =}$ 15.897 $_{min}$ (CH_3CN/H_2O, 45:55).

4-((2-(4-ethylbenzoyl)-1,2,3,4-tetrahydro-9*H*-pyrido[3,4-*b*]indol-9-yl)methyl)-*N*-hydroxybenzamide (**D19**).

Purity of 98.88%. HRMS (AP-ESI) m/z calcd for $C_{28}H_{27}N_3O_3$ $[M+H]^+$ 453.20524, found: 454.21204$[M+H]^+$. ^{1}H-NMR (400 MHz, DMSO). δ 11.15 (s, 1H), 9.01 (s, 1H), 7.67 (s, 2H), 7.50-7.46 (m, 2H), 7.44-7.39 (m, 3H), 7.13-6.85 (m, 5H), 5.50-5.26 (m, 2H), 4.77-4.61 (m, 2H), 3.97-3.65 (m, 2H), 2.82 (s, 2H), 2.68-2.65 (m, 2H), 1.21-1.16 (m, 3H). ^{13}C-NMR (400 MHz, DMSO). δ 170.82, 164.38, 146.03, 141.74, 137.04, 133.91, 132.14, 128.29, 127.75, 127.41, 126.73, 121.78, 119.62, 118.42, 110.20, 108.02, 60.24, 46.12, 28.46, 22.08, 21.24, 15.82 ppm. HPLC (λ = 210 nm): $t_{R\ =}$ 17.653 $_{min}$ (CH_3CN/H_2O, 45:55).

4-((2-(2-chlorobenzoyl)-1,2,3,4-tetrahydro-9*H*-pyrido[3,4-*b*]indol-9-yl)methyl)-*N*-hydroxybenzamide (**D20**).

Purity of 99.27%. HRMS (AP-ESI) m/z calcd for $C_{26}H_{22}ClN_3O_3$ $[M+H]^+$ 459.13497, found: 460.13953$[M+H]^+$. ^{1}H-NMR (400 MHz, DMSO) δ 11.16 (s, 1H), 9.03 (d, *J* = 10.3 Hz, 1H), 7.69 (d, *J* = 8.0 HZ, 1H), 7.59-7.55 (m, 1H), 7.52-7.42 (m, 4H), 7.34-7.21 (m, 3H), 7.16-7.02 (m, 2H), 6.83 (d, *J* = 8.0 HZ, 1H), 5.51-5.15 (m, 2H), 4.96-4.25 (m, 2H), 3.87-3.48 (m, 2H), 2.85-2.73 (m, 2H). ^{13}C-NMR (400 MHz, DMSO). δ 167.07, 166.66, 137.06, 136.19 (d, *J* = 37.9 Hz), 131.71, 130.96 (d, *J* = 31.6 Hz), 129.67 (d, *J* = 21.1 Hz), 128.27 (d, *J* = 15.8 Hz), 127.71 (d, *J* = 16.3 Hz), 126.90, 126.54 (d, *J* = 15.9 Hz), 121.83, 119.64, 118.46 (d, *J* = 8.5 Hz), 110.17 (d, *J* = 12.5 Hz), 108.43, 107.74, 46.18, 44.60 (d, *J* = 65.3 Hz), 21.90, 21.10 ppm. HPLC (λ = 210 nm): $t_{R\ =}$ 14.690 $_{min}$ (CH_3CN/H_2O, 45:55).

2-(2-(3-bromobenzoyl)-1,2,3,4-tetrahydro-9*H*-pyrido[3,4-*b*]indol-9-yl)-*N*-hydroxyacetamide (**D21**).

Purity of 97.53%. HRMS (AP-ESI) m/z calcd for $C_{20}H_{18}BrN_3O_3$ $[M+H]^+$ 427.05315, found: 428.05792$[M+H]^+$. ^{1}H-NMR (400 MHz, DMSO). δ 10.92 (d, *J* = 47.3 Hz, 1H), 9.03 (d, *J* = 38.0 Hz, 1H), 7.76-7.67 (m, 2H), 7.49-7.34 (m, 4H), 7.14-7.11 (m, 1H), 7.05-7.02 (m, 1H), 5.05-4.77 (m, 2H), 4.70-4.47 (m, 2H), 3.96-3.60 (m, 2H), 2.77 (s, 2H). ^{13}C-NMR (400 MHz, DMSO). δ 139.22, 138.25, 133.01, 131.39, 130.10, 126.72, 122.43, 121.52, 119.59, 118.25, 109.92, 107.34, 55.77, 44.11, 21.95 ppm. HPLC (λ = 210 nm): $t_{R\ =}$ 15.120 $_{min}$ (CH_3CN/H_2O, 45:55).

4-((2-(3-bromobenzoyl)-1,2,3,4-tetrahydro-9*H*-pyrido[3,4-*b*]indol-9-yl)methyl)-*N*-hydroxybenzamide (**D22**).

Purity of 97.45%. HRMS (AP-ESI) m/z calcd for $C_{26}H_{22}BrN_3O_3$ $[M+H]^+$ 503.08445, found: 504.08893$[M+H]^+$. ^{1}H-NMR (400 MHz, DMSO). δ 11.15 (s, 1H), 9.01 (s, 1H), 7.68 (d, J = 8.4 HZ, 3H), 7.59 (s, 1H), 7.49-7.26 (m, 4H), 7.14-6.91 (m, 4H), 5.50-5.25 (m, 2H), 4.79-4.55 (m, 2H), 3.97-3.61 (m, 2H), 2.81 (s, 2H). ^{13}C-NMR (400 MHz, DMSO). δ 168.91, 164.39, 141.83, 138.94, 137.04, 132.97, 132.31, 131.83, 129.89, 127.77, 126.82, 126.68, 126.12, 122.26, 121.82, 119.63, 118.45, 110.21, 107.87, 108, 46.14, 45.77, 21.95 ppm. HPLC (λ = 210 nm): $t_{R\ =}$ 16.097 $_{min}$ (CH_3CN/H_2O, 45:55).

4-((2-(2,4-difluorobenzoyl)-1,2,3,4-tetrahydro-9*H*-pyrido[3,4-*b*]indol-9-yl)methyl)-*N*-hydroxybenzamide (**D23**).

Purity of 95.67%. HRMS (AP-ESI) m/z calcd for $C_{26}H_{21}F_2N_3O_3$ $[M+H]^+$ 461.15510, found: HRMS m/z: 462.16037$[M+H]^+$. ^{1}H-NMR (400 MHz, DMSO). δ 11.16 (s, 1H), 9.02 (s, 1H), 7.70-7.53 (m, 2H), 7.50-7.33 (m, 3H), 7.24-7.03 (m, 4H), 6.98-6.65 (m, 1H), 5.54-5.28 (m, 2H), 4.84-4.34 (m, 2H), 3.39-3.56 (m, 2H), 2.84 (m, 2H). ^{13}C-NMR (400 MHz, DMSO). δ 164.66 (d, *J* = 42.5 Hz), 161.99 (d, *J* = 12.3 Hz), 159.90 (d, *J* = 12.3 Hz), 157.44 (d, *J* = 12.7 Hz), 141.60 (d, *J* = 26.1 Hz), 137.06, 132.25 (d, *J* = 18.6 Hz), 131.68, 127.71(d, *J* = 18.6 Hz), 126.89, 126.55 (d, *J* = 15.0 Hz), 121.85, 121.32 (d, *J* = 18.5 Hz), 119.66, 118.48 (d, *J* = 7.8 Hz), 112.74 (d, *J* = 17.5 Hz), 110.23, 108.46, 107.76, 105.05 (d, *J* = 17.4 Hz), 46.09 (d, *J* = 18.2 Hz), 45.34, 44.61, 21.51 (d, *J* = 94.3 Hz) ppm. HPLC (λ = 210 nm): $t_{R\ =}$ 16.067 $_{min}$ (CH_3CN/H_2O, 45:55).

2-(2-(3,5-difluorobenzoyl)-1,2,3,4-tetrahydro-9*H*-pyrido[3,4-*b*]indol-9-yl)-*N*-hydroxyacetamide (**D24**).

Purity of 95.49%. HRMS (AP-ESI) m/z calcd for $C_{20}H_{17}F_2N_3O_3$ $[M+H]^+$ 385.12380, found: 386.12924$[M+H]^+$. ^{1}H-NMR (400 MHz, DMSO). δ 10.92 (d, *J* = 50.0 Hz, 1H), 9.03 (d, *J* = 39.1 Hz, 1H), 7.45-7.33 (m, 3H), 7.27-7.26 (m, 2H), 7.12 (t, *J* = 7.2 Hz, 1H), 7.05-7.02 (m, 1H), 5.05-4.78 (m, 2H), 4.70-4.49 (m, 2H), 3.96-3.59 (m, 2H), 2.77 (s, 2H). ^{13}C-NMR (400 MHz, DMSO). δ 167.91, 164.75, 161.51, 137.23, 137.50 (d, *J* = 40.0 Hz), 130.75, 126.70, 121.53, 119.59, 118.27, 110.71 (d, *J* = 26.5 Hz), 109.87, 107.48, 45.70, 44.11, 21.83 ppm. HPLC (λ = 210 nm): $t_{R\ =}$ 14.477 $_{min}$ (CH_3CN/H_2O, 45:55).

4-((2-(3,5-difluorobenzoyl)-1,2,3,4-tetrahydro-9*H*-pyrido[3,4-*b*]indol-9-yl)methyl)-*N*-hydroxybenzamide (**D25**).

Purity of 95.87%. HRMS (AP-ESI) m/z calcd for $C_{26}H_{21}F_2N_3O_3$ $[M+H]^+$ 461.15510, found: 462.15964$[M+H]^+$. ^{1}H-NMR (400 MHz, DMSO). δ 11.16 (s, 1H), 9.01 (s, 1H), 7.70-7.57 (m, 2H), 7.49-7.40 (m, 3H), 7.26-6.93 (s, 2H), 7.24-7.03 (m, 4H), 5.50-5.27 (m, 2H), 4.79-4.54 (m, 2H), 3.97-3.59 (m, 2H), 2.80 (s, 2H). ^{13}C-NMR (400 MHz, DMSO). δ 167.94, 164.37, 164.01 (d, *J* = 11.5 Hz), 161.54 (d, *J* = 12.0 Hz),141.77, 140.15, 137.06, 132.33, 131.62, 127.78, 126.85, 126.67, 121.83, 119.64, 118.46, 110.71 (d, *J* = 26.6 Hz), 110.21, 107.97, 105.60, 105.50 (d, *J* = 51.5 Hz), 60.24, 45.91 (d, *J* = 47.8 Hz), 21.55 (d, *J* = 64.1 Hz), 14.55 ppm. HPLC (λ = 210 nm): $t_{R\ =}$ 15. 933 min (CH_3CN/H_2O, 45:55).

N-hydroxy-2-(2-(4-propylbenzoyl)-1,2,3,4-tetrahydro-9*H*-pyrido[3,4-*b*]indol-9-yl)acetamide (**D26**).

Purity of 98.35%. HRMS (AP-ESI) m/z calcd for $C_{23}H_{25}N_3O_3$ $[M+H]^+$ 391.1859, found: 392.19434$[M+H]^+$. ^{1}H-NMR (400 MHz, DMSO). δ 10.97 (s, 1H), 9.07 (s, 1H), 7.45-7.40 (m, 4H), 7.31-7.30 (m, 2H), 7.12 (t, *J* = 8.0 Hz, 1H), 7.05-7.02 (m, 1H), 5.04-4.85 (m, 2H), 4.69-4.47 (m, 2H), 3.94-3.63 (m, 2H), 2.78 (s, 2H), 2.62 (t, *J* = 8.0 Hz, 2H), 1.68-1.58 (m, 2H), 0.92 (t, *J* = 8.0 Hz, 3H). ^{13}C-NMR (400 MHz, DMSO). δ 170.81, 164.72, 144.47, 137.23, 134.05, 132.81, 128.88, 127.38, 126.77, 121.46, 119.55, 118.21, 109.87, 107.46, 60.23, 45.89, 44.10, 37.52, 24.37, 21.62 (d, *J* = 76.9 Hz), 14.14 ppm. HPLC (λ = 210 nm): $t_{R\ =}$ 16.550 $_{min}$ (CH_3CN/H_2O, 45:55).

N-hydroxy-4-((2-(4-propylbenzoyl)-1,2,3,4-tetrahydro-9*H*-pyrido[3,4-*b*]indol-9-yl)methyl)benzamide (**D27**).

Purity of 99.31%. HRMS (AP-ESI) m/z calcd for $C_{29}H_{29}N_3O_3$ $[M+H]^+$ 467.22089, found: 468.22525$[M+H]^+$. ^{1}H-NMR (400 MHz, DMSO). δ 11.15 (s, 1H), 9.01 (s, 1H), 7.67 (s, 2H), 7.49-7.43 (s, 2H), 7.38-7.29 (m, 3H), 7.12-6.85 (m, 5H), 5.49-5.24 (m, 2H), 4.77-4.59 (m, 2H), 3.96-3.64 (m, 2H), 2.82 (s, 2H), 2.60 (s, 2H), 1.60 (s, 2H), 0.90 (s, 3H). ^{13}C-NMR (400 MHz, DMSO). δ 170.82, 164.34, 144.44, 141.75, 137.03, 133.93, 132.27, 132.13, 128.85, 127.75, 127.31, 126.78, 121.78, 119.62, 118.43, 110.19, 107.74, 60.24, 45.99 (d, *J* = 24.6 Hz),37.48, 24.34, 21.65 (d, *J* = 83.3 Hz), 14.56, 14.11 ppm. HPLC (λ = 210 nm): $t_{R\ =}$ 17.960 $_{min}$ (CH_3CN/H_2O, 45:55).

2-(2-(2,5-difluorobenzoyl)-1,2,3,4-tetrahydro-9*H*-pyrido[3,4-*b*]indol-9-yl)-*N*-hydroxyacetamide (**D28**).

Purity of 95.86%. HRMS (AP-ESI) m/z calcd for $C_{20}H_{17}F_2N_3O_3$ $[M+H]^+$ 385.12380, found: 386.13004$[M+H]^+$. ^{1}H-NMR (400 MHz, DMSO). δ 10.91 (d, *J* = 56.9 Hz, 1H), 9.03 (d, *J* = 43.9 Hz, 1H), 7.47-7.35 (m, 5H), 7.15-7.10 (m, 1H), 7.04 (t, *J* = 8.0 Hz, 1H), 5.05-4.83 (m, 2H), 4.71-4.48 (m, 2H), 4.00-3.57 (m, 2H), 2.74 (s, 2H). ^{13}C-NMR (400 MHz, DMSO). δ 164.73, 164.31 (d, *J* = 29.9 Hz), 158.63 (d, *J* = 242.3 Hz), 154.36 (d, *J* = 240.8 Hz), 137.25, 132.19, 126.63, 126.20 (d, *J* = 10.8 Hz), 121.56, 118.28 (d, *J* = 8.8 Hz), 115.73 (d, *J* = 25.8 Hz), 109.89, 107.97, 107.33, 45.34, 44.13, 21.89, 21.06 ppm. HPLC (λ = 210 nm): $t_{R\ =}$ 14.470 $_{min}$ (CH_3CN/H_2O, 45:55).

2-(2-(2-chloro-6-fluorobenzoyl)-1,2,3,4-tetrahydro-9H-pyrido [3,4-b]indol-9-yl)-N-hydroxyacetamide (**D29**).

Purity of 99.09%. HRMS (AP-ESI) m/z calcd for $C_{20}H_{17}ClFN_3O_3$ $[M+H]^+$ 401.09425, found: 402.09875$[M+H]^+$. ^{1}H NMR (400 MHz, DMSO). δ 10.91 (d, *J* = 65.9, 1H), 9.03 (dd, *J* = 50.4, 1H), 7.60-7.56 (m, 1H), 7.54-7.32 (m, 4H), 7.15-7.10 (m, 1H), 7.03 (t, *J* = 7.6 Hz, 1H), 4.99 (dd, *J* = 42.0, 16.8 Hz, 2H), 4.71-4.47 (m, 2H), 4.04-3.54 (m, 2H), 2.82-2.67 (m, 2H). ^{13}C-NMR (400 MHz, DMSO). δ 164.73, 162.29, 158.58 (d, *J* = 247.4 Hz), 137.29, 132.25 (d, *J* = 9.6 Hz), 132.08, 131.01 (d, *J* = 6.1 Hz), 126.45 (d, *J* = 21.6 Hz), 124.78 (d, *J* = 23.3 Hz), 121.61, 119.62, 118.25, 115.50 (d, *J* = 21.2 Hz), 109.86 (d, *J* = 14.6 Hz), 107.91, 44.92, 44.17, 22.07, 21.15 ppm. HPLC (λ = 210 nm): $t_{R\ =}$ 16.050 $_{min}$ (CH_3CN/H_2O, 45:55).

Cell Culture

Human K562 myeloid lymphoblastoma cell line, human triple-negative breast cancer cell lines MDA-MB-231 and MDA-MB-468 were received from the Cell Bank of Shanghai (Shanghai in China) and maintained in (RPMI)-1640 supplemented with 10% fetal calf serum (FCS). The cells were incubated at 37°C in a humidified atmosphere containing 5% CO_2. Ubenimex (Cat. B8385) and 2′, 7′-Dichlorofluorescin diaceta (DCFH-DA) were purchased from Sigma. Paclitaxel (PTX, Cat. SP8020) and doxorubicin (Epirubicin Hydrochloride, Cat. IE 0640) were purchased from Solarbio. Carboplatin (CBP, Cat.C-0219027) and Cyclophosphamide (CTX, Cat.C-0232450) were purchased from HEOWNS. All the compounds were dissolved in sterile dimethyl sulfoxide (DMSO) to constitute 20 mM stock agents and the aliquots were stored at -20°C.

Enzyme Activity Screening Assay

K562 cells with overexpression of APN were added into PBS for ultrasonic crushing, centrifuged for 10 minutes, and supernatant was taken as enzyme source and added into 96-well plate. Different concentrations of compounds were added subsequently, and 1.6 mM L-leucine-p-nitro anilide was used as substrate. After 30 minutes of reaction, the APN enzyme activity was measured at 405 nm absorbance. The inhibition rate of APN activity was analyzed by the formula (Od control OD tested)/Od control 100%.

MTT Assay

MDA-MB-231 and MDA-MB-468 cells were added into 96-well plates (5X103 cells/well) and treated with PTX, PTX+Bestatin, or PTX+ various compounds at 37°C, 5% CO_2 for 48h. Then, 10μL of MTT solution (5 mg/mL) were added to each well. After incubation for 4h, the medium was carefully removed, and 100 μL DMSO was added to each well and fully dissolved in vibration for 10min. The optical density (OD) at 490 nm and 630 nm were measured with a microplate Spectrophotometer (M5, MD). IC_{50} values were obtained from at least 3 independent experiments.

Flow Cytometry of APN

The cells were seeded in 6-well plates (4 × 105 cells/well) and treated with tested compounds for 48 h. Then, cells were collected into 1.5 mL EP tubes, washed twice with PBS, and centrifuged at 2500rpm for 5minutes. Cells were resuspended with 100μlof PBS, then 2μL/tube of APN antibody was added, followed by incubation in dark for 30 minutes at 4°C. Then the cells were subjected to flow cytometry (FACSAria II, Becton-Dickinson) for the expression of APN.

Cellular Reactive Oxygen Species Detection

The cells were seeded in 6-well plates (4×10^5 cells/well) and treated with tested compounds for 48 h. Then, cells were resuspended with 500 μL of serum-free culture medium; after addition of10μMof DCFH-DA, cells were returned to the incubator for 30min. Finally, the cells were resuspended with PBS and subjected to flow cytometry.

Apoptosis Analysis

The cells were seeded in 6-well plates (3×10^5 cells/well) and treated with various compounds for 48 h. Then, cells were collected and washed twice with cold PBS. Annexin V-FITC staining solution was then added to the cells, and cells were incubated at 2-8°C for 15 minutes under dark conditions. Then, PI staining solution was added by gentle mix at 2-8°C. After 5 minutes of incubation under dark conditions, cells were tested with flow cytometry immediately.

Colony-Formation Assay

3000 cells were suspended in 2 mL medium, and seeded into the wells of six-well plate. After 12 hours of incubation, cells were treated with various compounds. Until each colony had more than 50 cells, this experiment terminated. Cells were washed twice with PBS and fixed with methanol for 10minutes. Then cells were stained with 1% crystal violet for 5minutes. Finally, colonies were washed and pictures were taken under a microscope (IX81, Olympus).

Spheroid-Formation Assay

MDA-MB-231 cells and MDA-MB-468 cells in logarithmic growth phase were collected, stem cell sphere culture medium without serum (containing 50X B-27Supplement,100X N-2

TABLE 2 | Primers in the RT-PCR study.

Gene	Forward (5'-3')	Reverse (5'-3')
SOX2	GACTTCACATGTCCCAGCACTA	CTCTTTTGCACCCCTCCCATT
NANOG	CCCCAGCCTTTACTCTTCCTA	CCAGGTTGAATTGTTCCAGGTC
OCT4	GAGAAGGATGTGGTCCGAGT	GTGCATAGTCGCTGCTTGAT

Supplement,20 μg/L epidermal growth factor (EGF), 20μg/L insulin-like growth factor (IGF-1), 10 μg/L fibroblast growth factor (b-FGF), 20X Knock Out SR, 2mM L-Glutamine, 5mg/L Heparin sodium, 1X PENICILLIN-STREPTOMYCIN and DMEM: F12 (1:1) medium was added for the re-suspension and fully blown into single-cell suspension. The cells were diluted to 5,000/2 mL, with stem cell sphere culture medium, and cultured in a 37°C, 5% CO_2 cell incubator. The number of stem cell spheres were observed every day. After about five days, stem cell microspheres could be visually confirmed, then various compounds were added every two days for ten days.

Quantitative Real-Time Reverse Transcription Polymerase Chain Reaction

Total RNA was extracted with TRIzol reagent, and the RNA concentration was detected by a Nano Drop instrument (2000C, NanoDrop). Single-strand cDNA was reverse-transcribed with a Hi Fi Script cDNA Synthesis Kit (CWBIO, China) following the manufacturer-provided instruction. The cDNA was amplified with a SYBR Green mixture (CWBIO, China) and gene-specific primers (**Table 2**). The primers used for QRT-PCR were OCT-4, SOX-2 and Nanog. The relative gene expression was calculated with the $2^{-\triangle\triangle Ct}$ method.

In vivo Imaging of Mice

Female Nude mice aged 3 weeks were purchased from Hunan SJA Experimental Animal Company and raised under SPF aseptic conditions. About 1×10^7 luciferase overexpressing MDA-MB-231 cells were injected subcutaneously into the right fat pad of the fourth mammary gland of each mouse. When the tumor volume reached100 mm^3, the mice were randomly divided into six groups (n = 4): PBS group, PTX group, PTX +Bestatin group, PTX+**D12** group, PTX+**D14** group, PTX+**D16** group. PBS group animals received PBS *via* intraperitoneal injection, while 10 mg/kg/3 days of PTX was administered to animals in the PTX group. 20 mg/kg/d of Bestatin, **D12**, **D14**, **D16**were administered in combination to10 mg/kg/3 days of PTX to the corresponding mice. After 3 weeks of administration, each mouse was intraperitoneally injected with 200uL of fluorescein substrate (d-fluorescein potassium salt, 150mg/kg), and then anesthetized with isoflurane. *In vivo* fluorescence imaging system (IVIS Spectrum, PerkinElmer) and SlideBook4.0 software were utilized for the result analysis. After the imaging analysis, mice were sacrificed and dissected for the detection of tumor size and calculation of liver/spleen indexes. All animal experiments were approved by the Animal Care and Use Committee of Weifang Medical University.

STATISTICAL ANALYSIS

All statistical analyses were performed with GraphPad Prism statistical software package. Quantitative data were presented as mean ± standard error of the mean (SEM). Statistical analysis was performed by one-way analysis of variance (ANOVA). When ANOVA returns significant results, post-hoc least significant different (LSD) tests were used be compare among the groups. $P < 0.05$ was considered statistically significant in all experiments.

DATA AVAILABILITY STATEMENT

The original contributions presented in the study are included in the article/**Supplementary Material**. Further inquiries can be directed to the corresponding authors.

ETHICS STATEMENT

The animal study was reviewed and approved by Animal Care and Use Committee of Weifang Medical University (ACUC-WFMU).

AUTHOR CONTRIBUTIONS

LEZ designed the project. XX and YH performed the enzymatic screening. FL synthesized the molecules. LIZ, QH and HQ performed the *in vitro* and *in vivo* anticancer experiments. QJ, CF and WJ analyzed the data and wrote the manuscript. All authors contributed to the article and approved the submitted version.

FUNDING

This work was supported by Science and technology support plan for youth innovation in universities of Shandong Province (Grant No. 2019KJM001), Natural Foundation of Shandong Province (Youth Found, Grant No. ZR2019QH005), National Natural Science Foundation of China (Youth Found, Grant No. 81803343).

SUPPLEMENTARY MATERIAL

The Supplementary Material for this article can be found online at: https://www.frontiersin.org/articles/10.3389/fonc.2022.894842/full#supplementary-material

REFERENCES

1. Taylor A. Aminopeptidases: Structure and Function. *FASEB J* (1993) 7 (2):290–8. doi: 10.1096/fasebj.7.2.8440407
2. Wickstrom M, Larsson R, Nygren P, Gullbo J. Aminopeptidase N (CD13) as a Target for Cancer Chemotherapy. *Cancer Sci* (2011) 102(3):501–8. doi: 10.1111/j.1349-7006.2010.01826.x
3. Santiago C, Mudgal G, Reguera J, Recacha R, Albrecht S, Enjuanes L, et al. Allosteric Inhibition of Aminopeptidase N Functions Related to Tumor Growth and Virus Infection. *Sci Rep-Uk* (2017) 7:46045. doi: 10.1038/srep46045
4. Bhagwat SV, Lahdenranta J, Giordano R, Arap W, Pasqualini R, Shapiro LH. CD13/APN is Activated by Angiogenic Signals and is Essential for Capillary Tube Formation. *Blood* (2001) 97(3):652–9. doi: 10.1182/blood.V97.3.652
5. Zhao Y, Wu H, Xing X, Ma Y, Ji S, Xu X, et al. CD13 Induces Autophagy to Promote Hepatocellular Carcinoma Cell Chemoresistance Through the P38/Hsp27/CREB/ATG7 Pathway. *J Pharmacol Exp Ther* (2020) 374(3):512–20. doi: 10.1124/jpet.120.265637
6. Dixon J, Kaklamanis L, Turley H, Hickson ID, Leek RD, Harris AL, et al. Expression of Aminopeptidase-N (CD 13) in Normal Tissues and Malignant Neoplasms of Epithelial and Lymphoid Origin. *J Clin Pathol* (1994) 47(1):43–7. doi: 10.1136/jcp.47.1.43
7. van Hensbergen Y, Broxterman HJ, Hanemaaijer R, Jorna AS, van Lent NA, Verheul HM, et al. Soluble Aminopeptidase N/CD13 in Malignant and Nonmalignant Effusions and Intratumoral Fluid. *Clin Cancer Res* (2002) 8(12):3747–54.
8. Hashida H, Takabayashi A, Kanai M, Adachi M, Kondo K, Kohno N, et al. Aminopeptidase N is Involved in Cell Motility and Angiogenesis: Its Clinical Significance in Human Colon Cancer. *Gastroenterology* (2002) 122(2):376–86. doi: 10.1053/gast.2002.31095
9. Zhai MY, Yang ZX, Zhang CR, Li JP, Jia J, Zhou LY, et al. APN-Mediated Phosphorylation of BCKDK Promotes Hepatocellular Carcinoma Metastasis and Proliferation via the ERK Signaling Pathway. *Cell Death Dis* (2020) 11 (5):396. doi: 10.1038/s41419-020-2610-1
10. Song YQ, Liu P, Wang CX, Zhang Q, Ge XC, Zhuang AS, et al. The Clinical Significance and Expression of TGF-Beta 1 and CD13 in Primary Lesion and Metastasis of Gastric Cancer. *Int J Clin Exp Med* (2017) 10(7):10643–51.
11. Amin SA, Adhikari N, Jha T. Design of Aminopeptidase N Inhibitors as Anti-Cancer Agents. *J Med Chem* (2018) 61(15):6468–90. doi: 10.1021/acs.jmedchem.7b00782
12. Zhang X, Fang H, Zhang J, Yuan Y, Xu W. Recent Advance in Aminopeptidase N (APN/CD13) Inhibitor Research. *Curr Med Chem* (2011) 18(32):5011–21. doi: 10.2174/092986711797535155
13. Schreiber CL, Smith BD. Molecular Imaging of Aminopeptidase N in Cancer and Angiogenesis. *Contrast Media Mol Imaging* (2018) 2018:5315172. doi: 10.1155/2018/5315172
14. Umezawa H, Aoyagi T, Suda H, Hamada M, Takeuchi T. Bestatin, an Inhibitor of Aminopeptidase B, Produced by Actinomycetes. *J Antibiot (Tokyo)* (1976) 29(1):97–9. doi: 10.7164/antibiotics.29.97
15. Zhang J, Fang C, Qu M, Wu H, Wang X, Zhang H, et al. CD13 Inhibition Enhances Cytotoxic Effect of Chemotherapy Agents. *Front Pharmacol* (2018) 9:1042. doi: 10.3389/fphar.2018.01042
16. Tsukamoto H, Shibata K, Kajiyama H, Terauchi M, Nawa A, Kikkawa F. Aminopeptidase N (APN)/CD13 Inhibitor, Ubenimex, Enhances Radiation Sensitivity in Human Cervical Cancer. *BMC Cancer* (2008) 8:74. doi: 10.1186/1471-2407-8-74
17. Yamashita M, Kajiyama H, Terauchi M, Shibata K, Ino K, Nawa A, et al. Involvement of Aminopeptidase N in Enhanced Chemosensitivity to Paclitaxel in Ovarian Carcinoma *In Vitro* and *In Vivo*. *Int J Cancer* (2007) 120(10):2243–50. doi: 10.1002/ijc.22528
18. Haraguchi N, Ishii H, Mimori K, Tanaka F, Ohkuma M, Kim HM, et al. CD13 Is a Therapeutic Target in Human Liver Cancer Stem Cells. *J Clin Invest* (2010) 120(9):3326–39. doi: 10.1172/JCI42550
19. Dou CH, Fang CY, Zhao Y, Fu XY, Zhang YF, Zhu DQ, et al. BC-02 Eradicates Liver Cancer Stem Cells by Upregulating the ROS-Dependent DNA Damage. *Int J Oncol* (2017) 51(6):1775–84. doi: 10.3892/ijo.2017.4159
20. Jin K, Zhang XP, Ma CH, Xu YY, Yuan YM, Xu WF. Novel Indoline-2,3-Dione Derivatives as Inhibitors of Aminopeptidase N (APN). *Bioorgan Med Chem* (2013) 21(9):2663–70. doi: 10.1016/j.bmc.2012.06.024
21. Hou JN, Jin K, Li J, Jiang YQ, Li XY, Wang XJ, et al. LJNK, an Indoline-2,3-Dione-Based Aminopeptidase N Inhibitor With Promising Antitumor Potency. *Anti-Cancer Drug* (2016) 27(6):496–507. doi: 10.1097/CAD.0000000000000351
22. Kalin JH, Butler KV, Akimova T, Hancock WW, Kozikowski AP. Second-Generation Histone Deacetylase 6 Inhibitors Enhance the Immunosuppressive Effects of Foxp3+ T-Regulatory Cells. *J Med Chem* (2012) 55(2):639–51. doi: 10.1021/jm200773h
23. Spindler A, Stefan K, Wiese M. Synthesis and Investigation of Tetrahydro-Beta-Carboline Derivatives as Inhibitors of the Breast Cancer Resistance Protein (Abcg2). *J Med Chem* (2016) 59(13):6121–35. doi: 10.1021/acs.jmedchem.6b00035
24. Mohamed HA, Girgis NM, Wilcken R, Bauer MR, Tinsley HN, Gary BD, et al. Synthesis and Molecular Modeling of Novel Tetrahydro-Beta-Carboline Derivatives With Phosphodiesterase 5 Inhibitory and Anticancer Properties. *J Med Chem* (2011) 54(2):495–509. doi: 10.1021/jm100842v
25. Zheng C, Fang YZ, Tong WG, Li GL, Wu HG, Zhou WB, et al. Synthesis and Biological Evaluation of Novel Tetrahydro-Beta-Carboline Derivatives as Antitumor Growth and Metastasis Agents Through Inhibiting the Transforming Growth Factor-Beta Signaling Pathway. *J Med Chem* (2014) 57(3):600–12. doi: 10.1021/jm401117t
26. Ran X, Zhao YJ, Liu L, Bai LC, Yang CY, Zhou B, et al. Structure-Based Design of Gamma-Carboline Analogues as Potent and Specific BET Bromodomain Inhibitors. *J Med Chem* (2015) 58(12):4927–39. doi: 10.1021/acs.jmedchem.5b00613
27. Liu H, Wang X, Yang H, Zhao Y, Ji S, Ma H, et al. New Method for Detecting the Suppressing Effect of Enzyme Activity by Aminopeptidase N Inhibitor. *Chem Pharm Bull (Tokyo)* (2019) 67(2):155–8. doi: 10.1248/cpb.c18-00667
28. Martinez JM, Prieto I, Ramirez MJ, Cueva C, Alba F, Ramirez M. Aminopeptidase Activities in Breast Cancer Tissue. *Clin Chem* (1999) 45 (10):1797–802. doi: 10.1093/clinchem/45.10.1797
29. Ji S, Ma Y, Xing X, Ge B, Li Y, Xu X, et al. Suppression of CD13 Enhances the Cytotoxic Effect of Chemotherapeutic Drugs in Hepatocellular Carcinoma Cells. *Front Pharmacol* (2021) 12:660377. doi: 10.3389/fphar.2021.660377
30. Yang F, Zhang J, Yang H. OCT4, SOX2, and NANOG Positive Expression Correlates With Poor Differentiation, Advanced Disease Stages, and Worse Overall Survival in HER2(+) Breast Cancer Patients. *Onco Targets Ther* (2018) 11:7873–81. doi: 10.2147/OTT.S173522

Conflict of Interest: The authors declare that the research was conducted in the absence of any commercial or financial relationships that could be construed as a potential conflict of interest.

frontiers | Frontiers in Oncology

ORIGINAL RESEARCH
published: 27 May 2022
doi: 10.3389/fonc.2022.912935

Long Non-Coding RNA TMPO-AS1 Promotes GLUT1-Mediated Glycolysis and Paclitaxel Resistance in Endometrial Cancer Cells by Interacting With miR-140 and miR-143

Peixin Dong[1†], Feng Wang[2†], Mohammad Taheri[3,4†], Ying Xiong[5], Kei Ihira[1], Noriko Kobayashi[1], Yosuke Konno[1*], Junming Yue[6,7*] and Hidemichi Watari[1]*

[1] Department of Obstetrics and Gynecology, Hokkaido University School of Medicine, Hokkaido University, Sapporo, Japan, [2] Department of Laboratory Medicine, Affiliated Hospital of Nantong University, Jiangsu, China, [3] Skull Base Research Center, Loghman Hakim Hospital, Shahid Beheshti University of Medical Sciences, Tehran, Iran, [4] Institute of Human Genetics, Jena University Hospital, Jena, Germany, [5] Department of Gynecology, State Key Laboratory of Oncology in South China, Sun Yat-sen University Cancer Center, Guangzhou, China, [6] Department of Pathology and Laboratory Medicine, University of Tennessee Health Science Center, Memphis, TN, United States, [7] Center for Cancer Research, University of Tennessee Health Science Center, Memphis, TN, United States

Increased glycolysis in tumor cells is frequently associated with drug resistance. Overexpression of glucose transporter-1 (GLUT1) promotes the Warburg effect and mediates chemoresistance in various cancers. Aberrant GLUT1 expression is considered as an essential early step in the development of endometrial cancer (EC). However, its role in EC glycolysis and chemoresistance and the upstream mechanisms underlying GLUT1 overexpression, remain undefined. Here, we demonstrated that GLUT1 was highly expressed in EC tissues and cell lines and that high GLUT1 expression was associated with poor prognosis in EC patients. Both gain-of-function and loss-of-function studies showed that GLUT1 increased EC cell proliferation, invasion, and glycolysis, while also making them resistant to paclitaxel. The long non-coding RNA TMPO-AS1 was found to be overexpressed in EC tissues and to be negatively associated with EC patient outcomes. RNA-immunoprecipitation and luciferase reporter assays confirmed that TMPO-AS1 elevated GLUT1 expression by directly binding to two critical tumor suppressor microRNAs (miR-140 and miR-143). Downregulation of TMPO-AS1 remarkably reduced EC cell proliferation, invasion, glycolysis, and paclitaxel resistance in EC cells. This study established that dysregulation of the TMPO-AS1-miR-140/miR-143 axis contributes to glycolysis and drug resistance in EC cells by up-regulating GLUT1 expression. Thus, inhibiting TMPO-AS1 and GLUT1 may prove beneficial in overcoming glycolysis-induced paclitaxel resistance in patients with EC.

Keywords: GLUT1, miR-140, miR-143, long non-coding RNA, TMPO-AS1, paclitaxel resistance, glycolysis, endometrial cancer

OPEN ACCESS

Edited by:
Zhe-Sheng Chen,
St. John's University, United States

Reviewed by:
Arjun Singh,
Memorial Sloan Kettering Cancer Center, United States
Fukang Sun,
Shanghai Jiao Tong University, China
Yang Chen,
Dalian Institute of Chemical Physics (CAS), China

***Correspondence:**
Peixin Dong
dpx1cn@gmail.com
Yosuke Konno
konsuke013@gmail.com
Junming Yue
jyue@uthsc.edu

†These authors have contributed equally to this work

Specialty section:
This article was submitted to Cancer Molecular Targets and Therapeutics, a section of the journal Frontiers in Oncology

Received: *05 April 2022*
Accepted: *29 April 2022*
Published: *27 May 2022*

Citation:
Dong P, Wang F, Taheri M, Xiong Y, Ihira K, Kobayashi N, Konno Y, Yue J and Watari H (2022) Long Non-Coding RNA TMPO-AS1 Promotes GLUT1-Mediated Glycolysis and Paclitaxel Resistance in Endometrial Cancer Cells by Interacting With miR-140 and miR-143. Front. Oncol. 12:912935. doi: 10.3389/fonc.2022.912935

INTRODUCTION

A hallmark of cancer is the remodeling of glucose metabolism (1). Even in the presence of abundant oxygen, cancer cells exhibit enhanced glycolysis to generate energy and supply intermediates for biosynthetic processes (1). Since cancer cells rely on increased glucose usage compared with normal healthy cells, inhibition of glucose metabolism represents a promising therapeutic option in combating cancer (2).

The glucose transporter (GLUT) proteins are a class of membrane proteins that aid in glucose transport across the plasma membrane (1). Cancer cells frequently overexpress GLUTs, particularly GLUT1, which significantly increases glucose import into the cytoplasm (3). Overexpression of GLUT1 has been observed in many types of cancers, and high GLUT1 expression is associated with unfavorable overall survival in human cancers (4, 5). GLUT1 has been shown to promote cancer cell proliferation, migration, invasion, and metastasis (6, 7). Accumulated reports indicate that aerobic glycolysis is linked to tumor chemoresistance (8, 9). Inhibition of GLUT1 sensitized tumor cells to the anti-cancer effects of chemotherapeutic drugs (10–12), although the mechanisms remain elusive.

GLUT1 expression is usually absent in benign endometrium (13, 14). However, GLUT1 expression was preferentially expressed in atypical hyperplasia and endometrial cancer (EC) specimens (13, 14), indicating a biological role for GLUT1 during the early stages of endometrial tumorigenesis. GLUT1 expression progressively increased from low-grade EC to high-grade EC (15). A recent study showed that treating spheroid cells derived from EC patients with BAY876, a specific GLUT1 inhibitor, could sensitize them to paclitaxel and suppress their glucose uptake (16). The potential roles of GLUT1 in regulating glycolysis and paclitaxel resistance in EC cells, as well as the underlying mechanisms, have not yet been elucidated.

Numerous non-coding RNAs, including microRNAs (miRNAs) and long non-coding RNAs (lncRNAs), have been identified to regulate cancer metabolism and chemoresistance (17). LncRNAs play an important role in regulating gene expression at multiple levels (including epigenetic, transcription, and post-transcriptional regulation) (18). Notably, lncRNAs act as competing endogenous RNAs, antagonizing the interactions of tumor suppressor miRNAs and target mRNAs (18). However, the epigenetic mechanisms underlying GLUT1 overexpression in EC, and the key molecular machinery by which lncRNAs mediate glycolysis and paclitaxel resistance *via* miRNAs, have not been identified.

In this study, we revealed a critical function of GLUT1 that facilitates glycolysis and confers paclitaxel resistance in EC cells. The interactions between lncRNA TMPO-AS1 and miR-140/miR-143 protect GLUT1 from miRNA inhibition, thus promoting glycolysis and paclitaxel resistance. This is the first report suggesting that TMPO-AS1 binds directly to miR-140/miR-143 to induce the expression of GLUT1 in EC cells, implying that GLUT1 is a downstream target of the TMPO-AS1-miR-140/miR-143 pathway. Furthermore, high GLUT1 and TMPO-AS1 expression is correlated with poor overall survival in EC patients. Our findings point to GLUT1 and TMPO-AS1 as potential therapeutic targets for improving the prognosis of EC patients by inhibiting glycolysis and overcoming paclitaxel resistance.

MATERIALS AND METHODS

Bioinformatic Analysis

The Oncomine database (https://www.oncomine.org/resource/login.html) was used to detect *GLUT1* expression in several types of cancer and normal tissues with the thresholds ($P < 0.05$, a 2-fold change, and a gene rank in the top 10%). The GEO datasets (GSE17025 and GSE63678) were combined to identify differentially expressed genes between EC and normal tissues using the ImaGEO database (https://imageo.genyo.es), which annotated the probes with gene identifiers, merged and normalized data. The Human Protein Atlas (HPA) is an open-access database that maps all human proteins in cells and tissue samples (https://www.proteinatlas.org/). Immunohistochemistry (IHC) pictures of EC tissues were retrieved from the HPA. The KM plotter database (http://kmplot.com/analysis/) was used to analyze the effects of *GLUT1* expression on the overall patient survival. The *P*-value was determined using the log-rank method. Genes associated with *GLUT1* were investigated using the LinkedOmics database (http://www.linkedomics.org). Kyoto Encyclopedia of Genes and Genomes (KEGG) and Wikipathway cancer enrichment analysis was carried out by Gene Set Enrichment Analysis (GSEA) in LinkedOmics. To select significantly enriched gene sets, 1000 simulations are conducted, and the false discovery rate (FDR < 0.05) was used. The expression of TMPO-AS1 in TCGA EC and normal tissues was examined using the ENCORI database (http://starbase.sysu.edu.cn) and Wanderer database (http://maplab.imppc.org/wanderer/). TANRIC database (https://www.tanric.org/) was applied to investigate the expression of TMPO-AS1 in TCGA EC patients with different tumor grades and stages.

Human Cell Lines and Cell Culture

Human EC cell lines (Ishikawa and HHUA) were derived from well-differentiated endometrioid EC. Ishikawa cells were obtained from the American Type Culture Collection (ATCC, Manassas, VA), and HHUA cells were purchased from the RIKEN cell bank (Tsukuba, Japan). An immortalized human endometrial epithelial cell line (EM) was a kind gift from Dr. Satoru Kyo (Shimane University, Japan). These cells were cultured in DMEM/F12 medium (Sigma-Aldrich, St. Louis, MO) that contained 10% fetal bovine serum (FBS, Invitrogen, Carlsbad, CA) and 100 μg/ml Normocin (Invitrogen, San Diego, CA, USA) at 37°C with 5% CO_2.

Plasmids and Transfection

To generate stable HHUA cell lines overexpressing GLUT1, the *GLUT1* cDNA expression vector pCMV6-GLUT1 (GLUT1-vec) or control vector was purchased from OriGene (Rockville, MD). Cell transfections were performed using Lipofectamine 3000 reagent (Invitrogen) following the manufacturer's instructions. The resulting cell lines were expanded after 14 days of selection with G418 (500 μg per ml, Sigma-Aldrich, St. Louis, MO).

GLUT1 silencing was conducted in the Ishikawa cell line using shRNA targeting GLUT1 (Santa Cruz Biotechnologies, Santa Cruz, CA) or control shRNA (Santa Cruz Biotechnologies) and Lipofectamine 3000 reagent. The transfected cells were expanded after being selected with puromycin (1 μg per ml, Sigma-Aldrich, St. Louis, MO) for 14 days. Western blotting analysis was used to evaluate forced GLUT1 overexpression or knockdown.

The control (NC) mimic, miR-140 mimic, miR-143 mimic, control inhibitor, miR-140 inhibitor, miR-143 inhibitor, control siRNA, and a specific siRNA against TMPO-AS1 were obtained from Invitrogen. Transfection of EC cells was performed using Lipofectamine 3000 reagent (Invitrogen). After transfection, cells were incubated for 48 hours before proceeding with the experiments.

Western Blotting Analysis

Whole-cell extracts were prepared in M-Per Mammalian Protein Extraction Reagent (Pierce, Rockford, IL), separated by SDS-polyacrylamide gels, and transferred to PVDF membranes (GE Healthcare Life Sciences, Piscataway, NJ). Membranes were incubated overnight with primary antibodies, including anti-GLUT1 (1:1000, Cell Signaling Technology, Beverly, MA) and anti-β-actin (1:5000, Cell Signaling Technology). Protein bands were detected with an ECL detection kit (Amersham Pharmacia Biotech, UK).

CCK-8 Assay

Cell proliferation was assessed using the Cell Counting Kit-8 (CCK-8) assay (Dojindo, Japan) according to the manufacturer's instructions. Five thousand cells were seeded per well in a 96-well plate and cultured for 72 hours. For the paclitaxel viability assays, 5000 cells per well were plated in 96-well plates for 24 hours and then treated with DMSO or varying doses of paclitaxel (Cell Signaling Technology). After 24 hours of paclitaxel treatment, cell viability was determined using the CCK-8 assay. The relative survival was calculated compared with cells treated with DMSO.

Matrigel Invasion Assay

Matrigel invasion assays were performed as previously reported (19). A total of 5×10^4 cells were plated in the upper wells of Matrigel–coated Transwell plates (8 μm pore size, Corning Costar Co., Lowell, CA) in 500 μl of serum-free DMEM/F12 medium containing 100 μg/ml of Normocin. The lower chambers of the plate were filled with 750 μl of DMEM/F12 medium containing 10% FBS and 100 μg/ml of Normocin. The cells were allowed to invade for 24 hours before being stained with 2% crystal violet for 15 minutes. Cells in the upper chamber were removed using a cotton swab, and cells migrating through the membrane were counted.

Measurement of Glucose Consumption and Lactate Production

Cells were cultured in DMEM/F12 medium in 6-well plates, and the medium was changed after 6 hours. Culture media was collected after incubation for 24 hours. The glucose concentration in the medium was determined using the Glucose Assay Kit-WST (Dojindo, Kumamoto, Japan) following the manufacturer's instructions. Lactate levels were measured using the Lactate Assay Kit-WST (Dojindo) according to the manufacturer's instructions. Glucose consumption and lactate production were normalized to cell numbers. The results were presented as fold-change over the respective controls.

Quantitative Reverse Transcription-PCR (qRT-PCR) Assay

Total RNA was isolated from cells with the TRIzol reagent (Invitrogen) and reverse-transcribed into cDNA using an M-MLV Reverse Transcriptase Kit (Invitrogen). Quantitative real-time PCR was carried out using SYBR Premix Ex Taq II (Takara, Shiga, Japan) in an ABI-7300 Real-Time PCR system (Applied Biosystems, Foster City, CA). The primers were as follows: human *GLUT1*, sense: 5′-GGCCAAGAGTGTGCTAAAGAA-3′, anti-sense: 5′-ACAGCGTTGATGCCAGACAG-3′; human *MMP-1*, sense: 5′-AAAATTACACGCCAGATTTGCC-3′, anti-sense: 5′-GGTGTGACATTACTCCAGAGTTG-3′; human *MMP-14*, sense: 5′-GGCTACAGCAATATGGCTACC-3′, anti-sense: 5′-GATGGCCGCTGAGAGTGAC-3′; human *Cyclin D1*, sense: 5′-GCTGCGAAGTGGAAACCATC-3′, anti-sense: 5′-CCTCCTTCTGCACACATTTGAA-3′; human TMPO-AS1, sense: 5′-GTGCTGCAGGACCGAGG-3′, anti-sense: 5′-GCTTTGTGTCCGCGAGTTTT-3′, and human *β-actin*, sense: 5′-CATGTACGTTGCTATCCAGGC-3′, anti-sense: 5′-CTCCTTAATGTCACGCACGAT-3′. Gene expression was normalized to *beta-actin* mRNA. The expression of miR-140 and miR-143 was measured using the NCode SYBR GreenER miRNA qRT-PCR analysis kit (Invitrogen). The forward primers for miRNA analysis had the same sequences as the mature miRNAs. The forward primer for U6 was 5′-CGCAAGGAT GACACGCAAATTCG-3′. The reverse primer was the NCode miRNA universal qPCR primer (Invitrogen). The expression of miRNAs was calculated relative to U6.

Subcellular Fractionation Assay

Cytoplasmic and nuclear RNA was extracted using the PARIS Kit (Thermo Fisher Scientific, Carlsbad, CA) according to the manufacturer's instructions. The qRT-PCR analysis was used to measure the expression ratio of TMPO-AS1 between the cytoplasmic and nuclear fractions. U6 served as the nuclear control, and *GAPDH* was used as the cytoplasmic control. The primers were as follows: human U6, sense: 5′-CTCGCTTCGGC AGCACA-3′; anti-sense: 5′-AACGCTTCACGAATTTGCGT-3′ and human *GAPDH* (sense: 5′-ACAACTTTGGTATCGTGGAA GG-3′; anti-sense: 5′-GCCATCACGCCACAGTTTC-3′).

Luciferase Reporter Assay

The wild-type (WT) human TMPO-AS1 fragment containing the predicted miRNA targeting sites was amplified and cloned into the pGL3-basic vector (Promega, Madison, WI). A human *GLUT1* 3′-untranslated region (3′-UTR) luciferase reporter vector was purchased from OriGene (Rockville, MD). The mutated (MUT) miRNA binding sites in TMPO-AS1 and the *GLUT1* 3′-UTR were generated using a QuickChange site-directed mutagenesis kit (Stratagene, La Jolla, CA). EC cells

were co-transfected with the WT or MUT TMPO-AS1 or *GLUT1* 3′-UTR luciferase reporter vector, miR-140/miR-143 mimic, miR-140/miR-143 inhibitor (or the respective control), and renilla luciferase plasmid pRL-CMV (Promega, Madison, WI) using the Lipofectamine 3000 reagent (Invitrogen). The activities of firefly and renilla luciferase in each group were measured 48 hours after transfection using a dual-luciferase reporter assay system (Promega). The firefly luciferase activities were normalized to renilla luciferase activities.

RNA Immunoprecipitation (RIP) Assay

The RIP assay was conducted using a Magna RIP RNA-Binding Protein Immunoprecipitation Kit (Millipore, Billerica, MA). Briefly, EC cells were re-suspended in RIP lysis buffer. Magnetic beads carrying protein A/G were incubated with anti-Ago2 antibody (Millipore) or control anti-IgG antibody (Millipore) for 30 minutes at room temperature. Lysates were incubated with the bead-antibody complexes in the RIP immunoprecipitation buffer at 4°C overnight. The next day, the RNA-protein-bead complexes were washed in the RIP wash buffer and incubated with proteinase K. After that, the immunoprecipitated RNAs were extracted and subjected to qRT-PCR analysis.

Statistical Analysis

The results are expressed as the mean ± SD of three independent experiments. Statistical analysis was performed using SPSS 22.0 statistical software (SPSS, Chicago). Differences between the two groups were analyzed using the two-tailed Student's *t*-tests and Mann-Whitney *U* tests. Comparisons among multiple groups were analyzed using a one-way ANOVA test. A P value < 0.05 was considered statistically significant.

RESULTS

The Clinical Importance of GLUT1 Expression in EC

To investigate the expression profiles of GLUT1 in human cancer and normal tissues, we used the Oncomine database to perform a pan-cancer transcriptome analysis on its available data sets. The mRNA differences between cancer and normal samples were analyzed using the default selection criteria. There were 448 Oncomine datasets involving GLUT1 (**Figure 1A**). Up-regulation of GLUT1 was observed in various cancer tissues (including bladder, breast, cervical, liver, ovarian, pancreatic cancer, and EC) (**Figure 1A**). To explore the clinical significance of GLUT1 in EC, we performed a meta-analysis of two GEO EC datasets (GSE17025 and GSE56026) using the ImaGEO database. As a result, we selected the differentially expressed genes in EC compared to normal tissues (**Figure 1B**). Remarkably, EC patients had higher levels of known oncogenes (including *STAT3* and *EZH2*) and lower

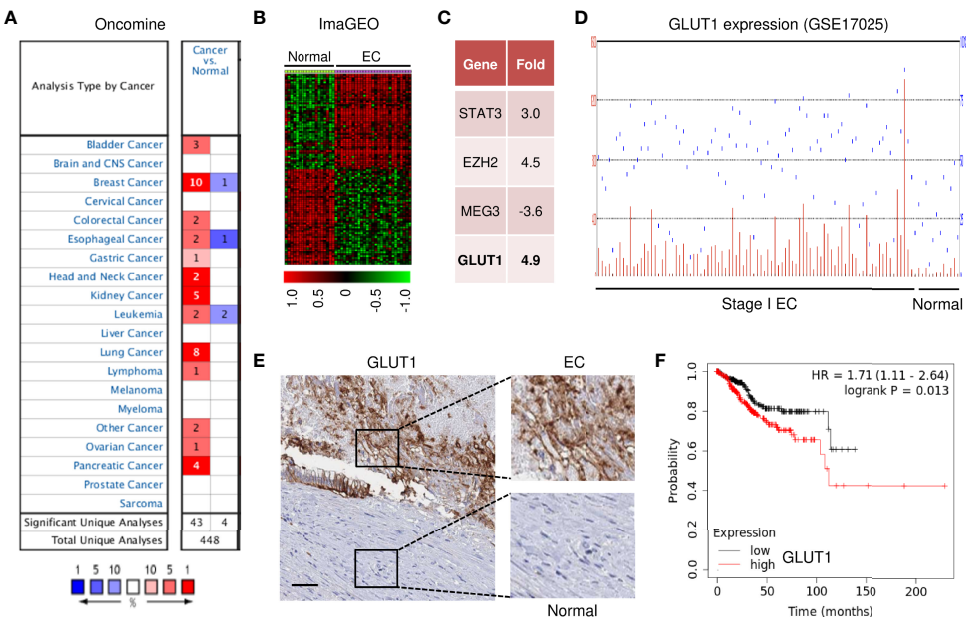

FIGURE 1 | GLUT1 Expression and Clinical Importance in EC. **(A)** The mRNA expression of *GLUT1* (cancer versus normal tissues) in pan-cancers was analyzed with the Oncomine database. The graphic demonstrates the number of datasets that meet our threshold for each cancer type. Red: up-regulation; blue: down-regulation. **(B)** The heatmap was generated by the ImaGEO database using two EC data sets (GSE17025 and GSE56026). **(C)** Up- or down-regulated genes in EC tissues compared to normal tissues (ImaGEO). **(D)** The GEO dataset was analyzed for *GLUT1* expression in stage I EC samples and normal endometrium samples. **(E)** The expression of GLUT1 protein was examined in EC tissue and adjacent normal tissues (Human Protein Atlas database; scale bar: 100 μm). **(F)** The probability of overall survival in EC patients expressing high or low *GLUT1* levels was assessed using the KM plotter database.

levels of the known tumor suppressor lncRNA MEG3 when compared to normal samples (**Figure 1C**). This analysis also showed a marked up-regulation of *GLUT1* in ECs (**Figure 1C**). Additionally, microarray gene expression data from the GEO website demonstrated that *GLUT1* was overexpressed in stage I EC tissues compared with normal endometrial tissues (**Figure 1D**). Furthermore, we assessed the expression of GLUT1 protein in an EC tissue microarray by extracting IHC images from the Human Protein Atlas database. GLUT1 exhibited both strong and diffuse positive staining in EC, but not in adjacent normal tissues (**Figure 1E**). Subsequently, we sought to determine the clinical relevance of GLUT1 expression in terms of prognosis in EC patients. Kaplan–Meier analysis using the KM plotter database showed that higher GLUT1 expression was significantly associated with worse overall survival in EC patients (**Figure 1F**). Interestingly, GLUT1 expression was low in non-malignant endometrial epithelial cell lines (EM), whereas GLUT1 expression was much higher in EC cell lines (**Figure 2A**). Together, these results suggest that increased GLUT1 expression is linked to EC tumorigenesis and progression, and its overexpression is correlated with poor clinical outcomes.

Critical Roles of GLUT1 in Promoting EC Cell Phenotypes

To establish the role of GLUT1 in EC cell phenotypes, we generated the HHUA cell line stably overexpressing GLUT1 (GLUT1-vec) and the control cell line (**Figure 2B**). On the

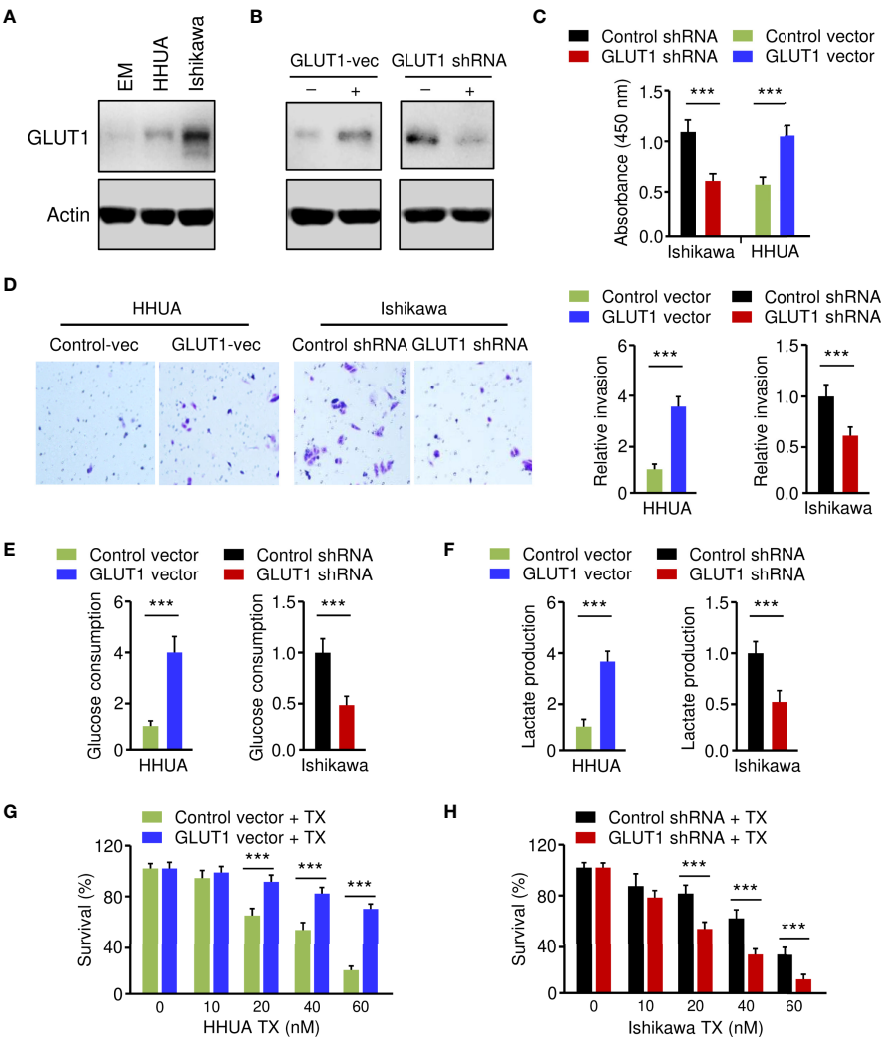

FIGURE 2 | Critical Roles of GLUT1 in Promoting EC Cell Phenotypes. **(A)** Western blotting analysis of GLUT1 protein expression in a normal endometrial cell line (EM) and human EC cell lines. **(B)** Western blotting analysis of GLUT1 expression in GLUT1-overexpressing HHUA cells and Ishikawa cells with GLUT1 silencing. **(C–F)** EC cell proliferation **(C)**, invasion **(D)**, glucose consumption **(E)**, and lactate production **(F)** assays following GLUT1 overexpression or knockdown. **(G, H)** GLUT1-overexpressing HHUA cells **(G)** and Ishikawa cells after knockdown of GLUT1 **(H)** were treated with different concentrations of paclitaxel, and cell viability was examined using the CCK-8 assay. Vec: vector. ***$P < 0.001$.

other hand, we knocked down the expression of GLUT1 in Ishikawa cells using shRNA for GLUT1 (**Figure 2B**). We first wanted to investigate how GLUT1 overexpression or silencing affects EC cell proliferation, invasion, glucose metabolism, and chemoresistance. Cell functional assays demonstrated that, when compared with control cells, HHUA GLUT1-vec cells showed a significant increase in cell growth, invasion, glucose consumption, lactate production, and paclitaxel resistance (**Figures 2C–G**). However, silencing of GLUT1 expression resulted in a marked decrease in cell proliferation, invasiveness, and glycolysis, as well as sensitization of EC cells to paclitaxel treatment (**Figures 2C–F, H**). These results suggest that GLUT1 is a key player that induces aggressive properties, glycolysis, and chemoresistance in EC cells.

Pathway Enrichment Analysis of Genes Related to GLUT1 Expression in EC

We investigated the genes associated with *GLUT1* in the TCGA EC dataset (n=304), as well as the pathways involved, using the LinkedOmics online database. There were 6648 genes, represented by red dots, which had a positive connection with *GLUT1*. Conversely, there were 13250 genes, represented by green dots, which had a notably negative correlation with *GLUT1* in TCGA EC tissues (**Figure 3A**). Then, we selected the top 100 positively and 100 negatively correlated genes, and performed Kyoto Encyclopedia of Genes and Genomes (KEGG) pathway enrichment analysis. The results of KEGG pathway analysis revealed that the genes that were positively related to *GLUT1* in EC tissues were mainly located in

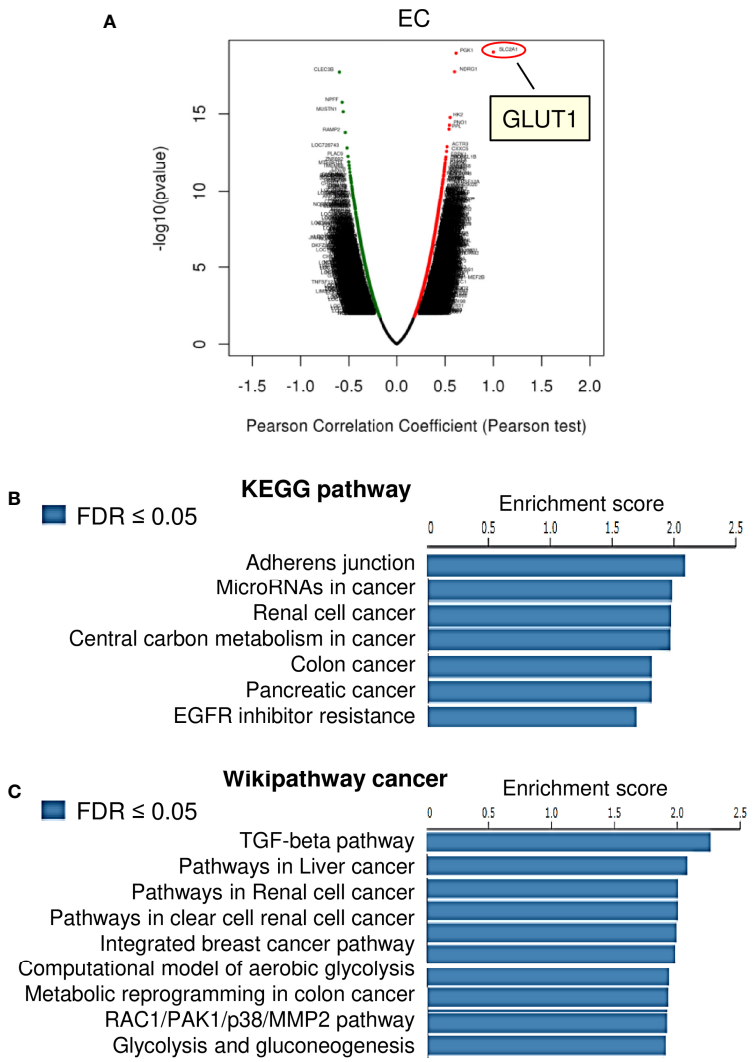

FIGURE 3 | KEGG Pathway and Wiki Pathway Enrichment Analysis of *GLUT1*-Associated Genes in EC. **(A)** Genes that were found to be highly co-expressed with *GLUT1* in the TCGA EC dataset from the LinkedOmics database were chosen. **(B, C)** Gene set enrichment analysis for positively correlated genes of *GLUT1* in TCGA EC tissues. Enrichment analysis for KEGG pathways **(B)** and Wikipathway cancer **(C)** was performed using the LinkedOmics database.

several pathways, including adherens junction, microRNAs in cancer, renal cell cancer, central carbon metabolism in cancer, colon cancer, pancreatic cancer, and EGFR inhibitor resistance (**Figure 3B**). Furthermore, using the GSEA tool in LinkedOmics, Wikipathway cancer enrichment of *GLUT1* co-expressed genes was performed. This enrichment analysis showed that those co-expressed genes were involved in the TGF-beta pathway, pathways in liver cancer, pathways in renal cell cancer, pathways in clear cell renal cell cancer, integrated breast cancer pathway, computational model of aerobic glycolysis, metabolic reprogramming in colon cancer, RAC1/PAK1/p38/MMP2 pathway, and glycolysis and gluconeogenesis (**Figure 3C**). These results indicate the broad impact of GLUT1 on the global transcriptome in EC cells, and support the notion that GLUT1 has a critical role in endometrial tumorigenesis, EC progression, and chemoresistance beyond working as a glucose transporter.

GLUT1 Is a Positive Upstream Regulator of MMP1, MMP14, and Cyclin D1

Using the KEGG enrichment analysis, based on the LinkedOmics database, we determined that several cancer-linked pathways (including MicroRNAs in Cancer Pathway) were among the top ten pathways that were significantly related to GLUT1 expression in TCGA EC tissues (**Figure 3B**). Importantly, Cyclin D1 is a key component of the MicroRNAs in the Cancer Pathway (**Figure 3B**), and it controls chemoresistance and glycolysis in human tumor cells (20, 21). In addition, MMP1, MMP14, and Cyclin D1 have important roles in increasing EC cell proliferation, migration, and invasion (22–25). Therefore, we studied whether the levels of MMP1/MMP14/Cyclin D1 were correlated with GLUT1 expression in ECs. By assessing EC samples in TCGA through the ENCORI database, we found that the expression of *GLUT1* was positively correlated with the expression of *MMP1*, *MMP14*, and *Cyclin D1* (**Figure 4A**), indicating that the mechanisms underlying the action of GLUT1 may be related to these genes.

To test this hypothesis, we evaluated the mRNA expression of *MMP1*, *MMP14*, and *Cyclin D1* in EC cells following overexpression or knockdown of GLUT1. By qRT-PCR assay, we found that the levels of *MMP1*, *MMP14*, and *Cyclin D1* were significantly higher in GLUT1-overexpressing cells than in control cells (**Figure 4B**). Additional qRT-PCR analysis also

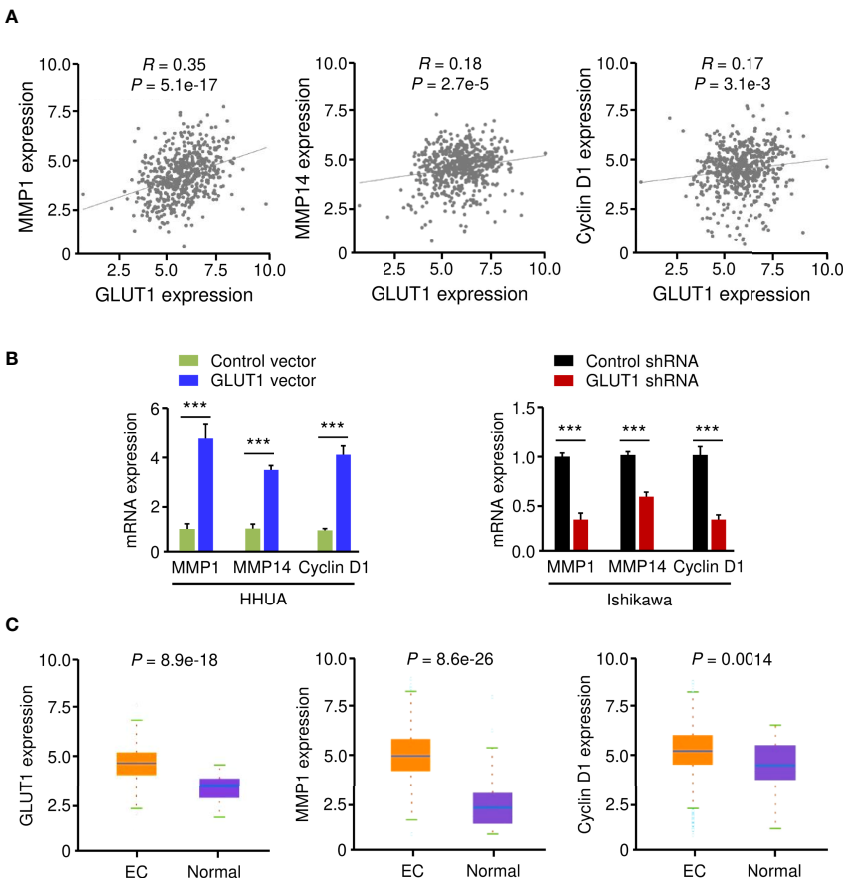

FIGURE 4 | GLUT1 is a Positive Upstream Regulator of MMP1, MMP14, and Cyclin D1. **(A)** The expression of *GLUT1* was positively correlated with the expression of *MMP1*, *MMP14*, and *Cyclin D1* in EC tissues from the TCGA dataset. **(B)** qRT-PCR analysis of the indicated genes in EC cells after overexpression or knockdown of GLUT1. **(C)** The expression of *MMP1*, *MMP14*, and *Cyclin D1* in TCGA EC and normal tissues (ENCORI database). ***$P < 0.001$.

showed that GLUT1 silencing significantly reduced the expression of *MMP1*, *MMP14*, and *Cyclin D1* (**Figure 4B**). We further analyzed the expression of these genes in TCGA EC and normal samples using the ENCORI database. *MMP1*, *MMP14*, and *Cyclin D1* were significantly higher in EC tissues than in normal tissues (**Figure 4C**). Together, these data suggest that MMP1, MMP14, and Cyclin D1 are critical downstream targets of GLUT1 in EC cells.

GLUT1 Is a Target Gene of MiR-140 and MiR-143

To determine whether overexpression of GLUT1 was caused by miRNA suppression, we searched miRNAs that might bind to the 3′-UTR of *GLUT1* mRNA using three online miRNA target prediction databases (TargetScan, ENCORI, and miRSystem) (**Figure 5A**). Six miRNAs were found in all three databases. Analysis of TCGA EC data from the miR-TV database (http://mirtv.ibms.sinica.edu.tw/) suggested that, among these 6 candidates, only miR-140 and miR-143 were significantly down-regulated in EC tissues compared to normal tissues (**Figures 5B, C**). Our qRT-PCR assay confirmed that EC cell lines had lower expression of miR-140 and miR-143 than EM cells (**Figure 5D**). The above results indicated that the dysregulation of miR-140 and miR-143 may be involved in GLUT1 overexpression in ECs. Thus, we tested the effects of miR-140 and miR-143 on GLUT1 protein expression in EC cells. The results from western blotting analysis showed that overexpression of miR-140 and miR-143 decreased, while inhibition of miR-140 and miR-143 increased the protein expression of GLUT1 in EC cells (**Figure 5E** and **Supplementary Figure 1**). To explore whether miR-140 and miR-143 directly bind to the 3′-UTR region of *GLUT1* mRNA, we performed a dual-luciferase reporter assay. The results showed that the introduction of miR-140 and miR-143 significantly decreased the luciferase activities of WT *GLUT1* 3′-UTR in Ishikawa cells, and had no effect on MUT *GLUT1* 3′-UTR (**Figure 5F**), proving that miR-140 and miR-143 directly target GLUT1 in EC cells. Overall, we confirmed that GLUT1 is a direct target of miR-140/miR-143, and that loss of miR-140/miR-143 expression contributes to GLUT1 up-regulation in ECs.

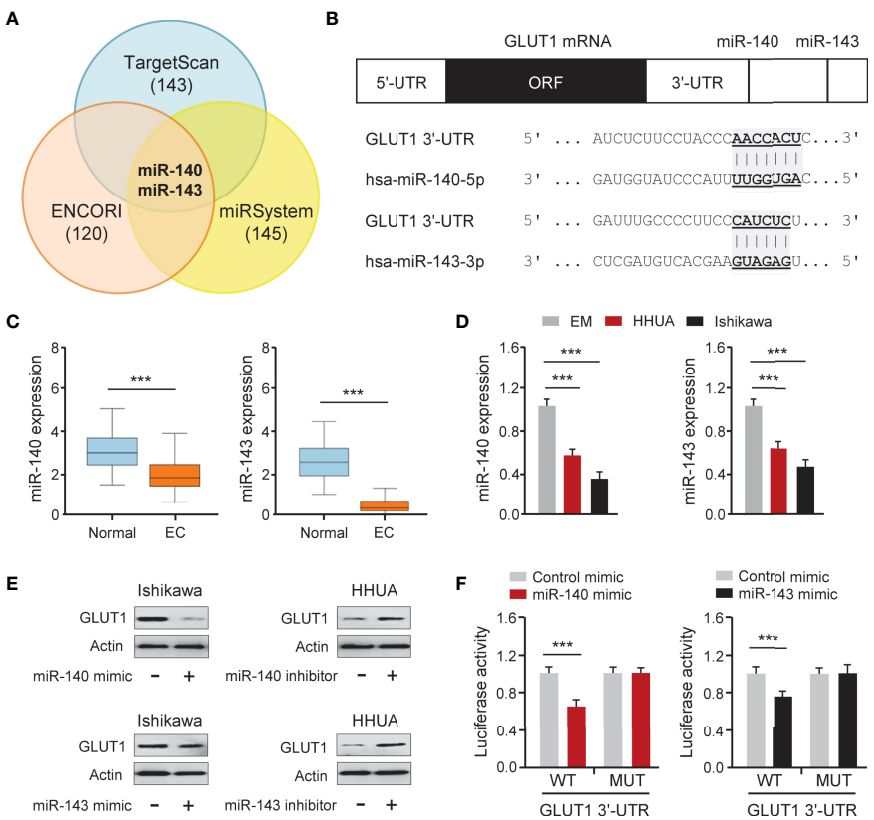

FIGURE 5 | GLUT1 is a Target Gene of MiR-140 and MiR-143. **(A)** Venn diagram showing the overlapping miRNAs predicted by three online databases. **(B)** Computational prediction of duplex formation between miR-140/miR-143 and the *GLUT1* 3′-UTR region. **(C)** The expression of miR-140/miR-143 in TCGA EC tissues and normal tissues (miR-TV database). **(D)** qRT-PCR analysis of miR-140/miR-143 in EC and EM cells. **(E)** GLUT1 protein expression was examined using western blotting assays in EC cells transfected as indicated. **(F)** Luciferase reporter assays in Ishikawa cells transfected with the wild-type (WT) or mutant (MUT) *GLUT1* 3′-UTR, as well as miR-140/miR-143 mimic or a control mimic. ***$P < 0.001$.

MiR-140 and MiR-143 Inhibit EC Cell Glycolysis and Chemotherapeutic Resistance

To elucidate the functional effect of miR-140 and miR-143 on EC cell phenotypes, we increased the expression of miR-140 and miR-143 in Ishikawa cells, while suppressing their expression in HHUA cells. The results from functional assays demonstrated that up-regulation of both miR-140 and miR-143 significantly inhibited the growth, invasion, glucose consumption, and lactate production of Ishikawa cells, whereas knockdown of miR-140 and miR-143 significantly enhanced these malignant phenotypes in HHUA cells (**Figures 6A–D**). We detected the impact of miR-140 and miR-143 expression on paclitaxel treatment and found that overexpression of miR-140 and miR-143 improved the sensitivity of EC cells to paclitaxel (**Figure 6E**), whereas suppression of miR-140 and miR-143 expression inhibited EC cell sensitivity (**Supplementary Figure 2A**). Since *MMP1*, *MMP14*, and *Cyclin D1* are downstream targets of GLUT1, we wanted to investigate whether miR-140 and miR-143 had any effect on their expression. Utilizing a qRT-PCR assay, we demonstrated that the expression of *MMP1*, *MMP14*, and *Cyclin D1* was increased in miR-140/miR-143-silenced HHUA cells, but decreased in Ishikawa cells overexpressing miR-140/miR-143 (**Figure 6F**; **Supplementary Figure 2B**). These results support the idea that miR-140 and miR-143 suppress EC cell proliferation, invasion, and glycolysis, and enhance the chemosensitivity of EC cells to paclitaxel by down-regulating GLUT1.

LncRNA TMPO-AS1 Interacts With MiR-140/MiR-143 to Inhibit Their Expression

LncRNAs have been shown to interact with miRNAs to regulate the expression of downstream genes (26, 27). To identify lncRNAs that might compete for the binding sites of miR-140/miR-143 with *GLUT1* mRNA, the ENCORI database was used for target prediction. We detected the binding sites for lncRNAs and miR-140/miR-143. In total, 9 lncRNAs may simultaneously bind to miR-140 and miR-143 (**Figure 7A**; **Supplementary Figure 4A**). According to the analysis of TCGA EC data ***via*** the ENCORI database and the Wanderer database, we found that 4 lncRNAs were highly expressed in EC tissues (**Figures 7A–C**). The data from the KM plotter database indicated that PVT1 and

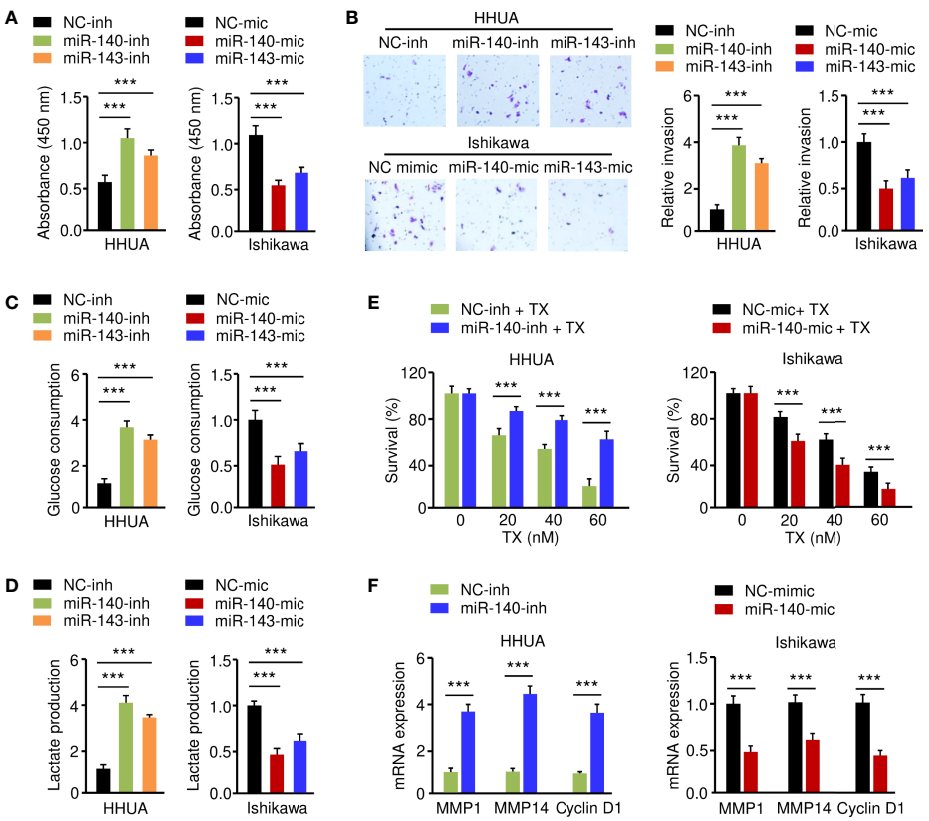

FIGURE 6 | MiR-140 and miR-143 Suppress Glycolysis and Chemoresistance of EC Cells. **(A–D)** Proliferation **(A)**, invasion **(B)**, glucose consumption **(C)**, and lactate production **(D)** assays in EC cells after miR-140 or miR-143 overexpression or knockdown. **(E)** HHUA cells transfected with miR-140 inhibitor (inh) and Ishikawa cells transfected with miR-140 mimic (mic) were treated with different concentrations of paclitaxel, and cell viability was examined using the CCK-8 assay. **(F)** The mRNA expression of the indicated genes was examined in Ishikawa cells after overexpression of miR-140, and in HHUA cells after the knockdown of miR-140. ***$P < 0.001$.

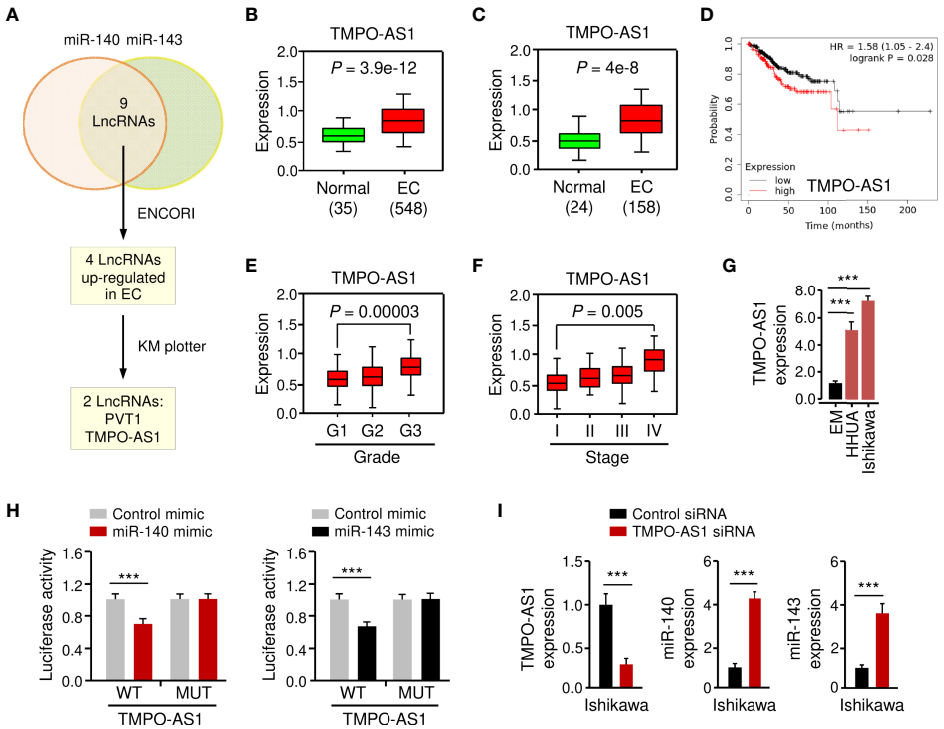

FIGURE 7 | LncRNA TMPO-AS1 Interacts with MiR-140 and MiR-143 to Inhibit Their Expression. **(A)** Workflow for identifying possible lncRNAs that regulate the expression of miR-140 and miR-143 simultaneously. **(B, C)** Expression of TMPO-AS1 in TCGA EC and normal tissues (**B**: ENCORI database; **C**: Wanderer database). **(D)** The probability of overall survival in EC patients expressing high or low TMPO-AS1 levels was examined using the KM plotter database. **(E, F)** TMPO-AS1 expression analysis in EC samples with varying histologic grades (**E**: well (G1), moderate (G2), and poor (G3)) and tumor stages (**F**: I–IV) (TANRIC database). **(G)** qRT-PCR analysis of TMPO-AS1 expression in EC and EM cells. **(H)** Luciferase reporter assays in Ishikawa cells transfected with wild-type (WT) or mutant (MUT) TMPO-AS1 fragments, as well as miR-140/miR-143 mimic or control mimic. **(I)** The expression of TMPO-AS1, miR-140, and miR-143 in Ishikawa cells transfected with TMPO-AS1 siRNA (or control siRNA) was examined using qRT-PCR analysis. ***$P < 0.001$.

TMPO-AS1 (but not the other two lncRNAs) were poor prognostic factors in EC patients (**Figure 7D**) and caught our attention. Because PVT1 functions as an oncogenic molecule in various cancers (28), TMPO-AS1 was chosen as the miR-140/miR-143-associated lncRNA in our study.

Basic information about TMPO-AS1 was obtained from the Lnc2Catlas database (https://lnc2catlas.bioinfotech.org). TMPO-AS1 is an intergenic lncRNA localized in chr12:98512973–988516422 and annotated as ENSG00000257167.2 in the ENSEMBL database (**Supplementary Figure 3A**). The lncATLAS database (https://lncatlas.crg.eu/) was applied to determine the subcellular localization of TMPO-AS1 in human cells. The results showed that TMPO-AS1 was mainly found in the cytoplasm of human cancer cells (including A549, HT1080, and MCF-7 cells) (**Supplementary Figure 3B**). Furthermore, qRT-PCR analysis of EC cell nuclear and cytoplasmic fractions revealed that TMPO-AS1 is mainly located in the cytoplasm (**Supplementary Figure 3C**).

To further explore whether TMPO-AS1 expression levels correlate with the clinicopathological characteristics of EC, we analyzed the expression of TMPO-AS1 in TCGA EC patients using the TANRIC database. We noticed that TMPO-AS1 expression was significantly increased in higher grade (grade 3) ECs than in lower grade (grade 1) ECs (**Figure 7E**). Furthermore, TMPO-AS1 levels were significantly increased in stage IV ECs compared to stage I ECs (**Figure 7F**). As expected, TMPO-AS1 expression was induced in EC cell lines when compared to normal EM cells (**Figure 7G**).

To confirm the relationship between TMPO-AS1 and miR-140/miR-143, we applied a luciferase assay. Transfection with miR-140 or miR-143 mimic markedly inhibited the WT TMPO-AS1-driven luciferase activities, but did not affect the MUT TMPO-AS1-driven luciferase activities (**Figure 7H**; **Supplementary Figure 4A**). Consistently, TMPO-AS1 negatively suppressed the expression of miR-140 and miR-143 in EC cells (**Figure 7I**; **Supplementary Figure 4B**). To further verify the binding of TMPO-AS1 and miR-140/miR-143, we performed an RIP assay. Endogenous TMPO-AS1 was significantly enriched in miR-140/miR-143 mimic-transfected EC cells compared with control cells transfected with control mimic (**Supplementary Figure 4C**). These results suggest that TMPO-AS1 negatively regulates the expression of miR-140 and miR-143 through direct interactions.

TMPO-AS1 Promotes GLUT1 Expression by Suppressing MiR-140 and MiR-143 Levels

Because TMPO-AS1 functions as a competing endogenous RNA for miR-140 and miR-143, we wondered whether TMPO-AS1 could modulate the expression of GLUT1 by negatively regulating these two miRNAs. To test this possibility, we transfected Ishikawa and HHUA cells with TMPO-AS1 siRNA or control siRNA, along with (or without) miR-140/miR-143 inhibitor, and measured the protein expression of GLUT1 using western blotting analysis. Knockdown of TMPO-AS1 decreased the expression of GLUT1, but inhibition of miR-140 and miR-143 restored GLUT1 expression in Ishikawa and HHUA cells (**Figure 8A**). qRT-PCR assays were used to estimate the impact of TMPO-AS1 silencing, in the presence (or absence) of the miR-140/miR-143 inhibitor, on *MMP1*, *MMP14*, and *Cyclin D1* expression. The mRNA levels of *MMP1*, *MMP14*, and *Cyclin D1* in EC cells were decreased greatly with the knockdown of TMPO-AS1 and increased when miR-140 and miR-143 were inhibited (**Figure 8B**). To investigate the clinical correlation between TMPO-AS1 and GLUT1 levels in EC patient tissues, we obtained the expression data of 548 EC samples from the TCGA project in the ENCORI database. Then, we calculated the Pearson correlation for TMPO-AS1 and *GLUT1* and found a positive and significant correlation between them (**Figure 8C**). Conversely, the levels of miR-140 and miR-143 were negatively correlated with TMPO-AS1 expression in our analysis (**Figure 8C**). These correlations in the TCGA EC dataset were highly consistent with our above results (**Figures 5**, **7**). Together, TMPO-AS1 promotes GLUT1 expression by negatively regulating miR-140 and miR-143.

Knockdown of TMPO-AS1 Inhibits Glycolysis and Reverses Chemoresistance of EC Cells

Finally, we investigated whether suppressing TMPO-AS1 expression is effective in inhibiting EC cell growth, invasion, glycolysis, and chemoresistance. CCK-8, invasion, glucose consumption, lactate production, and drug sensitivity assays demonstrated that siRNA-mediated TMPO-AS1 downregulation significantly reduced EC cell growth, invasion, glucose consumption, and lactate production, as well as reversing EC cell resistance to paclitaxel (**Figures 9A–F**). These results link the up-regulation of TMPO-AS1 to increased glycolytic metabolism

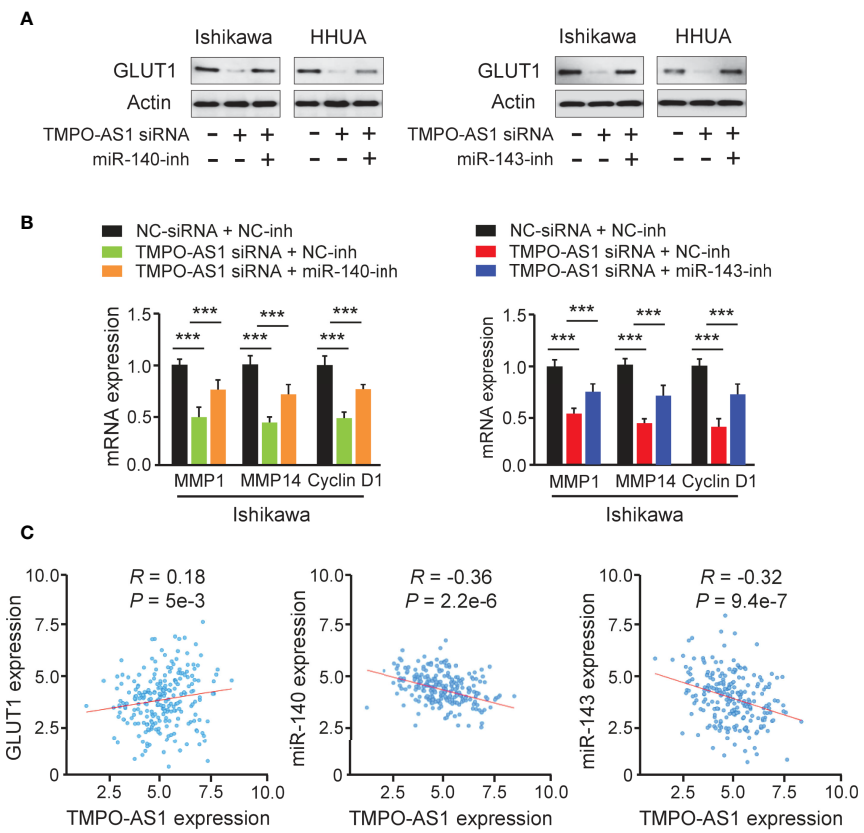

FIGURE 8 | TMPO-AS1 Induces GLUT1 Expression by Repressing MiR-140 and MiR-143 Levels. **(A)** GLUT1 protein expression was measured in Ishikawa and HHUA cells transfected with (or without) TMPO-AS1 siRNA, along with (or without) miR-140/miR-143 inhibitor. **(B)** Examination of *MMP1*, *MMP14*, and *Cyclin D1* expression in Ishikawa cells transfected as indicated. **(C)** Correlation analysis between TMPO-AS1 and GLUT1 or between TMPO-AS1 and miR-140/miR-143. ***$P < 0.001$.

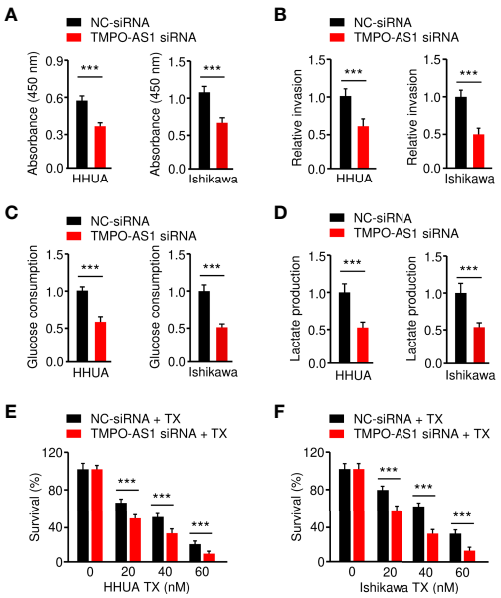

FIGURE 9 | Knockdown of TMPO-AS1 Inhibits Glycolysis and Reverses Chemoresistance of EC Cells.**(A–D)** *Proliferation* **(A)**, invasion **(B)**, glucose consumption **(C)**, and lactate production **(D)** assays in EC cells after the knockdown of TMPO-AS1. **(E, F)** HHUA **(E)** or Ishikawa cells **(F)** were transfected with TMPO-AS1 siRNA (or control siRNA) and treated with different concentrations of paclitaxel. Cell viability was examined using a CCK-8 assay. ***$P < 0.001$.

and the development of paclitaxel resistance, suggesting potential therapeutic strategies that target TMPO-AS1 to improve the treatment of paclitaxel-resistant EC.

DISCUSSION

With over 319,000 cases diagnosed worldwide, EC is the most common gynecologic cancer in developed countries (29). Early cancer detection is crucial for improving patient survival rates by providing care at the earliest possible stage. Although blood- and tissue-based biomarker candidates for EC detection have been reported, to date, there are no validated biological markers that can reliably detect EC at an early stage (30). The GLUT1 protein is rarely expressed in normal endometrium, but was abundant in pre-cancerous endometrial lesions and most EC tissues (13, 14). Here, we have shown that GLUT1 is exclusively expressed in stage I EC samples and not in normal endometrium, and high GLUT1 expression is closely related to unfavorable outcomes. These findings imply that GLUT1 could be used as a diagnostic and prognostic marker for EC. More importantly, GLUT1 expression is elevated across a wide range of cancer types, implying that GLUT1 could be used to screen for other cancers.

Several oncogenes and tumor suppressor genes, including p53 (31), HER2 (32), PI3KCA (32), and PTEN (32), have previously been identified as regulators in EC. However, most of these could be used to predict prognosis, and valuable therapeutic targets are still lacking in EC. In this study, we discovered that GLUT1 is required for EC cell proliferation, invasion, glucose consumption, and lactate production. Furthermore, shRNA-induced repression of GLUT1 results in a remarkable reduction in these malignant properties of EC cells, substantiating that GLUT1 is a potentially targetable biomarker for EC.

To date, many natural and synthetic GLUT1 inhibitors have shown anti-cancer effectiveness (10, 33, 34). A small-molecule inhibitor of GLUT1, WZB117, was shown to induce cell death in lung and breast cancer cells while having no effect on normal cells (35). Recently, BAY-876, a highly selective GLUT1 inhibitor, was recently reported to inhibit the tumorigenesis of ovarian cancer cells *in vivo* by blocking glycolysis and growth (36). Notably, treatment with BAY-876 suppresses cell viability and glucose uptake in spheroid cells derived from EC patient tissues (16), indicating the possibility that the blockade of GLUT1 might inhibit the characteristics of EC stem cells. In line with these results, we verified that inhibiting GLUT1 expression with shRNA could effectively sensitize the representative EC cell line Ishikawa to paclitaxel *in vitro*. Thus, inhibiting GLUT1 expression and its function might be explored as a potential therapeutic target to delay EC progression and combat chemoresistance in this cancer.

Aside from its well-characterized role in tumor glycolysis, GLUT1 exhibits diverse functions in different aspects of tumorigenesis and metastasis, including proliferation, motility, invasiveness, and epithelial-mesenchymal transition (6, 7, 10, 37). GLUT1 acts on tumor cells *via* a number of downstream signaling pathways, including the EGFR/ERK/PKM2 and integrin 1/Src/FAK signaling pathways (6, 7). In addition, GLUT1 has been shown to regulate many proteins, including Cyclin D1 (6, 7), MMP1 (37), MMP2 (38), and MMP14 (39). Cyclin D1 overexpression confers resistance to cisplatin- or paclitaxel-mediated apoptosis in human cancer cells (40, 41).

Both MMP1 (23) and MMP14 (24) are overexpressed in EC and are crucial for EC metastasis. Here, we found that up-regulation of GLUT1 significantly increases the expression of *MMP1*, *MMP14*, and *Cyclin D1* in EC cells, implying that GLUT1 promotes EC cell invasion and paclitaxel resistance, at least in part by increasing MMP1/MMP14/Cyclin D1 expression.

GLUT1 expression is controlled by transcription factors, lncRNAs, and tumor suppressor miRNAs (8). Transcription factors (including hypoxia-inducible factor HIF-1α and c-Myc) bind directly to the promoter region of *GLUT1* and activate its transcription (8). Activation of the RAS pathway and PI3K/AKT pathway is also implicated in the up-regulation of GLUT1 in cancer cells (8). Furthermore, lncRNA HOTAIR is able to up-regulate GLUT1 expression in hepatocellular carcinoma cells (8). Moreover, multiple miRNAs (such as miR-140 and miR-143) have been shown to directly regulate GLUT1 expression in breast cancer (42) and T cells (43), respectively. Interestingly, the aberrant expression of both miR-140 and miR-143 has been detected in various cancers, including EC (44, 45). MiR-143 is recognized as a powerful tumor suppressor miRNA that inhibits cancer progression, glycolysis, and chemoresistance by regulating a large number of oncogenes (44). MiR-140 is expressed at low levels in EC tissues (46, 47), but its cellular functions and its target genes remain poorly understood. Here, our study provided the first evidence showing that both miR-140 and miR-143 suppress the growth, invasion, glycolysis, and chemoresistance of EC cells by directly targeting GLUT1. Collectively, post-transcriptional modifications mediated by miR-140/miR-143 could influence GLUT1 expression levels in EC cells.

Considering the down-regulation of miR-140 and miR-143 in ECs, we investigated the mechanism involved in miR-140 and miR-143 regulation. Recent research has indicated the ability of lncRNAs to sponge miRNAs and modulate their expression (18). Consistent with these reports, we have shown that, by sponging miR-140 and miR-143, lncRNA TMPO-AS1 suppresses their expression to induce the expression of GLUT1. Interestingly, TMPO-AS1 is frequently up-regulated in tumor tissues, and it is functionally required for maintaining cell invasiveness and chemoresistance (48, 49). However, its biological functions in EC, as well as the relationship between TMPO-AS1 and glycolysis, are still unclear. Our results demonstrate for the first time that TMPO-AS1 predicts poor prognosis in EC patients, and has a pivotal oncogenic role in enhancing glycolysis and paclitaxel resistance in EC cells, by weakening the suppressive effects of miR-140/miR-143 on GLUT1. Future strategies targeting TMPO-AS1 and GLUT1 may represent a promising therapeutic option for treating paclitaxel-resistant EC.

There are several limitations to our study. One limitation is that, although aberrant overexpression of GLUT1 and TMPO-AS1 was detected in GEO and TCGA EC samples, future studies using primary EC and normal tissues will be needed to verify the clinical relevance of our findings. In addition, EC can be divided into two categories: type I and type II (32). Type I and type II EC exhibit distinct clinical behaviors and molecular mechanisms (50), and Ishikawa and HHUA cells serve as representative models for type I EC (51). Thus, another limitation of our investigation is that we are unable to determine whether this TMPO-AS1-miR-140/miR-143-GLUT1 pathway is functionally active in type II EC. We should evaluate the biological roles of GLUT1 and TMPO-AS1 in type II EC cells. Finally, mouse models of EC will be used to validate the results from the *in vitro* experiments.

CONCLUSION

In summary, our study reveals that GLUT1 and lncRNA TMPO-AS1 enhance glycolysis and paclitaxel resistance in EC. TMPO-AS1 acts as a sponge to compete with miR-140 and miR-143,

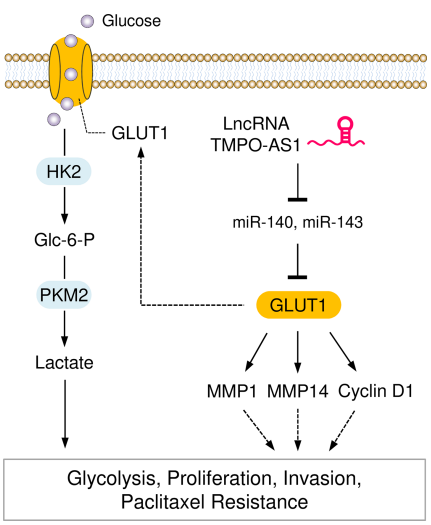

FIGURE 10 | Graphical Abstract showing that the LncRNA TMPO-AS1 Regulates Glycolysis and Paclitaxel Resistance in EC Cells by Affecting the MiR-140/MiR-143-GLUT1 Pathway.

thereby removing the depression of GLUT1 (**Figure 10**). Our findings link the dysregulation of the TMPO-AS1-miR-140/miR-143-GLUT1 pathway to the development of glycolysis and paclitaxel resistance. Therefore, interventions that target this signaling pathway may provide a better chance of slowing EC progression and inhibiting paclitaxel resistance.

DATA AVAILABILITY STATEMENT

The original contributions presented in the study are included in the article/**Supplementary Material**. Further inquiries can be directed to the corresponding authors.

AUTHOR CONTRIBUTIONS

PD, YK, and JY conceived the project. PD, FW, and MT performed the experiments and data collection. YX, YK, KI, NK, and HW analyzed the data. PD wrote the paper. All authors read and approved the final manuscript.

FUNDING

This work was supported by a grant from JSPS Grant-in-Aid for Scientific Research (C) (19K09769, 22K09541 and 22K09634), National Natural Science Foundation of China (81873978), Key Project of Social Development in Jiangsu Province (BE2019691), Postdoctoral Research Funding Project of Jiangsu Province (2021K012A), and an NIH/NCI grant 1R21CA216585-01A1 to JY.

ACKNOWLEDGMENTS

We thank Dr. Zhujie Xu for her excellent technical assistance.

SUPPLEMENTARY MATERIAL

The Supplementary Material for this article can be found online at: https://www.frontiersin.org/articles/10.3389/fonc.2022.912935/full#supplementary-material

REFERENCES

1. Hanahan D, Weinberg RA. Hallmarks of Cancer: The Next Generation. *Cell* (2011) 144(5):646–74. doi: 10.1016/j.cell.2011.02.013
2. Ganapathy-Kanniappan S, Geschwind JF. Tumor Glycolysis as a Target for Cancer Therapy: Progress and Prospects. *Mol Cancer* (2013) 12:152. doi: 10.1186/1476-4598-12-152
3. Zhao Y, Butler EB, Tan M. Targeting Cellular Metabolism to Improve Cancer Therapeutics. *Cell Death Dis* (2013) 4(3):e532. doi: 10.1038/cddis.2013.60
4. Ma L, Zong X. Metabolic Symbiosis in Chemoresistance: Refocusing the Role of Aerobic Glycolysis. *Front Oncol* (2020) 10:5. doi: 10.3389/fonc.2020.00005
5. Hsu PP, Sabatini DM. Cancer Cell Metabolism: Warburg and Beyond. *Cell* (2008) 134(5):703–7. doi: 10.1016/j.cell.2008.08.021
6. Oh S, Kim H, Nam K, Shin I. Glut1 Promotes Cell Proliferation, Migration and Invasion by Regulating Epidermal Growth Factor Receptor and Integrin Signaling in Triple-Negative Breast Cancer Cells. *BMB Rep* (2017) 50(3):132–7. doi: 10.5483/bmbrep.2017.50.3.189
7. Zhao H, Sun J, Shao J, Zou Z, Qiu X, Wang E, et al. Glucose Transporter 1 Promotes the Malignant Phenotype of Non-Small Cell Lung Cancer Through Integrin β1/Src/FAK Signaling. *J Cancer* (2019) 10(20):4989–97. doi: 10.7150/jca.30772
8. Zambrano A, Molt M, Uribe E, Salas M. Glut 1 in Cancer Cells and the Inhibitory Action of Resveratrol as A Potential Therapeutic Strategy. *Int J Mol Sci* (2019) 20(13):3374. doi: 10.3390/ijms20133374
9. Yu M, Yongzhi H, Chen S, Luo X, Lin Y, Zhou Y, et al. The Prognostic Value of GLUT1 in Cancers: A Systematic Review and Meta-Analysis. *Oncotarget* (2017) 8(26):43356–67. doi: 10.18632/oncotarget.17445
10. Tiemin P, Peng X, Qingfu L, Yan W, Junlin X, Zhefeng H, et al. Dysregulation of the miR-148a-GLUT1 Axis Promotes the Progression and Chemoresistance of Human Intrahepatic Cholangiocarcinoma. *Oncogenesis* (2020) 9(2):19. doi: 10.1038/s41389-020-0207-2
11. Song K, Li M, Xu XJ, Xuan L, Huang GN, Song XL, et al. HIF-1α and GLUT1 Gene Expression is Associated With Chemoresistance of Acute Myeloid Leukemia. *Asian Pac J Cancer Prev* (2014) 15(4):1823–9. doi: 10.7314/apjcp.2014.15.4.1823
12. Li P, Yang X, Cheng Y, Zhang X, Yang C, Deng X, et al. MicroRNA-218 Increases the Sensitivity of Bladder Cancer to Cisplatin by Targeting Glut1. *Cell Physiol Biochem* (2017) 41(3):921–32. doi: 10.1159/000460505
13. Wang BY, Kalir T, Sabo E, Sherman DE, Cohen C, Burstein DE. Immunohistochemical Staining of GLUT1 in Benign, Hyperplastic, and Malignant Endometrial Epithelia. *Cancer* (2000) 88(12):2774–81. doi: 10.1002/1097-0142(20000615)88:12<2774::AID-CNCR16>3.0.CO;2-I
14. Idrees MT, Schlosshauer P, Li G, Burstein DE. GLUT1 and P63 Expression in Endometrial Intraepithelial and Uterine Serous Papillary Carcinoma. *Histopathology* (2006) 49(1):75–81. doi: 10.1111/j.1365-2559.2006.02447.x
15. Goldman NA, Katz EB, Glenn AS, Weldon RH, Jones JG, Lynch U, et al. GLUT1 and GLUT8 in Endometrium and Endometrial Adenocarcinoma. *Mod Pathol* (2006) 19(11):1429–36. doi: 10.1038/modpathol.3800656
16. Mori Y, Yamawaki K, Ishiguro T, Yoshihara K, Ueda H, Sato A, et al. ALDH-Dependent Glycolytic Activation Mediates Stemness and Paclitaxel Resistance in Patient-Derived Spheroid Models of Uterine Endometrial Cancer. *Stem Cell Rep* (2019) 13(4):730–46. doi: 10.1016/j.stemcr.2019.08.015
17. Ghafouri-Fard S, Shoorei H, Taheri M. The Role of Long Non-Coding RNAs in Cancer Metabolism: A Concise Review. *Front Oncol* (2020) 10:555825. doi: 10.3389/fonc.2020.555825
18. Dong P, Xiong Y, Yue J, Hanley SJB, Kobayashi N, Todo Y, et al. Long Non-Coding RNA NEAT1: A Novel Target for Diagnosis and Therapy in Human Tumors. *Front Genet* (2018) 9:471. doi: 10.3389/fgene.2018.00471
19. Dong P, Xiong Y, Yue J, Hanley SJB, Watari H. miR-34a, miR-424 and miR-513 Inhibit MMSET Expression to Repress Endometrial Cancer Cell Invasion and Sphere Formation. *Oncotarget* (2018) 9(33):23253–63. doi: 10.18632/oncotarget.25298
20. Mizumoto H, Saito T, Ashihara K, Nishimura M, Tanaka R, Kudo R. Acceleration of Invasive Activity ***via*** Matrix Metalloproteinases by Transfection of the Estrogen Receptor-Alpha Gene in Endometrial Carcinoma Cells. *Int J Cancer* (2002) 100(4):401–6. doi: 10.1002/ijc.10504
21. Kornmann M, Danenberg KD, Arber N, Beger HG, Danenberg PV, Korc M. Inhibition of Cyclin D1 Expression in Human Pancreatic Cancer Cells is Associated With Increased Chemosensitivity and Decreased Expression of Multiple Chemoresistance Genes. *Cancer Res* (1999) 59(14):3505–11.
22. Caillot M, Bourgeais J, Dakik H, Costé É, Mazure NM, Lelièvre É, et al. Cyclin D1 Targets Hexokinase 2 to Control Aerobic Glycolysis in Myeloma Cells. *Oncogenesis* (2020) 9(7):68. doi: 10.1038/s41389-020-00253-3.
23. Lin CY, Chao A, Wang TH, Hsueh S, Lee YS, Wu TI, et al. A Dual Tyrosine Kinase Inhibitor Lapatinib Suppresses Overexpression of Matrix Metallopeptidase 1 (MMP1) in Endometrial Cancer. *J Mol Med (Berl)* (2014) 92(9):969–81. doi: 10.1007/s00109-014-1163-0
24. Nakamura M, Zhang X, Mizumoto Y, Maida Y, Bono Y, Takakura M, et al. Molecular Characterization of CD133+ Cancer Stem-Like Cells in

Endometrial Cancer. *Int J Oncol* (2014) 44(3):669–77. doi: 10.3892/ijo.2013.2230
25. Liu Y, LL W, Chen S, ZH Z, Guan X, Zhao Y. LncRNA ABHD11-AS1 Promotes the Development of Endometrial Carcinoma by Targeting Cyclin D1. *J Cell Mol Med* (2018) 22(8):3955–64. doi: 10.1111/jcmm.13675
26. Dong P, Xiong Y, Yue J, Hanley S JB, Kobayashi N, Todo Y, et al. Exploring lncRNA-Mediated Regulatory Networks in Endometrial Cancer Cells and the Tumor Microenvironment: Advances and Challenges. *Cancers (Basel)* (2019) 11:234. doi: 10.3390/cancers11020234
27. Dong P, Xiong Y, Konno Y, Ihira K, Kobayashi N, Yue J, et al. Long Non-Coding RNA DLEU2 Drives EMT and Glycolysis in Endometrial Cancer Through HK2 by Competitively Binding With miR-455 and by Modulating the EZH2/miR-181a Pathway. *J Exp Clin Cancer Res* (2021) 40(1):216. doi: 10.1186/s13046-021-02018-1
28. Lu D, Luo P, Wang Q, Ye Y, Wang B. lncRNA PVT1 in Cancer: A Review and Meta-Analysis. *Clin Chim Acta* (2017) 474:1–7. doi: 10.1016/j.cca.2017.08.038
29. Torre LA, Bray F, Siegel RL, Ferlay J, Lortet-Tieulent J, Jemal A. Global Cancer Statistics, 2012. *CA Cancer J Clin* (2015) 65(2):87–108. doi: 10.3322/caac.21262
30. Njoku K, Chiasserini D, Whetton AD, Crosbie EJ. Proteomic Biomarkers for the Detection of Endometrial Cancer. *Cancers (Basel)* (2019) 11(10):1572. doi: 10.3390/cancers11101572
31. Dong P, Karaayvaz M, Jia N, Kaneuchi M, Hamada J, Watari H, et al. Mutant P53 Gain-of-Function Induces Epithelial-Mesenchymal Transition Through Modulation of the miR-130b-ZEB1 Axis. *Oncogene* (2013) 32(27):3286–95. doi: 10.1038/onc.2012.334
32. Dong P, Kaneuchi M, Konno Y, Watari H, Sudo S, Sakuragi N. Emerging Therapeutic Biomarkers in Endometrial Cancer. *BioMed Res Int* (2013) 2013:130362. doi: 10.1155/2013/130362
33. Meng Y, Xu X, Luan H, Li L, Dai W, Li Z, et al. The Progress and Development of GLUT1 Inhibitors Targeting Cancer Energy Metabolism. *Future Med Chem* (2019) 11(17):2333–52. doi: 10.4155/fmc-2019-0052
34. Chen XY, Wang JQ, Yang Y, Li J, Chen ZS. Natural Product as Substrates of ABC Transporters: A Review. *Recent Pat Anticancer Drug Discovery* (2021) 16 (2):222–38. doi: 10.2174/1574892816666210218220943
35. Liu Y, Cao Y, Zhang W, Bergmeier S, Qian Y, Akbar H, et al. A Small-Molecule Inhibitor of Glucose Transporter 1 Downregulates Glycolysis, Induces Cell-Cycle Arrest, and Inhibits Cancer Cell Growth *In Vitro* and *In Vivo*. *Mol Cancer Ther* (2012) 11(8):1672–82. doi: 10.1158/1535-7163.MCT-12-0131
36. Ma Y, Wang W, Idowu MO, Oh U, Wang XY, Temkin SM, et al. Ovarian Cancer Relies on Glucose Transporter 1 to Fuel Glycolysis and Growth: Anti-Tumor Activity of BAY-876. *Cancers (Basel)* (2018) 11(1):33. doi: 10.3390/cancers11010033
37. Wang Y, Zhang X, Wang Z, Hu Q, Wu J, Li Y, et al. LncRNA-P23154 Promotes the Invasion-Metastasis Potential of Oral Squamous Cell Carcinoma by Regulating Glut1-Mediated Glycolysis. *Cancer Lett* (2018) 434:172–83. doi: 10.1016/j.canlet.2018.07.016
38. Ito S, Fukusato T, Nemoto T, Sekihara H, Seyama Y, Kubota S. Coexpression of Glucose Transporter 1 and Matrix Metalloproteinase-2 in Human Cancers. *J Natl Cancer Inst* (2002) 94(14):1080–91. doi: 10.1093/jnci/94.14.1080
39. Liao H, Wang Z, Deng Z, Ren H, Li X. Curcumin Inhibits Lung Cancer Invasion and Metastasis by Attenuating GLUT1/MT1-MMP/MMP2 Pathway. *Int J Clin Exp Med* (2015) 8(6):8948–57.
40. Biliran H Jr, Wang Y, Banerjee S, Xu H, Heng H, Thakur A, et al. Overexpression of Cyclin D1 Promotes Tumor Cell Growth and Confers Resistance to Cisplatin-Mediated Apoptosis in an Elastase-Myc Transgene-Expressing Pancreatic Tumor Cell Line. *Clin Cancer Res* (2005) 11(16):6075–86. doi: 10.1158/1078-0432.CCR-04-2419
41. Bao C, Chen J, Chen D, Lu Y, Lou W, Ding B, et al. MiR-93 Suppresses Tumorigenesis and Enhances Chemosensitivity of Breast Cancer *via* Dual Targeting E2F1 and CCND1. *Cell Death Dis* (2020) 11(8):618. doi: 10.1038/s41419-020-02855-6
42. He Y, Deng F, Zhao S, Zhong S, Zhao J, Wang D, et al. Analysis of miRNA-mRNA Network Reveals miR-140-5p as a Suppressor of Breast Cancer Glycolysis *via* Targeting GLUT1. *Epigenomics* (2019) 11(9):1021–36. doi: 10.2217/epi-2019-0072
43. Zhang T, Zhang Z, Li F, Ping Y, Qin G, Zhang C, et al. miR-143 Regulates Memory T Cell Differentiation by Reprogramming T Cell Metabolism. *J Immunol* (2018) 201(7):2165–75. doi: 10.4049/jimmunol.1800230
44. Farooqi AA, Qureshi MZ, Attar R, Alhewairini SS, Fayyaz S, Sabitaliyevich UY, et al. MicroRNA-143 as a New Weapon Against Cancer: Overview of the Mechanistic Insights and Long Non-Coding RNA Mediated Regulation of miRNA-143 in Different Cancers. *Cell Mol Biol (Noisy-le-grand)* (2019) 65 (6):1–5. doi: 10.14715/cmb/2019.65.6.1
45. Chang L, Zhang D, Shi H, Bian Y, Guo R. MiR-143 Inhibits Endometrial Cancer Cell Proliferation and Metastasis by Targeting MAPK1. *Oncotarget* (2017) 8(48):84384–95. doi: 10.18632/oncotarget.21037
46. Hiroki E, Suzuki F, Akahira J, Nagase S, Ito K, Sugawara J, et al. MicroRNA-34b Functions as a Potential Tumor Suppressor in Endometrial Serous Adenocarcinoma. *Int J Cancer* (2012) 131(4):E395–404. doi: 10.1002/ijc.27345
47. Hiroki E, Akahira J, Suzuki F, Nagase S, Ito K, Suzuki T, et al. Changes in microRNA Expression Levels Correlate With Clinicopathological Features and Prognoses in Endometrial Serous Adenocarcinomas. *Cancer Sci* (2010) 101(1):241–9. doi: 10.1111/j.1349-7006.2009.01385.x
48. Ning X, Zhao J, He F, Yuan Y, Li B, Ruan J. Long Non-Coding RNA TMPO-AS1 Facilitates Chemoresistance and Invasion in Breast Cancer by Modulating the miR-1179/TRIM37 Axis. *Oncol Lett* (2021) 22(1):500. doi: 10.3892/ol.2021.12761
49. Li H, Zhou Y, Cheng H, Tian J, Yang S. Roles of a TMPO-AS1/microRNA-200c/TMEFF2 ceRNA Network in the Malignant Behaviors and 5-FU Resistance of Ovarian Cancer Cells. *Exp Mol Pathol* (2020) 115:104481. doi: 10.1016/j.yexmp.2020.104481
50. Yeramian A, Moreno-Bueno G, Dolcet X, Catasus L, Abal M, Colas E, et al. Endometrial Carcinoma: Molecular Alterations Involved in Tumor Development and Progression. *Oncogene* (2013) 32(4):403–13. doi: 10.1038/onc.2012.76
51. Van Nyen T, Moiola CP, Colas E, Annibali D, Amant F. Modeling Endometrial Cancer: Past, Present, and Future. *Int J Mol Sci* (2018) 19 (8):2348. doi: 10.3390/ijms19082348

Conflict of Interest: The authors declare that the research was conducted in the absence of any commercial or financial relationships that could be construed as a potential conflict of interest.

Publisher's Note: All claims expressed in this article are solely those of the authors and do not necessarily represent those of their affiliated organizations, or those of the publisher, the editors and the reviewers. Any product that may be evaluated in this article, or claim that may be made by its manufacturer, is not guaranteed or endorsed by the publisher.

frontiers | Frontiers in Oncology

REVIEW
published: 30 May 2022
doi: 10.3389/fonc.2022.897895

Effects of N^6-Methyladenosine Modification on Cancer Progression: Molecular Mechanisms and Cancer Therapy

Yong-fu Zhu[1,2†], Shu-Jie Wang[3†], Jie Zhou[2], Ye-han Sun[1], You-mou Chen[1], Jia Ma[1], Xing-xing Huo[4] and Hang Song[5*]*

[1] The First Department of Oncology, The First Affiliated Hospital of Anhui University of Chinese Medicine, Hefei, China, [2] The Department of Acupuncture, The Third Affiliated Hospital of Zhejiang Chinese Medical University, Hangzhou, China, [3] Anhui Province Key Laboratory of Medical Physics and Technology, Institute of Health and Medical Technology, Hefei Institutes of Physical Science, Chinese Academy of Sciences, Hefei, China, [4] Experimental Center of Clinical Research, Scientific Research Department, The First Affiliated Hospital of Anhui University of Chinese Medicine, Hefei, China, [5] Department of Biochemistry and Molecular Biology, School of Integrated Chinese and Western Medicine, Anhui University of Chinese Medicine, Hefei, China

N^6-methyladenosine (m^6A) is a major internal epigenetic modification in eukaryotic mRNA, which is dynamic and reversible. m^6A is regulated by methylases ("writers") and demethylases ("erasers") and is recognized and processed by m^6A-binding proteins ("readers"), which further regulate RNA transport, localization, translation, and degradation. It plays a role in promoting or suppressing tumors and has the potential to become a therapeutic target for malignant tumors. In this review, we focus on the mutual regulation of m^6A and coding and non-coding RNAs and introduce the molecular mechanism of m^6A methylation involved in regulation and its role in cancer treatment by taking common female malignant tumors as an example.

Keywords: RNA modifications, N6-methyladenosine, female malignancies, molecular mechanisms, immunotherapy

OPEN ACCESS

Edited by:
Yan-yan Yan,
Shanxi Datong University, China

Reviewed by:
Zexian Liu,
Sun Yat-sen University Cancer Center (SYSUCC), China
Eshan Khan,
The Ohio State University, United States

***Correspondence:**
Hang Song
hangsong@ahtcm.edu.cn
Xing-xing Huo
hxx0520@ahtcm.edu.cn

†These authors have contributed equally to this work

Specialty section:
This article was submitted to Cancer Molecular Targets and Therapeutics, a section of the journal Frontiers in Oncology

Received: *16 March 2022*
Accepted: *21 April 2022*
Published: *30 May 2022*

Citation:
Zhu Y-f, Wang S-J, Zhou J, Sun Y-h, Chen Y-m, Ma J, Huo X-x and Song H (2022) Effects of N^6-Methyladenosine Modification on Cancer Progression: Molecular Mechanisms and Cancer Therapy. Front. Oncol. 12:897895. doi: 10.3389/fonc.2022.897895

INTRODUCTION

N^6-methyladenosine (m^6A) alteration is a methylation modification located on the 6th nitrogen atom of adenine. m^6A is the most abundant form of epigenetic modification in eukaryotic RNA, which exists in several different types of RNA, including mRNA and non-coding RNA. At present, the research on m^6A methylation and malignant tumors mainly focuses on the influence of m^6A

methylation on tumor cell proliferation, invasion, resistance to radiotherapy and chemotherapy, and prognosis of patients (1). The detection rate of malignant tumors is growing year by year, and the age of onset tends to be younger, thanks to the popularization of associated cancer screening tools and an increase in people's health awareness (2). The primary clinical treatment for malignant tumors is to select individualized surgery combined with postoperative radiotherapy and chemotherapy according to the patient's condition (3). However, for some patients with relapsed and refractory tumors, the treatment effect is often difficult to achieve the expected (4). Therefore, one of the most pressing issues to be addressed is elucidating the etiology of malignant tumors and finding novel therapeutic medications to overcome tumor resistance. In this review, we focus on the effect of m^6A methylation on the occurrence and development of malignant tumors and introduce the molecular mechanisms involved in the regulation of m^6A methylation and its role in cancer treatment by taking common female malignancies as an example.

OVERVIEW OF M^6A METHYLATION

The m^6A methylation modification of RNA is the most common internal modification in RNA modification. m^6A is the methylation modification of RNA on the 6th nitrogen atom of adenosine, and the process is dynamic and reversible. The proteins involved in the methylation and demethylation of m^6A are divided into three categories, namely methyltransferases ("writers"), demethylases ("erasers"), and m^6A recognition proteins ("readers") (**Figure 1**). Through RNA transcription, splicing, processing, translation, and degradation, it plays a role in the formation and spread of numerous malignant cancers. (5). Furthermore, studies have shown that m^6A methylation modification is closely related to the activation and inhibition of cancer-related signaling pathways, which mainly affect tumor progression by regulating related tumor biological functions (6).

Abbreviations: 3' -UTR, 3'-untranslation regions; 5'-UTR, 5'-untranslated region; YTH, YTH m6A RNA-binding protein; ALKBH5, AlkB homolog 5; ALKBH3, AlkB homolog 3; FZD7, Wnt receptor frizzled7; WTAP, associated protein; VIRMA, vir-like m6A methyltransferase associated; CC, Cervical cancer; circRNAs, Circular RNAs; EC, Endometrial cancer; eIF3, Eukaryotic initiation factor 3; FTO, Fat mass and obesity-associated protein; SRSF2, Serine and arginine-rich splicing factor 2; HNSCCs, Head and neck squamous cell carcinoma; HNRNPC, HNRNPG and HNRNPA2B1, Heterogeneous nuclear ribonucleoproteins; HGSOC, High-grade serous ovarian cancer; ICB, Immune checkpoint blockade; YAP, Yes-associated protein; IGFBP7, Insulin-like growth factor-binding protein-7; lncRNAs, Long non-coding RNAs; MA, Meclofenaic; mRNA, Messenger RNA; METTL3, Methyltransferase-like 3; METTL14, Methyltransferase-like 14; SKOV3, human ovarian cancer; m6A, N6-Methyladenosine; NPC, Nasopharyngeal carcinoma; ncRNAs, Non-coding RNAs; OC, Ovarian cancer; HMGA2, high mobility group A2; pre-miRNAs, Precursor miRNAs; pri-miRNAs, Primary miRNAs; PD-1, Programmed cell death protein-1; RBM15, RNA-binding motif protein 15; RBM15B, RNA-binding motif protein 15B; RISCs, RNA-induced silencing complexes; rRNAs, Ribosomal RNAs; snRNAs, Small nuclear RNAs; snoRNAs, Small nucleolar RNAs; TME, Tumor microenvironment; TIME, Tumor immune microenvironment; YTHDC1, YTHDC2, YTHDF1, YTHDF2, and YTHDF3, YTH domain protein family.

At present, m^6A RNA modification is increasingly used in cancer detection and related targeted molecules (7, 8).

m^6A Readers

For m^6A-modified mRNA to perform specific biological functions, a specific RNA-binding protein, methylation reader protein, is required. It mainly includes YTH m^6A RNA-binding protein (YTH) domain proteins (including YTHDF1, YTHDF2, YTHDF3, YTHDC1, and YTHDC2) (9), heterogeneous nuclear ribonucleoproteins (HNRNPC, HNRNPG, and HNRNPA2B1) and eukaryotic initiation factor (eIF). The functions of these reader proteins are mainly to alter protein-RNA interactions by impairing the homologous binding of m^6A to RNA-binding proteins and altering RNA secondary structure (10). Studies have found that YTHDF1 has a clear oncogenic role, and its high expression in cancer genes can accelerate the transformation of important oncogenic drivers in cancer *via* numerous methods, impacting cancer progression and prognosis. For example, in gastric cancer progression, mutated YTHDF1 enhances the expression of the key oncogenic factor Wnt receptor Frizzled7 (FZD7), leading to gastric cancer progression and poor prognosis (11).

m^6A Writers

The m^6A methyltransferase consists of methyltransferase-like 3 (METTL3), METTL14, WTAP, RBM15, ZC3H13, VIRMA, and the newly discovered METTL16, which are also called writers. Its primary function is to catalyze the m^6A modification of adenylate on mRNA. METTL3 and METTL14 have a critical catalytic domain (12), and the METTL3-METTL14 methyltransferase complex assembly during m^6A modification is a crucial factor initiating the modification. In addition, methyltransferases also include associated protein (WTAP), RBM15, ZC3H13, vir-like m^6A methyltransferase associated (VIRMA), and METTL16. These methyltransferases all play an important role in forming METTL3-METTL14 complexes in different links, affecting cancer cell proliferation and migration (13–16).

m^6A Erasers

m^6A modification is the earliest reversible modification found among many RNA modifications, and the reversibility of its modification is due to the existence of demethylases. In addition, their encoding genes are called "erasers". Fat mass and obesity-associated protein (FTO) is the first demethylase discovered and is a member of the Alkb protein family, which can affect the RNA-binding ability of the splicing factor serine and arginine-rich splicing factor 2 (SRSF2), thereby regulating the splicing process of pre-mRNA (17). ALKBH5, another member of the Alkb protein family, was found to have a demethylation function, which can directly catalyze m^6A-methylated adenosine to remove methyl groups, different from the oxidative demethylation of FTO (18).

THE ROLE OF M^6A MODIFICATIONS IN NON-CODING RNAS

In recent years, m^6A has been found to exist in various ncRNAs such as miRNAs, long non-coding RNAs (lncRNAs), circular

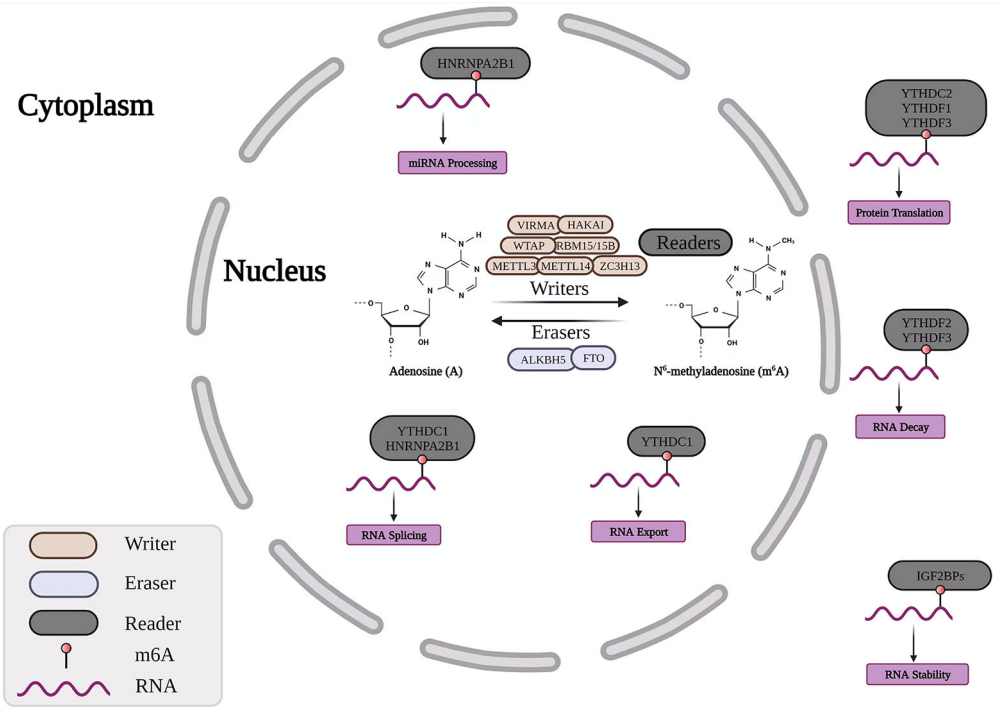

FIGURE 1 | Dynamic m6A RNA modifying process. The RNA modification of m6A is regulated by methyltransferases ("writers"), demethylases ("erasers") and m6A-binding proteins ("readers"). VIRMA, Vir Like m6A Methyltransferase Associated; HAKAI, Cbl Proto-Oncogene Like 1; WTAP, Wilms Tumor 1 Associated Protein; RBM15, RNA Binding Motif Protein 15; METTL3, Methyltransferase Like 3; METTL14, Methyltransferase Like 14; ZC3H13, Zinc Finger CCCH-Type Containing 13; ALKBH5, AlkB Homolog 5; FTO, Fat Mass And Obesity-Associated Protein; HNRNP, Heterogeneous Nuclear Ribonucleoprotein; YTHDF, YTH domain protein family; IGF2BP, Insulin Like Growth Factor 2 MRNA Binding Protein.

RNAs (circRNAs), ribosomal RNAs (rRNAs), and small nuclear RNAs (snRNAs), essential for its metabolism and function (19). Moreover, some m^{6}A regulatory proteins associated with aberrant m^{6}A modification of ncRNAs are also involved in cancer cells proliferation, invasion, and drug resistance, suggesting a potential link between cancer and m^{6}A-ncRNA modification (20).

The Effect of m^{6}A on LncRNA

LncRNAs, a type of ncRNAs of 200 or more nucleotides, can regulate gene expression at multiple levels (21). Many m^{6}A-modified lncRNAs have been found recently, and they can control gene expression and function in a variety of ways. They can act as transcriptional regulators, acting in cis or trans, regulating the transcription of adjacent genes (22). XIST, one of the first functionally annotated lncRNAs, plays a key role in X chromosome inactivation by recruiting multiple factors (23). A study shows that in head and neck squamous cell carcinoma, METTL3- and METTL14-mediated m^{6}A methylation contributes to the stability of LNCAROD, and LNCAROD overexpression promotes the malignant development of HNSCC by promoting YBX1-hspa1a interaction, thereby enhancing the stability of the YBX1 protein (24). Another study found that modifying lncRNAs with m^{6}A had the opposite effect on cancers. METTL14 suppressed colorectal cancer growth and metastasis by downregulating oncogenic long non-coding RNA XIST in the METTL14-YTHDF2-lncRNA regulatory axis (25). LncRNA GAS5 binds directly to Yes-associated protein (YAP), promoting its phosphorylation and ubiquitin-mediated degradation, thereby attenuating YAP-mediated transcription of YTHDF3 and inhibiting the progression of rectal cancer (26). LincRNA-p21 acts as a tumor inhibitor in the development of esophageal squamous cell carcinoma (27). In hepatocellular carcinoma, the m^{6}A methylation modification of LINC00152 is involved in the prognosis of LIHC patients through the cytoskeleton regulation pathway (28). Furthermore, in rectal cancer, m^{6}A modification of lncRNA RP11 can upregulate the translation of Zeb1 to trigger cancer cell dissemination (29); lncRNA-THOR enhances IGF2BP1-targeted mRNA expression and promotes human osteosarcoma cell survival and proliferation (30).

The Effect of m^{6}A Modification on MiRNA

MiRNAs are non-coding single-stranded RNAs of 21-25 nucleotides in length that regulate gene expression at the post-transcriptional level by building RNA-induced silencing complexes (RISCs) that bind to the 3'untranslated region of

target mRNAs (3'UTR) to regulate gene expression (31). In the nucleus, miRNAs are first transcribed into longer primary miRNAs (pri-miRNAs) and subsequently processed into precursor miRNAs (pre-miRNAs). It is then cleaved into mature single-stranded miRNAs by Dicer in the cytoplasm, and the participation and processing of such pri-miRNAs are m^{6}A-dependent. METTL3 tags pre-miRNAs through m^{6}A modification, enabling DGCR8 to recognize and bind its specific substrates, thereby promoting miRNA maturation and increased miRNA levels in cells (32).

The Role of m^{6}A Modification of CircRNA in Cancer

Circular RNAs (circRNAs) are a class of single-stranded covalently closed RNA molecules that participate in many physiological processes, including competing with endogenous RNAs as sponge miRNAs, forming RNA-protein complexes, regulating gene transcription, and even encoding proteins (33). In most cases, abnormal m^{6}A modification contributes to tumorigenesis and tumor progression. However, m^{6}A modification on circRNAs can suppress innate immunity; YTHDF2 sequesters m^{6}A-circRNA and is essential for suppressing innate immunity (34). Chen et al. found that m^{6}A modification of circNSUN2 promoted liver metastasis of colorectal cancer by promoting cytoplasmic export and forming a circNSUN2/IGF2BP2/HMGA2 RNA-protein triple complex to stabilize HMGA2 mRNA (35).

THE ROLE OF M^{6}A MODIFICATIONS IN CODING RNAS

m^{6}A affects all physiological processes such as mRNA processing, nuclear export, translation, and degradation. It mainly affects mRNA stability, which is also closely related to the occurrence and development of malignant tumors. At present, the research on m^{6}A and its participants in the reversible regulation process (m^{6}A-modifying enzymes and m^{6}A-binding proteins) and the mechanism of tumorigenesis and development has gradually become a hot spot.

Ries et al. found that m^{6}A-mRNA is regulated by compartments, including mRNA stability and reduced translation. This study demonstrates that the number and distribution of m^{6}A sites in cellular mRNA can modulate and influence the composition of the phase-separated transcriptome (36). Li et al. first elucidated the *in vivo* biological role of m^{6}A modification in T cell-mediated pathogenesis. They revealed a novel mechanism for T cell homeostasis and signal-dependent induction of mRNA degradation (37). RNA methyltransferase (METTL3) acts as a translation initiation complex, thereby enhancing the translation of target mRNAs (38). In addition, at different intracellular locations, m^{6}A exerts methyltransferase activity-dependent and -independent functions in gene regulation. Besides, the RNA methyltransferase METTL16 is in the nucleus, acting as an m^{6}A writer, depositing m^{6}A into its hundreds of a specific messenger RNA target. In the cytosol, METTL16 promotes translation in an m^{6}A-independent manner (39).

THE ROLE OF M^{6}A MODIFICATIONS IN COMMON FEMALE MALIGNANCIES

Common malignant tumors in women mainly include breast cancer (BC), ovarian cancer (OC), cervical cancer (CC), and endometrial cancer (EC). Despite advancements in examination methods in the prevention and treatment of common female malignant tumors, most patients are in the middle and late stages of their disease due to difficulties in early diagnosis and localization of tumors and a lack of effective efficacy evaluation and prognosis monitoring methods. Therefore, the mortality rate of common malignant tumors in women continues to increase. Genetic, epigenetic, and environmental factors drive its occurrence, development, and transfer, and epigenetic factors play an important role as a bridge between genetic and environmental factors. Epigenetics has multiple forms of expression, of which m^{6}A is the most abundant form of internal modification. In this review, we take common female malignant tumors as examples to introduce the molecular mechanism of m^{6}A modification in the occurrence and development of cancer and its application in cancer treatment (**Table 1**).

The Regulatory Role of m^{6}A Methyltransferase (Writers)

m^{6}A methyltransferases ("Writers") are an essential class of catalytic enzymes. METTL3 is a key regulator that promotes m^{6}A modification, and the abnormal regulation of METTL3 is also inextricably linked to tumor development. Some studies have confirmed that the overexpression of METTL3 may be an important factor in promoting the development of common malignant tumors in women. Pan et al. found that the expression of RBM15 and METTL3 in CESC (cervical squamous cell carcinoma) tissues was higher than that in normal tissues (49). In addition, Hua et al. found that METTL3 promoted the epithelial-to-mesenchymal transition of ovarian cancer cells and the proliferation, invasion, and tumor formation of ovarian cancer cells, affecting their prognosis and overall survival (50). Moreover, Ma et al. compared the expressions of METTL14, WTAP, and METTL3 in ovarian cancer and found that METTL3 independently regulates m^{6}A modification and thus affects the proliferation and metastasis (51). Besides, Li et al. found that METTL3 inhibited the viability of cervical cancer cells and enhanced their sensitivity to the chemotherapeutic drug cisplatin by downregulating the expression of the receptor for advanced glycation and its product in cervical cancer tissues (40); METTL3 modulated the m^{6}A modification of MALAT1. The expression of MALAT1 is upregulated, and MALAT1 can promote the expression of high mobility group A2 (HMGA2) by sponge miR-26b, thereby promoting the development of breast cancer (41). Regarding this, Wang et al. proposed that WTAP may promote the proliferation, invasion, and migration of ovarian cancer through two gene sequences of FAM76A and HBS1 (42).

The Regulatory Role of m^{6}A Methylation Reader Proteins (Readers)

As m^{6}A methylation reading proteins, "Readers" can recognize the information of RNA methylation modification and

TABLE 1 | Dysregulation of m6A modification in common female malignant (CFM).

m^6A regulators	Target	Regulation in CFM	Fuction	Mechanisms
METTL3	RAGE	Down	writer	METTL3 increases cisplatin chemosensitivity of cervical cancer cells *via* downregulation of the activity of RAGE. Li, R. et al. (40);
	MALAT1	Down	writer	The m6A methyltransferase METTL3 controls epithelial-mesenchymal transition, migration and invasion of breast cancer through the MALAT1/miR-26b/HMGA2 axis. Zhao, C et al. (41)
WTAP	HBS1L/FAM76A	Up	writer	Identification of WTAP-related genes by weighted gene co-expression network analysis in ovarian cancer. Wang, J. et al. (42).
YTHDF1	RANBP2	Up	reader	YTHDF1 Aggravates the Progression of Cervical Cancer Through m(6)A-Mediated Up-Regulation of RANBP2. Wang, H. et al. (43).
	EIF3C	Up	reader	The m^6A reader YTHDF1 promotes ovarian cancer progression *via* augmenting EIF3C translation. Liu, T. et al. (9).
eIF3	WNT	Up	reader	The Immune-Related Gene ELF3 is a Novel Biomarker for the Prognosis of Ovarian Cancer. Xu, H., et al. (44).
FTO	miR-181b-3p	Up	ereaser	The FTO/miR-181b-3p/ARL5B signaling pathway regulates cell migration and invasion in breast cancer. Xu, Y. et al. (45).
	BNIP3	Up	ereaser	RNA N6-methyladenosine demethylase FTO promotes breast tumor progression through inhibiting BNIP3. Niu, Y. et al. (46).
	cAMP	Down	ereaser	FTO-Dependent N (6)-Methyladenosine Modifications Inhibit Ovarian Cancer Stem Cell Self-Renewal by Blocking cAMP Signaling. Huang, H. et al. (47).
ALKBH5	NANOG	Up	ereaser	RNA demethylase ALKBH5 promotes ovarian carcinogenesis in a simulated tumour microenvironment through stimulating NF-kappaB pathway. Jiang, Y. et al. (48).

participate in downstream mRNA translation, degradation, and miRNA processing. It mainly changes the interaction between protein and RNA by weakening the homologous binding of m^6A to RNA-binding protein and changing the secondary structure of RNA.

YTHDF1 acts as an important reading element in m^6A modification by recognizing m^6A-containing mRNAs and promoting their translation initiation and elongation (52). Wang et al. applied online data analysis to identify RANBP2 as a critical target of YTHDF1 in cervical cancer cells, and subsequent reduction of RANBP2 decreased cervical cancer cell proliferation, migration, and invasion (43). Overexpression of YTHDF1 promoted the growth, migration, and invasion of Hela and Siha cells. At the same time, knockdown of RANBP2 reversed the effect of overexpression of YTHDF1 on cervical cancer progression, indicating that YTHDF1 promotes cervical cancer progression by regulating RANBP2 expression in an m^6A-dependent manner. Some scholars have proposed that YTHDF1 directly targets eIF3C (a subunit of EIF3) and promotes ovarian cancer's occurrence, metastasis, and prognosis (51).

Heterogeneous ribonucleoproteins (hnRNPs) are a diverse family of RNA-binding proteins that function in most stages of RNA metabolism (53). Studies have shown that HNRNPC regulates target transcripts' abundance and alternative splicing through mA binding to RNA. Other researchers have proposed that hnRNPA2B1 can inhibit the growth of ovarian cancer cells, reduce the mobility of ovarian cancer cells *in vitro*, and hinder the formation of xenograft tumors *in vivo*. In addition, hnRNPA2B1 promotes the occurrence and development of malignant phenotypes of ovarian cancer by activating the expression of Lin28B (54). Moreover, Shi et al. found that lobaplatin induced apoptosis and cell cycle arrest by downregulating hnRNP A2/B1 in cervical cancer cells, and knockdown of hnRNP A2/B1 significantly reduced tumor growth in nude mice xenografts and increased cervical cancer Cellular sensitivity to lobaplatin and irinotecan (55). Eukaryotic initiation factor 3 (eIF3) can bind to m^6A-modified bases in the 5' UTR of RNA, promoting mRNA translation (56). The high expression of eLF3 in ovarian cancer is closely related to its poor prognosis (44); Zhu et al. concluded that eIF3B is highly expressed in cervical cancer tissues and is closely related to advanced FIGO in cervical cancer patients staging, shorter overall survival and lymph node metastasis (57).

The Regulatory Role of m^6A Demethylases (erasers)

Demethylase is an integral part of the reversible modification of m^6A, and FTO, as the first discovered demethylase, is widely present in adult and embryonic tissues, and its expression is exceptionally high in the brain. Moreover, recent studies have shown that FTO has an important effect on glioblastoma growth and self-renewal (58).

The expression level of FTO is also elevated in cervical squamous cell carcinoma, which can enhance chemoradiotherapy resistance *in vitro* and *in vivo* by reducing m^6A-regulated β-catenin expression (59). Zhao et al. believed that FTO accelerated the growth of cancer cells by promoting proliferation, inhibiting apoptosis, and activating autophagy in ovarian cancer (60). In the latest study, Huang et al. found that FTO expression in high-grade serous ovarian cancer (HGSOC) tumor cells were significantly lower than that in other tissues, and it had a significant inhibitory effect on ovarian cancer cells (47). It can be seen that FTO may have a bidirectional regulatory impact on ovarian cancer tissue, and the specific mechanism needs to be further studied. Furthermore some researchers believe that FTO primarily stimulates the oncogenic activity of breast cancer cell invasion and migration through the FTO/miR-181b-3p/ARL5B signaling pathway, promoting tumor proliferation (61). The tumor suppressor BNIP3 is a downstream target of FTO-mediated m^6A modification. FTO mediates m^6A demethylation in the 3'UTR of BNIP3 mRNA and induces its degradation through a YTHDF2-independent mechanism,

promoting breast cancer cell proliferation, colony formation, and *in vitro* and *in vivo* transfer (46).

Among them, ALKBH5, another member of the Alkb protein family, was found to have demethylation, which can directly catalyze m^{6}A-methylated adenosine to remove methyl groups is different from the oxidative demethylation of FTO (62). ALKBH5 affects tumor growth by regulating cell proliferation, migration, invasion, and metastasis. Recently, some scholars have proposed that ALKBH5 has dual roles in various cancers. ALKBH5 can reverse METTL3 autophagy in cells through down-regulation of mRNA stability. In epithelial ovarian cancer cells (63), overexpressed ALKBH5 in human ovarian cancer (SKOV3) cells enhanced the stability of BCL-2 mRNA and inhibited tumor cell growth and metastasis. In contrast, overexpressed ALKBH5 in A2780 cells had the exact opposite effect. In cervical cancer tissues, GAS5-AS1 was also low-expressed and inhibited the proliferation and metastasis of cervical cancer cells. And regulate GAS5 expression by interacting with RNA demethylase ALKBH5, thereby inhibiting CC cell proliferation, migration, and invasion (64).

M^{6}A RNA MODIFICATIONS AND COMMON FEMALE MALIGNANCIES THERAPY

The Role of m^{6}A RNA Modification Targeted Drugs in the Treatment of Common Female Malignant Tumors

Targeted therapy is at the cellular and molecular level to design corresponding therapeutic drugs for the already defined carcinogenic sites. The drug enters the body and will specifically select the carcinogenic sites to combine and act so that the tumor cells specifically die instead of normal tissue cells surrounding the tumor are affected. Early studies of targeting strategies based on m^{6}A modulators have focused on demethylases. Besides, previous studies have shown that m^{6}A plays an essential role in the occurrence and development of tumors. Therefore, it is of great scientific significance and clinical value to develop specific inhibitors of m^{6}A-related proteins. As the first discovered RNA-modifying demethylase, FTO is widely involved in various physiological processes, and its dysregulation is associated with multiple human diseases.

Due to its involvement in obesity and obesity-induced metabolic diseases and the occurrence, development and prognosis of various cancers, such as melanoma, acute myeloid leukemia, glioblastoma, lung cancer, hepatocellular carcinoma and breast cancer, studies have shown that rhein can induce apoptosis (65). Huang et al.. systematically investigated the effect of rhein on adipogenesis by transcriptional and post-transcriptional approaches and found that rhein regulates m^{6}A methylation rearrangement and adipogenesis in an independent manner, inhibiting fat mass and obesity-related (FTO) demethylase activity (66). It is indicated that rhein can inhibit the demethylation activity of FTO on m^{6}A on mRNA *in vitro* and *in vivo*, thereby increasing the level of m^{6}A in cells. ALKBH5 and FTO are both m^{6}A demethylases. Studies have found that in ovarian cancer, the core cytokine NANOG is a key target to promote the development of ovarian cancer (48). On the contrary, there is much evidence to prove the overexpression of METTL3 in tumor tissues (67), while studies targeting METTL3 have shown that it can effectively inhibit tumor growth, proliferation, and metastasis (68).

In the progression of common malignant tumors in women, drug resistance that often occurs in the later stage is also a significant difficulty in its treatment. Chemotherapy resistance, especially platinum resistance, is a major cause of poor prognosis in ovarian cancer. Bowen Li et al. found that m^{6}A can modulate the modification of anticancer drug resistance by modulating drug-target interactions and drug-mediated cell death signaling (69). The ethyl ester form of the FTO inhibitor Meclofenaic (MA2) inhibits FTO and enhances the effect of the chemotherapeutic drug temozolom by targeting the MYC-miR-155/23a cluster-MXI1 feedback circuit in gliomas anti-tumor effects (45) (**Table 2**).

m^{6}A RNA Modification and Immunotherapy

The tumor microenvironment (TME) is primarily responsible for mediating immunotherapy responses in tumor progression, and bioinformatics research has shown that m^{6}A alteration and its regulators may regulate the TME and are linked to immune checkpoint inhibition (ICB) (7, 72).

Yi et al. systematically studied head and neck squamous cell carcinoma (HNSCC) compared with adjacent normal pairs, concluded that m^{6}A regulators were upregulated in HNSCC, and found that m^{6}A regulators were associated with PDL in the tumor immune microenvironment (TIME) (73). The expression of -1 was positively correlated, which may provide a promising target for improving the responsiveness of HNSCC to immunotherapy. In addition, He et al. systematically analyzed RNA-sequencing data of 24 major m^{6}A methylation regulators in 775 breast cancer patients from the TCGA database and classified them for overall survival in the lower RNA methylation status group (RM1). The higher methylation status (RM2) group was significantly reduced (70). Moreover, the RM2 group displayed higher expression and higher numbers of tumor-infiltrating CD8$^+$ T cells, helper T cells, and activated NK cells. The expressions of PD-L2, TIM3, and CCR4 were lower than those of the RM1 group, so it can be considered that the regulator of m^{6}A is closely related to the malignant degree, prognosis, and anti-tumor immune response of breast cancer and can be used as a potential target and biological target for breast cancer immunotherapy.

In addition, anti-PD-1 immunotherapy is effective initially, but its efficacy is significantly reduced later due to FTO-mediated resistance (71). However, recent studies have shown that FTO knockdown can increase tumor sensitivity to anti-PD-1 immunotherapy, thereby improving efficacy (69). Therefore, the combined use of ICB and FTO inhibitors may block the development of drug resistance in individuals who develop adaptive immunity.

TABLE 2 | Therapeutic targets of M6A modification in common female malignant (CFM).

Remedy	Regulation of target	Target	Mechanisms
Rhein	inhibition	REEP3	FTO regulates the chemo-radiotherapy resistance of cervical squamous cell carcinoma (CSCC) by targeting beta-catenin through mRNA demethylation. Zhou, S. et al. (59).
Temozolomide	inhibition	MYC-miR-155/23a	FTO Inhibition Enhances the Antitumor Effect of Temozolomide by Targeting MYC-miR-155/23a Cluster-MXI1 Feedback Circuit in Glioma. Xiao, L. et al. (45).
Immune checkpoint inhibitor	inhibition	PD-L1, PD-L2, TIM3, and CCR4	Expression pattern of m(6)A regulators is significantly correlated with malignancy and antitumor immune response of breast cancer. He, X., et al. (70).
Immune checkpoint inhibitor PARP	upregulating	Wnt/β-catenin pathway	N(6)-Methylation of Adenosine of FZD10 mRNA Contributes to PARP Inhibitor Resistance. Fukumoto, T. et al. (71).

CONCLUSIONS

With the rapid development of high-throughput sequencing technology and bioinformatics, m^6A has been gradually revealed as an important epigenetic modification with reversible properties, modification-related enzyme system, and role in different disease processes. It provides infinite possibilities for subsequent tumor diagnosis and treatment. These m^6A-modified molecules are expected to become effective early diagnosis and prognostic markers for tumors and potential therapeutic targets, providing new ideas for tumor diagnosis and treatment.

Since m^6A research provides a new understanding of the molecular mechanisms of tumorigenesis, metastasis, immune response, and drug resistance and promotes the development of new therapeutics, the process from theory to clinical translation still needs to be explored. Currently, the understanding of how m^6A modification affects immune phenotype is still in its infancy. Although some methylase inhibitors have been discovered so far and provide new targets for tumor drugs, their mechanisms of action *in vitro* and *in vivo* are not fully understood and lack specificity. Therefore, the development of more inhibitors against m^6A-related proteins brings a new dawn for guiding tumor-targeted therapy based on RNA epigenetics. Targeted intervention in m^6A modification can promote basic research in related fields, show excellent application prospects in tumor treatment and other disease-related fields, and show important scientific significance in life sciences and new drug discovery.

AUTHOR CONTRIBUTIONS

HS and X-xH conceived and designed the study. Y-fZ, S-jW, JZ, Y-hS, JM, and Y-mC collected data and aided in writing the manuscript. HS and Y-fZ edited the manuscript. All authors read and approved the final manuscript.

FUNDING

This study was supported by the National Natural Science Foundation of China (No. 81802103, 81803938), Project of High-Level Talents in AHUTCM (Project code: 2019rcZD001), Excellent Young Scholars Project of Natural Science Foundation of Anhui Province in China (grant No. 2108085Y29), Natural Science Research Project of Colleges and Universities in Anhui Province (No. KJ2021A0557), Opening Project of Zhejiang Provincial Preponderant and Characteristic Subject of Key University (Chinese Traditional Medicine), and Zhejiang Chinese Medical University (No.ZYXZD2019004).

REFERENCES

1. Han X, Liu J, Cheng G, Cui S. Gene Signatures and Prognostic Values of M6a RNA Methylation Regulators in Ovarian Cancer. *Cancer Control* (2020) 27:1073274820960460. doi: 10.1177/1073274820960460
2. Sung H, Ferlay J, Siegel RL, Laversanne M, Soerjomataram I, Jemal A, et al. Global Cancer Statistics 2020: GLOBOCAN Estimates of Incidence and Mortality Worldwide for 36 Cancers in 185 Countries. *CA Cancer J Clin* (2021) 71:209–49. doi: 10.3322/caac.21660
3. Byrd DR, Brierley JD, Baker TP, Sullivan DC, Gress DM. Current and Future Cancer Staging After Neoadjuvant Treatment for Solid Tumors. *CA Cancer J Clin* (2021) 71:140–8. doi: 10.3322/caac.21640
4. Graillon T, Tabouret E, Chinot O. Chemotherapy and Targeted Therapies for Meningiomas: What Is the Evidence? *Curr Opin Neurol* (2021) 34:857–67. doi: 10.1097/WCO.0000000000001002
5. He L, Li H, Wu A, Peng Y, Shu G, Yin G. Functions of N6-Methyladenosine and its Role in Cancer. *Mol Cancer* (2019) 18:176. doi: 10.1186/s12943-019-1109-9
6. Zhou Z, Lv J, Yu H, Han J, Yang X, Feng D, et al. Mechanism of RNA Modification N6-Methyladenosine in Human Cancer. *Mol Cancer* (2020) 19:104. doi: 10.1186/s12943-020-01216-3
7. Kuai D, Zhu S, Shi H, Yang R, Liu T, Liu H, et al. Aberrant Expression of M(6)A mRNA Methylation Regulators in Colorectal Adenoma and Adenocarcinoma. *Life Sci* (2021) 273:119258. doi: 10.1016/j.lfs.2021.119258
8. Zhang B, Chen Z, Tao B, Yi C, Lin Z, Li Y, et al. M(6)A Target microRNAs in Serum for Cancer Detection. *Mol Cancer* (2021) 20:170. doi: 10.1186/s12943-021-01477-6
9. Liu S, Li G, Li Q, Zhang Q, Zhuo L, Chen X, et al. The Roles and Mechanisms of YTH Domain-Containing Proteins in Cancer Development and Progression. *Am J Cancer Res* (2020) 10(4):1068–84.
10. Liu N, Zhou KI, Parisien M, Dai Q, Diatchenko L, Pan T. N6-Methyladenosine Alters RNA Structure to Regulate Binding of a Low-Complexity Protein. *Nucleic Acids Res* (2017) 45:6051–63. doi: 10.1093/nar/gkx141
11. Pi J, Wang W, Ji M, Wang X, Wei X, Jin J, et al. YTHDF1 Promotes Gastric Carcinogenesis by Controlling Translation of FZD7. *Cancer Res* (2021) 81:2651–65. doi: 10.1158/0008-5472.CAN-20-0066
12. Zaccara S, Ries RJ, Jaffrey SR. Reading, Writing and Erasing mRNA Methylation. *Nat Rev Mol Cell Biol* (2019) 20:608–24. doi: 10.1038/s41580-019-0168-5
13. Wen J, Lv R, Ma H, Shen H, He C, Wang J, et al. Zc3h13 Regulates Nuclear RNA M(6)A Methylation and Mouse Embryonic Stem Cell Self-Renewal. *Mol Cell* (2018) 69:1028–1038 e1026. doi: 10.1016/j.molcel.2018.02.015

14. Lan Y, Liu B, Guo H. The Role of M(6)A Modification in the Regulation of Tumor-Related lncRNAs. *Mol Ther Nucleic Acids* (2021) 24:768–79. doi: 10.1016/j.omtn.2021.04.002
15. Mendel M, Delaney K, Pandey RR, Chen KM, Wenda JM, Vagbo CB, et al. Splice Site M(6)A Methylation Prevents Binding of U2AF35 to Inhibit RNA Splicing. *Cell* (2021) 184:3125–3142 e3125. doi: 10.1016/j.cell.2021.03.062
16. Zhu W, Wang JZ, Wei JF, Lu C. Role of M6a Methyltransferase Component VIRMA in Multiple Human Cancers (Review). *Cancer Cell Int* (2021) 21:172. doi: 10.1186/s12935-021-01868-1
17. Su R, Dong L, Li Y, Gao M, Han L, Wunderlich M, et al. Targeting FTO Suppresses Cancer Stem Cell Maintenance and Immune Evasion. *Cancer Cell* (2020) 38:79–96 e11. doi: 10.1016/j.ccell.2020.04.017
18. Wu X, Dai M, Li J, Cai J, Zuo Z, Ni S, et al. M(6)A Demethylase ALKBH5 Inhibits Cell Proliferation and the Metastasis of Colorectal Cancer by Regulating the FOXO3/miR-21/SPRY2 Axis. *Am J Transl Res* (2021) 13 (10):11209–22.
19. Li Y, Xiao J, Bai J, Tian Y, Qu Y, Chen X, et al. Molecular Characterization and Clinical Relevance of M(6)A Regulators Across 33 Cancer Types. *Mol Cancer* (2019) 18:137. doi: 10.1186/s12943-019-1066-3
20. Huang H, Weng H, Chen J. M(6)A Modification in Coding and Non-Coding RNAs: Roles and Therapeutic Implications in Cancer. *Cancer Cell* (2020) 37:270–88. doi: 10.1016/j.ccell.2020.02.004
21. Kopp F, Mendell JT. Functional Classification and Experimental Dissection of Long Noncoding RNAs. *Cell* (2018) 172:393–407. doi: 10.1016/j.cell.2018.01.011
22. Furlan G, Gutierrez Hernandez N, Huret C, Galupa R, Van Bemmel JG, Romito A, et al. The Ftx Noncoding Locus Controls X Chromosome Inactivation Independently of Its RNA Products. *Mol Cell* (2018) 70:462–472 e468. doi: 10.1016/j.molcel.2018.03.024
23. Lee JT, Bartolomei MS. X-Inactivation, Imprinting, and Long Noncoding RNAs in Health and Disease. *Cell* (2013) 152:1308–23. doi: 10.1016/j.cell.2013.02.016
24. Ban Y, Tan P, Cai J, Li J, Hu M, Zhou Y, et al. LNCAROD is Stabilized by M6a Methylation and Promotes Cancer Progression *via* Forming a Ternary Complex With HSPA1A and YBX1 in Head and Neck Squamous Cell Carcinoma. *Mol Oncol* (2020) 14:1282–96. doi: 10.1002/1878-0261.12676
25. Yang X, Zhang S, He C, Xue P, Zhang L, He Z, et al. METTL14 Suppresses Proliferation and Metastasis of Colorectal Cancer by Down-Regulating Oncogenic Long Non-Coding RNA XIST. *Mol Cancer* (2020) 19:46. doi: 10.1186/s12943-020-1146-4
26. Ni W, Yao S, Zhou Y, Liu Y, Huang P, Zhou A, et al. Long Noncoding RNA GAS5 Inhibits Progression of Colorectal Cancer by Interacting With and Triggering YAP Phosphorylation and Degradation and is Negatively Regulated by the M(6)A Reader YTHDF3. *Mol Cancer* (2019) 18:143. doi: 10.1186/s12943-019-1079-y
27. Zhang Y, Miao Y, Shang M, Liu M, Liu R, Pan E, et al. LincRNA-P21 Leads to G1 Arrest by P53 Pathway in Esophageal Squamous Cell Carcinoma. *Cancer Manag Res* (2019) 11:6201–14. doi: 10.2147/CMAR.S197557
28. Zhu HX, Lu WJ, Zhu WP, Yu S. Comprehensive Analysis of N(6) -Methyladenosine-Related Long Non-Coding RNAs for Prognosis Prediction in Liver Hepatocellular Carcinoma. *J Clin Lab Anal* (2021) 35: e24071. doi: 10.1002/jcla.24071
29. Wu Y, Yang X, Chen Z, Tian L, Jiang G, Chen F, et al. M(6)A-Induced lncRNA RP11 Triggers the Dissemination of Colorectal Cancer Cells *via* Upregulation of Zeb1. *Mol Cancer* (2019) 18:87. doi: 10.1186/s12943-019-1014-2
30. Chen W, Chen M, Xu Y, Chen X, Zhou P, Zhao X, et al. Long Non-Coding RNA THOR Promotes Human Osteosarcoma Cell Growth *In Vitro* and *In Vivo*. *Biochem Biophys Res Commun* (2018) 499:913–9. doi: 10.1016/j.bbrc.2018.04.019
31. Correia De Sousa M, Gjorgjieva M, Dolicka D, Sobolewski C, Foti M. Deciphering miRNAs' Action Through miRNA Editing. *Int J Mol Sci* (2019) 20(24):6249. doi: 10.3390/ijms20246249
32. Chen Y, Lin Y, Shu Y, He J, Gao W. Interaction Between N(6)-Methyladenosine (M(6)A) Modification and Noncoding RNAs in Cancer. *Mol Cancer* (2020) 19:94. doi: 10.1186/s12943-020-01207-4
33. Li X, Ding J, Wang X, Cheng Z, Zhu Q. NUDT21 Regulates circRNA Cyclization and ceRNA Crosstalk in Hepatocellular Carcinoma. *Oncogene* (2020) 39:891–904. doi: 10.1038/s41388-019-1030-0
34. Chen YG, Chen R, Ahmad S, Verma R, Kasturi SP, Amaya L, et al. N6-Methyladenosine Modification Controls Circular RNA Immunity. *Mol Cell* (2019) 76:96–109 e109. doi: 10.1016/j.molcel.2019.07.016
35. Chen RX, Chen X, Xia LP, Zhang JX, Pan ZZ, Ma XD, et al. N(6)-Methyladenosine Modification of Circnsun2 Facilitates Cytoplasmic Export and Stabilizes HMGA2 to Promote Colorectal Liver Metastasis. *Nat Commun* (2019) 10:4695. doi: 10.1038/s41467-019-12651-2
36. Ries RJ, Zaccara S, Klein P, Olarerin-George A, Namkoong S, Pickering BF, et al. M(6)A Enhances the Phase Separation Potential of mRNA. *Nature* (2019) 571:424–8. doi: 10.1038/s41586-019-1374-1
37. Li HB, Tong J, Zhu S, Batista PJ, Duffy EE, Zhao J, et al. M(6)A mRNA Methylation Controls T Cell Homeostasis by Targeting the IL-7/STAT5/SOCS Pathways. *Nature* (2017) 548:338–42. doi: 10.1038/nature23450
38. Lin S, Choe J, Du P, Triboulet R, Gregory RI. The M(6)A Methyltransferase METTL3 Promotes Translation in Human Cancer Cells. *Mol Cell* (2016) 62:335–45. doi: 10.1016/j.molcel.2016.03.021
39. Su R, Dong L, Li Y, Gao M, He PC, Liu W, et al. METTL16 Exerts an M(6)A-Independent Function to Facilitate Translation and Tumorigenesis. *Nat Cell Biol* (2022) 24:205–16. doi: 10.1038/s41556-021-00835-2
40. Li R, Song Y, Chen X, Chu M, Wang ZW, Zhu X. METTL3 Increases Cisplatin Chemosensitivity of Cervical Cancer Cells *via* Downregulation of the Activity of RAGE. *Mol Ther Oncolytics* (2021) 22:245–55. doi: 10.1016/j.omto.2021.05.013
41. Zhao C, Ling X, Xia Y, Yan B, Guan Q. The M6a Methyltransferase METTL3 Controls Epithelial-Mesenchymal Transition, Migration and Invasion of Breast Cancer Through the MALAT1/miR-26b/HMGA2 Axis. *Cancer Cell Int* (2021) 21:441. doi: 10.1186/s12935-021-02113-5
42. Wang J, Xu J, Li K, Huang Y, Dai Y, Xu C, et al. Identification of WTAP-Related Genes by Weighted Gene Co-Expression Network Analysis in Ovarian Cancer. *J Ovarian Res* (2020) 13:119. doi: 10.1186/s13048-020-00710-y
43. Wang H, Luo Q, Kang J, Wei Q, Yang Y, Yang D, et al. YTHDF1 Aggravates the Progression of Cervical Cancer Through M(6)A-Mediated Up-Regulation of RANBP2. *Front Oncol* (2021) 11:650383. doi: 10.3389/fonc.2021.650383
44. Xu H, Wang H, Li G, Jin X, Chen B. The Immune-Related Gene ELF3 Is a Novel Biomarker for the Prognosis of Ovarian Cancer. *Int J Gen Med* (2021) 14:5537–48. doi: 10.2147/IJGM.S332320
45. Xiao L, Li X, Mu Z, Zhou J, Zhou P, Xie C, et al. FTO Inhibition Enhances the Antitumor Effect of Temozolomide by Targeting MYC-miR-155/23a Cluster-MXI1 Feedback Circuit in Glioma. *Cancer Res* (2020) 80:3945–58. doi: 10.1158/0008-5472.CAN-20-0132
46. Niu Y, Lin Z, Wan A, Chen H, Liang H, Sun L, et al. RNA N6-Methyladenosine Demethylase FTO Promotes Breast Tumor Progression Through Inhibiting BNIP3. *Mol Cancer* (2019) 18:46. doi: 10.1186/s12943-019-1004-4
47. Huang H, Wang Y, Kandpal M, Zhao G, Cardenas H, Ji Y, et al. FTO-Dependent N (6)-Methyladenosine Modifications Inhibit Ovarian Cancer Stem Cell Self-Renewal by Blocking cAMP Signaling. *Cancer Res* (2020) 80:3200–14. doi: 10.1158/0008-5472.CAN-19-4044
48. Jiang Y, Wan Y, Gong M, Zhou S, Qiu J, Cheng W. RNA Demethylase ALKBH5 Promotes Ovarian Carcinogenesis in a Simulated Tumour Microenvironment Through Stimulating NF-kappaB Pathway. *J Cell Mol Med* (2020) 24:6137–48. doi: 10.1111/jcmm.15228
49. Pan J, Xu L, Pan H. Development and Validation of an M6a RNA Methylation Regulator-Based Signature for Prognostic Prediction in Cervical Squamous Cell Carcinoma. *Front Oncol* (2020) 10:1444. doi: 10.3389/fonc.2020.01444
50. Hua W, Zhao Y, Jin X, Yu D, He J, Xie D, et al. METTL3 Promotes Ovarian Carcinoma Growth and Invasion Through the Regulation of AXL Translation and Epithelial to Mesenchymal Transition. *Gynecol Oncol* (2018) 151:356–65. doi: 10.1016/j.ygyno.2018.09.015
51. Ma Z, Li Q, Liu P, Dong W, Zuo Y. METTL3 Regulates M6a in Endometrioid Epithelial Ovarian Cancer Independently of METTl14 and WTAP. *Cell Biol Int* (2020) 44:2524–31. doi: 10.1002/cbin.11459
52. Lin X, Chai G, Wu Y, Li J, Chen F, Liu J, et al. RNA M(6)A Methylation Regulates the Epithelial Mesenchymal Transition of Cancer Cells and Translation of Snail. *Nat Commun* (2019) 10:2065. doi: 10.1038/s41467-019-09865-9
53. Levengood JD, Tolbert BS. Idiosyncrasies of hnRNP A1-RNA Recognition: Can Binding Mode Influence Function. *Semin Cell Dev Biol* (2019) 86:150–61. doi: 10.1016/j.semcdb.2018.04.001
54. Yang Y, Wei Q, Tang Y, Yuanyuan W, Luo Q, Zhao H, et al. Loss of Hnrnpa2b1 Inhibits Malignant Capability and Promotes Apoptosis *via*

Down-Regulating Lin28B Expression in Ovarian Cancer. *Cancer Lett* (2020) 475:43–52. doi: 10.1016/j.canlet.2020.01.029
55. Shi X, Ran L, Liu Y, Zhong SH, Zhou PP, Liao MX, et al. Knockdown of hnRNP A2/B1 Inhibits Cell Proliferation, Invasion and Cell Cycle Triggering Apoptosis in Cervical Cancer *via* PI3K/AKT Signaling Pathway. *Oncol Rep* (2018) 39:939–50. doi: 10.3892/or.2018.6195
56. Bhardwaj U, Powell P, Goss DJ. Eukaryotic Initiation Factor (eIF) 3 Mediates Barley Yellow Dwarf Viral mRNA 3'-5' UTR Interactions and 40S Ribosomal Subunit Binding to Facilitate Cap-Independent Translation. *Nucleic Acids Res* (2019) 47:6225–35. doi: 10.1093/nar/gkz448
57. Zhu P, Tan Q, Jiang W, Ou Y, Xu P, Yuan L. Eukaryotic Translation Initiation Factor 3B is Overexpressed and Correlates With Deteriorated Tumor Features and Unfavorable Survival Profiles in Cervical Cancer Patients. *Cancer biomark* (2019) 26:123–30. doi: 10.3233/CBM-182114
58. Huff S, Tiwari SK, Gonzalez GM, Wang Y, Rana TM. M(6)A-RNA Demethylase FTO Inhibitors Impair Self-Renewal in Glioblastoma Stem Cells. *ACS Chem Biol* (2021) 16:324–33. doi: 10.1021/acschembio.0c00841
59. Zhou S, Bai ZL, Xia D, Zhao ZJ, Zhao R, Wang YY, et al. FTO Regulates the Chemo-Radiotherapy Resistance of Cervical Squamous Cell Carcinoma (CSCC) by Targeting Beta-Catenin Through mRNA Demethylation. *Mol Carcinog* (2018) 57:590–7. doi: 10.1002/mc.22782
60. Zhao L, Kong X, Zhong W, Wang Y, Li P. FTO Accelerates Ovarian Cancer Cell Growth by Promoting Proliferation, Inhibiting Apoptosis, and Activating Autophagy. *Pathol Res Pract* (2020) 216:153042. doi: 10.1016/j.prp.2020.153042
61. Xu Y, Ye S, Zhang N, Zheng S, Liu H, Zhou K, et al. The FTO/miR-181b-3p/ARL5B Signaling Pathway Regulates Cell Migration and Invasion in Breast Cancer. *Cancer Commun (Lond)* (2020) 40:484–500. doi: 10.1002/cac2.12075
62. Gao R, Ye M, Liu B, Wei M, Ma D, Dong K. M6a Modification: A Double-Edged Sword in Tumor Development. *Front Oncol* (2021) 11:679367. doi: 10.3389/fonc.2021.679367
63. Zhu H, Gan X, Jiang X, Diao S, Wu H, Hu J. ALKBH5 Inhibited Autophagy of Epithelial Ovarian Cancer Through miR-7 and BCL-2. *J Exp Clin Cancer Res* (2019) 38:163. doi: 10.1186/s13046-019-1159-2
64. Wang X, Zhang J, Wang Y. Long Noncoding RNA GAS5-AS1 Suppresses Growth and Metastasis of Cervical Cancer by Increasing GAS5 Stability. *Am J Transl Res* (2019) 11(8):4909–21.
65. Heo SK, Noh EK, Kim JY, Jegal S, Jeong Y, Cheon J, et al. Rhein Augments ATRA-Induced Differentiation of Acute Promyelocytic Leukemia Cells. *Phytomedicine* (2018) 49:66–74. doi: 10.1016/j.phymed.2018.06.027
66. Huang L, Zhang J, Zhu X, Mi X, Li Q, Gao J, et al. The Phytochemical Rhein Mediates M(6)A-Independent Suppression of Adipocyte Differentiation. *Front Nutr* (2021) 8:756803. doi: 10.3389/fnut.2021.756803
67. Yankova E, Blackaby W, Albertella M, Rak J, De Braekeleer E, Tsagkogeorga G, et al. Small-Molecule Inhibition of METTL3 as a Strategy Against Myeloid Leukaemia. *Nature* (2021) 593:597–601. doi: 10.1038/s41586-021-03536-w
68. Wang Q, Chen C, Ding Q, Zhao Y, Wang Z, Chen J, et al. METTL3-Mediated M(6)A Modification of HDGF mRNA Promotes Gastric Cancer Progression and has Prognostic Significance. *Gut* (2020) 69:1193–205. doi: 10.1136/gutjnl-2019-319639
69. Li B, Jiang J, Assaraf YG, Xiao H, Chen ZS, Huang C. Surmounting Cancer Drug Resistance: New Insights From the Perspective of N(6)-Methyladenosine RNA Modification. *Drug Resist Update* (2020) 53:100720. doi: 10.1016/j.drup.2020.100720
70. He X, Tan L, Ni J, Shen G. Expression Pattern of M(6)A Regulators Is Significantly Correlated With Malignancy and Antitumor Immune Response of Breast Cancer. *Cancer Gene Ther* (2021) 28:188–96. doi: 10.1038/s41417-020-00208-1
71. Fukumoto T, Zhu H, Nacarelli T, Karakashev S, Fatkhutdinov N, Wu S, et al. N(6)-Methylation of Adenosine of FZD10 mRNA Contributes to PARP Inhibitor Resistance. *Cancer Res* (2019) 79:2812–20. doi: 10.1158/0008-5472.CAN-18-3592
72. Gu J, Bi F. Significance of N6-Methyladenosine RNA Methylation Regulators in Immune Infiltrates of Ovarian Cancer. *Front Genet* (2021) 12:671179. doi: 10.3389/fgene.2021.671179
73. Yi L, Wu G, Guo L, Zou X, Huang P. Comprehensive Analysis of the PD-L1 and Immune Infiltrates of M(6)A RNA Methylation Regulators in Head and Neck Squamous Cell Carcinoma. *Mol Ther Nucleic Acids* (2020) 21:299–314. doi: 10.1016/j.omtn.2020.06.001

Conflict of Interest: The authors declare that the research was conducted in the absence of any commercial or financial relationships that could be construed as a potential conflict of interest.

Publisher's Note: All claims expressed in this article are solely those of the authors and do not necessarily represent those of their affiliated organizations, or those of the publisher, the editors and the reviewers. Any product that may be evaluated in this article, or claim that may be made by its manufacturer, is not guaranteed or endorsed by the publisher.

frontiers | Frontiers in Pharmacology

ORIGINAL RESEARCH
published: 01 June 2022
doi: 10.3389/fphar.2022.902305

Anticancer Effects of Amlodipine Alone or in Combination With Gefitinib in Non-Small Cell Lung Cancer

Bingjie Fu[1†], Xiaojing Dou[1†], Miao Zou[1], Hao Lu[1], Kaixuan Wang[1], Qingxia Liu[1], Yao Liu[2], Wei Wang[2], Meihua Jin[1] and Dexin Kong[1]**

[1]Tianjin Key Laboratory of Technologies Enabling Development of Clinical Therapeutics and Diagnostics, School of Pharmacy, Key Laboratory of Immune Microenvironment and Diseases (Ministry of Education), Tianjin Medical University, Tianjin, China, [2]Department of Otorhinolaryngology Head and Neck Surgery, Key Laboratory of Auditory Speech and Balance Medicine, Institute of Otolaryngology of Tianjin, Tianjin First Central Hospital, Tianjin, China

Amlodipine is a Ca^{2+} channel blocker commonly used to cardiovascular diseases such as hypertension and angina; however, its anticancer effects in lung cancer A549 cells remain unknown. In the present study, we explored the antitumor effects and molecular mechanisms underlying the action of amlodipine in non-small cell lung cancer (NSCLC) A549 cells *in vitro* and *in vivo*. We observed that amlodipine suppressed the proliferation of A549 lung cancer cells by arresting the tumor cell cycle. Mechanistically, our results revealed that amlodipine could attenuate the phosphoinositide 3 kinase (PI3K)/Akt and Raf/MEK/extracellular signal-regulated kinase (ERK) pathways through epidermal growth factor receptor (EGFR) and modulated cell cycle-related proteins such as cyclin D1, p-Rb, p27, and p21. Subsequently, amlodipine combined with gefitinib could synergistically inhibit cell proliferation by arresting the cell cycle. Moreover, amlodipine combined with gefitinib effectively attenuated the growth of A549 lung cancer xenografts when compared with monotherapy, affording an excellent therapeutic effect. Collectively, our results indicate that amlodipine alone or combined with the novel anticancer drug gefitinib might be a potential therapeutic strategy for NSCLC patients with wild-type EGFR.

Keywords: amlodipine, gefitinib, lung cancer, synergistic anticancer effect, cell cycle arrest

OPEN ACCESS

Edited by:
Yunkai Zhang,
Vanderbilt University Medical Center, United States

Reviewed by:
Nuno Bernardes,
University of Lisbon, Portugal
Kubhushan Tikoo,
National Institute of Pharmaceutical Education and Research, India

****Correspondence:***
Meihua Jin
jinmeihua@tmu.edu.cn
Dexin Kong
kongdexin@tmu.edu.cn

[†]These authors have contributed equally to this work

Specialty section:
This article was submitted to Experimental Pharmacology and Drug Discovery, a section of the journal Frontiers in Pharmacology

Received: *23 March 2022*
Accepted: *17 May 2022*
Published: *01 June 2022*

Citation:
Fu B, Dou X, Zou M, Lu H, Wang K, Liu Q, Liu Y, Wang W, Jin M and Kong D (2022) Anticancer Effects of Amlodipine Alone or in Combination With Gefitinib in Non-Small Cell Lung Cancer. Front. Pharmacol. 13:902305. doi: 10.3389/fphar.2022.902305

INTRODUCTION

Calcium channel blockers (CCBs) inhibit calcium flux through voltage-gated calcium channels (Wang et al., 2021) and are widely used to treat cardiovascular diseases such as angina, hypertension, and supraventricular arrhythmias (Sica, 2006). CCBs are classified as dihydropyridines or non-dihydropyridines. Dihydropyridines include nifedipine, nicardipine, felodipine, and amlodipine, while non-dihydropyridines include diltiazem and verapamil (Eisenberg et al., 2004). CCBs, such as diltiazem and verapamil, were shown to decrease tumor growth in a xenograft mouse meningioma tumor model (Jensen and Wurster, 2001), and verapamil could reversibly decrease human melanoma cell invasion and metastasis (Yohem et al., 1991). In addition, dihydropyridine derivatives, such as amlodipine, nicardipine, and nimodipine, reportedly suppressed the growth of human epidermoid carcinoma cells, whereas verapamil, diltiazem, and dihydropyridine nifedipine failed to inhibit human epidermoid carcinoma cell growth at the same concentration (Yoshida et al., 2003). However, the anticancer effect of amlodipine against non-small cell lung cancer (NSCLC) A549 cells remains unknown.

Lung cancer is the most frequent and leading cause of cancer-related deaths globally, and NSCLC constitutes approximately 75% of all lung cancers (Cersosimo, 2002; Hirsch et al., 2017). Epidermal growth factor receptor (EGFR) is a transmembrane protein with cytoplasmic kinase activity commonly overexpressed in various human cancers, including NSCLC (da Cunha Santos et al., 2011; Wee and Wang, 2017). EGFR tyrosine kinase inhibitors (TKIs), gefitinib and erlotinib, are targeted therapies, used as first-line treatments for patients with NSCLC harboring EGFR mutations (Shukuya et al., 2011; De Mello et al., 2016). EGFR-TKIs have demonstrated insufficient efficacy in patients with wild-type EGFR (Hirai et al., 2017). However, it has been reported that shikonin could enhance the anticancer efficacy of gefitinib/erlotinib in wild-type EGFR NSCLC cells (Li et al., 2018). And recently, we also reported that proton pump inhibitor, lansoprazole, in combination with gefitinib showed synergistic antitumor effect on NSCLC A549 cells and mouse xenograft models with wild-type EGFR (Zhao et al., 2021). Therefore, potential EGFR-TKI sensitizers and treatment strategies to improve the prognosis of lung cancer patients with wild-type EGFR are essential.

Combination therapy, rather than monotherapy, can afford synergistic clinical benefits. Amlodipine attenuates phosphorylation of EGFR in human epidermoid carcinoma A431 cells *in vitro* and *in vivo* (Yoshida et al., 2010). Therefore, we hypothesized that simultaneous treatment with amlodipine and gefitinib might have synergistic anticancer effects. In the present study, we investigated the anticancer effects and preliminary mechanisms of amlodipine alone or in combination with gefitinib in NSCLC A549 cells with wild-type EGFR. Our study provides a promising new therapeutic agent or combination treatment strategy for patients with NSCLC.

MATERIALS AND METHODS

Cell Culture

A549 cells were obtained from the Cell Resource Center of Peking Union Medical College (Beijing, China). This cell line has been authenticated using STR profiling within the last 3 years. In addition, A549 cells were confirmed to be free of *mycoplasma* contamination by PCR. Briefly, A549 cells were cultured in RPMI 1640 medium containing 10% fetal bovine serum (FBS), 100 U/ml penicillin, and 100 μg/ml streptomycin. The cell cultures were maintained in a humidified atmosphere containing 5% CO_2 at 37°C.

Reagents

Amlodipine and gefitinib were purchased from Selleck Chemicals (Houston, TX, United States) and TopScience (Shanghai, China), respectively. Propidium iodide (PI) was obtained from Sigma-Aldrich (St. Louis, MO, United States). The Annexin V/FITC-PI apoptosis detection kit was obtained from BD Biosciences (San Jose, CA, United States of America). RPMI 1640 and FBS were purchased from Biological Industries (Beit Haemek, Israel). The enhanced chemiluminescence (ECL) reagent was purchased from Thermo Fisher Scientific (Waltham, MA, United States). Antibodies against phospho-EGFR, phospho-PDK1 (Ser241), PDK1, phospho-Akt (Ser473), phospho-Akt (Thr308), Akt, phospho-mammalian target of rapamycin complex 1 (mTORC1) (Ser2448), mTOR, phospho-glycogen synthase kinase 3 (GSK-3) β, phospho-p70 S6K (Thr389), p27, cyclin D1, phospho-retinoblastoma protein (Rb), phospho-extracellular signal-regulated kinase (ERK) 1/2, phospho-c-Raf, *β*-actin, and horseradish peroxidase (HRP)-conjugated goat anti-rabbit and horse anti-mouse secondary antibodies were purchased from Cell Signaling Technology Inc. (Danvers, MA, United States). Antibody specific for p21 was obtained from Santa Cruz Biotechnology Inc. (Dallas, TX, United States).

Determination of Cell Viability

Cell viability was determined using an 3-(4,5-dimethylthiazol-2-yl)-2,5-diphenyltetrazolium bromide (MTT) assay. Briefly, A549 cells were seeded into 96-well plates at a density of 4×10^3 cells/well and then treated with amlodipine and/or gefitinib for 48 h, followed by the addition of 20 μl MTT (5 mg/ml) to each well and further incubation for 4 h. Dimethyl sulfoxide (DMSO) was used to dissolve purple crystals after incubation. Optical density was measured at 490 nm using an iMark microplate reader (Bio-Rad, Hercules, CA, United States).

Flow Cytometric Analysis

Briefly, A549 cells were plated in 6-well plates at a density of 2×10^5 cells/well and treated with amlodipine or gefitinib for 48 h. For cycle analysis, the cells were harvested with trypsin, washed with PBS, resuspended in 75% pre-chilled ethanol, and stored at 4 °C overnight. After 24 h, the fixed cells were collected and stained with PI. Then, 20,000 cells were collected for each sample and analyzed using a BD Accuri C6 flow cytometer (BD Biosciences, San Jose, CA, United States).

To analyze cell apoptosis, Annexin V-FITC/PI double staining was performed as previously reported, with minor modifications (Zhang et al., 2021). The drug-pretreated cells were harvested with trypsin, resuspended in Annexin V-FITC/PI (BD Biosciences, San Jose, CA, United States) mixture, and incubated in the dark for 15 min. Subsequently, cells were analyzed using a BD Accuri C6 flow cytometer (10,000 cells were analyzed for each sample).

Data were quantified with BD Accuri C6 Software.

Wound-Healing Assay

Briefly, A549 cells were seeded in 24-well plates at a density of 6×10^5 cells/well and a micropipette tip was used to create a vertical scratch (wound) in the cell monolayer. Subsequently, cells were treated with different concentrations of amlodipine for 48 h. Wound areas were imaged under a microscope.

Western Blotting

Western blot analysis was performed as previously described (Shao et al., 2021). Briefly, cells were lysed with RIPA lysis buffer, and the protein concentration of each sample was determined using a BCA protein assay kit. Protein extracts were separated by 10% sodium dodecyl sulfate-polyacrylamide gel electrophoresis (SDS-PAGE) and transferred to a PVDF membrane. Membranes were blocked with 5% non-fat milk, incubated with primary

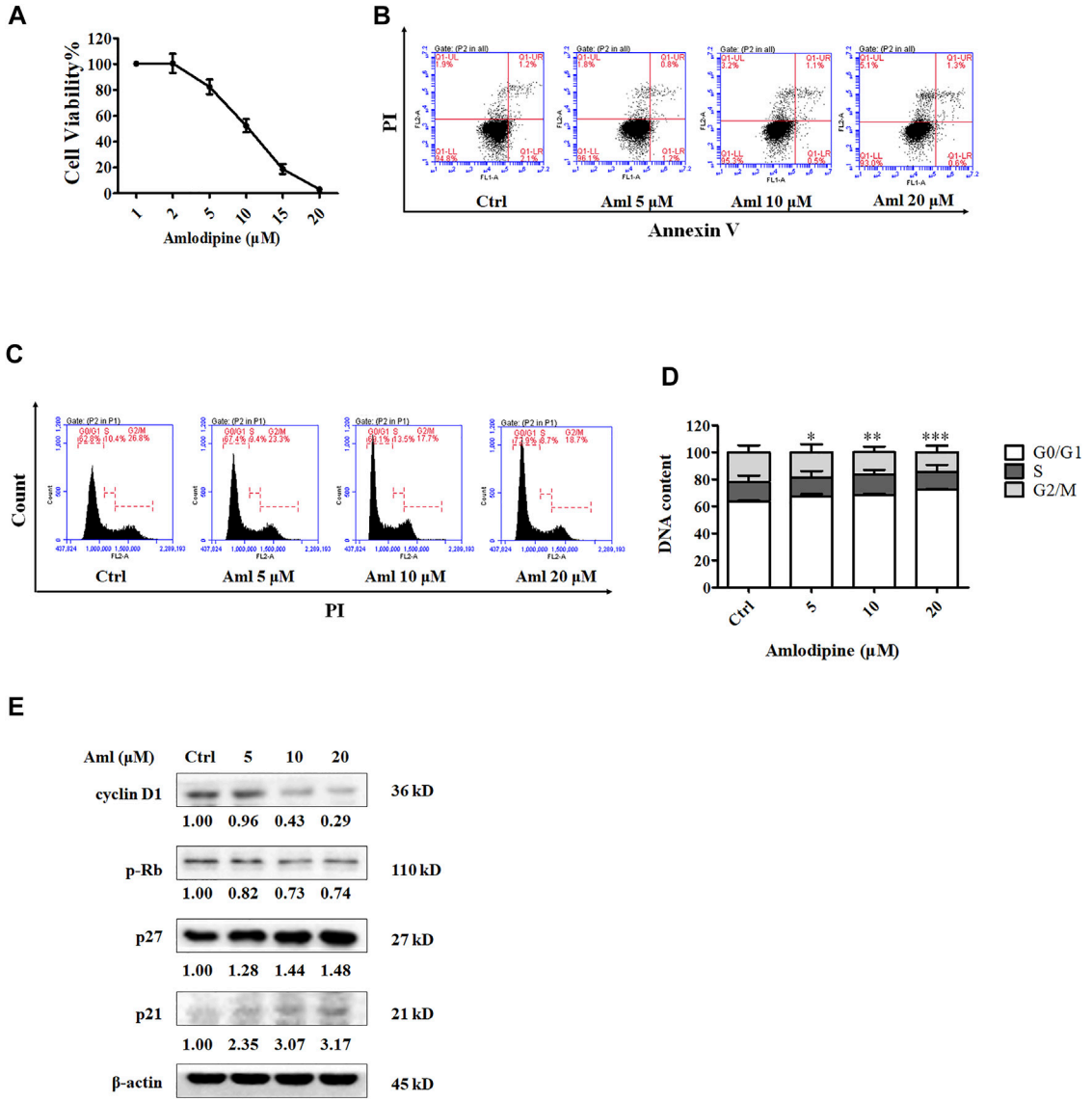

FIGURE 1 | Amlodipine inhibits A549 cell proliferation by blocking the cell cycle G0/G1 phase. **(A)** Incubation of A549 with various concentrations (1, 2, 5, 10, 15, and 20 μM) of amlodipine (Aml) for 48 h. The effects of amlodipine on A549 cell proliferation were determined by MTT assay. **(B)** A549 cells were harvested 48 h after treatment with indicated concentrations of amlodipine, and apoptotic cells were measured by flow cytometry analysis. **(C)** Cells were pre-incubated with different concentrations of amlodipine for 48 h, and the induction of cell cycle arrest was detected by flow cytometry analysis. **(D)** The percentage of total cells at G0/G1, S, and G2/M phases. **(E)** The expressions levels of cell cycle-related proteins were determined by Western blotting after treatment with amlodipine. Data are presented as mean ± SD of three independent experiments. $^{*}p < 0.05$, $^{**}p < 0.01$ and $^{***}p < 0.001$.

antibodies at 4 °C overnight, washed four times with Tris-buffered saline (TBS) containing Tween-20 (TBST), and incubated with the respective HRP-conjugated secondary antibody for 1 h. Protein bands were visualized using ECL reagents on a Bio-Rad ChemiDoc™ XRS + system (Bio-Rad, Hercules, CA, United States).

Nude Mouse Xenograft Tumor Experiments

All animal experiments were conducted at the Laboratory Animal Center of the Institute of Radiation Medicine, Chinese Academy of Medical Sciences, and were maintained in a pathogen-free environment. The experiments were performed under the Institutional Animal Care and Use Committee guidelines. Six-week-old male BALB/c nude mice were injected subcutaneously (s.c.) with 1×10^7 A549 cells, and then the sufficiently grown tumor tissue was divided into equal pieces, followed by subcutaneous implantation into the mice. Mice were randomly divided into four groups ($n = 4$) when tumors reached 20–30 mm^3, and then orally administered amlodipine (10 mg/kg) or gefitinib (50 mg/kg) alone or in combination every other day for 15 days. The growth of implanted tumors was monitored every other day, tumor volumes were measured

using a caliper, and the tumor volume was calculated using the formula $V = 1/2 \times Length \times Width^2$.

Immunohistochemistry Analyses

At the end of the experimental period, animals were euthanized, and tumors were excised and fixed in paraformaldehyde for IHC analysis. Tumors were embedded in paraffin, sectioned at 5-μm thickness, and stained with hematoxylin and eosin (H&E) for morphological assessment. The formalin-fixed tissue was heated in an antigen retrieval solution before incubation with the antibody Ki67, and bound antibodies were detected with Bond Polymer (anti-rabbit poly-HRP-IgG) and visualized using diaminobenzidine (DAB) peroxidase substrate. Specimen images were examined using an Olympus BX51 microscope.

Statistical Analysis

Data values are expressed as the mean ± standard deviation (SD) of triplicate values. One-way ANOVA followed by Tukey's multiple comparison test was used to determine statistical significance using GraphPad Prism 5 (GraphPad, San Diego, CA, United States). Differences were considered statistically significant at $p < 0.05$.

RESULTS

Amlodipine Inhibits the Proliferation of NSCLC A549 Cells *Via* Cell Cycle Arrest at the G0/G1 Phase

The MTT assay was used to detect the inhibitory effect of amlodipine on A549 cell proliferation. A549 cells were treated with a series of amlodipine concentrations for 48 h. As shown in **Figure 1A**, amlodipine significantly suppressed the proliferation of A549 cells in a concentration-dependent manner, with an IC_{50} of 9.641 μM. Apoptosis is a common mechanism of cell death. We first determined whether amlodipine induces apoptosis in A549 cells. A flow cytometry assay with double staining using Annexin-V FITC/PI was performed to detect the percentage of apoptotic cells. A549 cells were treated with 5, 10, and 20 μM amlodipine for 48 h. As shown in **Figure 1B**, incubation with amlodipine showed no significant changes. To explore the effects of amlodipine on the cell cycle, flow cytometry was used to evaluate cell cycle phase distribution in A549 cells following amlodipine treatment for 48 h. As shown in **Figures 1C,D**, amlodipine-treated cells exhibited significantly enhanced cell cycle arrest at the G0/G1 phase when compared with the non-treated group. To further explore these findings, the levels of cyclin D1, p27, and p21, as well as the phosphorylation of their downstream protein Rb, were determined using Western blotting after treatment with 5, 10, and 20 μM amlodipine for 48 h. Cyclin D-cyclin dependent kinase (CDK) 4/6 complex phosphorylates Rb to facilitate cell cycle progression from G1 to S phase (Sherr, 1994; Shapiro, 2006). As shown in **Figure 1E**, the expression of cyclin D1 and level of p-Rb were decreased, while the expression levels of p27 and p21 (CDK inhibitors) were increased in a dose-dependent manner, compared with the non-treated group. These findings indicated that amlodipine inhibited A549 cell proliferation by inducing cell cycle arrest but did not significantly affect apoptosis.

Amlodipine Suppresses A549 Cell Migration

Metastasis is associated with poor prognosis, and cancer cell migration and invasion are recognized as the initial steps in metastasis. To examine the effects of amlodipine on A549 cell migration, a scratch-wound assay was performed using evenly space 24-well plates covered with A549 cells. Amlodipine was then administered at concentrations of 2, 5, and 10 μM (to avoid interference between cell proliferative activity and migration, we selected a concentration less than the IC_{50}), and scratches were examined after 48 h of culture. As shown in **Figures 2A,B**, cell migration was notably lower in the amlodipine group than in the untreated group, with amlodipine treatment exhibiting a concentration-dependent effect.

Amlodipine Inhibits PI3Ks/Akt and Raf/MEK/ERK MAPKs Pathways by Inhibiting EGFR Phosphorylation in A549 Cells

The phosphatidylinositol-3 kinase (PI3K) pathway plays an important role in regulating cell migration, proliferation, cell cycle progression, and apoptosis (Martini et al., 2014). Therefore, to explore the molecular mechanism underlying amlodipine-mediated inhibition of A549 cell proliferation and cell cycle arrest, cells were treated with 5, 10, and 20 μM amlodipine for 48 h, and Western blotting was performed to detect PI3Ks pathway proteins. As shown in **Figure 2C**, amlodipine treatment at 20 μM for 48 h significantly decreased phosphorylation levels of PDK1, Akt (both Ser473 and Thr308), mTOR, p70 S6K, and GSK-3β, without changes in total PDK1, Akt and mTOR levels.

The Ras/Raf/MEK/ERK pathway is the most pivotal signaling cascade among all MAPK signal transduction pathways and regulates the survival, growth, differentiation, and development of tumor cells (Degirmenci et al., 2020; Guo et al., 2020). In addition, to examine the role of MAPK signaling inhibition and the effects of amlodipine on proliferation and migration, A549 cells were pretreated with several amlodipine concentrations for 48 h. As shown in **Figure 2D**, phosphorylation levels of c-Raf and ERK were reduced in a concentration-dependent manner in cells treated with 10 and 20 μM amlodipine with no variation detected in total ERK, when compared with untreated cells.

EGFR is a receptor tyrosine kinase that plays a critical role in carcinogenesis, including cell proliferation, survival, and differentiation (da Cunha Santos et al., 2011). PI3K and MAPK signaling pathways are involved in EGFR signal transduction. To determine whether amlodipine affects the upstream regulator EGFR, we assessed EGFR phosphorylation after amlodipine treatment using Western blotting. As shown in **Figure 2C**, amlodipine significantly suppressed the level of p-EGFR when compared with the untreated control group, and the inhibitory effects were particularly significant following treatment with 10 and 20 μM amlodipine with no variation detected in total EGFR.

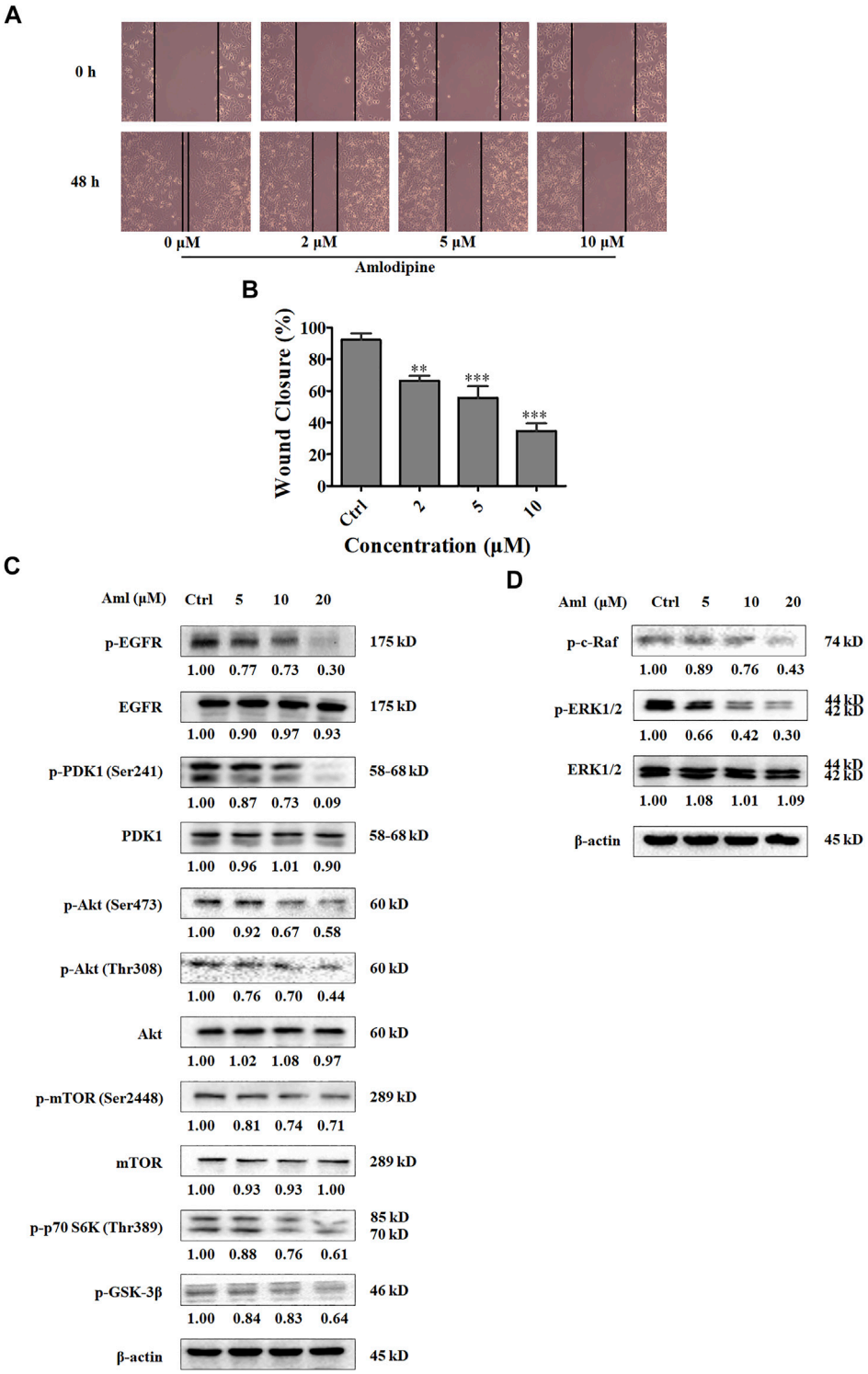

FIGURE 2 | Amlodipine suppresses A549 cells migration and PI3K/Akt and Raf/ERK MAPK pathways. **(A)** The effect of amlodipine on cell migration was detected by performing a wound-healing assay at 48 h. **(B)** Quantification of results in **(A). (C)** The levels of Akt pathway proteins were analyzed by Western blotting after treatment with amlodipine. **(D)** The phosphorylation of Raf and phosphorylation and total ERK1/2 were analyzed by Western blotting after treatment with amlodipine. Data are presented as mean ± SD of three independent experiments. $^{**}p < 0.01$ and $^{***}p < 0.001$.

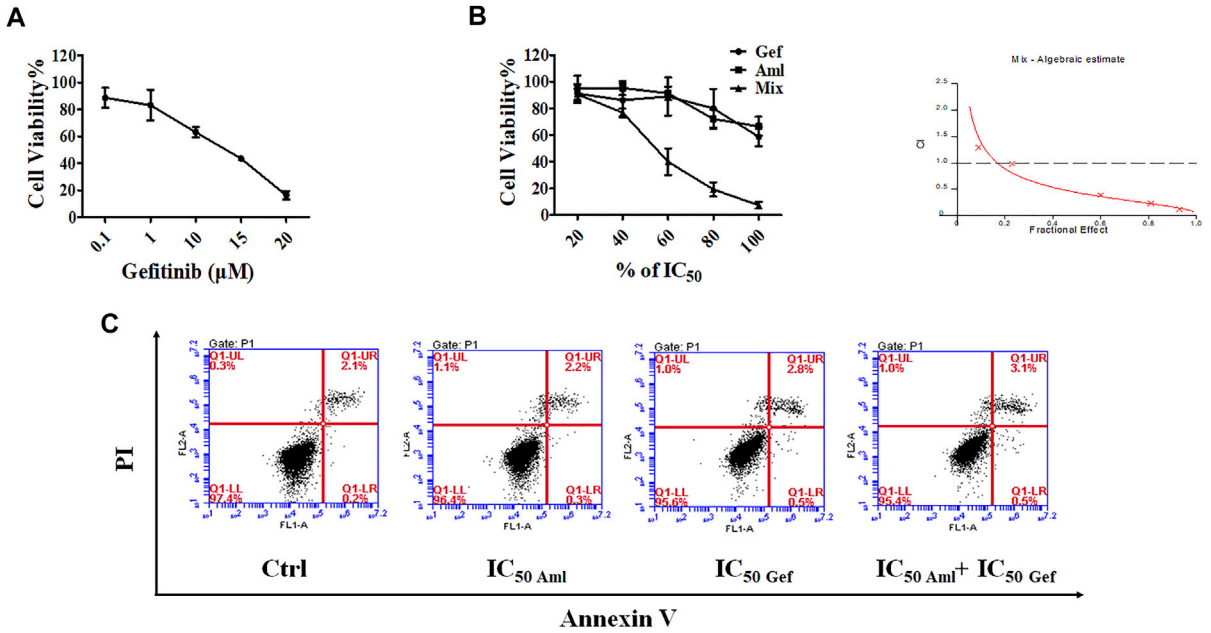

FIGURE 3 | Amlodipine combined with gefitinib led to a synergistic anti-proliferative effect on A549 cells. **(A)** MTT assay was used to detect the inhibitory effect of gefitinib (Gef) on cell proliferation. **(B)** A549 cells were treated with amlodipine, gefitinib, or a combination of these agents for 48 h. A549 cells were treated with amlodipine and gefitinib, with several percentages of IC_{50} value. **(C)** A549 cells were harvested 48 h after treatment with amlodipine, gefitinib, or a combination of these agents, and apoptotic cells were examined by flow cytometry analysis.

Amlodipine in Combination With Gefitinib Synergistically Reduces Cell Proliferation Through Cell Cycle Arrest at G0/G1 by Attenuating PI3K/Akt Signaling Pathway in A549 Cells

Several reports have shown that combination therapies afford synergistic antitumor effects when compared with the efficacy of either agent alone, such as a combination of cisplatin and vinorelbine, which is superior to cisplatin monotherapy in patients with advanced NSCLC (Wozniak et al., 1998). Therefore, gefitinib was selected and combined with amlodipine. First, the IC_{50} of gefitinib at 48 h was detected using the MTT assay, as shown in **Figure 3A**, notably inhibiting cell proliferation at an IC_{50} of 12.52 μM. To quantify the interaction between amlodipine and gefitinib, the multiple-drug effect evaluation introduced by Chou-Talalay was employed. The MTT assay was performed to measure the inhibitory activities of a series of drug concentration combinations (20, 40, 60, 80, and 100% of IC_{50} values of each drug) (**Figure 3B**). To detect the efficacy of the two-drug combination, combination index (CI) plots were generated using CalcuSyn software, and CI values were defined as follows; CI < 1, synergism; CI = 1, additive; and CI > 1, antagonism. The CI values for ED_{50}, ED_{75}, and ED_{90} were 0.43812, 0.26170, and 0.16192, respectively. Therefore, we fixed the ratio of $IC_{50\ amlodipine}$:$IC_{50\ gefitinib}$ (9.641 μM:12.52 μM) combination to perform a subsequent mechanistic study for examining the synergistic anti-proliferative effect.

We evaluated the effect of amlodipine combined with gefitinib on A549 cell apoptosis using Annexin V-FITC/PI staining. A549 cells were treated with amlodipine and gefitinib, either alone or in combination, for 48 h. The results revealed no significant changes following treatment with either amlodipine or a combination of amlodipine and gefitinib (**Figure 3C**). We further analyzed the effects of amlodipine in combination with gefitinib on the cell cycle. It has been reported that gefitinib, as well as amlodipine, can block the A549 cell cycle at the G0/G1 phase. Therefore, to clarify the combined anti-proliferation activity detected in the MTT assays, flow cytometry was performed to assess A549 cells treated with the two drugs alone or in combination for 48 h; the percentage of each cell cycle was determined by PI staining. As shown in **Figures 4A,B**, treatment of A549 cells with amlodipine combined with gefitinib significantly increased the proportion of cells in the G0/G1 phase (80.1%) when compared with amlodipine or gefitinib alone. A mechanistic assessment was performed using Western blotting, and the results indicated that the combined use of amlodipine and gefitinib significantly reduced levels of p-Rb and enhanced p27 when compared with amlodipine or gefitinib alone (**Figure 4C**).

In addition, the mechanism of action was investigated using Western blotting. Compared with amlodipine or gefitinib treatment alone, amlodipine combined with gefitinib could downregulate PI3K/Akt signaling pathway proteins, including phosphorylation of Akt (Ser473), Akt (Thr308), and mTOR (**Figure 4D**) with no variation detected in total Akt and mTOR levels. Furthermore, amlodipine combined with

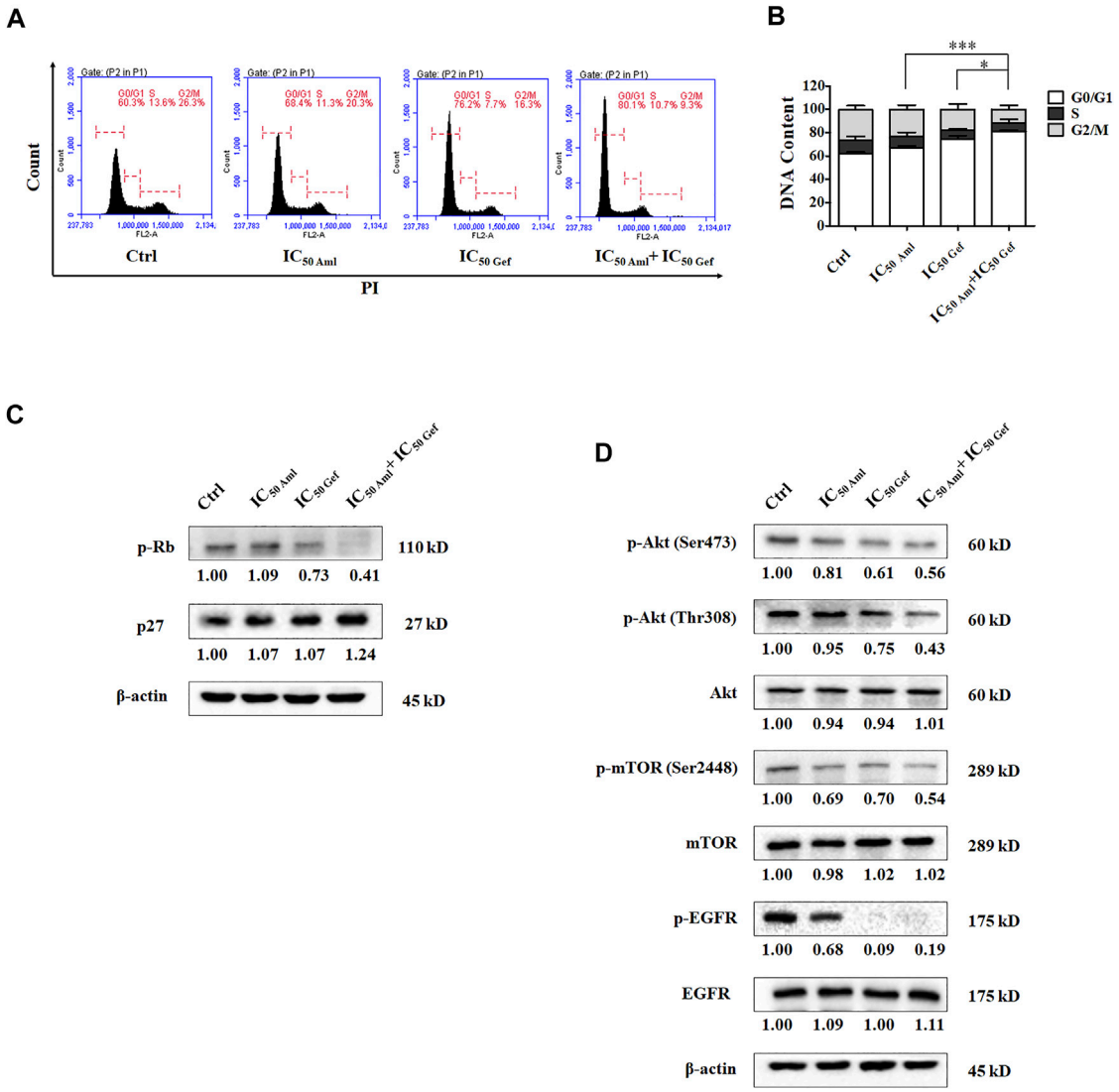

FIGURE 4 | Amlodipine combined with gefitinib induces cycle arrest in A549 cells. **(A)** Amlodipine combined with gefitinib increased the proportion of cells in the G0/G1 phase. **(B)** The percentage of total cells at G0/G1, S, and G2/M phases. **(C)** The levels of p-Rb and p27 were measured by Western blotting after treatment with amlodipine, gefitinib, or a combination of the two agents. **(D)** Phosphorylation and total levels of Akt, mTOR, and EGFR were analyzed by Western blotting after treatment with amlodipine, gefitinib, or a combination of the two agents. Data are presented as mean ± SD of three independent experiments. $^{*}p < 0.05$ and $^{***}p < 0.001$.

gefitinib decreased the phosphorylation of EGFR in A549 cells without any change in total EGFR when compared with the amlodipine alone group (**Figure 4D**).

Amlodipine Alone or in Combination With Gefitinib Suppresses A549 Xenograft Tumor Growth

Based on the aforementioned results from *in vitro* experiments, we speculated whether amlodipine or its combination with gefitinib could afford antitumor effects *in vivo*. Therefore, we examined the efficacy of amlodipine alone and in combination with gefitinib in an A549 xenograft mouse model. Tumor-bearing xenograft mice were orally administered amlodipine (10 mg/kg) or gefitinib (50 mg/kg), alone or in combination, every other day for 15 days. As shown in **Figures 5A,B**, amlodipine alone showed significant antitumor activity against A549 tumors, and this dose resulted in no significant weight loss when compared with the non-treated control group (**Figure 5C**). This result suggests that the test does not induce severe side effects. In addition, treatment with amlodipine combined with gefitinib markedly inhibited the growth of A549 tumors when compared with monotherapy with either agent, with no significant differences in body weight. Furthermore, we compared the histological findings following treatment with amlodipine alone or combined with gefitinib with the untreated group. H&E staining was used to confirm the tissue morphology (**Figure 5D**). Tumor tissue sections stained with the tumor cell proliferation marker Ki67 are shown in **Figure 5E**.

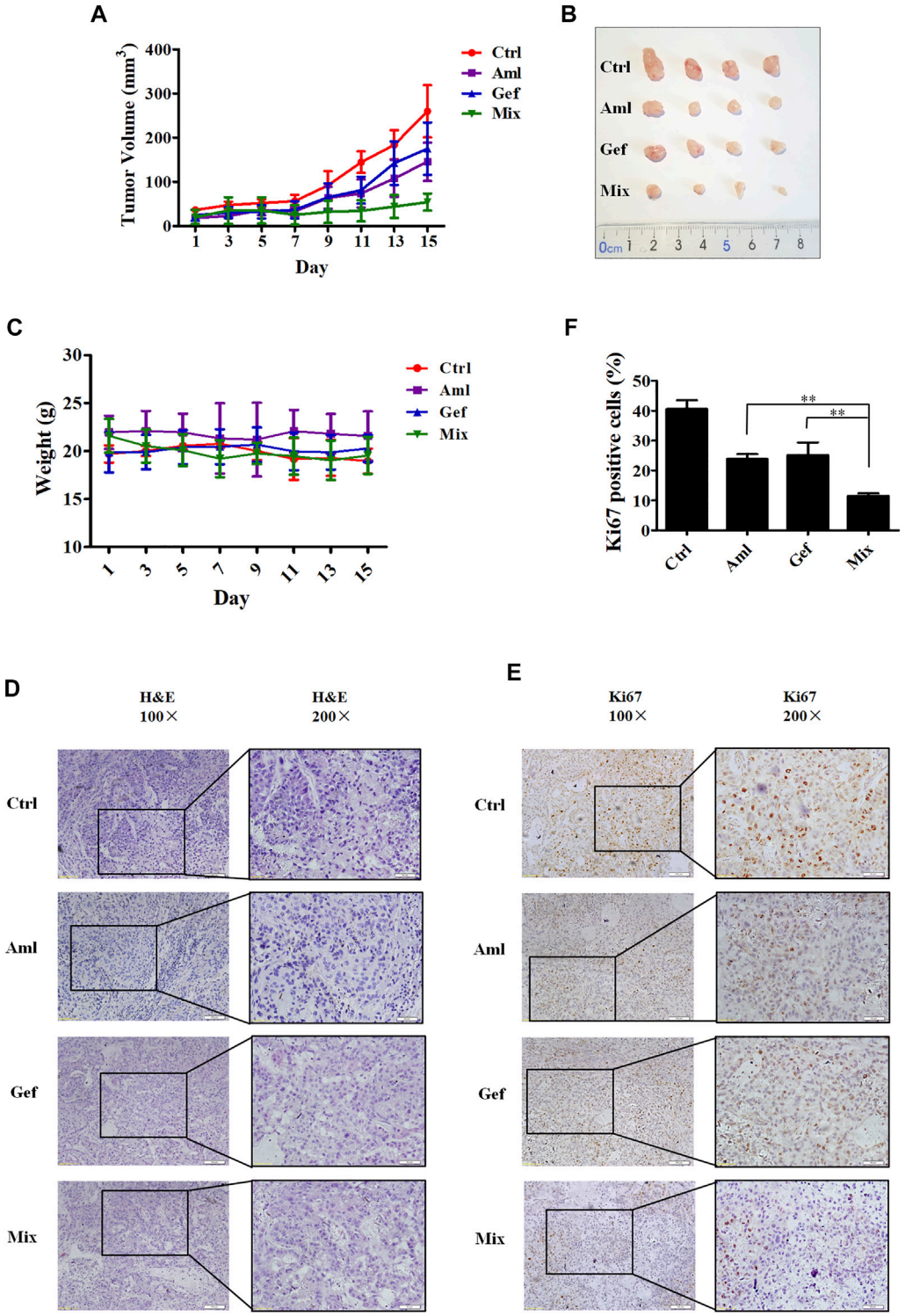

FIGURE 5 | Amlodipine combined with gefitinib inhibits tumor growth in nude mice bearing A549 xenograft. Tumor-bearing xenograft mice were orally administered amlodipine (10 mg/kg every other day) and gefitinib (50 mg/kg every other day), alone or in combination, for 15 days. **(A)** Tumor volumes were measured every alternate day. **(B)** Photographs of the isolated tumors in each group. **(C)** Representative body weights of mice in each group. **(D)** Tumor tissues were stained with H&E. **(E)** Tumor tissues were stained for the proliferation marker Ki67. **(F)** Quantitative analysis of the Ki67 positive cells in tumor sections from mice. Data are presented as mean ± SD obtained from at least 3 mice. $^{**}p < 0.01$.

Amlodipine combined with gefitinib reduced Ki67 positive brown cells when compared with either amlodipine or gefitinib alone (**Figure 5F**).

DISCUSSION

Amlodipine, a Ca^{2+} channel blocker, is frequently used to treat cardiovascular diseases, such as hypertension and angina (Sheraz et al., 2016). The efficacy and safety of long-term amlodipine combined with lisinopril were previously reported in patients with hypertension (Arslanagic et al., 2005). Recent studies have shown that amlodipine exhibits antitumor activity; for example Yoshida *et al.* have reported that amlodipine inhibits proliferation of human epidermoid carcinoma A431 cells, induces G1 phase A431 cell accumulation, retards tumor growth, and prolongs the survival of A431 tumor cell-bearing xenograft mice (Yoshida et al., 2003; 2004; 2007). However, the antitumor effects of amlodipine in NSCLC and its underlying antitumor effects have not been reported. In the present study, we found that amlodipine exhibited beneficial antitumor effects against lung A549 cancer cells both *in vitro* and *in vivo*, with no significant side effects. The mechanistic study revealed that amlodipine attenuated cell proliferation through cell cycle arrest at the G0/G1 phase without marked apoptosis induction. This result is consistent with that of Yoshida *et al.*, who reported that the anti-proliferative effect of amlodipine could not be attributed to cytotoxicity (Yoshida et al., 2003), and caused G1 cell cycle arrest and cell growth inhibition in human epidermoid carcinoma cells (Yoshida et al., 2007). In addition, we found that amlodipine arrested the cell cycle by regulating the cell cycle pathway. Western blot analysis revealed that cyclin D1 and p-Rb were significantly downregulated, while p27 and p21 were upregulated in amlodipine-treated A549 cells. There are three known D-type cyclins (D1, D2, and D3) that form active complexes with either CDK4 or CDK6, as well as cyclin E-CDK2 complexes, which phosphorylate Rb to facilitate the G1 to S phase transition (Shapiro, 2006; Qie and Diehl, 2016). CDK activity is negatively modulated by the INK4 and CIP/KIP families, which include p21 and p27 (Donjerkovic and Scott, 2000; Roskoski, 2019). In addition, reduced protein expression of p21 and p27 has been documented in breast, colon, and gastric tumors (Roskoski, 2019). Our present findings indicate that amlodipine could inhibit A549 cell proliferation by inducing cell cycle arrest *via* modulation of cyclin D1, p-Rb, p27, and p21.

Furthermore, we observed that amlodipine attenuated EGFR phosphorylation in A549 cells, and this finding is consistent with the report by Yoshida *et al.* who suggested that amlodipine suppresses the phosphorylation of EGFR in A431 cells (Yoshida et al., 2010). EGFR activation transduces multiple downstream pro-oncogenic signaling pathways, including the PI3K/Akt/mTOR and Ras/Raf/MEK/ERK pathways (Wee and Wang, 2017), which results in the progression of the G1/S cell cycle (Wee and Wang, 2017).

Subsequently, we noted that amlodipine could affect A549 cells by inhibiting the phosphorylation of PI3K/Akt pathway proteins such as PDK1, Akt (both Thr308 and Ser473), mTOR, p70 S6K, and GSK-3β. The PI3K/Akt/mTOR signaling pathway is one of the most frequently activated signal transduction pathways in human cancers (Martini et al., 2014; Alzahrani, 2019). PI3K phosphorylates phosphatidylinositol 4,5-bisphosphate (PIP2) and converts it to the secondary messenger, phosphatidylinositol 3,4,5-triphosphate (PIP3). PIP3 then recruits a subset of signaling proteins with pleckstrin homology domains, such as PDK1 and Akt, to the plasma membrane (Porta et al., 2014). PDK1 phosphorylates Akt in its activation loop at threonine 308 (Thr308), and full activation of Akt requires phosphorylation at serine 473 (Ser473) *via* mTORC2 activation (Martini et al., 2014; Alzahrani, 2019). Akt directly phosphorylates mTORC1 at Ser2448 (Navé et al., 1999), and activated mTORC1 regulates protein synthesis and cell survival by directly phosphorylating 4E-binding protein 1 and p70 S6K (Gibbons et al., 2009). Akt triggers a network that positively regulates G1/S cell cycle progression via GSK-3β inactivation, leading to increased cyclin D1 and decreased p27Kip1 (Liang and Slingerland, 2003). Dynamic regulated phosphorylation, which reduces the activity of GSK-3, occurs on Ser 9 of GSK-3β, and this N-terminal serine phosphorylation is mediated by Akt (Hermida et al., 2017).

Additionally, we observed that amlodipine effectively inhibited the phosphorylation of c-Raf and ERK, without impacting total ERK levels. The Ras/Raf/MEK/ERK pathway also plays an important role in cell proliferation and survival during several stages of cancer (Asati et al., 2016). Raf proteins are crucial components of the Ras/Raf/MEK/ERK signaling cascade and contain three isoforms; C-Raf (also called Raf-1), B-Raf, and A-Raf (Degirmenci et al., 2020). Activated C-Raf phosphorylates downstream MEK, which activates ERK by phosphorylating both Tyr and Thr regulatory sites (Vandamme et al., 2014; Muta et al., 2019; Guo et al., 2020). ERK1/2 are terminal kinases in MAPK signaling and are located in the cytoplasm when the signaling pathway is inactive. Once activated, ERK1/2 translocates to the nucleus and regulates the activity of several transcription factors, finally mediating cell growth, differentiation, and migration (Shin et al., 2018; Guo et al., 2020). In the present study, we found that amlodipine decreased A549 cell migration in a wound-healing assay. Thus, our results suggest that amlodipine suppresses A549 cell proliferation and migration by inhibiting EGFR-mediated PI3K/Akt and Raf/ERK pathways.

Several clinical studies have indicated that a single agent can present several limitations during the treatment of various cancers. Combination therapy involves the simultaneous administration of two or more therapeutic agents. Combination therapy has shown promising activity in cancer treatment; for example, sorafenib combined with other targeted agents, chemotherapy, and radiotherapy exhibits synergistic antitumor activity (Ibrahim et al., 2012), and gefitinib combined with carboplatin plus pemetrexed can improve progression-free survival when compared with gefitinib alone in patients with NSCLC (Hosomi et al., 2020). Our group has recently reported that combination therapy is beneficial in cancer treatment, such as biomimetic small-molecule self-assembly of the PI3K inhibitor, ZSTK474, integrated with the immunomodulator indomethacin to amplify anticancer

efficacy (Zhang et al., 2022) and hydroxychloroquine combined with the PI3K inhibitor BKM120 to induce synergistic effects against tumor cells by manipulating reactive oxygen species clearance and homologous recombination repair processes independent of autophagy (Peng et al., 2021). Herein, we demonstrated that amlodipine acts synergistically with gefitinib by inducing cell cycle arrest in the G0/G1 phase of A549 cells. Compared with amlodipine or gefitinib treatment alone, combination therapy with amlodipine and gefitinib could significantly decrease p-Rb and increase p27 levels. In addition, amlodipine acts synergistically with gefitinib to downregulate the phosphorylation of Akt (Ser473), Akt (Thr308), and mTOR without impacting total Akt and mTOR levels, compared with either amlodipine or gefitinib alone, thus leading to the inhibition of cell cycle progression. Our results indicate that combined treatment with amlodipine and gefitinib exhibited a more potent antitumor effect than monotherapy suppressing A549 cell proliferation.

Furthermore, we investigated the tumor-inhibitory effect of amlodipine in combination with gefitinib in an *in vivo* mouse model. We found that combining amlodipine and gefitinib could enhance the antitumor effects without inducing evident toxicity. Tumors size was decreased, along with a reduction in Ki67-positive staining of the tumor tissue.

Collectively, these findings indicate that amlodipine is a distinct antitumor agent in combination with gefitinib against NSCLC proliferation both *in vivo* and *in vitro*. To the best of our knowledge, this is the first study to combine amlodipine with gefitinib. However, the precise molecular targets of amlodipine alone and in combination with gefitinib on anticancer effects in A549 cells remain elusive in the present study and will be investigated in our future work. Our findings support the potential utility of amlodipine treatment for NSCLC, and amlodipine in combination with gefitinib may be feasible for clinical use, potentially providing a new therapeutic strategy for NSCLC.

DATA AVAILABILITY STATEMENT

The original contributions presented in the study are included in the article/Supplementary Material, further inquiries can be directed to the corresponding authors.

ETHICS STATEMENT

The animal study was reviewed and approved by the Laboratory Animal Center of the Institute of Radiation Medicine, Chinese Academy of Medical Sciences.

AUTHOR CONTRIBUTIONS

MJ and DK designed the experiments and acquired funding for the study; BF, XD, MZ, HL, KW, and QL performed the experiments; MJ, YL, and WW provided technical assistance; BF and MJ wrote the manuscript; DK edited the manuscript.

FUNDING

This project was supported by grants from the National Natural Science Foundation of China (81672809 to MJ, 82061148017, 82073890, and 81673464 to DK), and the Tianjin Science and Technology Commission (20JCYBJC00670).

REFERENCES

Alzahrani, A. S. (2019). PI3K/Akt/mTOR Inhibitors in Cancer: At the Bench and Bedside. *Semin. Cancer Biol.* 59, 125–132. doi:10.1016/j.semcancer.2019.07.009

Arslanagic, A., Zulic, I., and Bajraktarevic, A. (2005). Clinical Study on Safety and Efficacy of the Administration of Amlodipine in a Combination with Lisinopril in Hypertensive Patients. *Med. Arh.* 59, 346–348.

Asati, V., Mahapatra, D. K., and Bharti, S. K. (2016). PI3K/Akt/mTOR and Ras/Raf/MEK/ERK Signaling Pathways Inhibitors as Anticancer Agents: Structural and Pharmacological Perspectives. *Eur. J. Med. Chem.* 109, 314–341. doi:10.1016/j.ejmech.2016.01.012

Cersosimo, R. J. (2002). Lung Cancer: a eview. *Am. J. Health Syst. Pharm.* 59, 611–642. doi:10.1093/ajhp/59.7.611

Da Cunha Santos, G., Shepherd, F. A., and Tsao, M. S. (2011). EGFR Mutations and Lung Cancer. *Annu. Rev. Pathol.* 6, 49–69. doi:10.1146/annurev-pathol-011110-130206

De Mello, R. A., Liu, D. J., Aguiar, P. N., and Tadokoro, H. (2016). EGFR and EML4-ALK Updated Therapies in Non-small Cell Lung Cancer. *Recent Pat. Anticancer Drug Discov.* 11, 393–400. doi:10.2174/1574892811666160803090944

Degirmenci, U., Wang, M., and Hu, J. (2020). Targeting Aberrant RAS/RAF/MEK/ERK Signaling for Cancer Therapy. *Cells* 9, 198. *Cells* 9. doi:10.3390/cells9010198

Donjerkovic, D., and Scott, D. W. (2000). Regulation of the G1 Phase of the Mammalian Cell Cycle. *Cell. Res.* 10, 1–16. doi:10.1038/sj.cr.7290031

Eisenberg, M. J., Brox, A., and Bestawros, A. N. (2004). Calcium Channel Blockers: an Update. *Am. J. Med.* 116, 35–43. doi:10.1016/j.amjmed.2003.08.027

Gibbons, J. J., Abraham, R. T., and Yu, K. (2009). Mammalian Target of Rapamycin: Discovery of Rapamycin Reveals a Signaling Pathway Important for Normal and Cancer Cell Growth. *Semin. Oncol.* 36 (Suppl. 3), S3–s17. doi:10.1053/j.seminoncol.2009.10.011

Guo, Y. J., Pan, W. W., Liu, S. B., Shen, Z. F., Xu, Y., and Hu, L. L. (2020). ERK/MAPK Signalling Pathway and Tumorigenesis. *Exp. Ther. Med.* 19, 1997–2007. doi:10.3892/etm.2020.8454

Hermida, M. A., Dinesh Kumar, J., and Leslie, N. R. (2017). GSK3 and its Interactions with the PI3K/AKT/mTOR Signalling Network. *Adv. Biol. Regul.* 65, 5–15. doi:10.1016/j.jbior.2017.06.003

Hirai, F., Edagawa, M., Shimamatsu, S., Toyozawa, R., Toyokawa, G., Nosaki, K., et al. (2017). Evaluation of Erlotinib for the Treatment of Patients with Non-small Cell Lung Cancer with Epidermal Growth Factor Receptor Wild Type. *Oncol. Lett.* 14, 306–312. doi:10.3892/ol.2017.6118

Hirsch, F. R., Scagliotti, G. V., Mulshine, J. L., Kwon, R., Curran, W. J., Jr., Wu, Y. L., et al. (2017). Lung Cancer: Current Therapies and New Targeted Treatments. *Lancet* 389, 299–311. doi:10.1016/s0140-6736(16)30958-8

Hosomi, Y., Morita, S., Sugawara, S., Kato, T., Fukuhara, T., Gemma, A., et al. (2020). Gefitinib Alone versus Gefitinib Plus Chemotherapy for Non-small-cell Lung Cancer with Mutated Epidermal Growth Factor Receptor: NEJ009 Study. *J. Clin. Oncol.* 38, 115–123. doi:10.1200/jco.19.01488

Ibrahim, N., Yu, Y., Walsh, W. R., and Yang, J. L. (2012). Molecular Targeted Therapies for Cancer: Sorafenib Mono-Therapy and its Combination with

Other Therapies (Review). *Oncol. Rep.* 27, 1303–1311. doi:10.3892/or.2012.1675

Jensen, R. L., and Wurster, R. D. (2001). Calcium Channel Antagonists Inhibit Growth of Subcutaneous Xenograft Meningiomas in Nude Mice. *Surg. Neurol.* 55, 275–283. doi:10.1016/s0090-3019(01)00444-x

Li, Y. L., Hu, X., Li, Q. Y., Wang, F., Zhang, B., Ding, K., et al. (2018). Shikonin Sensitizes Wild-type EGFR NSCLC C-ells to E-rlotinib and G-efitinib T-herapy. *Mol. Med. Rep.* 18, 3882–3890. doi:10.3892/mmr.2018.9347

Liang, J., and Slingerland, J. M. (2003). Multiple Roles of the PI3K/PKB (Akt) Pathway in Cell Cycle Progression. *Cell. Cycle* 2, 339–345. doi:10.4161/cc.2.4.433

Martini, M., De Santis, M. C., Braccini, L., Gulluni, F., and Hirsch, E. (2014). PI3K/AKT Signaling Pathway and Cancer: an Updated Review. *Ann. Med.* 46, 372–383. doi:10.3109/07853890.2014.912836

Muta, Y., Matsuda, M., and Imajo, M. (2019). Divergent Dynamics and Functions of ERK MAP Kinase Signaling in Development, Homeostasis and Cancer: Lessons from Fluorescent Bioimaging. *Cancers (Basel)* 11, 513. doi:10.3390/cancers11040513

Navé, B. T., Ouwens, M., Withers, D. J., Alessi, D. R., and Shepherd, P. R. (1999). Mammalian Target of Rapamycin Is a Direct Target for Protein Kinase B: Identification of a Convergence Point for Opposing Effects of Insulin and Amino-Acid Deficiency on Protein Translation. *Biochem. J.* 344 Pt 2, 427–431.

Peng, X., Zhang, S., Jiao, W., Zhong, Z., Yang, Y., Claret, F. X., et al. (2021). Hydroxychloroquine Synergizes with the PI3K Inhibitor BKM120 to Exhibit Antitumor Efficacy Independent of Autophagy. *J. Exp. Clin. Cancer Res.* 40, 374. doi:10.1186/s13046-021-02176-2

Porta, C., Paglino, C., and Mosca, A. (2014). Targeting PI3K/Akt/mTOR Signaling in Cancer. *Front. Oncol.* 4, 64. doi:10.3389/fonc.2014.00064

Qie, S., and Diehl, J. A. (2016). Cyclin D1, Cancer Progression, and Opportunities in Cancer Treatment. *J. Mol. Med. Berl.* 94, 1313–1326. doi:10.1007/s00109-016-1475-3

Roskoski, R., Jr. (2019). Cyclin-dependent Protein Serine/threonine Kinase Inhibitors as Anticancer Drugs. *Pharmacol. Res.* 139, 471–488. doi:10.1016/j.phrs.2018.11.035

Shao, C., Huang, Y., Fu, B., Pan, S., Zhao, X., Zhang, N., et al. (2021). Targeting C-Jun in A549 Cancer Cells Exhibits Antiangiogenic Activity *In Vitro* and *In Vivo* through Exosome/miRNA-494-3p/PTEN Signal Pathway. *Front. Oncol.* 11, 663183. doi:10.3389/fonc.2021.663183

Shapiro, G. I. (2006). Cyclin-dependent Kinase Pathways as Targets for Cancer Treatment. *J. Clin. Oncol.* 24, 1770–1783. doi:10.1200/jco.2005.03.7689

Sheraz, M. A., Ahsan, S. F., Khan, M. F., Ahmed, S., and Ahmad, I. (2016). Formulations of Amlodipine: A Review. *J. Pharm. (Cairo)* 2016, 8961621. doi:10.1155/2016/8961621

Sherr, C. J. (1994). G1 Phase Progression: Cycling on Cue. *Cell.* 79, 551–555. doi:10.1016/0092-8674(94)90540-1

Shin, M., Franks, C. E., and Hsu, K. L. (2018). Isoform-selective Activity-Based Profiling of ERK Signaling. *Chem. Sci.* 9, 2419–2431. doi:10.1039/c8sc00043c

Shukuya, T., Takahashi, T., Kaira, R., Ono, A., Nakamura, Y., Tsuya, A., et al. (2011). Efficacy of Gefitinib for Non-adenocarcinoma Non-small-cell Lung Cancer Patients Harboring Epidermal Growth Factor Receptor Mutations: a Pooled Analysis of Published Reports. *Cancer Sci.* 102, 1032–1037. doi:10.1111/j.1349-7006.2011.01887.x

Sica, D. A. (2006). Pharmacotherapy Review: Calcium Channel Blockers. *J. Clin. Hypertens. (Greenwich)* 8, 53–56. doi:10.1111/j.1524-6175.2005.04140.x

Vandamme, D., Herrero, A., Al-Mulla, F., and Kolch, W. (2014). Regulation of the MAPK Pathway by Raf Kinase Inhibitory Protein. *Crit. Rev. Oncog.* 19, 405–415. doi:10.1615/critrevoncog.2014011922

Wang, J., Mcdonagh, D. L., and Meng, L. (2021). Calcium Channel Blockers in Acute Care: The Links and Missing Links between Hemodynamic Effects and Outcome Evidence. *Am. J. Cardiovasc. Drugs* 21, 35–49. doi:10.1007/s40256-020-00410-4

Wee, P., and Wang, Z. (2017). Epidermal Growth Factor Receptor Cell Proliferation Signaling Pathways. *Cancers (Basel)* 9. doi:10.3390/cancers9050052

Wozniak, A. J., Crowley, J. J., Balcerzak, S. P., Weiss, G. R., Spiridonidis, C. H., Baker, L. H., et al. (1998). Randomized Trial Comparing Cisplatin with Cisplatin Plus Vinorelbine in the Treatment of Advanced Non-small-cell Lung Cancer: a Southwest Oncology Group Study. *J. Clin. Oncol.* 16, 2459–2465. doi:10.1200/jco.1998.16.7.2459

Yohem, K. H., Clothier, J. L., Montague, S. L., Geary, R. J., Winters, A. L., 3rd, Hendrix, M. J., et al. (1991). Inhibition of Tumor Cell Invasion by Verapamil. *Pigment. Cell. Res.* 4, 225–233. doi:10.1111/j.1600-0749.1991.tb00445.x

Yoshida, J., Ishibashi, T., and Nishio, M. (2003). Antiproliferative Effect of Ca2+ Channel Blockers on Human Epidermoid Carcinoma A431 Cells. *Eur. J. Pharmacol.* 472, 23–31. doi:10.1016/s0014-2999(03)01831-4

Yoshida, J., Ishibashi, T., and Nishio, M. (2004). Antitumor Effects of Amlodipine, a Ca2+ Channel Blocker, on Human Epidermoid Carcinoma A431 Cells *In Vitro* and *In Vivo*. *Eur. J. Pharmacol.* 492, 103–112. doi:10.1016/j.ejphar.2004.04.006

Yoshida, J., Ishibashi, T., and Nishio, M. (2007). G1 Cell Cycle Arrest by Amlodipine, a Dihydropyridine Ca2+ Channel Blocker, in Human Epidermoid Carcinoma A431 Cells. *Biochem. Pharmacol.* 73, 943–953. doi:10.1016/j.bcp.2006.12.011

Yoshida, J., Ishibashi, T., Yang, M., and Nishio, M. (2010). Amlodipine, a Ca2+ Channel Blocker, Suppresses Phosphorylation of Epidermal Growth Factor Receptor in Human Epidermoid Carcinoma A431 Cells. *Life Sci.* 86, 124–132. doi:10.1016/j.lfs.2009.11.014

Zhang, S., Peng, X., Li, X., Liu, H., Zhao, B., Elkabets, M., et al. (2021). BKM120 Sensitizes Glioblastoma to the PARP Inhibitor Rucaparib by Suppressing Homologous Recombination Repair. *Cell. Death Dis.* 12, 546. doi:10.1038/s41419-021-03805-6

Zhang, Z., Hou, L., Yu, Z., Xu, Z., Li, S., Wang, Y., et al. (2022). Biomimetic Small-Molecule Self-Assembly of PI3K Inhibitor Integrated with Immunomodulator to Amplify Anticancer Efficacy. *Chem. Eng. J.* 433, 133747. doi:10.1016/j.cej.2021.133747

Zhao, X., Zhang, N., Huang, Y., Dou, X., Peng, X., Wang, W., et al. (2021). Lansoprazole Alone or in Combination with Gefitinib Shows Antitumor Activity against Non-small Cell Lung Cancer A549 Cells *In Vitro* and *In Vivo*. *Front. Cell. Dev. Biol.* 9, 655559. doi:10.3389/fcell.2021.655559

Conflict of Interest: The authors declare that the research was conducted in the absence of any commercial or financial relationships that could be construed as a potential conflict of interest.

Publisher's Note: All claims expressed in this article are solely those of the authors and do not necessarily represent those of their affiliated organizations, or those of the publisher, the editors and the reviewers. Any product that may be evaluated in this article, or claim that may be made by its manufacturer, is not guaranteed or endorsed by the publisher.

frontiers | Frontiers in Oncology

REVIEW
published: 06 June 2022
doi: 10.3389/fonc.2022.906372

Targeting TMEM88 as an Attractive Therapeutic Strategy in Malignant Tumors

Ming Cai[1,2†], *Wei-Jian Ni*[3,4*†], *Ying-Hong Wang*[5], *Jing-Ji Wang*[2] *and Hong Zhou*[5*]

[1] Department of Pharmacy, The Second Affiliated Hospital of Anhui University of Chinese Medicine, Hefei, China, [2] Anhui Acupuncture and Moxibustion Clinical Medicine Research Center, The Second Affiliated Hospital of Anhui University of Chinese Medicine, Hefei, China, [3] Inflammation and Immune Mediated Diseases Laboratory of Anhui Province, The Key Laboratory of Anti-inflammatory of Immune Medicines, Ministry of Education, Anhui Institute of Innovative Drugs, School of Pharmacy, Anhui Medical University, Hefei, China, [4] Anhui Provincial Hospital, The First Affiliated Hospital of USTC, Division of Life Sciences and Medicine, University of Science and Technology of China, Hefei, China, [5] Department of Pharmacy, Anhui Provincial Cancer Hospital, The First Affiliated Hospital of USTC, Division of Life Sciences and Medicine, University of Science and Technology of China, Hefei, China

According to authoritative surveys, the overall morbidity and mortality of malignant tumors show an upward trend, and it is predicted that this trend will not be well contained in the upcoming new period. Since the influencing factors, pathogenesis, and progression characteristics of malignant tumors have not been fully elucidated, the existing treatment strategies, mainly including surgical resection, ablation therapy and chemotherapy, cannot achieve satisfactory results. Therefore, exploring potential therapeutic targets and clarifying their functions and mechanisms in continuous research and practice will provide new ideas and possibilities for the treatment of malignant tumors. Recently, a double-transmembrane protein named transmembrane protein 88 (TMEM88) was reported to regulate changes in downstream effectors by mediating different signaling pathways and was confirmed to be widely involved in cell proliferation, differentiation, apoptosis and tumor progression. At present, abnormal changes in TMEM88 have been found in breast cancer, ovarian cancer, lung cancer, thyroid cancer and other malignant tumors, which has also attracted the attention of tumor research and attempted to clarify its function and mechanism. However, due to the lack of systematic generalization, comprehensive and detailed research results have not been comprehensively summarized. In view of this, this article will describe in detail the changes in TMEM88 in the occurrence and development of malignant tumors, comprehensively summarize the corresponding molecular mechanisms, and explore the potential of targeting TMEM88 in the treatment of malignant tumors to provide valuable candidate targets and promising intervention strategies for the diagnosis and cure of malignant tumors.

Keywords: malignant tumor, transmembrane protein 88 (Tmem88), Wnt/β-catenin, target, therapeutic strategy

OPEN ACCESS

Edited by:
Jian-ye Zhang,
Guangzhou Medical University, China

Reviewed by:
Xiangyu Yang,
Beijing Chao-yang Hospital Affiliated with Capital Medical University, China
Maicol Mancini,
U1194 Institut de Recherche en Cancérologie de Montpellier (INSERM), France
Hannah Hylton,
The Ohio State University, United States

***Correspondence:**
Wei-Jian Ni
niweijian@ustc.edu.cn
Hong Zhou
zhouhong@ahmu.edu.cn

[†]These authors have contributed equally to this work and share first authorship

Specialty section:
This article was submitted to Cancer Molecular Targets and Therapeutics, a section of the journal Frontiers in Oncology

Received: *28 March 2022*
Accepted: *09 May 2022*
Published: *06 June 2022*

Citation:
Cai M, Ni W-J, Wang Y-H, Wang J-J and Zhou H (2022) Targeting TMEM88 as an Attractive Therapeutic Strategy in Malignant Tumors. Front. Oncol. 12:906372. doi: 10.3389/fonc.2022.906372

INTRODUCTION

In recent years, membrane proteins have been studied and have become a research hotspot because they are widely distributed in tissues and play important and complex roles in various physiological processes and multiple diseases. Authoritative studies have shown that membrane proteins are distributed in the membranes of various cells and organelles, accounting for approximately 25% of the human proteome (1, 2), and exert undeniable effects on signal transduction in the cell-external environment and cell-cell interactions (3). Several studies have pointed out that membrane proteins can be classified into peripheral membrane proteins, lipid-anchored membrane proteins and integral membrane proteins according to their own structure and how they bind to biological membranes. The integral membrane protein contains at least one transmembrane fragment, which is also a transmembrane protein. These transmembrane proteins are not only involved in the body's metabolism and functional regulation (4–7) but also perform considerable regulatory roles in the tumorigenesis and progression of several tumors (8–11). For example, ATG9A, the only transmembrane protein currently in the core machinery of autophagy, can affect pathophysiological events such as cell growth, proliferation, stress and injury by regulating autophagy (12). In addition, endoplasmic reticulum-associated transmembrane protein 166 (TMEM166) was found not only in a variety of normal tissues and organs but also involved in multiple pathological processes, including cancer, infection, neurodegeneration, autoimmune disease, and sexually transmitted diseases, by regulating programmed cell death (13). Moreover, a transmembrane protein called the tyrosine kinase receptor may be abnormally activated to affect tumor cell growth, metastasis, invasion and malignant transformation by regulating multiple subprotein families and downstream signaling pathways (14). The aforementioned findings have made the transmembrane protein family a research focus that has received extensive attention. As an indispensable transmembrane protein family member, transmembrane protein 88 (TMEM88) has also been found to affect the growth and development of the body in normally expressed tissues, such as the development of cardiomyocytes and the activation of hematopoietic stem cells, while abnormal expression can affect the progression of various diseases, such as the inflammatory response, extracellular matrix secretion and drug resistance (15–21) (**Figure 1**). As an important tumor suppressor gene, TMEM88 benefits from the regulation of the Wnt signaling pathway and its downstream target genes and is widely involved in various biological events of malignant tumor cells, which has potential research value (22, 23). However, the current research on TMEM88 is still in its infancy, and there is no complete summary to help researchers fully understand the important role of TMEM88 in tumor research and prevention. In these circumstances, exploring TMEM88 as a new biomarker for tumor diagnosis and confirming that TMEM88 has become a promising target will be the research and prevention of tumors. In view of this, this review comprehensively describes the structure and function of TMEM88 and discusses its progress in the study of malignant tumors to provide important references and directions for subsequent research.

GENERAL STRUCTURE AND BIOLOGICAL FUNCTION OF TMEM88

The TMEM88 gene is a plus strand gene consisting of 1214 bases located at the p13.1 position on chromosome 17, and the corresponding TMEM88 protein is a 159 amino acid residue with a molecular weight of 17251 Da. An initial study found that the TMEM88 molecule is expressed on the Xenopus embryonic cell membrane (24). Meanwhile, the study also found that when the expression of TMEM88 was significantly upregulated in human embryonic kidney cells, the downstream Wnt/β-catenin signal transduction process was inhibited, while silencing TMEM88 could activate the Wnt/β-catenin signal transduction process. Another study found that TMEM88 can inhibit Wnt/β-catenin signal activation in human embryonic stem cells to a certain extent, thereby regulating the differentiation and development of embryonic stem cells into cardiomyocytes (21). With the progress of research, it was found that the TMEM88 protein is widely present in a variety of tumors, but its functions are different due to the different tissue and subcellular locations (**Table 1**). One study found that cytoplasmic localization of TMEM88 was positively correlated with TNM stage and lymph node metastasis in triple-negative breast cancer, whereas nuclear localization was negatively correlated with lymph node metastasis in nontriple-negative breast cancer (30); in ovarian cancer, TMEM88 was found to downregulate the levels of c-Myc and Cyclin D1, thereby inhibiting the proliferation of ovarian cancer cells (19). In non-small-cell lung cancer (NSCLC), the high expression of TMEM88 is positively correlated with a better prognosis of patients, but the detailed mechanism needs to be further clarified (28).

ROLE AND MECHANISM OF TMEM88 IN MALIGNANT TUMORS

In recent years, an increasing number of research results have shown that abnormal expression of TMEM88 exists in several malignant tumors (ovarian cancer, breast cancer, lung cancer, etc.) and has actively participated in the abnormality of tumor cell proliferation, invasion, metastasis and apoptosis. Meanwhile, with the development of structural biology, biochemistry and other disciplines, breakthroughs and progress have been made in the isolation and characterization of transmembrane proteins, which indicates that it may become a promising molecular marker and valuable intervention target for tumor diagnosis, therapy and prognosis (**Figure 2**).

TMEM88 in Ovarian Cancer

Ovarian cancer has become a malignant tumor in the female germline that seriously threatens women's health, with its third incidence rate (after cervical cancer and endometrial cancer) and

TABLE 1 | The landscape of the roles of TMEM88 in various human tissues.

Tissue localization	Disease types	Associated tissues or cells	Alterations	Target	Function	References
Human embryo	cell development	Human embryonic stem cells	Upregulation	DVL	Regulate cardiomyocyte specification	Lee, Heejin et al. (22) Lee, Ho-Jin et al. (24) Palpant, Nathan J et al. (21)
Ovarian	ovarian cancer	CP70 and PEO4 A2780 and PEO1	Upregulation Downregulation	JUN, PTIX2, β-catenin, c-Myc and cyclin-D1	Regulate platinum resistance	de Leon, Maria et al. (19)
Thyroid	thyroid cancer	BCPAP, TPC1, K1 and NPA87	Downregulation	TCF/LEF, c-Myc and cyclin D1	Suppress tumor process	Geng, Qianqian et al. (25)
Lung	Lung cancer	A549, H1299, H460, H292, SPC-A-1 and LTEP-A-2	Downregulation	DVL, FZD and ROR1	Suppress tumor process	Zhang, Xiupeng et al. (26) Stewart, David J. (27) Ma, Rongna etal. (28)
Skin	keloids	Keloid fibroblasts	Downregulation	β-catenin, c-Myc and cyclin D1	Inhibit extracellular matrix expression	Zhao, Huafei et al. (16)
Bladder	bladder cancer	5637, UM-UC-3, T24 and SW780	Downregulation	GSK-3β, β-catenin and TCF/LEF	Suppress tumor process	Zhao, Xu et al. (29)
Breast	triple-negative breast cancer	MCF-7, HER18, MDA-MB-231 and MDA-MB-468	Upregulation	DVL, Snail, Occludin and Zo-1	Promote tumor process	Yu, Xinmiao et al. (30)
Liver	liver fibrosis	LX-2 and human liver fibrotic tissues	Downregulation	β-catenin, Wnt3a, Wnt2b, Wnt10b, p-JNK and p-P38	Regulate proinflammatory cytokine secretion and inhibit HSC excitation	Xu, Tao et al. (17) Xu, Tao et al. (31)

c-Myc, c-Myc proto-oncogene; DVL, PDZ domain of Dishevelled-1; FZD, Wnt receptor Frizzled; GSK-3β, glycogen synthase kinase-3β; HSC, hepatic stellate cell; JNK, c-Jun N-terminal kinase; JUN, jun proto-oncogene; >PITX2, paired-like homeodomain 2; ROR1, receptor tyrosine kinase-like orphan receptor 1; TCF/LEF, T-cell factor/lymphoid enhancer-binding factor; TMEM88, transmembrane protein 88.

the highest mortality rate. On the one hand, due to the lack of typical clinical manifestations in the early stage, a large proportion of patients are already in the middle and late stages when they are diagnosed, and even the tumor cells have metastasized far away. On the other hand, platinum-based chemotherapy is the main means to maintain the survival of such patients, but many patients suffer from drug resistance, tumor recurrence and metastasis after chemotherapy (32). Based on this, exploring the pathogenesis and drug resistance mechanism of ovarian cancer and finding effective targets are of great significance for improving treatment and improving the 5-year survival rate of ovarian cancer patients. Maria de Leon et al. used an Illumina 450k DNA methylation array to detect methylated genes and levels in ovarian cancer xenografts and found that compared with platinum-sensitive transplanted tumors, the promoter region of the TMEM88 gene in platinum-resistant transplanted tumors in nude mice was significantly hypomethylated, while TMEM88 mRNA showed a substantial increase (19). Meanwhile, the application of the DNA methyltransferase inhibitor SGI-110 can significantly increase the TMEM88 mRNA level and corresponding protein expression in platinum-sensitive ovarian cancer cells. Both *in vitro*, *in vivo* and clinical studies have shown that the level of TMEM88 is significantly increased in platinum-resistant ovarian cancer xenograft nude mice, platinum-resistant ovarian cancer cells and recurrent ovarian cancer tissue, while knockdown or decrease the expression of TMEM88 can resensitize tumor cells to platinum drugs. Mechanistic studies found that silencing TMEM88 alleviated the inhibition of canonical Wnt/β-catenin signaling by reducing the interaction of the C-terminal VWV (Val-Trp-Val) sequence with the PDZ domain of Dishevelled-1 (Dvl-1) (19, 23). The activation of Wnt/β-catenin signaling increased the expression of the downstream target genes c-Myc and β-catenin to increase ovarian cancer cell proliferation and the proportion of S-phase cells throughout the cell cycle and reincreased platinum sensitivity. Meanwhile, the aforementioned studies also found that TMEM88 overexpression induced cell dormancy to help it evade the lethal effects of chemotherapy and trigger recurrent tumors. These studies suggest that TMEM88 may have an important regulatory role in the process of ovarian cancer resistance and may also be used to identify epigenetic modifiers associated with platinum resistance, which may provide new clues and insights for predicting ovarian cancer recurrence and overall cancer patient survival.

TMEM88 in Breast Cancer

Authoritative research estimates that breast cancer has become the most prevalent cancer type among female cancer patients in the United States, and death also ranks second among female cancer-related death types, with a true proportion of 15% in 2022

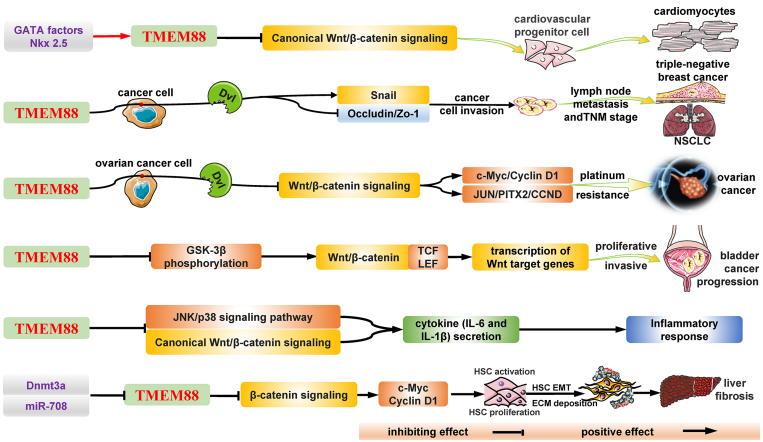

FIGURE 1 | The structure and general biological functions of TMEM88 in humans. As a secondary transmembrane protein, TMEM88 is widely distributed in many types of cells and tissues and plays an important regulatory role in various diseases and pathological processes, such as cancers, fibrosis, and inflammatory responses. Under stimulation, including DNA methylation, noncoding RNA and the inflammatory environment, the mRNA and protein levels of TMEM88 changed significantly. Subsequently, the significantly changed TMEM88 regulates the classical and noncanonical Wnt/β-catenin signaling pathways through different mechanisms in the cytoplasm and nucleus, such as the interaction with DVL proteins, thereby affecting the transcription and expression of downstream target genes. Ultimately, these effector target molecules affect the growth and development of tissues and organs and the progression of diseases, such as tumors by regulating various cellular life activities, such as cell proliferation, migration, invasion, and drug resistance. CCND, Cyclin D1; c-Myc, c-Myc proto-oncogene; Dnmt3a, DNA (cytosine-5)-methyltransferase 3a; DVL, PDZ domain of Dishevelled-1; ECM, extracellular matrix; EMT, epithelial-mesenchymal transition; GATA, GATA transcription factor; GSK-3β, glycogen synthase kinase-3β; HSC, hepatic stellate cell; JNK, c-Jun N-terminal kinase; JUN, jun proto-oncogene; NSCLC, non-small-cell lung cancer; PITX2, paired-like homeodomain 2; TCF/LEF, T-cell factor/lymphoid enhancer-binding factor; TMEM88, transmembrane protein 88; TNM, tumor node metastasis.

(33). According to the latest data released by the National Cancer Center, the incidence of breast cancer in China is 7.11%, and the mortality rate is 2.81%, ranking fifth and seventh, respectively (34). Based on the above statistical results, breast cancer is a serious public health issue in current society and needs to be given great attention. Although great progress has been made in clinical treatment strategies, including surgery, chemotherapy, radiotherapy and hormone therapy, the long-term clinical

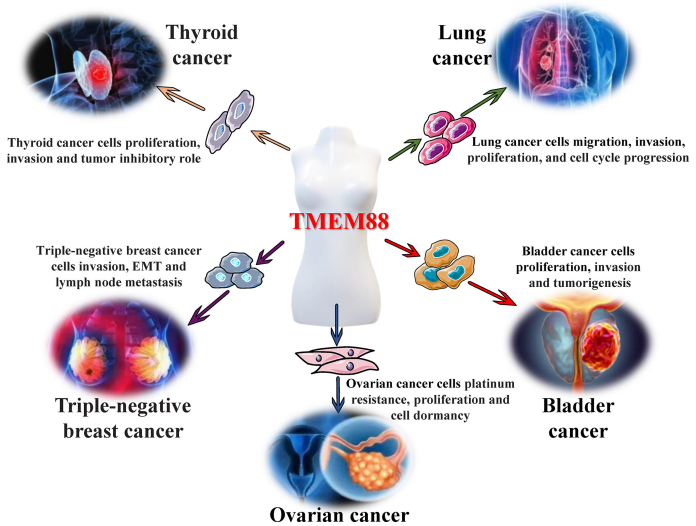

FIGURE 2 | Regulatory effects of TMEM88 in malignant tumors. Different tumor microenvironments, such as inflammation and oxidative stress, can cause significant changes in the levels of TMEM88 in tissues and cells, which will affect tumor cell properties, including abnormal cell proliferation, invasion, migration, and epithelial-mesenchymal transition (EMT), through canonical and noncanonical Wnt/β-catenin signaling and other signal transduction pathways. These tumor cell properties lead to the occurrence, growth, invasion, and metastasis of various tumors, including ovarian cancer, thyroid cancer, triple-negative breast cancer, bladder cancer, and lung cancer, and ultimately affect tumor progression and poor prognosis.

prognosis and the survival rate of patients are still not satisfactory (35, 36). Therefore, it has become an urgent problem to be solved in breast cancer research to explore new therapeutic targets and develop effective intervention strategies. During the process of exploring new targets for breast cancer, Yu et al. conducted a study that first performed a correlation analysis between 139 breast cancer tissues and normal breast tissues. The results showed that the overall expression level of TMEM88 in breast cancer tissues (71.22%, 99/139) was significantly higher than that in normal tissue (11.4%, 4/35; $P < 0.001$), and the specific expression differences were not the same. Specifically, expression and localization analysis revealed that TMEM88 was moderately elevated in breast cancer *in situ* and highly elevated in invasive breast ductal carcinoma compared with negative or low expression in normal breast tissue, which suggests that the expression of TMEM88 has potential as a marker for breast cancer classification. In addition, the study also found that the cytoplasmic localization of TMEM88 was positively correlated with advanced TNM stage ($P = 0.038$) and lymph node metastasis ($P = 0.01$), while nuclear localization was inversely related to lymph node metastasis ($P = 0.046$). These results indicate that TMEM88 plays different functions depending on different subcellular localizations in the development of breast cancer (cytoplasmic TMEM88 promotes tumors, while nuclear TMEM88 suppresses tumors), suggesting that TMEM88 has important research value and needs to be considered (30). When using breast cancer cells (MDA-MB-231 and MCF-7) as the object to explore the mechanism, Yu et al. also found that TMEM88 and Dvl colocalized in the cytoplasm and TMEM88 can interact with Dvl to promote the expression of Snail protein and inhibit the expression of Zo-1 and Occludin, thereby reducing the invasion and metastasis of breast cancer cells. The above results show that the expression level of TMEM88 has certain differences in different types of breast cancer, and the cytoplasmic level and nuclear expression of TMEM88 have obvious tissue distribution specificity, which may facilitate TMEM88 becoming a promising therapeutic target for the treatment of breast cancer; however, the specific mechanism and intervention potential need further research to clarify.

TMEM88 in Lung Cancer

Lung cancer has become the malignant tumor with the greatest threat to human health and life worldwide due to its higher incidence and mortality than other malignant tumors, accounting for 11.6% of cancer patients and 18.4% of total cancer deaths (37, 38). Among all lung cancer patients, NSCLC accounts for approximately 80%-85% of the total population. Although surgical resection is an effective treatment for early-stage lung cancer, the 5-year survival rate is still unsatisfactory (approximately 30-60%) (39, 40). What is even more regrettable is that most patients are already in the middle stage when they are diagnosed, most are even in the advanced stage, and they have lost the opportunity for surgical treatment, which accounts for one of the main reasons for the poor prognosis and high mortality of lung cancer patients (41). Therefore, exploring new targets and researching new treatment methods are urgently needed and will also provide a large number of theoretical and research foundations for the development of clinical treatments for lung cancer. In a study of 214 cases of NSCLC, Zhang et al. found that the expression of TMEM88 in the adjacent tissue was negative or weakly positive compared with the tissue of NSCLC patients by immunohistochemical analysis. The correlation analysis results of clinicopathological characteristics showed that high expression of TMEM88 in the cytoplasm was directly correlated with the tissue differentiation, lymph node metastasis and tumor stage of NSCLC patients ($P < 0.001$, $P = 0.032$ and $P = 0.012$), but there was no obvious correlation with sex, age, or histological type ($P = 1$, $P = 0.884$ and $P = 1$). Kaplan-Meier survival analysis showed that the overall survival of lung cancer patients (38.8 ± 4.83 months) with high TMEM88 expression was significantly lower than that of patients (58.64 ± 4.24 months) with low TMEM88 expression (26). This study preliminarily demonstrated the potential role and promising research value of TMEM88 in the development and exploration of NSCLC, but the specific pathogenesis needs to be further clarified. Subsequently, Zhang et al. used Western blotting to analyze the changes in TMEM88 in 40 fresh NSCLC specimens and found that TMEM88 expression was higher than that in normal lung tissue, which is also consistent with previous findings. Immunofluorescence staining of 7 types of lung cancer cells (A549, LTE, SPC, H292, H1299, BE1 and LH7 cells) found that the content of TMEM88 was significantly higher than that in human bronchial epithelial cells (HBE), while TMEM88 was found in the other two lung cancer cell types (LK2 and H460 cells) and was interestingly lower than that in HBE cells, and TMEM88 was predominantly located on the cell membrane in all types of lung cancer cells studied. Taking LK2 cells as the research object to study the effect of TMEM88, it was found that overexpression of TMEM88 can inhibit the excessive proliferation, invasion and migration of LK2 cells, thus preventing the growth of transplanted tumors in nude mice (26). Another study analyzed the NSCLC tissues and adjacent normal tissues of 12 patients and found that the degree of TMEM88 methylation in NSCLC tissues (82.2% ± 10.3%) was higher than that in normal tissues (65.9% ± 7.2%, $P < 0.01$), which was negatively correlated with overall survival ($P = 0.021$) (28). Subsequently, researchers used 5-aza-2'-deoxycytidine (DAC) to treat A549 and H1299 cells to further evaluate the functional alterations of TMEM88 methylation in lung cancer. The experimental results show that the degree of methylation of TMEM88 decreases while the expression level of TMEM88 increases after treatment with DAC. Scratch experiments, migration experiments and cell cycle experiments have found that TMEM88 can potently inhibit abnormal lung cancer cell proliferation, invasion and migration (26, 28), indicating that TMEM88 can exert a tumor suppressor effect and can be considered a candidate therapeutic target for the prognosis and cure of lung cancer, opening up a new avenue for the prevention of lung cancer.

TMEM88 in Thyroid Cancer

Thyroid cancer (TC) has become one of the most common malignancies of the endocrine system over the past few decades, with a steady increase in global morbidity and mortality and a

strong female predominance, which is well validated by the finding that the incidence in women in most populations is approximately three times that in men (42). Since 2003, the incidence of thyroid cancer in China has suddenly started to rise rapidly and has maintained an annual percentage change of approximately 14.51 from 2003 to 2007, while urban women have witnessed a faster rate of change, and by 2012, thyroid cancer had become one of the ten most common cancers (43–45). Meanwhile, one study also predicts that thyroid cancer may become the fourth most common malignant tumor in the world by 2030 (46). From a pathological point of view, thyroid cancer is mainly divided into papillary carcinoma, follicular carcinoma, anaplastic carcinoma and medullary carcinoma, among which papillary carcinoma is the most common (47). Most papillary thyroid carcinomas have a good prognosis, but local recurrence or distant metastasis after treatment is also common, and some patients die due to disease progression. Many studies have shown that various factors, such as radiation exposure, environmental and industrial pollution, and family inheritance, may promote the occurrence and development of thyroid cancer, but its pathogenesis is still unclear (43, 48). Therefore, exploring the pathogenesis of thyroid cancer and finding potential targets will provide an important basis for the preclinical study and clinical treatment of thyroid cancer. In one study, the researchers found that TMEM88 was significantly reduced in thyroid cancer by analyzing the gene expression profile interactive analysis database (25). In addition, Geng et al. also showed that the expression levels of TMEM88 were significantly decreased in 8 thyroid cancer patient specimens as well as in 4 thyroid cancer cell lines, BCPAP, TPC1, K1 and NPA87. Various experimental methods, such as Western blotting, qRT-PCR, cell counting kit-8 assay and colony formation experiments, found that restoration of TMEM88 by vector transfection can markedly suppress the proliferation, colony formation and invasion ability of thyroid cancer cells. In contrast, depletion of TMEM88 can accelerate the proliferation and invasion ability of thyroid cancer cells. The results of tumor formation experiments in nude mice also suggested that TMEM88 overexpression can significantly inhibit the growth of thyroid cancer, which is associated with the downregulation of active β-catenin expression. The above results show that TMEM88 exerts a nonnegligible role in the occurrence and development of thyroid cancer, and in-depth research on the mechanism of TMEM88 will offer new targets and ideas for the research and prevention of thyroid cancer.

TMEM88 in Bladder Cancer

An authoritative analysis found that bladder cancer, the fifth most common cancer in Western countries, has an increasing incidence with age and is found in the highest proportion in individuals over the age of 65 (49). In China, the incidence of bladder cancer ranks second among male genitourinary malignancies and 7th among all malignant tumors (50). Clinical studies have shown that bladder cancer is a highly malignant tumor that is prone to recurrence and progresses rapidly, especially muscle-invasive BC (MIBC), which often recurs after the first resection and has a poor prognosis (51, 52). Therefore, it is particularly urgent to explore the possible pathogenesis and potential therapeutic targets of bladder cancer. In one study, research found that TMEM88 is closely relevant to the pathogenesis and development of bladder cancer, and inhibition of the TMEM88/Wnt axis can significantly affect abnormal bladder cancer cell proliferation and the regulation of the cell cycle (29), which suggests that targeting TMEM88 for bladder cancer research will be a new strategy and direction. Moreover, the study conducted bioinformatic analysis of the GEPIA2 and ENCORI databases and found that the expression of TMEM88 in bladder cancer tissues was significantly reduced compared to that in normal tissues. In the detection of 6 bladder cancer patient tissues, it was found that the expression of TMEM88 in patient tissues indeed showed a downward trend compared with adjacent normal tissues. *In vitro*, depletion of TMEM88 in bladder cancer cells, such as UM-UC-3 and T24 cells, can enhance their invasive and proliferative capacity, while restoring TMEM88 levels can reverse these effects. In *in vivo* experiments in nude mice, overexpression of TMEM88 exhibited a certain inhibitory action on bladder cancer cell growth and tumor formation (53). The above results show that TMEM88 is most likely to become the specific target and that targeting TMEM88 may effectively treat bladder cancer.

Possible Mechanism of TMEM88 in Malignant Tumors

The relatively conserved Wnt signaling pathway is one of the major factors regulating development across the animal kingdom and is a key driver of stem cells in most types of tissues (54, 55). While regulating embryonic development and maintaining tissue homeostasis, it mediates downstream signals to participate in various biological/pathological processes and the genesis and development of cancer (53, 56, 57). During the research process of TMEM88, studies have pointed out that the C-terminal tripeptide Val-Trp-Val sequence of a subtype of TMEM88 CRA-a can bind to the PDZ domain of the scrambled protein and prohibit the Wnt/β-catenin signaling pathway, which exerts a nonnegligible effect in regulating tumor cell proliferation, metastasis and host antitumor immunity (22, 27, 58). For example, it can be coexpressed in the cytoplasm with scattered proteins in NSCLC and breast cancer to elevate the levels of Snail and thereby promote tumor progression. Analysis of the transcriptome information of ovarian cancer patients in the TCGA database shows that TMEM88 is closely correlated with the mRNA expression levels of c-Myc and β-catenin mRNA (P = 0.01252 and 0.0128) (19). In addition, Geng et al. found that the overexpression of TMEM88 significantly reduced the transcriptional activity of TCF/LEF and inhibited the expression of the downstream target genes c-Myc and cyclin D1 of the Wnt/β-catenin signaling pathway (25). Furthermore, reactivation of Wnt/β-catenin signaling by transfection of the pENTRN90-β-catenin vector partially reversed the inhibitory effect of TMEM88 on the proliferation and invasion of thyroid cancer cells, indicating that TMEM88 exerts an anti-thyroid cancer effect in the presence of Wnt/β-catenin protein signaling. A study in bladder cancer

found that overexpression of TMEM88 also inhibited the activation of the Wnt/β-catenin signaling pathway by reducing the phosphorylation level of GSK-3β (Ser9 site) (29). However, in a study of triple-negative breast cancer, transfection of MCF-7 and MDA-MB-231 cells to overexpress or silence TMEM88 did not affect the activity of the canonical Wnt signaling pathway or the expression of corresponding target genes such as MMP-7, c-Myc and cyclin D1 (30). Taken together, the above studies suggest that TMEM88, as an important linker in the genesis and development of various cancer diseases, can function by regulating different downstream oncogenic signals and effector molecules. It transmits upstream signals and regulates downstream signal transduction, such as Wnt signaling pathways, to interfere with the occurrence and progression of tumors and then has an anticancer effect. Based on this, TMEM88 should be considered a novel and important research target in cancer research, which needs to be deeply explored for its potential.

TARGETING TMEM88 POTENTIAL FOR TREATING MALIGNANT TUMORS

With the deepening of people's understanding of tumor research and clinical, molecular targeted therapy has also received increasing attention and aroused the interest of researchers. At present, the most common molecular targeted therapeutic drugs mainly include small molecular epidermal kinase inhibitors, such as gefitinib (AstraZeneca, UK) (59); anti-EGFR monoclonal antibodies, such as cetuximab (Merck & Leone Pharmaceutical Co, Germany) (60); anti-HER-2 monoclonal antibodies, such as trastuzumab (Roche Group, Switzerland) (61); Bcr-Abl tyrosine kinase inhibitors, such as imatinib (Novartis, Switzerland) (62); anti-CD20 monoclonal antibodies, such as rituximab (Roche Group, Switzerland) (63); and vascular endothelial growth factor receptor inhibitors, such as bevacizumab (Roche Group, Switzerland) (64). When the above drugs exert antitumor effects, they can significantly reduce the toxicity to normal cells, which provides a new direction for molecular targeted therapy of tumors. However, due to the heterogeneity of cancers, the current targeted therapeutic drugs benefit only a portion of cancer patients, which forces us to explore a broader spectrum of malignant tumor therapeutic targets and develop promising therapeutic drugs to address the urgent issue in tumor research and current clinical practice.

To date, a variety of transmembrane proteins have become powerful targets for drug development and have even entered clinical trials and clinical applications. As a representative, the G protein coupled receptor (GPCR) family is the largest transmembrane protein family in humans and is also an important target of many drugs (65). Currently, 475 drugs targeting GPCR have been approved by the FDA, accounting for 34% of all FDA approved drugs. Meanwhile, 321 drugs targeting GPCRs are in clinical studies (66, 67). The above drugs are mainly distributed in small molecule drugs, polypeptide drugs, monoclonal antibodies, and recombinant proteins. Four-transmembrane proteins, CD20 and Claudin 18.2, are important targets for disease treatment and drug development. CD20 is a transmembrane phosphorin located on the surface of B lymphocytes, mainly in the preceding B-cell to mature B-cell stage (68). Currently, the antitumor drug antibody and inflammatory immune regulatory antibody drugs that target CD20 have entered the fast lane developed by the product (69). Claudin18.2 is the most important member of the Claudin transmembrane protein family. In the normal physiological state, Claudin18.2 protein is only expressed on the surface of human gastric epithelial shorthearter cells. However, in the pathological state, Claudin18.2 protein is highly expressed in gastric cancer, esophageal cancer, pancreatic cancer, and other solid tissues (15, 70–72). The significant differences and high tissue specificity make Claudin 18.2 an ideal target for solid tumor immunotherapy(2016). Currently, it has been close to 20 drugs targeting Claudin18.2 in the clinical phase, such as zolbetuximab (Phase III: NCT03653507, Astellas Pharma Inc., Japan), TST001 (Phase I: NCT04495296, MabSpace Biosciences, China) and AMG910 (Phase I: NCT04260191, Amgen Inc., USA), and these drugs are primarily concentrated on monoclonal antibody and bispecific antibody, antibody-drug conjugate (ADC), and chimeric antigen receptor T-cell immunotherapy (CAR-T) (72–75). The abovementioned drug development of transmembrane proteins has laid a solid foundation for the research and exploration of targeted TMEM88 to treat malignant tumors. Meanwhile, we should be more aware of the current gaps in the development of drugs targeting TMEM88 for the treatment of tumors: 1. Insufficient analysis of the three-dimensional and crystal structure of the TMEM88 protein makes the structural information of the protein lacking. 2. Research on the full length of the TMEM88 protein polypeptide and the recognition epitope is insufficient, and information on the active site and affinity is lacking. We believe that the resolution of these problems will greatly promote the development of drugs targeting TMEM88.

However, due to the surface area of the transmembrane protein structure, its expression level is difficult to meet the requirements. Furthermore, it is difficult for us to achieve high-purity multitransmembrane proteins with natural conformations and activity. These difficulties make targeted TMEM88 antitumor drug development difficult. Based on this, various strategies can be considered to increase the development of antitumor drugs targeting TMEM88: 1. Novel protein purification, isolation and characterization systems and techniques need to be applied; 2. Artificial intelligence and computer simulation need to be more invested; 3. Drug diversity needs to be constantly tried, such as antibody drugs, nanodrugs, small-molecule drugs, traditional Chinese medicines and proteolysis targeting-chimeras (PROTAC). In any case, as a two-transmembrane protein, TMEM88 has significant differences and specificities between multiple malignant tumor and adjacent tissues and tumor and normal cells, which makes TMEM88 a potential therapeutic target through different strategies during tumor treatment.

PROSPECTIVE AND CONCLUSIONS

In recent years, tumors have been the main cause of human death, and the occurrence and development of many kinds of tumors are closely related to the imbalance of signal transduction in the body (76). Therefore, it is extremely important to clarify the signal transduction mechanism and find potential new tumor therapeutic targets. In the current literature, TMEM88 is considered to play an important role in the development of breast cancer, lung cancer, thyroid cancer and other tumors by inhibiting Wnt signal transduction and participates in the occurrence and development of tumors, but it needs to be pointed out that TMEM88 research is not deep enough, and many issues remain to be studied. Specifically, TMEM88 has different expression levels in different tumors and has tissue specificity, but what are the specific characteristics; when there are multiple influencing factors, will the role of TMEM88 in malignant tumors be different? TMEM88 methylation affects tumor biology However, what is the specific mechanism? In the process of cancer development, TMEM88 not only regulates the Wnt/β-catenin signaling pathway and participates in it but also affects other signal transduction processes. Therefore, more basic research needs to be carried out to further confirm the specific role of TMEM88 in tumor development, improve its credibility as a potential therapeutic target, and prove its potential to transform from basic research to clinical application in tumor treatment. In any case, the results of multiple studies have shown that TMEM88 may be a tumor diagnosis and prognostic indicator, which will provide new clues and directions for the diagnosis and treatment of clinical malignant tumors. We look forward to using advanced technologies for in-depth research, such as microarray analysis, tissue sample sequencing, high-throughput DNA methylation analysis and other new technologies, revealing the function of TMEM88 regulation in more malignant tumors and elucidating the pathogenesis of TMEM88 in tumors. This will further promote the progress of the diagnosis and treatment of malignant tumors.

AUTHOR CONTRIBUTIONS

HZ, W-JN, and MC designed the "idea"; MC and W-JN wrote the manuscript; Y-HW and J-JW collected the information; W-JN and HZ revised the manuscript. All authors read and approved the final manuscript.

FUNDING

This work was supported by the Science Foundation of Anhui Provincial Cancer Hospital (No. 2020YJQN008), the National Natural Science Foundation of China (No. 81803602), the Natural Science Foundation of Anhui Province (No. 1708085QH207), and the Fundamental Research Funds for the Central Universities (No. WK9110000018). Key Project of the Clinical Research Fund of Anhui University of Chinese Medicine (No. 2021efylc03).

ACKNOWLEDGMENTS

We thank American Journal Experts (AJE) for their guidance on the grammar and language of this article.

REFERENCES

1. Li C, Ou R, Chen Y, Gu X, Wei Q, Cao B, et al. Mutation Analysis of TMEM Family Members for Early-Onset Parkinson's Disease in Chinese Population. *Neurobiol Aging* (2021) 101:299.e1–6. doi: 10.1016/j.neurobiolaging.2020.11.005
2. Marx S, Dal Maso T, Chen JW, Bury M, Wouters J, Michiels C, et al. Transmembrane (TMEM) Protein Family Members: Poorly Characterized Even If Essential for the Metastatic Process. *Semin Cancer Biol* (2020) 60:96–106. doi: 10.1016/j.semcancer.2019.08.018
3. Liu Y, Zheng Q, He G, Zhang M, Yan X, Yang Z, et al. Transmembrane Protein 215 Promotes Angiogenesis by Maintaining Endothelial Cell Survival. *J Cell Physiol* (2019) 234(6):9525–34. doi: 10.1002/jcp.27641
4. Zhang Z, Luo S, Barbosa GO, Bai M, Kornberg TB, Ma DK. The Conserved Transmembrane Protein TMEM-39 Coordinates With COPII to Promote Collagen Secretion and Regulate ER Stress Response. *PloS Genet* (2021) 17(2): e1009317. doi: 10.1371/journal.pgen.1009317
5. Fuhrmann DC, Wittig I, Brune B. TMEM126B Deficiency Reduces Mitochondrial SDH Oxidation by LPS, Attenuating HIF-1alpha Stabilization and IL-1beta Expression. *Redox Biol* (2019) 20:204–16. doi: 10.1016/j.redox.2018.10.007
6. Beasley HK, Rodman TA, Collins GV, Hinton AJ, Exil V. TMEM135 Is a Novel Regulator of Mitochondrial Dynamics and Physiology With Implications for Human Health Conditions. *Cells* (2021) 10(7):1750–66. doi: 10.3390/cells10071750
7. Picotto G, Morse LR, Nguyen N, Saltzman J, Battaglino R. TMEM176A and TMEM176B Are Candidate Regulators of Inhibition of Dendritic Cell Maturation and Function After Chronic Spinal Cord Injury. *J Neurotrauma* (2020) 37(3):528–33. doi: 10.1089/neu.2019.6498
8. Xu J, Su Z, Ding Q, Shen L, Nie X, Pan X, et al. Inhibition of Proliferation by Knockdown of Transmembrane (TMEM) 168 in Glioblastoma Cells *via* Suppression of Wnt/beta-Catenin Pathway. *Oncol Res* (2019) 27(7):819–26. doi: 10.3727/096504018X15478559215014
9. Shen K, Yu W, Yu Y, Liu X, Cui X. Knockdown of TMEM45B Inhibits Cell Proliferation and Invasion in Gastric Cancer. *Biomed Pharmacother* (2018) 104:576–81. doi: 10.1016/j.biopha.2018.05.016
10. Li Y, Guo W, Liu S, Zhang B, Yu BB, Yang B, et al. Silencing Transmembrane Protein 45b (TNEM45B) Inhibits Proliferation, Invasion, and Tumorigenesis in Osteosarcoma Cells. *Oncol Res* (2017) 25(6):1021–6. doi: 10.3727/096504016X14821477992177
11. Zhang X, Wan JX, Ke ZP, Wang F, Chai HX, Liu JQ. TMEM88, CCL14 and CLEC3B as Prognostic Biomarkers for Prognosis and Palindromia of Human Hepatocellular Carcinoma. *Tumour Biol* (2017) 39(7):1010428317708900. doi: 10.1177/1010428317708900
12. Guardia CM, Tan XF, Lian T, Rana MS, Zhou W, Christenson ET, et al. Structure of Human ATG9A, the Only Transmembrane Protein of the Core Autophagy Machinery. *Cell Rep* (2020) 31(13):107837. doi: 10.1016/j.celrep.2020.107837
13. Yang Y, Zhou L, Xue F, An L, Jin M, Li L. Transmembrane Protein 166 and Its Significance. *Protein Pept Lett* (2021) 28(4):382–7. doi: 10.2174/0929866527666201002150316
14. Du Z, Lovly CM. Mechanisms of Receptor Tyrosine Kinase Activation in Cancer. *Mol Cancer* (2018) 17(1):58. doi: 10.1186/s12943-018-0782-4
15. Xu B, Liu F, Liu Q, Shi T, Wang Z, Wu N, et al. Highly Expressed Claudin18.2 as a Potential Therapeutic Target in Advanced Gastric Signet-Ring Cell Carcinoma (SRCC). *J Gastrointest Oncol* (2020) 11(6):1431–9. doi: 10.21037/jgo-20-344

16. Zhao H, Lu F, Cui S, Zhang X, Wang W, Si E, et al. TMEM88 Inhibits Extracellular Matrix Expression in Keloid Fibroblasts. *Biomed Pharmacother* (2017) 95:1436–40. doi: 10.1016/j.biopha.2017.09.047
17. Xu T, Pan LX, Ge YX, Li P, Meng XM, Huang C, et al. TMEM88 Mediates Inflammatory Cytokines Secretion by Regulating JNK/P38 and Canonical Wnt/beta-Catenin Signaling Pathway in LX-2 Cells. *Inflammopharmacology* (2018) 26(5):1339–48. doi: 10.1007/s10787-017-0419-z
18. Li LY, Yang CC, Li SW, Liu YM, Li HD, Hu S, et al. TMEM88 Modulates the Secretion of Inflammatory Factors by Regulating YAP Signaling Pathway in Alcoholic Liver Disease. *Inflamm Res* (2020) 69(8):789–800. doi: 10.1007/s00011-020-01360-y
19. de Leon M, Cardenas H, Vieth E, Emerson R, Segar M, Liu Y, et al.). Transmembrane Protein 88 (TMEM88) Promoter Hypomethylation Is Associated With Platinum Resistance in Ovarian Cancer. *Gynecol Oncol* (2016) 142(3):539–47. doi: 10.1016/j.ygyno.2016.06.017
20. Cai SP, Cheng XY, Chen PJ, Pan XY, Xu T, Huang C, et al. Transmembrane Protein 88 Attenuates Liver Fibrosis by Promoting Apoptosis and Reversion of Activated Hepatic Stellate Cells. *Mol Immunol* (2016) 80:58–67. doi: 10.1016/j.molimm.2016.11.002
21. Palpant NJ, Pabon L, Rabinowitz JS, Hadland BK, Stoick-Cooper CL, Paige SL, et al. Transmembrane Protein 88: A Wnt Regulatory Protein That Specifies Cardiomyocyte Development. *Development* (2013) 140(18):3799–808. doi: 10.1242/dev.094789
22. Lee H, Evans T.). TMEM88 Inhibits Wnt Signaling by Promoting Wnt Signalosome Localization to Multivesicular Bodies. *iScience* (2019) 19:267–80. doi: 10.1016/j.isci.2019.07.039
23. Ge YX, Wang CH, Hu FY, Pan LX, Min J, Niu KY, et al. New Advances of TMEM88 in Cancer Initiation and Progression, With Special Emphasis on Wnt Signaling Pathway. *J Cell Physiol* (2018) 233(1):79–87. doi: 10.1002/jcp.25853
24. Lee HJ, Finkelstein D, Li X, Wu D, Shi DL, Zheng JJ. Identification of Transmembrane Protein 88 (TMEM88) as a Dishevelled-Binding Protein. *J Biol Chem* (2010) 285(53):41549–56. doi: 10.1074/jbc.M110.193383
25. Geng Q, Chen X, Chen N. Transmembrane Protein 88 Exerts Tumorinhibitory Role Thyroid Cancer Through Restriction Wnt/beta-Catenin Signaling *Exp Cell Res* (2020) 395(2):112193. doi: 10.1016/j.yexcr.2020.112193
26. Zhang X, Yu X, Jiang G, Miao Y, Wang L, Zhang Y, et al. Cytosolic TMEM88 Promotes Invasion and Metastasis in Lung Cancer Cells by Binding DVLS. *Cancer Res* (2015) 75(21):4527–37. doi: 10.1158/0008-5472.CAN-14-3828
27. Stewart DJ. Wnt Signaling Pathway in Non-Small Cell Lung Cancer. *J Natl Cancer Inst* (2014) 106(1):djt356. doi: 10.1093/jnci/djt356
28. Rongna M, Nannan F, Xiao Y, Hongyan L, Xiaohong Z, Oumin S, et al. Promoter Methylation of Wnt/β-Catenin Signal Inhibitor TMEM88 Is Associated With Unfavorable Prognosis of Non-Small Cell Lung Cancer. *Cancer Biol Med* (2017) 14(4):377–86. doi: 10.20892/j.issn.2095-3941.2017.0061
29. Zhao X, Li G, Chong T, Xue L, Luo Q, Tang X, et al. TMEM88 Exhibits an Antiproliferative and Anti-Invasive Effect in Bladder Cancer by Downregulating Wnt/beta-Catenin Signaling. *J Biochem Mol Toxicol* (2021) 35(8):e22835. doi: 10.1002/jbt.22835
30. Yu X, Zhang X, Zhang Y, Jiang G, Mao X, Jin F. Cytosolic TMEM88 Promotes Triple-Negative Breast Cancer by Interacting With Dvl. *Oncotarget* (2015) 6 (28):25034–45. doi: 10.18632/oncotarget.4379
31. Xu T, Pan L, Li L, Hu S, Zhou H, Yang C, et al. MicroRNA-708 Modulates Hepatic Stellate Cells Activation and Enhances Extracellular Matrix Accumulation *via* Direct Targeting TMEM88. *J Cell Mol Med* (2020) 24 (13):7127–40. doi: 10.1111/jcmm.15119
32. Zhou F, Yang X, Zhao H, Liu Y, Feng Y, An R, et al. Down-Regulation of OGT Promotes Cisplatin Resistance by Inducing Autophagy in Ovarian Cancer. *Theranostics* (2018) 8(19):5200–12. doi: 10.7150/thno.27806
33. Siegel RL, Miller KD, Fuchs HE, Jemal A. Cancer Statistic. *CA Cancer J Clin* (2022) 72(1):7–33. doi: 10.3322/caac.21708
34. Zhang SZ, Zhang L, Xie L. Cancer Burden in China During 1990-2019: Analysis of the Global Burden of Disease. *BioMed Res Int* (2022) 2022:3918045. doi: 10.1155/2022/3918045
35. Liang Y, Zhang H, Song X, Yang Q. Metastatic Heterogeneity of Breast Cancer: Molecular Mechanism and Potential Therapeutic Targets. Semin. *Cancer Biol* (2020) 60:14–27. doi: 10.1016/j.semcancer.2019.08.012
36. Tray N, Taff J, Adams S. Therapeutic Landscape of Metaplastic Breast Cancer. *Cancer Treat Rev* (2019) 79:101888. doi: 10.1016/j.ctrv.2019.08.004
37. Bray F, Ferlay J, Soerjomataram I, Siegel RL, Torre LA, Jemal A. Global Cancer Statistics 2018: GLOBOCAN Estimates of Incidence and Mortality Worldwide for 36 Cancers in 185 Countries. *CA Cancer J Clin* (2018) 68(6):394–424. doi: 10.3322/caac.21492
38. Kibudde S, Kirenga BJ, Nabwana M, Okuku F, Walusansa V, Orem J. Clinical Profile and Initial Treatment of Non-Small Cell Lung Cancer: A Retrospective Cohort Study at the Uganda Cancer Institute. *Afr Health Sci* (2021) 21 (4):1739–45. doi: 10.4314/ahs.v21i4.30
39. Hirsch FR, Scagliotti GV, Mulshine JL, Kwon R, Curran WJ, Wu YL, et al. Lung Cancer: Current Therapies and New Targeted Treatments. *Lancet* (2017) 389(10066):299–311. doi: 10.1016/S0140-6736(16)30958-8
40. Blandin KS, Crosbie PA, Balata H, Chudziak J, Hussell T, Dive C. Progress and Prospects of Early Detection in Lung Cancer. *Open Biol* (2017) 7(9):170070. doi: 10.1098/rsob.170070
41. Duma N, Santana-Davila R, Molina JR. Non-Small Cell Lung Cancer: Epidemiology, Screening, Diagnosis, and Treatment. *Mayo Clin Proc* (2019) 94(8):1623–40. doi: 10.1016/j.mayocp.2019.01.013
42. Pizzato M, Li M, Vignat J, Laversanne M, Singh D, La Vecchia C, et al. The Epidemiological Landscape of Thyroid Cancer Worldwide: GLOBOCAN Estimates for Incidence and Mortality Rates in 2020. *Lancet Diabetes Endocrinol* (2022) 10(4):264–72. doi: 10.1016/S2213-8587(22)00035-3
43. Fei X, Chen W, Zhang S, Liu Q, Zhang Z, Pei Q. The Spatio-Temporal Distribution and Risk Factors of Thyroid Cancer During Rapid Urbanization-A Case Study in China. *Sci Total Environ* (2018) 630:1436–45. doi: 10.1016/j.scitotenv.2018.02.339
44. Liu Y, Lai F, Long J, Peng S, Wang H, Zhou Q, et al. Screening and the Epidemic of Thyroid Cancer in China: An Analysis of National Representative Inpatient and Commercial Insurance Databases. *Int J Cancer* (2021) 148 (5):1106–14. doi: 10.1002/ijc.33298
45. Mammen J, Cappola AR. Autoimmune Thyroid Disease in Women. *JAMA* (2021) 325(23):2392–3. doi: 10.1001/jama.2020.22196
46. Rahib L, Smith BD, Aizenberg R, Rosenzweig AB, Fleshman JM, Matrisian LM. Projecting Cancer Incidence and Deaths to 2030: The Unexpected Burden of Thyroid, Liver, and Pancreas Cancers in the United States. *Cancer Res* (2014) 74(11):2913–21. doi: 10.1158/0008-5472.CAN-14-0155
47. Dabravolski SA, Nikiforov NG, Zhuravlev AD, Orekhov NA, Mikhaleva LM, Orekhov AN. The Role of Altered Mitochondrial Metabolism in Thyroid Cancer Development and Mitochondria-Targeted Thyroid Cancer Treatment. *Int J Mol Sci* (2021) 23(1):460–75. doi: 10.3390/ijms23010460
48. Sandler JE, Huang H, Zhao N, Wu W, Liu F, Ma S, et al. Germline Variants in DNA Repair Genes, Diagnostic Radiation, and Risk of Thyroid Cancer. *Cancer Epidemiol Biomarkers Prev* (2018) 27(3):285–94. doi: 10.1158/1055-9965.EPI-17-0319
49. Adeyelu TT, Moya-Garcia AA, Orengo C. Exploiting Protein Family and Protein Network Data to Identify Novel Drug Targets for Bladder Cancer. *Oncotarget* (2022) 13:105–17. doi: 10.18632/oncotarget.28175
50. Li HZ, Zheng RS, Du LB, Zhang SW, Zhu C, Wei WW, et al. Bladder Cancer Incidence, Mortality and Temporal Trends in China. *Zhonghua Zhong Liu Za Zhi* (2021) 43(3):293–8. doi: 10.3760/cma.j.cn112152-20200421-00362
51. Wang Q, Zhang T, Wu J, Wen J, Tao D, Wan T, et al. Prognosis and Risk Factors of Patients With Upper Urinary Tract Urothelial Carcinoma and Postoperative Recurrence of Bladder Cancer in Central China. *BMC Urol* (2019) 19(1):24. doi: 10.1186/s12894-019-0457-5
52. Ghandour R, Singla N, Lotan Y. Treatment Options and Outcomes in Nonmetastatic Muscle Invasive Bladder Cancer. *Trends Cancer* (2019) 5 (7):426–39. doi: 10.1016/j.trecan.2019.05.011
53. Nusse R, Clevers H. Wnt/beta-Catenin Signaling, Disease, and Emerging Therapeutic Modalities. *Cell* (2017) 169(6):985–99. doi: 10.1016/j.cell.2017.05.016
54. Qu Y, Olsen JR, Yuan X, Cheng PF, Levesque MP, Brokstad KA, et al. Small Molecule Promotes Beta-Catenin Citrullination and Inhibits Wnt Signaling in Cancer. *Nat Chem Biol* (2018) 14(1):94–101. doi: 10.1038/nchembio.2510
55. Russell JO, Monga SP. Wnt/beta-Catenin Signaling in Liver Development, Homeostasis, and Pathobiology. *Annu Rev Pathol* (2018) 13:351–78. doi: 10.1146/annurev-pathol-020117-044010

56. Eubelen M, Bostaille N, Cabochette P, Gauquier A, Tebabi P, Dumitru AC, et al. A Molecular Mechanism for Wnt Ligand-Specific Signaling. *Science* (2018) 361(6403):eaat1178. doi: 10.1126/science.aat1178
57. Galluzzi L, Spranger S, Fuchs E, Lopez-Soto A. WNT Signaling in Cancer Immunosurveillance. *Trends Cell Biol* (2019) 29(1):44–65. doi: 10.1016/j.tcb.2018.08.005
58. Sun Z, Ning Q, Li H, Hu T, Tang L, Wen Q, et al. Transmembrane Protein 88 Inhibits Transforming Growth Factor-Beta1-Induced-Extracellular Matrix Accumulation and Epithelial-Mesenchymal Transition Program in Human Pleural Mesothelial Cells Through Modulating TGF-Beta1/Smad Pathway. *J Recept Signal Transd Res* (2022) 42(1):60–6. doi: 10.1080/10799893.2020.1843493
59. Noronha V, Patil VM, Joshi A, Menon N, Chougule A, Mahajan A, et al. Gefitinib Versus Gefitinib Plus Pemetrexed and Carboplatin Chemotherapy in EGFR-Mutated Lung Cancer. *J Clin Oncol* (2020) 38(2):124–36. doi: 10.1200/JCO.19.01154
60. Pietrantonio F. Encorafenib, Binimetinib, and Cetuximab in BRAF V600E-Mutated Colorectal Cancer. *N Engl J Med* (2020) 382(9):876–7. doi: 10.1056/NEJMc1915676
61. Altundag K. Association Between HER2 Status in Residual Disease and Sensitivity to Trastuzumab Emtansine. *Ann Oncol* (2021) 32(9):1191. doi: 10.1016/j.annonc.2021.05.794
62. Cohen P, Cross D, Janne PA. Kinase Drug Discovery 20 Years After Imatinib: Progress and Future Directions. *Nat Rev Drug Discov* (2021) 20(7):551–69. doi: 10.1038/s41573-021-00195-4
63. Nair R, Radhakrishnan VS, Mallath MK. Rituximab Biosimilars for B-Cell Lymphomas: A Decade of Real-World Experience From India. *Lancet Haematol* (2021) 8(8):e548–9. doi: 10.1016/S2352-3026(21)00212-X
64. Garcia-Romero N, Palacin-Aliana I, Madurga R, Carrion-Navarro J, Esteban-Rubio S, Jimenez B, et al. Bevacizumab Dose Adjustment to Improve Clinical Outcomes of Glioblastoma. *BMC Med* (2020) 18(1):142. doi: 10.1186/s12916-020-01610-0
65. Shimada I, Ueda T, Kofuku Y, Eddy MT, Wuthrich K. GPCR Drug Discovery: Integrating Solution NMR Data With Crystal and Cryo-EM Structures. *Nat Rev Drug Discov* (2019) 18(1):59–82. doi: 10.1038/nrd.2018.180
66. Insel PA, Sriram K, Gorr MW, Wiley SZ, Michkov A, Salmeron C, et al. GPCRomics: An Approach to Discover GPCR Drug Targets. *Trends Pharmacol Sci* (2019) 40(6):378–87. doi: 10.1016/j.tips.2019.04.001
67. Hauser AS, Attwood MM, Rask-Andersen M, Schioth HB, Gloriam DE. Trends in GPCR Drug Discovery: New Agents, Targets and Indications. *Nat Rev Drug Discov* (2017) 16(12):829–42. doi: 10.1038/nrd.2017.178
68. Kumar A, Planchais C, Fronzes R, Mouquet H, Reyes N. Binding Mechanisms of Therapeutic Antibodies to Human CD20. *Science* (2020) 369(6505):793–9. doi: 10.1126/science.abb8008
69. Pavlasova G, Mraz M. The Regulation and Function of CD20: An "Enigma" of B-Cell Biology and Targeted Therapy. *Haematologica* (2020) 105(6):1494–506. doi: 10.3324/haematol.2019.243543
70. Arnold A, Daum S, von Winterfeld M, Berg E, Hummel M, Rau B, et al. Prognostic Impact of Claudin 18.2 in Gastric and Esophageal Adenocarcinomas. *Clin Transl Oncol* (2020) 22(12):2357–63. doi: 10.1007/s12094-020-02380-0
71. Türeci, Mitnacht-Kraus R, Woll S, Yamada T, Sahin U. Characterization of Zolbetuximab in Pancreatic Cancer Models. *Oncoimmunology* (2019) 8(1):e1523096. doi: 10.1080/2162402X.2018.1523096
72. Katoh M, Katoh M. Precision Medicine for Human Cancers With Notch Signaling Dysregulation (Review). *Int J Mol Med* (2020) 45(2):279–97. doi: 10.3892/ijmm.2019.4418
73. Kyuno D, Takasawa A, Takasawa K, Ono Y, Aoyama T, Magara K, et al. Claudin-18.2 as a Therapeutic Target in Cancers: Cumulative Findings From Basic Research and Clinical Trials. *Tissue Barriers* (2022) 10(1):1967080. doi: 10.1080/21688370.2021.1967080
74. Jiang H, Shi Z, Wang P, Wang C, Yang L, Du G, et al. Claudin18.2-Specific Chimeric Antigen Receptor Engineered T Cells for the Treatment of Gastric Cancer. *J Natl Cancer Inst* (2019) 111(4):409–18. doi: 10.1093/jnci/djy134
75. Zhang J, Dong R, Shen L. Evaluation and Reflection on Claudin 18.2 Targeting Therapy in Advanced Gastric Cancer. *Chin J Cancer Res* (2020) 32(2):263–70. doi: 10.21147/j.issn.1000-9604.2020.02.13
76. Feng RM, Zong YN, Cao SM, Xu RH. Current Cancer Situation in China: Good or Bad News From the 2018 Global Cancer Statistics? *Cancer Commun (Lond)* (2019) 39(1):22. doi: 10.1186/s40880-019-0368-6

Conflict of Interest: The authors declare that the research was conducted in the absence of any commercial or financial relationships that could be construed as a potential conflict of interest.

Publisher's Note: All claims expressed in this article are solely those of the authors and do not necessarily represent those of their affiliated organizations, or those of the publisher, the editors and the reviewers. Any product that may be evaluated in this article, or claim that may be made by its manufacturer, is not guaranteed or endorsed by the publisher.

frontiers | Frontiers in Oncology

SYSTEMATIC REVIEW
published: 06 June 2022
doi: 10.3389/fonc.2022.922838

ANO1: More Than Just Calcium-Activated Chloride Channel in Cancer

*Saisai Guo, Linna Zhang and Na Li**

Department of Oncology, The Second Affiliated Hospital of Dalian Medical University, Dalian, China

ANO1, a calcium-activated chloride channel (CACC), is also known as transmembrane protein 16A (TMEM16A). It plays a vital role in the occurrence, development, metastasis, proliferation, and apoptosis of various malignant tumors. This article reviews the mechanism of ANO1 involved in the replication, proliferation, invasion and apoptosis of various malignant tumors. Various molecules and Stimuli control the expression of ANO1, and the regulatory mechanism of ANO1 is different in tumor cells. To explore the mechanism of ANO1 overexpression and activation of tumor cells by studying the different effects of ANO1. Current studies have shown that ANO1 expression is controlled by 11q13 gene amplification and may also exert cell-specific effects through its interconnected protein network, phosphorylation of different kinases, and signaling pathways. At the same time, ANO1 also resists tumor apoptosis and promotes tumor immune escape. ANO1 can be used as a promising biomarker for detecting certain malignant tumors. Further studies on the channels and the mechanism of protein activity of ANO1 are needed. Finally, the latest inhibitors of ANO1 are summarized, which provides the research direction for the tumor-promoting mechanism of ANO1.

Keywords: ANO1, cancer, protein network, signal pathway, tumor microenvironment, inhibitor, miRNA

OPEN ACCESS

Edited by:
Jian-ye Zhang,
Guangzhou Medical University, China

Reviewed by:
Arjun Singh,
Memorial Sloan Kettering Cancer Center, United States
Senthilkumar Rajagopal,
REVA University, India

***Correspondence:**
Na Li
linaonly828@163.com

Specialty section:
This article was submitted to Cancer Molecular Targets and Therapeutics, a section of the journal Frontiers in Oncology

Received: *18 April 2022*
Accepted: *09 May 2022*
Published: *06 June 2022*

Citation:
Guo S, Zhang L and Li N (2022) ANO1: More Than Just Calcium-Activated Chloride Channel in Cancer. Front. Oncol. 12:922838. doi: 10.3389/fonc.2022.922838

INTRODUCTION

ANO1, as a calcium-activated chloride channel (CaCC), also known as transmembrane protein 16A (TMEM16A), is a voltage-sensitive calcium-activated chloride channel with ten transmembrane fragments with amino and carboxyl-terminal structure (1). It is widely expressed in many cells, including epithelial cells, airways, smooth muscle cells, vascular endothelial cells, and myocardium. ANO1 also modulates several physiological functions, such as fluid and electrolyte secretion, intestinal motility, cardiac and neuronal excitability, vascular smooth muscle contraction, and heat pain (2, 3). Abnormal circulating ANO1 is associated with susceptibility and pathogenesis of several human diseases and pathological entities, including cystic fibrosis, various cancers, hypertension, and gastrointestinal motility disorders (4–6).

ANO1 also has a crucial role in tumor occurrence, development, metastasis, proliferation, anti-apoptosis, and epigenetic regulation is often overexpressed in tumor tissues and is an experimental target for antitumor therapies. However, the biological functions of malignant tumors remain a controversial issue. The present review aims to explore the role of ANO1 in cancer pathogenesis and therapeutics and to elucidate the mechanisms underlying the relation between ANO1 and malignancy.

ANO1 AS A POTENTIAL BIOMARKER IN CANCER

Through research on Human Protein Atlas and GEPIA database, ANO1 overexpression in various malignancies tissues (**Figure 1**). At the same time, up-regulation of ANO1 expression is associated with a worse prognosis in many malignant tumors (**Figures 2**, **3**). ANO1 was reported as a promising biomarker of malignant potential, stage progression, and prognosis, aiding the monitoring of certain malignancies.

The tumor growth and metastasis were observed by transplantation of nude mice and tumor cell culture *in vivo* and vitro. **Table 1** summarizes the role of ANO1 in different tumors. ANO1 was significantly upregulated in various malignant tumors and promotes the invasion of cancer cells. ANO1 overexpression is associated with lymph node metastasis, disease grading and poor prognosis in gastric cancer, liver cancer, and colon cancer (28, 36, 40). Overexpression of ANO1 promoted the growth and invasion of lung cancer, Head and Neck squamous cell carcinoma (HNSCC), breast cancer and pancreatic cancer through the epidermal growth factor receptor(EGFR)signal pathway (11, 22, 39). Especially in breast cancer cells, ANO1 and EGFR-signal transducer and activator of transcription 3(STAT3) signaling pathways form a positive feedback path to promote the proliferation and growth of breast cancer cells. At the same time, ANO1 also activates the Ras-Raf-MEK-ERK1/2 signaling pathway to promote HNSCC and colon cancer (22, 28). ANO1 can regulate the tumor growth factor-β(TGF-β) signaling pathway to promote Esophageal squamous cell carcinoma (ESCC) proliferation, migration, and invasion (17). Silencing or inhibition of ANO1 upregulates tumor necrosis factor-α (TNF-α) expression in prostate cancer cells (27). ANO1 can promote Hepatocellular carcinoma (HCC) and Ovarian cancer metastasis by activating the phosphatidylinositol three kinase-protein kinase B (PI3K-AKT) signaling pathway (23, 41). Meanwhile, ANO1 participates in immune escape in gastrointestinal stromal tumors (42). Finally, neutralization of ANO1 activity with gene knockdown or ANO1 inhibitors has shown anti-neoplastic actions both *in vivo* and *in vitro* models of cancer (**Table 1**).

In summary, it shows that ANO1 is related to cancer risk and progression in the following aspects: 1) its upregulation in a variety of tumor tissues; 2) its correlation with tumor proliferation, invasion depth, lymph node metastasis, distant metastasis, and apoptosis;3) the gene expression level of ANO1 is closely related to tumor size and differentiation; 4) its association with advanced stage and poor prognosis; 5) its interacts with various oncogenic signaling networks; 6) it regulate tumor microenvironmental tumorigenic signaling pathways.

The expression of ANO1 seems to be controlled by various molecules and stimuli. Different cells have different regulatory mechanisms and signaling pathways. ANO1 can participate in various signal pathways not only with the interaction with various proteins but also with the ion pathway that regulates the ion homeostasis of tumor cells, thereby promoting the critical functions of tumor cells. Further studies to clarify the molecular mechanism are required, for up-regulated tumors, promoting proliferation, metastasis, invasion, and avoiding apoptosis. The mechanism of ANO1's involvement in malignant tumors will be reviewed.

THE MECHANISM OF ANO1 INVOLVED IN CANCER

Previous studies have shown that ten biological functions formed during the multi-stage development of human tumors constitute the characteristics of cancer (43). These ten characteristics include self-sufficiency in growth signals, insensitivity to anti-growth signals, evading apoptosis, Limitless replicative potential, sustained angiogenesis, tissue invasion & metastasis, genome instability and mutation, tumor-Promoting inflammation,

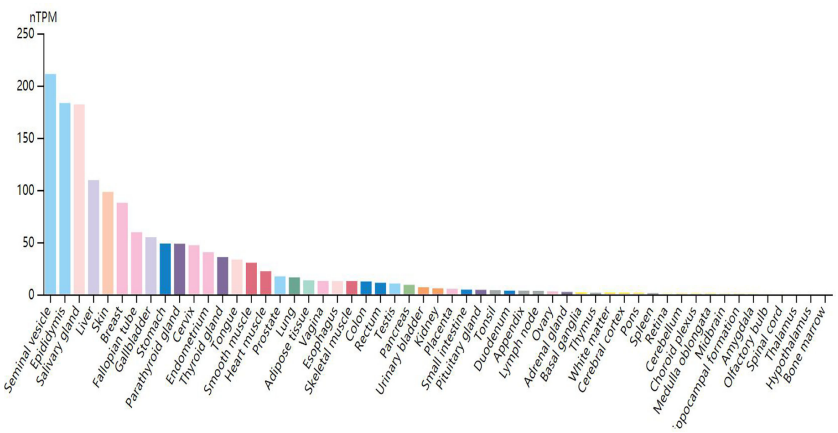

FIGURE 1 | Expression level of ANO1 in tissues.

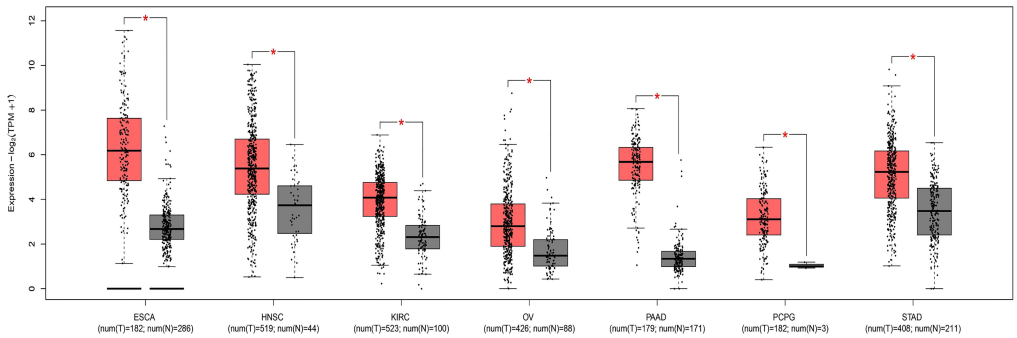

FIGURE 2 | The expression of ANO1 was up-regulated in various malignant tumor ESCA Esophageal carcinoma; HNSC, Head and Neck squamous cell carcinoma; KIRC, Kidney renal clear cell carcinoma; OV, Ovarian serous cystadenocarcinoma; PAAD, Panecreatic adenocarcinoma; PCPG, Pheochromocytoma and Paraganglioma; STAD, Stomach adenocarcinoma. * indicates that the expression of ANO1 is statistically significant between groups.

deregulating cellular energetics, avoiding immune destruction. The involvement of ANO1 in tumorigenesis is currently related to the following aspects (**Figure 4**).

ANO1 Overexpression Is Involved in the Unlimited Replication and Proliferation of Tumor Cells

ANO1 is upregulated in various tumor tissues and correlates with proliferation, invasion depth, lymph node metastasis, distant metastasis, and apoptosis. Multiple mechanisms can explain the overexpression of ANO1. ANO1 is located on human chromosome 11q13, commonly amplified in several cancers, and participates in tumorigenesis, invasion, and migration. Therefore, the most common mechanism of ANO1 overexpression in cancer amplifies the 11q13 locus (10, 44). This expansion has been described in some cancer types, including breast, gastric, esophageal, and lung carcinoma. However, it is essential to mention that 11q13 amplification resulted in a higher TMEM16A expression in human breast cancer and HNSCC than in non-11q13-amplified tumors. Meanwhile, ANO1 is sufficient to promote cell proliferation without 11q13 amplification, which shows that 11q13 gene amplification is not the only factor that promotes ANO1 overexpression (18).

ANO1 Interacts With Various Proteins to Promote Tumor Proliferation and Invasion

EGFR is overexpressed in many tumors such as HNSCC, breast cancer, and pancreatic cancer and is involved in tumorigenesis. ANO1 was also observed as a core protein in the STRING protein network pathway, which can regulate EGFR constitutive protein phosphorylation and related signal pathways, such as protein tyrosine kinase (SRC), protein kinase B (AKT), promote the proliferation of cancer cells (18,

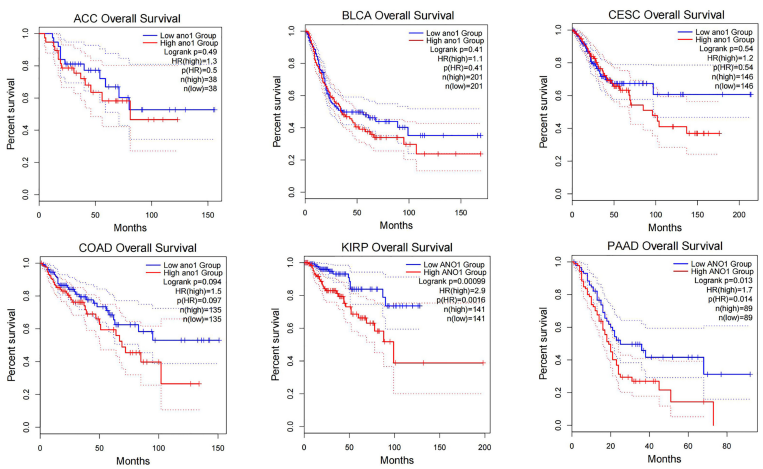

FIGURE 3 | The increased expression of ANO1 is associated with poor prognosis in many malignat tumors ACC, Adrenocortical carcinoma; BLCA, Bladder Urothelial Carcinoma; CESC, Cervical squamous cell carcinoma and endocervical adenocarcinoma; COAD, Colon adenocarcinoma; KIRP, Kidney renal papillary cell carcinoma.

TABLE 1 | The role of ANO1 in different malignant tumors.

Cancer type	Author/year	Tumor cells	ANO1 Overexpression				ANO1 Inhibition				Clinical outcome of ANO1 over expression
			P	M	I	A	P	M	I	A	
HNSCC	Ayoub (7) (2010)	HEP-2, SCC-25		+	+	+		-			It is related to DNA methylation, 11q13 chromosome amplification, EGFR signaling, MAPK signaling; Its overexpression association with poor prognosis
	Duvvuri (8) (2012)	UM-SCC1	+				-				
	Ruiz (9) (2012)	BHY		+			-		-		
	Dixit (10) (2015)	PE/CE-PJ34	+				-				
	Bill (11) (2015)	Te11	+								
	Reddy (12) (2016)	SCC-25, CAL-27 CAL-33, BHY		+							
	Wanitchakool (13) (2017)	BHY, CAL-133, HT-29, T84	+	+							
	Finegersh (14) (2017)	NOK	+								
	Hermida (15) (2018)	HPV(-)patient tissue	+	+	+						
ESCC	Shi (16) (2013)	KYSE30, KYSE510	+								It is associated with 11q13 chromosome amplification and TGF-βsignaling; correlation with lymph node metastasis and stage;
	Yu (17) (2019)	kyse30, kyse70, KYSE140, KYSE180	+	+	+		-				
Breast cancer	Britschgi (18) (2013)	ZR75-1, HCC1954, MDA-MB-415	+				-	-		+	It is associated with 11q13 chromosome amplification, EGFR signaling, PI3K-AKT-mTOR signaling, EGFR-STAT3 signaling; and association with poor prognosis;
	Wu (19)(2015)	Patient tissue	+				-			+	
	Fujimoto (20) (2018)	YMB-1, BT-549 MD, A-MB-453									
	Wu (21) (2017)	MCF7, MDA-MB-453	+								
	Wang (22) (2019)	Mcf7, T47d	+								
Ovarian cancer	Liu (23)(2018)	SKOU3, ES2	+		+		-		-		It is associated with PI3K-AKT signaling and related to the clinical FIGO stage and grade;
Prostate cancer	Liu (24) (2014)	PC3, LNCaP, DU145	+	+	+		-	-	-		Its correlation with PI3K-AKT signaling, TGF-a signaling, and related to tumor stage;
	Cha (25) (2015)	PC3, LnCaP, RWPE-1,	+	+			-	-			
	Seo (26) (2015)	PC3, HT29, DU145					-	-	-	-	
	Song (27) (2018)	PC3					-	-		+	
Colorectal cancer	Sui (28) (2014)	SW620, HCT116, LS174t	+	+			-	-	-	+	It is associated with 11q13 chromosome amplification, MAPK signaling, Wnt/β-catenin signaling, AKT-ERK signaling, EGFR-MAPK signaling; and correlation with lymph node metastasis and stage;
	Mokutani (29) (2016)	DLD1, HCT116					-		-		
	Jiang (30) (2019)	Caco-2, SW620, HCT116, SW480, LoVo					-	-			
	Park (31) (2019)	HTC116					-	-	-	+	
Lung cancer	Jia (32)(2015)	NCIH520, H1299, GLC82	+		+		-		-		It is associated with EGFR-MAPK signaling

(Continued)

TABLE 1 | Continued

Cancer type	Author/year	Tumor cells	ANO1 Overexpression				ANO1 Inhibition				Clinical outcome of ANO1 over expression
			P	M	I	A	P	M	I	A	
	Hu (33) (2019)	H1299	+	+	+		-	-	-		
Glioma	Liu (34) (2014)	U87MG	+	+	+						It is associated with NF-κB signaling, MAPK signaling, and ANO1 channel activities
	Lee (35) (2016)	U251, T98g, U138	+	+				-	-		
Gastric cancer	liu (36) (2015)	AGS, BGC823	+	+	+						Its correlation with TGF-β signaling and related to lymph node metastasis, stage and poor prognosis;
	Cao (37) (2017)	AGS, MKN45, MKN28, BGC823	+	+	+			-	-		
Pancreatic adenocarcinoma	Sauter (38) (2015)	BXPC3, ASPC1		+							Its correlation with EGFR signaling and association with lymph node metastasis, stage;
	David (39) (2019)	ASPC1		+	+						
Hepatocellular carcinoma	Deng (40) (2016)	SMC7721	+	+							Its correlation with PI3K-AKT, MAPK signaling, and related with lymph node metastasis and stage; and association with poor prognosis;
	Zhang (41) (2020)	Patient tissue	+	+	+	-	-	-	-	+	

P, proliferation; M metastasis; I, invasion; A, apoptosis; + promotes; - inhibit.
ANO1, a calcium-activated chloride channel; AKT, Protein Kinase B; EGFR, Epidermal Growth Factor Receptor; ERK, Extracellular Regulated Protein Kinases; ESCC, Esophageal squamous cell carcinoma; HPV, Human Papilloma Virus; MAPK, Mitogen-Activated Kinase; MEK, Mitogen-Activated Extracellular Signal-Regulated Kinase; MTOR, Mechanistic Target of Rapamycin; NF-κB, Nuclear Factor Kappa-B; PI3K Phosphatidylinositol 3 Kinase; STAT3, Signal Transducer and Activator of Transcription three; TGF-a, Tumor Necrosis Factor-α; TGF-β, Tumor Growth Factor-β; FIGO, Federation International of Gynecology and Obstetrics.

45) (**Figure 5**). The interaction between ANO1 and EGFR can also increase ANO1 protein stability. At the same time, ANO1 also has a significant effect on the remodeling of EGF-induced protein phosphorylation. The study also found that the AKT and extracellular regulated protein kinases (ERK) signaling pathways are not affected by the expression of ANO1, which was further confirmed by the STRING pathway of ANO1. So, the relationship between the expression of ANO1 and EGFR in different signaling pathways is different (39). Therefore, it is crucial to understand how ANO1 regulates the EGFR signaling pathway.

Recent data in pancreatic cancer show that ANO1 is necessary to promote EGF-induced EGFR signal transduction, EGF-mediated $Ca2^+$ storage depends on ANO1, and the ANO1-

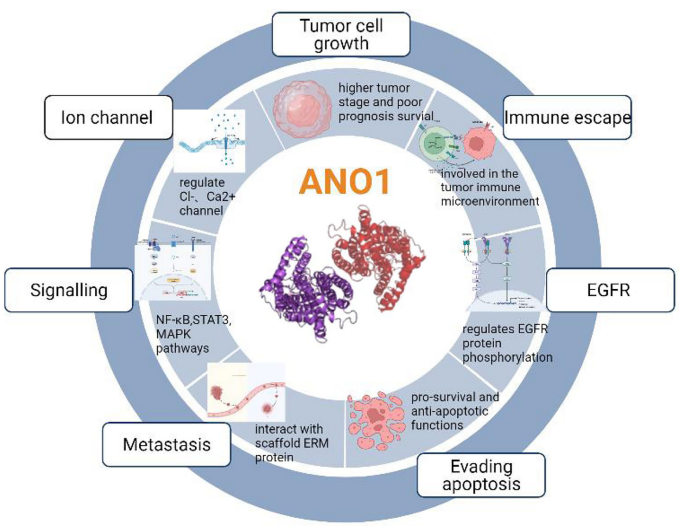

FIGURE 4 | The involvement of ANO1 in tumorigenesis.

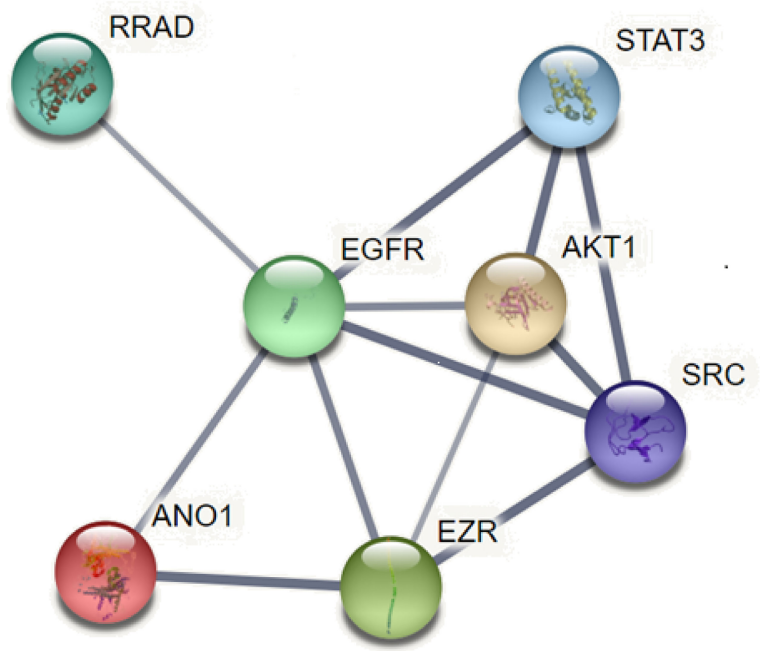

FIGURE 5 | ANO1 interacts with various proteins.

mediated $Ca2^{+}$ signaling pathway regulates EGF-induced may be involved in the proliferation of pancreatic cancer cells, and may dramatically impact the migration (46, 47). It can be seen that ANO1 provides a new entry point for treating pancreatic cancer.

In the study of breast cancer cells, EGF initiates EGFR/STAT3 signal transduction, which promotes the overexpression of ANO1, while ANO1 overexpression further activates the EGFR-STAT3 signal transduction of breast cancer cells. The positive feedback loop between ANO1 and EGFR-STAT3 promotes the proliferation and migration of breast cancer cells. Knockout of ANO1 will reduce the phosphorylation of EGFR in breast cancer cells, further inhibit the activation of AKT, SRC, and ERK, and reduce the autocrine of EGFR ligands, EGF and TGF-β, suggesting that ANO1 may increase EGFR ligands The autocrine activates EGFR signal transduction (22). Therefore, we considered that ANO1 could activate the EGFR signaling pathway by increasing EGFR expression, phosphorylation, and EGFR ligand autocrine. More research is needed to confirm the connection between ANO1 and EGFR.

ANO1 also regulates cell morphology and volume and directly interacts with scaffold ERM protein (Ezrin/Radixin/Moesin) (48) (**Figure 5**). The ERM protein connects the plasma membrane with the actin cytoskeleton, affects the cell morphology of cancer cells, and regulates the movement, metastasis, and invasion of tumor cells. At the same time, ERM can be activated by many ligands as scaffold proteins to promote the signal transduction of membrane proteins, including EGF ligands, to promote the deformation and invasion of cancer cells. Studies have found that ANO1 may interact with EGFR to recruit ERM proteins, promoting EGFR signal transduction and activation of the MAPK/AKT pathway (11). The ANO1 inhibitor Des inhibited the activity and migration of non-small-cell lung carcinoma by decreasing the levels of Ano1, p-ERK1/2 and p-EGFR (49).

ANO1 Activates Multiple Signaling Pathways Involved in Tumor Proliferation, Migration and Invasion

There is ample evidence that ANO1 triggers numerous signaling pathways and stimulates many biological effects in various cell types (**Figure 6**). Overexpression of ANO1 promoted the growth and invasion of lung cancer cells through the EGFR-MAPK signal pathway (33). ANO1 also activates the Ras-Raf-MEK-ERK1/2 signaling pathway to promote tumor cell growth of HNSCC (8). At the same time, ANO1 can regulate the TGF-β signaling pathway to promote ESCC cells proliferation, migration, and invasion (17). Silencing or inhibition of ANO1 inhibits cell growth, induces apoptosis, and upregulates TNF-α expression in prostate cancer cells (22). Calcium ions (SOCE) that activate ANO1 and ANO1-dependent storage can enter cells and regulate EGFR ligands to promote pancreatic cancer cell migration (39). The higher the expression level of ANO1 in HCC is accompanied by higher tumor grades, lesions, metastases, and a poor prognosis (40, 41). ANO1 can promote HCC metastasis by activating EGFR phosphorylation and subsequent PI3K-AKT signaling pathway (41). In breast cancer cells, ANO1 and EGFR-STAT3 signaling pathways form a positive feedback path to promote the proliferation of breast cancer cells (22). At the same time, ANO1 mediated the PI3K-AKT-mTOR and JAK-STAT3 signaling pathways of HER2-positive breast cancer cells by regulating intracellular Cl^{-} to participate in HER2 transcription

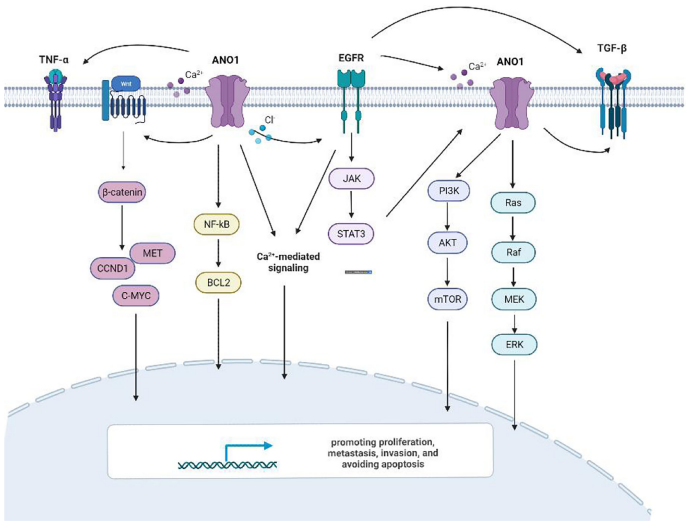

FIGURE 6 | ANO1activating multiple signaling pathways.

and promote tumor proliferation (21). Inhibit of ANO1 can inhibit PI3K-AKT signaling and inhibit the Ovarian cancer cell proliferation and invasion (23). ANO1 affects GBM cell proliferation by regulating NF-κB mediated genes. In the meantime, it is involved in cell proliferation cyclin D1, cyclin E and c-myc, and matrix metalloproteinase (MMP) 2 and MMP 9 induce GBM cell invasion and migration (34, 35). Higher expression of ANO1 was related to gastric and colorectal cancer lymph node metastasis, advanced tumor stage and poor prognosis. Knockout or pharmacological inhibition of ANO1 inhibits the proliferation and induces apoptosis of colorectal cancer cells *via* the Wnt/β-catenin signaling pathway (50).ANO1 is a direct target and negatively correlates with miR-9, miR-144 and miR-381 (30, 31, 37). Overexpression of miR-9 suppressed the expression of p-AKT, cyclin D1, and p-ERK. MiR-144 can inhibit colorectal cancer by inhibiting the EGFR-ERK signaling pathway targeting ANO1. Meanwhile, miR381 directly targets ANO1 to regulate the TGF-β pathway. ANO1 also has been considered an independent prognostic factor affecting the prognosis of gastric cancer patients.

ANO1 participates in various signaling pathways to promote proliferation, metastasis, and invasion. The signal pathway involved in each tumor is not unique, and one signal pathway can correspond to multiple tumor types. To this end, it would be significant to determine the ANO1 receptor and clarify its signaling pathway in tumor promotion.

Meanwhile, ion channels also participate in ANO1 regulated signaling pathways. Some scholars believe that ANO1 may regulate EGF through $Ca2^+$ signaling to promote pancreatic cancer cell migration (39). Some scholars have also found that silencing the expression of ANO1 reduces the intracellular Cl^-, thereby reducing the secretion of TGF-β and inhibiting the metastasis and invasion of gastric cancer cells (36). At the same time, in breast cancer cells, a decrease in the activity of the Cl^- channel can down-regulate the EGFR signaling pathway (18). The mechanism of ANO1 in each tumor is different, so that it may constitute the heterogeneity of ANO1 overexpressing cancer cells. However, further studies are needed to clarify whether specific cancer types have unique ionic states.

Alteration of ANO1 Protein Level and Ion Channel Activity Promotes Cancer Cell Proliferation and Migration

Many studies are researching how the increase in ANO1 protein level and channel activity is involved in the proliferation and migration of malignant tumor cells. The gating characteristics of ANO1 are complex because it involves the increase in intracellular calcium ion concentration, membrane depolarization, and the interaction between extracellular chloride or transition anions and intracellular protons (11).

ANO1 contains ten putative transmembrane domains, intracellular NH2 and COOH end, and two calmodulin-binding domains (51). E702 and E705 are presumed to be Ca2+ binding sites, and ANO1 expresses multiple splice variants with variable sensitivity to cytoplasmic $Ca2^+$. Studies have found an X-ray crystal structure (52) (a fungus with $Ca2^+$ activated lipid interfering enzyme activity nhTMEM16) ANO1 subtype has 39-42% homology with mammalian ANO1 (53, 54). nhTMEM16 contains ten transmembrane subunit fragments and six residues (including glutamic acid and aspartic acid). Exploring the fungal model of ANO1 will help determine the $Ca2^+$ binding site. However, the exact Ca2+ binding mechanism of ANO1 still needs to be further explored, even identifying the Ca2+ binding site and ionic conductive hole of ANO1.

For the structural study of ANO1, the current research shows two main ion phenomena: A) ANO1 is activated by voltage when $Ca2^+$ is absent in tumor cells. B) After reducing the concentration of extracellular Cl^-, the conductivity of Cl^- in ANO1 decreases (55).

The intracellular $Ca2^+$ signaling is an essential regulator of cell proliferation, and ANO1 can control intracellular $Ca2^+$ levels by regulating Ras-Raf-MEK-ERK1/2, PIK3-AKT, and DAG-IP3 receptor signals (11, 51). In many systems, the transient increase of intracellular $Ca2^+$ and the continuous activation of the Ras-Raf-MEK-ERK1/2 pathway are the central links in cell proliferation (51, 56, 57). The steady-state regulation of $Ca2^+$ and chloride ion conductance in ANO1 channel activity is also involved in the EGF-induced EGFR pathway. In addition, Cepharanthine significantly inhibits cell proliferation, migration and induces apoptosis in lung adenocarcinoma cells *via* endogenous ANO1 currents (58). Change and regulation of $Ca2^+$ concentration play an essential role in the ANO1 function of cancer cells.

At the same time, the Cl^- channel is the key to maintaining cell volume, so it is crucial in tumor cell migration and invasion (44, 59, 60). In cancer, related changes in intracellular water content can regulate cell volume, and the resulting morphological changes are critical to cell division, migration, invasion, and prevention of cell death (61, 62). The osmotic adjustment represents a mechanism that links ion flux to different cancer cell functions. Some reports have observed that inhibiting ANO1 can affect the size or morphology of cancer cells (7, 60, 63). Furthermore, the activation of Cl- concentration in ANO1 can regulate cell proliferation, and the overexpression of cell ANO1 protein and the increase of channel activity may lead to changes in Cl- concentration. Intracellular Cl^- can function as a second messenger, regulating various proteins in many signaling pathways (48, 64). So far, it is still unclear whether the overexpression of ANO1 will increase or decrease the concentration of Cl^-. Some scholars have put forward the hypothesis: If ANO1 overexpression can reduce the concentration of Cl^-, it may be by increasing the outflow of Cl- in the cell. Experiments have shown that the Cl^- channel associated with glioblastoma can be transported to the plasma membrane and act as an ion channel, explicitly participating in tumorigenesis (65).

Next, we determined that the homeostasis regulation of $Ca2^+$ and Cl^- currents also has a more significant effect on ANO1 in cancer cells. Some scholars established a 12-state Markov chain model by studying the mechanism of membrane potential, Ca^{2+}, and Cl^- on ANO1 ion channel gating (54). This model interprets the activation of ANO1 as 2 Ca^{2+} dependent on the membrane voltage, directly and continuously coupled with the external Cl^- dependent on the membrane potential, and transition into a voltage-dependent state. This model assumes that further experiments prove no significant change in extracellular Cl^- affinity for ANO1 $Ca2^+$. However, experiments have also found that extracellular Cl^- can promote voltage-dependent activation by stabilizing the open configuration induced by Ca^{2+}. The establishment of the model helped to understand the ion channel mechanism of ANO1. However, the related mechanism of ANO1 channel activity and tumor also needs to be confirmed in other models.

While most reports have confirmed the role of ANO1 overexpression in cancer cell proliferation and migration, there is insufficient information on the role of ANO1 in cell proliferation and migration, mainly due to the increase in ANO1 protein level or the increase in channel activity. Studies have found that reducing the expression level of ANO1 protein may be more critical than blocking the activity of ANO1 channels (66).

ANO1 Induces Tumor Cells to Escape Apoptosis and Regulate the Cell Cycle

Apoptosis is a highly regulated process of cells, essential for cell growth and tissue development (67, 68). Exogenous pathways can trigger apoptosis, including extracellular, pro-apoptotic, ligand-receptor interaction, and endogenous (69). In breast cells, the expression of ANO1 increased anti-apoptotic proteins BCL2 and MCL-1, indicating that ANO1 has pro-survival and anti-apoptotic functions (18). TNF-α expression was negatively correlated with ANO1 expression in prostate cancer cells. Inhibition of ANO1 can activate the TNF-α signaling and induce apoptosis *via* caspase activation (27). ANO1 also may regulate HCC cell apoptosis through the control AKT/MAPK signaling pathway (41). ANO1 expression correlates with increased ERK 1/2 activity and less apoptotic activity in HNSCC (70). ANO1 inhibitors can cause the overexpression of miR9 to inhibit the proliferation of colorectal cancer cells and induce cell cycle arrest at the GO/G1 phase leading to cell apoptosis (31). At the same time, inhibiting ANO1 can reduce the chloride channel activity and the expression of EGFR and calmodulin dependent kinase (CAMKII), thus promoting breast cancer cell apoptosis (18). Therefore, Suppression of ANO1 overexpression induces apoptosis and offers a promising new modality for the future treatment of malignant tumors.

The G1 phase arrest of the cell cycle can slow cell proliferation. Studies have found that inhibiting ANO1 can induce cell cycle G2/M phase arrest. Nevertheless, it does not affect cell cycle distribution (71). Meanwhile, changes in ANO1 expression affect proteins used explicitly for transcription or cell division. Such as cyclin A2, cyclin D1, and cyclin E. Up-regulation of cyclin-dependent kinases 1 and 2 (CDK1 and CDK2) in cancer cells can cause an increase in the expression of ANO1 (34, 52). The above data indicate that ANO1 may be involved in the cell cycle process, but it remains to be clarified how ANO1 induces tumor cell cycle arrest. Existing studies have found that the ANO1 inhibitor Caccinh-A01 may reduce the chloride current in gastric cancer cells and cause the G1 phase of the cell cycle block (72). At the same time, research on colorectal cancer found that cyclin D1 protein expression was positively correlated with ERK1/2 and ANO1.ANO1 inhibits G1 to S phase progression by down-regulating the expression of the ANO1, which is consistent with the decreased expression of cyclin D1 (28). Suppressing ANO1 expression also had significantly lower cyclin D1, leading to changes in $p27^{Kip1}$ distribution and correlated with a cell cycle arrest phenotype in HNSCC (8, 73).

ANO1 Is Involved in Tumor Immune Evasion

Tumor immune escape signifies that tumor cells escape recognition and attack by the immune system through various mechanisms to survive and proliferate (74). Future development of cancer immunotherapy depends on the crosstalk between cytokines produced by the tumor microenvironment and

biology. In the study of gastrointestinal stromal tumors, ANO1 gene expression was significantly negatively correlated with plasma cells and activated memory $CD4^+$ T cells, implying that ANO1 may be involved in the functional inhibition of helper T cells (42). We consider that ANO1 may be related to the immune microenvironment of malignant tumors. These specific mechanisms also remain to be systematically investigated.

PERSPECTIVES AND FUTURE DIRECTIONS OF ANO1

As a calcium-activated chloride channel, ANO1's expression is affected by various molecular mechanisms. Current research shows that ANO1 may be involved in malignant tumours' occurrence, development, and metastasis. Finally, novel, more effective, and safer ANO1-centered therapeutic interventions may open new horizons in oncotherapy and provide a new cancer treatment strategy. Some compounds such as cepharanthine (58), Ani9 (36, 75), cinobufagin (76), luteolin (77), Aa3 (78), theaflavin (79), 2-aminothiophene-3-carboxamidederivatives (80), matrine (76), have been identified as inhibitors of ANO1 Agent. It has been validated in multiple *in vitro* and vivo tumor models (**Table 2**).

Simultaneously, microRNAs (miRNAs) can also directly target and inhibit ANO1 expression suppressing tumor cells. MiRNA is small non-coding RNAs with about 22 nucleotides. miRNAs play an essential regulatory role in various cancers, including gastric cancer, pancreatic cancer, and hepatocellular carcinoma. They bind to the 3'-untranslated region (3'-UTR) of target genes, resulting in irreversible inhibition of transcription or translation. Because abnormally expressed miRNA also contributes to cancer cells' proliferation, apoptosis, and metastasis (87–89). Moreover, miRNA expression is considered a promising biomarker of cancer diagnosis, prognosis, and therapy (90).

Existing studies have found that luciferase detection shows that ANO1 is a direct target and is negatively correlated with miR132, miR144, miR381, and miR9 (**Figure 7**). High miR144 and miR9 directly target ANO1 to inhibit colorectal cell proliferation and migration and promote apoptosis (30, 31). miR9 overexpression inhibits ANO1 miRNA and protein expression and inhibits the expression of P-AKT, CD1, and P-ERK proteins in colorectal cancer cells (31). miR381 expression is related to gastric cancer proliferation, lymph node metastasis, advanced stage, and poor prognosis by directly targeting ANO1 to regulate the TGF-β pathway (37). MiR144 also down-regulates the expression of PTEN to activate the Ras-Raf-MEK-ERK1/2 pathway to inhibit breast cell proliferation and survival (30). Exploring the relationship between ANO1 and microRNA has broad prospects for the occurrence and development of tumors.

SUMMARY

ANO1 has recently attracted considerable attention because of its potential role in cancer chemoprevention and chemotherapy.

TABLE 2 | ANO1 inhibitor and its antitumor mechanism.

ANO1 inhibitors	Tumor cells	Mechanisms	Year
Cepharanthine (58)	LA795	reduced ANO1 channel activity	2021
Diethylstilbestrol (DES) (49)	PC9	1. reduced both ANO1 channel activity and cell viability 2. reduction of p-ERK1/2 and p-EGFR levels. 3. induced apoptosis by increasing caspase-3 activity and PARP-1 cleavage	2021
Ani9 (75, 80)	PC3, MCF7, BxPC3, DU145, LNCaP, 22RV1	1. reduced the protein levels 2. TNF-α signaling, activation of JNK and JUN	2016 2018
new2-aminothiophene-3-carboxamide derivatives (9c and 10q) (81)	U251	1. suppress ANO1 channel activities 2.combination of ANO1 inhibitor (9c or 3) and temozolomide (TMZ) brings about remarkable synergistic effects	2020
T16A(inh)-A01 (38, 82)	Panc-1, Mia PaCa2, Capan-1, AsPC-1, BxPC-3, HEK-293T, UM-SCC1, T24 DU145, LNCaP, 22RV1	1. suppress ANO1 channel activities 2. regulated ERK1/2 activation and cyclin D1 3. TNF-α signaling, activation of JNK and JUN	2012 2018
Arctigenin (83)	LA795	Inhibited MAPK pathway	2020
CaCCinh-A01 (38)	Panc-1, Mia PaCa2, Capan-1, AsPC-1, BxPC-3, DU145, LNCaP, 22RV1	TNF-α signaling, activation of JNK and JUN	2015 2018
NS3728 (38)	Panc-1, Mia PaCa2, Capan-1, AsPC-1, BxPC-3	altered ATP-induced [Ca2+]i signals	2015
Cinobufagin (76)	CAL-27	1. reduced phosphorylation of STAT3 2. induced caspase-3 activation and PARP cleavage	2021
Luteolin (77)	PC3	inhibited ANO1 channel activity and protein expression levels	2017
Matrine (84)	LA795	NR	2019
benzophenanthridine alkaloids (85)	LA795	inhibited ANO1 channel activity	2020
Avermectins (86)	LA795	NR	2020
Aa3 (78)	A549, NCI-H460	NR	2020
Theaflavin (79)	LA795	block the ion conduction pore	2021

NR, not reported.

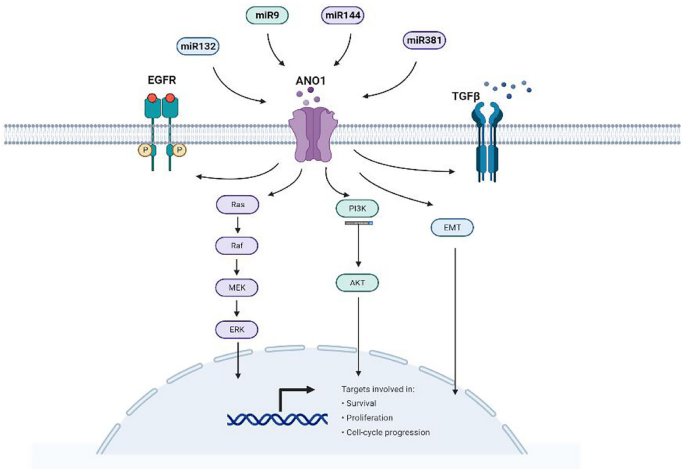

FIGURE 7 | miRNA directly targets ANO1and participates in tumorigenesis.

ANO1 can participate in various signal pathways by interacting with a variety of proteins or by regulating the ion conduction of malignant tumor cell ion homeostasis, thereby affecting the biological behavior of malignant tumors. Moreover, ANO1 expression can constitute a vital diagnosis and therapy monitoring marker. Advances in ANO1 biology and ANO1 inhibitors may hold promise for ANO1 use as a potential cancer biomarker and therapeutic target. The development of ANO1 inhibitors is currently desirable and validated in multiple *in vitro* and vivo tumor models and used in clinical trials. Simultaneously, many questions remain to be answered, yet other fields need additional exploration.

DATA AVAILABILITY STATEMENT

The original contributions presented in the study are included in the article/supplementary material. Further inquiries can be directed to the corresponding author.

AUTHOR CONTRIBUTIONS

All authors made a significant contribution to the work reported, whether that is in the conception, study design, execution, acquisition of data, analysis, and interpretation, or in all these areas; took part in drafting, revising or critically reviewing the article; gave final approval of the version to be published; have agreed on the journal to which the article has been submitted; and agree to be accountable for all aspects of the work.

FUNDING

This study was partially supported by China's National Natural Science Foundation(81900198), the Dalian Science and Technology Innovation Program, and the Natural Science Foundation of Liaoning Province(2020-MS-257).

REFERENCES

1. Paulino C, Neldner Y, Lam AK, Kalienkova V, Brunner JD, Schenck S, et al. Structural Basis for Anion Conduction in the Calcium-Activated Chloride Channel TMEM16A. *Elife* (2017) 6:1–23. doi: 10.7554/eLife.26232
2. Schroeder BC, Cheng T, Jan YN, Jan LY. Expression Cloning of TMEM16A as a Calcium-Activated Chloride Channel Subunit. *Cell* (2008) 134:1019–29. doi: 10.1016/j.cell.2008.09.003
3. Caputo A, Caci E, Ferrera L, Pedemonte N, Barsanti C, Sondo E, et al. TMEM16A, a Membrane Protein Associated With Calcium-Dependent Chloride Channel Activity. *Science* (2008) 322:590–4. doi: 10.1126/science.1163518
4. Pedemonte N, Galietta LJV. Structure and Function of TMEM16 Proteins (Anoctamins). *Physiol Rev* (2014) 94:419–59. doi: 10.1152/physrev.00039.2011
5. Oh U, Jung J. Cellular Functions of TMEM16/anoctamin. *Pflugers Archiv* (2016) 468:443–53. doi: 10.1007/s00424-016-1790-0
6. Qu ZQ, Yao WC, Yao RY, Liu XP, Yu K, Hartzell C. The Ca(2+) -Activated Cl (-) Channel, ANO1 (TMEM16A), Is a Double-Edged Sword in Cell Proliferation and Tumorigenesis. *Cancer Med* (2014) 3:453–61. doi: 10.1002/cam4.232
7. Ayoub C, Wasylyk C, Li Y, Thomas E, Marisa L, Robe A, et al. ANO1 Amplification and Expression in HNSCC With a High Propensity for Future Distant Metastasis and Its Functions in HNSCC Cell Lines. *Br J Cancer* (2010) 103:715–26. doi: 10.1038/sj.bjc.6605823
8. Duvvuri U, Shiwarski DJ, Xiao D, Bertrand C, Huang X, Edinger RS, et al. TMEM16A Induces MAPK and Contributes Directly to Tumorigenesis and Cancer Progression. *Cancer Res* (2012) 72:3270–81. doi: 10.1158/0008-5472.CAN-12-0475-T
9. Ruiz C, Martins JR, Rudin F, Schneider S, Dietsche T, Fischer CA, et al. Enhanced Expression of ANO1 in Head and Neck Squamous Cell Carcinoma Causes Cell Migration and Correlates With Poor Prognosis. *PloS One* (2012) 7:e43265. doi: 10.1371/journal.pone.0043265

10. Dixit R, Kemp C, Kulich S, Seethala R, Chiosea S, Ling S, et al. TMEM16A/ANO1 is Differentially Expressed in HPV-Negative Versus HPV-Positive Head and Neck Squamous Cell Carcinoma Through Promoter Methylation. *Sci Rep* (2015) 5:16657. doi: 10.1038/srep16657
11. Bill A, Gaither LA. The Mechanistic Role of the Calcium-Activated Chloride Channel ANO1 in Tumor Growth and Signaling. *Adv Exp Med Biol* (2017) 966:1–14. doi: 10.1007/5584_2016_201
12. Reddy RB, Bhat AR, James BL, Govindan SV, Mathew R, Ravindra DR, et al. Meta-Analyses of Microarray Datasets Identifies ANO1 and FADD as Prognostic Markers of Head and Neck Cancer. *PloS One* (2016) 11: e0147409. doi: 10.1371/journal.pone.0147409
13. Wanitchakool P, Wolf L, Koehl GE, Sirianant L, Schreiber R, Kulkarni S, et al. Role of Anoctamins in Cancer and Apoptosis. *Philos Trans R Soc Lond B Biol Sci* (2014) 369:20130096. doi: 10.1098/rstb.2013.0096
14. Finegersh A, Kulich S, Guo T, Favorov AV, Fertig EJ, Danilova LV, et al. DNA Methylation Regulates TMEM16A/ANO1 Expression Through Multiple CpG Islands in Head and Neck Squamous Cell Carcinoma. *Sci Rep* (2017) 7:15173. doi: 10.1038/s41598-017-15634-9
15. Hermida PF, Menéndez ST, Afanasiev PA, Diaz RG, Teijeiro SÁ., Villaronga MÁ., et al. Distinctive Expression and Amplification of Genes at 11q13 in Relation to HPV Status With Impact on Survival in Head and Neck Cancer Patients. *J Clin Med* (2018) 7:1–14. doi: 10.3390/jcm7120501
16. Shi ZZ, Shang L, Jiang YY, Hao JJ, Zhang Y, Zhang TT, et al. Consistent and Differential Genetic Aberrations Between Esophageal Dysplasia and Squamous Cell Carcinoma Detected by Array Comparative Genomic Hybridization. *Clin Cancer Res* (2013) 19:5867–78. doi: 10.1158/1078-0432.CCR-12-3753
17. Yu Y, Cao J, Wu WB, Zhu Q, Tang Y, Zhu CX, et al. Genome-Wide Copy Number Variation Analysis Identified ANO1 as a Novel Oncogene and Prognostic Biomarker in Esophageal Squamous Cell Cancer. *Carcinogenesis* (2019) 40:1198–208. doi: 10.1093/carcin/bgz077
18. Britschgi A, Bill A, Brinkhaus H, Rothwell C, Clay I, Duss S, et al. Calcium-Activated Chloride Channel ANO1 Promotes Breast Cancer Progression by Activating EGFR and CAMK Signaling. *Proc Natl Acad Sci U.S.A.* (2013) 110: E1026–34. doi: 10.1073/pnas.1217072110
19. Wu HZ, Guan S, Sun ML, Yu ZJ, Zhao L, He M, et al. Ano1/TMEM16A Overexpression Is Associated With Good Prognosis in PR-Positive or HER2-Negative Breast Cancer Patients Following Tamoxifen Treatment. *PloS One* (2015) 10:e0126128. doi: 10.1371/journal.pone.0126128
20. Fujimoto M, Kito H, Kajikuri J, Ohya S. Transcriptional Repression of Human Epidermal Growth Factor Receptor 2 by ClC-3 Cl (-) /H (+) Transporter Inhibition in Human Breast Cancer Cells. *Cancer Sci* (2018) 109:2781–91. doi: 10.1111/cas.13715
21. Wu HZ, Wang H, Guan S, Zhang J, Chen QC, Wang XD, et al. Cell-Specific Regulation of Proliferation by Ano1/TMEM16A in Breast Cancer With Different ER, PR, and HER2 Status. *Oncotarget* (2017) 8:84996–5013. doi: 10.18632/oncotarget.18662
22. Wang H, Yao F, Luo SY, Ma K, Liu MI, Bai LC, et al. A Mutual Activation Loop Between the Ca (2+)-Activated Chloride Channel TMEM16A and EGFR/STAT3 Signaling Promotes Breast Cancer Tumorigenesis. *Cancer Lett* (2019) 455:48–59. doi: 10.1016/j.canlet.2019.04.027
23. Liu ZT, Zhang SS, Hou F, Zhang CX, Gao JJ, Wang KW. Inhibition of Ca (2+) -Activated Chloride Channel ANO1 Suppresses Ovarian Cancer Through Inactivating PI3K/Akt Signaling. *Int J Cancer* (2019) 144:2215–26. doi: 10.1002/ijc.31887
24. Liu W, Lu M, Liu BG, Huang Y, Wang KW. Inhibition of Ca (2+)-Activated Cl (-) Channel ANO1/TMEM16A Expression Suppresses Tumor Growth and Invasiveness in Human Prostate Carcinoma. *Cancer Lett* (2012) 326:41–51. doi: 10.1016/j.canlet.2012.07.015
25. Cha JY, Wee JW, Jung JY, Jang YW, Lee B, Hong GS, et al. Anoctamin 1 (TMEM16A) is Essential for Testosterone-Induced Prostate Hyperplasia. *Proc Natl Acad Sci U.S.A.* (2015) 112:9722–7. doi: 10.1073/pnas.1423827112
26. Seo Y, Ryu K, Park J, Jeon DK, Jo S, Lee HK, et al. Inhibition of ANO1/TMEM16A Chloride Channel by Idebenone and Its Cytotoxicity to Cancer Cell Lines. *PloS One* (2015) 10:e0133656. doi: 10.1371/journal.pone.0133656
27. Song Y, Gao J, Guan LZ, Chen XL, Gao JJ, Wang KW. Inhibition of ANO1/TMEM16A Induces Apoptosis in Human Prostate Carcinoma Cells by Activating TNF-Alpha Signaling. *Cell Death Dis* (2018) 9:703. doi: 10.1038/s41419-018-0735-2
28. Sui YJ, Sun MY, Wu F, Yang LF, Di WH, Zhang GZ, et al. Inhibition of TMEM16A Expression Suppresses Growth and Invasion in Human Colorectal Cancer Cells. *PloS One* (2014) 9:e115443. doi: 10.1371/journal.pone.0115443
29. Mokutani Y, Uemura M, Munakata K, Okuzaki D, Haraguchi N, Takahashi H, et al. Down-Regulation of microRNA-132 is Associated With Poor Prognosis of Colorectal Cancer. *Ann Surg Oncol* (2016) 23:599–608. doi: 10.1245/s10434-016-5133-3
30. Jiang YS, Cai YH, Shao WW, Li F, Zhou Y, Tang C, et al. MicroRNA144 Suppresses Aggressive Phenotypes of Tumor Cells by Targeting ANO1 in Colorectal Cancer. *Oncol Rep* (2019) 41:2361–70. doi: 10.3892/or.2019.7025
31. Park YR, Lee ST, Kim SL, Zhu SM, Lee MR, Kim SH. Down-Regulation of miR-9 Promotes Epithelial Mesenchymal Transition via Regulating Anoctamin-1 (ANO1) in CRC Cells. *Cancer Genet* (2019) 231-232:22–31. doi: 10.1016/j.cancergen.2018.12.004
32. Jia L, Liu W, Guan L, Lu M, Wang K. Inhibition of Calcium-Activated Chloride Channel ANO1/TMEM16A Suppresses Tumor Growth and Invasion in Human Lung Cancer. *PloS One* (2015) 10:e0136584. doi: 10.1371/journal.pone.0136584
33. Hu C, Zhang RG, Jiang DP. Tmem16a as a Potential Biomarker in the Diagnosis and Prognosis of Lung Cancer. *Arch Iran Med* (2019) 22:32–8.
34. Liu J, Liu Y, Ren YG, Kang L, Zhang LH. Transmembrane Protein With Unknown F Unction 16A Overexpression Promotes Glioma Formation Through the Nuclear Factor-Kappa B Signaling Pathway. *Mol Med Rep* (2014) 9:1068–74. doi: 10.3892/mmr.2014.1888
35. Lee YS, Lee JK, Bae Y, Lee BS, Kim E, Cho CH, et al. Suppression of 14-3-3gamma-Mediated Surface Expression of ANO1 Inhibits Cancer Progression of Glioblastoma Cells. *Sci Rep* (2016) 6:26413. doi: 10.1038/srep26413
36. Liu F, Cao Q-H, Lu DJ, Luo B, Lu X-F, Luo RC, et al. TMEM16A Overexpression Contributes to Tumor Invasion and Poor Prognosis of Human Gastric Cancer Through TGF-β Signaling. *Oncotarget* (2015) 6:11585–99. doi: 10.18632/oncotarget.3412
37. Cao QH, Liu F, Ji KY, Liu N, He Y, Zhang WH, et al. MicroRNA-381 Inhibits the Metastasis of Gastric Cancer by Targeting TMEM16A Expression. *J Exp Clin Cancer Res* (2017) 36:29. doi: 10.1186/s13046-017-0499-z
38. Sauter DRP, Novak I, Pedersen SF, Larsen EH, Hoffmann EK. ANO1 (TMEM16A) in Pancreatic Ductal Adenocarcinoma (PDAC). *Pflugers Arch* (2015) 467:1495–508. doi: 10.1007/s00424-014-1598-8
39. Crottès D, Lin YT, Peters CJ, Gilchrist JM, Wiita AP, Jan YN, et al. TMEM16A Controls EGF-Induced Calcium Signaling Implicated in Pancreatic Cancer Prognosis. *Proc Natl Acad Sci U.S.A.* (2019) 116:13026–35. doi: 10.1073/pnas.1900703116
40. Deng L, Yang JH, Chen HW, Ma B, Pan KM, Su CK, et al. Knockdown of TMEM16A Suppressed MAPK and Inhibited Cell Proliferation and Migration in Hepatocellular Carcinoma. *Onco Targets Ther* (2016) 9:325–33. doi: 10.2147/OTT.S95985
41. Zhang CT, Liu JX, Han ZY, Cui X, Peng D, Xing YF. Inhibition of TMEM16A Suppresses Growth and Induces Apoptosis in Hepatocellular Carcinoma. *Int J Clin Oncol* (2020) 25:1145–54. doi: 10.1007/s10147-020-01653-6
42. Gasparotto D, Sbaraglia M, Rossi S, Baldazzi D, Brenca M, Mondello A, et al. Tumor Genotype, Location, and Malignant Potential Shape the Immunogenicity of Primary Untreated Gastrointestinal Stromal Tumors. *JCI Insight* (2020) 5:1–17. doi: 10.1172/jci.insight.142560
43. Hanahan D. Hallmarks of Cancer: New Dimensions. *Cancer Discovery* (2022) 12:31–46. doi: 10.1158/2159-8290.CD-21-1059
44. Kunzelmann K, Ousingsawat J, Benedetto R, Cabrita I, Schreiber R. Contribution of Anoctamins to Cell Survival and Cell Death. *Cancers (Basel)* (2019) 11:1–24. doi: 10.3390/cancers11030382
45. Basu A, Haldar S. The Relationship Between Bcl2, Bax and P53: Consequences for Cell Cycle Progression and Cell Death. *Mol Hum Reprod* (1998) 4:1099–109. doi: 10.1093/molehr/4.12.1099
46. Fernald K, Kurokawa M. Evading Apoptosis in Cancer. *Trends Cell Biol* (2013) 23:620–33. doi: 10.1016/j.tcb.2013.07.006
47. Locksley RM, Killeen N, Lenardo MJ. The TNF and TNF Receptor Superfamilies: Integrating Mammalian Biology. *Cell* (2001) 104:487–501. doi: 10.1016/s0092-8674(01)00237-9

48. Cornejo PP, Gokhale A, Duran C, Cui YY, Xiao QH, Hartzell HC. Anoctamin 1 (Tmem16A) Ca2+-Activated Chloride Channel Stoichiometrically Interacts With an Ezrin-Radixin-Moesin Network. *Proc Natl Acad Sci U.S.A.* (2012) 109:10376–81. doi: 10.1073/pnas.1200174109
49. Seo Y, Jeong SB, Woo JH, Kwon OB, Lee S, Oh HI, et al. Diethylstilbestrol, a Novel ANO1 Inhibitor, Exerts an Anticancer Effect on Non-Small Cell Lung Cancer *via* Inhibition of ANO1. *Int J Mol Sci* (2021) 22:7100. doi: 10.3390/ijms22137100
50. Yan YF, Ding XY, Han CH, Gao JJ, Liu ZT, Liu YN, et al. Involvement of TMEM16A/ANO1 Upregulation in the Oncogenesis of Colorectal Cancer. *Biochim Biophys Acta Mol Basis Dis* (2022) 868:166370. doi: 10.1016/j.bbadis.2022.166370
51. Henry E. The Activated Complex and the Absolute Rate of Chemical Reactions. *J Chem Phys* (1935) 3:107–15. doi: 10.1063/1.1749604
52. Guan LZ, Song Y, Gao J, Gao JJ, Wang KW. Inhibition of Calcium-Activated Chloride Channel ANO1 Suppresses Proliferation and Induces Apoptosis of Epithelium Originated Cancer Cells. *Oncotarget* (2016) 7:78619–30. doi: 10.18632/oncotarget.12524
53. Bill A, Gutierrez A, Kulkarni S, Kemp C, Bonenfant D, Voshol H, et al. ANO1/TMEM16A Interacts With EGFR and Correlates With Sensitivity to EGFR-Targeting Therapy in Head and Neck Cancer. *Oncotarget* (2015) 6:9173–88. doi: 10.18632/oncotarget.3277
54. Navas C, Porras IH, Schuhmacher AJ, Sibilia M, Guerra C, Barbacid M. EGF Receptor Signaling is Essential for K-Ras Oncogene-Driven Pancreatic Ductal Adenocarcinoma. *Cancer Cell* (2012) 22:318–30. doi: 10.1016/j.ccr.2012.08.001
55. Ardito CM, Grüner BM, Takeuchi KK, Martellato CL, Teichmann N, Mazur PK, et al. EGF Receptor is Required for KRAS-Induced Pancreatic Tumorigenesis. *Cancer Cell* (2012) 22:304–17. doi: 10.1016/j.ccr.2012.07.024
56. Betto G, Cherian OL, Pifferi S, Cenedese V, Boccaccio A, Menini A. Interactions Between Permeation and Gating in the TMEM16B/anoctamin2 Calcium-Activated Chloride Channel. *J Gen Physiol* (2014) 143:703–18. doi: 10.1085/jgp.201411182
57. Ferrera L, Caputo A, Ubby I, Bussani E, Moran OZ, Ravazzolo R, et al. Regulation of TMEM16A Chloride Channel Properties by Alternative Splicing. *J Biol Chem* (2009) 284:33360–8. doi: 10.1074/jbc.M109.046607
58. Zhang X, Zhang GH, Zhao ZJ, Xiu RL, Jia J, Chen PP, et al. Cepharanthine, a Novel Selective ANO1 Inhibitor With Potential for Lung Adenocarcinoma Therapy. *Biochim Biophys Acta Mol Cell Res* (2021) 1868:119132. doi: 10.1016/j.bbamcr.2021.119132
59. Vite JAC, Rangel SC, Jesús-Pérez JJD, Figueroa IAA, Menchaca AAR, Cornejo PP, et al. Revealing the Activation Pathway for TMEM16A Chloride Channels From Macroscopic Currents and Kinetic Models. *Pflugers Arch* (2016) 468:1241–57. doi: 10.1007/s00424-016-1830-9
60. Carpenter G. The EGF Receptor: A Nexus for Trafficking and Signaling. *Bioessays* (2020) 22:697–707. doi: 10.1002/1521-1878(200008)22:8<697::AID-BIES3>3.0.CO;2-1
61. Hodeify R, Yu F, Courjaret R, Nader N, Dib M, Sun L, et al. Regulation and Role of Store-Operated Ca 2+ Entry in Cellular Proliferation. *Calcium Entry Channels Non-Excitable Cells* (2018) 12:1–18. doi: 10.1201/9781315152592-12
62. Kunzelmann K. Tmem16, Lrrc8a, Bestrophin: Chloride Channels Controlled by Ca(2+) and Cell Volume. *Trends Biochem Sci* (2015) 40:535–43. doi: 10.1016/j.tibs.2015.07.005
63. Agell N, Bachs O, Rocamora N, Villalonga P. Modulation of the Ras/Raf/MEK/ERK Pathway by Ca (2+), and Calmodulin. *CellSignal* (2002) 14:649–54. doi: 10.1016/s0898-6568(02)00007-4
64. Darling NJ, Cook SJ. The Role of MAPK Signaling Pathways in the Response to Endoplasmic Reticulum Stress. *Biochim Biophys Acta* (2014) 1843:2150–63. doi: 10.1016/j.bbamcr.2014.01.009
65. Peretti M, Angelini M, Savalli N, Florio T, Yuspa SH, Mazzanti M. Chloride Channels in Cancer: Focus on Chloride Intracellular Channel 1 and 4 (CLIC1 AND CLIC4) Proteins in Tumor Development and as Novel Therapeutic Targets. *Biochim Biophys Acta* (2015) 1848:2523–31. doi: 10.1016/j.bbamem.2014.12.012
66. Wang H, Zou L, Ma K, Yu JK, Wu HZ, Wei MJ, et al. Cell-Specific Mechanisms of TMEM16A Ca (2+)-Activated Chloride Channel in Cancer. *Mol Cancer* (2017) 16:152. doi: 10.1186/s12943-017-0720-x
67. Wang L, Yu PW. miR-300 Promotes Proliferation and EMT-Mediated Colorectal Cancer Migration and Invasion by Targeting P53. *Oncol Rep* (2016) 36:3225–32. doi: 10.3892/or.2016.5193
68. Liu MJ, He XS, Xiao XJ, Wang YC. Overexpression of miR-422a Inhibits Cell Proliferation and Invasion, and Enhances Chemosensitivity in Osteosarcoma Cells. *Oncol Rep* (2016) 36:3371–8. doi: 10.3892/or.2016.5182
69. Chi YD, Zhou DM. MicroRNAs in Colorectal Carcinoma–From Pathogenesis to Therapy. *J Exp Clin Cancer Res* (2016) 35:43. doi: 10.1186/s13046-016-0320-4
70. Godse NR, Khan N, Yochum ZA, Gomez CR, Kemp C, Shiwarski DJ, et al. TMEM16A/ANO1 Inhibits Apoptosis Via Downregulation of Bim Expression. *Clin Cancer Res* (2017) 23):7324–32. doi: 10.1158/1078-0432.CCR-17-1561
71. Zhang AL, Yan XX, Li HL, Gu ZF, Zhang P, Zhang HL, et al. TMEM16A Protein Attenuates Lipopolysaccharide-Mediated Inflammatory Response of Human Lung Epithelial Cell Line A549. *Exp Lung Res* (2014) 40:237–50. doi: 10.3109/01902148.2014.905655
72. Fröbom R, Sellberg F, Xu C, Zhao A, Larsson C, Lui WO, et al. Biochemical Inhibition of DOG1/TMEM16A Achieves Antitumoral Effects in Human Gastrointestinal Stromal Tumor Cells. *In Vitro. Anticancer Res* (2019) 39:3433–42. doi: 10.21873/anticanres.13489
73. Filippou A, Pehkonen H, Karhemo PR, Väänänen J, Nieminen AI, Klefström J, et al. ANO1 Expression Orchestrates P27kip1/MCL1-Mediated Signaling in Head and Neck Squamous Cell Carcinoma. *Cancers (Basel).* (2021) 13):1170. doi: 10.3390/cancers13051170
74. Lippitz BE. Cytokine Patterns in Patients With Cancer: A Systematic Review. *Lancet Oncol* (2013) 14:e218–28. doi: 10.1016/S1470-2045(12)70582-X
75. Seo Y, Kim J, Chang J, Kim SS, Namkung W, Kim L. Synthesis and Biological Evaluation of Novel Ani9 Derivatives as Potent and Selective ANO1 Inhibitors. *Eur J Med Chem* (2018) 160:245–55. doi: 10.1016/j.ejmech.2018.10.002
76. Jo S, Yang E, Lee Y, Jeon D, Namkung W. Cinobufagin Exerts Anticancer Activity in Oral Squamous Cell Carcinoma Cells Through Downregulation of ANO1. *Int J Mol Sci* (2021) 22:12037. doi: 10.3390/ijms222112037
77. Seo Y, Ryu K, Park J, Jeon DK, Jo S, Lee HK, et al. Inhibition of ANO1 by Luteolin and its Cytotoxicity in Human Prostate Cancer PC-3 Cells. *PloS One* (2017) 12:e0174935. doi: 10.1371/journal.pone.0174935
78. Kim T, Cho S, Oh H, Hur J, Kim H, Choi YH, et al. Design of Anticancer 2,4-Diaminopyrimidines as Novel Anoctamin 1 (ANO1) Ion Channel Blockers. *Molecules* (2020) 25:5180. doi: 10.3390/molecules25215180
79. Shi S, Ma B, Sun F, Qu C, An HL. Theaflavin Binds to a Druggable Pocket of TMEM16A Channel and Inhibits Lung Adenocarcinoma Cell Viability. *J Biol Chem* (2021) 297:101016. doi: 10.1016/j.jbc.2021.10
80. Seo Y, Lee HK, Park J, Jeon DK, Jo S, Jo M, et al. Ani9, A Novel Potent Small-Molecule ANO1 Inhibitor With Negligible Effect on ANO2. *PloS One* (2016) 11:e0155771. doi: 10.1371/journal.pone.0155771
81. Choi SH, Ryu SS, Sim K, Song C, Shin L, Kim SS, et al. Anti-Glioma Effects of 2-Aminothiophene-3-Carboxamide Derivatives, ANO1 Channel Blockers. *Eur J Med Chem* (2020) 208:112688. doi: 10.1016/j.ejmech.2020.112688
82. Mazzone A, Eisenman ST, Strege PR, Yao Z, Ordog T, Gibbons SJ, et al. Inhibition of Cell Proliferation by a Selective Inhibitor of the Ca (2+)-Activated Cl (-) Channel, Ano1. *Biochem Biophys Res Commun* (2012) 427:248–53. doi: 10.1016/j.bbrc.2012.09.022
83. Guo S, Chen YF, Shi S, Wang XZ, Zhang HL, Zhan Y, et al. Arctigenin, a Novel TMEM16A Inhibitor for Lung Adenocarcinoma Therapy. *Pharmacol Res* (2020) 155:104721. doi: 10.1016/j.phrs.2020.104721
84. Guo S, Chen YF, Pang CL, Wang XZ, Shi S, Zhang HL, et al. Matrine is a Novel Inhibitor of the TMEM16A Chloride Channel With Antilung Adenocarcinoma Effects. *J Cell Physiol* (2019) 234:8698–708. doi: 10.1002/jcp.27529
85. Zhang GH, Zhu L, Xue YC, Zhao ZJ, Li H, Niu ZY, et al. Benzophenanthridine Alkaloids Suppress Lung Adenocarcinoma by Blocking TMEM16A Ca 2+-Activated Cl - Channels. *Pflugers Arch* (2020) 472:1457–67. doi: 10.1007/s00424-020-02434-w
86. Zhang X, Zhang GH, Zhai WJ, Zhao ZJ, Wang S, Yi JF. Inhibition of TMEM16A Ca 2+-Activated Cl - Channels by Avermectins Is Essential for

Their Anticancer Effects. *Pharmacol Res* (2020) 156:104763. doi: 10.1016/j.phrs.2020.104763
87. Bartel DP. Micronase: Genomics, Biogenesis, Mechanism, and Function. *Cell* (2004) 116:281–97. doi: 10.1016/s0092-8674(04)00045-5
88. Chen L, Luo L, Chen W, Xu HX, Chen F, Chen LZ, et al. MicroRNA-24 Increases Hepatocellular Carcinoma Cell Metastasis and Invasion by Targeting P53: miR-24 Targeted P53. *BioMed Pharmacother* (2016) 84:1113–8. doi: 10.1016/j.biopha.2016.10.051
89. Wang YF, Liu LL, Liu XQ, Zhang H, Liu JM, Feng B, et al. Shugoshin1 Enhances Multidrug Resistance of Gastric Cancer Cells by Regulating MRP1, Bcl-2, and Bax Genes. *Tumor Biol* (2013) 34:2205–14. doi: 10.1007/s13277-013-0758-3
90. Feng H, Wang YL, Su JJ, Liang HW, Zhang CY, Chen X, et al. MicroRNA-148a Suppresses the Proliferation and Migration of Pancreatic Cancer Cells by Down-Regulating ErbB3. *Pancreas* (2016) 45:1263–71. doi: 10.1097/MPA.0000000000000677

Conflict of Interest: The authors declare that the research was conducted in the absence of any commercial or financial relationships that could be construed as a potential conflict of interest.

Publisher's Note: All claims expressed in this article are solely those of the authors and do not necessarily represent those of their affiliated organizations, or those of the publisher, the editors and the reviewers. Any product that may be evaluated in this article, or claim that may be made by its manufacturer, is not guaranteed or endorsed by the publisher.

frontiers | Frontiers in Pharmacology

ORIGINAL RESEARCH
published: 15 June 2022
doi: 10.3389/fphar.2022.893151

PNA-Modified Liposomes Improve the Delivery Efficacy of CAPIRI for the Synergistic Treatment of Colorectal Cancer

Wenbin Diao[1,2], Ben Yang[1,2], Sipeng Sun[1,2], Anping Wang[1,2], Rongguan Kou[1], Qianyun Ge[1,2], Mengqi Shi[1,2], Bo Lian[1,2], Tongyi Sun[1,2], Jingliang Wu[1,2], Jingkun Bai[1,2], Meihua Qu[3], Yubing Wang[1,2], Wenjing Yu[1,2]* and Zhiqin Gao[1,2]**

[1]School of Life Science and Technology, Weifang Medical University, Weifang, China, [2]Shandong Universities Key Laboratory of Biopharmaceuticals, Weifang, China, [3]Translational Medical Center, Second People's Hospital of Weifang, Weifang, China

OPEN ACCESS

Edited by:
Zhe-Sheng Chen,
St. John's University, United States

Reviewed by:
Weicheng Liang,
Sun Yat-Sen University, China
Alessandro Ottaiano,
G. Pascale National Cancer Institute Foundation (IRCCS), Italy

***Correspondence:**
Yubing Wang
ybwang@wfmc.edu.cn
Wenjing Yu
yuwjwf@163.com
Zhiqin Gao
zhiqingao2013@163.com

Specialty section:
This article was submitted to Experimental Pharmacology and Drug Discovery, a section of the journal Frontiers in Pharmacology

Received: 10 March 2022
Accepted: 09 May 2022
Published: 15 June 2022

Citation:
Diao W, Yang B, Sun S, Wang A, Kou R, Ge Q, Shi M, Lian B, Sun T, Wu J, Bai J, Qu M, Wang Y, Yu W and Gao Z (2022) PNA-Modified Liposomes Improve the Delivery Efficacy of CAPIRI for the Synergistic Treatment of Colorectal Cancer. Front. Pharmacol. 13:893151. doi: 10.3389/fphar.2022.893151

Tumor-associated antigen mucin 1 (MUC1) is highly expressed in colorectal cancer and is positively correlated with advanced stage at diagnosis and poor patient outcomes. The combination of irinotecan and capecitabine is standard chemotherapy for metastatic colorectal cancer and is known as XELIRI or CAPIRI, which significantly prolongs the progression-free survival and overall survival of colorectal cancer patients compared to a single drug alone. We previously reported that peanut agglutinin (PNA)-conjugated liposomes showed enhanced drug delivery efficiency to MUC1-positive liver cancer cells. In this study, we prepared irinotecan hydrochloride (IRI) and capecitabine (CAP)-coloaded liposomes modified by peanut agglutinin (IRI/CAP-PNA-Lips) to target MUC1-positive colorectal cancer. The results showed that IRI/CAP-PNA-Lips showed an enhanced ability to target MUC1-positive colorectal cancer cells compared to unmodified liposomes. Treatment with IRI/CAP-PNA-Lips also increased the proportion of apoptotic cells and inhibited the proliferation of colorectal cancer cells. The targeting specificity for tumor cells and the antitumor effects of PNA-modified liposomes were significantly increased in tumor-bearing mice with no severe cytotoxicity to normal tissues. These results suggest that PNA-modified liposomes could provide a new delivery strategy for the synergistic treatment of colorectal cancer with clinical chemotherapeutic agents.

Keywords: colorectal cancer, liposomes, peanut agglutinin, combination therapy, irinotecan, capecitabine

INTRODUCTION

The 2020 Global Cancer Report showed that the incidence of colorectal cancer ranks third among all cancers (Engstrand et al., 2018; Xu, Fan, et al., 2019; Sung et al., 2021). The main treatment for colorectal cancer is surgical resection combined with chemotherapy (Chau and Cunningham, 2002). The topoisomerase I inhibitor irinotecan (IRI) mainly relies on its active metabolite SN-38 to exert tumor-suppressive effects and is widely used in the treatment of colorectal and pancreatic cancers but with toxic effects of neutrophil reduction and diarrhea (de Man et al., 2018). IRI is often used in combination with 5-FU and its derivatives in the clinical treatment of cancer (Paulík et al., 2020). Studies have shown that capecitabine (CAP) is a precursor of 5-FU, and its combination with irinotecan (XELIRI or CAPIRI) is as effective as other synergistic treatments in colorectal cancer

patients. The therapy is well tolerated with fewer toxic side effects and a higher safety profile at the same level of efficacy (Goldberg, 2005; Walko and Lindley, 2005; Lam et al., 2016). Due to the limitations of conventional chemotherapeutic drugs, such as poor targeting, short drug clearance half-life, low bioavailability, and poor solubility, there is much room to improve the efficacy of chemotherapy. Liposomes are ideal carriers to encapsulate chemotherapy drugs, not only to reduce drug toxicity and improve drug stability but also to enhance antitumor efficacy through surface modifications for active targeting and precise drug delivery (Harashima et al., 1999; Barenholz, 2012; Mitragotri et al., 2015).

Mucin 1 (MUC1) is a type of tumor-associated carbon antigen (TACA), which is a highly glycosylated mucin, and studies have shown that it is an important biomarker in colorectal cancer (Nabavinia et al., 2017; Gao et al., 2020). Altered expression of MUC1 glycosyltransferase results in a Thomsen–Friedenreich (TF) structure, which reduces the adhesion between tumor cells. Studies have shown that high expression of MUC1 promotes tumor cell proliferation and metastasis, and its expression is proportional to tumor malignancy and is associated with poor prognosis in patients (Li et al., 2019). Thus, using MUC1-specific ligands to modify liposomes could enable targeted delivery of drugs to MUC1-positive colorectal cancer tissue. Peanut agglutinin (PNA) is a homotetrameric plant agglutinin extracted from peanuts that can bind to a variety of disaccharides containing β-D-galactosyl-(1–3)-N-acetyl-D-galactosamine [Gal-β(1–3)GalNAc]. Studies have found that the core component of the TF structure is Gal-β(1–3)GalNAc, which is the core structure of MUC1 (Beack et al., 2017; Kumagai et al., 2019). Therefore, PNA-modified liposomes can actively target MUC1-positive colorectal cancers to deliver drugs centrally. Previously, we reported that PNA-modified liposomes showed enhanced drug delivery efficiency toward MUC1-positive liver cancer cells, which suggested the feasibility of using PNA-modified liposomes targeting MUC1 as a means to enhance its antitumor effects (Li, Diao, et al., 2020).

In this study, we prepared PNA-modified liposomes coloaded with IRICAP (IRI/CAP-PNA-Lips), achieved targeted codelivery of drugs, and improved the effectiveness of the anti-colorectal cancer effect. PNA-modified liposomes coloaded with drugs are important as a novel drug delivery strategy to enhance the efficacy of the clinical synergistic treatment of colorectal cancer.

MATERIALS AND METHODS

Synthesis and Identification of DSPE-PEG2K-PNA

Ten milligrams of peanut agglutinin (PNA, Medicago, Uppsala, Sweden) was weighed and dissolved in 2 ml of pH 7.4 PBS, and 0.2 ml (5.0 eq.) of DSPE-PEG2K-NHS (Xi'an Rui Xi Biotechnology Corporation, Xi'an, China) was added to DMSO solution. The reaction solution was transferred to a dialysis bag (cutoff molecular weight 8,000–14,000 Da) after 4 h of reaction at room temperature and then dialyzed with pure water for 12 h. The dialysate was collected and freeze-dried to obtain DSPE-PEG2K-PNA.

SDS–polyacrylamide gel electrophoresis (SDS–PAGE) was used for the analysis of PNA and DSPE-PEG2K-PNA. The gel was stained with 0.25% Coomassie Brilliant Blue solution for 3 h and then decolorized with the decolorizing solution until the bands were clear. The successful linkage of PNA and DSPE-PEG2K was determined using infrared spectroscopy analysis.

Analysis of the Optimal Synergistic Ratio of Irinotecan Hydrochloride (IRI) and Capecitabine (CAP) Using the Combination Index Method

The CI method was used to analyze the optimal synergistic ratio of irinotecan hydrochloride (IRI, Yuanye Biotechnology Corporation, Shanghai, China) and capecitabine (CAP, Ark Pharm, Chicago, United States) (Meng et al., 2015). Four colorectal cancer cell lines, Caco-2, HCT116, HT29, and SW620 (Cell Resource Center, Institute of Basic Medical Sciences, Chinese Academy of Medical Sciences, Beijing, China), were treated with different concentrations of IRI or CAP alone for 72 h to obtain the half-maximal inhibitory concentration (IC50) of IRI and CAP, respectively. The concentrations of the main drug, IRI, were determined as 1 μg/ml, 3 μg/ml, 9 μg/ml, 27 μg/ml, and 81 μg/ml, and the amounts of CAP were added at ratios of IRI:CAP equal to 8:1, 4:1, 3:1, 2:1, 1:1, 1:2, 1:3, 1:4, and 1:8 to obtain forty-five different concentrations and ratios of IRI and CAP mixture. Concentrations of IRI equal to 1 μg/ml, 3 μg/ml, 9 μg/ml, 27 μg/ml, and 81 μg/ml, and equivalent concentrations of CAP alone were used as controls. The four cell lines were treated with forty-five different concentration conditions for 72 h, and the IC50 values were calculated for the combination of the two drugs at different ratios. Six replicate wells were used in each group.

Based on the IC50 values, CI at different IRI/CAP ratios was calculated using the following equation:

$$CI = IC_1/IC_{m1} + IC_2/IC_{m2}.$$

IC_1 and IC_2 represent the IC50 values of IRI and CAP when the two drugs are combined to treat cells. IC_{m1} and IC_{m2} represent the IC50 values of IRI and CAP when they are treated alone (Guo et al., 2020). If the CI is greater than 1, it means that the two drugs have an antagonistic effect, less than 1 means that the two drugs have a synergistic effect, and equal to 1 means that the two drugs have an additive effect.

Preparation of PNA-Modified Liposomes Coloaded With IRICAP

Blank liposomes (Lips) were prepared by a thin-film dispersion method (Gao et al., 2021). Lecithin and cholesterol (Avet Pharmaceutical Corporation, Shanghai, China) were dissolved in 4 ml of chloroform at a mass ratio of 4:1, and the organic solvent was removed by heating and evaporating in a rotary evaporator (Yarmato Technology & Trading Corporation, Shanghai, China) to form lipid films. Then, 70 mg/ml ammonium sulfate was hydrated and homogenized for particle size using an ultrasonic cell crusher (Sonics & Materials,

United States). The liposome extruders were passed over 0.2 and 0.1 μm filter membranes, repeatedly extruded 10 times, and dialyzed with ddH_2O for 6 h to obtain unmodified blank liposomes.

Liposomes coloaded with IRICAP (IRI/CAP-Lips) and PNA-modified liposomes coloaded with IRICAP (IRI/CAP-PNA-Lips) were prepared by thin-film dispersion combined with the ammonium sulfate gradient method (Abraham et al., 2005; Zhang and Yao, 2012). Capecitabine was dissolved in chloroform according to the mass ratio (phospholipid:CAP = 1.3:1) to obtain loaded capecitabine liposomes (CAP-Lips). Then, CAP-Lips were mixed with IRI according to the mass ratio (phospholipid:IRI = 10:1), and IRI/CAP-Lips were obtained after hydration and dialysis. DSPE-PEG2K-PNA was used according to the mass ratio (phospholipid:PNA = 10:1) in chloroform, and IRI/CAP-PNA-Lips were obtained based on the IRI/CAP-Lip preparation procedure.

Characterization of PNA-Modified Liposomes Coloaded With IRICAP

The liposomes of each type were ultrasonically crushed for 10 min and then passed through 0.2 and 0.1 μm membrane filters ten times, diluted 10-fold with ddH_2O, and prepared for use. The morphological observation was performed using transmission electron microscopy (HITACHI High-Tech Corporation, Japan) after phosphotungstic acid staining (Feng et al., 2019). Particle size and potential were determined using a Malvern particle size meter (Malvern Panalytical Corporation, UK) (Sarisozen et al., 2012).

The encapsulation efficiency (EE) and drug loading (DL) of the coloaded liposomes were measured by using high-performance liquid chromatography (HPLC, Thermo Fisher Scientific, Massachusetts, United States) (Wang et al., 2019). After 6.8 g of potassium dihydrogen phosphate was dissolved in 800 ml of water, 10 ml of triethylamine was added, and the pH was adjusted to 4.0 with phosphoric acid. Water was then added to 1,000 ml to configure the phosphate buffer with a mobile phase ratio of methanol:acetonitrile:phosphate buffer equal to 55:5:45. After diluting the liposomes 10-fold, 0.2% Triton X-100 was added to permeabilize the membrane for 15 min, and the absorption peaks of IRI and CAP were detected at 254 and 307 nm, respectively. The EE and DL of liposomes were calculated using the following equations:

Encapsulation efficiency (EE) % = Mass of the drug loaded/Total mass of the drug used × 100%

Drug loading (DL) % = Mass of the drug loaded/Total mass of liposomes × 100%

Stability and Drug Release Analysis of PNA-Modified Liposomes Coloaded With IRICAP

Each type of liposome was stored in saline and 3% BSA at 4°C for 16 days. The changes in particle size and potential over 16 days were measured using a Malvern particle size meter.

The *in vitro* dialysis method was used for the drug release analysis of liposomes (Liu et al., 2017; Li, Hou, et al., 2020). For this, 2 ml of each type of liposome was placed in a dialysis bag (with molecular weight cutoff at 8,000–14,000 Da), placed in a conical flask containing 100 ml of phosphate-buffered saline (PBS), and incubated at 37°C on a shaker at 100 rpm. At each time point (15 min, 30 min, 1, 8, 12, and 24 h), samples (2 ml) were taken from the PBS and immediately replenished with an equal volume of fresh PBS. The levels of IRI and CAP in the samples and the cumulative drug release were analyzed by HPLC.

Identification of MUC1-Positive Colorectal Cancer Cell Lines

Caco-2, HCT116, HT29, and SW620 cells were cultured overnight in 6-well plates (3×10^5 cells/well). Total RNA that had been extracted by the TRIzol method was used as the template to produce cDNA by using an RT-PCR kit (Toyobo Life Science, Shanghai, China). Furthermore, the cDNA was used as a template for real-time quantitative PCR, using a program that was set to 95°C, 30 s→95°C, 5 s; 60°C, 10 s; and 72°C, 15 s (40 cycles). The Ct values of each group were recorded, and the relative expression of each group was calculated by the 2^{-}(-Delta Delta C(T)) method.

The four cell lines were cultured overnight in 6-well plates (3×10^5 cells/well), and RIPA lysis was performed to extract cellular protein. Western blot analysis identified MUC1 expression in the four cell lines.

Furthermore, all four cell lines were inoculated into cell crawls (5×10^4 cells/well) for 24 h, fixed in 4% tissue cell fixative for 10 min, permeabilized with 0.1% Triton X-100 for 10 min, blocked with 3% BSA for 2 h, incubated overnight at 4°C with MUC1-specific antibody (Cell Signaling Technology, Danvers, Massachusetts, United States), and further incubated with fluorescent secondary antibody for 1 h. DAPI was used to stain the nuclei. The four cell lines were then visualized with a confocal laser scanning microscope (CLSM, Leica Microscope Imaging System, Germany) to observe MUC1 expression. After each step of the aforementioned treatment, the cells were rinsed with PBS three times.

Targeting Property Analysis of PNA-Modified Liposomes *In Vitro*

To study the cellular uptake of liposomes by cells *in vitro*, FITC and rhodamine (Rhb) were used to replace the CAP and IRI to prepare liposomes coloaded with FITCRhb (FITC/Rhb-Lips) and PNA-modified liposomes coloaded with FITCRhb (FITC/Rhb-PNA-Lips). Caco-2, HCT116, HT29, and SW620 cells were inoculated into cell crawls (5×10^4 cells/well) overnight. The cells were incubated for 4 h with the addition of complete medium containing equal concentrations of FITC/Rhb, FITC/Rhb-Lips, and FITC/Rhb-PNA-Lips (Khan et al., 2020). We used 0.1% Triton X-100 to permeabilize the cell membrane and nuclear membrane. DAPI was utilized to stain the nucleus and an anti-fluorescence quencher as a sealant. Images were taken to observe the fluorescence distribution and intensity of different cells with CLSM. Each of the aforementioned steps was performed in the dark, and the cells were rinsed with PBS three times after the treatment (Xu et al., 2019).

Cytotoxicity Analysis of PNA-Modified Liposomes Coloaded With IRICAP *In Vitro*

Caco-2, HCT116, HT29, and SW620 cells were inoculated into 96-well plates (1×10^4 cells/well) overnight. The old medium was discarded, and Lips, IRI/CAP, IRI/CAP-Lips, and IRI/CAP-PNA-Lips were added to a 1.5-fold concentration gradient of IRI for 72 h. The old medium was replaced with a medium containing MTS and incubated for 15 min at 37°C. Enzyme-linked immunoassay (BIO-RAD, Hercules, California, United States) was used to detect optical density (OD) values. Inhibition of cell viability and IC50 values were calculated after 72 h of treatment with PNA-modified liposomes.

The four cell lines were treated with complete medium containing Lips, IRI/CAP, IRI/CAP-Lips, and IRI/CAP-PNA-Lips (C_{IRI} = 25 μg/ml, 50 μg/ml, 100 μg/ml) for 24 h. The MTS assay was used to analyze the inhibition of cell viability (Wang et al., 2015; Thapa et al., 2017).

$$\text{Cell Viability}(\%) = OD_{sample} - OD_{blank} / OD_{control} - OD_{blank} \times 100\%$$

Analysis of the Targeting Property of PNA-Modified Liposomes Coloaded With IRICAP *In Vivo*

To study the targeting property of liposomes *in vivo*, fluorescent-labeled liposomes were prepared by using Cy7 (Meilun Biotechnology Corporation, Dalian, China) at a mass ratio of phospholipid:Cy7 of 50:1 instead of the drugs encapsulated into the hydrophilic phase of liposomes.

BALB/C-nu mice (male, 4–5 weeks old, 14 ± 2 g, Viton River Laboratory Animal Technology Corporation, Beijing, China) were selected. All experiments met the institution's animal care standards and were approved by the Ethical Review Committee of Weifang Medical College. SW620 cells in the logarithmic growth phase were resuspended to 5×10^7cells/mL with saline and subcutaneously injected with 0.2 ml of cell suspension to construct a subcutaneous tumor-bearing nude mouse model.

When the mean tumor volume reached 100 mm^3, tumor-bearing nude mice were divided equally into three groups (n = 6) for targeted property analysis *in vivo* (Jiang et al., 2016). The distribution of fluorescence signals was observed at 1, 2, 4, 8, 12, 24, and 48 h after tail vein injection of Cy7, Cy7-Lips, and Cy7-PNA-Lips (2.5 mg/kg) by using a small animal imaging system *in vivo* (PerkinElmer Inc., United States) (Song et al., 2014; Xiong et al., 2017). Nude mice were euthanized 48 h after injection, and the heart, liver, spleen, lung, and kidney tumors were photographed to analyze the distribution of fluorescence in vital organs and tumor tissues.

Analysis of the Antitumor Ability of PNA-Modified Liposomes Coloaded With IRICAP *In Vivo*

Tumor-bearing nude mice were separated equally into 4 groups (n = 6) for antitumor experiments *in vivo*. Normal saline, IRI/CAP, IRI/CAP-Lips, and IRI/CAP-PNA-Lips (C_{IRI} = 20 mg/kg) were injected intraperitoneally every 4 days starting from the first day of grouping, and the body weight and tumor volume of nude mice were measured every other day (Guichard et al., 2001). After 20 days of treatment, tumor-bearing nude mice were euthanized; vital organs and tumor tissues were taken, photographed, and weighed; and the tumor inhibition rate (TIR) was calculated for each treatment group. The tumor tissues were fixed, embedded, and sectioned, and Ki-67 staining was performed to analyze the inhibitory ability of different treatments on the proliferation of tumor cells.

$$\text{Tumor volume}\left(mm^3\right) = \text{length} \times \text{width}^2 \times 0.5$$

$$\text{Tumor inhibition rate (TIR)} = 1 - V_{\text{treatment group}} / V_{\text{control group}} \times 100\%$$

Systemic Toxicity Assessment of PNA-Modified Liposomes Coloaded With IRICAP

Heart, liver, spleen, lung, and kidney tumors from the euthanized tumor-bearing nude mice were fixed, paraffin-embedded, and sectioned. H&E staining was performed on the tissue sections, and the sections were observed under a 20× microscope to determine whether obvious organic lesions appeared in each vital organ.

Heart blood was drawn from the SW620 tumor-bearing nude mouse model after 20 days of treatment, and the plasma was centrifuged for serum biochemical parameter analysis (Yu et al., 2019).

RESULTS

Synthesis and Characterization of DSPE-PEG2K-PNA

DSPE-PEG2K was bonded to peanut agglutinin (PNA) through an amide bond (-CO-NH-). The presence of the characteristic peaks of both DSPE-PEG2K and PNA in the infrared spectroscopy (IR) spectrum of DSPE-PEG2K-PNA (**Figure 1B**) indicated that DSPE-PEG2K-PNA was successfully synthesized. The SDS–PAGE results also indicated that PNA was ligated to DSPE-PEG2K. PNA is a homotetramer with a molecular weight of approximately 120 kDa and a monomeric molecular weight of approximately 32 kDa, which was consistent with the band on the SDS–PAGE gel. The band of DSPE-PEG2K-PNA showed that the molecular weight was heavier than the molecular weight of PNA. In addition, PEG-specific staining clearly marked the DSPE-PEG2K-PNA band in yellow, while the PNA band had no color. These results suggest that we successfully synthesized DSPE-PEG2K-PNA (**Figure 1C**; **Supplementary Figure S1D**).

The Optimal Synergistic Ratio of Irinotecan Hydrochloride and Capecitabine Is 3:1

The ratio of irinotecan hydrochloride (IRI) and capecitabine (CAP) in clinical synergistic treatment is approximately 1:8 (Kerr, 2002). To evaluate the optimal synergistic ratio of IRI

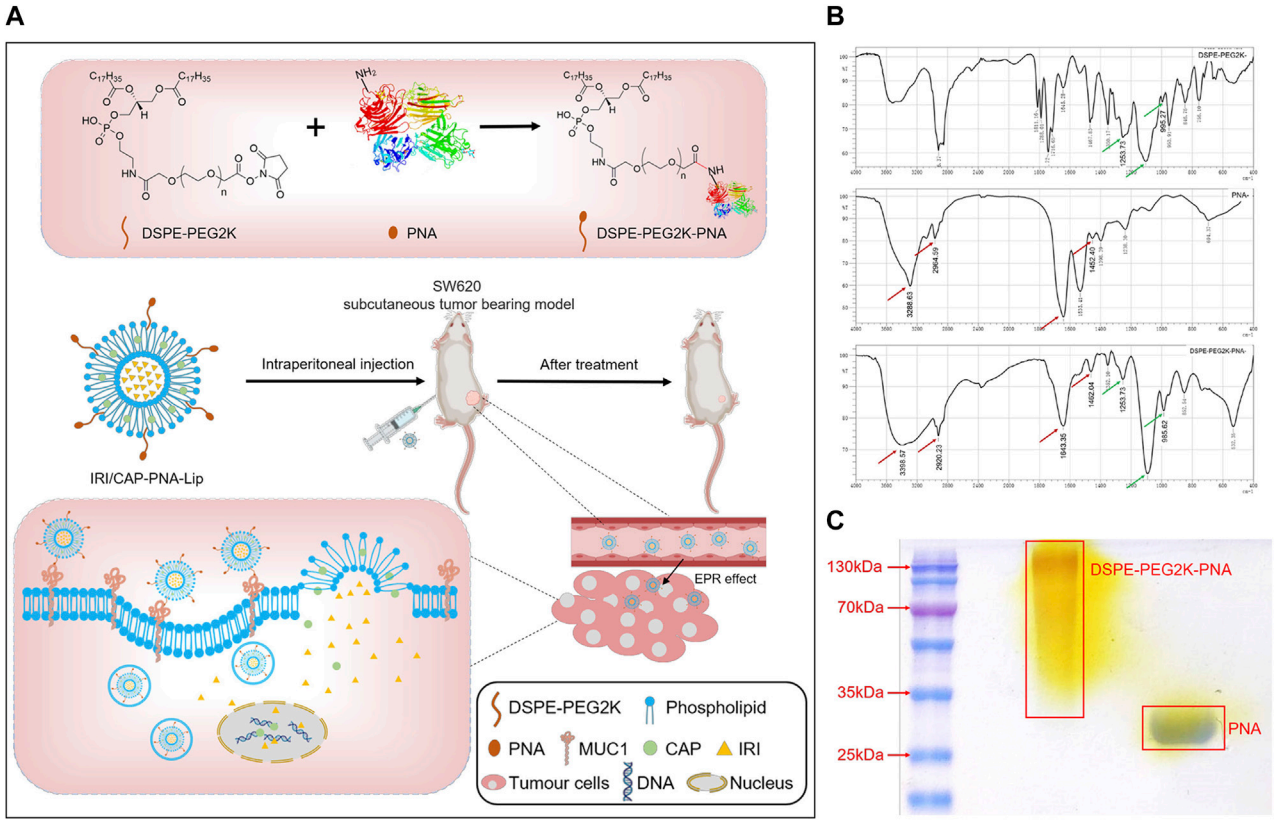

FIGURE 1 | (A) Schematic diagram of the preparation of PNA-modified liposomes and ligand–receptor-mediated targeting mechanisms for tumor tissue recognition. Liposomes loaded with IRICAP were modified with PNA as the ligand. PNA specifically interacts with MUC1, which is highly expressed in colorectal cancer cells. IRI and CAP are released into cells and bind to DNA to inhibit nucleic acid synthesis, thus enhancing the efficacy of anti-colorectal cancer. **(B)** Infrared spectroscopy identified the successful synthesis of DSPE-PEG2K-PNA. **(C)** SDS–PAGE to identify PNA was ligated to DSPE-PEG2K.

and CAP in the four colorectal cancer cell lines *in vitro*, the cell viability assay was performed by the MTS assay, and the combination index (CI) was compared (**Figure 2**). The CI of the four cell lines at different ratios was less than 1, suggesting that the combination of IRI and CAP exerted a synergistic effect. Caco-2, HT29, and SW620 had the lowest CI values when IRI: CAP was 3:1. The low CI values of HCT116 were 0.52 and 0.58 at IRI:CAP of 1:8 and 3:1, respectively (**Table 1**). The lowest CI values for Caco-2, HT29, and SW620 cells were observed at IRI: CAP of 3:1, and the lowest CI values were observed in HCT116 cells. We determined this ratio as the optimal synergistic ratio of the two drugs.

Characterization of PNA-Modified Liposomes Coloaded With CAPIRI

The particle size of PNA-modified liposomes coloaded with IRICAP (IRI/CAP-PNA-Lips) was 122.6 ± 0.58 nm. The polymer dispersity index (PDI) of coloaded PNA-modified liposomes was less than 0.2, which indicated that the particle size was dispersed equally (**Figures 3A,B**). For IRI/CAP-PNA-Lips, the encapsulation efficiency (EE) of IRI and CAP was 89.45 ± 0.015% and 7.56 ± 0.014%, respectively. The drug load (DL) of IRI and CAP was 17.98 ± 0.003% and 6.18 ± 0.013%, respectively (**Table 2**; **Supplementary Figures S1A–C**). The DL ratio of IRI and CAP in the coloaded PNA-modified liposomes was 3:1, which was consistent with the optimal synergistic ratio.

A drug release assay was performed *in vitro* to evaluate the sustained release effect and maximum cumulative release of coloaded liposomes. The maximum cumulative release of free drugs was achieved at 8 h, with over 80% of IRI and 60% of CAP. The cumulative release curves of IRI and CAP in coloaded liposomes can be divided into two phases: initial rapid release and sustained release. IRI in IRI/CAP-PNA-Lips and IRI/CAP-Lips had a rapid release in the first 8 h, and the rapid release phase of CAP in IRI/CAP-PNA-Lips and IRI/CAP-Lip was reached in the first hour. After that, the curve gradually changed to a sustained release phase. Finally, the maximum cumulative release of IRI was reached at 24 h in IRI/CAP-PNA-Lips and IRI/CAP-Lips, with maximum release rates of 72.9 ± 5.3% and 64.6 ± 2.9%, respectively. The maximum cumulative release of CAP in IRI/CAP-PNA-Lips and IRI/CAP-Lips had maximum release rates of 50.7 ± 3.2% and 53.6 ± 5.5%, respectively (**Figures 3C,D**). The particle size and potential of each type of liposome were stable, and no significant changes were observed after

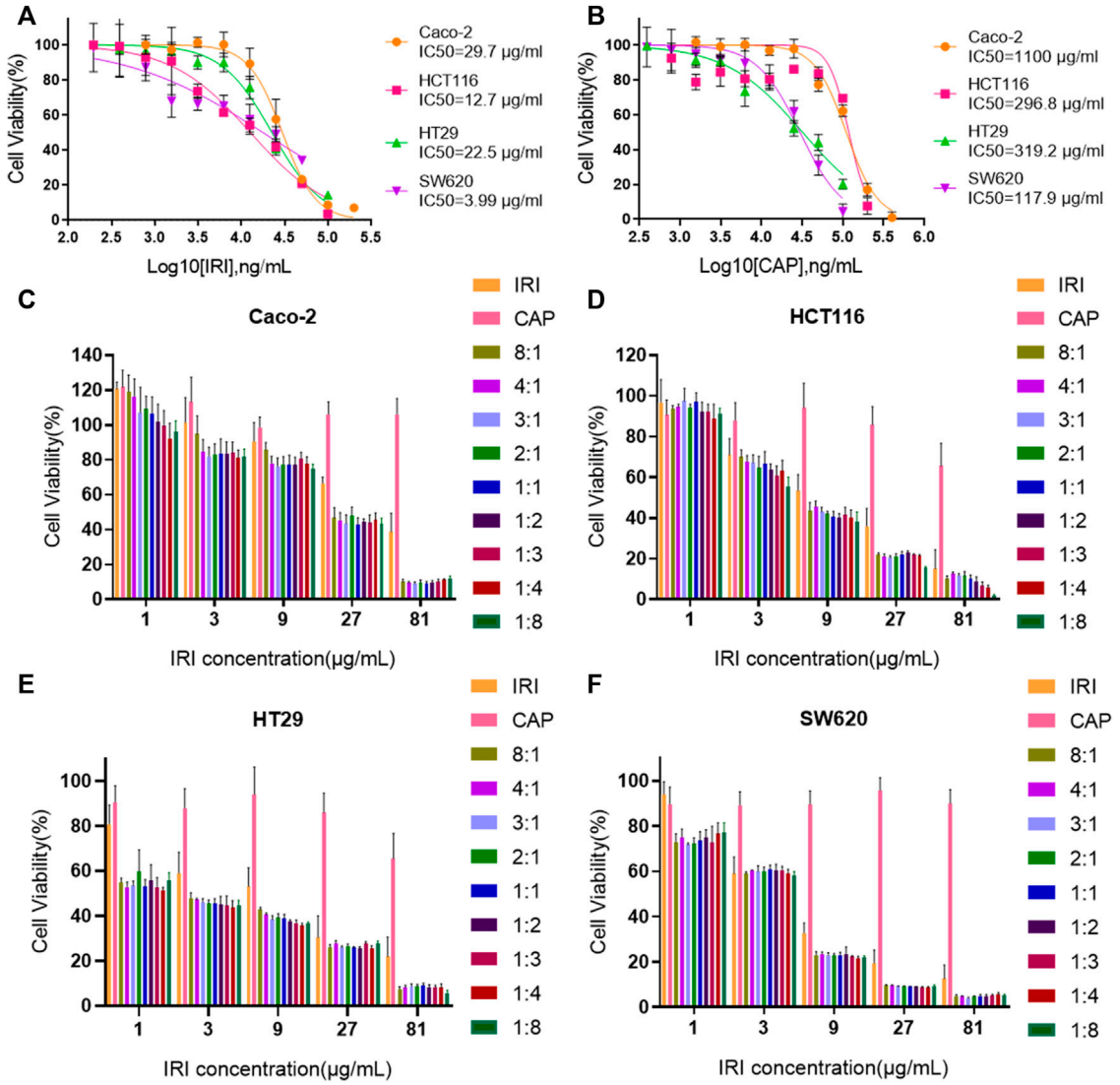

FIGURE 2 | The optimal synergistic ratio of irinotecan hydrochloride and capecitabine was 3:1. **(A,B)** IC50 value analysis of CAP and IRI alone in Caco-2, HCT116, HT29, and SW620 cell lines. **(C–F)** Effect of IRI and CAP on the viability of Caco-2, HCT116, HT29, and SW620 cells at different ratios.

TABLE 1 | CI values for four colorectal cancer cell lines at different combination ratios of IRI/CAP.

	Caco-2			HCT116			HT29			SW620		
	IC50 (IRI)	IC50 (CAP)	CI	IC50 (IRI)	IC50 (CAP)	CI	IC50 (IRI)	IC50 (CAP)	CI	IC50 (IRI)	IC50 (CAP)	CI
IRI	29.69	–	–	12.6	–	–	22.5	–	–	9.35	–	–
CAP	–	1100	–	–	296.8	–	–	319.2	–	–	117.9	–
8:01	26.3	3.29	0.89	7.44	0.93	0.59	5.01	0.63	0.22	3.2	0.4	0.35
4:01	22.1	5.53	0.75	7.57	1.9	0.61	5.11	1.28	0.23	2.9	0.725	0.32
3:01	20.1	6.7	0.68	7.22	2.41	0.58	4.89	1.63	0.22	2.7	0.9	0.29
2:01	22.2	11.1	0.76	6.78	3.39	0.55	4.98	2.49	0.22	3.1	1.55	0.34
1:01	20.4	20.4	0.71	6.94	6.94	0.57	5.08	5.08	0.24	2.7	2.7	0.31
1:02	20.6	41.2	0.73	6.44	12.88	0.55	5.12	10.24	0.26	2.7	5.4	0.33
1:03	21.4	64.2	0.78	6.17	18.51	0.55	4.96	14.88	0.26	2.5	7.5	0.33
1:04	20.6	82.4	0.77	6.03	24.12	0.56	4.89	19.56	0.27	2.3	9.2	0.32
1:08	19.5	156	0.8	4.9	39.2	0.52	4.86	38.88	0.33	2.6	20.8	0.45

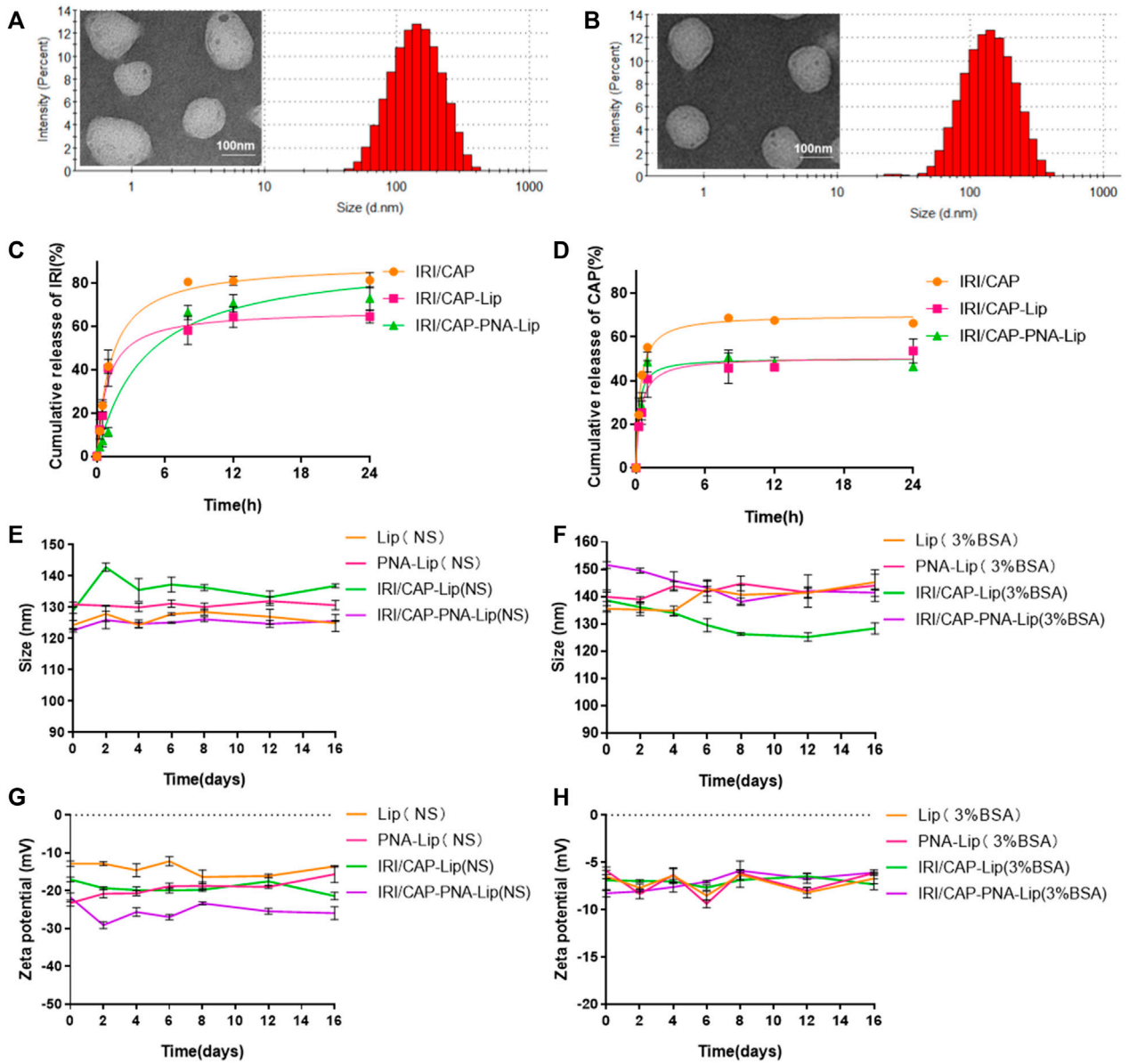

FIGURE 3 | Analysis of the drug release capacity and stability of different types of drug-loaded liposomes. **(A,B)** Particle size histograms and transmission electron microscopy (TEMik) images of IRI/CAP-Lips and IRI/CAP-PNA-Lips. **(C)** Cumulative drug release profiles of IRI-loaded liposomes in PBS at 37°C. **(D)** Cumulative release curves of CAP-loaded liposomes in PBS at 37°C. **(E,F)** Folding graphs of particle size changes of different types of liposomes stored in saline or 3% BSA at 4°C for 16 days. **(G,H)** Folding graphs of potential changes of different types of liposomes stored in saline or 3% BSA at 4°C for 16 days. The data are presented as the mean ± SD (n = 3).

TABLE 2 | Characteristics of different types of liposomes (mean ± SD, n = 3).

	Size (nm)	PDI	Zeta (mV)	EE IRI (%)	EE CAP (%)	DL IRI (%)	DL CAP (%)
Lips	126.6 ± 1.58	0.16 ± 0.04	−12.9 ± 0.70	–	–	–	–
PNA-Lips	130.9 ± 0.80	0.12 ± 0.02	−23.3 ± 0.81	–	–	–	–
IRI/CAP-Lips	126.7 ± 2.51	0.18 ± 0.05	−15.5 ± 0.56	57.67 ± 0.090	4.63 ± 0.020	11.53 ± 0.020	3.79 ± 0.010
IRI/CAP-PNA-Lips	122.6 ± 0.58	0.17 ± 0.03	−21.3 ± 0.49	89.45 ± 0.015	7.56 ± 0.014	17.98 ± 0.003	6.18 ± 0.013

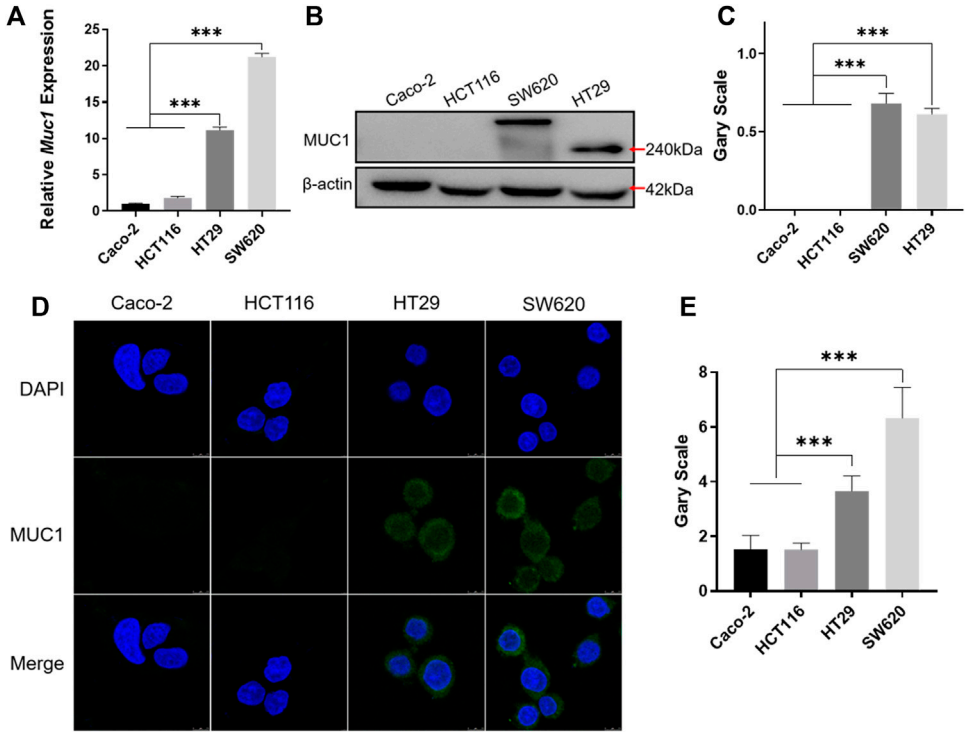

FIGURE 4 | Identification of MUC1 expression in colorectal cancer cells. **(A)** Real-time quantitative PCR analysis of MUC1 expression at the mRNA level in Caco-2, HCT116, HT29, and SW620 cell lines. **(B)** Western blot analysis of MUC1 expression in four cell lines. **(C)** Quantitative histogram of Western blot results. **(D)** Cellular immunofluorescence assay for the identification of MUC1 expression in four cell lines. **(E)** Quantitative histogram of cellular immunofluorescence results. ***$p < 0.001$.

storage in physiological saline or 3% BSA for half a month at 4°C (**Figures 3E–H**).

MUC1 Was Highly Expressed in the Colorectal Cancer Cell Lines HT29 and SW620

The results of real-time quantitative PCR and Western blotting showed that MUC1 was highly expressed in HT29 and SW620 cells (**Figures 4A–C**). Furthermore, immunofluorescence using a MUC1-specific antibody showed that the green fluorescence intensity was significantly higher in HT29 and SW620 cells than in Caco-2 and HCT116 cells (**Figures 4D,E**). The experiments showed that MUC1 was not expressed in the colorectal cancer cell lines Caco-2 and HCT116, while it was highly expressed in the colorectal cancer cell lines HT29 and SW620.

Enhanced Cellular Uptake of PNA-Modified Liposomes by MUC1-Positive Colorectal Cancer Cell Lines

To explore the targeting efficiency of PNA-modified liposomes to MUC1-positive cells, PNA-modified liposomes loaded with FITC and rhodamine (Rhb) were prepared. The cellular uptake of FITC and Rhb in the four cell lines showed distinct results. Two MUC1-negative cell lines, Caco-2 and HCT116, showed no significant difference in the cellular uptake of FITC and Rhb in the FITC/Rhb-PNA-Lip groups compared to the FITC/Rhb-Lip groups. The fluorescence signals of the FITC/Rhb-PNA-Lip groups were significantly enhanced in HT29 and SW620 cells, which are MUC1-positive cell lines (**Figure 5**; **Supplementary Figures S2A–D**). The aforementioned results suggest that PNA-modified liposomes exhibit effective MUC1-targeting properties in colorectal cancer cells and could work as efficient drug delivery carriers to MUC1-positive colorectal cancer.

PNA-Modified Liposomes Coloaded With IRICAP Significantly Inhibited the Viability of MUC1-Positive Colorectal Cancer Cell Lines *In Vitro*

Based on the effectiveness of cellular uptake, the MTS assay was used to further evaluate the inhibitory effect of PNA-modified liposomes coloaded with IRICAP on the viability of colorectal cancer cell lines. The results showed that in the MUC1-positive colorectal cancer cell line HT29, the IC50 values for the IRI/CAP-Lip and IRI/CAP-PNA-Lip groups were 5.8 μg/ml and 5.1 μg/ml, respectively. Another MUC1-positive colorectal cancer cell line, SW620, had IC50 values for the IRI/CAP-Lip and IRI/CAP-PNA-Lip groups of 5.4 μg/ml and 4.7 μg/ml, respectively. There was no significant difference in the cytotoxicity of the IRI/CAP-Lip and IRI/CAP-PNA-Lip treatment groups (**Figures 6A–D**).

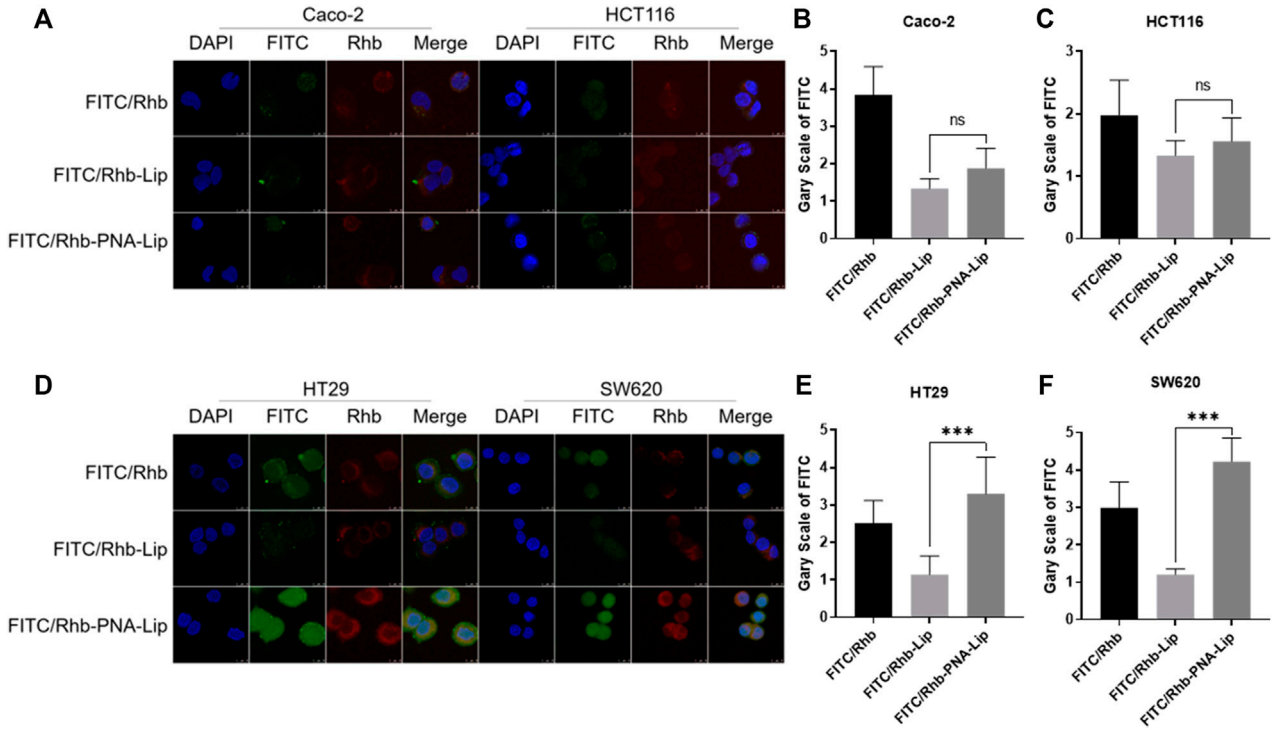

FIGURE 5 | CLSM analysis showed that PNA-modified liposomes enhance the cellular uptake of drugs by MUC1-positive cells. **(A)** CLSM observation of the distribution of fluorescence signals in Caco-2 and HCT116 cells. **(B,C)** Quantitative histograms of FITC fluorescence signals in Caco-2 and HCT116 cells. **(D)** CLSM observation of the distribution of fluorescence signals in HT29 and SW620 cells. **(E,F)** Quantitative histograms of FITC fluorescence signals in HT29 and SW620 cells. The data are presented as the mean ± SD (n = 3). ***$p < 0.001$.

This result may be due to the complete cellular uptake of the liposomes coloaded with CAPIRI by all cells after 72 h. Therefore, HT29 and SW620 cells were treated individually for 24 h, and we discovered that IRI/CAP-PNA-Lips had a stronger inhibitory effect at IRI concentrations up to 50 μg/ml (**Supplementary Figures S3A,B**).

When a single concentration of coloaded liposomes (C_{IRI} = 50 μg/ml) was used to treat cells for 24 h, the viability of HT29 and SW620 cells was significantly inhibited by PNA-modified liposomes coloaded with IRICAP compared to unmodified liposomes, which was consistent with the result of 100 μg/ml IRI in coloaded liposomes (**Figures 6E–H**; **Supplementary Figures S3C–J**).

PNA-Modified Liposomes Coloaded With IRICAP Promote Apoptosis in MUC1-Positive Colorectal Cancer Cells *In Vitro*

Based on the results of the MTS assays, we treated Caco-2, HCT116, HT29, and SW620 cells with coloaded liposomes at an IRI concentration of 50 μg/ml for 24 h. The effect of coloaded liposomes on the apoptosis of cells was evaluated using the Annexin V/PI double-staining method. The effects of IRI/CAP-Lips and IRI/CAP-PNA-Lips on the apoptosis of MUC1-negative Caco-2 and HCT116 cells were not significant. For MUC1-positive HT29 and SW620 cells, the apoptosis rate in the IRI/CAP-PNA-Lip group was 1.3-fold and 1.9-fold higher than that in the IRI/CAP-Lip group, respectively. The results suggested that PNA-modified liposomes coloaded with IRICAP significantly upregulated the apoptosis in MUC1-positive colorectal cancer cell lines (**Figure 7**).

PNA-Modified Liposomes Significantly Increase MUC1-Targeting Properties in Colorectal Cancer Tumors *In Vivo*

Small animal live-imaging techniques were used to observe the distribution of Cy7 in tumor uptake to assess the targeting ability of PNA-modified liposomes *in vivo*. Fluorescence signals could be observed in the whole body 1 h after tail vein injection of Cy7, which barely disappeared after 12 h in the tumor tissue. For the Cy7-Lip and Cy7-PNA-Lip groups, fluorescence signals were observed in the whole body between 1 and 2 h after injection. However, there was slower decay of fluorescence signals in the tumor tissue, which was different from the free drug conditions. After 2 h, the fluorescence signals of the Cy7-Lip and Cy7-PNA-Lip groups were consistently stronger than those of the Cy7 group, and the fluorescence signal of the Cy7-PNA-Lip group was consistently stronger than that of the Cy7-Lip group.

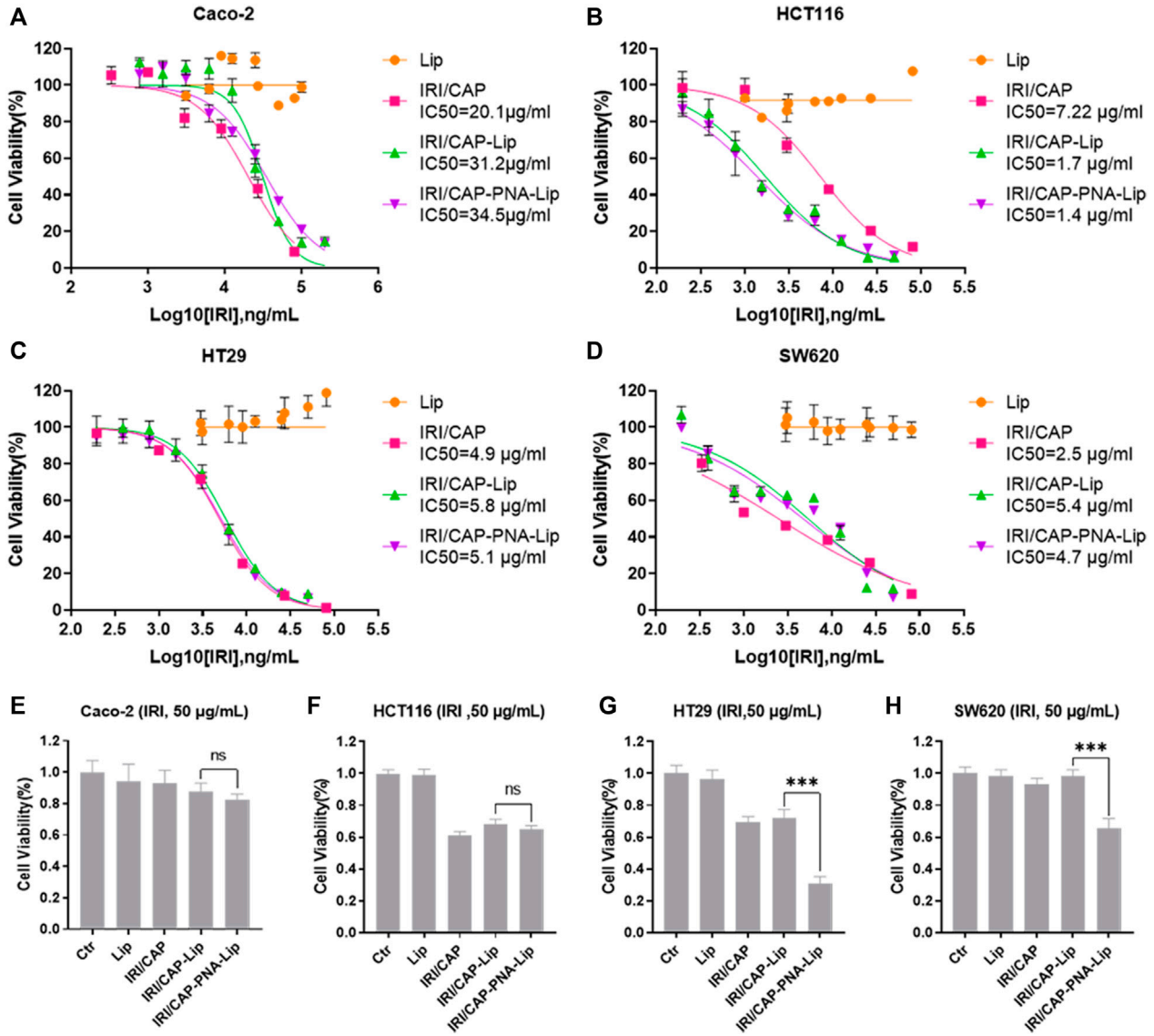

FIGURE 6 | IRI/CAP-PNA-Lips significantly inhibited the viability of MUC1-positive colorectal cancer cell lines *in vitro*. **(A–D)** Cytotoxicity analysis of coloaded liposomes in Caco-2, HCT116, HT29, and SW620 cell lines. **(E–H)** Effect of an IRI concentration of 50 μg/ml on cell viability after treatment of Caco-2, HCT116, HT29, and SW620 cell lines for 24 h. The data are presented as the mean ± SD (n = 3). ***p < 0.001.

The Cy7-PNA-Lip group showed the strongest fluorescence signals in the tumor tissue at 4 h after injection, which persisted in the tumor tissues up to 48 h after injection (**Figure 8B**). To verify that Cy7-PNA-Lips could improve the accumulation of drugs in tumor tissues and the targeted delivery efficiency, tumor-bearing nude mice were euthanized 48 h after injection (**Figure 8C**; **Supplementary Figure S2E**). Fluorescence accumulation was observed in the primary organs and tumor tissues. The Cy7-PNA-Lip group showed the strongest signals (**Figure 8D**). The results were consistent with the trend observed with cellular uptake, which suggested that PNA-modified liposomes could deliver targets and improve cellular uptake to improve drug accumulation in tumor tissues.

PNA-Modified Liposomes Coloaded With IRICAP Have Shown Improved Antitumor Ability *In Vivo*

Four groups of tumor-bearing nude mice were treated with physiological saline, IRI/CAP, IRI/CAP-Lips, or IRI/CAP-PNA-Lips to evaluate the antitumor ability of PNA-modified liposomes coloaded with IRICAP *in vivo*. There was no significant variation in the bodyweight of mice in the four groups after treatment (**Figure 9C**). All three dosing groups exhibited antitumor properties, but the tumor volume and weight of the IRI/CAP-PNA-Lip group were the lowest and were even lower than those of the IRI/CAP-Lip group (**Figures 9B,D**). The results showed that the IRI/CAP-PNA-

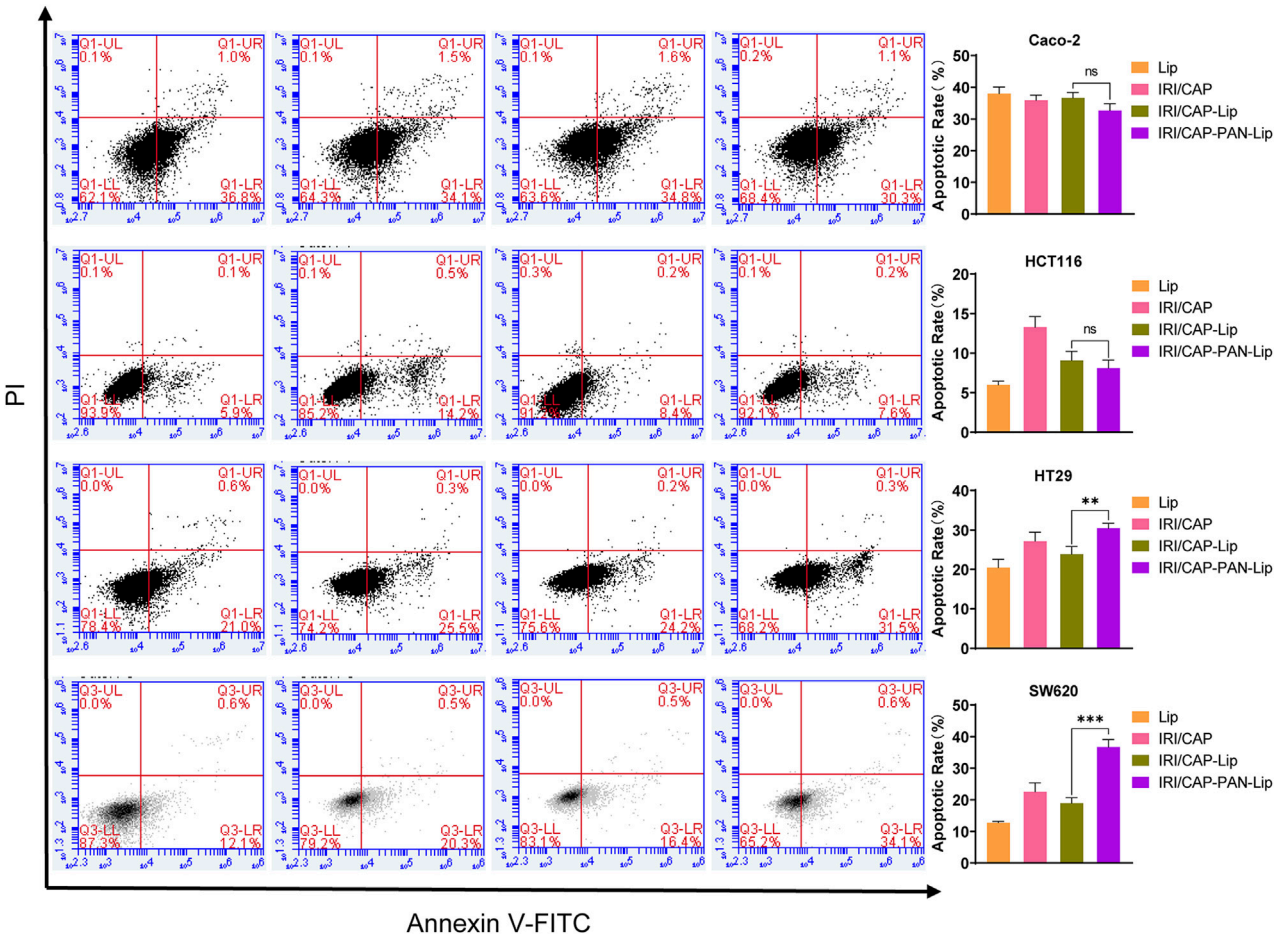

FIGURE 7 | IRI/CAP-PNA-Lips significantly induced apoptosis compared to IRI/CAP-Lips in HT29 and SW620 cell lines. The effects of Lips, IRI/CAP, IRI/CAP-Lips, and IRI/CAP-PNA-Lips on the apoptosis of colorectal cancer cell lines and their quantitative histograms. The data are presented as the mean ± SD ($n = 3$). $^{**}p < 0.01$. $^{***}p < 0.001$.

Lip group had the strongest antitumor effect, with the tumor inhibition rate (TIR) reaching 12.69%, which was 9.6-fold better than that of the free drug group (**Figures 9E,F**).

Systemic Toxicity of PNA-Modified Liposomes Coloaded With IRICAP *In Vivo*

To evaluate the systemic toxicity of IRI/CAP-PNA-Lips *in vivo*, H&E staining was performed on the heart, liver, spleen, lung, and kidney. No histopathological abnormalities were observed in the four groups (**Figure 10A**). The tumor tissues of the saline group were closely arranged with large nuclei, while the tumor tissues of the IRI/CAP-PNA-Lip group presented the highest degree of apoptosis and necrosis, reduced cytokinesis, agglutination of chromatin in the nuclei, and a large number of vacuoles. Immunohistochemistry results showed that Ki-67 expression was decreased in the tumor tissues of the IRI/CAP-PNA-Lip group compared to the IRI/CAP-Lip group, which suggested that PNA-modified liposomes coloaded with IRICAP had a stronger antitumor cell proliferative effect (**Figure 10B**).

Plasma biochemical analyses were used to assess the effects of PNA-modified liposomes coloaded with IRICAP on the major metabolic organs of tumor-bearing mice. The results showed that except for the creatinine (Cr) value in the free drug group, which was slightly higher than that in the saline group ($p < 0.01$), the biochemical indices of urea, alanine aminotransferase (ALT), alkaline phosphatase (ALP), and aspartate aminotransferase (AST) showed no significant variation. The aforementioned results suggest that PNA-modified liposomes coloaded with IRICAP do not produce any systemic toxicity in the experimental mice (**Figures 10C–G**).

DISCUSSION

The desired synergistic effect relies on well-controlled drug dose matching and duration of effect. Peng et al. (2021) used liposomes to codeliver adriamycin and sorafenib, and the results showed that liposomes could achieve codelivery of the drugs and effectively improve the synergistic effect of the drugs.

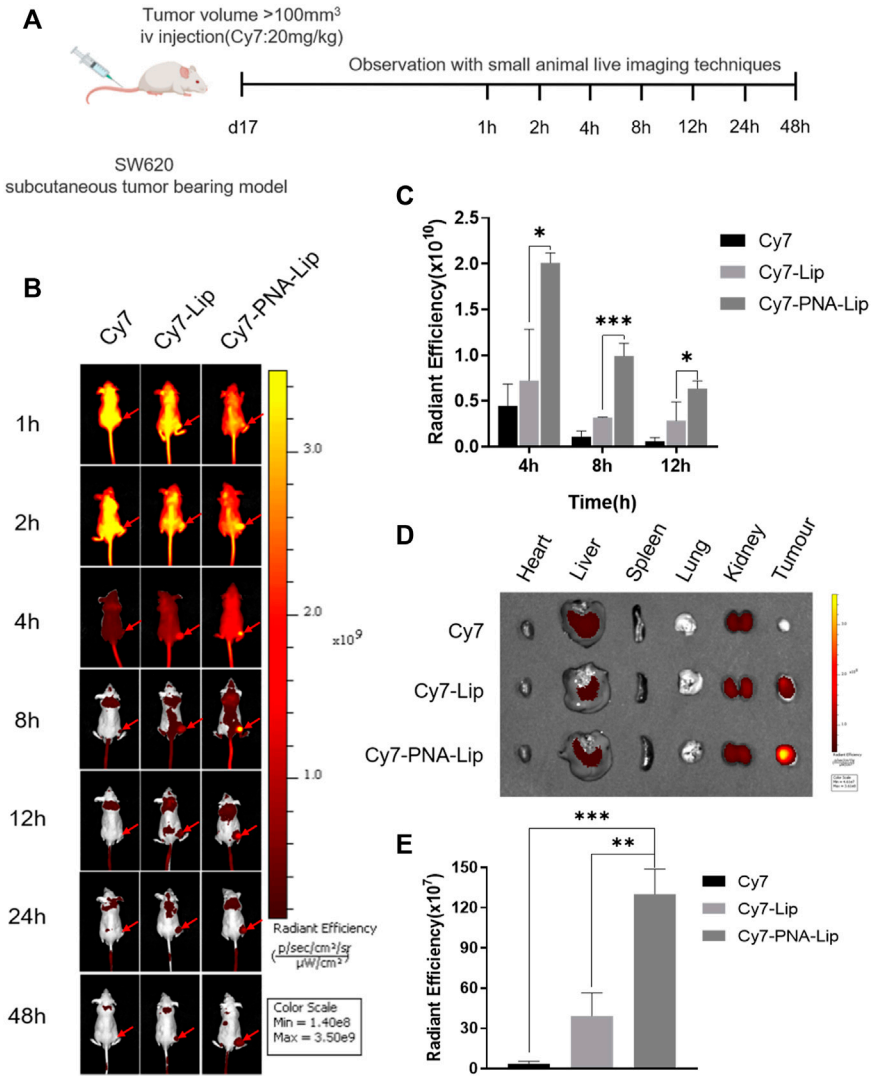

FIGURE 8 | PNA-modified liposomes exhibited effective MUC1-targeting properties in colorectal cancer tumors. **(A)** Design principles for the analysis of the targeting ability of PNA-modified liposomes *in vivo*. **(B)** Distribution of Cy7 in tumor-bearing nude mice after tail vein injection. **(C)** Quantitative histogram of fluorescence signals at tumor sites at different points in time. **(D)** Distribution of Cy7 in vital organs and tumor tissues after 48 h. **(E)** Quantitative histograms of fluorescence signals in tumors. The data are presented as the mean ± SD (n = 3). $^{*}p < 0.05$. $^{**}p < 0.01$. $^{***}p < 0.001$.

Although coloaded liposomes could improve drug efficacy, they are not specific for tumor tissue. Therefore, ligand-modified liposomes for active targeted drug delivery to enhance antitumor ability can be synthesized. IRI and CAP are synergistic chemotherapies approved by the FDA for treating colorectal cancer, but ligand-modified liposomes coloaded with IRICAP have not been reported (Chiorean et al., 2020). In this study, PNA-modified liposomes coloaded with IRICAP were prepared to specifically and actively target MUC1-positive colorectal cancer tumor tissue to further improve the synergistic efficacy. This drug delivery system can improve drug efficacy and reduce drug dosage while reducing drug concentrations in normal tissues and toxic side effects (Caliskan et al., 2019).

Taking into account the different water solubilities of CAP and IRI, they were encapsulated in hydrophobic or hydrophilic phases. This construction contributed to protecting the chemical stability of the two drugs during preparation, preservation, and blood transport while facilitating the stability of coloaded liposomes (Huang et al., 2019). Nanomedicines with particle size less than 200 nm can accumulate in tumor tissues through the enhanced permeability and retention effect (EPR). In this study, the particle size of each type of liposome fluctuated within approximately 120–130 nm, which is also close to the range reported in other studies (Kalyane et al., 2019; Park et al., 2019; Tan et al., 2019). The PDI of drug-loaded liposomes was between 0.1 and 0.3 in most studies, and the PDI of the liposomes in this study ranged between 0.12 and 0.18 (<0.2), indicating a

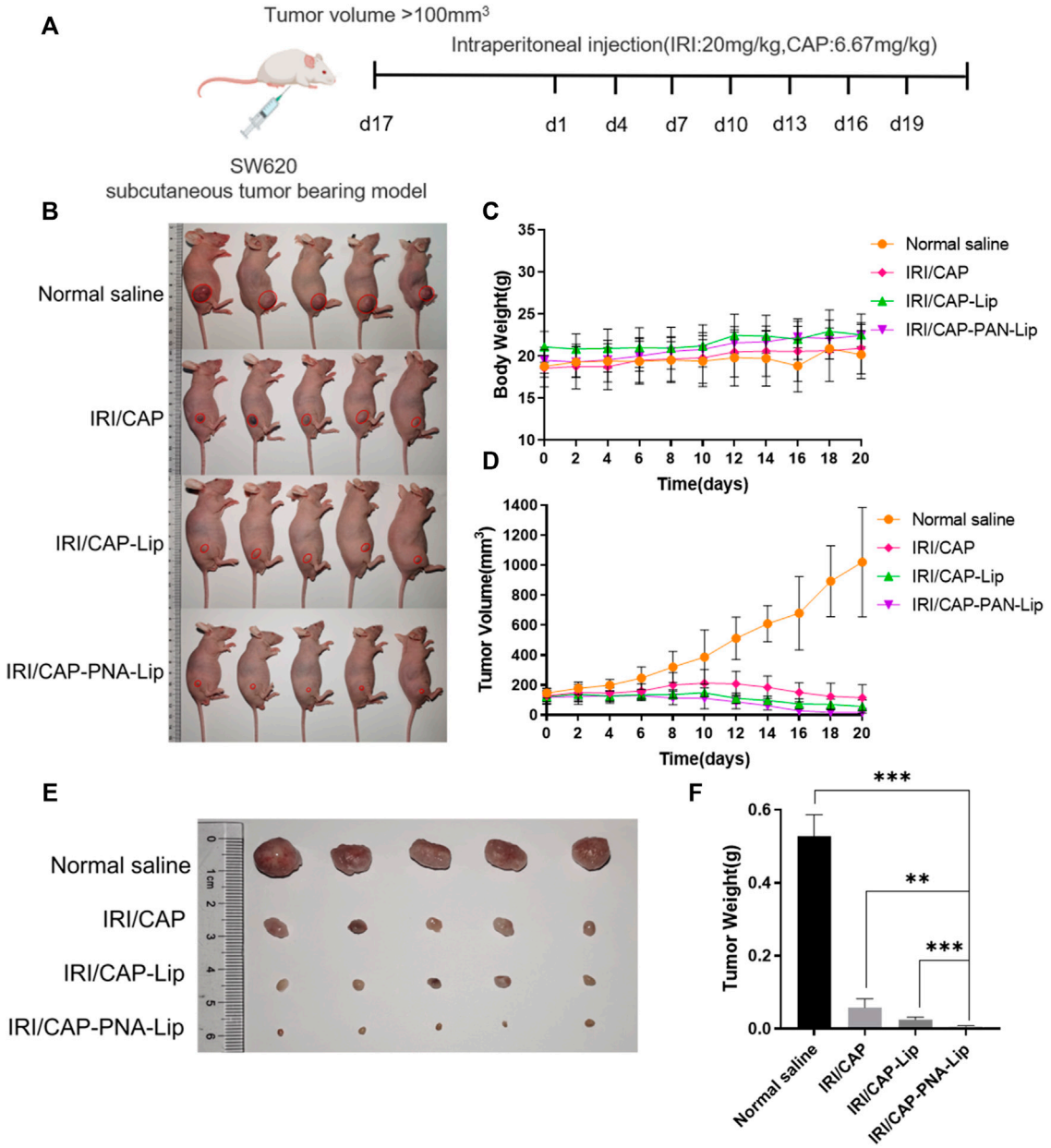

FIGURE 9 | PNA-modified liposomes significantly enhance the antitumor efficacy of the drug. **(A)** Design principles for the analysis of the antitumor abilities of PNA-modified liposomes *in vivo*. **(B)** Photos of tumor-bearing nude mice in each group after 20 days of treatment. **(C)** Changes in the bodyweight of the tumor-bearing nude mice. **(D)** Folding line graph of the change in tumor volume. **(E)** Photographs of tumors. **(F)** Histograms of tumor weights. The data are presented as the mean ± SD (n = 5). $^{**}p < 0.01$. $^{***}p < 0.001$.

good dispersion of the liposomes (Yang et al., 2015; Li et al., 2017). To enhance the efficacy of coloaded liposomes, we prepared negative potential liposomes that can protect liposomes from the reticuloendothelial system (RES) and effectively improve the circulation time in the blood (Ghosh et al., 2021). In addition, we hoped that the coloaded liposomes will accumulate and release as much of the drug as possible in the tumor tissue during circulation in blood. The 24-h maximum cumulative drug release of IRI and CAP in IRI/CAP-PNA-Lips was less than 60%, and sustained drug release was successfully achieved compared to the free drug *in vitro*, which reduced unnecessary drug release during circulation in blood (Allen and Cullis, 2013; Yalcin et al., 2018).

By Western blotting, we found that the molecular weight of MUC1 in HT29 and SW620 cells was not consistent, which was consistent with other studies showing that the different degrees of extracellular glycosylation of MUC1 cause the molecular weight to range from 240 to 500 kDa (Nath and Mukherjee, 2014; Apostolopoulos et al., 2015). Subsequently, cellular uptake experiments showed that the coloaded liposomes achieved

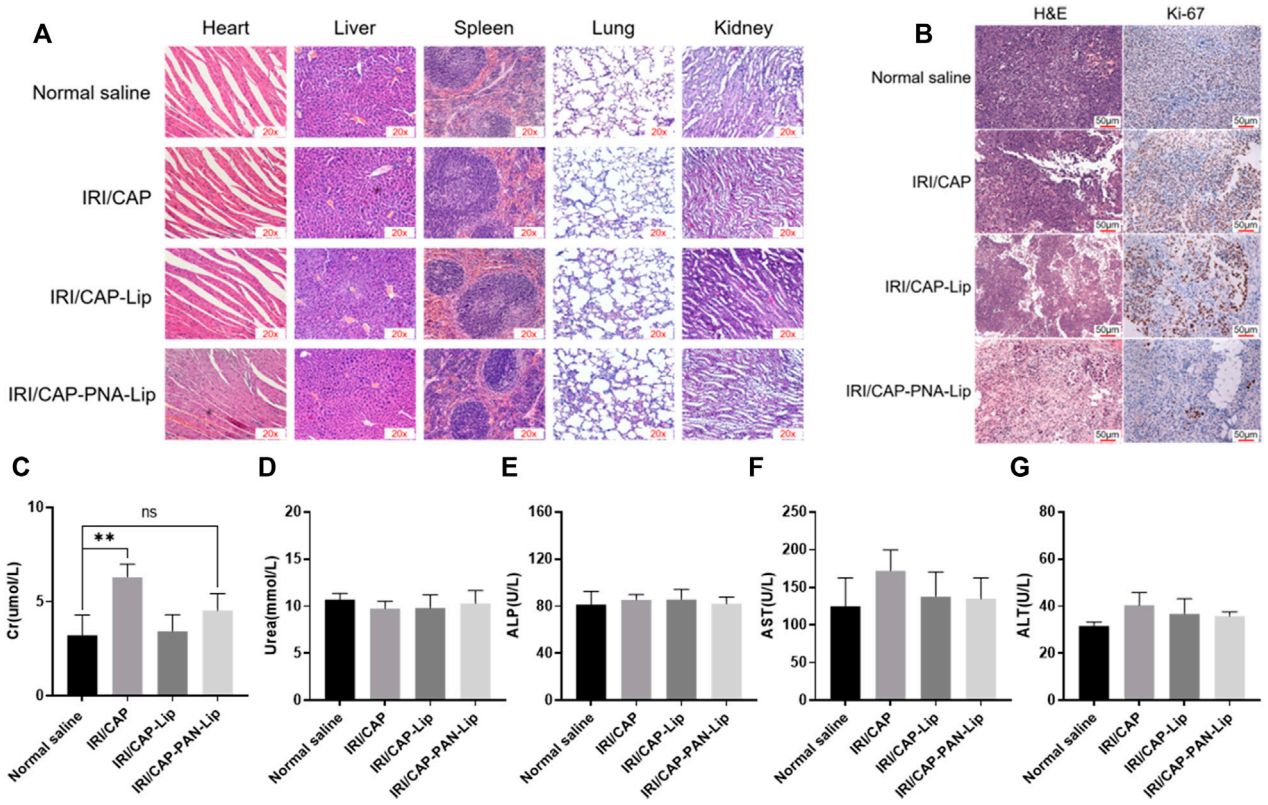

FIGURE 10 | PNA-modified liposomes had no systemic toxicity and enhanced the antiproliferative ability of drugs on MUC1-positive tumors. **(A)** H&E staining of vital organs. No significant pathological changes were observed in any group except for the tumor tissue. 20x **(B)** Ki-67 staining of tumors in different treatment groups. The plasma biochemical analysis of the tumor-bearing nude mice showed no significant difference compared with the saline group except for Cr. **(C)** Creatinine, Cr. **(D)** Urea. **(E)** Alkaline phosphatase, ALP. **(F)** Aspartate aminotransferase, AST. **(G)** Alanine aminotransferase, ALT. $^{**}p < 0.01$.

same-time and same-place drug delivery, which was beneficial in improving the synergistic drug efficacy (Zhang et al., 2017; Du et al., 2020). Meanwhile, the fluorescence signals of FITC/Rhb-PNA-Lips were significantly higher than those of the FITC/Rhb-Lip group due to the specific binding of PNA-modified liposomes to MUC1, which enhanced the cellular uptake of liposomes, and the *in vivo* targeting analyses were consistent with the results *in vitro* (Tang et al., 2020). When we further analyzed the ability of PNA-modified liposomes coloaded with IRICAP to inhibit cell viability *in vitro*, interestingly there was no significant difference in MUC1-positive cells in the IRI/CAP-PNA-Lip group compared to the IRI/CAP-Lip group, which has also been reported in other studies (Zhang et al., 2018). Based on the analysis of the cellular uptake results, we reduced the drug treatment time to 24 h after each group, and IRI/CAP-PNA-Lips showed significant cell viability inhibition compared to the control group. The IRI/CAP-PNA-Lip group showed excellent results in the antitumor assay *in vivo*, with a continuous decrease in tumor volume with a tendency to completely disappear. As a result, we had to euthanize the nude mice no longer than 20 days after treatment. Combined with our previous studies, we suggest that the potential antitumor mechanism of IRI/CAP-PNA-Lips is that colorectal cancer cells improve their uptake of liposomes through receptor-mediated endocytosis, promoting drug entry into the nucleus and inhibiting DNA replication and synthesis, which specifically blocks the S phase of the cell cycle, thereby inhibiting the proliferation of colorectal cancer cells (Li et al., 2020).

There are some limitations of IRI/CAP-PNA-Lips in this study. CAP can be classified as both a water-soluble and a fat-soluble drug, which leads to a lower encapsulation rate in the hydrophobic phase compared to other studies. In this study, we were unable to fully mimic the dose and dosing cycle of IRI in combination with CAP as in clinical treatment. The administration was through intraperitoneal injection for the *in vivo* experiments, and although other studies have shown that small molecules with particle size less than 300 nm can be absorbed through the intestine and IRI/CAP-PNA-Lips exert excellent antitumor effects, there is still a gap in comparison with the effectiveness of clinical intravenous drug administration (Eloy et al., 2016; Kopeckova et al., 2019).

In summary, well-characterized PNA-modified liposomes loaded with IRICAP (IRI/CAP-PNA-Lips) were successfully prepared to achieve synergistic drug delivery and enhanced the synergistic treatment effect in this study. The local drug concentrations and retention times in tumor tissues are increased through targeting ability that further enhances the antitumor effect of the drugs. Both *in vitro* and *in vivo* experiments are suggestive of the excellent antitumor effect of IRI/CAP-PNA-Lips. Therefore, this study is

important for optimizing clinical combination treatment protocols, improving the antitumor effect of drugs, and reducing the drug delivery concentration required to achieve beneficial tumor treatment effects. PNA-modified liposomes could be a potential strategy for the treatment of colorectal cancer.

DATA AVAILABILITY STATEMENT

The original contributions presented in the study are included in the article/**Supplementary Material**; further inquiries can be directed to the corresponding authors.

ETHICS STATEMENT

The animal study was reviewed and approved by the Ethical Review Committee of Weifang Medical University.

AUTHOR CONTRIBUTIONS

WD designed the research and participated in the experimental performance, data analysis, and drafting of the manuscript. BY participated in the experimental performance of HPLC. SS and AW participated in the assessment of cellular uptake and data analysis. RK, QG, and MS participated in the construction of the tumor-bearing nude mouse model. BL, TS, JW, and JB provided guidance on experimental techniques. MQ, YW, and WJ participated in the research design and revised the manuscript. ZG provided technical support and all of the reagents and chemicals. All authors have read and approved the final manuscript.

FUNDING

This project was supported by the National Natural Science Foundation of China (Nos. 81274093, 81871892, and 82070856) and Natural Science Foundation of Shandong Province (No. ZR20180709017).

SUPPLEMENTARY MATERIAL

The Supplementary Material for this article can be found online at: https://www.frontiersin.org/articles/10.3389/fphar.2022.893151/full#supplementary-material

REFERENCES

Abraham, S. A., Waterhouse, D. N., Mayer, L. D., Cullis, P. R., Madden, T. D., and Bally, M. B. (2005). The Liposomal Formulation of Doxorubicin. *Methods Enzymol.* 391, 71–97. doi:10.1016/S0076-6879(05)91004-5

Allen, T. M., and Cullis, P. R. (2013). Liposomal Drug Delivery Systems: from Concept to Clinical Applications. *Adv. Drug Deliv. Rev.* 65 (1), 36–48. doi:10.1016/j.addr.2012.09.037

Apostolopoulos, V., Stojanovska, L., Gargosky, S. E., Muc, Á., and Muc, Á. (2015). MUC1 (CD227): a Multi-Tasked Molecule, *Cell. Mol. Life Sci.* 72, 4475, 4500. doi:10.1007/s00018-015-2014-z

Barenholz, Y. (2012). Doxil®--the First FDA-Approved Nano-Drug: Lessons Learned. *J. Control Release* 160 (2), 117–134. doi:10.1016/j.jconrel.2012.03.020

Beack, S., Cho, M., Kim, Y. E., Ahn, G. O., and Hahn, S. K. (2017). Hyaluronate-Peanut Agglutinin Conjugates for Target-specific Bioimaging of Colon Cancer. *Bioconjug Chem.* 28 (5), 1434–1442. doi:10.1021/acs.bioconjchem.7b00126

Caliskan, Y., Dalgic, A. D., Gerekci, S., Gulec, E. A., Tezcaner, A., Ozen, C., et al. (2019). A New Therapeutic Combination for Osteosarcoma: Gemcitabine and Clofazimine Co-loaded Liposomal Formulation. *Int. J. Pharm.* 557, 97–104. doi:10.1016/j.ijpharm.2018.12.041

Chau, I., and Cunningham, D. (2002). Chemotherapy in Colorectal Cancer: New Options and New Challenges. *Br. Med. Bull.* 64, 159–180. doi:10.1093/bmb/64.1.159

Chiorean, E. G., Nandakumar, G., Fadelu, T., Temin, S., Alarcon-Rozas, A. E., Bejarano, S., et al. (2020). Treatment of Patients with Late-Stage Colorectal Cancer: ASCO Resource-Stratified Guideline. *JCO Glob. Oncol.* 6, 414–438. doi:10.1200/JGO.19.00367

de Man, F. M., Goey, A. K. L., van Schaik, R. H. N., Mathijssen, R. H. J., and Bins, S. (2018). Individualization of Irinotecan Treatment: A Review of Pharmacokinetics, Pharmacodynamics, and Pharmacogenetics. *Clin. Pharmacokinet.* 57 (10), 1229–1254. doi:10.1007/s40262-018-0644-7

Du, C., Li, S., Li, Y., Galons, H., Guo, N., Teng, Y., et al. (2020). F7 and Topotecan Co-loaded Thermosensitive Liposome as a Nano-Drug Delivery System for Tumor Hyperthermia. *Drug Deliv.* 27 (1), 836–847. doi:10.1080/10717544.2020.1772409

Eloy, J. O., Petrilli, R., Topan, J. F., Antonio, H. M. R., Barcellos, J. P. A., Chesca, D. L., et al. (2016). Co-loaded Paclitaxel/rapamycin Liposomes: Development, Characterization and *In Vitro* and *In Vivo* Evaluation for Breast Cancer Therapy. *Colloids Surf. B Biointerfaces* 141, 74–82. doi:10.1016/j.colsurfb.2016.01.032

Engstrand, J., Nilsson, H., Strömberg, C., Jonas, E., and Freedman, J. (2018). Colorectal Cancer Liver Metastases - a Population-Based Study on Incidence, Management and Survival. *BMC Cancer* 18 (1), 78–11. doi:10.1186/s12885-017-3925-x

Feng, C., Zhang, H., Chen, J., Wang, S., Xin, Y., Qu, Y., et al. (2019). Ratiometric Co-encapsulation and Co-delivery of Doxorubicin and Paclitaxel by Tumor-Targeted Lipodisks for Combination Therapy of Breast Cancer. *Int. J. Pharm.* 560, 191–204. doi:10.1016/j.ijpharm.2019.02.009

Gao, B., Luo, J., Liu, Y., Su, S., Fu, S., Yang, X., et al. (2021). Intratumoral Administration of Thermosensitive Hydrogel Co-loaded with Norcantharidin Nanoparticles and Doxorubicin for the Treatment of Hepatocellular Carcinoma. *Int. J. Nanomedicine* 16, 4073–4085. doi:10.2147/IJN.S308057

Gao, T., Cen, Q., and Lei, H. (2020). A Review on Development of MUC1-Based Cancer Vaccine. *Biomed. Pharmacother.* 132, 110888. doi:10.1016/j.biopha.2020.110888

Ghosh, S., Lalani, R., Maiti, K., Banerjee, S., Bhatt, H., Bobde, Y. S., et al. (2021). Synergistic Co-loading of Vincristine Improved Chemotherapeutic Potential of Pegylated Liposomal Doxorubicin against Triple Negative Breast Cancer and Non-small Cell Lung Cancer. *Nanomedicine* 31, 102320. doi:10.1016/j.nano.2020.102320

Goldberg, R. M. (2005). Advances in the Treatment of Metastatic Colorectal Cancer. *Oncologist* 10 (S3), 40–48. doi:10.1634/theoncologist.10-90003-40

Guichard, S., Arnould, S., Hennebelle, I., Bugat, R., and Canal, P. (2001). Combination of Oxaliplatin and Irinotecan on Human Colon Cancer Cell Lines: Activity *In Vitro* and *In Vivo*. *Anticancer Drugs* 12 (9), 741–751. doi:10.1097/00001813-200110000-00006

Guo, W., Song, Y., Song, W., Liu, Y., Liu, Z., Zhang, D., et al. (2020). Co-delivery of Doxorubicin and Curcumin with Polypeptide Nanocarrier for Synergistic Lymphoma Therapy. *Sci. Rep.* 10 (1), 7832–7848. doi:10.1038/s41598-020-64828-1

Harashima, H., Tsuchihashi, M., Iida, S., Doi, H., and Kiwada, H. (1999). Pharmacokinetic/pharmacodynamic Modeling of Antitumor Agents Encapsulated into Liposomes. *Adv. Drug Deliv. Rev.* 40 (1–2), 39–61. doi:10.1016/s0169-409x(99)00039-3

Huang, M., Liang, C., Tan, C., Huang, S., Ying, R., Wang, Y., et al. (2019). Liposome Co-encapsulation as a Strategy for the Delivery of Curcumin and Resveratrol. *Food Funct.* 10 (10), 6447–6458. doi:10.1039/c9fo01338e

Jiang, H., Geng, D., Liu, H., Li, Z., and Cao, J. (2016). Co-delivery of Etoposide and Curcumin by Lipid Nanoparticulate Drug Delivery System for the Treatment of Gastric Tumors. *Drug Deliv.* 23 (9), 3665–3673. doi:10.1080/10717544.2016.1217954

Kalyane, D., Raval, N., Maheshwari, R., Tambe, V., Kalia, K., and Tekade, R. K. (20192018). Employment of Enhanced Permeability and Retention Effect (EPR): Nanoparticle-Based Precision Tools for Targeting of Therapeutic and Diagnostic Agent in Cancer. *Mater Sci. Eng. C Mater Biol. Appl.* 98, 1252–1276. doi:10.1016/j.msec.2019.01.066

Kerr, D. J. (2002). Capecitabine/irinotecan Combination Regimens in Colorectal Cancer. *Oncol. Willist. Park)* 16 (4), 27–29.

Khan, M. M., Madni, A., Tahir, N., Parveen, F., Khan, S., Jan, N., et al. (2020). Co-delivery of Curcumin and Cisplatin to Enhance Cytotoxicity of Cisplatin Using Lipid-Chitosan Hybrid Nanoparticles. *Int. J. Nanomedicine* 15, 2207–2217. doi:10.2147/IJN.S247893

Kopeckova, K., Eckschlager, T., Sirc, J., Hobzova, R., Plch, J., Hrabeta, J., et al. (2019). Nanodrugs Used in Cancer Therapy. *Biomed. Pap. Med. Fac. Univ. Palacky. Olomouc Czech Repub.* 163 (2), 122–131. doi:10.5507/bp.2019.010

Kumagai, H., Yamada, K., Nakai, K., Kitamura, T., Mohri, K., Ukawa, M., et al. (2019). Tumor Recognition of Peanut Agglutinin-Immobilized Fluorescent Nanospheres in Biopsied Human Tissues. *Eur. J. Pharm. Biopharm.* 136, 29–37. doi:10.1016/j.ejpb.2019.01.007

Lam, S. W., Guchelaar, H. J., and Boven, E. (2016). The Role of Pharmacogenetics in Capecitabine Efficacy and Toxicity. *Cancer Treat. Rev.* 50, 9–22. doi:10.1016/j.ctrv.2016.08.001

Li, C., Zuo, D., Liu, T., Yin, L., Li, C., and Wang, L. (2019). Prognostic and Clinicopathological Significance of MUC Family Members in Colorectal Cancer: A Systematic Review and Meta-Analysis. *Gastroenterology Res. Pract.* 2019, 1–16. doi:10.1155/2019/2391670

Li, R., Deng, L., Cai, Z., Zhang, S., Wang, K., Li, L., et al. (2017). Liposomes Coated with Thiolated Chitosan as Drug Carriers of Curcumin. *Mater Sci. Eng. C Mater Biol. Appl.* 80, 156–164. doi:10.1016/j.msec.2017.05.136

Li, X., Diao, W., Xue, H., Wu, F., Wang, W., Jiang, B., et al. (2020). Improved Efficacy of Doxorubicin Delivery by a Novel Dual-Ligand-Modified Liposome in Hepatocellular Carcinoma. *Cancer Lett.* 489, 163–173. doi:10.1016/j.canlet.2020.06.017

Li, Y., Hou, H., Zhang, P., and Zhang, Z. (2020). Co-delivery of Doxorubicin and Paclitaxel by reduction/pH Dual Responsive Nanocarriers for Osteosarcoma Therapy. *Drug Deliv.* 27 (1), 1044–1053. doi:10.1080/10717544.2020.1785049

Liu, K., Chen, W., Yang, T., Wen, B., Ding, D., Keidar, M., et al. (2017). Paclitaxel and Quercetin Nanoparticles Co-loaded in Microspheres to Prolong Retention Time for Pulmonary Drug Delivery. *Int. J. Nanomedicine* 12, 8239–8255. doi:10.2147/IJN.S147028

Meng, H., Wang, M., Liu, H., Liu, X., Situ, A., Wu, B., et al. (2015). Use of a Lipid-Coated Mesoporous Silica Nanoparticle Platform for Synergistic Gemcitabine and Paclitaxel Delivery to Human Pancreatic Cancer in Mice. *ACS Nano* 9 (4), 3540–3557. doi:10.1021/acsnano.5b00510

Mitragotri, S., Anderson, D. G., Chen, X., Chow, E. K., Ho, D., Kabanov, A. V., et al. (2015). Accelerating the Translation of Nanomaterials in Biomedicine. *ACS Nano* 9 (7), 6644–6654. doi:10.1021/acsnano.5b03569

Nabavinia, M. S., Gholoobi, A., Charbgoo, F., Nabavinia, M., Ramezani, M., and Abnous, K. (2017). Anti-MUC1 Aptamer: A Potential Opportunity for Cancer Treatment. *Med. Res. Rev.* 37 (6), 1518–1539. doi:10.1002/med.21462

Nath, S., and Mukherjee, P. (2014). MUC1: A Multifaceted Oncoprotein with a Key Role in Cancer Progression. *Trends Mol. Med.* 20 (6), 332–342. doi:10.1016/j.molmed.2014.02.007

Park, J., Choi, Y., Chang, H., Um, W., Ryu, J. H., and Kwon, I. C. (2019). Alliance with EPR Effect: Combined Strategies to Improve the EPR Effect in the Tumor Microenvironment. *Theranostics* 9 (26), 8073–8090. doi:10.7150/thno.37198

Paulík, A., Nekvindová, J., and Filip, S. (2020). Irinotecan Toxicity during Treatment of Metastatic Colorectal Cancer: Focus on Pharmacogenomics and Personalized Medicine. *Tumori* 106 (2), 87–94.

Peng, Y., Su, Z., Wang, X., Wu, T., Xiao, H., Shuai, X., et al. (2021). Near-Infrared Light Laser-Triggered Release of Doxorubicin and Sorafenib from TemperatureSensitive Liposomes for Synergistic Therapy of Hepatocellular Carcinoma. *J. Biomed. Nanotechnol.* 16 (9), 1381–1393.

Sarisozen, C., Vural, I., Levchenko, T., Hincal, A. A., and Torchilin, V. P. (2012). Long-circulating PEG-PE Micelles Co-loaded with Paclitaxel and Elacridar (GG918) Overcome Multidrug Resistance. *Drug Deliv.* 19 (8), 363–370. doi:10.3109/10717544.2012.724473

Song, W., Tang, Z., Zhang, D., Zhang, Y., Yu, H., Li, M., et al. (2014). Anti-tumor Efficacy of c(RGDfK)-Decorated Polypeptide-Based Micelles Co-loaded with Docetaxel and Cisplatin. *Biomaterials* 35 (9), 3005–3014. doi:10.1016/j.biomaterials.2013.12.018

Sung, H., Ferlay, J., Siegel, R. L., Laversanne, M., Soerjomataram, I., Jemal, A., et al. (2021). Global Cancer Statistics 2020: GLOBOCAN Estimates of Incidence and Mortality Worldwide for 36 Cancers in 185 Countries. *CA A Cancer J. Clin.* 71 (3), 209–249. doi:10.3322/caac.21660

Tan, X., Fang, Y., Ren, Y., Li, Y., Wu, P., Yang, X., et al. (2019). D-α-tocopherol Polyethylene Glycol 1000 Succinate-Modified Liposomes with an siRNA Corona Confer Enhanced Cellular Uptake and Targeted Delivery of Doxorubicin via Tumor Priming. *Int. J. Nanomedicine* 14, 1255–1268. doi:10.2147/IJN.S191858

Tang, H., Chen, J., Wang, L., Li, Q., Yang, Y., Lv, Z., et al. (2020). Co-delivery of Epirubicin and Paclitaxel Using an Estrone-Targeted PEGylated Liposomal Nanoparticle for Breast Cancer. *Int. J. Pharm.* 573, 118806. doi:10.1016/j.ijpharm.2019.118806

Thapa, R. K., Byeon, J. H., Choi, H. G., Yong, C. S., and Kim, J. O. (2017). PEGylated Lipid Bilayer-Wrapped Nano-Graphene Oxides for Synergistic Co-delivery of Doxorubicin and Rapamycin to Prevent Drug Resistance in Cancers. *Nanotechnology* 28 (29), 295101. doi:10.1088/1361-6528/aa7997

Walko, C. M., and Lindley, C. (2005). Capecitabine: A Review. *Clin. Ther.* 27 (1), 23–44. doi:10.1016/j.clinthera.2005.01.005

Wang, B., Yu, X. C., Xu, S. F., and Xu, M. (2015). Paclitaxel and Etoposide Co-loaded Polymeric Nanoparticles for the Effective Combination Therapy against Human Osteosarcoma. *J. Nanobiotechnology* 13 (1), 22–11. doi:10.1186/s12951-015-0086-4

Wang, Y., Qian, J., Yang, M., Xu, W., Wang, J., Hou, G., et al. (2019). Doxorubicin/cisplatin Co-loaded Hyaluronic Acid/chitosan-Based Nanoparticles for *In Vitro* Synergistic Combination Chemotherapy of Breast Cancer. *Carbohydr. Polym.* 225, 115206. doi:10.1016/j.carbpol.2019.115206

Xiong, Q., Cui, M., Bai, Y., Liu, Y., Liu, D., and Song, T. (2017). A Supramolecular Nanoparticle System Based on β-cyclodextrin-conjugated Poly-L-Lysine and Hyaluronic Acid for Co-delivery of Gene and Chemotherapy Agent Targeting Hepatocellular Carcinoma. *Colloids Surf. B Biointerfaces* 155, 93–103. doi:10.1016/j.colsurfb.2017.04.008

Xu, C., Wang, Y., Guo, Z., Chen, J., Lin, L., Wu, J., et al. (2019). Pulmonary Delivery by Exploiting Doxorubicin and Cisplatin Co-loaded Nanoparticles for Metastatic Lung Cancer Therapy. *J. Control Release* 295, 153–163. doi:10.1016/j.jconrel.2018.12.013

Xu, J., Fan, J., Qin, X., Cai, J., Gu, J., Wang, S., et al. (2019). Chinese Guidelines for the Diagnosis and Comprehensive Treatment of Colorectal Liver Metastases (Version 2018). *J. Cancer Res. Clin. Oncol.* 145 (3), 725–736. doi:10.1007/s00432-018-2795-1

Yalcin, T. E., Ilbasmis-Tamer, S., Ibisoglu, B., Özdemir, A., Ark, M., and Takka, S. (2018). Gemcitabine Hydrochloride-Loaded Liposomes and Nanoparticles: Comparison of Encapsulation Efficiency, Drug Release, Particle Size, and Cytotoxicity. *Pharm. Dev. Technol.* 23 (1), 76–86. doi:10.1080/10837450.2017.1357733

Yang, Z., Liu, J., Gao, J., Chen, S., and Huang, G. (2015). Chitosan Coated Vancomycin Hydrochloride Liposomes: Characterizations and Evaluation. *Int. J. Pharm.* 495 (1), 508–515. doi:10.1016/j.ijpharm.2015.08.085

Yu, T., Huang, X., Liu, J., Fu, Q., Wang, B., and Qian, Z. (2019). Polymeric Nanoparticles Encapsulating α-mangostin Inhibit the Growth and Metastasis in Colorectal Cancer. *Appl. Mater. Today* 16, 351–366. doi:10.1016/j.apmt.2019.06.014

Zhang, B., Song, Y., Wang, T., Yang, S., Zhang, J., Liu, Y., et al. (2017). Efficient Co-delivery of Immiscible Hydrophilic/hydrophobic Chemotherapeutics by Lipid

Emulsions for Improved Treatment of Cancer. *Int. J. Nanomedicine* 12, 2871–2886. doi:10.2147/IJN.S129091

Zhang, Z., Qian, H., Huang, J., Sha, H., Zhang, H., Yu, L., et al. (2018). Anti-EGFR-iRGD Recombinant Protein Modified Biomimetic Nanoparticles Loaded with Gambogic Acid to Enhance Targeting and Antitumor Ability in Colorectal Cancer Treatment. *Int. J. Nanomedicine* 13, 4961–4975. doi:10.2147/IJN.S170148

Zhang, Z., and Yao, J. (2012). Preparation of Irinotecan-Loaded Folate-Targeted Liposome for Tumor Targeting Delivery and its Antitumor Activity. *AAPS PharmSciTech* 13 (3), 802–810. doi:10.1208/s12249-012-9776-5

Conflict of Interest: The authors declare that the research was conducted in the absence of any commercial or financial relationships that could be construed as a potential conflict of interest.

Publisher's Note: All claims expressed in this article are solely those of the authors and do not necessarily represent those of their affiliated organizations, or those of the publisher, the editors, and the reviewers. Any product that may be evaluated in this article, or claim that may be made by its manufacturer, is not guaranteed or endorsed by the publisher.

frontiers | Frontiers in Oncology

ORIGINAL RESEARCH
published: 16 June 2022
doi: 10.3389/fonc.2022.890154

SEMA3C Supports Pancreatic Cancer Progression by Regulating the Autophagy Process and Tumor Immune Microenvironment

*Dalin Zhang[1], Aaron Lindstrom[1], Edward J Kim[2], Chang-il Hwang[3], Madison Lee Hall[3], Tzu-Yin Lin[2] and Yuanpei Li[1]**

[1] Department of Biochemistry and Molecular Medicine, UC Davis Comprehensive Cancer Center, University of California, Davis, Sacramento, CA, United States, [2] Division of Hematology and Oncology, Department of Internal Medicine, University of California, Davis, Sacramento, CA, United States, [3] Department of Microbiology and Molecular Genetics, University of California, Davis, Davis, CA, United States

To date, driver genes for pancreatic cancer treatment are difficult to pursue therapeutically. Targeting mutated KRAS, the most renowned driver gene in pancreatic cancer, is an active area of study. We discovered a gene named SEMA3C was highly expressed in pancreatic cancer cell lines and patients with a G12D mutation in KRAS. High expression of SEMA3C in patients was significantly associated with the decreased survival of pancreatic cancer patients based on the TCGA database. In pancreatic cancer cells, SEMA3C knockdown or inhibition exhibited growth/colony inhibition and cell cycle arrest. In addition, SEMA3C inhibition sensitized KRAS or MEK1/2 inhibition in pancreatic cancer cells. Overexpression of SEMA3C resulted in the induction of autophagy, whereas depletion of SEMA3C compromised induction of autophagy. SEMA3C modified the PD-L1 expression in tumor and immune cells and is correlated with the M2-like macrophage marker ARG1/CD163 expression, which could reshape the tumor microenvironment. Inhibition of SEMA3C decreased tumor formation in the xenograft model *in vivo*. Taken together, our data suggest that SEMA3C plays a substantial role in promoting cancer cell survival by regulating the autophagy process and impacting the tumor environment immune response. SEMA3C can be used as a novel target or marker with therapeutic or diagnostic potential in pancreatic cancer especially in tumors harboring the specific KRAS G12D mutation.

Keywords: TCGA, SEMA3C, KRAS G12D, Pancreatic Cancer, Autophagy, Tumor Immune Microenvironment

OPEN ACCESS

Edited by:
Jian-ye Zhang,
Guangzhou Medical University, China

Reviewed by:
Wenting Du,
University of Michigan, United States
Abhijit Aithal,
University of Nebraska Medical Center, United States

***Correspondence:**
Yuanpei Li
lypli@ucdavis.edu

Specialty section:
This article was submitted to Cancer Molecular Targets and Therapeutics, a section of the journal Frontiers in Oncology

Received: *05 March 2022*
Accepted: *16 May 2022*
Published: *16 June 2022*

Citation:
Zhang D, Lindstrom A, Kim EJ, Hwang C-i, Hall ML, Lin T-Y and Li Y (2022) SEMA3C Supports Pancreatic Cancer Progression by Regulating the Autophagy Process and Tumor Immune Microenvironment. Front. Oncol. 12:890154. doi: 10.3389/fonc.2022.890154

INTRODUCTION

Pancreatic cancer is the fourth highest cause of cancer deaths in men and women in the United States. It is predicted to be the second leading cause of cancer-related death by 2030 (1). The median survival is less than a year with the most aggressive type of pancreatic cancer. Despite advances in targeted therapies for many other cancers, the only option for treating the majority of pancreatic cancers remains chemotherapy (2). Overall, pancreatic tumors have a limited response to cytotoxic

drugs, which contributes to the persistently poor prognosis for pancreatic cancer patients. Recently the 5-year survival rate for all stages of pancreatic cancer is 11%, and patients who are diagnosed at a late stage have a 5-year survival rate of only 3% (3). Gemcitabine is a standard treatment for pancreatic cancer, with a history of more than 20 years, but no longer a standard monotherapy treatment except in selected cases of frail patients who cannot tolerate the more aggressive regimens like Folfirinox and Gem/nab-paclitaxel (4). To date, there are few therapeutically targetable driver genes for pancreatic cancer. A limited number of molecularly targeted drugs, such as *PARP*, *BRCA*, and *NTRK* inhibitors, are in the clinical trial stage for pancreatic cancer (5).

More than 90% of pancreatic tumors harbor a KRAS mutation, which is considered an early driver mutation essential in the initiation of pancreatic carcinogenesis (6). Substantial evidence shows that mutated KRAS is essential for PDAC growth, but the K*RAS* protein has been generally considered undruggable for many years because it does not have a suitable pocket for the compound binding with high affinity. Recently, sotorasib (AMG510), a compound directly targeted to KRAS with the G12C mutation, was shown to cause the regression of KRAS G12C lung carcinoma. AMG510 is the first KRAS (G12C) inhibitor in clinical development and treatment and was recently approved by FDA for the lung cancer therapy (7). Nonetheless, AMG510 was not effective on the KRAS G12D mutation types because of the changed binding pocket (8) and the tumor will quickly acquire resistance to KRAS G12C inhibition. Therefore, new therapeutic strategies are needed to develop and overcome this drug resistance in patients with cancer (9). Furthermore, evidence shows that the origins and genetic interactions of KRAS mutations are allele and tissue specific (10). For instance, increased AKT phosphorylation was observed in KRAS G12D expressing cell lines, whereas increased RAL-GTP was detected in G12C cell lines (11). In colon cancer, DCLK1 and the MET are upregulated in KRAS G12 mutant expressing KRAS cells, whereas ZO-2 is upregulated in KRAS G13D (12). These studies illustrate that individual KRAS mutants can mediate different signaling pathways and require unique pharmacological targeting for different subtypes. Recently, efforts have centered on alternative strategies to inhibit the different KRAS mutation signaling pathway, such as STK33 (13), GATA2 (14), p38 (15), SLC7A11 (16),and PI3K (17). These proteins mediate different signaling pathways that support cancer progression and have been explored for the KRAS mutation dependent genes. Exploring new dependent genes or pathways for different *KRAS* mutation subtypes could lead to the identification of targetable vulnerabilities and the development of new treatments.

SEMA3C was reported as an oncogene and could support the tumor progression in pancreatic cancers. SEMA3C promotes tumor growth and metastasis in pancreatic cancer by activating the ERK 1/2 signaling pathway (18). In other tumors, SEMA3C is also reported to be an oncogene. For example, SEMA3C is one of the top 20 most frequently altered genes and its expression is markedly increased compared to astrocytoma tissues and this increase was significantly associated with the shorter overall survival of patients in glioblastomas (19, 20). In addition, high expression of SEMA3C is associated with poor prognosis and progression in prostate, breast, liver, gastric, pancreatic, and lung cancer (21). SEMA3C also plays an important role in the maintenance of cancer stem-like cells. For example, SEMA3C is selectively expressed in Glioblastoma stem cells but not in their counterpart neural progenitor cells or non-stem tumor cells (22). Overexpression of SEMA3C in prostate cancer cell lines facilitates stem cell marker CD44 expression and tumor-sphere formation, suggesting a role for SEMA3C in maintaining prostate CSCs (23). SEMA3C also can take part in the migration or metastasis of cancer cells. SEMA3C is highly expressed in aggressive, highly metastatic Her2-positive breast cancer and SEMA3C depletion reduced cell migration (24, 25).

Here, we found that SEMA3C was highly expressed in pancreatic cancer and associated with the KRAS G12D mutation. Knockdown of SEMA3C expression significantly decreased tumor growth *in vitro* and *in vivo*. SEMA3C regulates the autophagy process and enhances the tumor immunosuppressive related genes expression of macrophage, thus targeting the SEMA3C is a promising target in pancreatic cancer therapy.

MATERIALS AND METHODS

Reagents

Anti-ACTIN, Anti-ULK1, Anti-p-ULK1, Anti-p62, and Anti-LC3B were purchased from Cell Signaling Technology (Danvers, MA). The SEMA3C and GAPDH antibodies were purchased from Proteintech (Rosemont, IL). The Anti-KRAS antibody was from ABclonal (Woburn, MA). CellTiter-Glo®2.0 was purchased from Sigma-Aldrich (St. Louis, MO). ECL Chemiluminescence kit was obtained from National Diagnostics (Atlanta, Georgia). Recombinant Human SEMA3C protein was purchased from the R&D Systems (Minneapolis, MN). EasySep™ Mouse CD8+ T Cell Isolation Kit was from Stem Cell (Cambridge, MA). Human *KRAS* (G12D) Expression Lentivirus was from GenTarget Inc (San Diego, CA). *SEMA3C* plasmids were purchased from Sino Biological (Wayne, PA). The SEMA3C inhibitor, 3,5,4'-Tribromosalicylanilide (CAS: 87-10-5), was purchased from TCI chemicals (Portland, OR) (26).

Bioinformatics Analysis

The GEO, TCGA, cBioPortal (27), GEPIA (28), Timer (29), KM plot (30), and Oncomine databases (31) were retrieved and applied for analysis according to the respective website guidelines.

Cell Culture and Transfection

BxPC3, PANC1, PACA2, 3T3, and 293T cells were obtained from the American Tissue Culture Collection. KPC cells were kindly provided by Dr. Chang-il Hwang's lab in UC Davis. The KPC-Luc cells were transfected by the lentivirus-luciferase and 2 mg/ml of puromycin was added for stable cell selection. A549 GFP-RFP-LC3B and Hela GFP-RFP-LC3B were kindly provided

by Dr. Jeremy Chien's lab in UC Davis. Cells were cultured in Dulbecco's modified Eagle's medium or RPMI 1640 (Gibco) supplemented with 10% fetal bovine serum (Sigma), 100 U/ml penicillin, and 100 mg/ml streptomycin (Sigma). Pancreatic cancer cells were transfected with target siRNA using a transfection reagent (GeneCopoeia) according to the manufacturer's protocol. The *SEMA3C* siRNA sequences were 5′-CACCAUCCUUUAGACUACA-3′, *KRAS* siRNA sequences 5′-CUAUGGUCCUAGUAGGAAA-3′, and the Universal Negative Control siRNA was from Sigma-Aldrich.

Immunoblotting Analysis

Immunoblotting analysis was performed as previously described (32). Cells were harvested, washed, and lysed in the RIPA buffer (Thermo fisher). Cell lysates were subjected to SDS-PAGE and transferred to PVDF membranes. PVDF membranes were then incubated with 5% (w/v) nonfat dry milk in TBST washing buffer (20 mM Tris-Cl, pH 7.6, 150 mM NaCl, and 0.1% Tween 20) for 1 h at 37°C to block nonspecific protein binding. Primary antibodies (1:1000) were diluted in the washing buffer containing 5% BSA and applied to the membranes overnight at 4°C. After extensive washing, the membranes were incubated with peroxidase-conjugated antibodies for 1 h at room temperature and washed again. Immunoreactive bands were visualized with the ECL Chemiluminescence kit.

Growth Assay

Cells were seeded in 96-well plates at a density of 3000 cells/well. CellTiter-Glo®2.0 was used for detecting the cell numbers every 24 hours with a plate reader (Molecular Devices, San Jose, CA).

Confocal Image

2×10^4 A549 or Hela with GFP/RFP-LC3B cells were seeded in a culture dish with a glass-bottom plate overnight and treated with the SEMA3C inhibitor 25 μM 24 hours. Confocal laser scanning microscopy (LSM 800, ZEISS) was employed to monitor the patterns and changes of GFP and RFP fluorescence in cells.

RT-PCR

Quantitative RT-PCR assays were performed as previously described (33). The total RNA was isolated using the TRIZOL reagent (Thermo Scientific, Waltham, MA) and the phenol-chloroform extraction method according to the manufacturer's instructions. The cDNA was synthesized by the SuperScript reverse transcriptase (I Thermo Scientific, Waltham, MA) with 2 μg total RNA. qPCR was carried out with the SYBR Green PCR Master Mix (Thermo Fisher) on a CFX96 Real-Time PCR Detection System (Bio-Rad, Hercules, CA). GAPDH was used as a housekeeping gene to normalize the level of mRNA expression.

Colony Assay

The cells were seeded into 6-well plates with a density of 2×10^3 per well. On day 14, 0.005% crystal violet was added to make the colonies visible. Each assay was repeated three times.

Conditional Medium

Cell conditioned media was collected from 90% confluent cultures following 48 hours of conditioning. To remove cellular debris, conditioned media underwent differential centrifugation before concentration (20X, 30kDa filter, Millipore) (34).

T Cell Proliferation

CD8+ T cells were isolated from the spleen with the EasySep™ Mouse CD8+ T Cell Isolation Kit (Stem cell, MA). T cells then were activated by the anti-CD3 and anti-CD28 co-stimulation for 24 hours. 3T3 and KPC cells were transfected with the Vehicle or *SEMA3C* plasmid for 24 hours and then collected for co-culturing with the activated CD8+ T cells for 48 hours. Suspended live T cells numbers were counted by trypan blue staining.

Animal Studies

All animal experiments were strictly in compliance with the guidelines of the Animal Use and Care Administrative Advisory Committee of the University of California, Davis (IACUC #20265). C57/BL6 mice were purchased from the Jackson Laboratory (Bar Harbor, ME). The subcutaneous tumor models were established by inoculating KPC cells (5×10^5) into the flank of mice. After subcutaneous tumors reached approximately 50 mm^3, SEMA3C inhibitor or saline were given by IP every other day (20 mg/kg) for a total of 7 doses (n=5/group). The body weight and volume of tumors were measured every three days. Animal spirit, hair coat, and behavior were also closely monitored. Animals were terminated two weeks after the therapy. Tumors and organs were then harvested and fixed for microscopic analysis. KPC cells transfected with vehicle and *SEMA3C* sgRNA 9# and 17# were subcutaneously injected into the C57/BL6 mice(n=6) and after the tumor reached around 50mm^3, tumor volume was recorded every 3 days for 6 times.

Statistical Analysis

All statistical analyses were conducted using GraphPad Prism (GraphPad Software, La Jolla, CA). Statistically significant differences between two independent groups were determined by Student's *t*-test. The survival analysis was determined by the log-rank test. A value of $P<0.05$ was considered statistically significant.

RESULTS

KRAS G12D Mutation Status and Expression Level are Associated With Poor Prognosis

There is still a lack of clear understanding of the prognostic value of different KRAS mutation subtypes in pancreatic cancer. There are several studies on the KRAS mutation related prognosis and multiple studies stated that poor outcomes were identified in patients with KRAS G12D mutant pancreatic cancer (35, 36). However, other studies found no significant association between the G12D mutation and prognosis in pancreatic cancer patients

(37, 38). Therefore, we first investigated the relationship between the KRAS mutation subtype and prognosis with the TCGA for pancreatic cancer patients and confirmed the prognosis benefit of the mutation type. As expected, KRAS was overexpressed in pancreatic cancer compared with non-tumor and KRAS expression caused a worse clinical outcome in pancreatic cancer (**Figures 1A, B**). Patients with KRAS mutated tumors were also significantly associated with a worse prognosis in overall survival of pancreatic cancer patients compared with KRAS WT tumors (**Figure 1C**). Interestingly, the ratio of KRAS mutation types varies in different cancers and the *KRAS* G12D mutation type made up the highest proportion of tumors harboring a KRAS mutation (**Figure 1D**). We next investigated whether the different subtypes of KRAS mutation in patients were associated with prognosis. We found that KRAS G12D mutation significantly correlated with worse survival when compared to KRAS wild type, KRAS G12R, and KRAS G12V mutations (**Figure 1E**). We also found that different KRAS mutations induced distinctly specific gene enrichment patterns and signaling pathway alterations in KRAS WT and Mutation cell lines. The 20 most different genes expression in KRAS-WT and MUTATION is different from different mutation types (**Figures S1, S2** and **Table S1**). Previous studies have shown that tumor KRAS gene expression levels are influenced by the KRAS mutational status and *KRAS* mutation leads to an increase in KRAS mRNA level, which can enhance the downstream signaling pathways (39). We confirmed this observation that the *KRAS* G12D mutation can lead to increased KRAS expression level in pancreatic cancer patient samples (**Figure 1F**).

SEMA3C Expression is Associated With KRAS G12D Mutation and Highly Expressed in Pancreatic Cancers With a Poor Clinical Outcome

An alternative method for targeting the KRAS signaling pathway is to discover the vulnerable genes associated with different KRAS mutations. Since patients with the KRAS G12D mutation suffered a shorter survival time, we next explored potential KRAS G12D dependent genes in pancreatic carcinogenesis. The differentially expressed genes (DEGs) were compared between KRAS WT and KRAS G12D pancreatic cancer cell lines and TCGA patients. Aberrantly expressed genes in cancer can be regarded as oncogenes that could promote or support cancer progression. Then we combined KRAS G12D associated DEGs with the genes that are highly

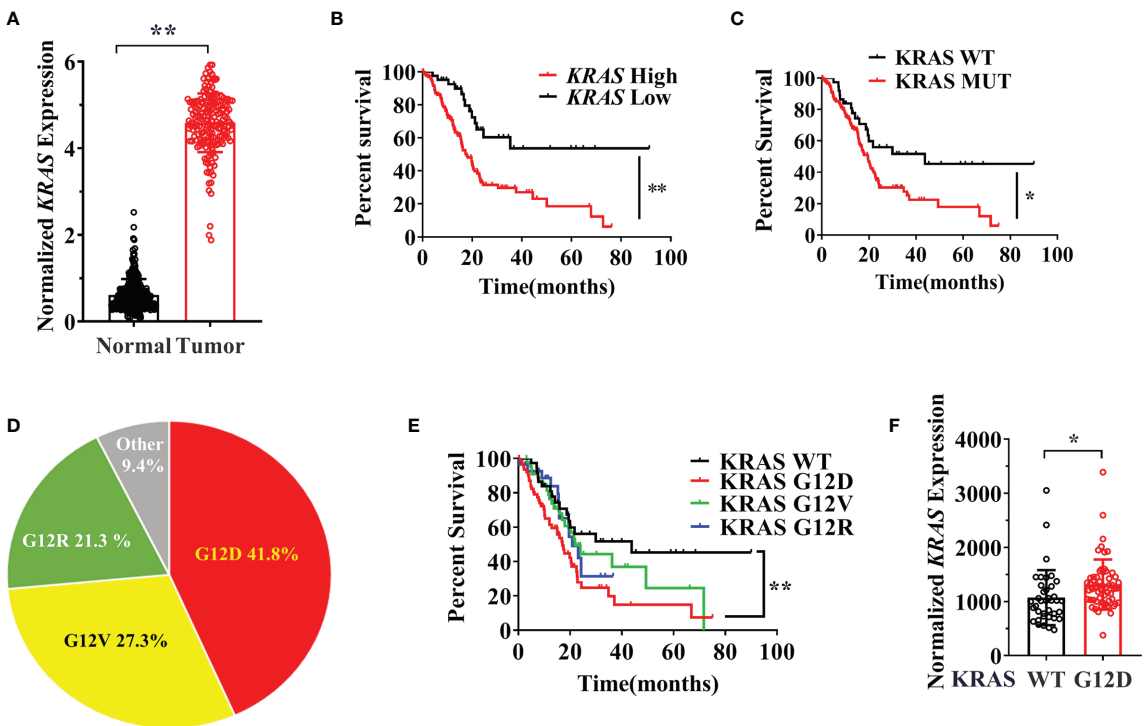

FIGURE 1 | **(A)** The expression data are first log2(TPM+1) transformed for differential analysis and the log2FC is defined as median (Tumor) and median (TCGA normal + GTEx normal), data were collected and analyzed from GEPIA. **(B)** The overall survival of the KRAS expression. Data from KM plot, significance vs cutoff values between lower and upper quartiles of expression. **(C)** Survival analysis of the pancreatic cancer patients between the KRAS wildtype and KRAS mutation. **(D)**The proportion of different mutation types in pancreatic cancer. **(E)** Survival analysis of the pancreatic cancer patients among different KRAS mutation and wild type. **(F)** KRAS expression level in G12D mutation and wild type group. These data were from the cBioPortal database and http://firebrowse.org/. Data are representative of three independent experiments. T-tests or log-rank Test for the measurements between the two groups; *P < 0.05, **P < 0.01.

expressed in pancreatic cancer patients in other 3 cohorts (TCGA/GSE62125/GSE71989). AHNAK2, ARL4C, ASAP2, SEMA3C were identified as being highly expressed in both KRAS G12D cell lines and pancreatic cancer patients (**Figure 2A**). Next, we chose SEMA3C for further analysis and verified that SEMA3C was highly expressed in both patients (TCGA) and cell lines with *KRAS* mutations (**Figures 2B, C**). Significantly, overexpression of the KRAS G12D in cultured cancer cells was found to increase the SEMA3C expression (**Figure 2D**). To further validate the expression of SEMA3C associated with *KRAS* G12D mutation, we analyzed KPC cell lines with or without KRAS G12D mutation from the GEO database (41). SEMA3C expression was significantly higher in pancreatic cancer cell lines derived from the KRAS G12D mutation mice than that from the WT mice (**Figure 2E**). Significantly, knockdown of the KRAS expression resulted in decreased SEMA3C expression (**Figure 2F**). Higher SEMA3C expression was correlated with KRAS expression and KRAS related signaling pathways (**Figures 2G, H**). Patients with high expression levels of both SEMA3C and KRAS had shorter survival times compared to those with high levels of either alone in pancreatic cancer patients (**Figure 2I**) (42). As expected, SEMA3C was highly expressed in pancreatic cancer, compared to paired normal tissue in three pancreatic cancer cohorts from TCGA/GSA/Oncomine (**Figures 2J–L**). SEMA3C expression is positively correlated with the clinical stages of pancreatic cancers, while patients with advanced stages of pancreatic cancer have a significantly shorter survival rate (**Figures 2M, N**). Consistent with the previous observations, high SEMA3C expression in pancreatic cancer was linked with a shorter survival time based on the analysis of the TCGA database (**Figure 2O**). Similarly, AHNAK2, ARL4C, ASAP2 were all highly expressed in pancreatic cancers, correlated with KRAS G12D mutation and could predict survival in pancreatic cancers (**Figure S3**).

SEMA3C Knockdown Impairs Cell Growth, Colony Formation, and Cell Cycle Arrest

We next explored the function of SEMA3C in pancreatic cancer. si*NC* and si*SEMA3C* were transfected into BXPC3 and PANC1 cells and the expression of SEMA3C was measured by RT-PCR to confirm the silencing of endogenous SEMA3C mRNA expression (**Figures 3A**, **S5A**). Knockdown of SEMA3C by siRNA resulted in the impairment of both growth and colony formation in PANC1 cells and BXPC3 cells (**Figures 3B, C**). Inhibition of SEMA3C with the SEMA3C special inhibitor 3,5,4'-Tribromosalicylanilide resulted in cell cycle arrest and apoptosis increase in pancreatic cancer cell lines (**Figures 3D, E**). Simultaneous suppression of KRAS and SEMA3C by siRNA shows a superimposed inhibition effect in cell growth and colony formation (**Figures 3F, G**). Furthermore, the combination of trametinib (MEK inhibitor, downstream of *KRAS)* and SEMA3C inhibitor can induce synergistic effect in KRAS G12D cells calculated by the combenefit software (**Figure 3H**),while no synergy effect in KRAS WT cells(**Figure S5C**).

SEMA3C Promotes Tumor Cell Survival by Autophagy Induction

KRAS mutant tumors have been shown to be dependent on autophagy for growth and survival (44). Next, we investigated whether the SEMA3C expression could mediate autophagy progress. We first evaluated the TCGA data and found that SEMA3C expression shows a strong correlation with the autophagy pathway expression (**Figures 4A, B**). We then overexpressed SEMA3C in 293T and PANC1 cells and found that the RNA expression levels of the autophagy induction genes ATG3 and Beclin1 were upregulated, which represented the initiation of autophagy (**Figures 4C, D** and **S5B**). Moreover, overexpression of SEMA3C in 293T cells showed autophagy induction by evaluating ULK1 phosphorylation levels and p62 protein expression (**Figure 4E**). Knockdown of SEMA3C resulted in a decrease of ATG3 and ATG5 in the mRNA level (**Figure 4F**). Knockdown of SEMA3C resulted in a significant accumulation of LC3B and P62 protein (**Figure 4G**), which indicated autophagy was inhibited based on previous reports that indicate that these proteins accumulate when autophagy is disrupted (45, 46). Furthermore, the upregulation of LC3B and P62 was cumulative and dose-dependent in different pancreatic cells (**Figures 4H, I**). Stably expressing GFP/RFP-LC3B cells are commonly used for evaluating autophagy flux progress representing the autophagy induction or inhibition (47), and we found that treating these cells with SEMA3C inhibitors increased more yellow puncta which meant the autophagy process was blocked (**Figure 4J**).

SEMA3C Leads to an Immunosuppressive Environment by Upregulation of PD-L1 and Macrophage Polarization

Preclinical reports have shown evidence linking oncogenic KRAS mutations and PD-L1 expression in cancers, which reduces the tumor-specific T cell's function in the tumor microenvironment (TME) (48). KRAS up-regulation of PD-L1 has further been shown to occur through ERK signaling pathways (49). Interestingly, SEMA3C knockdown also could control the ERK signaling pathway (18), which led us to inquire whether SEMA3C could mediate or be involved in the regulation of PD-L1 expression in tumor and tumor associated macrophages (TAMs). NRP1, one of the receptors of SEMA3C, was highly expressed on TAMs. NRP1 on macrophages triggers VEGFR1 activation and migration of macrophages to become TAMs (50). We checked the expression of the NRP1 in different cell types in pancreatic cancer (51). NRP1 are not only expressed in pancreatic cancer but also in macrophages/monocytes, this suggests that SEMA3C could affect the macrophage polarization by binding the NRP1 expressed in macrophages (**Figure S4**). We then examined the correlated expression of both *PD-L1* and SEMA3C in pancreatic cancer with TCGA data by Timer software (**Figure 5A**). We found that immunosuppressive genes (M2 makers: CD274, CD206, CD163) which are mainly expressed in macrophages were higher in the SEMA3C^{high} group (**Figure 5B**). To confirm that SEMA3C expression could affect the PD-L1 expression, we overexpressed SEMA3C in PANC1

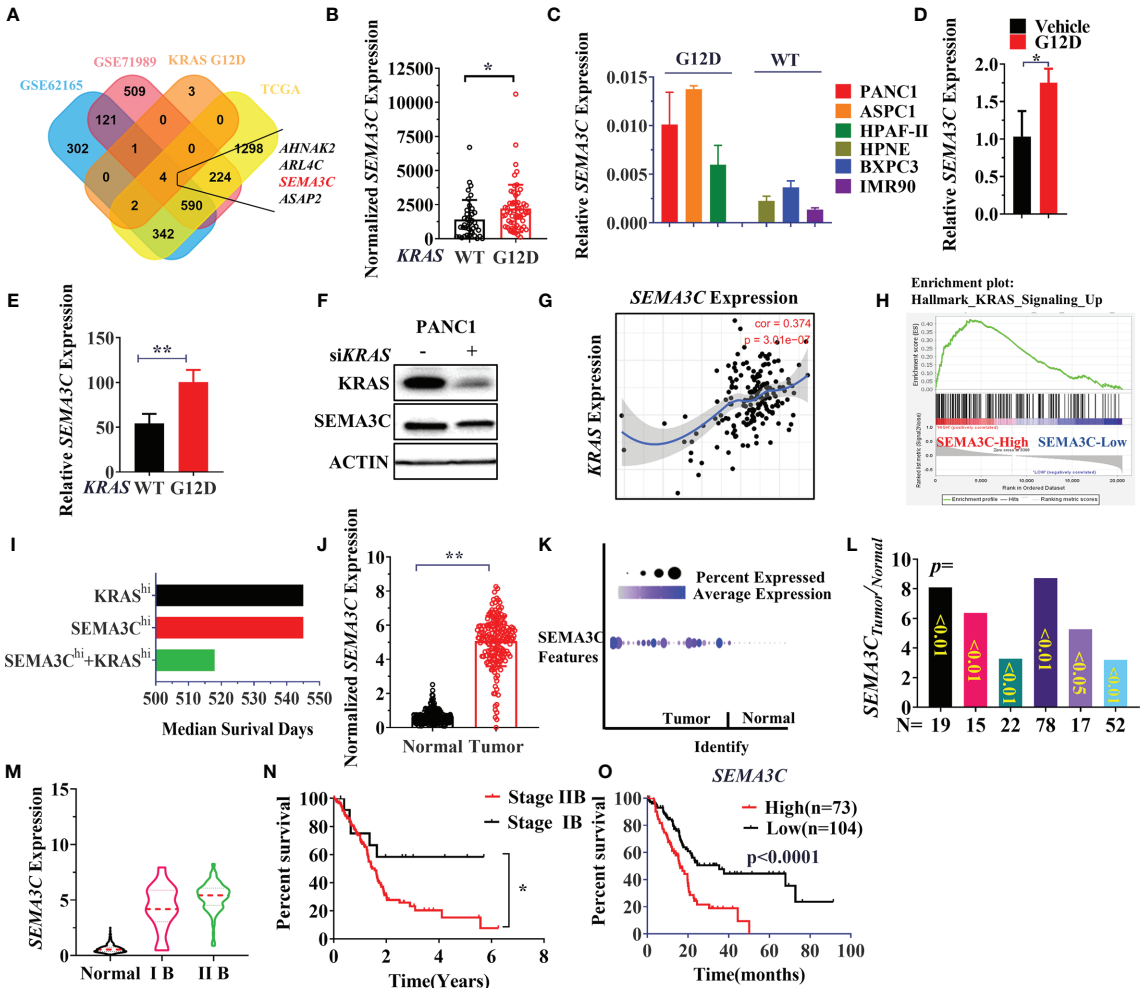

FIGURE 2 | **(A)** Simultaneous highly expressed genes in KRAS G12D mutation patients/cells, TCGA and GEO datasets (GSE62125/GSE71989). The normalized gene expression data were used for the comparison of two groups, the FC (fold change)>=1.5, p-Value<=0.05. **(B)** SEMA3C expression in *KRAS* WT and G12D mutation patients from TCGA data. **(C)** SEMA3C expression in cell lines with or without KRAS G12D mutation evaluated by the qPCR assay (KRAS WT cell lines: HPNE, BxPC3, IMR90; KRAS G12D cell lines: PANC1, ASPC1, HPAF-II). **(D)** SEMA3C expression was detected by qPCR after overexpression of the KRAS G12D for 48 hours. **(E)** SEMA3C expression in KPC cell lines with or without KRAS G12D mutation, data was collected in the GSE63348 database. **(F)** SEMA3C protein expression after depletion of *KRAS* in PANC1 cells. **(G)** The correlation between *KRAS* and SEMA3C expression analyzed by Timer software **(H)** High expressed or low expressed of SEMA3C enriched signaling pathway by the GSEA analysis. **(I)** Survival analysis of the patient group with high expression of SEMA3C, KRAS and both high expressions by the PROGgeneV2. **(J)** The expression data are first log2(TPM+1) transformed for differential analysis and the log2FC is defined as median (Tumor) and median (TCGA normal + GTEx normal), data were collected and analyzed by GEPIA. **(K)** The expression analysis of the SEMA3C from GSA: CRA001160 data (40). **(L)** SEMA3C expression data from the Oncomine in different groups (Segara; Logsdon; Grutzmann; Badea; Iacobuzio Donahue; Pei). **(M)** SEMA3C expression analyzed in different clinical stages of pancreatic cancer from www.aclbi.com. **(N)** The overall survival of patients analyzed in different stages of pancreatic cancer. **(O)** The overall survival of the SEMA3C expression. Data from KM plot, significance vs. cutoff values between lower and upper quartiles of expression. Data are representative of three independent experiments. T-tests or log-rank Test for the measurements between the two groups; *P < 0.05, **P < 0.01.

and 293T cell lines, and observed upregulated PD-L1 in these two cell lines after SEMA3C overexpression (**Figure 5C**). Knocking down SEMA3C led to PD-L1 decrease (**Figure 5D**). Additionally, treatment with a SEMA3C inhibitor significantly decreased the PD-L1 expression in KPC cells in a dose dependent manner (**Figure 5E**). Since SEMA3C is a secreted glycoprotein, tumor secreted SEMA3C may impact host myeloid/macrophage PD-L1 expression or polarization through modulation of the tumor-suppressive environment (52). THP1 and BMDM (Bone Marrow Derived Macrophage) were used as myeloid/macrophage models to test the PD-L1 expression or polarization *in vitro*. These cells were treated by the conditional medium collected from the PANC1 or KPC cells with or without the SEMA3C overexpression and we observed an increase in the PD-L1, CD163 or ARG1 mRNA levels (**Figures 5F, G**). Moreover, PD-L1 high expression can mediate T cell anergy by stimulating the PD1/PD-L1 signaling pathway, which could lead to the T cell death (53). To test this,

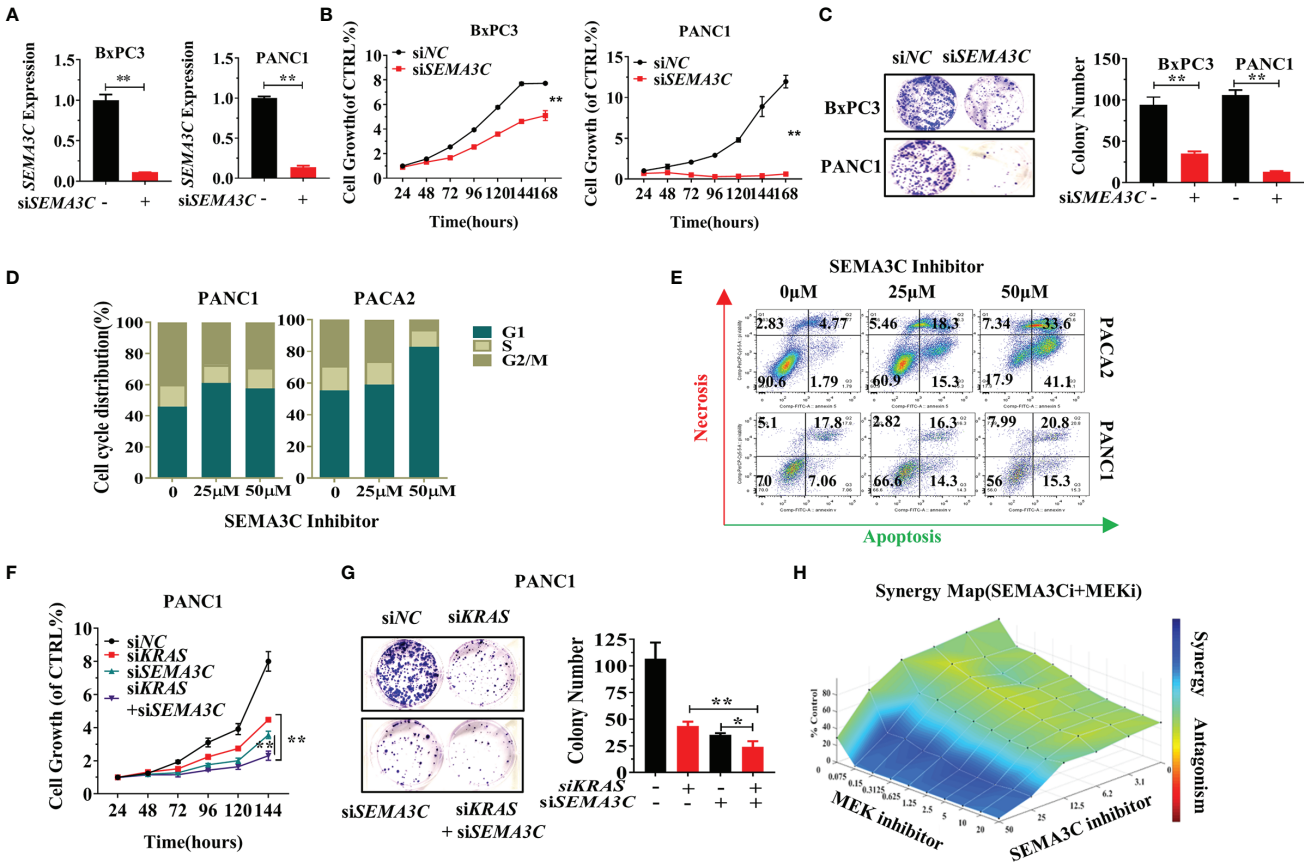

FIGURE 3 | **(A)** Expression levels of SEMA3C detected by qPCR after treatment with *siSEMA3C*. **(B)** The cell growth of pancreatic cells evaluated by the CellTiter-Glo®2.0 assay. **(C)** Colony formation assays were assessed after the knockdown of the *SEMA3C* expression in pancreatic cancer cells. **(D)** Cell cycle evaluation in pancreatic cancer cells after treatment of SEMA3C inhibitor 24 hours. **(E)** Cell necrosis and apoptosis evaluation in pancreatic cancer cells after treatment of *SEMA3C* inhibitor 24 hours. **(F, G)** The synergistic effect of the si*KRAS* and si*SEMA3C* in cell growth and cell colony formation assessed after knocking down the expression of KRAS, SEMA3C, or both in PANC1 cells. **(H)** Synergistic effects on cell viability evaluated by combining trametinib and SEMA3C inhibitor in KPC cells calculated with combenefit software (43). Data are representative of three independent experiments. T-tests for the measurements between the two groups; *P < 0.05, **P < 0.01.

we co-cultured activated T cells with either 3T3 or KPC vehicle cells, or 3T3 or KPC cell overexpressed SEMA3C. We found that the SEMA3C high expression groups showed a significant decrease in live T cells relative to cells with normal SEMA3C expression (**Figure 5H**).

SEMA3C Inhibitor Retarded Tumor Growth *In Vivo* Pancreatic Cancer Model

To explore the role of SEMA3C in pancreatic cancer *in vivo*, we created a KPC tumor model by subcutaneously injecting 5×10^5 mouse KPC-Luc cells into C57/BL6 mice (Charles River). After the tumors became established, mice were treated with the vehicle or SEMA3C inhibitor (20 mg/kg every other day for a total of 7 doses). We found that the tumor volume and weight in the SEMA3C inhibition group were significantly smaller than that in the vehicle group (**Figures 6A, B**). H&E results showed that the tumor was dense in the vehicle group while there were fewer tumor cells and more stroma in the group treated with the SEMA3C inhibitor (**Figure 6C**). The expression of Ki67 is strongly associated with tumor cell proliferation and growth and our IHC results show that the level of Ki67 is much higher in the vehicle group than that in the SEMA3C inhibitor group. On the contrary, the levels of cleaved caspase 3, a common cell apoptosis marker, is much lower in the vehicle group. We also detected that the CD8a positive staining was much greater in the SEMA3C inhibitor treated group (**Figure 6D**). Together, these results indicated that the tumorigenesis of the KPC tumor bearing mice was inhibited by SEMA3C inhibition. We further explored the role of SEMA3C in regulating the autophagy process and PD-L1 expression in the tumors and found that the SEMA3C inhibitor can influence the expression levels of these proteins' expression *in vivo* (**Figure 6E**). The enhanced p62 and LC3B expression imply that the autophagy process was blocked by the SEMA3C inhibitor (**Figure 6E**). Meanwhile, PD-L1 expression was decreased after the treatment (**Figure 6E**). PD-L1 mRNA level was also decreased in the SEMA3C inhibitor treated group (**Figure 6F**). Importantly, the SEMA3C inhibitor had no observed toxicity in mice by measuring the body weight

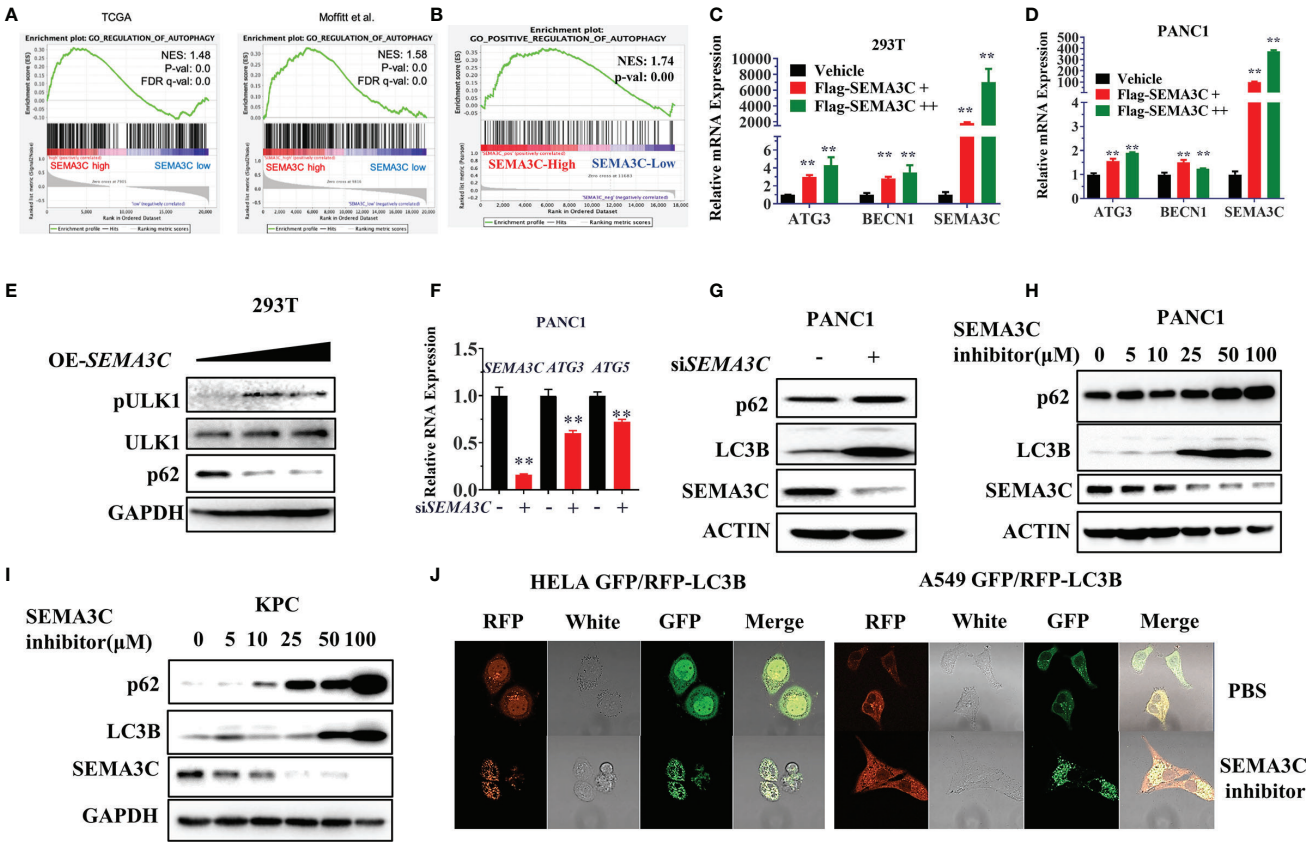

FIGURE 4 | **(A, B)** The correlation between SEMA3C expression and autophagy signaling pathway analyzed with TCGA and CRA001160 data by GSEA software. **(C, D)** Overexpression of the SEMA3C in 293T and PANC1 cells for 48 hours, autophagy induction genes mRNA levels were detected by the qPCR assay. **(E)** Overexpression of SEMA3C in 293T cells for 48 hours, autophagy initial protein ULK1 phosphorylation status and total protein were detected. **(F)** Knockdown of SEMA3C in PANC1 cells induces autophagy initial gene ATG3 and ATG5 mRNA expression. **(G)** Knocking down the SEMA3C in PANC1 cell lines, p62, and LC3B protein levels were detected by western blot. **(H, I)** Dose dependent on p62 and LC3B protein level after treatment by the SEMA3C inhibitors. **(J)** GFP-RFP-LC3B labeled cells were treated by the SEMA3C inhibitor, the LC3B puncta observed by the confocal image. Data are representative of three independent experiments. T-tests for the measurements between the two groups; **P < 0.01.

and the complete blood counts (**Figures 6G, H**). Knock down the SEMA3C expression by CRISPR-Cas9 in KPC cells and the xenograft model shows that SEMA3C impairs the growth *in vivo* (**Figures 6I, J**). These findings demonstrated that SEMA3C inhibition suppresses tumor growth *in vivo* by inhibiting cancer cell growth and altering the immune response within the tumor microenvironment. The Schematic illustration of probable mechanism of SEMA3C role in pancreatic cancer (**Figure 6K**).

DISCUSSION

There is currently no effective therapy that can cure pancreatic cancer. KRAS mutations occur in about 90% of pancreatic cancer and KRAS is a significant oncogene for the initiation of this cancer type. There are several types of KRAS mutations including the G12D, G12C, G12V, and G12R in pancreatic cancers which may play different roles. KRAS has been generally undruggable until the recent discovery of Sotorasib (AMG510, a specific covalent inhibitor of KRAS G12C mutation)), which has shown excellent therapeutic prospects. However, different KRAS mutations play different roles by allele-specific signaling pathways and the patient's survival time also varies from different mutation types. The KRAS G12D mutation is frequent in pancreatic cancer which makes targeting KRAS with the G12D mutation more prospective than the other mutations in pancreatic cancer therapy.

Autophagy is a cell survival mechanism induced by various conditions such as drug treatment, hypoxia or gene mutation, which helps cancer cells survive and induces drug resistance (54). High basal autophagy rates have been described in several human pancreatic ductal adenocarcinoma (PDAC) cell lines and autophagy is upregulated in the latter stages of pancreatic ductal neoplasia progressing to PDAC (55). Autophagy is elevated in KRAS-driven cancers but not normal tissue and is essential for tumor growth (56). Acute KRAS inhibition by the downstream effector increases rather than decreases autophagy. In addition, the ERK inhibition phenotype inhibits KRAS and

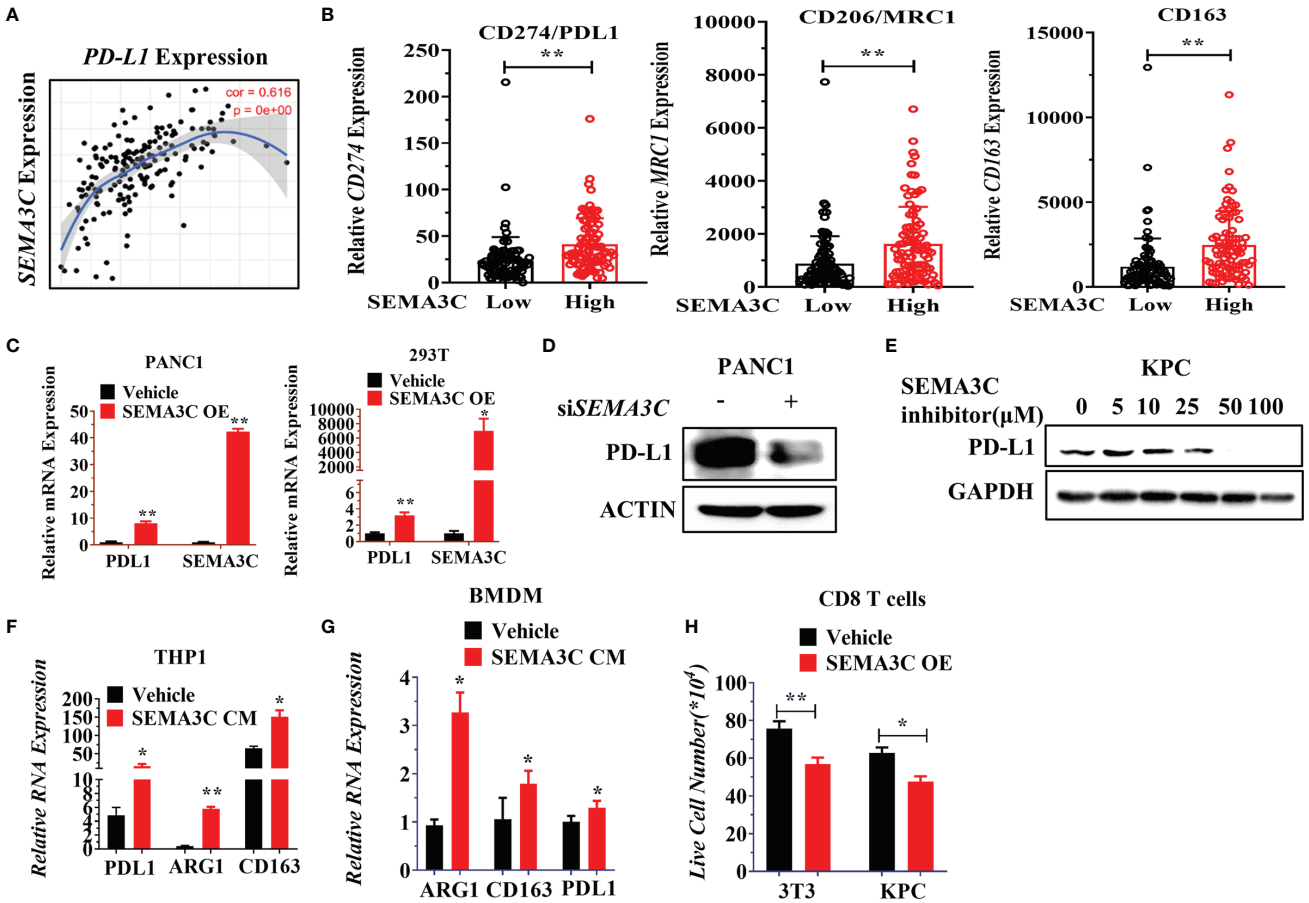

FIGURE 5 | **(A)** The correlation between SEMA3C and PD-L1 analyzed by Timer software. **(B)** PD-L1, MRC1, *CD163* expression in either SEMA3C high expression or low expression groups. The groups were divided into two groups by the mean of SEMA3C in the TCGA database. **(C)** PD-L1 mRNA expression detected after the overexpression of SEMA3C in different cell lines. **(D)** PD-L1 protein expression was detected after knocking down the SEMA3C expression. **(E)** PD-L1 protein expression was detected after treatment of different doses of SEMA3C inhibitor in the KPC cell line for 24 hours. **(F)** Expression of PD-L1, ARG1, and CD163 were detected by qPCR in THP1 cells after being treated by the conditional medium derived from either PANC1 cells or PANC1 cells overexpressing SEMA3C. **(G)** Expression of PD-L1, ARG1, and CD163 were detected by qPCR in BMDM cells after being treated by the conditional medium derived from KPC cells or KPC cells overexpressing SEMA3C. **(H)** Activated CD8+ T cells co-cultured with normal 3T3 and KPC cells or 3T3 and KPC cells with overexpressed SEMA3C for 24 hours before the suspended T cells number were counted. The error bars indicate the SD of three independent experiments: *P < 0.05, **P < 0.01.

stimulates increased autophagy flux. Inhibition of KRAS-RAF-MEK-ERK signaling triggers autophagy which could protect PDAC cells from the cytotoxic effects of KRAS pathway inhibition (57, 58).

Pancreatic cancer is known to have a highly immunosuppressive microenvironment (59). The immunosuppressive microenvironment allows tumor cells to escape immune surveillance and elimination of the anti-tumor immune system (60). One of the intrinsic determinants of immunogenicity is the expression of PD-L1 in tumors or tumor-related cells within the tumor microenvironments. Different signaling pathways change can induce the production of constitutive PD-L1 (61). PD-L1 is expressed not only in tumor cells (62) but also highly expressed in tumor-associated macrophages, which are the most abundant immune cell populations in the tumor microenvironment (63).

By multiple-genomics data mining we found that the KRAS G12D mutation was significantly associated with the survival of pancreatic patients and identified 4 genes that are associated with KRAS G12D mutation and highly expressed in pancreatic cancer and could regarded as promising targets for the pancreatic cancer therapy. Interestingly, very recent reports also reach a similar conclusion for these genes. For example, ASAP2 was identified as the novel driver gene and potential druggable target in pancreatic cancer (64). AHNAK2 was identified as differentially expressed proteins in KRAS mutants compared to cells lacking Ras pathway mutation (65). ARL4C was identified as RAF1-MEK/ERK pathway-dependent gene in ameloblastoma cell proliferation and osteoclast formation and as down localization of KRAS in pancreatic cancer (66, 67). Here we explored the SEMA3C role in pancreatic cancer. SEMA3C was highly expressed in pancreatic cancers, especially in cells and patients with high KRAS G12D expression, and high SEMA3C expression was enriched in the signaling pathways upregulated by KRAS. Both KRAS and SEMA3C high expression genotypes

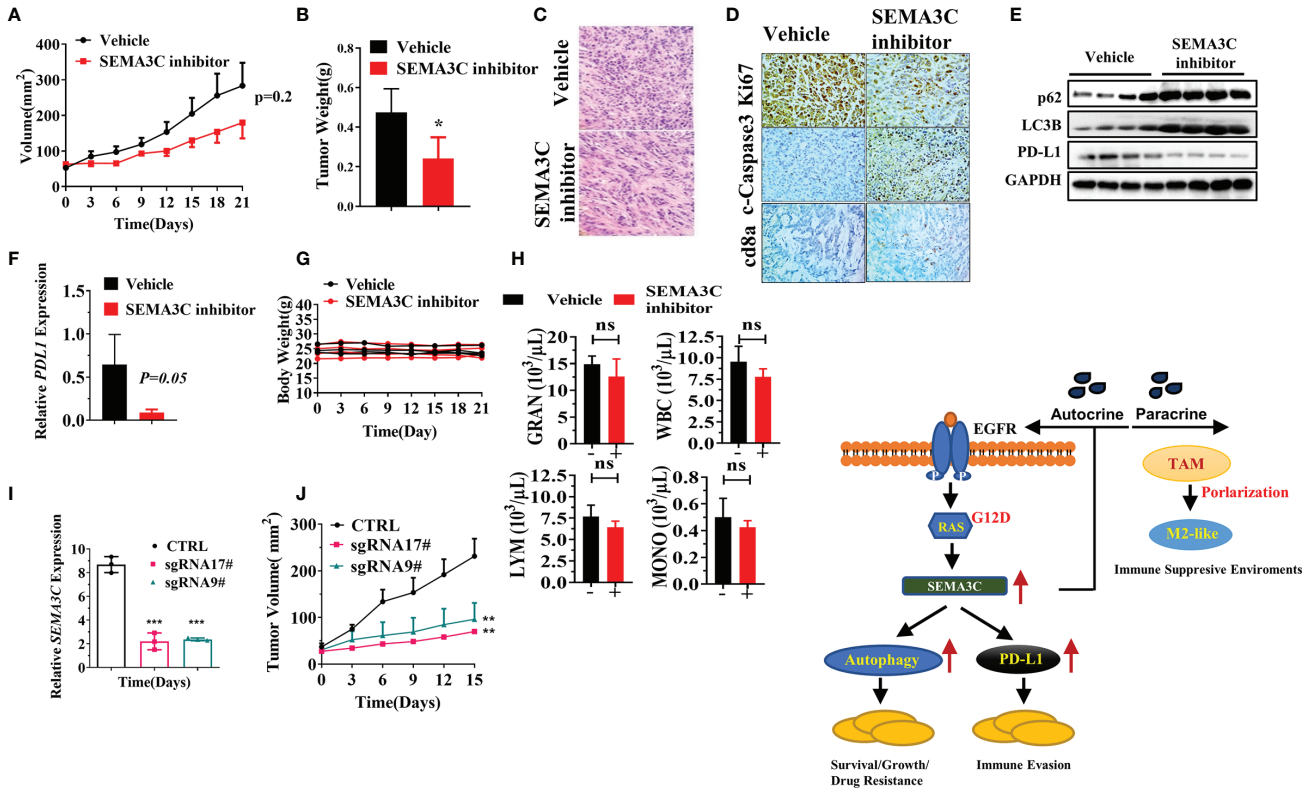

FIGURE 6 | **(A)** The tumor volume of the KPC tumor bearing mice model treated with SEMA3C inhibitor (20 mg/kg) or vehicle for 7 doses (n=5). The tumor length and width were measured every 3 days, and the tumor volume was calculated by the formula=1/2 length*width^2. **(B)** The weight of the tumors collected after euthanizing the mice treated with either the vehicle or SEMA3C inhibitor group. **(C)** H&E histology was evaluated in the vehicle and inhibitor groups. **(D)** Ki67 cleaved-Caspase3 and CD8a were evaluated in the vehicle and inhibitor groups. **(E)** Total proteins were extracted from the tumor, and autophagy related proteins p62, LC3B, and PD-L1 were detected by the western blot. **(F)** PD-L1 mRNA expression was detected by qPCR in tumors of KPC-Luc bearing mice. **(G)** The body weight of the Vehicle and SEMA3C inhibitor group were recorded every three days. **(H)** The complete blood counts were detected 48 hours after the inhibitor injection (HemaTrue, Loveland, Co). **(I)** SEMA3C expression were evaluated by qPCR in Vehicle, SEMA3C sgRNA 9# and 17#. **(J)** The tumor volume of the Vehicle, SEMA3C sgRNA 9# and 17# KPC cells subcutaneous model, the tumor length and width were measured every 3 days, and the tumor volume was calculated by the formula=1/2 length*width^2. **(K)** Schematic illustration of probable mechanism of SEMA3C role in pancreatic cancer. Data are representative of three independent experiments. T-tests for the measurements between the two groups; *P < 0.05, **P < 0.01, ***P < 0.001, ns, no significance.

shortened the survival time in pancreatic cancer patients. SEMA3C played a significant role in cell growth, cell colony formation, cell cycle arrest, and the increased apoptosis or necrosis of pancreatic cancer cells. Furthermore, a double knockdown of KRAS and SEMA3C shows significant synergistic inhibition of PANC1 cell growth and colony formation. We also demonstrated the synergistic effect in killing pancreatic cancer cells with the combination of MEK inhibitor and SEMA3C inhibitor. The process of autophagy is highly active in pancreatic cancer cells and autophagy is upregulated in KRAS mutated cells. Autophagy clears the dying organelles in damaged cancer cells to create the needed energy to survive and divide (68). The role of SEMA3C expression on autophagy regulation and immune modulation of TME has not been reported before. Herein, we found that high SEMA3C expression has enriched the autophagy process and SEMA3C played an active role in promoting autophagy. Next, we found that SEMA3C overexpression or inhibition can significantly regulate the expression of the autophagy-related markers in pancreatic cancer lines. Furthermore, SEMA3C expression can increase the PD-L1 expression in both tumor and immune cells which may mediate the immunosuppressive environment in pancreatic cancer. A SEMA3C inhibitor showed a significant inhibition effect on the growth of KPC-Luc bearing tumors *in vivo*. We further demonstrated the dramatic autophagy inhibition response by exploring the autophagy-related proteins and significant decrease in PD-L1 level in tumor tissue with treatment of SEMA3C inhibitor.

Overall, SEMA3C expression is associated with KRAS G12D mutation, which is highly expressed in pancreatic patients. Knocking down or inhibiting SEMA3C shows the tumor inhibition *in vitro* or *in vivo*. SEMA3C affects the regulation of autophagy and PD-L1. The study indicates that SEMA3C is a potentially promising and attractive target for pancreatic cancer therapy especially in patients with a G12D mutation in KRAS.

DATA AVAILABILITY STATEMENT

The raw data supporting the conclusions of this article will be made available by the authors, without undue reservation.

ETHICS STATEMENT

The animal study was reviewed and approved by The Animal Use and Care Administrative Advisory Committee of the University of California, Davis (IACUC #20265).

AUTHOR CONTRIBUTIONS

DZ and YL contributed to conception and design of the study. DZ collected the data and organized the database. DZ performed the statistical analysis. DZ wrote the first draft of the manuscript. DZ, AL, EK, C-IH, MH, TL and YL revise section of the manuscript. All authors contributed to manuscript revision, read, and approved the submitted version.

ACKNOWLEDGMENTS

The authors thank the financial support from NIH/NCI (Grant No. R01CA199668 and R01CA232845), NIH/NICHD (Grant No. R01HD086195), NIH/NIDCR (R01 DE029237, ACS IRG (Grant No. 95-125-13), and UC Davis Comprehensive Cancer Center Support Grant (CCSG) awarded by the National Cancer Institute (Grant No. NCI P30CA093373).

SUPPLEMENTARY MATERIAL

The Supplementary Material for this article can be found online at: https://www.frontiersin.org/articles/10.3389/fonc.2022.890154/full#supplementary-material

REFERENCES

1. Rahib L, Smith BD, Aizenberg R, Rosenzweig AB, Fleshman JM, Matrisian LM. Projecting Cancer Incidence and Deaths to 2030: The Unexpected Burden of Thyroid, Liver, and Pancreas Cancers in the United States. *Cancer Res* (2014) 74:2913–21. doi: 10.1158/0008-5472.CAN-14-0155
2. Conroy T, Hammel P, Hebbar M, Ben Abdelghani M, Wei AC, Raoul J-L, et al. FOLFIRINOX or Gemcitabine as Adjuvant Therapy for Pancreatic Cancer. *N Engl J Med* (2018) 379:2395–406. doi: 10.1056/NEJMoa1809775
3. Siegel RL, Miller KD, Fuchs HE, Jemal A. Cancer Statistics, 2022. *CA Cancer J Clin* (2022) 72:7–33. doi: 10.3322/caac.21708
4. Miller AL, Garcia PL, Yoon KJ. Developing Effective Combination Therapy for Pancreatic Cancer: An Overview. *Pharmacol Res* (2020) 155:104740. doi: 10.1016/j.phrs.2020.104740
5. Qian Y, Gong Y, Fan Z, Luo G, Huang Q, Deng S, et al. Molecular Alterations and Targeted Therapy in Pancreatic Ductal Adenocarcinoma. *J Hematol Oncol* (2020) 13:130. doi: 10.1186/s13045-020-00958-3
6. Giri B, Sethi V, Dudeja V, Banerjee S, Livingstone A, Saluja A. Genetics of Pancreatic Cyst-Cancer Progression: Standing on the Shoulders of Giants. *Curr Opin Gastroenterol* (2017) 33:404–10. doi: 10.1097/MOG.0000000000000382
7. Canon J, Rex K, Saiki AY, Mohr C, Cooke K, Bagal D, et al. The Clinical KRAS (G12C) Inhibitor AMG 510 Drives Anti-Tumour Immunity. *Nature* (2019) 575:217–23. doi: 10.1038/s41586-019-1694-1
8. Koga T, Suda K, Fujino T, Ohara S, Hamada A, Nishino M, et al. KRAS Secondary Mutations That Confer Acquired Resistance to KRAS G12C Inhibitors, Sotorasib and Adagrasib, and Overcoming Strategies: Insights From the *In Vitro* Experiments. *J Thorac Oncol* (2021) 16(8):1321–32. doi: 10.1016/j.jtho.2021.04.015
9. Awad MM, Liu S, Rybkin II, Arbour KC, Dilly J, Zhu VW, et al. Acquired Resistance to KRAS(G12C) Inhibition in Cancer. *N Engl J Med* (2021) 384:2382–93. doi: 10.1056/NEJMoa2105281
10. Cook JH, Melloni GEM, Gulhan DC, Park PJ, Haigis KM. The Origins and Genetic Interactions of KRAS Mutations Are Allele- and Tissue-Specific. *Nat Commun* (2021) 12:1808. doi: 10.1038/s41467-021-22125-z
11. Ihle NT, Byers LA, Kim ES, Saintigny P, Lee JJ, Blumenschein GR, et al. Effect of KRAS Oncogene Substitutions on Protein Behavior: Implications for Signaling and Clinical Outcome. *J Natl Cancer Inst* (2012) 104:228–39. doi: 10.1093/jnci/djr523
12. Hammond DE, Mageean CJ, Rusilowicz EV, Wickenden JA, Clague MJ, Prior IA. Differential Reprogramming of Isogenic Colorectal Cancer Cells by Distinct Activating KRAS Mutations. *J Proteome Res* (2015) 14:1535–46. doi: 10.1021/pr501191a
13. Scholl C, Frohling S, Dunn IF, Schinzel AC, Barbie DA, Kim SY, et al. Synthetic Lethal Interaction Between Oncogenic KRAS Dependency and STK33 Suppression in Human Cancer Cells. *Cell* (2009) 137:821–34. doi: 10.1016/j.cell.2009.03.017
14. Babij C, Zhang Y, Kurzeja RJ, Munzli A, Shehabeldin A, Fernando M, et al. STK33 Kinase Activity Is Nonessential in KRAS-Dependent Cancer Cells. *Cancer Res* (2011) 71:5818–26. doi: 10.1158/0008-5472.CAN-11-0778
15. Vitos-Faleato J, Real SM, Gutierrez-Prat N, Villanueva A, Llonch E, Drosten M, et al. Requirement for Epithelial P38alpha in KRAS-Driven Lung Tumor Progression. *Proc Natl Acad Sci USA* (2020) 117:2588–96. doi: 10.1073/pnas.1921404117
16. Hu K, Li K, Lv J, Feng J, Chen J, Wu H, et al. Suppression of the SLC7A11/glutathione Axis Causes Synthetic Lethality in KRAS-Mutant Lung Adenocarcinoma. *J Clin Invest* (2020) 130(4):1752–66. doi: 10.1172/JCI124049
17. Hobbs GA, Baker NM, Miermont AM, Thurman RD, Pierobon M, Tran TH, et al. Atypical KRAS(G12R) Mutant Is Impaired in PI3K Signaling and Macropinocytosis in Pancreatic Cancer. *Cancer Discovery* (2020) 10:104–23. doi: 10.1158/2159-8290.CD-19-1006
18. Xu X, Zhao Z, Guo S, Li J, Liu S, You Y, et al. Increased Semaphorin 3c Expression Promotes Tumor Growth and Metastasis in Pancreatic Ductal Adenocarcinoma by Activating the ERK1/2 Signaling Pathway. *Cancer Lett* (2017) 397:12–22. doi: 10.1016/j.canlet.2017.03.014
19. Brennan CW, Verhaak RG, McKenna A, Campos B, Noushmehr H, Salama SR, et al. The Somatic Genomic Landscape of Glioblastoma. *Cell* (2013) 155:462–77. doi: 10.1016/j.cell.2013.09.034
20. Vaitkiene P, Skiriute D, Steponaitis G, Skauminas K, Tamasauskas A, Kazlauskas A. High Level of Sema3C is Associated With Glioma Malignancy. *Diagn Pathol* (2015) 10:58. doi: 10.1186/s13000-015-0298-9
21. Hao J, Yu JS. Semaphorin 3C and Its Receptors in Cancer and Cancer Stem-Like Cells. *Biomedicines* (2018) 6(2):42. doi: 10.3390/biomedicines6020042
22. Man J, Shoemake J, Zhou W, Fang X, Wu Q, Rizzo A, et al. Sema3C Promotes the Survival and Tumorigenicity of Glioma Stem Cells Through Rac1 Activation. *Cell Rep* (2014) 9:1812–26. doi: 10.1016/j.celrep.2014.10.055
23. Tam KJ, Hui DHF, Lee WW, Dong M, Tombe T, Jiao IZF, et al. Semaphorin 3 C Drives Epithelial-to-Mesenchymal Transition, Invasiveness, and Stem-Like Characteristics in Prostate Cells. *Sci Rep* (2017) 7:11501. doi: 10.1038/s41598-017-11914-6
24. Cole-Healy Z, Vergani P, Hunter K, Brown NJ, Reed MW, Staton CA. The Relationship Between Semaphorin 3C and Microvessel Density in the Progression of Breast and Oral Neoplasia. *Exp Mol Pathol* (2015) 99:19–24. doi: 10.1016/j.yexmp.2015.03.041

25. Malik MF, Satherley LK, Davies EL, Ye L, Jiang WG. Expression of Semaphorin 3C in Breast Cancer and Its Impact on Adhesion and Invasion of Breast Cancer Cells. *Anticancer Res* (2016) 36:1281–6.
26. Lee CCW, Munuganti RSN, Peacock JW, Dalal K, Jiao IZF, Shepherd A, et al. Targeting Semaphorin 3C in Prostate Cancer With Small Molecules. *J Endocr Soc* (2018) 2:1381–94. doi: 10.1210/js.2018-00170
27. Cerami E, Gao J, Dogrusoz U, Gross BE, Sumer SO, Aksoy BA, et al. The Cbio Cancer Genomics Portal: An Open Platform for Exploring Multidimensional Cancer Genomics Data. *Cancer Discovery* (2012) 2:401–4. doi: 10.1158/2159-8290.CD-12-0095
28. Tang Z, Li C, Kang B, Gao G, Li C, Zhang Z. GEPIA: A Web Server for Cancer and Normal Gene Expression Profiling and Interactive Analyses. *Nucleic Acids Res* (2017) 45:W98–W102. doi: 10.1093/nar/gkx247
29. Li T, Fan J, Wang B, Traugh N, Chen Q, Liu JS, et al. TIMER: A Web Server for Comprehensive Analysis of Tumor-Infiltrating Immune Cells. *Cancer Res* (2017) 77:e108–10. doi: 10.1158/0008-5472.CAN-17-0307
30. Nagy A, Munkacsy G, Gyorffy B. Pancancer Survival Analysis of Cancer Hallmark Genes. *Sci Rep* (2021) 11:6047. doi: 10.1038/s41598-021-84787-5
31. Rhodes DR, Yu J, Shanker K, Deshpande N, Varambally R, Ghosh D, et al. ONCOMINE: A Cancer Microarray Database and Integrated Data-Mining Platform. *Neoplasia* (2004) 6:1–6. doi: 10.1016/S1476-5586(04)80047-2
32. Zhang D, Wang Q, Zhu T, Cao J, Zhang X, Wang J, et al. RACK1 Promotes the Proliferation of THP1 Acute Myeloid Leukemia Cells. *Mol Cell Biochem* (2013) 384:197–202. doi: 10.1007/s11010-013-1798-0
33. Zhang DL, Qu LW, Ma L, Zhou YC, Wang GZ, Zhao XC, et al. Genome-Wide Identification of Transcription Factors That Are Critical to non-Small Cell Lung Cancer. *Cancer Lett* (2018) 434:132–43. doi: 10.1016/j.canlet.2018.07.020
34. Lamano JB, Lamano JB, Li YD, DiDomenico JD, Choy W, Veliceasa D, et al. Glioblastoma-Derived IL6 Induces Immunosuppressive Peripheral Myeloid Cell PD-L1 and Promotes Tumor Growth. *Clin Cancer Res* (2019) 25:3643–57. doi: 10.1158/1078-0432.CCR-18-2402
35. Bournet B, Muscari F, Buscail C, Assenat E, Barthet M, Hammel P, et al. KRAS G12D Mutation Subtype Is A Prognostic Factor for Advanced Pancreatic Adenocarcinoma. *Clin Transl Gastroenterol* (2016) 7:e157. doi: 10.1038/ctg.2016.18
36. Qian ZR, Rubinson DA, Nowak JA, Morales-Oyarvide V, Dunne RF, Kozak MM, et al. Association of Alterations in Main Driver Genes With Outcomes of Patients With Resected Pancreatic Ductal Adenocarcinoma. *JAMA Oncol* (2018) 4:e173420. doi: 10.1001/jamaoncol.2017.3420
37. Miglio U, Oldani A, Mezzapelle R, Veggiani C, Paganotti A, Garavoglia M, et al. KRAS Mutational Analysis in Ductal Adenocarcinoma of the Pancreas and Its Clinical Significance. *Pathol Res Pract* (2014) 210:307–11. doi: 10.1016/j.prp.2014.01.011
38. Witkiewicz AK, McMillan EA, Balaji U, Baek G, Lin WC, Mansour J, et al. Whole-Exome Sequencing of Pancreatic Cancer Defines Genetic Diversity and Therapeutic Targets. *Nat Commun* (2015) 6:6744. doi: 10.1038/ncomms7744
39. Stephens RM, Yi M, Kessing B, Nissley DV, McCormick F. Tumor RAS Gene Expression Levels Are Influenced by the Mutational Status of RAS Genes and Both Upstream and Downstream RAS Pathway Genes. *Cancer Inform* (2017) 16:1176935117711944. doi: 10.1177/1176935117711944
40. Peng J, Sun BF, Chen CY, Zhou JY, Chen YS, Chen H, et al. Single-Cell RNA-Seq Highlights Intra-Tumoral Heterogeneity and Malignant Progression in Pancreatic Ductal Adenocarcinoma. *Cell Res* (2019) 29:725–38. doi: 10.1038/s41422-019-0195-y
41. Boj SF, Hwang CI, Baker LA, Chio II, Engle DD, Corbo V, et al. Organoid Models of Human and Mouse Ductal Pancreatic Cancer. *Cell* (2015) 160:324–38. doi: 10.1016/j.cell.2014.12.021
42. Goswami CP, Nakshatri H. PROGgeneV2: Enhancements on the Existing Database. *BMC Cancer* (2014) 14:970. doi: 10.1186/1471-2407-14-970
43. Di Veroli GY, Fornari C, Wang D, Mollard S, Bramhall JL, Richards FM, et al. Combenefit: An Interactive Platform for the Analysis and Visualization of Drug Combinations. *Bioinformatics* (2016) 32:2866–8. doi: 10.1093/bioinformatics/btw230
44. Eng CH, Wang Z, Tkach D, Toral-Barza L, Ugwonali S, Liu S, et al. Macroautophagy is Dispensable for Growth of KRAS Mutant Tumors and Chloroquine Efficacy. *Proc Natl Acad Sci USA* (2016) 113:182–7. doi: 10.1073/pnas.1515617113
45. Komatsu M, Waguri S, Koike M, Sou YS, Ueno T, Hara T, et al. Homeostatic Levels of P62 Control Cytoplasmic Inclusion Body Formation in Autophagy-Deficient Mice. *Cell* (2007) 131:1149–63. doi: 10.1016/j.cell.2007.10.035
46. Antonucci L, Fagman JB, Kim JY, Todoric J, Gukovsky I, Mackey M, et al. Basal Autophagy Maintains Pancreatic Acinar Cell Homeostasis and Protein Synthesis and Prevents ER Stress. *Proc Natl Acad Sci USA* (2015) 112:E6166–6174. doi: 10.1073/pnas.1519384112
47. Kaizuka T, Morishita H, Hama Y, Tsukamoto S, Matsui T, Toyota Y, et al. An Autophagic Flux Probe That Releases an Internal Control. *Mol Cell* (2016) 64:835–49. doi: 10.1016/j.molcel.2016.09.037
48. Hamarsheh S, Gross O, Brummer T, Zeiser R. Immune Modulatory Effects of Oncogenic KRAS in Cancer. *Nat Commun* (2020) 11:5439. doi: 10.1038/s41467-020-19288-6
49. Chen N, Fang W, Lin Z, Peng P, Wang J, Zhan J, et al. KRAS Mutation-Induced Upregulation of PD-L1 Mediates Immune Escape in Human Lung Adenocarcinoma. *Cancer Immunol Immunother* (2017) 66:1175–87. doi: 10.1007/s00262-017-2005-z
50. Roy S, Bag AK, Singh RK, Talmadge JE, Batra SK, Datta K. Multifaceted Role of Neuropilins in the Immune System: Potential Targets for Immunotherapy. *Front Immunol* (2017) 8:1228. doi: 10.3389/fimmu.2017.01228
51. Sun D, Wang J, Han Y, Dong X, Ge J, Zheng R, et al. TISCH: A Comprehensive Web Resource Enabling Interactive Single-Cell Transcriptome Visualization of Tumor Microenvironment. *Nucleic Acids Res* (2021) 49:D1420–30. doi: 10.1093/nar/gkaa1020
52. Tang F, Zheng P. Tumor Cells Versus Host Immune Cells: Whose PD-L1 Contributes to PD-1/PD-L1 Blockade Mediated Cancer Immunotherapy? *Cell Biosci* (2018) 8:34. doi: 10.1186/s13578-018-0232-4
53. Chen N, Fang W, Zhan J, Hong S, Tang Y, Kang S, et al. Upregulation of PD-L1 by EGFR Activation Mediates the Immune Escape in EGFR-Driven NSCLC: Implication for Optional Immune Targeted Therapy for NSCLC Patients With EGFR Mutation. *J Thorac Oncol* (2015) 10:910–23. doi: 10.1097/JTO.0000000000000500
54. Smith AG, Macleod KF. Autophagy, Cancer Stem Cells and Drug Resistance. *J Pathol* (2019) 247:708–18. doi: 10.1002/path.5222
55. Yang S, Wang X, Contino G, Liesa M, Sahin E, Ying H, et al. Pancreatic Cancers Require Autophagy for Tumor Growth. *Genes Dev* (2011) 25:717–29. doi: 10.1101/gad.2016111
56. Kimmelman AC. Metabolic Dependencies in RAS-Driven Cancers. *Clin Cancer Res* (2015) 21(8):1828–34. doi: 10.1158/1078-0432.CCR-14-2425
57. Bryant KL, Stalnecker CA, Zeitouni D, Klomp JE, Peng S, Tikunov AP, et al. Combination of ERK and Autophagy Inhibition as a Treatment Approach for Pancreatic Cancer. *Nat Med* (2019) 25:628–40. doi: 10.1038/s41591-019-0368-8
58. Kinsey CG, Camolotto SA, Boespflug AM, Guillen KP, Foth M, Truong A, et al. Protective Autophagy Elicited by RAF–>MEK–>ERK Inhibition Suggests a Treatment Strategy for RAS-Driven Cancers. *Nat Med* (2019) 25:620–7. doi: 10.1038/s41591-019-0367-9
59. Looi CK, Chung FF, Leong CO, Wong SF, Rosli R, Mai CW. Therapeutic Challenges and Current Immunomodulatory Strategies in Targeting the Immunosuppressive Pancreatic Tumor Microenvironment. *J Exp Clin Cancer Res* (2019) 38:162. doi: 10.1186/s13046-019-1153-8
60. von Ahrens D, Bhagat TD, Nagrath D, Maitra A, Verma A. The Role of Stromal Cancer-Associated Fibroblasts in Pancreatic Cancer. *J Hematol Oncol* (2017) 10:76. doi: 10.1186/s13045-017-0448-5
61. Kabacaoglu D, Ciecielski KJ, Ruess DA, Algul H. Immune Checkpoint Inhibition for Pancreatic Ductal Adenocarcinoma: Current Limitations and Future Options. *Front Immunol* (2018) 9:1878. doi: 10.3389/fimmu.2018.01878
62. Lu C, Paschall AV, Shi H, Savage N, Waller JL, Sabbatini ME, et al. The MLL1-H3K4me3 Axis-Mediated PD-L1 Expression and Pancreatic Cancer Immune Evasion. *J Natl Cancer Inst* (2017) 109(6):djw283. doi: 10.1093/jnci/djw283
63. Yang S, Liu Q, Liao Q. Tumor-Associated Macrophages in Pancreatic Ductal Adenocarcinoma: Origin, Polarization, Function, and Reprogramming. *Front Cell Dev Biol* (2020) 8:607209. doi: 10.3389/fcell.2020.607209
64. Fujii A, Masuda T, Iwata M, Tobo T, Wakiyama H, Koike K, et al. The Novel Driver Gene ASAP2 Is a Potential Druggable Target in Pancreatic Cancer. *Cancer Sci* (2021) 112:1655–68. doi: 10.1111/cas.14858

65. Kundu S, Ali MA, Handin N, Conway LP, Rendo V, Artursson P, et al. Common and Mutation Specific Phenotypes of KRAS and BRAF Mutations in Colorectal Cancer Cells Revealed by Integrative-Omics Analysis. *J Exp Clin Cancer Res* (2021) 40:225. doi: 10.1186/s13046-021-02025-2
66. Fujii S, Ishibashi T, Kokura M, Fujimoto T, Matsumoto S, Shidara S, et al. RAF1-MEK/ERK Pathway-Dependent ARL4C Expression Promotes Ameloblastoma Cell Proliferation and Osteoclast Formation. *J Pathol* (2022) 256(1):119–33. doi: 10.1002/path.5814
67. Harada A, Matsumoto S, Yasumizu Y, Akama T, Eguchi H, Kikuchi A. Localization of KRAS Downstream Target ARL4C to Invasive Pseudopods Accelerates Pancreatic Cancer Cell Invasion. *Elife* (2021) 10:e66721. doi: 10.7554/eLife.66721
68. Bigelsen S. Evidence-Based Complementary Treatment of Pancreatic Cancer: A Review of Adjunct Therapies Including Paricalcitol, Hydroxychloroquine, Intravenous Vitamin C, Statins, Metformin, Curcumin, and Aspirin. *Cancer Manag Res* (2018) 10:2003–18. doi: 10.2147/CMAR.S161824

Conflict of Interest: The authors declare that the research was conducted in the absence of any commercial or financial relationships that could be construed as a potential conflict of interest.

Publisher's Note: All claims expressed in this article are solely those of the authors and do not necessarily represent those of their affiliated organizations, or those of the publisher, the editors and the reviewers. Any product that may be evaluated in this article, or claim that may be made by its manufacturer, is not guaranteed or endorsed by the publisher.

frontiers | Frontiers in Oncology

REVIEW
published: 27 June 2022
doi: 10.3389/fonc.2022.829212

Targeting Adenylate Cyclase Family: New Concept of Targeted Cancer Therapy

Rui Guo[1†], *Tian Liu*[1†], *Marzieh Dehghan Shasaltaneh*[2†], *Xuan Wang*[3†], *Saber Imani*[1,3*] *and QingLian Wen*[1*]

[1] Department of Oncology, The Affiliated Hospital of Southwest Medical University, Luzhou, China, [2] Department of Biology, Faculty of Science, University of Zanjan, Zanjan, Iran, [3] China Regional Research Center, International Centre for Genetic Engineering and Biotechnology Taizhou, Jiangsu, China

The adenylate cyclase (ADCY) superfamily is a group of glycoproteins regulating intracellular signaling. ADCYs act as key regulators in the cyclic adenosine monophosphate (cAMP) signaling pathway and are related to cell sensitivity to chemotherapy and ionizing radiation. Many members of the superfamily are detectable in most chemoresistance cases despite the complexity and unknownness of the specific mechanism underlying the role of ADCYs in the proliferation and invasion of cancer cells. The overactivation of ADCY, as well as its upstream and downstream regulators, is implicated as a major potential target of novel anticancer therapies and markers of exceptional responders to chemotherapy. The present review focuses on the oncogenic functions of the ADCY family and emphasizes the possibility of the mediating roles of deleterious nonsynonymous single nucleotide polymorphisms (nsSNPs) in ADCY as a prognostic therapeutic target in modulating resistance to chemotherapy and immunotherapy. It assesses the mediating roles of ADCY and its counterparts as stress regulators in reprogramming cancer cell metabolism and the tumor microenvironment. Additionally, the well-evaluated inhibitors of ADCY-related signaling, which are under clinical investigation, are highlighted. A better understanding of ADCY-induced signaling and deleterious nsSNPs (p.E1003K and p.R1116C) in ADCY6 provides new opportunities for developing novel therapeutic strategies in personalized oncology and new approaches to enhance chemoimmunotherapy efficacy in treating various cancers.

Keywords: adenylate cyclase, cAMP signaling, molecular targeted therapy, chemoresistance, signaling pathway 4

OPEN ACCESS

Edited by:
Yan-Yan Yan,
Shanxi Datong University, China

Reviewed by:
Silvio Naviglio,
University of Campania Luigi Vanvitelli, Italy
Shuanshuan Xie,
Tongji University, China

***Correspondence:**
Saber Imani
saberimani@swmu.edu.cn
QingLian Wen
wql73115@hotmail.com

[†]*These authors have contributed equally to this work*

Specialty section:
This article was submitted to Cancer Molecular Targets and Therapeutics, a section of the journal Frontiers in Oncology

Received: *05 December 2021*
Accepted: *26 May 2022*
Published: *27 June 2022*

Citation:
Guo R, Liu T, Shasaltaneh MD, Wang X, Imani S and Wen Q (2022) Targeting Adenylate Cyclase Family: New Concept of Targeted Cancer Therapy. Front. Oncol. 12:829212. doi: 10.3389/fonc.2022.829212

1 INTRODUCTION

The latest global cancer burden data released by the International Agency for Research on Cancer (IARC) of the World Health Organization revealed 19.29 million new cancer cases and 9.96 million cancer deaths worldwide in 2020. The number of new cancer cases is predicted to increase to approximately 28.4 million worldwide in 2040, which is up by 47% compared to 2020. Following the development of targeted therapies and immunotherapy, cancer treatment modalities have long gone beyond surgery and radiotherapy. Outcomes for cancer patients are improved by applying tyrosine

kinase, cell cycle-dependent kinase (CDK), cell cycle, integrin signaling, and immune checkpoint inhibitors, although their efficacy significantly varies due to a variety of limiting factors (1). The effectiveness of targeted therapy depends on the correct matching between drug and target. The targets are expressed to varying degrees on tumor cells and act as the oncogenic driver mutations that provide cancer cells with growth and survival advantages. Therefore, the specific mechanisms of tumorigenesis should be further explored to identify novel therapeutic targets meeting the challenge related to the precision of oncology.

Based on the results of many studies since 1971, adenylate cyclase (AC) activity and cAMP levels are associated with the normalization of tumor cell morphology and restoration of contact inhibition, as well as the reduced growth rate (2, 3). AC activation, which drives the production of cAMP from adenosine triphosphate (ATP), leading to elevated intracellular cAMP levels (4), is accompanied by cancer through protein kinase A (PKA)-dependent and independent pathways. In addition to being involved in cell cycle inhibition, apoptosis, and growth, cAMP regulates angiogenesis by inhibiting vascular endothelial growth factor (VEGF), TGF-β, and epidermal growth factor receptor (EGFR) pathways (5). Targeting the upstream and downstream of the cAMP signaling pathway exhibits a range of anticancer effects such as the induction of mesenchymal-to-epithelial transition (EMT), inhibition of cell growth and migration, and enhanced sensitivity of cancer cells to conventional anticancer drugs (6–8).

The *adenylate cyclase* (*ADCY*) gene family, which encodes AC proteins, plays important regulatory roles in a spectrum of biological processes like cell proliferation, apoptosis, migration, invasion, angiogenesis, abnormal metabolism, and immune escape (9–11). AC compounds are already in clinical use for certain diseases such as neuropathic pain, neurodegenerative diseases, congestive heart failure, asthma, and male contraception (12). However, the studies on the role of the various isoforms of the ADCY family in cancer have been mainly limited to the screening of biomarkers for different cancers and the discovery of interactions with other genes or small molecules (13). Certain AC isoforms are expressed more or less in specific cancers and are associated in tumor development as pro- or anticancer factors, although specific mechanisms are unclear. In general, the potential role of the family in cancer therapy warrants attention and can yield important new targets for the treatment. The present study reviewed the current understanding of the ADCY family and the mechanism of ADCY activation in response to various types of chemotherapy. It highlighted the role of the family in the different signaling pathways regulating resistance to chemotherapy in tumorigenesis.

2 ACS AND CAMP LEVEL REGULATION

ACs are glycoproteins with important functions as intracellular signaling regulators. This large family contains 10 subtypes (AC I–IX and soluble AC (sAC)), each of which is encoded by an independent gene (*ADCY1–ADCY10*). *ADCY1–ADCY18* are located on different chromosomes, while *ADCY9* and *ADCY7* are locateded on chromosome 16 (14) (**Figure 1**). Membrane-bound ACs can be divided into four types according to the various regulatory characteristics (**Table 1**), the first of which is composed of AC1, AC3, and AC8, which are activated by cationic calcium (Ca^{2+}) and calmodulin (CAM). The second involves AC2, AC4, and AC7, which are activated by heterotrimeric GTP-binding protein (G-protein) βγ subunits, while they are insensitive to calcium. The next group, consisting of AC5 and AC6, is inhibited by Ca^{2+} and inhibitory G-protein (Gi), and AC9, as the only member of the

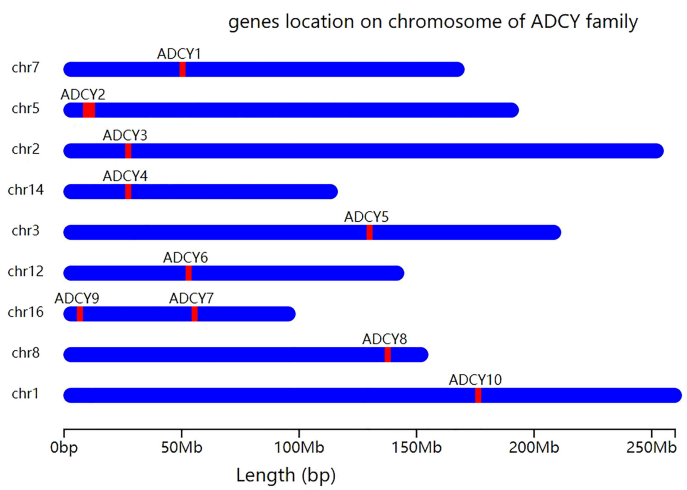

FIGURE 1 | Chromosomal localization of *ADCY* gene isoforms. Except for *ADCY7* and *ADCY9*, which are both located on chromosome 16, all other *ADCY* subtypes are located on different chromosomes. *ADCY1* is located on chromosome 7, *ADCY2* on chromosome 5, *ADCY3* on chromosome 2, *ADCY4* on chromosome 14, *ADCY5* on chromosome 3, *ADCY6* on chromosome 12, *ADCY8* on chromosome 8, and *ADCY10* on chromosome 1.

TABLE 1 | Activators or inhibitors for AC subtypes and related diseases.

Type of AC		Coded by	Related diseases	Activator[a]	Inhibitor[b]	Insensitive[c]
Membrane-bound AC						
Type 1	AC1	ADCY1	Long-term memory impairment	Ca^{2+}; CAM and forskolin		
	AC3	ADCY3	Motor dysfunction; renal function decline; obesity; diabetes			
	AC8	ADCY8	Long-term memory impairment; neuropsychiatric disorders			
Type 2	AC2	ADCY2	Breathing dysfunction; neuropsychiatric disorders; two-way emotional disorder	Heterotrimer G protein βγ subunits; forskolin		Calcium
	AC4	ADCY4	Breast cancer			
	AC7	ADCY7	Autoimmune diseases; depression			
Type 3	AC5	ADCY5	Renal function decline; alcohol addiction; extrapyramidal movement disorders	Forskolin	Ca^{2+},Giα	
	AC6	ADCY6	Nephrogenic diabetes insipidus; renal function decline; heart failure			
Type 4	AC9	ADCY9	Stroke in sickle cell disease; immune function disorders; different cancer	Calcineurin		Forskolin
Soluble AC						
Type 1	sAC	ADCY10	Prostate cancer; breast cancer; glaucoma; diabetes	Bicarbonate, calcium and ATP		Forskolin, heterotrimer G protein

AC/ADCY, adenylate cyclase; CAM, calcium-regulated proteins; Giα, the α subunit of the Gi protein; ATP, adenosine triphosphate.

[a]*Activator: the ADCY subtype of this classification is stimulated under the influence of such substances, thus activating the relevant downstream molecules for a subsequent series of reactions.*

[b]*Inhibitor: the ADCY subtype of this classification is inhibited under the influence of such substances, thereby reducing the occurrence of related downstream molecules and the subsequent series of reactions.*

[c]*Insensitive: the ADCY subtypes of this classification are sensitive to such foreign substances and can stimulate the ADCY subtype to react accordingly.*

cAMP-related pathways and biological function.

fourth type, is the only isomer that is not activated by forskolin, while it responds to calcineurin (15). In addition, sAC is stimulated by bicarbonate, calcium, and ATP, while it is insensitive to forskolin and heterotrimeric G-protein (16). ACs serve as the effectors of the G-protein-coupled system. Furthermore, at least two heterotrimeric G-proteins are responsible for regulating the activity of transmembrane adenylate cyclase (tmAC), which include stimulatory G-protein (Gs) and Gi, which activate and inhibit AC, respectively (17). It is worth noting that the differential regulation and unique distribution of various AC isomers can create completely different cellular signals, making them key enzymes in the signaling pathway (18). ACs are widely distributed, the diverse subtypes of which perform various physiological functions, and each subtype has nonspecific cross-coordination or antagonism properties. The results of some studies demonstrated that the regulation of ADCY expression is closely related to animal health, while it lacks effective selectivity (19). Furthermore, the nonselective inhibition of ACs causes a series of potential adverse reactions like long-term memory (LTM) impairment (AC1 and AC8), motor dysfunction (AC3), nephrogenic diabetes insipidus (AC6), renal function decline (AC3, AC5, and AC6), and higher mortality rate during sympathetic nerve maintenance stimulation (other ACs) (19).

The cAMP directly regulates many cellular functions (20). Intracellular cAMP is produced from ATP during a reaction catalyzed by ACs, while cAMP degradation is mediated by cAMP phosphodiesterase (PDE), which hydrolyses cAMP to produce adenosine 5′-monophosphate (21). Thus, the dynamic balance of intracellular cAMP levels is maintained by a combination of AC stimulation and PDE-mediated degradation. Additionally, cAMP acts as an intracellular signal for many hormones, neurotransmitters, and other signaling molecules, the production and degradation of which are accompanied by its sensitivity to a wide range of extracellular and intracellular signals. Some heterologous G-protein-coupled receptors (GPCR) such as nicotinic acetylcholine, beta-adrenergic, or adenosine receptors activate AC, leading to a rise in cAMP production (22). Similarly, forskolin directly stimulates AC, and theophylline and caffeine promote intracellular cAMP levels by inhibiting PDE (16), and consequently affect a range of pathophysiological functions.

3 AC-RELATED DISORDERS

Today, AC subtypes are known to be associated with different diseases (**Table 1**), such as autoimmune ones and depression (23), as well as stroke in sickle cell disease, immune function disorders, and different cancers (AC9) (24). Furthermore, AC1 and AC4 are respectively accompanied by LTM impairment (25) and breast cancer (26), while AC3 is related to motor dysfunction, renal function decline, obesity, and diabetes (18). An association is found between AC8 with LTM impairment and neuropsychiatric disorders (27). Some researchers found a relationship between AC2 with breathing dysfunction and neuropsychiatric and bipolar disorders (28), as well as another between AC5 with renal function decline, alcohol addiction, and extrapyramidal movement disorders (29). Furthermore, AC6 is accompanied by nephrogenic diabetes insipidus, renal function

decline, and heart failure (30). Finally, sAC is associated with prostate and breast cancer, glaucoma, and diabetes (31). Thus, AC subtypes are implied as important players in various diseases, suggesting that relevant diseases can be controlled by the specific targeting and regulation of AC isoforms.

4 cAMP-RELATED PATHWAYS AND BILOGICAL FUNCTION

The cAMP, as the first identified second messenger, regulates cellular transport by binding to PKAs, cAMP-activated guanine exchange factors (EPACs), and cyclic nucleotide-gated channels (CNGs) (32) (**Figure 2**). These cAMP sensors lead to the regulation of various physiological processes such as DNA degradation, cell proliferation, and apoptosis either alone or in cooperation with PKAs (33). PKAs and EPACs are the major targets of the cAMP signaling pathway (34). In addition, activated PKA-phosphatases regulate related metabolic and transcription factors like the activation of downstream cAMP response element-binding proteins (CREB) and consequently activate the WNT/β-catenin pathway, which is accompanied by cell cycle arrest, apoptosis, and survival (34). CREB regulates the inhibitory activity of apoptosis proteins (IAPs) to prevent apoptosis triggered by various stimuli and plays an important role in inhibiting cell death and regulating DNA damage in the cell cycle (35). Furthermore, the cAMP signaling pathway regulates sirtuin 6 expression through modulating the PKA-dependent Raf/mitogen-activated extracellular signal-regulated kinase/extracellular signal-regulated kinase (Raf-MEK-ERK) pathway as well as ubiquitin-protease-dependent degradation, causing apoptosis regulation (36). Similarly, the regulation of protein phosphatase 2A (PP2A) plays a crucial role in regulating apoptosis (37). PKA activation can protect cancer cells from apoptosis after exposure to radiation or chemotherapeutic agents by increasing parathyroid hormone-related protein expression (38). The higher PKA expression enhances the activity of the mitogen-activated protein kinase (MAPK) signaling pathway (39), which regulates cell proliferation. The results of a recent study demonstrated the important role of X-ray repair in complementing defective repair in repairing DNA in Chinese hamster cell 1 (XRCC1) and the ability of cAMP-mediated EPACs to repair DNA damage by regulating XRCC1 (40). Furthermore, EPACs regulate cell proliferation, differentiation, apoptosis, and inflammation as well as play a crucial role in endoskeletal remodeling, cell proliferation, adhesion, migration, and epithelial-mesenchymal transition by regulating downstream signaling molecules in the vascular cAMP signaling pathway (40). They can even act by preventing c-Jun N-terminal kinase (JNK) activation by inhibiting B-cell lymphoma-2 (Bcl-2) phosphorylation, downregulating cellular autophagy and phosphorylation, and subsequently leading to less ubiquitination and more histone deacetylase 8 (HDAC8) expression (41). Additionally, Bcl-2 is a well-known member of the antiapoptotic protein family, which serves by inhibiting the essential proapoptotic proteins that share multiple homology

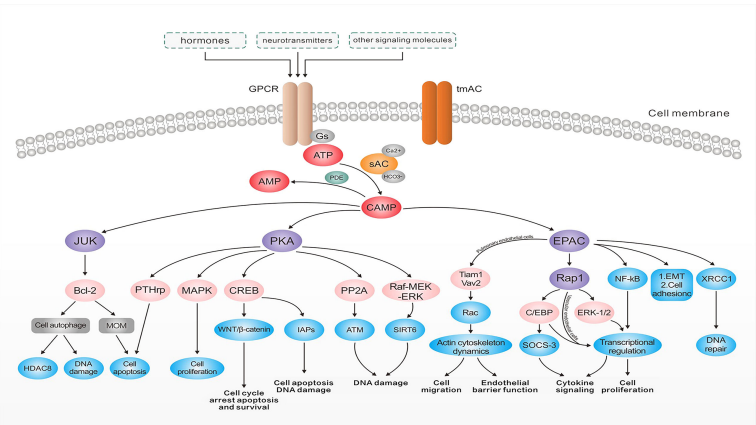

FIGURE 2 | The roles of adenylate cyclases in tumorigenesis. After binding to G protein-coupled receptors, hormones, neurotransmitters, and a number of other signaling molecules, cyclic adenosine 3′,5′-monophosphate (cAMP) is generated from ATP by the action of adenylate cyclase and degraded to the 5′-cAMP by the action of cyclic nucleotide phosphodiesterase (PDE). cAMP can increase DNA damage *via* a range of pathways and plays an important role in endoskeletal remodeling, cell proliferation, adhesion, and EMT. It also regulates the permeability of the mitochondrial outer membrane, affecting cell survival, activates the WNT/β-catenin pathway, and regulates the processes of cell cycle arrest, apoptosis, survival, and DNA damage. cAMP signaling pathways can also protect cancer cells from apoptosis after exposure to radiation or chemotherapeutic agents through related pathways. Abbreviations: EGFR, epidermal growth factor receptor; tmAC, transmembrane adenylate cyclase; Gs, stimulatory G-protein; sAC, soluble adenylate cyclase; ATP, adenosine triphosphate; PDE, phosphodiesterase; cAMP, cyclic adenosine phosphate; PKA, protein kinase A; JNK, c-Jun N-terminal kinase; Bcl-2, B-cell lymphoma-2; MOM, mitochondrial outer membrane; HDAC8, histone deacetylase 8; MAPK, mitogen-activated protein kinase; CREB, cAMP response element-binding proteins; IAPs, inhibitor of apoptosis proteins; PP2A, protein phosphatase 2A; ATM, the ataxia–telangiectasia–mutated protein; Raf-MEK-ERK, Raf/mitogen-activated extracellular signal-regulated kinase/extracellular signal-regulated kinase; EPAC, cAMP-EGF-I/II; ERK, extracellular signal-regulated kinase; XRCC1, X-ray repair complementing defective repair in Chinese hamster cell 1; EMT, epithelial-mesenchymal transition; SOCS-3, suppressor of cytokine signaling 3; C/EBP, CCAAT/enhancer-binding protein.

domains with Bcl-2 (42). It regulates mitochondrial outer membrane (MOM) permeability, which has a key role in apoptotic signaling and influences cell survival (43). Therefore, ACs regulate cAMP production, which results in modulating downstream signaling molecules to control various cellular physiological activities.

5 MUTATIONS IN ADCY FAMILY

5.1 Disease-Causing Effects of the Mutations in the ADCY Family

To date, at least 60 *ADCY* gene mutations have been reported in many genotype–phenotype databases, such as the Online Mendelian Inheritance in Man (OMIM) and Human Gene Mutation Database (HGMD), as well as the Database of Genotype and Phenotype (dbGAP). Mutations in ADCY1, ADCY2, ADCY3, ADCY4, ADCY6, and ADCY7 isoforms exhibit the most pathological effects and clinical significance. The disease-causing mutations are predominantly nonsense variants, partial and full deletions, and nonsense, insertion, and splice-site mutations. Nonsynonymous single nucleotide polymorphisms (nsSNPs, substitutions, and deletions) are considered the most common variants of *ADCY1* and *ADCY6*. Furthermore, exons 22 (22,896 bp of variants/length) and 23 (148,977 bp of variants/length) are the most affected exons. Some *ADCY* mutations were initially identified incorrectly due to the similarity between their symptoms and the other cancer-driver mutations. **Table 2** lists the most frequent disease-causing SNP mutation spectrums in *ADCY1* and *ADCY6*. As shown, the nonsynonymous mutations of G>A are more widely observed and change highly conserved amino acids in ADCY1 and ADCY6. The deleterious and pathogenic aspects of mutations were predicted by using an *in silico* prediction pipeline consisting of polymorphism phenotyping v2 (PolyPhen-2), mutation taster, I-Mutant, sorting intolerant from tolerant (SIFT), and ExAC programs. Furthermore, several online programs were applied to predict the pathogenicity of the selected variants of ADCY1 and ADCY6. Based on the predictions, *ADCY6* variants are disease-causing and damaging mutations, especially p.E1003K, p.R1116C, and p.Y992C, which were verified by more than two bioinformatics programs (**Table 2**). Three variants have a deleterious effect when using the SIFT and PolyPhen2 tools. Generally, the nsSNPs c. 3007G>A (p.E1003K), c. 3346C>T (p.R1116C), and c. 2975A>G (p.Y992C) are predicted to be pathogenic mutations with the potential as cancer-driver mutations.

5.2 Functional Effects of a Pathogenic Mutation in the ADCY Family

The analysis of the conserved domains of wild-type (WT) and mutant ADCY6 proteins is shown in **Figure 3**. In addition, the mutation sites were aligned to the ADCY6 protein sequence to explore the function-associated nsSNPs (**Figure 3A**). Most of the disease-driver mutations generate defective helicase proteins due to the changes in conserved residues (i.e., Y991, E1003, and

TABLE 2 | Predicted protein structure and disease-causing effects of mutations in AC family.

Gene	Exon	Variation				Polyphen-2 [sensitivity–specificity][b]	Mutation taster[c]	I-Mutant3.0 (kcal/mol)[d]	SIFT[e]	EXAC[f]	Overall evaluated pathogenicity
		Nucleotide[a]	Protein[a]	Type	Status						
ADCY1	22	c.2818 G>A	p.Ala940Thr	Missense	Homo	B (0.005) [0.97–0.740]	B (1.00)	DS (–0.45)	T (0.05)	Novel	Benign
	22	c. 3090G>A	p.Val984Met	Synonymous	Homo	PD (1.000) [0.00–1.00]	B (1.00)	DS (–1.37)	NT (0.05)	Novel	Benign
	22	c. 3184G>A	p.Gly1062Ser	Missense	Homo	PD (1.000) [0.00–1.00]	B (1.00)	DS (–1.37)	T (1.00)	Novel	Benign
ADCY6	23	c. 1640T>C	p.Ile547Thr	Missense	Hetro	PD (1.000) [0.00–1.00]	B (0.60)	DS (–2.22)	NT (0.05)	Novel	Benign
	23	c. 2029C>A	p.Leu677Met	Missense	Homo	PD (0.716) [0.86–0.92]	B (0.60)	DS –1.08)	T (0.05)	Novel	Benign
	23	c. 3007G>A	p.Glu1003Lys	Missense	Homo	PD (0.989) [0.72–0.97]	De (0.60)	DS (–0.63)	NT (1.00)	Pathogenic	Pathogenic
	23	c. 3346C>T	p.Arg1116Cys	Missense	Homo	PD (1.000) [0.00–1.00]	De (0.00)	DS (–1.21)	NT (1.00)	Pathogenic	Pathogenic
	23	c. 2975A>G	p.Tyr992Cys	Missense	Hetro	PD (1.000) [0.00–1.00]	De (0.60)	DS (–0.89)	NT (0.05)	Pathogenic	Likely pathogenic

c, variation at cDNA level; G, guvanin; G, guanine; A, adenine; T, thymine C, cytosine; p, variation at protein level; Ala, alanine; Thr, tyrosine; Val, valine; Met, methionine; Gly, glycine; Ser, serine; Ile, isoleucine; Leu, leucine; Glu, glutamic acid; Lys, lysine; Arg, arginine; Cys, cysteine; Tyr, tyrosine; Homo, homozygote; Hetro; heterozygous; B, benign; PD, probably damaging; DC, disease-causing; De, deleterious; DS, decrease stability; NT, not tolerated; T, tolerated.

[a]All nucleotide and amino acids are abbreviated according to the International Union of Pure and Applied Chemistry (IUPAC).

[b]Polymorphism phenotyping v2 (Polyphen-2) is used to predict the possible impact of amino acid substitutions on the stability and function of proteins using structural and comparative evolutionary considerations.

[c]Mutation taster is applied to evaluate the disease-causing potential of sequence alterations.

[d]I-Mutant3.0 support vector machine (SVM)-based tools were used for the automatic prediction of protein stability changes upon single-point mutations

[e]Sorting intolerant from tolerant (SIFT) program is used to predict whether an amino acid substitution affects protein function so that users can prioritize substitutions for further study.

[f]ExAC databases were used to identify individuals expected to exhibit a childhood disorder based on concordance with disease inheritance modes: heterozygous (for dominant), homozygous (for recessive), or hemizygous (for X-linked recessive conditions).

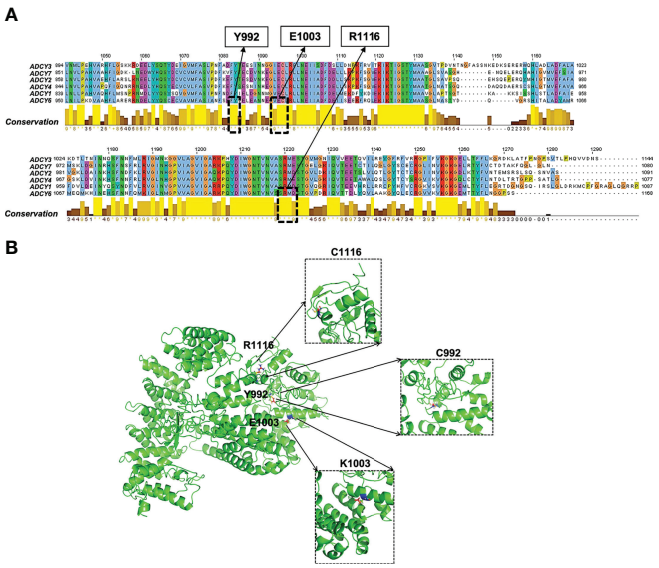

FIGURE 3 | Functional effects of pathogenic *ADCY6* SNPs. **(A)** Multiple sequence alignment of the ADCY protein family. **(B)** Surface and crystallographic imaging of the ADCY6 p.E1003K and p.R1116C SNPs located in the active site of the ADCY6 enzyme.

R111), as well as the degradation of the improperly folded protein or truncated mRNA. Structural–functional analysis revealed that all three disease-driver nsSNPs (p.E1003K, p.R1116C, and p.Y992C) are located in the topological domain of the ADCY6 protein (914–1,168 amino acid residues in the cytoplasmic domain). Based on the sequence conservation alignment, the nsSNP Y991, E1003, and R1116 are highly conserved in all organisms (**Figure 3A**). As shown in **Figure 3B**, the predicted crystal structures of the WT (left panel), and E1003K, R1116C, and Y992C mutant (right panel) ADCY6 proteins exhibit the mutation of a glutamic acid residue to lysine, arginine to cysteine, and tyrosine to cysteine at conserved positions 1003, 1116, and 992, respectively. Structurally, the active site is situated at the interface of the two topological domains, locating the three residues in the ADCY6 enzyme active site. The comparison between the protein structure homology-modeling of the WT and ADCY6 mutant (p.E1003K) demonstrated a change from a smaller Glu to a larger Lys at position 1003, leading to charge variation (positive charge). However, the other mutations result in introducing cysteine residues, which form disulfide bonds in the protein structure. Furthermore, the WT and mutant proteins were significantly different in terms of hydrophobicity and hydrophilicity. Therefore, the mutation may cause the loss of hydrophobic interactions and hydrogen bonds with other molecules, which alters the enzyme activity. In general, ADCY6 catalyzes the formation of the signaling molecule cAMP downstream of G-protein-coupled receptors, which act in the signaling cascade downstream of beta-adrenergic receptors in the heart and vascular smooth muscle cells. Given the crystal structure, the p.E1003 and p.R1116C substitutions are suggested to trigger a change in substrate conformation slightly, with the potential to affect the enzyme active center. In the present review, it is hypothesized that the ADCY6 (p.E1003 and p.R1116C) mutant loses its activity and attenuates the hydroxylation of substrates such as those in the cAMP-PKA-PP2A (37) and WNT/β-catenin pathways.

6 CROSSTALK BETWEEN ADCYS AND CANCER

The development, progression, metastasis, and drug resistance of most common cancers are mediated by the cAMP signal downstream of β-adrenergic receptors (β-ARs), which are coupled to stimulatory G-protein (Gs) (44). After hormones, neurotransmitters, and some other signaling molecules bind to G-protein-coupled receptors (**Figure 4**). Additionally, ATP is generated from cAMP through the action of AC and then involved in a range of pathophysiological activities. In contrast, 3′,5′-cAMP is degraded to 5′-cAMP by the action of PDE. The cAMP plays an important role in endoskeletal remodeling, cell proliferation, adhesion, and epithelial–mesenchymal transition (EMT) by preventing JNK activation, leading to the inhibition of Bcl-2 phosphorylation and, consequently, downregulation of cellular autophagy and phosphorylation. As a result, ubiquitination decreases, HDAC8 expression increases, and DNA damage increases (41). Furthermore, Bcl-2 regulates MOM permeability, which has a significant role in apoptotic signaling and affects cell survival (45). Activated PKA-phosphatases, which regulate related metabolic and transcription factors like CREB (34), are associated with cell cycle arrest, apoptosis, and survival through activating the WNT/

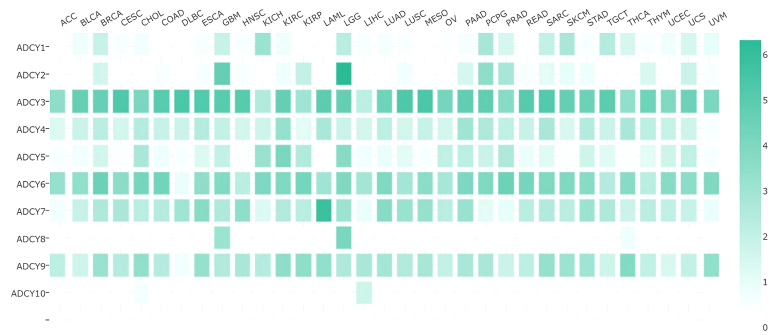

FIGURE 4 | Comparison of the expression of various *ACDY* isoforms in different cancers. The adenylate cyclase gene is expressed differently in each cancer, with darker color indicating higher expression and vice versa. ACC, adrenocortical carcinoma; BLCA, bladder urothelial carcinoma; BRCA, breast invasive carcinoma; CESC, cervical squamous cell carcinoma and endocervical adenocarcinoma; CHOL, cholangiocarcinoma; COAD, colon adenocarcinoma; DLBC, lymphoid neoplasm diffuse large B-cell lymphoma; ESCA, esophageal carcinoma; GBM, glioblastoma multiforme; HNSC, head and neck squamous cell carcinoma; KICH, kidney chromophobe; KIRC, kidney renal clear cell carcinoma; KIRP, kidney renal papillary cell carcinoma; LAML, acute myeloid leukemia; LGG, brain lower-grade glioma; LIHC, liver hepatocellular carcinoma; LUAD, lung adenocarcinoma; LUSC, lung squamous cell carcinoma; MESO, mesothelioma; OV, ovarian serous cystadenocarcinoma; PAAD, pancreatic adenocarcinoma; PCPG, pheochromocytoma and paraganglioma; PRAD, prostate adenocarcinoma; READ, rectum adenocarcinoma; SARC, sarcoma; SKCM, skin cutaneous melanoma; STAD, stomach adenocarcinoma; TGCT, testicular germ cell tumors; THCA, thyroid carcinoma; THYM, thymoma; UCEC, uterine corpus endometrial carcinoma; UCS, uterine carcinosarcoma; UVM, uveal melanoma.

β-catenin pathway. They control apoptosis and DNA damage by regulating the enhancer sequences of IAPs (35). Furthermore, the cAMP signaling pathway controls apoptosis and DNA damage by regulating the PKA-dependent Raf-MEK-ERK pathway as well as protecting cancer cells from apoptosis following exposure to radiation or chemotherapeutic agents by elevating the expression of parathyroid hormone-related proteins (38). A rise in PKA improves the activity of the MAPK signaling pathway, which regulates cell proliferation (39). In addition, EPACs regulate cell proliferation, migration, adhesion, EMT, and endoskeletal remodeling by regulating downstream signaling molecules. The cAMP-mediated EPACs can repair DNA damage by regulating XRCC1 (40).

In this regard, AC activates the formation of intracellular cAMP-activated PKA and transcription factor CREB, which induces the overexpression of growth factors such as epidermal growth factor (EGF), VEGF, arachidonic acid (AA), and proinflammatory cytokines, and consequently stimulates the growth, development, metastasis, and drug resistance of many cancers (44). Furthermore, the Gi-coupled receptor can inhibit this signaling cascade by blocking the activation of the ACs catalyzing cAMP formation, and acting as a physiological inhibitor of the cascade (44). Thus, AC overexpression or silencing may be a key event in processes like tumorigenesis, cell proliferation, migration, and invasion.

6.1 ADCY Isoforms in Tumorigenesis

The cAMP-mediated activation of PKA in many cancer cells leads to cell cycle arrest and growth inhibition *via* the apoptotic pathway (46). The blocking of ERK (47), inhibition of antiapoptotic proteins Bcl2 and Bcl-xl (48), upregulation of tumor suppressor gene p53, and suppression of oncogenes c-myc and erb-2 (49) can be addressed as other ways in which cAMP is linked to growth inhibition. Furthermore, the regulation of the angiogenic pathway through preventing VEGF, transforming growth factor-β (TGF-β), and EGFR is associated with higher cAMP levels (50). However, a lower level of ADCY and cAMP is found in many cancers, which promotes cancer formation and cancer cell proliferation, decreases apoptosis, and even increases neovascularization, cancer cell migration, and invasion.

6.2 ADCY Family in Cancer Recurrence and Prognosis

As already mentioned, the ADCY family is closely related to cancer recurrence and prognosis (**Figure 5**). Cancer recurrence is a common phenomenon involving numerous complex mechanisms, in which the ADCY family plays a crucial role. The results of the previous studies indicated less AC7 expression among relapsed acute promyelocytic leukemia (APL) patients than the newly diagnosed APL ones. Additionally, miR-192, which directly targets AC7 expression, is relatively high in the relapsed APL individuals, which suggests the important role of miR-192-mediated AC7 in APL cell differentiation, as well as implicating AC7 and miR-192 as novel biomarkers and therapeutic targets for these patients (51). Individuals with primary or relapsed APL have a relatively lower level of AC9 expression compared to those with complete remission and nonleukemic patients (52). Furthermore, the expression is strongly accompanied by leukemogenesis in APL, proposing the potential of AC9 as a biomarker in clinical diagnosis and leukemia relapse treatment (52). The less expression of phosphorylated CREB protein produced through cAMP regulation is associated with the aggressive and metastatic recurrence of melanoma (53). Moreover, the ADCY family, as the key genes in important signaling pathways, influences patient prognosis through a variety of mechanisms. Based on the results of a cohort study, the level of ADCY9 is greater in colon cancer

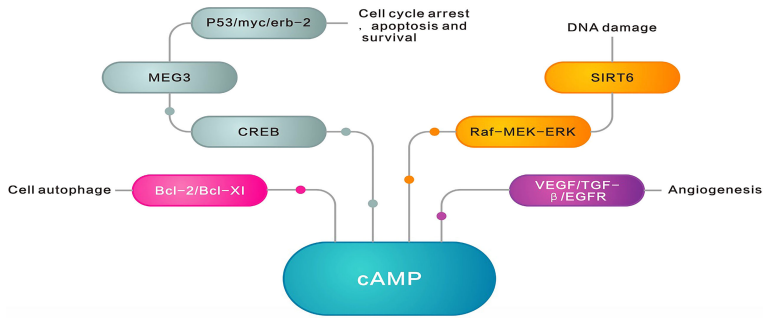

FIGURE 5 | ADCY family roles in cancer recurrence and prognosis. cAMP inhibits cancer formation by blocking extracellular signal-regulated kinase (ERK), inhibiting the antiapoptotic proteins Bcl2 and Bcl-XI, upregulating the cancer suppressor gene p53, inhibiting the oncogenes c-myc and erbB-2, and inhibiting the regulation of the angiogenic pathway by VEGF, TGF-β, and EGFR. However, many cancers exhibit lower AC levels and lower cAMP levels, promoting cancer formation as well as cancer cell proliferation, reducing apoptosis, and even promoting neovascularization, cancer cell migration, and invasion.

tissues than in the adjacent tissues (54). The low ADCY9 level in cancer tissues is attributed to longer disease-free survival (DFS), while high ADCY9 expression and distant metastasis indicate a poor prognosis after treatment (54).

6.3 ADCY Family in Chemo- and Radioresistance

Many treatment options are available for cancer, which include surgery, chemotherapy, radiotherapy, molecular targeted therapy, and immunotherapy. Specific cancer cell death induction and maximum remission are the ultimate goals of anticancer therapy. Currently, these goals still rely mainly on drug- or radiation-induced DNA-triggered death and antiproliferative signals. AC is activated by cAMP, which in turn activates PKA and CREB, which have roles in gene regulation, cell migration and proliferation, apoptosis, and mitochondrial homeostasis (55). In addition, forskolin, as an AC agonist, exerts several relevant anticancer effects such as inducing EMT, enhancing sensitivity to conventional antitumor drugs, and inhibiting the proliferation, motility, and migration of many types of cancer cells (50, 56).

In lung cancer, ADCY1 can modulate anticancer drugs and regulate apoptosis by regulating the expression of Bcl-2 family proteins, IAPs, and XRCC1 in human lung cancer cells (33). The expression of apoptosis inhibitors and inactivation of apoptosis promoters have been reported in human cancers. The results of the preclinical models suggested that functional defects in apoptosis signaling may translate into drug-resistant cells in cancer. The MOM permeability is known as a key step in apoptotic signaling, which is regulated by the Bcl-2 family of proteins, and targeting BCL in nonsmall cell lung cancer treatment leads to an initial improvement in chemoresistance (57). Further, ADCY1 catalyzes the elevation of cAMP and consequently inhibits the EPAC-dependent pathway degradation of XRCC1-induced DNA damage, DNA repair, and apoptosis in lung cancer cells (58). Ataxia-telangiectasia mutated (ATM) is a master regulator of the cellular response to the ionizing radiation-induced DNA damage, which can regulate multiple DNA damage responses like cell cycle, DNA repair, and apoptosis through activating downstream signaling pathways (59, 60). Gαs simulates ATM activation through the Gαs-cAMP-PKA-PP2A pathway, which results in declining the ATM protein-dependent nuclear factor kappa-B (NF-κB) activation, and increasing radiation-induced apoptosis in human and mouse lung cancer cells (37). Furthermore, the downregulation of cAMP-regulated Meg3 (an RNA gene) promotes cisplatin resistance in lung cancer cells by activating the WNT/β-catenin signaling pathway (61).

Breast cancer resistance to chemotherapeutic agent doxorubicin is generally accompanied by RAS/RAF/ERK activation (62). Additionally, AC activation can sensitize triple-negative breast cancer (TNBC) cells to doxorubicin *via* the cAMP/PKA-mediated mechanism of ERK inhibition, which greatly elevates doxorubicin-induced cell death (62). Forskolin can improve the sensitivity of MDA-MB-231 and MDA-MB-468 TNBC cells to 5-fluorouracil and taxol l (63).

Further, the cAMP signaling system inhibits DNA damage-induced apoptosis in leukemic cells by promoting p53 acetylation and turnover. The results of a study reflected an association between the upregulation of multidrug resistance gene (MDR1) expression through activating CREB by PKA with multidrug resistance in leukemia cells (64). EPAC1 and EPAC2 exhibit different expression patterns in mature and developing tissues. EPAC1 mRNA is widespread (65), while EPAC2 is mainly expressed in brain and endocrine tissues (66). Recently, some researchers have proposed the involvement of EPAC1 in regulating a variety of cancer cellular responses like cancer cell adhesion (67), proliferation (68), invasion (69), and migration (69, 70). Regarding ovarian cancer cells, roflumilast induces apoptosis and prevents tumor progression by activating the cAMP/PKA/CREB pathway and upregulating mitochondrial ferritin (FtMt) levels in the two types of cells (OVCAR3 and SKOV3) (55). Furthermore, ADCY4 is suggested to be accompanied by cetuximab insensitivity in colorectal cancer (71).

Table 3 presents an available spectrum of the multifunctional genes upregulated by ADCY in various radioresistant tumor

TABLE 3 | Role of adenylate cyclase-related pathways in cancer drug or radiotherapy sensitivity.

Types of cancer	Signaling axis of action	Cellular function	Drug/radial sensitivity	Phenotype function	References
Lung cancer	bcl-2-MOM	Modulate anticancer drugs and regulate apoptosis			[Willis et al. (45) and Mansilla Pareja et al. (40)]
	IAPs	Cell apoptosis			[Mansilla Pareja et al. (40)
	Epac-XRCC1	Induce DNA damage, DNA repair, and apoptosis	γ-ray		Mansilla Pareja et al. (40)]
	cAMP/PKA/PP2A-ATM-NF-κB	Enhance radiation-induced cell apoptosis			[Mansilla Pareja et al. (40)]
	cAMP-Meg3-WNT/β-catenin	Enhance drug resistance	Cisplatin		[Xia et al. (61)]
Breast cancer	cAMP/PKA/ERK	Induce cell apoptosis	Doxorubicin		[Abrams et al. (72)]
Leukemia	cAMP-p53	DNA damage-induced apoptosis			[Naderi et al. (73)] and [Kloster et al. (74)]
	cAMP/PKA/CREB1-MDR1			Multidrug resistance	(64)
Ovarian cancer	cAMP/PKA/CREB-FtMt	Induce cell apoptosis	Cisplatin	Reverse cisplatin resistance	[Gong et al. (55)]

Bcl-2, B-cell lymphoma-2; MOM, mitochondrial outer membrane; IAPs, inhibitor of apoptosis proteins; EPAC, cAMP-EGF-I/II; XRCC1, X-ray repair complementing defective repair in Chinese hamster cells 1; PP2A, protein phosphatase 2A; ATM, the ataxia–telangiectasia–mutated protein; NF-κB, nuclear factor kappa-B; PKA, protein kinase A; ERK, extracellular signal-regulated kinase; CREB, cAMP response element-binding proteins; MDR1, multidrug resistance gene.

cells. ADCY1 can modulate anticancer drugs and regulate cell apoptosis *via* the Bcl-2-MOM pathway in lung cancer (57). It can modulate cell apoptosis (35) and EPAC-XRCC1 through IAPs, both of which induce DNA damage (by increasing cell insensitivity to γ-ray), DNA repair, and apoptosis (40). In addition, it can enhance radiation-induced cell apoptosis *via* the cAMP-PKA-PP2A-ATM-NF-κB pathway (37) and cause more resistance to drugs such as cisplatin through the cAMP-Meg3-WNT/β-catenin pathway (61). All of the pathways in lung cancer involve changes in the sensitivity and effectiveness of chemotherapeutic drugs and radiotherapy. In breast cancer, it enhances the sensitivity of cancer cells to doxorubicin by improving the PKA-mediated activation of ERK to induce cell apoptosis and consequently promote the efficacy of the associated chemotherapy (63). Furthermore, it leads to the modulation of DNA damage-induced apoptosis *via* the cAMP-p53 pathway and cAMP/PKA/CREB1-MDR1 signaling axis in leukemia and is accompanied by multidrug resistance (64). In the case of ovarian cancer, it induces cell apoptosis and increases sensitivity to cisplatin, even reverses cisplatin resistance, through the cAMP/PKA/CREB-FtMt signaling axis (55). In general, the ADCY family results in improving the efficacy of cancer therapy because of modulating the downstream pathways which alter the sensitivity of cancer cells to chemotherapeutic agents and radiotherapy.

6.4 Role of ADCY Isoforms in Various Cancers

The expression of ADCY subtypes varies in various cancers so that some are highly expressed in tumors and participate in tumor formation and development as oncogenes, while the others may have low, or even no expression. Analyses have revealed that this variation may lead to antitumor effects and may even be related to tumor prognosis. The expression of each subtype of the ADCY family in different cancers is demonstrated in **Figure 4**. As displayed, the most significant variation in expression is observed in ADCY4 and ADCY9. ADCY4 mRNA expression is significantly downregulated in breast cancer compared to the normal tissues, while the level more than triples in invasive breast cancer. Furthermore, ADCY9 expression diminishes in colorectal and lung cancers in comparison with the normal tissues (26). The epigenetic changes in the ADCY family, as a gene family regulating the extensive and global physiological activities of organisms, play a certain role in the biological behavior of tumors and other pathological processes. The results of recent gene sequencing-based studies have introduced a new role for *ADCY1* mutations in influencing drug effectiveness in a variety of cancers like lung, esophageal, and colorectal ones (33). However, *ADCY4* is significantly silenced and highly methylated in many cancers. *ADCY5* has been less well studied, and the results of research knocking out the *AC5* gene in mice indicated a significant reduction in angiogenesis and a rise in cancer cell apoptosis, both of which prevent cancer growth (75). ADCY6 expression is negatively correlated to the signaling pathways associated with immune processes, as well as the activation of immune checkpoint receptors and ligands (76). It is a potentially key gene in regulating immune cell infiltration in luminal-like carcinomas (76). **Table 3** lists the cancers in which the AC subtype has been investigated so far.

6.4.1 Digest System Cancer

In gastric cancer cell lines and tissues, ADCY3 overexpression promotes tumorigenesis by upregulating the expression of matrix metalloproteinase-2 (MMP2) and metalloproteinase-9 (MMP9) *via* the cAMP/PKA/CREB pathway, which increases cell migration, invasion, proliferation, and colony formation (77, 78). *ADCY3* serves as an oncogene in gastric cancer formation, as an oncogene, with high ADCY3 expression regulated by DNA methylation accompanied by low survival (78). Additionally, the

ADCY3 gene is more expressed in primary pancreatic cancer and precancer tissues than the normal pancreatic tissues, while the expression of the *ADCY2* gene is downregulated in primary tumors and adjacent nontumor tissues (79). Unlike gastric cancer, a greater cAMP level in pancreatic cancer inhibits cell migration and invasion (80, 81), although it does not affect cell proliferation (81). In fact, AC3 may enhance cAMP levels in response to forskolin stimulation, which causes PKA to phosphorylate CREB, a primary binding protein for the cAMP response, and consequently inhibits cell migration and invasion. Its inhibitory effect is accompanied by the rapid formation of AC3/adenylate cyclase-associated protein 1 the (CAP1)/G-actin complex, which prevents filopodia generation and cell motility (79).

Certain subtypes of the ADCY family (ADCY2, 3, 8, and 9) are mutated in hepatocellular carcinoma, which may be key events in the formation of the carcinoma (82). The results of the genomic analysis of a patient with lung metastasis from colorectal cancer suggested ADCY2 and ADCY9 as potential metastasis prognostic biomarkers (83).

6.4.2 Breast Cancer

Based on the results in **Figure 4**, ADCY4 expression significantly decreased in breast cancer. The results of the previous studies have shown that Giα is highly expressed in breast cancer cells, especially in metastatic ones. A potential relationship is found between ADCY4 and Giα (7, 84). Furthermore, the proximal targets of cAMP are proteins with diverse functions, which regulate the transcription rates of many genes, such as those playing a role in EMT and inhibiting cell growth and migration, as well as anticancer drug transcription factors with biological roles in anticancer drug sensitivity (7, 84). Unlike gastric cancer, ADCY4 may impose a tumor inhibitory effect in breast cancer, although this effect is terminated by the gene silencing caused by DNA methylation (26). Thus, ADCY4 is a potential biomarker and therapeutic target to predict the prognosis of human breast cancer.

Furthermore, ADCY6 may be implicated in breast cancer progression and affect breast cancer prognosis through calcium-regulated immune and molecular signaling pathways (85). An association is observed between downregulated *ADCY6* gene expression and hypomethylation with a better prognosis in breast cancer patients (76).

Some researchers referred to the need for AC8 in breast cancer cell migration as well as the important role of the cAMP-PKA pathway in migrating MCF7 and MDA-MB-231 TNBC cells (86). In MDA-MB-231 cells, AC8 is required for focal adhesion kinase (FAK) phosphorylation, which may explain the role of AC8 in cell migration (87). AC8 and Orai1 interact to trigger the phosphorylation of Orai1 in MDA-MB-231 TNBCs, which results in inactivating Orai1 and stimulating breast cancer migration (86).

6.4.3 Leukemia

Previous studies have revealed the effectiveness of ADCY7 on intracellular cAMP levels and all-trans retinoic acid (ATRA)-induced cell differentiation in APL. The inhibition of ADCY7 elevates apoptosis, reduces cell growth, and declines c-myc expression (88). ADCY7 knockdown significantly inhibits inhibitor-mediated increases in CD11b expression and proliferation in NB4, an APL cell line (51). In addition, microRNA-192 (miRNA) directly targets AC7 expression, the knockdown of which promotes ATRA-induced APL cell differentiation by regulating AC7 expression (51).

Regarding acute myeloid leukemia (AML), CD300A (a type I transmembrane protein) is expressed in the myeloid cells (89). Furthermore, lymphoid lineages cause more proliferation and migration of U937 cells by improving the expression of platelet endothelial cell adhesion molecule (PECAM1) and ADCY7 and by activating the AKT/mTOR (autophagy classical pathway) signaling pathway (89).

6.4.4 Lung Cancer

ADCY1 is overexpressed in nonsmall cell lung cancer (90) and is only accompanied by patient prognosis. Furthermore, ADCY1-mediated cAMP can regulate multidrug resistance in lung cancer and other malignancies by regulating the specific long noncoding RNAs (lncRNAs) involved in different signaling pathways (33).

6.4.5 Melanoma

The low expression of miR-23a-3p (a miRNA) in a melanoma cell line is significantly related to poor prognosis, which significantly diminishes overall survival (OS) and DFS. MiR-23a-3p inhibits cAMP and MAPK signaling pathways because of its targeting of ADCY1 to prevent melanoma cell proliferation, migration, invasion, and tumorigenesis (9). Additionally, anal melanoma (MIS) is the most common malignant melanoma in the East Asian population. The sAC is mainly expressed in nuclei and nucleosomes, such as the deeply stained nuclei of melanoma cells, especially MIS, as well as the protruding nuclei in the vesicular nucleus (91). It may be associated with melanoma invasion, and cytological and nuclear changes in limbs end in melanoma progression (91). However, sAC can be implicated in melanocyte proliferation, apoptosis, and melanin synthesis through its catalytic product cAMP (91).

6.4.6 Laryngeal Cancer

In laryngeal cancer, ADCY6 is a biomarker with significantly different expressions in cancer and noncancer samples. Some researchers reported the involvement of ADCY6 in the cellular processes related to the cancer phenotype like cell cycle, apoptosis, DNA repair, protease inhibition, proteolysis, and transcriptional regulation (92).

6.4.7 Glioblastoma

ADCY8 polymorphisms are accompanied by the risk of glioma (brain tumor) in patients with neurofibromatosis type 1 (NF1), which is sex-specific (93). Based on the single nucleotide polymorphism (SNP) array analysis of cAMP pathway polymorphisms on DNA from NF1 patients with and without optic pathway glioma, polymorphisms in ADCY8 (AC8) lead to more glioma risk among female patients, although they exhibit a protective effect against glioma in male ones (94). Furthermore, ADCY activity and cAMP levels are higher in benign brain

tumors, while the lower levels are associated with a greater degree of malignancy (95). Therefore, there is a good reason to believe that a rise in cAMP will be an important tool in brain tumor treatment.

6.4.8 Cervical Cancer

ADCY8 is the most widely reported subtype implicated in cervical intraepithelial neoplasia. Regarding cervical cancer, miR-181b (a miRNA) promotes the growth of cervical cancer cells and inhibits apoptosis by increasing mRNA degradation and decreasing intracellular cAMP levels, which may be caused by binding to the 30′UTR#2 of AC9 (96). MiR-181b has different roles in tumor cells (97, 98). AC9, which produces cAMP, has been identified as a potential target of miR-181b, which negatively regulates AC9 by reducing AC9 mRNA levels (96). Furthermore, the DNA methylation of *ADCY8* in molecular Pap smears is considered a biomarker of high-grade cervical cytology (99).

6.4.9 Insulinoma

The expression of ADCY1 and calcium channel 2 (CACNA2) greatly enhances insulinoma with a YY1T372R mutation, while they are less expressed in normal β cells (100). The two gene products are involved in the key pathways regulating insulin secretion with the constitutive activation of cAMP and Ca^{2+} signaling pathways implied in insulin secretion (101). Accordingly, the higher expression of ADCY1 and CACNA2D2 may play a crucial role in the pathogenesis of insulinoma.

6.4.10 Prostate Cancer

Significant overexpression of sAC has been detected in prostate cancer. In addition, the inhibition of sAC activity prevents prostate cancer cell proliferation, leading to the release of lactate hydrogenase (LDH), as well as apoptosis. The regulation of sAC-dependent proliferation involves the EPAC/Rap1/B-RAF signaling pathway, and EPAC supports prostate cancer cell proliferation by promoting G2/M phase transition, while PKA has no role (99). The antiproliferative effect of sAC inhibition is seemingly ascribed to the inhibition of MEK1, a downstream target of Rap1/B-Raf signaling, which plays an important role in spindle organization and chromosome stabilization (102), and consequently, can impair spindle formation (103) and cause cell cycle arrest in the G2 phase (104).

7 FUTURE PROSPECTS

The ADCY family represents a wide range of functions and plays an important role in a variety of diseases such as neuropathic pain, neurodegenerative diseases, congestive heart failure, asthma, and male contraception. In addition, this family of proteins plays a crucial role in the development of different cancers (26). ADCY isoforms influence the biological behavior of cancer cells such as proliferation, differentiation, apoptosis, and invasive migration, and even have a critical role in cancer cell chemoresistance and sensitivity to radiation *via* cAMP-PKA and other pathways. In recent years, a relationship has been discovered between the family and cancer immunity. The high expression of some ADCY genes activates cancer-associated T-cell function and improves cancer cell immunity (105). This is another mechanism by which ADCYs exert their oncogenic effects, although the exact process is not well understood and should be clarified in continued research. However, better cancer immunity plays an important role in cancer therapy.

Furthermore, the family is expressed at varying levels in cancer cells, some of which are silenced as oncogenes due to DNA methylation. Therefore, a novel cancer treatment approach can involve the restoration of its expression and oncogenic effect by demethylating genes. Similarly, related protein products or specific protein activators can be developed as anticancer drugs to provide more treatment options for patients with various cancers. Currently, available AC agonists like forskolin exhibit some anticancer effects by elevating intracellular cAMP levels. Due to the extensive distribution of ADCYs and the wide range of involved biological functions, no targeted drugs are now available for ADCY isomers, and an urgent need is felt for the appropriate drugs for the various ADCY isomers that truly target cancer therapy.

The identification of a reagent that can be used to treat mutant ADCY indicates great scientific progress and provides important information for future targeted therapy. The present review introduced deleterious hotspot mutants p.E1003K and p.R1116C on ADCY6 as candidates for developing therapeutic strategies targeting cancer cells. The changes in amino acid positioning and H-bond strength can explain how the p.E1003K and p.R1116C mutations affect the complex interaction of ADCY6. Evidently, future studies on protein–protein docking, molecular dynamics, and conformational entropy, as well as principal component analysis, are required to reveal how the two hotspot mutants destroy the structure and function of the complex and increase the fluctuation range. This information presents an excellent basis for understanding the mechanism underlying an enhancement in p-Akt1 activity in carcinogenesis.

8 CONCLUSION

This review highlights the mechanistic functions of the AC family and cAMP in conferring chemoresistance, as well as cancer target therapy, which needs further comprehensive studies for full elucidation. The lower AC and cAMP levels have been reported in many cancers, which promote cancer formation and cancer cell proliferation, reduce apoptosis, and even increase neovascularization and cancer cell migration and invasion. Additionally, deleterious nsSNPs p.E1003K and p.R1116C on ADCY6 are candidates to develop potential therapeutic strategies targeting cancer cells. The possibility of targeting the AC family in oncology opens new opportunities for novel therapeutic strategy development and defines a new approach to improve chemoimmunotherapy efficacy in various cancers. The importance of immunotherapy and targeted therapies has become

growing in cancer treatment, and the anticancer therapies targeting the ADCY family, certainly ADCY1 and ADCY6, are becoming increasingly possible. Furthermore studies are required to elucidate the paradoxical effects of the other members of the family pathway in response to cancer therapy. In particular, further investigations should be conducted to clarify the interplay between the overexpression of ADCY signaling and cAMP-dependent genes in various tumors. Therefore, targeting the different isoforms of the ADCY family may be a new strategy for treating various cancers.

AUTHOR CONTRIBUTIONS

RG and TL checked the relevant literature and wrote the original draft of the manuscript. MD and XW performed the data interpretation and visualization in the form of diagrams and tables. SI and QW performed the project administration and funding acquisition. All authors have read and agreed to the published version of the manuscript and agreed to be accountable for all aspects of the work.

FUNDING

This research was funded by Southwest Medical University (SWMU), grant number HR21013.

ACKNOWLEDGMENTS

We gratefully acknowledge all the co-workers who provided technical support for the images and tables in this paper. We sincerely apologize that we cannot cite all contributions due to space limitations.

REFERENCES

1. Hamilton E, Infante JR. Targeting CDK4/6 in Patients With Cancer. *Cancer Treat Rev* (2016) 45:129–38. doi: 10.1016/j.ctrv.2016.03.002
2. Pluznick JL, Zou DJ, Zhang X, Yan Q, Rodriguez-Gil DJ, Eisner C, et al. Functional Expression of the Olfactory Signaling System in the Kidney. *Proc Natl Acad Sci U.S.A.* (2009) 106(6):2059–64. doi: 10.1073/pnas.0812859106
3. Aldehni F, Tang T, Madsen K, Plattner M, Schreiber A, Friis UG, et al. Stimulation of Renin Secretion by Catecholamines is Dependent on Adenylyl Cyclases 5 and 6. *Hypertension* (2011) 57(3):460–8. doi: 10.1161/HYPERTENSIONAHA.110.167130
4. Seamon KB, Padgett W, Daly JW. Forskolin: Unique Diterpene Activator of Adenylate Cyclase in Membranes and in Intact Cells. *Proc Natl Acad Sci U.S.A.* (1981) 78(6):3363–7. doi: 10.1073/pnas.78.6.3363
5. Tang G, Li S, Zhang C, Chen H, Wang N, Feng Y. Clinical Efficacies, Underlying Mechanisms and Molecular Targets of Chinese Medicines for Diabetic Nephropathy Treatment and Management. *Acta Pharm Sin B* (2021) 11(9):2749–67. doi: 10.1016/j.apsb.2020.12.020
6. Follin-Arbelet V, Torgersen ML, Naderi EH, Misund K, Sundan A, Blomhoff HK. Death of Multiple Myeloma Cells Induced by cAMP-Signaling Involves Downregulation of Mcl-1 *via* the JAK/STAT Pathway. *Cancer Lett* (2013) 335(2):323–31. doi: 10.1016/j.canlet.2013.02.042
7. Pattabiraman DR, Bierie B, Kober KI, Thiru P, Krall JA, Zill C, et al. Activation of PKA Leads to Mesenchymal-to-Epithelial Transition and Loss of Tumor-Initiating Ability. *Science* (2016) 351(6277):aad3680–aad3680. doi: 10.1126/science.aad3680
8. Zhang H, Kong Q, Wang J, Jiang Y, Hua H. Complex Roles of cAMP-PKA-CREB Signaling in Cancer. *Exp Hematol Oncol* (2020) 9(1):32. doi: 10.1186/s40164-020-00191-1
9. Ma M, Dai J, Tang H, Xu T, Yu S, Si L, et al. MicroRNA-23a-3p Inhibits Mucosal Melanoma Growth and Progression Through Targeting Adenylate Cyclase 1 and Attenuating cAMP and MAPK Pathways. *Theranostics* (2019) 9(4):945–60. doi: 10.7150/thno.30516
10. Johann K, Bohn T, Shahneh F, Luther N, Birke A, Jaurich H, et al. Therapeutic Melanoma Inhibition by Local Micelle-Mediated Cyclic Nucleotide Repression. *Nat Commun* (2021) 12(1):5981. doi: 10.1038/s41467-021-26269-w
11. Sanchez-Collado J, Lopez JJ, Jardin I, Salido GM, Rosado JA. Cross-Talk Between the Adenylyl Cyclase/cAMP Pathway and Ca(2+) Homeostasis. *Rev Physiol Biochem Pharmacol* (2021) 179:73–116. doi: 10.1007/112_2020_55
12. Dessauer CW, Watts VJ, Ostrom RS, Conti M, Dove S, Seifert R. International Union of Basic and Clinical Pharmacology. CI. Structures and Small Molecule Modulators of Mammalian Adenylyl Cyclases. *Pharmacol Rev* (2017) 69(2):93–139. doi: 10.1124/pr.116.013078
13. Wen DY, Lin P, Liang HW, Yang X, Li HY, He Y, et al. Up-Regulation of CTD-2547G23.4 in Hepatocellular Carcinoma Tissues and its Prospective Molecular Regulatory Mechanism: A Novel qRT-PCR and Bioinformatics Analysis Study. *Cancer Cell Int* (2018) 18:74. doi: 10.1186/s12935-018-0566-3
14. Pierre S, Eschenhagen T, Geisslinger G, Scholich K. Capturing Adenylyl Cyclases as Potential Drug Targets. *Nat Rev Drug Discovery* (2009) 8(4):321–35. doi: 10.1038/nrd2827
15. Boran AD, Chen Y, Iyengar R. Identification of New Gβγ Interaction Sites in Adenylyl Cyclase 2. *Cell Signal* (2011) 23(9):1489–95. doi: 10.1016/j.cellsig.2011.05.002
16. Seamon KB, Daly JW, Metzger H, de Souza NJ, Reden J. Structure-Activity Relationships for Activation of Adenylate Cyclase by the Diterpene Forskolin and its Derivatives. *J Med Chem* (1983) 26(3):436–9. doi: 10.1021/jm00357a021
17. Sabbatini ME, Gorelick F, Glaser S. Adenylyl Cyclases in the Digestive System. *Cell Signal* (2014) 26(6):1173–81. doi: 10.1016/j.cellsig.2014.01.033
18. Bogard AS, Birg AV, Ostrom RS. Non-Raft Adenylyl Cyclase 2 Defines a cAMP Signaling Compartment That Selectively Regulates IL-6 Expression in Airway Smooth Muscle Cells: Differential Regulation of Gene Expression by AC Isoforms. *Naunyn Schmiedebergs Arch Pharmacol* (2014) 387(4):329–39. doi: 10.1007/s00210-013-0950-4
19. Tang T, Lai NC, Wright AT, Gao MH, Lee P, Guo T, et al. Adenylyl Cyclase 6 Deletion Increases Mortality During Sustained Beta-Adrenergic Receptor Stimulation. *J Mol Cell Cardiol* (2013) 60:60–7. doi: 10.1016/j.yjmcc.2013.04.005
20. Beavo JA, Brunton LL. Cyclic Nucleotide Research – Still Expanding After Half a Century. *Nat Rev Mol Cell Biol* (2002) 3(9):710–8. doi: 10.1038/nrm911
21. Omori K, Kotera J. Overview of PDEs and Their Regulation. *Circ Res* (2007) 100(3):309–27. doi: 10.1161/01.RES.0000256354.95791.f1
22. Dang N, Meng X, Song H. Nicotinic Acetylcholine Receptors and Cancer. *BioMed Rep* (2016) 4(5):515–8. doi: 10.3892/br.2016.625
23. Ho D, Yan L, Iwatsubo K, Vatner DE, Vatner SF. Modulation of Beta-Adrenergic Receptor Signaling in Heart Failure and Longevity: Targeting Adenylyl Cyclase Type 5. *Heart Fail Rev* (2010) 15(5):495–512. doi: 10.1007/s10741-010-9183-5
24. Lee YS, Marmorstein LY, Marmorstein AD. Soluble Adenylyl Cyclase in the Eye. *Biochim Biophys Acta* (2014) 1842(12 Pt B):2579–83. doi: 10.1016/j.bbadis.2014.07.032
25. Wang H, Xu H, Wu LJ, Kim SS, Chen T, Koga K, et al. Identification of an Adenylyl Cyclase Inhibitor for Treating Neuropathic and Inflammatory Pain. *Sci Transl Med* (2011) 3(65):65ra63. doi: 10.1126/scitranslmed.3001269
26. Fan Y, Mu J, Huang M, Imani S, Wang Y, Lin S, et al. Epigenetic Identification of ADCY4 as a Biomarker for Breast Cancer: An Integrated Analysis of Adenylate Cyclases. *Epigenomics* (2019) 11(14):1561–79. doi: 10.2217/epi-2019-0207

27. Zachariou V, Liu R, LaPlant Q, Xiao G, Renthal W, Chan GC, et al. Distinct Roles of Adenylyl Cyclases 1 and 8 in Opiate Dependence: Behavioral, Electrophysiological, and Molecular Studies. *Biol Psychiatry* (2008) 63 (11):1013–21. doi: 10.1016/j.biopsych.2007.11.021
28. Li YR, Li J, Zhao SD, Bradfield JP, Mentch FD, Maggadottir SM, et al. Meta-Analysis of Shared Genetic Architecture Across Ten Pediatric Autoimmune Diseases. *Nat Med* (2015) 21(9):1018–27. doi: 10.1038/nm.3933
29. Niesor EJ, Benghozi R, Amouyel P, Ferdinand KC, Schwartz GG. Adenylyl Cyclase 9 Polymorphisms Reveal Potential Link to HDL Function and Cardiovascular Events in Multiple Pathologies: Potential Implications in Sickle Cell Disease. *Cardiovasc Drugs Ther* (2015) 29(6):563–72. doi: 10.1007/s10557-015-6626-1
30. Tang T, Lai NC, Wright AT, Gao MH, Lee P, Guo T, et al. Adenylyl Cyclase 6 Deletion Increases Mortality During Sustained β-Adrenergic Receptor Stimulation. *J Mol Cell Cardiol* (2013) 60:60–7. doi: 10.1016/j.yjmcc.2013.04.005
31. Holz GG, Leech CA, Chepurny OG. New Insights Concerning the Molecular Basis for Defective Glucoregulation in Soluble Adenylyl Cyclase Knockout Mice. *Biochim Biophys Acta* (2014) 1842(12 Pt B):2593–600. doi: 10.1016/j.bbadis.2014.06.023
32. Patel TB, Du Z, Pierre S, Cartin L, Scholich K. Molecular Biological Approaches to Unravel Adenylyl Cyclase Signaling and Function. *Gene* (2001) 269(1-2):13–25. doi: 10.1016/s0378-1119(01)00448-6
33. Zou T, Liu J, She L, Chen J, Zhu T, Yin J, et al. A Perspective Profile of ADCY1 in cAMP Signaling With Drug-Resistance in Lung Cancer. *J Cancer* (2019) 10(27):6848–57. doi: 10.7150/jca.36614
34. Bos JL. Epac: A New cAMP Target and New Avenues in cAMP Research. *Nat Rev Mol Cell Biol* (2003) 4(9):733–8. doi: 10.1038/nrm1197
35. Dong Z, Nishiyama J, Yi X, Venkatachalam MA, Denton M, Gu S, et al. Gene Promoter of Apoptosis Inhibitory Protein IAP2: Identification of Enhancer Elements and Activation by Severe Hypoxia. *Biochem J* (2002) 364(Pt 2):413–21. doi: 10.1042/bj20011431
36. Kim EJ, Juhnn YS. Cyclic AMP Signaling Reduces Sirtuin 6 Expression in non-Small Cell Lung Cancer Cells by Promoting Ubiquitin-Proteasomal Degradation *via* Inhibition of the Raf-MEK-ERK (Raf/mitogen-Activated Extracellular Signal-Regulated Kinase/Extracellular Signal-Regulated Kinase) Pathway. *J Biol Chem* (2015) 290(15):9604–13. doi: 10.1074/jbc.M114.633198
37. Cho EA, Kim EJ, Kwak SJ, Juhnn YS. cAMP Signaling Inhibits Radiation-Induced ATM Phosphorylation Leading to the Augmentation of Apoptosis in Human Lung Cancer Cells. *Mol Cancer* (2014) 13:36. doi: 10.1186/1476-4598-13-36
38. Luo K, Gu X, Liu J, Zeng G, Peng L, Huang H, et al. Inhibition of Disheveled-2 Resensitizes Cisplatin-Resistant Lung Cancer Cells Through Down-Regulating Wnt/beta-Catenin Signaling. *Exp Cell Res* (2016) 347(1):105–13. doi: 10.1016/j.yexcr.2016.07.014
39. Seino S, Shibasaki T. PKA-Dependent and PKA-Independent Pathways for cAMP-Regulated Exocytosis. *Physiol Rev* (2005) 85(4):1303–42. doi: 10.1152/physrev.00001.2005
40. Mansilla Pareja ME, Gaurón MC, Robledo E, Aguilera MO, Colombo MI. The cAMP Effectors, Rap2b and EPAC, are Involved in the Regulation of the Development of the Coxiella Burnetii Containing Vacuole by Altering the Fusogenic Capacity of the Vacuole. *PloS One* (2019) 14(2):e0212202. doi: 10.1371/journal.pone.0212202
41. Park JY, Juhnn YS. cAMP Signaling Increases Histone Deacetylase 8 Expression by Inhibiting JNK-Dependent Degradation *via* Autophagy and the Proteasome System in H1299 Lung Cancer Cells. *Biochem Biophys Res Commun* (2016) 470(2):336–42. doi: 10.1016/j.bbrc.2016.01.049
42. Khan N, Kahl B. Targeting BCL-2 in Hematologic Malignancies. *Target Oncol* (2018) 13(3):257–67. doi: 10.1007/s11523-018-0560-7
43. D'Orsi B, Mateyka J, Prehn JHM. Control of Mitochondrial Physiology and Cell Death by the Bcl-2 Family Proteins Bax and Bok. *Neurochem Int* (2017) 109:162–70. doi: 10.1016/j.neuint.2017.03.010
44. Schuller HM. Inhibitory Role of Gi-Coupled Receptors on cAMP-Driven Cancers With Focus on Opioid Receptors in Lung Adenocarcinoma and its Stem Cells. *Vitam Horm* (2019) 111:299–311. doi: 10.1016/bs.vh.2019.05.009
45. Willis SN, Fletcher JI, Kaufmann T, van Delft MF, Chen L, Czabotar PE, et al. Apoptosis Initiated When BH3 Ligands Engage Multiple Bcl-2 Homologs, Not Bax or Bak. *Science* (2007) 315(5813):856–9. doi: 10.1126/science.1133289
46. Ferretti AC, Tonucci FM, Hidalgo F, Almada E, Larocca MC, Favre C. AMPK and PKA Interaction in the Regulation of Survival of Liver Cancer Cells Subjected to Glucose Starvation. *Oncotarget* (2016) 7(14):17815–28. doi: 10.18632/oncotarget.7404
47. Ostojić J, Yoon YS, Sonntag T, Nguyen B, Vaughan JM, Shokhirev M, et al. Transcriptional Co-Activator Regulates Melanocyte Differentiation and Oncogenesis by Integrating cAMP and MAPK/ERK Pathways. *Cell Rep* (2021) 35(7):109136. doi: 10.1016/j.celrep.2021.109136
48. Liu C, Du Q, Zhang X, Tang Z, Ji H, Li Y. Clematichinenoside Serves as a Neuroprotective Agent Against Ischemic Stroke: The Synergistic Action of ERK1/2 and cPKC Pathways. *Front Cell Neurosci* (2015) 9:517. doi: 10.3389/fncel.2015.00517
49. Sonabend AM, Musleh W, Lesniak MS. Oncogenesis and Mutagenesis of Pituitary Tumors. *Expert Rev Anticancer Ther* (2006) 6 Suppl 9:S3–14. doi: 10.1586/14737140.6.9s.S3
50. Sun HJ, Liu TY, Zhang F, Xiong XQ, Wang JJ, Chen Q, et al. Salusin-β Contributes to Vascular Remodeling Associated With Hypertension *via* Promoting Vascular Smooth Muscle Cell Proliferation and Vascular Fibrosis. *Biochim Biophys Acta* (2015) 1852(9):1709–18. doi: 10.1016/j.bbadis.2015.05.008
51. He B, Chang Y, Yang C, Zhang Z, Xu G, Feng X, et al. Adenylate Cyclase 7 Regulated by miR-192 Promotes ATRA-Induced Differentiation of Acute Promyelocytic Leukemia Cells. *Biochem Biophys Res Commun* (2018) 506 (3):543–7. doi: 10.1016/j.bbrc.2018.10.125
52. Zhuang LK, Xu GP, Pan XR, Lou YJ, Zou QP, Xia D, et al. MicroRNA-181a-Mediated Downregulation of AC9 Protein Decreases Intracellular cAMP Level and Inhibits ATRA-Induced APL Cell Differentiation. *Cell Death Dis* (2014) 5:e1161. doi: 10.1038/cddis.2014.130
53. Rodríguez CI, Castro-Pérez E, Longley BJ, Setaluri V. Elevated Cyclic AMP Levels Promote BRAF(CA)/Pten(-/-) Mouse Melanoma Growth But pCREB is Negatively Correlated With Human Melanoma Progression. *Cancer Lett* (2018) 414:268–77. doi: 10.1016/j.canlet.2017.11.027
54. Li H, Liu Y, Liu J, Sun Y, Wu J, Xiong Z, et al. Assessment of ADCY9 Polymorphisms and Colorectal Cancer Risk in the Chinese Han Population. *J Gene Med* (2021) 23(2):e3298. doi: 10.1002/jgm.3298
55. Gong S, Chen Y, Meng F, Zhang Y, Li C, Zhang G, et al. Roflumilast Enhances Cisplatin-Sensitivity and Reverses Cisplatin-Resistance of Ovarian Cancer Cells *via* cAMP/PKA/CREB-FtMt Signalling Axis. *Cell Prolif* (2018) 51(5):e12474. doi: 10.1111/cpr.12474
56. Sapio L, Gallo M, Illiano M, Chiosi E, Naviglio D, Spina A, et al. The Natural cAMP Elevating Compound Forskolin in Cancer Therapy: Is It Time? *J Cell Physiol* (2017) 232(5):922–7. doi: 10.1002/jcp.25650
57. Wesarg E, Hoffarth S, Wiewrodt R, Kroll M, Biesterfeld S, Huber C, et al. Targeting BCL-2 Family Proteins to Overcome Drug Resistance in non-Small Cell Lung Cancer. *Int J Cancer* (2007) 121(11):2387–94. doi: 10.1002/ijc.22977
58. Ginsberg G, Angle K, Guyton K, Sonawane B. Polymorphism in the DNA Repair Enzyme XRCC1: Utility of Current Database and Implications for Human Health Risk Assessment. *Mutat Res* (2011) 727(1-2):1–15. doi: 10.1016/j.mrrev.2011.02.001
59. Lee Y, McKinnon PJ. ATM Dependent Apoptosis in the Nervous System. *Apoptosis* (2000) 5(6):523–9. doi: 10.1023/a:1009637512917
60. Derheimer FA, Kastan MB. Multiple Roles of ATM in Monitoring and Maintaining DNA Integrity. *FEBS Lett* (2010) 584(17):3675–81. doi: 10.1016/j.febslet.2010.05.031
61. Xia Y, He Z, Liu B, Wang P, Chen Y. Downregulation of Meg3 Enhances Cisplatin Resistance of Lung Cancer Cells Through Activation of the WNT/beta-Catenin Signaling Pathway. *Mol Med Rep* (2015) 12(3):4530–7. doi: 10.3892/mmr.2015.3897
62. Yang X, Shang P, Yu B, Jin Q, Liao J, Wang L, et al. Combination Therapy With Mir34a and Doxorubicin Synergistically Inhibits Dox-Resistant Breast Cancer Progression *via* Down-Regulation of Snail Through Suppressing Notch/NF-κb and RAS/RAF/MEK/ERK Signaling Pathway. *Acta Pharm Sin B* (2021) 11(9):2819–34. doi: 10.1016/j.apsb.2021.06.003
63. Illiano M, Sapio L, Salzillo A, Capasso L, Caiafa I, Chiosi E, et al. Forskolin Improves Sensitivity to Doxorubicin of Triple Negative Breast Cancer Cells

via Protein Kinase A-Mediated ERK1/2 Inhibition. *Biochem Pharmacol* (2018) 152:104–13. doi: 10.1016/j.bcp.2018.03.023
64. Yamagishi N, Nakao R, Kondo R, Nishitsuji M, Saito Y, Kuga T, et al. Increased Expression of Sorcin is Associated With Multidrug Resistance in Leukemia Cells *via* Up-Regulation of MDR1 Expression Through cAMP Response Element-Binding Protein. *Biochem Biophys Res Commun* (2014) 448(4):430–6. doi: 10.1016/j.bbrc.2014.04.125
65. de Rooij J, Zwartkruis FJ, Verheijen MH, Cool RH, Nijman SM, Wittinghofer A, et al. Epac is a Rap1 Guanine-Nucleotide-Exchange Factor Directly Activated by Cyclic AMP. *Nature* (1998) 396(6710):474–7. doi: 10.1038/24884
66. Kawasaki H, Springett GM, Mochizuki N, Toki S, Nakaya M, Matsuda M, et al. A Family of cAMP-Binding Proteins That Directly Activate Rap1. *Science* (1998) 282(5397):2275–9. doi: 10.1126/science.282.5397.2275
67. Rangarajan S, Enserink JM, Kuiperij HB, de Rooij J, Price LS, Schwede F, et al. Cyclic AMP Induces Integrin-Mediated Cell Adhesion Through Epac and Rap1 Upon Stimulation of the Beta 2-Adrenergic Receptor. *J Cell Biol* (2003) 160(4):487–93. doi: 10.1083/jcb.200209105
68. Misra UK, Pizzo SV. Epac1-Induced Cellular Proliferation in Prostate Cancer Cells is Mediated by B-Raf/ERK and mTOR Signaling Cascades. *J Cell Biochem* (2009) 108(4):998–1011. doi: 10.1002/jcb.22333
69. Almahariq M, Tsalkova T, Mei FC, Chen H, Zhou J, Sastry SK, et al. A Novel EPAC-Specific Inhibitor Suppresses Pancreatic Cancer Cell Migration and Invasion. *Mol Pharmacol* (2013) 83(1):122–8. doi: 10.1124/mol.112.080689
70. Baljinnyam E, Umemura M, De Lorenzo MS, Iwatsubo M, Chen S, Goydos JS, et al. Epac1 Promotes Melanoma Metastasis *via* Modification of Heparan Sulfate. *Pigment Cell Melanoma Res* (2011) 24(4):680–7. doi: 10.1111/j.1755-148X.2011.00863.x
71. Yu C, Hong H, Lu J, Zhao X, Hu W, Zhang S, et al. Prediction of Target Genes and Pathways Associated With Cetuximab Insensitivity in Colorectal Cancer. *Technol Cancer Res Treat* (2018) 17:1533033818806905. doi: 10.1177/1533033818806905
72. Abrams SL, Steelman LS, Shelton JG, Wong EW, Chappell WH, Basecke J, et al. The Raf/MEK/ERK Pathway Can Govern Drug Resistance, Apoptosis and Sensitivity to Targeted Therapy. *Cell Cycle* (2010) 9(9):1781–91. doi: 10.4161/cc.9.9.11483
73. Naderi EH, Jochemsen AG, Blomhoff HK, Naderi S. Activation of cAMP Signaling Interferes With Stress-Induced p53 Accumulation in ALL-Derived Cells by Promoting the Interaction Between p53 and HDM2. *Neoplasia* (2011) 13(7):653–63. doi: 10.1593/neo.11542
74. Kloster MM, Naderi EH, Haaland I, Gjertsen BT, Blomhoff HK, Naderi S. cAMP Signalling Inhibits p53 Acetylation and Apoptosis via HDAC and SIRT Deacetylases. *Int J Oncol* (2013) 42(5):1815–21. doi: 10.3892/ijo.2013.1853
75. Hanahan D, Weinberg RA. Hallmarks of Cancer: The Next Generation. *Cell* (2011) 144(5):646–74. doi: 10.1016/j.cell.2011.02.013
76. Li W, Sang M, Hao X, Jia L, Wang Y, Shan B. Gene Expression and DNA Methylation Analyses Suggest That Immune Process-Related ADCY6 is a Prognostic Factor of Luminal-Like Breast Cancer. *J Cell Biochem* (2020) 121 (7):3537–46. doi: 10.1002/jcb.29633
77. Hong SH, Goh SH, Lee SJ, Hwang JA, Lee J, Choi IJ, et al. Upregulation of Adenylate Cyclase 3 (ADCY3) Increases the Tumorigenic Potential of Cells by Activating the CREB Pathway. *Oncotarget* (2013) 4(10):1791–803. doi: 10.18632/oncotarget.1324
78. Zou J, Wu K, Lin C, Jie ZG. LINC00319 Acts as a microRNA-335-5p Sponge to Accelerate Tumor Growth and Metastasis in Gastric Cancer by Upregulating ADCY3. *Am J Physiol Gastrointest Liver Physiol* (2020) 318 (1):G10–g22. doi: 10.1152/ajpgi.00405.2018
79. Quinn SN, Graves SH, Dains-McGahee C, Friedman EM, Hassan H, Witkowski P, et al. Adenylyl Cyclase 3/Adenylyl Cyclase-Associated Protein 1 (CAP1) Complex Mediates the Anti-Migratory Effect of Forskolin in Pancreatic Cancer Cells. *Mol Carcinog* (2017) 56(4):1344–60. doi: 10.1002/mc.22598
80. Burdyga A, Conant A, Haynes L, Zhang J, Jalink K, Sutton R, et al. cAMP Inhibits Migration, Ruffling and Paxillin Accumulation in Focal Adhesions of Pancreatic Ductal Adenocarcinoma Cells: Effects of PKA and EPAC. *Biochim Biophys Acta* (2013) 1833(12):2664–72. doi: 10.1016/j.bbamcr.2013.06.011
81. Zimmerman NP, Roy I, Hauser AD, Wilson JM, Williams CL, Dwinell MB. Cyclic AMP Regulates the Migration and Invasion Potential of Human Pancreatic Cancer Cells. *Mol Carcinogenesis* (2015) 54(3):203–15. doi: 10.1002/mc.22091
82. Zhang Y, Qiu Z, Wei L, Tang R, Lian B, Zhao Y, et al. Integrated Analysis of Mutation Data From Various Sources Identifies Key Genes and Signaling Pathways in Hepatocellular Carcinoma. *PloS One* (2014) 9(7):e100854. doi: 10.1371/journal.pone.0100854
83. Fang LT, Lee S, Choi H, Kim HK, Jew G, Kang HC, et al. Comprehensive Genomic Analyses of a Metastatic Colon Cancer to the Lung by Whole Exome Sequencing and Gene Expression Analysis. *Int J Oncol* (2014) 44 (1):211–21. doi: 10.3892/ijo.2013.2150
84. Dong H, Claffey KP, Brocke S, Epstein PM. Inhibition of Breast Cancer Cell Migration by Activation of cAMP Signaling. *Breast Cancer Res Treat* (2015) 152(1):17–28. doi: 10.1007/s10549-015-3445-9
85. Liu S, Liu X, Wu J, Zhou W, Ni M, Meng Z, et al. Identification of Candidate Biomarkers Correlated With the Pathogenesis and Prognosis of Breast Cancer *via* Integrated Bioinformatics Analysis. *Med (Baltimore)* (2020) 99 (49):e23153. doi: 10.1097/MD.0000000000023153
86. Sanchez-Collado J, Lopez JJ, Jardin I, Camello PJ, Falcon D, Regodon S, et al. Adenylyl Cyclase Type 8 Overexpression Impairs Phosphorylation-Dependent Orai1 Inactivation and Promotes Migration in MDA-MB-231 Breast Cancer Cells. *Cancers (Basel)* (2019) 11(11):1624–48. doi: 10.3390/cancers11111624
87. Abrams SL, Steelman LS, Shelton JG, Wong EW, Chappell WH, Bäsecke J, et al. The Raf/MEK/ERK Pathway can Govern Drug Resistance, Apoptosis and Sensitivity to Targeted Therapy. *Cell Cycle* (2010) 9(9):1781–91. doi: 10.4161/cc.9.9.11483
88. Sun X, Huang S, Wang X, Zhang X, Wang X. CD300A Promotes Tumor Progression by PECAM1, ADCY7 and AKT Pathway in Acute Myeloid Leukemia. *Oncotarget* (2018) 9(44):27574–84. doi: 10.18632/oncotarget.24164
89. Li C, Xie J, Lu Z, Chen C, Yin Y, Zhan R, et al. ADCY7 Supports Development of Acute Myeloid Leukemia. *Biochem Biophys Res Commun* (2015) 465(1):47–52. doi: 10.1016/j.bbrc.2015.07.123
90. He RQ, Li XJ, Liang L, Xie Y, Luo DZ, Ma J, et al. The Suppressive Role of miR-542-5p in NSCLC: The Evidence From Clinical Data and *In Vivo* Validation Using a Chick Chorioallantoic Membrane Model. *BMC Cancer* (2017) 17(1):655. doi: 10.1186/s12885-017-3646-1
91. Li H, Kim SM, Savkovic V, Jin SA, Choi YD, Yun SJ. Expression of Soluble Adenylyl Cyclase in Acral Melanomas. *Clin Exp Dermatol* (2016) 41(4):425–9. doi: 10.1111/ced.12730
92. Warrington NM, Sun T, Rubin JB. Targeting Brain Tumor cAMP: The Case for Sex-Specific Therapeutics. *Front Pharmacol* (2015) 6:153–60. doi: 10.3892/or_00000268
93. Warrington NM, Sun T, Rubin JB. Targeting Brain Tumor cAMP: The Case for Sex-Specific Therapeutics. *Front Pharmacol* (2015) 6:153. doi: 10.3389/fphar.2015.00153
94. Warrington NM, Sun T, Luo J, McKinstry RC, Parkin PC, Ganzhorn S, et al. The Cyclic AMP Pathway is a Sex-Specific Modifier of Glioma Risk in Type I Neurofibromatosis Patients. *Cancer Res* (2015) 75(1):16–21. doi: 10.1158/0008-5472.Can-14-1891
95. Held-Feindt J, Krisch B, Forstreuter F, Mentlein R. Somatostatin Receptors in Gliomas. *J Physiol Paris* (2000) 94(3-4):251–8. doi: 10.1016/s0928-4257(00)00213-8
96. Yang L, Wang YL, Liu S, Zhang PP, Chen Z, Liu M, et al. miR-181b Promotes Cell Proliferation and Reduces Apoptosis by Repressing the Expression of Adenylyl Cyclase 9 (AC9) in Cervical Cancer Cells. *FEBS Lett* (2014) 588(1):124–30. doi: 10.1016/j.febslet.2013.11.019
97. Shi L, Cheng Z, Zhang J, Li R, Zhao P, Fu Z, et al. Hsa-Mir-181a and Hsa-Mir-181b Function as Tumor Suppressors in Human Glioma Cells. *Brain Res* (2008) 1236:185–93. doi: 10.1016/j.brainres.2008.07.085
98. Zhu W, Shan X, Wang T, Shu Y, Liu P. miR-181b Modulates Multidrug Resistance by Targeting BCL2 in Human Cancer Cell Lines. *Int J Cancer* (2010) 127(11):2520–9. doi: 10.1002/ijc.25260
99. Flacke JP, Flacke H, Appukuttan A, Palisaar RJ, Noldus J, Robinson BD, et al. Type 10 Soluble Adenylyl Cyclase is Overexpressed in Prostate Carcinoma

and Controls Proliferation of Prostate Cancer Cells. *J Biol Chem* (2013) 288 (5):3126–35. doi: 10.1074/jbc.M112.403279
100. Thorvaldsen JL, Weaver JR, Bartolomei MS. A YY1 Bridge for X Inactivation. *Cell* (2011) 146(1):11–3. doi: 10.1016/j.cell.2011.06.029
101. Cromer MK, Choi M, Nelson-Williams C, Fonseca AL, Kunstman JW, Korah RM, et al. Neomorphic Effects of Recurrent Somatic Mutations in Yin Yang 1 in Insulin-Producing Adenomas. *Proc Natl Acad Sci U.S.A.* (2015) 112(13):4062–7. doi: 10.1073/pnas.1503696112
102. Cao JN, Shafee N, Vickery L, Kaluz S, Ru N, Stanbridge EJ. Mitogen-Activated Protein/Extracellular Signal-Regulated Kinase Kinase 1act/Tubulin Interaction is an Important Determinant of Mitotic Stability in Cultured HT1080 Human Fibrosarcoma Cells. *Cancer Res* (2010) 70 (14):6004–14. doi: 10.1158/0008-5472.Can-09-4490
103. Feinstein TN, Linstedt AD. Mitogen-Activated Protein Kinase Kinase 1-Dependent Golgi Unlinking Occurs in G2 Phase and Promotes the G2/M Cell Cycle Transition. *Mol Biol Cell* (2007) 18(2):594–604. doi: 10.1091/mbc.e06-06-0530
104. Hayne C, Tzivion G, Luo Z. Raf-1/MEK/MAPK Pathway is Necessary for the G2/M Transition Induced by Nocodazole. *J Biol Chem* (2000) 275 (41):31876–82. doi: 10.1074/jbc.M002766200
105. Rodriguez G, Ross JA, Nagy ZS, Kirken RA. Forskolin-Inducible cAMP Pathway Negatively Regulates T-Cell Proliferation by Uncoupling the Interleukin-2 Receptor Complex. *J Biol Chem* (2013) 288(10):7137–46. doi: 10.1074/jbc.M112.408765

Conflict of Interest: The authors declare that the research was conducted in the absence of any commercial or financial relationships that could be construed as a potential conflict of interest.

Publisher's Note: All claims expressed in this article are solely those of the authors and do not necessarily represent those of their affiliated organizations, or those of the publisher, the editors and the reviewers. Any product that may be evaluated in this article, or claim that may be made by its manufacturer, is not guaranteed or endorsed by the publisher.

frontiers | Frontiers in Pharmacology

ORIGINAL RESEARCH
published: 06 July 2022
doi: 10.3389/fphar.2022.842316

Toxicological Properties of 7-Methylguanine, and Preliminary Data on its Anticancer Activity

*Kirill Kirsanov[1,2], Timur Fetisov[1], Elena Antoshina[1], Lubov Trukhanova[1], Tatiana Gor'kova[1], Olga Vlasova[1], Irina Khitrovo[1], Ekaterina Lesovaya[1,3], Nataliya Kulbachevskaya[1], Tatiana Shcherbakova[4], Gennady Belitsky[1], Marianna Yakubovskaya[1], Vytas Švedas[4,5] and Dmitry Nilov[4]**

[1]Blokhin Cancer Research Center, Moscow, Russia, [2]Peoples' Friendship University of Russia, Moscow, Russia, [3]Pavlov Ryazan State Medical University, Ryazan, Russia, [4]Belozersky Institute of Physicochemical Biology, Lomonosov Moscow State University, Moscow, Russia, [5]Faculty of Bioengineering and Bioinformatics, Lomonosov Moscow State University, Moscow, Russia

7-Methylguanine (7-MG) competitively inhibits the DNA repair enzyme poly(ADP-ribose) polymerase (PARP) and RNA-modifying enzyme tRNA-guanine transglycosylase (TGT) and represents a potential anticancer drug candidate. Furthermore, as a natural compound, it could escape the serious side effects characteristic for approved synthetic PARP inhibitors. Here we present a comprehensive study of toxicological and carcinogenic properties of 7-MG. It was demonstrated that 7-MG does not induce mutations or structural chromosomal abnormalities, and has no blastomogenic activity. A treatment regimen with 7-MG has been established in mice (50 mg/kg per os, 3 times per week), exerting no adverse effects or changes in morphology. Preliminary data on the 7-MG anticancer activity obtained on transplantable tumor models support our conclusions that 7-MG can become a promising new component of chemotherapy.

Keywords: 7-Methylguanine, inhibitor, cancer, carcinogenicity, toxicity

OPEN ACCESS

Edited by:
Zhe-Sheng Chen,
St. John's University, United States

Reviewed by:
Katia Mangano,
University of Catania, Italy
Harald Krenzlin,
Johannes Gutenberg University Mainz, Germany

****Correspondence:***
Dmitry Nilov
nilovdm@gmail.com

Specialty section:
This article was submitted to Experimental Pharmacology and Drug Discovery, a section of the journal Frontiers in Pharmacology

Received: *23 December 2021*
Accepted: *13 June 2022*
Published: *06 July 2022*

Citation:
Kirsanov K, Fetisov T, Antoshina E, Trukhanova L, Gor'kova T, Vlasova O, Khitrovo I, Lesovaya E, Kulbachevskaya N, Shcherbakova T, Belitsky G, Yakubovskaya M, Švedas V and Nilov D (2022) Toxicological Properties of 7-Methylguanine, and Preliminary Data on its Anticancer Activity. Front. Pharmacol. 13:842316. doi: 10.3389/fphar.2022.842316

1 INTRODUCTION

7-Methylguanine (7-MG) (Shapiro et al., 1968) is a degradation product of nucleic acids which is present in small amounts in human urine (Bromberg et al., 1957a; Bromberg et al., 1957b; Lothrop and Uziel, 1983; Svoboda and Kasai, 2004; Rodríguez-Gonzalo et al., 2013; Raćkowska et al., 2019) and may be considered an indicator of whole-body RNA turnover (Sander et al., 1986a; Sander et al., 1986b; Sander et al., 1986c; Topp et al., 1987). In mRNA the guanosine cap is methylated due to methyltransferase activity, that is required for maturation and translation (Shuman, 2002; Shafer et al., 2005; Topisirovic et al., 2011; Varshney et al., 2016). Furthermore, 7-MG adducts are normally present in DNA, exposed to various exogenous and endogenous methylating agents, and their number is increasing on aging (Park and Ames, 1988; Tan et al., 1990; Mustonen and Hemminki, 1992; O'Connor, 1993; Tamae et al., 2009). There is no evidence, however, for synthesis of nucleotides from free 7-MG base or for its direct incorporation into nucleic acids (Craddock et al., 1968; Kaina et al., 1983; Kerr, 1985; Kerr, 1990). A certain proportion of 7-MG is converted to

Abbreviations: 7-MG, 7-methylguanine; PARP, poly(ADP-ribose) polymerase; TGT, tRNA-guanine transglycosylase.

8-hydroxy-7-methylguanine by xanthine oxidase or demethylated (Weissmann and Gutman, 1957; Borowitz et al., 1965; Litwack and Weissmann, 1966; Skupp and Ayvazian, 1969).

Recently we have shown that 7-MG inhibits DNA repair enzymes poly(ADP-ribose) polymerases, PARP1 and PARP2, in a competitive manner and accelerates apoptotic death of cancer cells induced by cisplatin and doxorubicin (Nilov et al., 2016; Nilov et al., 2018a; Nilov et al., 2020a). These PARP enzymes bind to DNA breaks and synthesize a signal polymer poly (ADP-ribose) from NAD^+ molecules to activate the excision repair proteins (Hassler and Ladurner, 2012; Drenichev and Mikhailov, 2015; Ray Chaudhuri and Nussenzweig, 2017; Alemasova and Lavrik, 2019; Nilov et al., 2020b). Inhibitors of PARP1/2, therefore, can exert anti-proliferative effect and be combined with DNA damaging agents (Cepeda et al., 2006; Martin et al., 2008; Ferraris, 2010; Lord et al., 2015; Nilov et al., 2018b). We have demonstrated that 7-MG forms substrate-specific interactions with the Gly863 and Tyr907 residues in the PARP1/2 active site and suppresses DNA-dependent PARP activity in three different assays (biochemical assay with radiolabeled NAD^+, fluorescence anisotropy assay, and Förster resonance energy transfer microscopy assay with nucleosome particles) (Nilov et al., 2016; Nilov et al., 2020a). This results in the formation of nonproductive PARP–nucleosome complexes and likely prevents further steps in DNA repair, replication and transcription, leading to cancer cell death (Maluchenko et al., 2019; Nilov et al., 2020a). 7-MG is also known as a competitive inhibitor of RNA-modifying enzyme tRNA-guanine transglycosylase (TGT) which substitutes the guanine base with 7-deazaguanine derivative queuine (Farkas et al., 1984; Johannsson et al., 2018). In a recent paper, it was shown that TGT deficiency could significantly suppress the proliferation and migration of cancer cells (Zhang et al., 2020). From the point of view of polypharmacology, such a multitarget (PARP1/2, TGT) mechanism of a drug candidate may be promising, if adverse effects are negligible (Bolognesi, 2013; Medina-Franco et al., 2013).

FDA-approved synthetic PARP1/2 inhibitors olaparib, rucaparib, niraparib (Frampton, 2015; Mittica et al., 2018; Zimmer et al., 2018) can cause side effects likely related to the nonselective interaction with numerous NAD^+-binding proteins and nonspecific effects on the organism. Myelodysplastic syndrome/acute myeloid leukemia occurred in some patients after treatment with above-mentioned synthetic inhibitors, and some cases were fatal (Malyuchenko et al., 2015; Sonnenblick et al., 2015; Wang et al., 2016; Ohmoto and Yachida, 2017; Jain and Patel, 2019). 7-MG, being a natural compound, may have a more favorable toxicity profile, which is also supported by QSAR modeling (Nilov et al., 2016; Nilov et al., 2018a). In this article, we present the results of a comprehensive experimental study of toxicological and carcinogenic properties of 7-MG that establish the basis for further testing of its anticancer activity.

2 MATERIALS AND METHODS

2.1 Toxicology Studies

Six-week-old female CBA, BALB/c, and C57BL/6 mice were obtained from the Stolbovaya farm of the Federal Medical Biological Agency (http://www.scbmt.ru). These mouse strains are widely used in toxicology studies and in studies involving transplantable tumor models. 7-MG (Sigma-Aldrich, product No. 67073) was administered orally by gavage in experiments A and B (**Figure 1**). In experiment A, CBA mice were divided randomly to four treatment groups of 10 animals: control group I, drinking water (3 times per week for 4 weeks); group II, 50 mg/kg 7-MG (3 times per week for 4 weeks); group III, 200 mg/kg 7-MG (3 times per week for 1 week); group IV, 600 mg/kg 7-MG (single dose). Animals were euthanized by cervical dislocation 1 week after the last treatment. In experiment B, mice of each strain (CBA, BALB/c, C57BL/6) were divided into two groups, group I (drinking water) and group II (600 mg/kg 7-MG), and euthanized 4 weeks after single-dose administration. Lungs, heart, liver, spleen, thymus, kidneys, adrenal glands, pancreas, stomach, small and large intestines were collected from euthanized mice and inspected. The tissues were processed for light microscopy by fixing in 10% buffered formalin, dehydrating, and embedding in paraffin. Histological analysis was performed on sections stained by hematoxylin-eosin. Organ lesions were detected on the examined sections (representative microphotographs of the found abnormalities are shown in **Supplementary Figure S1**), and the number of lesions per animal was counted.

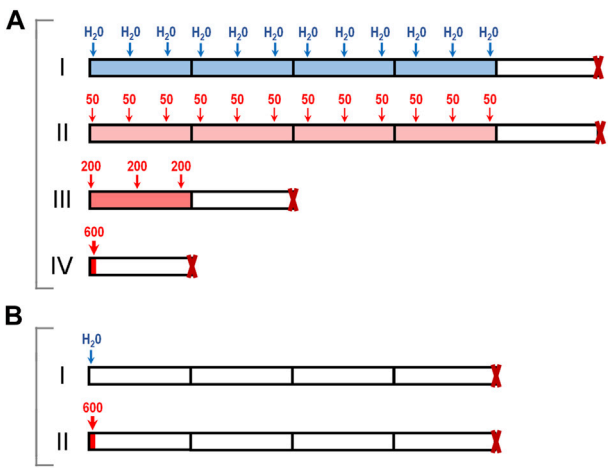

FIGURE 1 | Toxicology study of 7-MG: schematic representation of experiments. **(A)** CBA mice were treated either with water (group I) or with single and multiple doses of 7-MG (groups II–IV, total dose for each group was 600 mg/kg); **(B)** CBA, BALB/c, or C57BL/6 mice were treated with water (groups I) or a single 600 mg/kg dose of 7-MG (group II), and euthanized 4 weeks later.

2.2 Carcinogenicity Studies

The Ames test was performed in *S. typhimurium* strains TA98 and TA100 as described previously (Maron and Ames, 1983). Three 7-MG doses (1.4, 7.0, and 35.0 μg/plate) were tested with and without rat liver S9 fraction. Distilled water was used as a negative control; 3,4-benzopyrene (4.4 μg/plate), 2-acetylaminofluorene (22.0 μg/plate), 4,9-diazapyrene derivative (8.8 μg/plate), and sodium azide (8.8 μg/plate) served as positive

controls. Plates were incubated for 72 h and then revertant colonies were counted. The comet assay was performed as described previously (Singh et al., 1988). Immortalized human kidney epithelial cells (NKE-hTERT) were treated with different concentrations of 7-MG (0.02 and 0.2 mg/ml) for 24 h and then embedded in agarose on microscope slides. After cell lysis and electrophoresis, slides were stained with DNA dye (Vista Green) and the number of comets was counted. Distilled water was used as a negative control and cisplatin (25 μg/ml) served as a positive control. The somatic mutation and recombination test in *D. melanogaster* was based on previous work (Kirsanov et al., 2011). Five wild type males and 10 $wts^{P4}/TM3$ females were placed into vials for breeding. Heterozygous larvae were treated with 7-MG (1 and 2 mg/vial); distilled water and oxoplatin (0.2 mg/vial) were used as controls. Adult F1 males and females were examined for the presence of tumors using a binocular microscope.

The chromosomal aberration assay was performed using standard procedure (Albertini et al., 2000). C57BL/6 mice were divided to groups of 5 animals and treated with 7-MG (50–250 mg/kg per os). Distilled water was used as a negative control and cyclophosphamide (50 mg/kg i.p.) served as a positive control. Bone marrow cells were collected 24 h after the treatment; to arrest proliferating cells at metaphase, animals received colchicine (0.004% i.p.) 3 h prior to euthanasia. Cells were obtained from the femurs, stained on slides with Giemsa, and analyzed by microscopy.

2.3 Anticancer Activity

Six-week-old female CBA mice were obtained from the Stolbovaya farm. Uterine sarcoma US-322 and cervical squamous cell carcinoma RShM-5 (originally derived from CBA mice exposed to 1,2-dimethylhydrazine and 3-methylcholanthrene, respectively) (Treshalina et al., 2000; Turusov et al., 2005; Bunyatyan et al., 2019) were inoculated subcutaneously by injecting 0.5 ml of tumor cell suspension (0.1 g/ml in PBS) into the right axillary cavity. Mice with US-322 were divided into three treatment groups of 10 animals: control group I, PBS (s.c., 3 times per week); group II, 7-MG (50 mg/kg per os, 3 times per week); group III, cisplatin (2.5 mg/kg s.c., 2 times within a week after inoculation). Mice with RShM-5 were divided into five groups of 10 animals: group I, PBS (s.c., 3 times per week); group II, 7-MG (50 mg/kg per os, 3 times per week); group III, 7-MG for 1 week (50 mg/kg per os, 3 times within a week after inoculation); group IV, cisplatin (1.5 mg/kg s.c., 3 times within a week after inoculation); group V, cisplatin + 7-MG (1.5 mg/kg s.c. + 50 mg/kg per os, 3 times within a week after inoculation). For the combined treatment, 7-MG was administered 3 h prior to cisplatin. The length and width of a subcutaneous tumor were measured with a digital caliper, and the tumor volume was calculated as 1/2 (length×width^2).

The animal protocols were approved by the Local Committee for Ethics of Animal Experimentation (Blokhin Cancer Research Center, decision 2019-5 dated 11 February 2019), experiments were conducted in accordance with resolution 81 of the Eurasian Economic Commission and directive 2010/63/EU (on the protection of animals used for scientific purposes).

TABLE 1 | Histological abnormalities of internal organs (+) in CBA mice treated with 7-MG.

Group	Lungs	Liver	Spleen	Intestine
I control	—	—	—	—
II 50 mg/kg[a]	—	—	—	—
III 200 mg/kg[a]	—	—	—	+
IV 600 mg/kg	+	+	+	+

[a]*Multiple-dose administration.*

2.4 Statistical Analysis

Statistical significance of the difference between animal groups was assessed with the Pearson's chi-squared test (study of anticancer activity, study of chromosomal abnormalities in mice), Student's *t*-test (analysis of organ weights), and Fisher's exact test (study of blastomogenic activity in flies). Significant differences between cells in the comet assay were assessed with the Fisher's exact test. Data processing was carried out using the Statistica software (StatSoft Inc.).

3 RESULTS

3.1 Toxicology Studies

The adverse effects of 7-MG that can result either from a single or multiple exposures were assessed using four groups of female CBA mice, as presented in **Figure 1A**. A maximum dose of 600 mg/kg was chosen based on mouse/rat oral LD_{50} values (40–500 mg/kg) predicted for 7-MG with QSAR software ACD/Percepta (www.acdlabs.com). Oral administration of 7-MG to group II (50 mg/kg, 3 times per week for 4 weeks), group III (200 mg/kg, 3 times per week for 1 week), and group IV (600 mg/kg, single dose) was not lethal to any of the animals. Visual observation revealed no apparent lesions or abnormalities of internal organs in treated mice. However, a significant elevation in spleen weight was produced in group IV (**Supplementary Table S1**). Histological analysis of the heart, thymus, kidney, adrenal gland, pancreas and stomach showed no abnormalities in all treatment groups. Lung, liver, and spleen tissues were affected only in group IV (**Table 1**). In this group, small lymphoid infiltrates developed in the lungs and liver (**Supplementary Figures S1A,B**). The splenic white pulp had poorly defined follicles and lacked germinal centers, and the red pulp was infiltrated with lymphoid cells (**Supplementary Figure S1C**). In addition, focal lymphoid hyperplasia of the small and large intestines was found in groups III and IV (**Supplementary Figure S1D**).

The stimulating effect on lymphoid tissue caused by a single 600 mg/kg dose of 7-MG was then investigated in more detail using different mouse strains: CBA, BALB/c and C57BL/6. Animals were administered with either water or 7-MG (600 mg/kg), and samples of lung, liver, spleen, and intestine were collected after 4 weeks (**Figure 1B**). Microscopic examination revealed the persistence of lymphoid lesions produced by a high dose of 7-MG in all strains. Lung, liver and intestine abnormalities were found in

TABLE 2 | Study of the mutagenicity of 7-MG in *S. typhimurium* strains TA98 (detects frameshift mutagens) and TA100 (detects mutagens that cause base-pair substitutions).

Tested compound	Dose, μg/plate	TA98				TA100			
		−S9		+S9		−S9		+S9	
		M	MA	M	MA	M	MA	M	MA
Control	—	9 ± 1	—	16 ± 5	—	43 ± 9	—	53 ± 2	—
BP	4.4			139 ± 15	+			623 ± 23	+
AAF	22.0			448 ± 53	+			433 ± 33	+
DP	8.8	248 ± 42	+						
AZ	8.8					397 ± 31	+		
7-MG	1.4	11 ± 3	—	16 ± 0.4	—	45 ± 1	—	56 ± 3	—
	7.0	10 ± 1	—	14 ± 3	—	35 ± 8	—	44 ± 8	—
	35.0	11 ± 1	—	14 ± 2	—	41 ± 3	—	56 ± 2	—

7-MG, 3,4-benzopyrene (BP), 2-acetylaminofluorene (AAF), 4,9-diazapyrene derivative (DP), and sodium azide (AZ) were tested with and without rat liver S9 fraction. The number of revertant colonies (M) was counted to assess the mutagenic activity (MA). MA was considered positive if M in the treated plates exceeded that in the control more than twice.

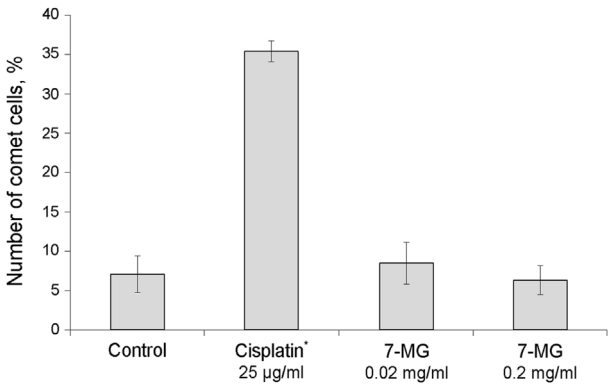

FIGURE 2 | Study of the ability of 7-MG to produce DNA strand breaks in immortalized human kidney epithelial cells using the comet assay (500 cells were analyzed per slide). *Significant difference from the control cells (Fisher's exact test, $p < 0.05$).

nearly all animals (**Supplementary Table S2**), and the splenic microarchitecture was affected in 33% of CBA mice, 30% of BALB/c, and 60% of C57BL/6. However, 7-MG treatment was not lethal to any of the animals and had no significant effect on body weight (**Supplementary Figure S2**). The median lethal dose (LD_{50}) is therefore expected to be substantially greater than 600 mg/kg, which allows us to classify 7-MG as only slightly toxic inhibitor.

These results lead to a conclusion that 50 mg/kg administration 3 times per week may be an optimal regimen, which is devoid of adverse effects and can be readily applied in further testing for anticancer activity of 7-MG in mice (see the **Section 3.3**).

3.2 Carcinogenicity Studies

The mutagenic and carcinogenic properties of 7-MG have been studied using various short term tests: the Ames test (uses bacterial strains to assess the mutagenic potential) (Maron and Ames, 1983), comet assay (detects DNA strand breaks at the level of the individual cell) (Collins, 2004), chromosomal aberration assay (detects structural chromosomal abnormalities in mice) (Albertini et al., 2000), and somatic mutation and recombination test (uses *Drosophila melanogaster* to assess the mutagenic, recombinogenic and blastomogenic potential) (Sidorov et al., 2001). The mutagenicity of 7-MG was tested in *Salmonella typhimurium* strains, TA98 and TA100, both with and without metabolic activation by rat liver S9 fraction. It was demonstrated that 7-MG does not induce frameshift mutations or base-pair substitutions (**Table 2**). The comet assay showed that 7-MG does not produce DNA damage in immortalized human kidney epithelial cells (**Figure 2**; **Supplementary Figure S3**), and the chromosomal aberration assay showed that it does not induce chromatid or chromosome breaks in bone marrow cells of C57BL/6 mice (**Table 3**; **Supplementary Figure S4**). The somatic mutation and recombination test detected no blastomogenic activity of 7-MG in *wts*/+ heterozygotes of *D. melanogaster* (**Table 4**).

3.3 Anticancer Activity

In previous sections, the following findings were made: 1) 7-MG is not carcinogenic and 2) it can be safely administered in an appropriate dosage. As molecular mechanisms of 7-MG are known (PARP1/2 and TGT inhibition), a thorough investigation of its anticancer properties could be initiated *in vivo*, involving various transplantable tumor models and a set of existing drugs as active controls. Below are two illustrative examples demonstrating the utility of 7-MG as a component of chemotherapy.

Preliminary studies of 7-MG anticancer activity at a safe dose were carried out using mouse transplantable tumor models of uterine sarcoma US-322 (**Figure 3**, **Supplementary Table S3**) and cervical cancer RShM-5 (**Figure 4**, **Supplementary Table S4**). Tumor nodes appeared in all control group animals within 3 and 7 days after inoculation, respectively. The US-322 model demonstrated a statistically significant inhibition of tumor growth by the treatment with 7-MG, 50 mg/kg 3 times per week (**Figure 3**, group II), and the effect of 7-MG was comparable to cisplatin (group III). In the case of RShM-5 model, an ineffective dose of cisplatin was used to test the ability of 7-MG to sensitize the tumor to DNA-damaging agents. It was revealed that the combined treatment with cisplatin and 7-MG within a week after inoculation inhibits tumor growth, whilst 7-MG or cisplatin administration alone

TABLE 3 | Study of the ability of 7-MG to induce chromosomal aberrations in C57BL/6 mice.

Group		Dose, mg/kg	Number of damaged cells per 500 cells			
			Chromatid breaks	Chromosome breaks	Multiple aberrations	Total number
1 day	I control, males	—	8	0	0	8
	II cyclophosphamide, males	50	30	1	11	42[a]
	III 7-MG, males	50	7	0	0	7
	IV 7-MG, males	250	7	0	0	7
5 days	V control, males	—	9	0	0	9
	VI control, females	—	10	0	0	10
	VII 7-MG, males	5 × 50[b]	7	0	0	7
	VIII 7-MG, females	5 × 50	9	0	0	9

Bone marrow cells were collected 24 h after the last treatment.
[a]*Significant difference from the control group (Pearson's chi-squared test,* $p < 0.01$*).*
[b]*50 mg/kg per day.*

TABLE 4 | Study of the blastomogenic activity of 7-MG in *D. melanogaster*.

Tested compound	Dose, mg/vial	Number of flies	Number of tumors	Tumor frequency, %
Control	—	452	14	3.1
Oxoplatin	0.2	564	128	22.7[a]
7-MG	1.0	488	14	2.9
	2.0	405	9	2.2

[a]*Significant difference from the control (Fisher's exact test,* $p < 0.01$*).*

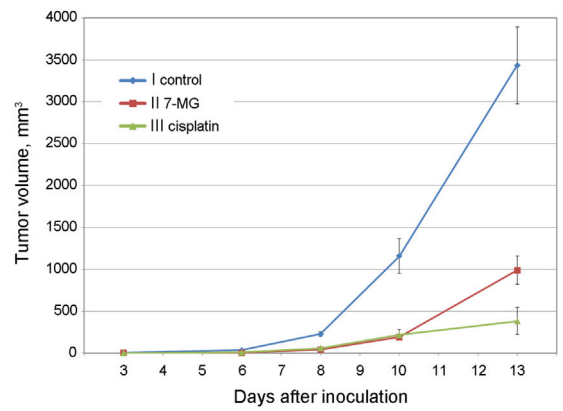

FIGURE 3 | Dynamics of US-322 tumor growth in female CBA mice at different treatment regimens.

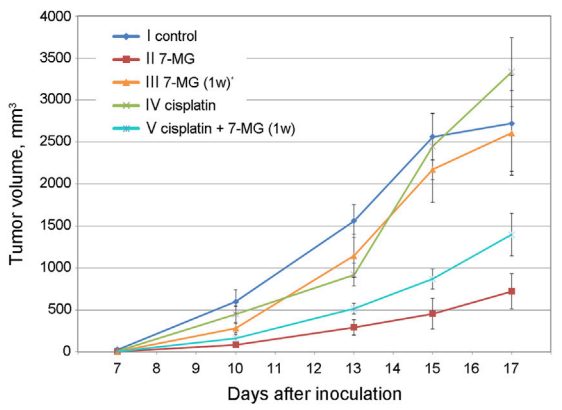

FIGURE 4 | Dynamics of RShM-5 tumor growth in female CBA mice at different treatment regimens. *7-MG was given for 1 week only.

exerted no significant effect (**Figure 4**, groups III–V). It is noteworthy that single-agent 7-MG treatment extended to more than 1 week (group II) had an even more pronounced antitumor effect compared to 1 week of combined treatment. Furthermore, group III (7-MG given for 1 week) clearly demonstrates that interruption of the 7-MG treatment results in accelerated tumor growth starting from the 10th day.

4 DISCUSSION

PARP1/2 inhibitors represent a novel class of anticancer agents. Although initially proposed for treatment of BRCA-deficient tumors in women (breast or ovarian cancer), these inhibitors have also demonstrated efficacy in other models such as prostate and gastric cancers (Underhill et al., 2011; Sachdev et al., 2019). Soft tissue sarcomas were also shown to be sensitive to PARP inhibition combined with genotoxic chemotherapy (Ordóñez et al., 2015). The strong PARP1/2 suppression seems to be inherently toxic due to an important role played by these proteins in the organism, but attempts are continuing to find the proper balance between efficacy and toxicity of inhibitors. Fatigue, anemia, nausea and neutropenia together with a risk of myelodysplastic syndrome/acute myeloid leukemia accompany the use of synthetic PARP1/2 inhibitors (Walsh, 2018). The recently described inhibitor 7-MG is a natural nitrogenous

base that could escape the serious side effects and become a promising new component of chemotherapy. Additionally, 7-MG inhibits the RNA-modifying enzyme TGT, which may enhance its anticancer activity.

The primary aim of this research was to outline the safety profile of 7-MG *in vivo*. We have established an oral regimen for 7-MG treatment in CBA mice (50 mg/kg, 3 times per week for up to 4 weeks) that exerts no adverse effects or changes in morphology. Adverse events were detected only at a maximum single dose of 600 mg/kg, in the form of small lymphoid infiltrates of non-inflammatory origin in the lungs and liver. These lesions may be resulted from the excessive inhibition of PARP (Beneke and Möröy, 2001; Ricks et al., 2015; Dasa et al., 2018) at concentrations much higher than therapeutic levels. The safety of 7-MG was also confirmed by the examination in four short-term carcinogenicity assays where it showed no mutagenic or blastomogenic effects.

Preliminary data obtained on mouse transplantable tumor models (uterine sarcoma, cervical carcinoma) demonstrated that 7-MG significantly reduces tumor growth at a safe dose and can also potentiate the activity of cisplatin. The interruption of the 7-MG treatment results in accelerated tumor growth, which highlights the advantages of a multiple-dose regimen. The molecular mechanism of 7-MG is fundamentally different from that of drugs like cisplatin. It acts by modulating the enzyme activity instead of causing DNA damage, and the multiple exposure to 7-MG is needed for the effective modulation. The present study of the natural 7-MG compound has confirmed its safety and potential tumor suppressing activity in mice. For further development, it would be important to identify the most sensitive tumors for the 7-MG treatment as well as to select DNA-damaging agents for the combination treatment.

DATA AVAILABILITY STATEMENT

The original contributions presented in the study are included in the article/**Supplementary Material**, further inquiries can be directed to the corresponding author.

ETHICS STATEMENT

The animal study was reviewed and approved by The Local Committee for Ethics of Animal Experimentation (Blokhin Cancer Research Center, Moscow, Russia).

AUTHOR CONTRIBUTIONS

Conceptualization and funding acquisition, DN; investigation, KK, TF, EA, LT, TG, OV, IK, EL, NK, and TS; writing—original draft, KK, EL, and DN; supervision and writing—review and editing, GB, MY, and VŠ.

FUNDING

This research was funded by the Russian Science Foundation, grant number 19-74-10072.

SUPPLEMENTARY MATERIAL

The Supplementary Material for this article can be found online at: https://www.frontiersin.org/articles/10.3389/fphar.2022.842316/full#supplementary-material

REFERENCES

Albertini, R. J., Anderson, D., Douglas, G. R., Hagmar, L., Hemminki, K., Merlo, F., et al. (2000). IPCS Guidelines for the Monitoring of Genotoxic Effects of Carcinogens in Humans. International Programme on Chemical Safety. *Mutat. Res.* 463, 111–172. doi:10.1016/s1383-5742(00)00049-1

Alemasova, E. E., and Lavrik, O. I. (2019). Poly(ADP-ribosyl)ation by PARP1: Reaction Mechanism and Regulatory Proteins. *Nucleic Acids Res.* 47, 3811–3827. doi:10.1093/nar/gkz120

Beneke, R., and Möröy, T. (2001). Inhibition of poly(ADP-Ribose) Polymerase Activity Accelerates T-Cell Lymphomagenesis in P53 Deficient Mice. *Oncogene* 20, 8136–8141. doi:10.1038/sj.onc.1205056

Bolognesi, M. L. (2013). Polypharmacology in a Single Drug: Multitarget Drugs. *Curr. Med. Chem.* 20, 1639–1645. doi:10.2174/0929867311320130004

Borowitz, I. J., Bloom, S. M., Rothschild, J., and Sprinson, D. B. (1965). Methylated Purines and Pyrimidines. I. Syntheses of 8-Hydroxy-7-Methylguanine and Methylation of a 5-(benzylideneamino) Pyrimidine. *Biochemistry* 4, 650–655. doi:10.1021/bi00880a006

Bromberg, P. A., Gutman, A. B., and Weissmann, B. (1957). The Purine Bases of Human Urine. II. Semiquantitative Estimation and Isotope Incorporation. *J. Biol. Chem.* 224, 423–434. doi:10.1016/s0021-9258(18)65041-0

Bromberg, P. A., Gutman, A. B., and Weissmann, B. (1957). The Purine Bases of Human Urine. I. Separation and Identification. *J. Biol. Chem.* 224, 407–422. doi:10.1016/s0021-9258(18)65040-9

Bunyatyan, N. D., Oborotova, N. A., Nikolaeva, L. L., Saprykina, N. S., Borisova, L. M., Kiseleva, M. P., et al. (2019). Comparative Analysis of Bioactivity of the Russian-made Antitumor Substances of the Nitrosourea Group. *Bull. Exp. Biol. Med.* 166, 456–460. doi:10.1007/s10517-019-04371-w

Cepeda, V., Fuertes, M. A., Castilla, J., Alonso, C., Quevedo, C., Soto, M., et al. (2006). Poly(ADP-ribose) Polymerase-1 (PARP-1) Inhibitors in Cancer Chemotherapy. *Recent Pat. Anticancer Drug Discov.* 1, 39–53. doi:10.2174/157489206775246430

Collins, A. R. (2004). The Comet Assay for DNA Damage and Repair: Principles, Applications, and Limitations. *Mol. Biotechnol.* 26, 249–261. doi:10.1385/MB:26:3:249

Craddock, V. M., Mattocks, A. R., and Magee, P. N. (1968). The Fate of 7[14C]-Methylguanine after Administration to the Rat. *Biochem. J.* 109, 75–78. doi:10.1042/bj1090075

Dasa, S. S. K., Diakova, G., Suzuki, R., Mills, A. M., Gutknecht, M. F., Klibanov, A. L., et al. (2018). Plectin-targeted Liposomes Enhance the Therapeutic Efficacy of a PARP Inhibitor in the Treatment of Ovarian Cancer. *Theranostics* 8, 2782–2798. doi:10.7150/thno.23050

Drenichev, M. S., and Mikhailov, S. N. (2015). Poly(ADP-ribose)--a Unique Natural Polymer Structural Features, Biological Role and Approaches to the Chemical Synthesis. *Nucleosides Nucleotides Nucleic Acids* 34, 258–276. doi:10.1080/15257770.2014.984073

Farkas, W. R., Jacobson, K. B., and Katze, J. R. (1984). Substrate and Inhibitor Specificity of tRNA-Guanine Ribosyltransferase. *Biochim. Biophys. Acta* 781, 64–75. doi:10.1016/0167-4781(84)90124-6

Ferraris, D. V. (2010). Evolution of poly(ADP-Ribose) Polymerase-1 (PARP-1) Inhibitors. From Concept to Clinic. *J. Med. Chem.* 53, 4561–4584. doi:10.1021/jm100012m

Frampton, J. E. (2015). Olaparib: A Review of its Use as Maintenance Therapy in Patients with Ovarian Cancer. *BioDrugs* 29, 143–150. doi:10.1007/s40259-015-0125-6

Hassler, M., and Ladurner, A. G. (2012). Towards a Structural Understanding of PARP1 Activation and Related Signalling ADP-Ribosyl-Transferases. *Curr. Opin. Struct. Biol.* 22, 721–729. doi:10.1016/j.sbi.2012.08.005

Jain, P. G., and Patel, B. D. (2019). Medicinal Chemistry Approaches of Poly ADP-Ribose Polymerase 1 (PARP1) Inhibitors as Anticancer Agents - A Recent Update. *Eur. J. Med. Chem.* 165, 198–215. doi:10.1016/j.ejmech.2019.01.024

Johannsson, S., Neumann, P., and Ficner, R. (2018). Crystal Structure of the Human tRNA Guanine Transglycosylase Catalytic Subunit QTRT1. *Biomolecules* 8, 81. doi:10.3390/biom8030081

Kaina, B., Heindorff, K., and Aurich, O. (1983). O6-methylguanine, but Not N7-Methylguanine or N3-Methyladenine, Induces Gene Mutations, Sister-Chromatid Exchanges and Chromosomal Aberrations in Chinese Hamster Cells. *Mutat. Res.* 108, 279–292. doi:10.1016/0027-5107(83)90126-4

Kerr, S. J. (1985). Induction of Adipocyte Formation in 10T1/2 Cells by 1-methylguanine and 7-methylguanine. *Tumour Biol.* 6, 115–121.

Kerr, S. J. (1990). Methylated Oxypurines and Induction of Differentiation of Murine Erythroleukemia Cells. *Mol. Cell. Biochem.* 92, 37–44. doi:10.1007/BF00220717

Kirsanov, K. I., Lesovaya, E. A., Sidorov, R. A., Belitsky, G. A., and Yakubovskaya, M. G. (2011). Analysis of Blastomogenic Activity of Mammal Carcinogens in Drosophila Using the Wts P4 Allele and RNA Interference-Induced P53 Silencing. *Russ. J. Genet.* 47, 409–416. doi:10.1134/s1022795411040065

Litwack, M. D., and Weissmann, B. (1966). Source of Urinary 8-Hydroxy-7-Methylguanine in Man. *Biochemistry* 5, 3007–3012. doi:10.1021/bi00873a033

Lord, C. J., Tutt, A. N., and Ashworth, A. (2015). Synthetic Lethality and Cancer Therapy: Lessons Learned from the Development of PARP Inhibitors. *Annu. Rev. Med.* 66, 455–470. doi:10.1146/annurev-med-050913-022545

Lothrop, C. D., Jr., and Uziel, M. (1983). RNA Turnover in Cultured Hamster Embryo Cells: Identification of Modified Nucleoside End Products. *J. Cell. Physiol.* 114, 111–116. doi:10.1002/jcp.1041140118

Maluchenko, N., Nilov, D., Feofanov, A., Lys, A., Kutuzov, M., Gerasimova, N., et al. (2019). 7-Methylguanine Traps PARP-1 on Nucleosomes: spFRET Microscopy Study. *Microsc. Microanal.* 25, 1282–1283. doi:10.1017/S1431927619007141

Malyuchenko, N. V., Kotova, E. Y., Kulaeva, O. I., Kirpichnikov, M. P., and Studitskiy, V. M. (2015). PARP1 Inhibitors: Antitumor Drug Design. *Acta Naturae* 7, 27–37. doi:10.32607/20758251-2015-7-3-27-37

Maron, D. M., and Ames, B. N. (1983). Revised Methods for the Salmonella Mutagenicity Test. *Mutat. Res.* 113, 173–215. doi:10.1016/0165-1161(83)90010-9

Martin, S. A., Lord, C. J., and Ashworth, A. (2008). DNA Repair Deficiency as a Therapeutic Target in Cancer. *Curr. Opin. Genet. Dev.* 18, 80–86. doi:10.1016/j.gde.2008.01.016

Medina-Franco, J. L., Giulianotti, M. A., Welmaker, G. S., and Houghten, R. A. (2013). Shifting from the Single to the Multitarget Paradigm in Drug Discovery. *Drug Discov. TodayToday* 18, 495–501. doi:10.1016/j.drudis.2013.01.008

Mittica, G., Ghisoni, E., Giannone, G., Genta, S., Aglietta, M., Sapino, A., et al. (2018). PARP Inhibitors in Ovarian Cancer. *Recent Pat. Anticancer Drug Discov.* 13, 392–410. doi:10.2174/1574892813666180305165256

Mustonen, R., and Hemminki, K. (1992). 7-Methylguanine Levels in DNA of Smokers' and Non-smokers' Total White Blood Cells, Granulocytes and Lymphocytes. *Carcinogenesis* 13, 1951–1955. doi:10.1093/carcin/13.11.1951

Nilov, D., Maluchenko, N., Kurgina, T., Pushkarev, S., Lys, A., Kutuzov, M., et al. (2020a). Molecular Mechanisms of PARP-1 Inhibitor 7-methylguanine. *Int. J. Mol. Sci.* 21, 2159. doi:10.3390/ijms21062159

Nilov, D. K., Pushkarev, S. V., Gushchina, I. V., Manasaryan, G. A., Kirsanov, K. I., and Švedas, V. K. (2020b). Modeling of the Enzyme-Substrate Complexes of Human poly(ADP-Ribose) Polymerase 1. *Biochem. (Mosc)* 85, 99–107. doi:10.1134/S0006297920010095

Nilov, D. K., Tararov, V. I., Kulikov, A. V., Zakharenko, A. L., Gushchina, I. V., Mikhailov, S. N., et al. (2016). Inhibition of poly(ADP-Ribose) Polymerase by Nucleic Acid Metabolite 7-methylguanine. *Acta Naturae* 8, 108–115. doi:10.32607/20758251-2016-8-2-108-115

Nilov, D., Kirsanov, K., Antoshina, E., Maluchenko, N., Feofanov, A., Kurgina, T., et al. (2018a). 7-Methylguanine: A Natural DNA Repair Inhibitor and a Promising Anticancer Compound. *FEBS Open Bio* 8. doi:10.1002/2211-5463.12453

Nilov, D. K., Yashina, K. I., Gushchina, I. V., Zakharenko, A. L., Sukhanova, M. V., Lavrik, O. I., et al. (2018b). 2,5-Diketopiperazines: A New Class of poly(ADP-Ribose)polymerase Inhibitors. *Biochem. (Mosc)* 83, 152–158. doi:10.1134/S0006297918020074

O'Connor, T. R. (1993). Purification and Characterization of Human 3-Methyladenine-DNA Glycosylase. *Nucleic Acids Res.* 21, 5561–5569. doi:10.1093/nar/21.24.5561

Ohmoto, A., and Yachida, S. (2017). Current Status of poly(ADP-Ribose) Polymerase Inhibitors and Future Directions. *Onco Targets Ther.* 10, 5195–5208. doi:10.2147/OTT.S139336

Ordóñez, J. L., Amaral, A. T., Carcaboso, A. M., Herrero-Martín, D., del Carmen García-Macías, M., Sevillano, V., et al. (2015). The PARP Inhibitor Olaparib Enhances the Sensitivity of Ewing Sarcoma to Trabectedin. *Oncotarget* 6, 18875–18890. doi:10.18632/oncotarget.4303

Park, J. W., and Ames, B. N. (1988). 7-Methylguanine Adducts in DNA Are Normally Present at High Levels and Increase on Aging: Analysis by HPLC with Electrochemical Detection. *Proc. Natl. Acad. Sci. U. S. A.* 85, 7467–7470. doi:10.1073/pnas.85.20.7467

Raćkowska, E., Bobrowska-Korczak, B., and Giebułtowicz, J. (2019). Development and Validation of a Rapid LC-MS/MS Method for Determination of Methylated Nucleosides and Nucleobases in Urine. *J. Chromatogr. B Anal. Technol. Biomed. Life Sci.* 1128, 121775. doi:10.1016/j.jchromb.2019.121775

Ray Chaudhuri, A., and Nussenzweig, A. (2017). The Multifaceted Roles of PARP1 in DNA Repair and Chromatin Remodelling. *Nat. Rev. Mol. Cell Biol.* 18, 610–621. doi:10.1038/nrm.2017.53

Ricks, T. K., Chiu, H. J., Ison, G., Kim, G., McKee, A. E., Kluetz, P., et al. (2015). Successes and Challenges of PARP Inhibitors in Cancer Therapy. *Front. Oncol.* 5, 222. doi:10.3389/fonc.2015.00222

Rodríguez-Gonzalo, E., Hernández-Prieto, R., García-Gómez, D., and Carabias-Martínez, R. (2013). Capillary Electrophoresis-Mass Spectrometry for Direct Determination of Urinary Modified Nucleosides. Evaluation of Synthetic Urine as a Surrogate Matrix for Quantitative Analysis. *J. Chromatogr. B Anal. Technol. Biomed. Life Sci.* 942–943, 21–30. doi:10.1016/j.jchromb.2013.10.022

Sachdev, E., Tabatabai, R., Roy, V., Rimel, B. J., and Mita, M. M. (2019). PARP Inhibition in Cancer: An Update on Clinical Development. *Target. Oncol.* 14, 657–679. doi:10.1007/s11523-019-00680-2

Sander, G., Hülsemann, J., Topp, H., Heller-Schöch, G., and Schöch, G. (1986). Protein and RNA Turnover in Preterm Infants and Adults: A Comparison Based on Urinary Excretion of 3-methylhistidine and of Modified One-Way RNA Catabolites. *Ann. Nutr. Metab.* 30, 137–142. doi:10.1159/000177186

Sander, G., Topp, H., Heller-Schöch, G., Wieland, J., and Schöch, G. (1986). Ribonucleic Acid Turnover in Man:RNA Catabolites in Urine as Measure for the Metabolism of Each of the Three Major Species of RNA. *Clin. Sci.* 71, 367–374. doi:10.1042/cs0710367

Sander, G., Topp, H., Wieland, J., Heller-Schöch, G., and Schöch, G. (1986). Possible Use of Urinary Modified RNA Metabolites in the Measurement of RNA Turnover in the Human Body. *Hum. Nutr. Clin. Nutr.* 40, 103–118.

Shafer, B., Chu, C., and Shatkin, A. J. (2005). Human mRNA Cap Methyltransferase: Alternative Nuclear Localization Signal Motifs Ensure Nuclear Localization Required for Viability. *Mol. Cell. Biol.* 25, 2644–2649. doi:10.1128/MCB.25.7.2644-2649.2005

Shapiro, R. (1968). "Chemistry of Guanine and its Biologically Significant Derivatives,". Editors J. N. Davidson and W. E. Cohn (New York, USA: Academic Press).*Prog. Nucleic Acid Res. Mol. Biol.*, Vol. 8, 73–112. doi:10.1016/s0079-6603(08)60544-9

Shuman, S. (2002). What Messenger RNA Capping Tells Us about Eukaryotic Evolution. *Nat. Rev. Mol. Cell Biol.* 3, 619–625. doi:10.1038/nrm880

Sidorov, R. A., Ugnivenko, E. G., Khovanova, E. M., and Belitsky, G. A. (2001). Induction of Tumor Clones in *D. melanogaster Wts/+* Heterozygotes with Chemical Carcinogens. *Mutat. Res.* 498, 181–191. doi:10.1016/s1383-5718(01)00277-7

Singh, N. P., McCoy, M. T., Tice, R. R., and Schneider, E. L. (1988). A Simple Technique for Quantitation of Low Levels of DNA Damage in Individual Cells. *Exp. Cell Res.* 175, 184–191. doi:10.1016/0014-4827(88)90265-0

Skupp, S., and Ayvazian, J. H. (1969). Oxidation of 7-methylguanine by Human Xanthine Oxidase. *J. Lab. Clin. Med.* 73, 909–916.

Sonnenblick, A., de Azambuja, E., Azim, H. A., Jr., and Piccart, M. (2015). An Update on PARP Inhibitors-Mmoving to the Adjuvant Setting. *Nat. Rev. Clin. Oncol.* 12, 27–41. doi:10.1038/nrclinonc.2014.163

Svoboda, P., and Kasai, H. (2004). Simultaneous HPLC Analysis of 8-hydroxydeoxyguanosine and 7-methylguanine in Urine from Humans and Rodents. *Anal. Biochem.* 334, 239–250. doi:10.1016/j.ab.2004.08.021

Tamae, K., Kawai, K., Yamasaki, S., Kawanami, K., Ikeda, M., Takahashi, K., et al. (2009). Effect of Age, Smoking and Other Lifestyle Factors on Urinary 7-methylguanine and 8-hydroxydeoxyguanosine. *Cancer Sci.* 100, 715–721. doi:10.1111/j.1349-7006.2009.01088.x

Tan, B. H., Bencsath, F. A., and Gaubatz, J. W. (1990). Steady-state Levels of 7-methylguanine Increase in Nuclear DNA of Postmitotic Mouse Tissues during Aging. *Mutat. Res.* 237, 229–238. doi:10.1016/0921-8734(90)90004-b

Topisirovic, I., Svitkin, Y. V., Sonenberg, N., and Shatkin, A. J. (2011). Cap and Cap-Binding Proteins in the Control of Gene Expression. *Wiley Interdiscip. Rev. RNA.* 2, 277–298. doi:10.1002/wrna.52

Topp, H., Sander, G., Heller-Schöch, G., and Schöch, G. (1987). Determination of 7-methylguanine, N2,N2-Dimethylguanosine, and Pseudouridine in Ultrafiltrated Serum of Healthy Adults by High-Performance Liquid Chromatography. *Anal. Biochem.* 161, 49–56. doi:10.1016/0003-2697(87)90650-6

Treshalina, H. M., Lukasheva, E. V., Sedakova, L. A., Firsova, G. A., Guerassimova, G. K., Gogichaeva, N. V., et al. (2000). Anticancer Enzyme L-Lysine α-Oxidase: Properties and Application Perspectives. *Abab* 88, 267–274. doi:10.1385/abab:88:1-3:267

Turusov, V. S., Siniak, IuE., Grigor'ev, A. I., Zaridze, D. G., Antoshina, E. E., Trukhanova, L. S., et al. (2005). Low-deuterium Water Effect on Transplantable Tumors. *Vopr. Onkol.* 51, 99–102.

Underhill, C., Toulmonde, M., and Bonnefoi, H. (2011). A Review of PARP Inhibitors: from Bench to Bedside. *Ann. Oncol.* 22, 268–279. doi:10.1093/annonc/mdq322

Varshney, D., Petit, A. P., Bueren-Calabuig, J. A., Jansen, C., Fletcher, D. A., Peggie, M., et al. (2016). Molecular Basis of RNA Guanine-7 Methyltransferase (RNMT) Activation by RAM. *Nucleic Acids Res.* 44, 10423–10436. doi:10.1093/nar/gkw637

Walsh, C. (2018). Targeted Therapy for Ovarian Cancer: the Rapidly Evolving Landscape of PARP Inhibitor Use. *Minerva Ginecol.* 70, 150–170. doi:10.23736/S0026-4784.17.04152-1

Wang, Y. Q., Wang, P. Y., Wang, Y. T., Yang, G. F., Zhang, A., and Miao, Z. H. (2016). An Update on poly(ADP-Ribose)polymerase-1 (PARP-1) Inhibitors: Opportunities and Challenges in Cancer Therapy. *J. Med. Chem.* 59, 9575–9598. doi:10.1021/acs.jmedchem.6b00055

Weissmann, B., and Gutman, A. B. (1957). The Identification of 6-succinoaminopurine and of 8-Hydroxy-7-Methylguanine as Normal Human Urinary Constituents. *J. Biol. Chem.* 229, 239–250. doi:10.1016/s0021-9258(18)70612-1

Zhang, J., Lu, R., Zhang, Y., Matuszek, Ż., Zhang, W., Xia, Y., et al. (2020). tRNA Queuosine Modification Enzyme Modulates the Growth and Microbiome Recruitment to Breast Tumors. *Cancers (Basel)* 12, 628. doi:10.3390/cancers12030628

Zimmer, A. S., Gillard, M., Lipkowitz, S., and Lee, J. M. (2018). Update on PARP Inhibitors in Breast Cancer. *Curr. Treat. Options Oncol.* 19, 21. doi:10.1007/s11864-018-0540-2

Conflict of Interest: DN and VŠ are named on a patent for using 7-methylguanine to suppress PARP activity.

The remaining authors declare that the research was conducted in the absence of any commercial or financial relationships that could be construed as a potential conflict of interest.

Publisher's Note: All claims expressed in this article are solely those of the authors and do not necessarily represent those of their affiliated organizations, or those of the publisher, the editors and the reviewers. Any product that may be evaluated in this article, or claim that may be made by its manufacturer, is not guaranteed or endorsed by the publisher.

frontiers | Frontiers in Oncology

ORIGINAL RESEARCH
published: 13 July 2022
doi: 10.3389/fonc.2022.922127

Gemcitabine Plus Anlotinib Is Effective and Safe Compared to Gemcitabine Plus Docetaxel in Advanced Soft Tissue Sarcoma

Zhiyong Liu, Xin Wang, Jiaqiang Wang, Peng Zhang, Chao Li, Bangmin Wang, Guancong Liu and Weitao Yao *

Department of Orthopedics, The Affiliated Cancer Hospital of Zhengzhou University and Henan Cancer Hospital, Zhengzhou, China

Objective: The aim of this study is to compare gemcitabine (G) plus docetaxel (D) versus G plus anlotinib (A) for advanced soft tissue sarcoma (STS).

Methods: We retrospectively investigated 122 patients with locally advanced or metastatic STS who were treated with either G+D or G+A between July 2016 and October 2021 and compared the efficacy and toxicity of G+D and G+A. The primary endpoints were median progression-free survival (PFS) and the proportion of patients with grade ≥3 adverse events. We also analyzed differences in the clinical efficacy of G+D and G+A in leiomyosarcoma, and the differences in the clinical efficacy of G+D and G+A as first-line therapy.

Results: Overall, 122 patients were included (81 patients receiving G+D and 41 patients receiving G+A) with a median age of 55 years. The main histological types are leiomyosarcoma, undifferentiated pleomorphic sarcoma, and liposarcoma. After a median follow-up of 25 months, PFS did not differ between patients treated with G+D and those treated with G+A (median PFS: 5.8 months and 6.8 months, $p = 0.39$), and overall survival (OS) was similar (median OS: 14.7 vs. 13.3 months, $p = 0.75$) with a similar objective response rate (18.5% vs. 14.6%, $p = 0.17$), whereas the proportion of patients with grade ≥3 adverse events treated with G+D was significantly higher than those treated with G+A (68% vs. 44%, $p < 0.05$). Subgroup analysis of leiomyosarcoma patients (47.5% of the patients) and first-line treatment patients (46.7% of the patients) shows that PFS was not significantly different between the two groups (LMS: median PFS: 6.5 months vs. 7.5 months, $p = 0.08$; first-line treatment: median PFS: 6.2 months vs. 7.1 months, $p = 0.51$).

Conclusion: Compared with gemcitabine plus docetaxel for advanced STS, gemcitabine plus anlotinib achieved a similar response rate on median PFS and OS, but lower toxicity. These results suggest that gemcitabine plus anlotinib may be an effective and safe strategy for advanced STS.

Keywords: efficacy, safety, anlotinib, gemcitabine, docetatxel, soft tissue sarcoma (STS)

OPEN ACCESS

Edited by:
Jian-ye Zhang, Guangzhou Medical University, China

Reviewed by:
Mustafa Benekli, Gazi University, Turkey
Purvish M. Parikh, Mahatma Gandhi Medical College Hospital, India

***Correspondence:**
Weitao Yao
yaoweitao1012@126.com

Specialty section:
This article was submitted to Cancer Molecular Targets and Therapeutics, a section of the journal Frontiers in Oncology

Received: *17 April 2022*
Accepted: *06 June 2022*
Published: *13 July 2022*

Citation:
Liu Z, Wang X, Wang J, Zhang P, Li C, Wang B, Liu G and Yao W (2022) Gemcitabine Plus Anlotinib Is Effective and Safe Compared to Gemcitabine Plus Docetaxel in Advanced Soft Tissue Sarcoma . Front. Oncol. 12:922127. doi: 10.3389/fonc.2022.922127

INTRODUCTION

Soft tissue sarcoma (STS) comprises rare and profound heterogeneous tumors of mesenchymal origin, with more than 50 different histological subtypes and an incidence of 10/1 million (1–3). Over 50% of STS originates in the trunk and limbs. Despite radical surgical excision with or without radiotherapy, approximately one-third of patients will eventually experience recurrence of locally unresectable or metastatic disease that threatens organ function and life (4). In the locally advanced or metastatic disease setting, patients have a poor prognosis, with a reported median overall survival (OS) of 12–20 months after diagnosis (5). The treatment of advanced disease with systemic therapy is limited, and cytotoxic chemotherapy has a prominent role in standard treatments consisting of doxorubicin monotherapy or doxorubicin plus ifosfamide (6). However, the cumulative cardiotoxicity of doxorubin increases significantly at doses above 450 mg/m^2, which limits the sustainability of clinical application (7). Taking into account the heterogeneous histomorphology and behavior of the disease, second-line treatment regimens are usually individualized based on histological subtypes and clinical behaviors (1), such as high-dose cyclophosphamide for synovial sarcoma (8), eribulin for liposarcoma (9), and tyrosine kinase inhibitors for non-adipogenic STS including pazopanib (10), regorafenib (11), and anlotinib (12). Apart from these drugs, gemcitabine (G) and/or docetaxel (D) is another widely used regimen for most patients with advanced STS (6).

Although G+D has shown moderate antitumor activity in advanced STS, the role of D remains controversial because multiple studies have yielded conflicting results with the exception of angiosarcomas (13). A Phase II study (14) published in 2002 including 119 patients with metastatic STS treated as one to four lines of chemotherapy showed that, compared with G monotherapy, G+D yielded statistically significant benefits in response rate (16% vs. 8%), median progression-free survival (PFS) (6.2 months vs. 3 months), and median OS (17.9 months vs. 11.5 months), but increased toxicity, where the toxicity results in at least one dose reduction in 46% of patients. In subtype analysis, the combination therapy could lead to superior survival in leiomyosarcoma (LMS) and undifferentiated pleomorphic sarcoma (UPS) compared with other subtypes. Moreover, a preclinical study showed that G followed by D is synergistic, and otherwise antagonistic (15). Hence, the current G+D regimen evolved into a most effective method for the treatment of advanced STS. However, several Phase II and retrospective studies showed that G+D showed moderate clinical efficacy similar to that of G alone, but with more adverse events (AEs). In 2012, the French Sarcoma Group conducted a randomized stratified Phase II study (16), which examined the efficacy and toxicity of G+D and G in 90 patients with metastatic or inoperable LMS (uterine and non-uterine) who had failed first-line therapy. For patients with non-uterine LMS, ORR was 5% and 14% for G+D and G treatment, and median PFS was 3.8 and 6.3 months, respectively. For patients with uterine LMS, G+D and G had similar effects, with ORR of 24% and 19% and median PFS of 4.7 and 5.5 months, respectively. However, less toxicity was observed in patients treated with G alone. Such results suggested that gemcitabine-based therapy is a treatment option for patients who have failed anthracycline therapy.

Chemotherapy and anti-angiogenesis play a crucial role in advanced malignant tumors. Increasing studies (17–20) have shown that anti-angiogenesis in combination with chemotherapy yielded synergetic effects in several malignancies including breast cancer, lung cancer, and sarcomas. Preclinical studies (21, 22) showed that anti-angiogenesis therapy not only induced tumor cell apoptosis but also induced tumor vascular normalization, improved hypoxia, and increased the delivery of chemotherapy drugs. In the ALTER0203 trial (12), anlotinib demonstrated superior ORR (10.13% vs. 1.33%) and median PFS (6.27 months vs. 1.47 months) over placebo in advanced STS after the failure of standard chemotherapy. Based on the above results, it was approved in China as a second-line treatment drug for advanced STS except for alveolar STS and clear cell sarcoma, in June 2019. Preclinical studies (23, 24) showed that anlotinib played a crucial part in tumor cell proliferation and migration, as well as angiogenesis, though selectively targeting VEGFR, PDGFR, FGFR, c- kit, and MET. The IC_{50} value was 0.2 nmol/L for VEGFR2, 0.7 nmol/L for VEGFR3, 8.7 nmol/L for PDFGFRβ, and 11.7 nmol/L for FGFR1. These data indicate that anlotinib has the potential to simultaneously inhibit phosphorylation of important tyrosine kinases and their downstream signaling pathways. Considering the poor outcome of advanced STS and the potential synergistic effect of gemcitabine and anlotinib (25), G+A has been used as a novel treatment for patients after failure of anthracycline-based regimen since the widespread use of anlotinib in China.

In this study, the efficacy and toxicity of G+D and G+A were retrospectively investigated, aiming to evaluate the feasibility of G+A as a novel treatment option for patients with locally advanced or metastatic STS who had failed adriamycin-based therapy.

MATERIALS AND METHODS

Study Design

Patients with locally advanced or metastatic STS were retrospectively collected between July 2016 and October 2021 at Henan Cancer Hospital, one of the largest hospitals for cancer patients in a province of about 100 million people. Medical records of the patients treated with G+D between July 2016 and October 2021 were reviewed, including patient characteristics, treatment regimens, imaging data, AEs, and survival data, and those of similar patients treated with G+A between July 2019 and October 2021. Partial survival data were followed up by telephone.

The inclusion criteria are as follows: (1) 18–70 years old; (2) histologically proven advanced STS (locally advanced or metastatic); (3) prior treatment with anthracyclines, and adjuvant therapy received within 1 year by patients with the recurrent disease was considered first-line therapy; (4) with

measurable lesions according to the Response Evaluation Criteria in Solid Tumors (RECIST) version 1.1; (5) an Eastern Cooperative Oncology Group (ECOG) performance status of 0–2; (6) with target lesions not suitable for complete surgical resection or radiotherapy; (7) adequate blood, renal, liver, and cardiac parameters; (8) available clinical data including medical history, treatment, and survival data; and (9) treated with G+D or G+A.

Exclusion criteria are as follows: (1) patients given other anti-tumor therapies during treatment including chemotherapy, radiotherapy, targeted therapy, surgery, and immunotherapy; (2) patients receiving G+D with a history of prior treatment with G and/or D within 6 months, and patients receiving G+A with a history of prior treatment with G and/or targeted agents within 6 months; (3) risk of active bleeding; (4) treatment interruption lasted more than 6 weeks.

Approval of this study was achieved from the institutional review board of Henan Cancer Hospital according to the Declaration of Helsinki. Written informed consent for treatment from each patient was obtained before either regimen.

Therapeutic Regimen

For patients treated with G+D, intravenous G 1,000 mg/m^2 was administered on days 1 and 8 and D 75 mg/m^2 was given on day 8 every 3 weeks. For G+A, G was administered at the same dose and schedule as the G+D regimen, and A was administered at a dose of 12 mg for 8–21 days every 3 weeks. The treatment schedule was formulated by the patient's physician and the dose of the respective drugs was reduced according to the toxicities. Granulocyte colony-stimulating factor or pegylated recombinant human granulocyte colony-stimulating factor was routinely given according to AEs. Patients were treated until the disease progressed or intolerable AEs occurred or they refused treatment. Multiple-dose reductions of regimens allowed were observed on an individual basis according to the toxicity. Generally, gemcitabine doses were reduced from 1000 mg/m^2 to 850 mg/m^2 and 723 mg/m^2, docetaxel doses were reduced from 75 mg/m^2 to 64 mg/m^2 and 54 mg/m^2, and anlotinib doses were reduced from 12 mg to 10 mg and 8 mg. Patients were informed of the potential efficacy and toxicity of the regimens before treatment initiation.

Study Assessments

The primary endpoints were median PFS and the proportion of patients with grade ≥3 AEs in two groups. Secondary endpoints were ORR, OS, and AEs. PFS was the interval from the start of either G+D or G+A to the time of the first occurrence of disease progression, death, or the last follow-up. OS was the interval from the beginning of treatment to the date of death or the last follow-up. The proportion of patients with AEs was the ratio of the number of patients who underwent AEs to the total number of patients. Treatment response was determined by CT scan, MRI scan, or both performed at baseline and then every 1.5–2 months. Tumor response was evaluated according to RECIST 1.1, including complete response (CR), partial response (PR), stable disease (SD), and progressive disease (PD). ORR was defined as the proportion of patients who gained a CR or PR. AEs were collected and evaluated based on the Common Terminology Criteria for Adverse Events (CTCAE) v4.0.

Statistical Analysis

Descriptive statistics and frequency were used to describe characteristics of patients and sarcomas. The differences in response rate, AEs, and other classification variables between the groups were analyzed by the Chi-square test or Fisher's exact test. Kaplan–Meier curve was plotted to estimate PFS and OS with 2-sided 95% confidence intervals (CIs), and log-rank test was used to calculate survival distributions. Bilateral $p < 0.05$ was considered statistically significant, and statistical analysis was conducted using GraphPad Prism version 9.0.1.

RESULTS

Demographics

From July 2016 to October 2021, 122 patients with locally advanced or metastatic STS who met the inclusion and exclusion criteria were retrospectively identified. Patient characteristics at baseline between two treatment groups were comparable and displayed in **Table 1**. Of 122 patients, 81 patients received G+D and 41 received G+A. The median (range) age was 53 (18–70) and 57 (20–70) years, 32 (39.5%) and 15 (36.6%) patients were men, and 73 (90.1%) and 35 (85.4%) patients had an ECOG PS of 0/1 in the G+D and G+A groups, respectively. The major histological subtypes in the G+D and G+A groups were represented: LMS (38 [46.9%] and 20 [48.7%] patients), UPS (11 [13.6%] and 6 [14.6%] patients), and liposarcoma (LPS) (12 [14.8%] and 4 [9.8%] patients). Seventy-three (90.3%) and 36 (87.8%) patients had received operations, and 30 (37%) and 13 (34.1%) patients had received radiotherapy in the G+D and G+A groups, respectively. In total, more than 70% of patients received either the regimen as a first or second line. Thirty-eight (31.1%) patients received anthracyclines and 84 (68.9%) received anthracyclines plus ifosfamide. Rare sarcoma subtypes with a frequency of 1–4 were defined as others. No significant differences were observed between the two groups in age, sex, histological type, and other characteristics at baseline.

Treatment Administered

The median of 6 (1–8) cycles of G and the median of 4 (1–7) cycles of D were given in the G+D regimen; G was administered at 1,000 mg/m^2 in 73 (90.1%) patients, 850 mg/m^2 in 6 (7.4%) patients, and 723 mg/m^2 in 2 (2.5%) patients as the beginning dose. D was administered at 75 mg/m^2 in 67 (82.7%) patients, 64 mg/m^2 in 11 (13.6%) patients, and 54 mg/m^2 in 3 (3.7%) patients as the beginning dose. Some patients were given day 1 G, but they were not given day 8 G and/or D; 15% and 30% of patients experienced dose reduction of G and D. While the median of 6 (range 1–8) cycles of G and the median of 6 (1–35) cycles of A were given in the G+A regimen, 34% of patients were treated with G+A followed by A alone because of the poor tolerability of G; 19.5% and 15% of patients experienced dose reductions of G and A, respectively. The main reasons for dose reduction in the

TABLE 1 | Demographics of patients.

Characteristics	Overall, *n* (%)	Gemcitabine+Docetaxel, *n* (%)	Gemcitabine+Anlotinib, *n* (%)	*p*-Value
No. of patients	122	81	41	
Age, median (range), years	55 (18–70)	53 (18–70)	57 (20–70)	0.35
Sex				
Female	75 (61.5%)	49 (60.5%)	26 (63.4%)	0.75
Male	47 (38.5%)	32 (39.5%)	15 (36.6%)	
ECOG				
0/1	108 (88.6%)	73 (90.1%)	35 (85.4%)	0.63
2	14 (11.5%)	8 (9.9%)	6 (14.6%)	
Stage				
Metastatic	94 (77%)	65 (80.5%)	29 (70.7%)	0.24
Locally advanced	28 (23%)	16 (19.5)	12 (29.3)	
Histological types				
Leiomyosarcoma	58 (47.5%)	38 (46.9%)	20 (48.8%)	0.85
Non-leiomyosarcoma	64 (52.5%)	43 (53.1%)	21 (51.3%)	
Undifferentiated pleomorphic sarcoma	17 (13.9%)	11 (13.6%)	6 (14.6%)	0.74
Liposarcoma	16 (13.1%)	12 (14.8%)	4 (9.8%)	
Others	31 (25.4%)	20 (24.7%)	11 (26.8%)	
Prior therapies received				
Radiotherapy	43 (35.2%)	30 (37%)	13 (34.1%)	0.60
Surgery	109 (89.3%)	73 (90.3%)	36 (87.8%)	0.94
Chemotherapy	122 (100%)	81 (100%)	41 (100%)	
Anthracyclines	38 (31.1%)	24 (29.6%)	14 (34.1%)	0.61
Anthracyclines+Ifosfamide	84 (68.9%)	57 (70.4%)	27 (65.9%)	
No. of lines of prior chemotherapy				
Neoadjuvant chemotherapy	57 (46.7%)	37 (45.7%)	20 (48.8%)	0.58
1	36 (29.5%)	23 (28.4%)	13 (31.7%)	
≥2	28 (23%)	21 (25.9%)	7 (17.1%)	

ECOG, Eastern Cooperative Oncology Group; Others, Synovial sarcoma, Undifferentiated rhabdomyosarcoma, Angiosarcoma, Epithelioid sarcoma, Fibrosarcoma, and Malignant peripheral nerve sheath tumor.

two regimens were febrile neutropenia, other hematological toxicities, and non-hematological toxicities (**Tables 2**, **Table 3**).

Treatment Responses and survival

Totally, the median follow-up time was 25 months (range, 3–38 months). At the time of the analysis, 117 patients (96%) have completed the treatment, 21 patients have achieved a CR or PR and 62 patients have obtained SD, yielding an ORR and disease control rate of 17.2% and 68%, respectively. The median PFS and OS were 6.3 months (95% CI 6.0–8.4) and 14.3 months (95% CI 14.1–17.4), respectively (**Table 4**). The common reasons for treatment discontinuations were PD in 88 (72.1%) patients, toxicity in 26 (21.3%) patients, and other reasons in 8 (6.6%) patients (**Table 2**).

Regarding differences in efficacy in total patients, no statistically significant difference in PFS was detected between the treatment groups, with a median PFS of 5.8 months (95% CI 6.0–8.4) vs. 6.8 months (95% CI 6.2–9.2) for the G+D and G+A groups, respectively (**Table 4** and **Figure 1**, $p = 0.39$). Similarly, no statistically significant difference in OS was detected between the treatment groups, with a median OS of 14.7 months (95% CI 13.9–17.9) vs. 13.3 months for the G+D and G+A groups (**Table 4** and **Figure 2**, $p = 0.75$). Response rates were similar between the G+D and the G+A groups, with an ORR of 18.5% (15/81) vs. 14.6% (6/41) (**Table 4**, $p = 0.17$) and a DCR of 66.7% (54/81) vs. 70.7% (29/41) (**Table 4**, $p = 0.75$), respectively.

Since nearly 50% of patients (45.7% and 48.8% for the G+D and G+A groups, respectively) were diagnosed with locally

TABLE 2 | Treated details.

	Gemcitabine+Docetaxel	Gemcitabine+Anlotinib
Median no. of cycles of G (range)	6 (1–8)	6 (1–8)
Median no. of cycles of D (range)	4 (1–5)	
Median no. of cycles of A (range)		7 (1–35)
Dose reduction of G+D, *n* (%)	25 (30.9%)	9 (22%)
Dose reduction of G, *n* (%)	12 (14.8%)	8 (19.5%)
Dose reduction of D, *n* (%)	24 (29.6%)	
Dose reduction of A, *n* (%)		6 (14.6%)
Treatment completed		
Disease progression, *n* (%)	57 (70.4%)	31 (75.6%)
Toxicity, *n* (%)	20 (24.7%)	6 (14.6%)
Other reasons, *n* (%)	4 (4.9%)	4 (9.8%)

G, Gemcitabine; D, Docetaxel; A, Anlotinib; Other reasons, refusal due to not toxicity.

TABLE 3 | Dose summary.

Gemcitabine+Docetaxel, *n* (%)		Gemcitabine+Anlotinib, *n* (%)	
Gemcitabine		**Gemcitabine**	
No. of cycles	400 (100%)	No. of cycles	236 (100%)
Day 1 dose		Day 1 dose	
1,000 mg/m^2	342 (85.5%)	1,000 mg/m^2	223 (94.5%)
850 mg/m^2	38 (9.5%)	850 mg/m^2	10 (4.2%)
723 mg/m^2	20 (5%)	723 mg/m^2	3 (1.2%)
Any dose reduction/Lowest dose administered	12 (14.8%)	Any dose reduction/Lowest dose administered	8 (19.5%)
850 mg/m^2	12 (37.5%)	850 mg/m^2	15 (62.5%)
723 mg/m^2	16 (50%)	723 mg/m^2	6 (25%)
615 mg/m^2	4 (12.5%)	615 mg/m^2	3 (12.5%)
Docetaxel	360 (100%)	Anlotinib	400 (100%)
No. of cycles (day 1 dose)		No. of cycles (day 1 dose)	
75 mg/m^2	318 (88.3%)	12 mg	390 (97.5%)
64 mg/m^2	36 (10%)	10 mg	10 (2.5%)
54 mg/m^2	6 (1.7%)	8 mg	0 (%)
Any dose reduction/Lowest dose administered	24 (30%)	Any dose reduction/Lowest dose administered	6 (14.6%)
64 mg/m^2	24	10 mg	13
54 mg/m^2	16	8 mg	6
46 mg/m^2	10		

advanced or metastatic LMS, we conducted a separate analysis to compare whether there were significant differences between LMS patients treated with the two regimens. There was no significant statistical difference in PFS and OS, with a median PFS of 6.2 months (95% CI 5.3–8.2) in the G+D group and 7.1 months (95% CI 5.9–9.9) in the G+A group (**Table 5** and **Figure 3**, p = 0.08), and a median OS of 15.7 months (95% CI 12.7–18.5) and 13.6 months (95% CI 10.5–17.9) in the G+D and G+A groups, respectively (**Table 5** and **Figure 4**, p = 0.76). There were too few patients with other histological subtypes to make a meaningful comparison of results between the two groups.

Approximately 50% of patients (45.7% and 48.8% for the G +D and G+A groups, respectively) received either G+D or G+A as first-line therapy (more than 1 year after adjuvant therapy). We conducted an exploratory analysis to compare the clinical outcomes between patients treated with the two regimens as first-line treatment. The PFS was not a statistically significant difference, with a median PFS of 6.5 months (95% CI 5.4–7.7) vs. 7.5 months (95% CI 6.2–10.6) for the G+D and G+A groups, respectively. (**Table 5** and **Figure 5**, p = 0.51). The OS was similar, with a median OS of 17.2 months (95% CI 14.4–20.1) vs. 16.2 months (95% CI 12.1–20.7) for the G+D and G+A groups, respectively (**Table 5**, and **Figure 6**, p = 0.62).

Toxicity

Both G+D and G+A were generally well tolerated. The grade 3/4 AEs are displayed in **Table 6**. The most frequent grade 3/4 AEs in the G+D and G+A groups were neutropenia (48% vs. 34%), thrombocytopenia (35% vs. 34%), anemia (25% vs. 12%), and transaminase elevation (15% vs. 17%). Although most types of AEs were consistent, the proportion of patients who experienced grade ≥3 AEs was higher in the G+D group than that in the G+A group (68% vs. 44%), especially hematological AEs observed in 45 (56%) vs. 14 (34%) patients in the G+D and G+A groups, respectively. It is worth noting that three patients experienced grade ≥3 pneumothorax events. The majority of the reasons for dose delay and dose reduction were febrile neutropenia, other hematological toxicities, and non-hematological toxicities. No deaths related to drugs have been reported.

TABLE 4 | Efficacy endpoints.

Endpoints	Two treatment regimens	Gemcitabine+Docetaxel	Gemcitabine+Anlotinib	*p*-Value
No. of patients	122	81	41	
Median PFS (95% CI), months	6.3 (6.0–8.4)	5.8 (6.0–8.4)	6.8 (6.2–9.2)	0.39
Median OS (95% CI), months	14.3 (14.1–17.4)	14.7 (13.9–17.9)	13.3 (12.8–18.0)	0.75
Best response, *n* (%)				
Complete response	1 (0.8%)	1 (1.2%)	0	NA
Partial response	15 (12.3%)	14 (17.3%)	6 (14.6%)	0.47
Stable disease	62 (50.8%)	39 (48.1%)	23 (56.1%)	0.22
Progressive disease	39 (32%)	27 (33.3%)	12 (29.3%)	0.43
Objective response rate	21 (17.2%)	15 (18.5%)	6 (14.6%)	0.17
Disease control rate	83 (68%)	54 (66.7%)	29 (70.7%)	0.58

95% CI, 95% confidence interval; PFS, progression-free survival; OS, overall survival.

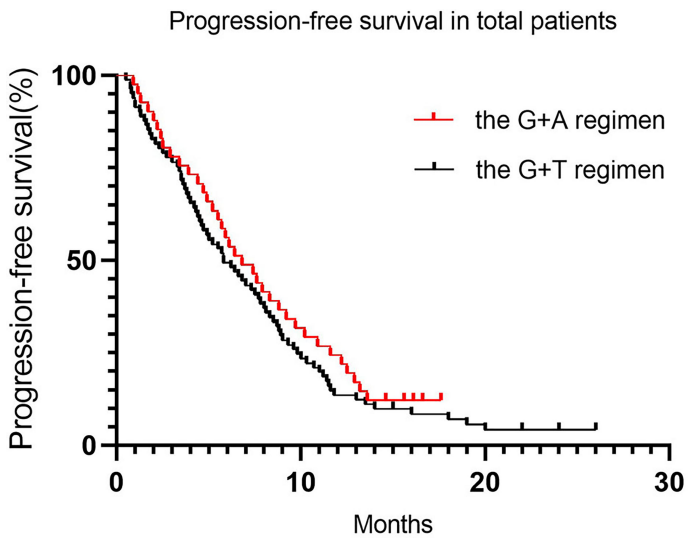

FIGURE 1 | Progression-free survival in total patients.

DISCUSSION

In this retrospective study, we collected and compared the efficacy and toxicity of G+D and G+A in patients with advanced STS; 122 patients (81 patients receiving G+D and 41 receiving G+A) were included. Patients' characteristics of the two groups were observed to be well balanced at baseline. G+D and G+A showed similar clinical efficacy (ORR: 15% and 14%, median PFS: 6.0 and 7.0 months, and median OS: 9.8 and 11.2 months, respectively), whereas G+A had a lower proportion of patients who experienced grade ≥3 AEs compared to G+D. These results suggest that G+A may be a novel treatment candidate for advanced STS, with similar efficacy to G+D but less toxicity.

The chemotherapy options for advanced STS are limited. The standard chemotherapy regimen is doxorubicin and/or ifosfamide. In recent decades, several exploratory studies (26–28) have shown that doxorubicin combined with other antineoplastic agents, in particular with the alkylating agent, may increase response rates or/and median PFS with increased AEs but fail to improve OS; although olaratumab (a PDGFR inhibitor) plus doxorubicin had a greater median OS than doxorubicin alone in advanced STS in the Phase IB/II study (29) (26.5 months vs. 14.7 months). Regrettably, the subsequent Phase III study including more similar patients did not provide an OS benefit (30) (20.4 months vs. 19.7 months). Since Hensley and colleagues (14) reported a response rate of 55% and a median

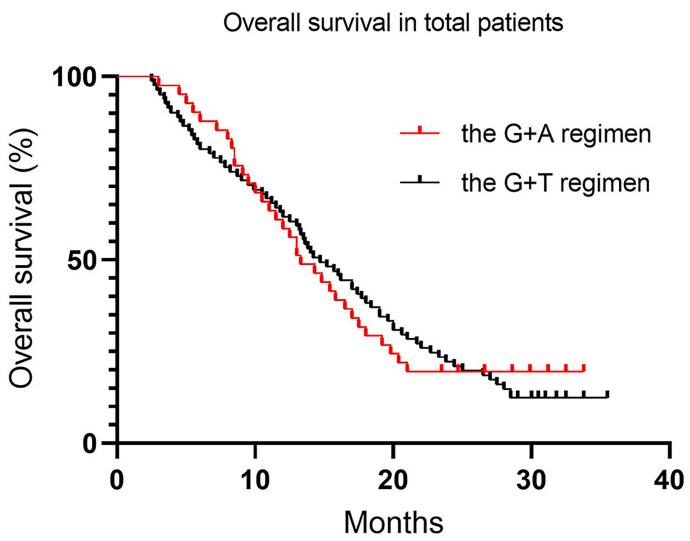

FIGURE 2 | Overall survival in total patients.

TABLE 5 | Efficacy of patients with leiomyosarcoma and treated as first-line treatment.

PFS and OS	G+D (Median, 95% CI) (months)	G+A (Median, 95% CI) (months)	*p*-Value
Leiomyosarcoma PFS	6.5 (5.4–7.7)	7.5 (6.2–10.6)	0.08
Leiomyosarcoma OS	17.2 (14.4–20.1)	16.2 (12.1–20.7)	0.76
First-line PFS	6.2 (5.3–8.2)	7.1 (5.9–9.9)	0.51
First-line OS	15.7 (12.7–18.5)	13.6 (10.5–17.9)	0.62

95% CI, 95% confidence interval; PFS, progression-free survival; OS, overall survival; G, gemcitabine; D, docetaxel.

PFS of 6.5 months in advanced LMS (uterus and others), the patients were given G 900 mg/m^2 on days 1 and 8 and D 100 mg/m^2 on day 8 for a 21-day cycle. G+D has been widely used in advanced LMS and STS with promising efficacy. In the first-line treatment setting, the GeDDiS study (31) showed that G+D (G 675 mg/m^2 on days 1 and 8 and D 75 mg/m^2 on day 8 every 3 weeks) achieved similar antitumor activity to doxorubicin (doxorubicin 75 mg/m^2 on day 1 every 3 weeks) in patients with unselected subtypes of STS, with a median PFS of 23.7 weeks and 23.3 weeks, and an ORR of 19% and 20%, respectively. However, G+D had higher costs, was more difficult to deliver, required more frequent and longer hospital visits, and caused more non-hematological toxicities than doxorubicin. With the failure of an anthracycline-based regimen setting, several studies compared the efficacy and toxicity of G+D versus G monotherapy in advanced sarcomas. In 2012, the TAXOGEM study (16) showed that G alone (G 1,000 mg/m^2 on days 1, 8, and 15 every 4 weeks) and G+D (G 900 mg/m^2 on days 1 and 8 and D 100 mg/m^2 on day 8 every 3 weeks) yielded an ORR of 19% and 24% in patients with uterine LMS, with a median PFS of 5.5 and 4.7 months, and an ORR of 14% and 5% in patients with non-uterine LMS, with a median PFS of 6.3 and 3.8 months, respectively. Meanwhile, a Phase II study (32) published by Maki showed that G+D yielded greater median PFS and OS than G alone in metastatic STS, but increased toxicity. These results suggest that both G monotherapy and G+D may be an option for advanced STS.

Our study showed that either the median PFS of 5.8 months for G+D or the median PFS of 6.5 months for G+A may be higher than those reported by Neeta Somaiah (33), but consistent with several previous reports including the GeDDis study (31), the LMS03 study (34), and Hensley's study (14). The different clinical outcomes may be due to differences in the initial dose, dose intensity and infusion rate of drugs, as well as patients' characteristics at baseline. In a randomized Phase II trial reported by Neeta Somaiah in 2021 including 90 patients with advanced STS who were randomized, 1:1 received either gemcitabine plus pazopanib (G+P) or gemcitabine plus docetaxel (G+D). Both G+D and G+P showed a median PFS of 4.1 months with similar toxicity. There may be many reasons why Neeta Somaiah's research differed from ours. Firstly, a larger proportion of advanced LMS patients were included in the present study (47.5% vs. 31%) than in Somaiah's study. Several studies (35, 36) have shown that LMS may be superior to non-LMS in chemotherapy sensitivity, with a greater response rate, and median PFS and OS. However, the results of the subgroup analysis of our study reveal that no significant differences were observed in ORR and median PFS between LMS and other subtypes. It should be noted that a large proportion of histopathological subtypes (LMS for 47.5%, UPS for 13.9%,

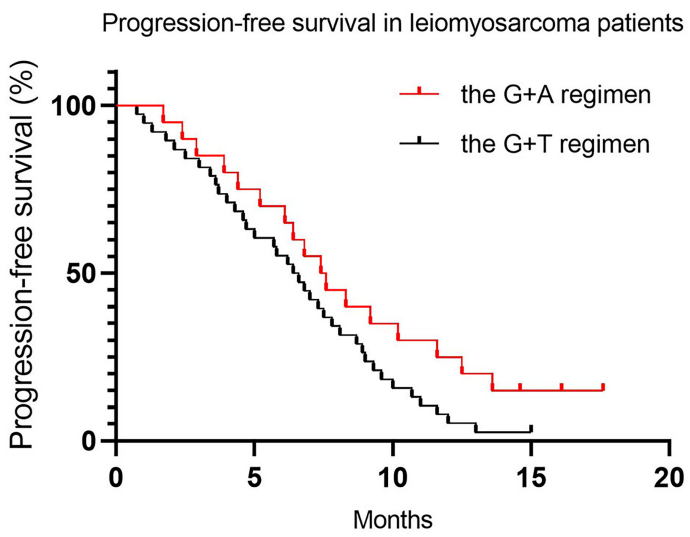

FIGURE 3 | Progression-free survival in leiomyosarcoma patients.

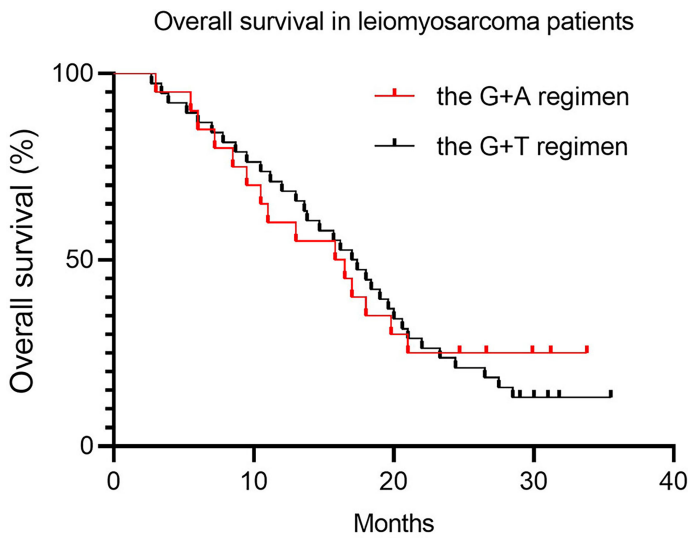

FIGURE 4 | Overall survival in leiomyosarcoma patients.

and LPS for 13.1%) may be considered to be chemosensitive to gemcitabine-based regimen in this study. Secondly, patients in our study experienced fewer dose reductions than Neeta Somaiah 's study (24% vs. 58%) due to toxicity. In Neeta Somaiah's study, 58% of patients in the G+D group underwent dose reduction and 80% of patients underwent dose reduction in the G+P group, while in our study, 30% of patients in the G+D group had dose reduction and 20% of patients in the G+A group underwent dose reduction, which may have an impact on efficacy. It is worth noting that only 20% of patients in the G +A group underwent dose reduction, significantly less than previously reported, which may be related to the fact that anlotinib avoided overlap with gemcitabine in this study and that there is little toxicity from anlotinib itself. According to the toxicities of targeted agents reported in previous studies (10, 37), the rate of grade ≥3 adverse reactions of anlotinib was significantly lower than that of pazopanib. Thirdly, there is a higher proportion of patients receiving the regimens as the first-line therapy (46.7% vs. 18%) in our study compared to Neeta Somaiah 's study. The high proportion of patients in this study is due to aggressive neoadjuvant chemotherapy based on anthracyclines in China. When the tumor recurred more than a year later, they were treated with G+D or G+A as first-line therapy. The efficacy of the present study is similar to that of the GeDDis study, with an ORR of 20% and a median PFS of 23.7 weeks.

Overall, the two treatment regimens were well tolerated, and the majority of AEs were consistent with previous studies and no

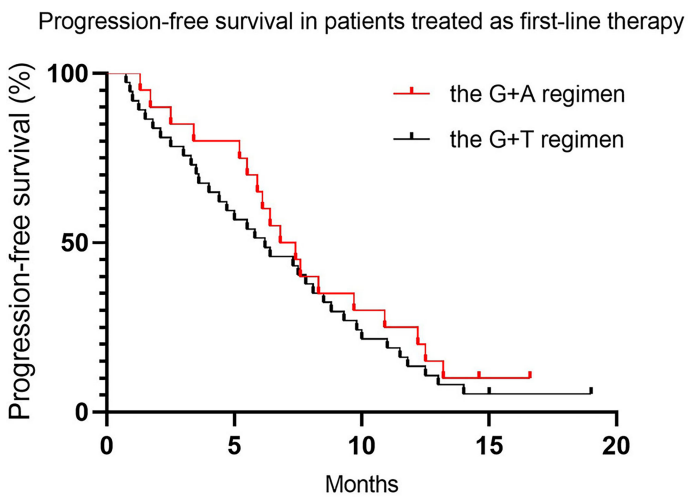

FIGURE 5 | Progression-free survival in patients treated as first-line therapy.

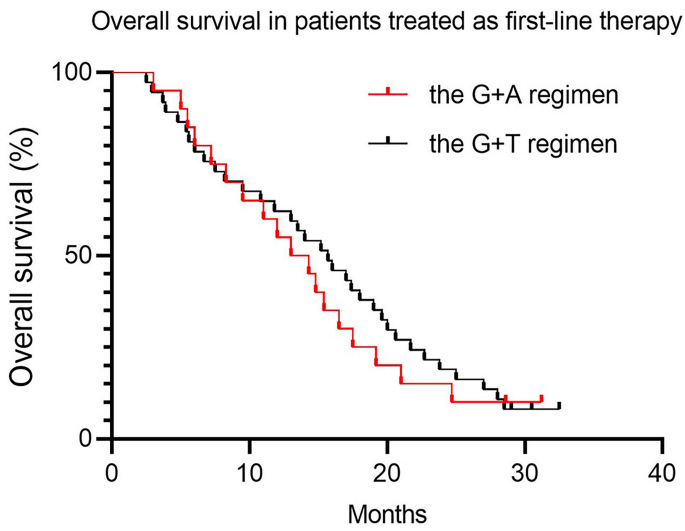

FIGURE 6 | Overall survival in patients treated as first-line therapy.

new AEs were observed. The common grade 3/4 AEs of G+D were neutropenia, thrombocytopenia, anemia, and febrile neutropenia, and the common grade 3/4 AEs of G+A were neutropenia, thrombocytopenia, transaminase elevation, and hypertension. Edema was mainly related to docetaxel, and fatigue and muscle soreness may be caused by long-term use of G+D, while pneumothorax and hypertension were mainly related to anlotinib. The proportion of patients with grade ≥3 AEs was higher in the G+D group than in the G+P group, and the major differential AEs were hematological AEs. Although there is no comparable study of docetaxel versus anlotinib in advanced STS, the rate of grade ≥3 hematological toxicity related to anlotinib reported by Chi (37) was lower than that related to docetaxel reported by van Hoesel (38) (0% vs. 89%). Thirty percent of patients in the G+D group needed at least one dose reduction due to adverse reactions, while only 20% did in the G +A group.

Palliative systemic treatment of advanced STS aims to reduce the tumor burden, thereby reducing symptoms and improving quality of life. To avoid primary resistance and acquired resistance to the tumor, as well as prolong the time of systemic therapy control, aggressive systemic therapy without significantly increased toxicity has become a treatment option. In this study, we explored the clinical efficacy and safety of G+A as a novel therapy for advanced STS, and the results show that G +A achieved similar efficacy to G+D with less toxicity, suggesting that G+A could be used as an alternative to G+D, and the therapy might be suitable for patients with poor physical quality

TABLE 6 | Toxicity.

Grade 3/4 adverse events (*n* = 122)	Patients, *n* (%)		*p*-Value
	Gemcitabine+Docetaxel (*n* = 81)	Gemcitabine+Anlotinib (*n* = 41)	
ALL	55 (68)	18 (44)	<0.01
Hematological AEs	45 (56)	14 (34)	0.03
Neutropenia	39 (48)	14 (34)	0.14
Febrile neutropenia	15 (19)	3 (7)	0.10
Anemia	20 (25)	5 (12)	0.10
Thrombocytopenia	28 (35)	14 (34)	0.96
Non-hematological AEs	30 (37)	13 (32)	0.32
Fatigue and muscle soreness	7 (9)	2 (5)	0.72
Diarrhea	5 (6)	2 (5)	1
Stomatitis	2 (2)	1 (2)	1
Vomiting	5 (6)	2 (5)	1
Transaminase elevation	12 (15)	7 (17)	0.75
Elevated bilirubin	2 (2)	4 (10)	0.19
Pneumothorax	1 (1)	3 (7)	0.21
Hypertension	4 (5)	6 (15)	0.14
Edema	4 (5)	0	NA
Thromboembolic	2 (2)	1 (2)	1

and intolerance to G+D or even the standard treatment. Both gemcitabine plus anti-tumor drugs and gemcitabine plus docetaxel combined with other anti-tumor drugs have been explored in advanced STS. Although few positive results have been reported in terms of efficacy, the results of some studies provide a reference for future studies. The LMS03 study (34) assessed the efficacy and safety of G plus pazopanib followed by pazopanib (G 1,000 mg/m^2 on days 1 and 8 and pazopanib 800 mg daily of each for 21 days, for no more than 8 cycles, followed by pazopanib) as the second-line treatment in advanced LMS; although the PFS rate at 9 months (PFR 9m) of 32% with a median PFS of 6.5 months failed to meet the target of 44%, a PFR 9m of 34.6% and a median PFS of 7.1 months in the per-protocol population were promising. The PAPAGEMO study (39) examined the efficacy of pazopanib plus G (pazopanib 800 mg once daily and G 1,000 mg/m^2 on days 1 and 8 every 3 weeks) and G (G 1,000 mg/m^2 on days 1 and 8 every 3 weeks) in advanced STS patients who failed with anthracycline and/or ifosfamide. The results show that compared with pazopanib alone, G+D significantly increased PFSR at 12 weeks (74% vs. 47%), with prolonged median PFS (5.6 months vs. 2.0 months), respectively. Interestingly, in a Phase III study (40), including 90 LMS patients, which evaluated the efficacy of G+D with or without bevacizumab as a first-line treatment for metastatic uterine LMS, the ORR was 31.5% and median PFS was 6.2 months in the G+D group, while the addition of bevacizumab to G+D did not improve the efficacy with an ORR of 35.8% and a median PFS of 4.2 months. These data suggest that although some antiangiogenic agents, particularly bevacizumab, may achieve a moderate antitumor activity in advanced STS, these agents may not be suitable for combination with chemotherapy.

The limitations of this study include the following: First, due to the retrospective and non-randomized nature of this study, documented toxicity may be incomplete. However, grade ≥3 AEs would be evaluated carefully and thoroughly, as such observations may contribute to clinical decision-making. Second, anlotinib is considered to inhibit the proliferation of pericytes and result in impaired tumor angiogenesis mainly through an EGFR2 signaling pathway. EGFR2 expression of the tumor and the relationship between EGFR2 and prognosis were not identified in this study. Third, due to the low number of non-LMS sarcomas, it was impossible to conduct a meaningful comparative analysis of the specific subtypes between the two groups.

CONCLUSION

In summary, our study shows that the G+A regimen obtains modest ORR, and median PFS and OS, similar to the G+D regimen, but less toxic. The prognosis of advanced STS remains poor, new therapeutic strategies need to be explored, and this study may serve as a benchmark for such trials in the future.

DATA AVAILABILITY STATEMENT

The original contributions presented in the study are included in the article/supplementary material. Further inquiries can be directed to the corresponding author.

ETHICS STATEMENT

The studies involving human participants were reviewed and approved by Henan Cancer Hospital. The patients/participants provided their written informed consent to participate in this study.

AUTHOR CONTRIBUTIONS

All authors listed have made a substantial, direct, and intellectual contribution to the work, and approved it for publication.

ACKNOWLEDGMENTS

The authors thank the patients for agreeing to publish this study and Dr. Ruina Zhao in Henan Cancer Hospital for her help in data collection.

REFERENCES

1. Gamboa AC, Gronchi A, Cardona K. Soft-Tissue Sarcoma in Adults: An Update on the Current State of Histiotype-Specific Management in an Era of Personalized Medicine. *CA Cancer J Clin* (2020) 70:200–29. doi: 10.3322/caac.21605
2. Liu Z, Yao W, Zhao Y, Liu O, Zhang P, Ge H. Efficacy and Safety of Anlotinib Combined With Liposomal Doxorubicin Followed by Anlotinib Maintenance in Metastatic Soft Tissue Sarcomas. *Cancer Manage Res* (2021) 13:1009–16. doi: 10.2147/CMAR.S286322
3. Liu Z, Liu C, Yao W, Gao S, Wang J, Zhang P, et al. Efficacy and Safety of Toripalimab Combined With Doxorubicin as First-Line Treatment for Metastatic Soft Tissue Sarcomas: An Observational Study. *Anticancer Drugs* (2021) 32:962–8. doi: 10.1097/CAD.0000000000001088
4. Gundle KR, Kafchinski L, Gupta S, Griffin AM, Dickson BC, Chung PW, et al. Analysis of Margin Classification Systems for Assessing the Risk of Local Recurrence After Soft Tissu E Sarcoma Resection. *J Clin Oncol* (2018) 36:704–9. doi: 10.1200/JCO.2017.74.6941
5. Frezza AM, Stacchiotti S, Gronchi A. Systemic Treatment in Advanced Soft Tissue Sarcoma: What Is Standard, What is New. *BMC Med* (2017) 15:109. doi: 10.1186/s12916-017-0872-y
6. Nakano K, Takahashi S. Precision Medicine in Soft Tissue Sarcoma Treatment. *Cancers* (2020) 12:221. doi: 10.3390/cancers12010221
7. Anjos Ferreira AL, Russell RM, Rocha N, Placido Ladeira MS, Favero Salvadori DM, Oliveira Nascimento MC, et al. Effect of Lycopene on Doxorubicin-Induced Cardiotoxicity: An Echocardiographic, Histological and Morp Hometrical Assessment. *Basic Clin Pharmacol Toxicol* (2007) 101:16–24. doi: 10.1111/j.1742-7843.2007.00070.x

8. Stacchiotti S, Van Tine BA. Synovial Sarcoma: Current Concepts and Future Perspectives. *J Clin Oncol* (2018) 36:180–7. doi: 10.1200/JCO.2017.75.1941
9. Demetri GD, Schöffski P, Grignani G, Blay JY, Maki RG, Van Tine BA, et al. Activity of Eribulin in Patients With Advanced Liposarcoma Demonstrated in a Subgroup Analysis From a Randomized Phase III Study of Eribulin Versus Dacarbazine. *J Clin Oncol* (2017) 35:3433–9. doi: 10.1200/JCO.2016.71.6605
10. van der Graaf WT, Blay JY, Chawla SP, Kim DW, Bui-Nguyen B, Casali PG, et al. Pazopanib for Metastatic Soft-Tissue Sarcoma (PALETTE): A Randomised, Double-Blind, Placebo-Controlle D Phase 3 Trial. *Lancet* (2012) 379:1879–86. doi: 10.1016/S0140-6736(12)60651-5
11. Brodowicz T, Mir O, Wallet J, Italiano A, Blay JY, Bertucci F, et al. Efficacy and Safety of Regorafenib Compared to Placebo and to Post-Cross-Over Regorafenib in Advanced Non-Adipocytic Soft Tissue Sarcoma. *Eur J Cancer* (2018) 99:28–36. doi: 10.1016/j.ejca.2018.05.008
12. Chi Y, Yao Y, Wang S, Huang G, Cai Q, Shang G, et al. Anlotinib for Metastasis Soft Tissue Sarcoma: A Randomized, Double-Blind, Placebo-Controlled and Multi-Centered Clinical Trial. *J Clin Oncol* (2018) 36:11503–3. doi: 10.1200/JCO.2018.36.15_suppl.11503
13. Nagano T, Yamada Y, Ikeda T, Kanki H, Kamo T, Nishigori C. Docetaxel: A Therapeutic Option in the Treatment of Cutaneous Angiosarcoma: Report of 9 Patients. *Cancer* (2007) 110:648–51. doi: 10.1002/cncr.22822
14. Hensley ML, Maki R, Venkatraman E, Geller G, Lovegren M, Aghajanian C, et al. Gemcitabine and Docetaxel in Patients With Unresectable Leiomyosarcoma: Results of a Phase II Trial. *J Clin Oncol* (2002) 20:2824–31. doi: 10.1200/JCO.2002.11.050
15. Leu KM, Ostruszka LJ, Shewach D, Zalupski M, Sondak V, Biermann JS, et al. Laboratory and Clinical Evidence of Synergistic Cytotoxicity of Sequential Treatment With Gemcitabine Followed by Docetaxel in the Treatment of Sarcoma. *J Clin Oncol* (2004) 22:1706–12. doi: 10.1200/JCO.2004.08.043
16. Pautier P, Floquet A, Penel N, Piperno-Neumann S, Isambert N, Rey A, et al. Randomized Multicenter and Stratified Phase II Study of Gemcitabine Alone Versus Gemcitabine and Doce Taxel in Patients With Metastatic or Relapsed Leiomyosarcomas: A Federation Nationale Des Centres De Lutte Contre Le Cancer (FNCLCC) French Sarcoma Group Study (TAXOGEM Study). *Oncologist* (2012) 17:1213–20. doi: 10.1634/theoncologist.2011-0467
17. Ren W, Korchin B, Lahat G, Wei C, Bolshakov S, Nguyen T, et al. Combined Vascular Endothelial Growth Factor Receptor/Epidermal Growth Factor Receptor Blockade With Chemotherapy for Treatment of Local, Uterine, and Metastatic Soft Tissue Sarcoma. *Clin Cancer Res An Off J Am Assoc Cancer Res* (2008) 14:5466–75. doi: 10.1158/1078-0432.CCR-08-0562
18. Tang J, Li XY, Liang JB, Peng L, Li X. Apatinib Plus Chemotherapy Shows Clinical Activity in Advanced NSCLC: A Retrospective Study. *Oncol Res* (2019) 27:635–41. doi: 10.3727/096504018X15288447760357
19. Shi J, Zhang Y, Wang J, Li J, Li Z. Anlotinib Combined With Chemoradiotherapy Exhibits Significant Therapeutic Efficacy in Esophageal Squamous Cell Carcinoma. *Front Oncol* (2020) 10:995. doi: 10.3389/fonc.2020.00995
20. Pignata S, Lorusso D, Scambia G, Sambataro D, Tamberi S, Cinieri S, et al. Pazopanib Plus Weekly Paclitaxel Versus Weekly Paclitaxel Alone for Platinum-Resistant or Platinum-Refractory Advanced Ovarian Cancer (MITO 11): A Randomised, Open-Label, Phase 2 Trial. *Lancet Oncol* (2015) 16:561–8. doi: 10.1016/S1470-2045(15)70115-4
21. Gao Q, Jiang Y, Li X, Chen H, Tang S, Chen H, et al. Intratumoral Injection of Anlotinib Hydrogel Combined With Radiotherapy Reduces Hypoxia in Lewis Lung Carcinoma Xenografts: Assessment by Micro Fluorine-18-Fluoromisonidazole Positron Emission Tomograp Hy/Computed Tomography Hypoxia Imaging. *Front Oncol* (2021) 11:628895. doi: 10.3389/fonc.2021.628895
22. Li S. Anlotinib: A Novel Targeted Drug for Bone and Soft Tissue Sarcoma. *Front Oncol* (2021) 11:664853. doi: 10.3389/fonc.2021.664853
23. Xie C, Wan X, Quan H, Zheng M, Fu L, Li Y, et al. Preclinical Characterization of Anlotinib, a Highly Potent and Selective Vascular Endothelial Growth Factor Receptor-2 Inhibitor. *Cancer Sci* (2018) 109:1207–19. doi: 10.1111/cas.13536
24. Lin B, Song X, Yang D, Bai D, Yao Y, Lu N. Anlotinib Inhibits Angiogenesis *via* Suppressing the Activation of VEGFR2, PDGFR¦Â and FGFR1. *Gene* (2018) 654:77–86. doi: 10.1016/j.gene.2018.02.026
25. Wang HY, Chu JF, Zhang P, Wang JQ, Yan Z, Yao SN, et al. Safety and Efficacy of Chemotherapy Combined With Anlotinib Plus Anlotinib Maintenance in Chinese Pat Ients With Advanced/Metastatic Soft Tissue Sarcoma. *Onco Targets Ther* (2020) 13:1561–8. doi: 10.2147/OTT.S235349
26. Tap WD, Papai Z, Van Tine BA, Attia S, Ganjoo KN, Jones RL, et al. Doxorubicin Plus Evofosfamide Versus Doxorubicin Alone in Locally Advanced, Unresectable or Metastati C Soft-Tissue Sarcoma (TH CR-406/SARC021): An International, Multicentre, Open-Label, Randomised Phase 3 Trial. *Lancet Oncol* (2017) 18:1089–103. doi: 10.1016/S1470-2045(17)30381-9
27. Ryan CW, Merimsky O, Agulnik M, Blay JY, Schuetze SM, Van Tine BA, et al. PICASSO III: A Phase III, Placebo-Controlled Study of Doxorubicin With or Without Palifosfamide in Pa Tients With Metastatic Soft Tissue Sarcoma. *J Clin Oncol* (2016) 34:3898–905. doi: 10.1200/JCO.2016.67.6684
28. Judson I, Verweij J, Gelderblom H, Hartmann JT, Sch?ffski P, Blay JY, et al. Doxorubicin Alone Versus Intensified Doxorubicin Plus Ifosfamide for First-Line Treatment of Advanced or Metastatic Soft-Tissue Sarcoma: A Randomised Controlled Phase 3 Trial. *Lancet Oncol* (2014) 15:415–23. doi: 10.1016/S1470-2045(14)70063-4
29. Tap WD, Jones RL, Van Tine BA, Chmielowski B, Elias AD, Adkins D, et al. Olaratumab and Doxorubicin Versus Doxorubicin Alone for Treatment of Soft-Tissue Sarcoma: An Open-Lab El Phase 1b and Randomised Phase 2 Trial. *Lancet* (2016) 388:488–97. doi: 10.1016/S0140-6736(16)30587-6
30. Tap WD, Wagner AJ, Sch?ffski P, Martin-Broto J, Krarup-Hansen A, Ganjoo KN, et al. Effect of Doxorubicin Plus Olaratumab vs Doxorubicin Plus Placebo on Survival in Patients With Advanc Ed Soft Tissue Sarcomas: The ANNOUNCE Randomized Clinical Trial. *Jama* (2020) 323:1266–76. doi: 10.1001/jama.2020.1707
31. Seddon B, Strauss SJ, Whelan J, Leahy M, Woll PJ, Cowie F, et al. Gemcitabine and Docetaxel Versus Doxorubicin as First-Line Treatment in Previously Untreated Advanced Unresectable or Metastatic Soft-Tissue Sarcomas (GeDDiS): A Randomised Controlled Phase 3 Trial. *Lancet Oncol* (2017) 18:1397–410. doi: 10.1016/S1470-2045(17)30622-8
32. Maki RG, Wathen JK, Patel SR, Priebat DA, Okuno SH, Samuels B, et al. Randomized Phase II Study of Gemcitabine and Docetaxel Compared With Gemcitabine Alone in Patients With Metastatic Soft Tissue Sarcomas: Results of Sarcoma Alliance for Research Through Collaborations Tudy 002 [Corrected]. *J Clin Oncol* (2007) 25:2755–63. doi: 10.1200/JCO.2006.10.4117
33. Somaiah N, Van Tine BA, Wahlquist AE, Milhem MM, Hill EG, Garrett-Mayer E, et al. A Randomized, Open-Label, Phase 2, Multicenter Trial of Gemcitabine With Pazopanib or Gemcitabine Wit H Docetaxel in Patients With Advanced Soft-Tissue Sarcoma. *Cancer* (2021) 127:894–904. doi: 10.1002/cncr.33216
34. Pautier P, Penel N, Ray-Coquard I, Italiano A, Bompas E, Delcambre C, et al. A Phase II of Gemcitabine Combined With Pazopanib Followed by Pazopanib Maintenance, as Second-Line T Reatment in Patients With Advanced Leiomyosarcomas: A Unicancer French Sarcoma Group Study (LMS03 Study). *Eur J Cancer* (2020) 125:31–7. doi: 10.1016/j.ejca.2019.10.028
35. Bay JO, Ray-Coquard I, Fayette J, Leyvraz S, Cherix S, Piperno-Neumann S, et al. Docetaxel and Gemcitabine Combination in 133 Advanced Soft-Tissue Sarcomas: A Retrospective Analysis. *Int J Cancer* (2006) 119:706–11. doi: 10.1002/ijc.21867
36. Patel SR, Gandhi V, Jenkins J, Papadopolous N, Burgess MA, Plager C, et al. Phase II Clinical Investigation of Gemcitabine in Advanced Soft Tissue Sarcomas and Window Evaluation of Dose Rate on Gemcitabine Triphosphate Accumulation. *J Clin Oncol* (2001) 19:3483–9. doi: 10.1200/JCO.2001.19.15.3483
37. Chi Y, Fang Z, Hong X, Yao Y, Sun P, Wang G, et al. Safety and Efficacy of Anlotinib, a Multikinase Angiogenesis Inhibitor, in Patients With Refractory Metastatic Soft-Tissue Sarcoma. *Clin Cancer Res An Off J Am Assoc Cancer Res* (2018) 24:5233–8. doi: 10.1158/1078-0432.CCR-17-3766
38. van Hoesel QG, Verweij J, Catimel G, Clavel M, Kerbrat P, van Oosterom AT, et al. Phase II Study With Docetaxel (Taxotere) in Advanced Soft Tissue Sarcomas of the Adult. EORTC Soft Tissue and Bone Sarcoma Group. *Ann Oncol* (1994) 5:539–42. doi: 10.1093/oxfordjournals.annonc.a058909
39. Schmoll HJ, Lindner LH, Reichardt P, Hei?ner K, Kopp HG, Kessler T, et al. Efficacy of Pazopanib With or Without Gemcitabine in Patients With

Anthracycline- and/or Ifosfamide-R Efractory Soft Tissue Sarcoma: Final Results of the PAPAGEMO Phase 2 Randomized Clinical Trial. *JAMA Oncol* (2021) 7:255–62. doi: 10.1001/jamaoncol.2020.6564

40. Hensley ML, Miller A, O'Malley DM, Mannel RS, Behbakht K, Bakkum-Gamez JN, et al. Randomized Phase III Trial of Gemcitabine Plus Docetaxel Plus Bevacizumab or Placebo as First-Line Tr Eatment for Metastatic Uterine Leiomyosarcoma: An NRG Oncology/Gynecologic Oncology Group Study. *J Clin Oncol* (2015) 33:1180–5. doi: 10.1200/JCO.2014.58.3781

Conflict of Interest: The authors declare that the research was conducted in the absence of any commercial or financial relationships that could be construed as a potential conflict of interest.

Publisher's Note: All claims expressed in this article are solely those of the authors and do not necessarily represent those of their affiliated organizations, or those of the publisher, the editors and the reviewers. Any product that may be evaluated in this article, or claim that may be made by its manufacturer, is not guaranteed or endorsed by the publisher.

frontiers | Frontiers in Oncology

TYPE Original Research
PUBLISHED 26 July 2022
DOI 10.3389/fonc.2022.898586

OPEN ACCESS

EDITED BY
Yunkai Zhang,
Vanderbilt University Medical Center,
United States

REVIEWED BY
Francesco Facchinetti,
Gustave Roussy Cancer
Campus, France
Nagla Abdel Karim,
Augusta University, United States

*CORRESPONDENCE
Junhui Wang
wangjunhui7526@163.com

SPECIALTY SECTION
This article was submitted to
Cancer Molecular Targets
and Therapeutics,
a section of the journal
Frontiers in Oncology

RECEIVED 17 March 2022
ACCEPTED 01 July 2022
PUBLISHED 26 July 2022

CITATION
Chen J, Wu X and Wang J (2022)
Double-dose icotinib may induce the
emergence of the EGFR exon 20
T790M mutation in non-small cell
lung cancer patients harboring EGFR-
sensitive mutation.
Front. Oncol. 12:898586.
doi: 10.3389/fonc.2022.898586

Double-dose icotinib may induce the emergence of the EGFR exon 20 T790M mutation in non-small cell lung cancer patients harboring EGFR-sensitive mutation

Jianxin Chen, Xilin Wu and Junhui Wang*

Department of Medical Oncology, The Quzhou Affiliated Hospital of Wenzhou Medical University, Quzhou People's Hospital, Quzhou, China

Background: Acquired resistance to epidermal growth factor receptor tyrosine kinase inhibitors (EGFR-TKIs) inevitably occurs in non-small cell lung cancer (NSCLC) patients harboring EGFR-sensitive mutations. There are approximately half of the patients who developed resistance to EGFR-TKIs treatment, the mechanism of which remains undiscovered. We occasionally found that double-dose icotinib as further-line salvage treatment may induce the emerging mutation of EGFR exon 20 T790M in NSCLC patients. The present study, therefore, was conducted to explore the probability of the emerging T790M mutation after exposure to double-dose icotinib in metastatic NSCLC patients.

Patients and Methods: Metastatic NSCLC patients who received double-dose icotinib as salvage treatment after progression on first-generation TKIs and systematic chemotherapy were screened. Thereafter, patients who received a repeated next-generation sequencing (NGS) test with tumor sample were further enrolled. The procedure of NGS was performed with the standard criteria. Finally, the clinical characteristics, treatment procedures, and outcomes of eligible patients were reviewed and presented.

Results: Three patients have been detected with the emerging T790M mutation after double-dose icotinib exposure, with a mutation frequency of 19.6%, 8.2%, and 87.5%. During the treatment of targetable TKIs including almonertinib or osimertinib, partial response was observed in two patients, and stable disease was observed in the other. The progression-free survival by targetable TKIs for the patients was 3.7+ months (still in extension), 4.9+ months (still in extension), and 6.3 months. Manageable adverse events were observed during the treatment of TKIs.

Conclusion: The results of the present study revealed that the emerging EGFR exon 20 T790M mutation might be induced by double-dose icotinib exposure in further-line treatment. Patients with the emerging T790M mutation responded well to the treatment of targetable TKIs including almonertinib or osimertinib.

KEYWORDS

icotinib, double dose, T790M mutation, lung cancer, epidermal growth factor receptor

Introduction

Epidermal growth factor receptor tyrosine kinase inhibitors (EGFR-TKIs) are the recommended treatment strategy in patients with non-small cell lung cancer (NSCLC) harboring EGFR-sensitive mutations, especially with common mutations including exon 19 deletion and exon 21 L858R mutation (1–4). However, acquired resistance to EGFR-TKIs inevitably occurs after 10 to 14 months of exposure. The most common mechanism of acquired resistance was the EGFR p.Thr790Met point mutation (T790M), which accounts for 40% to 50% (5, 6). Among patients with the acquired EGFR T790M mutation, osimertinib, an irreversible EGFR-TKI selective for both EGFR-sensitive mutations and T790M resistance mutations, has emerged as a standard treatment choice, with an objective response rate (ORR) of 61% and a progression-free survival (PFS) time of 12.3 months (7, 8). However, there are still approximately 50% of patients who developed resistance to EGFR-TKIs treatment, the mechanism of which remains unknown (9). Although systematic therapy with cytotoxic agents has been suggested as standard therapy for those patients without the T790M mutation, confined efficacy accompanied with related adverse events significantly limited its application, especially for patients with poor performance status.

Icotinib, a highly specific and selective EGFR-TKI, has been approved for treatment of advanced or metastatic NSCLC patients harboring EGFR-sensitive mutations in China (10). Recently, a randomized phase II trial (INCREASE), conducted to evaluate the efficacy and safety of double-dose icotinib as front-line treatment in NSCLC patients harboring EGFR exon 21 L858R mutation, reported its positive results (11). The results of the study demonstrated tolerable toxicities, as well as better PFS [12.9 versus 9.2 months, HR, 0.75; 95% confidence interval (CI): 0.53–1.05, $p < 0.05$] of double-dose icotinib in NSCLC patients with the EGFR exon 21 L858R mutation when compared with routine dose (11). However in the INCREASE trial, the probability of the acquired T790M mutation, as well as the subsequent treatment strategies between double-dose and routine-dose icotinib, was not reported. In clinical practice, we occasionally found that double-dose icotinib as further-line salvage treatment may induce the emerging/increasing mutation of EGFR exon 20 T790M in NSCLC patients (12). To address the question, we therefore performed a retrospective study to explore the probability of the emerging T790M mutation after exposure to double-dose icotinib in previous T790M-negative NSCLC patients.

Materials and methods

Patients

Patients were eligible to enroll in the present retrospective study if they met the listed criteria: (1) patients diagnosed with metastatic NSCLC harboring EGFR-sensitive mutations (exon 19 deletion/exon 21 L858R mutation) between July 2018 and December 2021 in our institute; (2) after progression on first-line treatment with first-generation EGFR-TKIs (without the acquired T790M mutation/or T790M mutation by frequency less than 5%) and systematic chemotherapy, patients who received double-dose icotinib as salvage treatment were further selected; (3) in addition, patients who received a repeated NGS test with tumor sample after double-dose icotinib exposure were finally enrolled; and (4) efficacy and safety of the treatment with third-generation TKIs should be evaluated by RECIST 1.1 and NCI CTCAE 4.0. The clinical and molecular characteristics including sex, age, Eastern Cooperative Oncology Group performance status (ECOG PS), disease stage, smoking history, brain metastases, EGFR mutations, and concurring mutation were reviewed. EGFR mutation testing was performed using commercially available next-generation sequencing (NGS) analysis (BioMed Diagnostics, China). The NGS tests (before/after double-dose icotinib) were performed using tumor tissue obtained from same-site biopsy to reduce the incidence of false-negative results by plasma or tumor heterogeneity by tumor location. Available gene tests in the NGS panel adopted in the present study included anaplastic lymphoma kinase (ALK), V-Ki-ras2 Kirsten rat sarcoma viral oncogene homolog (KRAS), ROS proto-oncogene 1 (ROS1), neuroblastoma RAS viral

oncogene homolog (NRAS), V-raf murine sarcoma viral oncogene homologB1 (BRAF), RET proto-oncogene (RET), receptor tyrosine-protein kinase erbB-2 (ERBB2), RAC-alpha serine/threonine-protein kinase (AKT1), MNNG HOS transforming gene (MET), discoidin domain receptor tyrosine kinase 2 (DDR2), phosphatidylinosito-4,5-bisphosphate 3-kinase (PIK3CA), fibroblast growth factor receptor 1 (FGFR1), phosphatase and tensin homolog (PTEN), and mitogen-activated protein kinase 1 (MAP2K1). The present study was approved by the Ethical Committee of People's Hospital of Quzhou. All experiments in the present study were performed in accordance with international ethical guidelines.

Next-generation sequencing analysis

For NGS analysis, the library was performed based on the OncoAim™ cancer 15 gene panel (BioMed Diagnostics, Inc., Shanghai, China). DNA fragment shearing was developed with Covaris M220, followed by phosphorylation, and adaptor ligation. The quality of the fragments was evaluated with bio-analyzer high-sensitivity DNA assay. The indexed samples were sequenced on Hiseq500 sequencer (Illumina, Inc., USA) with paired reads of 150 bp length. Local alignment optimization, variant calling, and annotation were conducted with GATK 3.2, MuTect, and VarScan; Tophat 2 and Factera 1.4.3 were adopted for the DNA translocation analysis.

Results

Between July 2018 and December 2021, 162 patients with metastatic NSCLC harboring EGFR-sensitive mutations (exon 19 deletion/exon 21 L858R mutation) were screened with electronic medical record system. After first-line administration of EGFR TKIs and systematic chemotherapy (with or without antiangiogenic agents), there were 11 patients who received double-dose icotinib as salvage treatment without the EGFR exon 20 T790M mutation. However, there were only four patients who received repeated NGS analysis after progression on double-dose icotinib. Finally, three patients were detected with the emerging/increasing T790M mutation after double-dose icotinib exposure (Figures 1A, 2A, and 3A). Clinical and molecular characteristics including sex, age, ECOG PS, disease stage, smoking history, brain metastases, EGFR mutations, and concurring mutation are summarized in Table 1.

Among the three included patients, two patients (Patient 1 and Patient 2) received gefitinib as first-line treatment, and the other one (Patient 3) received routine-dose icotinib as first-line therapy. The progression-free survival (PFS) time of the first-line TKIs for the three patients were 14.3 months, 21.6 months, and 8.1 months. The acquired T790M mutation was not detected by repeated NGS analysis using tumor tissue in two patients (Patient 1 and Patient 2). The other patient (Patient 3) was detected with the T790M mutation with a low frequency of 4.0%. Thereafter, all patients received systematic chemotherapy (Patient 3 received osimertinib followed by chemotherapy) as subsequent treatment. After progression, a further NGS test using fresh tumor specimen by re-biopsy was developed in two patients (Patient 1 and Patient 2), the results of which failed to detect the EGFR exon 20 T790M mutation. As salvage treatment, all patients received double-dose icotinib administration. As a result, two patients (Patient 1 and Patient 2) were evaluated to have disease progression on double-dose icotinib treatment in the first examination (PFS: 2.7 months and 1.6 months, respectively). Disease progression in brain was discovered in all of the three patients (Figures 1C, 2C, and 3C). A repeated NGS analysis was conducted again, the results of which suggested the emerging/increasing T790M mutation in the three patients, with a frequency of 19.6%, 8.2%, and 87.5% (Figures 1B, 2B, and 3B), respectively. Based on that, third-generation TKIs, including almonertinib and osimertinib, were prescribed as further-line treatment. Consequently, partial response was observed in two patients (Patient 1 and Patient 2), and stable disease was observed in Patient 3 (Figures 1D, 2D, and 3D). The PFS time by third-generation TKIs for the patients was 3.7+ months (still in extension), 4.9+ months (still in extension), and 6.3 months by 30 November 2021. In addition, an adverse event, cerebral infarction, was observed in Patient 2. Procedures, efficacy, and safety assessment of treatment for the three patients are presented in Table 2. The pathologic diagnosis, emerging T790M mutations, and efficacy evaluation in brain for the three patients are presented in Figures 1–3, respectively. The treatment procedure of the patients is presented in Figure 4.

Discussion

In the current study, our results indicated that there were selected NSCLC patients without the acquired EGFR exon 20 T790M mutation, but who might be induced by double-dose icotinib exposure in further-line treatment. Patients with the emerging T790M mutation responded well to third-generation TKIs including almonertinib or osimertinib.

In recent years, osimertinib has been recommended as the preferred first-line EGFR TKIs in metastatic NSCLC patients with EGFR-sensitive mutations because of the positive results of the trial FLAURA (13). However, in clinical practice, there were still several questions to be addressed. Firstly, there was a slight statistical difference on OS benefits for Asian patients receiving osimertinib as first-line treatment compared to gefitinib according to subgroup analysis (HR, 1.0; 95% CI, 0.75–1.32) (13). In the further expanded research for the Chinese cohort, there was still no statistical difference observed (HR, 0.85; 95% CI, 0.56–1.29) (14). Secondly, after progression on first-generation TKIs, there were approximately 50% patients who

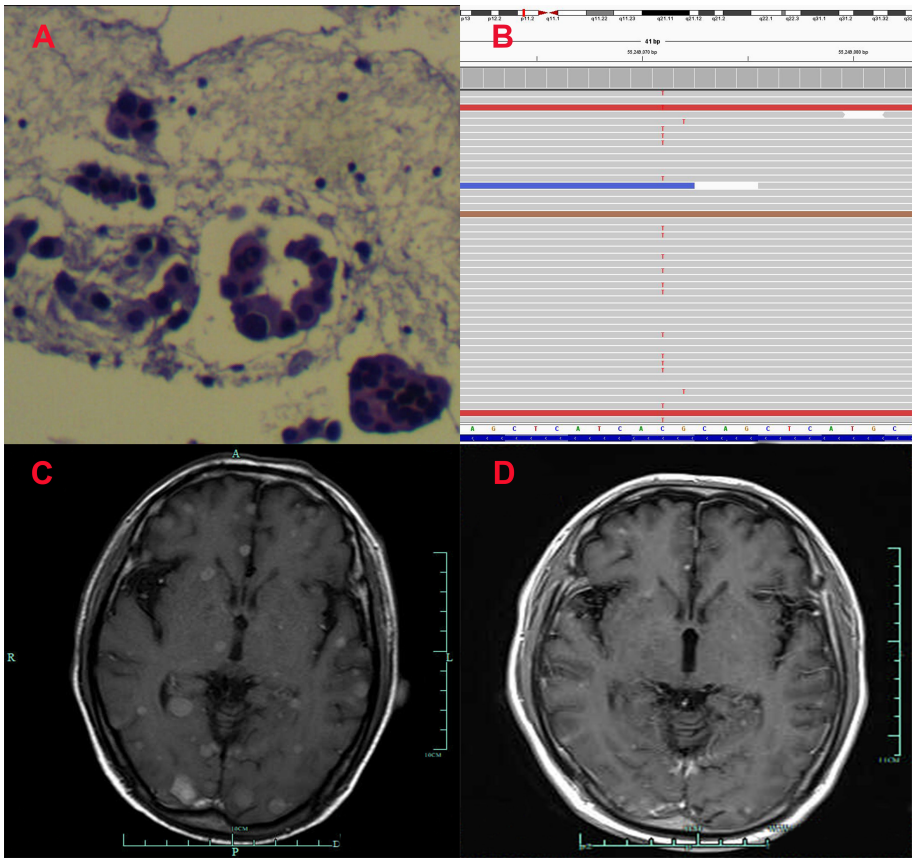

FIGURE 1
Pathological and clinical findings of Patient 1. **(A)** Pathological findings with HE staining. **(B)** NGS screenshots suggested emerging EGFR exon 20 T790M mutations. **(C)** Brain MRI image before salvage almonertinib treatment (after the emerging T790M mutation). **(D)** Brain MRI image after salvage almonertinib treatment.

may develop the acquired T790M mutation, who could obtain another opportunity to receive further-line osimertinib treatment, resulting in a PFS of 10.1 months according to the AURA 3 study (15). However, in patients who receive osimertinib as front-line treatment, systematic chemotherapy might be the only standard choice after progression, which usually resulted in limited efficacy but significant adverse events. Finally, the first-line choice of osimertinib might be more expensive than gefitinib/icotinib followed by osimertinib. The cost of medication is a significant aspect for making a final choice, especially in developing countries including China. Hence, in real-world practice, there are still a majority of patients receiving the regimen of gefitinib/icotinib followed by osimertinib. In such a situation, acquired resistance to first-/second-generation EGFR TKIs inevitably occurs, with molecular mechanisms remaining challenging. Currently, acquired resistance mechanisms to EGFR TKIs can be classified into EGFR-dependent mechanisms and EGFR-independent mechanisms, in which the EGFR exon 20 T790M mutation accounts for approximately 40% to 50% (16). Patients with the EGFR exon 20 T790M mutation responded well to third-generation TKIs including almonertinib and osimertinib, which is said to be a "lucky mutation". However, one-half of the patients still had a T790M-negative mutation; they commonly received chemotherapy, usually resulting in limited efficacy. Immune checkpoint inhibitors (ICIs) and anti-PD-1/PD-L1 monoclonal antibodies inhibit the interaction of PD-1 with their ligands, hence promoting an immunologic response by T cells against cancer cells, which failed to prove its efficacy as mono-therapy in patients harboring EGFR-sensitive mutations after resistance (17). Prospective clinical trials of combinational therapy of cytotoxic drugs combined with ICIs, including KEYNOTE 789 and CHECKMATE 722, are still ongoing. Current treatment strategies for NSCLC patients with T790M mutation-free TKIs resistance have not met clinical demands.

Recently, there was a prospective phase II clinical trial conducted to investigate the efficacy and safety of gefitinib as further-line re-challenge treatment for advanced NSCLC patients with EGFR-sensitive mutations (18). The study included stage IIIB/IV NSCLC patients with EGFR common mutations

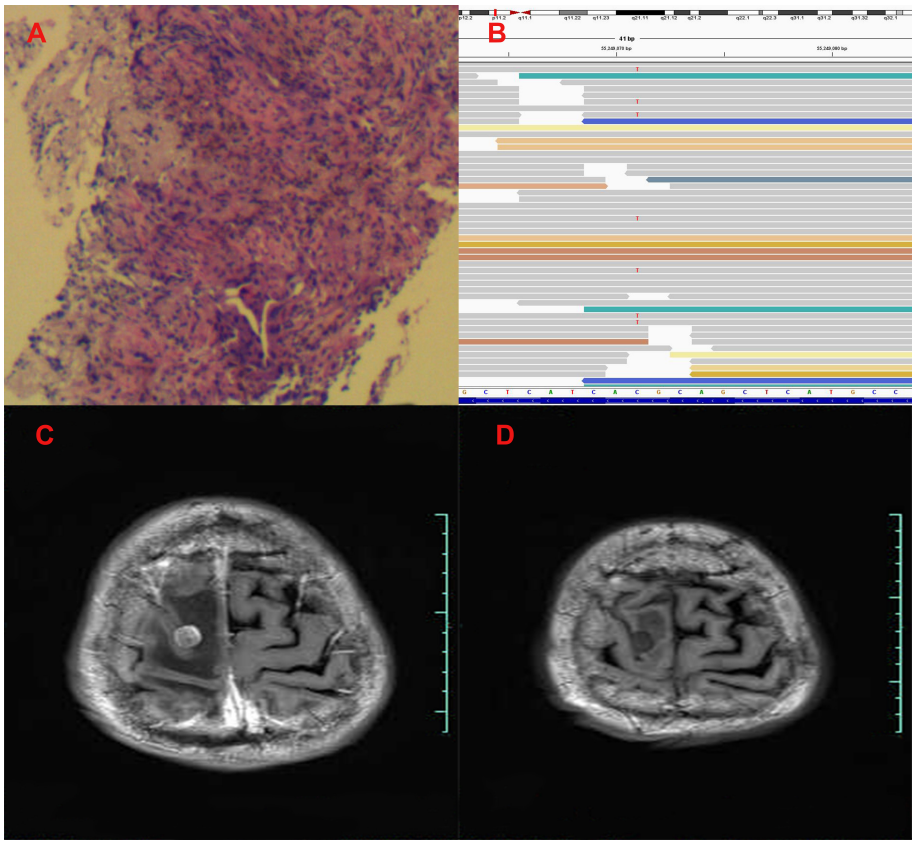

FIGURE 2
Pathological and clinical findings of Patient 2. **(A)** Pathological findings with HE staining. **(B)** NGS screenshots suggested emerging EGFR exon 20 T790M mutations. **(C)** Brain MRI image before salvage almonertinib treatment (after the emerging T790M mutation). **(D)** Brain MRI image after salvage almonertinib treatment.

including exon 19 deletion and exon 21 L858R mutation, who had benefited from first-line gefitinib treatment, and followed by further-line chemotherapy. Eligible patients received routine-dose gefinitib as re-challenge treatment. The results of the research showed that predefined disease control rate (DCR) was achieved in 69.8% (95% CI, 49.87–74.91) of patients. However, objective response rate (ORR) was reported merely in 4.7% (95% CI, 0.78–13.06) of patients, which suggested that anti-tumor efficacy of re-challenge of gefitinib was not satisfactory among the majority of the patients (18). In the present study, we also found that 2/3 patients (Patient 1 and Patient 2) suffered rapid progression of disease during the exposure of double-dose icotinib, the results of which were consistent with the former publication (18). However, we detected emerging T790M mutations unexpectedly after the exposure to double-dose icotinib, which was rarely reported in former literature. It should be pointed out that the NGS test using fresh tumor tissue from re-biopsy was also performed before the prescription of double-dose icotinib, the results of which did not reveal the T790M mutation. Based on this, it was most likely that the emerging T790M mutation was induced by the administration of double-dose icotinib. With the detection of the emerging T790M mutation, third-generation TKIs were prescribed as salvage treatment, which resulted in significant efficacy among the three patients. Therefore, the emerging T790M mutation might also be considered as a predictor to targetable TKIs. In addition, the emerging T790M mutations after the re-challenge of gefitinib in the CTONG 1304 trial were also reported (18). The authors reported that T790M-positive patients increased significantly (from 11 to 23, $p = 0.0081$) after the gefinitib re-challenge treatment. However, the sample adopted for the NGS test in that study was plasma, which may lead to a false-negative result before the re-challenge treatment of gefitinib. In the present study, fresh tumor tissue from re-biopsy was used for the NGS analysis, which may decrease the possibility of a potential false-negative result. Even so, we still suggested that a prospective, well-designed clinical trial might be essential to further address the issue of the emerging T790M mutation after double-dose icotinib treatment. In fact, the aforementioned study has been designed, with eligible patients being recruited in our institute.

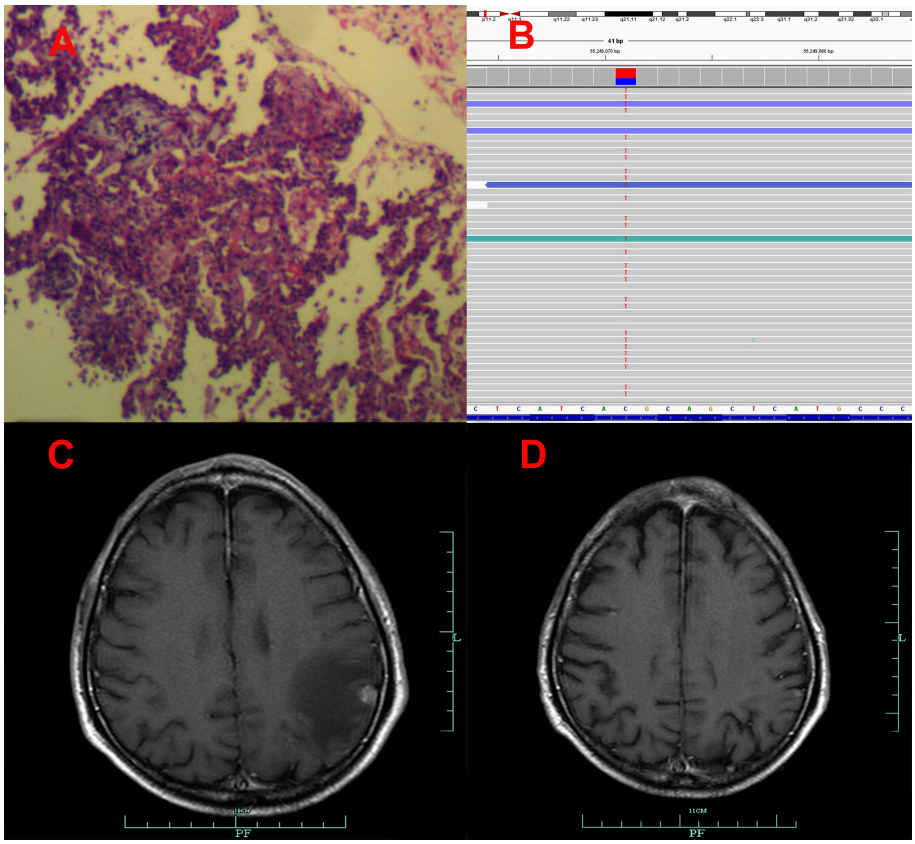

FIGURE 3
Pathological and clinical findings of Patient 3. **(A)** Pathological findings with HE staining. **(B)** NGS screenshots suggested increasing EGFR exon 20 T790M mutations (4% up to 87.5%). **(C)** Brain MRI image before salvage almonertinib treatment (after the emerging T790M mutation). **(D)** Brain MRI image after salvage osimertinib treatment (12).

Although the mechanism of the emerging T790M mutation after double-dose icotinib exposure remained unknown, we supposed that tumor heterogeneity might be the probable reason. In the AURA trial, 21% of patients with the T790M-negative mutation still responded to osimertinib, the specific T790M mutation inhibitor, which suggested that the T790M-negative results might appear to be the false-negative ones. The extremely low frequency of the T790M mutation led to false results (7). In addition, the TREM trial was conducted to evaluate the efficacy of osimertinib in patients progressing on standard EGFR-TKI treatment regardless of T790M status, the results of which showed that ORR was 28% (15% to 41%) for T790M-negative patients, with a PFS of 5.1 months (19). Hence, it was suggested that the T790M mutation could not be detected

TABLE 1 Baseline demographic and clinical/molecular characteristics of patients.

	Patient 1	Patient 2	Patient 3
Sex	Male	Male	Male
Age	59	62	67
ECOG PS	2	1	2
Stage	IVB	IVB	IVB
Smoking history	No	Yes	Yes
Brain metastases	Yes	Yes	Yes
EGFR mutation	Exon 21 L858R	Exon 19 deletion	Exon 19 deletion
Concurring mutation	TP53 S240G	ND	ND

ECOG PS, Eastern Cooperative Oncology Group Performance Status; EGFR, Epidermal Growth Factor Receptor; ND, Not Detected.

TABLE 2 Procedure, efficacy, and safety assessment of treatment for the patients.

	Patient 1	Patient 2	Patient 3
First-line TKIs	Gefitinib	Gefitinib	Icotinib
PFS for first-line TKI	14.3 months	21.6 months	8.1 months
PD lesions for TKI	Lung/pleura	Lung/lymph node	Lung/lymph node
PFS for double-dose icotinib	2.7 months	1.6 months	6.2 months
AEs for double-dose icotinib	Ileus	No	No
Frequency for the emerging T790M	19.6%	8.2%	87.5%
Salvage TKIs for T790M	Almonertinib	Almonertinib	Osimertinib
Best response for the salvage TKIs	PR	PR	SD
AEs for the salvage TKIs	No	Cerebral infarction	No
PFS for the salvage TKIs	3.7+ months	4.9+ months	6.3 months

TKI, tyrosine kinase inhibitor; PFS, progression-free survival; PD, progressive disease; AE, adverse event; T790M, EGFR exon20 T790M mutation; PR, partial response; SD, stable disease. +, the survival time is still in extension.

in a portion of patients, which may still respond to targetable TKIs. In the present study, the double-dose exposure of icotinib may rapidly eliminate T790M-negative subpopulations, which resulted in the elevated portion of the T790M mutation. For all these, basic experiments may still be essential to investigate the potential mechanisms of the emerging T790M mutations.

In addition, gefitinib and icotinib were approved as first-line treatment in metastatic NSCLC patients harboring EGFR-sensitive mutations because of their phase III, randomized research of the IPASS trial and the CONVINCE trial, respectively (4, 10). However in the present study, patients received gefitinib as first-line treatment, whose PFS was much better than that of icotinib. Based on the limited sample size, we still suggested that the difference in PFS between gefitinib and icotinib was coincidental. A "head to head" research (ICOGEN) was conducted to compare the efficacy between icotinib and gefitinib, the results of which did not suggest a statistical difference between icotinib and gefitinib (HR, 0.835; 95% CI, 0.667–1.046) (20). The comparative results among the first-line TKIs should be prudently concluded. Moreover, icotinib rather than other TKIs was adopted in the present study to induce treatment for emerging T790M mutations. In clinical practice, we have observed that the high-dose exposure of first-generation TKIs might be easier to induce that. Icotinib was the only TKI whose double-dose administration has been approved based on its clinical trial (11). However, for the other TKIs including gefitinib, erlotinib, and afatinib, high-dose exposure was not approved, which might lead to potential extra toxicities. This was the main reason why icotinib was chosen to induce treatment in the present study.

There were several limitations in the present study. The small sample size is the most obvious one. Owing to the frequent NGS tests using fresh tumor tissue, as well as the expensive cost of the serial gene tests, a majority of patients were excluded in the present retrospective study. We have noticed that the small sample size might limit its reliability in the present study. To address this, we have sponsored another prospective cohort study to further confirm the clinical phenomenon. In addition, the nature of a retrospective study may lead to a selection bias for the interpretation of the results.

Conclusion

In total, the results of the present study revealed that the EGFR exon 20 T790M mutation might be induced by double-dose

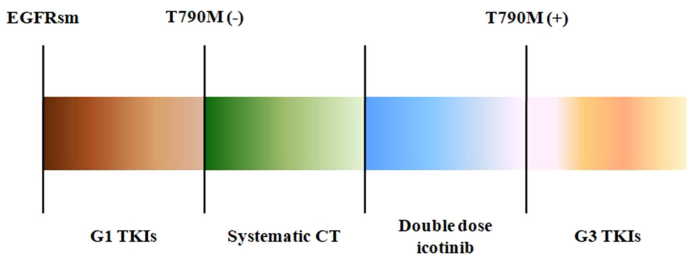

FIGURE 4
The treatment procedures of the three patients. EGFRsm, epidermal growth factor receptor sensitive mutation; TKIs, tyrosine kinase inhibitors; G1, first-generation TKIs; G3, third-generation TKIs; CT, chemotherapy.

icotinib exposure as further-line treatment in patients with former T790M-negative mutation. Patients with emerging T790M mutations responded well to the treatment of targetable TKIs including almonertinib or osimertinib.

Data availability statement

The original contributions presented in the study are included in the article/supplementary material. Further inquiries can be directed to the corresponding author.

Ethics statement

The studies involving human participants were reviewed and approved by Ethical Committee of People's Hospital of Quzhou. The patients/participants provided their written informed consent to participate in this study.

Author contributions

JC: Conceptualization, Methodology, Software, Writing-Original draft preparation, Software, Validation. XW: Data curation, Supervision. JW: Visualization, Investigation, Writing-Reviewing and Editing. All authors contributed to the article and approved the submitted version.

Funding

The study was supported by Instructional Project of Quzhou (2020057).

Acknowledgments

The authors thank the patients for their participation and agreement to publish the study.

Conflict of interest

The authors declare that the research was conducted in the absence of any commercial or financial relationships that could be construed as a potential conflict of interest.

Publisher's note

References

1. Wu YL, Zhou C, Hu CP, Feng J, Lu S, Huang Y, et al. Afatinib versus cisplatin plus gemcitabine for first-line treatment of Asian patients with advanced non-small-cell lung cancer harbouring EGFR mutations (LUX-lung 6): an open-label, randomised phase 3 trial. *Lancet Oncol* (2014) 15:213–22. doi: 10.1016/S1470-2045(13)70604-1

2. Sequist LV, Yang JC, Yamamoto N, O'Byrne K, Hirsh V, Mok T, et al. Phase III study of afatinib or cisplatin plus pemetrexed in patients with metastatic lung adenocarcinoma with EGFR mutations. *J Clin Oncol* (2013) 31:3327–34. doi: 10.1200/JCO.2012.44.2806

3. Rosell R, Carcereny E, Gervais R, Vergnenegre A, Massuti B, Felip E, et al. Erlotinib versus standard chemotherapy as first-line treatment for European patients with advanced EGFR mutation-positive non-small-cell lung cancer (EURTAC): a multicentre, open-label, randomised phase 3 trial. *Lancet Oncol* (2012) 13:239–46. doi: 10.1016/S1470-2045(11)70393-X

4. Mok TS, Wu YL, Thongprasert S, Yang CH, Chu DT, Saijo N, et al. Gefitinib or carboplatin-paclitaxel in pulmonary adenocarcinoma. *N Engl J Med* (2009) 361:947–57. doi: 10.1056/NEJMoa0810699

5. Oxnard GR, Arcila ME, Sima CS, Riely GJ, Chmielecki J, Kris MG, et al. Acquired resistance to EGFR tyrosine kinase inhibitors in EGFR-mutant lung cancer: Distinct natural history of patients with tumors harboring the T790M mutation. *Clin Cancer Res* (2011) 17:1616–22. doi: 10.1158/1078-0432.CCR-10-2692

6. Sun JM, Ahn MJ, Choi YL, Ahn JS, Park K. Clinical implications of T790M mutation in patients with acquired resistance to EGFR tyrosine kinase inhibitors. *Lung Cancer* (2013) 82:294–8. doi: 10.1016/j.lungcan.2013.08.023

7. Janne PA, Yang JC, Kim DW, Planchard D, Ohe Y, Ramalingam SS, et al. AZD9291 in EGFR inhibitor-resistant non-small-cell lung cancer. *N Engl J Med* (2015) 372:1689–99. doi: 10.1056/NEJMoa1411817

8. Yang JC, Ahn MJ, Kim DW, Ramalingam SS, Sequist LV, Su WC, et al. Osimertinib in pretreated T790M-positive advanced non-Small-Cell lung cancer: AURA study phase II extension component. *J Clin Oncol* (2017) 35:1288–96. doi: 10.1200/JCO.2016.70.3223

9. Xu J, Xu L, Wang B, Kong W, Chen Y, Yu Z. Outcomes in patients with lung adenocarcinoma with transformation to small cell lung cancer after EGFR tyrosine kinase inhibitors resistance: A systematic review and pooled analysis. *Front Oncol* (2021) 11:766148. doi: 10.3389/fonc.2021.766148

10. Shi YK, Wang L, Han BH, Li W, Yu P, Liu YP, et al. First-line icotinib versus cisplatin/pemetrexed plus pemetrexed maintenance therapy for patients with advanced EGFR mutation-positive lung adenocarcinoma (CONVINCE): a phase 3, open-label, randomized study. *Ann Oncol* (2017) 28:2443–50. doi: 10.1093/annonc/mdx359

11. Li X, Zhang L, Jiang D, Wang Y, Zang A, Ding C, et al. Routine-dose and high-dose icotinib in patients with advanced non-small cell lung cancer harboring EGFR exon 21-L858R mutation: the randomized, phase II, INCREASE trial. *Clin Cancer Res* (2020) 26:3162–71. doi: 10.1158/1078-0432.CCR-19-3064

12. Wang J, Chen J. Positive response to icotinib in metastatic lung adenocarcinoma with acquiring EGFR Leu792H mutation after AZD9291 treatment: A case report. *BMC Cancer* (2019) 19:131. doi: 10.1186/s12885-019-5352-7

13. Ramalingam SS, Vansteenkiste J, Planchard D, Cho BC, Gray JE, Ohe Y, et al. Overall survival with osimertinib in untreated, EGFR-mutated advanced NSCLC. *N Engl J Med* (2020) 382:41–50. doi: 10.1056/NEJMoa1913662

14. Wu YL, Tsuboi M, He J, John T, Grohe C, Majem M, et al. Osimertinib in resected EGFR-mutated non-Small-Cell lung cancer. *N Engl J Med* (2020) 383:1711–23. doi: 10.1056/NEJMoa2027071

15. Mok TS, Wu YL, Ahn MJ, Garassino MC, Kim HR, Ramalingam SS, et al. Osimertinib or platinum-pemetrexed in EGFR T790M-positive lung cancer. *N Engl J Med* (2017) 376:629–40. doi: 10.1056/NEJMoa1612674

16. Reita D, Pabst L, Pencreach E, Guerin E, Dano L, Rimelen V, et al. Molecular mechanism of EGFR-TKI resistance in EGFR-mutated non-small cell lung cancer: Application to biological diagnostic and monitoring. *Cancers (Basel)* (2021) 13. doi: 10.3390/cancers13194926

17. Hayashi H, Sugawara S, Fukuda Y, Sato Y, Miura S, Ota K, et al. A randomized phase II study comparing nivolumab (NIVO) with carboplatin-pemetrexed (CbPEM) for patients (pts) with EGFR mutation positive non-small cell lung cancer (NSCLC) who acquire resistance to tyrosine kinase inhibitors (TKIs) not due to a secondary T790M mutation (WJOG8515L). *J Clin Oncol* (2021) 39. doi: 10.1200/JCO.2021.39.15_suppl.9037

18. Song Y, Wu YL, Cao LJ, Chen JH, Ma ZY, Cui JW, et al. Efficacy and safety of gefitinib as third-line treatment in NSCLC patients with activating EGFR mutations treated with first-line gefitinib followed by second-line chemotherapy: A single-arm, prospective, multicenter phase II study (RE-CHALLENGE, CTONG1304). *Am J Clin Oncol* (2019) 42:432–9. doi: 10.1097/COC.0000000000000538

19. Eide IJZ, Helland A, Ekman S, Mellemgaard A, Hansen KH, Cicenas S, et al. Osimertinib in T790M-positive and -negative patients with EGFR-mutated advanced non-small cell lung cancer (the TREM-study). *Lung Cancer* (2020) 143:27–35. doi: 10.1016/j.lungcan.2020.03.009

20. Shi Y, Zhang L, Liu X, Zhou C, Zhang L, Zhang S, et al. Icotinib versus gefitinib in previously treated advanced non-small-cell lung cancer (ICOGEN): a randomised, double-blind phase 3 non-inferiority trial. *Lancet Oncol* (2013) 14:953–61. doi: 10.1016/S1470-2045(13)70355-3

frontiers | Frontiers in Oncology

TYPE Case Report
PUBLISHED 01 August 2022
DOI 10.3389/fonc.2022.884814

OPEN ACCESS

EDITED BY
Jian-ye Zhang,
Guangzhou Medical University, China

REVIEWED BY
Alessandro De Vita,
Scientific Institute of Romagna for the Study and Treatment of Tumors (IRCCS), Italy
Cecilia Garofalo,
Veneto Institute of Oncology (IRCCS), Italy

*CORRESPONDENCE
Xiu Nie,
niexiuyishi@126.com
Jun Fan,
fanjun0915@sina.com

†These authors have contributed equally to this work

SPECIALTY SECTION
This article was submitted to Cancer Molecular Targets and Therapeutics, a section of the journal Frontiers in Oncology

RECEIVED 27 February 2022
ACCEPTED 12 July 2022
PUBLISHED 01 August 2022

CITATION
Luo Y, Wu Y, Chang X, Huang B, Luo D, Zhang J, Zhang P, Shi H, Fan J and Nie X (2022) Identification of a novel *FGFR2-KIAA1217* fusion in esophageal gastrointestinal stromal tumours: A case report. *Front. Oncol.* 12:884814. doi: 10.3389/fonc.2022.884814

Identification of a novel *FGFR2-KIAA1217* fusion in esophageal gastrointestinal stromal tumours: A case report

Yuehao Luo[1†], Ying Wu[1†], Xiaona Chang[1], Bo Huang[1], Danju Luo[1], Jiwei Zhang[1], Peng Zhang[2], Heshui Shi[3], Jun Fan[1*] and Xiu Nie[1*]

[1]Department of Pathology, Union Hospital, Tongji Medical College, Huazhong University of Science and Technology, Wuhan, China, [2]Department of Gastrointestinal Surgery, Union Hospital, Tongji Medical College, Huazhong University of Science and Technology, Wuhan, China, [3]Department of Radiology, Union Hospital, Tongji Medical College, Huazhong University of Science and Technology, Wuhan, China

Background: Gastrointestinal stromal tumours (GISTs) rarely arise in the esophagus. The clinical course and treatment options for esophageal GISTs are poorly understood because of their rarity. In general, the mutation spectrum of esophageal GISTs resembles that of gastric GISTs. *Wild-type (WT)* GISTs lacking *KIT* and *PDGFRA* gene mutations occasionally occur in adults; primary esophageal GISTs are commonly *WT*.

Case presentation: Herein, we report the case of a 41-year-old female patient who presented with a 1-week history of anterior upper chest pain. Chest computed tomography revealed a 3.7 cm × 2.8 cm × 6.7 cm soft tissue mass in the right posterior mediastinum adjacent to the esophagus. The patient underwent thoracoscopic mediastinal tumor resection and was subsequently diagnosed with an esophageal GIST. Neither *KIT* nor *PDGFRA* mutations were detected by Sanger sequencing; however, next-generation sequencing (NGS) identified an *FGFR2-KIAA1217* gene fusion in the tumor tissue. No relapse was observed in this patient during the 8-month treatment-free follow-up period.

Conclusion: To the best of our knowledge, this report is the first to describe an *FGFR2-KIAA1217* fusion in a patient with a quadruple *WT* esophageal GIST. When *WT KIT/PDGFRA* GISTS are suspected, intensive genetic analysis is recommended, and obtaining a better molecular characterization of these tumours might reveal novel therapeutic avenues.

KEYWORDS

esophageal, quadruple *wild-type*, gastrointestinal stromal tumor, next-generation sequencing, *FGFR2-KIAA1217* fusion

Introduction

Gastrointestinal stromal tumours (GISTs) arise anywhere throughout the gastrointestinal tract and are seen most commonly in the stomach (40%–70%), small intestine (20%–40%), and colon and rectum (5%–15%) (1). Esophageal GISTs are extremely rare, accounting for 0.7% of all GISTs (2). Due to their rarity, clinicopathological data on esophageal GISTs are extremely limited, with only individual case reports or case series with small patient numbers available (3).

Most GISTs are characterized by oncogenic mutations in *c-KIT* (70% - 85%) or platelet-derived growth factor receptor-alpha (*PDGFRA*, 5%–15%) genes (4). The remaining 10-15% of GISTs lack *c-KIT* and *PDGFRA* mutations and are considered "*wild-type*" GISTs. These GISTs include *BRAF*-mutant GISTs, succinate dehydrogenase complex (SDH)-deficient GISTs, *KRAS*-mutant GISTs, and neurofibromatosis type 1 (NF1)-related GISTs.

The mutation status of esophageal GISTs has rarely been reported and is of increasing interest to researchers. Kang et al. found that the mutation spectrum of esophageal GISTs was similar to that of gastric GISTs in their case series, and most *KIT* mutations were detected in exon 11. Moreover, five (24%) of the 21 cases had *wild-type KIT* and *PDGFRA* genes, one of which was found to have the *BRAF* exon 15 V600E mutation by next-generation sequencing (NGS) (5).

Here, with the help of NGS detection technology, we found a rare *FGFR2-KIAA1217* fusion gene in the esophageal GIST of our patient, further expanding the *FGFR2* fusion variant spectrum.

Case report

A 41-year-old nonsmoker female was admitted to our hospital for chest pain that had persisted for over 1 week. Computed tomography (CT) imaging showed a soft tissue mass shadow in the right posterior mediastinum approximately 3.7 × 2.8 × 6.7 cm in size, and the boundary with the adjacent esophagus was unclear (Figures 1A, B). Endoscopic ultrasound examination showed a 3.5 cm × 3.3 cm submucosal eminence of the esophagus. The boundary remained clear with uniform hypoechoic changes (Figures 1C, D). Colour Doppler ultrasound of blood flow

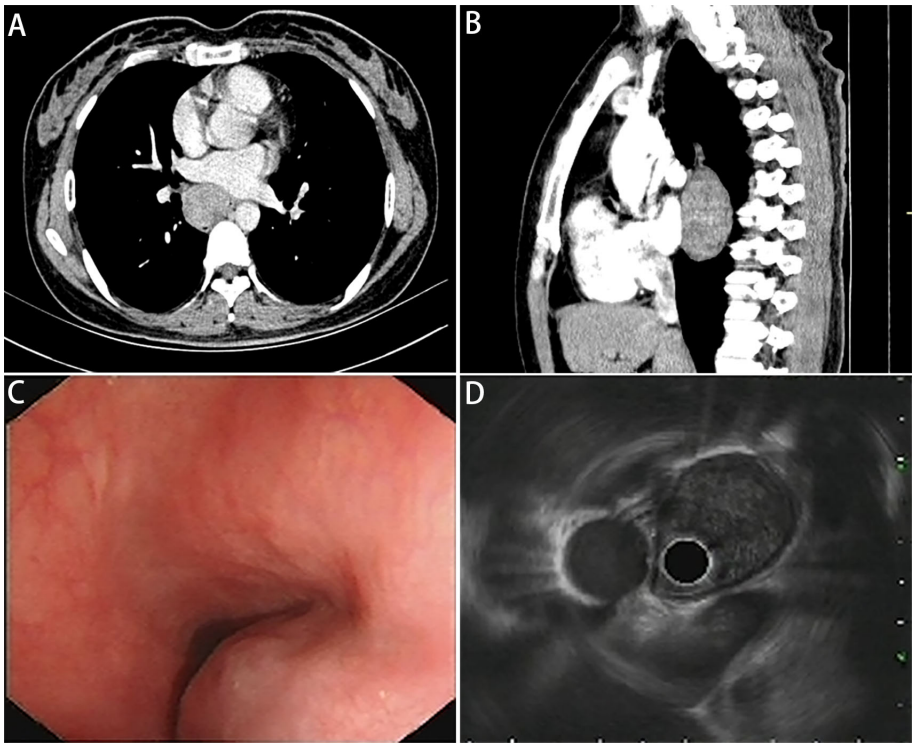

FIGURE 1
Images of pulmonary mediastinum CT and echogatstroscopy. **(A)** Transverse position and **(B)** sagittal position of pulmonary mediastinum CT show a mass located in the right posterior mediastinum approximately 37 × 28 × 67 mm in size, and the boundary with the adjacent esophagus is unclear. **(C)** The white light endoscopy view and **(D)** endoscopic ultrasound image show a 34.5 mm × 32.6 mm semispherical uplift with smooth surface mucosa and intraluminal growth pattern originating from the esophageal submucosal layer, with uniform hypoechoic change and a clear boundary.

displayed little blood flow signals inside the mass. Ultrasonic elastography showed that the texture of the lesion was soft, and the strain ratio (SR) value was 4.91. The disease was initially diagnosed as a mediastinal mass. After the preoperative examination, the patient underwent mediastinal mass enucleation by video-assisted thoracic surgery (VATS). The tumor was completely resected macroscopically, and postoperative pathology supported the diagnosis of esophageal GIST. The mass (6.0× 4.0× 3.0 cm) showed a complete capsule and weave-like dimensional structure upon gross examination. The histological examination revealed that the tumor consisted of short spindle cells with red homogeneous stroma and mucoid degeneration (Figure 2A) with a mitotic index of < 5/5 square mm2. Thus, according to the modified National Institute of Health (NIH) criteria, the tumor was considered a high-risk GIST.

On immunohistochemistry, the tumor cells were unequally positive for CD117 (Figure 2B), weakly positive for DOG1 (Figure 2C), negative for SMA (Figure 2D), strongly positive for CD34 (Figure 2E), and positive for SDHB (Figure 2F). The Ki-67 labelling index was 1% (Figure 2G). Sanger sequencing revealed no mutations in the exons corresponding to the *c-KIT* and *PDGFRA* genes, including exons 9, 11, 13 and 17 of *KIT* and exons 12, 14 and 18 of *PDGFRA* (Figures 3A, B). Next-generation sequencing (NGS) revealed the presence of an *FGFR2-KIAA1217* gene fusion (3.88% abundance in tissue, Figure 3C). A break-apart fluorescent *in situ* hybridization (FISH) assay confirmed the *FGFR2* translocation (Figure 2H). Follow-up was suggested for this patient. The patient did not experience relapse during the 8-month follow-up after surgery, and no further treatment was administered.

Materials and methods

Immunohistochemistry

The surgical specimens were fixed with 3.7% neutral formaldehyde and then routinely dehydrated, paraffin-embedded, sectioned at 4 μm, stained with HE and observed under a light microscope. Immunohistochemical staining was performed by the Envision two-step method. The primary antibodies were CD117 (Ventana Medical System, Inc., Tucson, AZ, USA; Clone: c-kit), DOG1 (MXB, Fuzhou, China; Clone: SP31), CD34 (Gene Tech, Shanghai, China; Clone: QBEnd 10), smooth muscle actin (SMA) (Gene Tech; Clone: 1A4), SDHB (ZSGB-BIO, Beijing, China; Clone: OTI1H6) and Ki-67 (MXB, Clone: MIB-5).

Sanger sequencing

The Sanger sequencing method was used to detect c-KIT and PDGFRA gene mutations. According to the kit (c-KIT and PDGFRA gene mutation detection kit of Xiamen Aide Co., Ltd, Xiamen, China) instructions, genomic DNA was extracted from the samples. c-KIT exons 9, 11, 13, and 17 and PDGFRA exons 12 and 18 were amplified with polymerase chain reaction (PCR). After detecting the PCR products by gel electrophoresis, the PCR products were sequenced using ABI 3730XL DNA sequencers. The sequencing results were compared with the standard template sequences of the BLAST program within the CHROMAS software to identify the gene mutation loci.

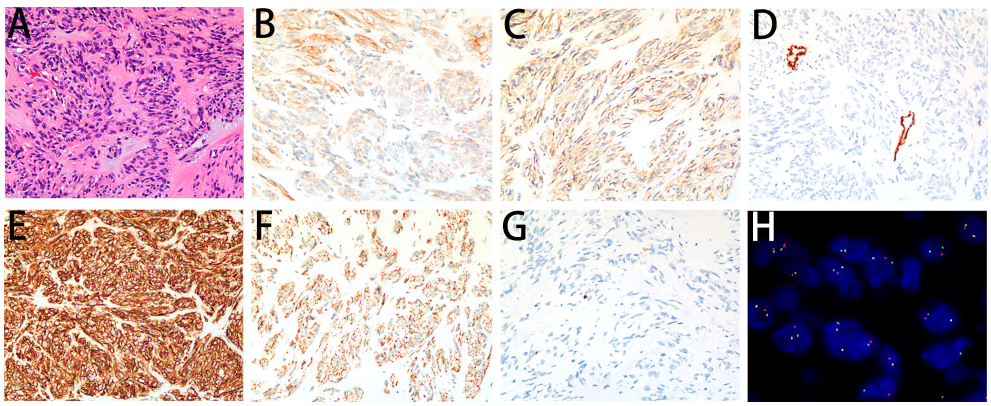

FIGURE 2
Microscopy images of the GIST. **(A)** The tumor demonstrated short spindle cells with red homogeneous stroma and pale blue mucus stained by H&E (200×). **(B)** The tumor cells showed an unequal positive cytoplasmic signal for CD117 (200×). **(C)** The tumor cells showed a weakly positive cytoplasmic signal for DOG1 (200×). **(D)** The tumor cells showed a negative cytoplasmic signal for SMA (200×). **(E)** The tumor cells showed a positive cytoplasmic signal for CD34 (200×). **(F)** The tumor cells showed a positive cytoplasmic signal for SDHB (200×). **(G)** The Ki-67 labelling index was 1% (200×). **(H)** A break-apart fluorescent *in situ* hybridization (FISH) assay found *FGFR2* translocation (100×).

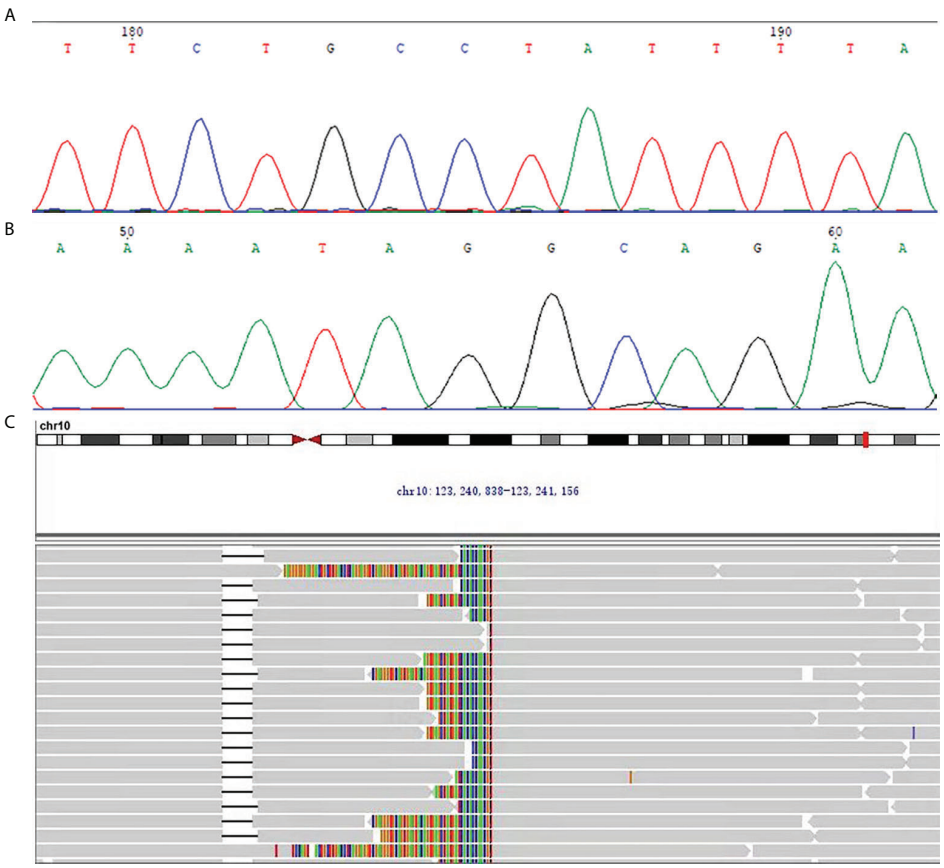

FIGURE 3
(A, B) The representative chromatogram of Sanger sequencing. **(A)** The forward sequencing result at exon 9 of *c-KIT* for the GIST in this case. **(B)** The reverse sequencing result at exon 9 of *c-KIT* for the GIST in this case. **(C)** NGS revealed the presence of the *FGFR2-KIAA1217* gene fusion (3.88% abundance in tissue).

Next-generation sequencing

NGS was performed by Tongshu Gene (Shanghai, China). The OncoPanel consists of targeted sequencing of 556 cancer-related genes. The FGFR2 gene in the 556 panel for the detection of gene rearrangement and mutation were detected by DNA sequencing.

Fluorescence *in situ* hybridization

Fluorescence *in situ* hybridization (FISH) was performed on 4-μm-thick FFPE sections using the Vysis dual-color FGFR2 break-apart probe kit (Abbott Molecular/Vysis, Des Plaines, IL) following the manufacturer's instructions. The results were considered positive for FGFR2 when more than 30% of tumor nuclei had evidence of FGFR2 rearrangement in at least 100 tumor cells. The split signal was counted when the space between the two signals was larger than that of one signal.

Discussion

Esophageal GISTs are a rare subtype, and limited data are available on the associated clinicopathologic features and clinical outcomes. The most common location of esophageal GISTs is the lower esophagus, followed by the middle esophagus; GISTs in the upper esophagus are rare (6). Esophageal GISTs are often found accidentally by oesophagoscopy or barium oesophagography (7). Dysphagia (36–51%) is the most frequent symptom in patients with esophageal GISTs, followed by weight loss (20%), chest pain (8–15%), and bleeding (1–10%) (1, 8). Here, the patient presented with atypical chest pain, and CT revealed a mass with a maximum diameter of 6.7 cm in the lower esophagus.

Spindle cell morphology is observed in 82.8% of esophageal GISTs, while 8–10% demonstrate epithelioid morphology and 8–10% mixed morphology (1). The vast majority of esophageal GISTs are positive for CD117, DOG-1 and CD34 (5). SDH-deficient cases are rare. Our patient's tumor demonstrated short

spindle-cell morphology and was highly positive for CD117, CD34 and DOG-1 expression. The current risk stratification systems are based on tumor size, mitotic counts per 50 high-power fields (5 mm2) and anatomical location (9). The risk for tumor recurrence was determined to be high according to the modified NIH criteria. Feng et al. reported that the majority of esophageal GISTs are classified into the high-risk category (70.83%) (1). On the other hand, when the risk classification system was established, only a few esophageal GISTs were included in the risk assessment, and the accuracy of these systems for determining the prognosis of patients with esophageal GISTs is unknown (10).

Data reported in the limited number of studies on esophageal GISTs suggest that the mutation spectrum of these GISTs resembles that of gastric GISTs. It was reported that the proportion of *KIT* exon 11 mutations is strikingly high in esophageal GISTs, usually involving codons 557 and/or 558 (5). However, our patient's tumor did not harbor detectable *KIT* or *PDGFRA* mutations, as determined by Sanger sequencing. Next, we performed an in-depth targeted investigation into the genetic status of the so-called *KIT/PDGFRA wild-type* GIST by NGS to uncover putative alterations in frequently mutated genes that conventional molecular diagnostic approaches can miss. A novel *FGFR2-KIAA1217* fusion with a complete *FGFR2* protein kinase structure was identified in the absence of SDH/*RAS* pathway mutations. Therefore, our patient's tumor was determined to be a quadruple *wild-type (qWT)* GIST. To date, only individual and rarely recurring alterations have been identified in this GIST subgroup, such as alterations in *ETV6-NTRK3*, *FGFR1*, *FGF4*, *MAX* and *MEN1 (*11). Here, we report the first case of a *qWT* GIST harboring the novel *FGFR2-KIAA1217* variant, enriching the *FGFR2* fusion spectrum.

There is increasing interest in deregulation of fibroblast growth factor (FGF)/FGF-receptor (FGFR) signaling in different molecular subgroups of GISTs, which has emerged as a relevant pathway driving oncogenic activity. FGF/FGFR pathway alterations have been observed in *qWT* GISTs, including two activating missense mutations identified in *FGFR1* (p.K656E and p.N546K) and two gene fusions, *FGFR1–HOOK3* and *FGFR1–TACC1*. In *c-KIT*-mutated GISTs, the activation of the FGF/FGFR signaling pathway and crosstalk with the KIT receptor provide an alternative mechanism of imatinib resistance, representing a route for tumor cells to acquire secondary resistance to imatinib (12, 13). FGFR2 gain has been suggested as an additional potential mechanism associated with imatinib resistance (14).

Because of this rarity, the treatment of esophageal GISTs remains a matter of debate. Surgical resection is the only potentially curative treatment for localized GISTs. A small-sample exploratory study indicated that thoracoscopic enucleation of esophageal GISTs seems to represent a viable therapeutic option, as the postoperative morbidity/mortality is low and the oncological outcome is good for low-to-intermediate grade malignant tumours (15). Although imatinib treatment for GIST has been regarded as the paradigm of precision oncology, there is far from a consensus on the treatment of *qWT* GIST. Moreover, clinical studies of adjuvant imatinib therapy following resection of GISTs seldom involved esophageal GISTs. Therefore, more studies are needed to determine the effectiveness of adjuvant therapy for *qWT* esophageal GISTs.

Recently, pemigatinib and infigratinib, targeted oral therapeutic agents that are competitive inhibitors of FGFR1, FGFR2, and FGFR3, have been approved by the Food and Drug Administration (FDA) for locally advanced or metastatic cholangiocarcinoma with *FGFR2* fusion or rearrangements (16, 17). A recent clinicogenomic analysis of FGFR2-Rearranged Cholangiocarcinoma (FIGHT-202) suggest that patients with specific co-occurring alterations, especially in tumor-suppressor genes (including BAP1, CDKN2A/B, TP53, PBRM1, ARID1A, or PTEN) may have worse outcomes with Pemigatinib treatment. In the research, the authors found acquired FGFR2 mutations in all 8 patients analyzed at progression, consistent with previous reports of resistance to other FGFR inhibitors (18). Further, according to Varghese et al., polyclonal acquired mutations in the FGFR2 kinase domain were identified in acquired resistance to FGFR Inhibition by detectable circulating tumor DNA. Therefore, genomic profiling enables a deeper understanding of the molecular basis for response and nonresponse to targeted therapy (19).

So far, efficacy of the selective FGFR inhibitors in heavily pretreated phase 1/2 patients' looks encouraging. A pivotal trial of derazantinib in advanced or inoperable FGFR2 gene fusion-positive intrahepatic cholangiocarcinoma reported an overall response rate of 20.7%, disease control rate of 82.8%. Estimated median progression-free survival was 5.7 months (20).In another phase I trial of advanced Solid Tumors harboring FGFR alterations, 58 patients receiving Debio 1347, there were 6 partial responses (3 with FGFR fusions) and 10 additional patients' tumor size regressions of ≤30% (21). The development of targeted drugs for FGFR2 subtypes, such as bemarituzumab, an afucosylated monoclonal antibody against FGFR2b, and alofanib, a predominantly FGFR2-selective allosteric small-molecule inhibitor, is underway (22, 23).

Also, FGFR4, another member of FGFR family, has gradually been noticed. Indeed, while it is well known that its mutations are recurrent in several pediatric and adult rhabdomyosarcoma cases (24), recently its role has been proved also in gastric cancers, showing that mutationally activated FGFR4 may act as an oncoprotein, therefore supporting its therapeutic targeting (25). Therefore, FGFR-specific tyrosine kinase inhibitors may also provide a new approach to treating GISTs with FGF/FGFR pathway mutations.

It is worth noting that Caruso C et al. mentioned, Pharmacogenomics (PGx) biomarkers that can predict drug response play an important role in the improvement of molecular diagnostics in clinical routines in GIST patients. Association of SNP and outcome of GIST patients cured with

imatinib and sunitinib was also highlighted by Kloth and colleagues. Thus, it is crucial to find novel prognostic biomarkers to stratify patients with improved risk for disease progression during imatinib therapy. Therefore, the potential role of FGFR2-KIAA1217 as pharmacogenomics biomarker in conventional chemotherapic protocol of GIST deserve further attention (26).

The clinical outcomes of esophageal GISTs from large case series studies indicated that 5-year disease-free survival (DFS) ranges from 57.0-65.3%. However, the overall survival (OS) results are controversial. Nakano et al. reported that the average time to recurrence was 40 months (5-year OS: 89%) and emphasized the need for long-term follow-up because recurrence occurred even 5 years after surgery (8). In contrast, Lott et al. reported that the 5-year OS of esophageal GISTs was 48.3%, suggesting a significantly worse prognosis than that of gastric GISTs. In our case, no recurrence occurred during the follow-up period of 8 months, and long-term follow-up was necessary.

This study is subject to several limitations. First, the duration of the follow-up was relatively short. Second, the therapeutic effects of the FGFR inhibitors or GIST targeted therapies were not clearly established.

Conclusion

In summary, this report is the first to describe a *qWT* esophageal GIST patient with a novel, potentially targetable *FGFR2-KIAA1217* fusion. The case highlights the importance of a comprehensive genomic profiling approach able to detect all classes of genomic alterations, including uncommon gene fusions, to reveal potentially targetable somatic alterations for mutation-matched therapy selection.

Data availability statement

The original contributions presented in the study are included in the article/supplementary material. Further inquiries can be directed to the corresponding authors.

Ethics statement

Written informed consent was obtained from the individual(s) for the publication of any potentially identifiable images or data included in this article.

Author contributions

XN and JF: conception and design of the work; acquisition and interpretation of data; revision of the manuscript critically for important intellectual content and scientific integrity. YL and YW: drafting of the manuscript and analysis of the patient's data. PZ and HS: clinical management of the patient and provision of patient's data. XC, BH, JZ and DL: elaboration and analysis of the pathology. All authors contributed to manuscript revision, read, and approved the submitted version.

Funding

This work was supported by grants from the National Natural Science Foundation of China (No. 81773022 and 82072333); Natural Science Foundation of Hubei Province (No. 2020CFB808).

Conflict of interest

The authors declare that the research was conducted in the absence of any commercial or financial relationships that could be construed as a potential conflict of interest.

Publisher's note

References

1. Feng F, Tian Y, Liu Z, Xu G, Liu S, Guo M, et al. Clinicopathologic features and clinical outcomes of esophageal gastrointestinal stromal tumor: Evaluation of a pooled case series. *Medicine* (2016) 95(2):e2446. doi: 10.1097/MD.0000000000002446

2. Monges G, Bisot-Locard S, Blay JY, Bouvier AM, Urbieta M, Coindre JM, et al. The estimated incidence of gastrointestinal stromal tumors in France Results of progist study conducted among pathologists. *Bull du Cancer* (2010) 97(3):E16–22. doi: 10.1684/bdc.2010.1041

3. Hihara J, Mukaida H, Hirabayashi N. Gastrointestinal stromal tumor of the esophagus: Current issues of diagnosis, surgery and drug therapy. *Trans Gastroenterol Hepatol* (2018) 3:6. doi: 10.21037/tgh.2018.01.06

4. Wozniak A, Rutkowski P, Piskorz A, Ciwoniuk M, Osuch C, Bylina E, et al. Prognostic value of Kit/Pdgfra mutations in gastrointestinal stromal tumours (Gist): Polish clinical gist registry experience. *Ann Oncol* (2012) 23(2):353–60. doi: 10.1093/annonc/mdr127

5. Kang G, Kang Y, Kim KH, Ha SY, Kim JY, Shim YM, et al. Gastrointestinal stromal tumours of the oesophagus: A clinicopathological and molecular analysis of 27 cases. *Histopathology* (2017) 71(5):805–12. doi: 10.1111/his.13292

6. Lott S, Schmieder M, Mayer B, Henne-Bruns D, Knippschild U, Agaimy A, et al. Gastrointestinal stromal tumors of the esophagus: Evaluation of a pooled case series regarding clinicopathological features and clinical outcome. *Am J Cancer Res* (2015) 5(1):333–43.

7. Nemeth K, Williams C, Rashid M, Robinson M, Rasheed A. Oesophageal gist-a rare breed case report and review of the literature. *Int J Surg Case Rep* (2015) 10:256–9. doi: 10.1016/j.ijscr.2015.02.023

8. Nakano A, Akutsu Y, Shuto K, Uesato M, Kono T, Hoshino I, et al. Giant esophageal gastrointestinal stromal tumor: Report of a case. *Surg Today* (2015) 45 (2):247–52. doi: 10.1007/s00595-014-0929-x

9. Joensuu H, Vehtari A, Riihimaki J, Nishida T, Steigen SE, Brabec P, et al. Risk of recurrence of gastrointestinal stromal tumour after surgery: An analysis of pooled population-based cohorts. *Lancet Oncol* (2012) 13(3):265–74. doi: 10.1016/S1470-2045(11)70299-6

10. Neofytou K, Costa Neves M, Giakoustidis A, Benson C, Mudan S. Effective downsizing of a Large oesophageal gastrointestinal stromal tumour with neoadjuvant imatinib enabling an uncomplicated and without tumour rupture laparoscopic-assisted ivor-Lewis oesophagectomy. *Case Rep oncological Med* (2015) 2015:165736. doi: 10.1155/2015/165736

11. Astolfi A, Indio V, Nannini M, Saponara M, Schipani A, De Leo A, et al. Targeted deep sequencing uncovers cryptic kit mutations in Kit/Pdgfra/Sdh/Ras-p wild-type gist. *Front Oncol* (2020) 10:504. doi: 10.3389/fonc.2020.00504

12. Javidi-Sharifi N, Traer E, Martinez J, Gupta A, Taguchi T, Dunlap J, et al. Crosstalk between kit and Fgfr3 promotes gastrointestinal stromal tumor cell growth and drug resistance. *Cancer Res* (2015) 75(5):880–91. doi: 10.1158/0008-5472.Can-14-0573

13. Li F, Huynh H, Li XY, Ruddy DA, Wang YZ, Ong R, et al. Fgfr-mediated reactivation of mapk signaling attenuates antitumor effects of imatinib in gastrointestinal stromal tumors. *Cancer Discovery* (2015) 5(4):438–51. doi: 10.1158/2159-8290.Cd-14-0763

14. Boichuk S, Galembikova A, Dunaev P, Valeeva E, Shagimardanova E, Gusev O, et al. A novel receptor tyrosine kinase switch promotes gastrointestinal stromal tumor drug resistance. *Molecules* (2017) 22(12):2152. doi: 10.3390/molecules22122152

15. Cohen C, Pop D, Icard P, Berthet JP, Venissac N, Mouroux J. Is there a place for thoracoscopic enucleation of esophageal gastrointestinal stromal tumors? *Thorac Cardiovasc surgeon* (2019) 67(7):585–8. doi: 10.1055/s-0038-1670662

16. Massironi S, Pilla L, Elvevi A, Longarini R, Rossi RE, Bidoli P, et al. New and emerging systemic therapeutic options for advanced cholangiocarcinoma. *Cells* (2020) 9(3):688. doi: 10.3390/cells9030688

17. Rizzo A, Ricci AD, Brandi G. Pemigatinib: Hot topics behind the first approval of a targeted therapy in cholangiocarcinoma. *Cancer Treat Res Commun* (2021) 27:100337. doi: 10.1016/j.ctarc.2021.100337

18. Silverman IM, Hollebecque A, Friboulet L, Owens S, Newton RC, Zhen H, et al. Clinicogenomic analysis of Fgfr2-rearranged cholangiocarcinoma identifies correlates of response and mechanisms of resistance to pemigatinib. *Cancer Discovery* (2021) 11(2):326–39. doi: 10.1158/2159-8290.CD-20-0766

19. Varghese AM, Patel J, Janjigian YY, Meng F, Selcuklu SD, Iyer G, et al. Noninvasive detection of polyclonal acquired resistance to fgfr inhibition in patients with cholangiocarcinoma harboring Fgfr2 alterations. *JCO Precis Oncol* (2021) 5:44–50. doi: 10.1200/PO.20.00178

20. Mazzaferro V, El-Rayes BF, Droz Dit Busset M, Cotsoglou C, Harris WP, Damjanov N, et al. Derazantinib (Arq 087) in advanced or inoperable Fgfr2 gene fusion-positive intrahepatic cholangiocarcinoma. *Br J Cancer* (2019) 120(2):165–71. doi: 10.1038/s41416-018-0334-0

21. Voss MH, Hierro C, Heist RS, Cleary JM, Meric-Bernstam F, Tabernero J, et al. A phase I, open-label, multicenter, dose-escalation study of the oral selective fgfr inhibitor debio 1347 in patients with advanced solid tumors harboring fgfr gene alterations. *Clin Cancer Res* (2019) 25(9):2699–707. doi: 10.1158/1078-0432.CCR-18-1959

22. Tyulyandina A, Harrison D, Yin W, Stepanova E, Kochenkov D, Solomko E, et al. Alofanib, an allosteric Fgfr2 inhibitor, has potent effects on ovarian cancer growth in preclinical studies. *Invest New Drugs* (2017) 35(2):127–33. doi: 10.1007/s10637-016-0404-1

23. Catenacci DV, Tesfaye A, Tejani M, Cheung E, Eisenberg P, Scott AJ, et al. Bemarituzumab with modified Folfox6 for advanced Fgfr2-positive gastroesophageal cancer: Fight phase iii study design. *Future Oncol* (2019) 15 (18):2073–82. doi: 10.2217/fon-2019-0141

24. De Vita A, Vanni S, Fausti V, Cocchi C, Recine F, Miserocchi G, et al. Deciphering the genomic landscape and pharmacological profile of uncommon entities of adult rhabdomyosarcomas. *Int J Mol Sci* (2021) 22(21):11564. doi: 10.3390/ijms222111564

25. Futami T, Kawase T, Mori K, Asaumi M, Kihara R, Shindoh N, et al. Identification of a novel oncogenic mutation of Fgfr4 in gastric cancer. *Sci Rep* (2019) 9(1):14627. doi: 10.1038/s41598-019-51217-6

26. Caruso C, Garofalo C. Pharmacogenomics biomarkers of soft tissue sarcoma therapies. *Front Oncol* (2020) 10:509. doi: 10.3389/fonc.2020.00509

frontiers | Frontiers in Oncology

TYPE Review
PUBLISHED 01 August 2022
DOI 10.3389/fonc.2022.923260

OPEN ACCESS

EDITED BY
Jian-ye Zhang,
Guangzhou Medical University, China

REVIEWED BY
Xin-Lin Chen,
Guangzhou University of Chinese Medicine, China
Xiaomeng Xie,
China-US (Henan) Hormel Cancer Institute, China

*CORRESPONDENCE
Yongqiang Xie
zhangzcmnwk@163.com
Zhenghua Gao
398815535@qq.com

†These authors have contributed equally to this work

SPECIALTY SECTION
This article was submitted to Cancer Molecular Targets and Therapeutics, a section of the journal Frontiers in Oncology

RECEIVED 19 April 2022
ACCEPTED 27 June 2022
PUBLISHED 01 August 2022

CITATION
Zhang Z, Li D, Yun H, Tong J, Liu W, Chai K, Zeng T, Gao Z and Xie Y (2022) Opportunities and challenges of targeting c-Met in the treatment of digestive tumors.
Front. Oncol. 12:923260.
doi: 10.3389/fonc.2022.923260

Opportunities and challenges of targeting c-Met in the treatment of digestive tumors

Zhengchao Zhang[1,2†], Dong Li[1†], Heng Yun[1†], Jie Tong[1], Wei Liu[1], Keqiang Chai[1], Tongwei Zeng[1], Zhenghua Gao[1*] and Yongqiang Xie[1*]

[1]Department of General Surgery, The Third Affiliated Hospital of Gansu University of Traditional Chinese Medicine, Baiyin, China, [2]Department of General Surgery, Second Hospital of Lanzhou University, Lanzhou, China

At present, a large number of studies have demonstrated that c-Met generally exerts a crucial function of promoting tumor cells proliferation and differentiation in digestive system tumors. c-Met also mediates tumor progression and drug resistance by signaling interactions with other oncogenic molecules and then activating downstream pathways. Therefore, c-Met is a promising target for the treatment of digestive system tumors. Many anti-tumor therapies targeting c-Met (tyrosine kinase inhibitors, monoclonal antibodies, and adoptive immunotherapy) have been developed in treating digestive system tumors. Some drugs have been successfully applied to clinic, but most of them are defective due to their efficacy and complications. In order to promote the clinical application of targeting c-Met drugs in digestive system tumors, it is necessary to further explore the mechanism of c-Met action in digestive system tumors and optimize the anti-tumor treatment of targeting c-Met drugs. Through reading a large number of literatures, the author systematically reviewed the biological functions and molecular mechanisms of c-Met associated with tumor and summarized the current status of targeting c-Met in the treatment of digestive system tumors so as to provide new ideas for the treatment of digestive system tumors.

KEYWORDS

c-Met, digestive system tumors, gastric cancer, hepatocellular carcinoma, pancreatic cancer, colorectal cancer, targeted therapy, adoptive immunotherapy

Introduction

Digestive system tumors (DSTs) mainly include gastric cancer(GC), hepatocellular carcinoma (HCC), pancreatic cancer(PC) and colorectal cancer(CRC), which are general cancers in worldwide (1). Although surgery, chemotherapy and molecular targeted therapy have been widely used in the treatment of DSTs, the prognosis of most advanced

DSTs patients is still poor (2). Therefore, it is crucial to explore effective therapeutic targets and strategies for middle-advanced DSTs. Several studies have shown that c-Met is a promising treating target for DSTs (3–5). In recent years, clinical trials of treating DSTs based on c-Met targets have achieved favourable security, and c-Met inhibitors have been found to be an efficient treatment regimen in combination with other drugs (6).

MET gene is involved not only in the proliferation, differentiation and invasion of various human tumor cells, but also in the resistance of anti-tumor drugs (7). It is overexpressed in many human tumors, including respiratory system tumors, DSTs (8–11), urinary system tumors (12, 13) and reproductive system tumors (14, 15). Previous researches have demonstrated that inhibition of c-Met signaling, such as non-small cell lung cancer (NSCLC), HCC, GC, PC, CRC, ovarian cancer, bladder cancer (16–25), is an efficient anti-tumor strategy for many tumors. c-Met has also been found to participate in the drug resistance of epidermal growth factor receptor-tyrosine kinase inhibitors (EGFR-TKIs) treating NSCLC patients (25). The combination of c-Met inhibitors and EGFR-TKIs might be considered a promising treatment option.

Researches have demonstrated that c-Met normally mediates downstream signals by combining with its corresponding ligand, hepatocyte growth factor (HGF), to promote the proliferation and differentiation of tumor cells. It was also found that c-Met can also activate downstream pathways through signaling interaction with some carcinogenic molecules in the absence of ligands (26, 27). Therefore, the mechanism of c-Met promoting tumor proliferation and drug resistance is complicated. In order to promote the clinical application of c-Met targeted drugs for DSTs, it is necessary to explore the mechanism of c-Met action in DSTs so as to optimize the anti-tumor activity and treatment regimens of c-Met drugs. This paper systematically reviews the biological functions of c-Met related to tumor formation and development, and summarizes the researches on targeting c-Met in the treatment of DSTs, in order to bring new ideas of targeting c-Met in the treatment of DSTs.

The structure of c-Met/HGF and its tumor-related signaling pathway

c-Met is a glycosylated membrane protein consisting of transmembrane β chains (145 kDa) and extracellular α chains (50 kDa). HGF, as a ligand of c-Met, is composed of a 103 kDa soluble heterodimer, which consists of α-chain and β-chain linked together by disulfide bonds (28). Binding of HGF and c-Met leads to autophosphorylation of tyrosine residues Y1234 and Y1235 in the tyrosine kinase domain, which further activates autophosphorylation of the Y1349 and Y1356 tyrosine domains near the COOH (Figure 1). For example, the adaptive molecule GRB2-associated-binding protein 1 (29) is a scaffold protein connector containing a c-Met binding site, which provides a binding site for effectors containing the SrC-Homology-2 domain. The same way as translational protein SH2, phosphoinositol 3 kinase, protein tyrosine phosphatase with SH2 domain, phospholipase Cc1, signal transduction and

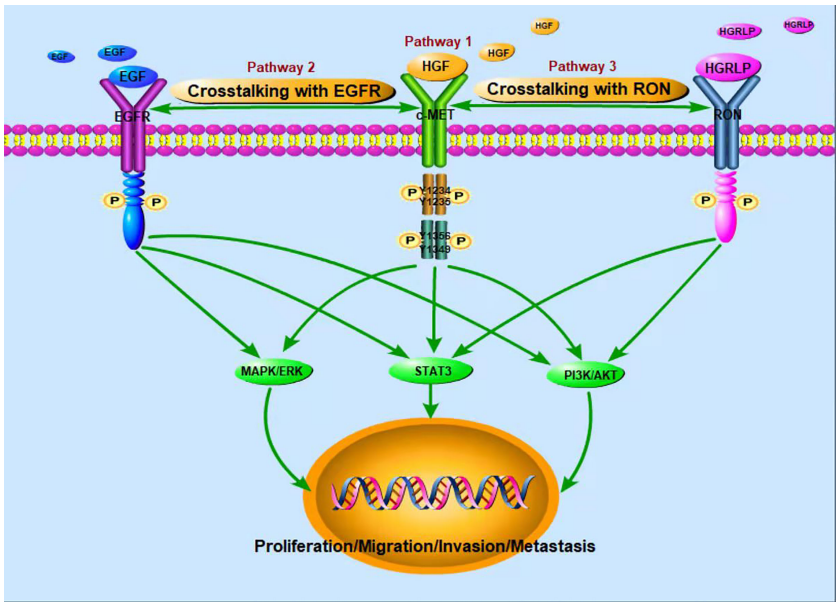

FIGURE 1
Activation of c-Met tumor-related signaling pathways.

transcription activator 3, etc. Therefore, the binding of HGF and c-Met regulates cellular biological functions by activating the above-mentioned downstream signaling pathways (30–34). The HGF/c-Met pathway is also regulated by other proteins, such as integrin, which promotes the activation of RAS, PI3K, plexinB1, signaling hormone and death receptor Fas (35). Through these second messengers, c-Met downstream signaling pathways trigger many biological activities, such as cell proliferation, cell survival, motor function and morphological changes (36, 37).

In recent years, studies have found that EGFR and c-Met are often co-expressed in tumors, and they share a common downstream signaling pathway, such as ERK, MAPK, PI3K, AKT pathways. The interaction between EGFR and c-Met has been reported in HCC (38). Besides, Yoshiaki Nakamura et al. (39)found that cetuximab induced MET gene mutation and amplification in advanced GC, suggesting that EGFR-targeted therapy may mediate drug resistance through MET amplification and/or proteinhyperactivation. Further studies showed that the signal interaction between c-Met and EGFR mediated anti-tumor resistance (40, 41). Yuying Zhu et al. (27) also found that up-regulated c-Met signal can be used as a compensation mechanism for weakening EGFR family signal so as to maintain the proliferation of chemotherapy resistant breast tumor cells. The combination of c-Met and EGFR targeted therapy was also found to synergistically inhibit proliferation of drug-resistant cells *in vitro* and *in vivo*. According to the above findings, simultaneous targeting of these two targets may be promising in the treatment of tumors. A number of clinical studies have also verified the antitumor activity of targeted EGFR and c-Met combination therapy (42–44). Therefore, in order to perfect the anti-tumor activity of c-Met targeted therapy and develop its function in treating drug-resistant tumors, future studies should further explore the interaction mechanism between c-Met and EGFR.

In addition, RON (Recepteur d 'Origine Nantais) receptor is a member of the tyrosine kinase receptor family. The homologous similarity between the extracellular domain and kinase domain and c-Met domain was 25% and 63%, respectively. The activation of RON can lead to the activation of MAPK, PI3K and other signaling pathways. RON ligand is hepatocyte growth factor-like protein (HGFLP) (45). According to the sequence homology with HGF, the cDNA encoding HGFLP was isolated for the first time and named HGFLP (46). HGFLP is mainly secreted by liver cells and is a single chain precursor with no biological activity. RON and c-Met, interactive activation between which has been demonstrated, are co-expressed in many tumors; what's more, recent studies have suggested that c-Met trans-activation of RON may be a hallmark of cancer cells (26). Both c-Met and RON play important functional roles in embryonic development and organogenesis, and are overexpressed or abnormally activated in various tumors (47). S Zhao et al. (48) found that RON knockout can increase the intensity and duration of c-Met signal, suggesting that c-Met signal could compensate for the loss of RON signal. Therefore, RON and c-Met exert a crucial role in tumor genesis and development through their dynamic complementarity.

Tumor-related biological functions and regulation of c-Met/HGF

c-Met is essential for several events including angiogenesis, myoblast migration, bone remodeling, and nerve germination during the processes of embryogenesis (49). In vertebrate adulthood, c-Met has been found to be constitutively expressed in epithelial cells during liver regeneration and wound healing (50). c-Met/HGF kinase pathway is inactivated in normal tissues, but activated in various tumor tissues (51). As a proto-oncogene, MET mediates tumor cell proliferation, invasion, angiogenesis, chemotherapy resistance, epithelial-mesenchymal transformation (52–55).

HGF is defined as a secretory factor responsible for enhancing cell motility, invasion and causing cell dispersal (56). HGF in tumor microenvironment can be derived from both tumor cells and tumor associated stromal cells (56). Binding of actived HGF and c-Met leads to oligomerization of receptors, activation, autophosphorylation of tyrosine residues, and substrate docking, thereby activating downstream signaling processes (36, 57). Activation of other tyrosine kinases is also found to be involved in enhancing the HGF/c-Met signaling pathway. EGFR plays a critical role in promoting c-Met mediated cell proliferation, cell invasion, and cell survival (58). EGFR activation can induce SRC-dependent c-Met activation, which is ligand-independent (59). Similarly, at the downstream of c-Met activation, the release of PGE2 induced by COX2 increases the activity of matrix metalloproteinases and releases EGFR ligands, such as bidirectional regulatory proteins (60). Therefore, EGFR and c-Met promote tumor progression through signal interaction. Other carcinogenic mechanisms have also been found to enhance the effects of c-Met. c-Met interacts with insulin-like growth factor 1 receptors could promote tumor cell invasion and migration (61). In addition, hypoxia positively regulates c-Met activity through tumor angiogenesis (62). These findings suggest a complex interaction system that regulates and controls the size and duration of c-Met signaling.

The association of c-Met activity with tumor growth, invasion, and poor prognosis has been demonstrated (35). C-Met aberrations occur in approximately 50% of HCC patients and can be caused by gene mutations, gene amplification, increased mRNA expression, and receptor overexpression (63). Although c-Met has a potentially beneficial role in chronic liver disease, increased activity may initiate or promote the development and progression of HCC. Therefore, c-Met is considered to be an important factor in the regulation of liver

disease and a carcinogen driver of HCC. In PC, increasing of MET transcription leads to c-Met overexpression, and c-Met increasing promotes tumor genesis and development through a variety of mechanisms (64). C-Met expression is 5-7 times higher in PC tissues than in adjacent tissues, providing a large therapeutic safety window for targeted c-Met therapy in PC (65). In addition, inappropriate activation of c-Met pathway in GC was found to be mainly due to the amplification and mutation of Met gene leading to c-Met protein overexpression (66). About 4-10% of gastric cancer patients have MET amplification, and 50% of advanced gastric cancer patients have C-MET protein overexpression (67, 68). High expression of c-Met was also detected in CRC and has been observed to be associated with tumor invasion, lymph node and liver metastasis. Therefore, c-Met plays an important role in the diagnosis and treatment of DSTs.

Application of c-Met inhibitors in DSTs

In the past few years, a number of c-Met inhibitors have been developed for therapeutic studies in tumors and have shown significant antitumor activity in preclinical studies of DSTs (69–73). Some c-Met inhibitors have been used in the clinical treatment of DSTs and achieved certain efficacy. In addition, several new c-Met inhibitors and drug therapy strategies are being developed for DSTs (Table 1). Therefore, it is of great importance to deeply understand the regulatory mechanism of HGF/c-Met pathway in finding effective c-Met inhibitors and therapeutic strategies for DSTs.

Hepatocellular carcinoma

In 2020, hepatocellular carcinoma (HCC) was the sixth most common cancer and the third leading cause of cancer deaths in worldwide, with approximately 906,000 new cases and 830,000 deaths (74). Conventional chemotherapy has limited efficacy, and the 5-year survival rate of advanced HCC is less than 10% (75). Therefore, it is urgent to develop effective treatments for advanced HCC. Researchers studied the expression of c-Met in 62 HCC patients and its correlation with prognosis, they found that the 5-year survival rate of HCC patients with high expression of c-Met was significantly lower than that with low expression of c-Met (76). The study also found that high c-Met expression in HCC was associated with an increased incidence of intrahepatic metastasis. The study suggests that c-Met plays an important role in the formation and development of HCC and may be a promising therapeutic target. In recent years, c-Met inhibitors, multikinase inhibitors and some new drugs have been used in the treatment of HCC.

Tivantinib, a selective small molecule inhibitor of c-Met, has shown significant antitumor activity in phase I clinical trials for the treatment of HCC. However, hematologic toxicity of tivantinib, mainly with neutropenia, was observed in phase II clinical trials (77). Santoro et al. conducted a study in which 97 patients with advanced HCC were randomized to tivantinib or placebo. The median time of progression was longer in the tivantinib group compared with the placebo one. 10 patients with neutropenia and 8 with anemia in the tivantinib group was also found (78). However, a recent randomized, double-blind Phase III clinical study conducted by Rimassa et al. showed that tivantinib did not improve the overall survival of c-Met positive patients with advanced HCC (79). These studies indicate that tivantinib may have some limitations in the treatment of HCC.

Sorafenib, as a multikinase inhibitor, is currently the only confirmed first-line treatment for advanced HCC (80). Sorafenib obviously perfected overall survival in patients with advanced HCC; however, its antitumor activity was generally hampered by the development of drug resistance (81). Since then, researchers have identified c-Met high-selective inhibitors in combination with Sorafenib as a potential therapeutic strategy for HCC. JIANG X et al. (82) found that a new c-Met inhibitor (DE605) combined with Sorafenib could effectively induce HCC cells apoptosis *in vitro* and inhibit HCC metastasis *in vivo*. MinKe He et al. (83) conducted a randomized clinical trial of Sorafenib combined with oxaliplatin, fluorouracil and calcium folate in the treatment of HCC patients with portal vein invasion. The results showed that Sorafenib combined with chemotherapy significantly improved overall survival and had an acceptable toxic effect compared with single Sorafenib treatment. Therefore, Sorafenib combination therapy may be a good strategy for the treatment of HCC.

Tepotinib, which has been shown to inhibit the progression of c-Met positive HCC *in vivo*, is a highly selective c-Met inhibitor*in vivo* (84). Baek-yeol Ryoo et al. (85) conducted a phase II clinical study (NCT01988493) to evaluate the role of Tepotinib in the treatment of advanced HCC. Patients treated with tepotinib had better progression-free survival and objective response rate than that with Sorafenib, and tepotinib showed better drug tolerance. Faced with the problem of Sorafenib resistance, Thomas Decaens et al. (86) conducted a phase II clinical study to evaluate the efficacy of Tepotinib in Sorafenib resistant patients with advanced HCC (NCT02115373). Tepotinib was generally well tolerated and showed good efficacy. These studies suggest that tepotinib may be more effective than Sorafenib in the treatment of advanced HCC, and tepotinib is effective in patients with Sorafenib resistance. Tepotinib has great potential in treating advanced HCC.

SU11274, a small molecule inhibitor of c-Met, could also inhibit the growth of HCC cells by inhibiting the activation of c-Met (87). Other c-Met inhibitors such as cabozantinib, Capmatinib, Golvatinib and foretiinib have also been reported

TABLE 1 Clinical studies on c-Met inhibitors in the treatment of DSTs.

Conditions	Interventions	First posted	Number enrolled	Phase	NCT number	State	Status
Gastric Cancer	Drug: crizotinib	May 6, 2015	2	Phase 2	NCT02435108	Korea	Completed
Advanced Solid Tumors	Drug:Capmatinib	October 5, 2016	36	Phase 1	NCT02925104	United States	Completed
Solid Tumors	Drug: Capmatinib	March 29, 2011	131	Phase 1	NCT01324479	United States	Completed
Gastric Cancer	Drug: MCLA-129	May 3, 2021	150	Phase 1 Phase 2	NCT04868877	United States	Recruiting
Solid Tumors	Genetic: SAIT301	November 20, 2014	16	Phase 1	NCT02296879	Korea	Completed
Solid Tumor, Adult	Drug: HLX55	November 19, 2019	98	Phase 1	NCT04169178	Taipei, Taiwan	Recruiting
Gastric Cancer Gastroesophageal Junction Adenocarcinoma	Drug: APL-101 Oral Capsules	June 5, 2017	201	Phase 1 Phase 2	NCT03175224	United States	Recruiting
Solid Tumors	Drug: tepotinib	April 16, 2013	12	Phase 1	NCT01832506	Japan	Completed
Advanced Solid Tumors Which Are cMET-dependent	Drug: capmatinib Drug: Nazartinib Drug: Gefitinib	February 2, 2017	40	Phase 2	NCT03040973	United States	Recruiting
Solid Tumor	Drug: SPH 3348	October 21, 2021	36	Phase 1	NCT05088070	China	Recruiting
Pancreatic Adenocarcinoma Metastatic	Drug: Cabozantinib Drug: Erlotinib	July 11, 2017	7	Phase 2	NCT03213626	United States	Terminated
Colorectal Cancer	Drug: MCLA-129	June 18, 2021	400	Phase 1 Phase 2	NCT04930432	China	Recruiting
Solid Tumors	Drug: tepotinib	November 17, 2009	149	Phase 1	NCT01014936	United States	Completed
Solid Cancers	Drug: bevacizumab •Drug: MetMAb	February 17, 2010	44	Phase 1	NCT01068977		Completed
Colorectal Cancer	Drug: PF-02341066 Drug: PD-0325901 Drug: Binimetinib	July 28, 2015	82	Phase 1	NCT02510001	United Kingdom	Completed
Solid Tumor	Drug: RC108	November 5, 2020	32	Phase 1	NCT04617314	China	Recruiting
Solid Tumors	Drug: HS-10241	May 3, 2016	7	Phase 1	NCT02759640	Australia	Completed
Solid Tumor	Drug: Tepotinib	December 1, 2020	100	Phase 2	NCT04647838	Korea	Recruiting
Hepatocellular Carcinoma	Drug: Tepotinib	April 16, 2014	66	Phase 1 Phase 2	NCT02115373	Germany	Completed
Liver Cancer	Drug: TIVANTINIB	January 7, 2014	386	Phase 3	NCT02029157	Japan	Completed
Advanced Solid Tumor	Drug: CAPMATINIB	March 7, 2012	44	Phase 1	NCT01546428	Japan	Completed
Solid Tumor	Drug: HS-10241	July 20, 2020	30	Phase 1	NCT04477057	China	Recruiting
Advanced Solid Tumors	Drug: AMG 337	December 3, 2010	111	Phase 1	NCT01253707	United States	Completed
Carcinoma, Hepatocellular	Drug: Foretinib	June 15, 2009	45	Phase 1	NCT00920192	Taiwan	Completed
Advanced Solid Tumors	Drug: ABT-700	November 16, 2011	74	Phase 1	NCT01472016		Completed

All clinicaltrials can be downloaded from www.clinicaltrials.gov (accessed February 28, 2022).

in HCC treatment (88–90). All of these c-Met inhibitors have shown antitumor activity in preclinical studies of HCC. However, the efficacy and safety of these drugs need to be tested in future clinical studies. The peptide LZ8, as a c-Met inhibitor, is extracted from ganoderma lucidum and has anti-tumor activity in breast cancer, lung cancer, cervical cancer and HCC (91–94). As a Chinese herbal ingredient, the peptide LZ8 has been certified as safe, but clinical trials are still needed to verify its safety and effectiveness in HCC patients. Although c-Met inhibitors have great potential in the treatment of HCC, more clinical studies are needed to optimize the treatment regimen and improve the prognosis of patients with advanced HCC.

Pancreatic cancer

Pancreatic cancer(PC) is a highly lethal disease with a 5-year survival rate of only 10% (95). The disease is often insidious, and most patients could not often be diagnosed until at advanced stage. In recent decades, with the advancement of diagnostic, treatment methods and techniques, the prognosis of PC patients has been significantly improved (96). However, its efficacy is still limited for advanced patients, and better treatment strategies need to be developed to solve the current situation. A large number of studies have confirmed that c-Met is involved in the formation and development of PC (91, 92, 97). Renzo et al. found that c-Met was up-regulated in most PDAC, while the

expression level was very low in normal pancreatic tissues (97). In addition, other studies have shown that the c-Met/HGF pathway plays a crucial role in the progression, invasion, metastasis and therapeutic drug resistance of PC (48, 93). Therefore, c-Met may be a promising therapeutic target for PC.

Chenwei Li et al. (94) evaluated the tumorigenicity of PC cells with high expression of c-Met in NOD SCID mice, the results showed that cells with high expression of c-Met were more likely to develop tumor than those with negative expression of c-Met. Studies *in vitro* also showed that c-Met inhibitor XL184 could significantly suppress the formation of tumor globules, suggesting that cells with high expression c-Met increased the tumorigenic potential of mice. In NOD SCID mice, the use of c-Met inhibitors slowed tumor growth in pancreatic tumors. In addition, other studies have found that c-Met inhibitors PHA665752 and AMG102 can not only block the HGF/c-Met axis by reducing the phosphorylation level of c-Met, but also weaken the epithelial mesenchymal transformation and chemotherapy resistance (98). Firuzi et al. (99) also found that pancreatic stellate cells increased resistance to gemcitabine through the c-Met/HGF signaling pathway. Besides, Zhihong Xu et al. (100)found in preclinical studies that c-Met inhibitors combined with chemotherapy drugs could completely eliminate metastasis and significantly reduce tumor growth *in vivo*. Therefore, these studies suggest that c-Met inhibitors can not only inhibit the growth of c-Met expressing PC, but also serve as an important therapeutic option for patients with chemotherapy-resistant PC.

Furthermore, the sequence of c-Met expression in PC cells changed after irradiation, and the expression of c-Met was induced by irradiation instantaneously (101). Irradiation also enhanced downstream phosphorylated MET expression in a mouse model of *in vivo* subcutaneous tumors. Compared with cells with low expression of c-Met, PC cells with enhanced expression of c-Met after radiation had a higher malignant potential, including invasion and migration. Capmatinib has been shown to reverse this enhanced malignant potential by inhibiting c-Met expression. These studies not only explain the possible mechanism of PC progression after radiotherapy, but also provide a theoretical basis for radiotherapy combined with c-Met inhibitor therapy for PC.

Soichi Takiguchi et al. (102) evaluated the effect of Crizotinib on peritoneal spread of PC *in vivo*, the study found that Crizotinib reduced tumor burden and ascites accumulation. So crizotinib may be an effective drug in treating PC patients with peritoneal metastasis. In addition, Enliang Li et al. (103) found that c-Met inhibitors combined with PD-1/PD-L1 inhibitors could achieve better efficacy against PC *in situ* and subcutaneous mouse models, indicating that combination of c-Met and PD-1/PD-L1 inhibitors may be a charming choice for PC treatment.

Gastric cancer

Gastric cancer (GC), causing more than 1 million new cases and an estimated 769,000 deaths in 2020, ranking respectively fifth and fourth globally in morbidity and mortality, remains an important cancer worldwide (74). Clinically, the prognosis of patients with advanced GC is still poor (104). Surgical resection, radiotherapy and chemotherapy for advanced GC patients have been widely used in clinical practice, but the efficacy is limited. Therefore, it is necessary to further explore the molecular mechanism of GC in order to find effective therapeutic targets. Researchers conducted Northern blot analysis, reverse transcription polymerase chain reaction and immunohistochemical staining on 45 patients with GC, and found that the expression of MET mRNA in GC tissues was 2 times and 7 times higher than that in normal adjacent tissues (105). c-Met was detected overexpression in 32 of all patients (71.1%), and was significantly overexpressed in GC tissue compared to normal ones. What's more GC patients with high c-Met expression have a poor overall prognosis (106, 107). Therefore, c-Met is a potential therapeutic target for GC.

Haiyan Liao et al. (108) found that Volitinib inhibited downstream PI3K/Akt and MAPK signaling pathways by selectively inhibiting c-Met phosphorylation, and significantly inhibited proliferation of MKN45 cell lines with high c-Met expression *in vitro* and *in vivo*. Paul R. Gavine et al. (109) also found that volitinib could lead to significantly GC tumor cell growth stagnation *in vitro* experiments, but its anti-tumor activity was negligible in xenograft tumor model. The above *in vivo* results*in vivo* may be related to different tumor models, such as MKN45-derived CDX model used by Haiyan Liao, and PDX model used by Paul R. Gavine. After all, there are certain differences in target expression between CDX model and PDX model. Therefore, the efficacy of Volitinib in GC needs to be verified by more PDX models or organoids with high c-Met expression.

Tivantinib and SAR125844 are also widely studied as selective c-Met inhibitors. Bum Jun Kim et al. (110) evaluated the inhibitory effect of tivantinib on proliferation and migration of GC cells, and discussed the mechanism of tivantinib through carcinogenic pathway analysis. Oncogenic pathway analysis showed that tivantinib inhibited the expression of VEGF signal in GC cells in addition to the c-Met signaling pathway. Studies have shown that tivantinib has anti-tumor effect not only on GC cells with high expression of c-Met, but also on ones with expression of non-c-Met. Tivantinib has been studied in clinical trials in several different tumors, including NSCLC, HCC and metastatic GC. In a multicenter Phase II trial, 31 Japanese and Korean patients with metastatic GC were enrolled, 11 of whom had disease control (111). However, adverse events remain serious. SHITARA K et al. conducted a phase I clinical

trial of SAR125844 treating GC. It involved 22 Asian patients with GC and showed moderate anti-tumor function in 2 of them, although adverse events were also common in these patients (112). Similar to the HCC treatment, most c-Met inhibitors still have Insufficient benefits for cancer treatment due to adverse events and limitations of c-Met positivity.

Tepotinib is an oral, potent, highly selective c-Met inhibitor. Sung-hwa Sohn et al. (113) evaluated the antitumor activity of Tepotinib in GC cell lines. Tepotinib showed good antitumor growth activity *in vitro* and in mouse models, with reduced levels of phosphorylated c-Met protein. The results of this study suggest that Tepotinib inhibits tumor growth and migration by negatively regulating c-Met induction. Kohei Shitara et al. (114) conducted a multi-center Phase I clinical trial (NCT01832506) to evaluate the dose tolerated by patients with solid tumors. Tepotinib was generally well tolerated, no dose-limiting toxicity was observed, and treatment-related adverse events were mainly in grade 1-2 GC patients. These studies suggest that Tepotinib may play a greater role in the treatment of GC due to its good tolerability.

Yashiro et al. (115) studied the clinical efficacy of SU11274 combined with irinotecan in the treatment of GC, and found that the effect of inhibiting tumor growth *in vivo* through combined administration was superior to that of any single drug therapy. SU11274 was found to inhibit the c-Met signaling pathway, thereby reducing the expression of uridine 50-bisphosphate-glucuronyltransferase 1A1 (UGT1A1), which is associated with irinotecan resistance. Since then, KRC-408, KRC-00715 and Simm530 have been identified as selective inhibitors of c-Met, all of which have been shown in preclinical studies to inhibit the growth of GC cells (69, 116–118). Still, more clinical studies are needed to verify its efficacy and safety.

Colorectal cancer (CRC)

Colorectal cancer (CRC) is the third most common malignancy in the world and a familiar cause of cancer-related death. It is estimated that there were more than 1.9 million new CRC cases and 935,000 deaths of CRC in the United States in 2020, accounting for about one in 10 cancer cases and deaths (74). In recent decades, great progress has been made in CRC early diagnosis measures, combination chemotherapy, targeted drugs and surgical treatment, but there are still limitations in efficacy. Existing targeted drugs have poor efficacy on some CRC subtypes (119), and further research on the molecular mechanism of tumor genesis is needed to optimize the efficacy of targeted drug. Studies have shown that the high expression of c-Met in CRC is associated with tumor invasion and liver metastasis (120). In recent years, a large number of studies have devoted to figure out the role of HGF-MET signaling pathway in CRC, and illuminated that this pathway is a therapeutic target. Liu et al. (121)observed that the expression of c-Met in CRC mucosal tissues was significantly higher than that in normal ones. Takeuchi et al. (122) used real-time quantitative polymerase chain reaction to study 36 patients with early CRC, and found that the expression of MET in CRC tissues was significantly higher than that in normal colon mucosal tissues, and the high expression of c-Met was related to the depth of intestinal wall invasion and regional lymph node metastasis. Therefore, c-Met inhibitors are widely used in the studies of CRC treating.

Crizotinib, Capmatinib and Tivantinib are also used as selective inhibitors of c-Met in the treatment of CRC. Feng Du et al. (123) found that crizotinib could block the HGF/STAT3/SOX13/c-Met axis and significantly inhibit SOX13-mediated CRC migration, invasion and metastasis. Kyle C. Cuneo et al. (124) evaluated the radiosensitization of crizotinib in cetuximab resistant CRC cell lines. The results showed that crizotinib effectively increased the sensitivity of cetuximab KRAS mutant CRC cell lines to radiotherapy. Besides, Jean-pierre Delord et al. (6) conducted a clinical study of Capmatinib combined with Cetuximab in the treatment of c-Met positive metastatic CRC (NCT02205398). 13 patients were found to have no dose-limiting toxicity and tumors shrank 29-44% in 4 patients. Capmatinib combined with cetuximab was well tolerated. However, in a phase II study reported by Cathy et al. (NCT01075048), tiantinib in combination with cetuximab did not significantly improve progression-free survival in metastatic CRC (125). This is consistent with the results of tivantinib study in liver cancer carried out by Rimassa et al. (79), indicating that tivantinib has limitations in treating DSTs.

In addition, SU11274 was found to have antitumor effects in CRC treatment by specifically inhibiting c-Met phosphorylation. GAO S H et al. reported that SU11274 can inhibit the proliferation of four colon cancer cell lines (126). At the same time, GAO W et al. also described that SU11274 could induce G1 block and inhibit the survival of CRC cells *in vitro*; what's more, the growth of xenograft tumors was inhibited *in vivo* (127). YITAO JIA et al. (120) also studied the effects of c-Met inhibitor PHA665752 on the irradiation activity of colon cancer cells and xenograft cells. The results show that c-Met inhibition makes CRC cells radiation-sensitive by enhancing the formation of DNA double-strand breaks and alleviating tumor hypoxia.

As a c-Met inhibitor, Nororitin (NCTD) is a demethylated analogue of Cantharidin and has strong anti-tumor activity (128, 129). Studies have shown that NCTD can inhibit CRC cell proliferation and induce G2/M growth arrest by reducing the levels of EGFR and c-Met (128). Therefore, NCTD may be also a promising therapeutic agent, and its clinical efficacy and safety are worth looking forward to.

Application of c-Met monoclonal antibody in DSTs

In recent years, c-Met monoclonal antibody has also been widely used in the treatment of DSTs. The studies mainly include the use of monoclonal antibodies alone, antibodies combination with other drugs and antibody-drug coupling in anti-DSTs (Table 2). However, due to its unimproved antitumor activity and high complication rate, it has not been widely applied in clinic.

Onartuzumab is a monoclonal antibody that has been evaluated clinically in a variety of human cancers, including targeted therapies alone or in combination (130–132). In 2014, Ravi Salgia et al. (133) evaluated the antitumor activity of onartuzumab in humans for the first time. Thirty-four patients with GC were treated in the study, and only one patient achieved a lasting complete response for nearly two years. In addition, MANISH A. SHAH et al. (134) conducted a Phase II clinical study of onartuzumab combined with oxaliplatin in treating metastatic human EGFR2 negative adenocarcinoma at the gastric or gastroesophageal junction (NCT01590719). The study found that the addition of onartuzumab to c-Met positive GC patients could not improve the outcome. Manish A. Shah, MD et al. (135) also conducted a similar clinical study (NCT01662869) and found that onartuzumab combined with first-line oxaliplatin did not significantly improve clinical prognosis in GC patients with c-Met immunohistochemistry of 2+ and 3+. These studies suggest that onartuzumab has limited efficacy in treating GC.

In addition, the current study found that complications of onartuzumab are also the main reasons limiting its widespread use in clinic. Clinical studies conducted by MANISH A. SHAH et al. found grade 3 adverse events in 88.3% of onartuzumab treated patients, and severe adverse events in 55% (134). Roland Morley et al. (136) conducted a study of complications in 773 solid tumor patients treated with ornatuzumab, all of which were reported possessing edema and venous thromboembolism. Hypoalbuminemia was also more common in the onartuzumab group, with an incidence between 77.8% and 98.3%. Compared with control group, patients treated with onartuzumab had higher rates of arterial venous thromboembolism, gastrointestinal perforation, hypoproteinemia and edema. Therefore, these complications are considered to be expected events of onartuzumab treatment.

Emibetuzumab is a bivalent monoclonal antibody against c-Met that blocks both ligand-dependent and non-ligand-dependent c-Met signaling. S. Betty Yan et al. (137) evaluated emibetuzumab using a c-Met positive GC xenograft model. Emibetuzumab therapy provided transient tumor regression (37.7%), though tumor emerged regrowing during treatment. Daisuke Sakai et al. (138) evaluated the activity and safety of emibetuzumab in the treatment of advanced GC through phase II clinical study. Emibetuzumab

TABLE 2 Clinical studies on c-Met MAbs in the treatment of DSTs.

Conditions	Interventions	First posted	Number enrolled	Phase	NCT number	State	Status
Neoplasms	Drug:4mg/kg/15mg/kg/30mg/kg Onartuzumab	January 9, 2014	30	Phase 1	NCT02031731	China	Completed
Solid Tumor	Drug: Onartuzumab Drug: Bevacizumab Drug: Erlotinib	July 2, 2015	12	Phase 3	NCT02488330	France	Completed
Colorectal Cancer	Drug: 5-FU Drug:FOLFOX regimen	August 17, 2011	194	Phase 2	NCT01418222	United States	Completed
Gastric Cancer	Drug: 5-Fluoruracil Drug: Folinic acid Drug: Onartuzumab	August 10, 2012	564	Phase 3	NCT01662869	United States	Completed
Hepatocellular Carcinoma	Drug: Onartuzumab Drug: Sorafenib	July 11, 2013	9	Phase 1	NCT01897038	United States	Completed
Gastric Cancer	Drug: Onartuzumab Drug: Oxaliplatin	May 3, 2012	123	Phase 2	NCT01590719	United States	Completed
Solid Cancers	Drug: bevacizumab Drug:MetMAb(PRO143966)	February 17, 2010	44	Phase 1	NCT01068977	United States	Completed
Advanced Cancer Gastric Adenocarcinoma Gastroesophageal Junction Adenocarcinoma	Drug: Emibetuzumab Drug: Ramucirumab	March 10, 2014	97	Phase 1 Phase 2	NCT02082210	United States	Completed
Solid Tumor	Drug: Merestinib	September 30, 2016	12	Phase 2	NCT02920996	United States	Active, not recruiting

All clinicaltrials can be downloaded from www.clinicaltrials.gov (accessed February 28, 2022).

was well tolerated in the treatment of advanced GC, but its anti-tumor activity was limited. Later, James J. Harding et al. (139) reported a Phase I/II clinical study of ramucirumab combined with emibetuzumab in the trement of HCC. The results show that the combination of the two antibodies is safe and possesses the activity of inhibiting tumor cells. These studies indicate that emibetuzumab alone has significantly limited antitumor activity and may achieve better efficacy in combination with other antitumor drugs.

Yangbing Jin et al. (140) constructed a new c-Met antibody-drug conjugate, SR-A1403, for the targeted treatment of pancreatic ductal adenocarcinoma with high c-Met expression. Studies have shown that SR-A1403 can significantly inhibit the proliferation, migration and invasion of PC cells, and induce cell cycle arrest and apoptosis. These changes are caused by the inhibition of intracellular cholesterol biosynthesis by SR-A1403. The results illustrate that the SR-A1403-targeting c-Met shows strong preclinical antitumor efficacy in PC. At the same time, Alex Cazes et al. (141) constructed a newly developed antibody drug conjugation, TR1801-ADC, which conjugated a c-Met antibody to a potent pyrrole benzodiazepine toxin conjugation. This study tested TR1801-ADC *in vitro* in PC cell lines and evaluated its preclinical efficacy. Results showed that TR1801-ADC induced a specific cytotoxicity in PC cell lines and produced profound inhibition of tumor growth, even in gemcitabine-resistant tumors. These results reaffirm the importance of c-Met monoclonal antibody in combination with other drugs in treating DSTs.

The application of adoptive immunotherapy targeting c-Met in DSTs' treatment

Since the success of CD19-targeting CAR-T in B-cell-derived lymphomas and leukemias, adoptive immunotherapy for solid tumors has been extensively studied. Adoptive immunotherapy has not made a breakthrough in the treatment of solid tumors due to the heterogeneity of solid tumors and inhibitory tumor microenvironment. However, with the rapid development of gene editing technology, it is possible to modify CAR-T cells to adapt to the suppressive tumor microenvironment while enhancing the persistence of tumor killing. Preclinical studies of c-Met-targeting CAR-T in the treatment of DSTs have been conducted mainly in GC and HCC. Two clinical studies of HCC and solid tumor are currently underway in China (NCT03672305 and NCT03638206) in order to evaluate the efficacy and safety of c-Met CAR-T cells and c-Met/PD-L1 CAR -T cells in the treatment of solid tumors.

Nakajima et al. (142) found that c-Met overexpression in GC patients was associated with tumor invasion depth, lymph node metastasis and poor survival rate. Therefore, c-Met has become a potential target for CAR-T cell therapy in GC. Chung Hyo Kang et al. (143) constructed CAR-T cells targeting c-Met, and when incubated with c-Met positive GC cell lines, the secretion of IL-2 and IFN-γ was significantly higher than that of c-Met negative expression ones. Intratumor injection of c-Met CAR-T cells effectively inhibited tumor growth in the xenograft tumor model. In addition, Xingxing Yuan et al. (144) used c-Met-CAR-T cells combined with PD-1 monoclonal antibody in the treatment of GC. By blocking PD-1-PD-L1 binding, novel bifunctional CAR-T cells maintain cytotoxicity to PD-L1+ tumor cells. In tumor tissue, bifunctional CAR-T cells exhibit stronger antitumor ability and prolongation of survival in the PD-L1+ tumor xenograft model compared with c-Met-CAR-T cells. Considering the immunosuppressive microenvironment of solid tumors could inhibit CAR T-cells, our research group constructed c-Met-CAR-T cells for GC and added PD1/CD28 fusion receptor (CSR) to it, aiming to transfer the immunosuppressive signal caused by PD-1 into T cell activation signal (145). PD1/CD28 CSR was found to further enhance the killing capacity of c-Met CAR-T (especially its long-term antitumor effect) and reduce il-6 release levels. CAR-T cells targeting c-Met were found to have no significant off-target toxicity in normal organs. These *in vivo* studies demonstrate antitumor activity by intratumoral injection of c-Met CAR-T cells. On the one hand, local injection in the tumor is not suitable for the later clinical application. On the other hand, it is not conducive to the killing of peripheral circulation and metastatic tumor cells. Therefore, c-Met-CAR-T cells need gene editing to enhance their proliferative activity and persistence.

Wei Jiang et al. (146) constructed bi-specific CAR-T cells targeting c-Met and PD-L1 in the study of HCC. *In vitro* and *in vivo* studies showed that c-Met/PD-L1 CAR-T cells exhibited better antitumor activity against c-Met and PD-L1 positive HCC cells than c-Met CAR T cells or PD-L1 CAR-T cells. These studies also suggest that bi-specific c-Met/PDL1 CAR-T cells are feasible in current T cell engineering techniques. In addition, BING LIU1 et al. (147) constructed c-Met-targeted CAR-NK cells and evaluated their specificity and efficacy for HCC *in vitro*. The results of cytotoxicity assay showed that c-Met CAR-NK cells had stronger specific cytotoxicity against high c-Met expression HCC cell line HepG2. These results suggest that c-Met may be an effective target for adoptive immunotherapy of HCC.

Discussion

At present, c-Met small molecule inhibitors are widely used in the treatment of DSTs. Most of the preclinical studies showed

excellent tumor killing activity, while most patients with c-Met inhibitors alone had limited benefit in clinical studies. Significant improvements in overall survival have been found in several studies when combine c-Met small molecule inhibitors with other antitumor approaches (82, 83, 100, 115, 125). Emibetuzumab was combined with VEGFR-2 monoclonal antibody in treating advanced HCC patients (139). These results may be related to the signal activation mode of c-Met. c-Met could not only bind HGF and then activate downstream signals to promote tumor progression, but also activate downstream oncogenic pathways through molecular interactions with other oncogenic molecules. According to this signal activation mechanism, c-Met can target escape by activating interacting oncogenic molecules (EGFR, RON, etc). Yoshiaki Nakamura et al. (39) demonstrated that cetuximab induces MET gene mutation and amplification in advanced GC. Therefore, the treatment of DSTs should be individualized according to the specific expression of cancer-causing molecules, and multi-target therapy can be combined when necessary. Such a treatment strategy can be as seamless as possible to block the biological signals that promote tumor proliferation and metastasis. It is expected to make breakthrough progress in the treatment of DSTs.

At present, adoptive immunotherapy targeting c-Met is relatively rare in the treatment of digestive system, which is only limited to GC and HCC. Preclinical studies have confirmed its antitumor activity, and some clinical studies are ongoing. According to the c-Met signal activation theory, CAR-T cells targeting c-Met may also target escape in the treatment of DSTs. After all, target escape is one of the major challenges adoptive immunotherapy faces in treating solid tumors. Therefore, according to c-Met-CAR T cells and its interacting molecules, targeted therapies may achieve better clinical efficacy.

Furthermore, complications also limit the widespread clinical use of small-molecule inhibitors and monoclonal antibodies targeting c-Met. The study of tivantinib in metastatic HCC found 10 neutropenia and 8 anemia in 48 patients in the tivantinib group (78). Phase I adverse events related to SAR125844 in GC were also common in these patients (112). Onartuzumab was found to have serious adverse events in 55% of patients with GC, with edema and venous thromboembolism reported in all treated patients (134, 136). Therefore, it is necessary to investigate the risk factors for these complications, so as to pave the way for the application of c-Met targeted therapy in DSTs.

Conclusion

In conclusion, existing preclinical trials have demonstrated the potential of targeting c-Met for DSTs. The majority of clinical studies using targeted c-Met therapy alone have failed to achieve better efficacy in treating DSTs, while the combination of targeted c-Met therapy with other antitumor methods demonstrates its great potential. According to the biological function of c-Met in promoting tumor progression and inducing drug resistance, targeted therapy with c-Met and its associated oncogenic molecules should be explored to achieve better efficacy It is believed that with the optimization of c-Met targeted therapy, the treatment of DSTs will make a breakthrough.

Author contributions

All authors conceptualized and wrote the manuscript. ZZ and DL additionally performed literature and data analysis. All authors contributed to the article and approved the submitted version.

Funding

This study was funded by the Third Affiliated Hospital of Gansu University of Chinese Medicine (Project Approval Number: 2016YG-06) and Baiyin City 2019 Science and technology plan project (Project Approval Number: 2019-1-22Y).

Acknowledgments

Thanks to all the authors who participated in the design and data analysis of this paper, as well as the Third Affiliated Hospital of Gansu University of Traditional Chinese Medicine for providing convenience.

Conflict of interest

The authors declare that the research was conducted in the absence of any commercial or financial relationships that could be construed as a potential conflict of interest.

Publisher's note

References

1. Zuo C, Sheng X, Ma M, Xia M, Oouyan L. ISG15 in the tumorigenesis and treatment of cancer: An emerging role in malignancies of the digestive system. *Oncotarget* (2016) 7(45):74393–409. doi: 10.18632/oncotarget.11911

2. Ang C, Doyle E, Branch A. Bisphosphonates as potential adjuvants for patients with cancers of the digestive system. *World J Gastroenterol* (2016) 22 (3):906–16. doi: 10.3748/wjg.v22.i3.906

3. Jiang Z, Cai Z, Ma Q, Shen C, Yin Y, Yin X, et al. Comparative efficacy and safety of anti-HGF/MET pathway agents plus chemotherapy versus chemotherapy alone as first-line treatment in advanced gastric cancer: A protocol for a systematic review and meta-analysis. *BMJ Open* (2021) 11(12):e049575. doi: 10.1136/bmjopen-2021-049575

4. Bang YJ, Su WC, Schuler M, Nam DH, Lim WT, Bauer TM, et al. Phase 1 study of capmatinib in MET-positive solid tumor patients: Dose escalation and expansion of selected cohorts. *Cancer Sci* (2020) 111(2):536–47. doi: 10.1111/cas.14254

5. Gao Y, Chen MK, Chu YY, Yang L, Yu D, Liu Y, et al. Nuclear translocation of the receptor tyrosine kinase c-MET reduces the treatment efficacies of olaparib and gemcitabine in pancreatic ductal adenocarcinoma cells. *Am J Cancer Res* (2021) 11(1):236–50.

6. Delord JP, Argilés G, Fayette J, Wirth L, Kasper S, Siena S, et al. A phase 1b study of the MET inhibitor capmatinib combined with cetuximab in patients with MET-positive colorectal cancer who had progressed following anti-EGFR monoclonal antibody treatment. *Invest New Drugs* (2020) 38(6):1774–83. doi: 10.1007/s10637-020-00928-z

7. Weinberg RA. How cancer arises. *Sci Am* (1996) 275(3):62–70. doi: 10.1038/scientificamerican0996-62

8. Yang Y, Wang C, Dai C, Liu X, Li W, Huang M, et al. Amplification and expression of c-MET correlate with poor prognosis of patients with gastric cancer and upregulate the expression of PDL1. *Acta Biochim Biophys Sin* (2021) 53 (5):547–57. doi: 10.1093/abbs/gmab026

9. Tang Y, Xu H, Dai Y, Wang F, Huang W, Liu P, et al. A novel peptide targeting c-met for hepatocellular carcinoma diagnosis. *J Mater Chem B* (2021) 9 (22):4577–86. doi: 10.1039/D1TB00408E

10. Kiehne K, Herzig KH, Fölsch UR. C-met expression in pancreatic cancer and effects of hepatocyte growth factor on pancreatic cancer cell growth. *Pancreas* (1997) 15(1):35–40. doi: 10.1097/00006676-199707000-00005

11. Lai X, Dong Q, Xu F, Wu S, Yang D, Liu C, et al. Correlation of c-MET expression with clinical characteristics and the prognosis of colorectal cancer. *J Gastrointest Oncol* (2021) 12(5):2203–10. doi: 10.21037/jgo-21-536

12. Giubellino A, Linehan WM, Bottaro DP. Targeting the met signaling pathway in renal cancer. *Expert Rev Anticancer Ther* (2009) 9(6):785–93. doi: 10.1586/era.09.43

13. Ornstein DK, Lubensky IA, Venzon D, Zbar B, Linehan WM, Walther MM, et al. Prevalence of microscopic tumors in normal appearing renal parenchyma of patients with hereditary papillary renal cancer. *J Urol* (2000) 163(2):431–3. doi: 10.1016/S0022-5347(05)67893-7

14. Ponzo MG, Lesurf R, Petkiewicz S, O'Malley FP, Pinnaduwage D, Andrulis IL, et al. Met induces mammary tumors with diverse histologies and is associated with poor outcome and human basal breast cancer. *Proc Natl Acad Sci U S A* (2009) 106(31):12903–8. doi: 10.1073/pnas.0810402106

15. Hass R, Jennek S, Yang Y, Friedrich K. C-met expression and activity in urogenital cancers - novel aspects of signal transduction and medical implications. *Cell Commun Signal* (2017) 15(1):10. doi: 10.1186/s12964-017-0165-2

16. Boromand N, Hasanzadeh M, Shahidsales S, Farazestanian M, Gharib M, Fiuji H, et al. Clinical and prognostic value of the c-Met/HGF signaling pathway in cervical cancer. *J Cell Physiol* (2018) 233(6):4490–6. doi: 10.1002/jcp.26232

17. Hu CT, Wu JR, Cheng CC, Wu WS. The therapeutic targeting of HGF/c-met signaling in hepatocellular carcinoma: Alternative approaches. *Cancers (Basel)* (2017) 9(6):2. doi: 10.3390/cancers9060058

18. Furge KA, Zhang YW, Vande Woude GF. Met receptor tyrosine kinase: Enhanced signaling through adapter proteins. *Oncogene* (2000) 19(49):5582–9. doi: 10.1038/sj.onc.1203859

19. Mo HN, Liu P. Targeting MET in cancer therapy. *Chronic Dis Trans Med* (2017) 3(3):148–53. doi: 10.1016/j.cdtm.2017.06.002

20. Bradley CA, Salto-Tellez M, Laurent-Puig P, Bardelli A, Rolfo C, Tabernero J, et al. Targeting c-MET in gastrointestinal tumours: Rationale, opportunities and challenges. *Nat Rev Clin Oncol* (2017) 14(9):562–76. doi: 10.1038/nrclinonc.2017.40

21. Xu X, Zhu Y, Liang Z, Li S, Xu X, Wang X, et al. c-Met and CREB1 are involved in miR-433-mediated inhibition of the epithelial-mesenchymal transition in bladder cancer by regulating Akt/GSK-3β/Snail signaling. *Cell Death Dis* (2016) 7(2):e2088. doi: 10.1038/cddis.2015.274

22. Kim HJ, Yoon A, Ryu JY, Cho YJ, Choi JJ, Song SY, et al. C-MET as a potential therapeutic target in ovarian clear cell carcinoma. *Sci Rep* (2016) 6:38502. doi: 10.1038/srep38502

23. Demkova L, Kucerova L. Role of the HGF/c-MET tyrosine kinase inhibitors in metastasic melanoma. *Mol Cancer* (2018) 17(1):26. doi: 10.1186/s12943-018-0795-z

24. Wang W, Dong J, Wang M, Yao S, Tian X, Cui X, et al. miR-148a-3p suppresses epithelial ovarian cancer progression primarily by targeting c-met. *Oncol Lett* (2018) 15(5):6131–6. doi: 10.3892/ol.2018.8110

25. Pasquini G, Giaccone G. C-MET inhibitors for advanced non-small cell lung cancer. *Expert Opin Investig Drugs* (2018) 27(4):363–75. doi: 10.1080/13543784.2018.1462336

26. Wang MH, Yoshimura T, Skeel A, Leonard EJ. Proteolytic conversion of single chain precursor macrophage-stimulating protein to a biologically active heterodimer by contact enzymes of the coagulation cascade. *J Biol Chem* (1994) 269 (5):3436–40. doi: 10.1016/S0021-9258(17)41881-3

27. Zhu Y, Zhang H, Han X, Wang Z, Cui Y, Tian R, et al. STAT3 mediated upregulation of c-MET signaling acts as a compensatory survival mechanism upon EGFR family inhibition in chemoresistant breast cancer cells. *Cancer Lett* (2021) 519:328–42. doi: 10.1016/j.canlet.2021.07.048

28. Ruco LP, Ranalli T, Marzullo A, Bianco P, Prat M, Comoglio PM, et al. Expression of met protein in thyroid tumours. *J Pathol* (1996) 180(3):266–70. doi: 10.1002/(SICI)1096-9896(199611)180:3<266::AID-PATH658>3.0.CO;2-Q

29. Ponzetto C, Bardelli A, Zhen Z, Maina F, dalla Zonca P, Giordano S, et al. A multifunctional docking site mediates signaling and transformation by the hepatocyte growth factor/scatter factor receptor family. *Cell* (1994) 77(2):261–71. doi: 10.1016/0092-8674(94)90318-2

30. Maroun CR, Holgado-Madruga M, Royal I, Royal I, Naujokas MA, Fournier TM, et al. The Gab1 PH domain is required for localization of Gab1 at sites of cell-cell contact and epithelial morphogenesis downstream from the met receptor tyrosine kinase. *Mol Cell Biol* (1999) 19(3):1784–99. doi: 10.1128/MCB.19.3.1784

31. Schaeper U, Gehring NH, Fuchs KP, Sachs M, Kempkes B, Birchmeier W, et al. Coupling of Gab1 to c-met, Grb2, and Shp2 mediates biological responses. *J Cell Biol* (2000) 149(7):1419–32. doi: 10.1083/jcb.149.7.1419

32. Awad A, Gassama-Diagne A. PI3K/SHIP2/PTEN pathway in cell polarity and hepatitis c virus pathogenesis. *World J Hepatol* (2017) 9(1):18–29. doi: 10.4254/wjh.v9.i1.18

33. Gual P, Giordano S, Williams TA, Rocchi S, Van Obberghen E, Comoglio PM, et al. Sustained recruitment of phospholipase c-gamma to Gab1 is required for HGF-induced branching tubulogenesis. *Oncogene* (2000) 19(12):1509–18. doi: 10.1038/sj.onc.1203514

34. Maroun CR, Naujokas MA, Holgado-Madruga M, Wong AJ, Park M. The tyrosine phosphatase SHP-2 is required for sustained activation of extracellular signal-regulated kinase and epithelial morphogenesis downstream from the met receptor tyrosine kinase. *Mol Cell Biol* (2000) 20(22):8513–25. doi: 10.1128/MCB.20.22.8513-8525.2000

35. Boccaccio C, Comoglio PM. Invasive growth: A MET-driven genetic programme for cancer and stem cells. *Nat Rev Cancer* (2006) 6(8):637–45. doi: 10.1038/nrc1912

36. Zhang YW, Vande Woude GF. HGF/SF-met signaling in the control of branching morphogenesis and invasion. *J Cell Biochem* (2003) 88(2):408–17. doi: 10.1002/jcb.10358

37. Rosário M, Birchmeier W. How to make tubes: Signaling by the met receptor tyrosine kinase. *Trends Cell Biol* (2003) 13(6):328–35. doi: 10.1016/S0962-8924(03)00104-1

38. Jo M, Stolz DB, Esplen JE, Dorko K, Michalopoulos GK, Strom SC, et al. Cross-talk between epidermal growth factor receptor and c-met signal pathways in transformed cells. *J Biol Chem* (2000) 275(12):8806–11. doi: 10.1074/jbc.275.12.8806

39. Nakamura Y, Sasaki A, Yukami H, Jogo T, Kawazoe A, Kuboki Y, et al. Emergence of concurrent multiple EGFR mutations and MET amplification in a patient with EGFR-amplified advanced gastric cancer treated with cetuximab. *JCO Precis Oncol* (2020) 4:PO.20.00263. doi: 10.1200/PO.20.00263

40. Wang Q, Yang S, Wang K, Sun SY. MET inhibitors for targeted therapy of EGFR TKI-resistant lung cancer. *J Hematol Oncol* (2019) 12(1):63. doi: 10.1186/s13045-019-0759-9

41. Dong Q, Du Y, Li H, Liu C, Wei Y, Chen MK, et al. EGFR and c-MET cooperate to enhance resistance to PARP inhibitors in hepatocellular carcinoma. *Cancer Res* (2019) 79(4):819–29. doi: 10.1158/0008-5472.CAN-18-1273

42. Bean J, Brennan C, Shih JY, Riely G, Viale A, Wang L, et al. MET amplification occurs with or without T790M mutations in EGFR mutant lung

tumors with acquired resistance to gefitinib or erlotinib. *Proc Natl Acad Sci U S A* (2007) 104(52):20932–7. doi: 10.1073/pnas.0710370104

43. Engelman JA, Zejnullahu K, Mitsudomi T, Song Y, Hyland C, Park JO, et al. MET amplification leads to gefitinib resistance in lung cancer by activating ERBB3 signaling. *Science (New York NY)* (2007) 316(5827):1039–43. doi: 10.1126/science.1141478

44. Sohn J, Liu S, Parinyanitikul N, Lee J, Hortobagyi GN, Mills GB, et al. cMET activation and EGFR-directed therapy resistance in triple-negative breast cancer. *J Cancer* (2014) 5(9):745–53. doi: 10.7150/jca.9696

45. Bhatt AS, Welm A, Farady CJ, Vásquez M, Wilson K, Craik CS, et al. Coordinate expression and functional profiling identify an extracellular proteolytic signaling pathway. *Proc Natl Acad Sci U S A* (2007) 104(14):5771–6. doi: 10.1073/pnas.0606514104

46. Waltz SE, Mcdowell SA, Muraoka RS, Air EL, Fuck LM, Chen YQ, et al. Functional characterization of domains contained in hepatocyte growth factor-like protein. *J Biol Chem* (1997) 272(48):30526–37. doi: 10.1074/jbc.272.48.30526

47. Lu Y, Yao HP, Wang MH. Multiple variants of the RON receptor tyrosine kinase: Biochemical properties, tumorigenic activities, and potential drug targets. *Cancer Lett* (2007) 257(2):157–64. doi: 10.1016/j.canlet.2007.08.007

48. Zhao S, Cao L, Freeman JW. Knockdown of RON receptor kinase delays but does not prevent tumor progression while enhancing HGF/MET signaling in pancreatic cancer cell lines. *Oncogenesis* (2013) 2(10):e76. doi: 10.1038/oncsis.2013.36

49. Klempner SJ, Borghei A, Hakimian B, Ali SM, Ou SI., et al. Intracranial activity of cabozantinib in MET exon 14-positive NSCLC with brain metastases. *J Thorac Oncol* (2017) 12(1):152–6. doi: 10.1016/j.jtho.2016.09.127

50. Tuck AB, Park M, Sterns EE, Boag A, Elliott BE, et al. Coexpression of hepatocyte growth factor and receptor (Met) in human breast carcinoma. *Am J Pathol* (1996) 148(1):225–32.

51. Yap TA, Sandhu SK, Alam SM, De Bono JS, et al. HGF/c-MET targeted therapeutics: Novel strategies for cancer medicine. *Curr Drug Targets* (2011) 12 (14):2045–58. doi: 10.2174/138945011798829348

52. Szturz P, Raymond E, Abitbol C, Albert S, de Gramont A, Faivre S, et al. Understanding c-MET signalling in squamous cell carcinoma of the head & neck. *Crit Rev Oncol Hematol* (2017), 39–51. doi: 10.1016/j.critrevonc.2017.01.004

53. Michikoshi H, Nakamura T, Sakai K, Suzuki Y, Adachi E, Matsugo S, et al. α-lipoic acid-induced inhibition of proliferation and met phosphorylation in human non-small cell lung cancer cells. *Cancer Lett* (2013) 335(2):472–8. doi: 10.1016/j.canlet.2013.03.008

54. Hartmann S, Bhola NE, Grandis JR. HGF/Met signaling in head and neck cancer: Impact on the tumor microenvironment. *Clin Cancer Res* (2016) 22 (16):4005–13. doi: 10.1158/1078-0432.CCR-16-0951

55. Balan M, Mier Y Teran E, Waaga-Gasser AM, Gasser M, Choueiri TK, Freeman G, et al. Novel roles of c-met in the survival of renal cancer cells through the regulation of HO-1 and PD-L1 expression. *J Biol Chem* (2015) 290(13):8110–20. doi: 10.1074/jbc.M114.612689

56. Basile JR, Afkhami T, Gutkind JS. Semaphorin 4D/plexin-B1 induces endothelial cell migration through the activation of PYK2, src, and the phosphatidylinositol 3-kinase-Akt pathway. *Mol Cell Biol* (2005) 25(16):6889–98. doi: 10.1128/MCB.25.16.6889-6898.2005

57. Gherardi E, Sandin S, Petoukhov MV, Finch J, Youles ME, Ofverstedt LG, et al. Structural basis of hepatocyte growth factor/scatter factor and MET signalling. *Proc Natl Acad Sci U S A* (2006) 103(11):4046–51. doi: 10.1073/pnas.0509040103

58. Ma PC, Kijima T, Maulik G, Fox EA, Sattler M, Griffin JD, et al. C-MET mutational analysis in small cell lung cancer: novel juxtamembrane domain mutations regulating cytoskeletal functions. *Cancer Res* (2003) 63(19):6272–81.

59. Dulak AM, Gubish CT, Stabile LP, Henry C, Siegfried JM. HGF-independent potentiation of EGFR action by c-met. *Oncogene* (2011) 30 (33):3625–35. doi: 10.1038/onc.2011.84

60. Stabile LP, Rothstein ME, Keohavong P, Jin Yin J, Land SR, et al. Therapeutic targeting of human hepatocyte growth factor with a single neutralizing monoclonal antibody reduces lung tumorigenesis. *Mol Cancer Ther* (2008) 7(7):1913–22. doi: 10.1158/1535-7163.MCT-07-2169

61. Bauer TW, Somcio RJ, Fan F, Liu W, Johnson M, Lesslie DP, et al. Regulatory role of c-met in insulin-like growth factor-I receptor-mediated migration and invasion of human pancreatic carcinoma cells. *Mol Cancer Ther* (2006) 5(7):1676–82. doi: 10.1158/1535-7163.MCT-05-0175

62. Cooke VG, Lebleu VS, Keskin D, Khan Z, O'Connell JT, Teng Y, et al. Pericyte depletion results in hypoxia-associated epithelial-to-mesenchymal transition and metastasis mediated by met signaling pathway. *Cancer Cell* (2012) 21(1):66–81. doi: 10.1016/j.ccr.2011.11.024

63. Lee SJ, Lee J, Sohn I, Mao M, Kai W, Park CK, et al. A survey of c-MET expression and amplification in 287 patients with hepatocellular carcinoma. *Anticancer Res* (2013) 33(11):5179–86.

64. Comoglio PM, Giordano S, Trusolino L. Drug development of MET inhibitors: Targeting oncogene addiction and expedience. *Nat Rev Drug Discov* (2008) 7(6):504–16. doi: 10.1038/nrd2530

65. Yu J, Ohuchida K, Mizumoto K, Ishikawa N, Ogura Y, Yamada D, et al. Overexpression of c-met in the early stage of pancreatic carcinogenesis; altered expression is not sufficient for progression from chronic pancreatitis to pancreatic cancer. *World J Gastroenterol* (2006) 12(24):3878–82. doi: 10.3748/wjg.v12.i24.3878

66. Liu X, Newton RC, Scherle PA. Developing c-MET pathway inhibitors for cancer therapy: Progress and challenges. *Trends Mol Med* (2010) 16(1):37–45. doi: 10.1016/j.molmed.2009.11.005

67. Hara T, Ooi A, Kobayashi M, Mai M, Yanagihara K, Nakanishi I. Amplification of c-myc, K-sam, and c-met in gastric cancers: Detection by fluorescence *in situ* hybridization. *Lab Invest J Tech Methods Pathol* (1998) 78 (9):1143–53.

68. Lordick F, Kang YK, Chung HC, Salman P, Oh SC, Bodoky G, et al. Capecitabine and cisplatin with or without cetuximab for patients with previously untreated advanced gastric cancer (EXPAND): A randomised, open-label phase 3 trial. *Lancet Oncol* (2013) 14(6):490–9. doi: 10.1016/S1470-2045(13)70102-5

69. Park CH, Cho SY, Ha JD, Jung H, Kim HR, Lee CO , et al. Novel c-met inhibitor suppresses the growth of c-met-addicted gastric cancer cells. *BMC Cancer* (2016) 16:35. doi: 10.1186/s12885-016-2058-y

70. He CX, Ai J, Xing WQ, Chen Y, Zhang HT, Huang M, et al. Yhhu3813 is a novel selective inhibitor of c-met kinase that inhibits c-met-dependent neoplastic phenotypes of human cancer cells. *Acta Pharmacol Sin* (2014) 35(1):89–97. doi: 10.1038/aps.2013.125

71. Balan M, Chakraborty S, Flynn E, Zurakowski D, Pal S. Honokiol inhibits c-Met-HO-1 tumor-promoting pathway and its cross-talk with calcineurin inhibitor-mediated renal cancer growth. *Sci Rep* (2017) 7(1):5900. doi: 10.1038/s41598-017-05455-1

72. Hsieh YS, Liao CH, Chen WS, Pai JT, Weng MS. Shikonin inhibited migration and invasion of human lung cancer cells *via* suppression of c-met-mediated epithelial-to-mesenchymal transition. *J Cell Biochem* (2017) 118 (12):4639–51. doi: 10.1002/jcb.26128

73. Wang L, Ai J, Shen Y, Zhang H, Peng X, Huang M, et al. SOMCL-863, a novel, selective and orally bioavailable small-molecule c-met inhibitor, exhibits antitumor activity both *in vitro* and *in vivo*. *Cancer Lett* (2014) 351(1):143–50. doi: 10.1016/j.canlet.2014.05.012

74. Sung H, Ferlay J, Siegel RL, Laversanne M, Soerjomataram I, Jemal A, et al. Global cancer statistics 2020: GLOBOCAN estimates of incidence and mortality worldwide for 36 cancers in 185 countries. *CA Cancer J Clin* (2021) 71(3):209–49. doi: 10.3322/caac.21660

75. Goyal L, Muzumdar MD, Zhu AX. Targeting the HGF/c-MET pathway in hepatocellular carcinoma. *Clin Cancer Res* (2013) 19(9):2310–8. doi: 10.1158/1078-0432.CCR-12-2791

76. Ueki T, Fujimoto J, Suzuki T, Yamamoto H, Okamoto E. Expression of hepatocyte growth factor and its receptor c-met proto-oncogene in hepatocellular carcinoma. *Hepatology (Baltimore Md)* (1997) 25(4):862–6. doi: 10.1002/hep.510250413

77. Porta C, Giglione P, Ferrari A, Reversi F, Liguigli W, Imarisio I, et al. Tivantinib (ARQ197) in hepatocellular carcinoma. *Expert Rev Anticancer Ther* (2015) 15(6):615–22. doi: 10.1586/14737140.2015.1050383

78. Santoro A, Rimassa L, Borbath I, Daniele B, Salvagni S, van Laethem JL, et al. Tivantinib for second-line treatment of advanced hepatocellular carcinoma: A randomised, placebo-controlled phase 2 study. *Lancet Oncol* (2013) 14(1):55–63. doi: 10.1016/S1470-2045(12)70490-4

79. Rimassa L, Assenat E, Peck-Radosavljevic M, Pracht M, Zagonel V, Mathurin P, et al. Tivantinib for second-line treatment of MET-high, advanced hepatocellular carcinoma (METIV-HCC): A final analysis of a phase 3, randomised, placebo-controlled study. *Lancet Oncol* (2018) 19(5):682–93. doi: 10.1016/S1470-2045(18)30146-3

80. Kuczynski EA, Lee CR, Man S, Chen E, Kerbel RS. Effects of sorafenib dose on acquired reversible resistance and toxicity in hepatocellular carcinoma. *Cancer Res* (2015) 75(12):2510–9. doi: 10.1158/0008-5472.CAN-14-3687

81. Llovet JM, Ricci S, Mazzaferro V, Hilgard P, Gane E, Blanc JF, et al. Sorafenib in advanced hepatocellular carcinoma. *N Engl J Med* (2008) 359(4):378–90. doi: 10.1056/NEJMoa0708857

82. Jiang X, Feng K, Zhang Y, Li Z, Zhou F, Dou H, et al. Sorafenib and DE605, a novel c-met inhibitor, synergistically suppress hepatocellular carcinoma. *Oncotarget* (2015) 6(14):12340–56. doi: 10.18632/oncotarget.3656

83. He M, Li Q, Zou R, Shen J, Fang W, Tan G, et al. Sorafenib plus hepatic arterial infusion of oxaliplatin, fluorouracil, and leucovorin vs sorafenib alone for hepatocellular carcinoma with portal vein invasion: A randomized clinical trial. *JAMA Oncol* (2019) 5(7):953–60. doi: 10.1001/jamaoncol.2019.0250

84. Bladt F, Faden B, Friese-Hamim M, Knuehl C, Wilm C, Fittschen C, et al. EMD 1214063 and EMD 1204831 constitute a new class of potent and highly selective c-met inhibitors. *Clin Cancer Res* (2013) 19(11):2941–51. doi: 10.1158/1078-0432.CCR-12-3247

85. Ryoo BY, Cheng AL, Ren Z, Kim TY, Pan H, Rau KM, et al. Randomised phase 1b/2 trial of tepotinib vs sorafenib in Asian patients with advanced hepatocellular carcinoma with MET overexpression. *Br J Cancer* (2021) 125 (2):200–8. doi: 10.1038/s41416-021-01380-3

86. Decaens T, Barone C, Assenat E, Wermke M, Fasolo A, Merle P, et al. Phase 1b/2 trial of tepotinib in sorafenib pretreated advanced hepatocellular carcinoma with MET overexpression. *Br J Cancer* (2021) 125(2):190–9. doi: 10.1038/s41416-021-01334-9

87. Inagaki Y, Qi F, Gao J, Qu X, Hasegawa K, Sugawara Y, et al. Effect of c-met inhibitor SU11274 on hepatocellular carcinoma cell growth. *Biosci Trends* (2011) 5 (2):52–6. doi: 10.5582/bst.2011.v5.2.52

88. Huynh H, Ong R, Soo KC. Foretinib demonstrates anti-tumor activity and improves overall survival in preclinical models of hepatocellular carcinoma. *Angiogenesis* (2012) 15(1):59–70. doi: 10.1007/s10456-011-9243-z

89. Nakagawa T, Tohyama O, Yamaguchi A, Matsushima T, Takahashi K, Funasaka S, et al. E7050: A dual c-met and VEGFR-2 tyrosine kinase inhibitor promotes tumor regression and prolongs survival in mouse xenograft models. *Cancer Sci* (2010) 101(1):210–5. doi: 10.1111/j.1349-7006.2009.01343.x

90. Xiang Q, Chen W, Ren M, Wang J, Zhang H, Deng DY, et al. Cabozantinib suppresses tumor growth and metastasis in hepatocellular carcinoma by a dual blockade of VEGFR2 and MET. *Clin Cancer Res* (2014) 20(11):2959–70. doi: 10.1158/1078-0432.CCR-13-2620

91. Nones K, Waddell N, Song S, Patch AM, Miller D, Johns A , et al. Genome-wide DNA methylation patterns in pancreatic ductal adenocarcinoma reveal epigenetic deregulation of SLIT-ROBO, ITGA2 and MET signaling. *Int J Cancer* (2014) 135(5):1110–8. doi: 10.1002/ijc.28765

92. Waddell N, Pajic M, Patch AM, Chang DK, Kassahn KS, Bailey P, et al. Whole genomes redefine the mutational landscape of pancreatic cancer. *Nature* (2015) 518(7540):495–501. doi: 10.1038/nature14169

93. Chen ST, Kuo TC, Liao YY, Lin MC, Tien YW, Huang MC. Silencing of MUC20 suppresses the malignant character of pancreatic ductal adenocarcinoma cells through inhibition of the HGF/MET pathway. *Oncogene* (2018) 37(46):6041–53. doi: 10.1038/s41388-018-0403-0

94. Li C, Wu JJ, Hynes M, Dosch J, Sarkar B, Welling TH, et al. C-met is a marker of pancreatic cancer stem cells and therapeutic target. *Gastroenterology* (2011) 141(6):2218–27.e5. doi: 10.1053/j.gastro.2011.08.009

95. Rahbari M, Rahbari N, Reissfelder C, Weitz J, Kahlert C. Exosomes: Novel implications in diagnosis and treatment of gastrointestinal cancer. *Langenbecks Arch Surg* (2016) 401(8):1097–110. doi: 10.1007/s00423-016-1468-2

96. Siegel RL, Miller KD, Jemal A. Cancer statistics, 2016. *CA Cancer J Clin* (2016) 66(1):7–30. doi: 10.3322/caac.21332

97. Di Renzo MF, Poulsom R, Olivero M, Comoglio PM, Lemoine NR. Expression of the met/hepatocyte growth factor receptor in human pancreatic cancer. *Cancer Res* (1995) 55(5):1129–38.

98. Xu J, Liu S, Yang X, Cao S, Zhou Y. Paracrine HGF promotes EMT and mediates the effects of PSC on chemoresistance by activating c-Met/PI3K/Akt signaling in pancreatic cancer *in vitro*. *Life Sci* (2020) 263:118523. doi: 10.1016/j.lfs.2020.118523

99. Firuzi O, Che PP, El Hassouni B, Buijs M, Coppola S, Löhr M, et al. Role of c-MET inhibitors in overcoming drug resistance in spheroid models of primary human pancreatic cancer and stellate cells. *Cancers (Basel)* (2019) 11(5):6. doi: 10.3390/cancers11050638

100. Xu Z, Pang TCY, Liu AC, Pothula SP, Mekapogu AR, Perera CJ, et al. Targeting the HGF/c-MET pathway in advanced pancreatic cancer: A key element of treatment that limits primary tumour growth and eliminates metastasis. *Br J Cancer* (2020) 122(10):1486–95. doi: 10.1038/s41416-020-0782-1

101. Mori S, Akita H, Kobayashi S, Iwagami Y, Yamada D, Tomimaru Y, et al. Inhibition of c-MET reverses radiation-induced malignant potential in pancreatic cancer. *Cancer Lett* (2021) 512:51–9. doi: 10.1016/j.canlet.2021.04.029

102. Takiguchi S, Inoue K, Matsusue K, Furukawa M, Teramoto N, Iguchi H. Crizotinib, a MET inhibitor, prevents peritoneal dissemination in pancreatic cancer. *Int J Oncol* (2017) 51(1):184–92. doi: 10.3892/ijo.2017.3992

103. Li E, Huang X, Zhang G, Liang T. Combinational blockade of MET and PD-L1 improves pancreatic cancer immunotherapeutic efficacy. *J Exp Clin Cancer Res* (2021) 40(1):279. doi: 10.1186/s13046-021-02055-w

104. Goscinski MA, Larsen SG, Warloe T, Stoldt S, Nesland JM, Suo ZH, et al. Adenocarcinomas on the rise–does it influence survival from oesophageal cancer? *Scand J Surg* (2009) 98(4):214–20. doi: 10.1177/145749690909800404

105. Huang TJ, Wang JY, Lin SR, Lian ST, Hsieh JS. Overexpression of the c-met protooncogene in human gastric carcinoma–correlation to clinical features. *Acta Oncol (Stockholm Sweden)* (2001) 40(5):638–43. doi: 10.1080/02841860170444204

106. Fuse N, Kuboki Y, Kuwata T, Nishina T, Kadowaki S, Shinozaki E, et al. Prognostic impact of HER2, EGFR, and c-MET status on overall survival of advanced gastric cancer patients. *Gastric Cancer* (2016) 19(1):183–91. doi: 10.1007/s10120-015-0471-6

107. Metzger ML, Behrens HM, Böger C, Haag J, Krüger S, Röcken C. MET in gastric cancer–discarding a 10% cutoff rule. *Histopathology* (2016) 68(2):241–53. doi: 10.1111/his.12745

108. Liao H, Tian T, Sheng Y, Peng Z, Li Z, Wang J, et al. The significance of MET expression and strategies of targeting MET treatment in advanced gastric cancer. *Front Oncol* (2021) 11:719217. doi: 10.3389/fonc.2021.719217

109. Gavine PR, Ren Y, Han L, Lv J, Fan S, Zhang W, et al. Volitinib, a potent and highly selective c-met inhibitor, effectively blocks c-met signaling and growth in c-MET amplified gastric cancer patient-derived tumor xenograft models. *Mol Oncol* (2015) 9(1):323–33. doi: 10.1016/j.molonc.2014.08.015

110. Kim BJ, Kim YJ, Sohn SH, Kim B, Sul HJ, Kim HS, et al. Tivantinib inhibits the VEGF signaling pathway and induces apoptosis in gastric cancer cells with c-MET or VEGFA amplification. *Invest New Drugs* (2020) 38(6):1633–40. doi: 10.1007/s10637-020-00940-3

111. Kang YK, Muro K, Ryu MH, Yasui H, Nishina T, Ryoo BY, et al. A phase II trial of a selective c-met inhibitor tivantinib (ARQ 197) monotherapy as a second- or third-line therapy in the patients with metastatic gastric cancer. *Invest New Drugs* (2014) 32(2):355–61. doi: 10.1007/s10637-013-0057-2

112. Shitara K, Kim TM, Yokota T, Goto M, Satoh T, Ahn JH, et al. Phase I dose-escalation study of the c-met tyrosine kinase inhibitor SAR125844 in Asian patients with advanced solid tumors, including patients with MET-amplified gastric cancer. *Oncotarget* (2017) 8(45):79546–55. doi: 10.18632/oncotarget.18554

113. Sohn SH, Sul HJ, Kim B, Kim BJ, Kim HS, Zang DY. Tepotinib inhibits the epithelial-mesenchymal transition and tumor growth of gastric cancers by increasing GSK3β, e-cadherin, and mucin 5AC and 6 levels. *Int J Mol Sci* (2020) 21(17):7. doi: 10.3390/ijms21176027

114. Shitara K, Yamazaki K, Tsushima T, Naito T, Matsubara N, Watanabe M, et al. Phase I trial of the MET inhibitor tepotinib in Japanese patients with solid tumors. *Jpn J Clin Oncol* (2020) 50(8):859–66. doi: 10.1093/jjco/hyaa042

115. Yashiro M, Nishii T, Hasegawa T, Matsuzaki T, Morisaki T, Fukuoka T, et al. A c-met inhibitor increases the chemosensitivity of cancer stem cells to the irinotecan in gastric carcinoma. *Br J Cancer* (2013) 109(10):2619–28. doi: 10.1038/bjc.2013.638

116. Toiyama Y, Yasuda H, Saigusa S, Matushita K, Fujikawa H, Tanaka K, et al. Co-Expression of hepatocyte growth factor and c-met predicts peritoneal dissemination established by autocrine hepatocyte growth factor/c-met signaling in gastric cancer. *Int J Cancer* (2012) 130(12):2912–21. doi: 10.1002/ijc.26330

117. Hong SW, Jung KH, Park BH, Zheng HM, Lee HS, Choi MJ, et al. KRC-408, a novel c-met inhibitor, suppresses cell proliferation and angiogenesis of gastric cancer. *Cancer Lett* (2013) 332(1):74–82. doi: 10.1016/j.canlet.2013.01.015

118. Wang Y, Zhan Z, Jiang X, Peng X, Shen Y, Chen F, et al. Simm530, a novel and highly selective c-met inhibitor, blocks c-met-stimulated signaling and neoplastic activities. *Oncotarget* (2016) 7(25):38091–104. doi: 10.18632/oncotarget.9349

119. Tsilimigras DI, Ntanasis-Stathopoulos I, Bagante F, Moris D, Cloyd J, Spartalis E, et al. Clinical significance and prognostic relevance of KRAS, BRAF, PI3K and TP53 genetic mutation analysis for resectable and unresectable colorectal liver metastases: A systematic review of the current evidence. *Surg Oncol* (2018) 27 (2):280–8. doi: 10.1016/j.suronc.2018.05.012

120. Jia Y, Dai G, Wang J, Gao X, Zhao Z, Duan Z, et al. C-MET inhibition enhances the response of the colorectal cancer cells to irradiation *in vitro* and *in vivo*. *Oncol Lett* (2016) 11(4):2879–85. doi: 10.3892/ol.2016.4303

121. Liu C, Park M, Tsao MS. Overexpression of c-met proto-oncogene but not epidermal growth factor receptor or c-erbB-2 in primary human colorectal carcinomas. *Oncogene* (1992) 7(1):181–5.

122. Takeuchi H, Bilchik A, Saha S, Turner R, Wiese D, Tanaka M, et al. C-MET expression level in primary colon cancer: A predictor of tumor invasion and lymph node metastases. *Clin Cancer Res* (2003) 9(4):1480–8.

123. Du F, Li X, Feng W, Qiao C, Chen J, Jiang M, et al. SOX13 promotes colorectal cancer metastasis by transactivating SNAI2 and c-MET. *Oncogene* (2020) 39(17):3522–40. doi: 10.1038/s41388-020-1233-4

124. Cuneo KC, Mehta RK, Kurapati H, Thomas DG, Lawrence TS, Nyati MK. Enhancing the radiation response in KRAS mutant colorectal cancers using the c-met inhibitor crizotinib. *Trans Oncol* (2019) 12(2):209–16. doi: 10.1016/j.tranon.2018.10.005

125. Eng C, Bessudo A, Hart LL, Severtsev A, Gladkov O, Müller L, et al. A randomized, placebo-controlled, phase 1/2 study of tivantinib (ARQ 197) in combination with irinotecan and cetuximab in patients with metastatic

colorectal cancer with wild-type KRAS who have received first-line systemic therapy. *Int J Cancer* (2016) 139(1):177–86. doi: 10.1002/ijc.30049

126. Gao SH, Liu C, Wei J, Feng Y. Effect of c-met inhibitor SU11274 on human colon cancer cell growth. *Chin Med J* (2013) 126(14):2705–9.

127. Gao W, Bing X, Li M, Yang Z, Li Y, Chen H. Study of critical role of c-met and its inhibitor SU11274 in colorectal carcinoma. *Med Oncol (Northwood London Engl)* (2013) 30(2):546. doi: 10.1007/s12032-013-0546-3

128. Qiu P, Wang S, Liu M, Ma H, Zeng X, Zhang M, et al. Norcantharidin inhibits cell growth by suppressing the expression and phosphorylation of both EGFR and c-met in human colon cancer cells. *BMC Cancer* (2017) 17(1):55. doi: 10.1186/s12885-016-3039-x

129. Mo L, Zhang X, Shi X, Wei L, Zheng D, Li H, et al. Norcantharidin enhances antitumor immunity of GM-CSF prostate cancer cells vaccine by inducing apoptosis of regulatory T cells. *Cancer Sci* (2018) 109(7):2109–18. doi: 10.1111/cas.13639

130. Catenacci DV, Henderson L, Xiao SY, Patel P, Yauch RL, Hegde P, et al. Durable complete response of metastatic gastric cancer with anti-met therapy followed by resistance at recurrence. *Cancer Discov* (2011) 1(7):573–9. doi: 10.1158/2159-8290.CD-11-0175

131. Surati M, Patel P, Peterson A, Salgia R. Role of MetMAb (OA-5D5) in c-MET active lung malignancies. *Expert Opin Biol Ther* (2011) 11(12):1655–62. doi: 10.1517/14712598.2011.626762

132. Spigel DR, Ervin TJ, Ramlau RA, Daniel DB, Goldschmidt JH, Blumenschein GR, et al. Randomized phase II trial of onartuzumab in combination with erlotinib in patients with advanced non-small-cell lung cancer. *J Clin Oncol* (2013) 31(32):4105–14. doi: 10.1200/JCO.2012.47.4189

133. Salgia R, Patel P, Bothos J, Yu W, Eppler S, Hegde P, et al. Phase I dose-escalation study of onartuzumab as a single agent and in combination with bevacizumab in patients with advanced solid malignancies. *Clin Cancer Res* (2014) 20(6):1666–75. doi: 10.1158/1078-0432.CCR-13-2070

134. Shah MA, Cho JY, Tan IB, Tebbutt NC, Yen CJ, Kang A, et al. A randomized phase ii study of FOLFOX with or without the MET inhibitor onartuzumab in advanced adenocarcinoma of the stomach and gastroesophageal junction. *Oncologist* (2016) 21(9):1085–90. doi: 10.1634/theoncologist.2016-0038

135. Shah MA, Bang YJ, Lordick F, Alsina M, Chen M, Hack SP, et al. Effect of fluorouracil, leucovorin, and oxaliplatin with or without onartuzumab in HER2-negative, MET-positive gastroesophageal adenocarcinoma: The MET gastric randomized clinical trial. *JAMA Oncol* (2017) 3(5):620–7. doi: 10.1001/jamaoncol.2016.5580

136. Morley R, Cardenas A, Hawkins P, Suzuki Y, Paton V, Phan SC, et al. Safety of onartuzumab in patients with solid tumors: Experience to date from the onartuzumab clinical trial program. *PloS One* (2015) 10(10):e0139679. doi: 10.1371/journal.pone.0139679

137. Yan SB, Um SL, Peek VL, Stephens JR, Zeng W, Konicek BW, et al. MET-targeting antibody (emibetuzumab) and kinase inhibitor (merestinib) as single agent or in combination in a cancer model bearing MET exon 14 skipping. *Invest New Drugs* (2018) 36(4):536–44. doi: 10.1007/s10637-017-0545-x

138. Sakai D, Chung HC, Oh DY, Park SH, Kadowaki S, Kim YH, et al. A non-randomized, open-label, single-arm, phase 2 study of emibetuzumab in Asian patients with MET diagnostic positive, advanced gastric cancer. *Cancer Chemother Pharmacol* (2017) 80(6):1197–207. doi: 10.1007/s00280-017-3445-z

139. Harding JJ, Zhu AX, Bauer TM, Choueiri TK, Drilon A, Voss MH, et al. A phase Ib/II study of ramucirumab in combination with emibetuzumab in patients with advanced cancer. *Clin Cancer Res* (2019) 25(17):5202–11. doi: 10.1158/1078-0432.CCR-18-4010

140. Jin Y, Zhang Z, Zou S, Li F, Chen H, Peng C, et al. A novel c-MET-targeting antibody-drug conjugate for pancreatic cancer. *Front Oncol* (2021) 11:634881. doi: 10.3389/fonc.2021.634881

141. Cazes A, Betancourt O, Esparza E, Mose ES, Jaquish D, Wong E, et al. A MET targeting antibody-drug conjugate overcomes gemcitabine resistance in pancreatic cancer. *Clin Cancer Res* (2021) 27(7):2100–10. doi: 10.1158/1078-0432.CCR-20-3210

142. Nakajima M, Sawada H, Yamada Y, Watanabe A, Tatsumi M, Yamashita J, et al. The prognostic significance of amplification and overexpression of c-met and c-erb b-2 in human gastric carcinomas. *Cancer* (1999) 85 (9):1894–902. doi: 10.1002/(SICI)1097-0142(19990501)85:9<1894::AID-CNCR3>3.0.CO;2-J

143. Kang CH, Kim Y, Lee DY, Choi SU, Lee HK, Park CH. C-Met-Specific chimeric antigen receptor T cells demonstrate anti-tumor effect in c-met positive gastric cancer. *Cancers (Basel)* (2021) 13(22):9. doi: 10.3390/cancers13225738

144. Yuan X, Sun Z, Yuan Q, Hou W, Liang Q, Wang Y, et al. Dual-function chimeric antigen receptor T cells targeting c-met and PD-1 exhibit potent anti-tumor efficacy in solid tumors. *Invest New Drugs* (2021) 39(1):34–51. doi: 10.1007/s10637-020-00978-3

145. Chen C, Gu YM, Zhang F, Zhang ZC, Zhang YT, He YD, et al. Construction of PD1/CD28 chimeric-switch receptor enhances anti-tumor ability of c-met CAR-T in gastric cancer. *Oncoimmunology* (2021) 10 (1):1901434. doi: 10.1080/2162402X.2021.1901434

146. Jiang W, Li T, Guo J, Wang J, Jia L, Shi X, et al. Bispecific c-Met/PD-L1 CAR-T cells have enhanced therapeutic effects on hepatocellular carcinoma. *Front Oncol* (2021) 11:546586. doi: 10.3389/fonc.2021.546586

147. Liu B, Liu ZZ, Zhou ML, Lin JW, Chen XM, Li Z, et al. Development of c–Met –specific chimeric antigen receptor–engineered natural killer cells with cytotoxic effects on human liver cancer HepG2 cells. *Mol Med Rep* (2019) 20(3):2823–31. doi: 10.3892/mmr.2019.10529

frontiers | Frontiers in Oncology

TYPE Hypothesis and Theory
PUBLISHED 29 November 2022
DOI 10.3389/fonc.2022.906197

OPEN ACCESS

EDITED BY
Yan-yan Yan,
Shanxi Datong University, China

REVIEWED BY
Luis E. Arias-Romero,
National Autonomous University of Mexico, Mexico
Raksha Bhat,
Baylor College of Medicine, United States

*CORRESPONDENCE
Jing Shen
crystal_stray@126.com
Zhangang Xiao
zhangangxiao@swmu.edu.cn
Qinglian Wen
wql73115@163.com

SPECIALTY SECTION
This article was submitted to Cancer Molecular Targets and Therapeutics, a section of the journal Frontiers in Oncology

RECEIVED 28 March 2022
ACCEPTED 07 November 2022
PUBLISHED 29 November 2022

CITATION
Dai Y, Yang L, Sakandar A, Zhang D, Du F, Zhang X, Zou L, Zhao Y, Wang J, Zhang Z, Wu X, Li M, Ling X, Yu L, Dong L, Shen J, Xiao Z and Wen Q (2022) Vemurafenib inhibits immune escape biomarker BCL2A1 by targeting PI3K/AKT signaling pathway to suppress breast cancer. *Front. Oncol.* 12:906197. doi: 10.3389/fonc.2022.906197

Vemurafenib inhibits immune escape biomarker BCL2A1 by targeting PI3K/AKT signaling pathway to suppress breast cancer

Yalan Dai[1], Liqiong Yang[2,3], Abass Sakandar[1], Duoli Zhang[2,3], Fukuan Du[2,3,4], Xinyi Zhang[5], Linglin Zou[1], Yueshui Zhao[2,3,4], Jigang Wang[6], Zhenhua Zhang[1], Xu Wu[2,3,4], Mingxing Li[2,3,4], Xiao Ling[7], Lei Yu[7], Lishu Dong[7], Jing Shen[2,3,4]*, Zhangang Xiao[2,3,4]* and Qinglian Wen[1]*

[1]Department of Oncology, Affiliated Hospital of Southwest Medical University, Luzhou, Sichuan Province, China, [2]Laboratory of Molecular Pharmacology, Department of Pharmacology, School of Pharmacy, Southwest Medical University, Luzhou, Sichuan, China, [3]Cell Therapy & Cell Drugs, Luzhou Key Laboratory, Luzhou, China, [4]South Sichuan Institute of Translational Medicine, Southwest Medical University, Luzhou, China, [5]School of Data Science, The Chinese University of Hong Kong, Shenzhen, China, [6]Shenzhen Municipal People's Hospital, Shenzhen, China, [7]Department of Obstetrics, Luzhou Maternal & Child Health Hospital (Luzhou Second People's Hospital), Luzhou, Sichuan, China

Objectives: To investigate the role of immune escape encoding genes on the prognosis of BC, and to predict the novel targeting agents.

Methods: Human immune genes and immune escape encoding genes were obtained from the IMMPORT database and the previous study. Sample information and clinical data on BC were obtained from the TCGA and GTEX databases. Obtaining differentially expressed protein data from cBioportal database. To construct a risk score model by lasso analysis, and nomogram was used to predict score core. GSCA, TIMER and CELLMINER databases were used for immune and drug susceptibility correlation analyses. Cell experiments were verified by MTT, Western blotting, and RT-qPCR.

Results: We found prognostic models consisting of eleven immune escape related protein-coding genes with ROC curves that performed well in the ontology data (AUC for TCGA is 0.672) and the external data (AUC for GSE20685 is 0.663 and for GES42568 is 0.706). Five core prognostic models are related to survival (EIF4EBP1, BCL2A1, NDRG1, ERRFI1 and BRD4) were summarized, and a nomogram was constructed to validate a C-index of 0.695, which was superior to other prognostic models. Relevant drugs targeting core genes were identified based on drug sensitivity analysis, and found that Vemurafenib downregulates the PI3K-AKT pathway and BCL2A1 protein in BC, as confirmed by external data and cellular assays.

Conclusions: Briefly, our work establishes and validates an 11-immune escape risk model, and five core prognostic factors that are mined deeply from this model, and elucidates in detail that Vemurafenib suppresses breast cancer by targeting the PI3K/AKT signaling pathway to inhibit the immune escape biomarker BCL2A1, confirms the validity of the prognostic model, and provides corresponding targeted agents to guide individualized treatment of BC patients.

KEYWORDS

Immune escape, breast cancer, prognostic model, bioinformatics, biomarker, BCL2A1, vemurafenib, PI3K/Akt signaling pathway

Introduction

The World Health Organization's International Agency for Research on Cancer (IARC) released the latest data on the global cancer burden in 2020. New cases of breast cancer (BC) increased rapidly to 2.26 million, accounting for 11.7% of all new cancer patients, officially overtaking lung cancer (2.2 million cases) as the world's leading cancer for the first time (1). Effective prevention, diagnosis, treatment, and whole-process management strategies for BC have become important mediums for improving the global cancer burden.

The efficacy of local and systemic treatment of BC has improved greatly in recent years, and avoid the underutilization of medical resources has become a focus (2). The clinical decision of BC is mainly dependent on the abnormal expression of estrogen, progesterone endocrine receptors (ER, PR) and HER2. Immunotherapy has been shown to have salvage implications in many cancers. Antibodies against the immunomodulators PD-L1/PD-1 and CTLA4 have had staged clinical success, but more in-depth studies of immunotherapy are still needed. Proper functioning of the immune system requires constant modulation to ensure protection against foreign factors and the tolerance of autoantigens (3).

Immune editing is a dynamic process that regulates tumor evolution through the immune system, including elimination, homeostasis and escape (4). Immune escape is key to the persistence of most solid tumors, and it is a key obstacle to the success of cancer (immune) treatment (5). The mechanisms of immune escape include a decrease in immune analysis, downregulation of co-stimulatory molecules, and overexpression of co-inhibitory molecules, causing a decrease in CD8+ T cell activity and weakening the body's anti-tumor immunity (6). Immune escape is a necessary condition for the formation and development of breast tumors and a key step in the transition from pre-invasive lesions to aggressive tumors (7).

Current work is focused on developing combination therapies to convert non-responders into responders, deepen existing responses, and overcome acquired immunotherapy resistance (8). The response elicited by immunotherapy is expected to clearly target and destroy tumor cells while preserving normal cells. Immunotherapeutic approaches include the use of antibodies to neutralize or block immune checkpoints, induction of proliferation and/or increased activity of tumor infiltrating lymphocytes (CTL), and it regulating the tumor microenvironment (TME) (9). Effective anti-tumor strategies must focus on targeting multiple immune pathways to fully activate endogenous tumor immunity (10, 11). In advanced BC patients, immunotherapy combined with targeted therapy is undergoing basic and clinical trials to confirm biomarkers in the tumor and TME, as well as to identify the pharmacokinetics and pharmacodynamics of drug combinations, and to optimize drug dosing in order to find the optimal combination of treatments for individual patients (12).

BC is extremely heterogeneous at the clinical and molecular level. Because of the use of various histological techniques (genomics, transcriptomics or proteomics, etc.), we have gained deep understanding of the complexity of the development of BC (13). Multiomic is an emerging analytical approach that combines next-generation DNA and RNA sequencing with protein characterization to provide features such as protein expression levels, post-translational modifications, and protein-protein interactions (14).

Keith A. Lawson et al. have found a key set of genes and pathways, which make tumor cells dodge CTL-mediated killing. They found 182 immune escape related genes by the genome wide CRISPR screen on a set of mouse BC cell lines cultured in the presence of CTL, and disrupting these genes alone increased the sensitivity and resistance of cancer cells to CTL killing (15). There are no comprehensive studies on the genes encoding immune escape in BC, and endocrine therapy plus CDK4/6 inhibitors have become the standard of care for estrogen receptor-positive (ER+) BC. Although immune checkpoint

inhibitors (ICIs) have shown promising antitumor activity in a variety of cancer types, only limited success has been achieved in patients with metastatic breast cancer (mBC), particularly the ER+ subtype, with typically exhibiting a lower tumor mutational load (TMB) compared to other subtypes and are therefore considered immunostasis. This may lead to missed treatment opportunities and overdosing (16, 17).

Targeted therapies have been greatly developed in BC, such as Toremifene and Pertuzumab (18). Vemurafenib is often used in BRAF-mutated melanoma and is gradually being explored in BC. A xenograft model of vemurafenib-treated MDA-MB-231 showed growth-inhibitory activity associated with inhibition of tumor angiogenesis (19). Magdalena Pircher et al. reported the first successful control of multiple lung metastases from triple-negative BC with vemurafenib (20). The specific mechanism by which vemurafenib inhibits breast cancer needs to be further explored.

The main objective of this study is to screen for immune escape related genes, and to identify hub genes that are associated with prognosis and efficacy of BC, and to provide new targets for the treatment of BC.

Materials and methods

Data

182 core immune escape encoding genes were extracted from a study by Keith A. Lawson. et al. IMMPORT database (https://www.immport.org/) provided 2483 immune encoding genes (21). Venn diagram was drawn by Hiplot mapping tool (https://hiplot.com.cn/) to identify two sets of intersection genes. Downloaded data from TCGA database (https://tcga-Data.Nci.nih.gov/TCGA/), GTEX database (https://www.Gtex-portal.org/home/) and UCSC database (http://xena.Ucsc.edu/), which provided us with clinical data from 1095 BC cases and 292 normal controls, and their matched transcriptome RNA second-generation sequencing data.

Differentially expressed protein analysis and enrichment analysis

The "t-test" of "GraphPad Prism 8" were used for differential expression analysis of normal and tumor samples, and the "survival" R package for survival analysis. The cBioportal database (http://www.cbioportal.org/) was used for further differentially expressed proteins analysis (22). Gene ontology (GO) and Kyoto Encyclopedia of Genes and Genomes (KEGG) enrichment analyses of differential expression of protein-coding genes were performed using "clusterprofiler" package. Category, Count, and -log10pvalue were used by GO analysis to obtain important metabolic pathways.

Cox regression analysis to establish a risk model

First, the gene sequencing data and patient survival data were combined, and univariate Cox analysis was performed using the "surviving" and "forestplot" R packages, and critical genes associated with prognosis were further explored using the "glmnet" R package. Multivariate cox analysis of candidate genes was performed with the "surv" package, and it constructed a prognostic risk assessment model.

$$Risk \quad score = \sum_{i=0}^{n}(Expi * Coei)$$

Then, risk prediction and risk score calculation were performed using a prediction model. Based on the risk scores, patients were divided into high- and low- risk groups.

Measure the risk model

The "Hiplot" plotting tool was used to show the distribution of survival situation of low- and high- risk patients. The "pheatmap" R package was used to observe the difference in expression levels between high- and low- risk groups. Kaplan-Meier Survival analysis was used to assess the survival rates of BC patients in both groups. The validity of candidate genes in predicting the prognosis of BC patients was measured by plotting ROC curves using the "pROC" R package, which based on survival status, survival time and candidate gene expression in BC patients. The TCIA database (https://tcia.at/home) was used to analysis the enrichment of immune cells in the high- and low- risk groups (23). The prognostic model was externally validated by GSE20685 and GES42568 datasets.

Screening of core prognostic factors and construction of nomogram

The "T test" of "GraphPad Prism 8" was used for differential expression analysis of normal and tumor samples, and "survival" package was used to obtain survive-related hub genes, and $P<0.05$ was regarded statistically significant. The nomogram was used to predict the effect of each differentially expressed protein coding genes on 1-, 3-, and 5- year overall survival. The nomogram is composed of central prognostic factors, whose point scale is assigned to each variable. We used a horizontal line to determine the points for each variable and calculated the total points for each patient by adding points for all variables by normalizing the distribution from 0 to 100. Then we established the performance of the calibration curve for the visual nomogram. We compared the predictions in the calibration curves with the observed results. The best prediction was when the slope was close to 1.

Immunoassay database

The "XY" of "GraphPad Prism 8" performed correlation analysis of central protein-encoding genes with immune checkpoints PD-1, PD-L1 and CTLA4 and showed the relationship between them using Hiplot's chord charts. The Gene Set Cancer Analysis (GSCA) database (http://bioinfo.life.hust.edu.cn/GSCA/) was used to analyze the expression of central protein-encoding genes and associated immune infiltration (24). The TIMER database (https://cistrome.shinyapps.io/timer/) was used to capture the immune cells and the correlation of tumor purity and quantity of gene expression, and represented by the heat map of the Hiplot (25).

Drug sensitivity analysis database

Used the CELLMINER database (https://discover.nci.nih.gov/cellminer/) download the processed data "Processed Data Set" (26), and the data was processed by the "readxl" package. There were some "NA" missing values in the drug sensitivity data, and the "impute. KNN ()" function was used to evaluate and complement the missing values. Pearson correlation coefficients between each gene expression and different drugs were calculated and the two groups of drugs with the maximum and minimum correlation for each protein-coding gene were found based on the correlation coefficients. Correlation analysis was performed using "XY" of "GraphPad Prism 8" for visualization and validation purposes. The GES97681 dataset was used to verify whether Vemurafenib affects the expression of B-cell lymphoma 2-associated protein A1 (BCL2A1) and to find the pathway of drug effects through the literature, integrating the genes and pathways in the KEGG data (https://www.genome.jp/kegg/) to discover the effects of drugs on genes.

Cell culture

Human BC lines (MCF-7, MDA-MB-231, SK-BR-3) were obtained from the School of Biomedical Sciences, Chinese University of Hong Kong. MCF-7 maintained in RPMI-1640 medium and MDA-MB-231 were cultured in Dulbecco's modified Eagle's medium (DMEM) (Gibco; Thermo Fisher Scientific, Inc.). Both media contained 10% fetal bovine serum (FBS; Thermo Fisher Scientific, Inc.) and 100 µg/ml streptomycin/100 U/ml penicillin (Gibco; Thermo Fisher Scientific, Inc.). SK-BR-3 were cultured in DMEM complete medium (iCell-h189-001b). Human breast epithelial cells (MCF-10A) purchased from iCell Bioscience Inc, China. MCF-10A was cultured in special medium (iCell-h131-001b). Vemurafenib (MedChemExpress, HY-12057) was dissolved in dimethyl sulfoxide (DMSO, final concentration is 0.1%) to prepare required concentrations. All cell lines were kept at 37°C in a humidified incubator with 5% CO2.

MTT assay

For the MTT assay, MCF-7, SK-BR-3 and MDA-MB-231 cells were detached by trypsinization and counted in a haemocytometer. Cells were seeded in 96-well plates at a density of 4000 cells/well in 100 µl medium per well. Twenty-four hours after incubation in the CO2 incubator, adherent cells were treated with increasing concentrations of drugs: vemurafenib (0, 20, 40, and 60 µM) in fresh 1640 and DMEM medium. For measuring the concentration of vemurafenib that resulted in 50% control growth inhibition (IC50), at 48 hours following drug treatment, 10 µl MTT (3-(4,5-Dimethylthiazol-2-yl)-2,5-diphenyltetrazolium bromide) (Sigma-Aldrich) solution (5 mg/ml in PBS) was added to each well after 48h of drug treatment. In addition, cell viability was measured by adding MTT at 0, 24, 48, 72h. Then incubation was continued for additional 4h in the CO2 incubator. The blue formazan product, formed by reduction in live attached cells, was dissolved by adding 100 µl of 100% DMSO per well. The plates were gently swirled at room temperature for 10 minutes to dissolve the precipitate. Absorbance was monitored at 490 nm using a microplate reader (CYTATION 3; Agilent Technologies, Inc.). The effect of vemurafenib on cell viability was assessed as the percent of cell viability compared with vehicle-treated control cells, which were arbitrarily assigned 100% viability. Dose-response curves and IC50 values were obtained using GraphPad Prism software. At least 3 dose-response experiments were performed for each compound, and the mean IC50 ± SD was calculated.

Real-Time Quantitative Polymerase Chain Reaction (RT-qPCR)

Cells were seeded at the density described above and incubated for 24 hours before the addition of vemurafenib. The compounds were added to the final concentrations of 0, 20, 40, and 60 µM. After 48 hours of treatment, Cell pellets were collected for experiments. Total RNA was isolated from MCF-7, SK-BR-3 and MDA-MB-231 by using Trizol reagent (Thermo Fisher Scientific, Inc.) according to the manufacturer's instructions. Total RNA (1 µg) from each group of treated cells was converted to cDNA using a FastKing RT reagent kit (Tiangen, Inc.). The RT reaction was performed at 42°C for 15 min and 95°C for 3 min. qPCR was performed with a SYBR Green Real Time PCR kit (Thermo Fisher Scientific, Inc.) on CFX96 Touch Real Time PCR System (BioRad Laboratories, Inc.) under the following conditions: 95°C for 1 min, then 40 cycles of 95°C for 5 sec and 60°C for 15 sec. The gene expression

level was calculated as $2(^{-\triangle\triangle Ct})$ method, and the $\triangle$Ct means the Ct of target gene minus the Ct of reference gene. The primers used for real-time PCR were BCL2A1 (forward) 5'-AAATTGC CCCGGATGTGGAT-3' and (reverse) 5'-ACAAAGC CATTTTCCCAGCCT-3'; GAPDH (forward) 5'-CTGGGC TACACTGAGCACC-3' and (reverse) 5'-AAGTGGTCGT TGAGGGCAATG-3'.

Western blot analysis

Western blotting was used to test the PI3K/AKT signaling pathway and BCL2A1 protein. RIPA lysis buffer (Beijing Solarbio Science & Technology Co., Ltd.) containing protease inhibitor PhosSTOP EASYpack (Roche Diagnostics) was used for total protein extraction according to the manufacturer's protocol. Protein concentration was measured by the BCA kit (Beyotime Biotechnology, China). Then, protein samples were separated by 10% SDS–PAGE gel and transformed into PVDF membranes (Millipore, USA). Afterwards, membranes were incubated using 5% bovine serum albumin (BSA, Sigma –Aldrich; Merck KGaA) at room temperature for 1h and incubated with primary antibodies under 4°C overnight. The antibodies are as follows: anti-PI3K (1: 1,000, 4249, CST), anti-AKT (1: 1,000, 9272S, CST), anti-phosphorylated (p)–AKT (1: 1,000, 9271S, CST), anti-BCL2A1 (1: 1,000, 14093, CST), and anti-GAPDH (1: 2,000, GTX100118, GENE TEX) with GAPDH being the endogenous control. Afterwards, membranes were incubated with HRP–conjugated secondary antibodies at room temperature for 1h using a secondary antibody (1: 3,000, A0208, Beyotime). Finally, ECL blotting detection reagents (Clarity; Bio –Rad Laboratories, Inc.) was utilized to observe protein blots and the signals were detected by the ChemiDoc™ Imaging System (Bio–Rad Laboratories, Inc.).

Datasource

Databases we used have: IMMPORT database, TCGA database, GTEX database, UCSC database, cBioportal database, TCIA database, GEO database (include GSE20685, GES42568 and GES97681 datasets), GSCA database, TIMER database, CELLMINER database. The softwares we used have: Hiplot mapping tool and GraphPad Prism.

Statistical analysis

Our research mainly used "GraphPad Prism 8" and "R language" for data difference analysis, visualization, etc. From the "GraphPad Prism 8", "T test" was used to compare the differences between two data sets, "one-way ANOVA" was used to compare differences between three or more groups of data, and "XY" was used for correlation analysis. $P<0.05$ was considered statistically significant, indicating significant differences between the data were used. R is the language and operating environment for statistical analysis and mapping. we used the "Pheatmap", "Survival", "GGPUBR" and "clusterprofiler " package fort expression analysis, survival analysis and enrichment analysis for differentially expressed genes and proteins. All experiment data are presented as the mean ± standard deviation (SD), further analyzing using GraphPad Prism 9.0. Differences in the results of two groups were evaluated using either two-tailed Student's t test or one-way ANOVA followed by *post-hoc* Dunnett's test. The differences with $P< 0.05$ were considered statistically significant.

Results

Fifteen immune escape encoding genes significantly associated with the survival and prognosis of BC

Venn plot was used to identify the overlap of 2483 human immune associated genes from Immport database with 182 immune escape associated genes from Keith A. Lawson's study (Figure 1A), yielded 31 crossover genes (Figure 1B). We compared the expression levels of immune escape encoding genes between BC patients and healthy individuals, found that 18 genes were significantly up-regulated and 12 genes were significantly down-regulated in BC patients, and ERAP1 was not significantly different in BC patients and healthy individuals (Figure 1C). BC patients were divided into high and low groups according to "res.cut" expression levels, and Kaplan-Meier survival analysis was performed for BC immune escape gene expression levels. Among them, 15 genes showed significant differences in survival and expression levels in BC patients (Figure 1D), and the survival curves of the other 16 genes were also shown (Figure S1A).

Immune escape in BC is mainly influenced by PI3K-Akt signaling pathway

We identified 181 differentially expressed proteins regulated by BC immune escape encoding genes through the cBioPortal database (Table S1). The volcanic plots (Figure 2A) show proteins with significant changes ($P<0.05$) and were used for further analysis. To determine which pathway differential proteins were mainly enriched, we performed GO and KEGG enrichment analysis using "clusterprofiler" R package, which showed that these differentially expressed proteins play important roles in protein serine/threonine kinase activity,

10.3389/fonc.2022.906197

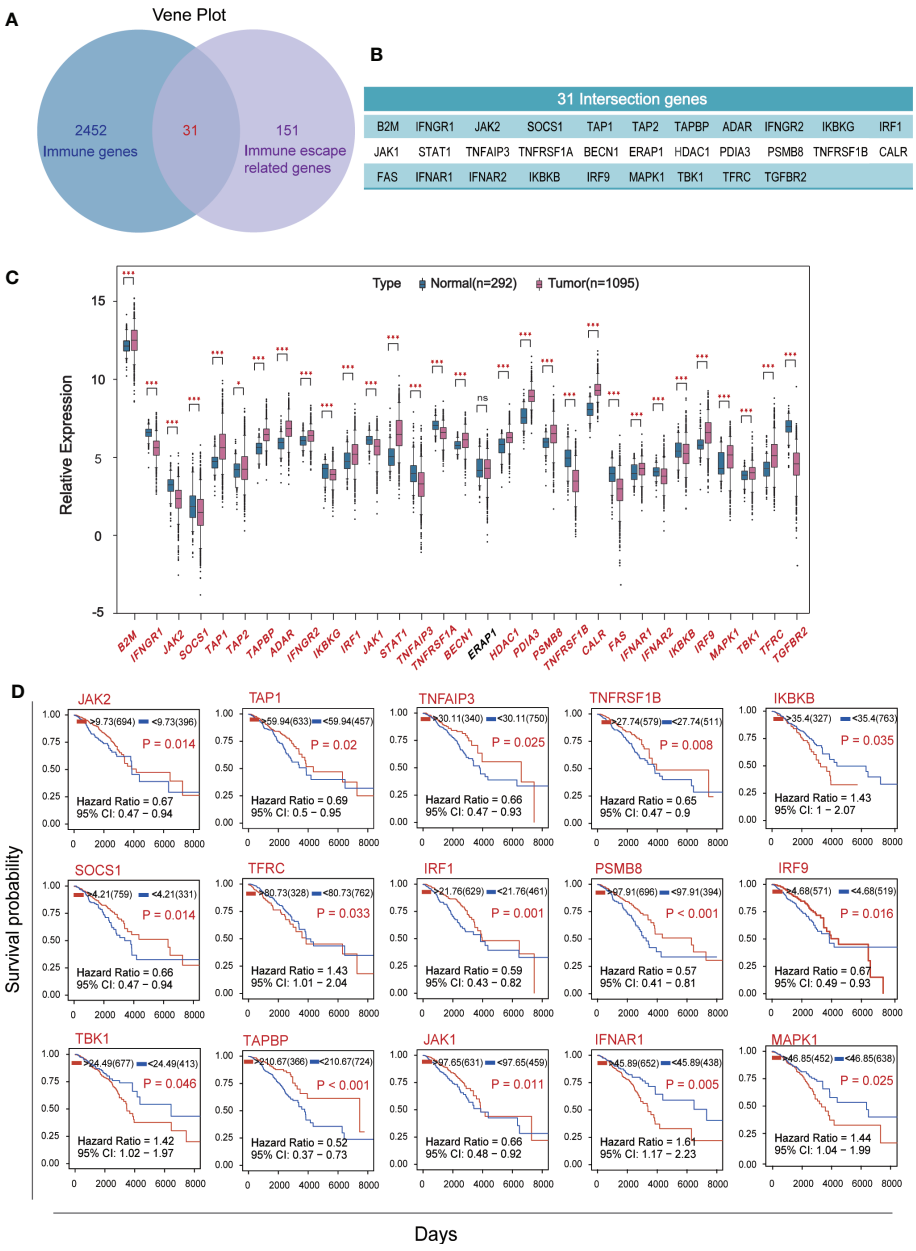

FIGURE 1
Screening for hub genes associated with immune escape from breast cancer. **(A)** The overlap of 2483 immune-related genes from Immport and 182 immune-escape related genes. **(B)** Display of 31 intersection genes. **(C)** The expression levels of breast cancer immune escape genes were analyzed using RNA sequencing data from 1095 cancer patients and 292 healthy subjects in the TCGA and GTEX databases. **(D)** Kaplan-Meier survival curve of immune escape genes in breast cancer based on expression level. Fifteen hub genes which P<0.05 and with significant differences in expression levels were shown. (★p<0. 05,★★p<0. 01 and★★★p< 0.001).

ubiquitin-like protein ligase binding, membrane raft, cell substrate connection, gland development andreproductive structure development. The PI3K-Akt signaling pathway is considered to be the most prominent downstream signaling pathway for immune escape related genes in BC (Figures 2B, C).

An 11-gene prognostic risk model was constructed and validated with external data sets

Univariate Cox analysis was performed on 181 differentially expressed protein coding genes associated with immune escape

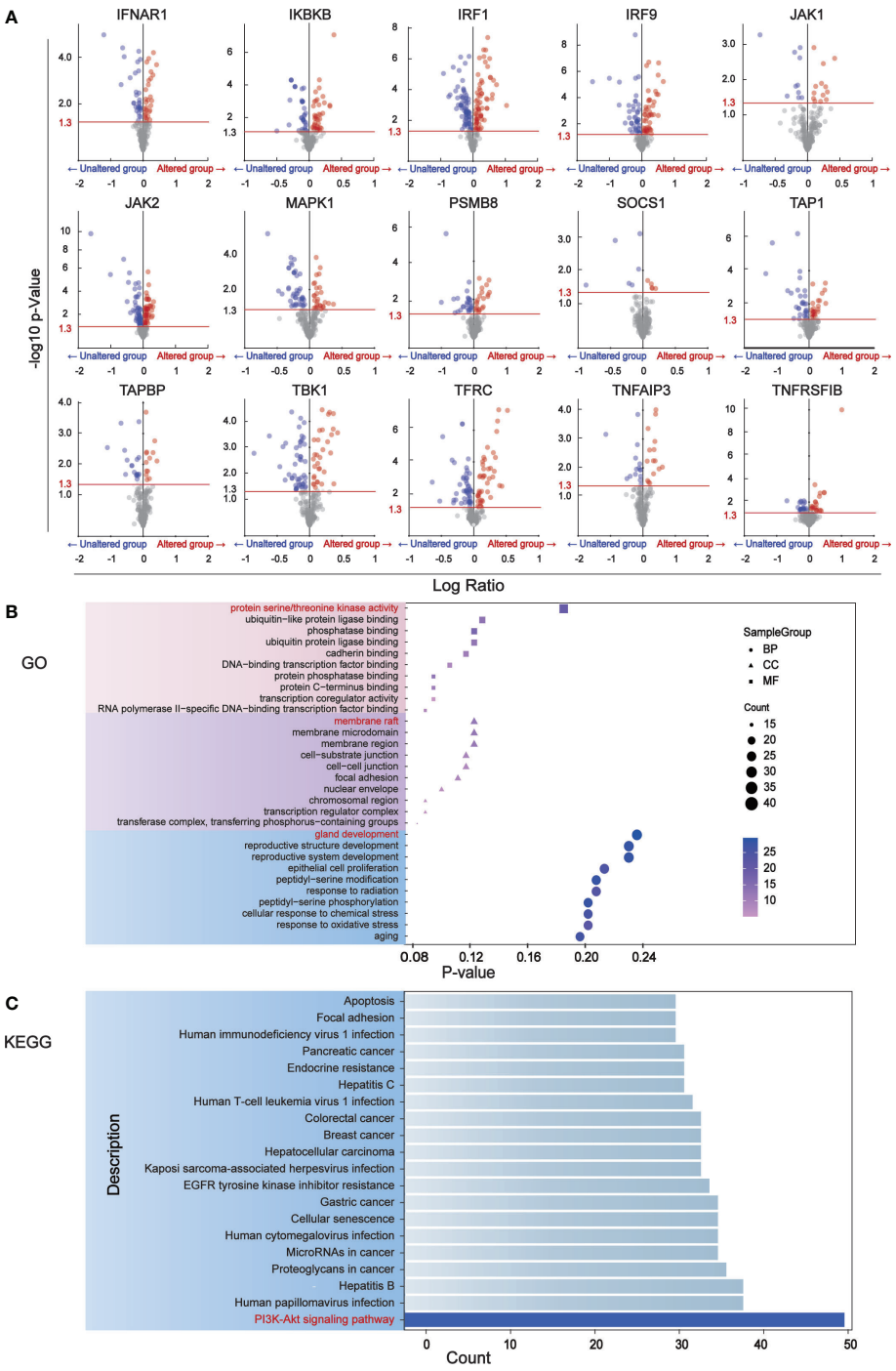

FIGURE 2
The major signaling pathway affected by genes associated with immune escape. **(A)** Volcano mapping to identify differential expressed proteins affected by immune escape related genes and analyzed by reverse phase protein array (RPPA) in cBioPortal. The Y-axis is the value that expresses the change in the horizontal fold, based on the logarithmic ratio (average of the changing expression/average of the constant expression). -log10 (p value)>1.30 is considered a significant difference. **(B)** The bubble diagram of GO enrichment analysis of immune escape gene was analyzed through clusterProfiler. Ten proteins have been shown to be important in biological processes, cell components, and molecular functions. **(C)** The downstream pathways related to immune escape gene changes were analyzed by KEGG pathway in clusterProfiler.

in BC, and 31 of them were identified to be associated with survival (Figure 3A). To evaluate differentially expressed protein-coding genes meaningfully associated with BC prognosis and to obtain a better-fitting model, we used LASSO to downscale the high-dimensional information by adding a constraint to the absolute value of the coefficients and further screening by 10-fold cross-validation. The optimal λ value (λmin=0.025) was obtained from the minimum local likelihood deviation, and 16 genes were found to be significantly associated with prognosis (Figures 3B, C). The previous one looks at each feature individually to see if it is related to survival, while multivariate cox regression is to test whether multiple features are related to survival at the same time. Multivariate Cox analysis recognized 11 excellent prognostic gene models, namely EIF4EBP1, BCL2A1, NDRG1, MRE11A, ERRFI1, CLDN7, PIK3CA, CASP9, BRD4, PDCD4, and G6PD (Figure 3D). The risk score of patients was reckoned based on the scoring formula: Risk score = (EIF4EBP1 expression level * 0.162425485) - (BCL2A1 expression level * 0.234522698) + (NDRG1 expression level * 0.158199675) + (MRE11A expression level * 0.3105604) - (ERRFI1 expression level * 0.268609023)+ (CLDN7 expression level * 0.173133629) + (PIK3CA expression level * 0.442654646) - (CASP9 expression level * 0.337535821) - (BRD4 expression level * 0.497664344) - (PDCD4 expression level * 0.140816004) + (G6PD expression level * 0.190558316). There were more deaths in the high-risk group than the low-risk group, while fewer patients survived longer than 5 years than in the low-risk group (Figure 4A). The heatmap shows the risk of prognostic genes with a multivariate outcome P value less than 0.05. As the risk score increased, the expression levels of MRE11A, PIK3CA, EIF4EBP1 and NDRG1 increased, while the expression levels of BCL2A1 and BRD4 decreased (Figure 4C). Kaplan-Meier survival curve assessed the difference in survival between high- and low-risk patients in the risk model, which showed that survival decreased more significantly over time in the high-risk group than in the low-risk group, and the mean prognosis was worse in the high-risk group than in the low-risk group (P<0.0001) (Figure 4E). The prognostic value of Kaplan-Meier survival curves was determined by the P-ROC curve, and the area under the curve (AUC) was 0.672, indicating the median reliability of the kaplan-Meier survival curve (Figure 4G). The AUC of the survival assessment model was 0.68 for 2 years, 0.71 for 5 years, 0.75 for 8 years, and 0.77 for 10 years (Figure 4I). The applicability of the prognostic model was externally validated using the GSE20685 dataset (Figures 4B, D, F, H, J) and GES42568 dataset (Figure S2), and the results further confirmed the reliability of the risk model. We imported the high- and low- risk groups into the TCIA database and found that the high-risk groups had a lower percentage of immune cells clustering (Figure S2).

Nomogram validates the predictive value of 5 core prognostic factors

Seven of the 11 prognostic indicators were statistically significant, when Kaplan-Meier survival analysis was performed on them according to expression level, six of them were significantly different (Figure 5A). Analysis of their expression levels in tumor patients and normal subjects identified five core prognostic markers, which were EIF4EBP1, BCL2A1, NDRG1, ERRFI1 and BRD4 (Figure 5B). We plotted the expression levels of five central prognostic factors based on 1069 TCGA-BC patients. By testing these parameters to obtain the corresponding assigned scores for their expression, the individual gene scores were summed to find the total score, which can predict the survival of BC patients for 1, 3, and 5 years (Figure 5C). A calibration curve was plotted to verify the accuracy of the prediction of the line graph. In the calibration diagram, the predicted result (blue line) was very close to the actual result (black line), with a c-index of 0.695, indicating that the prediction quality of Nomogram was very high (Figure 5D). In conclusion, five core prognostic markers can accurately predict the prognosis of BC patients.

BCL2A1 is significantly associated with BC immunity

Correlation analysis of 5 core prognostic factors and immune checkpoints (PD-1, PD-L1 and CTLA4) showed that BCL2A1 had the highest correlation with immune checkpoints, while other factors with no significant difference (Figure 5E). Correlation analysis of the 5 central protein-encoding genes with 26 immune cells showed that BCL2A1 had the highest correlation with immune cells (Figure 5F). The correlation of 5 central protein-coding genes with tumor purity and 6 kinds of immune cells (B cells, CD4+ T cells, CD8+ T cells, Neutrphils, Macrophages and Dendritic cells) was further analyzed. BCL2A1 was negatively correlated with tumor purity and positively correlated with immune cells (Figure 5G).

Analysis of the expression of five core prognostic factors in different BC subtypes

We analyzed the expression levels of five core prognostic factors in two sets of BC classification data from public databases TCGA (Figure 6A) and GSE96058 (Figure 6B). The expression levels of EIF4EBP1, BCL2A1, NDRG1, ERRFI1 and BRD4 in all BC patients are consistent. The expression levels of EIF4EBP1 and BCL2A1 in BC patients are significantly higher than those in

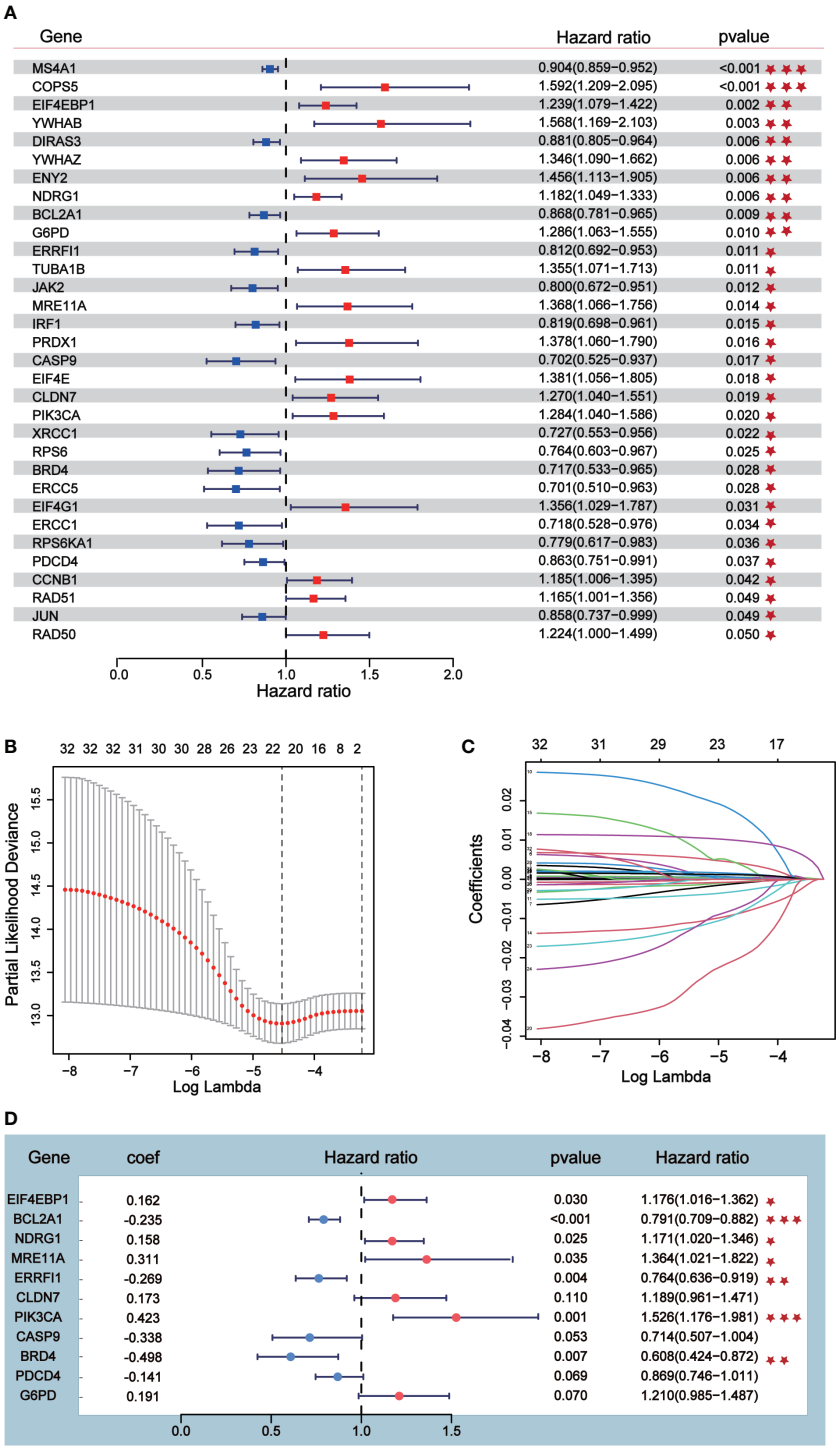

FIGURE 3
Prognostic risk model construction. **(A)** Univariate Cox analysis identified 31 differential expressed proteins coding genes related to survival. **(B, C)** Sixteen differential expressed proteins coding genes were further screened out from 31 genes by Lasso regression analysis and tenfold cross validation. **(D)** Multivariate Cox analysis was conducted according to Lasso results to obtain a risk model.

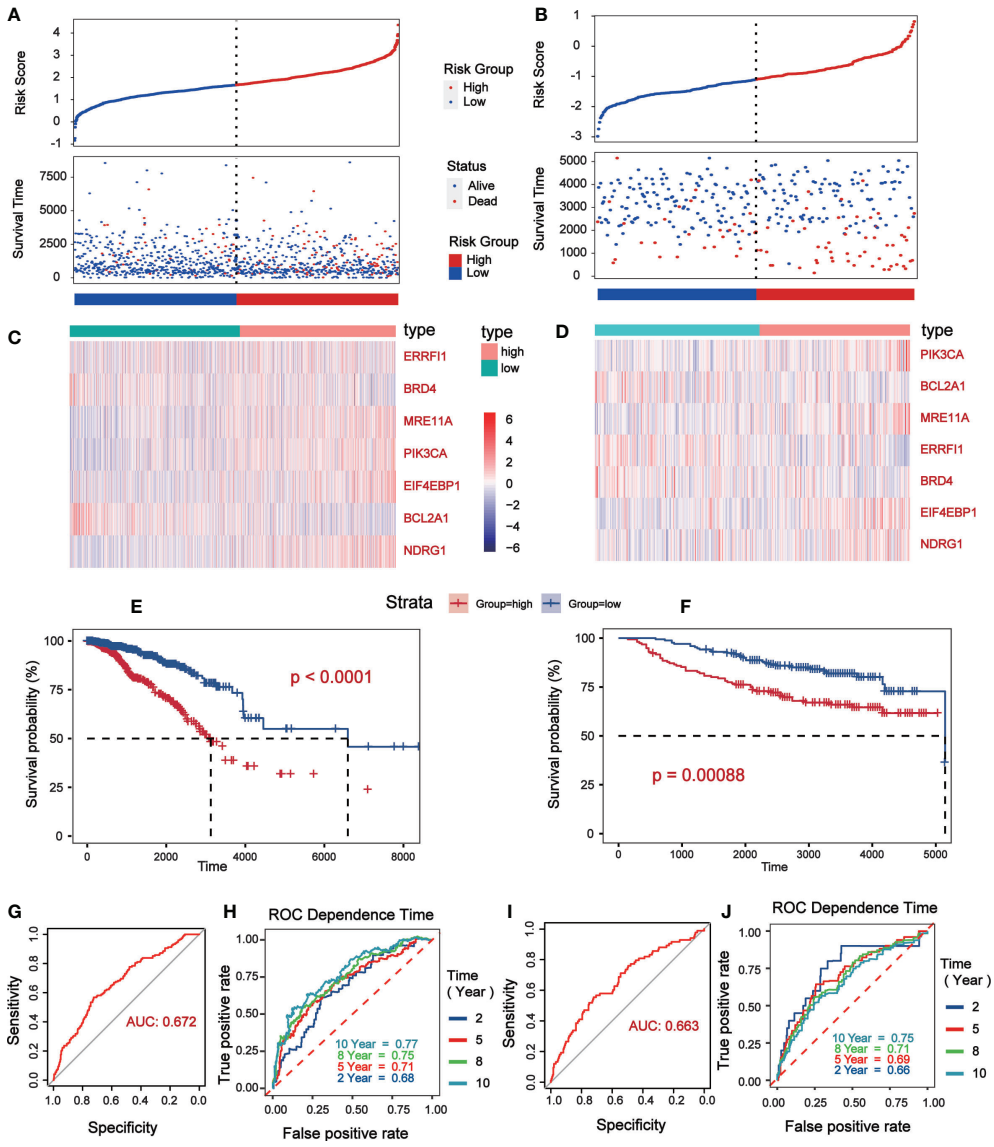

FIGURE 4
Verification of prognostic risk model based on TCGA database (Data were collected from low risk groups (n = 564) and high risk groups (n = 504)) and GSE20685 (Data were collected from low risk groups (n = 171) and high risk groups (n = 156)). **(A, B)** The status distribution of patients' survival between low and high risk groups. **(C, D)** Heat map showing expression levels of high and low genetic risk groups. **(E, F)** Kaplan–Meier curves of OS between the high risk and low risk groups. **(G, H)** The P-ROC curve verified the risk model, and the AUC>0.65 was considered to have good predictive value. **(I, J)** The time of 2- year, 5- year, 8- year and 10 - year survival forecasts depends on the ROC curve.

normal breast tissues, and with the increase of tumor malignancy. Its expression level increased.

Vemurafenib impacts the expression of BCL2A1 by affecting PI3K-AKT signaling pathway and inhibit BC cell growth

Analysis of the potential correlation between the expression of 5 core protein coding genes and drug sensitivity in different human cancer cell lines from CellMiner database, which showed that the expression of BCL2A1 was positively correlated with the drug sensitivity of Vemurafenib (Figure 7A). The results of the correlation between other drugs and gene expression are placed in the Supplementary Table (Table S2). We used RNA sequencing data from 78 BC patients in GSE97681, 24 without and 54 with Vemurafenib, the expression levels of BCL2A1 were analyzed and were found to be significantly reduced with the drug (Figure 7B). A review of the literature and the KEGG database

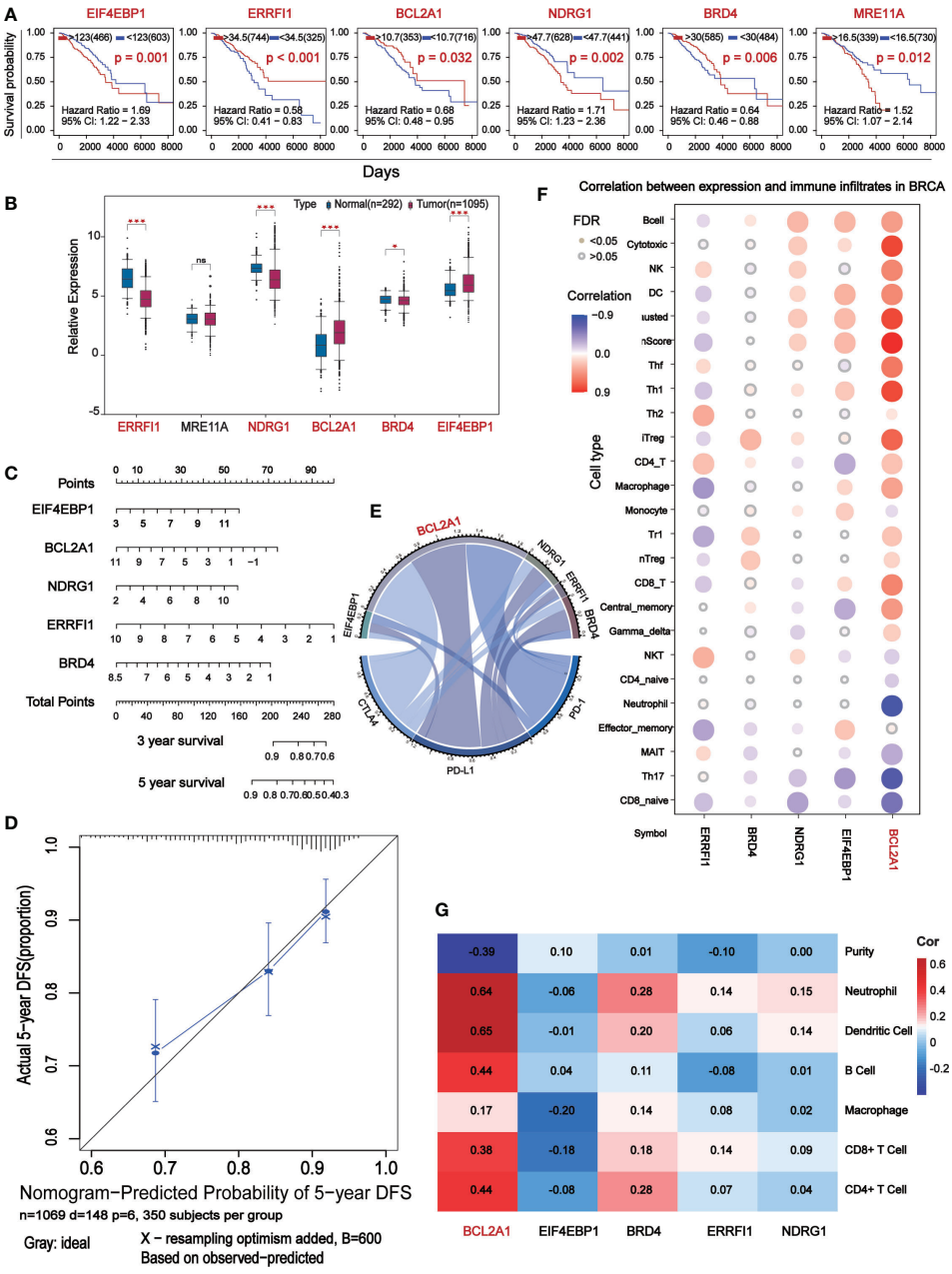

FIGURE 5
The central differential expressed proteins were further screened for immunocorrelation analysis. **(A)** Kaplan-Meier survival analysis based on the result of Multivariate Cox which P<0.05. **(B)** Box-plot analyze survival analysis for P<0.05 expression level of marker. **(C)** Prognostic maps of five central gene expression levels were established to predict overall survival at 1, 3, and 5 years. **(D)** Calibration chart of Nomogram. The black line represents the predicted results and the blue line represents the actual results. The high agreement between the two indicates that the prediction results are reliable. **(E)** Chord diagram shows the correlation between five central protein-coding genes and immune checkpoints. The longer arc and larger area with the better correlation. **(F)** Correlation analysis of the five central protein-coding genes and 26 immune cells: red represents positive correlation, blue represents negative correlation, the darker color show the stronger the correlation, and the small solid circles in color indicate FAD<0.05. **(G)** Correlation analysis (TIMER) between five central protein-coding genes and tumor purity and 6 immune cells.

revealed a map of the regulatory pathways of Vemurafenib on BCL2A1-sensitive targets (19) (Figure 7C).

We first detected the expression levels of PI3K, AKT, p-Akt and BCL2A1 in MCF7, MDA-MB-231, SKBR3 and MCF10A cells by Western Blot analysis. It was confirmed that the expression of these proteins in BC cells (MCF7, MDA-MB-231, SKBR3) was higher than that in normal breast cells (MCF10A)(Figure 7D).

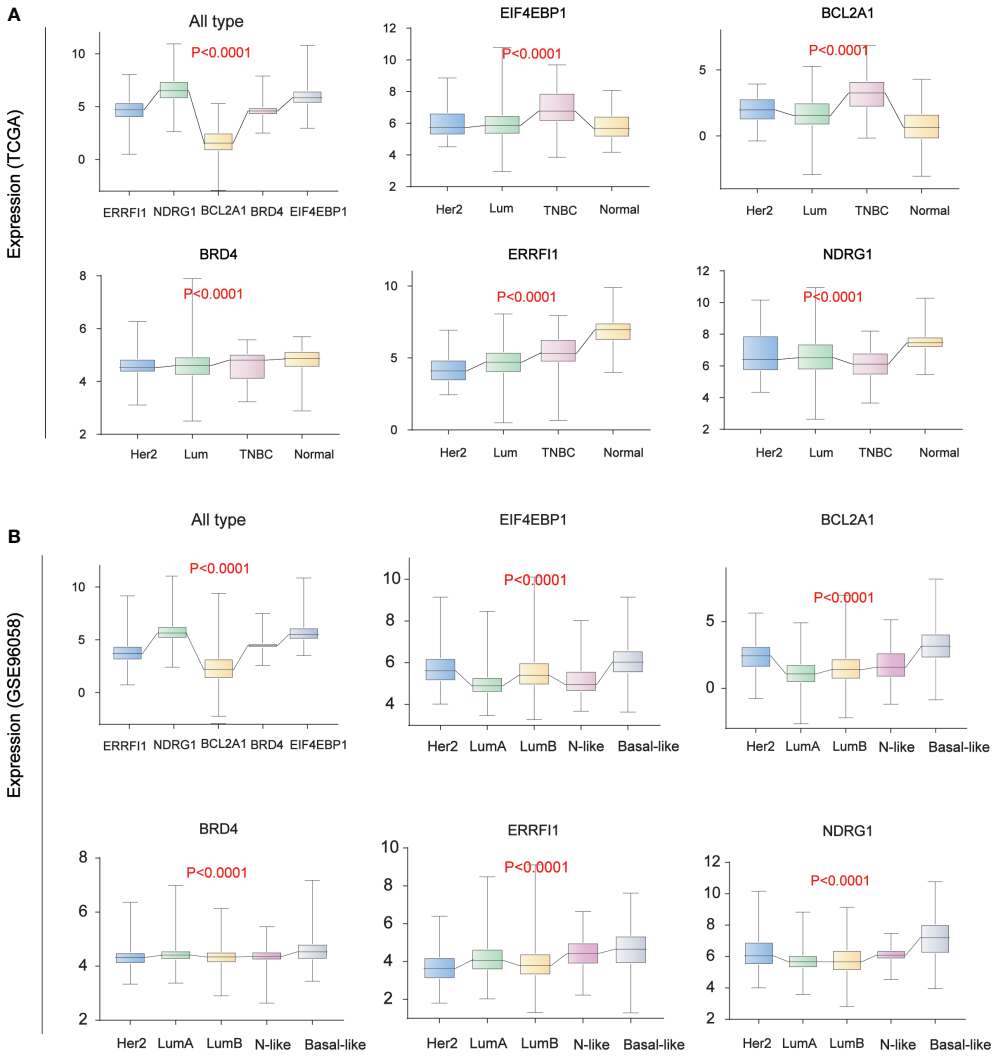

FIGURE 6
Breast Cancer Typing Expression. **(A)** Breast cancer typing expression in TCGA database. **(B)** Breast cancer typing expression in the GEO database (GSE96058).

To explore the effect of vemurafenib on BC cells, the concentration of vemurafenib that resulted in 50% control growth inhibition (IC50) of MCF7, MDA-MB-231 and SKBR3 cells was assessed by MTT (Figure 7E). The IC50 of MCF-7 is 42 μM, MDA-MB-231 is 34 μM and SKBR3 is 51 μM. Next, the inhibitory activity of different concentrations of vemurafenib (0, 20, 40, 60 μM) on MCF7, SKBR3 and MDA-MB-231 cells at 0, 24, 48, and 72 h were further studied by MTT (Figure 7F). The results showed that vemurafenib inhibited cell proliferation in a dose-dependent manner, and the inhibitory effect increased with time.

To further explore the mechanism by which vemurafenib inhibit the growth of MDA-MB-231, MCF7 and SKBR3 cells, the expression level of PI3K/AKT signaling pathway and BCL2A1 in vemurafenib treated cells was evaluated by western blot (Figures 8A–C). The expression level of PI3K, AKT, p-AKT and BCL2A1 were reduced in vemurafenib treated cells compared to without vemurafenib. This suggested that the drug inhibits the PI3K/AKT signaling pathway and BCL2A1. In addition, apoptosis-associated genes expression was detected. BCL2A1 downregulation was confirmed using RT-qPCR (Figures 8D–F), and the results indicated that vemurafenib promoted cell apoptosis of MDA-MB-231 and MCF-7.

Discussion

BC is a malignant tumor that seriously endangers women's health, and is occasionally seen in men. Most of the early symptoms of BC patients are not obvious and can be easily

10.3389/fonc.2022.906197

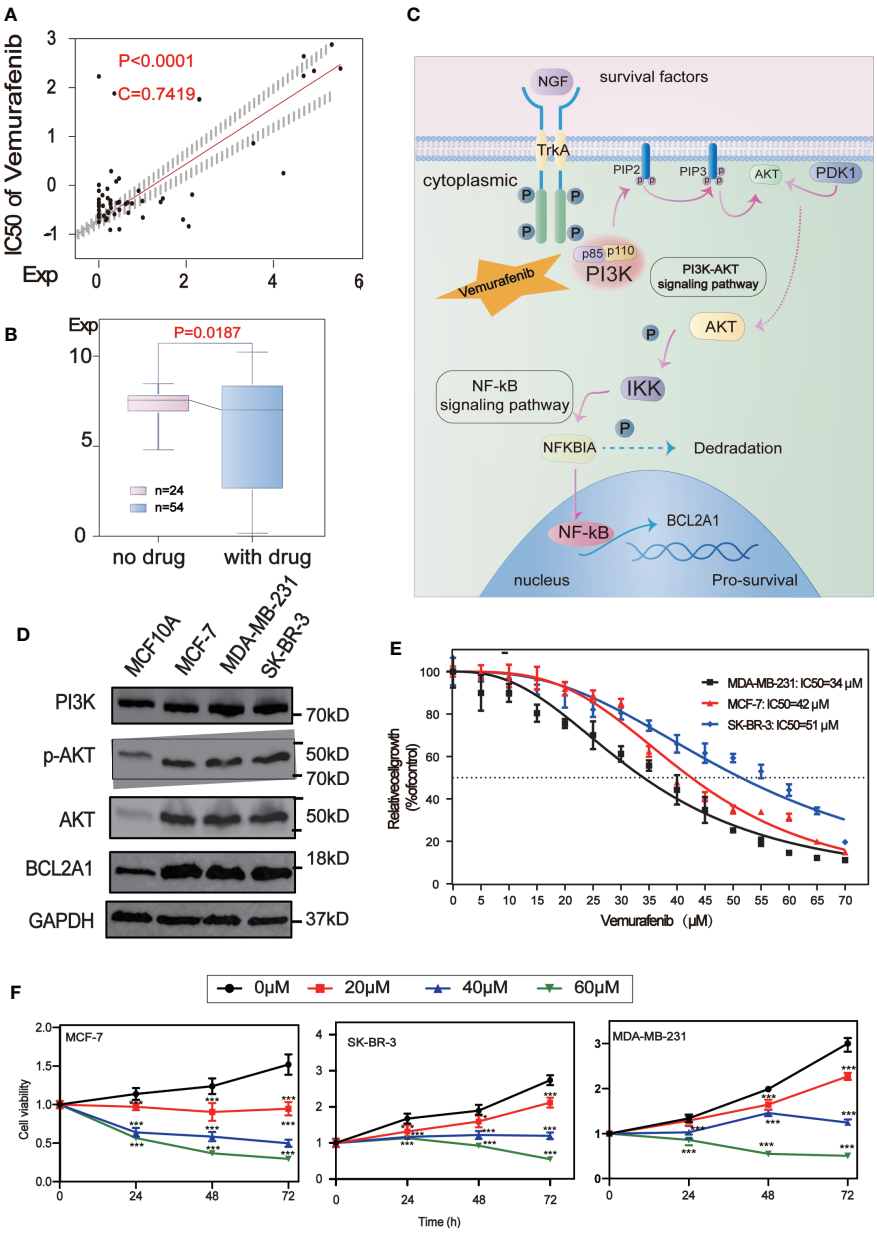

FIGURE 7
Drug sensitivity analysis of five central protein-coding genes. **(A)** Regulatory pathway map of BCL2A1 and the sensitive target of Vemurafenib. **(B)** The scatter plot shows the sensitivity analysis of BCL2A1 and the antitumor drug Vemurafenib. **(C)** Box-plot show the molecular formula of the Vemurafenib and the expression levels of BCL2A1 were analyzed using RNA sequencing data from 24 no drug and 54 with drug subjects in the GSE97681. **(D)** The expression levels of PI3K, AKT, P-Akt and BCL2A1 in MCF7, MDA-MB-231, SKBR3 and MCF10A cells were detected by Western Blot. **(E)** Vemurafenib inhibited cell viability in breast cancer cells. The concentration of vemurafenib resulting in 50% inhibition of control growth (IC50) was calculated. **(F)** Vemurafenib inhibit cell viability at different times. Vemurafenib (0, 20, 40, 60μM) inhibited MCF-7, SKBR3 and MDA-MB-231 cell viability at 0, 24, 48, and 72h. *P<0.05, **P<0.01, ***P<0.001.

ignored, and the failure to seek timely medical attention leads to poor prognosis of BC. Personalized treatment and other new therapies can help patients choose the most appropriate treatment among various therapies. Establishing an accurate patient prognosis prediction system to provide patients with a more optimal treatment approach in molecularly targeted therapy is essential for personalized treatment (27). Molecular prognostic markers can change with tumor progression, and monitoring these markers can dynamically reflect patient prognosis. In addition, some molecular prognostic markers are involved in tumor progression and may be potential targets for tumor therapy and diagnostic indicators for early tumors (28).

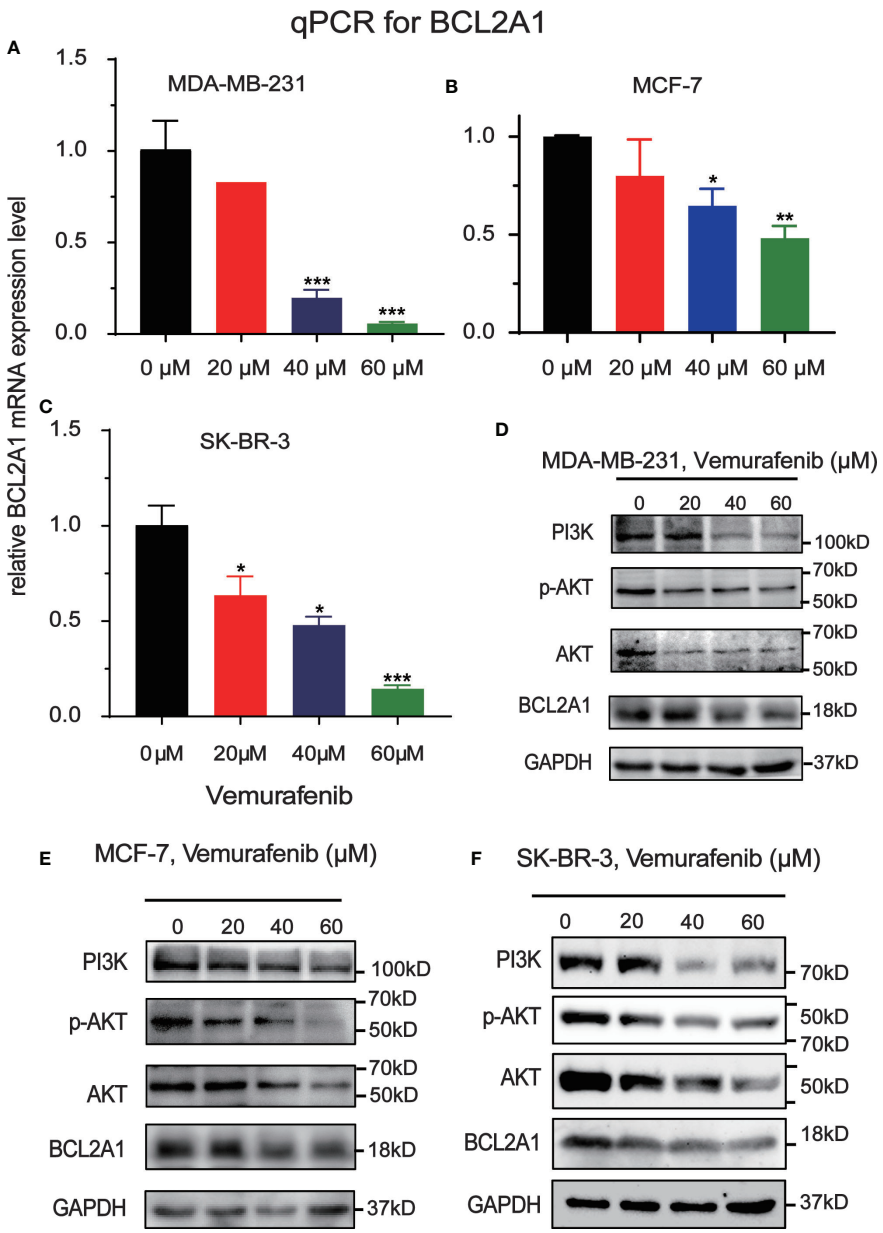

FIGURE 8
Inhibitory effect of Vemurafenib on different breast cancer cell lines. **(A)** Vemurafenib suppressed PI3K, AKT, p-AKT and BCL2A1 expression in MDA-MB-231cells. **(B)** Vemurafenib suppressed PI3K, AKT, p-AKT and BCL2A1 expression in MCF-7 cells. **(C)** Vemurafenib suppressed PI3K, AKT, p-AKT and BCL2A1 expression in SKBR3 cells. **(D)** Decreased levels of BCL2A1 in MDA-MB-231 cells treated with different concentrations of vemurafenib (0, 20, 40, 60 μM) were determined by RT-qPCR. **(E)** Decreased levels of BCL2A1 in MCF-7 cells treated with different concentrations of vemurafenib (0, 20, 40, 60 μM) were determined by RT-qPCR. **(F)** Decreased levels of BCL2A1 in SKBR3 cells treated with different concentrations of vemurafenib (0, 20, 40, 60 μM) were determined by RT-qPCR. (*P<0.05, **P<0.01, ***P<0.001.).

Molecular prognostic markers may be heterogeneous across patients, so that a group of molecular markers is superior to individual markers in terms of prognosis.

A large number of cancer and normal breast tissues were analyzed and screened in TCGA, GTEx, and GEO databases for broad applicability. 182 mouse immune escape related genes were obtained from Keith A. Lawson et al. and intersected with 2483 human immune escape related genes downloaded from the IMMPORT database, and 31 reliable immune escape related genes were identified. Fifteen of the immune escape related genes were significantly associated with survival and expression, and 181 differentially expressed proteins of the 15 hub genes were

identified through the cBioportal database. Gene enrichment analysis showed that differentially expressed proteins are involved in many important biological processes, such as protein serine/threonine kinase activity, ubiquitin-like protein ligase binding, membrane raft, cell substrate connection, gland development and reproductive structure development. In addition, they are associated with important tumor-related pathways such as the PI3K-AKT signaling pathway, Hepatitis B, and Human papillomavirus infection pathway. The PI3K-AKT signaling pathway mainly inhibits cell apoptosis and promotes cell proliferation, indicating that immune escape genes play an important role in the occurrence and development of tumors. In recent years, an increasing number of studies had found that PI3K/Akt signaling pathway is closely related to the occurrence and development of lung cancer, BC, colorectal cancer, prostate cancer, ovarian cancer, liver cancer and lymphoma (29).

To find the most representative survival-related differentially expressed proteins, univariate Cox analysis, lasso regression analysis and multivariate Cox analysis were used to analyze the genes encoding these differentially expressed proteins. The prognostic model consisted of EIF4EBP1, BCL2A1, NDRG1, MRE11A, ERRFI1, CLDN7, PIK3CA, CASP9, BRD4, PDCD4 and G6PD. According to these 11 genetic characteristics, BC patients can be divided into high- and low-risk group, the survival rate of high-risk group is significantly lower than that of low-risk group. Differential expression analysis and survival analysis were performed on the prognostic models, and five core prognostic models were summarized, including EIF4EBP1, BCL2A1, NDRG1, ERRFI1 and BRD4. EIF4EBP1, NDRG1 and BRD4 are associated with poor prognosis of BC, while BCL2A1 and ERRFI1 are associated with good prognosis of BC. The nomogram found that the five prognostic factors had good prediction accuracy at 1, 3 and 5 years of BC. Similarly, HPA database (Human Protein Atlas) was used to test the performance of the prognostic model based on the characteristics of these five protein-coding genes, and the results showed that they performed well in predicting the prognosis of BC.

EIF4EBP1 (also known as 4EBP1) gene encodes a translation repressor protein, which competitively binds to eukaryotic translation initiation factor 4E (EIF4E), and inhibits the assembly of the EIF4E complex, thereby suppressing cap-dependent translation (30). In BC and cervical cancer, EIF4EBP1 is considered to be a major factor in the signaling pathway related to prognosis and malignancy, which was not changed by the presence of other upstream carcinogens (31, 32), it is consistent with our findings. The Bromodomain and extra-Terminal Domain (BET) protein BRD4 was a transcriptional and epigenetic regulator that plays a key role in embryonic and cancer development. Aberrant degradation of the BRD4 protein in cancer leads to resistance to BET inhibitors, so BRD4 is emerging as a promising anticancer therapeutic target (33). Recent evidence suggests that BRD4 has additional non-transcriptional functions in cancer, affecting processes such as DNA damage repair, checkpoint activation, or telomere homeostasis (34). ERBB receptor feedback inhibitor 1(ERRFI1) was known as a tumor suppressor, and initiates cell growth by directly inhibiting the epidermal growth factor receptor and its downstream pathway. In addition, ERFFI1 inhibits another receptor family (Erbb), whose activation leads to cell survival, proliferation, migration, and invasion (35). A dual mechanism by which ERRFI1 regulates AKT has been identified. ERRF1 inhibits growth and enhances response to chemotherapy in cells expressing high levels of EGFR. This was partly mediated by ERRFI1-dependent direct inhibition of the negative regulation of AKT signaling by EGFR. In cells expressing low levels of EGFR, ERRFI1 positively regulates AKT by interfering with the interaction of the inactivated phosphatase PHLPP with AKT, thereby promoting cell growth and chemotherapy desensitization (36). N-myc Downstream regulated gene-1 (NDRG1) was a potent inhibitor of metastasis regulated by hypoxia, metal ions including iron, free radicals nitric oxide (NO), and various stress stimuli. This intriguing molecule had shown multiple functions in cancer, regulating a plethora of oncogenes through cellular signaling and inhibiting epithelial mesenchymal transition (EMT), cell migration and angiogenesis (37).

BCL2A1 is a member of the Bcl-2-associated protein family, as an anti-apoptotic protein associated with resistance to chemotherapeutic drugs and targeted drugs (38). The Bcl-2 protein family plays a key role in regulating the internal pathways apoptosis by inhibiting cytochrome C and releasing activated proteases (39). We found that BCL2A1 expression was higher in BC than in normal breast tissue, and the expression of BCL2A1 was upregulated as the malignancy of the molecular subtype of BC increased. We also found patients with high expression BC showed a better survival advantage, which may result from the high correlation of BCL2A1 with immune cells and immune checkpoints (CYLA4, PD-1, PD-L1). However, the tissue clump-based transcriptome sequencing data are indistinguishable between cancer cells and their surrounding machinery cells, suggesting that if BCL2A1 expression is increased in the machinery cells surrounding tumor cells, this could also lead to an increase in overall BCL2A1 expression levels. As there is no effective drugs to treat cancers that high expression BCL2A1 at present (40), the discovery of its target drug could provided value to guide clinical treatment. We found a significant correlation between BCL2A1 and vemurafenib by drug sensitivity analysis. We also analyzed the data of GSE97681 and found that the expression level of BCL2A1was significantly lower in the group using vemurafenib compared to the non-drug group.

BCL2A1 is present downstream of PI3K/AKT and is regulated by it, affecting survival. Vemurafenib (PLX4032) is a novel small molecule BRAF inhibitor that has been approved by

the US Food and Drug Administration for the treatment of patients with melanoma (41). One study found that applying Vemurafenib to a xenograft model of BC cells (MDA-MB-231) revealed that Vemurafenib treatment resulted in downregulation of PI3K-AKT signaling (19), which may be responsible for the downregulation of BCL2A1 expression after Vemurafenib. We found that vemurafenib had an inhibitory effect on the cell growth of MDA-MB-231, SKBR3 and MCF-7 cells by MTT assay. Further, we detected the level of PI3K/AKT signaling pathway in vemurafenib-treated cells by Western Blot and found that Vemurafenib significantly inhibited PI3K/AKT signaling pathway and the expression of BCL2A1. RT-qPCR confirmed the vemurafenib down-regulation of the expression of BCL2A1 too, and the results showed that vemurafenib inhibited the survival of MDA-MB-231, SKBR3 and MCF-7 cells.

In general, our study established an 11-gene prognostic model for predicting the efficacy of immunotherapy for BC, and further identified the 5 most core prognostic factors of the prognostic model, which plays a certain role in personalized treatment and accurate prognostic prediction for BC patients. In addition, this study also provides targeting reference drugs for the core prognostic genes to provide a reference for clinical practice, and the accuracy of drug targeting genes was verified by basic experiments and elucidates in detail that Vemurafenib suppresses BC by targeting the PI3K/AKT signaling pathway to inhibit the immune escape biomarker BCL2A1. However, further experimental studies and larger scale clinical trials are needed to further determine the applicability and accuracy of the 5 core factors that constitute prognostic markers for BC development and progression and the potential mechanisms of related drugs.

Conclusion

In summary, our 11-gene expression prediction model based on multiple data sets is more economical and clinically feasible than whole-gene sequencing. We also plotted histograms of five core prognostic factor prediction models, which can individually assess the prognosis of different patients by detecting the expression of genes. We also elucidate in detail that Vemurafenib suppresses BC by targeting the PI3K/AKT signaling pathway to inhibit the immune escape biomarker BCL2A1. Our findings will provide therapeutic targets for individualized treatment of BC and find its potential drugs, which will certainly be more beneficial for selecting effective treatments.

Data availability statement

The original contributions presented in the study are included in the article/Supplementary Material. Further inquiries can be directed to the corresponding author/s.

Author contributions

ZX, QW, and JS contributed to the concept, design, and review of the study. YD and DZ organize the database, LYa and DZ carry out statistical analysis. LYa, LZ conducted experiments, DL, YD and AS wrote the first manuscripts. All authors were involved in revising, reading, and approving the version of the submitted manuscript.

Funding

This work was supported by National Natural Science Foundation of China (No. 81972643, No. 82172962), Sichuan Science and Technology Project (2021YJ0201), Luzhou Science and Technology Bureau (2017LZXNYD-Z04), Sichuan Provincial Human Resources and Social Security Department (CW202002), Science and Technology Bureau of China (2017LZXNYD-Z04), Scientific Research Foundation for Doctors of the Affiliated Hospital of Southwest Medical University (20016) and Science and Technology Project founded by Southwest Medical University (2018- ZRZD-016).

Conflict of interest

The authors declare that the research was conducted in the absence of any commercial or financial relationships that could be construed as a potential conflict of interest.

Publisher's note

Supplementary material

The Supplementary Material for this article can be found online at: https://www.frontiersin.org/articles/10.3389/fonc.2022.906197/full#supplementary-material

FIGURE S1
The remaining Kaplan – Meier survival curve in Figure 1D and Figure 5A.

FIGURE S2
(A–E) GSE42568 verify the risk model. **(F)** Cluster analysis of high and low risk groups and 28 types of immune cells.

References

1. Sung H, Ferlay J, Siegel RL, Laversanne M, Soerjomataram I, Jemal A, et al. Global cancer statistics 2020: GLOBOCAN estimates of incidence and mortality worldwide for 36 cancers in 185 countries. *CA Cancer J Clin* (2021) 71(3):209–49. doi: 10.3322/caac.21660

2. Harbeck N, Gnant M. Breast cancer. *Lancet* (2017) 389(10074):1134–50. doi: 10.1016/s0140-6736(16)31891-8

3. Chen DS, Mellman I. Elements of cancer immunity and the cancer-immune set point. *Nature* (2017) 541(7637):321–30. doi: 10.1038/nature21349

4. Schreiber RD, Old LJ, Smyth MJ. Cancer immunoediting: integrating immunity's roles in cancer suppression and promotion. *Science* (2011) 331 (6024):1565–70. doi: 10.1126/science.1203486

5. De Jaeghere EA, Denys HG, De Wever O. Fibroblasts fuel immune escape in the tumor microenvironment. *Trends Cancer* (2019) 5(11):704–23. doi: 10.1016/j.trecan.2019.09.009

6. Wang S, Zhang Q, Yu C, Cao Y, Zuo Y, Yang L. Immune cell infiltration-based signature for prognosis and immunogenomic analysis in breast cancer. *Brief Bioinform* (2021) 22(2):2020–31. doi: 10.1093/bib/bbaa026

7. Waks AG, Winer EP. Breast cancer treatment: A review. *Jama* (2019) 321 (3):288–300. doi: 10.1001/jama.2018.19323

8. Emens LA. Breast cancer immunotherapy: Facts and hopes. *Clin Cancer Res* (2018) 24(3):511–20. doi: 10.1158/1078-0432.Ccr-16-3001

9. Jia H, Truica CI, Wang B, Wang Y, Ren X, Harvey HA, et al. Immunotherapy for triple-negative breast cancer: Existing challenges and exciting prospects. *Drug Resist Update* (2017) 32:1–15. doi: 10.1016/j.drup.2017.07.002

10. Uno T, Takeda K, Kojima Y, Yoshizawa H, Akiba H, Mittler RS, et al. Eradication of established tumors in mice by a combination antibody-based therapy. *Nat Med* (2006) 12(6):693–8. doi: 10.1038/nm1405

11. Smyth MJ, Ngiow SF, Ribas A, Teng MW. Combination cancer immunotherapies tailored to the tumour microenvironment. *Nat Rev Clin Oncol* (2016) 13(3):143–58. doi: 10.1038/nrclinonc.2015.209

12. Esteva FJ, Hubbard-Lucey VM, Tang J, Pusztai L. Immunotherapy and targeted therapy combinations in metastatic breast cancer. *Lancet Oncol* (2019) 20 (3):e175–e86. doi: 10.1016/s1470-2045(19)30026-9

13. Network CGA:. Comprehensive molecular portraits of human breast tumours. *Nature* (2012) 490(7418):61–70. doi: 10.1038/nature11412

14. Ruggles KV, Krug K, Wang X, Clauser KR, Wang J, Payne SH, et al. Methods, tools and current perspectives in proteogenomics. *Mol Cell Proteomics* (2017) 16(6):959–81. doi: 10.1074/mcp.MR117.000024

15. Lawson KA, Sousa CM, Zhang X, Kim E, Akthar R, Caumanns JJ, et al. Functional genomic landscape of cancer-intrinsic evasion of killing by T cells. *Nature* (2020) 586(7827):120–6. doi: 10.1038/s41586-020-2746-2

16. O'Leary B, Finn RS, Turner NC. Treating cancer with selective CDK4/6 inhibitors. *Nat Rev Clin Oncol* (2016) 13(7):417–30. doi: 10.1038/nrclinonc.2016.26

17. Wang R, Yang Y, Ye WW, Xiang J, Chen S, Zou WB, et al. Case report: Significant response to immune checkpoint inhibitor camrelizumab in a heavily pretreated advanced ER+/HER2- breast cancer patient with high tumor mutational burden. *Front Oncol* (2020) 10:588080. doi: 10.3389/fonc.2020.588080

18. Maughan KL, Lutterbie MA, Ham PS. Treatment of breast cancer. *Am Fam Physician* (2010) 81(11):1339–46.

19. Zhang ZX, Jin WJ, Yang S, Ji CL. BRAF kinase inhibitor exerts anti-tumor activity against breast cancer cells *via* inhibition of FGFR2. *Am J Cancer Res* (2016) 6(5):1040–52.

20. Pircher M, Winder T, Trojan A. Response to vemurafenib in metastatic triple-negative breast cancer harbouring a BRAF V600E mutation: A case report and electronically captured patient-reported outcome. *Case Rep Oncol* (2021) 14 (1):616–21. doi: 10.1159/000513905

21. Bhattacharya S, Andorf S, Gomes L, Dunn P, Schaefer H, Pontius J, et al. ImmPort: disseminating data to the public for the future of immunology. *Immunol Res* (2014) 58(2–3):234–9. doi: 10.1007/s12026-014-8516-1

22. Gao J, Aksoy BA, Dogrusoz U, Dresdner G, Gross B, Sumer SO, et al. Integrative analysis of complex cancer genomics and clinical profiles using the cBioPortal. *Sci Signal* (2013) 6(269):pl1. doi: 10.1126/scisignal.2004088

23. Charoentong P, Finotello F, Angelova M, Mayer C, Efremova M, Rieder D, et al. Pan-cancer immunogenomic analyses reveal genotype-immunophenotype relationships and predictors of response to checkpoint blockade. *Cell Rep* (2017) 18 (1):248–62. doi: 10.1016/j.celrep.2016.12.019

24. Liu CJ, Hu FF, Xia MX, Han L, Zhang Q, Guo AY. GSCALite: a web server for gene set cancer analysis. *Bioinformatics* (2018) 34(21):3771–2. doi: 10.1093/bioinformatics/bty411

25. Li T, Fan J, Wang B, Traugh N, Chen Q, Liu JS, et al. TIMER: A web server for comprehensive analysis of tumor-infiltrating immune cells. *Cancer Res* (2017) 77(21):e108–e10. doi: 10.1158/0008-5472.Can-17-0307

26. Reinhold WC, Sunshine M, Liu H, Varma S, Kohn KW, Morris J, et al. CellMiner: a web-based suite of genomic and pharmacologic tools to explore transcript and drug patterns in the NCI-60 cell line set. *Cancer Res* (2012) 72 (14):3499–511. doi: 10.1158/0008-5472.Can-12-1370

27. Jácome AA, Coutinho AK, Lima EM, Andrade AC, Dos Santos JS. Personalized medicine in gastric cancer: Where are we and where are we going? *World J Gastroenterol* (2016) 22(3):1160–71. doi: 10.3748/wjg.v22.i3.1160

28. Loumaye A, Thissen JP. Biomarkers of cancer cachexia. *Clin Biochem* (2017) 50(18):1281–8. doi: 10.1016/j.clinbiochem.2017.07.011

29. Lien EC, Dibble CC, Toker A. PI3K signaling in cancer: beyond AKT. *Curr Opin Cell Biol* (2017) 45:62–71. doi: 10.1016/j.ceb.2017.02.007

30. Gingras AC, Raught B, Sonenberg N. eIF4 initiation factors: effectors of mRNA recruitment to ribosomes and regulators of translation. *Annu Rev Biochem* (1999) 68:913–63. doi: 10.1146/annurev.biochem.68.1.913

31. Rojo F, Najera L, Lirola J, Jiménez J, Guzmán M, Sabadell MD, et al. 4E-binding protein 1, a cell signaling hallmark in breast cancer that correlates with pathologic grade and prognosis. *Clin Cancer Res* (2007) 13(1):81–9. doi: 10.1158/1078-0432.Ccr-06-1560

32. Castellvi J, Garcia A, Rojo F, Ruiz-Marcellan C, Gil A, Baselga J, et al. Phosphorylated 4E binding protein 1: a hallmark of cell signaling that correlates with survival in ovarian cancer. *Cancer* (2006) 107(8):1801–11. doi: 10.1002/cncr.22195

33. Jin X, Yan Y, Wang D, Ding D, Ma T, Ye Z, et al. DUB3 promotes BET inhibitor resistance and cancer progression by deubiquitinating BRD4. *Mol Cell* (2018) 71(4):592–605.e4. doi: 10.1016/j.molcel.2018.06.036

34. Donati B, Lorenzini E, Ciarrocchi A. BRD4 and cancer: going beyond transcriptional regulation. *Mol Cancer* (2018) 17(1):164. doi: 10.1186/s12943-018-0915-9

35. Baselga J, Swain SM. Novel anticancer targets: revisiting ERBB2 and discovering ERBB3. *Nat Rev Cancer* (2009) 9(7):463–75. doi: 10.1038/nrc2656

36. Cairns J, Fridley BL, Jenkins GD, Zhuang Y, Yu J, Wang L. Differential roles of ERRFI1 in EGFR and AKT pathway regulation affect cancer proliferation. *EMBO Rep* (2018) 19(3):e44767. doi: 10.15252/embr.201744767

37. Park KC, Paluncic J, Kovacevic Z, Richardson DR. Pharmacological targeting and the diverse functions of the metastasis suppressor, NDRG1, in cancer. *Free Radic Biol Med* (2020) 157:154–75. doi: 10.1016/j.freeradbiomed.2019.05.020

38. Vogler M. BCL2A1: the underdog in the BCL2 family. *Cell Death Differ* (2012) 19(1):67–74. doi: 10.1038/cdd.2011.158

39. García-Sáez AJ. The BCL-2 family saga. *Nat Rev Mol Cell Biol* (2020) 21 (10):564–5. doi: 10.1038/s41580-020-0276-2

40. Hiraki M, Maeda T, Mehrotra N, Jin C, Alam M, Bouillez A, et al. Targeting MUC1-c suppresses BCL2A1 in triple-negative breast cancer. *Signal Transduct Target Ther* (2018) 3:13. doi: 10.1038/s41392-018-0013-x

41. Hyman DM, Puzanov I, Subbiah V, Faris JE, Chau I, Blay JY, et al. Vemurafenib in multiple nonmelanoma cancers with BRAF V600 mutations. *N Engl J Med* (2015) 373(8):726–36. doi: 10.1056/NEJMoa1502309

Frontiers in Oncology

Advances knowledge of carcinogenesis and tumor progression for better treatment and management

The third most-cited oncology journal, which highlights research in carcinogenesis and tumor progression, bridging the gap between basic research and applications to imrpove diagnosis, therapeutics and management strategies.

Discover the latest Research Topics

See more →

Frontiers

Avenue du Tribunal-Fédéral 34
1005 Lausanne, Switzerland
frontiersin.org

Contact us

+41 (0)21 510 17 00
frontiersin.org/about/contact